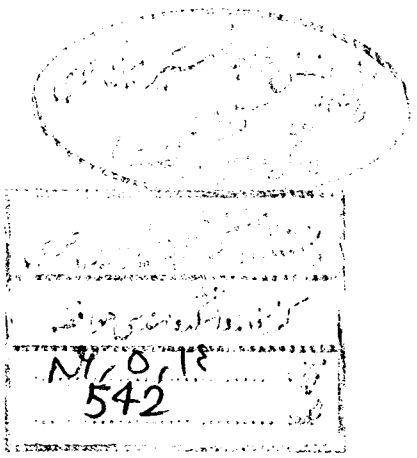

# Gas Dynamics

## Third Edition

James E. John

*President, Kettering University*
*Flint, Michigan*

Theo G. Keith

*Department of Mechanical*
*and Manufacturing Engineering*
*University of Toledo*
*Toledo, Ohio*


Pearson Education International

Vice President and Editorial Director, ECS: *Marcia J. Horton*
Executive Managing Editor: *Vince O'Brien*
Managing Editor: *David A. George*
Production Editor: *Wendy Kopf*
Director of Creative Services: *Paul Belfanti*
Creative Director: *Jayne Conte*
Cover Designer: *Bruce Kenselaar*
Art Editor: *Greg Dulles*
Manufacturing Buyer: *Lisa McDowell*



Pearson Prentice Hall
Pearson Education, Inc.
Upper Saddle River, New Jersey 07458



Printed in the United States of America

10 9 8 7 6 5 4 3 2 1

ISBN 0-13-202331-8

Pearson Education Ltd., *London*
Pearson Education Australia Pty. Ltd., *Sydney*
Pearson Education Singapore, Pte. Ltd.
Pearson Education North Asia Ltd., *Hong Kong*
Pearson Education Canada Inc., *Toronto*
Pearson Educación de Mexico, S.A. de C.V.
Pearson Education—Japan, *Tokyo*
Pearson Education Malaysia, Pte. Ltd.
Pearson Education, Inc., *Upper Saddle River, New Jersey*

*To Connie, the inspiration in my life*
*JEAJ*

*To Sandra and our daughters Robin and Nicole*
*TGK*

# Contents

# Preface

The first edition of *Gas Dynamics* appeared in 1969 and the second edition in 1984. Thus, at this writing, *Gas Dynamics* has been in print for over three and one-half decades and has not been revised in more than two decades. During this time-span, much has occurred technologically. Accordingly, it was decided that a substantial revision of the text was needed. To accomplish this task a second author (a former student and colleague as well as a lifelong friend of the first author) was added. It was apparent that given the book's long-term popularity, any revision had to build upon and retain many of the features of the previous editions. Hence, those who have used the earlier editions will find familiar material embedded in a more comprehensive treatment.

Albeit *Gas Dynamics*, Third Edition is an expanded version, it still retains the fundamental purpose that was described in the Preface of the first edition, *viz.*: This book is intended to provide the undergraduate and first-level graduate engineering student with a knowledge and understanding of the basic fundamentals of compressible flow and gas dynamics. The material covered should serve to bridge the gap between sophomore- or junior-level courses in thermodynamics and fluid mechanics as well as advanced courses in propulsion, turbomachinery, energy conversion, advanced fluid mechanics, and advanced aerodynamics.

*Gas Dynamics*, Third Edition contains a number of modifications and changes over the earlier versions. These new features include the following:

1. Makes exclusive use of spreadsheet computations (a first in books on gas dynamics).
    - Spreadsheet programs require no knowledge of any computer language (e.g., FORTRAN or C). Because every student in engineering is exposed to spreadsheet programming, they should be very comfortable with this computational tool.
    - Spreadsheet programs eliminate or at least minimize dependence on the use of tables and charts (along with the laborious table look-up and interpolation procedures required to solve gas dynamics problems) that are found in every book on gas dynamics.
    - Spreadsheet programs are used throughout the book to solve a wide variety of gas dynamic problems. For example, they are used to compute the

speed of sound in a real gas, to determine flow properties across shocks and expansion fans, to determine the confluence of shocks at the trailing edge of an supersonic airfoil, to numerically solve the Taylor–MacColl conical shock equation, to compute frictional flow through variable ducts, and many more.

- An appendix is included that provides details to assist with the development of spreadsheet solvers.

2. Introduces several computational procedures that have not previously appeared in gas dynamics texts. For example:
   - A noniterative method to locate a normal shock in a C–D nozzle.
   - An efficient numerical procedure to determine the flow properties across an oblique shock wave.
   - A noniterative method to locate a normal shock in a constant area duct with friction that is connected to a reservoir by a C–D nozzle.
3. Many example problems are included in each chapter. Every example problem is prefaced with a title, which provides a brief indication of the objective of the problem.
4. A chapter capstone application section is included in the first 10 chapters.
5. New chapters have been written on Moving Normal Shockwaves (Chapter 5) and on Exact Solutions (Chapter 12).
6. Expanded versions of chapters have been prepared on Characteristics (Chapter 14) and Measurements in Compressible Flow (Chapter 15).
7. An assortment of historical notes has been sprinkled throughout the text. These notes describe some of the individuals (several who may not be familiar to many) and their accomplishments in gas dynamics.

Eliminated from previous editions are two chapters entitled Applications I (Chapter 5) and Applications II (Chapter 8). The material within these chapters was incorporated into several of the current chapters. Also eliminated were Flow with Applied Electric and Magnetic Fields (Chapter 11), Imperfect Gas Effects (Chapter 12), and Rarefied Gas Dynamics (Chapter 16).

*Gas Dynamics*, Third Edition contains 50% more example and end-of-chapter problems than the second edition. The book also contains over 90% more references than earlier editions.

The authors wish to thank a number of individuals without whose help this book could not have been completed. These include a truly exceptional group of graduate students (most of whom at this writing have completed their Ph.D) at the University of Toledo: Sorin Cioc, Carmen Cioc, Anahita Ayasoufi, Ramin Rahmani, Laurentiu Morau, Nicolete Ene, Peter Kenney, Daniel Wang, and Ping Wang. The group always miraculously found time to provide their enthusiastic assistance. Special thanks go to a very special person: Karen Balog, who typed the draft chapters from the second edition and who was always supportive of the project.

The authors also wish to thank the reviewers: William W. Liou, Western Michican University; Gerald S. Jakubowski, Arizona State University; Jay M. Khodadadi, Auburn University; and Forman A. Williams, University of California at San Diego.

The authors also wish to acknowledge the excellent assistance provided to them by their production editor at Pearson Education/Prentice Hall, Wendy Kopf.

JAMES E. A. JOHN

THEO G. KEITH

# Chapter 1

# Basic Equations of Compressible Flow

## 1.1 FLUIDS: LIQUIDS AND GASES

A *fluid* is a substance that cannot sustain a shear stress: It is, in other words, a substance that deforms continuously when subjected to shear. This is unlike a solid, which, under the action of a shear stress, will deform and then remain at equilibrium. This difference between solids and fluids shows up in the tendency of fluids to flow under the action of shear, whereas solids remain rigid.

From a molecular point of view, in solids there exist very strong intermolecular attractive forces; in fluids, these intermolecular forces are very much weaker. The definition of a fluid, as previously stated, includes both liquids and gases. From common experience, we know that the difference between these is that, whereas liquids tend to occupy a more or less well-defined volume, gases will fill the volume allotted to them. In other words, the intermolecular attractive forces between gas molecules are much less than the forces between liquid molecules.

Because water and other liquids tend to occupy a fixed or well-defined volume, it is generally assumed that the *density* ($\rho$) of a liquid, defined as the mass per unit volume, remains constant under the action of an externally applied pressure. Actually, large pressures exerted on a liquid in a container can cause slight changes in the liquid volume (e.g., imposing a pressure of 200 times normal atmospheric pressure on liquid water raises the density by 1 percent). However, the rate of change of density with pressure is small enough so that, in a study of the flow of liquids, it is generally assumed that no changes in density occur as the result of the pressure variation. This type of flow is called *incompressible flow.*

With a gas, however, large density changes can occur as a result of an externally applied pressure. We have only to look at an equation of state for a gas (e.g., $p = \rho RT$)

molecules must be analyzed. This field of study is called *rarefied gas dynamics*, which is beyond the scope of this book; thus, continuum flow will be assumed throughout this text.

## 1.3 VISCOSITY AND THE BOUNDARY LAYER

The *coefficient of viscosity* of a fluid relates the shearing stress applied to a fluid to the resultant rate of shearing strain. In a continuum, when a viscous fluid flows over a fixed surface, layers of fluid next to the surface are held back by the viscous forces and stick to the surface; in other words, the velocity of the fluid at the fixed wall is zero. As we move away from the wall, the velocity increases to its free stream value and a velocity distribution is built up, as shown in Figure 1.1. The effects of viscosity are dominant in the region near the surface. For most fluids, and certainly for gases, this viscosity is quite small, so viscous effects are confined to a very thin layer in the vicinity of the surface, called the *boundary layer.* Outside the boundary layer, the fluid can be analyzed with *inviscid theory*.

In a boundary layer, the velocity components of a continuum flow at a fixed surface are zero, both normal and tangential to the wall surface. On the other hand, in an inviscid flow (zero viscosity), the normal component at the wall is zero, yet the tangential component need not be zero. The boundary-layer equations, unlike the inviscid-flow equations, have terms containing the viscous forces, which makes them far more difficult to handle. Fortunately, the boundary layer is usually thin enough that it can be assumed that there is no pressure gradient in the direction normal to the wall surface. Thus, the pressure distribution on a body, even in the presence of a boundary layer, can often be calculated using the simpler inviscid-flow equations. Furthermore, in considering the flow of a gas through an internal passage or nozzle, usually the boundary layer thickness can be taken as small enough so as not to appreciably affect the area available to the inviscid flow outside the boundary layer and thus not to require the tedious calculation of boundary-layer thickness along the walls, as illustrated in Figure 1.2.

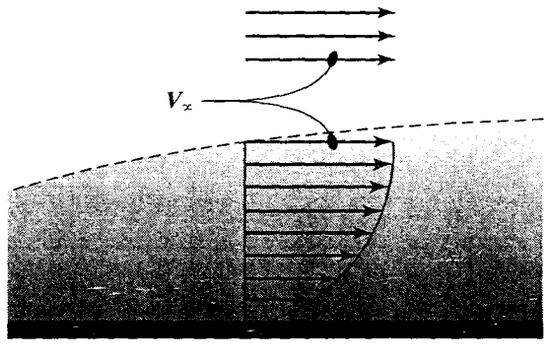


**Figure 1.1** Boundary-Layer Flow

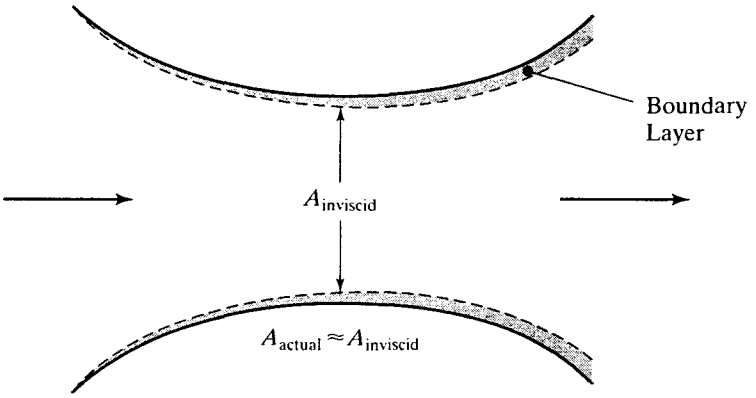


**Figure 1.2** Nozzle Flow

For a wide variety of cases, then, viscous forces can be neglected in the analysis of gas flows. However, in other cases, such as the calculation of convective heat-transfer coefficients, skin-friction drag, and flow separation, viscous forces are very important and play a large part in the resultant analysis.

## 1.4 EQUATIONS OF MOTION

In a study of basic fluid mechanics covering the flow of water and other liquids, incompressible flow can be assumed, and therefore density does not vary. For this type of flow, two equations are generally sufficient to solve the problems encountered: the continuity equation, or conservation of mass, and a form of the *Bernoulli equation* derivable from either momentum or energy considerations. The variables are generally pressure and velocity.

For a compressible flow, density becomes an additional variable; furthermore, significant variations in fluid temperature may occur as a result of density or pressure changes. There are four possible unknowns, and thus four equations are required for the solution of a problem in compressible-gas dynamics: equations for the conservation of mass, momentum, and energy, and a thermodynamic equation of state for the substance involved. Since a study of compressible flow necessarily involves an interaction between thermodynamics and fluid mechanics, the remainder of this chapter will be devoted to a review of the basic principles and equations of these two sciences. To simplify the working of problems involving the fundamental equations, the next section will discuss very briefly the system of units to be used throughout the text.

## 1.5 UNITS OF MEASUREMENT

In any engineering subject, considerable care must be exercised in the use of a consistent set of units. The primary dimensions for an engineer consist of mass, length, time, and temperature. The system of units to be used throughout this text will be the International System (SI). In SI units, the unit of mass is the kilogram (kg), the unit of length

**TABLE 1.1** Prefixes of Units

| **Factor** | $10^{12}$ | $10^{9}$ | $10^{6}$ | $10^{3}$ | $10^{-2}$ | $10^{-3}$ | $10^{-6}$ | $10^{-9}$ | $10^{-12}$ |
|---|---|---|---|---|---|---|---|---|---|
| **Prefix** | Tera | Giga | Mega | Kilo | Centi | Milli | Micro | Nano | Pico |
| **Symbol** | T | G | M | k | c | m | $\mu$ | n | p |

is the meter (m), the unit of time is the second (s), and the unit of temperature is the degree Kelvin (K). It is also common practice to express temperature in degrees Celsius (°C), where K = °C + 273.15. (**Calculation Note:** In the calculations that follow, we will use 273 for simplicity instead of the more accurate value of 273.15.)

The units of length, time, and temperature present little difficulty. However, the differentiation between units of force and mass is not as easily grasped and should be reviewed. Force and mass are related by Newton's second law of motion, $F = ma$. In SI units, the unit of force is the newton (N), defined as the force required to accelerate a mass of 1 kilogram at the rate of 1 meter per second per second:

$$1\ \text{N} = 1\ \text{kg} \cdot \text{m/s}^2$$

*Weight* is the force with which a mass is attracted to the earth or some other body. From the law of conservation of mass, the mass of a body remains constant, independent of distance from the earth's surface. However, body weight decreases as it is moved away from earth.

The multiplying prefixes in Table 1.1 will be used in conjunction with the various units. For example, 1 kN = 1000 N, 1 cm = 0.01 m, and 1 $\mu$g = 0.000001 g. Units of energy are joules (J), where 1 J = 1 N-m. *Power*, the rate of doing work, has units of watts (W), where 1 W = 1 J/s.

Pressure was defined in Section 1.2 as a normal force per unit area. Pressure in SI units is expressed in newtons per square meter ($\text{N/m}^2$). One $\text{N/m}^2$ is called 1 pascal (Pa). For comparison, 1 standard atmosphere is equal to 101,325 Pa, or 101.325 kPa, or 1.01325 bar, or 0.101325 MPa. Pressure given relative to zero pressure is called *absolute pressure*; pressure given relative to the atmospheric pressure of the surroundings is called *gauge pressure*. For example, a pressure gauge connected to a tank containing compressed air registers 100 kPa; if the local atmospheric pressure is 101 kPa, the absolute pressure inside the tank is 201 kPa. Unless indicated otherwise, pressures given in pascals throughout this text will refer to absolute pressures.

## 1.6 EQUATION OF STATE

An equation of state for a pure substance is a relation between pressure, density, and temperature for that substance. Depending on the phase of the substance and on the range of conditions to which the substance is subjected, one of a number of different equations of state is applicable. However, for liquids or solids, these equations become so cumbersome and have such a limited range of application that it is generally more

convenient to use tables of thermodynamic properties or a computer to solve them. For gases, an equation that does have a reasonably wide range of application exists: the *perfect-gas law.* (*Note*: This law is also referred to as *the ideal-gas law*—derived from Charles's and Boyle's laws.) In its usual form, it is expressed as

$$p = \rho RT \tag{1.2}$$

where $R$ is a gas constant whose value is dependent on the gas in question. For any perfect gas,

$$R = \frac{\mathbf{R}}{\mathrm{MM}} \tag{1.3}$$

where $\mathbf{R}$ (*the universal gas constant* = 8314.3 J/(kg–mole · K) and MM is the *molecular mass of gas.* For example, for air with MM = 28.97 kg/(kg–mole),

$$R = \frac{8314.3\left(\dfrac{\mathrm{J}}{\mathrm{kg\text{–}mole \cdot K}}\right)}{28.97\left(\dfrac{\mathrm{kg}}{\mathrm{kg\text{–}mole}}\right)}\left(\frac{1\ \mathrm{kJ}}{1000\ \mathrm{J}}\right) = 0.287\frac{\mathrm{kJ}}{\mathrm{kg \cdot K}}$$

In the derivation of the perfect-gas law from kinetic theory, the volume of the gas molecules and the forces between the molecules are neglected. A real gas only at very low pressures satisfies these assumptions. However, even at reasonably high pressures, a real gas approximates a perfect gas as long as the gas temperature is great enough.

For example, for steam at 6 MPa and 500°C, the deviation of a perfect gas from a real gas is only about 5 percent. As the steam is cooled at this pressure so that its state approaches the saturation line, the deviation becomes more marked.

More exact equations of state have been derived that account for molecular volumes (the *Clausius equation of state)* and intermolecular forces (the *van der Waals equation of state).* These equations are more complex than the perfect-gas law and lend added complications to the solutions of the flow equations. The perfect-gas law, simple as it is, yields uncomplicated expressions for the various thermodynamic properties and can be applied over a wide range of pressures and temperatures with a high degree of accuracy.

James Prescott Joule (1818–1889) demonstrated that the specific internal energy of a perfect gas is a function of temperature only:

$$u = u(T)$$

According to the definition of specific heat at constant volume,

$$c_v = \left(\frac{\partial u}{\partial T}\right)_v \tag{1.4}$$

so that, for a perfect gas,

$$du = c_v\, dT \tag{1.5}$$

*Enthalpy* is defined as

$$h = u + \frac{p}{\rho} \tag{1.6}$$

or

$$dh = du + d\left(\frac{p}{\rho}\right)$$

and, for a perfect gas,

$$dh = du + R\,dT \tag{1.7}$$

Therefore, the enthalpy of a perfect gas is also a function of temperature only.

The definition of specific heat at constant pressure is

$$c_p = \left(\frac{\partial h}{\partial T}\right)_p \tag{1.8}$$

so that, for a perfect gas,

$$dh = c_p\,dT \tag{1.9}$$

Thus, combining Eqs. (1.7), (1.5), and (1.9), we see that

$$c_p - c_v = R \tag{1.10}$$

where $c_p$ and $c_v$ are not necessarily constants, but can vary with temperature.

If a perfect gas undergoes a thermodynamic process between two equilibrium states, then

$$u_2 - u_1 = \int_1^2 c_v\,dT \tag{1.11}$$

and

$$h_2 - h_1 = \int_1^2 c_p\,dT \tag{1.12}$$

If a constant specific heat (or else a mean specific heat over the temperature range of interest) is assumed, then

$$u_2 - u_1 = c_v(T_2 - T_1) \tag{1.13}$$

and

$$h_2 - h_1 = c_p(T_2 - T_1) \tag{1.14}$$

## 1.7 CONTROL-VOLUME APPROACH

Two approaches are possible in writing the equations of motion of a fluid. One of these, *the Lagrangian approach*, follows a fixed mass of fluid particles as it moves throughout the flow field. The other, *the Eulerian approach*, considers a fixed control volume in the flow field and relates the movements of mass, momentum, and energy across the control-volume boundaries to changes taking place inside the control volume. A great majority of the problems that are encountered deal with steady flow, in which the flow properties at a point in the fluid do not change with time. Whereas a fluid particle can accelerate or decelerate as it moves from point to point in the flow field, steady flow requires that the velocity of all particles passing by a given point have the same value at that point. It is more convenient to use the control-volume approach so that, for steady flow, time is not an independent variable. This approach will be used exclusively throughout the text.

To use the familiar form of Newton's laws of motion, in which a fixed mass of particles is considered, it is necessary to relate the fixed-mass system to the control volume, as is shown in Figure 1.3. Let $S_1$ be the boundary of a system of particles at time $t$. The control volume is selected as the volume bounded by $S_1$. Hence, the system and control-volume boundaries are coincident at time $t$. Fluid passes through the control volume. After a time interval $\Delta t$, the mass of particles within $S_1$ at time $t$ will have moved to a new location in the flow field, bounded by $S_2$. Let $X(t)$ be the total mass, momentum, or energy possessed by the system of particles at time $t$. Divide regions $S_1$ and $S_2$ as shown in Figure 1.3, so that $\forall_1 + \forall_2$ equals the volume bounded by $S_1$, and $\forall_2 + \forall_3$ equals the volume bounded by $S_2$. Now we have

$$X(t) = X_{\forall_1}(t) + X_{\forall_2}(t) \tag{1.15}$$

where, for example, $X_{\forall 1}(t)$ represents the mass, momentum, or energy possessed by the fluid particles in $\forall_1$ at time $t$. At $t + \Delta t$,

$$X(t + \Delta t) = X_{\forall_2}(t + \Delta t) + X_{\forall_3}(t + \Delta t) \tag{1.16}$$

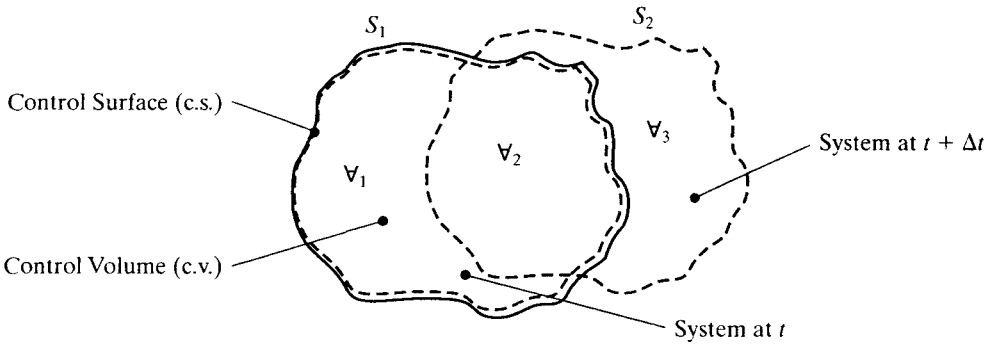


**Figure 1.3** Relation between the System and Control Volume

The change in $X$ of the system of particles during $\Delta t$ is determined by subtracting Eq. (1.15) from Eq. (1.16), yielding

$$X(t + \Delta t) - X(t) = X_{\forall_2}(t + \Delta t) - X_{\forall_2}(t) + X_{\forall_3}(t + \Delta t) - X_{\forall_1}(t) \quad (1.17)$$

or by adding and subtracting $X_{\forall_1}(t + \Delta t)$, yielding

$$\begin{aligned} X(t + \Delta t) - X(t) = {} & [X_{\forall_2}(t + \Delta t) + X_{\forall_1}(t + \Delta t)] - [X_{\forall_2}(t) + X_{\forall_1}(t)] \\ & + [X_{\forall_3}(t + \Delta t) - X_{\forall_1}(t + \Delta t)] \end{aligned}$$

Divide this equation by $\Delta t$ to get

$$\frac{\Delta X}{\Delta t} = \frac{\Delta X_{\forall_2 + \forall_1}}{\Delta t} + \frac{X_{\forall_3}(t + \Delta t) - X_{\forall_1}(t + \Delta t)}{\Delta t} \quad (1.18)$$

Let $\Delta t$ approach zero so that the volume $(\forall_1 + \forall_2)$ approaches that of the control volume. The left-hand side of Eq. (1.18) represents the time rate of change of $X$ within the system [i.e., $(dX/dt)_{\text{system}}$]. In fluid mechanics, this derivative is written as $DX/Dt$ and called either the *material* or *substantial derivative* because it represents the change of $X$ with time as a fixed amount of material moves with the fluid. (For more detail, refer to Chapter 11.) It is the time rate of change of $X$ in following the motion of the fluid. The first term on the right-hand side of Eq. (1.18) becomes the rate of change of $X$ within the control volume [i.e., $(\partial X/\partial t)_{\text{c.v.}}$]. A partial derivative appropriately appears because $X$ can be a function of both time and space.

The second term expresses the difference between the rate at which $X$ leaves the control volume and that at which it enters the control volume. This net rate of efflux can be expressed in more familiar terms. Let $x$ be equal to the value of $X$ per unit mass. Consider an elemental area $d\mathbf{A}$ on the surface of the control volume in Figure 1.4. (*Note:* The vector $d\mathbf{A}$ is assumed positive with the normal to the differential area pointing outward.) The rate at which mass flows across this area is given by the dot product

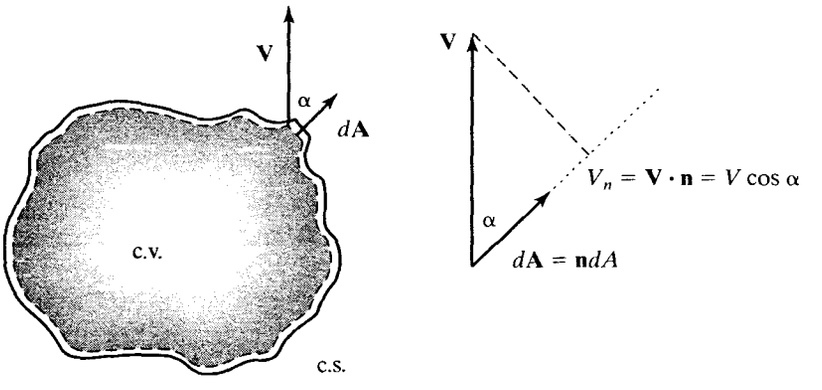


**Figure 1.4** Efflux from a Control Volume

$\rho \mathbf{V} \cdot d\mathbf{A}$, so the rate of efflux of $X$ across $d\mathbf{A}$ is given by $x\rho \mathbf{V} \cdot d\mathbf{A}$. To account for all the mass flow across the control surface, we must integrate over the boundary c.s. Now Eq. (1.18) can be written as

$$\left(\frac{dX}{dt}\right)_{\substack{\text{for fixed mass}\\ \text{system of}\\ \text{particles moving}\\ \text{with fluid}}} = \frac{DX}{Dt} = \left(\frac{\partial X}{\partial t}\right)_{\substack{\text{for fluid in}\\ \text{control}\\ \text{volume}}} + \left(\iint_{\text{c.s.}} x(\rho \mathbf{V} \cdot d\mathbf{A})\right)_{\substack{\text{integration around}\\ \text{surface bounding}\\ \text{control volume}}} \tag{1.19}$$

The time rate of change of $X$ within the control volume can also be written as an integral because for any small mass $dm$ within the control volume $dX_{\text{c.v.}} = xdm = x\rho d\forall$. Finally, we integrate over the entire control volume to get

$$\frac{DX}{Dt} = \frac{\partial}{\partial t} \iiint_{\text{c.v.}} x\rho d\forall + \iint_{\text{c.s.}} x(\rho \mathbf{V} \cdot d\mathbf{A}) \tag{1.20}$$

Equation (1.20), often referred to as the *Reynolds transport equation*, relates the properties of a fixed-mass system of fluid particles to the properties of the fluid inside of, and crossing, the boundaries of the control volume. The equations of conservation of mass, momentum, and energy for a fluid can now be related to the control volume.

## 1.8 CONSERVATION OF MASS

For the equation of conservation of mass, or the continuity equation, let $X$ equal the total mass $m$ of the system of fluid particles. For this fixed-mass system, $Dm/Dt = 0$, since mass can be neither created nor destroyed. Since $x$ refers to the total mass per unit mass, it is equal to 1. Equation (1.20) reduces to the following form, which is called the *continuity equation*:

$$0 = \frac{\partial}{\partial t} \iiint_{\text{c.v.}} \rho d\forall + \iint_{\text{c.s.}} \rho \mathbf{V} \cdot d\mathbf{A} \tag{1.21}$$

The rate of increase of mass within the control volume must equal the net rate of mass flux into the control volume. Note that if the density is uniform over the control volume, the first integral in Eq. (1.21) may be written as

$$\frac{\partial}{\partial t} \iiint_{\text{c.v.}} \rho d\forall = \frac{\partial}{\partial t}(\rho \forall)_{\text{c.v.}} = \frac{\partial}{\partial t}(m)_{\text{c.v.}} \tag{1.22}$$

The second integral in Eq. (1.21) is positive at outflow boundaries and negative at inflow boundaries; that is,

$$\iint_{\text{c.s.}} \rho \mathbf{V} \cdot d\mathbf{A} = \iint_{\text{outflow}} \rho V_n \, dA - \iint_{\text{inflow}} \rho V_n \, dA \tag{1.23}$$

This follows from the fact that if $\mathbf{V}$ is in the same direction as $d\mathbf{A} = \mathbf{n} \, dA$ (i.e., $\alpha = 0$), Eq. (1.23) is $+\rho V_n A$, whereas, on the other hand, if $\mathbf{V}$ and $\mathbf{n}$ are in opposite directions (i.e., $\alpha = \pi$), Eq. (1.23) yields $-\rho V_n A$. If $\mathbf{V}$ does not vary in either magnitude or direction across a cross-sectional area $A$ of the flow and if $\rho$ is uniform across $A$, then Eq. (1.23) can be written as

$$\iint_{\text{c.s.}} \rho \mathbf{V} \cdot d\mathbf{A} = \sum_{\text{outflow}} (\rho V_n A) - \sum_{\text{inflow}} (\rho V_n A) \tag{1.24}$$

where the summations account for flows across all inlets and exits to the control volume and where $V_n (= V \cos \alpha)$ is the normal velocity component to the flow area, as shown in Figure 1.4. The product $\rho V_n A$ is the mass-flow rate $\dot{m}$. Thus, Eq. (1.24) may also be expressed as

$$\iint_{\text{c.s.}} \rho \mathbf{V} \cdot d\mathbf{A} = \sum_{\text{outflow}} \dot{m} - \sum_{\text{inflow}} \dot{m} \tag{1.25}$$

Thus, for uniform conditions within and on the boundaries of the control volume, we may use the following instead of the integral version of the continuity equation, Eq. (1.21):

$$\frac{d}{dt}(m)_{\text{c.v.}} + \sum_{\text{outflow}} \dot{m} - \sum_{\text{inflow}} \dot{m} = 0 \tag{1.26}$$

Clearly, for steady flow, the properties within the control volume do not change with time; hence,

$$\frac{\partial}{\partial t} \iiint_{\text{c.v.}} \rho \, d\forall = \frac{d}{dt}(m)_{\text{c.v.}} = 0 \tag{1.27}$$

Therefore,

$$\iint_{\text{c.s.}} \rho \mathbf{V} \cdot d\mathbf{A} = \sum_{\text{outflow}} \dot{m} - \sum_{\text{inflow}} \dot{m} = 0 \tag{1.28}$$

**Example 1.1. Mass in a punctured air cylinder**

An air cylinder of volume $\forall$ is accidentally punctured. The puncture creates a hole having a cross-sectional area $A_e$. The air escapes through the hole according to the relation

$$\dot{m}_e = 0.040418 \frac{p}{\sqrt{T}} A_e$$

where $p$ is the tank pressure and $T$ is the tank temperature. (We will derive this expression in Chapter 3.) The constant 0.040418 is based on the properties of air, and the units are $N/m^2$ for pressure, K for temperature, $m^2$ for area, and kg/s for mass-flow rate. Assuming that the temperature of the air in the cylinder does not change with time, find the mass of air, $m_2$, in kg, that remains in the cylinder $\Delta t$ sec after the cylinder is punctured. How long would it take for the tank to lose one half of its mass?

**Solution**

Select a control volume as shown in Figure 1.5. Because the density may be assumed to be uniform within the fixed control volume, and the conditions on the boundary of the control volume are uniform, we may replace the continuity equation, Eq. (1.21), with Eq. (1.26), which for this application reduces to

$$\frac{dm}{dt} + \dot{m}_e = 0$$

Using the perfect-gas law (with $R = 287 \dfrac{\text{N} \cdot \text{m}}{\text{kg} \cdot \text{K}}$ for air; refer to Appendix H), we obtain

$$p = \frac{287mT}{\forall}$$

We can write the expression for mass-flow rate as

$$\dot{m}_e = 0.040418 \frac{287m\sqrt{T}}{\forall} A_e = 11.6000 \frac{mA_e\sqrt{T}}{\forall}$$

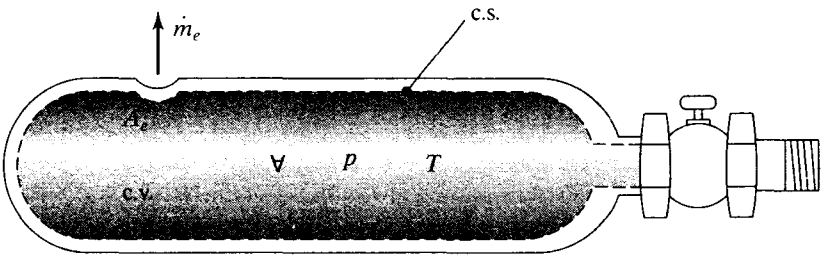


**Figure 1.5** Control Volume of Punctured Air Cylinder

Consequently, the mass-balance equation becomes

$$\frac{dm}{dt} = -11.6\frac{mA_e\sqrt{T}}{\forall}$$

This equation can be directly integrated to give

$$m_2 = m_1 e^{-11.6 A_e \sqrt{T}/\forall \Delta t}$$

Finally, the time increment for the cylinder to lose one half of its mass ($m_2 = 0.5m_1$) is

$$\Delta t_{\text{half}} = \frac{\forall}{11.6A_e\sqrt{T}} \ln 2 = 0.0598\frac{\forall}{A_e\sqrt{T}}$$

We observe that it will take longer to lose this amount of mass if $A_e$ is small, $\forall$ is large, or the air is cold.

---

**Example 1.2. Exit velocity from a liquid-propellant rocket**

In Figure 1.6, a steady flow of $\dot{m}_H$ kilograms per second of liquid hydrogen and $\dot{m}_O$ kg/s of liquid oxygen are injected into a rocket combustion chamber. A violent chemical reaction occurs, and the gaseous products of combustion are expelled at high velocity through the

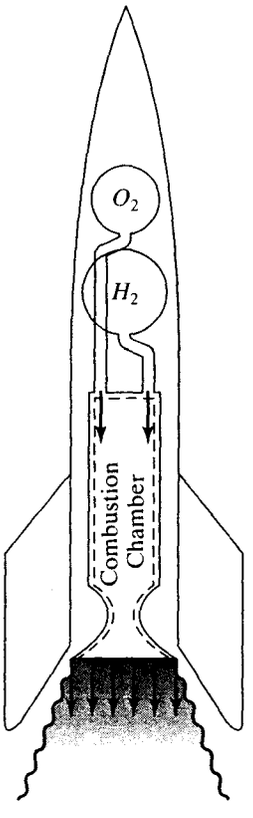


**Figure 1.6** Control Volume of Liquid Rocket

exhaust nozzle. Assuming uniform flow in the rocket nozzle exhaust plane, determine the exit velocity. The nozzle's exit diameter is $D_e$ m, and the density of the gases at the exit plane is $\rho_e$ kg/m$^3$.

**Solution**

Select a control volume as shown in Figure 1.6. Since this is a case of steady flow, Eq. (1.28) is applicable:

$$\iint_{\text{c.s}} \rho \mathbf{V} \cdot d\mathbf{A} = \sum_{\text{outflow}} \dot{m} - \sum_{\text{inflow}} \dot{m} = 0$$

There is a single outflow boundary for which we may write

$$\sum_{\text{outflow}} \dot{m} = \dot{m}_e = \rho_e A_e V_e$$

where $A_e = \frac{\pi}{4} D_e^2$. There are two inflow boundaries, and thus

$$\sum_{\text{inflow}} \dot{m} = \dot{m}_H + \dot{m}_O$$

Therefore,

$$\iint_{\text{c.s}} \rho \mathbf{V} \cdot d\mathbf{A} = \rho_e \mathbf{A_e} \mathbf{V_e} - (\dot{\mathbf{m}}_\mathbf{H} + \dot{\mathbf{m}}_\mathbf{O}) = \mathbf{0}$$

Accordingly,

$$V_e = \frac{\dot{m}_H + \dot{m}_O}{\rho_e A_e}$$

## 1.9 CONSERVATION OF MOMENTUM

Newton's second law of motion for an inertial reference, as applied to a fixed mass $m$, yields

$$\sum \mathbf{F} = m \frac{D\mathbf{V}}{Dt} = \frac{D(m\mathbf{V})}{Dt} = \frac{D\mathbf{P}}{Dt} \tag{1.29}$$

where $\mathbf{P}$ is the linear momentum of the system, $m\mathbf{V}$. This result can be applied to a control volume in a fluid by substituting $\mathbf{P}$ for $X$ in the Reynolds transport equation [i.e., Eq. (1.20)], with $x = \mathbf{P}/m = \mathbf{V}$:

$$\frac{D\mathbf{P}}{Dt} = \frac{\partial}{\partial t} \iiint_{\text{c.v.}} \rho \mathbf{V} d\forall + \iint_{\text{c.s.}} \mathbf{V}(\rho \mathbf{V} \cdot d\mathbf{A}) \tag{1.30}$$

But, as indicated in Eq. (1.29), the time rate of change of the linear momentum is equal to the sum of all external forces acting on the system. So,

$$\sum \mathbf{F} = \frac{\partial}{\partial t} \iiint_{\text{c.v.}} \rho \mathbf{V} d\forall + \iint_{\text{c.s.}} \mathbf{V}(\rho \mathbf{V} \cdot d\mathbf{A}) \tag{1.31}$$

It should be noted that because the Reynolds transport equation connects system equations to control-volume equations when the system and the control volume are coincident, the sum of the external forces acting on the system is identical to the sum of those forces acting on the control volume. No restrictions have been placed on the nature of the forces, so $\Sigma \mathbf{F}$ may involve pressure forces, viscous forces, gravity, magnetic forces, electric forces, surface tension, and so on.

It is important to recognize that, unlike the continuity equation, Eq. (1.21), the momentum equation is a vector equation. Thus, when performing a momentum balance, we must define a coordinate system. However, we will generally work with an individual component of the equation. Whereas the left-hand side of Eq. (1.31) represents the summation of all forces acting on the control volume, the right-hand side represents the rate of increase of linear momentum within the control volume added to the net rate of *efflux* (outflow – inflow) of linear momentum from the control volume.

A restriction is imposed on Eq. (1.31) by the use of Eq. (1.29) in the former's derivation. The acceleration in Eq. (1.29) must be measured relative to an inertial reference. Since fluid velocities in Eq. (1.30) are taken relative to the control volume, this equation is valid only for fixed control volumes or control volumes translating at a constant velocity relative to an inertial reference.

It is important to observe that two separate signs are contained within the momentum equation:

1. The forces and velocities are positive when pointing in the direction of the coordinate axis.
2. The scalar product $\mathbf{V} \cdot d\mathbf{A} = \mathbf{V} \cdot \mathbf{n} dA = V \cos(\alpha)\, dA$ is positive if $\alpha \leq 90$. (See Figure 1.4.)

It should be stressed that, because of sign (1), a coordinate system *must* be drawn for every problem involving the momentum equation. And, because of sign (2), a control surface *must* be drawn around the object that is being analyzed.

For steady flow, the time rate of change of linear momentum stored in the control volume vanishes; that is,

$$\frac{\partial}{\partial t}\left( \iiint_{\text{c.v.}} \rho \mathbf{V} d\forall \right) = 0$$

Hence, the momentum equation for steady-flow problems simplifies to

$$\sum \mathbf{F} = \iint_{\text{c.s.}} \mathbf{V}(\rho \mathbf{V} \cdot d\mathbf{A}) \tag{1.32}$$

If the conditions of flow are uniform on all flow boundaries on the control surface, the area integrals may be replaced with summations as follows:

$$\sum \mathbf{F} = \iint_{\text{c.s.}} \mathbf{V}(\rho \mathbf{V} \cdot d\mathbf{A}) = \sum_{\text{outflow}} \dot{m}\mathbf{V} - \sum_{\text{inflow}} \dot{m}\mathbf{V} \tag{1.33}$$

**Example 1.3. Thrust of a rocket engine on a stationary test stand**

A rocket motor is fired in place on a test stand. The rocket exhausts 10 kg/s at an exit velocity of 800 m/s through an area of 0.01 $m^2$. Assume uniform steady conditions at the exit plane, with an exit-plane static pressure of 50 kPa. For an ambient pressure of 101 kPa, determine the rocket motor thrust transmitted to the test stand as shown in Figure 1.7(a).

**Solution**

Select a control volume as shown in Figure 1.7(a). The forces acting on this control volume are the thrust and the unbalanced pressure force acting on the exit plane. Note that, as may be seen in Figure 1.7(b), the ambient pressure force cancels out over the entire surface of the rocket except over the area $A_e$. Also note that the pressure force is always drawn as a compressive force on the control surface. Applying Eq. (1.32), we obtain

$$\sum F_x = \mathbf{T} - p_e A_e + p_a A_e = \iint_{\text{c.s.}} V_x(\rho \mathbf{V} \cdot d\mathbf{A}) = \dot{m} V_e$$

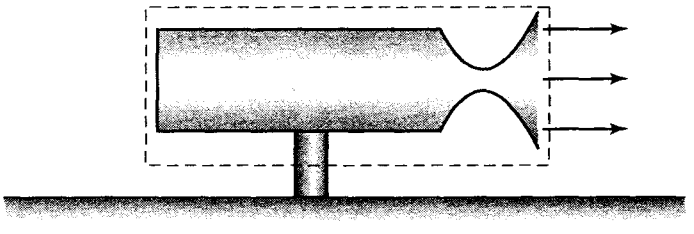

(a) Control Volume

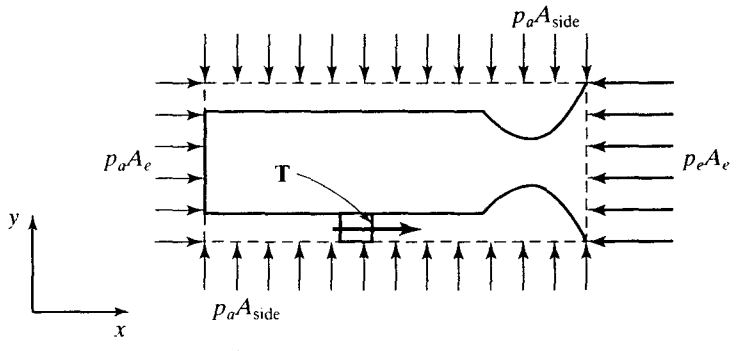


(b) Forces Acting on Control Volume

**Figure 1.7** Rocket on Stationary Test Stand

The *thrust* **T** (i.e., the force required to keep the rocket attached to the test stand) may therefore be written as

$$\mathbf{T} = \dot{m}V_e + (p_e - p_a)A_e$$

This expression may be replaced by an equivalent expression known as the *thrust equation*:

$$\mathbf{T} = \dot{m}V_{\text{eq}}$$

Here, we have introduced an *equivalent exhaust velocity* $V_{\text{eq}}$, which may be written as

$$V_{\text{eq}} = V_e + \frac{(p_e - p_a)A_e}{\dot{m}}$$

We first determine the equivalent velocity:

$$V_{\text{eq}} = 800 \text{ m/s} + \left[\frac{(50 - 101)\dfrac{\text{kN}}{\text{m}^2}\left(\dfrac{1000 \text{ N}}{\text{kN}}\right)(0.01 \text{ m}^2)}{10 \text{ kg/s}}\right]\left(\frac{1 \text{ kg} \cdot \text{m}}{\text{N} \cdot \text{s}^2}\right) = 749.0 \text{ m/s}$$

Therefore,

$$\mathbf{T} = \dot{m}V_{\text{eq}} = \left(10\frac{\text{kg}}{\text{s}}\right)\left(749.0\frac{\text{m}}{\text{s}}\right)\left(1\frac{\text{N} \cdot \text{s}^2}{\text{kg} \cdot \text{m}}\right) = 7{,}490 \text{ N} = 7.49 \text{ kN}$$

---

**Example 1.4. A momentum balance across a moving normal shockwave**

A normal shockwave moves at a speed of 570.2 m/s through still air at a pressure of 101.3 kPa and a temperature of 25°C. The pressure behind the shockwave is measured to be three times the ambient pressure. Determine the velocity behind the shock.

**Solution**

It can be easily shown that the velocity of the moving shock exceeds the velocity of sound and that therefore the shock travels at supersonic speed. (See Chapter 2.) Shockwaves in gases can occur only when the speed is supersonic. We will study this type of compressible-flow phenomena in later chapters.

The normal shock front is illustrated in Figure 1.8(a). The thickness of the shock front is extremely small, and across this small thickness, finite changes occur in the flow variables. The shock is taken to be a discontinuity in the flow, with accompanying abrupt changes in velocity, pressure, and temperature. The shock front allows the flow to immediately adjust to the rapidly changing flow conditions as the shock sweeps through the medium.

To solve the problem at hand, we must first immobilize the moving shock. This operation can be accomplished by superimposing on the flow a velocity equal to the shock speed $S$, but in the opposite direction. In essence, this approach defines a coordinate system on the shock front. By this approach, we reduce the problem to one of steady flow. We

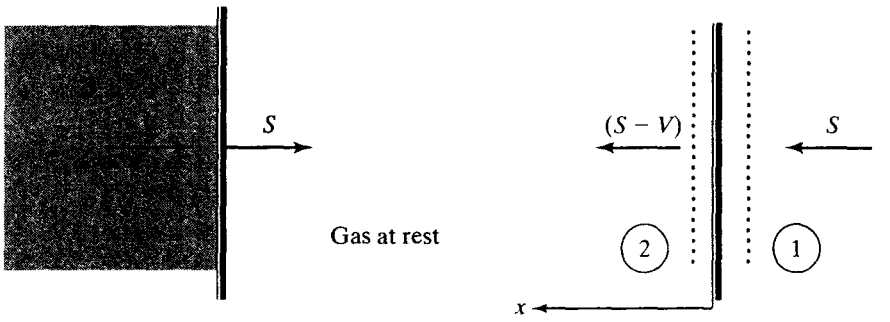


(a) Stationary Coordinate System (b) Moving Coordinate System

**Figure 1.8** Coordinate Systems for a Moving Normal Shockwave

now construct a control volume around the shock as shown in Figure 1.8(b), and we use Eqs. (1.28) and (1.33) to write the continuity and momentum equations, respectively, as

$$\sum_{\text{outflow}} \dot{m} - \sum_{\text{inflow}} \dot{m} = \rho_2(S - V)A - \rho_1 SA = 0$$

$$\sum F_x = p_1 A - p_2 A = \sum_{\text{outflow}} \dot{m}\mathbf{V} - \sum_{\text{inflow}} \dot{m}\mathbf{V} = \dot{m}(S - V) - \dot{m}\mathbf{S} = -\dot{m}V$$

Because the shock is so thin, the area on either side of the shock is the same. Therefore, it can be removed from the expressions, and, by combining the continuity and momentum equations together, we obtain

$$V = \frac{p_2 - p_1}{\rho_1 S}$$

Since $p_2 = 3p_1$ and since air is a perfect gas ($p_1/\rho_1 = RT_1$), the preceding equation reduces to the simple form

$$V = \frac{2RT_1}{S} = \frac{2\left(287\dfrac{\text{N}\cdot\text{m}}{\text{kg}\cdot\text{K}}\right)(298\text{K})\left(1\dfrac{\text{kg}\cdot\text{m}}{\text{N}\cdot\text{s}^2}\right)}{570.2\dfrac{\text{m}}{\text{s}}} = 300\frac{\text{m}}{\text{s}}$$

## 1.10 CONSERVATION OF ENERGY: THE FIRST LAW OF THERMODYNAMICS

For a system consisting of a fixed mass of particles, the law of conservation of energy can be expressed as

$$\delta Q - \delta W' = dE \tag{1.34}$$

where $\delta Q$ and $\delta W'$, small amounts of heat and work, respectively, are forms of energy that are defined as they cross the system boundaries, and $E$ is the total energy possessed

by the system in a given state. $W'$ is used in a broad sense to include not only simple mechanical work, but also, for example, electrical work and shaft work done by the system. The total energy $E$ includes the *total internal energy* ($U = mu$) associated with the random motions of the molecules possessed by the system, the *kinetic energy* ($\text{KE} = mV^2/2$) due to the speed $V$ of the entire system mass, and the *potential energy* ($\text{PE} = mgz$) due to the position of the mass of the system a distance $z$ above some datum. Other forms of storable energy that are characteristic of a fixed-mass system in a given state may also be included, such as chemical energy or electrical energy that can be stored, for example, in a capacitor.

The accepted sign convention for $Q$ and $W'$ is as follows: $Q$ is positive when it is added to the system, and $W'$ is positive when work is done by the system (i.e., is out of the system).

To apply these results to a control volume, use the Reynolds transport equation, Eq. (1.20). Replace $x$ with $e$, which is equal to the total energy, $E$, of the fixed-mass system per unit mass, so that

$$\frac{DE}{Dt} = \frac{\delta Q}{dt} - \frac{\delta W'}{dt} = \dot{Q} - \dot{W}' = \frac{\partial}{\partial t}\iiint_{\text{c.v.}} e\rho d\forall + \iint_{\text{c.s.}} e(\rho \mathbf{V} \cdot d\mathbf{A}) \tag{1.35}$$

If the system can be assumed to possess only internal, kinetic, and potential energies, then

$$E = U + mV^2/2 + mgz$$

and

$$e = E/m = u + V^2/2 + gz$$

Substituting into Eq. (1.35) yields

$$\dot{Q} - \dot{W}' = \frac{\partial}{\partial t}\iiint_{\text{c.v.}} e\rho d\forall + \iint_{\text{c.s.}} \left(u + \frac{V^2}{2} + gz\right)(\rho \mathbf{V} \cdot d\mathbf{A}) \tag{1.36}$$

For cases in which mass flows across the control-volume boundaries, it is convenient to divide the work $W'$ into two parts: (1) the work necessary to push the mass across the boundaries, and (2) all the other work $W$ crossing the control surface, such as shaft work, electric and magnetic work, viscous shear work, and so on.

A simple expression can be derived for the former type of work, which is called *flow work*. Consider a mass $\Delta m$, shown in Figure 1.9, that is to flow across the control surface. It is desired to find the work done by the system in pushing the mass across the boundaries (i.e., the work that acts against the external pressure at the boundaries). If the volume of the mass is $\Delta\forall$, then the work required is $p\Delta\forall$ (i.e., $F\Delta x = (pdA)\Delta x = p\Delta\forall$). Since the density $\rho = \Delta m/\Delta\forall$, the flow work done by the system per unit mass is $p/\rho$. For mass flowing into the control volume, the expression for flow work is negative, since work must be done by the surroundings on the system. Conversely, for the mass

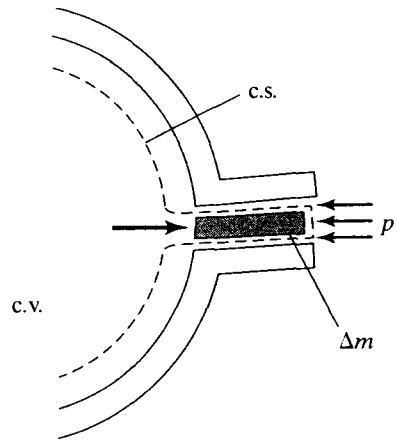


**Figure 1.9** Flow Work

flowing out of the control volume, the flow-work term is positive. Consequently, the sign of the flow work is positive for outflow and negative for inflow. Thus,

$$\text{flow work} = \pm\frac{p}{\rho}\Delta\forall\rho = \pm\left(\frac{p}{\rho}\right)dA\Delta x\rho$$

Hence, in the time $\Delta t$, the amount of flow work that crosses the control surface is given by

$$\pm\frac{p}{\rho}\rho V_n\,dA = \frac{\mathrm{p}}{\rho}(\rho\mathbf{V}\cdot d\mathbf{A})$$

(Note that $\Delta x/\Delta t = V_n$.) The flow work must be accounted for over the entire boundary of the control volume. This is accomplished by integrating the expression and writing Eq. (1.36) as

$$\dot{Q} - \dot{W} - \iint_{\text{c.s.}}\frac{p}{\rho}(\rho\mathbf{V}\cdot d\mathbf{A}) = \frac{\partial}{\partial t}\iiint_{\text{c.v.}}e\rho d\forall + \iint_{\text{c.s.}}\left(u + \frac{V^2}{2} + gz\right)(\rho\mathbf{V}\cdot d\mathbf{A}) \quad (1.37)$$

The last integral on the left-hand side of Eq. (1.37) (i.e., the flow-work term) is now brought to the right-hand side. Because flow work is transported across the control surface in the same manner as the internal energy, it is convenient to combine internal energy per unit mass, $u$, and flow work per unit mass, $p/\rho$, into the thermodynamic property enthalpy: $h = u + p/\rho$. Finally, the energy equation, Eq. (1.37), can be written as

$$\dot{Q} - \dot{W} = \frac{\partial}{\partial t}\iiint_{\text{c.v.}}e\rho d\forall + \iint_{\text{c.s.}}\left(h + \frac{V^2}{2} + gz\right)(\rho\mathbf{V}\cdot d\mathbf{A}) \quad (1.38)$$

where it is understood that $\dot{W}$ includes all power except for that associated with the flow work.

**Example 1.5. The charging of an empty storage tank**

A rigid, well-insulated tank is initially evacuated. A valve is opened in a pipeline connected to the tank, which allows air at 3 MPa and 300 K to flow into the vessel. The valve is closed when the pressure in the tank reaches 3 MPa. Determine the final equilibrium temperature of the air in the tank. Over the temperature range of interest, assume that $c_v = 0.716$ kJ/kg · K and $c_p = 1.005$ kJ/kg · K are constants.

**Solution**

Select a control volume as shown in Figure 1.10. With no heat transfer (*adiabatic*), no work, and negligible ΔKE and ΔPE, Eq. (1.38) simplifies to

$$\frac{\partial}{\partial t}\iiint_{\text{c.v.}} u\rho d\forall + \iint_{\text{c.s.}} h(\rho \mathbf{V} \cdot d\mathbf{A}) = 0$$

Because all properties are uniform on the boundary and within the interior of the control volume, this expression becomes

$$\frac{dU}{dt} - h_i \dot{m}_i = 0 \tag{1.39}$$

To proceed further, we perform a mass balance on the control that makes use of the continuity equation, Eq. (1.26), to obtain

$$\frac{dm}{dt} - \dot{m}_i = 0$$

where $m$ represents the mass inside the control volume and $\dot{m}_i$ is the mass-flow rate of the air crossing the control surface. We may use the expression to replace the mass-flow rate in

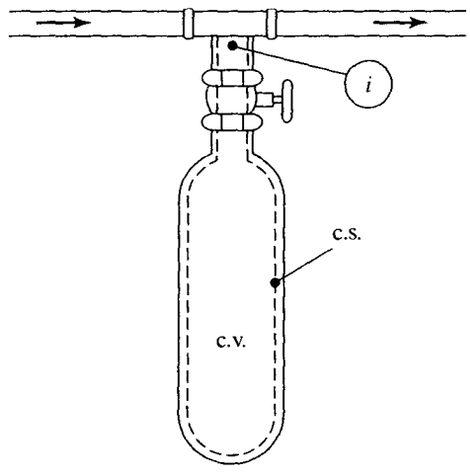


**Figure 1.10** Control Volume of an Empty Storage Cylinder during Charging

Eq. (1.39). Accordingly, we have

$$\frac{dU}{dt} - h_i \frac{dm}{dt} = 0$$

Because the conditions exterior to the tank do not change, and thus $h_i$ is constant, we may directly integrate this equation to obtain

$$U_2 - U_1 = m_2 u_2 - m_1 u_1 = h_i(m_2 - m_1)$$

Because the tank is initially evacuated, $m_1 = 0$. This value and the ideal-gas relations for internal energy and enthalpy produce

$$\begin{aligned} m_2 c_v T_2 &= m_2 c_p T_i \\ T_2 &= \frac{c_p}{c_v} T_i \\ &= \frac{\left(1.005 \dfrac{\text{kJ}}{\text{kg} \cdot \text{K}}\right)}{\left(0.716 \dfrac{\text{kJ}}{\text{kg} \cdot \text{K}}\right)} (300\ \text{K}) \\ &= 1.4036\ (300\ \text{K}) \\ &= 421.1\ \text{K} \end{aligned}$$

---

**Example 1.6. The power input to an air compressor**

Air ($R = 0.287$ kJ/kg · K and $c_p = 1.005$ kJ/kg · K) enters a compressor with a velocity of 30 m/s, a pressure of 1 bar, and an absolute temperature of 300 K. The inlet area is 0.1 $m^2$. At the outlet, the velocity is 10 m/s and the enthalpy is 450 kJ/kg. Assume a rate of heat loss from the compressor of 200 kJ/min, with negligible changes of potential energy. Determine the input power required to operate the compressor at steady state.

**Solution**

Select a control volume as shown in Figure 1.11.

For a steady flow with uniform conditions at inlet and outlet, Eq. (1.38) yields

$$\dot{Q} - \dot{W} = \dot{m}_e\left(h_e + \frac{V_e^2}{2}\right) - \dot{m}_i\left(h_i + \frac{V_i^2}{2}\right)$$

Since $\dot{m}_i = \dot{m}_e = \dot{m}$, this equation becomes

$$\dot{W} = \dot{Q} - \dot{m}\left[(h_e - h_i) + \left(\frac{V_e^2 - V_i^2}{2}\right)\right]$$

$$(h_e - h_i) = h_e - c_p T_i = 450 - (1.005)(300) = 148.500 \frac{\text{kJ}}{\text{kg}}$$

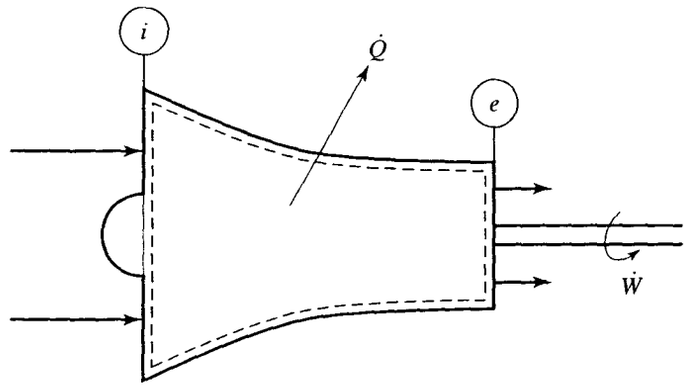


**Figure 1.11** Air Compressor Control Volume

$$\left(\frac{V_e^2 - V_i^2}{2}\right) = \frac{(V_e + V_i)(V_e - V_i)}{2} = \frac{(40)(-20)}{2}\left(\frac{\text{m}^2}{\text{s}^2}\right)\left(1\frac{\text{N}\cdot\text{s}^2}{\text{kg}\cdot\text{m}}\right)\left(\frac{1\text{ kJ}}{10^3\text{ N-m}}\right) = -0.4\frac{\text{kJ}}{\text{kg}}$$

$$\dot{m} = \rho_i A_i V_i = \frac{p_i}{RT_i}A_i V_i = \frac{\left(10^5\frac{\text{N}}{\text{m}^2}\right)}{\left(287\frac{\text{N-m}}{\text{kg}\cdot\text{K}}\right)(300\text{ K})}\left(0.1\text{ m}^2\right)\left(30\frac{\text{m}}{\text{s}}\right) = 3.4843\frac{\text{kg}}{\text{s}}$$

$$\dot{W} = -200\frac{\text{kJ}}{\text{min}}\left(\frac{1\text{ min}}{60\text{ s}}\right) - 3.4843\left(\frac{\text{kg}}{\text{s}}\right)(148.5 - 0.4)\frac{\text{kJ}}{\text{kg}}$$

$$= -519.3612\frac{\text{kJ}}{\text{s}}\left(1\frac{\text{kW}}{\text{kJ/s}}\right) = -519.4\text{ kW}$$

## 1.11 SECOND LAW OF THERMODYNAMICS

The *second law of thermodynamics* places a constraint on the direction thermodynamic processes may take; not all processes are possible even if they satisfy the First Law of Thermodynamics. The second law will be essential in the analysis of shockwaves.

Two concepts that are important to a study of compressible fluid flow are derivable from the second law of thermodynamics: the *reversible process* and the *property entropy*. For a thermodynamic system, a reversible process is a process after which the system can be restored to its initial state and leave no change in either system or surroundings. As a consequence of this definition, it can be shown that a reversible process is *quasistatic*: Changes occur at an infinitely slow rate, with no energy being dissipated. Since thermodynamics is a study of equilibrium states, definite thermodynamic equations for changes taking place during processes can be derived only for reversible processes; *irreversible processes* can be described thermodynamically

only with the use of inequalities. Irreversible processes involve, for example, the following:

- friction,
- heat transfer through a finite temperature difference,
- sudden expansion,
- magnetization with hysteresis,
- electrical resistance heating, and
- mixing of different gases.

In general, any natural process is irreversible, so the assumption of reversibility, while it may simplify the thermodynamic equations, necessarily yields an approximation. For many cases, the assumption of reversibility leads to very accurate results; yet it is well to keep in mind that the reversible process is always an idealization.

The thermodynamic property derivable from the second law is entropy, which is defined for a system undergoing a reversible process by

$$dS = \left(\frac{\delta Q}{T}\right)_{\text{rev}} \tag{1.40}$$

where $S$ denotes the total entropy in kJ/K. The *specific entropy* is the total entropy divided by the mass (i.e., $s = S/m$). For an irreversible process, entropy changes can arise from heat transfer or from irreversibilities. By considering a thermodynamic cycle consisting of one reversible process and one irreversible process and making use of Eq. (1.40), it is easy to show that

$$(S_2 - S_1)_{\text{system}} = \int_{\text{c.s.}} \frac{\delta Q}{T} + \sigma \tag{1.41}$$

where $\sigma$ accounts for any irreversibilities within the system and therefore must be either greater than zero (when irreversibilities are present) or equal to zero (when no irreversibilities are present). Equation (1.41) is called the *entropy balance for a closed system*. This equation reveals that the entropy of a system can increase, remain the same, or decrease. The latter can occur only if heat is removed from the system. During an *adiabatic process*, entropy either increases or remains constant. A process that is adiabatic and reversible involves no change in entropy and is called *isentropic*.

By making use of the Reynolds transport equation, Eq. (1.20), with $X = S$, $x = S/m = s$, and using the rate form of Eq. (1.41), in which $\delta Q/\Delta t = \dot{Q} = \dot{q}dA$, we obtain

$$\left(\frac{dS}{dt}\right)_{\text{system}} = \frac{DS}{Dt} = \iint_{\text{c.s.}} \frac{\dot{q}}{T} dA + \dot{\sigma}$$

We can write *the entropy balance for a control volume* as

$$\frac{DS}{Dt} = \frac{\partial}{\partial t} \iiint_{\text{c.v.}} \rho s d\forall + \iint_{\text{c.s.}} s(\rho \mathbf{V} \cdot d\mathbf{A}) = \iint_{\text{c.s.}} \frac{\dot{q}}{T} dA + \dot{\sigma} \tag{1.42}$$

For a control volume in which the entropy is uniformly distributed and has one inlet and one exit, Eq. (1.42) can be written as

$$\left(\frac{dS}{dt}\right)_{\text{c.v.}} = \iint_{\text{c.s.}} \frac{\dot{q}}{T} dA - \iint_{\text{c.s.}} s(\rho \mathbf{V} \cdot d\mathbf{A}) + \dot{\sigma} \tag{1.43}$$

$$= \iint_{\text{c.s.}} \frac{\dot{q}}{T} dA + \dot{m}_i s_i - \dot{m}_e s_e + \dot{\sigma} \tag{1.43a}$$

The left-hand side is the rate of entropy change within the control volume. The first integral on the right-hand side represents the entropy transfer rate accompanying heat transfer. The second integral in Eq. (1.43), which becomes the difference of mass-flow specific-entropy products in Eq. (1.43a), represents the entropy transfer rate. The final term on the right-hand side of Eqs. (1.43) and (1.43a) is the rate of entropy production.

Although we previously stated that the entropy of a system can increase, decrease, or remain constant, this is not true for an isolated system. There is no flow of mass or energy across the boundaries of an isolated system. Because there is no heat transfer across the boundary of an isolated system, we may write that

$$(\Delta S)_{\text{isolated}} = \sigma_{\text{isolated}}$$

Thus, the entropy can only increase. This phenomenon is known as the *increase of entropy*.

A useful thermodynamic equation for a pure substance, derivable from the first and second laws of thermodynamics, is

$$T ds = dh - \frac{dp}{\rho} \tag{1.44}$$

This equation contains only thermodynamic properties; it is independent of the path of a process. For example, Eq. (1.44) can be integrated between given end states to determine the entropy change regardless of whether the thermodynamic process involved is reversible or irreversible and of whether the process takes place in a closed container or in steady flow.

An expression for the entropy change of a perfect gas can be derived from Eq. (1.44):

$$\int_1^2 ds = s_2 - s_1 = \int_1^2 c_p \frac{dT}{T} - R \ln \frac{p_2}{p_1} \tag{1.45}$$

For an isentropic process ($s$ = constant),

$$0 = \int_1^2 c_p \frac{dT}{T} - R \ln \frac{p_2}{p_1}$$

If, in addition, the perfect gas is assumed to possess constant specific heats, then integration yields

$$\frac{c_p}{R}\ln\frac{T_2}{T_1} = \ln\frac{p_2}{p_1}$$

Let

$$\gamma = \frac{c_p}{c_v}$$

which is called the *ratio of specific heats.*

From Eq. (1.10), it is easy to show that

$$\frac{c_p}{R} = \frac{\gamma}{\gamma - 1}$$

For a perfect gas with constant specific heats undergoing an isentropic process, then

$$\frac{T_2}{T_1} = \left(\frac{p_2}{p_1}\right)^{(\gamma-1)/\gamma} = \left(\frac{\rho_2}{\rho_1}\right)^{\gamma-1}$$

or

$$\frac{p_2}{p_1} = \left(\frac{\rho_2}{\rho_1}\right)^{\gamma} \tag{1.46}$$

**Historical Note:** Various symbols for the ratio of specific heats have been used over the years. It appears that the symbol $\gamma$ was first used by William Rankine (1820–1872) in his study of normal shockwaves. In other studies of the shockwave, however, Georg Riemann (1826–1866) used the symbol $k$ and Pierre Hugoniot (1851–1887) used $m$ for this ratio. Refer to Table 4.1.

**Example 1.7. One-dimensional isentropic flow in a nozzle**

Hydrogen flows isentropically in a nozzle from an initial pressure of 500 kPa, with negligible velocity, to a final pressure of 100 kPa. Because the pressure falls during its journey through the nozzle, this flow is called an expansion. The initial gas temperature is 500 K. Assume steady flow, with the hydrogen behaving as a perfect gas with constant specific heats; $c_p$ = 14.5 kJ/kg · K. Determine the final velocity of the gas and the mass flow through the nozzle for an exit area of 500 cm$^2$.

**Solution**

With no heat or work terms, the energy equation for steady flow, Eq. (1.38), reduces to

$$\iint_{\text{C.S.}} \left(h + \frac{V^2}{2}\right)(\rho \mathbf{V} \cdot d\mathbf{A}) = 0$$

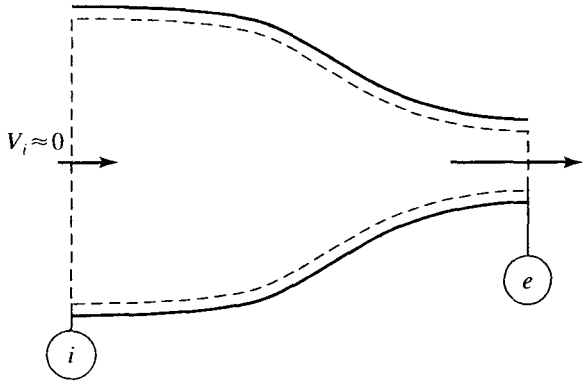


**Figure 1.12** Nozzle Control Volume

Select a control volume as shown in Figure 1.12. With $V_i \approx 0$, the preceding expression reduces to

$$h_i = h_e + \frac{V_e^2}{2}$$
$$V_e = \sqrt{2c_p(T_i - T_e)}$$

To find $T_e$, use Eq. (1.46):

$$\frac{T_e}{T_i} = \left(\frac{p_e}{p_i}\right)^{(\gamma-1)/\gamma}$$

For hydrogen, $R = 4.124$ kJ/kg · K, so

$$\gamma = c_p/c_v = c_p/(c_p - R) = 1.397$$

Now we have

$$\frac{T_e}{T_i} = \left(\frac{100 \text{ kPa}}{500 \text{ kPa}}\right)^{\frac{0.397}{1.397}} = (0.2)^{0.2842} = 0.6329$$

or

$$T_e = (500 \text{ K})(0.6329) = 316.45 \text{ K}$$

Thus,

$$V_e = \sqrt{2(14.5 \text{ kJ/(kg} \cdot \text{K)})(500 \text{ K} - 316.45 \text{ K})}$$
$$= \sqrt{5.32295 \times 10^6 \text{ N} \cdot \text{m/kg}}$$
$$= \sqrt{5.32295 \times 10^6 \text{ kg} \cdot \text{m}^2/(\text{s}^2 \cdot \text{kg})} = 2307 \text{ m/s}$$

The mass flow rate at the nozzle exit is given by

$$\begin{aligned}\dot{m}_e &= (\rho AV)_e \\ &= \frac{p_e}{RT_e} AV_e \\ &= \frac{(100\ \text{kN/m}^2)(500 \times 10^{-4}\ \text{m}^2)\ 2307\ \text{m/s}}{(4.124\ \text{kN} \cdot \text{m/kg K})(316.45\ \text{K})} \\ &= 8.8388\ \text{kg/s}\end{aligned}$$

**Example 1.8. Application of the second law of thermodynamics**

One kilogram of air is initially at a pressure of 100 kPa and a temperature of 327°C. Can a final state of 200 kPa and 27°C be attained in an adiabatic process? From Appendix H, we can find that $c_p = 1.02$ kJ/kg · K and $R = 0.287$ kJ/kg · K.

**Solution**

The entropy of an ideal gas with constant specific heat may be written from Eq. (1.45) as

$$\begin{aligned}s_2 - s_1 &= c_p \ln\frac{T_2}{T_1} - R \ln\frac{p_2}{p_1} \\ &= 1.02\frac{\text{kJ}}{\text{kg} \cdot \text{K}} \ln\left(\frac{27 + 273}{327 + 273}\right) - 0.287\frac{\text{kJ}}{\text{kg} \cdot \text{K}} \ln\left(\frac{200}{100}\right) \\ &= -1.307\frac{\text{kJ}}{\text{kg} \cdot \text{K}} \ln 2 = -0.906\frac{\text{kJ}}{\text{kg} \cdot \text{K}}\end{aligned}$$

However, the entropy balance for a closed system reveals that the entropy must increase or remain unchanged; that is,

$$m(s_2 - s_1) = \int \frac{\delta Q}{T} + \sigma = 0 + \sigma \geq 0$$

Thus, the process is impossible.

## 1.12 ONE-DIMENSIONAL FLOW

A complete solution of a problem in compressible fluid mechanics requires a three-dimensional analysis. However, even for incompressible flow, a complete solution in three dimensions is possible only for cases in which simple geometries are involved. Fortunately, a great many compressible flow problems can be solved to a good engineering approximation with the use of a one-dimensional analysis. One-dimensional flow implies that the flow variables are functions of only one space coordinate.

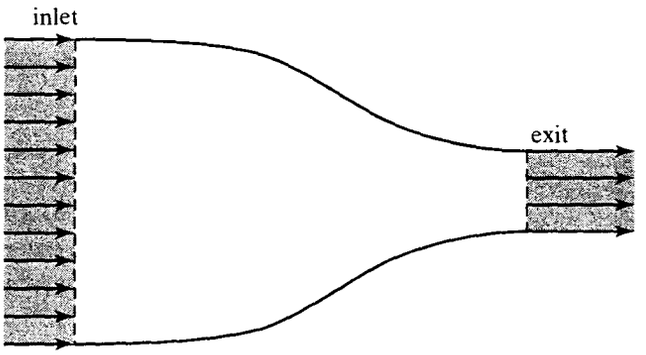


**Figure 1.13** One-Dimensional Flow

Consider the flow in a varying area channel. One-dimensional flow requires that the velocity profiles be as shown in Figure 1.13. Actually, due to viscosity, the flow velocity at the fixed wall must be zero. The velocity profiles in a real fluid are as shown in Figure 1.14.

By definition, one-dimensional flow prohibits velocity components in the $y$ or $z$ directions, as in area (b) in Figure 1.14. In true one-dimensional flow, area changes are not allowed. However, the more gradual the area change with $x$, the more exact the one-dimensional approximation becomes. The real case, illustrated by Figure 1.14, can be reduced to the one-dimensional case by assuming a mean velocity at each cross-section. Note that the one-dimensional approach can yield information only on variations in the $x$ direction; variations normal to the flow direction are assumed to be very small.

The value of the one-dimensional approximation lies in its simplifying the equations of fluid flow. Satisfactory engineering answers can be obtained for many complex problems that would otherwise be very difficult to solve.

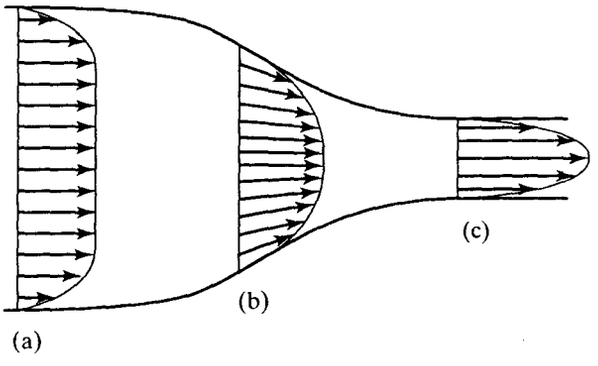


**Figure 1.14** Real Flow in a Varying Area Channel

## 1.13 CHAPTER CAPSTONE APPLICATION: THE JET EJECTOR

A *jet ejector* is a device that uses a high-pressure (or high-velocity) stream of fluid to entrain a low-pressure (or low-velocity) fluid and discharges the mixture at an intermediate velocity.

Figure 1.15 is a schematic diagram that shows two streams of air mixing in a mixing tube of constant area. The high-pressure, primary stream exits into the mixing tube at section $i$, and after it thoroughly mixes with the lower pressure, secondary stream, the combined gas exits the mixing tube at section $e$. The flows at both sections $i$ and $e$ are assumed to be one dimensional; that is, all properties are uniform across the tubes. The ejector is assumed to be operating at steady state. Because the velocity, pressure, density, and temperature of the compressible streams are unequal, we must employ the continuity, momentum, and energy equations, as well as the perfect-gas law, to determine the flow condition at section $e$. For the control volume shown in Figure 1.15, we may write the following:

*Continuity Equation*

$$\iint_{\text{c.s.}} \rho \mathbf{V} \cdot d\mathbf{A} = \sum_{\text{outflow}} (\rho V_n A) - \sum_{\text{inflow}} (\rho V_n A) = \dot{m}_e - \dot{m}_i$$

$$= \rho_e A_e V_e - (\rho_p A_p V_p + \rho_s A_s V_s) = 0 \tag{1.47}$$

*Momentum Equation*

$$\sum F_x = \iint_{\text{c.s.}} V_x (\rho \mathbf{V} \cdot d\mathbf{A})$$

$$p_p A_p + p_s A_s - p_e A_e = (\rho_e A_e V_e) V_e - [(\rho_s A_s V_s) V_s + (\rho_p A_p V_p) V_p] \tag{1.48}$$

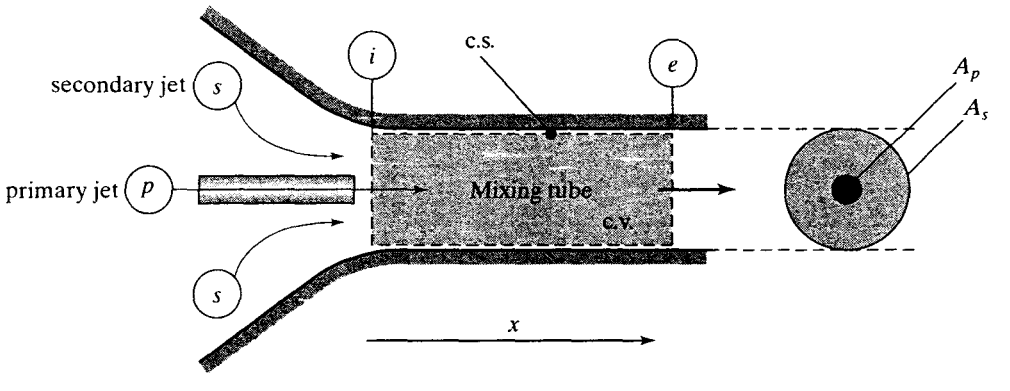


**Figure 1.15** Jet Ejector Control Volume

*Energy Equation*

$$\iint_{\text{c.s.}} \left(h + \frac{V^2}{2}\right)(\rho \mathbf{V} \cdot d\mathbf{A}) = 0$$

$$(\rho_e A_e V_e)\left(h_e + \frac{V_e^2}{2}\right) - \left[(\rho_p A_p V_p)\left(h_p + \frac{V_p^2}{2}\right) + (\rho_s A_s V_s)\left(h_s + \frac{V_s^2}{2}\right)\right] = 0 \quad (1.49)$$

Obviously, the preceding three equations contain many variables, and therefore we must simplify the expressions. First, we make use of the geometry and write

$$A_p + A_s = A_e$$

(Refer to Figure 1.15.) Further, we will assume that the ratio $A_s/A_p$ is known and equal to $\alpha$. Therefore, $A_s = \alpha A_p$, and $A_e = (1 + \alpha)A_p$. We will incorporate these geometric relations along with the ideal-gas law for density,

$$\rho = \frac{p}{RT}$$

into the governing equations. First, the continuity equation, Eq. (1.47), can be rewritten as

$$\frac{p_p}{T_p} V_p + \alpha \frac{p_s}{T_s} V_s = (\alpha + 1)\frac{p_e}{T_e} V_e$$

For later calculation, let

$$\frac{\left(\frac{p_p}{T_p} V_p + \alpha \frac{p_s}{T_s} V_s\right)}{(1 + \alpha)} = A$$

Thus, Eq. (1.47) becomes simply

$$\frac{p_e V_e}{T_e} = A \quad (1.50)$$

The geometric-area relations and the perfect-gas law again allow us to rewrite the momentum equation, Eq. (1.48), as

$$p_p + \alpha p_s - (\alpha + 1)p_e = (1 + \alpha)\frac{p_e}{RT_e} V_e^2 - \frac{p_p}{RT_p} V_p^2 - \alpha \frac{p_s}{RT_s} V_s^2$$

We then use Eq. (1.50) to produce

$$p_e + \frac{A}{R} V_e = \frac{1}{1 + \alpha}\left(p_p + \alpha p_s + \frac{p_p V_p^2}{RT_p} + \alpha \frac{p_s V_s^2}{RT_s}\right) = B$$

That is,

$$p_e + \frac{A}{R}V_e = B \tag{1.51}$$

The energy equation, Eq. (1.49), contains terms that include both the enthalpy and the kinetic energy. This sum is called the *total, or stagnation, enthalpy* and can be written as

$$h_o = h + \frac{V^2}{2} = c_pT + \frac{V^2}{2}$$

Using this relation along with the ideal-gas law and Eq. (1.49) yields

$$\frac{p_pV_p}{T_p}\left(c_{p_p}T_p + \frac{V_p^2}{2}\right) + \frac{\alpha p_sV_s}{T_s}\left(c_{p_s}T_s + \frac{V_s^2}{2}\right) = (1+\alpha)\frac{p_eV_e}{T_e}\left(c_{p_e}T_e + \frac{V_e^2}{2}\right)$$

We can rewrite the above as

$$c_{p_e}T_e + \frac{V_e^2}{2} = \frac{1}{(1+\alpha)A}\left[\left(\frac{p_pV_p}{T_p}\right)\left(c_{p_p}T_p + \frac{V_p^2}{2}\right) + \alpha\frac{p_sV_s}{T_s}\left(c_{p_s}T_s + \frac{V_s^2}{2}\right)\right] = C$$

or

$$c_{p_e}T_e + \frac{V_e^2}{2} = C \tag{1.52}$$

Hence, we have obtained three equations to solve for the three unknowns $V_e$, $p_e$, and $T_e$. Unfortunately, these equations are nonlinear, and we solve them using an iterative procedure as follows:

$$V_e = \frac{AT_e}{p_e} \tag{1.53}$$

$$p_e = B - \frac{A}{R}V_e \tag{1.54}$$

$$T_e = \frac{1}{c_{p_e}}\left(C - \frac{V_e^2}{2}\right) \tag{1.55}$$

Here,

$$A = \frac{1}{(1+\alpha)}\left(\frac{p_p}{T_p}V_p + \alpha\frac{p_s}{T_s}V_s\right) \tag{1.56}$$

$$B = \frac{1}{(1+\alpha)}\left[\left(1 + \frac{V_p^2}{RT_p}\right)p_p + \alpha\left(1 + \frac{V_s^2}{RT_s}\right)p_s\right] \tag{1.57}$$

$$C = \frac{1}{(1+\alpha)A}\left[\left(\frac{p_pV_p}{T_p}\right)\left(c_{p_p}T_p + \frac{V_p^2}{2}\right) + \alpha\left(\frac{p_sV_s}{T_s}\right)\left(c_{p_s}T_s + \frac{V_s^2}{2}\right)\right] \tag{1.58}$$

The strategy to solve this nonlinear set of equations is as follows:

1. From the given information, compute the constants $A$, $B$, and $C$ from Eqs. (1.56)–(1.58).
2. Using initial guess values of $p_e$ and $T_e$, determine $V_e$ from Eq. (1.53).
3. Using $V_e$ from Step 2, calculate $p_e$ from Eq. (1.54).
4. Using $V_e$ from Step 2, calculate $T_e$ from Eq. (1.55).
5. If the differences between the computed $V_e$, $p_e$, and $T_e$ do not differ from the previous values, terminate the computations; if they do differ, return to Step 3.

**Example 1.9. One-dimensional flow in a jet ejector**

Two streams of air mix in a constant-area mixing tube. The primary jet enters the tube with a speed of 300 m/s, a pressure of 300 kPa, and a temperature of 200°C. The secondary stream enters with a velocity of 10 m/s, a pressure of 101 kPa, and a temperature of 20°C. The ratio of the area of the secondary flow to the primary jet is 8:1. The air behaves as a perfect gas with constant specific heats and $c_p = 1.0045$ kJ/kg · K (from Appendix H); that is, the specific heat at constant pressure is the same for both jets and the exit, mixed, stream. Determine the velocity, pressure, and temperature of the air exiting the mixing tube.

**Solution**

From the given information, the values of the constants $A$, $B$, and $C$ in Eqs. (1.56)–(1.58), respectively, are computed:

$$A = 24{,}205.7370 \frac{\text{N}}{\text{m} \cdot \text{s} \cdot \text{K}}$$

$$B = 145{,}317.1585 \frac{\text{N}}{\text{m}^2}$$

$$C = 491{,}550.6260 \frac{\text{m}^2}{\text{s}^2}$$

**TABLE 1.2** Iteration Results from Example 1.9

| Iteration | $V_e$ (m/s) | $P_e$ (Pa) | $T_e$ (K) |
|---|---|---|---|
| 1 | 0.0000 | 101,000.0 | 293.1500 |
| 2 | 70.2566 | 139,391.7 | 486.8916 |
| 3 | 84.5500 | 138,186.2 | 485.7902 |
| 4 | 85.0947 | 138,140.2 | 485.7442 |
| 5 | 85.1149 | 138,138.5 | 485.7425 |
| 6 | 85.1157 | 138,138.5 | 485.7424 |
| 7 | 85.1157 | 138,138.5 | 485.7424 |

To begin the calculations, initial guesses for the pressure and temperature are required. Experimentation reveals that the convergence of this system of equations, Eqs. (1.53) through (1.55), is not greatly affected by the initial guess. Therefore, to begin the calculations, set the initial estimates for pressure and temperature at the secondary stream values (i.e., 101 kPa and 20°C, respectively). Table 1.2 is a summary of the calculations, which were performed with the use of a simple spreadsheet program that is easy to create.

A noniterative procedure is described in Problem 1.20.

## 1.14 SUMMARY

Compressible-fluid mechanics is a study of flow in which significant density variations occur throughout the fluid. With density and temperature as additional variables, the equations of incompressible-fluid mechanics must be supplemented with those of thermodynamics. A solution of a problem in compressible flow requires utilization of the continuity and momentum equations, as well as the first and second laws of thermodynamics and an equation of state for the substance involved. The additional complexities introduced by compressible flow require that approximations be made in order to simplify the problems so that satisfactory engineering answers can be obtained. The one-dimensional flow and perfect-gas approximations afford considerable simplicity to the equations involved and yield results that, for many engineering problems, are within a tolerable degree of accuracy.

## 1.15 REFERENCES

*Thermodynamics Texts*

**1.1** Moran, M. J., and Shapiro, H. N. *Fundamentals of Engineering Thermodynamics,* 4th ed., John Wiley & Sons, New York, 2000.

**1.2** Cengel, Y. A., and Boles, M. A. *Thermodynamics: An Engineering Approach,* 4th ed., McGraw-Hill Book Company, New York, 2002.

*Fluid Mechanics Texts*

**1.3** Alexandrou, A. N. *Principles of Fluid Mechanics,* Prentice Hall, Upper Saddle River, NJ, 2001.

**1.4** Munson, B. R., Young, D. F., and Okiishi, T. H., *Fundamentals of Fluid Mechanics,* 3d ed., John Wiley & Sons, New York, 1998.

*Gas Dynamics Texts*

**1.5** Hodge, B. K., and Koenig, K. *Compressible Fluid Dynamics with Personal Computer Applications*, Prentice Hall, Upper Saddle River, NJ, 1995.

**1.6** Oosthuizen, P. H., and Carscallen, W. E. *Compressible Fluid Flow,* McGraw-Hill Book Company, New York, 1997.

**1.7** Anderson, J. D., Jr. *Modern Compressible Flow with Historical Perspectives*, 3d ed., McGraw-Hill Book Company, New York, 2002.

**1.8** Zucker, R. D., and Biblarz, O. *Fundamentals of Gas Dynamics,* 2d ed., John Wiley & Sons, New York, 2002.

## 1.16 PROBLEMS

**1.1** Air is stored in a pressurized tank at a pressure of 120 kPa (gage) and a temperature of 27°C. The tank volume is 1 $m^3$. Atmospheric pressure is 101 kPa, and the local acceleration

of gravity is 9.81 m/s$^2$. Determine (a) the density and weight of the air in the tank, and (b) the density and weight of the air if the tank were located on the moon, where the acceleration of gravity is one sixth that on the earth.

**1.2** (a) Show that $p/\rho$ has units of velocity squared. (b) Show that $p/\rho$ has the same units as $h$ (kJ/kg). (c) Determine the units conversion factor that must be applied to kinetic energy, $V^2/2$ (m$^2$/s$^2$), in order to add this term to specific enthalpy $h$ (kJ/kg).

**1.3** Air flows steadily through a circular jet ejector. (Refer to Figure 1.15.) The primary jet flows through a 10-cm-diameter tube with a velocity of 20 m/s. The secondary flow is through the annular region that surrounds the primary jet. The outer diameter of the annular duct is 30 cm, and the velocity entering the annulus is 5 m/s. If the flows at both the inlet and exit are uniform, determine the exit velocity. Assume the air speeds are small enough that the flow may be treated as an incompressible flow (i.e., a flow in which the density is constant).

**1.4** A slow leak develops in a storage bottle, and oxygen slowly leaks out. The volume of the bottle is 0.1 m$^3$, and the diameter of the hole is 0.1 mm. The initial pressure is 10 MPa, and the temperature is 20°C. The oxygen escapes through the hole according to the relation

$$\dot{m}_e = 0.04248\frac{p}{\sqrt{T}}A_e$$

where $p$ is the tank pressure and $T$ is the tank temperature. The constant 0.04248 is based on the gas constant and the ratio of specific heats of oxygen. The units are N/m$^2$ for pressure, K for temperature, m$^2$ for area, and kg/s for mass-flow rate. Assuming that the temperature of the oxygen in the bottle does not change with time, determine the time it takes to reduce the pressure to one half of its initial value.

**1.5** A normal shockwave occurs in a nozzle in which air is steadily flowing. Because the shock has a very small thickness, changes in flow variables across the shock may be assumed to occur without change of cross-sectional area. The velocity just upstream of the shock is 500 m/s, the static pressure is 50 kPa, and the static temperature is 250 K. On the downstream side of the shock, the pressure is 137 kPa and the temperature is 343.3 K. Determine the velocity of the air just downstream of the shock.

**1.6** A gas flows steadily in a 2.0-cm-diameter circular tube with a uniform velocity of 1.0 cm/s and a density $\rho_0$. At a cross-section farther down the tube, the velocity distribution is given by $V = U_0[1 - (r/R)^2]$, with $r$ in centimeters. Find $U_0$, assuming the gas density to be $\rho_0[1 + (r/R)^2]$.

**1.7** For the rocket shown in Figure 1.6, determine the thrust. Assume that exit-plane pressure is equal to ambient pressure.

**1.8** Determine the force $F$ required to push the flat plate of Figure P1.8 against the round air jet with a velocity of $V = 10$ cm/s. The air jet velocity is $V_j = 100$ cm/s, with a jet diameter of 5.0 cm. Air density is 1.2 kg/m$^3$.

**1.9** A jet engine (see Figure P1.9) is traveling through the air with a forward velocity of 300 m/s. The exhaust gases leave the nozzle with an exit velocity of 800 m/s with respect to the nozzle. If the mass-flow rate through the engine is 10 kg/s, determine the jet engine thrust. Exit-plane static pressure is 80 kPa, inlet-plane static pressure is 20 kPa, ambient pressure surrounding the engine is 20 kPa, and the exit-plane area is 4.0 m$^2$.

**1.10** A high-pressure oxygen cylinder, typically found in most welding shops, is accidentally knocked over, and the valve on top of the cylinder breaks off. (See Figure P1.10.) This creates a hole with a cross-sectional area of $6.5 \times 10^{-4}$ m$^2$. Prior to the accident, the internal pressure of the oxygen is 14 MPa and the temperature is 27°C. Based on critical-flow calculations (the concept of critical flow will be discussed in Section 3.5), the velocity of

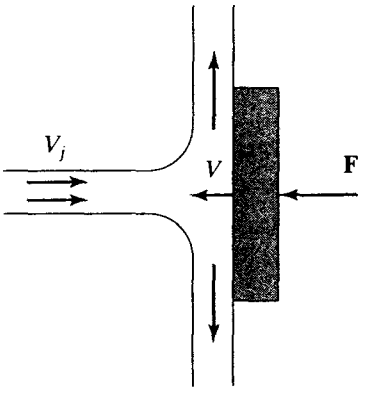


**Figure P1.8**

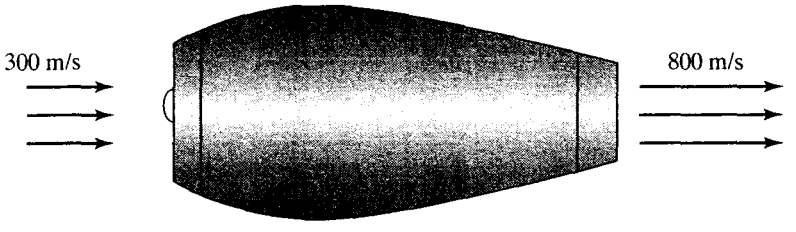


**Figure P1.9**

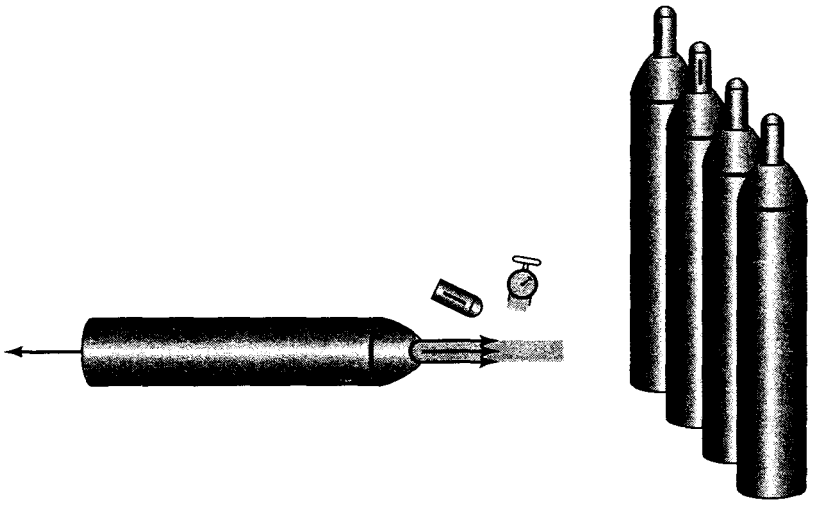

**Figure P1.10**

the oxygen exiting the cylinder is estimated to be 300 m/s, the exit pressure 7.4 MPa, and the exit temperature 250 K. How much thrust does the oxygen being expelled from the cylinder generate? What percentage is due to the pressure difference? What percentage is due to the exiting momentum? Atmospheric pressure is 101 kPa. To gain an idea of the size of this thrust force, also note that 0.2248 $lb_f$ = 1 N.

**1.11** Air enters a handheld hair dryer with a velocity of 3 m/s at a temperature of 20°C and a pressure of 101 kPa. (See Figure P1.11.) Internal resistance heaters warm the air, which exits through an area of 20 $cm^2$ with a velocity of 10 m/s at a temperature of 80°C. Assume that internal obstructions do not appreciably affect the pressure between inlet and exit and that heat transfer to the surroundings is negligible. Determine the power in kW needed to operate the hair dryer at steady state.

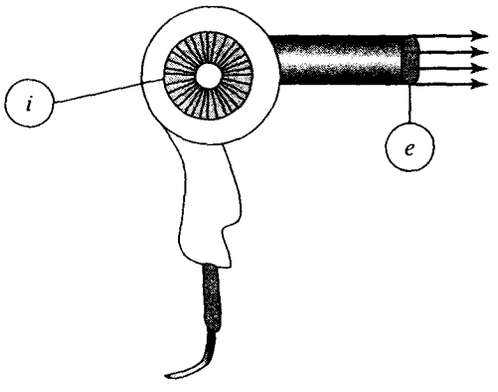


**Figure P1.11**

**1.12** Air is expanded isentropically in a horizontal nozzle from an initial pressure of 1.0 MPa and a temperature of 800 K to an exhaust pressure of 101 kPa. If the air enters the nozzle with a velocity of 100 m/s, determine the air's exhaust velocity. Assume that the air behaves as a perfect gas, with $R$ = 0.287 kJ/kg · K and $\gamma$ = 1.4. Repeat for a vertical nozzle with exhaust plane 2.0 m above the intake plane.

**1.13** Nitrogen is expanded isentropically in a nozzle from a pressure of 2000 kPa, at a temperature of 1000 K, to a pressure of 101 kPa. If the velocity of the nitrogen entering the nozzle is negligible, determine the exit-nozzle area required for a nitrogen flow of 0.5 kg/s. Assume that the nitrogen behaves as a perfect gas with constant specific heats, that it has a mean molecular mass of 28.0, and that $\gamma$ = 1.4.

**1.14** Air enters a compressor with a pressure of 100 kPa and a temperature of 20°C; the mass-flow rate is 0.25 kg/s. Compressed air is discharged from the compressor at 800 kPa and 50°C. Inlet and exit pipe diameters are 4.0 cm. Determine the exit velocity of the air at the compressor outlet and the compressor power required. Assume an adiabatic, steady flow and that the air behaves as a perfect gas with constant specific heats; $c_p$ = 1.005 kJ/kg · K and $R$ = 0.287 kJ/kg · K.

**1.15** Hot gases enter a jet engine turbine with a velocity of 50 m/s, a temperature of 1200 K, and a pressure of 600 kPa. The gases exit the turbine at a pressure of 250 kPa and a velocity of 75 m/s. Assume isentropic steady flow and that the hot gases behave as a perfect gas with constant specific heats (mean molecular mass = 25; $\gamma$ = 1.37). Find the turbine power output in kJ/(kg of mass flowing through the turbine).

**1.16** Hydrogen is stored in a tank at 1000 kPa and 30°C. A valve is opened, which vents the hydrogen and allows the pressure in the tank to fall to 200 kPa. Assuming that the hydrogen that remains in the tank has undergone an isentropic process, determine the amount of hydrogen left in the tank. Assume that hydrogen is a perfect gas with constant specific heats; the ratio of specific heats is 1.4, and the gas constant is 4.124 kJ/kg · K. The tank volume is 2.0 $m^3$.

**1.17** Methane enters a constant-diameter, 3-cm duct at a pressure of 200 kPa, a temperature of 250 K, and a velocity of 20 m/s. At the duct exit, the velocity reaches 25 m/s. For isothermal steady flow in the duct, determine the exit pressure, mass-flow rate, and rate at which heat is added to the methane. Assume that methane behaves as a perfect gas; the ratio of specific heats is 1.32 (constant) and the mean molecular mass is 16.0.

**1.18** Is it possible for air to be adiabatically compressed from a pressure of 300 kPa and a temperature of 27°C to a pressure of 600 kPa and a temperature of 327°C?

**1.19** Two streams of air mix in a constant-area mixing tube of a jet ejector. The primary jet enters the tube with a speed of 600 m/s, a pressure of 200 kPa, and a temperature of 400°C. The secondary stream enters with a velocity of 30 m/s, a pressure of 200 kPa, and a temperature of 100°C. The ratio of the area of the secondary flow to the primary jet is 5:1. The air behaves as a perfect gas with constant specific heats; $c_p$ = 1.0045 kJ/kg · K. Using the iterative numerical procedure described in Example 1.9, determine the velocity, pressure, and temperature of the air leaving the mixing tube.

**1.20** In this chapter, we determined the flow exiting a jet ejector by utilizing an iterative numerical procedure. A more direct approach is possible, however: Eliminate pressure $P_e$ between Eqs. (1.53) and (1.54). Solve for the temperature $T_e$ in the resulting expression, and equate it to Eq. (1.55). This procedure produces a quadratic equation for the velocity $V_e$. Solve the quadratic equation to determine $V_e$ for the same set of conditions given in Example 1.9.

# Chapter 2

# Wave Propagation in Compressible Media

## 2.1 INTRODUCTION

The method by which a flow adjusts to the presence of a body can be shown visually by a plot of the flow streamlines about the body. Figure 2.1 depicts the streamline patterns obtained for *ideal flow* (inviscid and incompressible) over an airfoil and over a circular cylinder. Note that the fluid particles are able to sense the presence of the body before actually reaching it. It may be observed that the fluid particles are displaced vertically at locations in the flow field ahead of the body. This result, true in the general case of any body inserted into an incompressible flow, suggests that a signaling mechanism exists whereby a fluid particle can be forewarned of a disturbance in the flow ahead of it. The velocity of signal waves sent from the body, relative to the moving fluid, apparently is greater than the absolute fluid velocity, since the flow is able to start to adjust to the presence of a body before reaching it. Thus, when a body is inserted into an incompressible flow, smooth, continuous streamlines result upstream of the body, which indicates gradual changes in fluid properties as the flow passes over the body. If the fluid particles were to move faster than the signal waves, the fluid would not be able to sense the body before actually reaching it, and very abrupt changes in velocity vectors and other properties would ensue.

In this chapter, the mechanism by which the signal waves are propagated through incompressible and compressible flows will be studied. An expression for the velocity of propagation of the waves will be derived. From this result, significant conclusions can be drawn concerning the basic differences between incompressible and compressible flows.

## 2.2 WAVE PROPAGATION IN ELASTIC MEDIA

Let us examine what happens when a solid elastic object, such as a steel bar, is subjected to a sudden, uniformly distributed compressive stress applied at one end, as shown

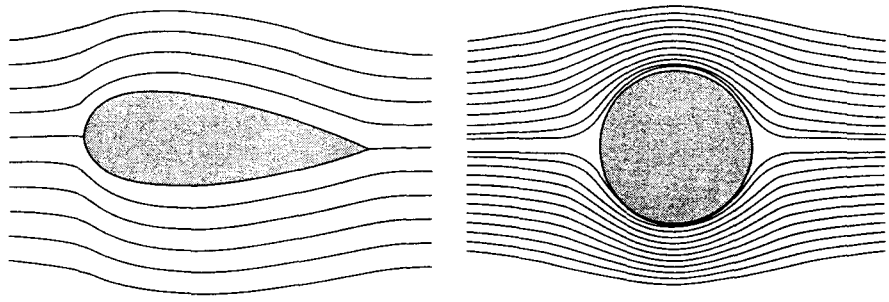

(a) A Symmetrical Airfoil (b) A Circular Cylinder

**Figure 2.1** Streamline Pattern of Ideal Flow Past Two Body Shapes

in Figure 2.2. In the first instant of time, a thin layer next to the point of application is compressed, while the remainder of the bar is unaffected. This compression is then transmitted to the next layer, and so on down the bar. Thus, a disturbance created at the left side of the bar is eventually sensed at the opposite end. The compression wave initiated at the left side of the bar takes a finite time to travel to the right side, the wave velocity being dependent on the elasticity and density of the medium.

Gases and liquids also are elastic substances, and *longitudinal waves* can be propagated through these media in the same way that waves are propagated through solids. Figure 2.3 depicts a gas that is confined in a long tube with a piston at the left-hand side. The piston is given a sudden push to the right. In the first instant, a layer of gas piles up next to the piston and is compressed; the remainder of the gas is unaffected. The compression wave created by the piston then moves through the gas until eventually all the gas is able to sense the movement of the piston. If the impulse given to the gas is infinitesimally small, the wave is called a *sound wave*, and the resultant compression wave moves through the gas at a velocity equal to the *velocity of sound*.

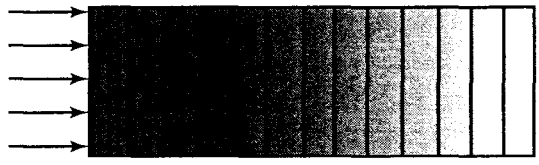

**Figure 2.2** Compression Waves in a Solid Bar

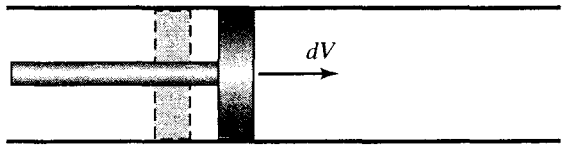


**Figure 2.3** Piston Motion into Gas

For a truly incompressible medium, no changes in density are allowed. If the piston in Figure 2.3 were moved to the right in an incompressible medium, no piling up of fluid, or density changes, would occur at any point in the fluid. All the fluid would have to move instantaneously with the piston. Thus, the velocity of wave propagation in an incompressible fluid is infinite. A disturbance created at any point in an incompressible fluid is sensed instantaneously at all other points in the fluid. However, no medium is actually incompressible, so the velocity of sound has a finite value in solids, liquids, and gases. The less compressible the substance through which the wave propagates, the larger will be the velocity of sound in that substance. Therefore, the velocity of sound in a solid is much greater than the velocity of sound in a liquid, and likewise, the velocity of sound in a liquid is much greater than the velocity of sound in a gas.

## 2.3 VELOCITY OF SOUND

If the piston in Figure 2.3 creates an infinitesimal disturbance, the wave propagates through the medium at the velocity of sound relative to the gas into which the wave is moving, as shown in Figure 2.4. Let the piston be given a steady velocity to the right, of magnitude $dV$, with the resultant sound wave moving at a velocity $a$. As a result of the compression created by the piston, the pressure and density next to the piston are infinitesimally greater than the pressure and density of the gas at rest ahead of the wave. The gas between piston and wave must move with the piston velocity $dV$. Thus, the wave, moving at speed $a$, divides the flow field into two parts: On the piston side, the fluid moves with the speed $dV$, and on the other side, the fluid is at rest, so $V = 0$. We must derive an expression for the velocity of sound, utilizing the flow equations reviewed in Sections 1.8 through 1.10.

Because the sound wave propagates into the gas at rest, the flow is unsteady, as conditions at a given point in the field do not remain constant in time. The problem can be turned into a steady-flow problem by redefining the coordinate system in which it is

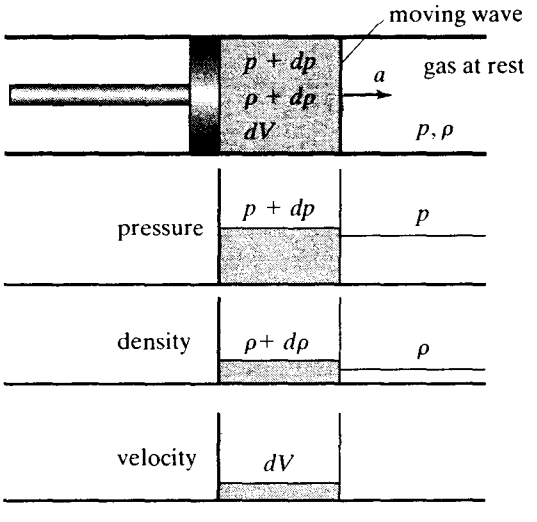


**Figure 2.4** Sound Wave

attached to the moving wave. From this vantage point, the wave does not move; on the right we would see the flow approaching the wave with a speed $a$, and on the left we would see the flow retreating from the wave with a speed $a - dV$. In essence, we are superimposing (i.e., adding) a velocity of $-a$ to all flow velocities. We can often obtain a steady flow from an unsteady flow if the object of interest (in this case, the sound wave; in Example 1.4, a moving normal shockwave) is traveling at a constant speed through an initially undisturbed medium. It should be noted that this transformation of coordinate systems does not affect the thermodynamic variables: pressure, temperature, density, enthalpy, and entropy. The transformed coordinate system is called a *Galilean reference system* (a system that moves with constant velocity).

Now choose a control volume containing the wave; all velocities must be expressed relative to this control volume. (See Figure 2.5.) Because this is a steady-flow problem in the new coordinate system, Eqs. (1.28) and (1.32) are applicable:

$$\iint_{\text{c.s.}} \rho \mathbf{V} \cdot d\mathbf{A} = 0 \tag{1.28}$$

$$\sum F_x = \iint_{\text{c.s.}} V_x(\rho \mathbf{V} \cdot d\mathbf{A}) \tag{1.32}$$

Since the sound wave initiated by the piston is a plane wave, changes in flow properties occur only in the flow direction. For this one-dimensional flow, Eq. (1.28) becomes

$$(\rho + d\rho)(a - dV)A - \rho aA = 0$$

Simplifying and dropping second-order terms (i.e., the product of the differentials, $dV\,d\rho$, which can be shown to be vanishingly small and therefore have no effect on the results) yields

$$a\,d\rho - \rho\,dV = 0 \tag{2.1}$$

The only forces acting on the control surface are pressure forces. (See Figure 2.6.) Applying Eq. (1.32) yields

$$pA - (p + dp)A = [(a - dV) - a]\rho Aa$$

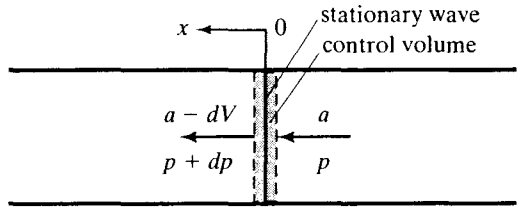


**Figure 2.5** Control Volume for Sound Wave

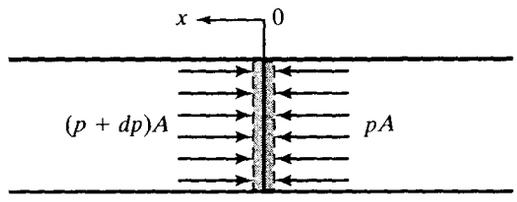


**Figure 2.6** Forces Acting on Control Surface of Wave

Simplifying, we obtain

$$dp = \rho a dV \tag{2.2}$$

Equation (2.2) indicates that the pressure rise across the wave is directly proportional to the fluid density, wave speed, and piston speed. Thus, given these three quantities, we can compute the pressure increment.

Eliminating the differential speed $dV$ between Eqs. (2.1) and (2.2) produces

$$dp = a^2 d\rho$$

or

$$a^2 = \frac{dp}{d\rho} \tag{2.3}$$

It should be observed that speed of sound involves only thermodynamic variables of the gas. It does not contain any geometric parameter, nor does it depend on the piston speed. In Eq. (2.3), $dp/d\rho$ should more properly be written as a *partial derivative*, since the manner in which pressure varies with density is dependent on the process occurring in the sound wave. For example, if the process were performed at constant temperature (isothermal), we would obtain a different result than if the process were performed such that entropy remained constant (isentropic). This is because

$$\left(\frac{\partial p}{\partial \rho}\right)_T \neq \left(\frac{\partial p}{\partial \rho}\right)_s$$

The sound wave is a *weak compression wave*, across which occur only infinitesimal changes in fluid properties. Therefore, the process occurring in the wave satisfies the definition of reversibility from Section 1.11. Furthermore, the wave itself is extremely thin, and changes in properties occur very rapidly. The rapidity of the process precludes the possibility of any heat transfer between the system of fluid particles and its surroundings. The sound-wave process is *reversible and adiabatic*; that is, it is *isentropic*. Hence, Eq. (2.3) may be more properly expressed as

$$a = \sqrt{\left(\frac{\partial p}{\partial \rho}\right)_s} \tag{2.4}$$

It should be noted that if the gas is subjected to high-frequency oscillation, the process cannot be regarded as isentropic, because the intermolecular motion due to the oscillation will generate internal frictional heating. Fortunately, this frequency is relatively high. [Reference (2.1) provides an order-of-magnitude estimate showing that the limiting frequency is $a^2\rho c_p/8k$, where $k$ is the thermal conductivity of the gas. A rough calculation shows that the limiting frequency is $\frac{1}{2}$ GHz for air and 1 THz for water]. Therefore, for most flows, the sound wave may be regarded as an adiabatic compression.

Equation (2.4) has been derived for the case of a weak compression wave; that is, the piston was pushed into the fluid with a speed $dV$. It is well known that an audible sound wave consists of *rarefactions,* or expansions, as well as compressions. The velocity of a weak expansion wave can be calculated using the same equations as were used with the compression wave. Allow the piston of Figure 2.4 to be drawn to the left with an infinitesimal velocity $dV$. This creates in the first instant a decrease in density of the gas at the piston face (same mass, but larger volume). The resulting weak expansion wave then moves to the right through the gas, traveling at the velocity of sound, as is illustrated in Figure 2.7.

To calculate the wave velocity, select a control volume that includes the wave, and express velocities relative to the control volume as shown in Figure 2.8.

Using the continuity and momentum equations, we see that the same expression is obtained for the velocity of the expansion sound wave as was obtained for the compression sound wave:

$$a = \sqrt{\left(\frac{\partial p}{\partial \rho}\right)_s}$$

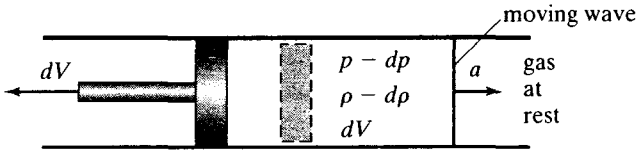


**Figure 2.7** Generation of an Expansion Wave

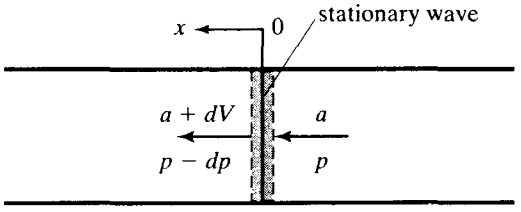


**Figure 2.8** Control Volume for an Expansion Wave

The velocity of sound for a perfect gas can be evaluated by using Eq. (1.46), which expresses the variation of pressure with density for a perfect gas undergoing an isentropic process:

$$\frac{p_2}{p_1} = \left(\frac{\rho_2}{\rho_1}\right)^{\gamma} \tag{1.46}$$

Alternatively, we have

$$\frac{p}{\rho^{\gamma}} = \text{constant} \tag{2.5}$$

Therefore, for a perfect gas,

$$\left(\frac{\partial p}{\partial \rho}\right)_s = \frac{\gamma p}{\rho}$$

and

$$a = \sqrt{\frac{\gamma p}{\rho}} \tag{2.6}$$

By making use of the perfect gas law, we have

$$a = \sqrt{\gamma RT} \tag{2.7}$$

Thus, the speed of sound for a perfect gas is dependent on the ratio of specific heats, the gas constant, and the absolute temperature. Hence, the velocity of sound in air at 25°C and 101 kPa is identical to that at 25°C and 50 kPa, or that at 25°C and 150 kPa. Also note that since the gas constant is $R = 8314.3\ \text{J/(kg} \cdot \text{K/MM)}$, where MM is the molecular mass [see Eq. (1.3)], light gases (small MM—e.g., hydrogen or helium) will have larger speed-of-sound values than heavier gases.

**Historical Note:** In 1635, Pierre Gassendi (1592–1655) made the first known measurement of the speed of sound in air, using firearms. Gassendi was a French Catholic priest, a philosopher, an astronomer, and a major figure of the scientific revolution. Isaac Newton (1642–1727) studied Gassendi's writings in his formative years. However, Gassendi's measured value was shown to be too large by French natural philosopher Marin Mersenne (1588–1648). Mersenne made more accurate measurements and produced a value of about 450 m/s. In 1738, the Academy of Sciences in Paris conducted more precise measurements, using cannon fire, and obtained a value of 332 m/s at 0°C. In 1698, Newton developed the first analytical expression of the speed of sound. However, he assumed the process to be isothermal, and therefore his predictions were low by about 15%. (See Problem 2.9.) In 1816, Pierre Simon Laplace (1749–1827) obtained the correct formula for the speed of sound by assuming that the process is adiabatic. He calculated the speed to be 331.5 m/s. Consequently, Eq. (2.7) is sometimes referred to as the *Newton–Laplace* equation or as the Laplace equation. For greater historical detail, see Ref. (2.2).

**Example 2.1. Speed-of-sound expression from dimensional analysis**

Use dimensional analysis to develop an equation for the speed of sound in terms of the pressure difference across the wave, $\Delta p$; the density difference across the wave, $\Delta\rho$; and the dimensional conversion constant $g_c$.

**Solution**

The speed of sound may be written as

$$a = f(\Delta p, \Delta\rho, g_c) \approx (\Delta p)^a(\Delta\rho)^b(g_c)^c$$

Inserting units of all quantities on both sides of the expression produces

$$\frac{L}{T} = \left(\frac{F}{L^2}\right)^a\left(\frac{M}{L^3}\right)^b\left(\frac{ML}{FT^2}\right)^c = F^{a-c}L^{-2a-3b+c}M^{b+c}T^{-2c}$$

Comparing like exponents yields a set of four equations for the three unknowns, and thus one equation will provide redundant information:

$$\begin{aligned} L:&\quad 1 = -2a - 3b + c \\ T:&\quad -1 = -2c \\ F:&\quad 0 = a - c \\ M:&\quad 0 = b + c \end{aligned}$$

Solving these equations produces: $c = a = -b = \frac{1}{2}$. Hence,

$$a = \sqrt{\frac{(\Delta p)g_c}{(\Delta\rho)}}$$

It is instructive to observe how the dimensional conversion constant $g_c$ enters the calculations for the speed of sound. In SI units (N, kg, m, and s), $g_c = 1\ (\text{kg}\cdot\text{m})/(\text{N}\cdot\text{s}^2)$ and therefore does not affect the numerical calculations for the speed of sound. However, for the engineering system of units ($\text{lb}_\text{f}$, $\text{lb}_\text{m}$, ft, and s), $g_c = 32.174\ (\text{lb}_\text{m}\cdot\text{ft})/(\text{lb}_\text{f}\cdot\text{s}^2)$ and therefore will numerically affect the value of $a$.

---

For a substance that is not a perfect gas, it is desirable to express the velocity of sound in terms of a physical property of the substance: the *compressibility*. Compressibility is a measure of relative volume change with pressure for a given process and is defined by

$$k_s = -\frac{1}{v}\left(\frac{\partial v}{\partial p}\right)_s = \frac{1}{\rho}\left(\frac{\partial\rho}{\partial p}\right)_s \tag{2.8}$$

$$k_T = -\frac{1}{v}\left(\frac{\partial v}{\partial p}\right)_T = \frac{1}{\rho}\left(\frac{\partial\rho}{\partial p}\right)_T \tag{2.9}$$

where $k_s$ and $k_T$ are, respectively, the *isentropic* and *isothermal compressibilities*. [See Ref. (2.3).] The speed of sound may therefore be written as

$$a = \sqrt{\left(\frac{\partial p}{\partial\rho}\right)_s} = \sqrt{\frac{1}{\rho k_s}} \tag{2.10}$$

It can be shown [see Ref. (2.3)] that

$$a = \sqrt{\gamma\left(\frac{\partial p}{\partial \rho}\right)_T} = \sqrt{\frac{\gamma}{\rho k_T}} \tag{2.11}$$

By comparing Eqs. (2.10) and (2.11), we see that

$$\frac{k_T}{k_s} = \gamma \tag{2.12}$$

For solids, the change in pressure with density is usually expressed in terms of the *bulk modulus* $\beta_s$, defined by

$$\beta_s = \rho\left(\frac{\partial p}{\partial \rho}\right)_s \tag{2.13}$$

Thus,

$$a = \sqrt{\frac{\beta_s}{\rho}} \tag{2.14}$$

Comparing Eqs. (2.8) and (2.13) shows that the bulk modulus is related to the isentropic compressibility by

$$\beta_s = \frac{1}{k_s} \tag{2.15}$$

The bulk modulus for solids can also be related to *Young's modulus* $E$ and *Poisson's ratio* $\nu$ through the following equation [see Ref. (2.4)]:

$$\beta_s = \frac{E}{3(1 - 2\nu)}$$

However, it is not uncommon for the bulk modulus to be taken to be equal to $E$. Tables 2.1, 2.2, and 2.3 present values [adapted from a table in Ref. (2.5)] of the

**TABLE 2.1** Speed-of-Sound Property Data for Various Gases

| Gases | $T$ (°C) | Molar mass | $R$ (N·m/kg·K) | $\rho$ (kg/m$^3$) | $\gamma$ | $\beta_s$ (kPa) | $k_s$ (1/GPa) | $k_T$ (1/GPa) | $a$ (m/s) |
|---|---|---|---|---|---|---|---|---|---|
| Air | 0 | 28.97 | 287.0 | 1.29 | 1.402 | 142.2 | 7,034 | 9,861 | 331.6 |
| Air | 20 | 28.97 | 287.0 | 1.21 | 1.402 | 142.4 | 7,025 | 9,849 | 343.0 |
| Helium | 20 | 4.003 | 2,076.9 | 0.16 | 1.667 | 169.0 | 5,919 | 9,866 | 1.015.0 |
| Hydrogen | 0 | 2.016 | 4,124.0 | 0.09 | 1.410 | 145.0 | 6,894 | 9,721 | 1,269.5 |
| Oxygen | 0 | 32.00 | 259.8 | 1.43 | 1.400 | 143.9 | 6,950 | 9,730 | 317.2 |
| Steam | 100 | 18.02 | 461.4 | 0.60 | 1.324 | 98.3 | 10,171 | 13,467 | 404.8 |

**TABLE 2.2** Speed-of-Sound Property Data for Various Liquids

| Liquids | $T$ (°C) | $\rho$ (kg/m$^3$) | $\gamma$ | $\beta_s$ (kPa) | $k_s$ (1/GPa) | $k_T$ (1/GPa) | $a$ (m/s) |
|---|---|---|---|---|---|---|---|
| Alcohol (ethyl) | 20 | 790 | — | 1.04 | 0.957 | — | 1,150 |
| Glycerine | 20 | 1,260 | — | 4.94 | 0.202 | — | 1,980 |
| Mercury | 20 | 13,600 | 1.13 | 28.59 | 0.035 | 0.040 | 1,450 |
| Seawater | 13 | 1,026 | 1.01 | 2.31 | 0.433 | 0.438 | 1,500 |
| Fresh water | 20 | 998 | 1.004 | 2.19 | 0.457 | 0.459 | 1,481 |
| Turpentine | 20 | 870 | 1.27 | 1.36 | 0.736 | 0.934 | 1,250 |

**TABLE 2.3** Speed-of-Sound Property Data for Various Solids

| Solids | $\rho$ (kg/m$^3$) | $\beta_s$ (kPa) | $k_s$ (1/GPa) | $a$ (m/s) |
|---|---|---|---|---|
| Aluminum | 2,700 | 71.61 | 0.014 | 5,150 |
| Brass | 8,500 | 104.13 | 0.010 | 3,500 |
| Copper | 8,900 | 121.84 | 0.008 | 3,700 |
| Lead | 11,300 | 16.27 | 0.061 | 1,200 |
| Steel | 7,700 | 196.37 | 0.005 | 5,050 |
| Glass (Pyrex) | 2,300 | 62.19 | 0.016 | 5,200 |
| Silver | 11,300 | 82.38 | 0.012 | 2,700 |
| Hard Rubber | 1,100 | 0.01 | 185.529 | 70 |

isentropic and isothermal compressibilities, the bulk modulus, and supporting information for a variety of materials.

**Example 2.2. Compute the speed of sound in a gas, a liquid, and a solid**

At 27°C and one atmosphere, determine the velocity of sound (a) in air ($R$ = 0.287 kJ/kg · K and $\gamma$ = 1.4), (b) in liquid water, which has an isothermal compressibility of $0.51 \times 10^{-6}$/kPa and a density of 1,000 kg/m$^3$ under these conditions, and (c) in copper, for which $\rho$ = 8,900 kg/m$^3$ and $\beta_s = 1.218 \times 10^8$ kPa at these conditions.

**Solution**

(a) From Eq. (2.5), we have

$$a = \sqrt{(1.4)(0.287\ \text{kN}\cdot\text{m/kg}\cdot\text{K})T} = \sqrt{(1.4)(287\ \text{kg}\cdot\text{m}^2/\text{kg}\cdot\text{K}\cdot\text{s}^2)T}$$
$$= 20.0449\sqrt{T}$$
$$= 20.0449\sqrt{300} = 347.1887\ \text{m/s} \tag{2.16}$$

(b) For water, $c_p \approx c_v$, so that $\gamma \approx 1.0$, and we can use Eq. (2.10) as follows:

$$a = \sqrt{\frac{1}{\rho k_s}} = \sqrt{\frac{1}{(1{,}000\ \text{kg/m}^3)\ 0.51 \times 10^{-6}(\text{kPa})^{-1}}} = \sqrt{\frac{(1{,}000\ \text{Pa})10^6}{510\ \text{kg/m}^3}}$$
$$= \sqrt{(1.96 \times 10^6)\ \text{kg/m}\cdot\text{s}^2/\text{kg/m}^3} = 1{,}400\ \text{m/s}$$

Thus, $a_{\text{water}} = 4.03a_{\text{air}}$.

(c) We can use Eq. (2.14) to calculate the velocity of sound in copper:

$$a = \sqrt{\frac{\beta_s}{\rho}} = \sqrt{\frac{1.218 \times 10^{11}\ \text{Pa}}{8{,}900\ \text{kg/m}^3}} = \sqrt{\frac{1.218 \times 10^{11}\ \text{kg/m}\cdot\text{s}^2}{0.8900 \times 10^4\ \text{kg/m}^3}} = 3{,}700\ \text{m/s}$$

Thus, $a_{\text{copper}} = 2.64a_{\text{water}} = 10.65a_{\text{air}}$.

---

**Example 2.3. The speed of sound in superheated steam**

Calculate the local speed of sound in a flow of superheated steam at a location where the pressure is 500 kPa and the temperature is 300°C. The accepted experimental value for this pressure and temperature is 582.46 m/s.

**Solution**

To accomplish this, we must have access to steam property data, which can be found in any text on thermodynamics. Table 2.4 is excerpted from Ref. (2.6).

There are several methods by which we can determine the speed of sound in this case. However, because we are dealing with a single phase, we must be assured that the steam is superheated. Since the saturation temperature at 500 kPa is 151.86°C, and since the local temperature exceeds this value, the steam is clearly superheated.

To begin, we will first assume that the steam is a perfect gas. From Table 2.1, we have $R = 8{,}314/18.02 = 461.4$ J/kg · K and $\gamma = 1.324$; therefore, using Eq. (2.7), we have

$$a = \sqrt{\gamma RT} = \sqrt{(1.324)(461.4)(300 + 273)} = 591.6\frac{\text{m}}{\text{s}}$$

Alternatively, we can make use of Eq. (2.6), as well as the steam property data. Entering Table 2.4 at the given $P$ and $T$, we find that $v = 0.5226\ \text{m}^3/\text{kg}$, and, therefore,

$$a = \sqrt{\frac{\gamma p}{\rho}} = \sqrt{\gamma p v} = \sqrt{(1.324)(500{,}000)(0.5226)} = 588.2\frac{\text{m}}{\text{s}}$$

**TABLE 2.4** Steam Property Data

| | $p = 400$ kPa ($T_{sat} = 143.63°C$) | | $p = 500$ kPa ($T_{sat} = 151.86°C$) | | $p = 600$ kPa ($T_{sat} = 158.85°C$) | |
|---|---|---|---|---|---|---|
| $T$ (°C) | $v$(m³/kg) | $s$(kJ/kg·K) | $v$(m³/kg) | $s$(kJ/kg·K) | $v$(m³/kg) | $s$(kJ/kg·K) |
| Sat. | 0.4625 | 6.8959 | 0.3749 | 6.8213 | 0.3157 | 6.7600 |
| 200 | 0.5342 | 7.1706 | 0.4249 | 7.0592 | 0.3520 | 6.9665 |
| 250 | 0.5951 | 7.3789 | 0.4744 | 7.2709 | 0.3938 | 7.1816 |
| **300** | 0.6548 | 7.5662 | **0.5226** | **7.4599** | 0.4344 | 7.3724 |
| 350 | 0.7726 | 7.8985 | 0.5701 | 7.6329 | 0.4742 | 7.5464 |
| 400 | 0.8893 | 8.1913 | 0.6173 | 7.7938 | 0.5137 | 7.7079 |

Another approach is based on first determining the compressibility of the steam through the use of a simple central finite-difference approximation of the derivative that appears in Eq. (2.9); that is,

$$k_T = -\frac{1}{v}\left(\frac{\partial v}{\partial p}\right)_T = -\frac{1}{v(p,T)}\left(\frac{v(p+\Delta p,T) - v(p-\Delta p,T)}{2\Delta p}\right)$$

Here, we use $\Delta p = 100$ kPa only because this is the available datum. A smaller increment would lead to improved results. So $p + \Delta p = 500 + 100 = 600$ kPa, and $p - \Delta p = 500 - 100 = 400$ kPa. Using the data in Table 2.4 yields the following:

$$k_T = -\frac{1}{0.5226}\left(\frac{0.4344 - 0.6548}{2(100{,}000)}\right) = 2.109 \times 10^{-6}\frac{1}{\text{Pa}}$$

Hence, using Eq. (2.11), we have

$$a = \sqrt{\gamma\left(\frac{\partial p}{\partial \rho}\right)_T} = \sqrt{\frac{\gamma}{\rho k_T}} = \sqrt{\frac{\gamma v}{k_T}} = \sqrt{\frac{(1.324)(0.5226)}{2.109 \times 10^{-6}}} = 572.8\frac{\text{m}}{\text{s}}$$

Finally, we may obtain the finite difference of the derivative in the isentropic compressibility relation, Eq. (2.8), to determine the speed of sound:

$$k_s = -\frac{1}{v}\left(\frac{\partial v}{\partial p}\right)_s = -\frac{1}{v(p,s)}\left(\frac{v(p+\Delta p,s) - v(p-\Delta p,s)}{2\Delta p}\right)$$

Now, at $p = 500$ kPa and $T = 300°C$, we see from Table 2.4 that $s = 7.4599$ kJ/kg·K. This value is then used to determine the specific volumes at the two side pressures.

To accomplish this, the property data must be interpolated, and we find that at 600 kPa, $v = 0.4544$ m$^3$/kg, and at 400 kPa, $v = 0.6209$ m$^3$/kg. Thus,

$$k_s = -\frac{1}{0.5226}\left(\frac{0.4544 - 0.6209}{2(100{,}000)}\right) = 1.593 \times 10^{-6}\frac{1}{\text{Pa}}$$

$$a = \sqrt{\left(\frac{\partial p}{\partial \rho}\right)_s} = \sqrt{\frac{1}{\rho k_s}} = \sqrt{\frac{v}{k_s}} = \sqrt{\frac{(0.5226)}{1.593 \times 10^{-6}}} = 572.8\frac{\text{m}}{\text{s}}$$

## 2.4 SUBSONIC AND SUPERSONIC FLOWS

It has been established that the presence of a small disturbance is signaled throughout a fluid by means of a wave traveling at the local velocity of sound of the fluid into which the wave is propagating. If a body travels through a fluid at a velocity greater than the velocity of sound, the fluid ahead of the body is unable to sense the presence of the body, and abrupt changes in flow properties occur as the flow passes over the body. If a body travels through a fluid at a velocity less than the velocity of sound, the presence of the body is signaled to the fluid ahead of it. Thus, the fluid is able to adjust to the movement of the body, and gradual changes in flow properties result, with smooth, continuous streamlines.

Let us now consider a simplified representation of this discussion. A point projectile is injected with velocity $V$ into a stationary fluid. Just as the piston of Figure 2.3 produced a compression wave ahead of it traveling at the velocity of sound, so the disturbance here creates a pressure wave propagating throughout the fluid in all directions (a spherical wave) at the velocity of sound.

The projectile is assumed to travel to the right with a velocity equal to some multiple of the velocity of sound. Points 0, 1, 2, and 3 denote the locations, given by $x = na\Delta t$, of the projectile after 0, 1, 2, and 3 equal time intervals, respectively. The projectile is continually issuing waves during its motion; the waves move radially outward from the point of emission at the velocity of sound. The locations of the waves emitted by the projectile while at points 0, 1, 2, and 3 are depicted after three time intervals. For example, while the projectile moves from 0 to 3, the wave emitted at 0 travels a distance $3a\Delta t$. Figure 2.9 shows magnified views of a subsonic and supersonic case. Figure 2.10 presents an assembly of cases for various projectile speeds.

**Historical Note:** Diagrams of the type shown in Figures 2.9 and 2.10 were drawn by Ernst Mach (1838–1916) in his research of projectile motion. As stated in Ref. (2.13), "To one familiar with the physics of shock waves, it is obvious how familiar Mach already was [in 1886] with these new supersonic phenomena. He interpreted the bow wave at once as the envelope of disturbances originating from the projectile and he supposed it to be a shock front." Figure 2.9(a) "displays the well-known construction illustrating the idea. The sine of the half-angle of the vertex of the cone is the ratio of the sound speed to the projectile speed, i.e., the reciprocal of the Mach number."

It should also be mentioned that Christian Johann Doppler (1803–1853) in 1847, some 40 years before Mach, had constructed diagrams such as Figures 2.9 and 2.10 to explain the phenomena. Thus, the geometry could be called a Doppler–Mach cone.

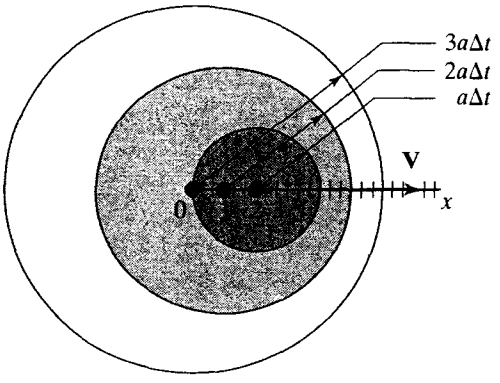


(a) Subsonic Velocity

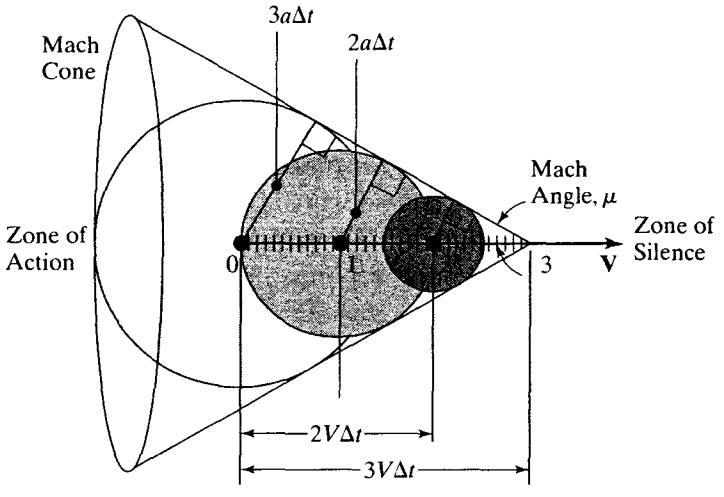


(b) Supersonic Velocity

**Figure 2.9** Sound Speeds Generated by a Disturbance Traveling at Subsonic and Supersonic Speeds

Lines have been drawn tangent to the spherical waves for the supersonic-projectile-speed case in Figure 2.9, with the projectile at the apex of the cone thus formed. As shown in Figure 2.10, the cone angle diminishes as the speed of the projectile is increased. This cone defines the flow region in which the fluid has "sensed" the projectile motion. Everywhere outside the cone, the fluid is "unaware of" the presence of the moving projectile. For this reason, von Karman termed the region inside the cone the *zone of action* and the region outside the cone the *zone of silence*. [See Ref. (2.7).] The nearness of the waves at any time signifies the strength of the resultant pressure disturbance at a point in the fluid. From Figure 2.9, it can be seen that the pressure disturbance is greatest in the vicinity of the cone.

For a subsonic projectile velocity, the pressure wave moves farther ahead of the projectile as time passes. This case is exemplified in Figure 2.10 (a)–(f). For subsonic cases, the point projectile has been made to travel to the right with a velocity $V$ equal

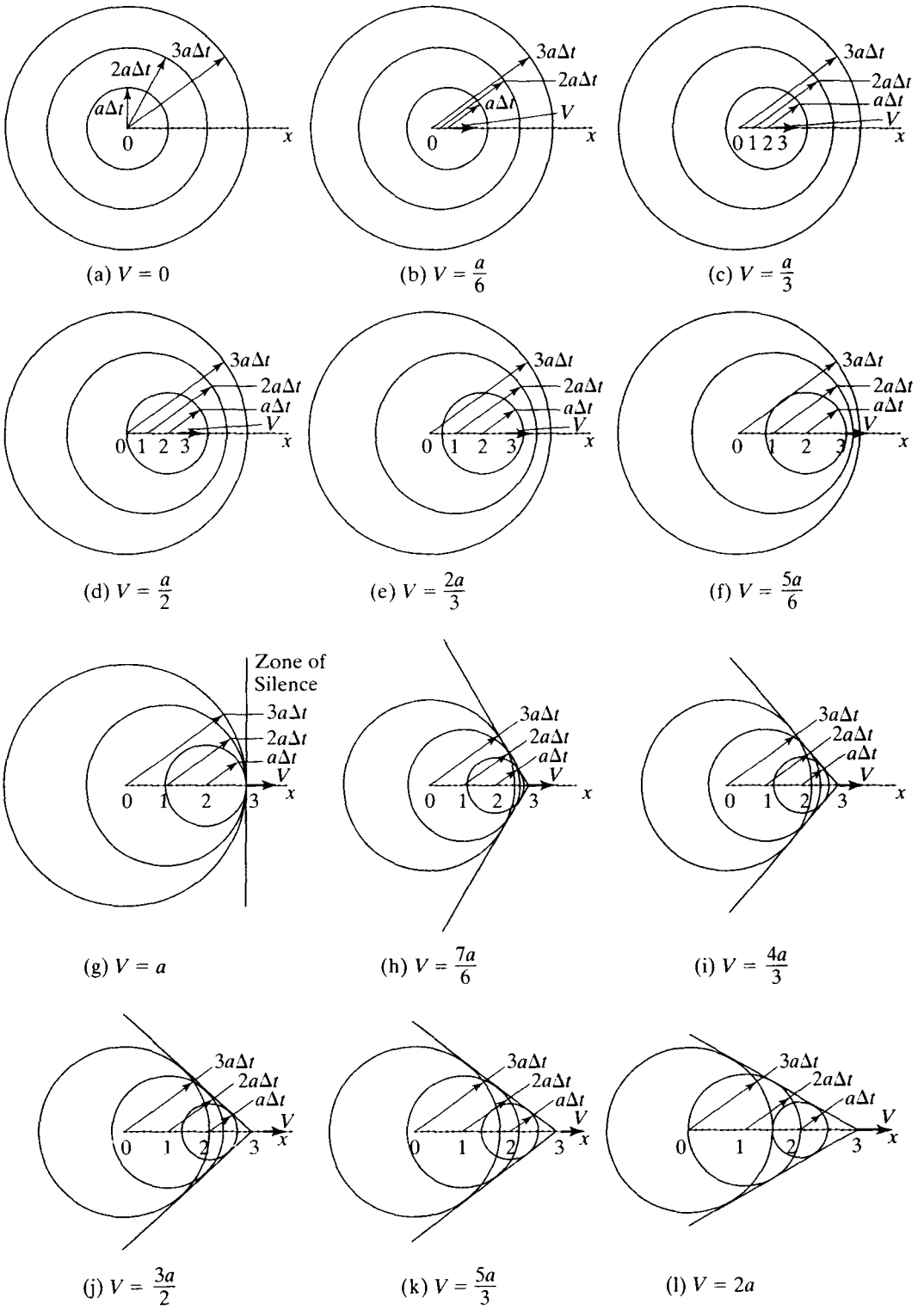


(a) $V = 0$ (b) $V = \frac{a}{6}$ (c) $V = \frac{a}{3}$

(d) $V = \frac{a}{2}$ (e) $V = \frac{2a}{3}$ (f) $V = \frac{5a}{6}$

(g) $V = a$ (h) $V = \frac{7a}{6}$ (i) $V = \frac{4a}{3}$

(j) $V = \frac{3a}{2}$ (k) $V = \frac{5a}{3}$ (l) $V = 2a$

**Figure 2.10** Taxonomy of Pressure Wave and Projectile Speeds

to various fractions of the velocity of sound. The location of the projectile and a pressure wave emitted by the projectile are depicted at one, two, and three equal time intervals $\Delta t$ after the projectile has emitted the wave. The spherical wave precedes the projectile into the fluid, with the distance between projectile and wave increasing with time [i.e., $(a - V)t$]. Eventually, all the fluid ahead of the projectile is able to "sense" its motion and thereby adjust to it.

Figure 2.10(g) depicts the case when the projectile travels at exactly the same speed as the wave. In this case, the pressure wave, which just keeps pace with the projectile, is unable to signal the undisturbed fluid that the projectile is about to arrive.

If the projectile travels at a velocity greater than the velocity of sound, it continually moves into a fluid that has not "sensed" its presence. At each instant, the disturbance must push aside undisturbed fluid. This case is illustrated in Figures 2.10(h)–(l).

The lines at which the pressure disturbance is concentrated and that generate the cone are called *Mach lines* or waves. The angle between the Mach line and the projectile direction is the *Mach angle* $\mu$, which can be computed from the triangles shown in Figure 2.10; that is,

$$\sin \mu = \frac{na\Delta t}{nV\Delta t} = \frac{a}{V}$$

or

$$\mu = \sin^{-1}\left(\frac{a}{V}\right) \tag{2.17}$$

For subsonic flow, no such zone of silence exists. The entire fluid is able to "sense" the projectile moving through it, since the signal waves move faster than the projectile. No concentration of pressure disturbances can occur for subsonic flow; Mach lines cannot be defined.

It should be noted that the motion of the projectile in the gas is an unsteady-flow problem. However, by the same reasoning that was used in Example 1.4 to immobilize a moving shockwave, as well as in Section 2.2 to change the unsteady motion of a sound wave into a steady-state problem, we may imagine that a velocity of $-V$ is superimposed onto the flow. In essence, we are changing the coordinate system by attaching it to the projectile, and in so doing, the projectile is made stationary in that coordinate system and the fluid approaches it from the right in all of the figures. Rather than the *projectile* traveling at some multiple of the speed of sound, in this situation the *fluid* is traveling at a speed above or below the speed of sound. It becomes harder for any disturbance signal to propagate upstream as the fluid speed approaches the speed of sound. For fluid velocities that equal or exceed the speed of sound, no signal can be propagated in that direction.

Let us now compare steady, uniform, subsonic, and supersonic flow over a finite wedge-shaped body. If the velocity of the fluid is less than the velocity of sound, flow ahead of the body is able to "sense" the presence of the body. As a result, gradual changes in flow properties take place, with smooth streamlines. (See Figure 2.11.)

If the velocity of the fluid is greater than the velocity of sound, the approaching flow, being in the zone of silence, is unable to "sense" the presence of the body. Unlike

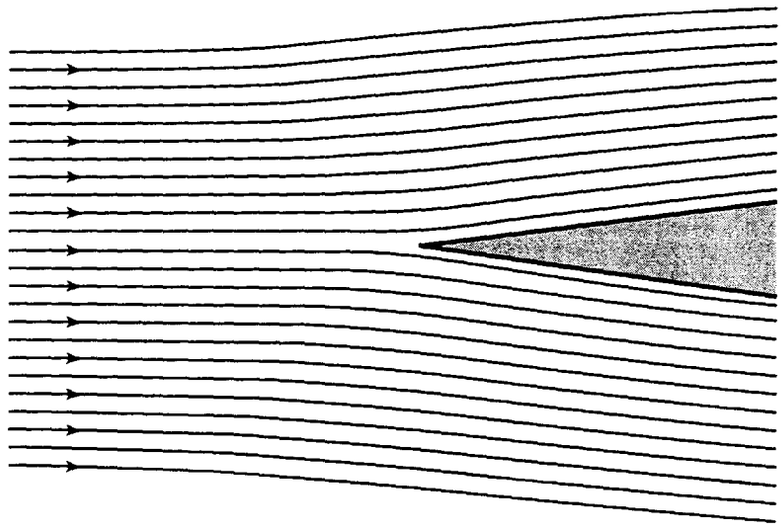

**Figure 2.11** Subsonic Wedge Flow

the point projectile discussed previously, the body now presents a finite disturbance to the flow. The wave pattern obtained is a result of the addition of the individual Mach waves emitted from each point on the wedge. This nonlinear addition yields a compression shockwave across which occur finite changes in velocity, pressure, and other flow properties. A typical flow pattern obtained for supersonic flow over the wedge is shown in Figure 2.12.

In this case, the adjustment of the flow to the body is not gradual, but takes place entirely in the shockwave itself, which is of infinitesimal thickness. As a result, discontinuous changes in flow direction, pressure, temperature, density, and so on, occur across the wave. In a real fluid, discontinuities cannot exist, since real fluid effects

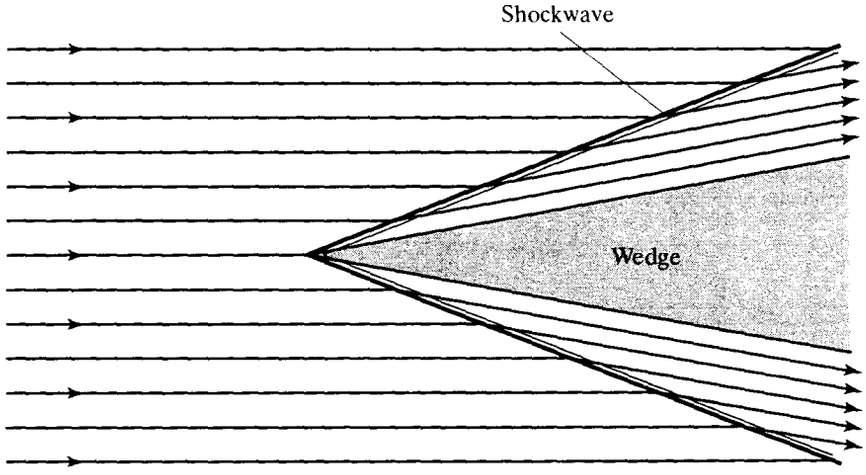


**Figure 2.12** Supersonic Wedge Flow

(viscosity and the like) tend to smooth them out. However, the measured thickness of a shock is on the order of the mean molecular free path, a small fraction of a millimeter. [See Ref. (2.8).]

The design of an airfoil, or even an aircraft, that operates in a subsonic flow is inherently different from the design for supersonic flow. For subsonic flow, a smooth shape is generally selected. (Figure 2.13 shows various subsonic aircraft.) However, for supersonic flow, the existence of shocks must be allowed for in design. A thin body with a pointed nose is preferable in order to minimize the strength of the shock in the vicinity of the front of the body. Figure 2.14 shows aircraft that fly at supersonic speeds. Clearly, subsonic and supersonic geometries are quite different.

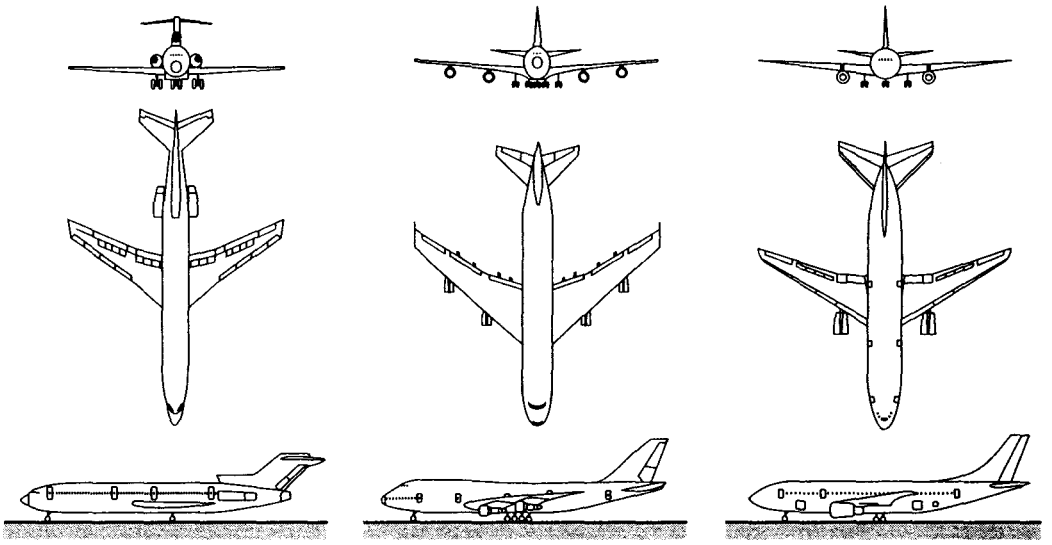


**Figure 2.13** Subsonic Aircraft

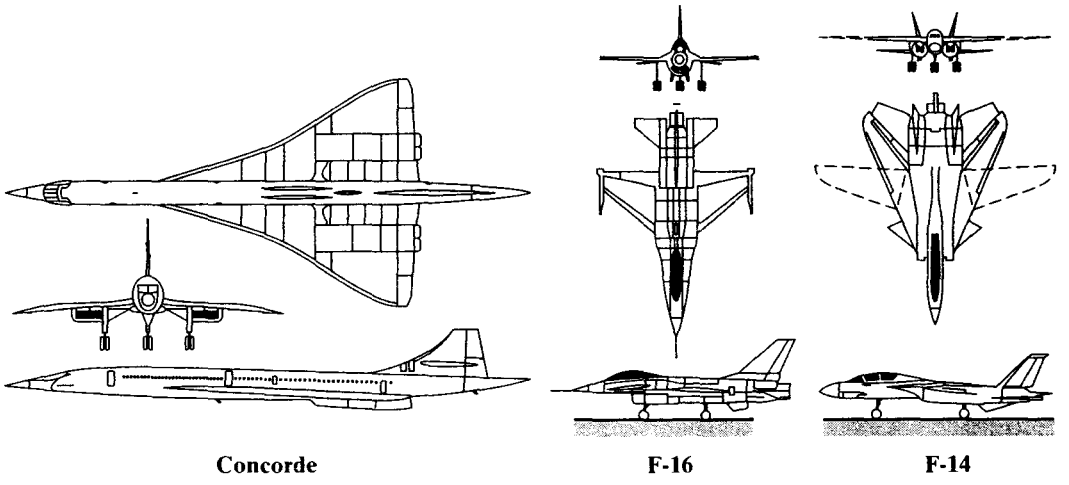


**Figure 2.14** Supersonic Aircraft

## 2.5 MACH NUMBER

From the discussion in the previous section, the significance of the difference between subsonic and supersonic flow can be appreciated. The criterion for the type of flow is *Mach number*, a nondimensional parameter defined by

$$M = \frac{V}{a} \tag{2.18}$$

The Mach number is the ratio of the speed of the gas divided by the *local* speed of sound. Because, as we have seen, the speed of sound depends upon thermodynamic variables of pressure, density or temperature, its value changes throughout the flow field as these variables change.

Gas flows can be classified according to the magnitude of the Mach number:

| | |
|---|---|
| Incompressible | $M \ll 1$ |
| Subsonic | $M < 1$ |
| Transonic | $M \sim 1$ |
| Sonic | $M = 1$ |
| Supersonic | $M > 1$ |
| Hypersonic | $M \gg 1$ |

As has just been described, the speed of sound of a truly incompressible substance is infinite. Therefore, the Mach number of a truly incompressible substance must be exactly zero. However, we will find in later chapters that flows with small Mach numbers physically behave like an incompressible fluid. In fact, only a relatively small error will be made in treating the compressible flow as an incompressible flow for $M$ below 0.2.

Mach number is an extremely important parameter in the study of compressible-fluid flow. In the development of the equations of motion of a compressible fluid, much of the analysis will appear in terms of Mach number. As a simple illustration, we write Eq. (2.17) for the Mach angle in terms of the Mach number

$$\mu = \sin^{-1}\left(\frac{1}{M}\right) \tag{2.19}$$

The significance of the point at which Mach number is equal to unity will be demonstrated again and again in future chapters.

Jakob Ackert

**Historical Note:** Mach did not coin the term *Mach number*. Rather, it was first publicized in 1929 when Swiss engineer **Jakob Ackeret** (1898–1981) named it in honor of Mach during a lecture at the Eidgenossiche Technische Hochschule in Zurich. The name was not immediately accepted. In fact, the Russians at one time preferred the term "Bairstow number" for the ratio, and years later, in 1947, the French proposed the term "Moisson number." The term "Mach number" first appeared in English publications in 1932, 16 years after Mach's death.

## 2.6 CHAPTER CAPSTONE APPLICATION: THE SPEED OF SOUND IN A REAL GAS

When gases are exposed to pressures and temperature far removed from atmospheric values, the perfect-gas equation of state does not provide an accurate relationship between the thermodynamic variables. Accordingly, an alternative equation of state should be used. However, these alternative equations do not possess the simplicity of $pv = RT$ and therefore are more difficult to work with. For example, the Beattie–Bridgeman equation contains eight groups of terms and five experimentally determined constants, and the Benedict–Webb–Rubin equation contains ten groups of terms and eight constants. To minimize the complexity, two-constant equations of state have been widely used. There are several members of the so-called two-constant family of equations of state. The oldest member is van der Waals's equation, which first appeared in 1873.

In this section, the speed of sound of a real gas, i.e., a nonperfect gas, will be determined using the van der Waals equation of state, which contains only two groups of terms and two constants. However, before proceeding in that direction, a few words regarding gas imperfection are in order.

Thermodynamically, a gas may be imperfect in two ways. If the gas does not satisfy the perfect-gas law, it is said to be *thermally imperfect*. If it does not have constant specific heats, it is said to be *calorically imperfect*. Eggers has pointed out two cases for which a gas may not be thermally perfect [see Ref. (2.9)]:

- There are densities in excess of 10 times the sea-level atmospheric value, in which case the molecules occupy an appreciable fraction of the available volume.
- There are sufficiently high pressures and low temperatures so as to cause intermolecular forces to be appreciable.

The *compressibility factor* $Z$ (not to be confused with compressibilities $k_s$ and $k_T$) is defined by

$$Z = \frac{pv}{RT} \tag{2.20}$$

Obviously, if $Z$ is close to unity, the conditions allow the perfect-gas equation to be used.

Next, we employ a two-constant equation of state. Van der Waals's equation was selected because it is relatively easy to work with. However, it is not the most accurate. It should be noted that the equation takes into account intermolecular forces, as well as molecular volumes. Van der Waals's equation may be written as

$$\left(p + \frac{\alpha}{v^2}\right)(v - \beta) = RT \tag{2.21}$$

The two constants that appear are generally written as $a$ and $b$; however, the symbol for the speed of sound is also $a$, and thus to avoid confusion, we will use $\alpha$ and $\beta$ for these constants. Note that for large values of specific volume, $v \gg \beta$, and for pressures such that $p \gg \alpha/v^2$, the equation reduces to the perfect-gas equation. One

method to determine values of $\alpha$ and $\beta$ (or the constants in any two-constant equation of state) is to make use of the fact that the isotherm passing through the critical point of a gas passes through an inflection point. This condition requires that

$$\left(\frac{\partial p}{\partial v}\right)_T = 0$$

and

$$\left(\frac{\partial^2 p}{\partial v^2}\right)_T = 0$$

By differentiating Eq. (2.21) according to these equations and rearranging, it is not difficult to show that

$$\alpha = \frac{9}{8}RT_c v_c = \frac{27}{64}\frac{R^2T_c^2}{p_c} = 3p_c v_c^2$$

$$\beta = \frac{v_c}{3} = \frac{1}{8}\frac{RT_c}{p_c}$$

$$v_c = \frac{3}{8}\frac{RT_c}{p_c}$$

Note the subscript $c$ is used to signify critical-point values. These values can be found in Refs. (2.3) and (2.6) for a variety of gases. It is well known that van der Waals's equation of state is not particularly accurate. For example, using this equation, we find the compressibility factor at the critical point to be

$$Z_c = \frac{p_c v_c}{RT_c} = \frac{3}{8} = 0.375$$

However, generally, $Z$ for most gases at the critical point is somewhere between 0.2 and 0.3. The accuracy of van der Waals's equation of state can be improved by developing values for $\alpha$ and $\beta$ by empirically fitting data in the temperature and pressure range of interest. Alternatively, a different equation of state can be explored. For example, the Redlich–Kwong equation of state is a two-constant equation of state that was developed in 1949:

$$\left(p + \frac{\alpha_o}{v(v+\beta)\sqrt{T}}\right)(v - \beta) = RT$$

This equation offers about the same simplicity, but better accuracy than, van der Waals's equation of state. Recently [see Ref. (2.10)], Redlich–Kwong equation was extended to provide even more accuracy.

Expanding Eq. (2.21) gives a cubic equation in terms of specific volume:

$$v^3 - \left(\beta + \frac{RT}{p}\right)v^2 + \frac{\alpha}{p}v - \frac{\alpha\beta}{p} = 0 \qquad (2.22)$$

Thus, given values of $p$ and $T$, we can obtain the specific volume by solving Eq. (2.22). To accomplish this, we will use *Newton–Raphson's method.* [See, for example, Ref. (2.11).] This is a very efficient trial-and-error method that yields a solution to many nonlinear expressions quite rapidly. We will employ this method at numerous times throughout the book.

A solution strategy for this method can be developed by first writing a functional equation in terms of the variable whose root we are attempting to find. In the present case, we would write Eq. (2.22) as

$$f(v) = 0$$

Since this is a trial-and-error method, a new value of the specific volume $v_{\text{new}}$ is obtained from a previous value $v_{\text{old}}$. One method to establish the link between these two values is to write a single-term Taylor series

$$f(v_{\text{new}}) = f(v_{\text{old}}) + \frac{df}{dv}(v_{\text{old}})(v_{\text{new}} - v_{\text{old}}) + \cdots = 0$$

Rearrangement gives

$$v_{\text{new}} = v_{\text{old}} - \frac{f(v_{\text{old}})}{\dfrac{df}{dv}(v_{\text{old}})} \tag{2.23}$$

The function $f(v)$ that appears in Eq. (2.23) is the cubic equation in Eq. (2.22). The denominator is the derivative of this function. Given a guess (say, the perfect-gas value), we are able to compute a value of $f(v)$ and its derivative. In turn, this result will provide an updated value that will allow us to calculate a new value of $f(v)$ and its derivative, and so on until convergence is obtained. In essence, we are successively obtaining an improved approximation of the root of Eq. (2.22) [i.e., the value of specific volume that brings $f(v)$ as close to zero as possible]. The specific volume, or density, is then used to compute the speed of sound.

**Historical Note:** Newton–Raphson's method has also been called Newton's method. Around 1669, Isaac Newton presented a method to algebraically solve polynomial equations. As an example, he sought to determine the root of $x^3 - 2x - 5 = 0$ between 2 and 3. The method involved guessing an initial value of the root, substituting the sum of the guess plus an additional small term into the polynomial, and then linearizing the equation by dropping higher-order terms. The added term is then readily calculated from the linear equation. The process is repeated for as many times as needed. In 1690, Joseph Raphson (1648–1715) presented a simplified, successive, approximate version that is similar to Eq. (2.23). In 1740, Thomas Simpson (1710–1761) greatly improved the method to iteratively solve nonlinear equations and generalized the method to systems of two equations. For more detail, refer to Ref. (2.12).

To determine the expression for speed of sound, $a$, we start with Eq. (2.11),

$$a = \sqrt{\gamma\left(\frac{\partial p}{\partial \rho}\right)_T}$$

Rewriting Eq. (2.21) in terms of density we get

$$p = \frac{\rho RT}{1 - \beta\rho} - \alpha\rho^2$$

This result allows us to easily determine the partial derivative of pressure with respect to density for a constant temperature; that is,

$$\left(\frac{\partial p}{\partial \rho}\right)_T = \frac{RT}{1 - \beta\rho} + \frac{RT\rho\beta}{(1 - \beta\rho)^2} - 2\alpha\rho$$

Hence,

$$a = \sqrt{\gamma\left[\frac{RT}{1 - \beta\rho} + \frac{RT\rho\beta}{(1 - \beta\rho)^2} - 2\alpha\rho\right]} \tag{2.24}$$

**Example 2.4. The speed of sound in a real gas**

Determine the speed of sound in nitrogen at a location where the pressure is 300 kPa and the temperature is 300K for both a perfect gas and a real gas, using van der Waals's equation of state. Repeat the calculations for the same temperature, but a pressure 100 times larger. The experimental values for these two cases are 353.47 m/s and 483.18 m/s, respectively.

**Solution**

To solve this example, we first develop a spreadsheet solver to determine the specific volume (density) using the numerical procedure just described and then compute the speed of sound from Eq. (2.24). The constants used in van der Waals's equation of state are as follows:

$$R = 296.82\ (\text{N} \cdot \text{m})/(\text{kg} \cdot \text{K})$$

$$\alpha = 174.11\ \text{N} \cdot \text{m}^4/\text{kg}^2$$

$$\beta = 0.001378\ \text{m}^3/\text{kg}$$

$$\gamma = 1.4$$

**Case 1:** $p = 300$ kPa, $T = 300$ K

The first step is to determine the specific volume for the given pressure and temperature, using the cubic equation in Eq. (2.22) and Newton–Raphson's method, Eq. (2.23). Once the density is known for the given pressure and temperature, Eq. (2.24) is used to compute the speed of sound. Table 2.5 shows the iterations for the real gas, starting from the perfect-gas value of $v$ as the initial guess.

**TABLE 2.5** Iteration Results for Case 1 of Example 2.4

| Iteration | $v$ | $f(v)$ | $df/dv$ | $v - f/(df/dv)$ | $\rho$ | $a$ |
|---|---|---|---|---|---|---|
| 1 | 0.2968 | 5.00E-05 | 8.7866E-02 | 0.29625 | 3.3690 | 352.4043 |
| 2 | 0.29625 | 1.92E-07 | 8.7192E-02 | 0.29625 | 3.3755 | 352.4030 |
| 3 | 0.296251 | 2.86E-12 | 8.7190E-02 | 0.296251 | 3.3755 | 352.4030 |

*Perfect gas:* $v = 0.2968\ \text{m}^3/\text{kg}$, $\rho = 3.3690\ \text{kg/m}^3$, $a = 353.08\ \text{m/s}$

*Real gas:* $v = 0.2963\ \text{m}^3/\text{kg}$, $\rho = 3.3755\ \text{kg/m}^3$, $a = 352.40\ \text{m/s}$

There is not a large difference between the results. This is not surprising, since the compressibility factor ($Z = pv/RT$) for the real gas is very close to unity. Actually, the speed of sound predicted by the perfect-gas model is slightly closer to the experimental value than the value predicted using van der Waals's equation. This is because the constants in van der Waals's equation were set at the critical conditions, which are far from the given pressure and temperature.

**Case 2:** $p = 30{,}000\ \text{kPa}$, $T = 300\ \text{K}$

Table 2.6 shows the iterations for the real gas.

**TABLE 2.6** Iteration Results for Case 2 of Example 2.4

| Iteration | $v$ | $f(v)$ | $df/dv$ | $v - f/(df/dv)$ | $\rho$ | $a$ |
|---|---|---|---|---|---|---|
| 1 | 0.002968 | −2.9130E-09 | 6.4330E-06 | 0.003421 | 336.9016 | 519.7548 |
| 2 | 0.003421 | 1.0275E-09 | 1.1176E-05 | 0.003329 | 292.3081 | 455.0607 |
| 3 | 0.003329 | 4.9235E-11 | 1.0114E-05 | 0.003324 | 300.3806 | 465.3416 |
| 4 | 0.003324 | 1.3357E-13 | 1.0059E-05 | 0.003324 | 300.8205 | 465.9189 |
| 5 | 0.003324 | 9.9202E-19 | 1.0059E-05 | 0.003324 | 300.8217 | 465.9205 |

*Perfect gas:* $v = 0.002968\ \text{m}^3/\text{kg}$, $\rho = 336.90\ \text{kg/m}^3$, $a = 353.08\ \text{m/s}$

*Real gas:* $v = 0.003324\ \text{m}^3/\text{kg}$, $\rho = 300.82\ \text{kg/m}^3$, $a = 465.92\ \text{m/s}$

The specific volume of the real gas is 12 percent larger than the perfect-gas value; however, the speed of sound of the real gas is 32 percent larger than that of the perfect gas. Note that the speed of sound of air, computed as a perfect gas, is the same in both cases. This is because, for nitrogen, $a = 20.385\sqrt{T}$ (i.e., depends only on temperature), and since the temperature for Case 1 is the same as in Case 2, the speed of sound must be identical

for both cases. Also, the speed of sound computed from van der Waals's equation of state differs from the experimental value by only 3.5 percent.

**Example 2.5. The speed of sound in a real gas using finite differences**

Use finite differences to determine the speed of sound of nitrogen, using van der Waals's equation of state and the data of Case 1 in Example 2.4.

**Solution**

Instead of calculating the speed of sound from an equation that we develop from the equation of state [e.g., Eq. (2.24) for van der Waals's equation of state], here we will start from Eq. (2.11):

$$a = \sqrt{\gamma\left(\frac{\partial p}{\partial \rho}\right)_T}$$

The foregoing partial derivative can be approximated using a central finite difference much as the speed of sound was computed for superheated steam in Example 2.3. In this case,

$$\left(\frac{\partial p}{\partial \rho}\right)_T \approx \frac{p(\rho + \Delta\rho, T) - p(\rho - \Delta\rho, T)}{2\Delta\rho}$$

For $p = 300$ kPa and $T = 300$ K, the density was determined, using van der Waals's equation, to be 3.3755 kg/m$^3$. The procedure is simply to add and subtract a small increment of density (i.e., $\Delta\rho$) to the computed value of density and then use van der Waals's equation to compute the pressure from

$$p = \frac{RT\rho}{1 - b\rho} - a\rho^2$$

The accuracy of any finite difference will depend on the size of $\Delta\rho$. Small increments will produce the best results. Use $\Delta\rho = 0.1$ kg/m$^3$, $p = 308{,}870.07$ N/m$^2$ ($\rho = 3.4755$ kg/m$^3$, $T = 300$ K), and $p = 291{,}128.94$ N/m$^2$ ($\rho = 3.2755$ kg/m$^3$, $T = 300$ K). Subtracting the pressures, dividing by $2\Delta\rho$, multiplying the ratio by $\gamma = 1.4$, and taking the square root of the result gives $a = 352.403$ m/s, which is the same value that was determined previously.

## 2.7 SUMMARY

As a body moves through a stationary fluid, waves are emitted from each point on the body and travel outward at the velocity of sound. In an incompressible fluid, the velocity of sound is infinite, so an entire body of fluid is able to instantaneously "sense" the motion of an object passing through it. In a compressible fluid, the velocity of sound has a finite value. If a body travels through a compressible fluid at a velocity *less* than that of sound, waves emitted by the body are able to move ahead of the body and signal the fluid to adjust to the oncoming disturbance. If a body travels at a velocity *greater* than that of sound, the waves are not able to signal the fluid ahead of the body. For the subsonic case, the fluid is able to adjust gradually to a moving object, and smooth, continuous

streamline patterns result. For the supersonic case, the fluid must adjust rapidly to a moving object. Shockwaves result, with discontinuous changes in fluid properties. Because of its importance, a variety of methods for determining the speed of sound were presented. The importance of Mach number for compressible flow is established.

## 2.8 REFERENCES


**2.1** Hall, D. E. *Basic Acoustics*, Harper & Row, New York, 1987, pp. 134–136.

**2.2** Rayleigh, J. W. S. *The Theory of Sound*, Vol. 1, Dover Publications, New York, 1945, pp. xvii–xx.

**2.3** Moran, M. J., and Shapiro, H. N. *Fundamentals of Engineering Thermodynamics*, 4th ed., John Wiley & Sons, New York, 2000, pp. 578–581.

**2.4** Wang, C. T. *Applied Elasticity*, McGraw-Hill, New York, 1953, p. 31.

**2.5** Kinsler, L. E., and Frey, A. R., *Fundamentals of Acoustics*, 2d ed., John Wiley & Sons, New York, 1962, pp. 502–503.

**2.6** Cengel, Y. A., and Boles, M. A. *Thermodynamics: An Engineering Approach*, 4th ed., McGraw-Hill Book Company, New York, 2002, p. 834.

**2.7** Von Karman, T. "Supersonic Aerodynamics: Principles and Applications," *J Aeronautl Sci* 1947; 14(7): 373.

**2.8** Shapiro, A. *The Dynamics and Thermodynamics of Compressible Fluid Flow*, Vol. 1, Ronald Press, New York, 1958, pp. 131–134.

**2.9** Eggers, A. J. "One-Dimensional Flows of an Imperfect Diatomic Gas," NACA Report 959, 1959.

**2.10** Aungier, R. H. "A Fast, Accurate Real Gas Equation of State for Fluid Dynamic Analysis Applications," ASME, *J Fluids Eng* 1995; 117: 277–281.

**2.11** Hoffman, J. D. *Numerical Methods for Engineers and Scientists*, 2d ed., Marcel Dekker, New York, 2001, p. 158.

**2.12** Chabert, J.-L., ed. *A History of Algorithms*, Springer-Verlag, Berlin, 1999, pp. 169–178.

**2.13** Reichenbach, H. "Contributions of Ernst Mach to Fluid Mechanics," *Ann Rev Fluid Mech* 1983; 15: 1–28.

**2.14** Gomes, M. F., and Trusler, J. P. M. "The Speed of Sound in Nitrogen at Temperatures Between $T = 250$ K and $T = 350$ K and at Pressures up to 30 MPa," *J Chem Thermodynam* 1998; 30: 527–534.


## 2.9 PROBLEMS

**2.1** Using the expansion wave and control volume depicted in Figures 2.7 and 2.8, along with the continuity and momentum equations, rederive Eq. (2.4).

**2.2** (a) Derive an expression for $k_s$ for a perfect gas, substitute the result into Eq. (2.10), and thereby demonstrate Eq. (2.7). (b) Derive an expression for $k_T$ for a perfect gas, substitute the result into Eq. (2.11), and thereby demonstrate Eq. (2.7). (c) Finally, derive an expression for $\beta_s$ for a perfect gas, substitute your result into Eq. (2.14), and thereby demonstrate Eq. (2.7).

**2.3** Use dimensional analysis to develop an expression for the speed of sound in terms of the isentropic compressibility, the density, and $g_c$.

**2.4** Using the data provided in Tables 2.1, 2.2, and 2.3 (i.e., the density and the isentropic compressibility or the bulk modulus), calculate the velocity of sound in (a) helium, (b) turpentine, and (c) lead at 20°C and one atmosphere pressure.

**2.5** In Example 2.3, the speed of sound of superheated steam was determined by using a finite-difference representation of the compressibility and steam-property data. (See Table 2.4.)

Using the same steam-property data, determine the speed of sound of superheated steam for the same pressure and temperature (i.e., at $p = 500$ kPa and T = 300°C). Then use the finite-difference method on the following equations to provide two estimates for the speed of sound:

$$a^2 = \frac{\gamma}{\left(\frac{\partial \rho}{\partial p}\right)_T} = \frac{\gamma}{\left[\frac{\partial (1/v)}{\partial p}\right]_T}$$

$$a^2 = \frac{1}{\left(\frac{\partial \rho}{\partial p}\right)_s} = \frac{1}{\left[\frac{\partial (1/v)}{\partial p}\right]_s}$$

**2.6** Equation (2.16) provides a convenient expression for calculating the speed of sound in air: $a = 20.05\sqrt{T}$, where $T$ is the absolute temperature in degrees Kelvin. Derive the following linear equation for the speed of sound in air, where $a_0$ is the speed of sound in air at 0°C and $T$ is °C:

$$a = a_0 + 0.6T$$

To accomplish this, use Eq. (2.16) and the expansion $(x + y)^n = x^n + nx^{n-1}y + \cdots$.

**2.7** Rather than measuring the bulk modulus directly, it may be easier to measure the speed of sound as the sound propagates though a material and then use the result to compute the bulk modulus. For a Lucite plastic of density 1,200 kg/m$^3$, the speed of sound is measured as 2,327 m/s. Determine the bulk modulus. What is the corresponding isentropic compressibility?

**2.8** An object of diameter $d$(m) is rotated in air at a speed of $N$ revolutions per minute. Draw a plot of the rotational speed required for the velocity at the outer edge of the object to just reach sonic velocity for a given diameter. Take the speed of sound of the air to be 331 m/s.

**2.9** (a) Newton assumed that the sound-wave process was isothermal rather than isentropic. Determine the size of error made in computing the speed of sound that occurs as a result of this assumption. (b) A flash of lightning occurs in the distance. Twenty seconds later, the sound of thunder is heard. The temperature in the area is 23°C. How far away was the lightning strike?

**2.10** (a) The pressure increase across a compression pulse moving into still air at one atmosphere pressure and 30°C is 100 Pa. Determine the velocity following the pulse. (b) The velocity changes by 0.1 m/s across a pressure wave that moves into hydrogen gas that is at rest at a pressure of 100 kPa and temperature 300 K. Determine the pressure behind the wave.

**2.11** (a) Helium at 35°C is flowing at a Mach number of 1.5. Find the velocity, and determine the local Mach angle. (b) Determine the velocity of air at 40°C to produce a Mach angle of 38°.

**2.12** (a) A jet plane is traveling at Mach 1.8 at an altitude of 10 km, where the temperature is 223.3 K. Determine the speed of the plane. (b) Air at 320 K flows in a supersonic wind tunnel over a two-dimensional wedge. From a photograph, the Mach angle is measured to be 45°. Determine the flow velocity, the local speed of sound, and the Mach number of the tunnel.

**2.13** A supersonic aircraft, flying horizontally a distance $H$ above the earth, passes overhead. A time interval $\Delta t$ later, the sound wave from the aircraft is heard. In this time increment, the plane has traveled a distance $L$. Show that the Mach number of the aircraft can be computed from:

$$M = \sqrt{\left(\frac{L}{H}\right)^2 + 1} = \sqrt{\left(\frac{V\Delta t}{H}\right)^2 + 1}$$

*Hint:* first show that the Mach angle $\mu$ can be expressed as $\tan^{-1}\left(1/\sqrt{M^2 - 1}\right)$, and then connect the Mach angle to the geometric parameters $H$ and $L$.)

**2.14** Given the following speeds and temperatures, determine the corresponding Mach numbers (*Note:* 1 mile = 5,280 ft = 1,609.3 m; 1 mi/h = 1.6093 km/h = 0.447 m/s):
(a) A cheetah running at top speed of 60 mi/h; the local temperature is 40°C
(b) A peregrine falcon in a dive at 217 mi/h; the local temperature is 25°C
(c) Maurice Greene, who in June 1999, in Athens, Greece, became the world's fastest human by running 100 m in 9.79 s; the temperature was 21°C
(d) Alexander Popov, who in June 1999 became the world's fastest swimmer by swimming 50 m in 21.64 s; the temperature of the water was 20°C

**2.15** Given the following speeds and Mach numbers, and assuming that air is a perfect gas, determine the corresponding local temperature (*Note*: 1 mi/h = 0.447 m/s):
(a) A *Boeing 747-400* at a cruise speed of 910 km/h; $M = 0.85$
(b) The *Concorde* at a cruise speed of 1,320 mi/h; $M = 2.0$
(c) The fastest airplane, the *Lockheed SR-71 Blackbird*, flying at 2,200 mi/h; $M = 3.3$
(d) The fastest boat, the *Spirit of Australia*, which averaged a speed of 317.6 mi/h; $M = 0.41$
(e) The fastest car, the *ThrustSSC*, which averaged a speed of 760.035 mi/h; $M = 0.97$

**2.16** A baseball, which has a mass of 145 grams and a diameter of 3.66 cm, when dropped from a very tall building reaches high speeds. If the building is tall enough, the speed will be controlled by the drag, as the baseball will reach terminal speed. At this state,

$$W = F_D$$

where $W$ (weight) = mg, $g$ (acceleration of gravity) = 9.81 m/s$^2$, $F_D$ (drag force) = $C_D \rho_{air} AV^2/2$, $C_D$ (drag coefficient) = 0.5, and $A$ (projected area of sphere) = $\pi R^2$. Find the terminal speed of the baseball and determine the corresponding Mach number if the ambient air temperature is 23°C and the ambient air pressure is 101 kPa.

**2.17** Berthelot's equation of state,

$$p = \frac{\rho RT}{1 - \beta\rho} - \frac{\alpha\rho^2}{T}$$

is a two-constant equation of state that provides more accuracy than van der Waals's equation, particularly at low pressures. Use this equation to derive the following equation for the speed of sound:

$$a = \sqrt{\gamma\left[\frac{RT}{1 - \beta\rho} + \frac{RT\rho\beta}{(1 - \beta\rho)^2} - \frac{2\alpha\rho}{T}\right]}$$

**2.18** Using the speed-of-sound expression from the previous problem and constants for nitrogen of $R = 296.82$ (N · m)/(kg · K), $\alpha = 21{,}972.68$ (N · m$^4$ · K)/kg$^2$, $\beta = 0.001378$ m$^3$/kg, and $\gamma = 1.4$, determine the speed of sound for the two cases described in Example 2.4.

**2.19** Employ the finite-difference method of Example 2.5 to determine the speed of sound in nitrogen, using the Redlich–Kwong equation of state, which is

$$p = \frac{RT\rho}{1 - \beta\rho} - \frac{\alpha_o \rho^2}{(1 + \beta\rho)\sqrt{T}}$$

where, for nitrogen

$R = 296.823\ (\mathrm{N \cdot m})/(\mathrm{kg \cdot K})$

$\alpha_o = 1979.453\ \left(\mathrm{N \cdot m^4 \cdot \sqrt{K}}\right)/(\mathrm{kg^2})$

$\beta = 0.0009557\ \mathrm{m^3/kg}$

$\gamma = 1.4$

Compute the speed of sound at a pressure of 30.1 MPa and a temperature of 300 K. Experimental values of the speed of sound of nitrogen may be found in Ref. (2.14). For the given conditions, the measured value is 483.730 m/s.

# Chapter 3

# Isentropic Flow of a Perfect Gas

## 3.1 INTRODUCTION

In this and subsequent chapters, the effect on compressible flow of area change, friction, heat transfer, and electromagnetic fields will be studied. In most physical situations, more than one of these effects occur simultaneously; for example, flow in a rocket nozzle involves area change, friction, and heat transfer. However, one of the effects is usually predominant; in the rocket nozzle, area change is the factor that has greatest influence on the flow. The frequent predominance of one factor provides a justification for separating the effects, including them one at a time in the equations of motion, and studying the resultant property variations.

Whereas a certain loss of generality is incurred by treating each effect individually, this procedure does simplify the equations of motion so that the result of each effect can be easily appreciated. Furthermore, this simplification enables approximate solutions to be derived for a wide range of problems in compressible flow; such solutions are sufficiently accurate for many engineering applications. Attempts to include all the effects simultaneously in the equations of motion lead to mathematical complexities that mask the physical situation. In many cases, exact solutions to these generalized equations of motion are impossible.

Chapter 3 is concerned with compressible, isentropic flow through varying area channels, such as nozzles, diffusers, and turbine-blade passages. Friction and heat transfer are nonexistent in these isentropic flows; variations in properties are brought about by area change. One-dimensional, steady flow of a perfect gas is assumed in order to reduce the equations to a workable form. For gas flows, changes in potential energy and gravitational forces are neglected. To fully understand the limitations imposed by the various assumptions, reference should be made to Chapter 1. The applicability and accuracy of the equations derived in this and subsequent chapters depend to a large extent on the manner in which the assumptions fit the physical situation involved in a given engineering problem.

## 3.2 EQUATIONS OF MOTION

For one-dimensional steady flow through a varying area channel, select a control volume, as shown in Figure 3.1. The continuity equation for this configuration [refer to Eq. (1.28)] is

$$\iint_{\text{C.S.}} \rho \mathbf{V} \cdot d\mathbf{A} = \dot{m}_{\text{outflow}} - \dot{m}_{\text{inflow}} = 0 \tag{3.1}$$

Thus, the mass rate of flow, $\dot{m}$ (kg/s), which is the product of the density, cross-sectional area, and velocity, is constant at all sections of the channel. Accordingly, for one-dimensional steady flow through a varying area channel,

$$\rho AV = \dot{m} = \text{constant} \tag{3.2}$$

To obtain a differential form of the continuity equation, take the natural logarithm of Eq. (3.2) and then differentiate to obtain

$$\frac{d\rho}{\rho} + \frac{dA}{A} + \frac{dV}{V} = 0 \tag{3.3}$$

An alternative derivation consists of performing a mass balance on the differential control volume in Figure 3.1, which produces

$$(\rho + d\rho)(A + dA)(V + dV) - \rho AV = 0$$

Expand, simplify, and divide the entire equation by $\rho AV$ to obtain Eq. (3.3).

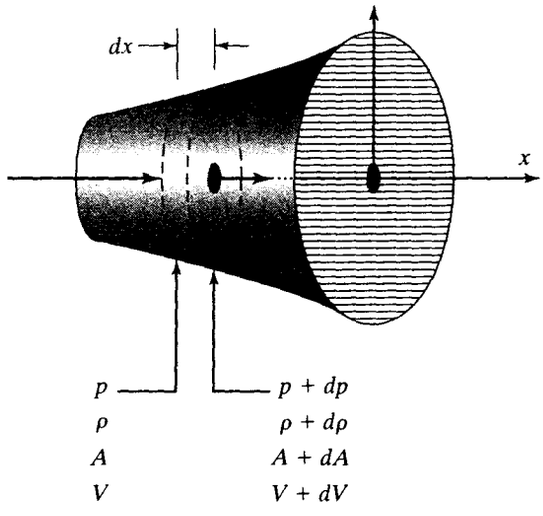


**Figure 3.1** Control Volume for Varying Area Flow

For steady flow, the momentum equation [refer to Eq. (1.33)] in the $x$ direction is

$$\Sigma F_x = \iint_{\text{C.S.}} V_x(\rho \mathbf{V} \cdot d\mathbf{A}) = (\dot{m}V)_{\text{outflow}} - (\dot{m}V)_{\text{inflow}} \tag{3.4}$$

In the absence of electromagnetic forces, and with negligible friction, the only forces acting on the control surface are pressure forces. As illustrated in Figure 3.2, these forces act compressively on the upstream face, the sidewall face, and the downstream face. It may be assumed that an average pressure equal to $p + dp/2$ acts on the sidewalls.

Thus, we have

$$\Sigma F_x = F_{\text{upstream}} + F_{\text{sidewall}} - F_{\text{downstream}}$$

where

$$F_{\text{upstream}} = pA$$

$$F_{\text{sidewall}} = \left(p + \frac{dp}{2}\right)\left(\frac{dA}{\sin\theta}\right)\sin\theta = \left(p + \frac{dp}{2}\right)dA$$

$$F_{\text{downstream}} = (p + dp)(A + dA)$$

Combining all terms and expanding gives

$$\Sigma F_x = -A\,dp$$

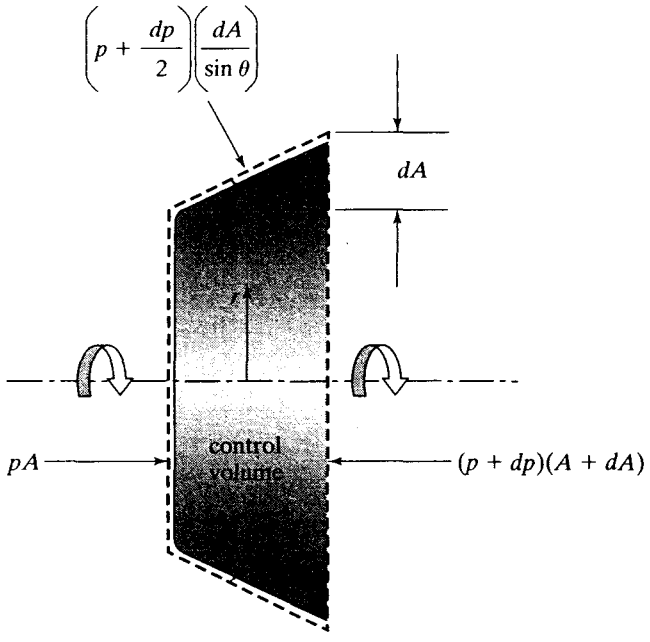


**Figure 3.2** Pressure Forces Acting on Control Volume

It should be noted that this is the same force balance that would be obtained for a constant-area duct. Completing the momentum balance using Eqs. (3.2) and (3.4), we get

$$\Sigma F_x = -A dp = [\dot{m}(V + dV)] - \dot{m}V = \dot{m}dV = \rho AV dV$$

Simplification produces the steady, one-dimensional, differential-momentum equation called *Euler's equation*, which is valid for both constant-area and variable-area geometries:

$$dp + \rho V dV = 0 \tag{3.5}$$

Because the flow is one dimensional, say, in the $x$ direction, Eq. (3.5) may also be written as

$$\frac{dp}{dx} + \rho V \frac{dV}{dx} = 0$$

Note that the pressure and the velocity act in opposite directions in Euler's equation. When the pressure increases, the velocity decreases, and vice versa. Also note that if the density were constant, integration of Eq. (3.5) would produce the well-known *Bernoulli equation*, which can be used for low-Mach-number flows:

$$p + \rho \frac{V^2}{2} = \text{constant}$$

The energy equation with negligible potential energy, no external heat transfer, and no work [refer to Eq. (1.38)] becomes

$$\iint_{\text{c.s.}} \left(h + \frac{V^2}{2}\right)(\rho \mathbf{V} \cdot d\mathbf{A}) = \left[\dot{m}\left(h + \frac{V^2}{2}\right)\right]_{\text{outflow}} - \left[\dot{m}\left(h + \frac{V^2}{2}\right)\right]_{\text{inflow}} = 0$$

for steady one-dimensional flow.

Performing an energy balance on the differential control volume of Figure 3.1 yields the differential energy equation

$$d\left(h + \frac{V^2}{2}\right) = dh + d\left(\frac{V^2}{2}\right) = 0 \tag{3.6}$$

Hence, the sum of the enthalpy and kinetic energy, like the mass-flow rate, is constant throughout the channel.

Now, from the Gibbs second identity [refer to Eq. (1.44)], we know that

$$Tds = dh - \frac{dp}{\rho} \tag{3.7}$$

For isentropic flow, $ds = 0$; hence, Eq. (3.7) becomes

$$dh = \frac{dp}{\rho}$$

Combining this equation with Eq. (3.6) produces

$$\frac{dp}{\rho} + d\left(\frac{V^2}{2}\right) = 0$$

or

$$dp + \rho V dV = 0$$

So, using the energy equation, we have again derived Euler's equation, Eq. (3.5).

## 3.3 SUBSONIC AND SUPERSONIC ISENTROPIC FLOW THROUGH A VARYING AREA CHANNEL

Combining the continuity and momentum equations for isentropic flow [i.e., Eqs. (3.3) and (3.5)], respectively, one obtains

$$dp + \rho V^2\left[-\frac{d\rho}{\rho} - \frac{dA}{A}\right] = 0 \tag{3.8}$$

But, as we have seen in the previous chapter,

$$\left(\frac{\partial p}{\partial \rho}\right)_s = a^2$$

For isentropic flow, there is no need to use the partial derivatives, and we may therefore write $d\rho = dp/a^2$. Replacing $d\rho$ in Eq. (3.8) yields

$$dp + \rho V^2\left(-\frac{dp}{\rho a^2} - \frac{dA}{A}\right) = 0$$

or

$$dp(1 - M^2) = \rho V^2 \frac{dA}{A} \tag{3.9}$$

Dividing by the pressure and using the perfect-gas expression for the speed of sound, $a^2 = \gamma p/\rho$, produces

$$\frac{dp}{dA} = \left[\frac{\gamma M^2}{(1 - M^2)}\right]\frac{p}{A} \tag{3.10}$$

The principal value of Eq. (3.10) is that it demonstrates the influence of Mach number on steady, isentropic, variable-area flow of a perfect gas.

For subsonic flow, $M < 1$, the coefficient on the right-hand side of Eq. (3.10) is positive. Therefore, $dp/dA > 0$, which informs us that area and pressure change in the same direction; that is an increase of one is accompanied by an increase in the other. Also, from Euler's equation, Eq. (3.5), if pressure increases, the velocity must decrease. So, for subsonic flow, a decrease in area results in a decrease in pressure (an expansion) and an increase in velocity (an acceleration). The results of this analysis are summarized in Figure 3.3.

For supersonic flow, $M > 1$, the term $(1 - M^2)$ makes the term on the right-hand side of Eq. (3.10) negative. Accordingly, $dp/dA < 0$, which indicates that the area and pressure change in opposite directions; that is, an increase of one is accompanied by a decrease of the other. In other words, for supersonic flow, pressure and cross-sectional area are inversely related: A decrease in area results in an increase in pressure (a compression) and therefore a decrease in velocity (a deceleration). These conditions represent opposite variations to the subsonic flow outcomes. The results of this analysis are summarized in Figure 3.4.

It is important to observe that, to accelerate a subsonic flow, we decrease the area, as we would expect; however, to accelerate a supersonic flow, we must actually increase the area!

The results illustrated in Figures 3.3 and 3.4 have several ramifications. For example, they indicate that a subsonic flow cannot be accelerated to a velocity greater than the velocity of sound (supersonic flow) in a converging nozzle, regardless of the pressure difference imposed on the flow through the nozzle. If it is desired to accelerate a stream from negligible velocity to supersonic velocity, a convergent–divergent channel must be used. That is, the flow must pass through a *throat*, or minimum area. (See Figure 3.5.)

That a minimum area must occur is mathematically realized by noting that to pass from $M < 1$ to $M > 1$, the velocity of the flow must reach sonic velocity; that is, the Mach number must be equal to unity. However, this means that we will divide

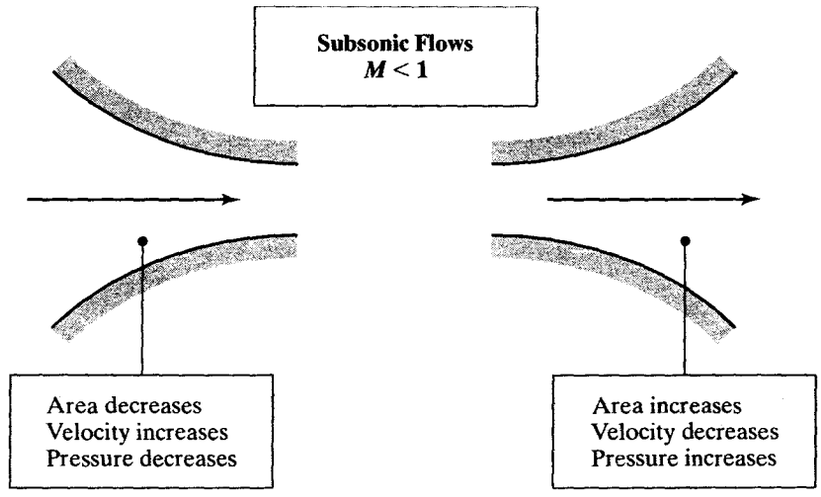


**Figure 3.3** Subsonic Flows

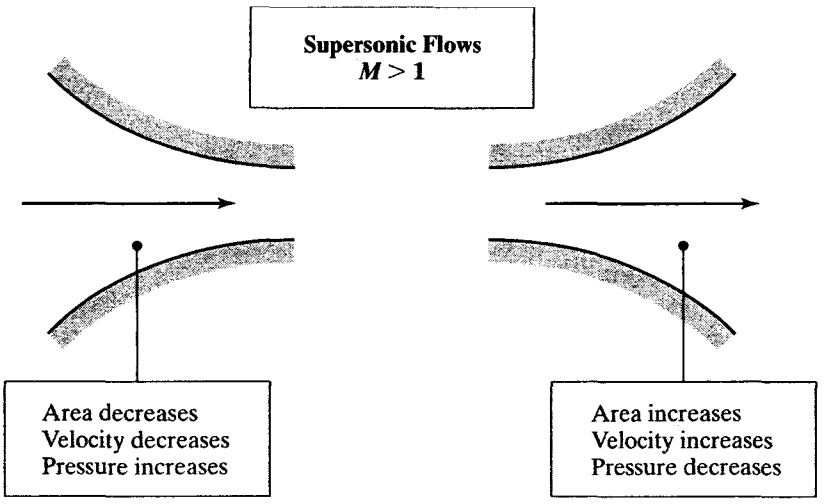


**Figure 3.4** Supersonic Flow

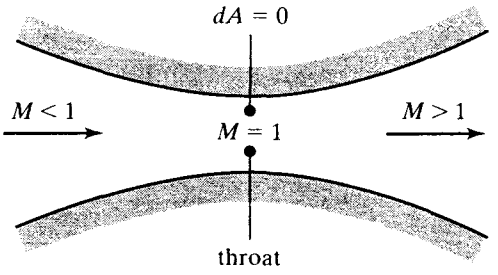


**Figure 3.5** Conversion of Subsonic–Supersonic Flows through the Minimum Area of a Duct

Eq. (3.10) by zero. For this equation not be to become infinite, $dA$ must equal zero. It can be shown that $d^2A > 0$ for this condition. [See Ref. (3.1).] Thus, the location where $M = 1$ occurs is at the position in the channel where $A$ is a minimum.

## 3.4 STAGNATION PROPERTIES

Stagnation properties are useful in that they define a reference state for compressible flow.

*Stagnation enthalpy*, or *total enthalpy*, $h_o$ at a point in a flow is the enthalpy attained by bringing the flow *adiabatically* to rest at that point. The stagnation enthalpy per unit mass is defined by

$$h_o = h + \frac{V^2}{2} \tag{3.11}$$

*Stagnation temperature*, or *total temperature*, $T_o$ is the temperature measured by bringing a flow *adiabatically* to rest at a point. For a perfect gas with constant specific heats, we have from Eq. (3.11)

$$h_o - h = c_p(T_o - T) = \frac{V^2}{2}$$

So,

$$T_o = \frac{V^2}{2c_p} + T = T\left(1 + \frac{V^2}{2c_pT}\right)$$

However,

$$c_p = \frac{\gamma R}{\gamma - 1}$$

Hence,

$$T_o = T\left[1 + \frac{(\gamma - 1)V^2}{2\gamma RT}\right]$$

Also,

$$\gamma RT = a^2$$

Combining terms, we obtain the following for a perfect gas with constant specific heats:

$$\frac{T_o}{T} = 1 + \frac{\gamma - 1}{2}M^2 \tag{3.12}$$

Equation (3.12) can provide the Mach number when the temperature ratio is known:

$$M = \sqrt{\frac{2}{\gamma - 1}\left(\frac{T_o}{T} - 1\right)} \tag{3.13}$$

*Stagnation pressure*, or *total pressure*, $p_o$ at a point in a flow is defined as the pressure attained if the flow at that point is brought *isentropically* to rest. From Eq. (1.46), for a perfect gas with constant specific heats undergoing an isentropic process, we obtain

$$\frac{p_2}{p_1} = \left(\frac{T_2}{T_1}\right)^{\gamma/(\gamma-1)} \tag{3.14}$$

Let state 2 be the stagnation state; then

$$\frac{p_o}{p} = \left(\frac{T_o}{T}\right)^{\gamma/(\gamma-1)}$$

Using Eq. (3.12), we obtain

$$\frac{p_o}{p} = \left(1 + \frac{\gamma - 1}{2}M^2\right)^{\gamma/(\gamma-1)} \tag{3.15}$$

Equation (3.15) can be used to determine the Mach number when the pressure ratio is known:

$$M = \sqrt{\frac{2}{\gamma - 1}\left[\left(\frac{p_o}{p}\right)^{\frac{\gamma-1}{\gamma}} - 1\right]} \tag{3.16}$$

*Stagnation density*, or *total density*, $\rho_o$ at a point in a flow is defined as the density that is attained if the flow at that point is brought *isentropically* to rest. The stagnation-to-static-density ratio is connected to the pressure ratio through the isentropic relation

$$\frac{\rho_o}{\rho} = \left(\frac{p_o}{p}\right)^{\frac{1}{\gamma}}$$

Utilizing Eq. (3.15) yields

$$\frac{\rho_o}{\rho} = \left(1 + \frac{\gamma - 1}{2}M^2\right)^{1/(\gamma-1)} \tag{3.17}$$

Solving Eq. (3.16) gives the Mach number in terms of the density ratio:

$$M = \sqrt{\frac{2}{\gamma - 1}\left[\left(\frac{\rho_o}{\rho}\right)^{(\gamma-1)} - 1\right]} \tag{3.18}$$

**Calculation Note:** Equations (3.12), (3.15), and (3.17) are often tabulated for three common ratios of specific heats: $\gamma = 1.4$, 1.3, and 5/3, as $T/T_o$, $p/p_o$, and $\rho/\rho_o$ versus $M$. See Appendix B. However, access to computers has made the use of tables of these ratios less valuable than in the past. Nevertheless, the isentropic-flow tables are convenient particularly when a computer is not available. Alternatively, it is an easy matter to create a spreadsheet program that replicates these tables and provides an isentropic-flow solver. (See Appendix A.) Furthermore, flow calculators are available on the World Wide Web.

**Example 3.1. Calculation of stagnation properties**

A perfect gas with $\gamma = 1.4$ is traveling at Mach 3 with a static temperature of 250 K, a static pressure of 101 kPa, and a static density of 1.4077 kg/m$^3$. Determine the stagnation temperature, pressure, and density values.

**Solution**

From Eqs. (3.12), (3.15), and (3.17), we find the static-to-stagnation-temperature ratio at $M = 3$ to be 0.3571, the static-to-stagnation-pressure ratio to be 0.02722, and the static-to-stagnation-density ratio to be 0.07623. Thus,

$$T_o = T\left(\frac{T_o}{T}\right) = 250\frac{1}{0.3571} = 700.0840 \text{ K}$$

$$p_o = p\left(\frac{p_o}{p}\right) = 101\frac{1}{0.02722} = 3{,}710.5070\ \text{kPa}$$

$$\rho_o = \rho\left(\frac{\rho_o}{\rho}\right) = 1.4077\frac{1}{0.07623} = 18.4665\frac{\text{kg}}{\text{m}^3}$$

Because of the high speed of the flow [$V = Ma = (3)(317.02) = 951.1$ m/s], there are large differences between the static and stagnation properties. Note that static properties are used to compute the speed of sound.

---

It can be difficult to understand the difference between static and stagnation properties. *Static pressure* and *static temperature* of a moving stream are properties experienced by an observer or instrument moving with the same velocity as the stream. They are thermodynamic properties of the flow. On the other hand, *stagnation pressure* and *stagnation temperature* are properties experienced by a fixed observer or instrument, the fluid having been brought to rest (isentropically and adiabatically, respectively) at the observer or instrument. The difference between static and stagnation properties is due to the velocity or kinetic energy of the flow.

For steady adiabatic flow in a variable area channel, we have shown [see Eq. (3.6)] that

$$dh + d\left(\frac{V^2}{2}\right) = d\left(h + \frac{V^2}{2}\right) = 0$$

But the sum of the static enthalpy and the kinetic energy is the stagnation enthalpy, Eq. (3.11), and therefore

$$dh_o = 0$$

So the stagnation enthalpy remains constant. Since for a perfect gas $h_o = c_p T_o$, this relationship informs us that the stagnation temperature is also constant for steady, adiabatic, and isentropic flow.

**Example 3.2. Stagnation pressure in steady isentropic flow**

Prove that the stagnation pressure of a perfect gas in a steady isentropic flow remains constant.

**Solution**

From the Gibbs second identity [Eq. (1.44)],

$$T_o ds_o = dh_o - \frac{dp_o}{\rho_o}$$

For steady adiabatic flow, $dh_o = 0$; hence,

$$ds_o = -\left(\frac{1}{T_o\rho_o}\right)dp_o = -\left(\frac{R}{p_o}\right)dp_o = -Rd(\ln p_o)$$

Integration between two arbitrary points in the flow produces the following arrangement:

$$\frac{p_{o2}}{p_{o1}} = e^{-(\Delta s_o/R)}$$

For isentropic flow, $\Delta s_o = \Delta s = 0$; hence, $p_{o2} = p_{o1}$. In other words, the stagnation pressure $p_o$ is constant for isentropic flow. Therefore, the stagnation pressure is a useful metric for evaluating the quality of the flow. For example, to access the value of a subsonic inlet of a gas turbine engine, the difference in internal and external stagnation pressures (stagnation pressure recovery) is determined.

---

The mass-flow rate at cross-sectional area $A$ can be expressed in terms of stagnation pressure and temperature by starting from Eq. (3.2):

$$\dot{m} = \rho AV$$

For a perfect gas with constant specific heats,

$$\dot{m} = \frac{p}{RT} AM\sqrt{\gamma RT}$$

where

$$p = \frac{p_o}{\left(1 + \dfrac{\gamma - 1}{2} M^2\right)^{\gamma/(\gamma-1)}}$$

and

$$T = \frac{T_o}{1 + \dfrac{\gamma - 1}{2} M^2}$$

Thus,

$$\dot{m} = \frac{p_o}{\sqrt{RT_o}} A\sqrt{\gamma} M\left(1 + \frac{\gamma - 1}{2} M^2\right)^{-\frac{\gamma+1}{2(\gamma-1)}} \tag{3.19}$$

or, more simply,

$$\dot{m} = \frac{p_o A}{\sqrt{RT_o}} F(\gamma, M) \tag{3.20}$$

where $F(\gamma, M)$ is given by

$$F(\gamma, M) = \sqrt{\gamma} M\left(1 + \frac{\gamma - 1}{2} M^2\right)^{-\frac{\gamma+1}{2(\gamma-1)}} \tag{3.21}$$

It is useful to determine the Mach number corresponding to the maximum value of $F(\gamma, M)$ because it will reveal the maximum flow rate for given values of $p_o$, $T_o$, and $A$. To accomplish this, differentiate Eq. (3.21) and set the result to zero to find that

$$\frac{dF}{dM} = \sqrt{\gamma}\left(1 + \frac{\gamma - 1}{2}M^2\right)^{-\frac{3\gamma-1}{2(\gamma-1)}}(1 - M^2) = 0$$

This equation is satisfied by $M = 1$. A second derivative evaluated at $M = 1$ will show that $d^2F/dM^2 < 0$, which is the requirement for this rate to be a maximum. Thus, for constant values of $p_o$, $T_o$, and $A$, the maximum flow rate is

$$\dot{m}_{\max} = \frac{p_o A}{\sqrt{RT_o}}F(\gamma, 1) = \frac{p_o A}{\sqrt{RT_o}}\sqrt{\gamma}\left(\frac{\gamma + 1}{2}\right)^{-\frac{\gamma+1}{2(\gamma-1)}}$$

Note that for air ($\gamma = 1.4$ and $R = 287\ \text{N} \cdot \text{m/kg} \cdot \text{K}$), the maximum flow rate is

$$\dot{m}_{\max} = 0.040418\frac{p_o A}{\sqrt{T_o}}$$

as used in Example 1.1.

For isentropic flow, in which $p_o$ and $T_o$ are both constant, the cross-sectional area $A$ can be related directly to Mach number. Select the area at which $M = 1$ as a reference area. Call this area $A^*$. For steady flow, the mass-flow rate is constant through a variable-area channel. Thus, the flow rate at area $A$, say, $\dot{m}_A$, is equal to the mass flow rate at $A^*$, say, $\dot{m}_{A^*}$. Hence, using Eq. (3.16), we get

$$\frac{p_o}{\sqrt{RT_o}}AF(\gamma, M) = \frac{p_o}{\sqrt{RT_o}}A^*F(\gamma, 1)$$

or

$$\frac{A}{A^*} = \frac{F(\gamma, 1)}{F(\gamma, M)} \tag{3.22}$$

where

$$\frac{F(\gamma, 1)}{F(\gamma, M)} = \frac{\sqrt{\gamma}\left(\frac{\gamma + 1}{2}\right)^{(\gamma+1)/(2-2\gamma)}}{M\sqrt{\gamma}\left(1 + \frac{\gamma - 1}{2}M^2\right)^{(\gamma+1)/(2-2\gamma)}} = \frac{1}{M}\left[\left(\frac{2}{\gamma + 1}\right)\left(1 + \frac{\gamma - 1}{2}M^2\right)\right]^{\frac{\gamma+1}{2(\gamma-1)}}$$

Therefore,

$$\frac{A}{A^*} = \frac{1}{M}\left[\left(\frac{2}{\gamma + 1}\right)\left(1 + \frac{\gamma - 1}{2}M^2\right)\right]^{\frac{\gamma+1}{2(\gamma-1)}} \tag{3.23}$$

Equation (3.23) is plotted in Figure 3.6 for $\gamma = 1.4$. As may be seen for each value of $M$, there is only one value of $A/A^*$; however, for a given $A/A^*$ there are two possible isentropic solutions, one subsonic and the other supersonic. Also, note that $A/A^*$ is never smaller than unity. Furthermore, around $M = 1$, the curve is relatively flat. Physically, this informs us that small changes in area can lead to relatively large changes in Mach number in the vicinity of the sonic point.

Numerical values of $A/A^*$ versus $M$, as with other isentropic ratios, are tabulated for $\gamma = 1.4, 1.3$, and $5/3$ in Appendix B. However, it is an easy matter to develop a spreadsheet program to create the isentropic-flow tables. (See Appendix A.) As a demonstration, from the tables in Appendix B, we find that for $\gamma = 1.4$ and $A/A^* = 1.5$, $M = 0.43$ and 1.85. The results of this example are shown in Figure 3.6, and the physics of this result are illustrated in Figure 3.7. Note that to determine the Mach numbers in this example from the tables, we would have had to use linear interpolation. If we desire more accurate results, an improved process is required. To accomplish this, we can use the numerical procedure, Newton–Raphson's method, which was introduced in Section 2.6 to solve a cubic equation for specific volume.

Here, we seek the Mach-number roots of Eq. (3.23), which is rewritten as

$$f(M) = \alpha M - c^b\left(1 + \frac{M^2}{2bc}\right)^b$$

$$\frac{df}{dM} = f' = \alpha - c^{b-1}M\left(1 + \frac{M^2}{2bc}\right)^{b-1}$$

where $\alpha = \dfrac{A}{A^*}$, $b = \dfrac{\gamma + 1}{2(\gamma - 1)}$, and $c = \dfrac{2}{\gamma + 1}$.

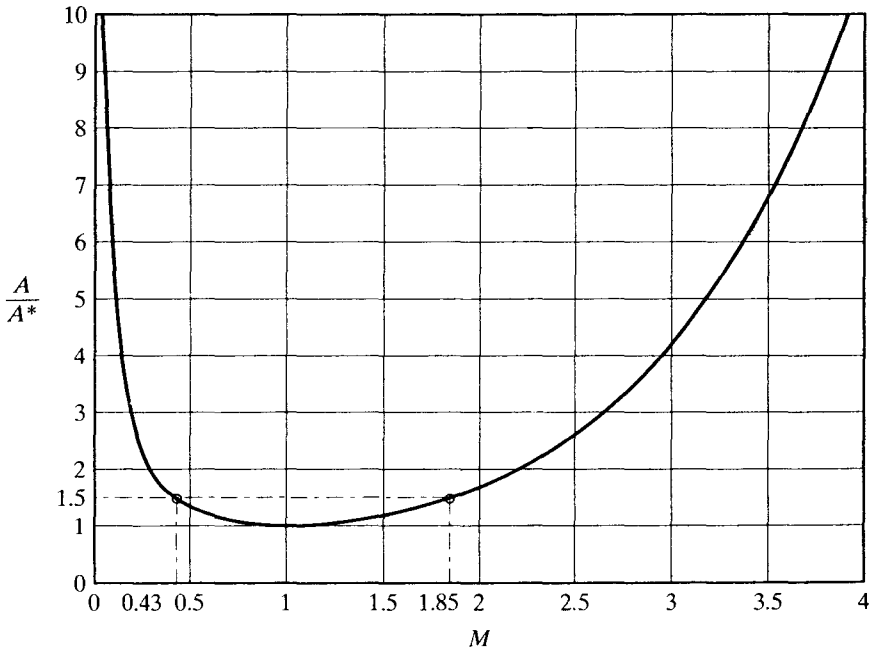


**Figure 3.6** Area Ratio $A/A^*$ versus Mach Number

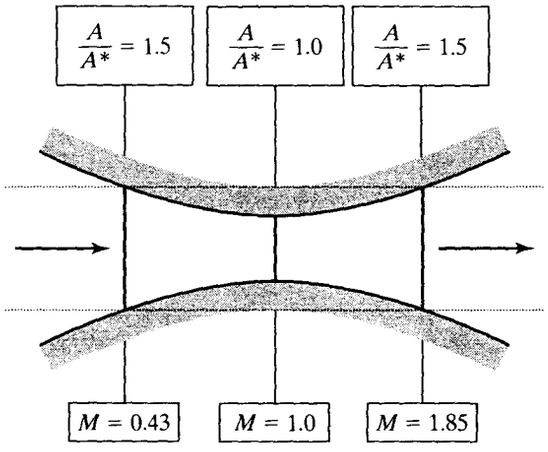


**Figure 3.7** Area Ratio and Mach Number in a Duct

The relation that provides the new value of Mach number from an assumed or previous value is

$$M_{\text{new}} = M_{\text{old}} - \frac{f(M_{\text{old}})}{\frac{df}{dM}(M_{\text{old}})} \tag{3.24}$$

A simple spreadsheet program can be used to determine the Mach number for a given $A/A^*$ and $\gamma$. The results for this numerical illustration for $A/A^* = 1.5$ and $\gamma = 1.4$ are presented in Table 3.1.

**TABLE 3.1** Summary of Iterations to Determine Mach Number for a Given Area Ratio

| Subsonic Solution | | | | | Supersonic Solution | | | | |
|---|---|---|---|---|---|---|---|---|---|
| Iteration | $M$ | $f(M)$ | $f'(M)$ | $M - f/f'$ | Iteration | $M$ | $f(M)$ | $f'(M)$ | $M - f/f'$ |
| 1 | 0.0000 | −0.578704 | 1.50 | 0.3858 | 1 | 3.0000 | −8.2037 | −14.83 | 2.4469 |
| 2 | 0.3858 | −0.053236 | 1.22 | 0.4296 | 2 | 2.4469 | −2.4707 | −6.71 | 2.0785 |
| 3 | 0.4296 | −0.000797 | 1.18 | 0.430262 | 3 | 2.0785 | −0.6304 | −3.52 | 1.8992 |
| 4 | 0.430262 | 0.000000 | 1.18 | 0.430262 | 4 | 1.8991 | −0.1030 | −2.41 | 1.8564 |
| | | | | | 5 | 1.8564 | −0.0049 | −2.18 | 1.8541 |
| | | | | | 6 | 1.8541 | −0.00001 | −2.17 | 1.854124 |
| | | | | | 7 | 1.854124 | 0.000000 | −2.17 | 1.854124 |

A few observations may be made regarding these results. First, it should be noted that an initial guess of $M < 1$ is required to obtain the subsonic solution, whereas an initial guess of $M > 1$ is required to obtain the supersonic solution. Clearly, better initial guesses than those in the table can reduce the number of iterations. It should also be noted that $f(M)$ becomes very small at convergence. Further, the slope of $f(M)$ [i.e., $f'(M)$] is positive for the subsonic case and negative for the supersonic case. Finally, it is seen that the results of $M = 0.4303$ and 1.8541 are in agreement with the results from the isentropic relations.

**Example 3.3. Isentropic relations at small Mach numbers**

When the Mach number is small, isentropic compressible-flow relationships may be written in a more compact form. Determine the limiting relation for the pressure ratio.

**Solution**

The stagnation-to-static-pressure ratio is given in Eq. (3.15) as

$$\frac{p_o}{p} = \left(1 + \frac{\gamma - 1}{2} M^2\right)^{\gamma/(\gamma-1)}$$

We can expand this expression by using the binomial theorem, which states that

$$(a + b)^n = a^n + na^{n-1}b + \frac{n(n-1)}{2} a^{n-2}b^2 + \cdots$$

**Memory Aid:** A useful method of recalling the binomial theorem is to begin by writing the first term on the right-hand side as $a^n b^0$. To obtain the next term, first differentiate $a^n$ to obtain $na^{n-1}$ and then integrate $b^0$ to obtain $b^1/1$. The succeeding terms are written by repeatedly differentiating the preceding $a$ term and integrating the preceding $b$ term.

Now, if $a = 1$ and $b = (\gamma - 1)M^2/2$, the foregoing expression forms a convergent series provided that $b/a < 1$; that is, $M < \sqrt{2/(\gamma - 1)}$, which, for $\gamma = 1.4$, is $\sqrt{5} = 2.236$ and therefore of no concern, since we are considering relatively small Mach numbers here. So expanding the pressure ratio yields

$$p_o = p\left[1 + \frac{\gamma}{2}M^2 + \frac{\gamma}{8}M^4 + \frac{\gamma(2-\gamma)}{48}M^6 + \cdots\right]$$

Thus, we may write

$$p_o = p + \frac{\gamma}{2}pM^2 + O\left(\frac{\gamma}{8}pM^4\right)$$

It should be noted that the second term in the series is actually $\rho V^2/2$, which is called the dynamic pressure. Thus, the first two terms in the series are $p + \rho V^2/2$ and consequently

represent the stagnation pressure of an incompressible flow. The term within the order-of-magnitude symbol $O(\ )$ represents the largest term neglected in the series.

Finally, dividing by the static pressure produces

$$\frac{p_o}{p} = 1 + \frac{\gamma}{2}M^2 + O\left(\frac{\gamma}{8}M^4\right)$$

It is observed that for negligibly small Mach numbers (speeds), the stagnation and the static pressures are virtually identical. Furthermore, for small Mach numbers, flows can be treated as incompressible. It is generally accepted that if $M < 0.2$, the error in neglecting density effects is only a few percent. However, some texts [e.g., Refs. (3.2) and (3.3)] state that flows can be treated as incompressible for Mach numbers below 0.3 to 0.4.

## 3.5 ISENTROPIC FLOW IN A CONVERGING NOZZLE

Consider steady flow through a varying-area nozzle, emanating from a very large reservoir, as shown in Figure 3.8. Because of the reservoir's size, the velocity is negligible. (For steady one-dimensional flow, $\rho AV$ = constant, and if $A$ is large, we expect $V$ to be correspondingly small.) Thus, the static pressure and temperature of the gas in the reservoir can be taken to be identical to the stagnation pressure and temperature.

As the flow is accelerated through the nozzle, the static pressure and temperature decrease. However, as we have seen in the energy analysis of the flow in a variable channel, if the flow is adiabatic, the stagnation temperature at any cross-section of the flow remains constant and therefore must equal the reservoir temperature, which, as we have determined, can be taken to be the stagnation value $T_o$. If the flow is reversible as well as adiabatic (i.e., isentropic), both the stagnation pressure and stagnation temperature are constant within the nozzle flow and must be equal to the reservoir values.

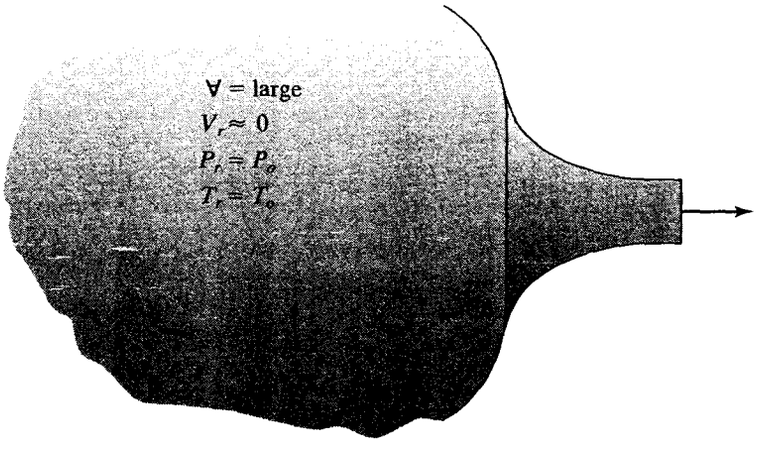


**Figure 3.8** Flow from a Large Tank through a Converging Nozzle

**Calculation Note:** In the next example, we employ a technique that we will use frequently in computational problems. In this method, we construct products of ratios to form the particular ratio that we are seeking. For example, suppose we seek the value of $p_2/p_1$ and we are given $M_1$ and $M_2$, as well as $p_{o2}/p_{o1}$. We can obtain the desired pressure ratio by first computing $p_{o2}/p_2$ and $p_{o1}/p_1$ from Eq. (3.15) by using $M_1$ and $M_2$, respectively. Then

$$\frac{p_2}{p_1} = \left(\frac{p_2}{p_{o2}}\right)\left(\frac{p_{o2}}{p_{o1}}\right)\left(\frac{p_{o1}}{p_1}\right)$$

Notice how the various terms cancel with each other to produce the desired pressure ratio.

**Example 3.4. Isentropic flow in a converging nozzle**

An airstream flows in a converging nozzle (see Figure 3.9) from a cross-sectional area $A_1$ of 50 cm$^2$ to a cross-sectional area $A_2$ of 40 cm$^2$. If $T_1$ = 300 K, $p_1$ = 100 kPa, and $V_1$ = 100 m/s, find $M_2$, $p_2$, and $T_2$. Assume steady, one-dimensional isentropic flow.

**Solution**

Over the temperature range of interest, air behaves as a perfect gas with $\gamma$ = 1.4, and the Mach number at section 1 can be computed from the given information:

$$M_1 = \frac{V_1}{a_1} = \frac{(100 \text{ m/s})}{\sqrt{(1.4)\left(0.287 \frac{\text{kN} \cdot \text{m}}{\text{kg} \cdot \text{K}}\right)(300 \text{ K})}} = 0.288$$

If isentropic flow in the converging nozzle were to be maintained with the duct extended, as shown in Figure 3.9, the flow would be accelerated to $M$ = 1, with the area at this point equal to the reference area $A^*$.

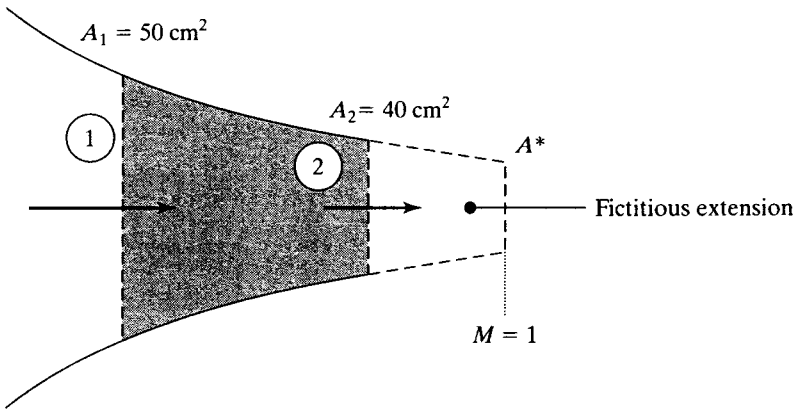


**Figure 3.9** Flow through a Converging Nozzle

At $M_1 = 0.288$, from Appendix B [or from Eq. (3.23)], with $\gamma = 1.4$, we obtain

$$\frac{A_1}{A^*} = 2.111$$

However,

$$\frac{A_2}{A_1} = \frac{40}{50} = 0.80$$

Next, we utilize a procedure that is widely used in gas-dynamic calculations: We determine the unknown ratio from a rearrangement of the products of known quantities, yielding

$$\frac{A_2}{A^*} = \frac{A_2}{A^*}\left(\frac{A_1}{A_1}\right) = \left(\frac{A_2}{A_1}\right)\left(\frac{A_1}{A^*}\right) = (0.80)(2.111) = 1.689$$

From Appendix B [or by using Newton–Raphson's method, Eq. (3.24), within a spreadsheet program], we have $M_2 = 0.372$. For isentropic flow, $p_o$ and $T_o$ are constant. At $M_1 = 0.288$, from Eqs. (3.12) and (3.15), we obtain

$$\frac{p_1}{p_{o1}} = 0.944$$

$$\frac{T_1}{T_{o1}} = 0.984$$

Therefore,

$$p_{o1} = \frac{100}{0.944} = 105.9 \text{ kPa} = p_{o2}$$

$$T_{o1} = \frac{300}{0.984} = 304.9 \text{ K} = T_{o2}$$

Similarly, at $M_2 = 0.372$,

$$\frac{p_2}{p_{o2}} = 0.909$$

$$\frac{T_2}{T_{o2}} = 0.973$$

or

$$p_2 = 0.909(105.9 \text{ kPa}) = 96.3 \text{ kPa}$$

$$T_2 = 0.973(304.9 \text{ K}) = 296.7 \text{ K}$$

Suppose that fluid stored in a very large reservoir is to be discharged through a converging nozzle. For a constant reservoir pressure $p_r$, we desire to determine the rate of mass flow through the nozzle as a function of the back pressure $p_b$ imposed on the nozzle.

Figure 3.10 depicts the pressure distribution obtained in the nozzle for six different values of back pressure. Figure 3.11 shows the mass-flow rate through the nozzle for each of the values of back pressure. For $p_b = p_r$ (Curve 1 in Figure 3.10), there is no flow in the nozzle (Point 1 in Figure 3.11), and pressure does not change with $x$. As $p_b$ is reduced below $p_r$, more and more flow is induced through the nozzle (Curves 2 and 3 in Figure 3.10, and Points 2 and 3 in Figure 3.11), and the static pressure decreases with $x$ for this subsonic flow. The velocity at the nozzle exit plane increases as $p_b$ is reduced, until eventually the velocity of sound is reached at the nozzle exit plane (Curve 4 of Figure 3.10).

The results of Section 3.3, illustrated by Figures 3.3 and 3.4, indicate that the flow in a converging nozzle cannot be accelerated to a velocity greater than the velocity of

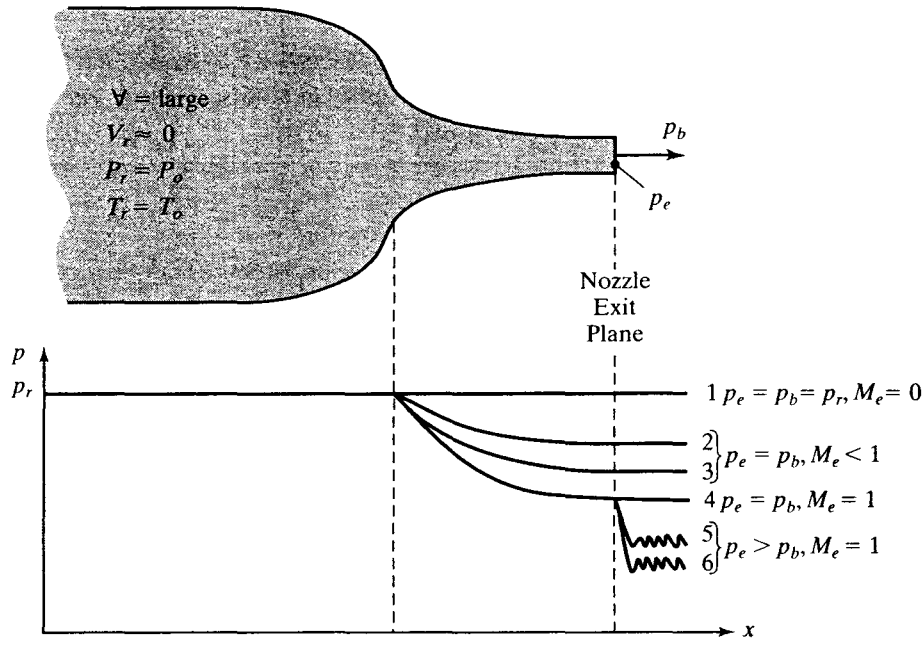


**Figure 3.10** Pressure Distributions in a Converging Nozzle

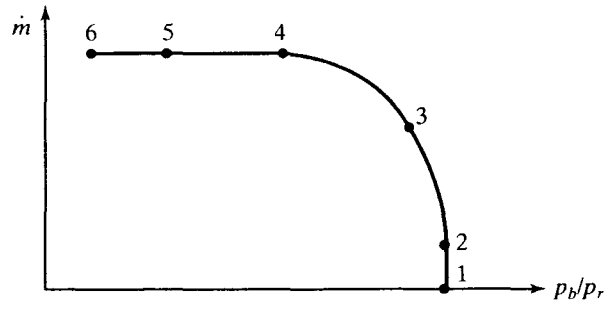


**Figure 3.11** Mass-Flow Rate versus Reservoir-to-Back-Pressure Ratio

sound. To understand the phenomena that occur after sonic velocity is reached at the nozzle exit plane, let us discuss how the flow is able to physically adjust to changes in back pressure. The presence of a disturbance, such as a change in back pressure, is signaled through a compressible fluid by means of a wave traveling at the velocity of sound relative to the moving fluid. For subsonic flow in the nozzle, the signal wave propagates at a greater velocity than the flow. Changes in back pressure can be "communicated" back upstream to the fluid in the reservoir in the same way that the motion of the point projectile in Chapter 2 is "felt" in the fluid ahead of it. For example, when a decrease in back pressure occurs, the change is telegraphed back through the fluid to the reservoir, and more flow is issued from the reservoir. The subsonic flow in the nozzle is able to adjust gradually to the back pressure; thus, for all values of $p_b/p_r$ greater than that corresponding to Curve 4, the back pressure is equal to the exit-plane pressure.

For $p_b/p_r$ equal to that of Curve 4 in Figure 3.10, sonic velocity occurs at the nozzle exit plane. The velocity of the signal wave is equal to the velocity of sound relative to the fluid into which the wave is propagating. If the fluid at a cross-section is moving at the velocity of sound, the absolute velocity of the signal wave at this cross-section is zero. In other words, the signal wave cannot travel past this cross-section. (See Figure 3.12.)

After sonic flow is attained at the nozzle exit plane, signal waves are unable to propagate from the back-pressure region to the reservoir. Therefore, as the back pressure is decreased below that of Curve 4 in Figure 3.10, with the reservoir fluid not able to "sense" the decrease, flow through the nozzle remains the same as that of Point 4 of Figure 3.11. Since the entire flow in the nozzle upstream of the exit plane is unable to "sense" changes in back pressure, the pressure distribution in the nozzle, $p$ versus $x$, likewise remains the same as Curve 4 in Figure 3.10. Under these conditions, flow inside the nozzle cannot adjust to the changes in back pressure. Therefore, for back pressures less than that of Curve 4, the exit-plane pressure is not equal to the back pressure; instead, the flow must adjust to the back pressure by means of an expansion occurring outside the nozzle.

Reductions in back pressure below that of Curve 4 in Figure 3.10 cannot cause any more flow to be induced through the nozzle. Under these conditions, the nozzle is said to be *choked*. The pressure ratio $p_b/p_r$ below which the nozzle is choked can be calculated for isentropic flow through the nozzle. For a perfect gas with constant specific heats,

$$p_o = p\left(1 + \frac{\gamma - 1}{2} M^2\right)^{\gamma/(\gamma-1)} \tag{3.15}$$

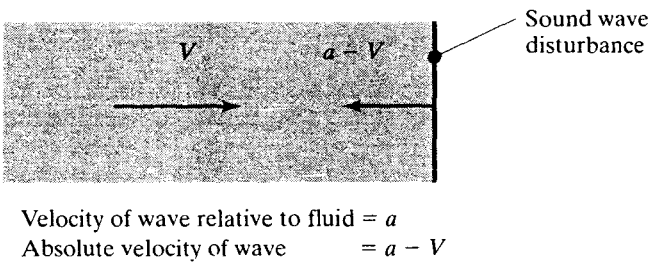


**Figure 3.12** Motion of a Sound Wave Propagating into a Moving Fluid

TABLE 3.2 Critical-Pressure Ratio for Three Values of the Ratio of Specific Heats

| $\gamma$ | $p_b/p_r$ |
|---|---|
| 1.3 | 0.5457 |
| 1.4 | 0.5283 |
| 1.67 | 0.4871 |

For isentropic flow in the nozzle, $p_o$ is constant and equal to $p_r$. Therefore, to just choke the nozzle, set the Mach number at the exit plane equal to unity (i.e., $M_e = 1$), and the static pressure at that location equal to the back pressure (i.e., $p_e = p_b$); hence,

$$\frac{p_r}{p_b} = \left(1 + \frac{\gamma - 1}{2}\right)^{\gamma/(\gamma-1)} = \left(\frac{\gamma + 1}{2}\right)^{\gamma/(\gamma-1)} \tag{3.25}$$

This ratio (actually, its reciprocal) below which the nozzle is choked is termed the *critical-pressure ratio.* For a perfect gas, the critical-pressure ratio is clearly dependent only on the ratio of specific heats. Table 3.2 provides values of the critical-pressure ratio for various $\gamma$.

**Example 3.5. Mass flow in a converging nozzle**

Air is allowed to flow from a large reservoir through a converging nozzle with an exit area of 50 $cm^2$. The reservoir is large enough so that negligible changes in reservoir pressure and temperature occur as fluid is exhausted through the nozzle. Assume isentropic, steady flow in the nozzle, with $p_r = 500$ kPa and $T_r = 400$ K. Assume also that air behaves as a perfect gas with constant specific heats; $\gamma = 1.4$. Determine the mass flow through the nozzle for back pressures of 0, 125, 250, and 375 kPa.

**Solution**

For $\gamma = 1.4$, the critical pressure ratio is 0.5283; therefore, for all back pressures below $(500)(0.5283) = 264.15$ kPa, the nozzle is choked. Under these conditions, the Mach number at the exit plane is unity, the pressure at the exit plane ($p_e$) is 264.15 kPa (does not equal the back pressure if $p_b < 264.15$ kPa), and the temperature at the exit plane ($T_e$) is $[(T/T_o)_e]T_r = (0.8333)(400) = 333.3$ K, where $(T/T_o)_e$ is obtained from Eq. (3.12) at $M_e = 1$ for $\gamma = 1.4$ (or from the tables in Appendix B). The mass-flow rate for all back pressures below the critical pressure is

$$\begin{aligned}
\dot{m} &= \rho_e A_e V_e \\
&= \left(\frac{p_e}{RT_e}\right) A_e \left(M_e \sqrt{\gamma RT_e}\right) \\
&= \left[\frac{(264.15\ \text{kN/m}^2)}{(0.287\ \text{kN} \cdot \text{m/kg})(333.3\ \text{K})}\right](50 \times 10^{-4}\ \text{m}^2) \\
&\quad \left[(1.0)\sqrt{(1.4)(287\ \text{N} \cdot \text{m/kg} \cdot \text{K})(333.3\ \text{K})}\right] \\
&= 5.053\ \text{kg/s}
\end{aligned}$$

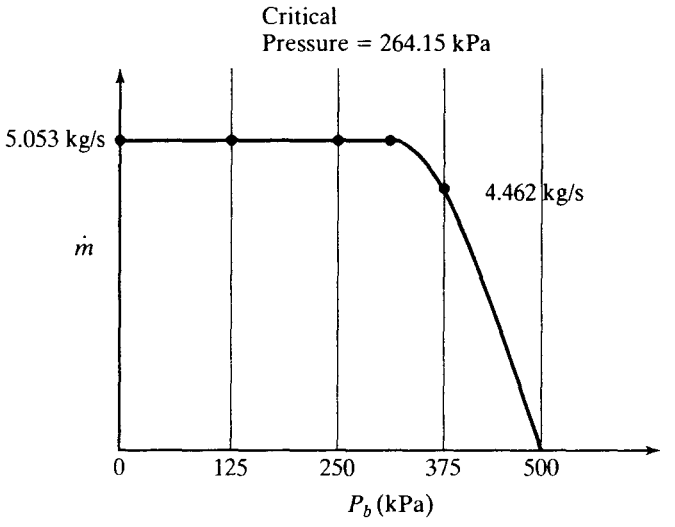


**Figure 3.13** Mass-Flow Rate versus Back Pressure for Example 3.5

This is the flow rate at back pressures of 0, 125, and 250 kPa. (See Figure 3.13.)

For a back pressure of 375 kPa, which is above the critical pressure, the nozzle is not choked, and the exit-plane pressure is equal to the back pressure. For $p_e/p_r = 375/500 = 0.75 = (p/p_o)_e$, we find that $M_e = 0.654$ [from Eq. (3.16) or from the tables in Appendix B] and use it to determine that $T_e/T_r = 0.921$. So,

$$\dot{m} = \left[\frac{375}{(0.287)(0.921)(400)}\right](50 \times 10^{-4})\left[(0.654)\sqrt{(1.4)(287)(0.921)(400)}\right] = 4.462 \text{ kg/s}$$

This flow rate is diagrammed in Figure 3.13.

## 3.6 ISENTROPIC FLOW IN A CONVERGING–DIVERGING NOZZLE

Fluid stored in a large reservoir is to be discharged through a converging–diverging (C–D) nozzle. It is desired to determine the mass flow and pressure distribution in the nozzle over a range of values of $p_b/p_r$. The reservoir pressure $p_r$ is maintained constant, with one-dimensional isentropic flow in the nozzle.

Figure 3.14 depicts the pressure distribution obtained in the nozzle for five different values of back pressure. Figure 3.15 shows the mass-flow rate for each value of $p_b/p_r$. For $p_b$ equal to $p_r$ (Curve 1 in Figure 3.14 and Point 1 in Figure 3.15), there is no flow in the nozzle, and pressure does not vary with $x$. For $p_b$ slightly less than $p_r$ (Curve 2 in Figure 3.14 and Point 2 in Figure 3.15), flow is induced through the nozzle, with subsonic velocities in both converging and diverging sections of the nozzle. Equation (3.10) tells us that, for subsonic flow, pressure decreases in the converging section and increases in the diverging section. As the back pressure is decreased, more flow is further induced through the nozzle (Curve 3 in Figure 3.14 and Point 3 in Figure 3.15)

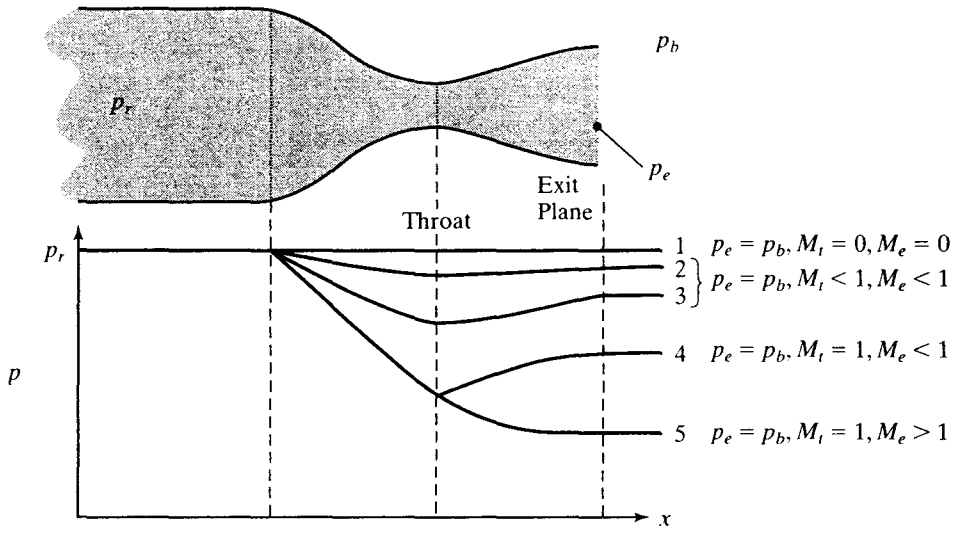


**Figure 3.14** Pressure Distributions for Isentropic Flow in a C–D Nozzle

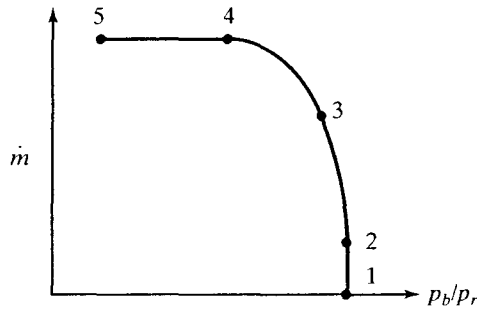


**Figure 3.15** Mass-Flow Rate versus Pressure Ratio for Isentropic Flow in a C–D Nozzle

until eventually sonic flow occurs at the throat (Curve 4 in Figure 3.14 and Point 4 in Figure 3.15). Further decreases in back pressure cannot be "sensed" upstream of the throat; thus, for all back pressures below that of Curve 4 in Figure 3.14, the reservoir continues to send out the same flow rate as Point 4 in Figure 3.15, and the pressure distribution in the nozzle up to the throat remains the same. For all back pressures below that of Curve 4, the converging–diverging nozzle is choked.

Note that for the same reservoir pressure, a converging–diverging nozzle is choked at a greater back pressure than a converging nozzle.

There are two possible isentropic solutions for a given area ratio $A/A^*$ (see Figure 3.6), one subsonic and the other supersonic. For a throat Mach number of 1, isentropic flow can either decelerate to a subsonic exit velocity or continue to accelerate to a supersonic exit velocity. Curve 4 in Figure 3.14 corresponds to the case of subsonic flow at the nozzle exit plane; Curve 5 corresponds to supersonic flow at the exit

plane. Thus, if the back pressure is lowered to that of Curve 5, pressure decreases with $x$ in both the converging and diverging portions of the nozzle, with supersonic flow at the exit plane.

For back pressures between those of Curves 4 and 5 in Figure 3.14, one-dimensional isentropic solutions to the equations of motion are not possible. These flows involve irreversible shockwaves in the diverging section of the nozzle. Nonisentropic solutions for flows through a converging–diverging nozzle will be discussed in some detail after the shock process has been introduced in Chapter 4 and the equations of motion for a shockwave have been derived.

**Example 3.6. Isentropic flow in a C–D nozzle**

A converging–diverging nozzle is designed to operate isentropically with an exit Mach number of 1.5. The nozzle is supplied from an air reservoir in which the pressure is 500 kPa; the temperature is 400 K. The nozzle throat area is 5 $cm^2$. Assume air to behave as a perfect gas, with $\gamma = 1.4$ and $R = 0.2870$ kJ/kg · K.

(a) Determine the ratio of exit area to throat area.

(b) Given the area ratio in part (a), find the range of back pressure over which the nozzle is choked.

(c) Determine the mass-flow rate for a back pressure of 450 kPa.

(d) Determine the mass-flow rate for a back pressure of 0 kPa.

**Solution**

(a) To produce a supersonic Mach number of 1.5 at the nozzle exit, the Mach number at the throat must be 1. Therefore, the throat area is equal to $A^* = 5$ $cm^2$. From the isentropic relation for $M_e = 1.5$, $A_e/A^* = 1.176$, so the ratio of exit area to throat area to produce this exit Mach number is 1.176, or $A_e = (1.176)(5) = 5.88$ $cm^2$.

(b) For all back pressures below that corresponding to Curve 4 of Fig 3.15, the nozzle is choked. For Curve 4, sonic flow is attained at the throat, followed by subsonic deceleration. The subsonic solution for $A/A^* = 1.176$ is found by solving for the Mach number, as indicated in Eq. (3.24): $M = 0.61$. At this Mach number, $p/p_o = 0.778$; therefore, the greatest back pressure at which the nozzle is choked is (0.778)(500 kPa) = 389 kPa. In other words, over the range $0 \leq p_b \leq 389$ kPa, the nozzle is choked.

(c) For a back pressure of 450 kPa, the nozzle is not choked; subsonic flow occurs throughout the nozzle. For this condition, the exit-plane pressure is equal to the back pressure. From isentropic relations, for $p_e/p_o = 0.90$, $M_e = 0.39$ and $T_e/T_o = 0.971$. Exit-plane pressure $p_e$ and temperature $T_e$ are, respectively, 450 kPa and 388.4 K. Using these values, we obtain

$$\dot{m} = \rho_e A_e V_e = \left(\frac{p_e}{RT_e}\right)(A_e)\left(M_e\sqrt{\gamma RT_e}\right)$$

$$= \left[\frac{450 \text{ kN/m}^2}{(0.287 \text{ kN} \cdot \text{m/kg} \cdot \text{K})(388.4 \text{ K})}\right][5.88 \times 10^{-4} \text{ m}^2]$$

$$\left[(0.39)\sqrt{(1.4)(287 \text{ N} \cdot \text{m/kg} \cdot \text{K})(388.4 \text{ K})}\right]$$

$$= \left(4.037 \text{ kg/m}^3\right)(5.88 \times 10^{-4} \text{ m}^2)(0.39)(395.0 \text{ m/s}) = 0.365 \text{ kg/s}$$

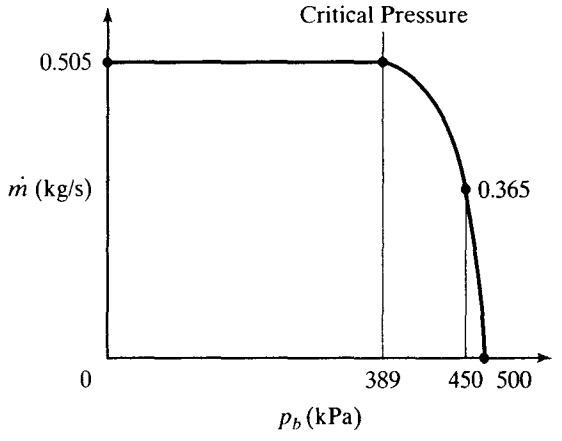


**Figure 3.16** Mass-Flow Rate versus Pressure Ratio for Isentropic Flow in the C–D Nozzle of Example 3.6

(d) For a back pressure of 0 kPa, the nozzle is choked, with the exit-plane pressure not equal to the back pressure. For this condition, the Mach number at the throat is 1, with the throat pressure and temperature equal to 264.2 kPa and 333.3 K, respectively. So,

$$\dot{m} = \rho_t A_t V_t = \left(\frac{p_t}{RT_t}\right) A_t (M_t)\left(\sqrt{\gamma RT_t}\right) = \frac{(p_t)(A_t)(M_t)\left(\sqrt{\gamma RT_t}\right)}{RT_t}$$

$$= \frac{(264.2\ \text{kN/m}^2)(5 \times 10^{-4}\ \text{m}^2)(1.0)\sqrt{(1.4)(287\ \text{N} \cdot \text{m/kg} \cdot \text{K})(333.3\ \text{K})}}{(0.287\ \text{kN} \cdot \text{m/kg} \cdot \text{K})(333.3\ \text{K})} = 0.505\ \text{kg/s}$$

The results of this example are plotted in Figure 3.16.

---

**Example 3.7. Isentropic flow in the nozzle of a supersonic wind tunnel**

A nozzle is to be designed for a supersonic helium wind tunnel as shown in Figure 3.17. Test section specifications are as follows:

Diameter, 10 cm

Mach number, 3.0

Static pressure, 12.1 kPa at 15 km altitude (from the table in Appendix I)

Static temperature, 216.7 K at 15 km altitude

Determine the mass flow that must be provided, the nozzle throat area, and the reservoir temperature and pressure. Assume isentropic flow in the nozzle at the design condition, and neglect boundary-layer effects. (See Figure 3.17.) Assume that helium behaves as a perfect gas, with $\gamma = 5/3$ (constant) and $R = 2.077\ \text{kJ/kg} \cdot \text{K}$.

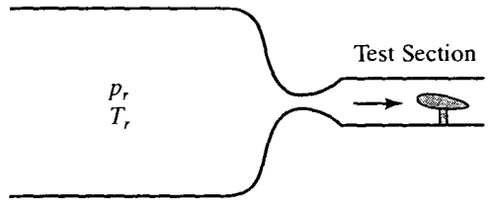


**Figure 3.17** Supersonic Wind Tunnel of Example 3.7

**Solution**

The mass flow of the test section is given by

$$\dot{m} = \rho AV = \left(\frac{p}{RT}\right)\left(\frac{\pi}{4}D^2\right)\left(M\sqrt{\gamma RT}\right)$$

$$= \left[\frac{(12.1 \text{ kN/m}^2)}{(2.077 \text{ kN} \cdot \text{m/kg} \cdot \text{K})(216.7 \text{ K})}\right](0.00785 \text{ m}^2)$$

$$\left[(3.0)\sqrt{\left(\frac{5}{3}\right)(2.077 \text{ kN} \cdot \text{m/kg} \cdot \text{K})(216.7 \text{ K})}\right]$$

$$= (0.269 \text{ kg/m}^3)(0.00785 \text{ m}^2)(2{,}598 \text{ m/s}) = 0.5487 \text{ kg/s}$$

From the isentropic flow relations at $M = 3.0$, we obtain

$$\frac{A}{A^*} = 3.00, \quad \frac{p}{p_o} = 0.03125, \quad \text{and} \quad \frac{T}{T_o} = 0.2500$$

Therefore,

$$A^* = \text{throat area} = \frac{\left(\frac{\pi}{4}D^2\right)}{\left(\frac{A}{A^*}\right)} = \frac{0.00785 \text{ m}^2}{3.0} = 0.002617 \text{ m}^2$$

$$p_r = \frac{12.1 \text{ kPa}}{0.03125} = 387.2 \text{ kPa}$$

$$T_r = \frac{216.7}{0.2500} = 866.8 \text{ K}$$

## 3.7 CHAPTER CAPSTONE APPLICATION: DEPRESSURIZATION OF A STORAGE RESERVOIR OF FINITE SIZE

The expulsion of gas through a valve or nozzle from a pressurized reservoir of a size that does not permit the reservoir pressure to remain constant with time is of considerable technical importance, since this situation is common in industry and military

applications. Often, an analysis of the depressurization process is required to determine the manner in which some system parameter varies with time.

The gas expulsion problem is well treated in the literature. The published papers may be divided into two groups: *unsteady-state analyses*, in which consideration is given to the effects of pressure gradients within the reservoir, and *spatially lumped analyses*, in which the pressure is considered uniform throughout the reservoir at any instant of time. We now perform the latter type of analysis.

The classical method of analysis is to disregard any heat transfer between the reservoir walls and the gas and to consider the gas as ideal. [See Ref. (3.4).]

Reynolds and Kays [see Ref. (3.5)] were the first to include heat transfer in the depressurization problem. In their analysis, which also considered the gas-charging process, a lumped method was used to characterize the gas state. Also, the heat stored in the walls was treated as being concentrated in a simple uniform-temperature heat capacitor. Excellent agreement between predictions and experiment was obtained using free convection as a means of heat transport between the gas and the cylinder walls.

Keith and John [see Ref. (3.6)] analyzed the depressurization of a high-pressure reservoir. They included real-gas and heat-transfer effects. Predictions were compared with perfect-gas predictions and with pressure and temperature measurements. Very good agreement was obtained between the predictions and the measurements.

Figure 3.18 is an illustration of the gas reservoir and the control volume. It is assumed

- that the gas within the cylinder can be treated as *spatially lumped* (i.e., that gas properties within the reservoir vary only with time),
- that the initial pressure and temperature of gas in the reservoir are $p_{o1}$ and $T_{o1}$,
- that the gas can be treated as a perfect gas with constant specific heats, and
- that the flow is isentropic (reversible and no heat transfer).

Since gas flows out of the control volume through only a single opening, we may write the mass conservation for a control volume, Eq. (1.26), as

$$\frac{dm}{dt} = -\dot{m} = -\rho_e A_e V_e \tag{3.26}$$

Equation (3.26) suggests a plan for the analysis: First, develop an expression for the time rate of change of mass within the reservoir in terms of the reservoir pressure.

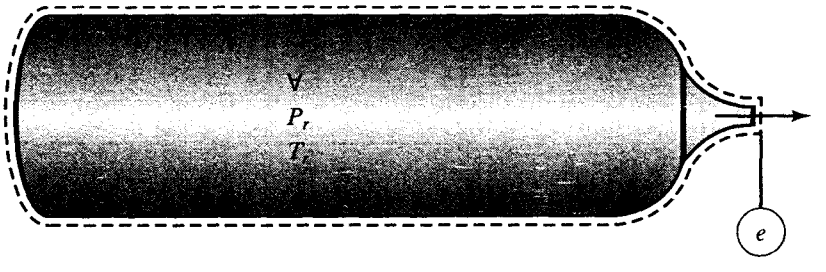


**Figure 3.18** Air Storage Cylinder

Second, develop an expression for the exiting mass-flow rate, also in terms of the reservoir pressure. Finally, equate these two expressions to provide a first-order ordinary differential equation that can be solved to determine the time history of the reservoir pressure.

The mass of the gas in the reservoir, $m_r$, is given by the product of the gas density in the reservoir, $\rho_r = \rho_o$, and the volume of the tank, $\forall$:

$$m_r = \rho_r \forall = \rho_o \forall$$

The reservoir density may be replaced using the isentropic relation

$$\frac{p_o}{\rho_o^\gamma} = \frac{p_{o1}}{\rho_{o1}^\gamma} = \frac{p_e}{\rho_e^\gamma} = \text{constant} \tag{3.27}$$

Equation (3.27) and the time rate of change of mass within the reservoir can be written as

$$\frac{dm}{dt} = \forall \frac{d\rho_o}{dt} = \frac{\rho_{o1}}{\gamma}\left(\frac{p_o}{p_{o1}}\right)^{1/\gamma} \frac{\forall}{p_o}\frac{dp_o}{dt} = \left[\frac{\rho_{o1}\forall}{\gamma p_{o1}^{1/\gamma}}\right] p_o^{(1-\gamma)/\gamma}\frac{dp_o}{dt} \tag{3.28}$$

Because the nozzle flow is steady and adiabatic, $h_o$ = constant; therefore,

$$h_o = h_r = h_{oe} = h_e + \frac{V_e^2}{2}$$

Hence, using perfect-gas relationships, we get

$$V_e^2 = 2(h_o - h_e) = 2c_p(T_o - T_e) = 2\frac{\gamma R}{\gamma - 1}(T_o - T_e) = 2\frac{\gamma}{\gamma - 1}\left(\frac{p_o}{\rho_o} - \frac{p_e}{\rho_e}\right)$$

Thus,

$$V_e = \sqrt{\left(\frac{2\gamma}{\gamma - 1}\right)\left(\frac{p_o}{\rho_o}\right)\left[1 - \left(\frac{p_e}{p_o}\right)^{(\gamma-1)/\gamma}\right]} \tag{3.29}$$

Next, the expression for the exiting mass-flow rate is determined from the product of the exit area, the exit velocity, and the exit density; however, because the exit conditions of the nozzle change as the reservoir pressure changes, this variation must be taken into account. Accordingly, the discharge period is divided into two stages, which have different exit conditions (see Figure 3.10):

Stage I: *Choked Nozzle*: $p_o = \left(\frac{\gamma + 1}{2}\right)^{\gamma/(\gamma-1)} p_e$, where $p_e > p_{\text{atm}}$ and $M_e = 1$

Stage II: *Unchoked Nozzle*: $p_{\text{atm}} \leq p_o \leq \left(\frac{\gamma+1}{2}\right)^{\gamma/(\gamma-1)} p_{\text{atm}}$, where $p_e = p_{\text{atm}}$ and $M_e < 1$

**Stage I**

Because $M_e = 1$ during this stage, the exit pressure is connected to the stagnation, or reservoir, pressure through Eq. (3.15):

$$\frac{p_o}{p_e} = \left(1 + \frac{\gamma-1}{2} M_e^2\right)^{\gamma/(\gamma-1)} = \left(\frac{\gamma+1}{2}\right)^{\gamma/(\gamma-1)} \tag{3.30}$$

Equation (3.30) simplifies the exit velocity, Eq. (3.29), and, with Eq. (3.27), produces

$$V_e = \sqrt{\left(\frac{2\gamma}{\gamma+1}\right)\left(\frac{p_o}{\rho_o}\right)} = \left[\sqrt{\frac{(2\gamma)p_{o1}^{1/\gamma}}{(\gamma+1)\rho_{o1}}}\right] p_o^{(\gamma-1)/2\gamma} \tag{3.31}$$

The exit density of the nozzle may be written using Eqs. (3.27) and (3.30):

$$\rho_e = \rho_o\left(\frac{p_e}{p_o}\right)^{1/\gamma} = \left[\frac{\rho_{o1}}{p_{o1}^{1/\gamma}}\left(\frac{2}{\gamma+1}\right)^{1/(\gamma-1)}\right] p_o^{1/\gamma} \tag{3.32}$$

Using Eqs. (3.31) and (3.32), we find that the mass-flow rate for Stage I can be written as

$$\begin{aligned}\dot{m} = \rho_e A_e V_e &= \left\{\left[\frac{\rho_{o1}}{p_{o1}^{1/\gamma}}\left(\frac{2}{\gamma+1}\right)^{1/(\gamma-1)}\right] p_o^{1/\gamma}\right\} A_e \left\{\left[\sqrt{\frac{(2\gamma)p_{o1}^{1/\gamma}}{(\gamma+1)\rho_{o1}}}\right] p_o^{(\gamma-1)/2\gamma}\right\} \\ &= \left[\frac{\rho_{o1}}{p_{o1}^{1/\gamma}}\left(\frac{2}{\gamma+1}\right)^{1/(\gamma-1)}\right] A_e \left[\sqrt{\frac{(2\gamma)p_{o1}^{1/\gamma}}{(\gamma+1)\rho_{o1}}}\right] p_o^{(\gamma+1)/2\gamma}\end{aligned} \tag{3.33}$$

Finally, the mass-flow rate leaving the reservoir [Eq. (3.33)] is set equal to the negative of the time rate of change of mass within the reservoir [Eq. (3.28)] and the result rearranged:

$$p_o^{(1-3\gamma)/2\gamma} \frac{dp_o}{dt} = C_1 \tag{3.34}$$

Here, $C_1$ is the Stage I constant, defined as

$$C_1 \equiv -\frac{\gamma A_e}{\forall}\left(\frac{2}{\gamma+1}\right)^{1/(\gamma-1)} \sqrt{\frac{(2\gamma)p_{o1}^{1/\gamma}}{(\gamma+1)\rho_{o1}}}$$

Equation (3.34) can be directly integrated to give

$$\left.\frac{p_o^{(1-\gamma)/2\gamma}}{\left(\frac{1-\gamma}{2\gamma}\right)}\right|_{p_{o1}}^{p_o} = C_I(t-0) \tag{3.35}$$

Let $b = (1-\gamma)/2\gamma$, which allows Eq. (3.35) to be written as

$$p_o = (p_{o1}^b + bC_I t)^{1/b} \tag{3.36}$$

Solving for time, we have

$$t = \frac{1}{bC_I}(p_o^b - p_{o1}^b) \tag{3.37}$$

or, in a more complete form,

$$t = \left(\frac{\forall}{A_e a_{o1}}\right)\left(\frac{2}{\gamma-1}\right)\left(\frac{\gamma+1}{2}\right)^{\frac{\gamma+1}{2(\gamma-1)}}\left[\left(\frac{p_{o1}}{p_o}\right)^{\frac{\gamma-1}{2\gamma}} - 1\right] \tag{3.37a}$$

where $a_{o1}$ is the speed of sound computed from initial reservoir conditions. Once the reservoir pressure is computed, the reservoir gas density or temperature can be computed from the isentropic relations:

$$\frac{\rho_o}{\rho_{o1}} = \left(\frac{p_o}{p_{o1}}\right)^{1/\gamma} = \frac{p_o/(RT_o)}{p_{o1}/(RT_{o1})} = \left(\frac{p_o}{p_{o1}}\right)\left(\frac{T_{o1}}{T_o}\right) \tag{3.38}$$

**Stage II**

At the beginning of this stage, the exit Mach number is 1 and $p_e = p_{\text{atm}}$ (see Curve 4 of Figure 3.10), and hence

$$\left(\frac{p_e}{p_o}\right)^{(\gamma-1)/\gamma} = \frac{2}{\gamma+1} = \left(\frac{p_{\text{atm}}}{p_o}\right)^{(\gamma-1)/\gamma} \tag{3.39}$$

Equation (3.39) is the lower limit for the integration that follows. The exit velocity equation [Eq. (3.29)] is rewritten as

$$V_e = \sqrt{\left(\frac{2\gamma}{\gamma-1}\right)\left(\frac{p_o}{\rho_o}\right)\left[1 - \left(\frac{p_{\text{atm}}}{p_o}\right)^{(\gamma-1)/\gamma}\right]}$$

$$= \sqrt{\left(\frac{2\gamma}{\gamma-1}\right)\left[\frac{p_o}{\rho_{o1}(p_o/p_{o1})^{1/\gamma}}\right]\left[1 - \left(\frac{p_{\text{atm}}}{p_o}\right)^{(\gamma-1)/\gamma}\right]} \tag{3.40}$$

The exit density is

$$\rho_e = \rho_o\left(\frac{p_{\text{atm}}}{p_o}\right)^{1/\gamma} = \rho_{o1}\left(\frac{p_o}{p_{o1}}\right)^{1/\gamma}\left(\frac{p_{\text{atm}}}{p_o}\right)^{1/\gamma} = \rho_{o1}\left(\frac{p_{\text{atm}}}{p_{o1}}\right)^{1/\gamma} \tag{3.41}$$

The mass-flow rate can therefore be expressed as

$$\dot{m} = \rho_e A_e V_e = \left[\rho_{o1}\left(\frac{p_{\text{atm}}}{p_{o1}}\right)^{1/\gamma}\right] A_e \left\{\sqrt{\left(\frac{2\gamma}{\gamma-1}\right)\left[\frac{p_o}{\rho_{o1}(p_o/p_{o1})^{1/\gamma}}\right]\left[1-\left(\frac{p_{\text{atm}}}{p_o}\right)^{(\gamma-1)/\gamma}\right]}\right\}$$

Equating this expression to the time rate of change of mass depletion within the reservoir, given by Eq. (3.28), yields

$$\begin{aligned}\frac{dm}{dt} &= \frac{\rho_{o1}}{\gamma}\left(\frac{p_o}{p_{o1}}\right)^{1/\gamma}\frac{\forall}{p_o}\frac{dp_o}{dt} = -\dot{m}_e \\ &= -\left[\rho_{o1}\left(\frac{p_{\text{atm}}}{p_{o1}}\right)^{1/\gamma}\right] A_e \left\{\sqrt{\left(\frac{2\gamma}{\gamma-1}\right)\left[\frac{p_o}{\rho_{o1}(p_o/p_{o1})^{1/\gamma}}\right]\left[1-\left(\frac{p_{\text{atm}}}{p_o}\right)^{(\gamma-1)/\gamma}\right]}\right\}\end{aligned} \tag{3.42}$$

Obviously, Eq. (3.42) is complicated, with a large number of terms. We can simplify it somewhat by introducing

$$\overline{p} \equiv \left(\frac{p_o}{p_{\text{atm}}}\right)$$

and defining a Stage II constant as

$$C_{\text{II}} \equiv -\frac{\gamma A_e}{\forall}\left(\frac{2}{\gamma-1}\right)^{1/2} a_{o1}\left(\frac{p_{\text{atm}}}{p_{o1}}\right)^{(\gamma-1)/2\gamma}$$

where $a_{o1}$ is the speed of sound based on the initial reservoir conditions. Thus, Eq. (3.42) can be rewritten as

$$\frac{1}{\overline{p}^{(\gamma-1)/\gamma}}\frac{d\overline{p}}{\sqrt{\overline{p}^{(\gamma-1)/\gamma}-1}} = C_{\text{II}}dt \tag{3.43}$$

Equation (3.43) can be integrated more readily by transforming variables as follows:

$$r \equiv \sqrt{\overline{p}^{(\gamma-1)/\gamma}-1}$$

Therefore,

$$\overline{p} = \frac{p_o}{p_{\text{atm}}} = (r^2+1)^{\gamma/(\gamma-1)}$$

$$d\overline{p} = \frac{\gamma}{\gamma - 1}(r^2 + 1)^{1/(\gamma-1)}2rdr$$

Equation (3.43) may be written as

$$\left(\frac{2\gamma}{\gamma - 1}\right)\int_{r^*}^{r}(r^2 + 1)^{(2-\gamma)/(\gamma-1)}dr = C_{\text{II}}\int_{t^*}^{t}dt = C_{\text{II}}(t - t^*) \tag{3.44}$$

where $r^* = \sqrt{(\gamma + 1)/2 - 1} = \sqrt{(\gamma - 1)/2}$ and $t^*$ is the time at which the nozzle unchokes [i.e., the last time value computed by Eq. (3.37a)]. In general, the integral on the left-hand side of Eq. (3.44) requires numerical integration. However, for $\gamma = 1.4$, the integration can be performed in closed form:

$$\begin{aligned} t - t^* &= \frac{2\gamma/(\gamma - 1)}{C_{\text{II}}}\int_{\sqrt{5}/5}^{r}(r^2 + 1)^{3/2}dr \\ &= \frac{2\gamma/(\gamma - 1)}{C_{\text{II}}}\left[\frac{r}{8}(2r^2 + 5)\sqrt{r^2 + 1} + \frac{3}{8}\ln\left(r + \sqrt{r^2 + 1}\right) - 0.49325\right] \end{aligned} \tag{3.45}$$

where

$$r \equiv \sqrt{(p_o/p_{\text{atm}})^{(\gamma-1)/\gamma} - 1} \text{ and } r^* = \sqrt{5}/5 = 0.4472 \text{ for } \gamma = 7/5.$$

**Example 3.8. Spatially lumped isothermal flow from a reservoir of finite size**

Nitrogen is stored in a tank 2 $m^3$ in volume at a pressure of 3 MPa and a temperature of 300 K. (See Figure 3.18.) The gas is discharged through a converging nozzle with an exit area of 12 $cm^2$. For a back pressure of 101 kPa, find the time required for the tank pressure to drop to 300 kPa. Assume isentropic nozzle flow and that the nitrogen is a perfect gas with $\gamma = 1.4$ (constant) and $R = 0.2968$ kJ/kg · K. Also assume that the reservoir gas is spatially lumped so that the reservoir gas has a single pressure at each instant of time [i.e., $p_r = p_r(t)$]. Finally, assume that the discharge process is slow enough so that $T_r$ is constant.

**Solution**

As the reservoir pressure drops from 3 MPa to 300 kPa, the ratio $p_b/p$ remains below the critical-pressure ratio, and the nozzle exit Mach number is 1. The exit pressure is given by the critical-pressure ratio times the reservoir pressure; therefore, for $\gamma = 1.4$, from Table 3.2 we have $p_e = 0.5283p_r$, and the static temperature in the exit plane of the nozzle is $T_e = 0.8333T_r = (0.8333)(300) = 250$ K. The exiting mass-flow rate is therefore

$$\begin{aligned} \dot{m} &= \rho_e A_e V_e \\ &= \left(\frac{p_e}{RT_e}\right)A_e a_e = \left(\frac{p_e}{RT_e}\right)A_e\sqrt{\gamma RT_e} \\ &= \frac{(0.5283p_r)(12 \times 10^{-4})\sqrt{(1.4)(296.8)(250)}}{(0.2968)(250)} = 0.002754p_r \end{aligned}$$

From Eq. (1.8), we have

$$\frac{\partial}{\partial t}\iiint_{\text{C.V.}} \rho d\forall + \iint_{\text{C.S.}} \rho \mathbf{V} \cdot d\mathbf{A} = 0 \tag{3.46}$$

where

$$\iiint_{\text{C.V.}} \rho d\forall = m = \frac{p_r \forall_r}{RT_r}$$

Here, $m$ is the mass inside the tank at any time. By substituting into Eq. (3.46), we obtain

$$\frac{\forall_r}{RT_r}\frac{dp_r}{dt} + 0.002754 p_r = 0$$

$$\frac{2}{(0.2968)(300)}\frac{dp_r}{dt} + 0.002754 p_r = 0$$

or

$$\frac{dp_r}{p_r} = -0.1226 dt$$

So,

$$t = -\int_{3000}^{300} 8.1554 \frac{dp_r}{p_r} = -8.1554 \ln\left(\frac{300}{3{,}000}\right) = 8.1554 \ln(10) = 18.78 \text{ s}$$

---

**Example 3.9. Spatially lumped isentropic flow from a reservoir of finite size**

Air ($\gamma = 1.4$ and $R = 287$ J/kg · K) is stored in a tank 0.037661 m$^3$ in volume at an initial pressure of 5,760.6 kPa and a temperature of 321.4 K. The gas is discharged through a converging nozzle with an exit area of $3.167 \times 10^{-5}$ m$^2$. For a back pressure of 101 kPa, assuming that the gas within the reservoir follows an isentropic process and that spatial lumping applies (i.e., $p_r = p_r(t)$ and $T_r = T_r(t)$), compare predicted tank pressures to the measured values contained in Table 3.3.

**Solution**

The critical-pressure ratio $p_b/p_r$ for air ($\gamma = 1.4$ from Table 3.2) is 0.5283. For this problem, as long as the reservoir pressure is above 101/0.5283 = 191 kPa, the nozzle is choked. Nondimensionalizing this value by the initial reservoir pressure gives a pressure ratio of 0.033. Thus, except for the value at $t = 19$ s in Table 3.3, we see that the nozzle remains

**TABLE 3.3** Experimental Pressure–Time Data for the Expulsion of Air from a Tank

| **Time (s)** | 0.0 | 1.0 | 2.0 | 3.0 | 4.0 | 5.0 | 6.0 | 7.0 | 9.0 | 11.0 | 13.0 | 15.0 | 17.0 | 19.0 |
|---|---|---|---|---|---|---|---|---|---|---|---|---|---|---|
| $p_o/p_{o1}$ | 1.000 | 0.717 | 0.551 | 0.448 | 0.358 | 0.281 | 0.241 | 0.199 | 0.142 | 0.104 | 0.078 | 0.059 | 0.044 | 0.033 |

**TABLE 3.4** Comparison of Predicted and Experimental Pressures for Example 3.9

| $t$ (sec) | $p_o/p_{o1}$ | $p_o/p_{o1}$ (exp) | % Error | $p_o$ | $p_o$ (exp) |
|---|---|---|---|---|---|
| 0.0 | 1.000 | 1.000 | 0.0 | 5,760.6 | 5,760.6 |
| 1.0 | 0.786 | 0.717 | 9.6 | 4,528.3 | 4,130.3 |
| 2.0 | 0.623 | 0.551 | 13.0 | 3,588.2 | 3,174.1 |
| 3.0 | 0.497 | 0.448 | 11.0 | 2,864.6 | 2,580.7 |
| 4.0 | 0.400 | 0.358 | 11.7 | 2,303.1 | 2,062.3 |
| 5.0 | 0.324 | 0.281 | 15.1 | 1,863.9 | 1,618.7 |
| 6.0 | 0.263 | 0.241 | 9.3 | 1,517.8 | 1,388.3 |
| 7.0 | 0.216 | 0.199 | 8.5 | 1,243.3 | 1,146.4 |
| 9.0 | 0.147 | 0.142 | 3.7 | 847.9 | 818.0 |
| 11.0 | 0.102 | 0.104 | −1.5 | 589.8 | 599.1 |
| 13.0 | 0.073 | 0.078 | −7.0 | 417.7 | 449.3 |
| 15.0 | 0.052 | 0.059 | −11.5 | 300.7 | 339.9 |
| 17.0 | 0.038 | 0.044 | −13.4 | 219.6 | 253.5 |
| 19.0 | 0.028 | 0.033 | −14.5 | 162.6 | 190.1 |

choked for all of the experimental values. Consequently, Eq. (3.37a) can be used to determine the pressure–time history of the expulsion. For the calculations, $a_{o1} = 20.05\sqrt{321.39} = 359.4$ m/s, $b = 1/7$, and $C_1 = -0.57870\ \text{s}^{-1}$. Inserting these constants into Eq. (3.37a), we can construct Table 3.4. (A spreadsheet program was written to accomplish the calculations.)

It can be seen that the computed values differ from the experimental values by approximately 10%. Some of the differences are a result of real-gas effects; others are due to the assumption of quasisteady flow. It is unlikely that heat transfer would have much of an impact, but nevertheless, some error results from neglect of heat-transfer effects, particularly towards the end of the expulsion process.

## 3.8 SUMMARY

In this chapter, the equations of continuity, momentum, and energy are presented for one-dimensional isentropic flow through a varying-area channel. The effect of Mach number on the flow is demonstrated; the variations of pressure, velocity, and temperature with area for supersonic flow are entirely different than for subsonic flow. For supersonic flow, the increase of velocity and decrease of pressure as area is increased seems to violate our intuition; however, our intuition is based mainly on liquid-water flow, in which density does not vary. For flow in a diverging channel at Mach numbers

greater than unity, density decreases are great enough to outweigh the increase in area so that, with $\rho AV$ = constant, the result is an increase in flow velocity.

The phenomenon of choking also seems contrary to our intuition. As the back pressure on a nozzle is lowered for a constant reservoir pressure, more flow is induced through the nozzle until a maximum flow rate is reached. Further decreases in back pressure then have no effect on the mass-flow rate; the nozzle is choked. Choking occurs when changes in back pressure can no longer be "sensed" in the reservoir. For subsonic flow, the reservoir is able to "sense" back pressure changes by means of sonic signal waves sent back through the fluid. Once the velocity of sound is reached at a point in the flow, the signal wave is not able to travel back to the reservoir; hence, the reservoir is unable to "sense" further decreases in back pressure.

It should be clear that certain intuitive notions gained from a knowledge of water flow cannot always be applied to a study of compressible-fluid mechanics. One should now begin to appreciate the significance of Mach number and the velocity of sound for compressible flow.

## 3.9 REFERENCES


**3.1** Saad, M. J. *Compressible Fluid Flow*, 2d ed., Prentice Hall, Upper Saddle River, NJ, 1993, p. 100.

**3.2** Zucrow, M. J., and Hoffman, J. D. *Gas Dynamics*, Vol. 1, John Wiley & Sons, New York, 1976, p. 132.

**3.3** Oosthuizen, P. H., and Carscallen, W. E. *Compressible Fluid Flow,* McGraw-Hill, New York, 1997, pp. 66–67.

**3.4** Owczarek, J. A. *Fundamentals of Gas Dynamics*, International Textbook Co., Scranton, PA, 1964, p. 254.

**3.5** Reynolds, W. C., and Kays, W. M. "Blowdown and Charging Processes in a Single Gas Receiver with Heat Transfer," *Transactions of the ASME* 1959; 80: 1160–1168.

**3.6** Keith, T. G., Jr., and John, J. E. A. "Calculation of Real-Gas Effects in the Depressurization of Air Storage Cylinders," *AIAA J Spacecr Rockets* 1970; 7(7): 890–894.


## 3.10 PROBLEMS

**3.1** Air flows at Mach 0.25 through a circular duct with a diameter of 60 cm. The stagnation pressure of the flow is 500 kPa; the stagnation temperature is 175°C. Calculate the mass-flow rate through the channel, assuming that $\gamma = 1.4$ and that the air behaves as a perfect gas with constant specific heats.

**3.2** Helium flows at Mach 0.50 in a channel with cross-sectional area of 0.16 $m^2$. The stagnation pressure of the flow is 1 MPa, and stagnation temperature is 1,000 K. Calculate the mass-flow rate through the channel, with $\gamma = 5/3$.

**3.3** In Problem 3.2, the cross-sectional area is reduced to 0.12 $m^2$. Calculate the Mach number and flow velocity at the reduced area. What percent of further reduction in area would be required to reach Mach 1 in the channel?

**3.4** (a) For small Mach numbers, determine an expression for the density ratio $\rho/\rho_o(b)$. Using Eqs. (3.15) and (3.17), prove that

$$\left(\frac{p_o}{p}\right)\left(\frac{\rho}{\rho_o}\right) = \left(\frac{T_o}{T}\right) = \left(\frac{a_o}{a}\right)^2$$

**3.5** An airflow at Mach 0.6 passes through a channel with a cross-sectional area of 50 $cm^2$. The static pressure in the airstream is 50 kPa; the static temperature is 298 K.

(a) Calculate the mass-flow rate through the channel.
(b) What percent of reduction in area would be necessary to increase the flow Mach number to 0.8? to 1.0?
(c) What would happen if the area were reduced more than necessary to reach Mach 1?

**3.6** A converging nozzle with an exit area of 1.0 $cm^2$ is supplied from an oxygen reservoir in which the pressure is 500 kPa and the temperature is 1,200 K. Calculate the mass-flow rate of oxygen for back pressures of 0, 100, 200, 300, and 400 kPa. Assume that $\gamma = 1.3$.

**3.7** Compressed air is discharged through the converging nozzle, as shown in Figure P3.7. The tank pressure is 500 kPa, and local atmospheric pressure is 101 kPa. The inlet area of the nozzle is 100 $cm^2$; the exit area is 34 $cm^2$. Find the force of the air on the nozzle, assuming the air to behave as a perfect gas with constant $\gamma = 1.4$. Take the temperature in the tank to be 300 K.

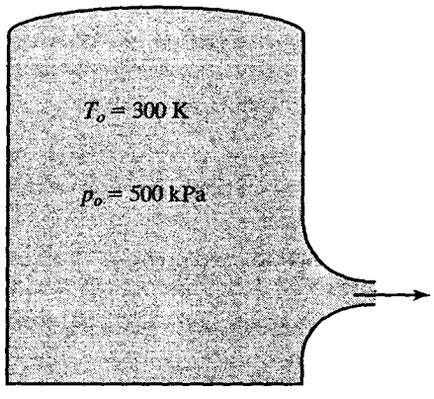


**Figure P3.7**

**3.8** A converging nozzle has an exit area of 56 $cm^2$. Nitrogen stored in a reservoir is to be discharged through the nozzle to an ambient pressure of 100 kPa. Determine the flow rate through the nozzle for reservoir pressures of 120 kPa, 140 kPa, 200 kPa, and 1 MPa. Assume isentropic nozzle flow. In each case, determine the increase in mass flow to be gained by reducing the back pressure from 100 to 0 kPa. The reservoir temperature is 298 K.

**3.9** Pressurized liquid water flows from a large reservoir through a converging nozzle. Assuming isentropic nozzle flow with a negligible inlet velocity and a back pressure of 101 kPa, calculate the reservoir pressure necessary to choke the nozzle. Assume that the isothermal compressibility of water is constant at $5 \times 10^{-7}$ $(kPa)^{-1}$ and equal to the isentropic compressibility. The exit density of the water is 1,000 $kg/m^3$.

**3.10** Calculate the stagnation temperature in an airstream traveling at Mach 5 with a static temperature of 273 K. (See Figure P3.10.) An insulated flat plate is inserted into this flow,

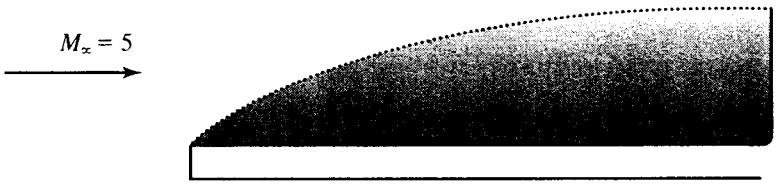


**Figure P3.10**

aligned parallel with the flow direction, with a boundary layer building up along the plate. Since the absolute velocity at the plate surface is zero, would you expect the plate temperature to reach the free stream stagnation temperature? Explain.

**3.11** A gas stored in a large reservoir is discharged through a converging nozzle. For a constant back pressure, sketch a plot of mass-flow rate versus reservoir pressure. Repeat for a converging–diverging nozzle.

**3.12** A converging–diverging nozzle with an exit area is 0.12 $m^2$ is designed to operate isentropically with air at an exit Mach number of 1.75. For a constant chamber pressure and temperature of 5 MPa and 200°C, respectively, calculate the following:

(a) the maximum back pressure to choke the nozzle,
(b) the flow rate in kilograms per second for a back pressure of 101 kPa, and
(c) the flow rate for a back pressure of 1 MPa.

**3.13** A supersonic flow is allowed to expand indefinitely in a diverging channel. Does the flow velocity approach a finite limit, or does it continue to increase indefinitely? Assume a perfect gas with constant specific heats.

**3.14** A converging–diverging frictionless nozzle is used to accelerate an airstream emanating from a large chamber. The nozzle has an exit area of 30 $cm^2$ and a throat area of 15 $cm^2$. If the ambient pressure surrounding the nozzle is 101 kPa and the chamber temperature is 500 K, calculate the following:

(a) the minimum chamber pressure to choke the nozzle,
(b) the mass-flow rate for a chamber pressure of 400 kPa, and
(c) the mass-flow rate for a chamber pressure of 200 kPa.

**3.15** Sketch $p$ versus $x$ for the case shown in Figure P3.15.

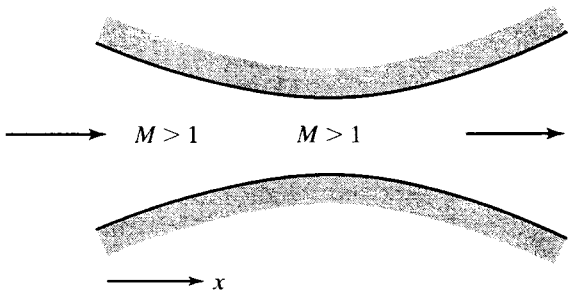


**Figure P3.15**

**3.16** Steam is to be expanded to Mach 2.0 in a converging–diverging nozzle from an inlet velocity of 100 m/s. The inlet area is 50 $cm^2$, and the inlet static temperature is 500 K. Assuming isentropic flow, determine the throat and exit areas required. Assume the steam to behave as a perfect gas with constant $\gamma = 1.3$.

**3.17** Write a computer program that will yield values of $T/T_o$, $p/p_o$, and $A/A^*$ for isentropic flow of a perfect gas with constant $\gamma = 1.27$. Use Mach-number increments of 0.05 over the range $M = 0$ to $M = 2.0$.

**3.18** A gas is known to have a molecular mass MM of 18, with $c_p = 2.0$ kJ/kg · K. The gas is expanded from negligible initial velocity through a converging–diverging nozzle with an area ratio of 5.0. Assuming an isentropic expansion in the nozzle with initial stagnation pressure and temperature of 1 MPa and 1,000 K, respectively, determine the exit nozzle velocity.

**3.19** A jet plane is flying at 10 km with a cabin pressure of 101 kPa and a cabin temperature of 20°C. Suddenly, a bullet is fired inside the cabin and pierces the fuselage; the resultant hole is 2 cm in diameter. Assume that the temperature within the cabin remains constant and that the flow through the hole behaves as that through a converging nozzle with an exit diameter of 2.0 cm. Take the cabin volume to be 100 $m^3$. Calculate the time for the cabin pressure to decrease to one half the initial value. At 10 km, $p = 26.5$ kPa and $T = 223.3$ K. (Refer to the altitude table in Appendix I.)

**3.20** A rocket nozzle is designed to operate isentropically at 20 km with a chamber pressure of 2.0 MPa and chamber temperature of 3,000 K. If the products of combustion are assumed to behave as a perfect gas with constant specific heats and with exhaust properties of $\gamma = 1.3$ and MM = 20, determine the design thrust for a nozzle throat area of 0.25 $m^2$.

**3.21** A converging nozzle has a rectangular cross-section of a constant width of 10 cm. For ease of manufacture, the side walls of the nozzle are straight, making an angle of 10° with the horizontal, as shown in Figure P3.21. Determine and plot the variation of $M$, $T$, and $p$ with $x$, taking $M_1 = 0.4$, $p_{o1} = 200$ kPa, and $T_{o1} = 350$ K. Assume the working fluid to be air, which behaves as a perfect gas with constant specific heats and $\gamma = 1.4$, and that the flow is isentropic.

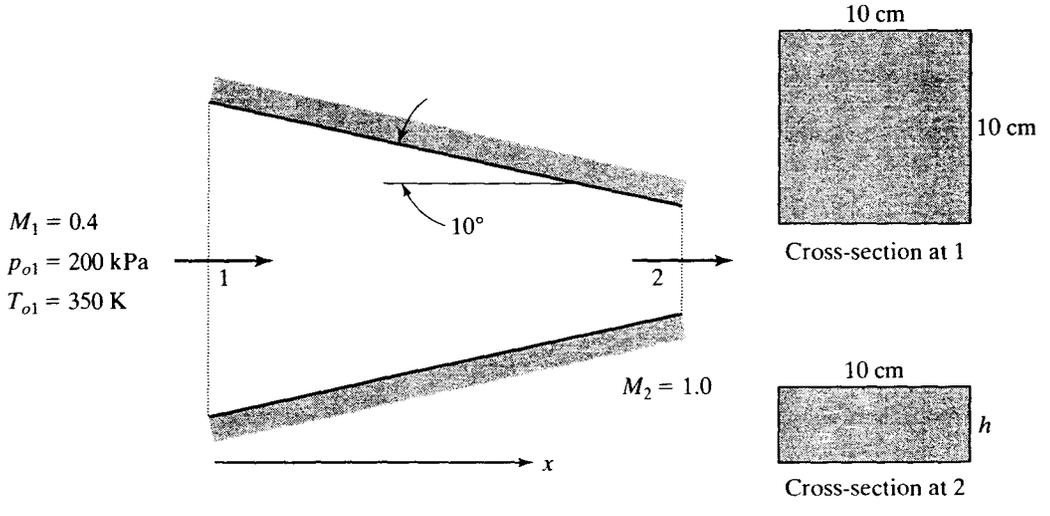


**Figure P3.21**

**3.22** A spherical tank contains compressed air at 500 kPa; the volume of the tank is 20 $m^3$. A 5-cm burst diaphragm in the side of the tank ruptures, causing air to escape from the tank. Find the time required for the tank pressure to drop to 200 kPa. Assume that the temperature of the air in the tank is 280 K, the ambient pressure is 101 kPa, and the airflow through the opening can be treated as isentropic through a converging nozzle with a 5-cm exit diameter.

**3.23** A converging–diverging nozzle has an area ratio of 3.3 to 1 (exit area to throat area). The nozzle is supplied from a tank containing helium at 100 kPa and 270 K. (See Figure P3.23.) Find the maximum mass flow possible through the nozzle and the range of back pressures over which the mass flow can be attained. Repeat with hydrogen as the working fluid. (Use data from Table H.1 in Appendix H.)

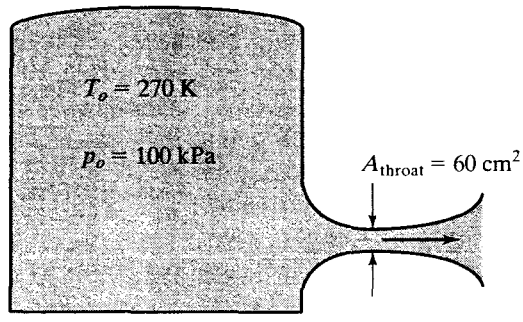


**Figure P3.23**

**3.24** Superheated steam is stored in a large tank at 6 MPa and 800°C. The steam is exhausted isentropically through a converging–diverging nozzle. Determine the velocity of the steam flow when the steam starts to condense, assuming the steam to behave as a perfect gas with $\gamma = 1.3$.

**3.25** Air is stored in a tank 0.037661 $m^3$ in volume at an initial pressure of 5,760.6 kPa and a temperature of 321.4 K. The gas is discharged through a converging nozzle with an exit area of $3.167 \times 10^{-5}$ $m^2$. For a back pressure of 101 kPa, assuming quasisteady polytropic flow in the tank (i.e., $pv^n$ = constant) and isentropic flow in the nozzle (i.e., $pv^\gamma$ = constant) compare predicted tank pressures with the measured values contained in Table P3.25. Try various values of the polytropic exponent $n$ from 1.0 (isothermal) to 1.4 (isentropic) to obtain the best results.

**TABLE P3.25**

| **Time (s)** | 0.0 | 1.0 | 2.0 | 3.0 | 4.0 | 5.0 | 6.0 | 7.0 | 9.0 | 11.0 | 13.0 | 15.0 | 17.0 | 19.0 |
|---|---|---|---|---|---|---|---|---|---|---|---|---|---|---|
| $p_o/p_{o1}$ | 1.000 | 0.717 | 0.551 | 0.448 | 0.358 | 0.281 | 0.241 | 0.199 | 0.142 | 0.104 | 0.078 | 0.059 | 0.044 | 0.033 |

# Chapter 4

# Stationary Normal Shockwaves

## 4.1 INTRODUCTION

The *shock process* represents an abrupt change in fluid properties in which finite variations in pressure, temperature, and density occur over a shock thickness comparable to the mean free path of the gas molecules involved. It has been established that supersonic flow adjusts to the presence of a body by means of such shockwaves, whereas subsonic flow can adjust by gradual changes in flow properties. Shocks may also occur in the flow of a compressible medium through nozzles or ducts and thus may have a decisive effect on these flows. An understanding of the shock process and its ramifications is essential in the study of compressible flow.

Chapter 4 is devoted to a consideration of the stationary *normal shockwave*, a plane shock normal to the flow direction. This case represents the simplest example of a shock in that changes in flow properties occur only in the direction of flow; thus, it can be treated with the equations of one-dimensional gas dynamics. Chapter 6 will cover the oblique shockwave, positioned at an angle to the flow direction.

It was pointed out in Section 2.4 that a series of weak compression waves can coalesce to form a finite-compression shockwave. In this chapter, the mechanism by which this process occurs will be discussed in detail. The thermodynamics of the shock process will be reviewed, and the one-dimensional equations of continuity, momentum, and energy applied to the normal shock. Solutions of these equations will be presented to enable the working of practical engineering problems.

## 4.2 FORMATION OF A NORMAL SHOCKWAVE

It was shown in Section 2.3 that, when a piston in a tube is given a small constant velocity increment to the right of magnitude $dV$ (see Figure 2.4), a sound wave travels

ahead of the piston through the medium in the tube. Suppose the piston is now given a second increment of velocity $dV$, causing a second wave to move into the compressed gas behind the first wave. The location of the waves and the pressure distribution in the tube after three times $t_1 > t_2 > t_3$ are shown in Figure 4.1. Each wave

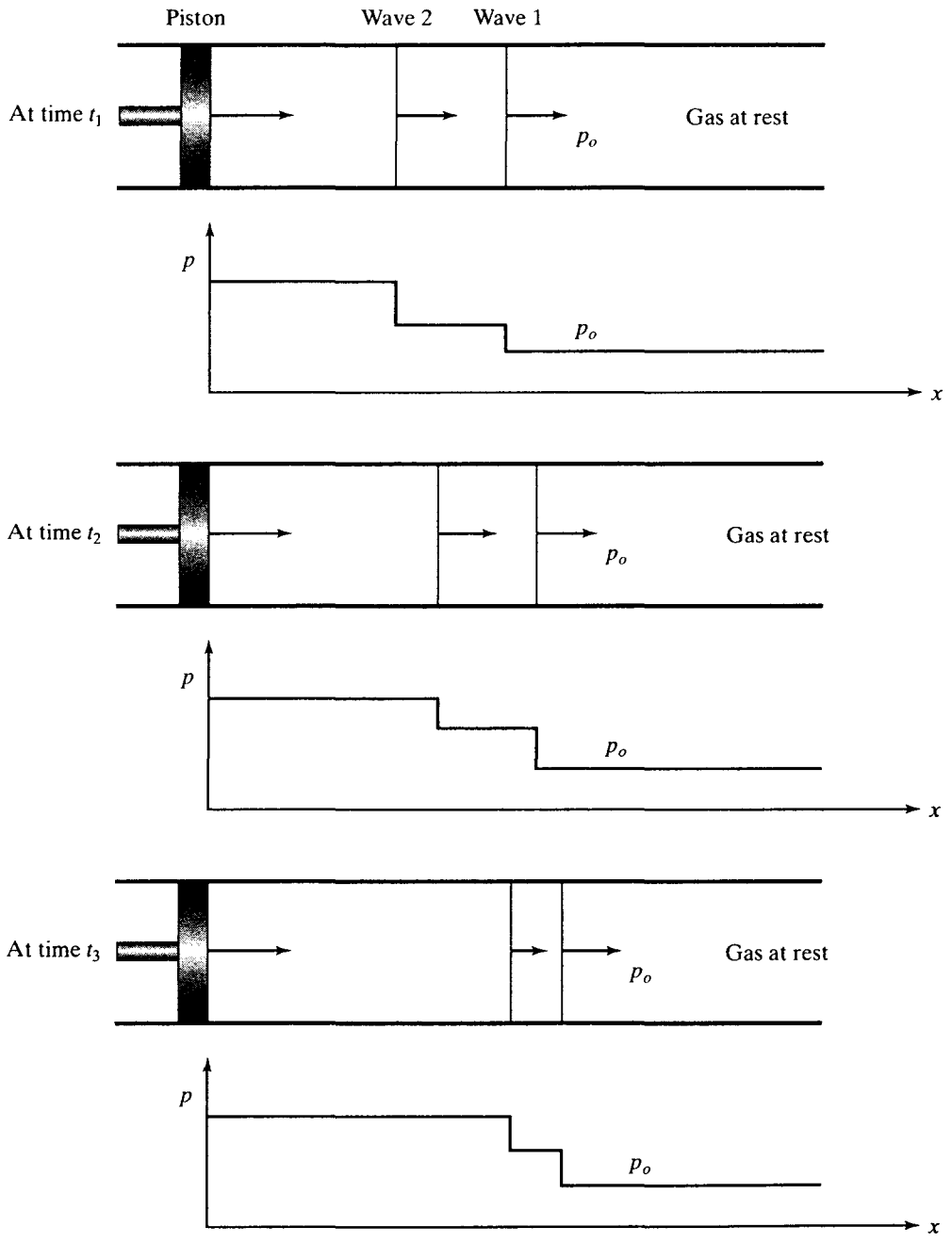


**Figure 4.1** The Gradual Overtaking of One Compression Wave by Another Compression Wave

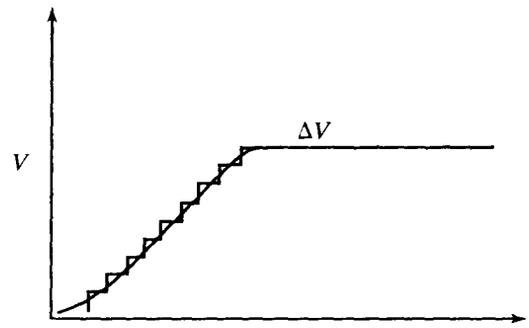


**Figure 4.2** Piston Velocity Increments as a Function of Time

travels at the velocity of sound with respect to the gas into which it is moving. Since the second wave is moving into a gas that is already moving to the right with velocity $dV$, and since it is moving into a compressed gas having a slightly elevated temperature, the second wave travels with a greater absolute velocity than the first wave and gradually overtakes it.

Now suppose the piston is accelerated from rest to a *finite* velocity increment of magnitude $\Delta V$ moving to the right. This finite velocity increment can be thought to consist of a large number of infinitesimal increments, each of magnitude $dV$. Figure 4.2 shows the velocity of the piston versus time, with the incremental velocities $dV$ superimposed. As was demonstrated in Figure 4.1, the waves next to the piston tend to overtake those farther down the tube. (See Figure 4.3.)

As time passes, the compression wave steepens. The tendency of the higher density parts of the wave to overtake the lower density parts is finally counteracted by heat conduction and viscous effects taking place internal to the wave. The resultant constant-shape compression *shockwave* produced by the addition of the weak compression waves then moves through the undisturbed gas ahead of the piston. The slopes of temperature and pressure versus distance in the wave itself are very large (yet not truly infinite), and so the shock can be approximated by a discontinuity. (See Figure 4.4.)

If the piston in Figure 4.5 is suddenly given an incremental velocity $dV$ to the left, a weak expansion wave propagates to the right at the velocity of sound. When the piston is given a second increment of velocity, a second expansion wave moves into the expanded gas behind the first wave, as illustrated in the figure. Again, each wave travels at the velocity of sound with respect to the gas into which it is moving. In this case, the waves and gas are moving in opposite directions. Furthermore, the second wave is traveling into a gas that has already been expanded and cooled, which lowers the velocity of the sound. Both effects reduce the absolute wave velocity and cause the second wave to fall farther and farther behind the first. In this manner, expansion waves spread out; they are not able to reinforce one another. (See Figure 4.6.) The creation of a finite-expansion shockwave is impossible.

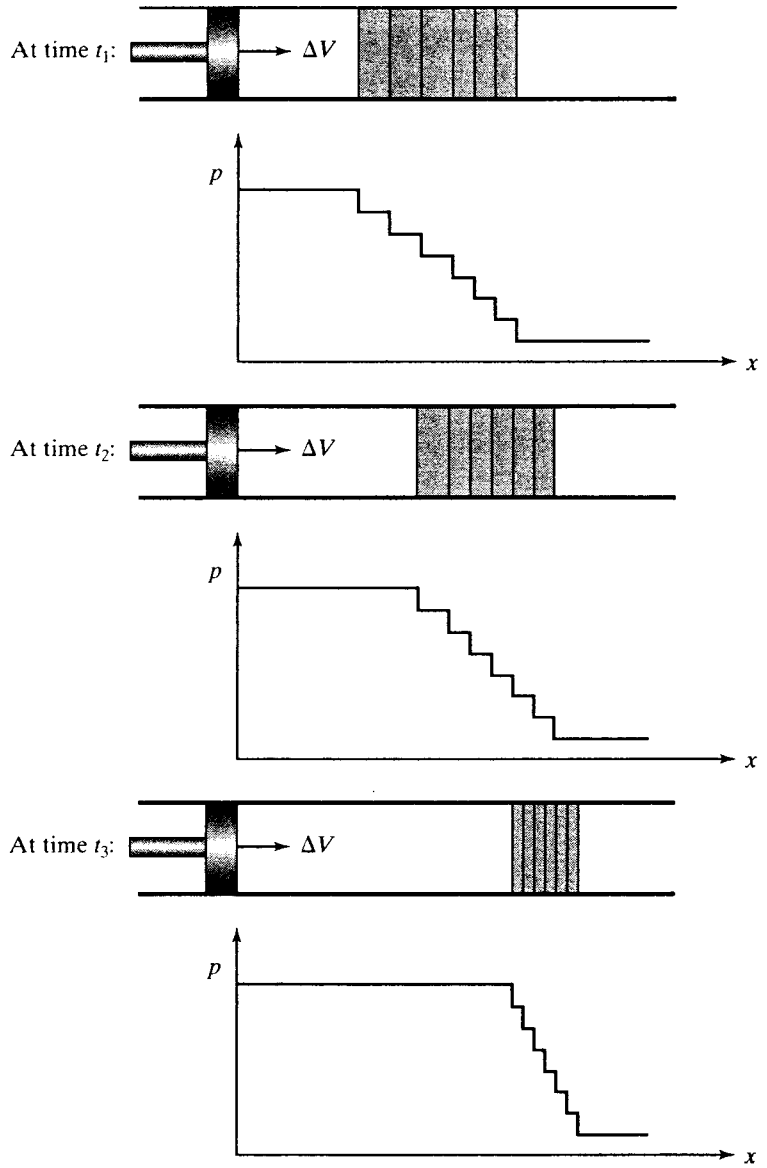


**Figure 4.3** The Steepening of Compression Waves

## 4.3 EQUATIONS GOVERNING A STATIONARY NORMAL SHOCKWAVE

A shock involves *finite* changes in flow variables (velocity, pressure, temperature, and density), and these changes occur at virtually the same location. The processes taking place inside the wave itself are extremely complex and cannot be studied on the basis of equilibrium thermodynamics. Temperature and velocity gradients internal to the shock provide heat conduction and viscous dissipation that render the shock process internally irreversible. In a practical sense, however, primary interest is not generally focused on the interior details of the shockwave, but on the net changes in fluid

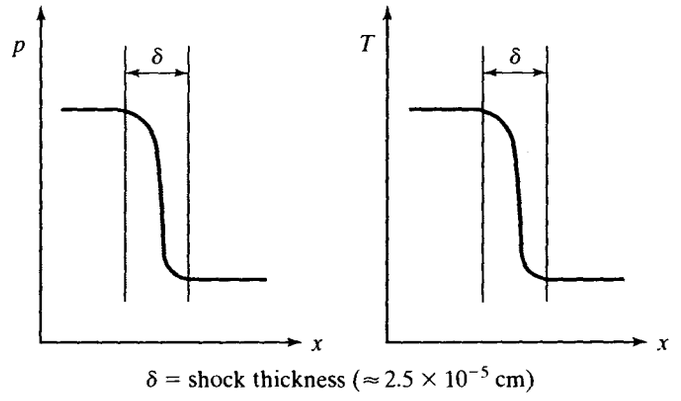


**Figure 4.4** Pressure and Temperature Distributions through a Shock Wave

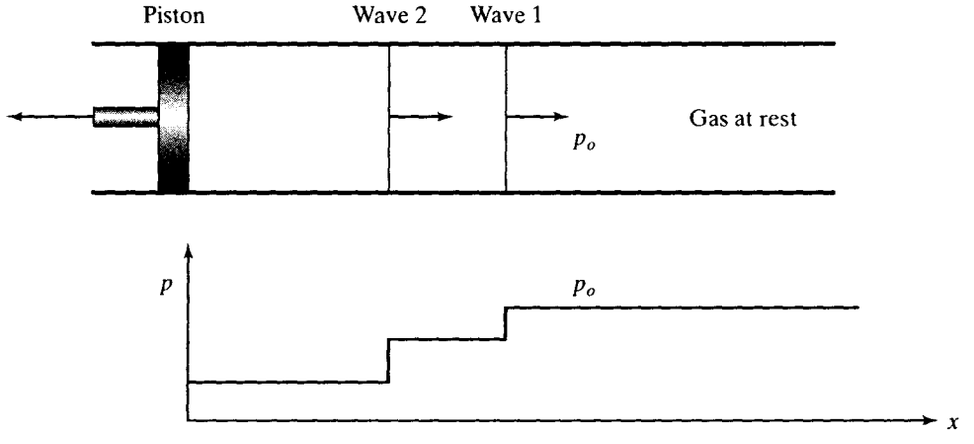


**Figure 4.5** Two Expansion Waves Moving through a Tube

properties taking place across the entire wave. If one chooses a control volume encompassing the shockwave, the flow equations can be written without regard to the complexities of the internal processes. For this purpose, it is sufficient to note that the shock process is thermodynamically irreversible. Furthermore, with the shock-temperature gradient inside the control volume, there is no external heat transfer across the control volume boundaries, so the shock process is adiabatic.

Suppose a fixed-plane shock occurs in one-dimensional, steady flow, as shown in Figure 4.7. The shock is assumed thin enough so that, even though it may occur in a varying area channel, as in Figure 4.8, there is no area change across the wave.

If one refers to the control volume indicated in Figure 4.7, the steady-state continuity equation, with uniform conditions on the control surfaces, Eq. (1.28), yields

$$\rho_1 V_1 = \rho_2 V_2 \tag{4.1}$$

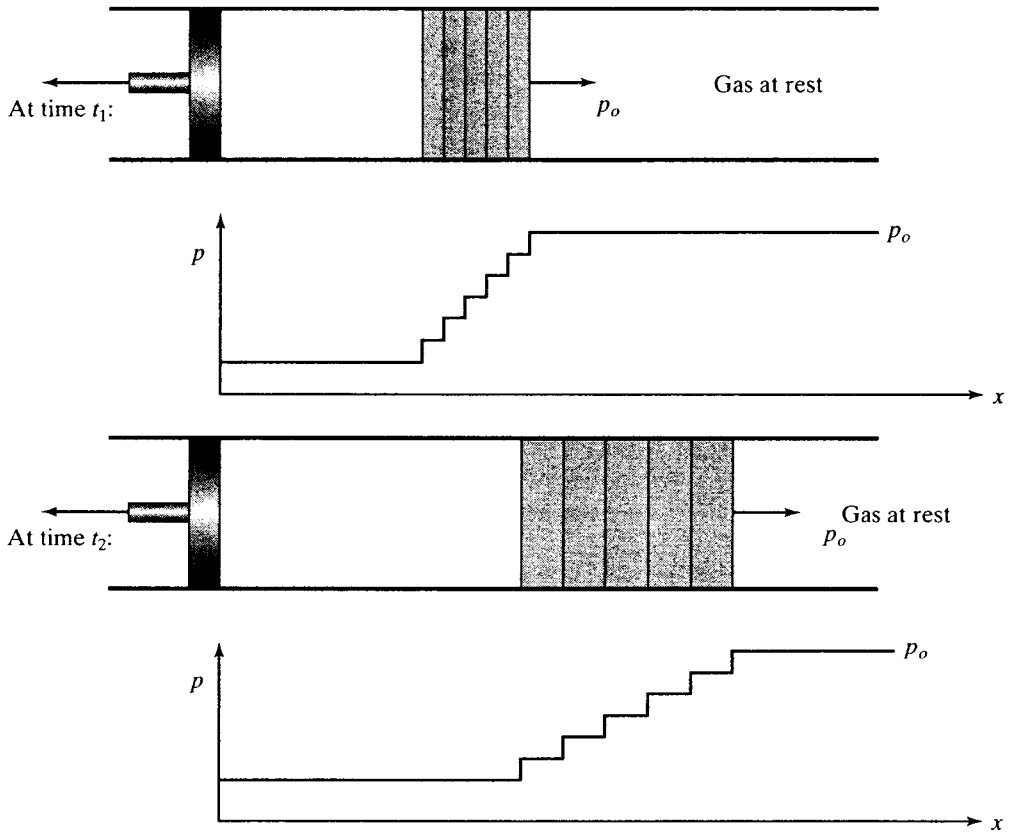


**Figure 4.6** The Spreading Out of Expansion Waves

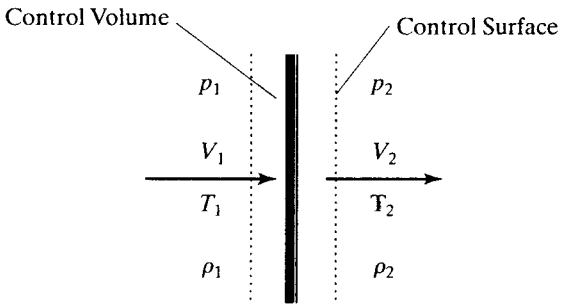


**Figure 4.7** Control Volume Placed around a Normal Shockwave

With pressure forces being the only external forces acting on the control volume, the momentum equation, Eq. (1.31), becomes

$$p_1A_1 - p_2A_2 = \iint_{\text{C.S.}} V_x(\rho \mathbf{V} \cdot d\mathbf{A})$$
$$= \rho_2A_2V_2^2 - \rho_1A_1V_1^2$$

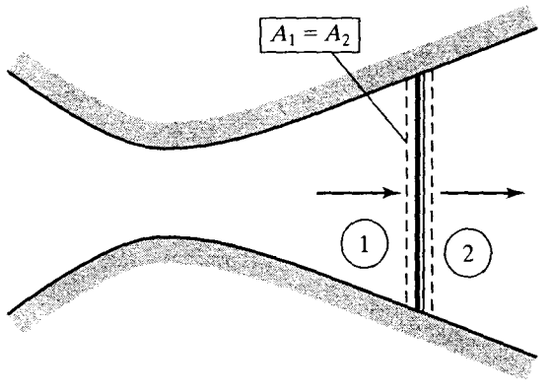


**Figure 4.8** A Normal Shock in a Varying Area Channel

or

$$p_1 + \rho_1 V_1^2 = p_2 + \rho_2 V_2^2 \tag{4.2}$$

For an adiabatic process, the energy equation, Eq. (1.38), for steady flow simplifies to

$$h_1 + \frac{V_1^2}{2} = h_2 + \frac{V_2^2}{2} \tag{4.3}$$

Therefore, from Eqs. (4.1), (4.2), and (4.3), across the stationary normal shockwave, we have

$$\begin{aligned} (\rho_2 V_2 - \rho_1 V_1) &= 0 \\ (p_2 + \rho_2 V_2^2) - (p_1 + \rho_1 V_1^2) &= 0 \\ \left(h_2 + \frac{V_2^2}{2}\right) - \left(h_1 + \frac{V_1^2}{2}\right) &= 0 \end{aligned} \tag{4.4}$$

Collectively, these equations are known as the *jump conditions* and must be satisfied to preserve conservation of mass, momentum, and energy across the shock.

To obtain a solution of this system of equations, it is necessary to incorporate an equation of state for the medium in which the shock occurs. Because of its reasonably wide range of application and its inherent simplicity, the perfect-gas equation of state with constant specific heats will be assumed for the medium. So, we have

$$p = \rho RT$$

$$dh = c_p dT = \left(\frac{\gamma R}{\gamma - 1}\right) dT$$

and, from Eq. (2.7), we have

$$a^2 = \gamma RT$$

For a perfect gas with constant specific heats undergoing an adiabatic process, it was shown in Section 3.4 that the stagnation temperature remains constant. In other words, Eq. (4.3) simplifies to

$$T_1\left(1 + \frac{\gamma - 1}{2}M_1^2\right) = T_2\left(1 + \frac{\gamma - 1}{2}M_2^2\right) \tag{4.5}$$

For a perfect gas,

$$p + \rho V^2 = p(1 + \gamma M^2)$$

so Eq. (4.2) becomes

$$p_1(1 + \gamma M_1^2) = p_2(1 + \gamma M_2^2) \tag{4.6}$$

Combining Eqs. (4.6) and (4.5) with Eq. (4.1) yields

$$\rho_1 V_1 = \rho_2 V_2$$

$$\frac{p_1}{RT_1}M_1\sqrt{\gamma RT_1} = \frac{p_2}{RT_2}M_2\sqrt{\gamma RT_2}$$

$$\frac{M_1}{1 + \gamma M_1^2}\sqrt{1 + \frac{\gamma - 1}{2}M_1^2} = \frac{M_2}{1 + \gamma M_2^2}\sqrt{1 + \frac{\gamma - 1}{2}M_2^2} \tag{4.7}$$

Equation (4.7) can be solved to yield $M_2$ in terms of $M_1$. Squaring both sides gives

$$\frac{M_1^2\left(1 + \frac{\gamma - 1}{2}M_1^2\right)}{(1 + \gamma M_1^2)^2} = \frac{M_2^2\left(1 + \frac{\gamma - 1}{2}M_2^2\right)}{(1 + \gamma M_2^2)^2} \tag{4.8}$$

Expressed in terms of a quadratic in $M_2^2$, the result is

$$M_2^4\left(\frac{\gamma - 1}{2} - \gamma^2 L\right) + M_2^2(1 - 2\gamma L) - L = 0$$

where $L$ is equal to the left-hand side of Eq. (4.8). Solving the quadratic equation for $M_2^2$, we obtain

$$M_2^2 = \frac{-(1 - 2\gamma L) \pm \sqrt{(1 - 2\gamma L)^2 + 4L\left(\frac{\gamma - 1}{2} - \gamma^2 L\right)}}{2\left(\frac{\gamma - 1}{2} - \gamma^2 L\right)}$$

The radical simplifies to $(M_1^2 - 1)/(1 + \gamma M_1^2)$. If the negative sign is selected, we find that $M_2^2 = M_1^2$. This solution is trivial, as it involves no change in properties in a constant-area flow and thus corresponds to isentropic flow and so is not of interest for the irreversible normal shock. The positive sign leads to the following;

$$M_2^2 = \frac{M_1^2 + \dfrac{2}{\gamma - 1}}{\dfrac{2\gamma}{\gamma - 1} M_1^2 - 1} \tag{4.9}$$

The result of Eq. (4.9) is plotted in Figure 4.9 for $\gamma = 1.4$.

For $M_1 > 1$, $M_2$ is less than unity, and vice versa. From Eq. (4.6), $M_1 > 1$ is the case of a *compression shock*—that is, $p_2 > p_1$; $M_1 < 1$ is the case of an *expansion shock*—that is, $p_2 < p_1$.

Equations (4.5) and (4.9) can be combined to yield $T_2/T_1$ as a function of $M_1$ and $\gamma$; in the same way, Eqs. (4.6) and (4.9) can be combined to yield $p_2/p_1$ as a function of $M_1$ and $\gamma$. The entropy change for a perfect gas with constant specific heats is given by Eq. (1.45):

$$s_2 - s_1 = c_p \ln \frac{T_2}{T_1} - R \ln \frac{p_2}{p_1} \tag{4.10}$$

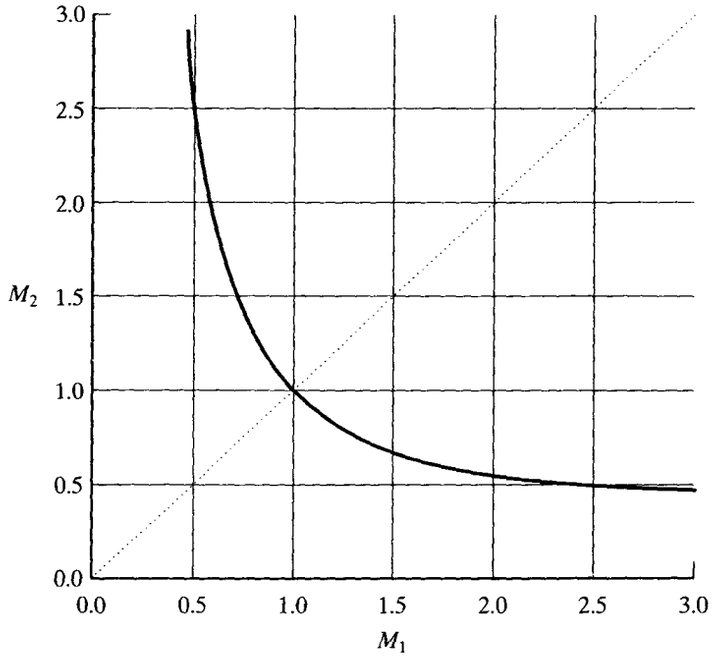


**Figure 4.9** Downstream Mach Number versus Upstream Mach Number

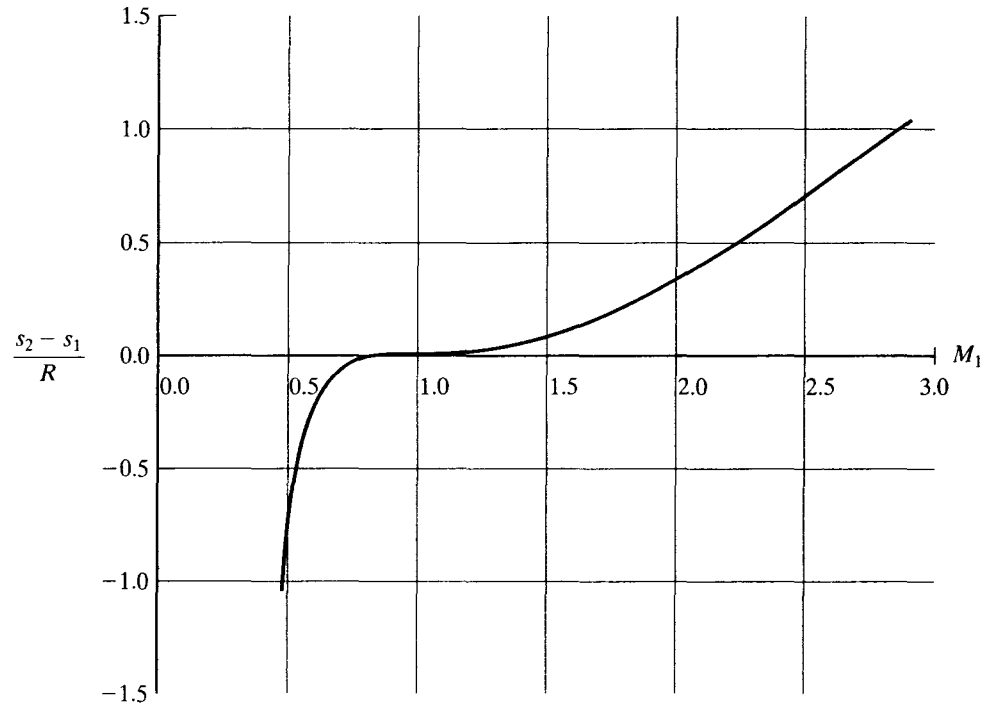


**Figure 4.10** Entropy Difference across a Normal Shock versus Mach Number Upstream of Shock

With $p_2/p_1$ and $T_2/T_1$ as functions of $M_1$, $\Delta s$ can be expressed in terms of $M_1$ alone. (The development of this expression will be presented shortly.) The result is plotted in Figure 4.10. The shock process has been determined to be adiabatic and irreversible. From the second law of thermodynamics, for an irreversible process,

$$dS > \frac{\delta Q}{T} \tag{1.41}$$

For an adiabatic process, $\delta Q = 0$, and since $dS = mds$, $ds > 0$; that is, the entropy must increase across a shockwave.

From Figure 4.10, $s_2 - s_1$ is greater than zero for $M_1$ greater than unity. Thus, the only solutions to the normal shock equations that do not violate the second law are those for which $M_1$ is greater than unity; the approach flow must be supersonic with respect to the wave. The static pressure increases across the shock. Thus, for the conditions of this analysis, an expansion shockwave violates the second law of thermodynamics and is therefore impossible. However, it has been found experimentally that an expansion or rarefaction shock can be generated in certain types of fluid called *dense gases*; for example, see Refs. (4.1) and (4.2).

From the normal shock equations for a perfect gas with constant specific heats, as derived in Eqs. (4.9), (4.6), and (4.5), $M_2$, $p_2/p_1$, $T_2/T_1$, and $\rho_2/\rho_1$ can be expressed as a function of $M_1$ alone for a given $\gamma$.

For example, from Eq. (4.5),

$$\frac{T_2}{T_1} = \frac{1 + \dfrac{\gamma - 1}{2} M_1^2}{1 + \dfrac{\gamma - 1}{2} M_2^2}$$

Combining the preceding equation with Eq. (4.9) yields

$$\begin{aligned} \frac{T_2}{T_1} &= \frac{\left(1 + \dfrac{\gamma - 1}{2} M_1^2\right)\left(\dfrac{2\gamma}{\gamma - 1} M_1^2 - 1\right)}{M_1^2\left(\dfrac{2\gamma}{\gamma - 1} + \dfrac{\gamma - 1}{2}\right)} \\ &= \frac{\left(1 + \dfrac{\gamma - 1}{2} M_1^2\right)\left(\dfrac{2\gamma}{\gamma - 1} M_1^2 - 1\right)}{\left[\dfrac{(\gamma + 1)^2}{2(\gamma - 1)}\right] M_1^2} \end{aligned} \tag{4.11}$$

From Eq. (4.6),

$$\frac{p_2}{p_1} = \frac{1 + \gamma M_1^2}{1 + \gamma M_2^2}$$

Combining this equation with Eq. (4.9) yields

$$\frac{p_2}{p_1} = \frac{2\gamma M_1^2}{\gamma + 1} - \frac{\gamma - 1}{\gamma + 1} \tag{4.12}$$

Finally,

$$\frac{\rho_2}{\rho_1} = \frac{V_1}{V_2} = \frac{M_1}{M_2}\sqrt{\frac{T_1}{T_2}}$$

Substituting from Eqs. (4.9) and (4.11), we obtain

$$\frac{\rho_2}{\rho_1} = \frac{M_1}{\sqrt{\dfrac{M_1^2 + \dfrac{2}{\gamma - 1}}{\dfrac{2\gamma}{\gamma - 1} M_1^2 - 1}}} \sqrt{\frac{M_1^2\left(\dfrac{2\gamma}{\gamma - 1} + \dfrac{\gamma - 1}{2}\right)}{\left(1 + \dfrac{\gamma - 1}{2} M_1^2\right)\left(\dfrac{2\gamma}{\gamma - 1} M_1^2 - 1\right)}}$$

Simplifying, we get,

$$\frac{\rho_2}{\rho_1} = \frac{V_1}{V_2} = \frac{(\gamma + 1) M_1^2}{(\gamma - 1) M_1^2 + 2} \tag{4.13}$$

**Computational Note:** Numerical values of $M_2$, $p_2/p_1$, $T_2/T_1$, and $\rho_2/\rho_1$ may readily be put in tabular form as a function of $M_1$ for various ratios of specific heats. (See Appendix C.) Usually, the latter are taken to be $\gamma = 1.4$, $\gamma = 1.3$, and $\gamma = 5/3$. Also, refer to Appendix A for guidance in developing a spreadsheet program.

Changes in stagnation properties across a stationary normal shock can also be related to $M_1$. For steady flow of a perfect gas with constant specific heats, there is no change in stagnation temperature for the adiabatic shock process. Physically, the increase of static temperature accompanying the compression process is compensated for by a decrease in kinetic energy of the gas, which yields no net change in total or stagnation temperature.

Stagnation pressure variations across a fixed normal shock can be related directly to the entropy rise across the shock. From Eq. (4.10),

$$\frac{s_2 - s_1}{R} = \frac{c_p}{R}\ln\frac{T_2}{T_1} - \ln\frac{p_2}{p_1}$$

Expressing $s_2 - s_1$ in terms of stagnation properties for an adiabatic process, we make use of

$$T_o = T\left(1 + \frac{\gamma - 1}{2}M^2\right)$$

$$p_o = p\left(1 + \frac{\gamma - 1}{2}M^2\right)^{\gamma/(\gamma-1)}$$

so that

$$\frac{s_2 - s_1}{R} = \frac{c_p}{R}\ln\frac{1 + \frac{\gamma - 1}{2}M_1^2}{1 + \frac{\gamma - 1}{2}M_2^2} - \ln\left\{\frac{p_{o2}}{p_{o1}}\left[\frac{1 + \frac{\gamma - 1}{2}M_1^2}{1 + \frac{\gamma - 1}{2}M_2^2}\right]^{\gamma/(\gamma-1)}\right\}$$

Since $c_p/R = \gamma/(\gamma - 1)$, this expression reduces to

$$\frac{s_2 - s_1}{R} = -\ln\frac{p_{o2}}{p_{o1}} \tag{4.14}$$

But, from the second law, $s_2 > s_1$, so that $p_{o2} < p_{o1}$ for a fixed normal shock. To obtain the total pressure ratio across the shock, we may form a string of pressure ratios consisting of the stagnation-to-static-pressure ratio on the downstream side of the shock, the static-pressure ratio across the shock and the static-to-stagnation-pressure

ratio on the upstream side of the shock. As may be observed, the string contains considerable flow physics:

$$\frac{p_{o2}}{p_{o1}} = \left(\frac{p_{o2}}{p_2}\right)\left(\frac{p_2}{p_1}\right)\left(\frac{p_1}{p_{o1}}\right)$$

$$= \left(1 + \frac{\gamma - 1}{2} M_2^2\right)^{\gamma/(\gamma-1)} \left(\frac{2\gamma M_1^2}{\gamma + 1} - \frac{\gamma - 1}{\gamma + 1}\right) \left(\frac{1}{1 + \dfrac{\gamma - 1}{2} M_1^2}\right)^{\gamma/(\gamma-1)}$$

Substituting for $M_2$ from Eq. (4.9), we obtain

$$\frac{p_{o2}}{p_{o1}} = \left[\frac{\dfrac{\gamma + 1}{2} M_1^2}{1 + \dfrac{\gamma - 1}{2} M_1^2}\right]^{\gamma/(\gamma-1)} \left[\frac{1}{\dfrac{2\gamma}{\gamma + 1} M_1^2 - \dfrac{\gamma - 1}{\gamma + 1}}\right]^{1/(\gamma-1)} \tag{4.15}$$

Values of $p_{o2}/p_{o1}$ versus $M_1$ may be tabulated. For an adiabatic process, stagnation pressure represents a measure of available energy of the flow in a given state. A decrease in stagnation pressure, or an increase in entropy, denotes an energy dissipation or loss of available energy.

In the preceding explanation, all ratios of parameters across the normal shock were written in terms of $M_1$, the Mach number on the upstream side of the shock. It is, however, possible to write the equations in terms of some other independent variable (e.g., the static-pressure ratio across the shock, $p_2/p_1$). Towards that end, we next develop an expression connecting the static-pressure ratio to the density ratio across the shock:

$$\frac{\rho_2}{\rho_1} = f\left(\frac{p_2}{p_1}\right)$$

This expression is known as the *Rankine–Hugoniot* (the latter name is pronounced who-GO-knee-oh) *relation*. Note that this relation involves only thermodynamic quantities; that is, it contains no Mach numbers or other kinematic variables. To develop the relation, use the continuity equation, Eq. (4.1), to rewrite the momentum equation, Eq. (4.2):

$$\frac{p_1}{\rho_1 V_1} - \frac{p_2}{\rho_2 V_2} = V_2 - V_1$$

Multiply this expression by $(V_2 + V_1)$ to obtain

$$V_1^2 - V_2^2 = (p_2 - p_1)\left(\frac{1}{\rho_1} + \frac{1}{\rho_2}\right)$$

Now, from the energy equation, Eq. (4.3), and the perfect-gas equations, we have

$$V_1^2 - V_2^2 = 2(h_2 - h_1) = 2c_p(T_2 - T_1)$$
$$= 2\frac{\gamma}{\gamma - 1}(RT_2 - RT_1) = 2\frac{\gamma}{\gamma - 1}\left(\frac{p_2}{\rho_2} - \frac{p_1}{\rho_1}\right)$$

Equating the two expressions and rearranging produces the Rankine–Hugoniot relation

$$\frac{p_2}{p_1} = \frac{\left(\frac{\gamma + 1}{\gamma - 1}\right)\frac{\rho_2}{\rho_1} - 1}{\left(\frac{\gamma + 1}{\gamma - 1}\right) - \frac{\rho_2}{\rho_1}} \tag{4.16a}$$

or

$$\frac{\rho_2}{\rho 1} = \frac{\left(\frac{\gamma + 1}{\gamma - 1}\right)\frac{p_2}{p_1} + 1}{\left(\frac{\gamma + 1}{\gamma - 1}\right) + \frac{p_2}{p_1}} \tag{4.16b}$$

We now derive a relation that will be useful in some of the calculations, as well as in some of the developments that follow. Begin with Eq. (4.2), which has been rearranged and modified using Eq. (4.1):

$$\left(\frac{p_1}{\rho_1 V_1} + \frac{\rho_1 V_1^2}{\rho_1 V_1}\right) - \left(\frac{p_2}{\rho_2 V_2} + \frac{\rho_2 V_2^2}{\rho_2 V_2}\right) = 0$$

Next, replace the pressure–density ratios using the perfect-gas equation of state to get

$$\frac{RT_1}{V_1} - \frac{RT_2}{V_2} + (V_1 - V_2) = 0 \tag{4.17}$$

Now, from the definition of stagnation enthalpy ($h_o = h + V^2/2$) and perfect-gas relations [$h = c_pT = (\gamma RT)/(\gamma - 1) = a^2/(\gamma - 1)$], we may write

$$\frac{RT_1}{V_1} = \frac{1}{\gamma V_1}\left(\gamma RT_o - \frac{\gamma - 1}{2}V_1^2\right)$$
$$\frac{RT_2}{V_2} = \frac{1}{\gamma V_2}\left(\gamma RT_o - \frac{\gamma - 1}{2}V_2^2\right) \tag{4.18}$$

Combining Eqs. (4.17) and (4.18) gives

$$\frac{1}{\gamma V_1}\left(\gamma RT_o - \frac{\gamma - 1}{2}V_1^2\right) - \frac{1}{\gamma V_2}\left(\gamma RT_o - \frac{\gamma - 1}{2}V_2^2\right) + (V_1 - V_2) = 0$$

Rearranging this equation produces the simple expression

$$\left(-\frac{\gamma RT_o}{V_1 V_2} + \frac{\gamma + 1}{2}\right)(V_1 - V_2) = 0 \tag{4.19}$$

Equation (4.19) can be satisfied in either of two ways: If $V_1 = V_2$, the solution is a trivial result and therefore of no interest; on the other hand, if

$$V_1 V_2 = \frac{2}{\gamma + 1} a_o^2 \tag{4.20}$$

we obtain a simple result that is known as *Prandtl's relation* for normal shockwaves. (In Chapter 6, a relation for oblique shockwaves will be developed.) We will make use of Prandtl's relation in subsequent developments. It should be noted, however, that

$$a_o^2 = \gamma RT_o = (\gamma - 1)h_o = (\gamma - 1)\left(h + \frac{V^2}{2}\right)$$
$$= \gamma RT + (\gamma - 1)\frac{V^2}{2} = a^2 + (\gamma - 1)\frac{V^2}{2}$$

There are various ways to write Eq. (4.20), such as

$$V_1 V_2 = \frac{2}{\gamma + 1} a_o^2 = \frac{2}{\gamma + 1} a_1^2 + \frac{\gamma - 1}{\gamma + 1} V_1^2 = \frac{2}{\gamma + 1} a_2^2 + \frac{\gamma - 1}{\gamma + 1} V_2^2 \tag{4.20a}$$

**Example 4.1. Limiting forms of the relations for stationary normal shockwaves**

Develop limiting expressions for the flows in which the upstream conditions produce (i) a strong shock and (ii) a weak shock.

**Solution**

The *strength of a normal shock* is defined as the ratio of the pressure difference $p_2 - p_1$ across the shock divided by the upstream pressure $p_1$. Equation (4.12) can be rearranged as follows:

$$\frac{p_2 - p_1}{p_1} = \frac{2\gamma}{\gamma + 1}(M_1^2 - 1)$$

For *strong shocks*, the left-hand side is large, and therefore $M_1$ must be very large, whereas for *weak shocks*, the strength is close to zero, and thus $M_1$ is close to unity.

*Strong normal shocks*

We may examine each normal-shock expression to determine the limiting form for large values of the upstream Mach number. For example, consider the expression for the downstream Mach number, Eq. (4.9):

$$M_2^2 = \frac{M_1^2 + \dfrac{2}{\gamma - 1}}{\dfrac{2\gamma}{\gamma - 1} M_1^2 - 1}$$

Now, for large values of $M_1$, the numerator is dominated by $M_1^2$, whereas the denominator is dominated by $2\gamma M_1^2/(\gamma - 1)$. Thus, the limiting expression for $M_2$ is

$$M_2 \cong \sqrt{\frac{\gamma - 1}{2\gamma}}$$

So, for $\gamma = 1.4$, $M_2$ cannot fall below 0.378, even if $M_1$ is infinite. The limiting expressions for the strong shock case for the other flow variables are found in the same way and written as

$$\frac{T_2}{T_1} \cong \frac{2\gamma(\gamma - 1)}{(\gamma + 1)^2} M_1^2$$

$$\frac{p_2}{p_1} \cong \frac{2\gamma}{\gamma + 1} M_1^2$$

$$\frac{\rho_2}{\rho_1} = \frac{V_1}{V_2} \cong \frac{(\gamma + 1)}{(\gamma - 1)}$$

$$\frac{p_{o2}}{p_{o1}} = e^{-[(s_2 - s_1)/R]} \cong \left(\frac{\gamma + 1}{\gamma - 1}\right)^{\gamma/(\gamma-1)} \left(\frac{\gamma + 1}{2\gamma M_1^2}\right)^{1/(\gamma-1)}$$

From this list, we see that the temperature ratio, pressure ratio, and entropy change all become infinitely large for infinite $M_1$, whereas the density ratio, the downstream Mach number, and the velocity ratio approach limit values that depend on $\gamma$. The ratio of the stagnation pressure tends to zero as $M_1$ becomes very large. Of course, these relations apply only if perfect-gas conditions remain valid. In reality, at large values of $M_1$, gases will dissociate.

*Weak normal shocks*

For a weak shock, the pressure change across the shock tends to zero and the pressure ratio $p_2/p_1$ approaches unity, and therefore the quantity $(M_1^2 - 1)$ is a very small number, say, $\varepsilon$. To illustrate the process of determining the weak shock relations, let us reconsider the expression for $M_2$:

$$M_2^2 = \frac{M_1^2 + \dfrac{2}{\gamma - 1}}{\dfrac{2\gamma}{\gamma - 1} M_1^2 - 1}$$

Replace $M_1^2$ with $1 + \varepsilon$. Expand using the binomial-expansion relation where appropriate (see Example 3.3), dropping all second-order and higher terms in $\varepsilon$:

$$M_2^2 = \frac{1 + \varepsilon + \dfrac{2}{\gamma - 1}}{\dfrac{2\gamma}{\gamma - 1}(1 + \varepsilon) - 1} = \frac{\dfrac{\gamma + 1}{\gamma - 1} + \varepsilon}{\dfrac{\gamma + 1}{\gamma - 1} + \dfrac{2\gamma}{\gamma - 1}\varepsilon}$$

$$= \left(1 + \frac{\gamma - 1}{\gamma + 1}\varepsilon\right)\left(1 + \frac{2\gamma}{\gamma + 1}\varepsilon\right)^{-1} = \left(1 + \frac{\gamma - 1}{\gamma + 1}\varepsilon\right)\left(1 - \frac{2\gamma}{\gamma + 1}\varepsilon \cdots\right)$$

$$\cong 1 + \left(\frac{\gamma - 1}{\gamma + 1} - \frac{2\gamma}{\gamma + 1}\right)\varepsilon = 1 - \varepsilon$$

$$= 2 - M_1^2$$

The limiting weak shock expressions for the other flow variables are found in the same manner and written as

$$\frac{p_2}{p_1} = 1 + \frac{2\gamma}{\gamma + 1}(M_1^2 - 1)$$

$$\frac{\rho_2}{\rho_1} \cong 1 + \frac{2}{\gamma + 1}(M_1^2 - 1)$$

$$\frac{V_2}{V_1} \cong 1 - \frac{2}{\gamma + 1}(M_1^2 - 1)$$

$$\frac{T_2}{T_1} \cong 1 - 2\left(\frac{\gamma - 1}{\gamma + 1}\right)(M_1^2 - 1)$$

From Eq. (4.15), we see that the ratio of stagnation pressures is equal to unity at the limiting value of $M_1 = 1$, and therefore, from Eq. (4.14), there is no change in entropy. Hence, the flow tends toward isentropic flow for weak shocks. We can place this result on a firmer analytical base as follows: Using Eqs. (4.13) and (4.14), we can write the change in entropy across a shock as

$$\frac{s_2 - s_1}{R} = \ln\left\{\left[\frac{(\gamma + 1)M_1^2}{2 + (\gamma - 1)M_1^2}\right]^{-\gamma/(\gamma-1)}\left[\frac{2\gamma}{\gamma + 1}(M_1^2 - 1) + 1\right]^{1/(\gamma-1)}\right\}$$

Again replace $(M_1^2 - 1)$ with $\varepsilon$. After a small amount of algebra, the foregoing expression becomes

$$\frac{s_2 - s_1}{R} = \ln\left\{\left[1 + \frac{(\gamma - 1)}{(\gamma + 1)}\varepsilon\right]^{\gamma/(\gamma-1)}[1 + \varepsilon]^{-\gamma/(\gamma-1)}\left[1 + \frac{2\gamma}{\gamma + 1}\varepsilon\right]^{1/(\gamma-1)}\right\}$$

$$= \frac{\gamma}{\gamma - 1}\ln\left[1 + \frac{(\gamma - 1)}{(\gamma + 1)}\varepsilon\right] - \frac{\gamma}{\gamma - 1}\ln[1 + \varepsilon] + \frac{1}{\gamma - 1}\ln\left[1 + \frac{2\gamma}{\gamma + 1}\varepsilon\right]$$

Next, we will use the series representation of the natural logarithmic function:

$$\ln(1 + x) = x - \frac{x^2}{2} + \frac{x^3}{3} + \cdots$$

The coefficients of the $\varepsilon$ and $\varepsilon^2$ terms both sum to zero, whereas the sum of the coefficients of $\varepsilon^3$ produce

$$\frac{s_2 - s_1}{R} \cong \frac{2\gamma}{(\gamma + 1)^2}\frac{\varepsilon^3}{3} + O(\varepsilon^4) \cong \frac{2\gamma}{3(\gamma + 1)^2}(M_1^2 - 1)^3$$

Replacing the $(M_1^2 - 1)$ with $\left(\frac{\gamma + 1}{2\gamma}\right)\left(\frac{p_2 - p_1}{p_1}\right)$, we get

$$\frac{s_2 - s_1}{R} \cong \frac{(\gamma + 1)}{12\gamma^2}\left(\frac{p_2 - p_1}{p_1}\right)^3$$

The implication is that the change of entropy across a weak shock may be neglected. Moreover, the change of entropy across a shock of moderate strength, say, up to a $\Delta p/p_1 \sim 3$, may also be ignored without serious error. This may be verified either by showing that the

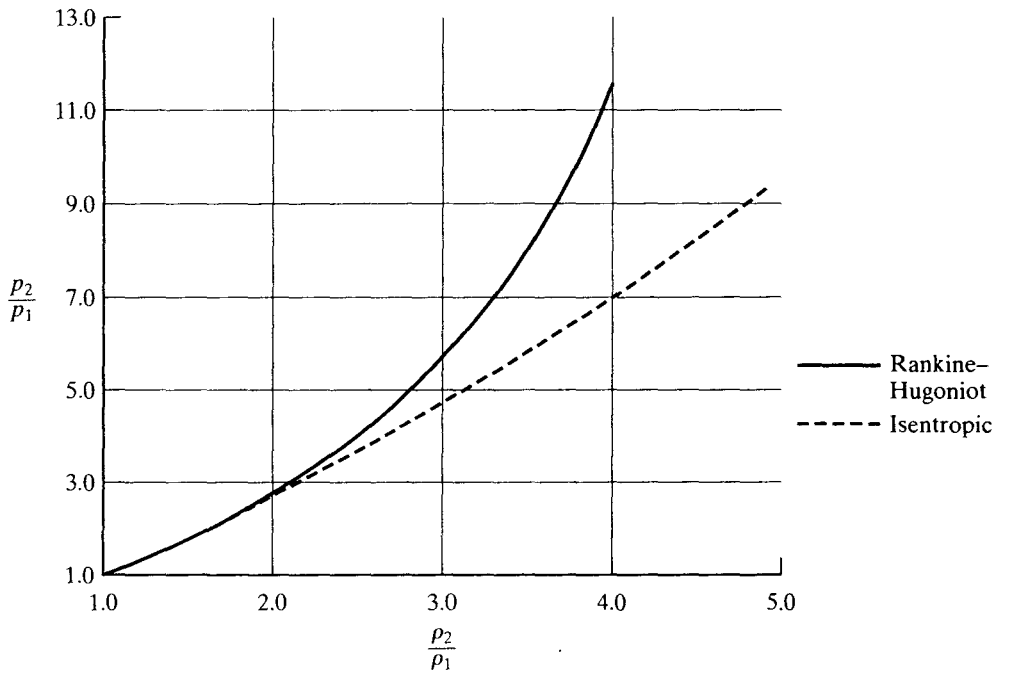


**Figure 4.11** Comparison of Rankine–Hugoniot and Isentropic Relations

Rankine–Hugoniot relation of Eq. (4.16a) reduces to $\Delta p/p = \gamma\, \Delta\rho/\rho$ for a weak shock or by plotting the Rankine–Hugoniot relation and the isentropic relation $p_2/p_1 = (\rho_2/\rho_1)^\gamma$ (as shown in Figure 4.11), from which we observe that the curves merge as the pressure ratio approaches unity. A concise discussion of this material is given in Ref. (4.3).

---

**Example 4.2. Calculation of properties behind a stationary normal shockwave**

An airstream ($\gamma = 1.4$, $R = 287$ J/kg·K) with a velocity of 500 m/s, a static pressure of 50 kPa, and a static temperature of 250 K undergoes a normal shock. Determine the air velocity and the static and stagnation conditions after the wave.

**Solution**

The Mach number upstream of the shock, $M_1$, is given by

$$M_1 = \frac{V_1}{a_1} = \frac{V_1}{\sqrt{\gamma R T_1}} = \frac{500 \text{ m/s}}{\sqrt{1.4(287 \text{ J/kg} \cdot \text{K})250 \text{ K}}} = \frac{500}{316.9385} = 1.5776$$

From Eqs. (4.11), (4.12), (4.13), and (4.9), respectively, we get

$$\frac{T_2}{T_1} = 1.3726, \quad \frac{p_2}{p_1} = 2.7370, \quad \frac{\rho_2}{\rho_1} = 1.9940, \text{ and } M_2 = 0.6753$$

However,

$$\frac{V_2}{V_1} = \frac{\rho_1}{\rho_2}$$

so the gas velocity after the wave is

$$V_2 = \frac{500}{1.994} = 250.7523 \text{ m/s}$$

Also,

$$p_2 = 50(2.737) = 136.8500 \text{ kPa}$$
$$T_2 = 250(1.3726) = 343.1500 \text{ K}$$

Because the flow is adiabatic across the shock, $T_{o1} = T_{o2}$. From the isentropic-flow–temperature relation,

$$\frac{T_1}{T_{o1}} = 0.6677$$

So

$$T_{o1} = \frac{250}{0.6677} = 374.4196 \text{ K} = T_{o2}$$

From the isentropic-flow–stagnation-static-pressure relation,

$$\frac{p_1}{p_{o1}} = 0.2432$$

or

$$p_{o1} = \frac{50}{0.2432} = 205.5921 \text{ kPa}$$

Unlike the stagnation temperature, the stagnation pressure is not constant across the shock. The value of the stagnation pressure is a measure of losses in the flow. Thus, $p_{o2} < p_{o1}$, whereas $p_2 > p_1$ across the shock. From normal-shock relations,

$$\frac{p_{o2}}{p_{o1}} = 0.9034$$

$$p_{o2} = (0.9034)(205.5921) = 185.7319 \text{ kPa}$$

---

The normal shock is a discontinuity in the flow that separates isentropic flows on either side of it. For isentropic flow, the area at which the Mach number is equal to unity was defined as $A^*$, with this area (which varies with Mach number) being used as a reference. A normal shock, however, is not an isentropic process; so, for example, if a shock occurs in a channel [Figure 4.12(a)], flow areas downstream of the shock (between locations from 2 to $e$) cannot be referenced to the value of $A^*$ for the upstream flow (between locations from $i$ to 1). Mathematically, we have

$$(A_i^* = A_1^*) \neq (A_2^* = A_e^*)$$

Note that the upstream reference area is labeled $A_1^*$, whereas the downstream reference area is labeled $A_2^*$. Next, we develop a relationship between these two reference areas. From Figure 4.12(b), apply the continuity equation between $A_1^*$ and $A_2^*$, assuming a perfect gas with constant specific heats. From Eq. (3.20), with $\dot{m}(A_1^*) = \dot{m}(A_2^*)$, we may write

$$\frac{p_{o1}A_1^*}{\sqrt{T_{o1}}} f(\gamma, M = 1) = \frac{p_{o2}A_2^*}{\sqrt{T_{o2}}} f(\gamma, M = 1)$$

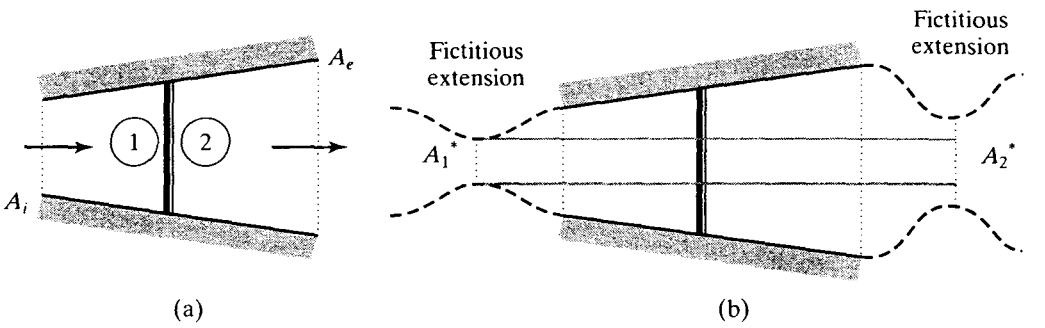


**Figure 4.12** Critical Throat Areas on Both Sides of a Normal Shockwave

This expression incorporates the fact that $M = 1$ at $A_1^*$ and at $A_2^*$. Thus, $f(\gamma, 1)$ drops out of the expression; also, since the flow is steady and adiabatic, $T_{o1} = T_{o2}$. Thus,

$$p_{o1}A_1^* = p_{o2}A_2^* \tag{4.21}$$

It should be noted that because of the losses through the shockwave, $p_{o1}$ is larger than $p_{o2}$. It therefore follows from Eq. (4.21) that $A_1^*$ must be smaller than $A_2^*$, as illustrated in Figure 4.12(b). Also, it must be borne in mind that every isentropic flow has a critical throat area $A^*$, even though it may not physically exist in the flow field. Thus, the areas $A_1^*$ and $A_2^*$ are sketched with dashed lines in Figure 4.12(b).

**Example 4.3. A stationary normal shockwave in a diverging channel**

An airstream ($\gamma = 1.4$, $R = 0.287$ kJ/kg · K) at Mach 2.0 with a pressure of 100 kPa and a temperature of 270 K enters a diverging channel with a ratio of exit area to inlet area of 3.0. (See Figure 4.13.) Determine the back pressure $p_b$ necessary to produce a normal shock in the channel at an area equal to twice the inlet area. Assume one-dimensional, steady flow, with the air behaving as a perfect gas with constant specific heats; also assume isentropic flow, except for the normal shock.

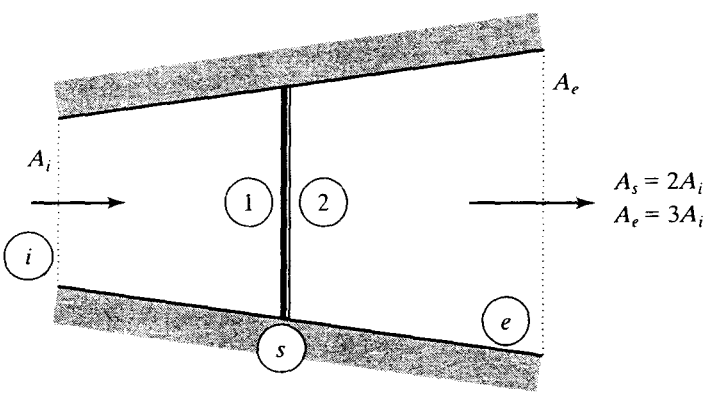


**Figure 4.13** A Stationary Normal Shock in a Diverging Channel

**Historical Note:** The theory of shockwaves presented in this chapter was developed during a period of just over 100 years. This period marked "... the rich and complex process by which incremental discoveries are made and fundamental understanding is advanced." The major contributions during this period and biosketches of the persons making the contributions are presented in this table. It is hoped that this presentation will address the material of this chapter in a somewhat different light. "The object lesson here is that scientific discovery and progress are slow, even for the recognized greats in the field." Ref. (4.5)

**TABLE 4.1** Milestones and Personalities in the Study of Normal Shockwaves

| Year/Event | Person/Biographical Sketch |
|---|---|
| **1808** Poisson publishes MÉMOIRE SUR LA THEORIE DU SON (Paper on the Theory of Sound). In it, he attempts to find solutions to the nonlinear wave equation where the convective terms give rise to solutions of the form $u = f[x - (a + u)t]$ for simple waves moving in the $x$ direction. Here, $u$ is defined by the velocity potential $\varphi$ as $u = \partial\varphi/\partial x$. The speed of sound, $a$, is assumed constant set forth by *isothermal conditions* and Boyle's law. Challis (1848) observed this equation cannot always be uniquely solved for $u$. Refs. (4.5) and (4.9) |  **Siméon-Denis Poisson** Born: 21 June 1781 in Pithiviers, France Died: 25 April 1840 in Sceaux, France Poisson was taught to read and write by his father. The senior Poisson guided his son into medicine, but the younger Poisson lacked both the skills and interest to become a surgeon. Returning to school, the latter demonstrated great mathematical talent. He entered the École Polytechnique in 1798, graduated in 1800, and immediately took the position of répétiteur (coach) there. In 1806, he became a full professor. Although he devised no innovative theories, he made major contributions to further developing the theories of others, often being the first to exhibit the real significance of the theory. During his career, he addressed problems in the theory of sound, astronomy, electricity and magnetism, elasticity, vibrations, heat propagation, and probability. Refs. (4.5) and (4.6) |
| **1848** Stokes publishes ON A DIFFICULTY IN THE THEORY OF SOUND in response to Challis's claim that there existed a contradiction in the accepted theory of sound (in gases). Stokes was the first to introduce the concept of surfaces of discontinuity (shocks) to account for the situation that develops when waves steepen to the point of infinite gradient. Later, Kelvin and Rayleigh convinced him that such discontinuities could not exist, as conservation of mass, momentum, and energy could not be satisfied in concert. The problem here lay in the assumption that the same pressure–density relationship that applied to continuous motion must also apply to discontinuous motion and that the shock would thus be isentropic. Basic concepts of irreversibility were likely being developed at this time. Taylor and Rayleigh later sorted out the problem after reading the works of Rankine and Hugoniot. Ref. (4.5) |  **George Gabriel Stokes** Born: 13 August 1819 in Skreen, County Sligo, Ireland Died: 1 February 1903 in Cambridge, Cambridgeshire, England Stokes received his early education from his father, a Protestant rector. In 1832, he went to school in Dublin; in 1835, he entered Bristol College in Bristol, England; and in 1837, he entered Pembroke College, Cambridge. In 1838, he began to read with the famous tutor Wm. Hopkins. In 1841, Stokes graduated and took a fellowship from Pembroke. Hopkins advised him to do hydro dynamic research, so he began by seeking to account for internal friction in moving fluids. After he had deduced the correct equations of motion in 1845, he found that Navier, Poisson, and Saint-Venant had already considered the problem. Considering the motion of a pendulum in a fluid, he (1) published a work on geodesy of major importance entitled "On the variation of gravity at the surface of the earth" in 1849, the year he became Lucasian Professor of Mathematics, and (2) developed a fundamental paper on hydrodynamics in 1851, the year during which he also published his law of viscosity. In addition, he published papers concerning the wave theory of light and named and explained the phenomenon of fluorescence in 1852. Refs. (4.5) and (4.6) |

(*Continued*)

**TABLE 4.1** (Continued)

| Year/Event | Person/Biographical Sketch |
|---|---|
| **1860** Earnshaw publishes ON THE MATHEMATICAL THEORY OF SOUND. Earnshaw considered a simple wave solution for a more general gas flow in which the pressure and density were related: $p = p(\rho)$. He observed that since the local velocity of propagation was higher in the compressive part of a continuous disturbance, the density gradient would steepen (perpetually gaining on its front) with time and eventually form a discontinuous pressure front. Refs. (4.8) and (4.9) |  **Rev. Samuel Earnshaw** Born: 1 February 1805 in Sheffield, England Died: 6 December 1888 in Sheffield, England Earnshaw, the son of a file cutter and schoolmaster, was homeschooled until the age of 8. In 1827, he was admitted to St. John's College, Cambridge. He finished as the top mathematician in 1831. He received an M.A. in 1834. From 1831 to 1847, he easily supported his family as a notable coach. He was also a rising cleric. In 1847, his health failed and he became chaplain of Queen Mary's foundation in Sheffield—a post he held the rest of his life. He published two texts—*Dynamics* and *Statics*—plus papers in mathematics and physics. He also published some sermons and lectures. In 1874, the University Extension Movement reached Sheffield. Firth College grew out of this program in 1879. He was elected its vice president and, later, president. Refs. (4.5) and (4.7) |
| **1860** Riemann publishes UEBER DIE FORTPFLANZUNG EBENER LUFTWELLEN VON ENDLICHER SCHWINGUNGSWEITE (Propagation of Planar Air Waves of Finite Amplitude). Laplace successfully calculated the speed of sound waves of infinitesimal amplitude as an isentropic process in 1816. Thus, as a first attempt to calculate shock properties (waves of finite amplitude where pressure was an arbitrary function of density), Riemann assumed an isentropic process. This assumption, of course, was incorrect, as shock waves are irreversible processes caused by viscosity and thermal conduction effects inside the shockwave. His work was independent of Earnshaw's. Rankine correctly derived the proper flow equations across a normal shockwave 12 years later. Refs. (4.10) and (4.11) |  **Georg Friedrich Bernard Riemann** Born: 17 Sept 1826 in Breselenz, Hanover (now Germany) Died: 20 July 1866 in Selasca, Italy Riemann was taught by his father, a Lutheran minister, until age 10. In 1840, he entered preparatory schools and showed a talent in mathematics. At age 20, he entered the University of Göttingen to study theology. There he attended mathematics lectures, changed his major to mathematics, and moved to the University of Berlin in the spring of 1847. His work was based on intuitive reasoning, which was less rigorous than the reasoning required for firm proofs, but his ideas were much clearer, as his work was not filled with long computations. In 1849, he returned to Göttingen, and he submitted his dissertation in late 1851. He delivered his inaugural presentation—a classic on the foundations of geometry—as a lecturer in 1854. Einstein later justified this work by using it as a frame to fit his own ideas of general relativity. In 1862, Riemann developed tuberculosis. He made many trips to Sicily and Italy for the sake of his health and died in northern Italy. Refs. (4.5) and (4.6) |
| **1870** Rankine publishes ON THE THERMODYNAMIC THEORY OF WAVES OF FINITE LONGITUDINAL DISTURBANCE. In this major breakthrough in shock theory, Rankine successfully derived a relation ship for the thermodynamic changes across a shock. In the paper, he clearly presented the proper normal shock equations for continuity, momentum, and energy. Further, he properly assumed that the internal structure of the shockwave was not isentropic (contrary to Riemann's assumption), but rather that |  **William John Macquorn Rankine** Born: 5 July 1820 in Edinburgh, Ayrshire, Scotland Died: 24 Dec 1872 in Glasgow, Scotland Rankine's childhood health was poor, and he attended school only for short periods. His early schooling was from his father, who was a railroad superintendent and who probably introduced his son to civil engineering. He studied chemistry, botany, and natural history and gave much attention to music theory. When he was 14, he was given Newton's *Principia* (in Latin), which he eagerly read. At age 16, he entered the University of Edinburgh, where he studied a variety of subjects for two years. He skipped mathematics lectures and seems to have taught himself. During this time, he also worked with his father. In 1838, he left school without a |

(*Continued*)

**TABLE 4.1** (Continued)

| Year/Event | Person/Biographical Sketch |
|---|---|
| it was a dissipation region. He was thinking of thermal conduction, not the companion effect of viscosity within the shock. Rankine showed that no steady adiabatic process having forces due only to pressure can represent a continuous change over a small infinite region from one constant state to another. He proposed that across this region a non-adiabatic process occurs subject to the condition that heat may be communicated from one particle to another, but that no outside heat is received. Hugoniot subsequently pointed out that an adiabatic process would in fact violate the principle of conservation of energy. Refs. (4.8), (4.9), and (4.11) | degree to apprentice as a civil engineer to J. MacNeill and others working on various waterworks, harbor, and railroad projects in Ireland and Scotland. In 1855, he was appointed Regius Professor of Civil Engineering and Mechanics at Glasgow University. During his lifetime, he wrote on railway-axle metal fatigue, earth pressures, stability of retaining walls, cooling of the earth, thermodynamic cycles, the dynamical theory of heat and energy, ship hull resistance and motions, explosions in grain mills, force distributions in framed structures, prediction of the true value of the specific heat of air, water compressibility, and the oscillatory theory of light. He also wrote manuals on applied mechanics, steam engines and other prime movers, civil engineering, machinery and millwork, and useful rules and tables. He also was a writer, composer, and singer of humorous and patriotic songs, as well as a keen cellist, pianist, and vocalist. His health deteriorated rapidly during the final six months of his life. Refs. (4.6), (4.11), and (4.13) |
| **1887** Hugoniot publishes SUR LA PROPAGATION DU MOUVEMENT DANS LES CORPS ET SPÉCIALEMENT DANS LES GAZ PARFAITS (On the Propagation of Motion in Bodies and in Perfect Gases in Particular)–Part I. In 1889, Part II was published. Unaware of Rankine's work, this ballistician independently discovered the normal shock equations. To this day, the governing equations for flow across a shock wave are called the Rankine–Hugoniot equations, in their honor. Rankine's condition agrees with the first law of thermodynamics, but Hugoniot clearly showed that an adiabatic reversible transition in a shock would violate the first law. He showed that in the absence of viscosity and heat conduction (outside the shock), the first law implies conservation of entropy in continuous flow, as well as a change of entropy across a shock. From the first law, he also deduced the third shock condition in its customary form, which is preferable to Rankine's form, although in the case of a perfect gas, Rankine's three shock conditions are equivalent to those of Hugoniot. Refs. (4.8)–(4.11) | **Pierre Henri Hugoniot**<br>  <br>Born: 5 June 1851 in Allenjoie, Doubs, France<br>Died: 1887 in Nantes, Loire-Inférieure, France<br>Hugoniot, the son of a metallist in a small village, was very successful in his studies and by the age of 18 had graduated in the mathematical sciences. At age 19, he was admitted to the École Polytechnique. His academic performance there steadily progressed until he was declared acceptable for public service in 1872 and, finally, was accepted in the marine artillery service. He devoted all of his energies to this service for the remainder of his life. He became professor of mechanics and ballistics at the Lorient Artillery School in 1879 and, in 1882, assistant director of the central laboratory of the Marine Artillery. In January 1884, he was appointed captain of the Marine Artillery, and a few months later he was appointed an auxiliary assistant in mechanics at the École Polytechnique. There, he finally found the time and surroundings to settle the question with which he was constantly faced as a gunner: *the propagation of movements in bodies, particularly in perfect gases.* It took him only 15 months to find the answer, and in October 1885 he submitted his work—a memoir that was published in two volumes, the first in 1887. The second volume (1889) was delayed, as Hugoniot died suddenly on a trip to Nantes and "was unable to make the necessary changes and additions to his original text which it seems he had the intention of making." Ref. (4.5) |

(*Continued*)

**TABLE 4.1** (Continued)

| Year/Event | Person/Biographical Sketch |
|---|---|
| **1910** Rayleigh publishes AERIAL PLANE WAVES OF FINITE AMPLITUDE. The works of both Rankine and Hugoniot did not tell us the direction of the changes across a shockwave. Both works allow the mathematical possibility of either compression or rarefaction shocks. It was not until 1910 that this ambiguity was resolved. In two almost simultaneous and independent papers, first Rayleigh (in the paper cited here) and then Taylor invoked the second law of thermodynamics to show that only compression shocks are physically possible; that is, the Rankine–Hugoniot relations apply physically only to the case where the pressure behind the shock is greater than the pressure in front of the shock. Besides applying the second law of thermodynamics, Rayleigh also showed that viscosity played as essential a role in the structure of a shock as conduction. As noted previously, Rankine considered conduction only; Hugoniot obtained his results without reference to any dissipative mechanism. Ref. (4.11) |  <br>**Lord Rayleigh (John William Strutt)**<br>Born: 12 Nov 1842 in Langford Grove (near Maldon), Essex, England<br>Died: 30 June 1919 in Terling Place, Witham, Essex, England<br>As a boy, Rayleigh was sickly, and his schooling was disrupted. In 1861, he entered Trinity College, Cambridge, graduated in 1865, and became a fellow in 1866. After returning from a trip to America, he set up a laboratory at his family estate in Terling. Soon after marrying in 1871, he developed rheumatic fever and was advised to travel to Egypt for his health. Shortly after he returned from Egypt, his father died and he succeeded to the title Third Baron Rayleigh. From 1879 to 1884, Rayleigh was Cavendish Professor of Experimental Physics at Cambridge, but in 1884, he resigned to return to his first passion: scientific research at Terling. He helped to found the National Physical Laboratory, which opened at Teddington in 1900. From 1908 until his death, he served as chancellor of Cambridge. During his lifetime, he wrote on many topics in applied mathematics and physics: electro-magnetic phenomena, theory of sound, establishment of the ohm, scattering of light (which explained why the sky is blue), the method of reproducing colors by photography, aerodynamic drag theory, and hydrodynamic similarity theory. He also wrote on unusual topics such as insects and the color of flowers, the irregular flight of a tennis ball, the soaring of birds, the sailing flight of the albatross, and "the problem of the whispering gallery." Rayleigh is perhaps most famous for his discovery and isolation of argon in 1895, which earned him a Nobel Prize in 1904. He donated the proceeds of the prize to build an extension to the Cavendish laboratories. Refs. (4.5) and (4.6) |
| **1910** G. I. Taylor publishes a short paper entitled THE CONDITIONS NECESSARY FOR DISCONTINUOUS MOTION IN GASES one month after Rayleigh published his aforementioned paper in the same journal. This paper supported Rayleigh's conclusions. So, finally, the theory of shockwaves was fully established. Taylor would go on to become one of the leading fluid dynamicists of the 20th century. The blast wave associated with an explosion is essentially a shockwave of spherical form initiated by the impulsive release of a fixed quantity of energy. The finite-energy condition complicates the flow structure behind the blast wave, particularly if the wave is a strong one. This problem was discussed by Taylor (1950), who compares his theoretical estimates with observations made when the first atomic bomb was exploded in New Mexico in 1945. Refs. (4.8) and (4.11) |  <br>**Geoffrey Ingram Taylor**<br>Born: 7 March 1886 in St. John's Wood, London, England<br>Died: 27 June 1975 in Cambridge, England<br>In 1899, Taylor entered Trinity College, Cambridge, to read mathematics, and he stayed at Cambridge for the rest of his life. His early research was in optics and discontinuous motion in gases. The *Scotia* was the first vessel sent on the International Ice Patrol in 1913, and Taylor served as its meteorologist for six months. There, he studied lower-atmosphere mixing processes by taking pressure, humidity, and temperature data. He based his theoretical model of turbulent mixing on these data. His studies of turbulence are considered his most important scientific contributions. During World War I, he worked on the stress distribution in propeller shafts. This research led him to consider the limiting strengths of materials and his theory of dislocations in metals. Afterwards, he returned to Trinity College. During World War II, Taylor worked on the propagation of blast waves and shockwaves in the air and underwater. He retired in 1952, yet continued his work at Cambridge until 1972, when he suffered a stroke. During his lifetime, he worked on solid and fluid mechanics topics and their application in meteorology, oceanography, aeronautics, metal physics, mechanical and chemical engineering, and applied mathematics. He was a keen botanist and took great pleasure in plants. Refs. (4.5) and (4.6) |

**Solution**

At $M_i = 2.0$, from the isentropic relations with $\gamma = 1.4$, we have

$$\frac{A_i}{A_1^*} = 1.6875$$

Therefore,

$$\frac{A_1}{A_1^*} = \left(\frac{A_1}{A_i}\right)\left(\frac{A_i}{A_1^*}\right) = (2)(1.6875) = 3.3750$$

Using the Newton–Raphson iterative procedure discussed in Section 3.4, and taking the supersonic root because the flow on the upstream side of the shock must be supersonic, we obtain $M_1 = 2.7617$. With the upstream shock Mach number determined, ratios of properties across the shock can be found from normal shock relations, which are then combined with Eq. (4.21) to give

$$\frac{p_{o2}}{p_{o1}} = 0.4022 = \frac{A_1^*}{A_2^*}$$

or

$$\frac{A_e}{A_2^*} = \left(\frac{A_e}{A_i}\right)\left(\frac{A_i}{A_1^*}\right)\left(\frac{A_1^*}{A_2^*}\right) = (3.0)(1.6875)(0.4022) = 2.0361$$

Again, using the Newton–Raphson procedure, we see that this area ratio produces the following subsonic value at the exit: $M_e = 0.2998$. We can now solve for the exit pressure $p_e$:

$$\frac{p_e}{p_i} = \left(\frac{p_e}{p_{o2}}\right)\left(\frac{p_{o2}}{p_{o1}}\right)\left(\frac{p_{o1}}{p_{oi}}\right)\left(\frac{p_{oi}}{p_i}\right) = (0.9395)(0.4022)(1.0)\left(\frac{1}{0.1278}\right) = 2.9567$$

With subsonic flow at the channel exit, the channel back pressure is equal to the exit-plane pressure:

$$p_e = 100(2.9567) = 295.6705 \text{ kPa} = p_b$$

## 4.4 STATIONARY NORMAL SHOCKWAVE IN A CONVERGING–DIVERGING NOZZLE

Isentropic flow in a converging–diverging nozzle was examined in Section 3.6. It was pointed out that for certain ratios of back pressure to supply pressure, isentropic, one-dimensional solutions to the equations of motion are not possible. Returning to the system illustrated in Figure 3.14, we consider the case in which a fluid stored in a large reservoir is to be discharged through a converging–diverging nozzle. It is desired to find the pressure distribution in the nozzle over a range of values of $p_b/p_r$, with $p_r$ maintained constant, as illustrated in Figure 4.14.

With $p_b = p_r$, there is no flow in the nozzle. As $p_b$ is reduced below $p_r$, subsonic flow is induced through the nozzle, with pressure decreasing until the throat and then increasing in the diverging portion of the nozzle.

For subsonic flow, the pressure is at a minimum at the throat, which we can prove as follows: It was pointed out in Section 3.3 that the condition $dA/dx = 0$ was

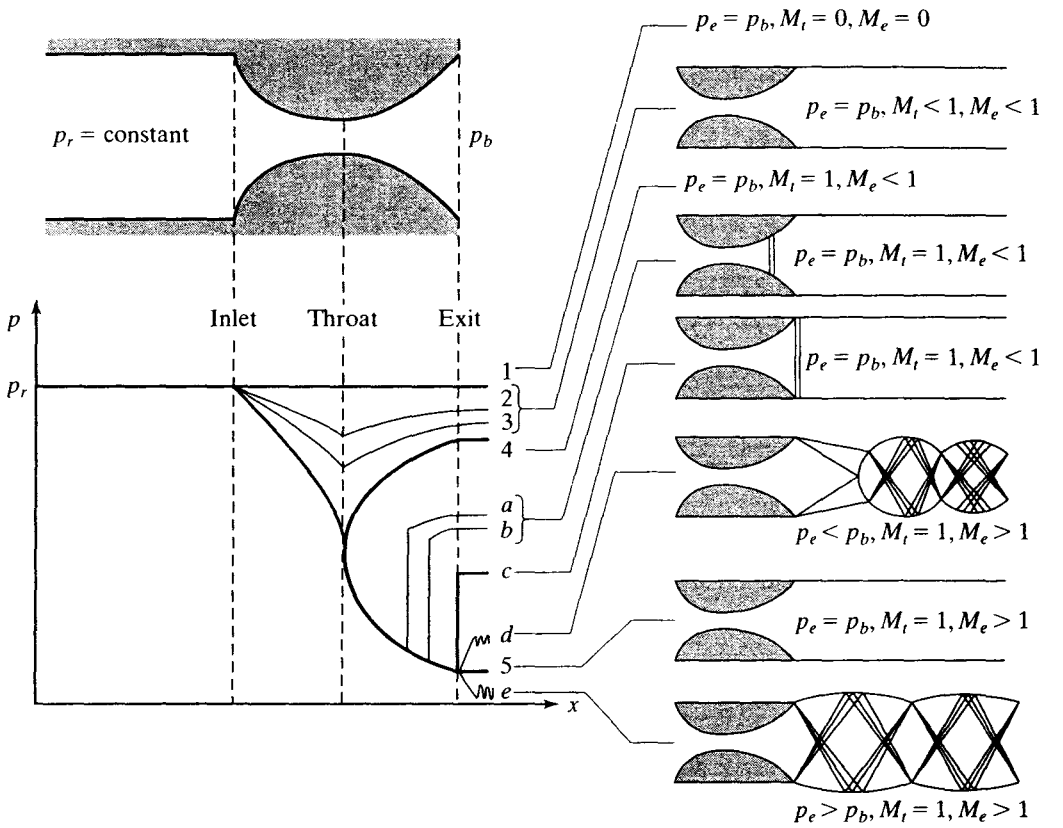


**Figure 4.14** Pressure Distribution in a C–D Nozzle

required at the throat in order to avoid the mathematical problem with Eq. (3.9) when $M = 1$,

$$\frac{dp}{dx} = \frac{\rho V^2}{A(1 - M^2)} \frac{dA}{dx} \tag{3.9}$$

Consequently, we may use the chain rule to obtain

$$\frac{dA}{dx} = \left(\frac{dA}{dp}\right)\left(\frac{dp}{dx}\right) = 0$$

Because this expression is a product of two terms, it can be satisfied if either term vanishes. However, from Eq. (3.9), at $M \neq 1$, $dA/dp \neq 0$. Therefore, $dp/dx$ must be zero. Further analysis reveals that $d^2p/dx^2 > 0$, which indicates that the pressure distribution for steady, one-dimensional, isentropic, subsonic flow in a C–D nozzle has a minimum value at the throat.

When the back pressure is lowered to that of Curve 4, sonic flow occurs at the nozzle throat. Further reductions in back pressure can induce no more flow through the nozzle. As the back pressure is reduced below that of Curve 4, a normal shock appears in the nozzle just downstream of the throat (Curve *a*). Further reduction of $p_b$ results in the shock being pushed farther downstream (for example, Curve *b*), until, for

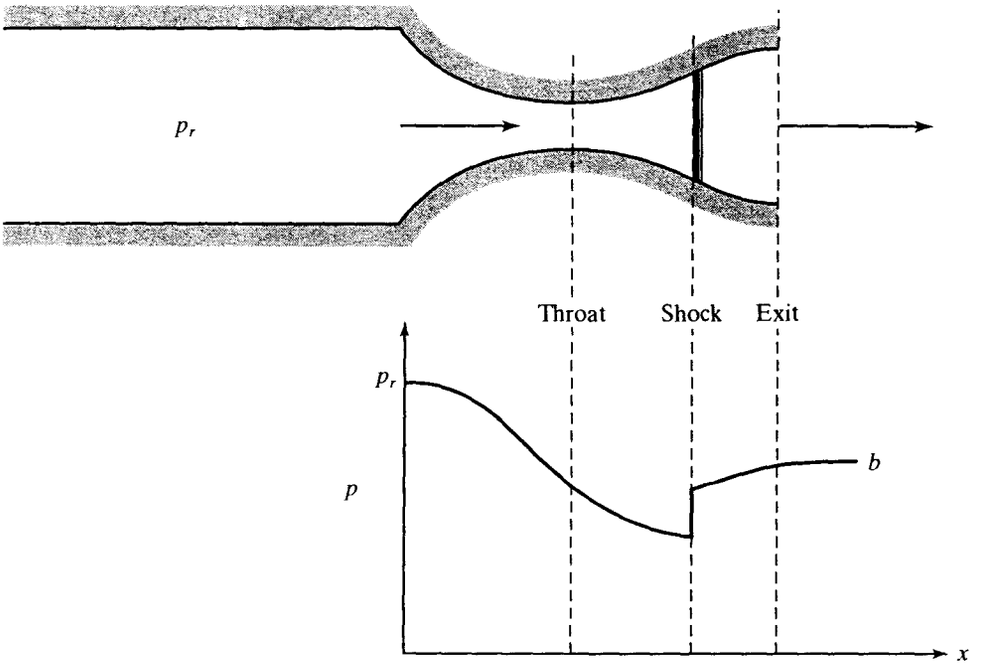


**Figure 4.15** Pressure Distribution in a C–D with a Shockwave

a low-enough back pressure, the normal shock positions itself at the nozzle exit plane (Curve *c*).

Consider in detail a curve of $p$ versus $x$ with a shock in the nozzle. (See Figure 4.15.) The static pressure decreases in the converging portion of the nozzle, with $M = 1$ at the throat. In the diverging portion, with the flow supersonic, the pressure continues to decrease up to the normal shock. After the shock, flow in the diverging part of the nozzle is subsonic, and the static pressure increases to the exit plane pressure. With subsonic flow at the exit, the exit-plane pressure is equal to the back pressure.

As the back pressure is lowered below that of Curve *c* in Figure 4.14, a shockwave inclined at an angle to the flow appears at the exit plane of the nozzle. (See Figure 4.16.) This discontinuity, weaker than a normal shock, is called an *oblique shock.*

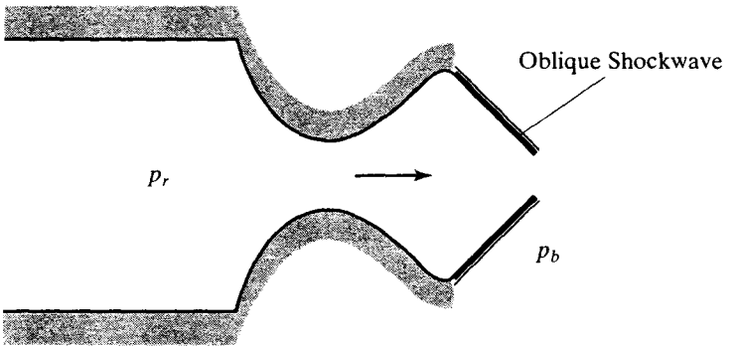


**Figure 4.16** Oblique Shocks at the Exit of a C–D Nozzle

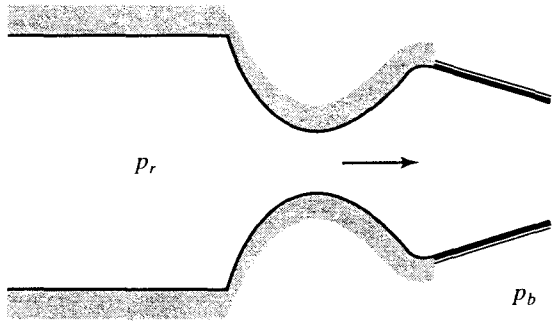


**Figure 4.17** Oblique Shocks at the Exit of a C–D Nozzle

Further reductions in back pressure cause the angle between the oblique shock and the flow to decrease, thus decreasing the shock strength (see Figure 4.17), until eventually the isentropic case, Curve 5 in Figure 4.14, is reached.

Curve 5 corresponds to the design condition in which the flow is perfectly expanded in the nozzle to the back pressure. For back pressures below that of Curve 5, the exit-plane pressure is greater than the back pressure. A pressure decrease occurs outside the nozzle in the form of expansion waves. (See Figure 4.18.) Oblique shockwaves and expansion waves represent flows that are not one dimensional and therefore cannot be treated directly with the methods of Chapters 3 and 4. These flows will be analyzed in detail in Chapters 6 and 7.

It is important to realize that, for all back pressures below that of Curve *c* in Figure 4.14, the flow downstream of the exit plane adjusts to the back pressure outside the nozzle. Over this range of back pressures (below Curve *c*), flow inside the nozzle remains unchanged as the back pressure is diminished. Accordingly, the exit-plane pressure and exit velocity are the same for all back pressures below Curve *c*. If a rocket nozzle is designed to operate isentropically at sea level, the rocket exhaust velocity and exit-plane pressure do not change as the rocket moves upward through the atmosphere (assuming constant chamber temperature and pressure).

Figure 4.19 depicts the variation of exit-plane pressure with back pressure. For subsonic flow at the exit plane (Curves 1 to 4 and *a* to *c* in Figure 4.14) and for the

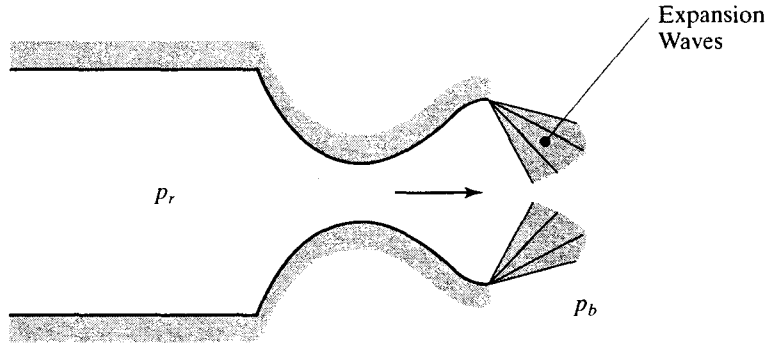


**Figure 4.18** Expansion Waves at the Exit of a C–D Nozzle

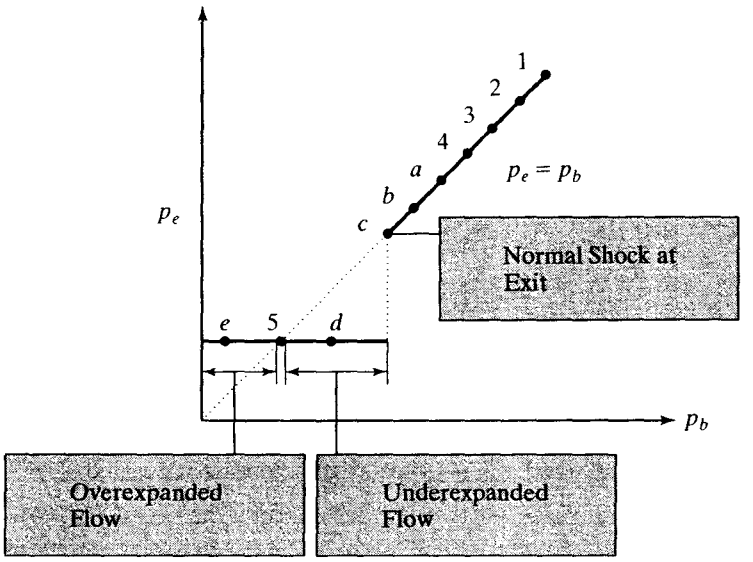


**Figure 4.19** Exit Pressure versus Back Pressure for a C–D Nozzle

supersonic design condition (Curve 5), the exit-plane pressure is equal to the back pressure. For supersonic flow at the exit plane (Curves *d*, 5, and *e*), the exit-plane pressure is equal to that for the design condition. For back pressures between Curves *c* and 5 in Figure 4.14, the exit-plane pressure is less than the back pressure, so the nozzle is termed *overexpanded*. For back pressures below Curve 5, with the exit-plane pressure greater than the back pressure, the nozzle is termed *underexpanded*.

Nozzle design and operation have been studied up to this point by means of a one-dimensional flow analysis. Although this method of analysis is adequate for the solution of many engineering problems, certain limitations become apparent. For example, in the design of a supersonic nozzle, area ratios can be determined for a given supersonic Mach number. However, the length of the nozzle or the rate of change of area with axial distance cannot be prescribed from one-dimensional-flow considerations. Furthermore, due to the presence of boundary layers on the nozzle walls, the area available to the main flow is somewhat reduced; the areas calculated from a one-dimensional flow analysis may have to be enlarged to account for boundary layers. For an exact and complete analysis of the operation and design of a converging–diverging nozzle, a study of two- and three-dimensional compressible flow is required. However, this work should not detract from the one-dimensional analysis under study; good engineering approximations can be obtained for the solution of a wide range of compressible-flow problems.

As we have seen under certain conditions, a normal shockwave can exist within the diverging section of a C–D nozzle.

The upper pressure ratio limit (Curve 4 in Figure 4.14) occurs when the throat area $A_t = A^*$—that is, the throat Mach number is unity. The subsonic solution of Eq. (3.23) for the given $A_e/A_t$, where the Newton–Raphson method is used to solve Eq. (3.24), yields the corresponding exit Mach number $M_e$. With this Mach number in Eq. (3.15), we can determine the overall pressure ratio $p_e/p_{o1} = p_b/p_{o1}$.

The lower pressure ratio limit (Curve $c$ in Figure 4.14) occurs when a normal shock stands in the exit plane of the C–D nozzle. In this case, we first obtain the supersonic solution of Eq. (3.23) for the given $A_e/A_t$, using the Newton–Raphson method. This produces the Mach number just upstream of the shock. From this Mach number, we can then find the static-pressure ratio across the shock, $p_2/p_1$, from Eq. (4.12), as well as $p_1/p_{o1}$ from Eq. (3.15). A shock appears at the exit of the nozzle for an overall pressure ratio $p_b/p_{o1} = (p_2/p_1)(p_1/p_{o1})$.

**Example 4.4. Calculations of a stationary normal shockwave in a C–D nozzle**

A converging–diverging nozzle is designed to operate with an exit Mach number of 1.75. The nozzle is supplied from an air reservoir at 5 MPa. Assuming one-dimensional, steady flow with $\gamma = 1.4$, calculate the following:

(a) the maximum back pressure to choke the nozzle;

(b) the range of back pressures over which a normal shock will appear in the nozzle;

(c) the back pressure for the nozzle to be perfectly expanded to the design Mach number;

(d) the range of back pressures for supersonic flow at the nozzle exit plane.

**Solution**

The nozzle is designed for $M_e = 1.75$. From the isentropic-area–Mach-number relation, Eq. (3.23), at $M_e$, we find that $A_e/A_t = A_e/A^* = 1.3865$.

(a) The nozzle is choked with $M = 1$ at the throat, followed by subsonic flow in the diverging portion of the nozzle. From the isentropic relations at $A/A^* = 1.3865$, we have $M_e = 0.4770$ and $(p/p_o)_e = 0.8558$. Therefore, the nozzle is choked for $p_b \leq (0.8558)(5) = 4.2790$ MPa.

(b) For a normal shock at the nozzle exit plane (see Figure 4.20), $M_1 = 1.75$ and $(p/p_o)_1 = 0.1878$. Therefore, $p_1 = (0.1878)(5) = 0.9390$ MPa. From the normal shock relations at $M_1 = 1.75$, we have $p_2/p_1 = 3.4063$. For a normal shock at the nozzle exit, $p_b = p_2 = (3.4063)(0.9390) = 3.1985$ MPa. Referring to Figure 4.14, for a shock just downstream of the nozzle throat (Curve $a$), we find that $p_b = 4.279$ MPa. A normal shock will appear in the nozzle over the range of back pressures from 3.1985 to 4.2790 MPa.

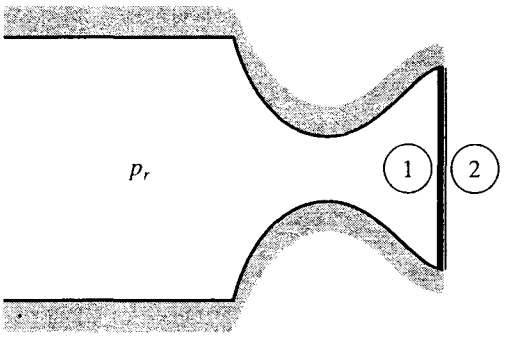


**Figure 4.20** Normal Shock Standing in the Exit Plane of a C–D Nozzle

(c) From the isentropic relations at $M_e = 1.75$, we have $(p/p_o)_e = 0.1878$. For a perfectly expanded, supersonic nozzle, $p_e = p_b = (0.1878)(5) = 0.9390$ MPa.

(d) Referring again to Figure 4.14, we find that supersonic flow will exist at the nozzle exit plane for all back pressures less than 3.1985 MPa.

## 4.5 DETERMINING THE LOCATION OF A STATIONARY NORMAL SHOCK IN A C–D NOZZLE

There are two procedures for locating a stationary normal shock in a C–D nozzle. For both methods, it is assumed here that we are given the area ratio (exit to throat), $A_e/A_t$, and the pressure ratio $p_b/p_{o1}$.

In one method, the location of the shock is specified as $A_s/A_t$, where $A_s$ is the cross-sectional area at the location of the shock. In this method, the corresponding properties are determined based on this location. If the computed values do not agree with the given information, the shock is moved to a new location and the calculations are repeated. Ultimately, this trial-and-error procedure can lead to the correct solution. The following detailed set of steps describes how to perform the calculations:

Trial-and-Error Procedure When the Shock Location Is Specified:

1. From $A_1/A_1^*$, use the Newton–Raphson method, Eq.(3.23), to determine $M_1$.
2. Use $M_1$ to determine $p_{o2}/p_{o1}$ from Eq. (4.15).
3. Note from Eq. (4.21) that $A_2^*/A_1^* = p_{o1}/p_{o2}$.
4. Compute $A_e/A_2^* = (A_e/A_1^*)(A_1^*/A_2^*)$.
5. From $A_e/A_2^*$, use the Newton–Raphson method, Eq. (3.23), to determine $M_e$.
6. Use $M_e$ in Eq. (3.15) to determine $p_e/p_{o2}$.
7. Note that $p_e/p_{o1} = (p_e/p_{o2})(p_{o2}/p_{o1})$.
8. (a) If $(p_e/p_{o1})_{\text{computed}} < (p_b/p_{o1})_{\text{given}}$, move the shock upstream; or
   (b) if $(p_e/p_{o1})_{\text{computed}} > (p_b/p_{o1})_{\text{given}}$ move the shock downstream.

One method to accomplish either Step 8(a) or 8(b) is to compute the following:

$$(A_1/A_1^*)_{\text{new}} = [(p_e/p_{o1})_{\text{computed}}/(p_b/p_{o1})_{\text{given}} - 1](A_1/A_1^*)_{\text{old}}$$

Typically, only a few iterations are required to locate the position of the shock to a reasonable degree of accuracy.

In the second method, the actual location of the shock is determined either graphically, as in Ref. (4.4), or analytically, as will be explained next. To develop a direct method of solution, we will utilize some of the same equations that were used in the trial-and-error method. We begin by writing the pressure ratio from Step 7 in the trial-and-error method. Then the total pressure ratio is replaced, using the reference area relation, Eq. (4.21), and we have

$$\frac{p_b}{p_{o1}} = \left(\frac{p_e}{p_{o2}}\right)\left(\frac{p_{o2}}{p_{o1}}\right) = \left(\frac{p_e}{p_{o2}}\right)\left(\frac{A_1^*}{A_2^*}\right) = \left(\frac{p_e}{p_{o2}}\right)\left(\frac{A_1^*}{A_e}\right)\left(\frac{A_e}{A_2^*}\right) \tag{4.22}$$

But from Eqs. (3.15) and (3.23) evaluated at the exit plane, we have

$$\frac{p_{o2}}{p_e} = \left(1 + \frac{\gamma - 1}{2} M_e^2\right)^{\gamma/(\gamma-1)} \tag{4.23}$$

$$\frac{A_e}{A_2^*} = \frac{1}{M_e}\left[\left(\frac{2}{\gamma + 1}\right)\left(1 + \frac{\gamma - 1}{2} M_e^2\right)\right]^{\frac{\gamma+1}{2(\gamma-1)}} \tag{4.24}$$

Combining Eqs. (4.22), (4.23), and (4.24) and rearranging the result yields

$$\left(\frac{p_b}{p_{o1}}\right)\left(\frac{A_e}{A_t}\right) = \left(\frac{p_b}{p_{o1}}\right)\left(\frac{A_e}{A_1^*}\right) = \frac{1}{M_e}\left(\frac{2}{\gamma + 1}\right)^{\frac{\gamma+1}{2(\gamma-1)}}\left(1 + \frac{\gamma - 1}{2} M_e^2\right)^{\frac{\gamma+1}{2(\gamma-1)} - \frac{\gamma}{(\gamma-1)}}$$

$$\left(\frac{p_b}{p_{o1}}\right)\left(\frac{A_e}{A_t}\right) = \frac{1}{M_e}\left(\frac{2}{\gamma + 1}\right)^{\frac{\gamma+1}{2(\gamma-1)}}\left(1 + \frac{\gamma - 1}{2} M_e^2\right)^{-\frac{1}{2}} \tag{4.25}$$

Note that the left-hand side of Eq. (4.25) is the product of the given information, while the right-hand side depends only on $\gamma$ and $M_e$. Equation (4.25) is a quadratic in terms of $M_e^2$, which can be solved to produce

$$M_e^2 = -\frac{1}{\gamma - 1} + \sqrt{\left(\frac{1}{\gamma - 1}\right)^2 + \left(\frac{2}{\gamma - 1}\right)\left(\frac{2}{\gamma + 1}\right)^{(\gamma+1)/(\gamma-1)}\left(\frac{p_{o1}}{p_b}\right)^2\left(\frac{A_t}{A_e}\right)^2} \tag{4.26}$$

Once the exit Mach number is computed, the remaining portion of the problem is straightforward:

*Direct Procedure When the Shock Location Is Not Specified*

1. Determine $M_e$ from Eq. (4.26).
2. Use $M_e$ to determine $p_e/p_{o2}$ from Eq. (4.23).
3. Since $M_e < 1$, $p_e = p_b$, so form the product $(p_b/p_{o1})(p_{o2}/p_e) = p_{o2}/p_{o1}$.
4. Use the Newton–Raphson method to solve Eq. (4.15), given $p_{o2}/p_{o1}$ from Step 3, to determine $M_1$.
5. Determine $A_s/A_1^* = A_s/A_t$ from Eq. (3.23).

**Example 4.5. Determining the location of a stationary normal shock wave in a C–D nozzle**

The back-pressure-to-reservoir-pressure ratio is 0.7 for a C–D nozzle, with an exit-to-throat-area ratio of 2.0. Determine the cross-sectional area location of a normal shock for $\gamma = 1.4$.

**Solution**

The first step in the process is to find the range of pressure ratios that will produce a shock in the diverging portion. Using the area ratio, we find the upper limit (i.e., the pressure ratio that will produce a shock just downstream of the throat) to be $p_b/p_{o1} = 0.9372$. Using the Newton–Raphson method, we find that this procedure requires the subsonic solution for the given area ratio. Next, the lower limit is determined in which a shock stands in the

exit plane. This task is accomplished first by determining the Mach number just upstream of the shock (using the Newton–Raphson method to find the supersonic solution for the given area ratio) to be $M_1 = 2.1972$, from which we find the static-to-stagnation-pressure ratio $p_1/p_{o1} = 0.0939$ and the static-pressure ratio across the shock $p_2/p_1 = 5.4656$. Thus, taking the product of these gives the lower pressure ratio limit of 0.5134.

Accordingly, since the given pressure ratio of 0.7 is between the upper limit 0.9372 and the lower limit 0.5134, a shock will reside somewhere within the nozzle. To determine its location, we will use the five-step direct procedure described previously. Using the given information, we obtain

1. $M_e = 0.4067$,
2. $p_e/p_{o2} = 0.8923$,
3. $p_{o2}/p_{o1} = 0.7/0.8923 = 0.7845$,
4. $M_1 = 1.8627$, and
5. $A_s/A_t = 1.5101$.

A spreadsheet program may be easily constructed to perform the calculations. To check these calculations, we could use our result (i.e., $A_s/A_t$) and the trial-and-error procedure, for the situation when the shock location is specified, to make certain that we have not made an error. This operation will be left as an exercise. (See Problem 4.25.)

## 4.6 CONVERGING–DIVERGING SUPERSONIC DIFFUSER

In an air-breathing jet-propulsion engine, forward thrust is provided by the acceleration of an airstream. In both the turbojet and ramjet, the air is compressed, energy is added from the combustion of a fuel, and the resultant products are ejected from the exhaust nozzle at high velocity. (See Figure 4.21.) With the jet engine, the inlet or diffuser must take the incoming air, traveling at high velocity with respect to the engine, and slow it down before entrance to the axial compressor of the turbojet or the combustion zone of the ramjet engine. The amount of static-pressure rise achieved during deceleration of the flow in the diffuser is of prime importance to the operation of the jet engine, since the pressure of the air entering the nozzle determines to a large extent the magnitude of the nozzle exhaust velocity. The maximum pressure that can be achieved in the diffuser is the isentropic stagnation pressure. Any loss in available energy (or stagnation pressure) in the diffuser, or, for that matter, in any other component of the engine, will have a harmful effect on the operation of the engine as a whole. For a supersonic diffuser, it would be highly desirable to provide shock-free isentropic flow.

A first approach to obtaining shock-free flow is to operate a converging–diverging nozzle in reverse. (See Figure 4.22.) At the design Mach number $M_D$ for such a diffuser, there is no loss in stagnation pressure (neglecting friction). However, off-design performance has to be considered, since the external flow must be accelerated to the design condition. For example, if a supersonic converging–diverging diffuser is to be designed for a flight Mach number of 2.0, the ratio $A(\text{inlet})/A(\text{throat}) = A_i/A_t = A_i/A^* = 1.6875$ [from Eq. (3.23)]. However, for a supersonic-flight Mach number less than the design Mach number, $A/A^*$ is less than 1.6875, which indicates that the throat area is not large enough to handle this flow. Under these conditions, flow must be bypassed around the diffuser. A normal shock stands in front of the

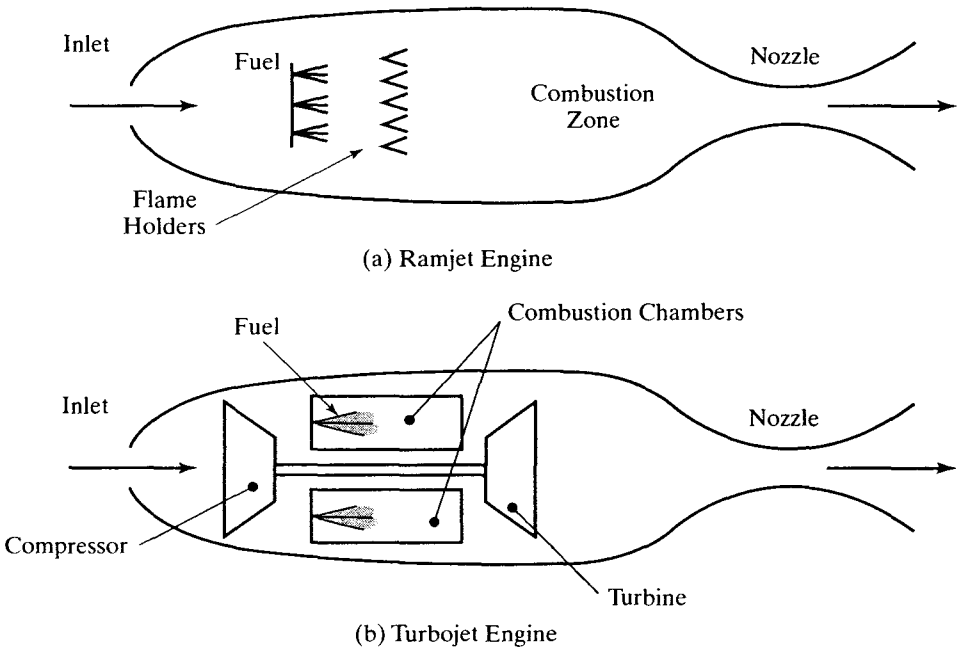


**Figure 4.21** Two Jet-Propulsion Engines

diffuser, with subsonic flow after the shock able to sense the presence of the inlet. Now, an appropriate amount of the flow "spills over," or bypasses, the inlet. (See Figure 4.23.)

As the flight Mach number is increased, the normal shock moves toward the inlet lip. When the design Mach number $M_D$ is reached during startup, however, with a normal shock in front of the diffuser, some of the flow must still be bypassed, since the throat area of less than $A_2$ is still not able to handle the entire subsonic flow after the shock. As the flight Mach number is increased above $M_D$, the shock eventually moves to the inlet lip. A further increase in $M$ causes the shock to reach a new equilibrium position in the diverging portion of the diffuser; in other words, the shock is *swallowed.* Once the shock has been swallowed, a decrease in flight Mach number causes the shock to move back toward the throat, where it reaches an equilibrium position for $M$

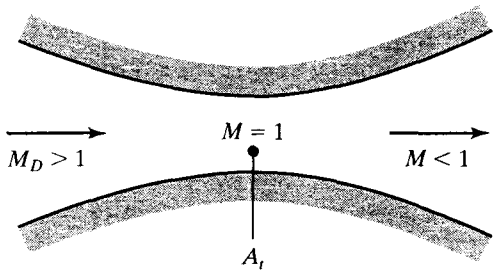


**Figure 4.22** C–D Nozzle Operated in Reverse

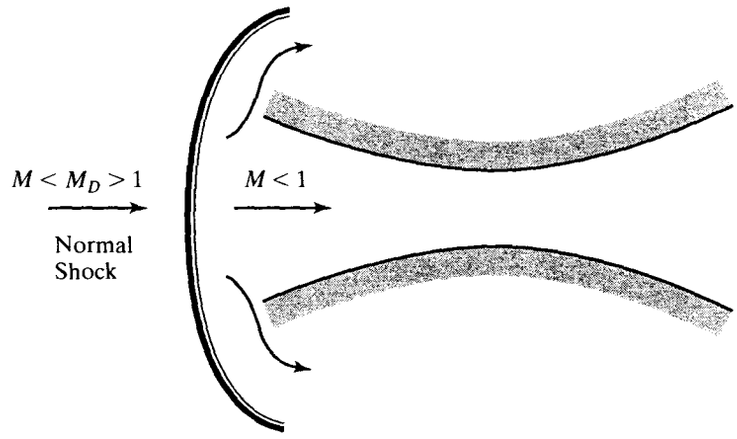


**Figure 4.23** Bypass Inlet Flow Phenomena for Flight Mach Numbers below the Design Value

equal to $M_D$. At this position, the shock is of vanishing strength, occurring at $M = 1.0$, so no loss in stagnation pressure occurs at the design condition. In actual operation, it is desirable to operate with the shock slightly past the throat; operation at the design condition is unstable in that a slight decrease in Mach number results in the shock's moving back out in front of the inlet. In this case, the operation of *overspeeding* to swallow the shock would have to be repeated. This process is summarized in Figure 4.24.

Another method for swallowing the shock is to use a variable throat area. With a shock in front of the diffuser, the throat area would be increased (say, from $A_1^*$ to $A_2^*$), which would allow more flow to pass through the inlet and consequently bring the

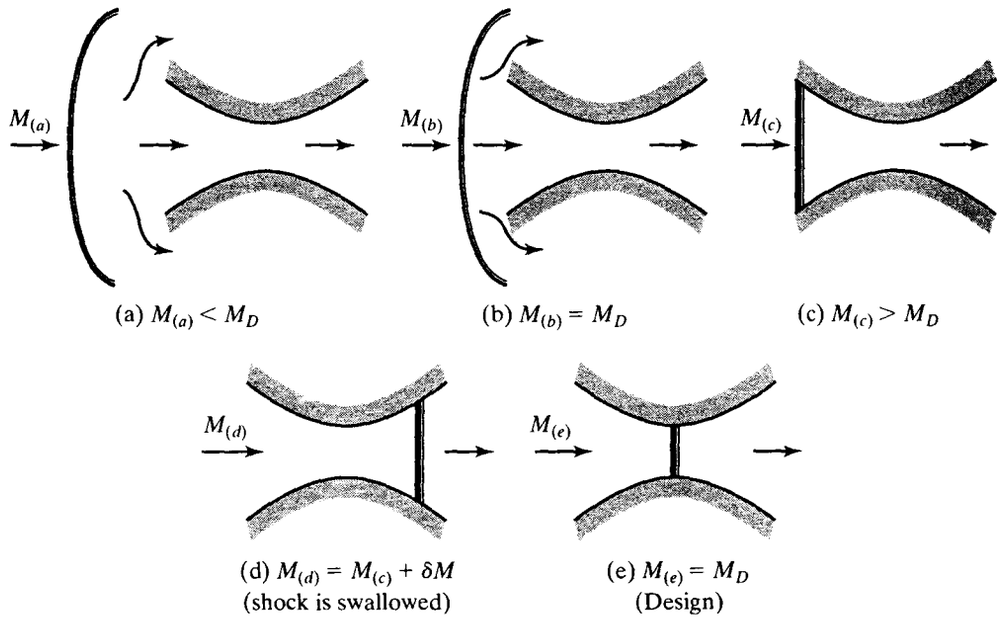


**Figure 4.24** Overspeeding of a Supersonic Inlet to Swallow a Startup Normal Shock

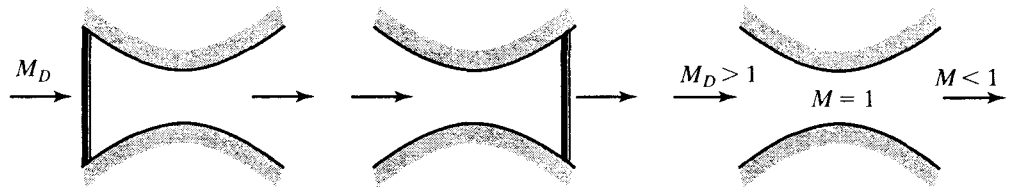


**Figure 4.25** Varying the Throat Area of a Supersonic Inlet to Swallow a Startup Normal Shock

shock closer to the inlet lip. To swallow the shock, the throat area would have to be slightly larger than the area required to accept the flow with a shock at $M_D$ at the inlet lip (i.e., slightly larger than $A_2^*$, with a normal shock at the design Mach number). For $M_D = 2.0$, from normal-shock relations, we have

$$\frac{A_{t1}}{A_{t2}} = \frac{A_1^*}{A_2^*} = \frac{p_{o2}}{p_{o1}} = 0.7209$$

Therefore, an increase of greater than $(1 - 0.7209)/0.7209 \approx 39$ percent is required to swallow the shock. Once the shock is swallowed, the throat area must be decreased to reach the design condition, as shown in Figure 4.25.

It can be readily seen that, although the converging–diverging diffuser has favorable operating characteristics at the design condition, off-design operation of such a device involves severe losses. Operation with a normal shock in front of an inlet entails prohibitive losses in stagnation pressure. To swallow this shock, the inlet flow must be accelerated beyond its design speed, or a variable throat area must be provided. Except for very low supersonic Mach numbers, the amount of overspeeding required to swallow the shock during startup becomes large enough to be totally impractical. Furthermore, the incorporation of a variable throat area into a diffuser presents many mechanical difficulties. For these reasons, the converging–diverging diffuser is not commonly used; most engines utilize the oblique-shock type described in Chapter 6.

**Example 4.6. Determination of the amount of overspeeding to swallow a normal shock**

A supersonic converging–diverging diffuser is designed to operate at a Mach number of 1.7. To what Mach number would the inlet have to be accelerated in order to swallow the shock during startup?

**Solution**

From Eq. (3.23), we find that at $M_1 = 1.7$, $A_i/A_t = A_i/A^* = 1.3376$, so the diffuser is designed with an inlet-to-throat-area ratio of 1.3376. The inlet flow must be accelerated to a Mach number slightly greater than that required to position the shock at the inlet lip. (See Figure 4.26.)

For $M = 1.0$ at the diffuser throat, with subsonic flow after a shock at the inlet lip, $A_i/A^* = 1.3376$. Using this area ratio and the Newton–Raphson procedure to determine the subsonic Mach number, we find that $M_2 = 0.5012$. From Eq. (4.9), we have $M_1 = 2.6316$.

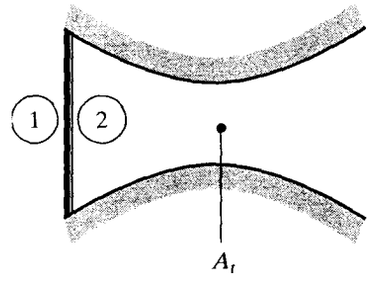


**Figure 4.26** Normal Shock at Inlet Lip

If the back-pressure conditions imposed on the diffuser are such that a Mach number of 1.0 cannot be achieved at the throat, then $M_2$ will be less than 0.5012, and a value of $M_1$ greater than 2.6316 will be required. However, with $M = 1.0$ at the diffuser throat, the diffuser must be accelerated to a Mach number slightly greater than 2.6316 in order to swallow the initial shock during startup. The impracticality of overspeeding, at least at the flight Mach numbers discussed here and for greater Mach numbers, can be readily seen from this example.

## 4.7 CHAPTER CAPSTONE APPLICATION: SUPERSONIC WIND TUNNELS

In a wind tunnel, it is desired to subject a test object to the flow conditions that the object will undergo in actual flight. The creation of a uniform supersonic flow in a test section of appreciable size, and the maintenance of this flow for a sufficient time to make meaningful measurements on a test object, may involve a large consumption of power. This section is concerned with the use of a supersonic diffuser to recover the fluid pressure after the test section and to improve the operation and reduce the power requirements of the wind tunnel.

An *intermittent, or blow-down, supersonic wind tunnel* can be constructed by allowing air at atmospheric pressure to pass through a converging–diverging nozzle into a vacuum tank. (See Figure 4.27.) With this setup, constant conditions are maintained in the test section until the back pressure in the vacuum tank rises to a value such that

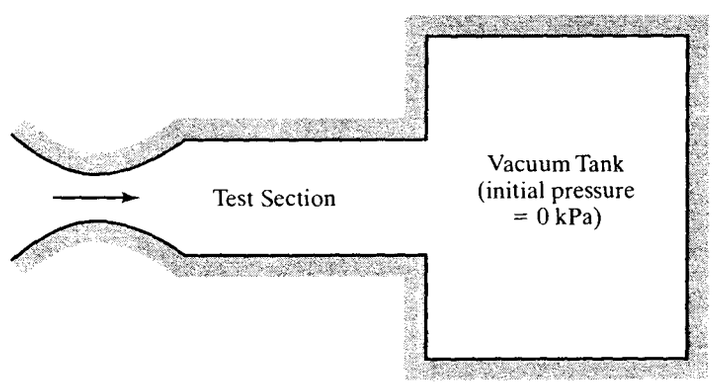


**Figure 4.27** A Blow-Down Supersonic Wind Tunnel without Diffuser

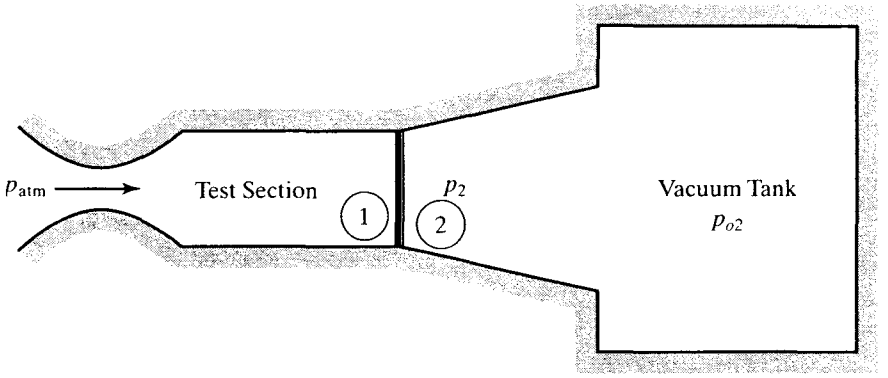


**Figure 4.28** A Blow-Down Supersonic Wind Tunnel with Diffuser

a normal shock appears in the test section (corresponding to Curve *c* of Figure 4.13). To provide a longer running time at the design Mach number, a diffuser can be placed at the test section exit. Isentropic flow in the diffuser provides a recovery of static pressure. Ideally, the wind tunnel can now be run until the pressure in the vacuum tank rises to the stagnation pressure after a shock at the design Mach number. This limiting condition is illustrated in Figure 4.28. Intermittent wind tunnels present the problem of providing only a relatively short test time before the back pressure rises to a limiting value, at which point flow in the test section ceases to be supersonic.

In a *continuous closed-circuit tunnel*, test conditions can be maintained almost indefinitely. A compressor is used to boost the air pressure from a somewhat reduced value after the test section to the inlet stagnation pressure $p_{o1}$. (See Figure 4.29.) Naturally, the greater the pressure recovery after the test section, the smaller are the compressor power requirements. The use of a normal shock pressure recovery, as shown in Figure 4.28, has the disadvantage of always entailing a loss in stagnation pressure. Even if a perfect diffuser were provided after the shock, causing a rise in pressure to $p_{o2}$, the compressor would still need to provide the pressure difference $p_{o1} - p_{o2}$, which increases as the test section Mach number is increased.

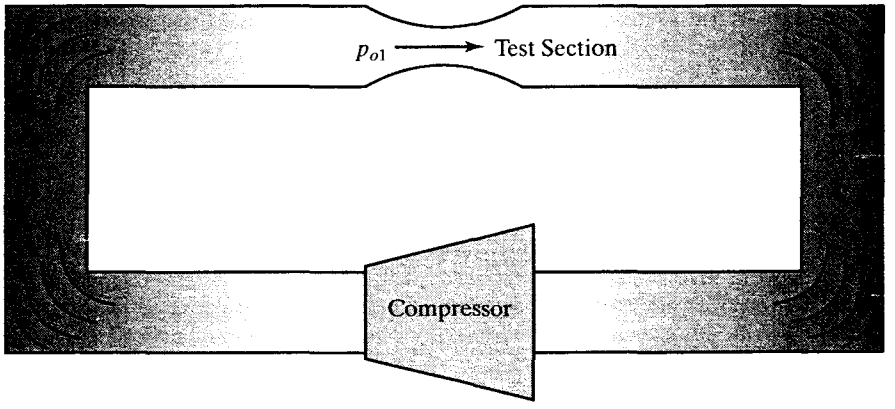


**Figure 4.29** Continuous, Closed-Circuit, Supersonic Wind Tunnel

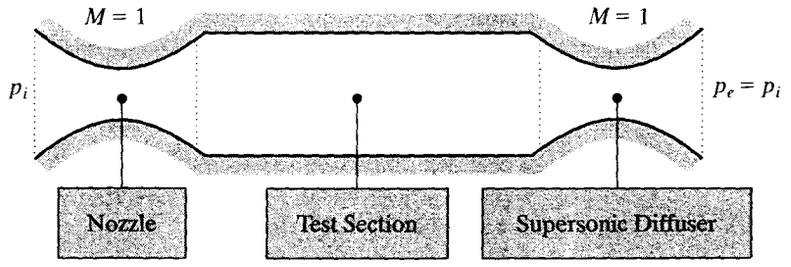


**Figure 4.30** Ideal Case of a Double-Throated Supersonic Wind Tunnel

To provide isentropic deceleration and complete pressure recovery after the test section, consider the system shown in Figure 4.30, with a second throat after the test section. In the configuration shown, neglecting friction and boundary-layer effects, the wind tunnel could be run at design conditions indefinitely, with no pressure difference required to maintain the flow. However, difficulties arise during startup of the system. To initiate flow, a pressure difference must be maintained across the entire system. As the pressure ratio $p_b/p_i$ is decreased from 1.0, the situation for the converging–diverging nozzle is the same as that discussed in Section 4.4. Eventually, the flow condition shown in Figure 4.31 is attained.

Now a decrease in overall pressure ratio $p_b/p_i$ causes a shock to appear downstream of the nozzle throat [see Figure 4.32(a)], with a further decrease moving the shock downstream to the nozzle exit [test section entrance; see Figure 4.32(b)]. With a shock in the diverging portion of the nozzle, there is a loss in stagnation pressure in the system. To pass the flow after the shock, the second throat must be at least $A_2^*$. The

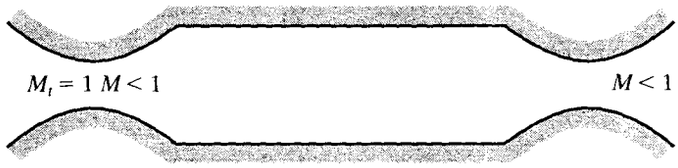


**Figure 4.31** Flow in a Double-Throated Supersonic Wind Tunnel Prior to the Appearance of a Shock

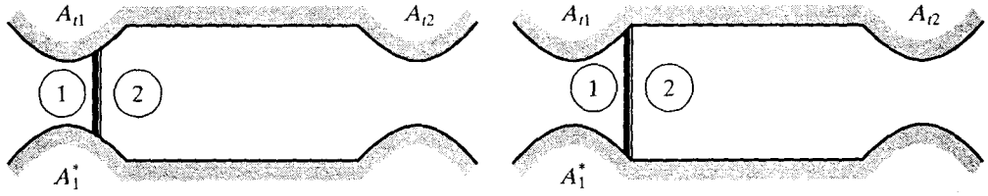


(a) Shock Downstream of Nozzle Throat (b) Shock at Nozzle Exit

**Figure 4.32** Location of Shocks in a Double-Throated Supersonic Wind Tunnel

worst possible case, involving the maximum loss in stagnation pressure, is that of a normal shock in the test section. [See Figure 4.32(b).] For this case, the second throat area must be at least $A_2^*$, with a shock at the test section Mach number. If the second throat area is less than $A_2^*$, it cannot pass the required flow, and the shock can never reach the test section and will remain in the diverging part of the nozzle. Under these conditions, supersonic flow can never be established in the test section.

For example, if the test section Mach number is 2.0,

$$\frac{p_{o2}}{p_{o1}} = 0.7209 = \frac{A_1^*}{A_2^*} = \frac{A_{t1}}{A_{t2}}$$

During startup, then, the second throat must be larger than the first by a factor of 1/0.7209, or 1.3872. This condition is illustrated in Figure 4.33. As the ratio $p_o/p_i$ is further lowered, the shock jumps to an area in the diverging part of the diffuser greater than the test section area; the shock is "swallowed" by the diffuser. (See Figure 4.34.)

To maximize the pressure recovery in the diffuser, the pressure ratio $p_o/p_i$ can now be increased, which moves the shock upstream to the diffuser throat, the position at which the shock strength is at a minimum. (See Figure 4.35.)

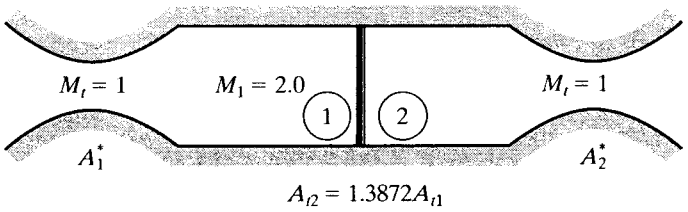


**Figure 4.33** Relation of Throat Areas Needed to Produce Supersonic Flow in the Test Section at $M = 2.0$

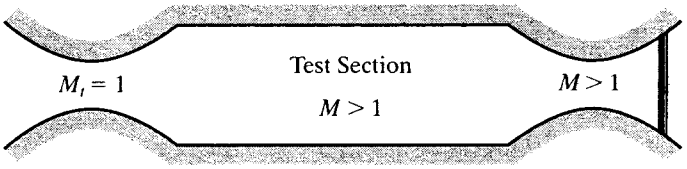


**Figure 4.34** Shock Swallowed by Diffuser

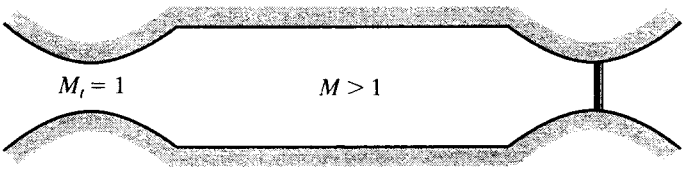


**Figure 4.35** Optimal Operating Condition of a Double-Throated Supersonic Wind Tunnel

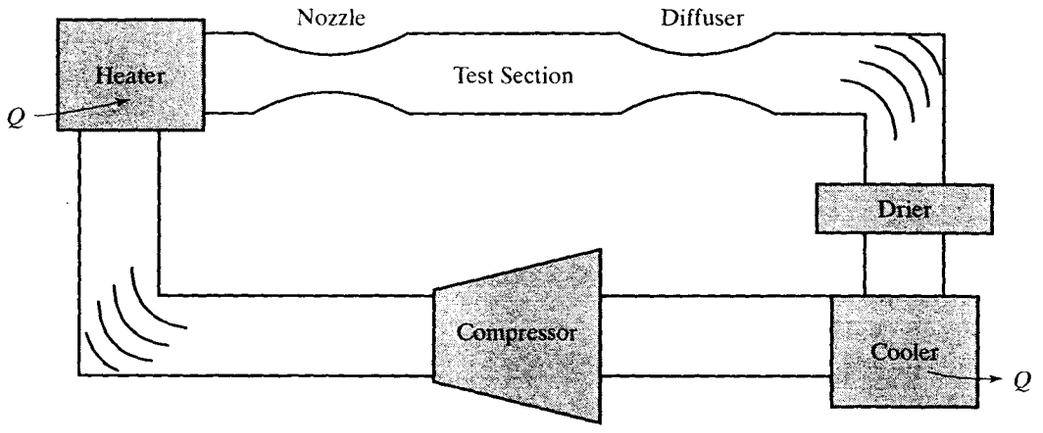


**Figure 4.36** Continuous Closed-Circuit Supersonic Wind Tunnel

Figure 4.35 represents the optimal operating condition for a fixed-geometry diffuser. There is still a loss of stagnation pressure across the shock at the diffuser throat, which must be made up for by a compressor.

An improvement can be obtained with a variable-area diffuser throat. After the initial shock has been "swallowed," we reduce the diffuser throat area to that of the nozzle throat and again raise the overall pressure ratio $p_b/p_i$ so as to bring the shock to the diffuser throat. But at the diffuser throat, the Mach number is unity, so the shock is of vanishing strength. This situation approaches the ideal of Figure 4.30.

To complete this discussion of supersonic wind tunnels, several of the components required for a continuous, cyclic system should be reviewed. (See Figure 4.36.) Besides the compressor, nozzle, and diffuser, a drier must be provided to remove water vapor from the air so as to prevent its condensation at the low static temperatures encountered in the test section. The condensation of water can lead to shockwaves, negate any measurements made in the test section, and possibly damage the test object. At higher Mach numbers, a heater may be required to raise the stagnation temperature of the inlet air and prevent condensation of the air gases (oxygen and nitrogen) in the test section. If this is impractical, a gas with low boiling point (such as helium) may have to be used in place of air. Finally, for a cycle, $\oint \delta Q = \oint \delta W$, so that an amount of energy equal to that supplied to the air by the compressor and the heater must be rejected by a cooler.

**Example 4.7. Calculation of compressor power requirements in a supersonic wind tunnel**

A continuous supersonic wind tunnel is designed to operate at a test section Mach number of 2.0, with static conditions duplicating those at an altitude of 20 km ($\gamma = 1.4$ and $c_p = 1.004$ kJ/kg·K). The test section is to be circular, 25 cm in diameter, with a fixed geometry and with a supersonic diffuser downstream of the test section. Neglecting friction and boundary-layer effects, determine the power requirements of the compressor during startup and during steady-state operation. [See Figure 4.37(a).] Assume an isentropic compressor, with a cooler located between compressor and nozzle (after the compressor), so the compressor inlet static temperature can be assumed equal to the test section stagnation temperature.

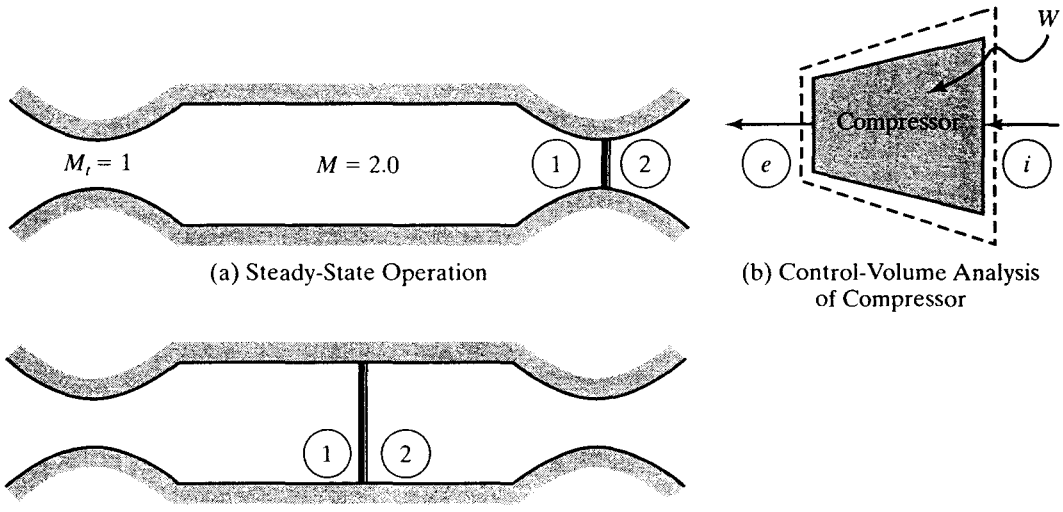


**Figure 4.37** Continuous Supersonic Wind Tunnel of Example 4.7

**Solution**

During startup, the worst possible case [see Figure 4.37(c)] is that of a shock in the test section with $M_1 = 2.0$. For this situation, which fixes the ratio of the two throat areas, we have

$$\frac{p_{o2}}{p_{o1}} = 0.7209 = \frac{A_1^*}{A_2^*} = \frac{A_{t1}}{A_{t2}}$$

To fix the size of the diffuser throat area, we first use the design Mach number to find $(A/A^*)_{\text{test}} = 1.6875$. The throat area is then determined from the following string of area ratios:

$$A_{t2} = \frac{A_{t2}}{A_{t1}}\frac{A_{t1}}{A_{\text{test}}^*}\frac{A_{\text{test}}^*}{A_{\text{test}}}A_{\text{test}} = \left(\frac{1}{0.7209}\right)(1)\left(\frac{1}{1.6875}\right)(0.04909) = 0.4035 \text{ m}^2$$

During steady-state operation [see Figure 4.37(a)], the mass flow through the test section is given by

$$\dot{m} = \rho AV = \frac{p}{RT}AM\sqrt{\gamma RT}$$

At 20 km, from Appendix H, $p = 5.5$ kPa and $T = 216.7$ K. Therefore,

$$\dot{m} = \left[\frac{5.5 \text{ kN/m}^2}{(0.287 \text{ kN/kg} \cdot \text{K})(216.7 \text{ K})}\right]\left[\frac{\pi}{4}0.25^2 \text{ m}^2\right]\left[2.0\sqrt{1.4(287 \text{ N/kg} \cdot \text{K})(216.7 \text{ K})}\right]$$

$$= (0.08843 \text{ kg/m}^3)(0.04909 \text{ m}^2)(590.1527 \text{ m/s}) = 2.5619 \text{ kg/s}$$

At the design Mach number of 2.0, $T/T_o = 0.5556$. So, the test section stagnation temperature during steady-state operation is 216.7/0.5556 = 390.0288 K.

For this fixed geometry (i.e., $A_{t2}/A_{t1} = 0.7209$), the optimum condition for steady-state operation is a normal shock at the diffuser throat. Since $M_{t1} = 1$, $A_{t1} = A^*$. Consequently, $(A/A^*)_{t2} = 1/0.7209 = 1.3872$. Using the Newton–Raphson method, we find that

$M_{t2} = 1.7506$. At steady state, this is the upstream Mach number of the shock at the diffuser throat [i.e., $M_1$ in Figure 4.37(a)]. Now from Eq. (4.15), we obtain $p_{o2}/p_{o1} = 0.8343$, where it should again be pointed out that the "1" and "2" in the subscripts are the locations within Figure 4.37(a). The loss in stagnation pressure must be compensated for by the compressor. [See Figure 4.37(b).] Performing an energy balance on the compressor, we have

$$w = h_o - h_i = c_p(T_o - T_i)$$

For an isentropic compressor,

$$\frac{T_o}{T_i} = \left(\frac{p_o}{p_i}\right)^{(\gamma-1)/\gamma}$$

$$T_o - T_i = T_i\left[\left(\frac{p_o}{p_i}\right)^{(\gamma-1)/\gamma} - 1\right] = 390.0288\left[\left(\frac{1}{0.8343}\right)^{0.2857} - 1\right] = 20.7197 \text{ K}$$

$$w = c_p(T_o - T_i) = (1.004 \text{ kJ/kg} \cdot \text{K})(20.7197 \text{ K}) = 20.8026 \text{ kJ/kg}$$

or

$$\text{Power required} = \dot{m}w = (2.5619 \text{ kg/s})(20.8026 \text{ kJ/kg}) = 53.2941 \text{ kW}$$

As mentioned previously, during startup, $p_{o2}/p_{o1} = 0.7209$. Now the isentropic compressor work required is determined as follows

$$T_o - T_i = T_i\left[\left(\frac{p_o}{p_i}\right)^{(\gamma-1)/\gamma} - 1\right] = 390.0288\left[\left(\frac{1}{0.7209}\right)^{0.2857} - 1\right] = 38.2276 \text{ K}$$

$$w = c_p(T_o - T_i) = (1.004 \text{ kJ/kg} \cdot \text{K})(38.2276 \text{ K}) = 38.3805 \text{ kJ/kg}$$

or

$$\text{Power required} = \dot{m}w = (2.5619 \text{ kg/s})(38.3805 \text{ kJ/kg}) = 98.3269 \text{ kW}$$

Hence, 84.5% more power is required during startup.

## 4.8 SUMMARY

The normal shock represents a sudden, almost discontinuous, change in fluid properties that takes place in the direction of flow. Although the shock process is adiabatic, viscous dissipation and heat conduction effects occurring internal to the wave render the shock wave an irreversible process. Thus, from the second law of thermodynamics, there must be an accompanying rise in entropy across the wave. The equations of continuity, momentum, and energy applied to the fixed shockwave reveal the variations of pressure, temperature, density, velocity, Mach number, entropy, and so on, across the wave. For an increase of entropy, the Mach number of the flow ahead of the wave must be supersonic with respect to the wave, and the flow behind the wave must be subsonic, corresponding to a compression shock. Possible solutions to the equations of motion corresponding to an expansion shock that involve a decrease of entropy are generally impossible, since they would violate the second law of thermodynamics.

The stationary normal shock often appears in supersonic flows. Thus, the ability to determine when a normal shock is present, to determine properties across it, and to determine its location is a fundamental and important gas dynamics skill.

## 4.9 REFERENCES


**4.1** Cramer, M. S., and Fry, R. N. "Nozzle Flows of Dense Gases," *Physics of Fluids*, Vol. A5, 1993, pp. 1246–1259.

**4.2** Brown, B. P., and Argrow, B. M. "Two-Dimensional Shock Tube Flow in Dense Gases," *J Fluid Mech* 1997; 349: 95–115.

**4.3** Chapman, C. J. *High Speed Flow*, Cambridge University Press, Cambridge, UK, 2000, pp. 87–98.

**4.4** Sullivan, J. A., and Hansen, A. G. "A Method for Locating the Position of a Normal Shock in a Converging–Diverging Nozzle," *Bull Mech Engng Educ* 1964; 3: 119–122.

**4.5** Johnson, J. N., and Chéret, R., eds. *Classic Papers in Shock Compression Science*, Springer-Verlag, New York, 1998.

**4.6** MacTutor, School of Mathematics and Statistics, University of St. Andrews, Fife, Scotland. http://www-groups.dcs.st-and.ac.uk.

**4.7** Department of Chemistry Web site, Yale University, New Haven, CT. http://www.chem.yale.edu/~chem125/levitron/Earnshaw.html.

**4.8** Pain, H. J., and Rogers, H. J. "Shock Waves in Gases," *Reports on Progress in Physics* 1962; 25(1): 287–336.

**4.9** Courant, R., and Friedrichs, K. O. *Supersonic Flow and Shock Waves*, Interscience Publishers, New York, 1948, pp. 118–119.

**4.10** Anderson, J. D., Jr. "Research in Supersonic Flight and the Breaking of the Sound Barrier," NASA SP-4219, Chapter 3.

**4.11** Anderson, J. D., Jr. *Modern Compressible Flow with Historical Perspective*, McGraw-Hill, New York, 1982.

**4.12** Glasgow Digital Library, Memoirs and Portraits of One Hundred Glasgow Men.


## 4.10 PROBLEMS

**4.1** A helium flow with a velocity of 2,500 m/s and static temperature of 300 K undergoes a normal shock. Determine the helium's velocity and the static and stagnation temperatures after the wave. Assume the helium to behave as a perfect gas with constant $\gamma = 5/3$ and $R = 2{,}077$ J/kg · K.

**4.2** A normal shock occurs at the inlet to a supersonic diffuser, as shown in Figure P4.2. $A_e/A_i$ is equal to 3.0. Find $M_e$, $p_e$, and the loss in stagnation pressure $(p_{oi} - p_{oe})$. Repeat for a shock at the exit. Assume $\gamma = 1.4$.

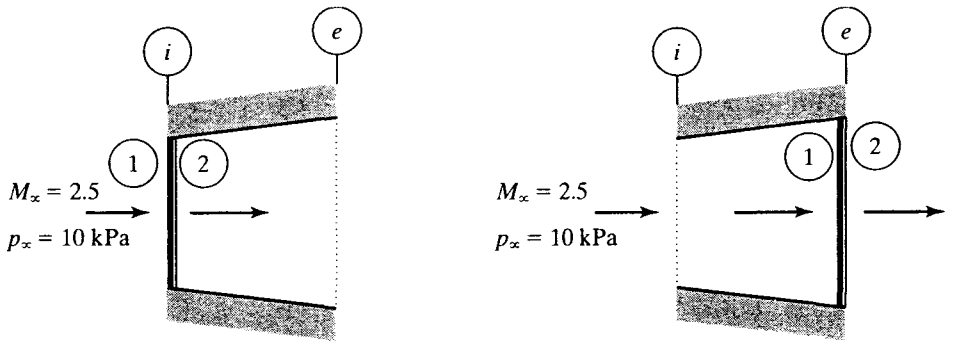


**Figure P4.2**

**4.3** Sketch $p$ versus $x$ for the three cases shown in Figure P4.3. Assume isentropic flow except for flow across the normal shocks.

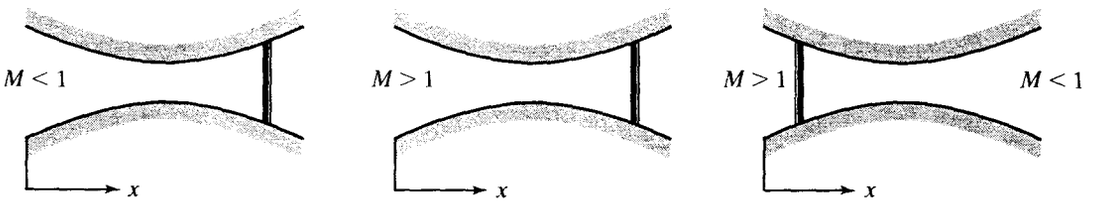


**Figure P4.3**

**4.4** Air expands from a storage tank through a converging–diverging nozzle. (See Figure P4.4.) Under certain conditions, it is found that a normal shock exists in the diverging section of the nozzle at an area equal to twice the throat area, with the exit area of the nozzle equal to four times the throat area. Assuming isentropic flow except for the shockwaves, that the air behaves as a perfect gas with constant $\gamma = 1.4$, and that the storage tank pressure and temperature are 200 kPa and 300 K, respectively, determine the following:

(a) $A^*$ for flow from inlet to shock,
(b) $A^*$ for flow from shock to exit,
(c) the mach number at the nozzle exit plane,
(d) the stagnation pressure at the nozzle exit plane,
(e) the exit plane static pressure, and
(f) the exit plane velocity.

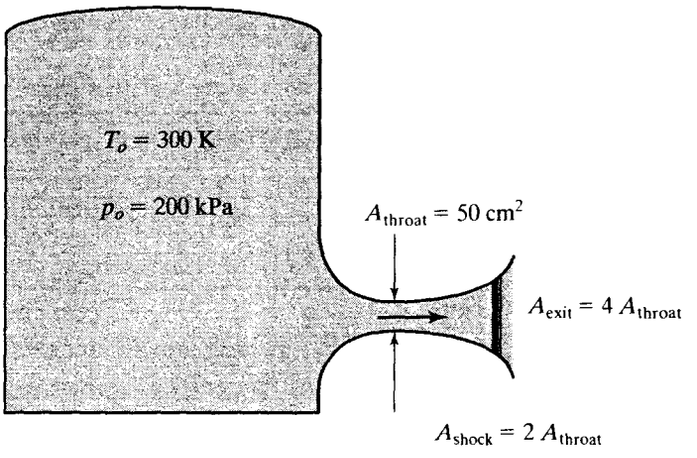


**Figure P4.4**

**4.5** A supersonic flow at Mach 3.0 and $\gamma = 1.4$ is to be slowed down via a normal shock in a diverging channel. For the conditions shown in Figure P4.5, find $p_2/p_1$ and $p_e/p_i$.

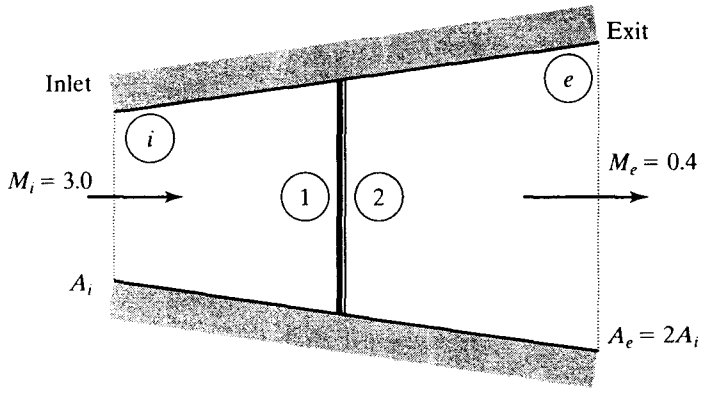


**Figure P4.5**

**4.6** A body is reentering the earth's atmosphere at a Mach number of 20. In front of the body is a shockwave, as shown in Figure P4.6. Opposite the nose of the body, the shock can be seen to be normal to the flow direction. Determine the stagnation pressure and temperature to which the nose is subjected. Assume that the air behaves as a perfect gas (neglect dissociation) with constant $\gamma = 1.4$. The ambient pressure and temperature are 1.0 kPa and 220 K, respectively.

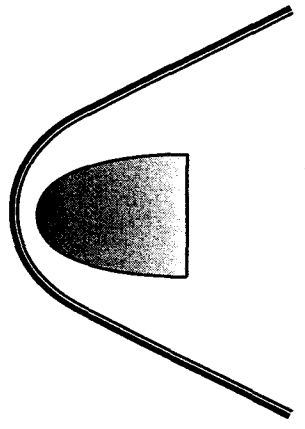

**Figure P4.6**

**4.7** Determine the back pressure necessary for a normal shock to appear at the exit of a converging–diverging nozzle, as shown in Figure P4.7. Assume that $\gamma = 1.4$.

**4.8** A normal shock is found to occur in the diverging portion of a converging–diverging nozzle at an area equal to 1.1 times the throat area. If the nozzle has a ratio of exit area to throat area of 2.2, determine the percent of decrease in nozzle exit velocity caused by the presence of the shock (compared with the exit velocity of a perfectly expanded isentropic supersonic nozzle flow). Assume that the flow is expanded from negligible velocity, that the stagnation temperature of the flow is the same for both cases, and that the working fluid is steam, which behaves as a perfect gas with constant $\gamma = 1.3$.

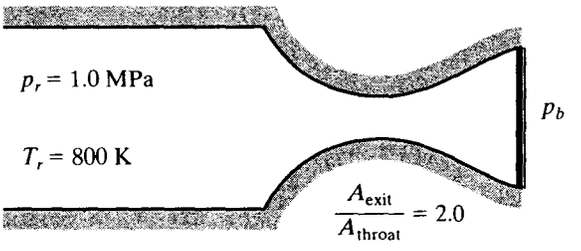


**Figure P4.7**

**4.9** A flow system consists of two converging–diverging nozzles in series, separated by a duct. [See Figure P4.9(a).] If the area ratio (exit to throat) of each nozzle is 3 to 1, find the area ratio $A_3/A_1$ necessary to produce sonic flow at the second throat, with a shock at $A_2$. Assume isentropic flow except for the normal shock. Find the percentage of loss in stagnation pressure for this flow. At another operating condition, a shock appears at $A_3$. [See Figure P4.9(b).] Find the percentage of loss of stagnation pressure for this condition for the same geometry.

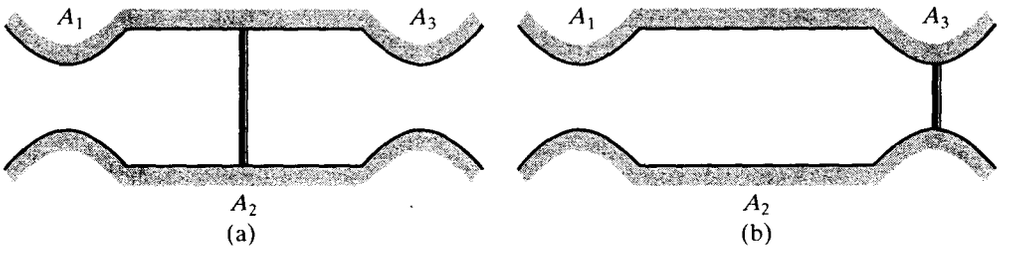


**Figure P4.9**

**4.10** For the system shown in Figure P4.10, $M_a = 2.0$, $A_a = 20\ \text{cm}^2$, throat area $= 15\ \text{cm}^2$, shock area $= 22\ \text{cm}^2$, and exit area $= 25\ \text{cm}^2$. With the working fluid behaving as a perfect gas with constant $\gamma = 1.3$, find the following:

(a) the throat Mach number,

(b) the exit Mach number, and

(c) the ratio of exit static pressure to static pressure at *i*.

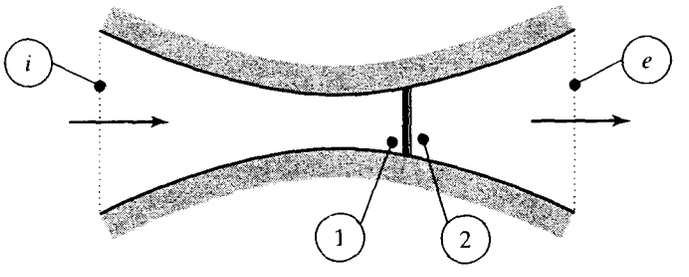


**Figure P4.10**

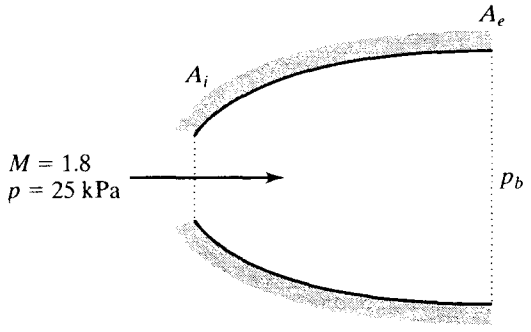


**Figure P4.11**

**4.11** A jet engine uses a diverging passage as a diffuser. (See Figure P4.11.) For a flight Mach number of 1.8, determine the range of back pressures over which a normal shock will appear in the diffuser. Ambient pressure and temperature are 25 kPa and 220 K, respectively. Find the mass-flow range handled by the diffuser for the determined back-pressure range. Also, the inlet and exit areas are $A_i = 250\ \text{cm}^2$ and $A_e = 500\ \text{cm}^2$, respectively. Assume isentropic flow except for the shocks. Take $\gamma = 1.4$.

**4.12** Air ($\gamma = 1.4$) enters a converging–diverging diffuser with a Mach number of 2.8, static pressure $p_i$ of 100 kPa, and static temperature of 20°C. For the flow situation shown in Figure P4.12, find the exit velocity, exit static pressure, and exit stagnation pressure.

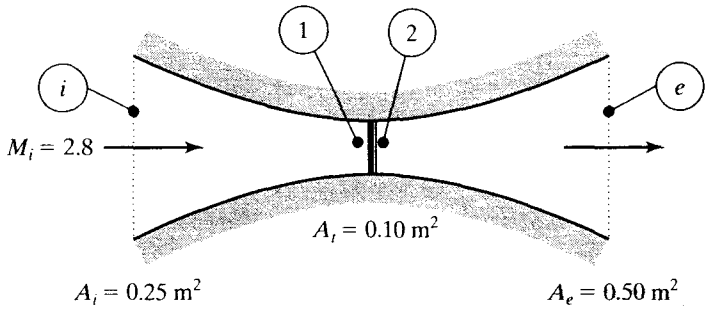


**Figure P4.12**

**4.13** Write a computer program that will yield values of $p_2/p_1$, $\rho_2/\rho_1$, $T_2/T_1$, and $p_{o2}/p_{o1}$ for a fixed normal shock with a working fluid consisting of a perfect gas with constant $\gamma = 1.20$. Use Mach number increments of 0.05 over the range $M = 1.0$ to $M = 2.5$.

**4.14** A converging–diverging nozzle has an area ratio (exit to throat) of 3.0. The nozzle is supplied from an air ($\gamma = 1.4$, $R = 287\ \text{J/kg} \cdot \text{K}$) reservoir in which the pressure and temperature are maintained at 270 kPa and 35°C, respectively. The nozzle is exhausted to a back pressure of 101 kPa. Find the nozzle exit velocity and nozzle exit-plane static pressure.

**4.15** A supersonic nozzle possessing an area ratio (exit to throat) of 3.0 is supplied from a large reservoir and is allowed to exhaust to atmospheric pressure (101 kPa). Determine the

range of reservoir pressures over which a normal shock will appear in the nozzle. For what value of reservoir pressure will the nozzle be perfectly expanded, with supersonic flow at the exit plane? Find the minimum reservoir pressure to produce sonic flow at the nozzle throat. Assume isentropic flow except for shocks, with $\gamma = 1.4$.

**4.16** A converging–diverging nozzle with an area ratio (exit to throat) of 3.0 exhausts air ($\gamma = 1.4$) from a large high-pressure reservoir to a region of back pressure $p_b$. Under a certain operating condition, a normal shock is observed in the nozzle at an area equal to 2.2 times the throat area. What percent of decrease in back pressure would be necessary to rid the nozzle of the normal shock?

**4.17** Due to variations in fuel flow rate, it is found that the stagnation pressure at the inlet to a jet-engine nozzle varies with time according to $p_o = 200[1 + 0.1 \sin(\pi/4)t]$, with $t$ in seconds and $p_o$ in kilopascals. Determine the resultant variation in nozzle flow rate, nozzle exhaust velocity, and exit-plane static pressure. Assume the nozzle area ratio (exit to throat) to be 2.0 to 1, with inlet stagnation temperature of 600 K and negligible inlet velocity. The nozzle exhausts to an ambient pressure of 30 kPa; $\gamma = 1.4$; the nozzle exit area is 0.3 $m^2$; and $R = 0.3$ kJ/kg · K.

**4.18** Helium enters a converging–diverging nozzle with a negligible velocity; stagnation pressure is 500 kPa and stagnation temperature is 300 K. The nozzle throat area is 50 $cm^2$, and the exit area is 300 $cm^2$. Determine the range of nozzle back pressures over which a normal shock will appear in the nozzle. Also, find the nozzle exit velocity if the nozzle exhausts into a vacuum.

**4.19** A jet engine uses a diverging passage as a diffuser. (See Figure P4.19.) For a flight Mach number of 1.92, determine the range of back pressures over which a normal shock will appear in the diffuser. Ambient pressure and temperature are 70 kPa and 270 K, respectively. Find the mass-flow rates handled by the diffuser for the determined back-pressure ranges, with $A_{inlet} = 100\ cm^2$ and $A_{exit} = 200\ cm^2$. Assume isentropic airflow ($\gamma = 1.4$, $R = 287$ J/kg · K) except for across the shocks.

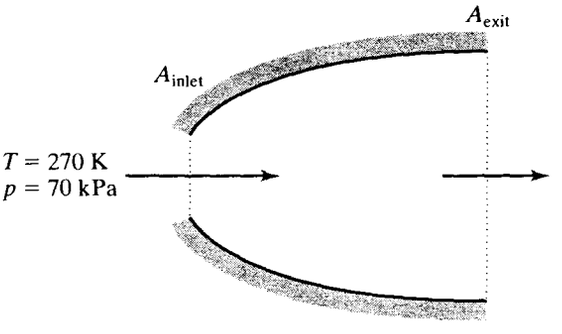


**Figure P4.19**

**4.20** For the converging–diverging nozzle shown in Figure P4.20, find the range of back pressures for which $p_e > p_b$, the range of back pressures for which $p_e < p_b$, and the range of back pressures over which the nozzle is choked. Take $\gamma = 1.4$.

**4.21** Nitrogen ($\gamma = 1.4$, $R = 296.8$ J/kg · K) expands in a converging–diverging nozzle from negligible velocity, a stagnation pressure of 1 MPa, and a stagnation temperature of 1,000 K to supersonic velocity in the diverging portion of the nozzle. If the area ratio (exit to throat) of the nozzle is 4.0, determine the back pressure necessary for a normal shock to position itself at an area equal to twice the throat area. For this condition, find the nozzle exit velocity.

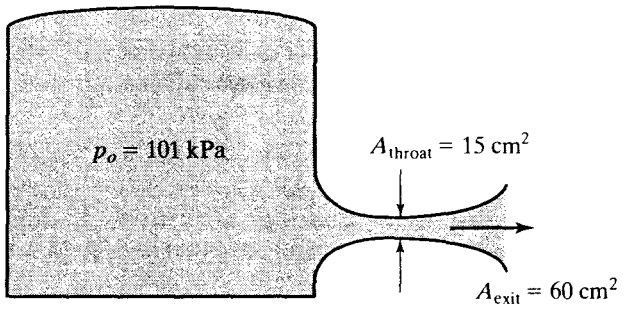


**Figure P4.20**

**4.22** (a) Develop a relation for the upstream Mach number $M_1$ in terms of the downstream Mach number $M_2$. (b) Use the result from part (a) and Eq. (4.12) to prove that

$$M_2^2 = \left(\frac{\gamma + 1}{2\gamma}\right)\left(\frac{\gamma - 1}{\gamma + 1} + \frac{p_1}{p_2}\right)$$

**4.23** Prove that the Rankine–Hugoniot relation reduces to the equation for an isentropic process for very weak shocks. [*Hint*: Start from Eq. (4.16b) and replace $p_2$ with $p + dp$ and $p_1$ with $p$. Repeat this operation for the densities. Then use the expansion technique employed in Example 4.1. Note that to properly use the expansion approach, we must first express the term to be expanded as 1 + (small quantity).]

**4.24** The back-pressure-to-reservoir-pressure ratio is 0.7 for a C–D nozzle, with an exit to throat area ratio of 2.0. Use the procedure for cases in which the shock location is not specified (i.e., the direct approach to determine the location of a normal shock for a ratio of specific heats equal to 1.3). Repeat the problem for $\gamma = 5/3$. Draw a conclusion regarding shock location and the value of $\gamma$.

**4.25** The back-pressure-to-reservoir-pressure ratio is 0.7 for a C–D nozzle, with an exit to throat area ratio of 2.0. Use the procedure for cases in which the shock location is specified (i.e., the trial-and-error approach to determine the location of a normal shock for a ratio of specific heats equal to 1.4). To start, assume that the shock is at the exit of the nozzle.

**4.26** A converging–diverging supersonic diffuser is to be used at Mach 3.0. The diffuser is to use a variable throat area so as to swallow the starting shock. What percentage of increase in throat area will be necessary? Solve for air ($\gamma = 1.4$) and for helium ($\gamma = 5/3$) as working fluids.

**4.27** A supersonic wind tunnel is to be constructed as shown in Figure 4.27, with air ($\gamma = 1.4$, $R = 287$ J/kg · K) at atmospheric pressure passing through a converging–diverging nozzle into a constant-area test section and then into a large vacuum tank. The test run is started with a pressure 0 kPa in the tank. How long can uniform flow conditions be maintained in the test section? That is, how long will it be before the tank pressure rises to a value such that a shock will appear in the test section? Assume the test section to be circular, 10 cm in diameter, with a design Mach number of 2.4. The tank volume is 3 m$^3$, with atmospheric conditions of 101 kPa and 20°C. Assume the air to be brought to rest adiabatically in the tank.

**4.28** Repeat Problem 4.27, but assume that there is a diffuser of area ratio 2 to 1 between the test section and the tank.

# Chapter 5

# Moving Normal Shockwaves

## 5.1 INTRODUCTION

Chapters 3 and 4 covered the subjects of isentropic flow and stationary normal shockwaves. Compressible flows can also involve moving shocks. Accordingly, we will next consider the unsteady problem of a moving normal shockwave and then use the material developed to study the flow physics of a shock tube, an unusually simple experimental device that is widely used to study transient wave and high-temperature phenomena.

## 5.2 MOVING NORMAL SHOCKWAVES

In the previous chapter, we dealt exclusively with stationary normal shockwaves. However, many physical situations arise in which a normal shock is moving. For example, when an explosion occurs, a shockwave propagates through the atmosphere from the point of the explosion. As a blunt body reenters the atmosphere from space, a shock travels a short distance ahead of the body. When a valve in a gas line is suddenly closed, a shock propagates back through the gas. To treat these cases, it is necessary to extend the procedures already developed for the stationary normal shockwave.

**The Fundamental Problem:** *A normal shock moving at constant speed into a motionless gas.*

Consider a normal shock moving at constant velocity into a motionless gas. [See Figure 5.1(a).] Although the arrangement is not the most general, it does represent the most widely encountered case. Moreover, we will repeatedly transform other cases to this arrangement, and for that reason, we regard this case as the *fundamental problem.* Define $S$ to be the shock velocity and $V$ to be the velocity of the gas behind the shock; both velocities are measured with respect to a stationary observer. For a stationary observer, the flow is not steady, since conditions at a point are dependent on whether the shock has passed over that point.

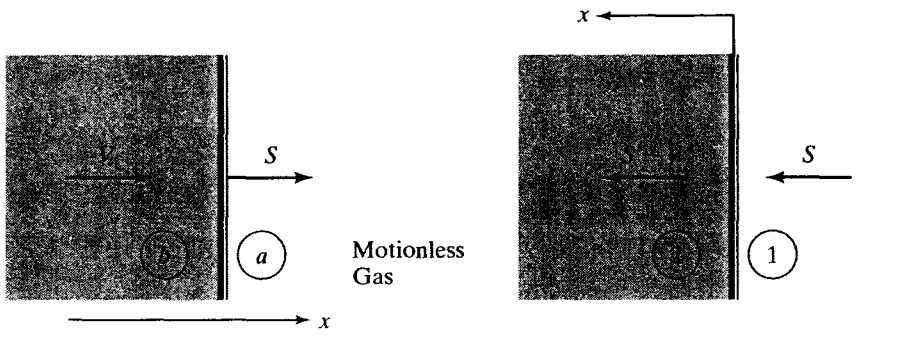


(a) Moving Shock
Stationary Coordinate System

(b) Stationary Shock
Moving Coordinate System

**Figure 5.1** Normal Shockwave Moving into a Gas at Rest

Now consider the same physical situation with an observer moving at a speed that is identical to that of the shockwave velocity—a situation, for instance, with the observer "sitting on the shockwave." Accordingly, the shock is now stationary with respect to the observer. [See Figure 5.1(b).] Example 1.4 served as an introduction to this type of coordinate change.

The strategy behind the coordinate change is that the flow is now unchanging with time; that is, the problem is steady in this moving coordinate system. So, we may utilize the relations and results that were obtained in Sections 4.2 and 4.3 for the stationary normal shockwave. However, in order to apply these results to moving normal shocks, consideration must be given to the effect of observer velocity on static and stagnation properties.

As may be recalled, static-flow properties are defined as properties measured with an instrument moving at the absolute flow velocity. Thus, static properties are independent of the velocity of the observer. Hence, comparing Figure 5.1(a) with Figure 5.1(b), we may write that

$$\frac{p_2}{p_1} = \frac{p_b}{p_a} \text{ and } \frac{T_2}{T_1} = \frac{T_b}{T_a}$$

Stagnation properties, on the other hand, are measured by bringing the flow to rest. Comparing the situations shown in Figure 5.1, we find that if $T_1 = T_a$ and $p_1 = p_a$, it is evident that $T_{o1} > T_{oa}$ and $p_{o1} > p_{oa}$, since the gas at state 1 has velocity $S$, while the gas at state $a$ has zero velocity. Thus, stagnation properties are dependent on the observer velocity. To calculate the variation of stagnation properties across a moving shockwave, static conditions and velocities must first be determined. (See Example 5.1.)

Because of the transformation of a stationary coordinate system to a coordinate system that moves with the shock, analysis of the moving normal shock is reduced to consideration of the steady-flow situation shown in Figure 5.1(b). We may apply the jump conditions across the shock and arrive at the following set of conservation relations:

$$\rho_2(S - V) = \rho_1 S \tag{5.1}$$

$$p_2 + \rho_2(S - V)^2 = p_1 + \rho_1 S^2 \tag{5.2}$$

$$h_2 + \frac{(S - V)^2}{2} = h_1 + \frac{S^2}{2} \tag{5.3}$$

We also require an equation of state. The perfect-gas model with constant specific heats will be employed, and therefore we have, in addition to the jump conditions,

$$\begin{aligned} \frac{p_2}{\rho_2 T_2} &= \frac{p_1}{\rho_1 T_1} \\ c_p &= \frac{\gamma R}{\gamma - 1} \\ h &= c_p T \\ a^2 &= \gamma RT = \gamma \frac{p}{\rho} \end{aligned} \tag{5.4}$$

Since only static properties appear in it, we may use the Rankine–Hugoniot relation, eq. (4.16b) written as

$$\frac{\rho_2}{\rho_1} = \frac{(\gamma + 1)p_2 + (\gamma - 1)p_1}{(\gamma + 1)p_1 + (\gamma - 1)p_2} \tag{5.5}$$

Now the preceding set of equations can be algebraically manipulated to obtain the following set of equations:

$$\frac{\rho_1}{\rho_2} = 1 - \frac{V}{S} \tag{5.6}$$

$$\frac{p_2}{p_1} = 1 + \frac{\gamma SV}{a_1^2} \tag{5.7}$$

$$\frac{p_2}{p_1} = \frac{2\gamma}{\gamma + 1}\left(\frac{S}{a_1}\right)^2 - \frac{\gamma - 1}{\gamma + 1} \tag{5.8}$$

$$\frac{V}{S} = \frac{2}{\gamma + 1}\left[1 - \left(\frac{a_1}{S}\right)^2\right] \tag{5.9}$$

$$S = \left(\frac{\gamma + 1}{4}\right)V + \sqrt{\left[\left(\frac{\gamma + 1}{4}\right)V\right]^2 + a_1^2} \tag{5.10}$$

$$S = \sqrt{\left(\frac{\gamma - 1}{2}\right)\left(\frac{p_1}{\rho_1}\right) + \left(\frac{\gamma + 1}{2}\right)\left(\frac{p_1}{\rho_1}\right)\left(\frac{p_2}{p_1}\right)} \tag{5.11}$$

$$\frac{p_2}{p_1} = 1 + \gamma\left(\frac{\gamma + 1}{4}\right)\left(\frac{V}{a_1}\right)^2 + \left(\frac{\gamma V}{a_1}\right)\sqrt{1 + \left(\frac{\gamma + 1}{4}\right)^2\left(\frac{V}{a_1}\right)^2} \tag{5.12}$$

$$\frac{T_2}{T_1} = \frac{a_2^2}{a_1^2} = 1 + \frac{(\gamma - 1)}{a_1^2}\left(SV - \frac{V^2}{2}\right) \tag{5.13}$$

**TABLE 5.1** Summary of a Process to Develop Eqs. (5.6) to (5.13)

| To Obtain | Use |
|---|---|
| Eq. (5.6) | Eq. (5.1) |
| Eq. (5.7) | Eqs. (5.2), (5.1), and (5.6) |
| Eq. (5.8) | Eqs. (5.2), (5.1), and (5.5) |
| Eq. (5.9) | Eqs. (5.7) and (5.8) |
| Eq. (5.10) | Eq. (5.9), solve quadratic |
| Eq. (5.11) | Eq. (5.8) and $a_1 = \sqrt{\gamma \frac{p_1}{\rho_1}}$ |
| Eq. (5.12) | Eqs. (5.7), (5.8), and (5.9) |
| Eq. (5.13) | Eq. (5.3) and $h = \frac{a^2}{(\gamma - 1)}$ |

The development of most of these relations is not difficult. Table 5.1 summarizes their development. Combinations of equations other than those shown in Table 5.1 are possible as well.

**Example 5.1. Calculation of properties behind a moving normal shock using physical variables**

An explosion occurs which produces a normal shockwave that propagates at a speed of 600 m/s into still air (a perfect gas with $\gamma = 1.4$). The pressure and temperature of the motionless air in front of the shock are 101.3 kPa and 20°C, respectively. Determine the velocity, static pressure, and static temperature of the air following the shock.

**Solution**

Examination of Eqs. (5.6) to (5.13) in relation to the given information ($S$, $p_1$, and $T_1$), as well as the expected results ($V$, $p_2$, and $T_2$), reveals that we may use Eqs. (5.9), (5.7), and (5.13) in turn. First, we must compute the speed of sound $a_1$:

$$a_1 = \sqrt{\gamma R T_1} = \sqrt{(1.4)(287)(293)} = 343.1143 \text{ m/s}$$

Therefore,

$$V = \frac{2S}{\gamma + 1}\left[1 - \left(\frac{a_1}{S}\right)^2\right] = \frac{(2)(600)}{2.4}\left[1 - \left(\frac{343.1143}{600}\right)^2\right] = 336.4897 \text{ m/s}$$

$$p_2 = p_1\left(1 + \frac{\gamma S V}{a_1^2}\right) = (101.3)\left[1 + \frac{(1.4)(600)(336.4897)}{(343.1143)^2}\right] = 344.5109 \text{ kPa}$$

$$T_2 = T_1\left[1 + \frac{(\gamma - 1)}{a_1^2}\left(SV - \frac{V^2}{2}\right)\right]$$

$$= (293)\left\{1 + \frac{0.4}{(343.1143)^2}\left[(600)(336.4897) - \frac{(336.4897)^2}{2}\right]\right\}$$

$$= 437.6303 \text{ K}$$

*Note:* Had we been given the speed of the gas trailing the shock, $V$, instead of the shock speed $S$, the procedure would be essentially the same, except that the solution of Eq. (5.9) would be replaced with the solution of Eq. (5.10).

Rather than proceeding with an entirely new analysis, as in the foregoing solution, we may also use the results developed for the stationary normal shock in the previous chapter. Table 5.2 contains appropriate relations for the stationary shock and contrasts them with the moving-shock relations just developed.

In the moving-shock equations, $p$, $T$, and $\rho$ are properties that refer to the thermodynamic state of the flowing fluid and are the static properties of the fluid. (Again, static properties are those properties that would be measured by instruments at rest with respect to the fluid.) As has been mentioned, changing the coordinate system from stationary to moving does not affect the static properties, but this transformation will have an impact on the stagnation properties. We can easily demonstrate these effects by calculating the change in static temperature across the shock for a stationary normal shock.

Since for a normal shock that is stationary in a moving coordinate system,

$$T_{o1} = T_{o2}$$

**TABLE 5.2** Comparison of Equations across Moving and Stationary Normal Shocks

| Moving Normal-Shock Relations | Stationary Normal-Shock Relations |
|---|---|
| $M_1 = \dfrac{0}{a_1} = 0$ | $M_1 = \dfrac{S}{a_1}$ |
| $p_{o1} = p_1$ | $p_{o1} = p_1\left(1 + \dfrac{\gamma - 1}{2}M_1^2\right)^{\gamma/(\gamma-1)}$ |
| $T_{o1} = T_1$ | $T_{o1} = T_1\left(1 + \dfrac{\gamma - 1}{2}M_1^2\right)$ |
| $T_2 = T_1\left[1 + \dfrac{\gamma - 1}{2a_1^2}(2SV - V^2)\right]$ | $T_2 = T_1\dfrac{2(\gamma - 1)}{(\gamma + 1)^2}\dfrac{\left(1 + \dfrac{\gamma - 1}{2}M_1^2\right)\left(\dfrac{2\gamma}{\gamma - 1}M_1^2 - 1\right)}{M_1^2}$ |
| $M_2 = \dfrac{V}{a_2}$ | $M_2 = \dfrac{S - V}{a_2} = \sqrt{\dfrac{M_1^2 + \dfrac{2}{\gamma - 1}}{\dfrac{2\gamma}{\gamma - 1}M_1^2 - 1}}$ |
| $p_2 = p_1\left(1 + \gamma\dfrac{SV}{a_1^2}\right)$ | $p_2 = p_1\left[\dfrac{2\gamma}{\gamma + 1}M_1^2 - \dfrac{(\gamma - 1)}{(\gamma + 1)}\right]$ |
| $p_{o2} = p_2\left(1 + \dfrac{\gamma - 1}{2}\dfrac{V^2}{a_2^2}\right)^{\gamma/\gamma-1}$ | $p_{o2} = p_2\left(1 + \dfrac{\gamma - 1}{2}M_2^2\right)^{\gamma/(\gamma-1)}$ |
| $T_{o2} = T_2\left(1 + \dfrac{\gamma - 1}{2}\dfrac{V^2}{a_2^2}\right)$ | $T_{o2} = T_2\left(1 + \dfrac{\gamma - 1}{2}M_2^2\right)$ |

and hence

$$T_1\left(1 + \frac{\gamma - 1}{2}M_1^2\right) = T_2\left(1 + \frac{\gamma - 1}{2}M_2^2\right)$$

rearranging gives

$$\begin{aligned}(T_2 - T_1)_{\text{stationary}} &= \frac{\gamma - 1}{2}(T_1M_1^2 - T_2M_2^2) = \frac{\gamma - 1}{2}\left[T_1\left(\frac{S}{a_1}\right)^2 - T_2\left(\frac{S - V}{a_2}\right)^2\right] \\ &= \frac{\gamma - 1}{2}\left[\frac{S^2}{\gamma R} - \frac{(S - V)^2}{\gamma R}\right] \\ &= \frac{(\gamma - 1)T_1}{2a_1^2}(2SV - V^2) = (T_2 - T_1)_{\text{moving}}\end{aligned}$$

On the other hand,

$$\begin{aligned}(T_{o2} - T_{o1})_{\text{moving}} &= T_2\left(1 + \frac{\gamma - 1}{2}M_2^2\right) - T_1 = (T_2 - T_1) + \frac{\gamma - 1}{2\gamma R}V^2 \\ &= \frac{2SV - V^2}{2c_p} + \frac{V^2}{2c_p} = \frac{SV}{c_p} \\ &\neq (T_{o2} - T_{o1})_{\text{stationary}}\end{aligned}$$

**Example 5.2. Calculation of properties behind a moving normal shock, using stationary normal shock relations**

An explosion occurs which produces a normal shockwave that propagates at a speed of 600 m/s into still air (a perfect gas with $\gamma = 1.4$). The pressure and temperature of the motionless air in front of the shock are 101.3 kPa and 20°C, respectively. Use the relations for a stationary normal shock, and determine the static and stagnation conditions present in the air after passage of the wave, as well as the gas velocity behind the wave.

**Solution**

For the normal shock in the coordinate system moving with the shock,

$$M_1 = \frac{S}{a_1} = \frac{S}{\sqrt{\gamma RT_1}} = \frac{600 \text{ m/s}}{\sqrt{(1.4)(287 \text{ J/kg} \cdot \text{K})(293 \text{ K})}} = 1.7487$$

From the isentropic relations and stationary normal-shock relations at this Mach number, we have

$$\frac{p_1}{p_{o1}} = 0.18820 \text{ and } \frac{T_1}{T_{o1}} = 0.6205$$

$$\frac{p_2}{p_1} = 3.4009, \frac{T_2}{T_1} = 1.4936, \frac{p_{o2}}{p_{o1}} = 0.8351, \text{ and } M_2 = 0.6284$$

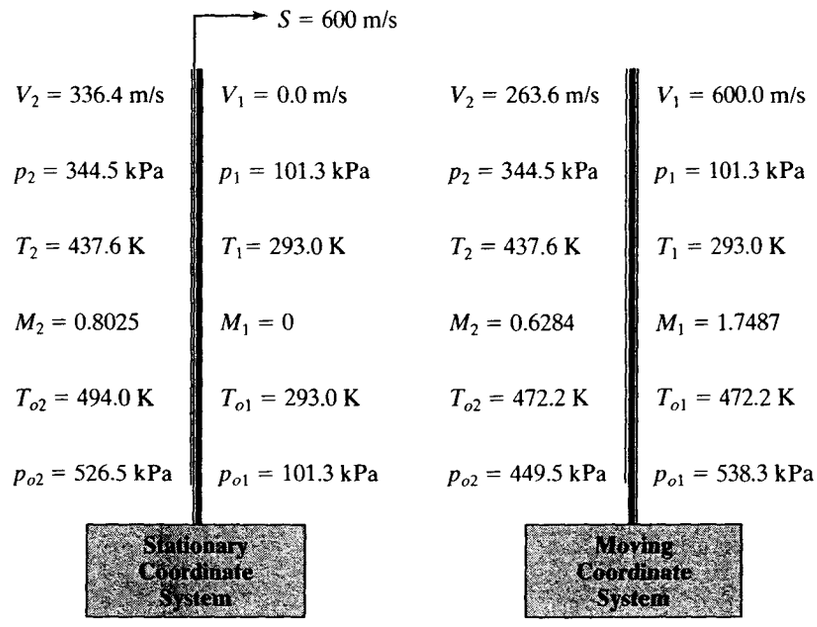


**Figure 5.2** Computed Properties on Both Sides of the Moving Normal Shock in Two Coordinate Systems of Example 5.2

Using $p_1 = 101.3$ kPa and $T_1 = 293$, we compute parameters within the moving coordinate system:

$$T_{o1} = \frac{T_1}{(T_1/T_{o1})} = \frac{293}{0.6205} = 472.1998 \text{ K} = T_{o2}$$

$$p_{o1} = \frac{p_1}{(p_1/p_{o1})} = \frac{101.3}{0.18820} = 538.2572 \text{ kPa}$$

$$p_{o2} = \left(\frac{p_{o2}}{p_{o1}}\right)p_{o1} = (0.8351)(538.2572) = 449.4986 \text{ kPa}$$

$$p_2 = \left(\frac{p_2}{p_1}\right)p_1 = (3.4009)(101.3) = 344.5112 \text{ kPa}$$

$$T_2 = \left(\frac{T_2}{T_1}\right)T_1 = (1.4936)(293) = 437.6248 \text{ K}$$

$$a_2 = \sqrt{\gamma R T_2} = 419.3300 \text{ m/s}$$

$$S - V = a_2 M_2 = (419.3300)(0.6284) = 263.5070 \text{ m/s}$$

$$V = S - (S - V) = 600 - 263.5070 = 336.4930 \text{ m/s}$$

Now, for the moving shock in the stationary coordinate system,

$$M_2 = \frac{V}{a_2} = \frac{336.4930}{419.3300} = 0.8025$$

From the isentropic flow relations at $M_2 = 0.8025$, we obtain

$$\frac{p_2}{p_{o2}} = 0.6544 \text{ and } \frac{T_2}{T_{o2}} = 0.8859$$

$$p_{o2} = \frac{p_2}{(p_2/p_{o2})} = \frac{344.5112}{0.6544} = 526.4535 \text{ kPa}$$

$$T_{o2} = \frac{T_2}{(T_2/T_{o2})} = \frac{437.6248}{0.8859} = 493.9889 \text{ K}$$

Figure 5.2 compares the computed values for both the stationary and moving coordinate systems for this example.

---

**Example 5.3. Relations for a normal shock moving into a gas in motion**

Develop expressions for the case of a normal shock traveling at a constant speed $S$ into a gas that is moving with a speed $W$. The shock induces a speed $V$ of the gas it passes over, as shown in Figure 5.3.

**Solution**

To begin, we must transform the coordinate system to one in which the shock is stationary. This can be accomplished by locating the coordinate system on the shock and therefore obtaining the arrangement shown in Figure 5.3(b).

We could next perform an analysis in which we write the jump conditions across the shock and perform the algebraic manipulations to obtain the desired results. However, by contrasting the arrangement in Figure 5.3(b) with that in Figure 5.1(b), it can be seen that if the shock speed $S$ and the gas speed $V$ are replaced with $S - W$ and $V - W$, respectively, in Eqs. (5.6)–(5.13), we will obtain the desired results.

**Analysis Aid:** It is helpful to perform an intermediate step in the coordinate transformation process, in which the gas ahead of the shock is made motionless by superimposing on the entire flow field the speed of this gas (for the case at hand, $W$), but in the opposite direction. This intermediate step would result in the arrangement shown in Figure 5.4. It should be more apparent why $S - W$ and $V - W$ are used to replace $S$ and $V$, respectively, in the relations developed for the fundamental problem.

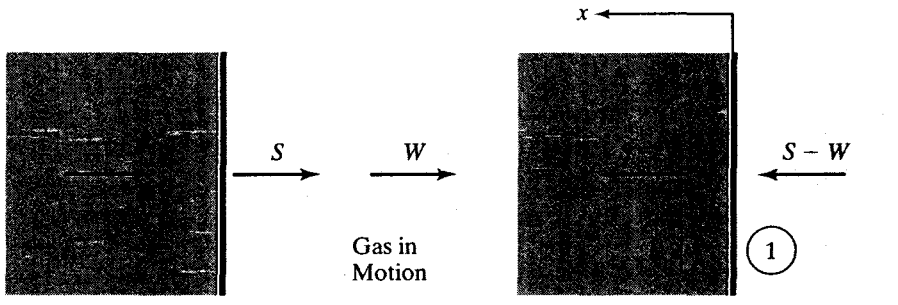


(a) Moving Shock
Stationary Coordinate System

(b) Stationary Shock
Moving Coordinate System

**Figure 5.3** Normal Shock Moving into a Gas in Motion

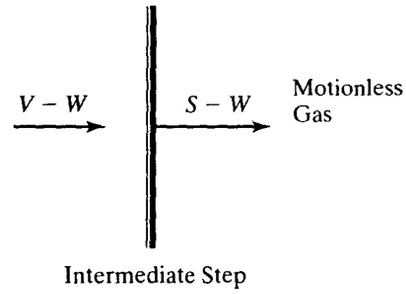


**Figure 5.4** Transformed Normal Shock Moving into a Motionless Gas

To demonstrate the utility of the various transformations, consider Eq. (5.7), which can be immediately written for the problem under consideration as

$$\frac{p_2}{p_1} = 1 + \frac{\gamma(S - W)(V - W)}{a_1^2} \tag{5.14}$$

If we set $W$ to zero, the pressure ratio for the fundamental problem is obtained. Next, we can develop an expression of the speed of the shock from Eq. (5.10), which can be rewritten as

$$S - W = \left(\frac{\gamma + 1}{4}\right)(V - W) + \sqrt{\left[\left(\frac{\gamma + 1}{4}\right)(V - W)\right]^2 + a_1^2}$$

or

$$\begin{aligned} S &= W + \left(\frac{\gamma + 1}{4}\right)(V - W) + \sqrt{\left[\left(\frac{\gamma + 1}{4}\right)(V - W)\right]^2 + a_1^2} \\ &= \frac{(\gamma + 1)V + (3 - \gamma)W}{4} + \sqrt{\left[\left(\frac{\gamma + 1}{4}\right)(V - W)\right]^2 + a_1^2} \end{aligned} \tag{5.15}$$

Other relations may be readily obtained in the same manner.

---

**Example 5.4. Calculation of properties behind two moving normal shocks in a tube**

A piston in a tube is suddenly accelerated to a constant velocity of 50 m/s, which causes a normal shock to move into the air at rest in the tube. [See Figure 5.5(a).] Several seconds


(a) Generation of the First Shock (b) Flow Field Involving Both Shocks

**Figure 5.5** Two Normal Shocks Moving into a Motionless Gas

later, the piston is suddenly accelerated from 50 to 100 m/s, which causes a second shock to move down the tube. [See Figure 5.5(b).] Calculate the velocities of the two shockwaves if the temperature of the air ($\gamma = 1.4$, $R = 287$ J/kg · K) at rest is 300 K.

**Solution**

This example involves three zones of uniform flow conditions and two shocks, as opposed to the two zones and one shock in previous examples, and therefore the notation requires some care. We take Zone 1 to be downstream of the first shock, Zone 2 between the two shocks, and Zone 3 upstream of the second shock. The first shock travels at a speed $S_F$, whereas the second shock has the speed $S_S$.

The air next to the piston must move at the same velocity as the piston, since it can neither move through the face of the piston nor move away from the piston and leave a vacuum behind.

*First Shock:*

For a moving observer fixed to the shock, the air velocities after the first shock has been generated are as shown in Figure 5.6.

Now, from Eq. (5.10), with $V_2 = 50$ m/s and $a_1 = \sqrt{\gamma RT_1} = \sqrt{1.4(287)300} = 347.1887$ m/s, we have

$$S_F = \left(\frac{\gamma + 1}{4}\right)V_2 + \sqrt{\left[\left(\frac{\gamma + 1}{4}\right)V_2\right]^2 + a_1^2}$$

$$= \frac{2.4(50)}{4} + \sqrt{\frac{(2.4)^2(50)^2}{16} + (347.1887)^2} = 378.4824 \text{ m/s}$$

The Mach number within Zone 1 is

$$M_1 = \frac{S_F}{a_1} = \frac{378.4824}{347.1887} = 1.0901$$

With $M_1$, we can determine the temperature in Zone 2 from Eq. (4.11) or Eq. (5.13):

$$T_2 = \left(\frac{T_2}{T_1}\right)T_1 = (1.05865)(300) = 317.5950 \text{ K}$$

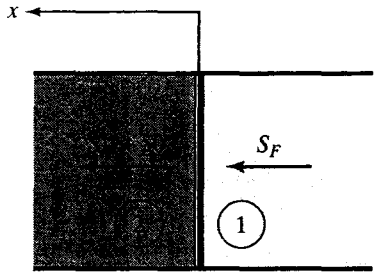


**Figure 5.6** First Shock in a Coordinate System

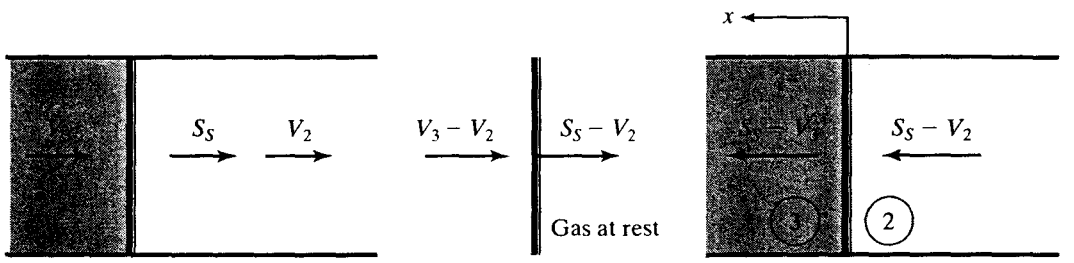


(a) Moving Normal Shock Stationary Coordinate System

(b) Intermediate Step

(c) Moving Normal Shock Moving Coordinate System

**Figure 5.7** Transforming the Second Shock to a Coordinate System Moving with the Shock

*Second Shock:*

To determine the speed of the second shock, we must fix the shock by defining a new coordinate system equivalent to superimposing a speed $S_S - V_2 = S_S - 50$ on the entire flow, as shown in Figure 5.7. As previously indicated, it may be helpful to perform this operation in separate steps. First, superimpose a speed $V_2$, to the left, to bring the gas in front of the moving shock to rest. (This condition allows us to use the results from the fundamental problem.) Second, bring the shock to rest by superimposing a speed $S_S - V_2$, to the left, on the entire flow.

Employing Eq. (4.13), we have

$$\frac{\rho_3}{\rho_2} = \frac{S_S - V_2}{S_S - V_3} = \frac{(\gamma + 1)M_2^2}{(\gamma - 1)M_2^2 + 2} = \frac{(\gamma + 1)\left(\dfrac{S_S - V_2}{a_2}\right)^2}{(\gamma - 1)\left(\dfrac{S_S - V_2}{a_2}\right)^2 + 2}$$

Expanding this expression yields the quadratic equation

$$S_S^2 + bS_S + c = 0$$

where

$$V_2 = 50 \text{ m/s}, V_3 = 100 \text{ m/s, and } a_2 = \sqrt{\gamma RT_2} = \sqrt{1.4(287)317.6} = 357.2 \text{ m/s}$$

So, we have

$$\begin{aligned} b &= (\gamma - 1)V_2 + \frac{(\gamma + 1)}{2}(V_2 + V_3) \\ &= (0.4)50 - 1.2(50 + 100) = -160 \\ c &= -a_2^2 - \left(\frac{\gamma - 1}{2}\right)V_2^2 + \left(\frac{\gamma + 1}{2}\right)V_2V_3 \\ &= -(357.2)^2 - (0.2)(50)^2 + (1.2)(50)(100) = -122{,}091.8 \end{aligned}$$

Solution yields

$$S_S = 438.5 \text{ m/s}$$

Alternatively, we can avoid having to solve the quadratic by modifying Eq. (5.15) with $V = V_3 = 100$ m/s and $W = V_2 = 50$ m/s [compare Figure 5.7(c) with Figure 5.3(b)] and replacing $a_1$ with $a_2 = 357.2$ m/s to obtain

$$S_S = \frac{(\gamma + 1)V_3 + (3 - \gamma)V_2}{4} + \sqrt{\left[\left(\frac{\gamma + 1}{4}\right)(V_3 - V_2)\right]^2 + a_2^2}$$

$$= \frac{(2.4)100 + (1.6)50}{4} + \sqrt{\left[\left(\frac{2.4}{4}\right)(100 - 50)\right]^2 + 357.2^2} = 438.5 \text{ m/s}$$

Thus, the second wave travels at a greater velocity than the first and eventually overtakes it. This result is a demonstration of the principles discussed in Section 4.2: Compression waves are able to overtake and reinforce one another. In this example, the second wave travels at a greater velocity because it is both moving into the compressed, higher temperature gas behind the first wave and moving into a gas stream already traveling in the same direction with a velocity of 50 m/s.

## 5.3 REFLECTED NORMAL SHOCKWAVES

To continue our study of moving normal shockwaves, consider a wave impinging on the end of a tube. Two physical arrangements should be considered: a closed-end tube and a tube open to the atmosphere. (See Figure 5.8.) In both cases, it is desired to determine whether the reflected wave is a compression shockwave or a series of weak expansion waves.

For case (a) in Figure 5.9(a), the gas next to the closed end of the tube must be at rest, with the gas behind the incident shock moving to the right with velocity $V$. For an observer moving with the reflected wave, the physical situation is as shown in Figure 5.9(b), which indicates a decrease in velocity and a corresponding increase in static pressure across the reflected wave, which is physically the situation for a normal shock. Therefore, an incident normal shock reflects from the solid surface of a closed tube as a normal shock.

For case (b) in Figure 5.8, the static pressure at the end of the tube is the boundary condition imposed on the system. Because the flow in front of the moving shock is subsonic, the back pressure and the exit pressure must be the same. From Figure 5.8(b),

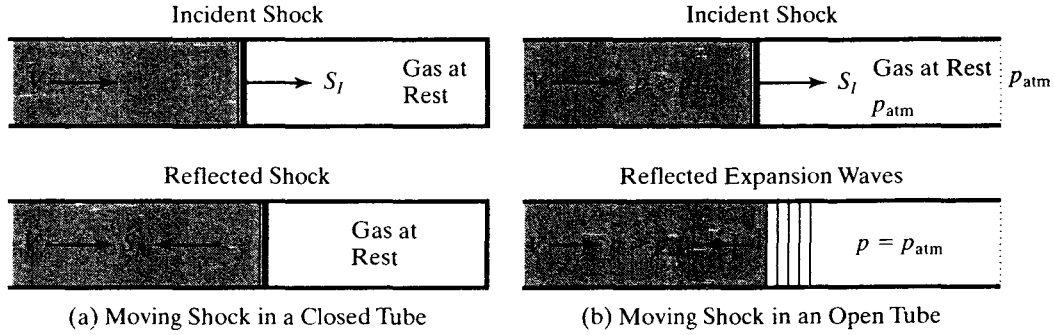


(a) Moving Shock in a Closed Tube (b) Moving Shock in an Open Tube

**Figure 5.8** Moving Normal Reflections from a Closed- and Open-ended Tube

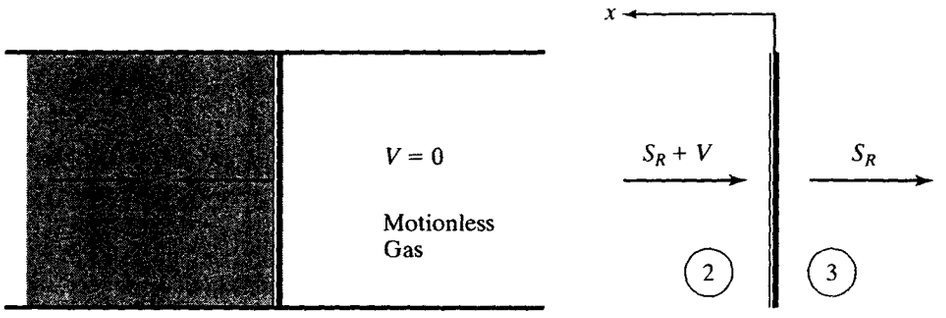


(a) Moving Reflected Shock Stationary Coordinate System

(b) Moving Reflected Shock Moving Coordinate System

**Figure 5.9** Transformation of the Coordinate System for a Reflected Normal Shock

we see a decrease in pressure across the reflected wave. Consequently, a normal shock reflects from an open end of a tube as a series of expansion waves.

In order to analyze a normal shock reflected from a solid surface, consider both the incident and reflected shocks in moving and stationary coordinate systems. (See Figure 5.10.) As noted in the previous example, when the system includes various shock speeds and zones, we must exercise care with the notation. Moreover, because we will be combining these analyses, we must be consistent and assign the same direction to the coordinate axes in both incident and reflected systems. We will take the positive direction to be towards the solid surface.

To initiate the analysis, we will use Prandtl's relation, Eq. (4.20a), in which $V_1$ and $V_2$ (the speeds in front of and behind the incident shock, respectively) have been replaced with $V_f$ and $V_b$, respectively:

$$V_f V_b = \frac{2}{\gamma + 1} a_o^2 = \frac{\gamma - 1}{\gamma + 1} V_f^2 + \frac{2}{\gamma + 1} a_f^2 = \frac{\gamma - 1}{\gamma + 1} V_b^2 + \frac{2}{\gamma + 1} a_b^2$$

Therefore, referring to Figure 5.10(a), we find that for the incident-shock case,

$$\begin{aligned} V_f &= -S_I \\ V_b &= V_2 - S_I \\ a_b &= a_2 \end{aligned}$$

Thus, for the incident shock,

$$(-S_I)(V_2 - S_I) = \left(\frac{\gamma - 1}{\gamma + 1}\right)(V_2 - S_I)^2 + \left(\frac{2}{\gamma + 1}\right) a_2^2 \tag{5.16}$$

Referring to Figure 5.10(b), we find that for the reflected-shock case,

$$\begin{aligned} V_f &= S_R + V_2 \\ V_b &= S_R \\ a_f &= a_3 \end{aligned}$$

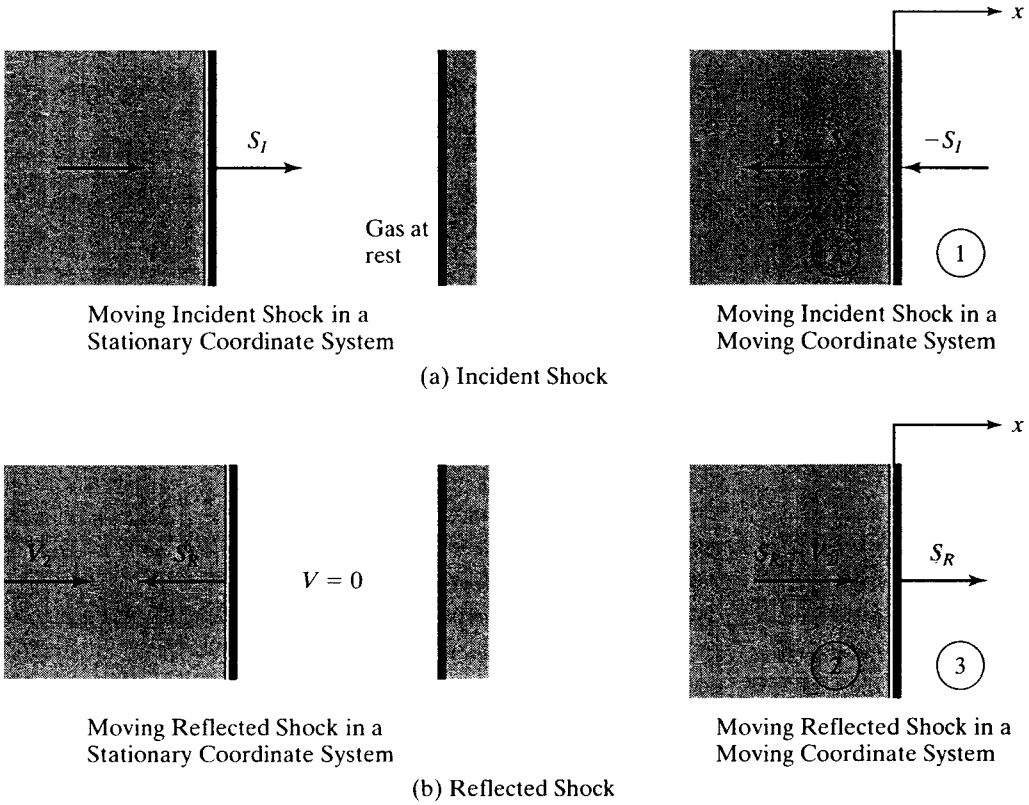


**Figure 5.10** Transformation of Coordinate Systems for Moving Incident and Reflected Shocks

So, for the reflected-shock case,

$$(S_R + V_2)(S_R) = \left(\frac{\gamma - 1}{\gamma + 1}\right)(S_R + V_2)^2 + \left(\frac{2}{\gamma + 1}\right)a_3^2 \tag{5.17}$$

Equations (5.16) and (5.17) can be rearranged as

$$\left(\frac{V_2 - S_I}{a_2}\right)^2 - 1 = \left(\frac{\gamma + 1}{2}\right)\left(\frac{V_2}{a_2}\right)\left(\frac{V_2 - S_I}{a_2}\right) \tag{5.18}$$

and

$$\left(\frac{S_R + V_2}{a_2}\right)^2 - 1 = \left(\frac{\gamma + 1}{2}\right)\left(\frac{V_2}{a_2}\right)\left(\frac{S_R + V_2}{a_2}\right) \tag{5.19}$$

respectively. Divide Eq. (5.18) by Eq. (5.19) to get

$$\frac{\left(\frac{S_R + V_2}{a_2}\right)^2 - 1}{\left(\frac{S_R + V_2}{a_2}\right)} = \frac{\left(\frac{V_2 - S_I}{a_2}\right)^2 - 1}{\left(\frac{V_2 - S_I}{a_2}\right)} \tag{5.20}$$

Equation (5.20) is a quadratic in terms of $(S_R + V_2)/a_2$. To see this, let $(S_R + V_2)/a_2 = x$ and $(V_2 - S_I)/a_2 = y$. The right-hand side of Eq. (5.20) can be written as $(y^2 - 1)/y$, which we will set equal to $b$ for convenience. Thus, Eq. (5.20) may be simply written as

$$x^2 - bx - 1 = 0$$

Solution of this equation produces two roots, one possible and one impossible:

$$x = \frac{b \pm \sqrt{b^2 + 4}}{2} = \frac{\left(\frac{y^2 - 1}{y}\right) \pm \sqrt{\left(\frac{y^2 - 1}{y}\right)^2 + 4}}{2} = \frac{(y^2 - 1) \pm (y^2 + 1)}{2y}$$

So,

$$x_+ = y$$

$$x_- = -\frac{1}{y}$$

Substituting back the physical terms of the problem, we get

$$\frac{S_R + V_2}{a_2} = \frac{(V_2 - S_I)}{a_2}$$

$$\frac{S_R + V_2}{a_2} = -\frac{1}{\frac{(V_2 - S_I)}{a_2}}$$

Since $\frac{S_R + V_2}{a_2} > 1$ and $\frac{V_2 - S_I}{a_2} < 0$, only the second solution is possible:

$$\frac{S_R + V_2}{a_2} = -\frac{a_2}{V_2 - S_I} \tag{5.21}$$

Now, across a stationary shock,

$$\frac{p_2}{p_1} = \frac{2\gamma}{\gamma + 1} M_1^2 - \frac{(\gamma - 1)}{(\gamma + 1)}$$

Therefore, for a reflection,

$$\frac{p_3}{p_2} = \frac{2\gamma}{\gamma + 1}\left(\frac{S_R + V_2}{a_2}\right)^2 - \frac{(\gamma - 1)}{(\gamma + 1)} \tag{5.22}$$

It can be shown (see Problem 4.22) that

$$M_2^2 = \left(\frac{\gamma + 1}{2\gamma}\right)\left(\frac{\gamma - 1}{\gamma + 1} + \frac{p_1}{p_2}\right)$$

Hence, for the incident shock,

$$\frac{p_1}{p_2} = \left(\frac{2\gamma}{\gamma + 1}\right)\left(\frac{V_2 - S_I}{a_2}\right)^2 - \frac{\gamma - 1}{\gamma + 1} \tag{5.23}$$

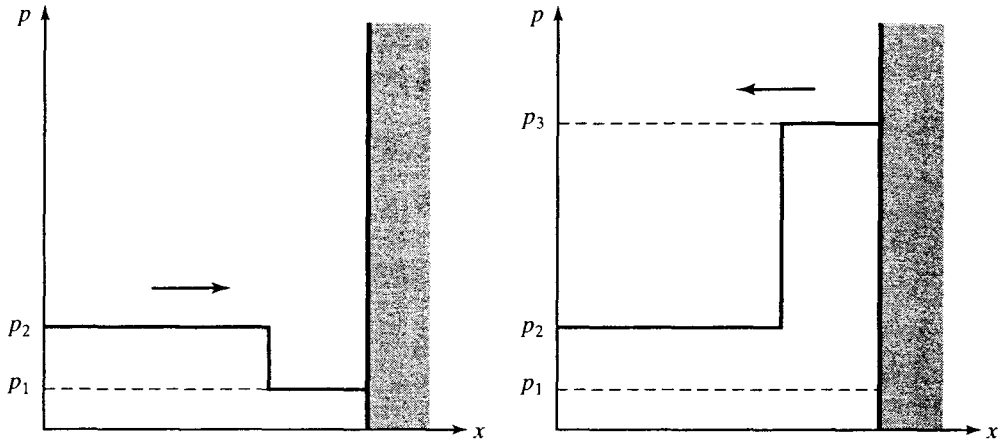


(a) Incident Normal Shock (b) Reflected Normal Shock

**Figure 5.11** Reflection of a Normal Shock

Eliminating $(V_2 - S_I)/a_2$ and $(S_R + V_2)/a_2$ between Eqs. (5.22) and (5.23), using Eq. (5.21), produces

$$\frac{p_3}{p_2} = \frac{\left(\frac{3\gamma - 1}{\gamma + 1}\right) - \left(\frac{\gamma - 1}{\gamma + 1}\right)\left(\frac{p_1}{p_2}\right)}{\left(\frac{p_1}{p_2}\right) + \left(\frac{\gamma - 1}{\gamma + 1}\right)} = \frac{\left(\frac{3\gamma - 1}{\gamma + 1}\right)\left(\frac{p_2}{p_1}\right) - \left(\frac{\gamma - 1}{\gamma + 1}\right)}{1 + \left(\frac{\gamma - 1}{\gamma + 1}\right)\left(\frac{p_2}{p_1}\right)} \tag{5.24}$$

Figure 5.11 illustrates the magnification effect on pressure caused by reflection of a normal shock from a solid surface.

**Example 5.5. Calculation of shock speeds and pressures for a normal shock reflecting off a solid surface**

A normal shockwave with pressure ratio of 4.5 impinges on a plane wall. (See Figure 5.10.) Determine the speeds of the incident and reflected shocks, the speed of the gas behind the incident shock, and the static-pressure ratio for the reflected normal shockwave. The air ($\gamma = 1.4$, $R = 287$ J/kg · K) temperature in front of the incident wave is 20°C.

**Solution**

To solve this problem, we utilize a coordinate system moving with the shock, as shown in Figure 5.10. For $p_2/p_1 = 4.5$ and $\gamma = 1.4$, we find that $M_1 = 2.0$. The speed of the incident shock is determined from $S_I = M_1 a_1 = 2.0\sqrt{(1.4)(287)293} = 686.2285$ m/s. From the normal-shock relations, we have

$$\frac{\rho_2}{\rho_1} = 2.6667 \text{ and } \frac{T_2}{T_1} = 1.6875$$

and from the continuity equation, we get

$$\frac{S_I}{S_I - V_2} = \frac{\rho_2}{\rho_1}$$

Therefore, the velocity of the air behind the incident wave is

$$V_2 = S_I\left(\frac{\frac{\rho_2}{\rho_1} - 1}{\frac{\rho_2}{\rho_1}}\right) = 686.2285\left(\frac{2.6667 - 1}{2.6667}\right) = 428.8960 \text{ m/s}$$

$$T_2 = \left(\frac{T_2}{T_1}\right)T_1 = (1.6875)293 = 494.4375 \text{ K}$$

$$a_2 = \sqrt{\gamma R T_2} = \sqrt{(1.4)(287)(494.4375)} = 445.7185 \text{ m/s}$$

From Eq. (5.21), we obtain

$$S_R = -V_2 - \frac{a_2^2}{(V_2 - S_I)} = -428.896 + \frac{445.7185^2}{686.2285 - 428.896} = 343.1207 \text{ m/s}$$

Finally, from Eq. (5.24), we can compute the static-pressure ratio across the reflected shock:

$$\frac{p_3}{p_2} = \frac{\left(\frac{3\gamma - 1}{\gamma + 1}\right)\left(\frac{p_2}{p_1}\right) - \left(\frac{\gamma - 1}{\gamma + 1}\right)}{1 + \left(\frac{\gamma - 1}{\gamma + 1}\right)\left(\frac{p_2}{p_1}\right)} = \frac{\frac{4}{3}(4.5) - \frac{1}{6}}{1 + \frac{1}{6}(4.5)} = 3.3333$$

The pressure in Zone 3 is 15 [(3.3333)(4.5)] times larger than the pressure in Zone 1.

For a more comprehensive treatment of unsteady flows involving moving normal shockwaves, see Ref. (5.1).

## 5.4 CHAPTER CAPSTONE APPLICATION: THE SHOCK TUBE (THE RIEMANN PROBLEM)

The *shock tube* [see Refs. (5.2) and (5.3)] is a device in which normal shockwaves are generated by the rupture of a diaphragm separating a high-pressure gas from a gas at low pressure. As such, the shock tube is a useful research tool for investigating not only shock phenomena, but also the behavior of materials and objects when subjected to the extreme conditions of pressure and temperature prevalent in the gas flow behind the wave. Thus, the kinetics of a chemical reaction taking place at high temperature can be studied, as well as the performance, for example, of a body during reentry from space back into the earth's atmosphere.

A shock tube is shown in Figure 5.12. After rupture of the diaphragm, the system eventually approaches thermodynamic equilibrium, with the final state in the closed-end tube determined from the first law of thermodynamics. With no external heat transfer, the total internal energy of the gases at the final state is equal to the sum of the internal energies of the gases initially present on either side of the diaphragm.

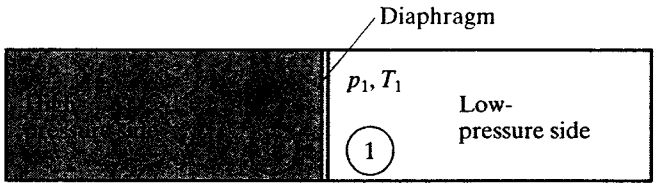


**Figure 5.12** Shock Tube Geometry

However, of primary interest is not the final equilibrium state of the gases, but the transient shock phenomena occurring immediately after rupture of the diaphragm. Upon rupture of the diaphragm, a normal shockwave moves into the low-pressure side, while a series of expansion waves propagates into the high-pressure gas. Curves of $p$ versus $x$ and $T$ versus $x$ shortly after rupture of the diaphragm are shown in Figure 5.13. Following the initial normal shockwave down the tube is a *contact surface,* a temperature discontinuity separating the gases compressed by the shock from the gases cooled by the expansion. The contact surface is a remnant of the diaphragm. The gases in Zones 2

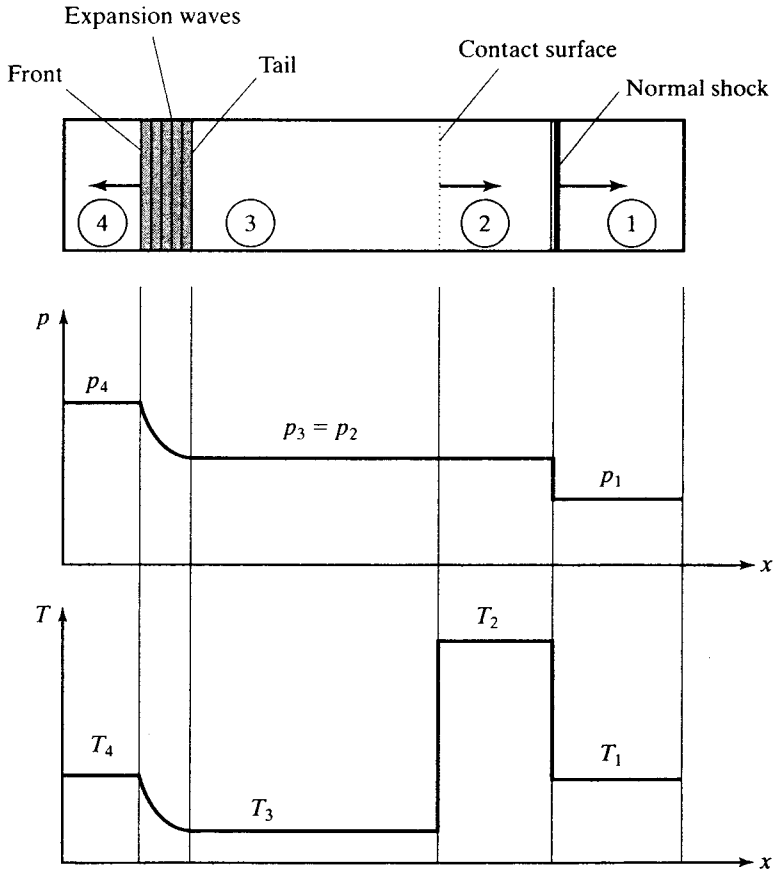


**Figure 5.13** Shock Tube Pressure and Temperature Distributions Shortly after Rupture of the Diaphragm

and 3 move with the same velocity and are at the same pressure, yet there is a density and temperature difference distinguishing these regions. The shock strength and gas velocities are dependent on the initial pressure ratio across the diaphragm, the properties of the gases involved, and the initial temperatures of the gases.

For shock-tube operation, it is of prime interest to develop an expression for shock strength $p_2/p_1$ as a function of the initial pressure ratio $p_4/p_1$ set across the diaphragm. The method we shall use in this analysis will be first to obtain an expression for $p_4/p_3$ across the expansion-wave system as a function of $V_3$, then to develop an expression for the normal-shock pressure ratio $p_2/p_1$ in terms of $V_2$, and finally to match the two solutions at the contact surface where $V_2 = V_3$ and $p_2 = p_3$, thus obtaining a resultant equation relating $p_2/p_1$ and $p_4/p_1$. (See Figure 5.14.)

First, we shall determine the variation of properties across the expansion waves. Let us consider the general case of an infinitesimal wave moving leftward down a tube into a gas stream moving toward the wave. As usual, assume that the gas behaves as a perfect gas, with constant specific heats. The wave moves at the velocity of sound with respect to the gas into which it is moving, so the absolute velocity of the wave will be $(a - V)$ (see Figure 5.15.). Following our usual procedure, let us fix this wave, as shown in Figure 5.16. From the continuity equation, we have

$$\rho a = (\rho + d\rho)(a + dV)$$

or

$$\frac{d\rho}{\rho} = -\frac{dV}{a} \tag{5.25}$$

For an infinitesimal wave, the flow is isentropic (i.e., $p/\rho^\gamma$ = constant), so we may write

$$p = C_1\rho^\gamma = C_2T^{\gamma/\gamma-1} = C_3a^{2\gamma/(\gamma-1)}$$

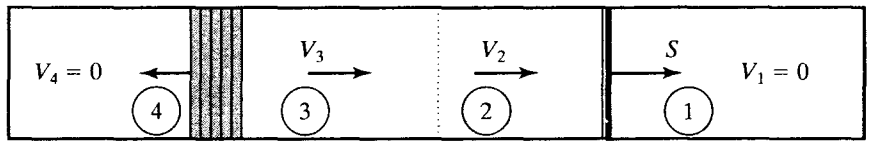


**Figure 5.14** Speeds within a Shock Tube

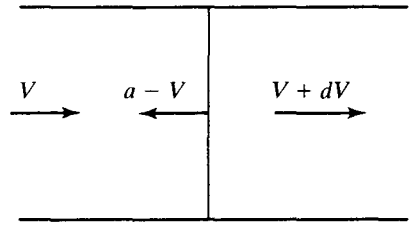


**Figure 5.15** Left-running Expansion Wave

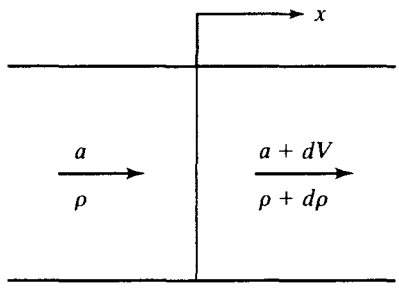


**Figure 5.16** Left-Running Expansion Wave in a Moving Coordinate System

Therefore,

$$\rho = Ca^{2/(\gamma-1)}$$

Take the logarithm of this expression and then differentiate to obtain

$$\frac{d\rho}{\rho} = \frac{2}{\gamma - 1}\frac{da}{a}$$

Combine this result with Eq. (5.25) to find for the left-moving wave

$$\frac{2}{\gamma - 1}da + dV = 0 \tag{5.26}$$

Equation (5.26) can be directly integrated to produce

$$\frac{2}{\gamma - 1}a + V = \text{constant} = Q_1 \tag{5.27}$$

If the infinitesimal wave were moving to the right, as shown in Figure 5.17, a similar analysis yields

$$\frac{2}{\gamma - 1}a - V = \text{constant} = Q_2 \tag{5.28}$$

The quantities $[2/(\gamma - 1)]a \pm V$, appearing in Eqs. (5.27) and (5.28), are constants $Q_1$ and $Q_2$ and called the *Riemann invariants*. They play a critical role in the numerical analysis of unsteady compressible-flow problems.

Returning to the shock-tube flow of Figure 5.12, we see that Eq. (5.27) can be applied between Zone 3 and Zone 4. Note that the gas is at rest in Zone 4 (i.e., $V_4 = 0$) and that $\gamma_3 = \gamma_4$. Therefore,

$$\frac{2}{\gamma_4 - 1}a_4 + 0 = \frac{2}{\gamma_4 - 1}a_3 + V_3 \tag{5.29}$$

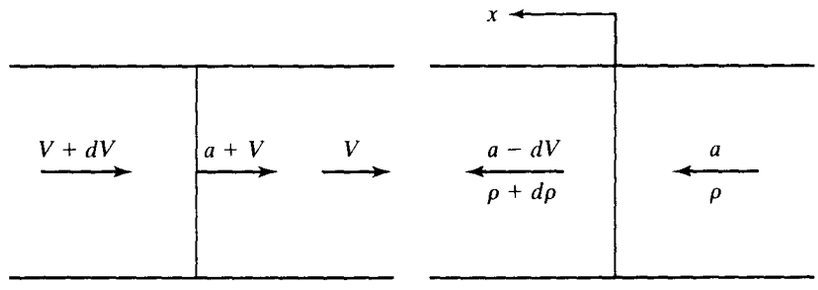


(a) Stationary Coordinate System (b) Moving Coordinate System

**Figure 5.17** Right-Running Expansion Wave in Stationary and Moving Coordinate Systems

In the region separating Zones 3 and 4, the expansion waves do not coalesce, but rather spread out as they move down the tube. Therefore, we can assume that the flow from within this region is isentropic, and so

$$\left(\frac{p_3}{p_4}\right) = \left(\frac{\rho_3}{\rho_4}\right)^{\gamma_4} = \left(\frac{T_3}{T_4}\right)^{\gamma_4/(\gamma_4-1)} = \left(\frac{a_3}{a_4}\right)^{2\gamma_4/(\gamma_4-1)} \tag{5.30}$$

Combining the isentropic relations with a rearranged version of Eq. (5.29) yields

$$V_3 = \frac{2a_4}{\gamma_4 - 1}\left(1 - \frac{a_3}{a_4}\right) = \frac{2a_4}{\gamma_4 - 1}\left[1 - \left(\frac{p_3}{p_4}\right)^{(\gamma_4-1)/2\gamma_4}\right] \tag{5.31}$$

This completes the first portion of the analysis.

We may now proceed to determine the velocity $V_2$ of the gas behind the rightward-moving normal shock as a function of the shock-pressure ratio. [See Figure 5.18(a).] To reduce the problem to one of steady flow, first we must redefine the coordinate system to fix the shock. [See Figure 5.18(b).]

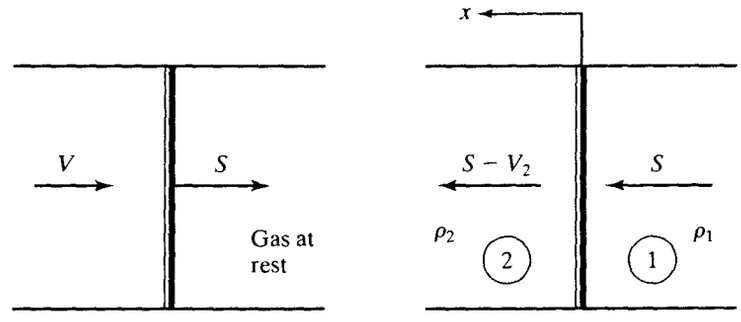


(a) Moving Shock in a Stationary Coordinate System (b) Moving Shock in a Moving Coordinate System

**Figure 5.18** Normal Shock in Fixed and Moving Coordinate Systems

Because the shock is moving into a gas at rest, this is the same problem that was treated in Section 5.2, and therefore we may utilize the expressions developed there. The pressure ratio across the shock is related to the shock Mach number ($M_1 = M_s = S/a_1$) by Eq. (5.8):

$$\frac{p_2}{p_1} = \frac{2\gamma_1}{\gamma_1 + 1}\left(\frac{S}{a_1}\right)^2 - \frac{\gamma_1 - 1}{\gamma_1 + 1}$$

This equation may be rewritten as

$$S = a_1\sqrt{\left(\frac{\gamma_1 + 1}{2\gamma_1}\right)\frac{p_2}{p_1} + \left(\frac{\gamma_1 - 1}{2\gamma_1}\right)} \tag{5.32}$$

The continuity equation, written as Eq. (5.6), may be used to introduce $V_2$ into the analysis:

$$\frac{\rho_2}{\rho_1} = 1 - \frac{V_2}{S} \tag{5.33}$$

To eliminate the density ratio, we may make use of the Rankine–Hugoniot relation, Eq. (5.5):

$$\frac{\rho_2}{\rho_1} = \frac{\dfrac{(\gamma_1 + 1)}{(\gamma_1 - 1)}\dfrac{p_2}{p_1} + 1}{\dfrac{(\gamma_1 + 1)}{(\gamma_1 - 1)} + \dfrac{p_2}{p_1}} \tag{5.34}$$

Combining Eqs. (5.32)–(5.34) yields

$$V_2 = \frac{a_1}{\gamma_1}\left(\frac{p_2}{p_1} - 1\right)\sqrt{\frac{\left(\dfrac{2\gamma_1}{\gamma_1 + 1}\right)}{\dfrac{p_2}{p_1} + \left(\dfrac{\gamma_1 - 1}{\gamma_1 + 1}\right)}} \tag{5.35}$$

To complete the solution to the problem, Eqs. (5.35) and (5.31) are equated, since $V_2 = V_3$:

$$V_2 = \frac{a_1}{\gamma_1}\left(\frac{p_2}{p_1} - 1\right)\sqrt{\frac{\left(\dfrac{2\gamma_1}{\gamma_1 + 1}\right)}{\dfrac{p_2}{p_1} + \left(\dfrac{\gamma_1 - 1}{\gamma_1 + 1}\right)}} = V_3 = \frac{2a_4}{\gamma_4 - 1}\left[1 - \left(\frac{p_3}{p_4}\right)^{(\gamma_4 - 1)/2\gamma_4}\right]$$

Finally, making use of the fact that $p_2 = p_3$ and rearranging terms produces

$$\frac{p_4}{p_1} = \frac{p_2}{p_1}\left[1 - \frac{(\gamma_4 - 1)\left(\dfrac{a_1}{a_4}\right)\left(\dfrac{p_2}{p_1} - 1\right)}{\sqrt{2\gamma_1}\sqrt{2\gamma_1 + (\gamma_1 + 1)\left(\dfrac{p_2}{p_1} - 1\right)}}\right]^{-[2\gamma_4/(\gamma_4 - 1)]} \tag{5.36}$$

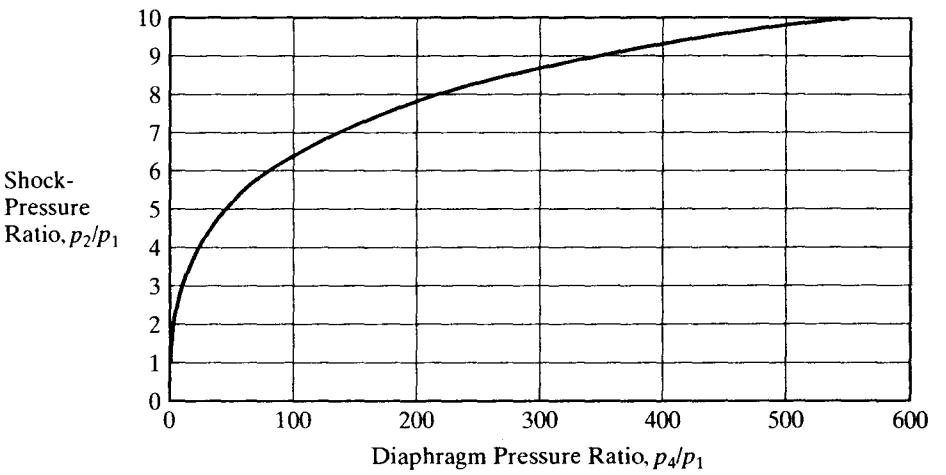


**Figure 5.19** Shock-pressure Ratio Versus Diaphragm-pressure Ratio.

It should be noted that if the shock-pressure ratio $p_2/p_1$ is known, it is a simple matter to obtain the diaphragm pressure ratio $p_4/p_1$ for given values of $\gamma_1$, $\gamma_4$, $a_1$, and $a_4$. However, the opposite is the case; that is, generally, we seek the shock-pressure ratio given the diaphragm ratio. Unfortunately, this is not as simple as we might think, because Eq. (5.36) is highly nonlinear. It is this fact that makes the shock tube (*the Riemann problem*) computationally difficult. To determine the shock-pressure ratio from Eq. (5.36), some form of iterative procedure will be required. (See Example 5.6.) Figure 5.19 provides a plot of the shock-pressure ratio versus the diaphragm-pressure ratio for a shock tube, with $\gamma = 1.4$ and $T_1 = T_4$.

Once the shock-pressure ratio is known, the temperature ratio across the shock can be determined by combining the perfect law with the Rankine–Hugoniot relation to obtain

$$\frac{T_2}{T_1} = \frac{\dfrac{(\gamma_1 - 1)}{(\gamma_1 + 1)}\dfrac{p_2}{p_1} + 1}{1 + \dfrac{(\gamma_1 - 1)}{(\gamma_1 + 1)}\dfrac{p_1}{p_2}} = \left(\frac{a_2}{a_1}\right)^2 \tag{5.37}$$

The temperature ratio across the expansion is determined from the isentropic relations of Eq. (5.30):

$$\frac{T_3}{T_4} = \left(\frac{p_3}{p_4}\right)^{(\gamma_4 - 1)/\gamma_4} = \left(\frac{\dfrac{p_2}{p_1}}{\dfrac{p_4}{p_1}}\right)^{(\gamma_4 - 1)/\gamma_4} = \left(\frac{a_3}{a_4}\right)^2 \tag{5.38}$$

The following is a summary of the computational procedure to determine the shock-tube parameters following rupture of the diaphragm:

Given: $\gamma_1$, $\gamma_4$, $R_1$, $R_4$, $T_1$, $T_4$, $p_1$, and $p_4$; also, $V_1 = V_4 = 0$
Determine:

1. $a_1$, $a_4$, $\rho_1$, and $\rho_4$ from the perfect-gas relations,
2. $p_2/p_1$ by solving Eq. (5.36),
3. S from Eq. (5.32),
4. $V_2$ and $V_3$ from Eq. (5.35) (note that $V_3 = V_2$),
5. $T_2/T_1$ from Eq. (5.37),
6. $\rho_2/\rho_1$ from Eq. (5.34),
7. $T_3/T_4$ from Eq. (5.38), and
8. $\rho_4/\rho_3$ from Eq. (5.30).

**Example 5.6. Calculation of the shock pressure ratio in a shock tube**

Develop a numerical procedure to determine the shock-pressure ratio from the diaphragm-pressure ratio. As an example, find $p_2/p_1$ given $\gamma_1 = \gamma_4 = 1.4$, $a_1 = a_4$, and $p_4/p_1 = 50$.

**Solution:**

The Newton–Raphson method will be used to determine the shock-pressure ratio. This root-solving technique has been frequently used in previous chapters. To utilize the method, we rewrite Eq. (5.36) as

$$f\left(\frac{p_2}{p_1}\right) = \frac{p_4}{p_1}\left[1 - \frac{(\gamma_4 - 1)\left(\frac{a_1}{a_4}\right)\left(\frac{p_2}{p_1} - 1\right)}{\sqrt{2\gamma_1}\sqrt{2\gamma_1 + (\gamma_1 + 1)\left(\frac{p_2}{p_1} - 1\right)}}\right]^{2\gamma_4/(\gamma_4 - 1)} - \frac{p_2}{p_1} = 0$$

or

$$f(p) = \left(\frac{p_4}{p_1}\right)\left[1 - \frac{c_1(p - 1)}{\sqrt{1 + c_2(p - 1)}}\right]^{c_3} - p = 0 \tag{5.39}$$

where $p_2/p_1$ has been replaced by $p$ for convenience, and the constants within the function are

$$c_1 = \frac{\gamma_4 - 1}{2\gamma_1}\left(\frac{a_1}{a_4}\right)$$

$$c_2 = \frac{\gamma_1 + 1}{2\gamma_1}$$

$$c_3 = \frac{2\gamma_4}{\gamma_4 - 1}$$

The Newton–Raphson method for this case may be expressed as

$$p_{\text{new}} = p_{\text{old}} - \frac{f(p_{\text{old}})}{\frac{df}{dp}(p_{\text{old}})}$$

**TABLE 5.3** Spreadsheet Calculations Used to Determine the Shock-Pressure Ratio of Example 5.6

| $p_{old}$ | $f$ | $f(p + \Delta p)$ | $f(p - \Delta p)$ | $df/dp$ | $p_{new}$ |
|---|---|---|---|---|---|
| 2.00000 | 21.03105 | 20.87650 | 21.18696 | −15.52281 | 3.35485 |
| 3.35485 | 7.72947 | 7.66697 | 7.79230 | −6.26662 | 4.58828 |
| 4.58828 | 1.84580 | 1.80926 | 1.88246 | −3.65990 | 5.09261 |
| 5.09261 | 0.15297 | 0.12219 | 0.18385 | −3.08291 | 5.14223 |
| 5.14223 | 0.00119 | −0.02911 | 0.03159 | −3.03503 | 5.14263 |
| 5.14263 | 0.00000 | −0.03030 | 0.03039 | −3.03466 | 5.14263 |

Because the derivative of the function is somewhat complicated, a central finite-difference representation will be used to compute the required derivative:

$$\frac{df}{dp} = \frac{f(p + \Delta p) - f(p - \Delta p)}{2\Delta p}$$

The computations for the given conditions are contained within Table 5.3, which has been prepared using a simple spreadsheet program. An arbitrary initial guess of 2.00 was used to begin the process. The following constants were used:

$$c_1 = 0.14286$$
$$c_2 = 0.85714$$
$$c_3 = 7.0$$
$$\Delta p = 0.01$$

Thus, the shock pressure ratio $p_2/p_1$ is 5.1426. With this value, it is a relatively easy task to determine all other shock-tube parameters, as will be shown in the following example.

**Example 5.7. Calculation of speeds and flow properties in a shock tube**

The air pressure on the high-pressure side (also called the driver side) of the diaphragm in a shock tube is set at 500 kPa, and the air pressure on the low-pressure side (also called the driven side) is 20 kPa; the initial air temperature on both sides of the diaphragm is 30°C. The diaphragm is suddenly broken, which causes a normal shock to propagate rightward into the low-pressure air and a series of expansion waves to propagate leftward into the high-pressure air, as shown in Figures 5.13 and 5.14. Determine the following:

(a) the velocity of the normal shock,
(b) the velocity of the air behind the normal shock,
(c) the velocity of the contact surface,
(d) the static temperature behind the normal shock,
(e) the static temperature behind the contact surface, and
(f) the velocity of the expansion waves at front and tail of the system of expansion waves.

**Solution**

(a) Following the shock-tube calculation procedure just delineated, we first determine the speed of sound of the low-pressure, driven air:

$$a_1 = \sqrt{\gamma_1 R_1 T_1} = \sqrt{(1.4)(287)(303)} = 348.9203 \text{ m/s}$$

For $p_4/p_1 = 500/20 = 25$, using the procedure described in Example 5.6, we find that $p_2/p_1 = 4.0471$. The shock speed can be determined from Eq. (5.32):

$$S = a_1\sqrt{\left(\frac{\gamma_1 + 1}{2\gamma_1}\right)\frac{p_2}{p_1} + \left(\frac{\gamma_1 - 1}{2\gamma_1}\right)} = 348.9203\sqrt{\left(\frac{2.4}{2.8}\right)(4.0471) + \left(\frac{0.4}{2.8}\right)}$$
$$= (348.9203)(1.9005) = 663.1138 \text{ m/s}$$

Note that the shock Mach number $M_s = S/a_1$ is 1.9005.

(b) The speed of the gas behind the shock is computed from Eq. (5.35):

$$V_2 = \frac{a_1}{\gamma_1}\left(\frac{p_2}{p_1} - 1\right)\sqrt{\frac{\left(\frac{2\gamma_1}{\gamma_1 + 1}\right)}{\frac{p_2}{p_1} + \left(\frac{\gamma_1 - 1}{\gamma_1 + 1}\right)}}$$
$$= \left(\frac{348.9203}{1.4}\right)(3.0471)\sqrt{\frac{1.1667}{(4.0471 + 0.1667)}}$$
$$= 399.6019 \text{ m/s}$$

(c) The contact surface moves at the same velocity as that of the air behind the normal shock.

(d) The static temperature behind the shock is determined from Eq. (5.37):

$$\frac{T_2}{T_1} = \frac{\frac{(\gamma_1 - 1)}{(\gamma_1 + 1)}\frac{p_2}{p_1} + 1}{1 + \frac{(\gamma_1 - 1)}{(\gamma_1 + 1)}\frac{p_1}{p_2}} = \frac{\frac{4.0471}{6} + 1}{1 + \frac{1}{6(4.0471)}} = 1.6083$$

Alternatively, since the Mach number behind the shock is $M_1 = M_s = 1.9005$, the ratio of static temperatures across the shock can be determined from Eq. (4.11). Hence,

$$T_2 = 1.6083(303) = 487.3149 \text{ K}$$

(e) For the expansion flow, the region between Zones 3 and 4 in Figure 5.14,

$$\frac{T_3}{T_4} = \left(\frac{p_3}{p_4}\right)^{(\gamma_4 - 1)/\gamma_4} = \left(\frac{\frac{p_2}{p_1}}{\frac{p_4}{p_1}}\right)^{(\gamma_4 - 1)/\gamma_4} = \left(\frac{4.0471}{25}\right)^{0.2857} = 0.5944$$

Hence,

$$T_3 = 0.5944(303) = 180.1032 \text{ K}$$

(f) The wave at the front of the system of expansion waves moves at the velocity of sound with respect to the air ahead of it. Since $V_4 = 0$ and $a_4 = a_1$ (because $T_4 = T_1$ and $\gamma_4 = \gamma_1$), the velocity of the front wave is equal to $a_4 = 348.9203$ m/s.

At the tail of the expansion-wave system,

$$a_3 = \sqrt{\gamma_3 R_3 T_3} = \sqrt{(1.4)(287)(180.1032)} = 269.0083 \text{ m/s}$$

The absolute velocity of the last wave is $a_3 - V_3 = 269.0083 - 399.6019 = -130.5936$ m/s. (The negative sign indicates that the wave is moving rightward.)

---

An $x$–$t$ diagram showing the location of normal shock, contact surface, and expansion waves as a function of time is given in Figure 5.20.

In a shock tube, it is often desirable to be able to subject a test object to uniform conditions of high pressure and temperature for as long a period of time as possible. Uniform conditions prevail behind the initial shock until the passage of either the contact surface, the shock reflected from the closed end of the tube, or the front of the expansion waves reflected from the opposite end. Figure 5.21 depicts the location of each of these waves as a function of time from rupture of the diaphragm for a typical shock-tube system. For the system shown, the position at which the test object should be placed in order to subject it to uniform conditions for a maximum time interval is indicated in Figure 5.21. The test object is exposed to the pressure and temperature behind the initial shock for a period $t_{max}$ from passage of the initial wave to passage

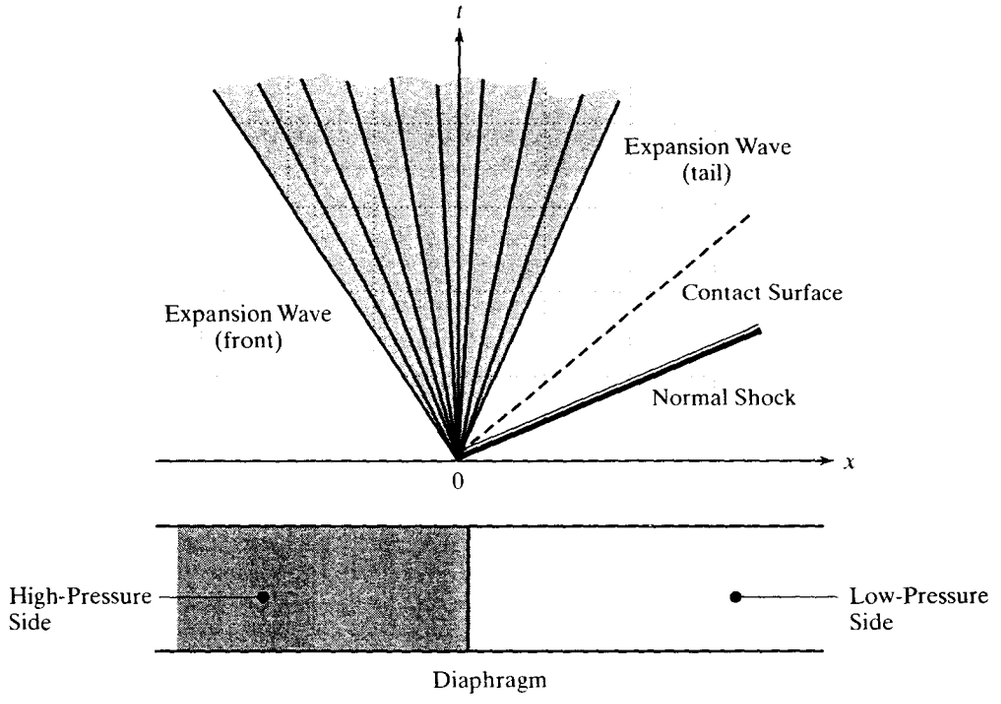


**Figure 5.20** Shock Tube $x$–$t$ Diagram

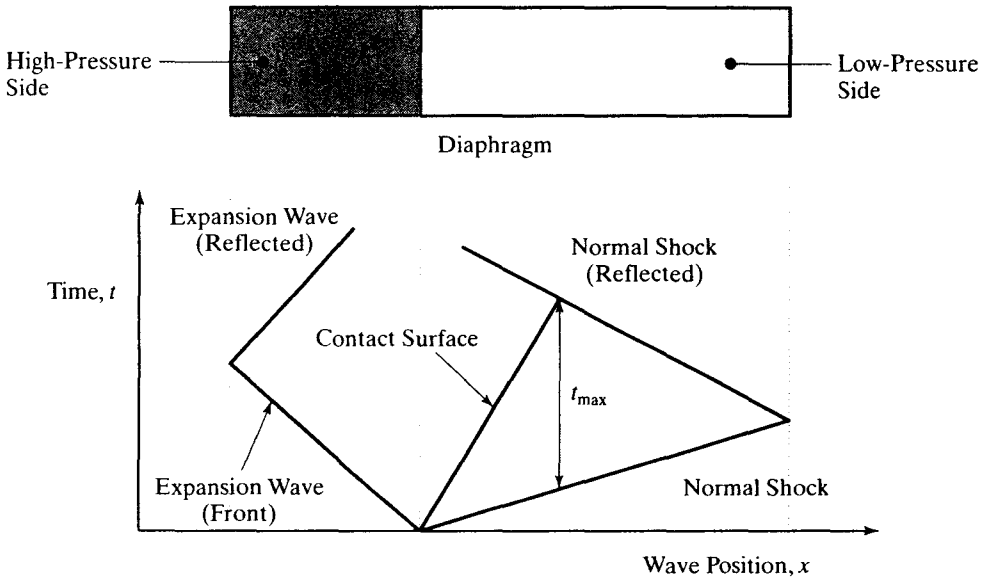


**Figure 5.21** *x–t* Diagram of Wave Motion within a Shock Tube

over the object of the contact surface. The test time is clearly a function of the shock-tube length, as well as of the shock and expansion velocities. An object can be tested under uniform conditions for periods up to several milliseconds in a shock tube, which is sufficient in many cases to make meaningful measurements on a test object.

## 5.5 SUMMARY

In this chapter, the case of moving normal shockwaves has been considered in some detail. The governing equations were developed in both stationary (attached to the earth) and moving (attached to the moving wave) coordinate systems. Numerous illustrations of the transformation between the two coordinate systems were provided. These illustrations allowed a clear picture to emerge of the distinction between stagnation and static fluid properties. Finally, the simple, but very useful, test device the shock tube was analyzed. This analysis was accompanied by the introduction of expansion waves and the contact discontinuity. Both will be studied in greater depth in subsequent chapters.

## 5.6 REFERENCES

**5.1** Owczarek, J. A. *Fundamentals of Gas Dynamics,* International Textbook Co., Scranton, PA, 1964, pp. 366–434.

**5.2** Glass, I. I. "Theory and Performances of Simple Shock Tubes," Institute of Aerophysics, University of Toronto, *UTIA Review*, No. 12, 1958.

**5.3** Wright, J. K. *Shock Tubes*, Methuen's Monographs on Physical Subjects, John Wiley & Sons, New York, 1961.

## 5.7 PROBLEMS

**5.1** A projectile moves down a gun barrel with a velocity of 500 m/s. (See Figure P5.1.) Calculate the velocity of the normal shock that would precede the projectile. Assume the pressure in the undisturbed air ($\gamma = 1.4$, $R = 287$ J/kg·K) to be 101 kPa and the temperature to be 25°C. How fast would the projectile have to be moving in order for the shock velocity to be two times the projectile velocity?

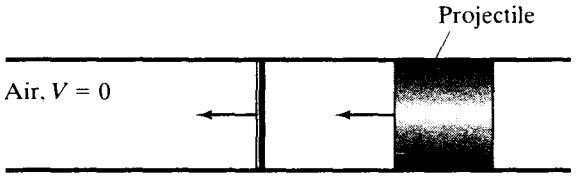


**Figure P5.1**

**5.2** A normal shock moves into still air ($\gamma = 1.4$, $R = 287$ J/kg·K) with a velocity of 1,000 m/s. The motionless air is at 101 kPa and 20°C. Calculate the following:

(a) the velocity of the air flow behind the wave,
(b) the static pressure behind the wave, and
(c) the stagnation temperature behind the wave.

**5.3** A normal shock is observed to move through a constant-area tube into air ($\gamma = 1.4$, $R = 287$ J/kg·K) at rest at 25°C. (See Figure P5.3.) The velocity of the air behind the wave is measured to be 150 m/s. Calculate the shock velocity.

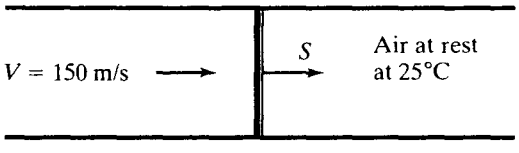


**Figure P5.3**

**5.4** A piston in a tube is suddenly accelerated to a velocity of 25 m/s, causing a normal shock to move into helium ($\gamma = 5/3$, $R = 2{,}077$ J/kg·K) at rest in the tube and at a temperature of 27°C in the tube. One second later, the piston is suddenly accelerated from 25 to 50 m/s, causing a second shock to move down the tube. How much time will elapse from the initial acceleration of the piston to the intersection of the two shocks?

**5.5** Air ($\gamma = 1.4$, $R = 287$ J/kg·K) at 100 kPa and 290 K is flowing in a constant-area tube with a velocity of 100 m/s. (See Figure P5.5.) Suddenly, the end of the tube is closed, which causes a normal shock to propagate back through the airstream. Find the absolute velocity of this shock.

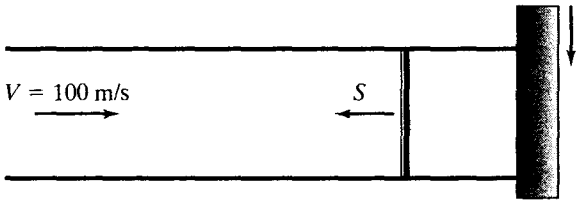


**Figure P5.5**

**5.6** A normal shock traveling at 1,000 m/s into still air ($\gamma = 1.4$, $R = 287$ J/kg · K) at 0°C and 101 kPa reflects from a plane wall. Determine the velocity of the reflected shock. Compare the pressure ratio across the reflected shock with that across the incident shock. Find the stagnation pressure that would be measured by a stationary observer behind the reflected wave.

**5.7** Under a certain operating condition, the piston speed in an auto engine is 10 m/s. We will approximate engine knock as the occurrence of a normal shockwave traveling at 1,000 m/s downward, as shown in Figure P5.7, into the unburned mixture at 700 kPa and 500 K. Determine the pressure acting on the piston face after the shock reflects from it. Assume that the gas has the properties of air ($R = 287$ J/kg · K) and acts as a perfect gas, with $\gamma = 1.4$.

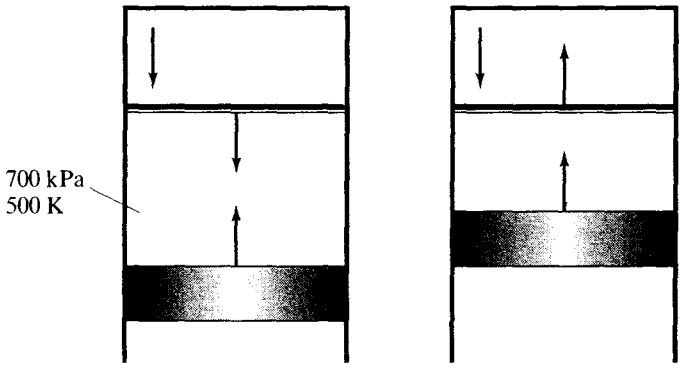


**Figure P5.7**

**5.8** A normal shock moves down a tube with a velocity of 600 m/s into a gas with a static pressure of $p = 50$ kPa and a static temperature of 300 K. At the end of the tube, a piston is moving with a velocity of 60 m/s, as shown in Figure P5.8. Calculate the velocity of the reflected wave and the static pressure behind the reflected wave. Assume that the gas has the properties of air ($\gamma = 1.4$, $R = 287$ J/kg · K).

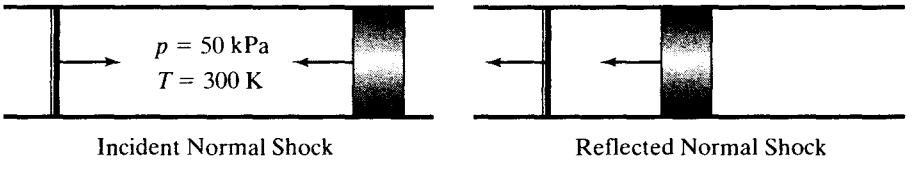


**Figure P5.8**

**5.9** For both $\gamma = 7/5$ and $5/3$, determine the limits of the static-pressure ratio of a reflected normal shock (i.e., $p_3/p_2$) (a) for a strong incident shock (i.e., $p_2/p_1 \rightarrow \infty$) and (b) for a weak incident wave (i.e., $p_2/p_1 \rightarrow 1$).

**5.10** A shock tube is to be used to subject an object to momentary conditions of high pressure and temperature. To provide an adequate measuring time, the tube is to be made long enough so that a period of 100 ms is provided between the time of passage over the body of the initial shock and the time of passage of the shock reflected from the closed end of the tube. The initial pressure ratio across the diaphragm is 400 to 1, with the object located 3 m from the diaphragm. The initial temperature of the air ($\gamma = 1.4$, $R = 287$ J/kg · K) in the shock tube is 35°C. Determine a suitable length for the low-pressure end of the tube.

**5.11** Air ($\gamma = 1.4$, $R = 287$ J/kg · K) is stored in a tube at 200 kPa and 300 K. (See Figure P.5.11.) A diaphragm at the end of the tube separates the high-pressure air and the ambient air, which has a pressure of 101 kPa. The diaphragm is suddenly ruptured, which causes expansion waves to move down the duct. Determine both the time required for the first expansion wave to reach the closed end of the tube and the velocity of the air behind the expansion waves.

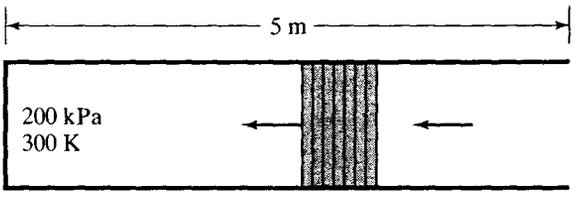


**Figure P5.11**

**5.12** Write a computer program that will yield values of the diaphragm-pressure ratio for given values of the shock-pressure ratio for a shock tube with helium ($\gamma = 5/3$) at the same temperature on both sides of the diaphragm. Determine values of diaphragm-pressure ratios for shock-pressure ratios from 1.0 to 5.0, using increments of 0.2.

**5.13** A circular tube of length 1.5 m is evacuated to a pressure of 2.5 kPa, with the ambient pressure at 101 kPa. A diaphragm at the end of the tube is ruptured, which causes a normal shock to move down the tube. Determine the velocity of the initial shock that moves down the tube, the velocity and Mach number of the air ($\gamma = 1.4$, $R = 287$ J/kg · K) behind the shock, and the velocity of the shock that reflects from the closed end. The initial air temperature before diaphragm rupture is 300 K. A test object is located midway along the tube. Determine the time that this object is subjected to the pressure and temperature conditions behind the initial shock (before the arrival of the reflected shock). Find the static pressure and temperature behind the initial shock.

**5.14** The pressure ratio across the diaphragm in a shock tube is set at 10. The diaphragm is then ruptured. Determine the velocity of the initial normal shock, the Mach number of the gas behind the shock, and the static pressure and temperature behind the shock for air ($\gamma = 1.4$, $R = 287$ J/kg · K) as the working fluid and for helium ($\gamma = 5/3$, $R = 2{,}077$ J/kg · K) as the working fluid. Assume the initial temperatures on each side of the diaphragm to be 25°C and the initial pressure in the low-pressure end to be 25 kPa.

**5.15** A normal shock moves down an open-ended tube with a velocity of 1,000 m/s. (See Figure P5.15.) The ambient pressure and temperature are 101 kPa and 25°C, respectively. Determine the velocities of the first and last expansion waves that move down the tube after reflection of the shock from the open end.

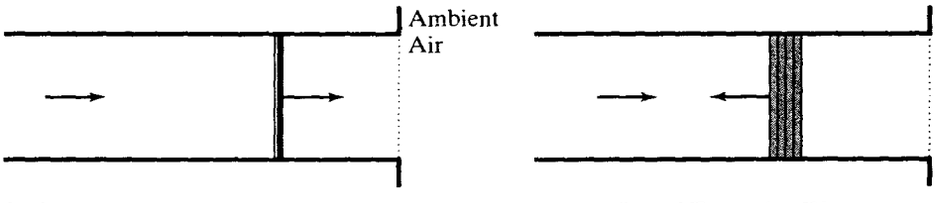


Incident Normal Shock on the Open End of a Tube

Reflected Expansion Waves

**Figure P5.15**

**5.16** A shock tube is 10 m long, with a 30-cm diameter. The high-pressure section is 4 m long and contains air ($\gamma = 1.4$, $R = 287$ J/kg · K) at 200 kPa; the low-pressure section is 6 m long and contains air at 5 kPa. A test object is placed in the low-pressure section 3 m from the diaphragm. Both sections initially contain air at 25°C. The diaphragm is suddenly ruptured, which causes a shock to move into the low-pressure section. Determine the following:

(a) the shock velocity,
(b) the contact-surface velocity,
(c) the Mach number of air behind the shock,
(d) the time between passage of the normal shock and the contact surface over the test object, and
(e) the time between passage of the normal shock and the reflected shock over the test object.
(f) Provide an $x$–$t$ diagram showing the location of the initial shock, the reflected shock, and the contact surface as a function of time.

# Chapter 6

# Oblique Shockwaves

## 6.1 INTRODUCTION

In Chapter 4, the stationary normal shockwave, a compression discontinuity normal to the flow direction, was studied in some detail. However, in a wide variety of physical situations, a compression shockwave occurs that is inclined at an angle to the flow. Such a wave is called an *oblique shock*.

An oblique shockwave, either straight or curved, can occur in such varied examples as supersonic flow over a thin airfoil, as explained in Chapter 2, or in supersonic flow through an overexpanded nozzle, as mentioned in Chapter 4. The frequency of occurrence of such oblique waves makes the material presented in this chapter essential to an understanding of compressible supersonic flow.

A study of the multidimensional oblique shockwave represents a departure from the one-dimensional flow covered previously, yet, in many ways, the method of handling the oblique shock parallels that of handling the normal shock. Even though inclined to the flow direction, the oblique shock still represents a sudden, almost discontinuous change in fluid properties, with the shock process itself being adiabatic. In this chapter, attention will be focused on the two-dimensional straight oblique shockwave, a type that might occur because of the presence of a wedge in a supersonic stream [see Figure 6.1(a)] or during a supersonic compression in a corner [see Figure 6.1(b)]. Note that in either case the surface is directed into the flow.

As with the normal shockwave, the conservation equations of mass, momentum, and energy will first be derived. An additional variable is introduced because of the change in flow direction across the wave. However, momentum is a vector quantity, so two momentum equations are derivable for this two-dimensional flow. With the additional variable and equation, the analysis of two-dimensional shock flow is more complex than that for normal shock flow. However, as with the normal shockwave, solutions to the equations of motion will be presented in a form suitable for the working of practical engineering problems. Moreover, utilization of the spreadsheet computation can remove tedious calculations and the reliance on graphical methodology that generally accompany work with oblique shocks.

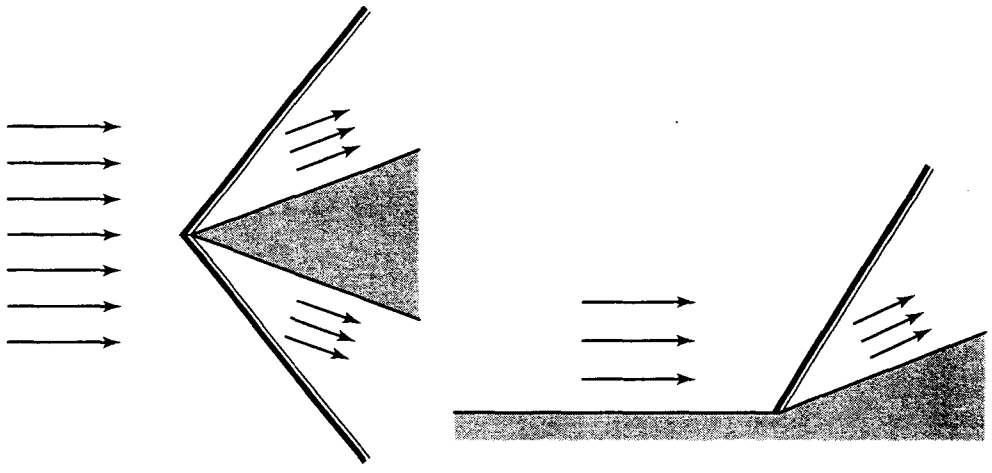

(a) A Symmetrical Wedge (b) A Concave Corner

**Figure 6.1** Geometries Involving Straight Oblique Shocks

## 6.2 EQUATIONS OF MOTION FOR A STRAIGHT OBLIQUE SHOCKWAVE

When a uniform supersonic stream is forced to undergo a finite change in direction due to the presence of a body in the flow, the stream cannot adjust gradually to the presence of the body; rather, a shockwave or sudden change in flow properties must occur, as described in Chapter 2.

A simple case is that of supersonic flow about a two-dimensional wedge whose axis is aligned parallel to the flow direction. For small *wedge angles*, designated by $\Delta$, the flow is turned by means of an oblique shockwave attached to the apex of the wedge and inclined at an angle $\theta$ to the flow direction. $\theta$ is called the *shockwave angle*. Flow behind the shock is uniform, parallel to the wedge surface (as shown in Figure 6.2), with the entire flow having been turned through the wedge half-angle. Since the flow is turned or deflected through the angle $\delta$, it is also referred to as the *deflection angle*. In this simple case, it is seen that $\delta = \Delta$. It must be kept in mind that $\delta$ is the amount of turn the flow makes relative to the upstream flow angle ($\alpha_1$) and that $\theta$ is measured relative to this flow direction. (See Figure 6.3.)

It should be noted that there is no standard notation for the shockwave and deflection angles. Reference to a variety of texts reveals that the shockwave angle has been given numerous symbols. Usually, the deflection angle is designated by the symbol $\delta$; however, $\theta$ has also been used. Thus, when referring to other texts, it is imperative to make certain of the notation being used.

Before proceeding with the analysis of the flow through an oblique shockwave, it is important to assume a sign convention for the angles involved in the problems. Towards that end, the counterclockwise (CCW) direction will be taken as the positive angular direction and the clockwise direction (CW) as the negative angular direction.

The equations of continuity, momentum, and energy will now be written for uniform, supersonic flow turned through a given deflection. If one selects the control volume

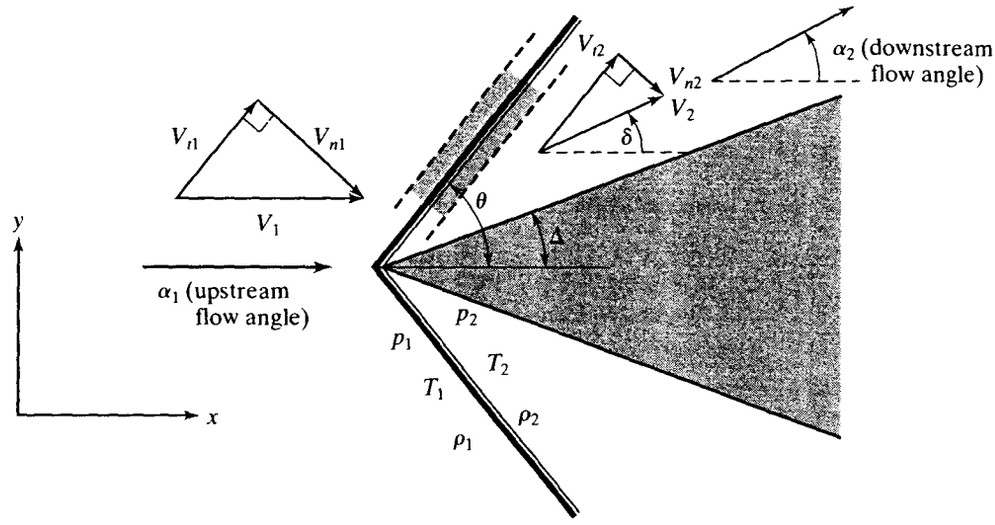


**Figure 6.2** Notation and Control Volume for an Oblique Shock

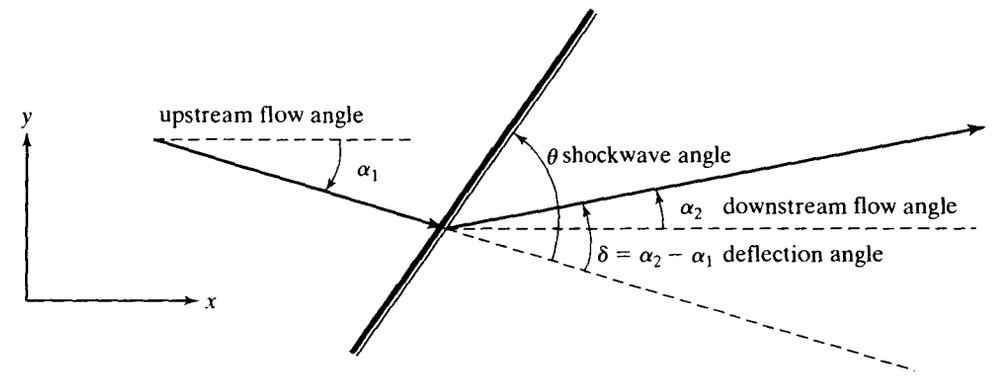


**Figure 6.3** Relationship between Flow Directions and the Deflection and Shockwave Angles

drawn around a portion of the shockwave as indicated in Figure 6.2, the continuity equation for steady flow is

$$\iint_{\text{C.S.}} \rho \mathbf{V} \cdot d\mathbf{A} = 0 \tag{1.28}$$

For the control volume under study, this expression simplifies to

$$\rho_1 V_{n1} = \rho_2 V_{n2} \tag{6.1}$$

where $V_{n1}$ and $V_{n2}$ are the velocity components normal to the wave on the upstream and downstream sides of the shock, respectively. The momentum equation for steady flow is

$$\sum \mathbf{F} = \iint_{\text{C.S.}} \mathbf{V}(\rho \mathbf{V} \cdot d\mathbf{A}) \tag{1.32}$$

Momentum is a vector quantity, so momentum balance equations can be written both in the direction normal to the wave and in the direction tangential to the wave. The normal momentum equation yields

$$p_1A_1 - p_2A_2 = \rho_2A_2V_{n2}^2 - \rho_1A_1V_{n1}^2$$

The shock is very thin so that $A_1 = A_2$. Thus, the areas drop out, leaving

$$p_1 - p_2 = \rho_2V_{n2}^2 - \rho_1V_{n1}^2 \tag{6.2}$$

In the tangential direction there is no change in pressure; thus, there are no external forces acting on the control volume, and so the flux of tangential momentum must sum to zero:

$$\iint_{\text{C.S.}} V_t(\rho\mathbf{V}\cdot d\mathbf{A}) = 0$$

This expression can be rewritten as

$$V_{t1}(\rho_1A_1V_{n1}) - V_{t2}(\rho_2A_2V_{n2}) = 0$$

where $V_{t1}$ and $V_{t2}$ are the velocity components tangential to the wave. Canceling the mass-flow rate, we obtain

$$V_{t1} = V_{t2} \tag{6.3}$$

Because the tangential component is the same on both sides of the shock, there is no momentum transfer along the shock front, and consequently there is no need to apply subscripts 1 and 2 to the tangential velocity components.

The energy equation for adiabatic steady flow simplifies to

$$h_1 + \frac{V_1^2}{2} = h_2 + \frac{V_2^2}{2}$$

Expanding this equation, we obtain

$$h_1 + \frac{V_{n1}^2 + V_t^2}{2} = h_2 + \frac{V_{n2}^2 + V_t^2}{2}$$

Canceling the tangential velocity component gives

$$h_1 + \frac{V_{n1}^2}{2} = h_2 + \frac{V_{n2}^2}{2} \tag{6.4}$$

Equations (6.1), (6.2), and (6.4) can be written as

$$\begin{aligned}(\rho_2V_{n2} - \rho_1V_{n1}) &= 0\\ (p_2 + \rho_2V_{n2}^2) - (p_2 + \rho_1V_{n1}^2) &= 0\end{aligned} \tag{6.5}$$

and

$$\left(h_2 + \frac{V_{n2}^2}{2}\right) - \left(h_1 + \frac{V_{n1}^2}{2}\right) = 0$$

which are the jump conditions across an oblique shockwave. Comparing this set of conditions to the jump conditions across a normal shockwave [see Eq. (4.4)], we observe that the only difference between the two is that the normal velocity component appears in the oblique shock equations where the absolute velocity appeared in the normal shock equations. From a physical standpoint, this observation means that an oblique shock acts as a normal shock for the component normal to the wave, while the tangential velocity component remains unchanged. From an analytical standpoint, the results from the normal shock analysis may be used by appropriately modifying normal shockwave expressions, which can save a considerable amount of effort. Towards that end, from the geometry of the flow, we have (see Figure 6.4)

$$V_t = V_1 \cos\theta \tag{6.6a}$$

$$V_{n1} = V_1 \sin\theta \tag{6.6b}$$

$$V_t = V_2 \cos(\theta - \delta) \tag{6.7a}$$

$$V_{n2} = V_2 \sin(\theta - \delta) \tag{6.7b}$$

We can form the following equations from these various Mach number relations:

$$M_t = \frac{V_t}{a_1} = \frac{V_1 \cos\theta}{a_1} = M_1 \cos\theta \tag{6.8a}$$

$$M_{n1} = M_1 \sin\theta \tag{6.8b}$$

$$M_t = M_2 \cos(\theta - \delta) \tag{6.9a}$$

$$M_{n2} = M_2 \sin(\theta - \delta) \tag{6.9b}$$

The expressions for the pressure ratio, temperature ratio, and so on, across an oblique shock are simply obtained by replacing $M_1$ in the corresponding normal shock relations

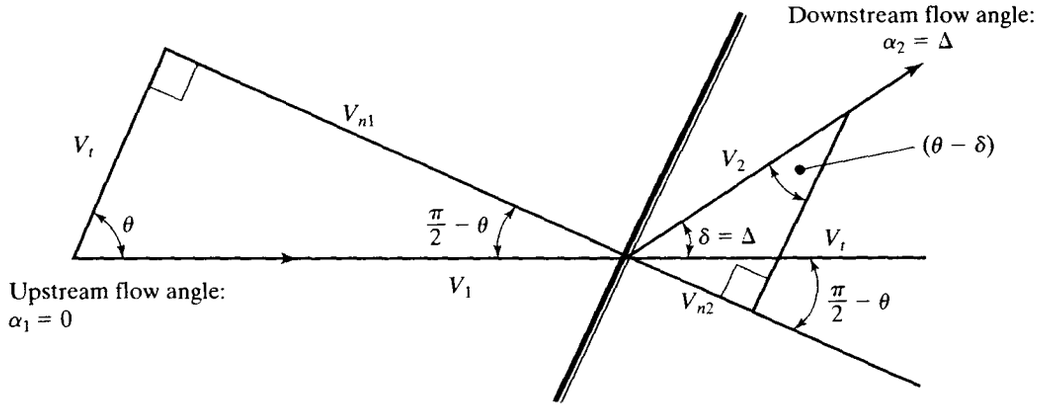


**Figure 6.4** Oblique Shock Geometry

with $M_1 \sin\theta$ and by replacing $M_2$ with $M_2 \sin(\theta - \delta)$. Thus, the working relations for an oblique shock are

$$\frac{p_2}{p_1} = \frac{2\gamma M_1^2 \sin^2\theta}{\gamma + 1} - \frac{\gamma - 1}{\gamma + 1} \tag{6.10}$$

$$\frac{\rho_2}{\rho_1} = \frac{V_{n1}}{V_{n2}} = \frac{V_1 \sin\theta}{V_2 \sin(\theta - \delta)} = \frac{(\gamma + 1)M_1^2 \sin^2\theta}{(\gamma - 1)M_1^2 \sin^2\theta + 2} \tag{6.11}$$

$$\frac{T_2}{T_1} = \left(\frac{a_2}{a_1}\right)^2 = \frac{\left(1 + \dfrac{\gamma - 1}{2} M_1^2 \sin^2\theta\right)\left(\dfrac{2\gamma}{\gamma - 1} M_1^2 \sin^2\theta - 1\right)}{\left[\dfrac{(\gamma + 1)^2}{2(\gamma - 1)}\right] M_1^2 \sin^2\theta} \tag{6.12}$$

$$\frac{p_{o2}}{p_{o1}} = e^{-(\Delta s/R)} = \left[\frac{\dfrac{\gamma+1}{2} M_1^2 \sin^2\theta}{1 + \dfrac{\gamma-1}{2} M_1^2 \sin^2\theta}\right]^{\gamma/(\gamma-1)} \left[\frac{1}{\dfrac{2\gamma}{\gamma+1} M_1^2 \sin^2\theta - \dfrac{\gamma-1}{\gamma+1}}\right]^{1/(\gamma-1)} \tag{6.13}$$

$$\frac{T_{o2}}{T_{o1}} = 1 \tag{6.14}$$

**Example 6.1. Obtaining Prandtl's relation for an oblique shock by transforming the relation for a normal shock**

Derive Prandtl's relation for an oblique shockwave by making use of the expression already developed in Chapter 4, Eq. (4.20), for a stationary normal shockwave.

**Solution**

The classical development of Prandtl's relation was performed for a stationary normal shockwave in Chapter 4. The result obtained connects the velocities on either side of the shock to the speed of sound at stagnation conditions:

$$V_1 V_2 = \frac{2}{\gamma + 1} a_o^2 \tag{4.20}$$

To develop the relation for an oblique shockwave, we could pursue the traditional approach (see Problem 6.17), in which we write the energy equation at locations both ahead of and behind the shock, solve for the pressure on both sides, and incorporate the results with the momentum equation. Finally, by using the continuity equation, we obtain the relationship. Alternatively, however, we may take advantage of the relationship between normal shocks and oblique shocks and simply rewrite Prandtl's expression. We now make the following replacements (indicated by the $\rightarrow$ symbol) in Eq. (4.20):

$$V_1 \rightarrow V_{n1}$$
$$V_2 \rightarrow V_{n2}$$

$$a_o^2 = \gamma RT_o = (\gamma - 1)h_o = (\gamma - 1)\left(h_1 + \frac{V_1^2}{2}\right)$$

$$(\gamma - 1)\left(h_1 + \frac{V_1^2}{2}\right) \rightarrow (\gamma - 1)\left(h_1 + \frac{V_{n1}^2}{2}\right)$$

$$(\gamma - 1)\left(h_1 + \frac{V_{n1}^2}{2}\right) = (\gamma - 1)\left(h_1 + \frac{V_{n1}^2}{2} + \frac{V_t^2}{2} - \frac{V_t^2}{2}\right)$$

$$= (\gamma - 1)\left(h_o - \frac{V_t^2}{2}\right) = a_o^2 - (\gamma - 1)\frac{V_t^2}{2}$$

$$a_o^2 \rightarrow a_o^2 - \frac{(\gamma - 1)}{2}V_t^2$$

Replacing all the parameters in Eq. (4.20) with their oblique shock counterparts gives

$$V_{n1}V_{n2} = \frac{2}{\gamma + 1}a_o^2 - \left(\frac{\gamma - 1}{\gamma + 1}\right)V_t^2$$

---

It must be kept in mind that transformations of relationships from normal to oblique shocks will affect velocities, Mach numbers, and stagnation values. Transformations do not affect static property values. Accordingly, for example, the Rankine–Hugoniot relation, which connects the static pressure ratio to the density ratio across an oblique shock, is exactly the same as for the normal shock:

$$\frac{p_2}{p_1} = \frac{\left(\frac{\gamma + 1}{\gamma - 1}\right)\frac{\rho_2}{\rho_1} - 1}{\left(\frac{\gamma + 1}{\gamma - 1}\right) - \frac{\rho_2}{\rho_1}} \tag{4.16a}$$

The Mach number downstream of the shock, $M_2$, can be obtained by employing the following strategy:

$$M_2^2 = \left(\frac{V_2}{a_2}\right)^2 = \left(\frac{V_2}{V_1}\right)^2\left(\frac{a_1}{a_2}\right)^2\left(\frac{V_1}{a_1}\right)^2 = \left(\frac{V_2}{V_1}\right)^2\left(\frac{T_1}{T_2}\right)\left(\frac{V_1}{a_1}\right)^2 \tag{6.15}$$

However,

$$V_2^2 = V_{n2}^2 + V_t^2 = \left(\frac{V_{n2}}{V_{n1}}\right)^2 V_{n1}^2 + V_t^2 = \left(\frac{\rho_1}{\rho_2}\right)^2 V_1^2 \sin^2\theta + V_1^2\cos^2\theta$$

Thus,

$$\frac{V_2^2}{V_1^2} = \left(\frac{\rho_1}{\rho_2}\right)^2 \sin^2\theta + \cos^2\theta \tag{6.16}$$

Now insert Eq. (6.16) into Eq. (6.15) and make use of Eqs. (6.11) and (6.12) to find, after some algebraic effort, that

$$M_2^2 = \frac{1 + \frac{\gamma - 1}{2} M_1^2}{\gamma M_1^2 \sin^2\theta - \frac{(\gamma - 1)}{2}} + \frac{M_1^2 \cos^2\theta}{1 + \frac{\gamma - 1}{2} M_1^2 \sin^2\theta} \tag{6.17}$$

Normal shock theory requires that $M_1 \geq 1$ and $M_2 \leq 1$ in order not to violate the second law of thermodynamics. For the oblique shock, these conditions apply only to the velocity component normal to the shock. Therefore, $M_1 \sin\theta \geq 1$ and $M_2 \sin(\theta - \delta) \leq 1$. Because $\sin\theta$ is less then or equal to unity, the first relation indicates that $M_1$ *must* be supersonic; further, the relation on the upstream side of the shock provides a range of possible shock angles: $\theta_{\min} = \sin^{-1}(1/M_1)$, which is the relation for a Mach wave [see Eq. (2.19)], whereas $\theta_{\max} = \sin^{-1}(1) = \frac{\pi}{2}$ (i.e., the normal shock). Accordingly, the range of values over which the shock angle may vary is given by

$$\sin^{-1}\left(\frac{1}{M_1}\right) \leq \theta \leq \frac{\pi}{2}$$

So, for example, if $M_1 = 2.0$, all shock angles must lie in the range from 30° to 90°.

On the other hand, the Mach number downstream of the oblique shock, $M_2$, need not be subsonic, as it must be for the normal shock, because the downstream relation requires that the product of $M_2$ and $\sin(\theta - \delta)$ be smaller than unity. This enables $M_2$ to be greater than, equal to, or less than unity.

We can determine an expression that connects the deflection angle $\delta$ $(= \alpha_2 - \alpha_1)$ to the upstream Mach number $M_1$ and the shock angle $\theta$ by taking the ratio of Eqs. (6.6a) and (6.6b) to obtain

$$\frac{V_{n1}}{V_t} = \tan\theta$$

Similarly, from Eqs. (6.7a) and (6.7b), we get

$$\frac{V_{n2}}{V_t} = \tan(\theta - \delta) = \frac{\tan\theta - \tan\delta}{1 + \tan\theta \tan\delta}$$

Eliminate $V_t$ between these two expressions and make use of the density relation of Eq. (6.11) to find that

$$\tan\delta = \cot\theta \frac{M_1^2 \sin^2\theta - 1}{\frac{\gamma + 1}{2} M_1^2 - (M_1^2 \sin^2\theta - 1)} \tag{6.18}$$

For a normal shockwave, which is actually a special case of an oblique shock in which the shock angle is always $\pi/2$, only one independent parameter (generally, $M_1$) is needed to determine the other shock parameters (the downstream Mach number, the pressure ratio, the temperature ratio, and so forth). Examination of the equations for

the oblique shock reveals that two independent parameters are required to fully describe the conditions on either side of the front. In the preceding expressions, $M_1$ and the shock angle $\theta$ are used to determine the various parameters; that is, for any parameter (pressure ratio, temperature ratio, etc.) $\xi = f(M_1, \theta)$. It is not much more difficult to develop working relations for oblique shocks in terms of the deflection angle and the shock angle—that is, $\xi = f(\delta, \theta)$. [See Refs. (6.1) and (6.2).] In most cases, the shock angle is not known, but rather $M_1$ and $\delta$ appear as the independent variables. Therefore, it is more advantageous to be able to express the working relations as $\xi = f(M_1, \delta)$. Unfortunately, development of an explicit set of oblique shock relations of this form is not possible.

A procedure that was presented in Ref. (6.3) can, however, be used to numerically extract the shock angle from Eq. (6.18), which will enable the other parameters to be determined in turn. To utilize this procedure, which we will call *Collar's method*, first rewrite Eq. (6.18) as the cubic equation

$$f(x) = x^3 + Cx^2 - Ax + (B - AC) = 0 \tag{6.19}$$

where $x = \cot\theta$, $A = M_1^2 - 1$, $B = [(\gamma + 1)/2]M_1^4 \tan\delta$, and $C = \{1 + [(\gamma + 1)/2]M_1^2\}\tan\delta$.

In deriving Eq. (6.19), it should be mentioned that the identity $\sin^2\theta = 1/(1 + x^2)$ was used. The validity of Eq. (6.19) can be substantiated by substituting $x$, $A$, $B$, and $C$ into Eq. (6.19) and rearranging it to obtain Eq. (6.18).

Because Eq. (6.19) is a third-order equation, it will have three roots, or zeros. If we were to plot $f(x)$, with the coefficients $A$, $B$, and $C$ determined from the given values of $\gamma$, $\delta$, and $M_1$, it would cross the $x$-axis three times. Each crossing is a root of the equation. Note that $A$, $B$, $C$, and $(B - AC)$ are positive for all values of $M_1$ and $\delta$. According to *Descartes's Rule of Signs*, since the coefficients in Eq. (6.19) change sign twice, the equation has two positive roots and one negative root. The largest root can be found from a simple successive approximation method, which can be developed by rewriting Eq. (6.19) as

$$x^2(x + C) - A(x + C) + B = 0$$

This expression can be rearranged to produce an iterative algorithm:

$$x_{n+1} = \sqrt{A - \frac{B}{(x_n + C)}} \tag{6.20}$$

Now, for a starting value of $x$ (i.e., $x_0$), the right-hand side of Eq. (6.20) may be computed to yield $x_1$. This value is then used to determine $x_2$. The process continues similarly until the value used on the right, $x_n$, yields virtually the same value as that on the left, $x_{n+1}$. A good starting value for this root is $\sqrt{A} = \sqrt{M_1^2 - 1}$.

The second positive root is obtained by root extraction. To accomplish this operation, simply divide Eq. (6.19) by the term $(x - x_1)$, where $x_1$ is the root obtained by the iterative procedure of Eq. (6.20). This division yields a quadratic equation for $x$. In other words, we can rewrite Eq. (6.19) as

$$(x - x_1)[x^2 + (x_1 + C)x + (x_1 + C)x_1 - A] = 0 \tag{6.21}$$

Solution of the quadratic portion of Eq. (6.21) yields the second root:

$$x_{II} = \frac{1}{2}\left[-(x_I + C) + \sqrt{(x_I + C)(C - 3x_I) + 4A}\right] \tag{6.22}$$

Note that the negative root was discarded as not meaningful. The following example demonstrates the iterative procedure.

**Example 6.2. Use of Collar's method to determine parameters behind an oblique shock**

A uniform supersonic flow ($\gamma = 1.3$) traveling horizontally ($\alpha_1 = 0$) at Mach 2.0 passes over a wedge with a half-angle of 9°. (See Figure 6.5.) An oblique shock is attached to the wedge under these flow conditions. If the static pressure and temperature in the uniform flow are, respectively, 20 kPa and −10°C, determine the shock angle, the static pressure, the temperature behind the wave, and the Mach number of the flow passing over the wedge.

**Solution**

We may incorporate Collar's successive-approximation technique into a simple spreadsheet program. The given information, along with the computed coefficients of Eq. (6.19), are contained in Table 6.1. The results of the calculations within the program are provided in Table 6.2.

Thus, the shockwave angle is $\theta = \cot^{-1}(1.2885768) = 37.81°$. The second root is determined from Eq. (6.22), which yields $\theta = \cot^{-1}(0.0869245) = 85.03°$. With these shock angles, Eqs. (6.10), (6.11), (6.12), and (6.17) can be used to determine the values in Table 6.3.

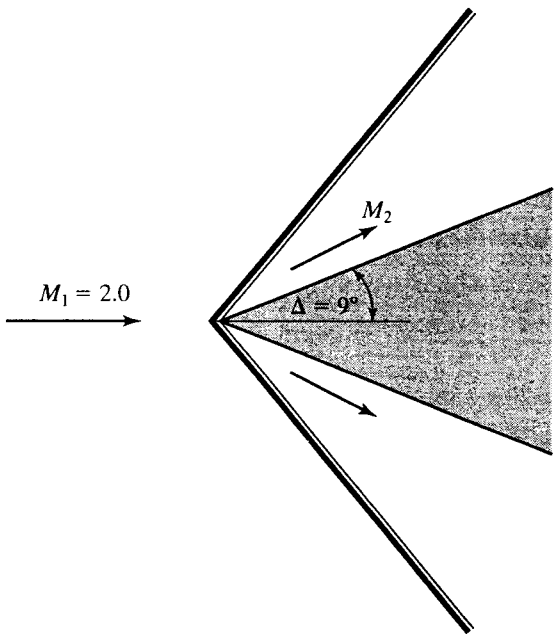


**Figure 6.5** Configuration for Example 6.2

**TABLE 6.1** Parameters (Given and Computed) for Use in Collar's Method of Example 6.2

| $\gamma$ | $M_1$ | $\delta$ | $A$ | $B$ | $C$ | $B-AC$ | First Guess |
|---|---|---|---|---|---|---|---|
| 1.3 | 2.0 | 9.0 | 3.0 | 2.914274 | 0.886953 | 0.253415 | 1.7320508 |

**TABLE 6.2** Results of Calculations for Example 6.2

| Iteration | $x_n$ | $x_{n+1}$ |
|---|---|---|
| 1 | 1.7320508 | 1.3737753 |
| 2 | 1.3737753 | 1.3080190 |
| 3 | 1.3080190 | 1.2931727 |
| 4 | 1.2931727 | 1.2896721 |
| 5 | 1.2896721 | 1.2888384 |
| 6 | 1.2888384 | 1.2886393 |
| 7 | 1.2886393 | 1.2885918 |
| 8 | 1.2885918 | 1.2885804 |
| 9 | 1.2885804 | 1.2885777 |
| 10 | 1.2885777 | 1.2885771 |
| 11 | 1.2885771 | 1.2885769 |
| 12 | 1.2885769 | 1.2885769 |

**TABLE 6.3** Oblique Shock Results of Example 6.2

| $\cot\theta = 1.2885768$ | | $\theta = 37.81°$ | | $\cot\theta = 0.0869245$ | | $\theta = 85.03°$ | |
|---|---|---|---|---|---|---|---|
| $p_2/p_1$ | $\rho_2/\rho_1$ | $T_2/T_1$ | $M_2$ | $p_2/p_1$ | $\rho_2/\rho_1$ | $T_2/T_1$ | $M_2$ |
| 1.5692 | 1.4109 | 1.1122 | 1.7099 | 4.3574 | 2.8615 | 1.5228 | 0.5815 |

Thus, for the smaller root,

$$p_2 = \left(\frac{p_2}{p_1}\right)p_1 = (1.5692)20 = 31.38\ \text{kPa}$$

$$T_2 = \left(\frac{T_2}{T_1}\right)T_1 = (1.1122)263 = 292.5\ \text{K}$$

Further discussion regarding this choice accompanies description of Figure 6.7.

As already mentioned, the Mach number downstream of the oblique shockwave, $M_2$, can have a value greater than unity without violating the second law of thermodynamics. However, the normal component of $M_2$ must be subsonic. To verify this condition, we compute the following:

$$M_{n2} = M_2 \sin(\theta - \delta) = (1.7099)\sin(37.81 - 9) = 0.8240$$

It should be pointed out that the successive approximation method [i.e., Eq. (6.20)] used in Collar's method is not unique, and other methods may be created from Eq. (6.19). Collar experimented with several others, but found that the procedure in Eq. (6.20) worked the best. Alternatively, Newton's method can be used to solve Eq. (6.19). (See Problem 6.14.) You will find that Newton's method requires fewer iterations than Collar's method. However, for spreadsheet computations, this is not a significant advantage.

**Historical Note: Arthur Roderick Collar** (1908–1986), aeronautical engineer: After graduating from Cambridge in 1929, Dr. Collar worked in the aerodynamics department, National Physical Laboratory, Teddington, and at the Royal Aircraft Establishment, Farnborough. His early papers involved application of matrix methods to a variety of engineering problems. Along with R. A. Frazer and W. J. Duncan, he co-authored *Elementary Matrices and Some Applications to Dynamics and Differential Equations*, Cambridge University Press, 1938 [7th (paperback) printing, 1963]. Later papers reveal that he had a research interest in aeroelasticity. In 1946, he was appointed the first Sir George White Professor of Aeronautical Engineering at Bristol University, where he remained for the rest of his career. He served in the Vice Chancellor's Office at Bristol for a period of three years. From 1936, Collar was also involved with the work of the Aeronautical Research Committee (later the Aeronautical Research Council). He served in various capacities with the council and its subcommittees until its abolition in 1980, holding the chairmanship from 1964–1968. He was elected a fellow of the Royal Society in 1965. See Ref. (6.4).

Detailed oblique-shock charts for $\gamma = 1.4$ [for example, see Appendix D, Refs. (6.5) and (6.6)] have traditionally been used along with normal-shockwave tables as the basis for most oblique-shock computations. The use of Collar's method in conjunction with spreadsheet computation eliminates the need for these charts because this method enables us to directly connect the deflection angle to the shock angle. Nevertheless, the form of one oblique-shock chart will be examined as several important characteristics of the solution to the oblique-shock equations emerge. In particular, we will consider the plot of shock angle against deflection angle for given values of $M_1$ and $\gamma$.

From Eq. (6.18), at the minimum value of the shock angle [i.e., the angle of inclination of a Mach wave, $\theta = \sin^{-1}(1/M_1)$], we find that $\delta = 0$, so the flow at this angle is not turned. [See Figure 6.6(a).] At the maximum value of the shock angle (i.e., $\theta = \pi/2$), Eq. (6.18) again reveals that the flow is not turned through an angle. [See Figure 6.6(b).] At angles between these two extremes, the deflection is positive, which suggests that a maximum value of $\delta$ lies somewhere between the limiting values. To determine the maximum value of the deflection angle that will allow a solution for given values of $M_1$ and $\gamma$, rewrite Eq. (6.18) as

$$\cot \delta = \tan \theta \left[ \left( \frac{\gamma + 1}{2} \right) \frac{M_1^2}{(M_1^2 \sin^2 \theta - 1)} - 1 \right] \tag{6.23}$$

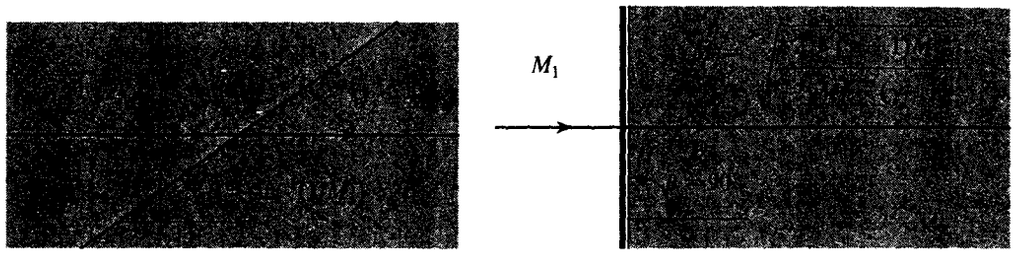


(a) Mach wave (b) Normal shock

**Figure 6.6** Limiting Shock Angles at which the Deflection Is Zero

Differentiate Eq. (6.23) to obtain

$$\frac{d(\cot\delta)}{d\theta} = \sec^2\theta\left[\left(\frac{\gamma+1}{2}\right)\frac{M_1^2}{(M_1^2\sin^2\theta-1)}-1\right] + \tan\theta\left(\frac{\gamma+1}{2}\right)M_1^2\left[\frac{-2M_1^2\sin\theta\cos\theta}{(M_1^2\sin^2\theta-1)^2}\right]$$

Since we seek the maximum value of $\delta$, we set this expression equal to zero and rearrange the remaining expression to obtain the following quadratic equation:

$$(\gamma M_1^4)\sin^4\theta + \left[2M_1^2 - \left(\frac{\gamma+1}{2}\right)M_1^4\right]\sin^2\theta - \left(1+\frac{\gamma+1}{2}M_1^2\right) = 0$$

Solution of this quadratic yields the value of $\theta$ at $\delta_{max}$, which we define as $\theta_{max}$:

$$\sin^2\theta_{max} = \left(\frac{1}{\gamma M_1^2}\right)\left\{\left(\frac{\gamma+1}{4}\right)M_1^2 - 1 + \sqrt{(\gamma+1)\left[\frac{(\gamma+1)}{16}M_1^4 + \frac{(\gamma-1)}{2}M_1^2 + 1\right]}\right\} \quad (6.24)$$

From Eq. (6.24), the shock angle at this location can be determined and the result used to find $\delta_{max}$ from Eq. (6.18). Table 6.4 contains a sampling of values of these angles that were determined from a spreadsheet calculation of Eqs. (6.24) and (6.18) for three values of $\gamma$.

It is of interest to determine where on the $\theta$–$\delta$ plot the downstream Mach number is unity. This location divides the subsonic and supersonic solutions. To determine this point, Eq. (6.17), with $M_2 = 1$, can be rearranged into a quadratic equation of the form

$$(\gamma M_1^4)\sin^4\theta - \left[\left(\frac{\gamma-3}{2}\right)M_1^2 + \left(\frac{\gamma+1}{2}\right)M_1^4\right]\sin^2\theta - 1 = 0$$

**TABLE 6.4** Maximum Deflection and Shock Angles for Various $\gamma$ and $M_1$ Values

| $\gamma$ | $M_1$ | $\theta_{max}$ (deg) | $\delta_{max}$ (deg) | $\gamma$ | $M_1$ | $\theta_{max}$ (deg) | $\delta_{max}$ (deg) | $\gamma$ | $M_1$ | $\theta_{max}$ (deg) | $\delta_{max}$ (deg) |
|---|---|---|---|---|---|---|---|---|---|---|---|
| 1.3 | 1.0 | 90 | 0 | 1.4 | 1.0 | 90 | 0 | 1.667 | 1.0 | 90 | 0 |
| | 1.5 | 66.86 | 12.89 | | 1.5 | 66.59 | 12.11 | | 1.5 | 66.01 | 10.43 |
| | 2.0 | 65.34 | 24.73 | | **2.0** | **64.67** | **22.97** | | 2.0 | 63.27 | 19.34 |
| | 2.5 | 65.82 | 32.28 | | 2.5 | 64.78 | 29.8 | | 2.5 | 62.69 | 24.79 |
| | 3.0 | 66.56 | 37.07 | | 3.0 | 65.24 | 34.07 | | 3.0 | 62.64 | 28.14 |
| | 3.5 | 67.21 | 40.22 | | 3.5 | 65.69 | 36.87 | | 3.5 | 62.71 | 30.3 |
| | 4.0 | 67.74 | 42.39 | | 4.0 | 66.06 | 38.77 | | 4.0 | 62.81 | 31.76 |
| | 4.5 | 68.15 | 43.94 | | 4.5 | 66.35 | 40.13 | | 4.5 | 62.9 | 32.79 |
| | 5.0 | 68.48 | 45.08 | | 5.0 | 66.58 | 41.12 | | 5.0 | 62.97 | 33.54 |
| | 10 | 69.68 | 48.93 | | 10 | 67.45 | 44.43 | | 10 | 63.3 | 36.02 |

This quadratic can be readily solved to produce the value of $\theta$ at $M_2 = 1$, which we define as $\theta_{sonic}$:

$$\sin^2\theta_{sonic} = \left(\frac{1}{\gamma M_1^2}\right)\left\{\left(\frac{\gamma+1}{4}\right)M_1^2 - \left(\frac{3-\gamma}{4}\right) + \sqrt{(\gamma+1)\left[\frac{(\gamma+1)}{16}M_1^4 + \frac{(\gamma-3)}{8}M_1^2 + \frac{(\gamma+9)}{16}\right]}\right\} \quad (6.25)$$

Equation (6.25) can be used in a spreadsheet program to determine the values contained in Table 6.5.

Comparison of the values contained in Tables 6.4 and 6.5 reveals that either as $M_1 \rightarrow 1$ or as $M_1 \rightarrow$ large, $\theta_{sonic} \cong \theta_{max}$ and $\delta_{sonic} \cong \delta_{max}$. For other values of $M_1$, $\theta_{sonic} < \theta_{max}$ and $\delta_{sonic} < \delta_{max}$. Therefore, the location where the downstream Mach number is unity does not coincide with the location of the maximum value of the deflection angle. There is a small region below the maximum deflection angle where the downstream flow is subsonic.

For the given values of $M_1 = 2$ and $\gamma = 1.4$, a plot of the oblique shock angle versus the deflection angle can be constructed as shown in Figure 6.7. To understand the shape of the curve within this figure, begin at the point where $\theta = \sin^{-1}\left(\frac{1}{2}\right) = 30°$ and $\delta = 0$ (the Mach wave limit). As we have seen, at this point, $M_2 = M_1 = 2$. Increasing $\theta$ above 30° results in $\delta$ increasing and $M_2$ decreasing, but remaining supersonic. Eventually, the

**TABLE 6.5** Deflection and Shock Angles Required to Produce $M_2 = 1$ for Various $\gamma$ and $M_1$ Values

| $\gamma$ | $M_1$ | $\theta_{sonic}$ (deg) | $\delta_{sonic}$ (deg) | $\gamma$ | $M_1$ | $\theta_{sonic}$ (deg) | $\delta_{sonic}$ (deg) | $\gamma$ | $M_1$ | $\theta_{sonic}$ (deg) | $\delta_{sonic}$ (deg) |
|---|---|---|---|---|---|---|---|---|---|---|---|
| 1.3 | 1.0 | 90 | 0 | 1.4 | 1.0 | 90 | 0 | 1.667 | 1.0 | 90 | 0 |
| | 1.5 | 62.52 | 12.45 | | 1.5 | 62.26 | 11.69 | | 1.5 | 61.69 | 10.07 |
| | 2.0 | 62.21 | 24.45 | | **2.0** | **61.49** | **22.71** | | 2.0 | 60 | 19.11 |
| | 2.5 | 63.76 | 32.15 | | 2.5 | 62.65 | 29.67 | | 2.5 | 60.42 | 24.67 |
| | 3.0 | 65.16 | 37 | | 3.0 | 63.77 | 34.01 | | 3.0 | 61.02 | 28.08 |
| | 3.5 | 66.22 | 40.19 | | 3.5 | 64.62 | 36.83 | | 3.5 | 61.51 | 30.27 |
| | 4.0 | 67 | 42.37 | | 4.0 | 65.26 | 38.75 | | 4.0 | 61.89 | 31.74 |
| | 4.5 | 67.58 | 43.93 | | 4.5 | 65.73 | 40.11 | | 4.5 | 62.17 | 32.78 |
| | 5.0 | 68.02 | 45.07 | | 5.0 | 66.08 | 41.11 | | 5.0 | 62.39 | 33.53 |
| | 10 | 69.57 | 48.93 | | 10 | 67.34 | 44.43 | | 10 | 63.15 | 36.02 |

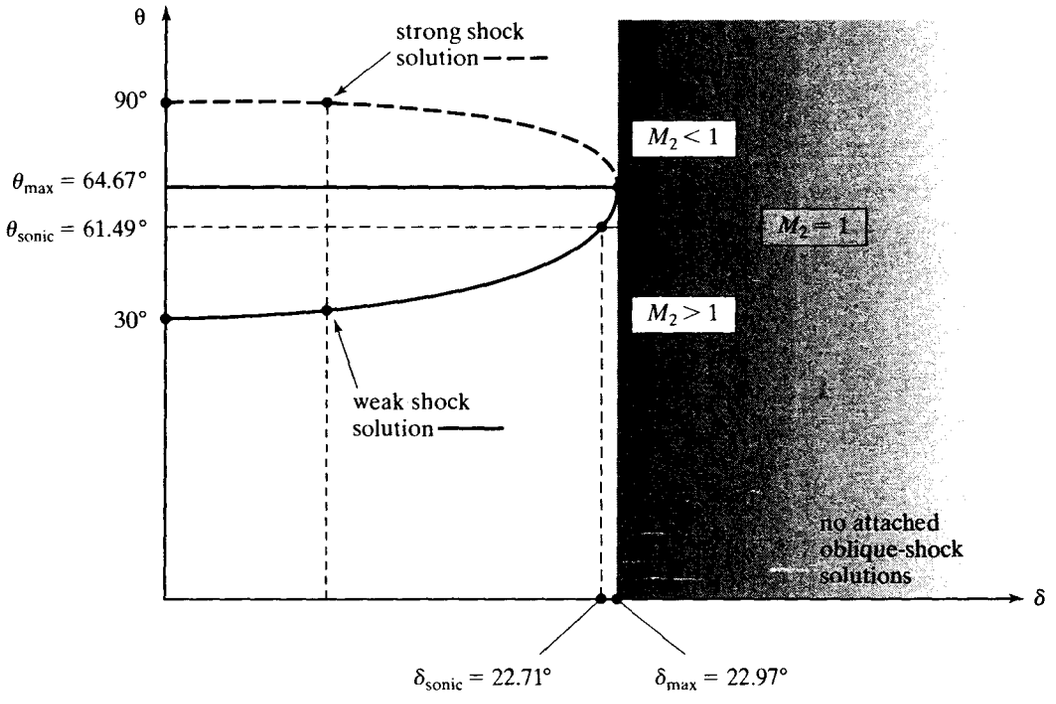


**Figure 6.7** Shock Angle versus Deflection Angle for $M_1 = 2$ and $\gamma = 1.4$

increase in $\theta$ results in the downstream Mach number becoming sonic (i.e., $M_2 \equiv 1$). This occurs at the location where $\theta_{sonic} = 61.49°$ and $\delta_{sonic} = 22.71°$. For values of $\theta$ beyond $\theta_{sonic}$, $M_2$ is subsonic. A slight increase in $\theta$ beyond $\theta_{sonic}$ brings us to the point of maximum deflection at the location where $\theta_{max} = 64.67°$ and $\delta_{max} = 22.97°$. By continuously increasing $\theta$ beyond $\theta_{max}$, we find that the normal shock limit will be reached at the point where $\theta = 90°$ and $\delta = 0$.

Because of the shape of the curve, as may be seen in Figure 6.7, for values of $M_1$, $\gamma$, and $\delta$, either two, one, or no attached oblique shock solutions are possible. If a solution exists, there may be a *weak oblique shock*, with $M_2$ either supersonic or slightly less than unity, or a *strong shock*, with $M_2$ subsonic. For the strong shock, the wave makes a large angle $\theta$ (close to 90°) with the approach flow; for the weak shock, the angle is much smaller. (See Figure 6.8.) The supersonic flow is turned through the same angle in both cases, yet the characteristics of the oblique shocks are quite different. The weak shock is accompanied, for example, by a relatively small pressure ratio, and the strong shock by a large pressure ratio.

Since the characteristics of the strong and weak oblique shocks are so different, it is essential to have an understanding of which solution will occur in a given flow situation. It is instructive at this point to refer back to a similar discussion about the possibility of occurrence of a normal shock. It was shown in Chapter 4 that the normal shock equations are satisfied by the trivial solution $M_2 = M_1$ [refer to the development of Eq. (4.9)], which corresponds to isentropic flow. This condition prompts the question, What determines whether isentropic flow or a normal shock will occur in a supersonic

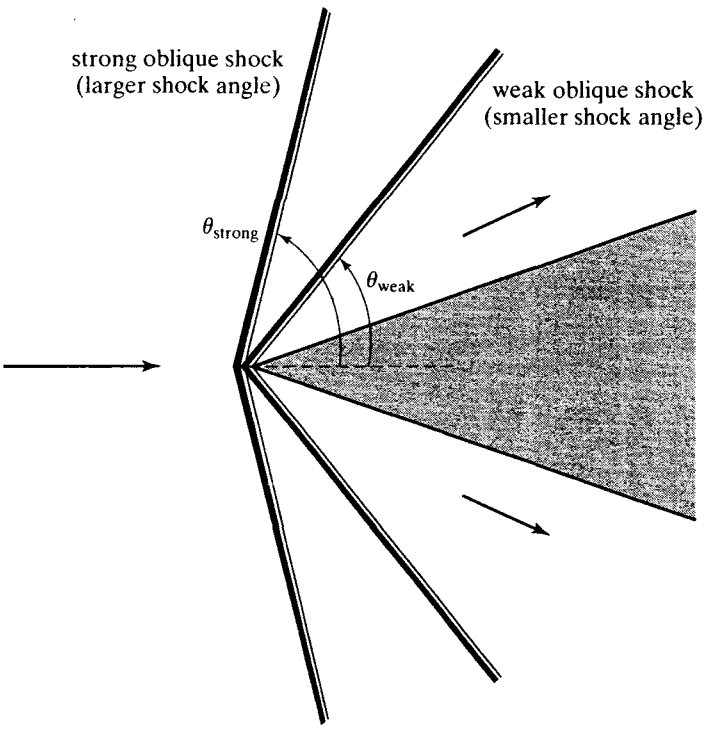


**Figure 6.8** Strong versus Weak Oblique Shocks

flow? The answer, at least for flow through converging–diverging nozzles, was presented in Section 4.4: For low-enough back pressures, isentropic flow occurs in the nozzle; for higher back pressures, a normal shock takes place in the diverging section of the nozzle. Thus, for supersonic flow in varying area channels, it is the pressure boundary conditions imposed on the channel that determine the type of solution.

The normal shock represents the limiting case of a strong oblique shock ($\delta = 0$), whereas the limiting case of a weak oblique shock ($\delta = 0$) is isentropic flow. Therefore, the result presented for the normal wave can be generalized to the oblique shock. The strong oblique shock occurs when a large back pressure is imposed on a supersonic flow, as might possibly take place during flow through a duct or inlet. When a wedge or airfoil travels through the atmosphere at supersonic velocities with an oblique shock attached to the body, however, only the weak shock solution is found to occur, since in this physical situation, with a uniform pressure after the shock, large pressure differences cannot be supported.

Another characteristic of the oblique-shock equations is that, for a great-enough turning angle $\delta$, no solution is possible. Under these conditions, it is observed that the shock is no longer attached to the wedge, but stands detached, in front of the body. (See Figure 6.9.) The detached shock is curved, as shown in the figure, with the shock strength diminishing progressively from that of a normal shock at the apex of the wedge to that of a Mach wave far from the body. Thus, with a detached shock, the entire range of oblique-shock solutions is obtained for the given Mach number $M_1$. The shape of the wave and the shock-detachment distance are dependent on the Mach number and the body shape. Flow over the body is subsonic in the vicinity of the wedge apex, where the strong oblique shocks occur, and it is supersonic farther back along the wedge, where the weak oblique shocks are present.

A detached oblique shock can also occur with supersonic flow in a concave corner. Again, if the turning angle is too great, an oblique-shock solution cannot be found,

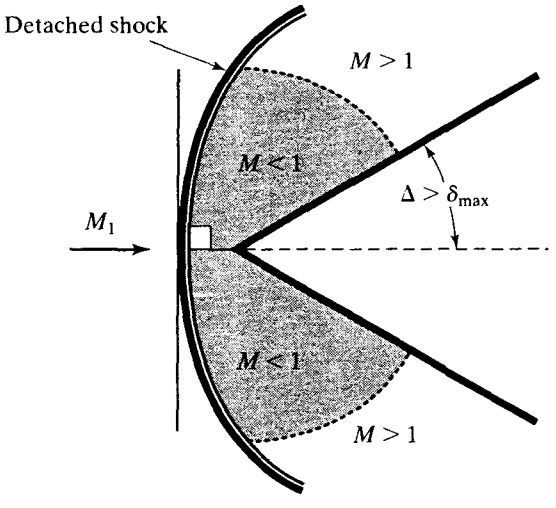


**Figure 6.9** A Detached Shock from a Wedge

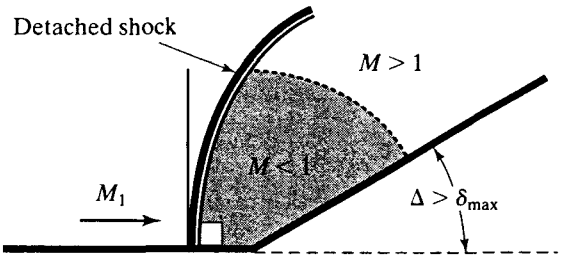


**Figure 6.10** Detached Flow in a Corner

so a detached shock forms ahead of the corner. (See Figure 6.10.) The characteristics of this shock are exactly the same as those of the upper half of the detached shock shown in Figure 6.9. This can be seen if one replaces the center streamline of Figure 6.9 with a plane wall. (The boundary conditions of the flow are not altered, since there can be no flow across a streamline.) Thus, flow after the shock is subsonic near the wall and supersonic farther out in the flow.

**Example 6.3. Determination of the minimum value of $M_1$ to keep shock attached**

Develop a method to determine the minimum upstream Mach number that is required if the shock is to remain attached.

**Solution**

We have seen that an oblique shock will detach itself from a wedge or concave corner if the upstream supersonic flow has to be turned through too large of an angle (i.e., $\delta > \delta_{max}$) for a given $M_1$ and $\gamma$. Alternatively, a shock can become detached if $M_1$ is too small for a given $\delta$ and $\gamma$. The distinction between the problem under consideration here and that previously analyzed is illustrated in Figure 6.11.

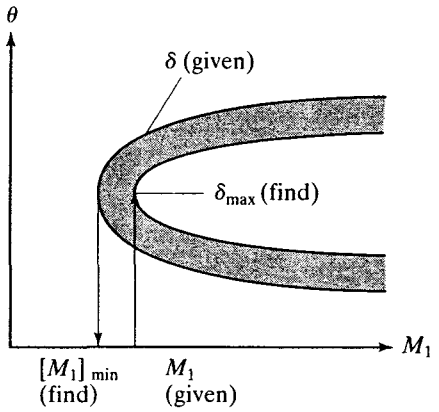


**Figure 6.11** Relation between $\delta_{max}$ and $(M_1)_{min}$ Problems

The analysis begins as follows from Eq. (6.18):

$$\cot\delta = \tan\theta\left[\left(\frac{\gamma+1}{2}\right)\frac{M_1^2}{(M_1^2\sin^2\theta - 1)} - 1\right] \tag{6.23}$$

Considerable rearrangement yields

$$\frac{1}{M_1^2} = \sin^2\theta - \left(\frac{\gamma+1}{2}\right)\frac{1}{1 + (\cot\delta)(\cot\theta)} \tag{6.26}$$

Keeping in mind that $\delta$ is given and therefore may be treated as a constant, we may differentiate Eq. (6.26) to obtain

$$\frac{d\left(\frac{1}{M_1^2}\right)}{d\theta} = 2\sin\theta\cos\theta - \left(\frac{\gamma+1}{2}\right)\cot\delta\frac{1}{\sin^2\theta(1 + \cot\delta\cot\theta)^2} = 0$$

Expanding and rearranging produces

$$f(\theta) = (\sin 2\delta)\sin^2 2\theta + \sin 2\theta + \left(\frac{\cos 2\delta}{2}\right)\sin 4\theta - \left(\frac{\gamma+1}{2}\right)\sin 2\delta = 0 \tag{6.27}$$

We must find the shock angle that satisfies Eq. (6.27) and then use it to compute $(M_1)_{\min}$. In the problem in which $M_1$ was given and $\delta_{\max}$ was to be found, this was accomplished by first finding an analytical expression for the shock angle and then using Eq. (6.23). For this problem, however, no explicit analytical solution for the shock angle can be found. On the other hand, it is not very difficult to find the solution numerically using spreadsheet calculations; we may use Newton's method to do so. This task requires that we possess the derivative of Eq. (6.27), which is easily found to be

$$\frac{df}{d\theta} = f' = 2(2\sin 2\delta\sin 2\theta + 1)\cos 2\theta + 2\cos 2\delta\cos 4\theta$$

The shock angle we seek is found from the iterative algorithm

$$\theta_{\text{new}} = \theta_{\text{old}} - \frac{f(\theta_{\text{old}})}{f'(\theta_{\text{old}})}$$

One problem with obtaining the solution to Eq. (6.27) via this approach is that because it involves sines and cosines, the function can cross the $\theta$-axis at a number of values. To avoid running into trouble, we require a good starting value for the initial guess. This can be accomplished very easily by simply substituting values into $f(\theta)$ [i.e., into Eq. (6.27)] and locating where it changes sign, which indicates a potential root.

As a concrete example, suppose $\delta = 20°$ and $\gamma = 1.4$. The first step would be to input $f(\theta)$ into a spreadsheet program and systematically increase $\theta$ to determine where the root we seek might lie. These computations produce the results shown in Table 6.6.

It is seen that $f(\theta)$ changes sign for a shock angle somewhere between 60° and 70°. Thus, using 60° as the initial guess, we find that the computations yield a solution in just a few tries, as may be seen in Table 6.7.

**TABLE 6.6** Method to Approximately Determine the Root of Eq. (6.27)

| $\theta$ (deg) | 20 | 30 | 40 | 50 | 60 | 70 | 80 | 90 |
|---|---|---|---|---|---|---|---|---|
| $f(\theta)$ | 0.5142 | 0.9085 | 0.9679 | 0.7059 | 0.2451 | −0.2402 | −0.6003 | −0.7713 |

**TABLE 6.7** Spreadsheet Calculations to Determine the Root of Eq. (6.27)

| Iteration | $\theta$ (deg) | $f(\theta)$ | $df/d\theta$ | $\theta_{new}$ | $M_1$ |
|---|---|---|---|---|---|
| 1 | 60.0 | 0.24506 | −2.87939 | 64.87643 | 1.840049 |
| 2 | 64.87643 | 0.00078 | −2.82208 | 64.89229 | 1.840049 |
| 3 | 64.89229 | 0.00000 | −2.82152 | 64.89229 | 1.840049 |

Note that with the shock angle of 64.892° and a deflection angle of 20°, Eq. (6.26) was used to compute the minimum upstream Mach number for which the shock remains attached. Thus, for a wedge angle of 20°, $\gamma = 1.4$, and $M_1 < 1.84$, an oblique shock is detached from the body. For the same deflection angle, but $\gamma = 1.3$, $(M_1)_{min}$ is readily found to be 1.775, whereas for $\gamma = 5/3$, $(M_1)_{min}$ is 2.048.

### Example 6.4. Oblique-shock relations for $M_1 \to \infty$

Develop working relations across an oblique shock for situations in which $M_1 \gg 1$.

**Solution**

Cases where the upstream Mach number is large are important—for example, in hypersonic flows. This exercise is a companion to Example 4.1, in which we found limiting forms of the relations for normal shocks. Therefore, we may utilize the results of that example by replacing the upstream Mach number $M_1$ with $M_1 \sin\theta$ to obtain

$$\frac{p_2}{p_1} \cong \frac{2\gamma}{\gamma + 1} M_1^2 \sin^2\theta$$

$$\frac{\rho_2}{\rho_1} = \frac{V_{n1}}{V_{n2}} \cong \frac{(\gamma + 1)}{(\gamma - 1)}$$

$$\frac{T_2}{T_1} \cong \frac{2\gamma(\gamma - 1)}{(\gamma + 1)^2} M_1^2 \sin^2\theta$$

On the other hand, the limiting form of the Mach number downstream of the oblique shock, $M_2$, is obtained by analyzing

$$M_2^2 = \frac{1 + \dfrac{\gamma - 1}{2} M_1^2}{\gamma M_1^2 \sin^2\theta - \dfrac{(\gamma - 1)}{2}} + \frac{M_1^2 \cos^2\theta}{1 + \dfrac{\gamma - 1}{2} M_1^2 \sin^2\theta} \tag{6.17}$$

As $M_1 \to \infty$, this expression reduces to

$$M_2^2 = \frac{(\gamma - 1)}{2\gamma \sin^2\theta} + \frac{2}{(\gamma - 1)\sin^2\theta} - \frac{2}{(\gamma - 1)} = \frac{(\gamma + 1)^2}{2\gamma(\gamma - 1)\sin^2\theta} - \frac{2}{(\gamma - 1)}$$

Unlike $M_2$ for the normal shock, which reduces to a particular value that depends only on $\gamma$, the limiting form of $M_2$ for the oblique shock also depends on the shock angle. The relation between the shock angle and the deflection angle for a flow with an infinite upstream Mach number can be determined as follows:

$$\tan\delta = \cot\theta \frac{M_1^2 \sin^2\theta - 1}{\frac{\gamma + 1}{2} M_1^2 - (M_1^2 \sin^2\theta - 1)} \tag{6.18}$$

Now, as $M_1 \to \infty$, this expression becomes

$$\tan\delta = \frac{\cos\theta}{\sin\theta} \frac{2\sin^2\theta}{(\gamma + 1) - 2\sin^2\theta} = \frac{\sin 2\theta}{\gamma + \cos 2\theta} \tag{6.28}$$

The largest deflection angle for this limiting Mach number can be found by differentiating the foregoing equation, setting the result to zero, and then solving for $\theta$. (See Problem 6.18.) Alternatively, we may find the limit value from Eq. (6.24), which, for an infinite $M_1$, yields

$$\sin^2\theta_{max} = \left(\frac{\gamma + 1}{4\gamma}\right) + \left(\frac{\gamma + 1}{4\gamma}\right) = \left(\frac{\gamma + 1}{2\gamma}\right)$$

Thus,

$$\theta_{max} = \sin^{-1}\sqrt{\frac{\gamma + 1}{2\gamma}} \tag{6.29}$$

For $\gamma = 1.4$, this equation yields the solution 67.792°. Note further that examining the shock angle where the downstream flow is sonic [see Eq. (6.25)] for this limiting case reveals that $\theta_{sonic} = \theta_{max}$. The maximum deflection angle is found by using Eq. (6.29) in Eq. (6.28) to obtain, for $M_1 \to \infty$,

$$\delta_{max} = \tan^{-1}\left(\frac{1}{\sqrt{\gamma^2 - 1}}\right)$$

For $\gamma = 1.4$, this equation yields the solution 45.585°.

---

**Example 6.5. Comparison of the pressure recovery in two supersonic inlets**

A supersonic two-dimensional inlet is to be designed to operate at Mach 3.0. Two possibilities will be considered, as shown in Figure 6.12. In one, the compression and slowing down of the flow take place through a single normal shock; in the other, a wedge-shaped diffuser, the deceleration occurs through two weak oblique shocks, followed by a normal shock. The wedge turning angles are each 8°. Compare the loss in stagnation pressure for the two cases.

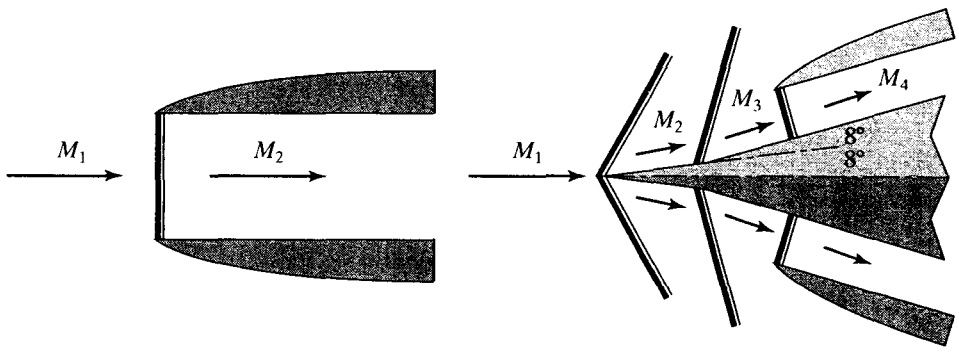


(a) Normal-Shock Diffuser (b) Wedge-Shaped Diffuser

**Figure 6.12** Flow in Two Supersonic Inlets

**Solution**

*Case 1: Normal-Shock Diffuser:* For the normal-shock diffuser, the ratio $p_{o2}/p_{o1}$ can be found from the stagnation pressure ratio for a normal shock through Eq. (4.15) at $M_1 = 3.0$: $p_{o2}/p_{o1} = 0.3283$.

*Case 2: Wedge-Shaped Diffuser:* For the first oblique shock with $M_1 = 3.0$ and $\delta = 8°$, we obtain from Appendix D or from the numerical procedure that the shock angle is $\theta = 25.61°$ and, in turn, from Eq. (6.17), that $M_2 = 2.6031$. We also find from Eq. (6.13) that $p_{o2}/p_{o1} = 0.9799$. The process is then repeated using $M_2 = 2.6031$ and $\delta = 8°$ to obtain a shock angle of $\theta = 28.94°$, a downstream Mach number $M_3 = 2.2595$, and $p_{o3}/p_{o2} = 0.9858$. At $M_3 = 2.2595$, from the normal-shock relations, we find that $p_{o4}/p_{o3} = 0.6013$. Finally, we obtain

$$\frac{p_{o4}}{p_{o1}} = \left(\frac{p_{o4}}{p_{o3}}\right)\left(\frac{p_{o3}}{p_{o2}}\right)\left(\frac{p_{o2}}{p_{o1}}\right) = (0.6013)(0.9858)(0.9799) = 0.5808$$

Therefore, the overall stagnation pressure ratio is 0.5808. The advantage of diffusing through several oblique shocks rather than one normal shock can be seen: The greater the number of oblique shocks, the less the overall loss in stagnation pressure is. Theoretically, if the flow is allowed to pass through an extremely large number of oblique shocks, each turning the flow through a very small angle, the inlet flow should approach that of an isentropic compression. The oblique-shock diffuser will be discussed in detail in Chapter 8.

## 6.3 OBLIQUE-SHOCK REFLECTIONS

When a weak, two-dimensional oblique shock impinges on a plane wall, the presence of a reflected wave is required to straighten the flow, since the boundary condition at the wall imposes the restriction that there can be no flow across the wall surface. (See Figure 6.13.) Flow after the incident wave is deflected toward the wall. Hence, a reflected oblique shockwave must be present to deflect the flow back through the same angle and restore the flow direction parallel to the wall. Although the deflection angle

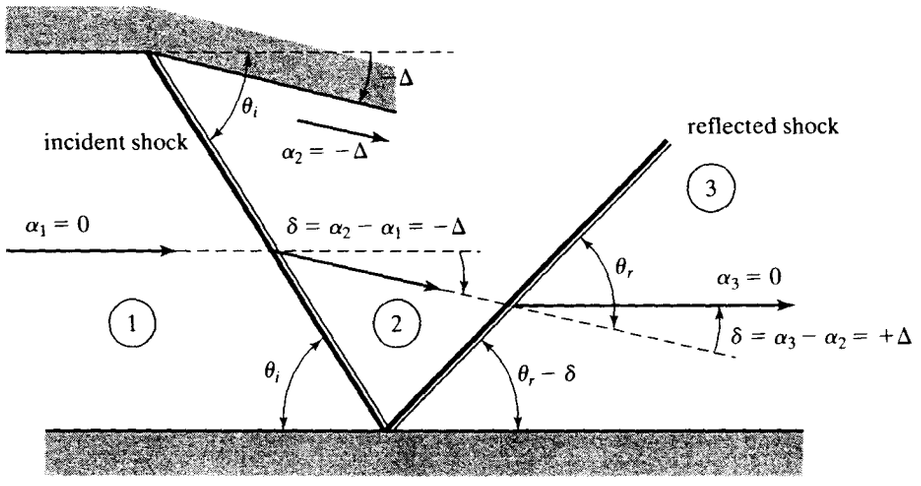


**Figure 6.13** Regular Oblique-Shock Reflection from a Plane Wall

$\delta$ has the same magnitude for both the incident and reflected shocks, the pressure ratios across them are not the same, since $M_2 < M_1$ (that is, the reflected shock is weaker than the incident shock). The overall static pressure ratio may computed from

$$\frac{p_3}{p_1} = \left(\frac{p_3}{p_2}\right)\left(\frac{p_2}{p_1}\right)$$

Experiments reveal that the reflected shock is always a weak shock. In general, the angle that the incident shock makes with the wall—in this case, $\theta_i$ —is not equal to the angle that the reflected shock makes with the wall—in this case, $\theta_r - \delta$.

**Example 6.6. Computations of a reflected oblique shock**

For a horizontal flow ($\alpha_1 = 0$), $M_1 = 2.0$, $\gamma = 1.4$, and $\theta_i = -40°$, determine $\theta_r$, $M_2$, and $M_3$. Refer to Figure 6.13.

**Solution**

As shown in Figure 6.13, the flow field is divided into three angular regions, each having uniform properties. For $M_1 = 2.0$ and $\theta = -40°$, the weak shock deflection angle $\delta$ may be readily computed from Eq. (6.18) as $-10.6229°$. (The deflection angle has the same sign as the shock angle.) This corresponds to the angle through which the flow is turned after the incident wave, as well as the angle through which the flow is turned back after the reflected wave. For the given shockwave angle and upstream Mach number, $M_2$ is determined from Eq. (6.17) to be 1.6173. With this value of $M_2$ and with $\delta = 10.6229°$ from Collar's method, we find the weak shock angle $\theta_r$ to be 51.3846° and $M_3$ to be 1.2331. The shockwave angle $\theta_r$ is the angle between the flow direction in region 2 and the reflected wave. From geometrical consideration, the angle of reflection is $\theta_r - \delta = 51.3846° - 10.6229° = 40.7617°$. The accuracy obtained in these computations was realized through the use of spreadsheet computation.

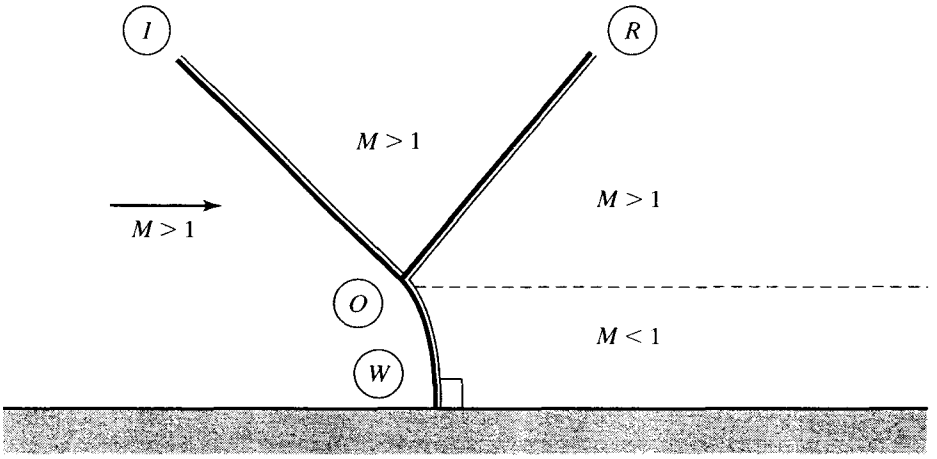


**Figure 6.14** A Mach Reflection at a Plane Wall

If $M_2$ is low enough, a regular shock reflection, as shown in Figure 6.13, may be impossible. That is, for a given $M_2$, the required turning angle may be great enough so that no solution exists. In this case, a *Mach reflection*, named after Ernst Mach, who was the first person to observe this phenomena in experiments performed in 1878 [see Ref. (6.7)], occurs. (See Figure 6.14.) A curved, strong oblique shock forms in the stream, extending from $O$ to the wall at $W$. At $W$, the shock must be normal to the wall to prevent the possibility of any flow deflection and hence satisfy the wall boundary condition at this point. Flow after the curved shock $OW$ is subsonic, with this flow adjusting smoothly to the presence of the wall. A weak oblique shock $OR$ also appears, with flow after this shock supersonic. The combination of supersonic and subsonic flow after the waves makes an analysis of the Mach reflection extremely difficult, and certainly beyond the scope of this text.

In a real fluid, the problem of oblique-shock reflections is complicated by the presence of a boundary layer on the wall. The interaction of the incident oblique shock with the wall boundary layer may have a pronounced effect on the resultant flow. It must be emphasized, then, that the analysis presented here of oblique-shock reflections is an approximate one that neglects real fluid effects.

## 6.4 CHAPTER CAPSTONE APPLICATION: THE INTERSECTION OF TWO OBLIQUE SHOCKS

In the previous section, we considered the turning of a supersonic flow as it passed through a system of shocks composed of incident and reflected oblique shocks. In essence, the solution of this problem amounted to solving flow through an oblique-shock twice, but under differing conditions. It should be mentioned that not all oblique-shock problems are as straightforward. In fact, depending upon the geometry and the flow conditions, oblique-shock problems can become very difficult, requiring the solution of high-order polynomials.

In this section, we will consider two additional oblique-shock problems. Figure 6.15(a) concerns the confluence of two supersonic streams at the trailing edge of an airfoil; Figure 6.15(b) deals with the crossing of two oblique shocks of

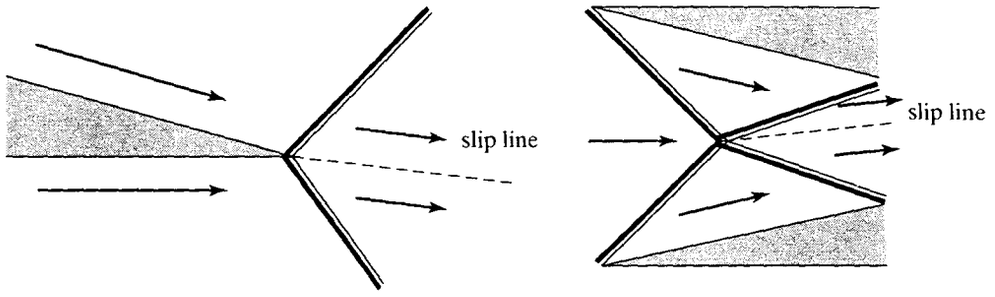


(a) Confluence of Two Oblique Shocks (b) Interaction of Two Oblique Shocks

**Figure 6.15** Two Oblique-Shock Systems

different strengths in the mouth of a supersonic inlet. Both problems result in the introduction of another type of flow discontinuity. This discontinuity is distinct from a compression discontinuity (the shockwave) in that no flow crosses it. Across this discontinuity, the pressure is continuous, but other flow variables (velocity, density, entropy, and temperature) need not be. The discontinuity has been given various names: *slip line*, contact discontinuity, and vortex sheet.

To assist us with the solution of these types of problems, we use a *pressure-deflection diagram*. The diagram, which is also called a *shock polar diagram*, will be useful in visualizing the solution we seek. Basically, the pressure-deflection diagram is a plot of all viable downstream oblique-shock pressures against corresponding deflection angles for a given set of upstream conditions. We now develop the equation to construct this figure.

The expression for the pressure ratio across an oblique shock is

$$\frac{p_2}{p_1} = \frac{2\gamma M_1^2 \sin^2\theta}{\gamma + 1} - \frac{\gamma - 1}{\gamma + 1} \tag{6.10}$$

This expression can be rearranged to obtain

$$M_1^2 \sin^2\theta = \left(\frac{\gamma + 1}{2\gamma}\right)\left(\frac{p_2}{p_1} - 1\right) + 1 \tag{6.30}$$

The following identity is also used in this development:

$$\cot\theta = \pm\sqrt{\frac{1}{\sin^2\theta} - 1} \tag{6.31}$$

Now the deflection angle is connected to the shockwave angle and the upstream Mach number:

$$\tan\delta = \cot\theta \frac{M_1^2 \sin^2\theta - 1}{\frac{\gamma + 1}{2} M_1^2 - (M_1^2 \sin^2\theta - 1)} \tag{6.18}$$

Combining Eqs. (6.18), (6.30), and (6.31) yields the *pressure-deflection* equation:

$$\tan\delta = \tan(\alpha_2 - \alpha_1) = \pm\frac{\dfrac{p_2}{p_1} - 1}{(1 + \gamma M_1^2) - \dfrac{p_2}{p_1}}\sqrt{\frac{\left(\dfrac{2\gamma}{\gamma+1}M_1^2 - \dfrac{\gamma-1}{\gamma+1}\right) - \dfrac{p_2}{p_1}}{\left(\dfrac{\gamma-1}{\gamma+1}\right) + \dfrac{p_2}{p_1}}} \tag{6.32}$$

This relation may be written in an a more compact form, called the *pressure-flow direction* equation, as

$$x = \alpha_1 \pm \tan^{-1}\left(\frac{y-1}{a-y}\sqrt{\frac{b-y}{c+y}}\right) \tag{6.33}$$

where $x = \alpha_2$, $y = \left(\dfrac{p_2}{p_1}\right)$, $a = (1 + \gamma M_1^2)$, $b = \left(\dfrac{2\gamma}{\gamma+1}M_1^2 - \dfrac{\gamma-1}{\gamma+1}\right)$,

and $c = \left(\dfrac{\gamma-1}{\gamma+1}\right)$.

Both the pressure-deflection equation [Eq. (6.32)] and the pressure-flow direction equation [Eq. (6.33)] describe a closed curve known as *Descartes's loop*. Figure 6.16

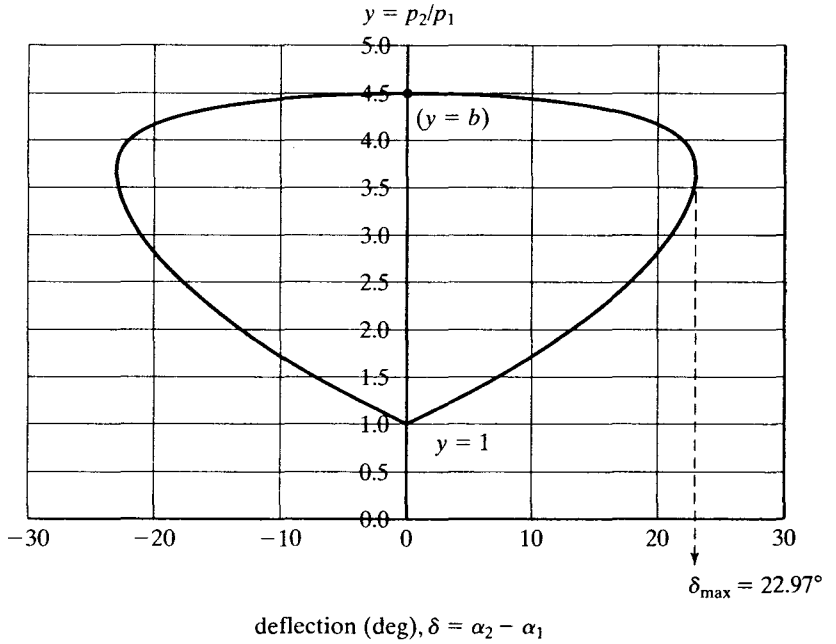


**Figure 6.16** Pressure-Deflection Diagram for $M_1 = 2.0$ and $\gamma = 1.4$

shows the plot of Eq. (6.32) for $M_1 = 2.0$ and $\gamma = 1.4$. Note that the constants $a$, $b$, and $c$ in Eq. (6.33) depend only upon $M_1$ and $\gamma$. By virtue of the $\pm$ sign that appears in the equations, the curve is symmetrical about $\delta = 0$ for Eq. (6.32) and about the line $x = \alpha_1$ for Eq. (6.33). The positive sign corresponds to the right lobe of the curve, while the negative sign corresponds to the left lobe.

It is useful to recognize several features of the diagram. First, it can be seen from Eq. (6.33) that at $y = p_2/p_1 = 1, \delta = 0(\alpha_2 = \alpha_1)$. This point corresponds to a Mach wave. The shockwave angle for this point is $\theta_{\min} = \sin^{-1}(1/M_1)$. For $\delta < \delta_{\max}$, there is the possibility of two pressure ratios (the smaller one for the weak shock solution and the larger one for the strong shock solution). If $\delta = \delta_{\max}$, which for $M_1 = 2$ and $\gamma = 1.4$ from Table 6.4 is 22.97°, the flow has a unique pressure ratio. If $\delta > \delta_{\max}$, no attached shock solution exists. When $y = p_2/p_1 = b$, the deflection is again zero. This point corresponds to that of the normal shock. It is also important to recognize that in order to avoid the possibility of the square root of a negative number, $y$ can never exceed $b$. Thus, we see that $b \geq y \geq 1$, which is in complete agreement with Eq. (6.10).

It is instructive to demonstrate the solution of the regular oblique-shock reflection problem of Example 6.6 by way of the pressure-deflection diagram. Figure 6.17 was drawn to show the solution process. Figure 6.17(a) is a repeat of Figure 6.16 because the upstream conditions are the same; that is, $M_1 = 2$ and $\gamma = 1.4$. Example 6.6 indicates that after passing through the oblique shock, which is inclined at an angle of 40° to the horizontal, the flow is deflected downwards by 10.6229°. The pressure ratio $p_2/p_1$ across the incident oblique shock is readily computed from Eq. (6.10) to be 1.7615. So in Figure 6.17(a), the coordinates corresponding to region 2 have been drawn. The origin for this region is labeled the *anchor point* and has the coordinates $\alpha_3 = \alpha_2 = -10.623$ and $p_3/p_1 = p_2/p_1 = 1.762$. In Figure 6.17(b), we now construct a second pressure-flow direction diagram based on the conditions of region 2, viz., $M_2 = 1.6173$ and $\alpha_2 = -10.6229°$. The equation for the diagram of Figure 6.17(b) is

$$x = \alpha_3 = \alpha_2 \pm \tan^{-1}\left[\frac{\left(\frac{y}{p_2/p_1} - 1\right)}{\left(a - \frac{y}{p_2/p_1}\right)}\sqrt{\frac{\left(b - \frac{y}{p_2/p_1}\right)}{\left(c + \frac{y}{p_2/p_1}\right)}}\right] \tag{6.34}$$

This expression provides all possible pressure-flow direction states within region 3. It is extremely important to note that $y = p_3/p_1$. When $y = p_3/p_1 = p_2/p_1, \alpha_3 = \alpha_2$, and therefore the deflection is zero. The downstream condition in region 3 requires that the flow be parallel to the horizontal wall (i.e., $\alpha_3 = 0°$). Thus, intersection with the ordinate axis provides the downstream pressure ratio, which is 2.9881. Unless these diagrams are drawn to a small scale, they do not provide accurate results. They can be replaced by numerical procedures that are guided by the diagrams. This approach is illustrated in the next two examples.

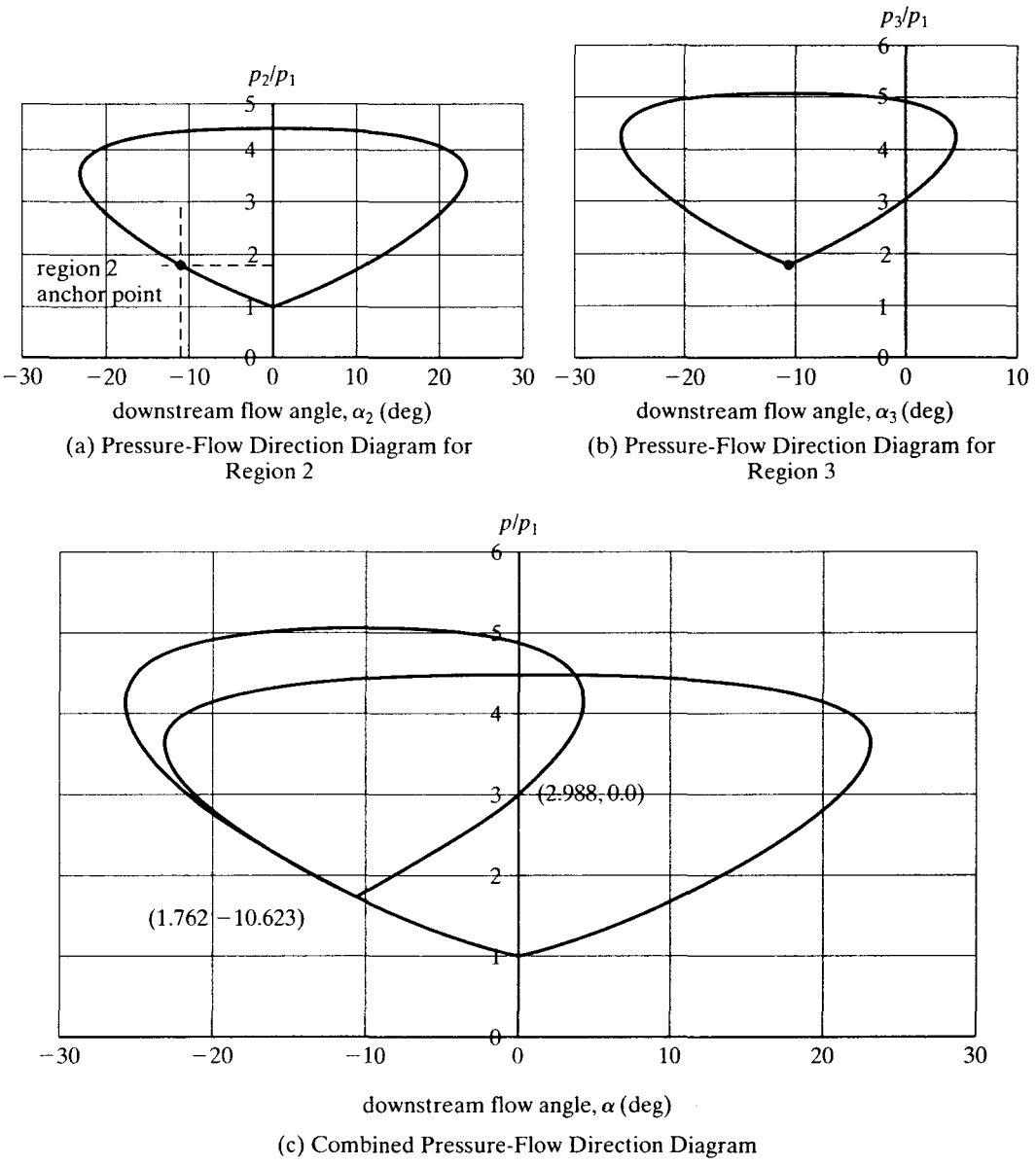


(a) Pressure-Flow Direction Diagram for Region 2

(b) Pressure-Flow Direction Diagram for Region 3

(c) Combined Pressure-Flow Direction Diagram

**Figure 6.17** Pressure-Flow Direction Diagrams for a Regular Reflection for Example 6.6

**Example 6.7. Confluence of two oblique shocks**

Figure 6.18 shows two supersonic flows, from the upper and lower surfaces of an airfoil, merging at the trailing edge. Because the flows must be turned in order to flow in the same direction, they pass through oblique shocks that reside at the trailing edge. Moreover, because each flow passes through a shock of different strength, each will possess different properties, and therefore a contact discontinuity or slip line will separate the two merged streams.

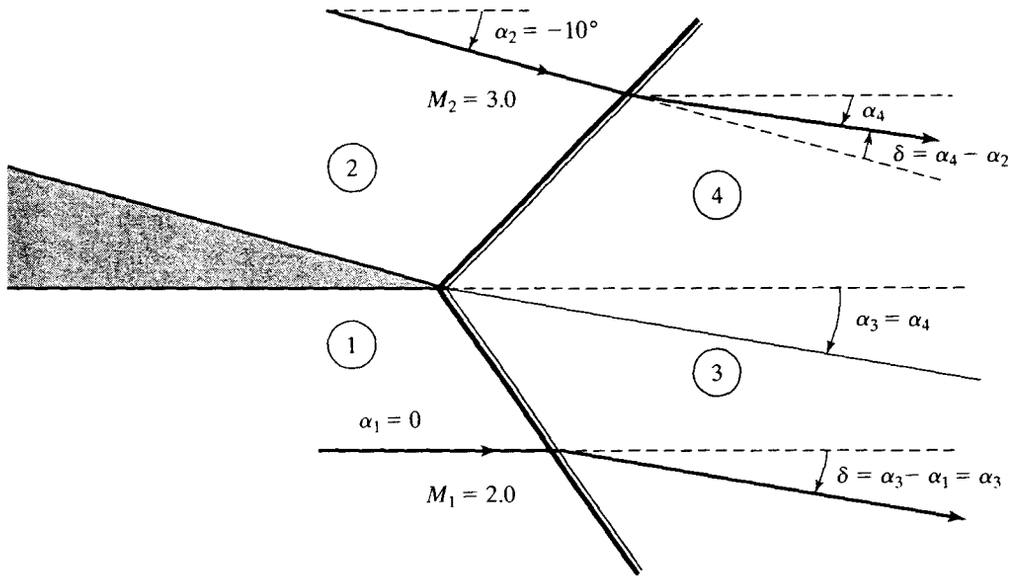


**Figure 6.18** Merging of Two Supersonic Flows at the Trailing Edge of an Airfoil

Find the resulting flow direction and downstream fluid properties in regions 3 and 4 if the flow in region 1 follows the horizontal lower surface ($\alpha_1 = 0$) with $M_1 = 2.0$ and the flow in region 2 follows the upper surface ($\alpha_2 = -10$) with $M_2 = 3.0$. Assume that both streams have the same pressure, so that $p_2/p_1 = 1$, and let $\gamma = 1.4$ for both streams.

**Solution**

To solve this problem, we first draw the pressure-flow direction diagram, as it will serve as a guide to subsequent numerical solutions.

The first step in this procedure is to create two data files, using Eq. (6.33). The coefficients within this expression ($a$, $b$, and $c$) are computed using $M_1$ and $\gamma$ for one set and $M_2$ and $\gamma$ for the other. Choose the number of points that will be ultimately plotted. (Fifty points should be more than adequate.) Take this number and divide it into the difference between $b$ and unity. The result provides the plot increment. Starting from $y = b$, reduce $y$ by this increment until the value of unity is reached. For each $y$ value and the computed coefficients $a$, $b$, and $c$, determine the value of $x$. Repeat the process starting from $y = 1$ and returning to $b$ by adding the increment to each previous $y$. Prior to calculating $x$ with these $y$ values, change the sign of the arctangent in Eq. (6.33). This sign change will provide data for both lobes of the curve. Once the data files have been developed, follow the chart-drawing procedure in the spreadsheet program.

Because the flow conditions are the same as those used to draw Figures 6.16 and 6.17(a), the diagram for region 1 is already known. The same procedure can be used to plot the pressure-flow direction diagram for region 2. Superimposing these two diagrams provides a reasonably accurate solution to this problem. The combined diagram is shown in Figure 6.19. It is seen that the curves intersect twice; the lower pressure intersection, at the

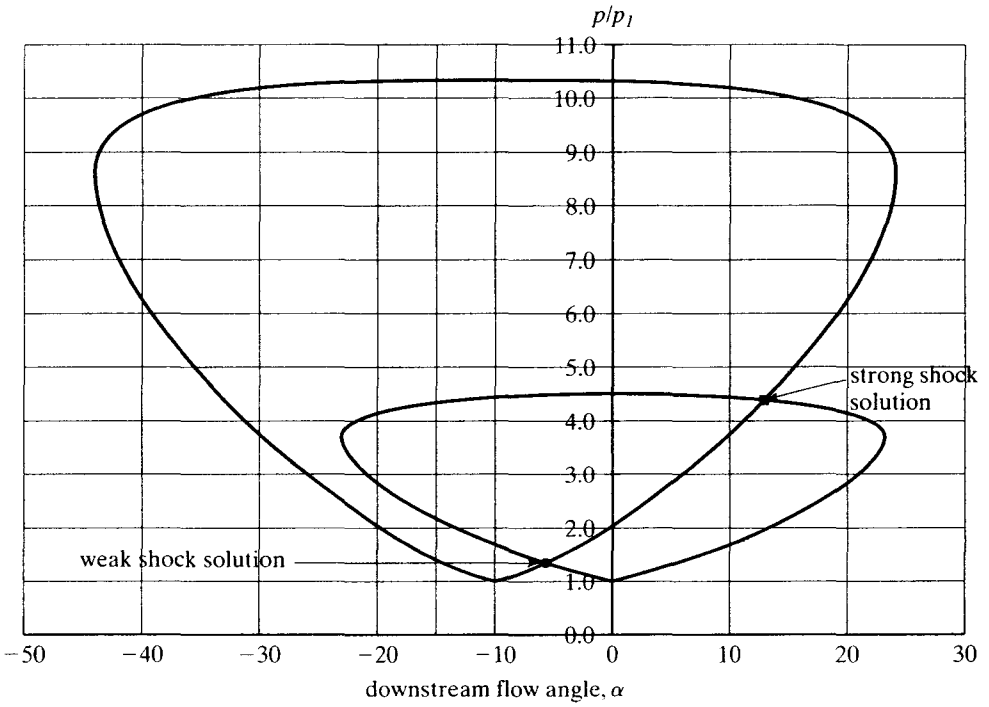


**Figure 6.19** Combined Pressure-Flow Direction Diagram for the Confluence of Two Shocks for Example 6.7

negative flow angle, is the weak shock solution, and the larger pressure intersection, at the positive flow angle, is the strong shock solution.

The accuracy of the results can be improved by using spreadsheet computations. A solution is realized when the following two downstream flow conditions are satisfied:

- the pressure is the same in regions 3 and 4: $p_3/p_1 = p_4/p_1$; and
- the flow direction is the same in regions 3 and 4: $\alpha_3 = \alpha_4$.

Using versions of Eq. (6.33), we see that a function that is dependent upon the pressure may be formulated as

$$f(y) = \alpha_3 - \alpha_4 = \left[\alpha_1 \pm \tan^{-1}\left(\frac{y-1}{a_1 - y}\sqrt{\frac{b_1 - y}{c + y}}\right)\right] - \left[\alpha_2 \pm \tan^{-1}\left(\frac{y-1}{a_2 - y}\sqrt{\frac{b_2 - y}{c + y}}\right)\right] \tag{6.35}$$

where $a_1$ and $b_1$ are computed using $M_1$ and $\gamma$, and $a_2$ and $b_2$ computed using $M_2$ and $\gamma$. The solution procedure is to vary $y$ until $f(y)$ becomes zero. This condition will occur for two values: one for the weak shock solution and the other for the strong shock solution. The Newton–Raphson method may be used to find these values:

$$y_{new} = y_{old} - \frac{f(y_{old})}{df(y_{old})/dy} \tag{6.36}$$

Because of the complexity of $f(y)$ in Eq. (6.35), the derivative required in the Newton–Raphson method is best computed using a central finite difference rather than actually differentiating Eq. (6.35):

$$\frac{df}{dy} \cong \frac{f(y + \Delta y) - f(y - \Delta y)}{2\Delta y}$$

Here, $\Delta y$ is a small number.

The results of the computations are shown in Tables 6.8 and 6.9. Thus, the weak-shock solution requires that the pressure ratio $p_3/p_1 = p_4/p_1 = 1.3723$ and that the flow direction $\alpha_3 = \alpha_4 = -5.7977°$.

The strong shock solution requires two revisions to the foregoing procedure. In both of these revisions, the pressure-flow direction diagram is of great assistance. First, a sign change within $f(y)$ must be made. This change is necessary because the strong shock solution for this case is an intersection of the right lobes of the two individual diagrams; therefore, select the + sign for both $\tan^{-1}$ functions. On the other hand, the weak shock solution was an intersection of the right lobe of one diagram (use the $+\tan^{-1}$) and the left lobe of the other (use the $-\tan^{-1}$). Second, because of the slopes involved, an initial guess close to the solution must be used for the strong shock solution. An inadequate guess causes the value of $y$ to be corrected beyond the value of $b_1$, which results in a

**TABLE 6.8** Results of Pressure-Deflection Diagram Spreadsheet Computations for Example 6.7

Weak Shock Solution

| Iteration | $y_{old}$ | $y + \Delta$ | $y - \Delta$ | $f(y)$ | $f(y + \Delta)$ | $f(y - \Delta)$ | $df/dy$ | $y_{new}$ | $x$ | $x$ (deg) |
|---|---|---|---|---|---|---|---|---|---|---|
| 1 | 2.0000 | 2.0001 | 1.9999 | 0.2224 | 0.2224 | 0.2223 | 0.3049 | 1.27081 | −0.07602 | −4.3555 |
| 2 | 1.2708 | 1.2709 | 1.2707 | −0.0434 | −0.0434 | −0.0435 | 0.4411 | 1.36925 | −0.10045 | −5.7551 |
| 3 | 1.3692 | 1.3693 | 1.3691 | −0.0013 | −0.0012 | −0.0013 | 0.4156 | 1.37233 | −0.10119 | −5.7976 |
| 4 | 1.3723 | 1.3724 | 1.3722 | 0.0000 | 0.0000 | 0.0000 | 0.4149 | 1.37233 | −0.10119 | −5.7977 |
| 5 | 1.3723 | 1.3724 | 1.3722 | 0.0000 | 0.0000 | 0.0000 | 0.4149 | **1.37233** | −0.10119 | **−5.7977** |

**TABLE 6.9** Results of Pressure-Flow Direction Diagram Spreadsheet Computations for Example 6.7

Strong Shock Solution

| Iteration | $y_{old}$ | $y + \Delta$ | $y - \Delta$ | $f(y)$ | $f(y + \Delta)$ | $f(y - \Delta)$ | $df/dy$ | $y_{new}$ | $x$ | $x$ (deg) |
|---|---|---|---|---|---|---|---|---|---|---|
| 1 | 4.2500 | 4.2501 | 4.2499 | −0.1051 | −0.1050 | −0.1051 | 0.4864 | 4.4660 | 0.1382 | 7.9175 |
| 2 | 4.4660 | 4.4661 | 4.4659 | 0.0909 | 0.0911 | 0.0907 | 1.9939 | 4.4205 | 0.2038 | 11.6764 |
| 3 | 4.4205 | 4.4206 | 4.4204 | 0.0219 | 0.0220 | 0.0218 | 1.1931 | 4.4021 | 0.2228 | 12.7666 |
| 4 | 4.4021 | 4.4022 | 4.4020 | 0.0015 | 0.0016 | 0.0014 | 1.0377 | 4.4007 | 0.2242 | 12.8457 |
| 5 | 4.4007 | 4.4008 | 4.4006 | 0.0000 | 0.0001 | −0.0001 | 1.0272 | **4.4007** | 0.2242 | **12.8461** |

negative square-root error. The problem is easily resolved by trying various values for the initial guess. Again, the pressure-flow direction diagram is of great assistance, since the approximate location of the intersection point for the strong shock solution is available from Figure 6.19. Thus, the strong shock solution requires that the pressure ratio $p_3/p_1 = p_4/p_1 = 4.4007$ and that the flow direction $\alpha_3 = \alpha_4 = +12.8461°$.

From the flow angles, it is straightforward to determine the deflection angles, and with $M_1$ and $M_2$, all parameters in regions 3 and 4 can be readily computed. (See Problem 6.22.)

---

**Example 6.8. Intersection of two oblique shocks of different strengths**

A supersonic stream with $M = 3.5$ flows into an inlet. The geometry is similar to that in Figure 6.15(b). The lower lip of the inlet has a wedge angle of 10°, while the upper lip has a wedge angle of −15°. The oblique shocks formed on these inlet lips intersect with each other, and two shocks and a slip line emanate from the point of intersection. Five angular regions of uniform properties are created and numbered as shown in Figure 6.20. Determine the downstream flow directions and pressures for the weak shock solution. Take $\gamma = 1.3$ for all flows.

**Solution**

A pressure-flow direction diagram is first drawn for $M_1 = 3.5$ and $\gamma = 1.3$. This is accomplished by using Eq. (6.33) to create a file of data of $y$ versus $x$ (as discussed in the solution of Example 6.7) and then employing the chart-drawing portion of a spreadsheet program. The result is Figure 6.21.

Shown on the curve within Figure 6.21 are two bullets. One represents the anchor point for region 2 ($y = p_2/p_1 = 2.1587$ and $x = \alpha_2 = 10°$) and the other the anchor point for region 3 ($y = p_3/p_1 = 3.0227$ and $x = \alpha_3 = -15°$). The Mach numbers within regions

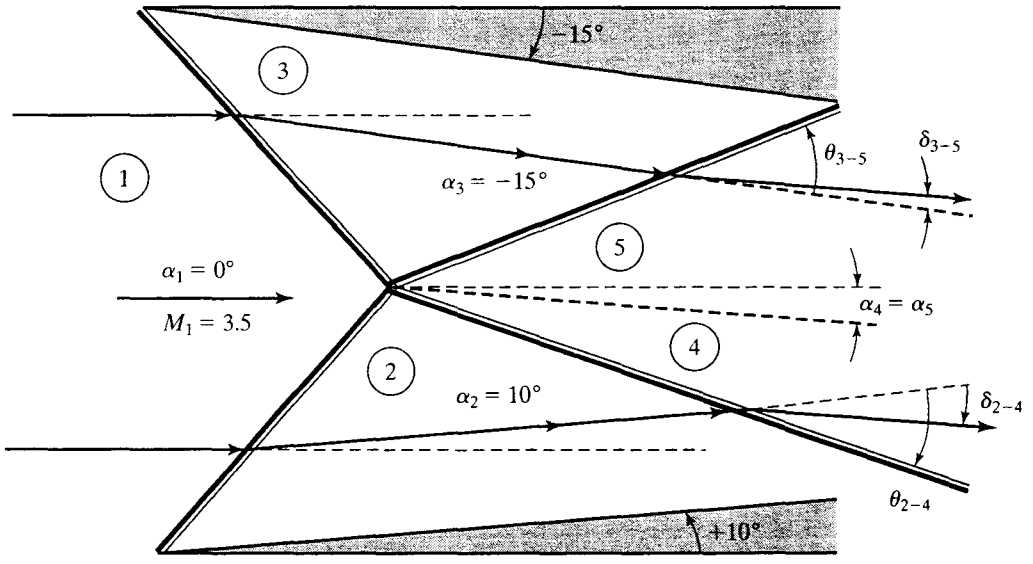


**Figure 6.20** Intersection of Oblique Shocks within an Inlet

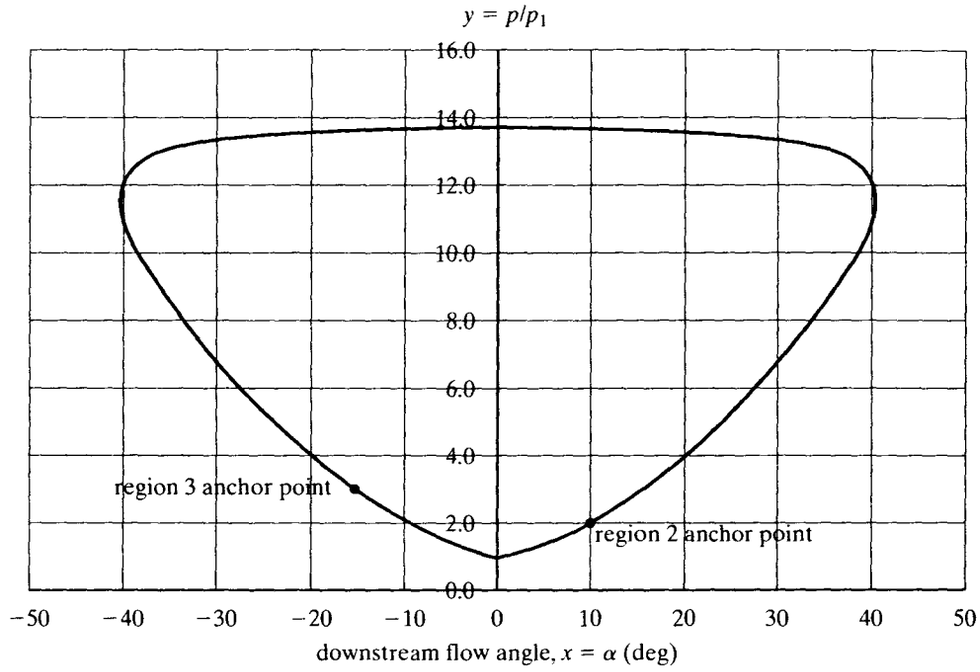


**Figure 6.21** Pressure-Flow Direction Diagram for Region 1 of Example 6.8 ($M_1 = 3.5, \gamma = 1.3$)

2 and 3 are 2.9976 and 2.7361, respectively. With these Mach numbers, pressure ratios, and $\gamma$, we can compute two more data files, using Eq. (6.34). This enables us to draw two additional pressure-flow direction diagrams that are shown as Figure 6.22(a) and 6.22(b) for regions 3 and 2, respectively. Finally, the two diagrams are united as shown in Figure 6.22(c).

The development of the diagram for the shock interaction problem is similar to that for the shock confluence problem of Example 6.7. The principal difference lies in the anchor points. In the confluence problem, both anchor points were at $y = 1$. Here, the points are at two different pressure ratios. Note carefully that all pressures on these diagrams have been nondimensionalized using $p_1$.

It is seen that the weak shock solution occurs at $y = p_4/p_1 = p_5/p_1 \cong 6$ and $\alpha_4 = \alpha_5 \cong -5°$.

To improve the accuracy of the results, we next employ a numerical procedure. Generally, the approach for problems involving shock interactions is to assume a range of possible flow directions for the slip line that are thought to blanket the actual solution and then to use interpolation of the pressure result to obtain an equality of pressure in regions 4 and 5. While the accuracy using this approach is better than the graphical results just described, it could be even better, as will be shown next.

Here, we write a function $f(y)$ just as we did in the previous example, where $y$ is the pressure, and we numerically determine (as in example 6.7) the value of $y$ that will cause the function to go to zero. The function is created using Eq. (6.34) as follows:

$$f(y) = \alpha_4 - \alpha_5$$

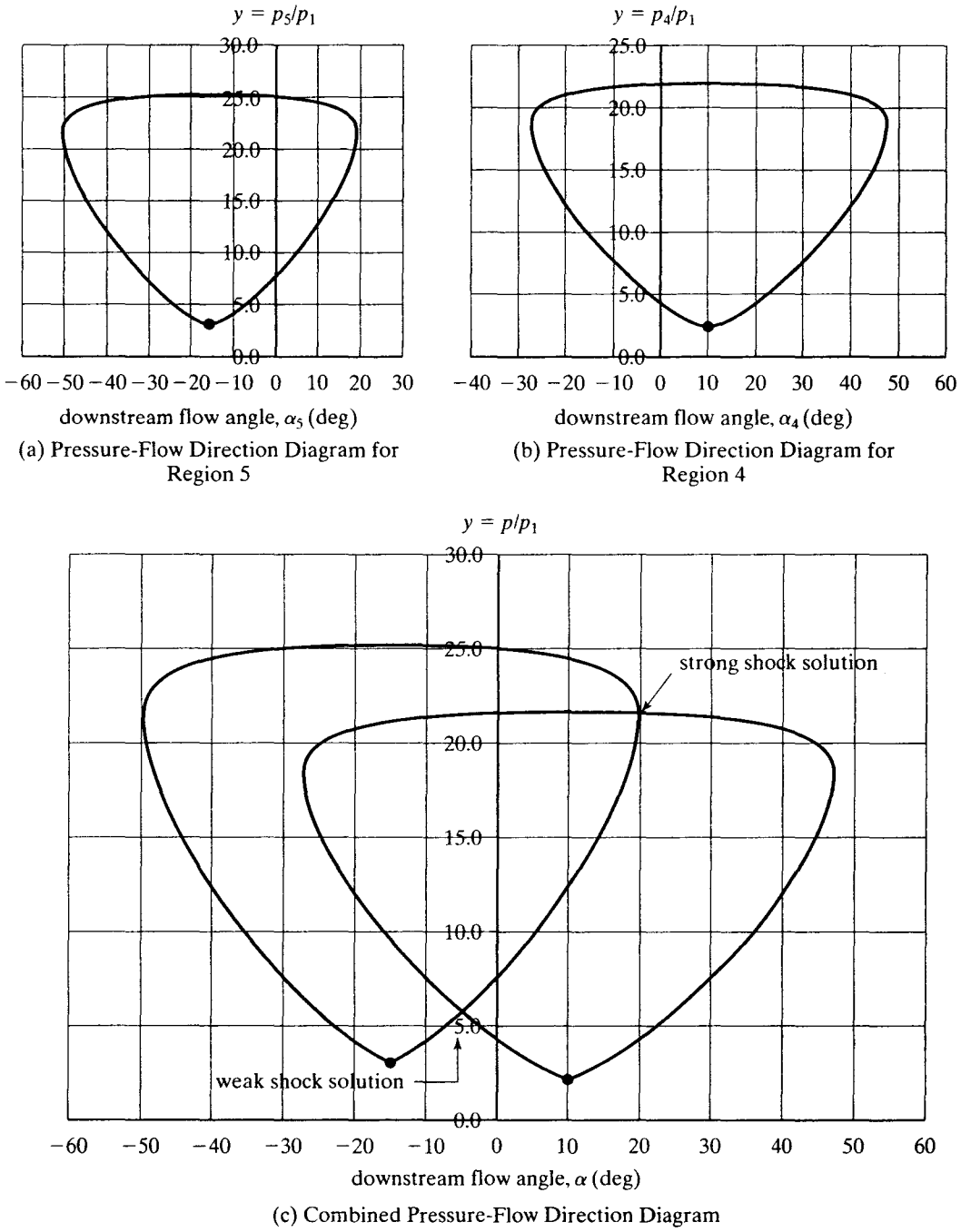


(a) Pressure-Flow Direction Diagram for Region 5

(b) Pressure-Flow Direction Diagram for Region 4

(c) Combined Pressure-Flow Direction Diagram

**Figure 6.22** Pressure-Flow Direction Diagram for the Intersection of Two Oblique Shocks of Unequal Strength

Here,

$$\alpha_4 = \alpha_2 \pm \tan^{-1}\left[\frac{\left(\frac{y}{p_2/p_1} - 1\right)}{\left(a_2 - \frac{y}{p_2/p_1}\right)}\sqrt{\frac{\left(b_2 - \frac{y}{p_2/p_1}\right)}{\left(c + \frac{y}{p_2/p_1}\right)}}\right]$$

$$\alpha_5 = \alpha_3 \pm \tan^{-1}\left[\frac{\left(\frac{y}{p_3/p_1} - 1\right)}{\left(a_3 - \frac{y}{p_3/p_1}\right)}\sqrt{\frac{\left(b_3 - \frac{y}{p_3/p_1}\right)}{\left(c + \frac{y}{p_3/p_1}\right)}}\right]$$

Table 6.10 provides the results of the numerical iterations from the spreadsheet program developed to solve this problem.

**TABLE 6.10** Results of Pressure-Flow Direction Diagram Spreadsheet Computations for Example 6.8

| $y_{old}$ | $y + \Delta$ | $y - \Delta$ | $f(y)$ | $f(y + \Delta)$ | $f(y - \Delta)$ | $df/dy$ | $y_{new}$ | $\alpha_4$ |
|---|---|---|---|---|---|---|---|---|
| 2.0000 | 2.0001 | 1.9999 | 0.5589 | 0.5588 | 0.5589 | −0.2409 | 4.3197 | 11.0514 |
| 4.3197 | 4.3198 | 4.3196 | 0.1597 | 0.1597 | 0.1597 | −0.1299 | 5.5486 | −0.3082 |
| 5.5486 | 5.5487 | 5.5485 | 0.0147 | 0.0146 | 0.0147 | −0.1079 | 5.6845 | −4.4705 |
| 5.6845 | 5.6846 | 5.6844 | 0.0001 | 0.0001 | 0.0001 | −0.1060 | 5.6857 | −4.8889 |
| 5.6857 | 5.6858 | 5.6856 | 9.83E–09 | 0.0000 | 0.0000 | −0.1060 | 5.6857 | −4.8926 |
| 5.6857 | 5.6858 | 5.6856 | 0.00E+00 | 0.0000 | 0.0000 | −0.1060 | 5.6857 | −4.8926 |

**TABLE 6.11** Property Values in the Various Regions for Example 6.8

Region 1 to Region 2 to Region 4

| $\gamma$ | $M_1$ | $\delta_{1\text{-}2}$ | $\theta_{1\text{-}2}$ | $p_2/p_1$ | $\rho_2/\rho_1$ | $T_2/T_1$ | $p_{o2}/p_{o1}$ | |
|---|---|---|---|---|---|---|---|---|
| 1.3000 | 3.5000 | 10.0000 | 23.9901 | 2.1587 | 1.7862 | 1.2085 | 0.9500 | |
| | $M_2$ | $\delta_{2\text{-}4}$ | $\theta_{2\text{-}4}$ | $p_4/p_2$ | $\rho_4/\rho_2$ | $T_4/T_2$ | $p_{o4}/p_{o2}$ | $M_4$ |
| | 2.9976 | −14.8926 | −31.4440 | 2.6339 | 2.0575 | 1.2802 | 0.9032 | 2.3580 |

Region 1 to Region 3 to Region 5

| $\gamma$ | $M_1$ | $\delta_{1\text{-}3}$ | $\theta_{1\text{-}3}$ | $p_3/p_1$ | $\rho_3/\rho_1$ | $T_3/T_1$ | $p_{o3}/p_{o1}$ | |
|---|---|---|---|---|---|---|---|---|
| 1.3000 | 3.5000 | −15.0000 | −28.5011 | 3.0227 | 2.2615 | 1.3366 | 0.8598 | |
| | $M_3$ | $\delta_{3\text{-}5}$ | $\theta_{3\text{-}5}$ | $p_5/p_3$ | $\rho_5/\rho_3$ | $T_5/T_3$ | $p_{o5}/p_{o3}$ | $M_5$ |
| | 2.7361 | 10.1074 | 29.1782 | 1.8810 | 1.6152 | 1.1646 | 0.9719 | 2.3422 |

It is seen that the solution is quickly obtained to be $y = p_4/p_1 = p_5/p_1 = 5.6857$ and that the flow direction is $\alpha_4 = \alpha_5 = -4.8926°$. With these values, it is not difficult to determine all other parameters and obtain the results in Table 6.11.

## 6.5 SUMMARY

Chapter 6 has presented an analysis of the oblique shockwave. Emphasis has been placed on demonstrating how accurate values of the oblique-shock properties and geometries can be determined by using spreadsheet computation. With this approach, the oblique shock and resultant two-dimensional flow can be readily found with the equations derived in this chapter.

The student should now appreciate the importance of recognizing the boundary conditions in a given flow situation. It is the boundary conditions, for example, that determine whether the strong or weak oblique-shock solution is to occur; again, it is the boundary conditions that determine the characteristics of the flow after impingement of an oblique shock on a plane wall.

Finally, the importance and usefulness of the pressure-deflection or pressure-flow direction shock-polar diagrams was illustrated through the solution of systems of oblique shocks. Most texts employ tedious trial-and-error methods. Here, the pressure-flow direction diagram provided reasonably accurate results, which were subsequently improved by more accurate numerical computations using spreadsheet methods.

## 6.6 REFERENCES


**6.1** Ames Research Staff. *Equations, Tables and Charts for Compressible Flow*, NACA Report 1135, 1953.

**6.2** Chapman, A. J., and Walker, W. F. *Introductory Gas Dynamics*, Holt, Rinehart, and Winston, New York, 1971, pp. 461–463.

**6.3** Collar, A. R. "Iterative Solutions of the Equations for Plane Oblique Shock Waves," *J Royal Aeronaut Soc* 1959; 63: 669–672.

**6.4** National Cataloguing Unit for the Archives of Contemporary Scientists (NCUACS). The Library, University of Bath, Claverton Down, Bath, UK. http://www.bath.ac.uk/ncuacs/guidec.htm#ARCollar.

**6.5** Rosenhead, L. *A Selection of Graphs for Use in Calculations of Compressible Flow*, Clarendon Press, Oxford, UK, 1954.

**6.6** Shapiro, A. H. *The Dynamics and Thermodynamics* of *Compressible Fluid Flow,* Vol. 1, Ronald Press, New York, 1953.

**6.7** Reichenbach, H. "Contributions of Ernst Mach to Fluid Mechanics," *Ann Rev Fluid Mech* 1983; 15: 1–28.

**6.8** Pai, S. I. *Introduction to the Theory of Compressible Flow*, D. Van Nostrand Company, Princeton, NJ, 1959, p. 272.

**6.9** Landau, L. D., and Lifshitz, E. M. *Fluid Mechanics*, Addison-Wesley Publishing Company, Reading, MA, 1959, p. 412.

**6.10** Courant, R., and Friedrichs, K. O. *Supersonic Flow and Shock Waves*, Interscience Publishers, New York, 1948, p. 32.

## 6.7 PROBLEMS

**6.1** Uniform air flow at Mach 3 passes into a concave corner of angle 15°, as shown in Figure P6.1. The pressure and temperature in the supersonic flow are, respectively, 72 kPa and 290 K. Determine the tangential and normal components of velocity and Mach number upstream and downstream of the wave. Also, find the static and stagnation pressure ratios across the wave. How great would the corner angle have to be before the shock would detach from the corner?

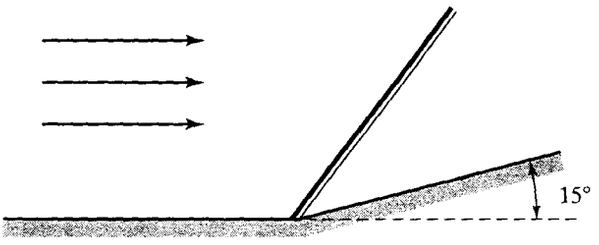


**Figure P6.1**

**6.2** In a helium wind tunnel, flow at Mach 4.0 passes over a wedge of unknown half-angle aligned symmetrically with the flow. An oblique shock is observed attached to the wedge, making an angle of 30° with the flow direction. Determine the half-angle of the wedge and the ratios of stagnation pressure and stagnation temperature across the wave.

**6.3** A wedge is to be used as an instrument to determine the Mach number of a supersonic airstream; that is, with the wedge axis aligned to the flow, the shock angle of the attached oblique shock is measured, permitting a determination of the incident Mach number. If the total included angle of such a wedge is 45°, give the Mach number range over which such an instrument would be effective.

**6.4** The leading edge of a supersonic wing is wedge shaped, with a total included angle of 10°. (See Figure P6.4.) If the wing is flying at zero angle of attack, determine the lift and drag force on the front portion of the wing per meter of span. Repeat for an angle of attack of 3°. Assume that the wing is traveling at Mach 2.5.

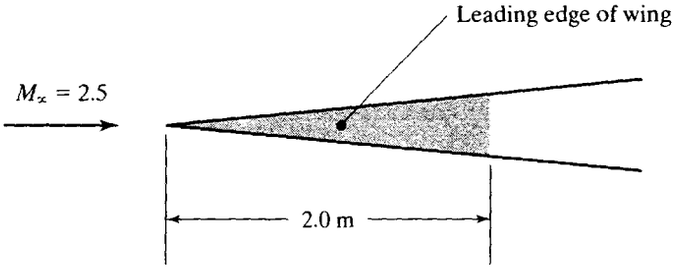


**Figure P6.4**

**6.5** An oblique shockwave is incident on a solid boundary, as shown in Figure P6.5. The boundary is to be turned through such an angle that there will be no reflected wave. Determine the angle $\beta$.

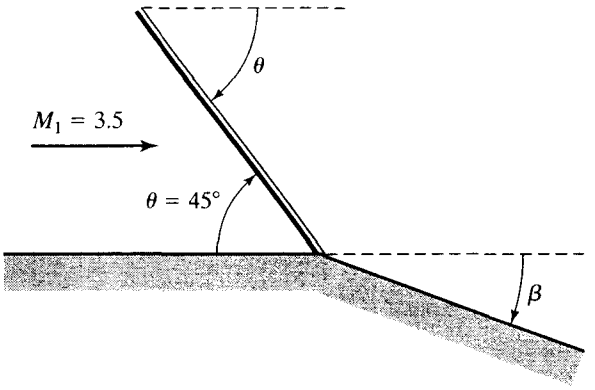


**Figure P6.5**

**6.6** Explain in physical terms why the angle of incidence and the angle of reflection of a reflected oblique shock are not equal.

**6.7** A converging–diverging nozzle is designed to provide flow at Mach 2.0. With the nozzle exhausting to a back pressure of 80 kPa and a reservoir pressure of 280 kPa, the nozzle is overexpanded, with oblique shocks at the exit. (See Figure P6.7.) Determine the flow direction and flow Mach number in region *R* with air as the working fluid.

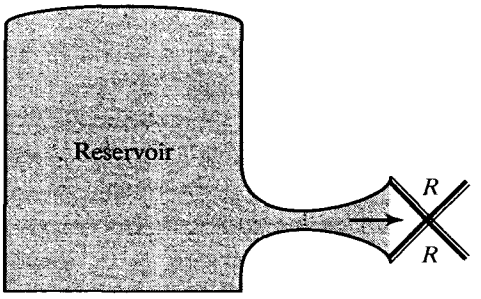


**Figure P6.7**

**6.8** Oblique shockwaves appear at the exit of a supersonic nozzle, as shown in Figure P6.8. Air is the working fluid. The stagnation temperature of the flow is 500 K. The nozzle throat area is 50 $cm^2$, and the nozzle exit area is 120 $cm^2$. If the nozzle back pressure is 101 kPa, (a) determine the nozzle inlet stagnation pressure; (b) find the velocity at the nozzle exit plane; and (c) find the mass-flow rate through the nozzle.

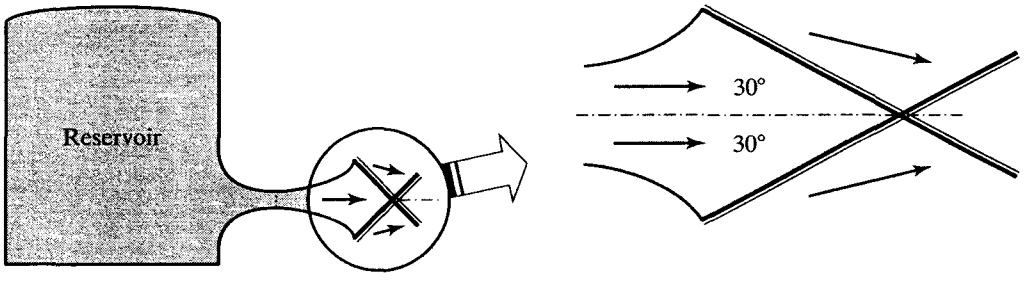


**Figure P6.8**

**6.9** A supersonic flow leaves a two-dimensional nozzle as parallel, horizontal flow (region *A*) with a Mach number of 2.6 and static pressure of 50 kPa. The pressure of the atmosphere

into which the jet discharges is 101 kPa. Find the pressures in regions $B$ and $C$ of Figure P6.9.

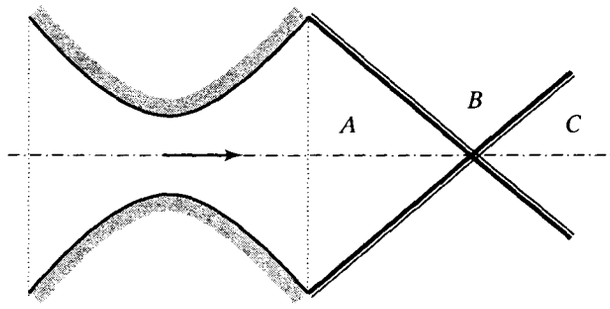


**Figure P6.9**

**6.10** For the two-dimensional diffuser shown in Figure P6.10, find $V_i$ and $p_{oi}$.

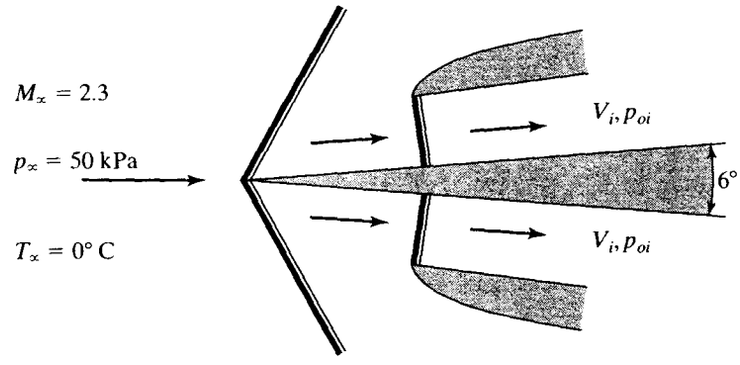


**Figure P6.10**

**6.11** A two-dimensional supersonic inlet is to be designed to operate at Mach 2.4. Deceleration is to occur through a series of oblique shocks followed by a normal shock, as shown in Figure 6.12(b). Determine the loss of stagnation pressure for the cases of two, three, and four oblique shocks. Assume that the wedge turning angles are each 6°.

**6.12** Two oblique shocks intersect as shown in Figure P6.12. Determine the flow conditions after the intersection, with $\gamma = 1.4$.

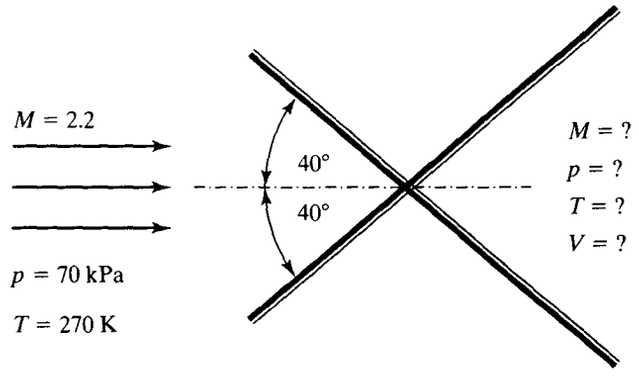


**Figure P6.12**

**6.13** Show that the entropy increase across an oblique shock is given by the following [see Ref. (6.8)]:

$$\frac{\Delta s}{c_v} = \ln\left[\left(\frac{2\gamma}{\gamma+1}M_1^2\sin^2\theta - \frac{\gamma-1}{\gamma+1}\right)\left(\frac{\gamma-1}{\gamma+1} + \frac{2}{(\gamma+1)M_1^2\sin^2\theta}\right)^{\gamma}\right]$$

**6.14** Repeat the computations of Example 6.2. However, instead of using the successive-substitution method proposed by Collar and described in Section 6.2, solve the problem by using the Newton–Raphson method.

**6.15** For the two-dimensional case shown in Figure P6.15, where $\gamma = 1.4$, determine $M_3$ and $p_3$.

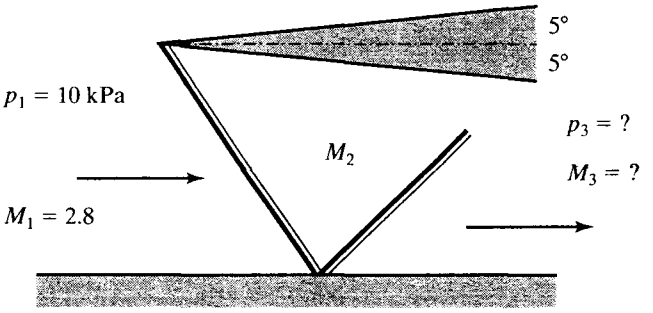


**Figure P6.15**

**6.16** Prove that (a) at the minimum shock angle, $M_2 = M_1$, and (b) at the maximum value of the shock angle, Eq. (6.17) becomes Eq. (4.9).

**6.17** Develop Prandtl's relation for oblique shocks from conservation principles.

**6.18** Show that the largest deflection angle for the limiting upstream Mach number $M_1 \rightarrow \infty$ can be found by differentiating Eq. (6.26), setting the result to zero, and then solving for $\theta$. In other words, verify that Eq. (6.27) is correct.

**6.19** In general, the angle of incidence, $\theta_i$, and the angle of reflection, $\theta_r$, of an oblique shock reflected from a flat surface are not equal. However, there is an angle $\theta^*$ such that the two angles are equal. [See Refs. (6.9) and (6.10).] Also, if $\theta_i < \theta^*$, then $(\theta_r - \delta) < \theta_i$, and if $\theta_i > \theta^*$, then $(\theta_r - \delta) > \theta_i$. Computationally verify that for $M_1 = 2, 3$, and 4 at $\gamma = 1.4$, the angle of incidence and the angle of reflection of an oblique shock reflected from a flat surface will be equal if

$$\theta_i = \theta^* = \frac{1}{2}\cos^{-1}\left(\frac{\gamma-1}{2}\right)$$

**6.20** Repeat the computations of Example 6.8 to find the angle the slip line makes with the horizontal for $\gamma = 1.4$ and 1.667. How does the angle vary with $\gamma$?

**6.21** Derive the pressure-deflection equation [i.e., Eq. (6.32)].

**6.22** Complete the computations of Example 6.7; that is, use the computed flow angles to determine the deflection angles, and with $M_1$ and $M_2$, determine all parameters in regions 3 and 4 of Figure 6.18.

# Chapter 7

# Prandtl–Meyer Flow

## 7.1 INTRODUCTION

When a supersonic compression takes place at a *concave corner* an oblique shock is known to occur at the corner. [See Figure 7.1(a).] When supersonic flow passes over a *convex corner* it is evident that some sort of supersonic expansion must take place. [See Figure 7.1(b).] Previous results indicate that, except for the unusual case involving dense gases [see Ref. (7.1)], an expansion normal shock is impossible. However, a means must be available for the supersonic flow of Figure 7.1(b) to negotiate the corner. This chapter will present an analysis of the mechanism of two-dimensional, supersonic expansion flow, as might occur, for example, during supersonic flow over a convex corner or at the exit of an underexpanded supersonic nozzle.

## 7.2 THERMODYNAMIC CONSIDERATIONS

Two-dimensional, supersonic flow is to be turned through a finite angle at a convex corner. The mechanism of the resultant flow is of interest. Consider first the possibility of an expansion oblique shockwave occurring at the corner. Figure 7.2 shows the velocity vectors normal and tangential to such a wave. For this two-dimensional adiabatic

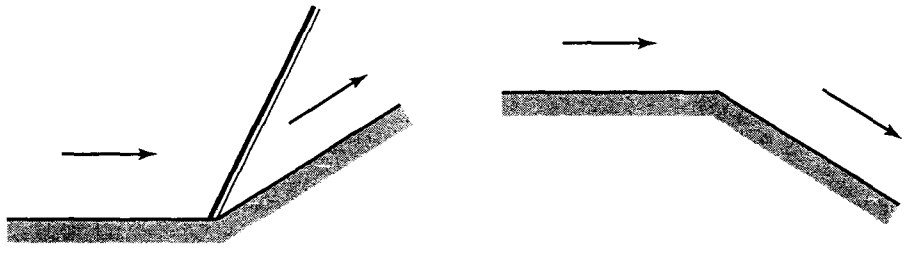

(a) Supersonic flow over a concave corner (b) Supersonic flow over a convex corner

**Figure 7.1** Supersonic Flow over Two Types of Corners

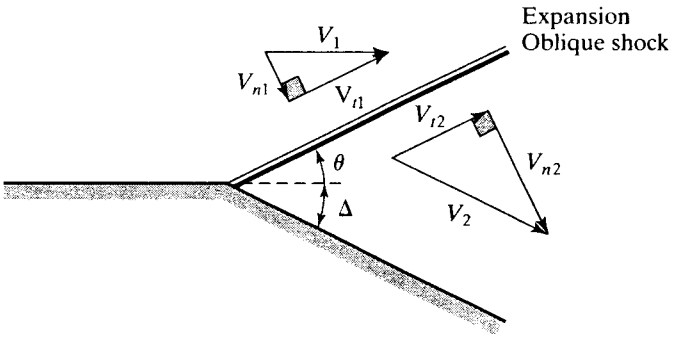


**Figure 7.2** Supersonic Flow around a Convex Corner

flow, uniform conditions prevail upstream and downstream of the wave. The equations of motion are exactly the same as those presented in Chapter 6 for the oblique compression shock. Again, with no pressure gradient in the direction tangential to the wave, the tangential momentum equation yields $V_{t1} = V_{t2}$. From geometrical considerations, then, it follows that $V_{n2}$ must be greater than $V_{n1}$ (Problem 7.1). The normal momentum equation, Eq. (6.2), yields

$$p_1 + \rho_1 V_{n1}^2 = p_2 + \rho_2 V_{n2}^2$$

Combining this with the continuity equation, Eq. (6.1), we obtain

$$p_2 - p_1 = \rho_1 V_{n1}(V_{n1} - V_{n2})$$

Since $V_{n2} > V_{n1}$, it follows that $p_2 < p_1$, indicating that the resultant flow must be an expansion. It has been shown that an oblique shock reduces to a normal shock for the velocity component normal to the wave, with the tangential component remaining unchanged. The ratios of pressure, temperature, and density across an oblique shock are functions of $M_{n1}$ alone. (See Section 6.2.) The entropy change across an oblique shock can be written, then, in terms of $M_{n1}$, the resultant variation of $\Delta s$ with $M_{n1}$ being exactly the same as that shown in Figure 4.11 for the normal shock. Hence, an oblique expansion shock of a perfect gas ($V_{n2} > V_{n1}$), just as a normal expansion shock of a perfect gas, would involve a decrease in entropy during an adiabatic process. This violates the second law of thermodynamics and is impossible. Therefore, the expansion shock of a perfect gas, with sudden changes in flow properties, cannot occur at the convex corner. Instead, a more gradual type of supersonic expansion must take place.

## 7.3 GRADUAL COMPRESSIONS AND EXPANSIONS

When a supersonic stream undergoes a compression due to a finite, sudden change of direction at a concave corner, an oblique shock occurs at the corner. However, if the flow is allowed to change direction in a more gradual fashion, the compression can approach an isentropic process. Allowing supersonic flow to pass through several weak oblique shocks rather than one strong shock (see Figure 7.3) has been shown to reduce the resultant loss in stagnation pressure (or entropy rise) for a given change in flow direction. In the limit, as the number of oblique shocks becomes larger, with

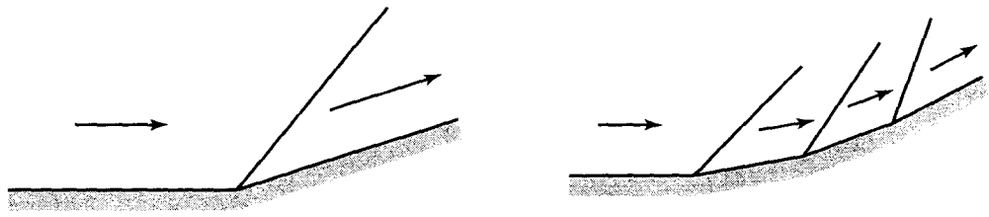

**Figure 7.3** Supersonic Flow through Weak Oblique Shockwaves

each shock turning the flow through a smaller and smaller angle, the oblique shocks approach the Mach waves, as discussed in Chapter 2. The Mach wave, brought about by the presence of an infinitesimal disturbance in a supersonic flow, here corresponds to an oblique shock of vanishing strength, with infinitesimally small changes of velocity, flow direction, entropy, and so on, taking place across the wave. (See Figure 7.4.) As we have seen in Section 6.2, the wave angle of an oblique shock of vanishing strength is given by $\theta = \mu = \sin^{-1}(1/M)$. So, by employing a smooth turn, with the resultant oblique shocks approaching Mach waves, we see that a continuous compression is achieved in the vicinity of the wall with vanishingly small entropy rise. (See Figure 7.5.)

Away from the wall, however, the compression waves converge, coalescing to form a finite oblique shockwave. (See Figure 7.6.) The characteristics of this shock are the same as those already discussed in Chapter 6 for an oblique shockwave of given $M_1$

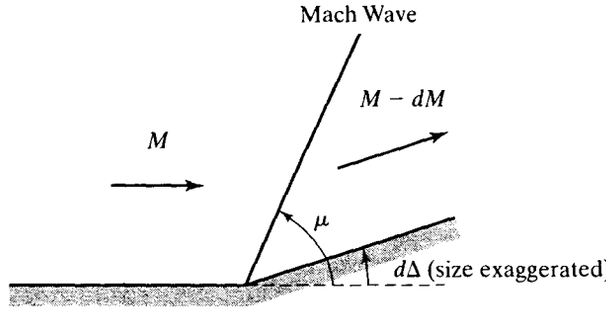


**Figure 7.4** Supersonic Flow through a Mach Wave

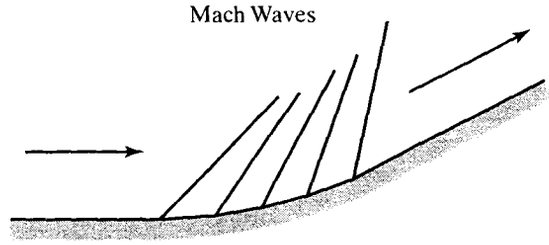


**Figure 7.5** Supersonic Flow through Weak Oblique Shocks in a Smooth Turn

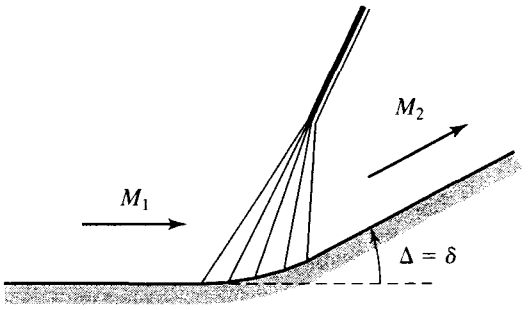


**Figure 7.6** Coalescing of Mach Waves into an Oblique Shock in a Concave Corner

and a deflection or turning angle $\delta$. In fact, far enough away from the wall, flow about the smooth turn cannot be distinguished from the flow about a sharp, concave corner of angle $\Delta = \delta$. It is important to note that here, again, the weak compression waves, each involving only an infinitesimal entropy rise, are able to reinforce one another to form a compression shockwave, with the resultant shock process involving a finite increase of entropy.

Now consider a supersonic expansion through a series of infinitesimally small convex turns. (See Figure 7.7.) Mach waves are generated at each corner, with each wave inclined at an angle to the flow direction. For this expansion flow, unlike the compressive flow previously discussed, waves do not coalesce, but rather spread out. The divergent waves cannot reinforce one another; an expansion oblique shock is physically impossible. Flow between each of the waves in Figure 7.7 is uniform, so the length of the wall between waves has no effect on the variation of flow properties. Thus, the lengths of the wall segments can be made vanishingly small, without affecting the overall variation of flow properties across the expansion. By thus reducing the wall segments, the series of convex turns becomes a sharp corner. (See Figure 7.8.) The resultant series of expansion waves, centered at the corner, is called a *Prandtl–Meyer expansion fan*. It is named after Ludwig Prandtl and Theodor Meyer. Prandtl, who originated the boundary-layer concept, studied simple waves in supersonic flows in the early 1900s. Meyer, one of Prandtl's students, wrote his doctoral dissertation on the topic in 1908. [See Refs. (7.2), (7.3), and (7.4); the latter reference contains Meyer's Ph.D. dissertation (in German).]

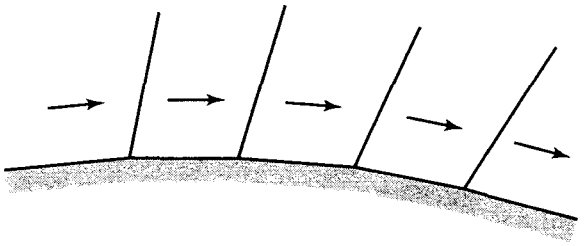

**Figure 7.7** Supersonic Flow around a Segmented Convex Corner

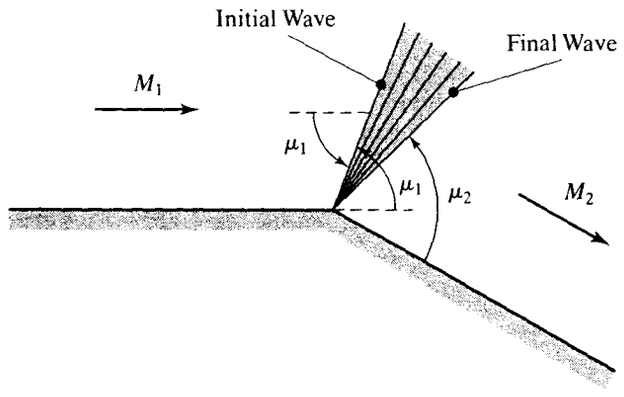


**Figure 7.8** Centered Expansion Fan at a Convex Corner

**Historical Note: Ludwig Prandtl** (1875–1953) was born in Freising, Germany. Because his mother was very sickly during most of his youth, Prandtl spent much time with his father, an Agricultural Central School Professor, who encouraged him to observe nature and think about his observations.

In 1894 in Munich, Prandtl began studying Mechanical Engineering at the Technische Hochschule (TH) and became an assistant of August Föppl—his advisor and future father-in-law. After completing his thesis (on elastic stability) and graduating in early 1900, Prandtl worked for less than two years at a Nuremburg factory. While there, he failed to improve the suction of sawdust from a wood-cutting machine because he used a diffuser with too large of a diverging angle. This haunted him until he invented boundary layer theory and used it to describe flow separation.

In 1901, Prandtl was appointed Professor at the TH in Hanover. There he made friends with Carle Runge (see **Historical Note** in Section 9.7). In 1904, Felix Klein, the reknowned mathematician at Göttingen, based on the strong recommendation of Föppl, enticed Prandtl to Göttingen in order to organize a new department of mechanics.

In August 1904, Prandtl delivered a revolutionary paper (it contained just eight equations) describing his boundary layer theory entitled *Ueber Flussigkeitsbewegung Bei Sehr Kleiner Reibung* ("Fluid Flow in Very Little Friction"). He became Director of the Institute for Technical Physics at the University of Göttingen later that year.

In 1906, Prandtl published the first estimate of the thickness of a shock wave and, during WWI, created his thin-airfoil theory for determining lift of thin, cambered airfoils. Prandtl worked with Albert Betz and Max Munk for almost ten years to solve the induced drag problem. The result was his lifting line theory to describe the lift and drag of wings of finite span which revealed the third source of subsonic drag. This was published in 1918–1919. English scientist Frederick Lanchester published the foundation for Prandtl's theory years earlier and this theory is also referred to as the Lanchester-Prandtl theory. In 1922 Prandtl contributed to a method that describes the compressibility effects at high speeds (Prandtl-Glauert rule for subsonic airflow). Prandtl also made important contributions to the theories of supersonic flow and turbulence, and contributed much to the development of wind tunnels and other aerodynamic equipment. In addition, he devised the soap-film analogy for the torsion of noncircular sections and wrote on the theories of plasticity and of meteorology.

By the 1920s Göttingen was an unparalleled scientific institution; it eventually turned into the Kaiser Wilhelm Institute for Fluid Mechanics (now the Max Planck Institute). Many of Prandtl's

(*Continued*)

*(Continued)*

students and colleagues went on to make many fundamental contributions to fluid dynamics. A list of their names reads like a who's who of fluid mechanics. A partial list includes: Jacob Ackeret, Albert Betz, Heinrich Blasius, Adolf Busemann, Henry Görtler, Karl Hiemenz, Theodore von Kármán, Theodor Meyer, Klaus Oswatitsch, Karl Pohlhausen, Hans Reichardt, Hermann Schlichting and Walther Tollmien. Prandtl would become recognized as the father of modern fluid mechanics and the father of aerodynamic theory.

Prandtl, also an accomplished pianist, remained at Gottingen as Professor of Applied Mechanics for 49 years until his death on August 15, 1953. See Refs. (7.5) – (7.7).

## 7.4 FLOW EQUATIONS FOR A PRANDTL–MEYER EXPANSION FAN

It has been shown that supersonic expansion flow around a convex corner involves a smooth, gradual change in flow properties. The Prandtl–Meyer expansion fan consists of a series of Mach waves, centered at the convex corner. The initial wave is inclined to the approach flow at an angle $\mu_1 = \sin^{-1}(1/M_1)$, see Figure 7.8. The final wave in the fan is inclined to the downstream flow at an angle $\mu_2 = \sin^{-1}(1/M_2)$, with the component of velocity normal to the wave at each point in the flow equal to the local velocity of sound. (See Section 2.4.) Flow conditions along each Mach wave are uniform; the variation of pressure, velocity, and so on, through the expansion is only a function of angular position.

The equations for two-dimensional Prandtl–Meyer flow will now be presented so that, just as with oblique shock flow, the variation of flow properties can be determined for a given flow turning angle. A perfect gas with constant specific heats will be assumed in the following analysis.

Consider first a single Mach wave, expanding and deflecting the supersonic flow through a very small angle of magnitude $\Delta = d\nu$. With no pressure gradient in the tangential direction, again, there is no change of the tangential velocity component across the wave. Equating the expressions for $V_t$ upstream and downstream of the Mach wave (see Figure 7.9), we have

$$\begin{aligned} V_t &= V\cos\mu \\ &= (V + dV)\cos(\mu + d\nu) \\ &= (V + dV)(\cos d\nu\cos\mu - \sin d\nu\sin\mu) \end{aligned} \tag{7.1}$$

Since $d\nu$ is a very small angle, we may use the following approximations:

$$\begin{aligned} \cos d\nu &\approx 1 \\ \sin d\nu &\approx d\nu \end{aligned}$$

Therefore, Eq. (7.1) can be written as

$$V\cos\mu = (V + dV)(\cos\mu - d\nu\sin\mu)$$

Expanding yields

$$V\cos\mu = V\cos\mu + (\cos\mu)dV - (V\sin\mu)d\nu - (\sin\mu)dV\,d\nu$$

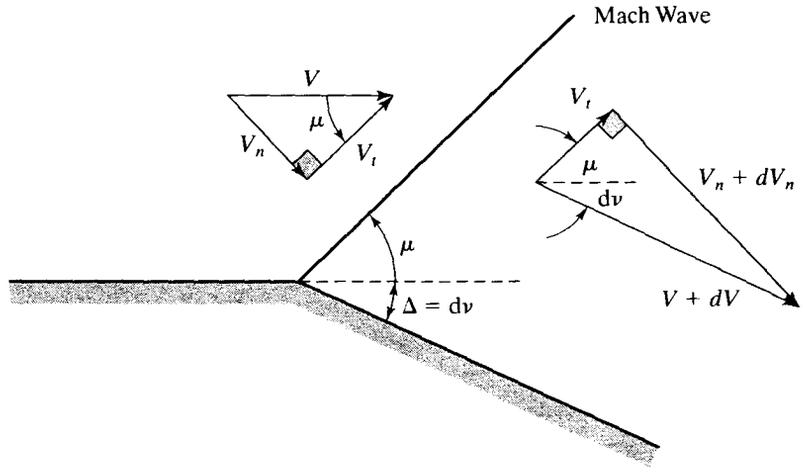


**Figure 7.9** Supersonic Flow through a Mach Wave at a Convex Corner

The last term, containing the product of two differentials, can be dropped in comparison with the other terms of the equation. Simplifying, we obtain

$$\frac{dV}{V} = (\tan\mu)d\nu$$

Since $\sin\mu = 1/M$, it follows that

$$\tan\mu = \frac{\sin\mu}{\cos\mu} = \frac{\sin\mu}{\sqrt{1 - \sin^2\mu}} = \frac{1}{\sqrt{M^2 - 1}}$$

Therefore,

$$\frac{dV}{V} = \frac{1}{\sqrt{M^2 - 1}}d\nu \tag{7.2}$$

To obtain an expression for $M$ as a function of the angle $\nu$, $V$ must be written in terms of $M$. From the definition of the Mach number for a perfect gas with constant specific heats, we have

$$V = M\sqrt{\gamma RT}$$

Taking the logarithm of each side and differentiating, we obtain

$$\frac{dV}{V} = \frac{dM}{M} + \frac{1}{2}\frac{dT}{T} \tag{7.3}$$

But, for this adiabatic flow, there is no change in stagnation temperature. So,

$$T_o = \text{constant} = T\left(1 + \frac{\gamma - 1}{2}M^2\right)$$

Taking the logarithm of each side and differentiating, we find that

$$0 = \frac{dT}{T} + \frac{(\gamma - 1)MdM}{1 + \frac{\gamma - 1}{2}M^2} \tag{7.4}$$

Equations (7.3) and (7.4) are combined to produce

$$\frac{dV}{V} = \frac{dM}{M} - \frac{1}{2}\left[\frac{(\gamma - 1)MdM}{1 + \frac{\gamma - 1}{2}M^2}\right] \tag{7.5}$$

or

$$\frac{dV}{V} = \left(\frac{1}{1 + \frac{\gamma - 1}{2}M^2}\right)\frac{dM}{M} \tag{7.6}$$

Substituting Eq. (7.6) into Eq. (7.2) yields

$$d\nu = \left(\frac{\sqrt{M^2 - 1}}{1 + \frac{\gamma - 1}{2}M^2}\right)\frac{dM}{M} \tag{7.7}$$

Equation (7.7) can be integrated to determine the change of Mach number associated with the turning of the supersonic flow through a finite angle. For the physical arrangement of Figure 7.10 for a finite turning angle $\Delta = (\nu_2 - \nu_1)$, we have

$$\int_{\nu_1}^{\nu_2} d\nu = \int_{M_1}^{M_2} \frac{\sqrt{M^2 - 1}}{1 + \frac{\gamma - 1}{2}M^2}\frac{dM}{M} \tag{7.8}$$

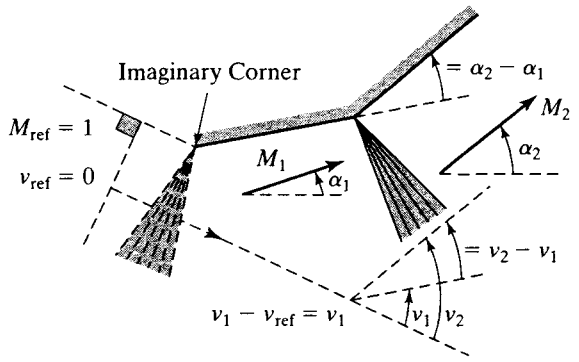


**Figure 7.10** Angles and Nomenclature for a Prandtl–Meyer Expansion

Formal integration leads to the following (see Problem 7.3):

$$\nu_2 - \nu_1 = \left| \sqrt{\frac{\gamma+1}{\gamma-1}} \tan^{-1}\left[ \sqrt{\frac{\gamma-1}{\gamma+1}\left(M^2-1\right)} \right] - \tan^{-1}\left(\sqrt{M^2-1}\right) \right|_{M_1}^{M_2} \tag{7.9}$$

For the purpose of tabulating this result, it is convenient to define a reference state, so that

$$\nu - \nu_{\text{ref}} = \left| \sqrt{\frac{\gamma+1}{\gamma-1}} \tan^{-1}\left[ \sqrt{\frac{\gamma-1}{\gamma+1}\left(M^2-1\right)} \right] - \tan^{-1}\left(\sqrt{M^2-1}\right) \right|_{M_{\text{ref}}}^{M}$$

Let the reference state be $\nu = 0$ at $M = 1$ so that

$$\nu = \left\{ \sqrt{\frac{\gamma+1}{\gamma-1}} \tan^{-1}\left[ \sqrt{\frac{\gamma-1}{\gamma+1}(M^2-1)} \right] - \tan^{-1}\left(\sqrt{M^2-1}\right) \right\} \tag{7.10}$$

The symbol $\nu$, which is called the *Prandtl–Meyer function* [see Appendix E and Refs. (7.8)–(7.11)], represents the angle through which a stream, initially at Mach 1, must be expanded to reach a supersonic Mach number $M$. (See Figure 7.10.) Note that the Prandtl–Meyer function depends only on $\gamma$ and $M$. A plot of $\nu$ against $M$ reveals that the Prandtl–Meyer function increases with increasing Mach number.

To determine the angle through which a flow would have to be turned to expand from $M_1$ to $M_2$, with $M_1$ not equal to 1, it is necessary only to subtract the value of $\nu_1$ at $M_1$ from the value of $\nu_2$ at $M_2$, (see Figure 7.10). The change in the Prandtl-Meyer function is connected to the change of the flow angle through

$$\Delta = \alpha_2 - \alpha_1 = \nu_2 - \nu_1 \tag{7.11}$$

Equation (7.11) applies to the case in which an isentropic supersonic stream is turned through a positive angle (counterclockwise),

$$\nu_2 = \nu_1 + (\alpha_2 - \alpha_1) = \nu_1 + \Delta \tag{7.12}$$

For a supersonic expansion about a convex corner in which $\alpha_2 - \alpha_1 = \Delta < 0$ (clockwise), use $\nu_2 = \nu_1 - \Delta$. In either case, the static pressure decreases, ($p_2 < p_1$) whereas the Mach number increases, ($M_2 > M_1$), therefore, the Prandtl-Meyer function must always increase, (i.e., $\nu_2 > \nu_1$).

The variation of pressure, temperature, and other thermodynamic properties through the expansion can be found from the usual thermodynamic relations for isentropic flow, presented in Chapter 3. For this isentropic process, with no change in stagnation pressure ($p_{o2} = p_{o1}$),

$$\frac{p_2}{p_1} = \frac{p_2/p_{o2}}{p_1/p_{o1}} = \left( \frac{1 + \dfrac{\gamma-1}{2} M_1^2}{1 + \dfrac{\gamma-1}{2} M_2^2} \right)^{\gamma/(\gamma-1)} \tag{7.13}$$

Since the expansion is adiabatic, there is no change of stagnation temperature, and, therefore,

$$\frac{T_2}{T_1} = \frac{T_2/T_{o2}}{T_1/T_{o1}} = \left(\frac{1 + \dfrac{\gamma - 1}{2}M_1^2}{1 + \dfrac{\gamma - 1}{2}M_2^2}\right) \tag{7.14}$$

**Example 7.1. A method to determine the Mach number from the Prandtl–Meyer function**

Develop a method to determine the Mach number in Eq. (7.9) for a given value of $\nu$. Use the procedure to find $M$ (a) for the case in which $\nu = 70°$ and $\gamma = 1.4$ and (b) for the case in which $\nu = 10°$ and $\gamma = 5/3$.

**Solution**

Equation (7.9) can be written in the following form:

$$f(M) = \left[\sqrt{\frac{\gamma + 1}{\gamma - 1}}\tan^{-1}\left[\sqrt{\frac{\gamma - 1}{\gamma + 1}(M^2 - 1)}\right] - \tan^{-1}\left(\sqrt{M^2 - 1}\right)\right] - \nu$$

For given values of $\nu$ and $\gamma$, we seek a value of $M$ that will result in $f(M) = 0$. To accomplish this task, use will again be made of the Newton–Raphson method. The derivative required in this method is readily obtained by reference to Eqs. (7.8) and (7.9) and is

$$\frac{df}{dM} = \left(\frac{\sqrt{M^2 - 1}}{1 + \dfrac{\gamma - 1}{2}M^2}\right)\frac{1}{M}$$

Alternatively, the derivative may be found by taking a central finite difference of $f(M)$:

$$\frac{df}{dM} = \frac{f(M + \Delta M) - f(M - \Delta M)}{2\Delta M}$$

The task of finding the value of $M$ that will satisfy $f(M) = 0$ for given values of $\nu$ and $\gamma$ is readily performed using spreadsheet computations. Table 7.1 provides the calculation details for the test case.

Case (a): $\nu = 70°$ and $\gamma = 1.4$

**TABLE 7.1** Results of the Computations in Example 7.1, Case (a), to Determine $M$ for a Given Value of $\nu$

| Iteration | $M_{old}$ | $f(M)$ | $f(M+\Delta M)$ | $f(M-\Delta M)$ | $\Delta f/\Delta M$ | $M_{new}$ |
|---|---|---|---|---|---|---|
| 1 | 2.0000 | −0.7613 | −0.7565 | −0.7661 | 0.4811 | 3.5824 |
| 2 | 3.5824 | −0.1777 | −0.1750 | −0.1804 | 0.2692 | 4.2423 |
| 3 | 4.2423 | −0.0201 | −0.0180 | −0.0222 | 0.2113 | 4.3374 |
| 4 | 4.3374 | −0.0003 | 0.0017 | −0.0024 | 0.2043 | 4.3390 |
| 5 | 4.3390 | −9.692E−08 | 0.0020 | −0.0020 | 0.2042 | 4.3390 |
| 6 | 4.3390 | −2.711E−13 | 0.0020 | −0.0020 | 0.2042 | 4.3390 |
| 7 | 4.3390 | 0.000E+00 | 0.0020 | −0.0020 | 0.2042 | 4.3390 |

Clearly, the iterations could be reduced with a better initial guess. Nevertheless, an initial guess of $M = 2.0$ is satisfactory for most problems. The Mach number for this case is 4.3390.

Case (b): $\nu = 10°$ and $\gamma = 5/3$

**TABLE 7.2** Results of the Computations in Example 7.1, Case (b), to Determine $M$ for a Given Value of $\nu$

| Iteration | $M_{old}$ | $f(M)$ | $f(M+\Delta M)$ | $f(M-\Delta M)$ | $\Delta f/\Delta M$ | $M_{new}$ |
|---|---|---|---|---|---|---|
| 1 | 2.0000 | 0.2057 | 0.2094 | 0.2020 | 0.3712 | 1.4457 |
| 2 | 1.4457 | −0.0192 | −0.0150 | −0.0235 | 0.4256 | 1.4909 |
| 3 | 1.4909 | 1.601E−05 | 0.0043 | −0.0042 | 0.4260 | 1.4909 |
| 4 | 1.4909 | −4.768E−10 | 0.0043 | −0.0043 | 0.4260 | 1.4909 |
| 5 | 1.4909 | 1.402E−14 | 0.0043 | −0.0043 | 0.4260 | 1.4909 |
| 6 | 1.4909 | 0.000E+00 | 0.0043 | −0.0043 | 0.4260 | 1.4909 |

The spreadsheet program developed for this example is of value for problems involving expansions, as will be demonstrated in the following example.

**Example 7.2. Computations of an expansion fan at a convex corner**

A uniform supersonic flow at Mach 2.0 and $\gamma = 1.4$, with static pressure of 75 kPa and a temperature of 250 K, expands around a 10° convex corner. Determine the downstream Mach number $M_2$, pressure $p_2$, temperature $T_2$, and the fan angle. See Figure 7.11.

**Solution**

For a $M_1 = 2.0$ and $\gamma = 1.4$, Eq. (7.9) gives $\nu_1 = 26.3798°$. From Eq. (7.10) with $\alpha_1 = 0°$ and $\alpha_2 = -10°$,

$$\nu_2 = \nu_1 - (\alpha_2 - \alpha_1) = 26.3798 - (-10) + 0 = 36.3798°$$

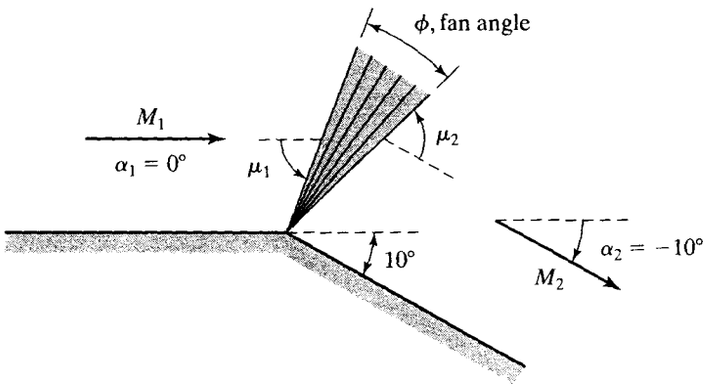


**Figure 7.11** Flow Configuration for Example 7.2

Again, because this is an expansion, $\nu_2 > \nu_1$. Using Appendix E or the solver developed in Example 7.1, we obtain

$$M_2 = 2.3849$$

From the isentropic-flow relations for $\gamma = 1.4$ at $M_2 = 2.3849$,

$$\frac{p_2}{p_{o2}} = 0.07003, \frac{T_2}{T_{o2}} = 0.4678$$

and at $M_1 = 2.0$,

$$\frac{p_1}{p_{o1}} = 0.1278, \frac{T_1}{T_{o1}} = 0.5556$$

Then

$$\frac{p_2}{p_1} = \frac{p_2}{p_{o2}} \frac{p_{o2}}{p_{o1}} \frac{p_{o1}}{p_1} = (0.07003)(1.0)\left(\frac{1}{0.1278}\right) = 0.5480$$

Since $p_1 = 75$ kPa,

$$p_2 = 41.0974 \text{ kPa}$$

and since $T_1 = 250$ K,

$$\frac{T_2}{T_1} = \frac{T_2}{T_{o2}} \frac{T_{o2}}{T_{o1}} \frac{T_{o1}}{T_1} = (0.4678)(1.0)\left(\frac{1}{0.5556}\right) = 0.8420$$

$$T_2 = 210.4932 \text{ K}$$

The included angle of the expansion fan may be computed as follows (refer to Figure 7.12):

$$\phi = \mu_1 - (\mu_2 - \Delta) = \mu_1 - \mu_2 + \Delta$$

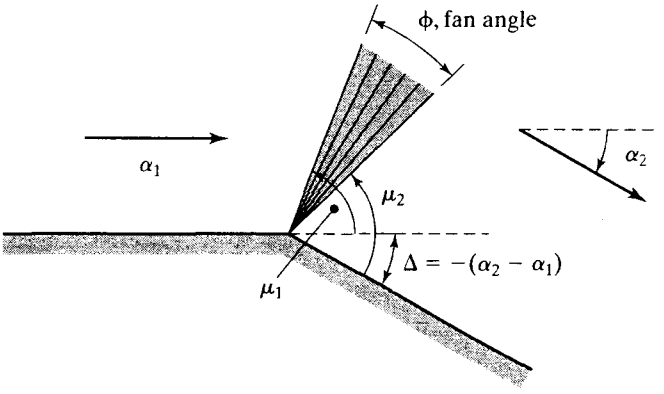


**Figure 7.12** Flow Configuration for Example 7.2

The wave angles $\mu_1$ and $\mu_2$ are computed from the Mach numbers:

$$\mu_1 = \sin^{-1}\left(\frac{1}{M_1}\right) = \sin^{-1}\left(\frac{1}{2}\right) = 30°$$

$$\mu_2 = \sin^{-1}\left(\frac{1}{M_2}\right) = \sin^{-1}\left(\frac{1}{2.3849}\right) = 24.7908°$$

Also, according to Eq. (7.10),

$$(\alpha_2 - \alpha_1) = -(\nu_2 - \nu_1) = -10°$$

Thus,

$$\phi = 30° - 24.7908° + 10° = 15.2092°$$

---

**Example 7.3. Supersonic flow through expansion fans at two convex corners**

Flow in Example 7.2 is expanded through a second convex turn of angle 10°. (See Figure 7.13.) Determine the downstream Mach number $M_3$ and the angle of the second fan.

**Solution**

The initial wave of the second fan must be parallel to the final wave of the first fan. Again, the distance between waves can have no effect on the resultant flow, since the flow between the waves is uniform. Therefore, the variation of properties is the same whether the flow is expanded through two 10° turns or one 20° turn:

$$\nu_3 = \nu_2 + 10° = 36.3798° + 10° = 46.3798°$$

Using the Prandtl–Meyer functions in Appendix E or the solver of Example 7.1, we find that

$$M_3 = 2.8306$$

Alternatively,

$$\nu_3 = \nu_1 + 20° = 26.3798° + 20° = 46.3798°$$

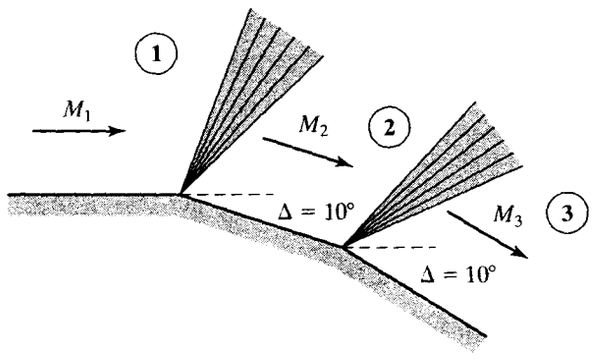


**Figure 7.13** Configuration for Example 7.3

Note the difference between Prandtl–Meyer flow and oblique-shock flow. In the latter, there was an advantage to be derived from compressing through several weak shocks rather than one strong shock.

The fan angle for the second fan is $\phi_2 = \mu_1 - \mu_2 + \Delta = 24.7908° - 20.6882° + 10° = 14.1026°$.

---

**Example 7.4. Supersonic flow from an underexpanded nozzle**

An underexpanded, two-dimensional, supersonic nozzle exhausts into a region where $p = 100$ kPa. (See Figure 7.14.) Flow at the nozzle exit plane is uniform, with $p_1 = 200$ kPa and $M_1 = 2.0$. Determine the flow direction and Mach number after the initial expansion (i.e., $M_2$.)

**Solution**

From the isentropic flow relations at $M_1 = 2.0$, we have

$$\frac{p_1}{p_{o1}} = 0.1278$$

Since $p_{o2} = p_{o1}$ for this isentropic expansion,

$$\frac{p_2}{p_{o2}} = \left(\frac{p_1}{p_{o1}}\right)\left(\frac{p_2}{p_1}\right)\left(\frac{p_{o1}}{p_{o2}}\right) = (0.1278)\left(\frac{100}{200}\right) = 0.0639$$

In addition, from the isentropic flow relations, we find that

$$M_2 = 2.4436$$

Now, at $M_1$ and $M_2$, the Prandtl–Meyer functions in regions 1 and 2 are, respectively,

$$\nu_1 = 26.3798°$$
$$\nu_2 = 37.7935°$$

Thus, the supersonic flow that passes through the expansion fan at the nozzle exit is turned through the angle $\alpha_2 - \alpha_1 = -(\nu_2 - \nu_1) = -11.4137°$. The minus sign indicates that the flow is turned in a clockwise direction.

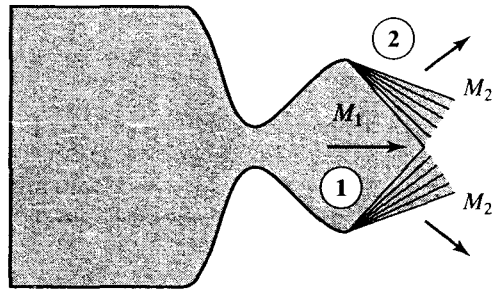


**Figure 7.14** Flow Configuration for Example 7.4

---

## 7.5 PRANDTL–MEYER FLOW IN A SMOOTH COMPRESSION

It was described in Section 7.3 that, at a smooth compressive turn in supersonic flow, Mach waves emanate from the wall, coalescing farther out in the stream to form an oblique shockwave. In the region from the wall out to the point of coalescence of the waves (see Figure 7.6), the flow is isentropic and possesses the same characteristics as Prandtl–Meyer flow. Therefore, the equations derived for Prandtl–Meyer flow can be applied to the isentropic flow region at a concave corner, even though a compression takes place at the corner. Naturally, the turning angle $\Delta\nu$ will here be negative, corresponding to a decrease in Mach number. The extent of the isentropic flow region at a concave corner depends on the curvature of the wall. For a sharp turn, the region that can be treated as Prandtl–Meyer flow is negligible; for a gradual turn, with a large radius of curvature, a much greater region has the characteristics of Prandtl–Meyer flow.

## 7.6 MAXIMUM TURNING ANGLE FOR PRANDTL–MEYER FLOW

As $M_2 \to \infty$ (or, equivalently, as the static pressure $p_2 \to 0$), the arctangents in Eq. (7.9) approach $\pi/2$. Consequently, the turning angle approaches the following finite value that only depends upon $\gamma$:

$$\nu_{\max} = \left(\sqrt{\frac{\gamma+1}{\gamma-1}} - 1\right)\frac{\pi}{2} = \left(\sqrt{\frac{\gamma+1}{\gamma-1}} - 1\right)\frac{\pi}{2}\frac{180^\circ}{\pi} = \left(\sqrt{\frac{\gamma+1}{\gamma-1}} - 1\right)90^\circ \quad (7.15)$$

For $\gamma = 1.4$, the maximum turning angle is 130.4541°. This represents the largest turn that a stream initially at Mach 1 can make. If the flow is initially supersonic, the maximum turn can be obtained by first determining the value of the Prandtl–Meyer function at the given Mach number and then subtracting this value from $\nu_{\max}$. For example, if $M_1 = 2.0$, $\nu_1 = 26.3798^\circ$, and, therefore, $\Delta\nu_{\max} = 130.4541^\circ - 26.3798^\circ = 104.0743^\circ$. This is illustrated in Figure 7.15.

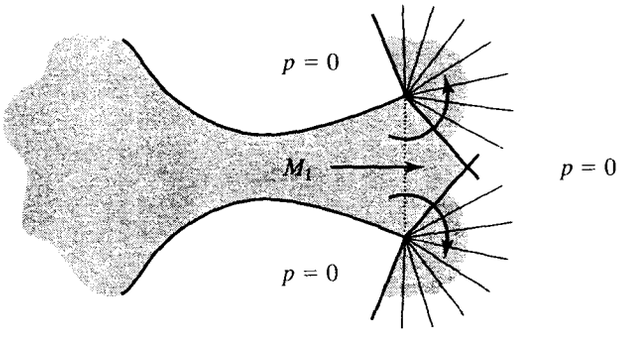


**Figure 7.15** Maximum Turning Angle for a Supersonic Flow Exiting a Nozzle into a Vacuum

This result has significance, for example, in the determination of the shape of the exhaust plume of an underexpanded nozzle discharging into the vacuum of space. To prevent the impingement of rocket exhaust gases on a part of a spacecraft, the designer must have knowledge of the shape of the rocket-nozzle exhaust plume; modification of a spacecraft geometrical design may be required to prevent possible damage from the hot exhaust gases. Furthermore, the axial thrust of a rocket depends on the direction of the exhaust velocity vectors.

The actual magnitude of the maximum turning angle presented here has only academic interest, in that effects such as liquefaction of air or gases and other departures from perfect-gas flow would occur long before the ultimate pressure could be attained. However, the result does indicate the presence of a maximum turning angle for a supersonic expansion.

## 7.7 REFLECTIONS

When a Prandtl–Meyer expansion flow impinges on a plane wall, as shown in Figure 7.16, sufficient waves must be generated to maintain the wall boundary condition; that is, at the wall surface, the flow must be parallel to the wall. Each Mach wave of the initial Prandtl–Meyer fan, then, must reflect as an expansion Mach wave. The resultant wave interactions present complexities that render an exact analysis of the flow extremely difficult; however, the general nature of the flow can be recognized. An application is the expansion that takes place at the exit of an underexpanded, two-dimensional nozzle. Since, from symmetry, there can be no flow across the center streamline, this streamline can be replaced by a plane wall. The resultant flow situation is shown in Figure 7.17.

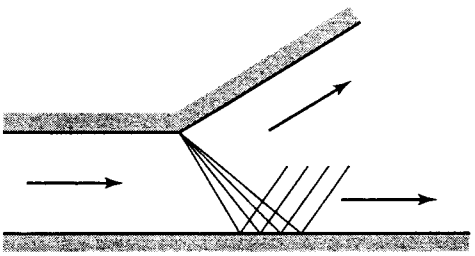

**Figure 7.16** Reflection of a Prandtl–Meyer Expansion Fan from a Plane Wall

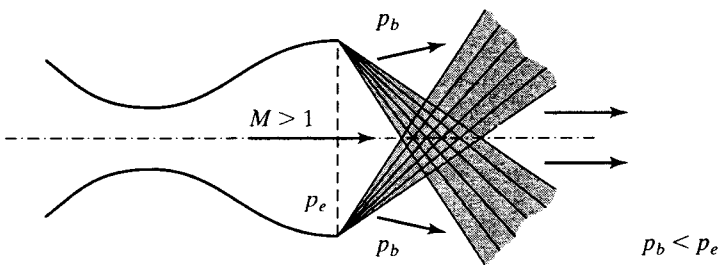


**Figure 7.17** Supersonic Flow from an Underexpanded Nozzle

## 7.8 CHAPTER CAPSTONE APPLICATION: CONFLUENCE OF AN OBLIQUE SHOCK AND AN EXPANSION FAN

When a thin body, taken here to be a flat plate of zero thickness, is placed at an angle of attack within a supersonic stream, both oblique shocks and expansion fans will appear at various locations on the body. (See Figure 7.18.) Oblique shocks will appear at locations where the flow must be turned because the plate forms a concave corner with the stream (on the bottom of the plate at the leading edge and on the top of the plate at the trailing edge). Expansion fans will appear at locations where the flow must be turned because the plate forms a convex corner with the stream (on the top of the plate at the leading edge and the bottom of the plate at the trailing edge). This type of problem will be studied in some detail in Section 8.5.

Here, we are interested only in the flow at the trailing edge of the plate. At this location, there is a confluence of an oblique shock and an expansion fan, as shown in Figure 7.18. Moreover, because the streams that pass over the top and bottom surfaces of the plate will not have the same value of entropy as after they have passed through the shock and expansions on each side of the plate, a contact discontinuity, originating at the trailing edge, will separate the two streams. The flow direction of the contact discontinuity is determined by requiring that the flow on either side of the discontinuity have the same flow angle and that the pressure across the discontinuity remain constant. This same approach was used in the previous chapter to determine the flow direction of the contact discontinuity involved with the confluence of two oblique shocks at the trailing edge of an airfoil. In that problem, the flow angles of the two streams differed so that the streams were each turned through a concave corner.

Because the flow through a Prandtl–Meyer expansion fan is isentropic, the Mach number in Eq. (7.9) may be replaced with the stagnation-to-static-pressure ratio from

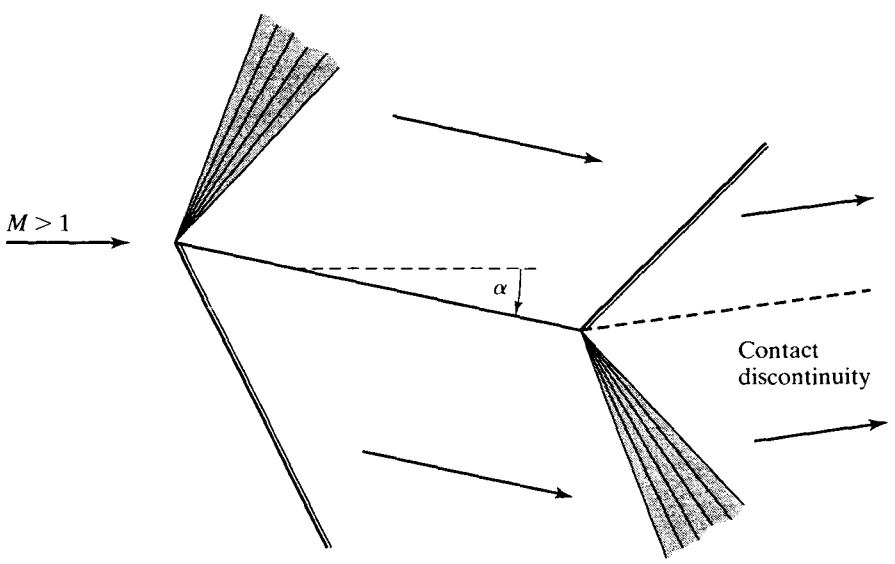


**Figure 7.18** Supersonic Flow past a Flat Plate at an Angle of Attack to the Flow

Eq. (3.15), which may be written in a form that is convenient for substitution:

$$M^2 = \frac{2}{\gamma - 1}\left[\left(\frac{p_o}{p}\right)^{(\gamma-1)/\gamma} - 1\right] = \frac{2}{\gamma - 1}\left(\frac{p_o}{p}\right)^{(\gamma-1)/\gamma} - \left(\frac{\gamma + 1}{\gamma - 1}\right) + 1$$

Accordingly, Eq. (7.9) can be written as

$$\nu = \left\{\sqrt{\frac{\gamma + 1}{\gamma - 1}}\tan^{-1}\left[\sqrt{\frac{2}{\gamma + 1}\left(\frac{p_o}{p}\right)^{(\gamma-1)/\gamma} - 1}\right]\right.$$
$$\left. - \tan^{-1}\left(\sqrt{\frac{2}{\gamma - 1}\left(\frac{p_o}{p}\right)^{\gamma-1/\gamma} - \left(\frac{\gamma + 1}{\gamma - 1}\right)}\right)\right\} \tag{7.16}$$

As will be demonstrated in the following example, this relation may be used along with that of the pressure-flow deflection equation for an oblique shock, Eq. (6.30), on the pressure-flow angle shock–polar diagram, to determine the flow direction beyond the trailing edge of a flat plate in supersonic flow.

**Example 7.5. Determination of the flow direction at the rear of a flat plate in supersonic flow**

The Mach number on the lower side of a flat plate, placed at an angle of attack of $-10°$ to the horizontal, is 2.0. The pressure on the lower side is 4 times the ambient pressure. The Mach number on the upper side of the plate is 3.0, and the pressure is equal to the ambient pressure. The ratio of specific heats is 1.4. For these conditions, determine the flow angle, the pressure ratios, and the Mach numbers downstream of the trailing edge.

**Solution**

Figure 7.19 shows the flow field in the trailing edge region. It may be seen that the region is divided into four zones. The flow properties within each of the zones are uniform.

The flow angle within zone 3 is

$$\alpha_3 = \alpha_1 + \nu_3 - \nu_1 \tag{7.17}$$

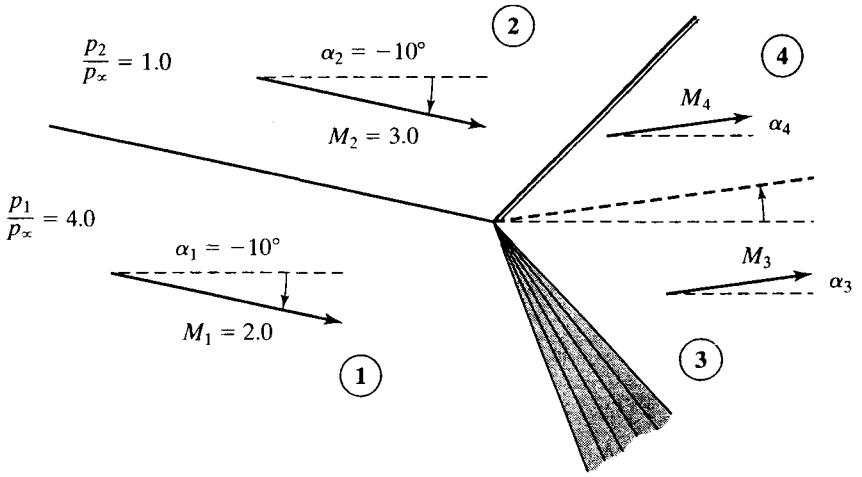


**Figure 7.19** Given Information and Nomenclature for Example 7.5

where $\nu_1$ is 26.3798°, which is determined from $M_1$, and $\alpha_1$ is given as $-10°$. The value of $\nu_3$ depends upon the value of $p_3$, as may be seen by reference to Eq. (7.16), and therefore is unknown. Consequently, $\alpha_3 = \alpha_3(p_3)$.

The flow direction within zone 4 is

$$\alpha_4 = \alpha_2 + \delta_{2\text{-}4} \tag{7.18}$$

where $\alpha_2$ is $-10°$. The value of the flow deflection through the shock, $\delta_{2\text{-}4}$, depends upon the value of $p_4$, as may be seen by Eq. (6.30), and therefore is also unknown. Consequently, $\alpha_4 = \alpha_4(p_4)$.

Because $p_3$ must equal $p_4$, by equating Eq. (7.16) and Eq.(7.17), we produce a single equation that contains only one unknown, $p_3$. The task of this example will be to solve the resulting expression for the unknown pressure and in turn determine the flow angle from either $\alpha_3 = \alpha_3(p_3)$ or $\alpha_4 = \alpha_4(p_4)$. To accomplish this, we form the following desired expression, which is a combination of Eqs. (7.16), (7.17), (7.18), and (6.30):

$$f(p_3) = [\nu_3(p_3) - \nu_1 + \alpha_1] - [\delta_{2\text{-}4}(p_3) + \alpha_2] = \nu_3(p_3) - \nu_1 - \delta_{2\text{-}4}(p_3) \tag{7.19}$$

Here,

$$\nu_3 = \left\{\sqrt{\frac{\gamma+1}{\gamma-1}}\tan^{-1}\left[\sqrt{\frac{2}{\gamma+1}\left(\frac{p_o}{p_1}\frac{p_1}{p_\infty}\frac{p_\infty}{p_3}\right)^{(\gamma-1)/\gamma} - 1}\right]\right.$$

$$\left. - \tan^{-1}\left(\sqrt{\frac{2}{\gamma-1}\left(\frac{p_o}{p_1}\frac{p_1}{p_\infty}\frac{p_\infty}{p_3}\right)^{(\gamma-1)/\gamma} - \left(\frac{\gamma+1}{\gamma-1}\right)}\right)\right\}$$

In this expression, $p_o/p_1$ is determined from the isentropic relations equation, Eq. (3.15), for the given $M_1$, and the value of $p_1/p_\infty$ is specified in the statement of the problem. Further, using Eq. (6.30), we get

$$\delta_{2\text{-}4} = \alpha_4 - \alpha_2 = \pm\tan^{-1}\left[\frac{\left(\frac{p_4/p_\infty}{p_2/p_\infty} - 1\right)}{\left(a_2 - \frac{p_4/p_\infty}{p_2/p_\infty}\right)}\sqrt{\frac{\left(b_2 - \frac{p_4/p_\infty}{p_2/p_\infty}\right)}{\left(c + \frac{p_4/p_\infty}{p_2/p_\infty}\right)}}\right]$$

These values can be plotted on a pressure-flow angle diagram to obtain all possible pressure-flow angle combinations. The result is shown in Figure 7.20. The intersection of the two curves provides a graphical result $p_3/p_\infty = p_4/p_\infty \approx 2.1$ and $\alpha_3 = \alpha_4 \approx 0.5°$.

Next, we obtain a more accurate result by solving Eq. (7.19) numerically, using the Newton–Raphson method to determine the root of an equation involving a single unknown. As in other problems, we developed a spreadsheet program to solve this problem. Furthermore, because $f(p_3)$ is rather complicated, we use a central finite difference instead of the derivative in the Newton–Raphson algorithm. Table 7.3 contains the results of the iterations required to numerically determine the unknown pressure. In this table, $y$ is the pressure ratio $p_3/p_\infty$ and $x$ is the flow angle $\alpha_3$.

The intersection of the two curves is numerically found to be at $y = p_3/p_\infty = p_4/p_\infty = 2.1229$ and $x = \alpha_3 = \alpha_4 = 0.4964°$. With these values, it is not difficult to obtain other flow variables. For example, $M_3 = 2.4054$ and $M_4 = 2.4805$.

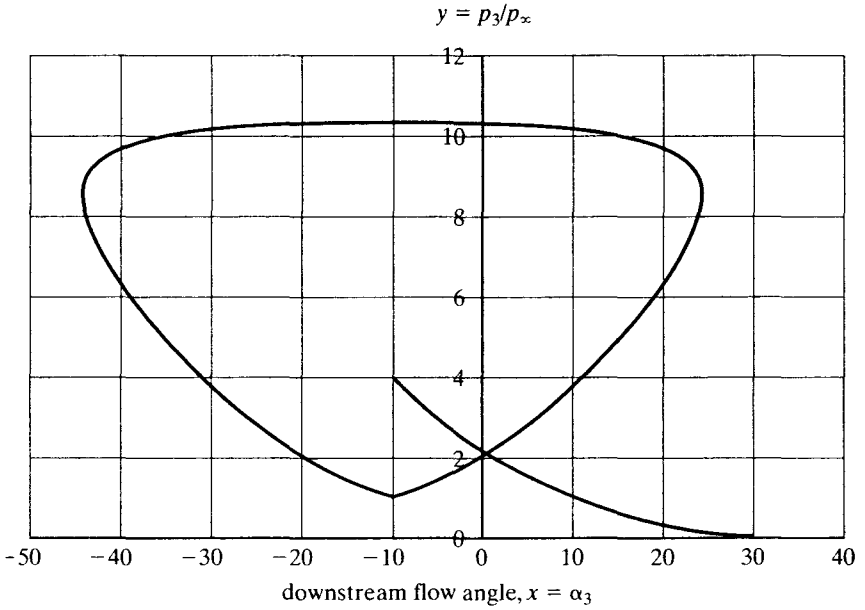


**Figure 7.20** Pressure versus Flow Angle for the Confluence of an Oblique Shock and Expansion Fan

**TABLE 7.3** Iteration Results to Determine the Direction of the Flow behind a Flat Plate in Example 7.5

| Iteration | $y_{old}$ | $y+\Delta$ | $y-\Delta$ | $f(y)$ | $f(y+\Delta)$ | $f(y-\Delta)$ | $\Delta f/\Delta y$ | $y_{new}$ | $x$ | $x$ (deg) |
|---|---|---|---|---|---|---|---|---|---|---|
| 1 | 1.0000 | 1.0001 | 0.9999 | −0.3715 | −0.3715 | −0.3715 | 0.4561 | 1.81451 | 0.14234 | −1.8444 |
| 2 | 1.8145 | 1.8146 | 1.8144 | −0.0826 | −0.0825 | −0.0826 | 0.2847 | 2.10453 | 0.18089 | 0.3643 |
| 3 | 2.1045 | 2.1046 | 2.1044 | −0.0047 | −0.0046 | −0.0047 | 0.2540 | 2.12284 | 0.18319 | 0.4960 |
| 4 | 2.1228 | 2.1229 | 2.1227 | −1.54E−05 | 0.0000 | 0.0000 | 0.2523 | 2.12290 | 0.18320 | 0.4964 |
| 5 | 2.1229 | 2.1230 | 2.1228 | −1.68E−10 | 0.0000 | 0.0000 | 0.2523 | 2.12290 | 0.18320 | 0.4964 |

## 7.9 SUMMARY

Just as Chapter 6 presented an analysis of supersonic, compressive oblique flow, so Chapter 7 has provided a study of supersonic, oblique expansion flow. A discussion of expansion and compression supersonic flows around convex and concave corners bears many similarities to the previous discussion of wave motion in constant-area tubes. In Chapter 4, it was shown that weak compression waves moving down a tube overtake one another and eventually coalesce to form a finite normal shock; expansion waves move farther apart and hence cannot reinforce one another. At a convex turn, the expansion waves diverge from the corner and, again, no reinforcement is possible; at a concave turn, the

compression waves converge to form a finite oblique shock. It was shown, in each case, that the expansion shock represents a violation of the second law of thermodynamics.

So, at a convex corner in supersonic flow, an isentropic expansion takes place. This flow consists of a large number of expansion Mach waves; across each wave, the changes in flow properties are infinitesimally small. The resultant flow is analyzed by using the equations of continuity, momentum, and energy for a perfect gas with constant specific heats. The result of this analysis has been presented in a form that allows the development of useful numerical tools. These tools may be readily employed to obtain the change in Mach number occurring for a given flow turning angle. The use of the isentropic relationships then permits an evaluation of the change of pressure and temperature taking place through the expansion. Moreover, these tools and a numerical procedure that uses spreadsheet calculations enables more complex problems to be undertaken.

## 7.10 REFERENCES


**7.1** Cramer, M. S., and Fry, R. N. "Nozzle Flows of Dense Gases," *Physics of Fluids,* A5, 1993, pp. 1246–1259.

**7.2** Anderson, Jr., J. D. *Modern Compressible Flow with Historical Perspectives*, 3d ed., McGraw-Hill Book Company, New York, 2002, pp. 183–186.

**7.3** Thompson, P. A. *Compressible-Fluid Dynamics,* McGraw-Hill Book Company, New York, 1972, p. 446.

**7.4** Carrier, G.F. *Foundations of Aerodynamics of High Speed: Facsimiles of Nineteen Fundamental Studies as They Were Originally Reported in the Scientific Journals*, Dover Publications, New York, 1951, pp. 50–89.

**7.5** Cramer, M.S. "Ludwig Prandtl: Father of Modern Fluid Mechanics," *Fluid Mechanics*, Cambridge University Press. http://www.fluidmech.net/msc/prandtl.htm.

**7.6** Oswatitsch, K., and Wieghardt, K. "Ludwig Prandtl and His Kaiser-Wilhelm-Institute," *Ann Rev Fluid Mech* 1987; 19: 1–25.

**7.7** Johnston, D. "The Work of Ludwig Prandtl," U.S. Centennial of Flight Commission Essays. http://www.centennialofflight.gov/essay/Theories_of_Flight/Prandtl/TH10.htm.

**7.8** Cheers, F. *Elements of Compressible Flow,* John Wiley & Sons, New York, 1963, pp. 66–76.

**7.9** Liepmann, H. W., and Roshko, A. *Elements of Gas Dynamics,* John Wiley & Sons, New York, 1957, pp. 93–100.

**7.10** Shapiro, A. H. *The Dynamics and Thermodynamics of Compressible Fluid Flow,* Vol. 1, Ronald Press, New York, 1953, pp. 463–477.

**7.11** Zucrow, M. J., and Hoffman, J. D. Gas *Dynamics,* Vol. 1, John Wiley & Sons, New York, 1976, pp. 422–441.


## 7.11 PROBLEMS

**7.1** Use a trigonometric development to demonstrate that, for an expansion flow around a convex corner, $V_{n2} > V_{n1}$. (See Figure 7.2 in Section 7.2.)

**7.2** A uniform supersonic flow of air ($\gamma = 1.4$) at Mach 2.6, with stagnation pressure of 5 MPa and stagnation temperature of 1000 K, expands around a 20° convex corner. Determine the downstream Mach number, the stagnation pressure and temperature, and the static pressure and temperature.

**7.3** Integrate Eq. (7.7). To accomplish this, first use a transformation in which $x^2 = M^2 - 1$, and then use the method of partial fractions to break the transformed integrand into two groups of terms, which may be integrated using:

$$\int \frac{du}{a^2 + b^2u^2} = \frac{1}{ab}\tan^{-1}\left(\frac{bu}{a}\right)$$

**7.4** A reservoir containing air at 2 MPa is connected to ambient air ($\gamma = 1.4$) at 101 kPa through a C–D nozzle designed to produce flow at Mach 2.0, with axial flow at the nozzle exit plane. (See Figure P7.4.) Under these conditions, the nozzle is underexpanded, with a Prandtl–Meyer expansion fan at the exit. Find the flow direction after the initial expansion fan. How does this turning angle affect the net axial thrust forces exerted by the fluid on the nozzle?

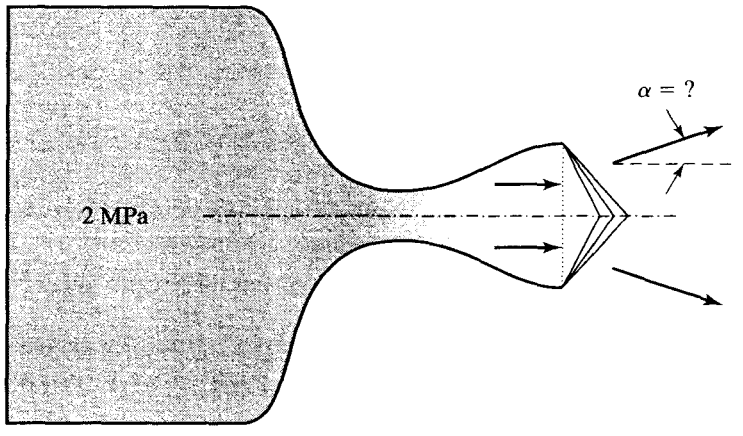


**Figure P7.4**

**7.5** Develop a computer program that will yield values of $\nu$ and $\mu$ versus $M$ for Prandtl–Meyer flow for $\gamma = 1.3$ over the range $M = 1.0$ to $M = 2.5$, using Mach-number increments of 0.1.

**7.6** A uniform supersonic flow of a perfect gas with $\gamma = 1.3$ and Mach number 3.0 expands around a 5° convex corner. Determine the downstream Mach number, the ratio of downstream to upstream velocity, and the ratio of downstream to upstream stagnation temperature.

**7.7** For flow at Mach 2.5 and $\gamma = 1.4$ over the symmetrical protrusion shown in Figure P7.7, find $M_2$, $M_3$, $M_4$, $T_2$, $T_3$, and $T_4$.

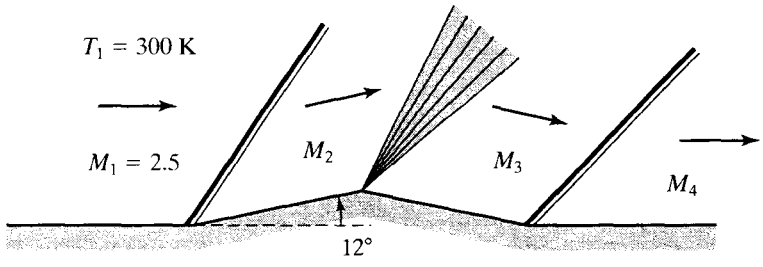


**Figure P7.7**

**7.8** A uniform supersonic flow of a perfect gas with $\gamma = 1.4$, a Mach number of 3.0, and an upstream static pressure of 100 kPa flows over a geometry as shown in Figure P7.8. Determine the downstream static pressure for both profiles.

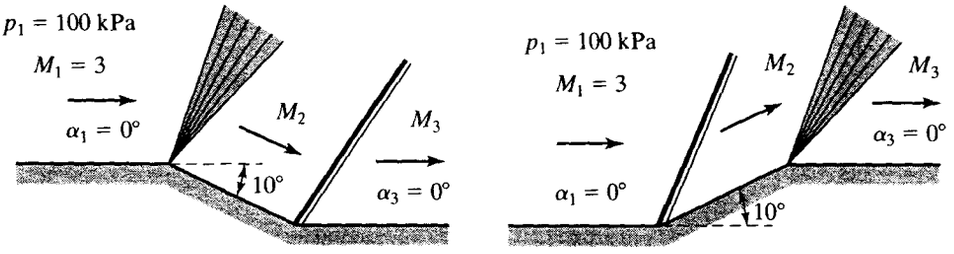


(a) Expansion Fan–Oblique Shock Geometry (b) Oblique Shock–Expansion Fan Geometry

**Figure P7.8**

**7.9** A two-dimensional, flat plate is inclined at a positive angle of attack in a supersonic airstream of Mach 2.0. (See Figure P7.9.) Below the plate, an oblique shockwave starts at the leading edge, making an angle of 42° with the stream direction. On the upper side, an expansion occurs at the leading edge.

(a) Find the angle of attack (AoA) of the plate.
(b) What is the pressure on the lower surface of the plate?
(c) What is the pressure on the upper surface of the plate?

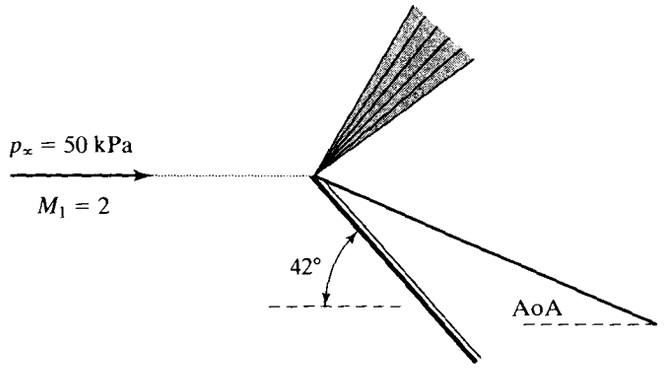


**Figure P7.9**

**7.10** A two-dimensional supersonic wing has the profile shown in Figure P7.10. At zero angle of attack, determine the drag force on the wing per unit length of span at Mach 2 and at Mach 4. Repeat for the lift force. Assume $\gamma = 1.4$.

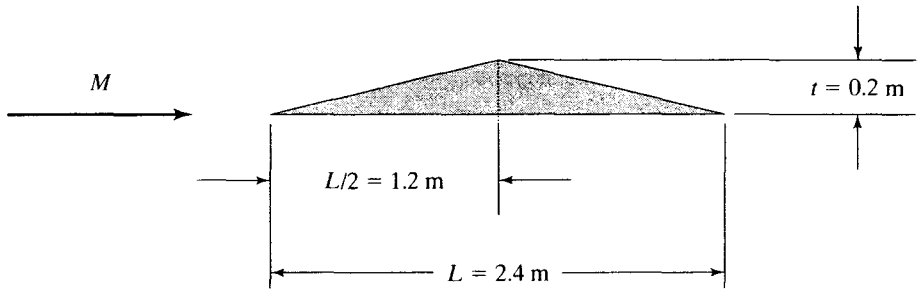


**Figure P7.10**

**7.11** In Problem 7.10, a compression occurs at the trailing edge, with the resultant parallel flows in regions 4 and 5. (See Figure P7.11.) Is there any difference in pressure, velocity, or entropy between regions 4 and 5? Discuss.

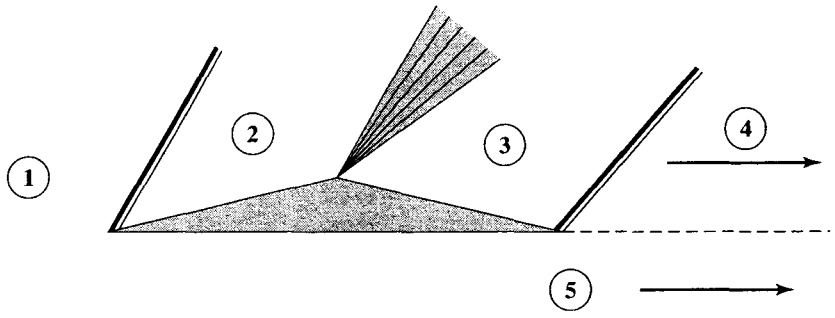


**Figure P7.11**

**7.12** A reservoir containing air (a perfect gas with constant $\gamma = 1.4$) at 10 MPa is discharged through a C–D nozzle of area ratio 3.0. An expansion fan is observed at the exit, with the flow immediately downstream of the fan turned through an angle of 10°. Determine the pressure of the region into which the nozzle is exhausting.

**7.13** Determine the value of $\gamma$ for which $\nu_{max} = 180°$.

**7.14** For the geometry shown in P7.14 and the given values of the fan angle and the deflection angle, determine $M_1$ and $M_2$.

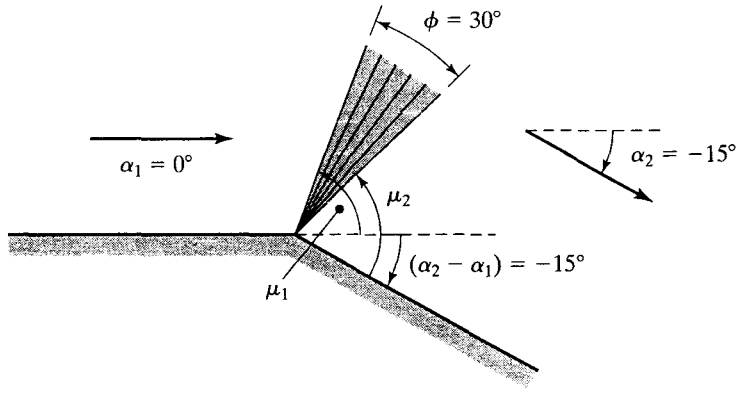


**Figure P7.14**

**7.15** For the geometry of Figure P7.14 and for given values of the wall turning angle $\Delta$ and the static pressure ratio across the expansion fan, $p_2/p_1$, define a process that will yield $M_1$ and $M_2$. Use the process to solve for these Mach numbers if $p_2 = 0.4p_1$ and $\Delta = 10°$. Assume that $\gamma = 1.4$.

**7.16** A gas ($\gamma = 1.44$; $R = 256\ \text{J/kg} \cdot \text{K}$) flows towards a convex corner with $M_1 = 3$ and $T_1 = 300\ \text{K}$. Determine the downstream Mach number $M_2$ and the downstream velocity $V_2$ if the wall is turned 15°. Repeat the calculations if the wall is turned 30°.

**7.17** Air ($\gamma = 1.4$) at $M_1 = 2$ and $p_1 = 150\ \text{kPa}$ flows in a duct as shown in Figure 7.15. The upper wall turns the uniform supersonic stream through 5° "away" from the flow, resulting in the formation of a Prandtl–Meyer fan at the corner. Waves of the fan reflect off the lower surface of the duct. Determine the Mach number and pressure downstream of the leading reflected expansion wave.

**7.18** When Theodor Meyer presented his dissertation in 1908, the Mach number had not been named; it appeared 20 years later. (See the Historical Note in Section 2.5.) Accordingly, at the time Meyer's thesis was written, the static-to-total-pressure ratio was used. Use the pressure ratio to write the Prandtl–Meyer function much as Meyer would have.

**7.19** Obtain the following pressure–Mach number relation from the continuity and normal momentum equations applied to a control volume containing a Mach wave:

$$\frac{dp}{p} = -\frac{\gamma M^2}{1 + \dfrac{\gamma - 1}{2} M^2} \frac{dM}{M}$$

Integrate this relation to derive the expression for the pressure ratio across the Mach wave $p_2/p_1$ in terms of $M_1$ and $M_2$; that is, obtain Eq. (7.13).

**7.20** Repeat Example 7.5 for $\gamma = 1.25$. [Note that this problem would best be performed using a numerical method, as there is no table for this value of $\gamma$.]

# Chapter 8

# Applications Involving Shocks and Expansion Fans

## 8.1 INTRODUCTION

Chapters 6 and 7 presented cases of two-dimensional flow: the oblique shockwave and the Prandtl–Meyer expansion. To analyze supersonic flow over a finite body in which changes in flow direction must occur, it is necessary to apply the characteristics of Prandtl–Meyer flow and oblique-shock flow to a physical situation. It is appropriate, then, at this point in the text, to present several applications in which the two-dimensional flows discussed in the previous chapters are present. Several such examples have already been considered in the text. The oblique-shock diffuser and the expansion or compression flows that take place at the exit of an underexpanded or overexpanded supersonic nozzle have been introduced in previous chapters.

In the current chapter, we will extend consideration of supersonic flows in diffusers by investigating the shock diffuser and a spike-type inlet. This examination will be followed by an investigation of the plug nozzle, a jet-propulsion system flow component that essentially replaces the diverging portion of a conventional supersonic nozzle with a Prandtl–Meyer expansion so as to increase the off-design performance of the nozzle. Finally, an analysis of a variety of supersonic airfoils that involve both oblique shocks and Prandtl–Meyer flow will be presented. The latter material is often termed *shock-expansion theory*.

## 8.2 SUPERSONIC OBLIQUE-SHOCK DIFFUSER

For a turbojet or ramjet traveling at high velocity, it is necessary to provide an inlet, or diffuser, that will perform the function of slowing down the incoming air with a minimum loss of stagnation pressure. The use of a converging–diverging passage as an inlet for supersonic flow was studied in Chapter 4. Because such an internal deceleration device can operate isentropically only at the design speed, this type of diffuser has been found to be impractical during startup and when operating in an off-design condition. In fact,

without provisions for either varying the throat area or overspeeding, the design condition could not be attained.

To eliminate the starting problem involved with the converging–diverging passage, the internal throat must be removed. Thus, a possible design is the normal-shock diffuser, where the deceleration takes place through a normal shock followed by subsonic diffusion in a diverging passage. (See Figure 8.1.) The disadvantage of this setup is the large loss in stagnation pressure incurred by the normal shock. Only at Mach numbers close to unity would this design be practicable.

In Chapter 6, the advantage of decelerating through several oblique shocks rather than one normal shock was demonstrated. (See Example 6.5.) The oblique-shock spike-type diffuser takes advantage of this condition and hence represents a practical device for decelerating a supersonic flow. The operation of a single oblique-shock inlet at design speed is depicted in Figure 8.2. External deceleration is accomplished through an oblique shock attached to the spike. Further deceleration takes place through a normal shock at the engine cowl inlet, with subsonic deceleration occurring internally. Even though a normal shock occurs in this system, the flight Mach number $M_\infty$ has been reduced by the oblique shock, thus reducing the normal-shock strength and resultant stagnation pressure loss.

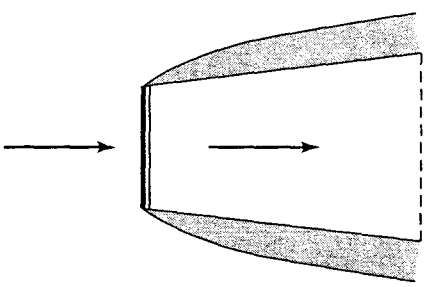

**Figure 8.1** A Normal-Shock Diffuser

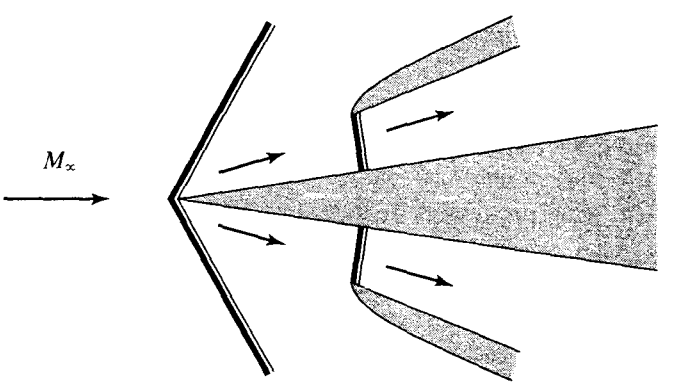


**Figure 8.2** A Single Oblique-Shock Spike-Type Inlet at Design Speed

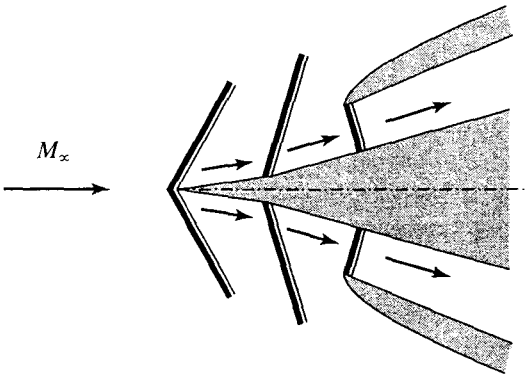


**Figure 8.3** A Two-Oblique-Shock Spike-Type Inlet at Design Speed

Theoretically, the greater the number of oblique shocks, the less the resultant total loss in stagnation pressure becomes. For example, a two-shock inlet is shown in Figure 8.3. Note, however, that along the surface of the spike, the boundary layer increases in thickness. The adverse pressure gradient created by the second shock may be sufficient to cause flow separation, with resultant loss of available energy.

The greater the number of shocks, then, the greater the tendency toward flow separation is. It is necessary to effect a compromise in supersonic diffuser design between the increased total-pressure recovery achieved by increasing the number of oblique shocks through which the flow must be diffused and the increased tendency toward separation brought about by the shocks. For this reason, with flight Mach numbers up to 2.0, a single-shock diffuser is generally employed, whereas multiple-shock inlets are required for higher flight Mach numbers.

Several different modes of operation of the spike diffuser may occur, depending on the downstream engine conditions such as nozzle opening, turbine speed, and fuel flow rate. This situation is in contrast to the converging–diverging inlet, where operation was dependent on the inlet's geometry. The spike diffuser's modes of operation are termed *subcritical*, *critical*, and *supercritical*, depending on the location of the normal shock.

*Critical operation* occurs with the normal shock at the cowl inlet, as shown in Figure 8.4(a), with the engine operating at design speed. If the flow resistance downstream of the inlet is increased, with the engine still at the design flight Mach number, the normal shock moves ahead of the inlet, with some of the subsonic flow after the shock able to spill over or bypass the inlet. [See Figure 8.4(b).] For this *subcritical condition*, the inlet is not handling the maximum flow rate; furthermore, the pressure recovery is unfavorable, since at least some of the inlet air passes through a normal shock at the design Mach number. If the downstream resistance is reduced below that for critical operation, the normal shock reaches an equilibrium position inside the diffuser. For this *supercritical condition* [see Figure 8.4(c)], the inlet is still handling maximum mass flow, yet the pressure recovery is less than that for critical operation, since the normal shock occurs at a higher Mach number in the diverging passage.

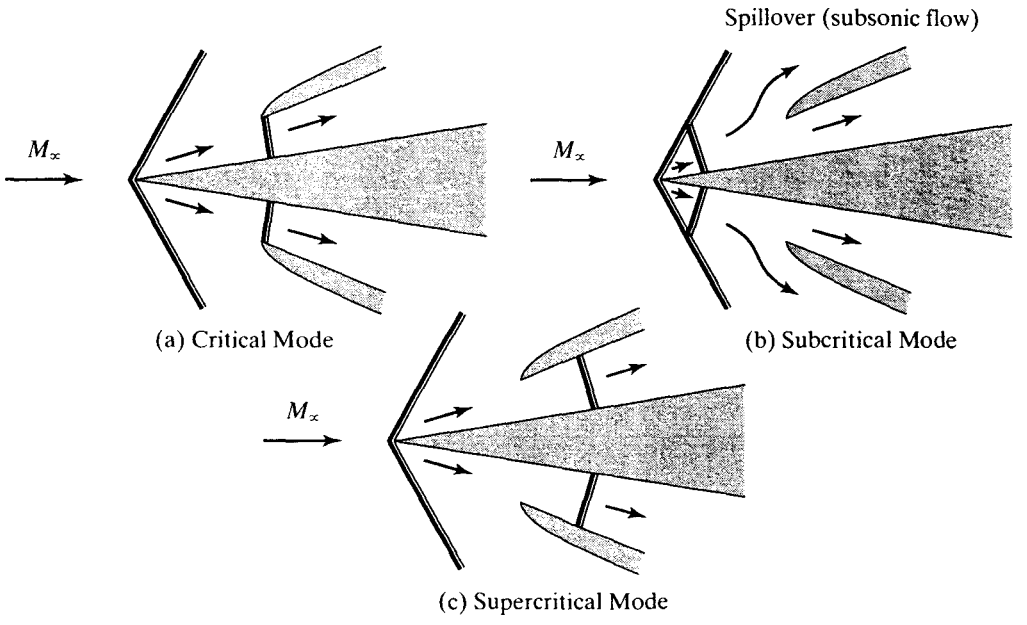


**Figure 8.4** Modes of Operation of the Spike Diffuser

A turbojet engine must be able to operate efficiently both at other-than-design speeds and at different angles of attack. An engine operating at the critical mode may be pushed over into the undesirable subcritical mode by a small change of speed or angle of attack. For this reason, in actual operation, it is more practical to operate in the supercritical mode. While not providing quite as good a pressure recovery as critical operation, the supercritical mode still yields maximum engine-mass flow and furnishes a safety margin so that a small decrease in engine speed will not cause a transition to the subcritical mode. Thus, the supercritical mode provides a more stable engine operation.

**Example 8.1. Computation of pressure recovery in one- and two-shock spike inlets**

Compare the loss in total pressure incurred by a one-shock spike diffuser (two dimensional) with that incurred by a two-shock diffuser operating at Mach 2.0. Repeat at Mach 4.0. (See Figure 8.5.) Assume that each oblique shock turns the flow through an angle of 10°. Take $\gamma = 1.4$.

**Solution**

From the charts in Appendix D [or an oblique-shock solver using Collar's method (see Chapter 6)] at $M_1 = 2.0$ and $\delta = 10°$, the weak solution yields $\theta = 39.3139°$. Moreover, the Mach number downstream of the shock is $M_2 = 1.6405$. For the one-shock diffuser,

$$\left(\frac{p_{o3}}{p_{o1}}\right)_{\text{one shock}} = \left(\frac{p_{o3}}{p_{o2}}\right)\left(\frac{p_{o2}}{p_{o1}}\right)$$

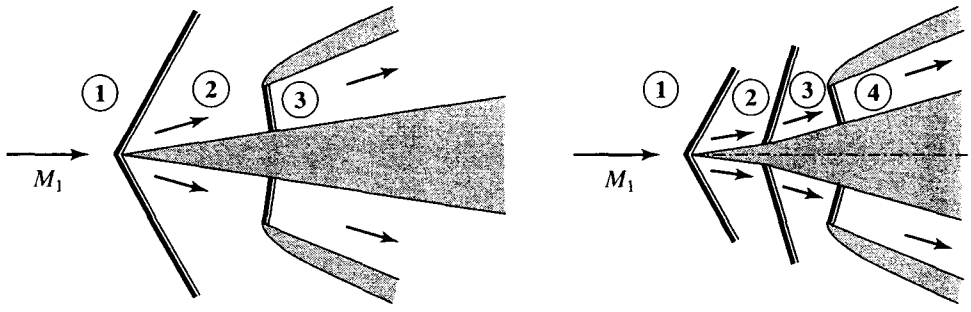


(a) One-shock inlet (b) Two-shock inlet

**Figure 8.5** Flow Regions within the Spike Diffusers of Example 8.1

From the oblique-shock relations at $M_1 = 2.0$, $p_{o2}/p_{o1} = 0.9846$, and from the normal-shock relations at $M_2 = 1.6405$, $p_{o3}/p_{o2} = 0.8797$. Hence,

$$\left(\frac{p_{o3}}{p_{o1}}\right)_{\text{one shock}} = (0.8797)(0.9846) = 0.8662$$

For the two-shock inlet, $M_2 = 1.6405$. At the latter Mach number and $\delta = 10°$, the wave angle for the weak-shock solution $\theta = 49.3849°$, $p_{o3}/p_{o2} = 0.9877$, and $M_3 = 1.2849$. At $M_3$, from the normal-shock relations, $p_{o4}/p_{o3} = 0.9819$. Thus,

$$\left(\frac{p_{o4}}{p_{o1}}\right)_{\text{two shocks}} = \left(\frac{p_{o4}}{p_{o3}}\right)\left(\frac{p_{o3}}{p_{o2}}\right)\left(\frac{p_{o2}}{p_{o1}}\right) = (0.9819)(0.9877)(0.9846) = 0.9549$$

Now, at $M_1 = 4.0$ and $\delta = 10°$, the weak solution (again, either from the charts in Appendix D or from Collar's method, described in Chapter 6) yields $\theta = 22.2341°$, $p_{o2}/p_{o1} = 0.9254$, and $M_2 = 3.2861$. From the normal-shock relations at $M_2 = 3.2861$, we have $p_{o3}/p_{o2} = 0.2563$. Therefore, for the one-oblique-shock diffuser,

$$\left(\frac{p_{o3}}{p_{o1}}\right)_{\text{one shock}} = \left(\frac{p_{o3}}{p_{o2}}\right)\left(\frac{p_{o2}}{p_{o1}}\right) = (0.2563)(0.9254) = 0.2372$$

For the two-shock inlet, $M_2 = 3.2861$. At $M_2 = 3.2861$ and $\delta = 10°$, $\theta = 25.5371°$, $p_{o3}/p_{o2} = 0.9539$, and $M_3 = 2.7358$. Using $M_3$ in the normal-shock relations gives $p_{o4}/p_{o3} = 0.4111$. For this case,

$$\left(\frac{p_{o4}}{p_{o1}}\right)_{\text{two shocks}} = \left(\frac{p_{o4}}{p_{o3}}\right)\left(\frac{p_{o3}}{p_{o2}}\right)\left(\frac{p_{o2}}{p_{o1}}\right) = (0.4111)(0.9539)(0.9254) = 0.3629$$

It can be seen that, whereas the improvement in total-pressure ratio gained by using a two-shock inlet over a one-shock inlet is only about 10 percent at Mach 2, this improvement amounts to 53 percent at Mach 4. Thus, at flight Mach numbers of 2.0 and below, the use of an inlet with one oblique shock is satisfactory; at flight Mach numbers of 4.0, an inlet with two oblique shocks (or more) is necessary.

**Example 8.2. Pressure recovery in a spike inlet operating at the supercritical mode**

A two-dimensional, spike-type inlet is operating in the supercritical mode at a flight Mach number of 3.0. The local static pressure and temperature are 50 kPa and 260 K, respectively. The flow cross-sectional area at the cowl inlet $A_2$ is 0.1 $m^2$; the cross-sectional area at the location where the normal shock occurs in the diverging passage $A_3 = A_4$ is 0.12 $m^2$. (See Figure 8.6.) Calculate the mass-flow rate and total-pressure ratio $p_{o4}/p_{o3}$. Neglect friction. The spike half-angle is 10°, and the ratio of specific heats is $\gamma = 1.4$.

**Solution**

From the oblique charts in Appendix D or an oblique-shock solver at $M_1 = 3.0$ and $\delta = 10°$, the weak solution yields $\theta = 27.3827°$. Moreover, the Mach number downstream of the shock is $M_2 = 2.5050$, and the total-pressure ratio across the shock $p_{o2}/p_{o1} = 0.9631$. The flow from region 2 to region 3 is assumed to be isentropic. Thus,

$$\frac{A_3}{A_3^*} = \left(\frac{A_3}{A_2}\right)\left(\frac{A_2}{A_2^*}\right)\left(\frac{A_2^*}{A_3^*}\right)$$

Using the isentropic area relations at $M_2 = 2.5050$, we have

$$\frac{A_3}{A_3^*} = \left(\frac{0.12}{0.10}\right)(2.6491)(1.0) = 3.1789$$

The Mach number corresponding to this value is determined to be

$$M_3 = 2.6986$$

Next,

$$\frac{p_{o4}}{p_{o1}} = \left(\frac{p_{o4}}{p_{o3}}\right)\left(\frac{p_{o3}}{p_{o2}}\right)\left(\frac{p_{o2}}{p_{o1}}\right)$$

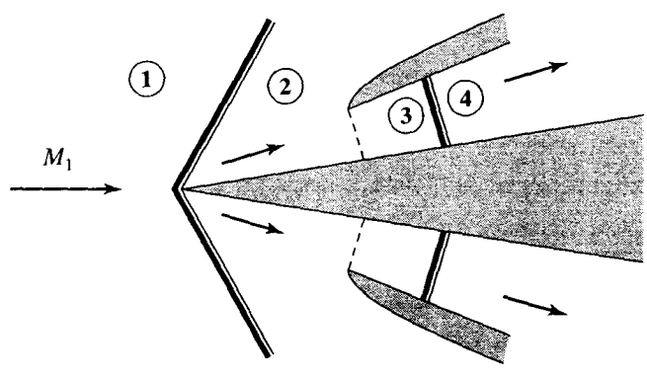


**Figure 8.6** Flow Regions within a Spike Diffuser Operating in the Supercritical Mode

From the normal-shock relations at $M_3$,

$$\frac{p_{o4}}{p_{o3}} = 0.4241$$

Therefore,

$$\frac{p_{o4}}{p_{o1}} = (0.4241)(1.0)(0.9631) = 0.40845$$

$$p_{o1} = \left(\frac{p_{o1}}{p_1}\right)p_1 = \left(\frac{1}{0.0272}\right)50 = 1{,}838.2353 \text{ kPa}$$

So

$$p_{o2} = \left(\frac{p_{o2}}{p_{o1}}\right)p_{o1} = 0.9631(1838.2) = 1{,}770.4044 \text{ kPa}$$

Since

$$p_2 = \left(\frac{p_2}{p_{o2}}\right)p_{o2}$$

where $p_2/p_{o2} = 0.0581$ at $M_2 = 2.5050$, we have

$$p_2 = (0.0581)(1770.4) = 102.8605 \text{ kPa}$$

Since no change in stagnation temperature occurs across a normal shock,

$$T_2 = \left(\frac{T_2}{T_{o2}}\right)\left(\frac{T_{o2}}{T_{o1}}\right)\left(\frac{T_{o1}}{T_1}\right)T_1 = (0.4435)(1.0)\left(\frac{1}{0.3571}\right)260 = 322.9067 \text{ K}$$

$$\dot{m} = \rho_2 A_2 V_2 = \left(\frac{p_2}{RT_2}\right)A_2 M_2 \sqrt{\gamma R T_2}$$

$$= \left[\frac{102.8605}{(0.287)(322.9067)}\right](0.10)\left[2.505\sqrt{(1.4)(287)(322.9067)}\right]$$

$$= 100.1477 \text{ kg/s}$$

## 8.3 EXIT FLOW FOR UNDEREXPANDED AND OVEREXPANDED SUPERSONIC NOZZLES

In Chapters 3 and 4, the flow through a converging–diverging nozzle was studied in detail. The variation in flow patterns inside the nozzle obtained by changing the back pressure, with a constant reservoir pressure, was discussed. It was shown that, over a certain range of back pressures, the flow inside the nozzle was unable to adjust to the prescribed back pressure inside the nozzle, but rather adjusted externally in the form of compression waves or expansion waves. Having studied oblique waves in Chapter 6 and Prandtl–Meyer flow in Chapter 7, we can now discuss in detail the wave pattern occurring at the exit of an underexpanded or overexpanded nozzle.

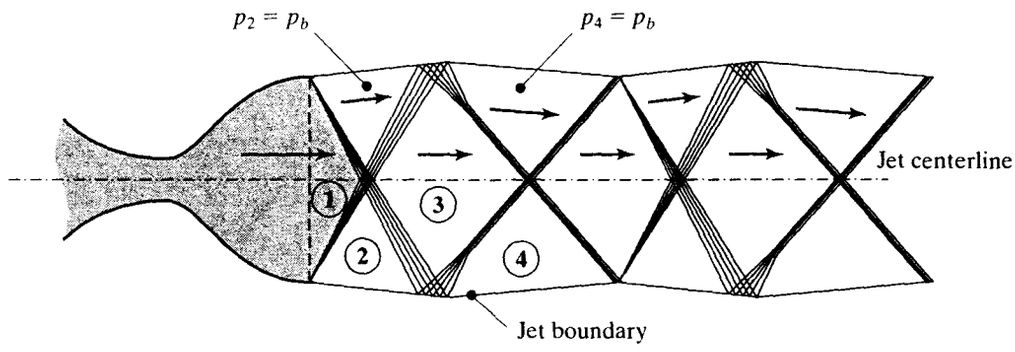


**Figure 8.7** Underexpanded Supersonic Nozzle

Consider first the flow at the exit plane of an underexpanded, two-dimensional nozzle. (See Figure 8.7.) Since the pressure drop due to the expansion inside the nozzle was less than the back pressure, expansion fans form at the nozzle exit plane. As is shown in Figure 8.7, flow at the exit plane is assumed to be uniform and parallel, with $p_1 > p_b$. For this case, from symmetry, there can be no flow across the centerline of the jet. Thus, the boundary conditions along the centerline are the same as those at a plane wall in nonviscous flow, and the normal velocity component must be equal to zero. The pressure is reduced to the prescribed value of back pressure in region 2 by the expansion fans. However, the flow in region 2 is turned away from the exhaust-jet centerline. To maintain the zero normal-velocity component along the centerline, the flow must be turned back toward the horizontal. Thus, the intersection of the expansion fans centered at the nozzle exit lip yields another set of expansion waves, just as did the reflection of the expansion fan from a plane wall discussed in Section 7.7. The second expansion, however, produces a pressure in region 3 that is less than the back pressure, so the expansion waves reflect from the external air as oblique shocks. These compression waves produce a static pressure in region 4 equal to the back pressure, but again turn the flow away from the centerline. The intersection of the oblique shocks from either side of the jet then requires another set of oblique shocks to turn the flow back toward the horizontal, with the shocks reflecting from the external air as expansion waves. The process thus goes through a complete cycle and continues to repeat itself, with an appropriate reduction in the stagnation pressure. The flow pattern discussed appears as a series of diamonds, often visible at the exit of rocket nozzles. Theoretically, the wave pattern should extend to infinity. Actually, however, mixing of the jet with ambient air along the jet boundaries eventually causes the wave pattern to die out.

Flow at the exit of an overexpanded nozzle is shown in Figure 8.8. Since the exit-plane pressure is less than the back pressure, oblique shockwaves form at the nozzle exit. The intersection of these shocks at the centerline yields a second set of oblique shocks, which in turn reflect from the ambient air as expansion waves. Thus, except for being out of phase with the wave pattern from the underexpanded nozzle, the jet flow of the overexpanded nozzle exhibits the same characteristics as the underexpanded nozzle.

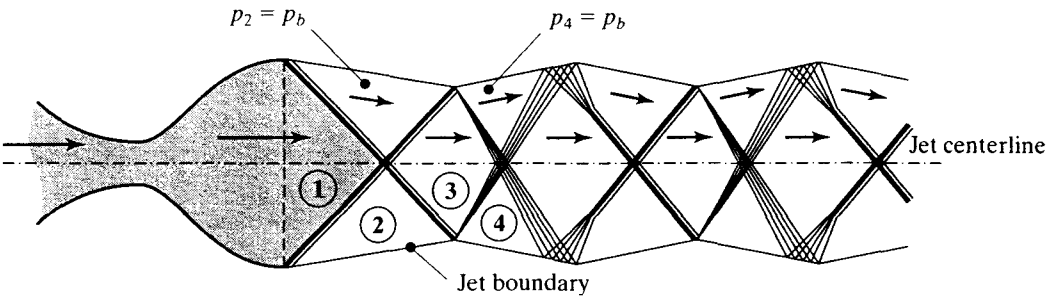


**Figure 8.8** Overexpanded Supersonic Nozzle

**Example 8.3. Computations involving an overexpanded supersonic nozzle**

A supersonic nozzle is designed to operate at Mach 2.0. Under a certain operating condition, however, an oblique shock making a 45° angle with the flow direction is observed at the nozzle exit plane. What percent of increase in stagnation pressure would be necessary to eliminate this shock and maintain supersonic flow at the nozzle exit? (See Figure 8.9.)

**Solution**

For $M_1 = 2.0$, $p_1/p_{o1} = 0.1278$. For this case, then, $p_1$ is equal to $(0.1278)p_{o1}$. The component of $M_1$ normal to the oblique wave is $M_1 \sin 45° = 1.4142$. From the normal-shock relations, $p_b/p_1 = 2.1667$. Of course, this pressure ratio can also be found using the oblique-shock solver described in Chapter 6. Therefore, with the oblique shock, the ratio $p_b/p_{o1} = (p_b/p_1)(p_1/p_{o1}) = (2.1667)(0.1278) = 0.2769$. With the shock, $p_{o1} = (1/0.2769)p_b = (3.6114)p_b$. On the other hand, for supersonic exit flow with no shocks (i.e., the perfectly expanded case), $p_{o1} = (1/0.1278)p_b = 7.8247p_b$. Thus, an increase of $[(7.8247 - 3.6114)/3.6114]100 = 116.7$ percent in stagnation pressure is required.

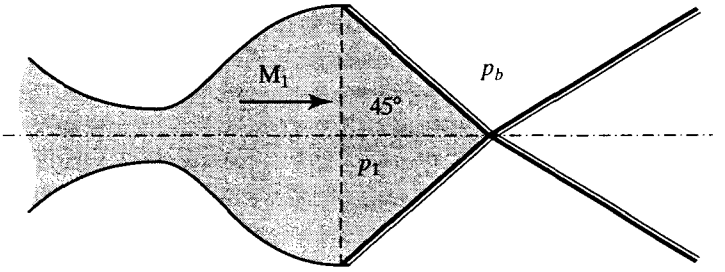


**Figure 8.9** Supersonic Nozzle of Example 8.3

## 8.4 PLUG NOZZLE

The enormous expense of sending a payload into space provides the basis for exploration of propulsion systems and propulsion components that can reduce costs. One approach for future space transportation systems is to employ a single-stage-to-orbit, reusable launch vehicle. It has been estimated that this type of vehicle will diminish the costs by a factor of 10; see Ref. (8.1).

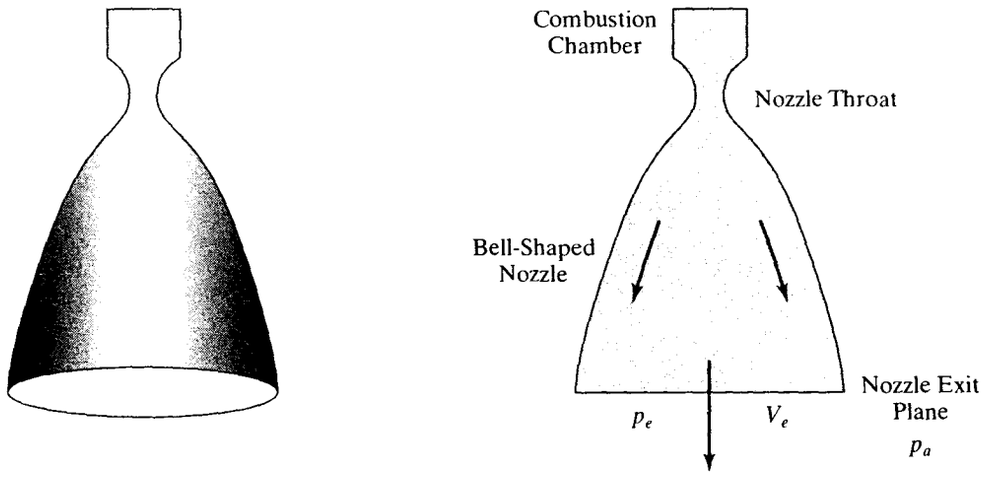


**Figure 8.10** Conventional Bell-Shaped Nozzle

An essential component of any space transportation system is the *exit nozzle.* Over the years, various nozzle profiles have been used. Early rockets employed conical shapes. Currently, the conventional shape of the exit nozzle on rockets has the profile of a bell. (See Figure 8.10.) The bell nozzle is essentially a converging–diverging nozzle; see Ref. (8.2).

The expansion of a high-pressure gas through a converging–diverging nozzle has been shown, at least over a reasonably wide range of operating pressure ratios, to be independent of back pressure. The adjustment to the back pressure in these cases occurs outside the nozzle in the form of expansion waves and oblique shockwaves, as shown in the previous section. Hence, the actual expansion of the gases in the nozzle is controlled solely by the nozzle walls. For example, in an underexpanded nozzle, the gases continue to expand to pressures well below the ambient pressure.

The *thrust* developed by a nozzle is dependent on the nozzle exhaust velocity and the pressure at the nozzle exit plane. (See Example 1.3.) In a jet propulsion device, for example, an exit-plane pressure greater than ambient gives a positive contribution to the thrust of the device, whereas an exit-plane pressure less than ambient gives a negative thrust component.

Let us consider a rocket moving at constant velocity and write the momentum equation for a control volume as shown in Figure 8.11. If one assumes one-dimensional flow at the nozzle exit, then

$$\mathbf{T} - (p_e - p_a)A_e = \dot{m}V_e$$

or

$$\mathbf{T} = (p_e - p_a)A_e + \dot{m}V_e \tag{8.1}$$

When a supersonic nozzle is operating in the under- or overexpanded regimes, with flow in the nozzle independent of back pressure, the exit velocity is unaffected by back pressure. Thus, over this range of back pressures, Eq. (8.1) shows that larger thrusts

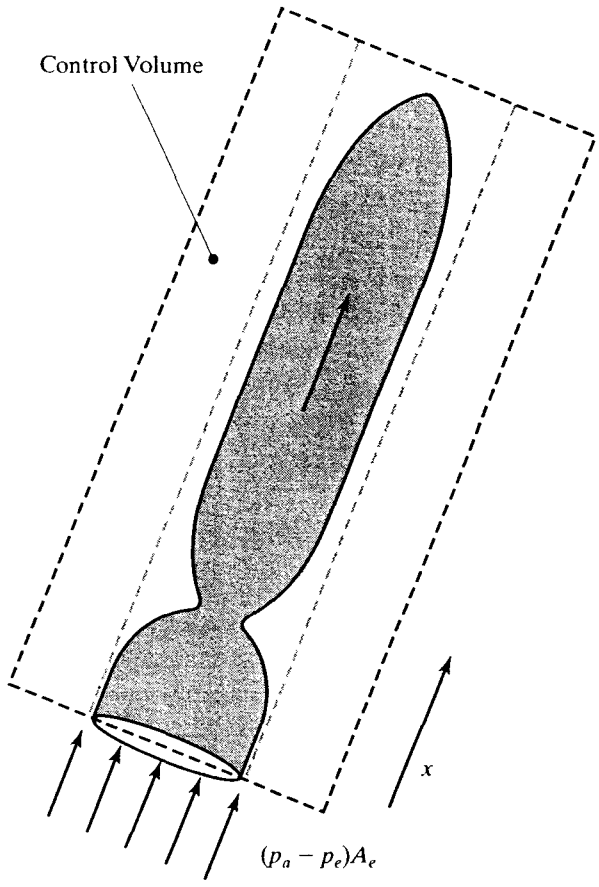


**Figure 8.11** Net Force Acting on the Control Surface of a Rocket Moving at Constant Velocity

are developed in the underexpanded case ($p_e > p_a$) and smaller thrusts in the overexpanded case ($p_e < p_a$).

A conceptual plot of thrust versus back pressure for a converging–diverging nozzle is shown in Figure 8.12. For back pressures greater than the upper limit indicated, a normal shock appears in the diverging portion of the nozzle, the exit velocity becomes subsonic, and this analysis no longer applies.

The *plug nozzle* (sketched in Figure 8.13a) was studied in the 1950s and '60s [see Refs. (8.3)–(8.6)] and reconsidered for use on the RLV X-33 in the 1990s. This device is intended to allow the flow to be directed or controlled by the ambient pressure (since ambient pressure varies with altitude, this mechanism is termed *altitude adaptation*) rather than by the nozzle walls. In this nozzle, the supersonic flow is not confined within solid walls, but is exposed to the ambient pressure.

Plug nozzle operation at the design pressure ratio is depicted in Figure 8.14. Figure 8.14(a) shows the expansion wave pattern, and Figure 8.14(b) shows the streamlines at the nozzle exit. The annular flow first expands internally up to Mach 1 at

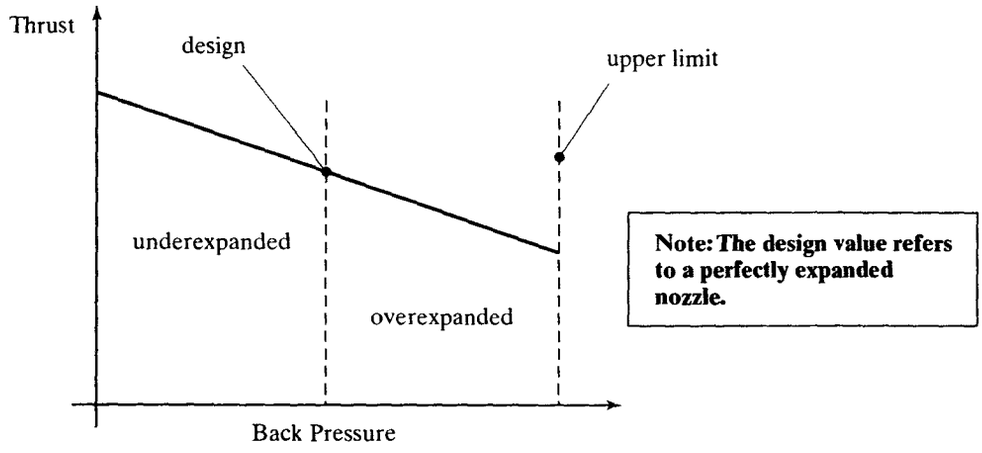


**Figure 8.12** Conceptual Diagram of Thrust versus Back Pressure for a C–D Nozzle

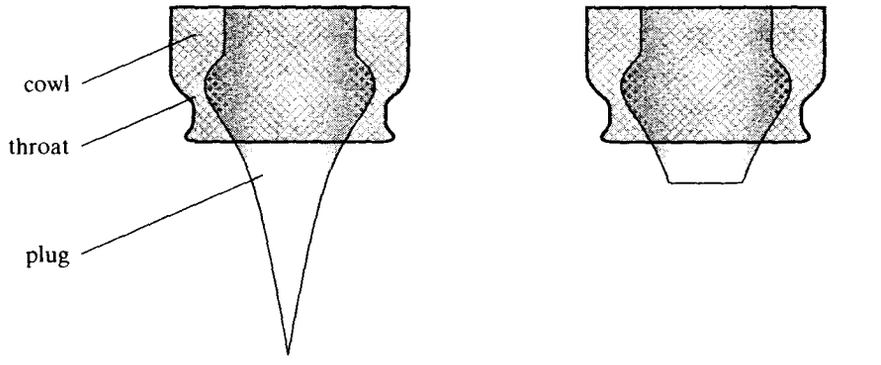


(a) Annular Plug Nozzle (b) Truncated Annular Plug Nozzle

**Figure 8.13** Plug Nozzles

the throat. The remainder of the expansion to the back pressure occurs with the flow exposed to ambient pressure. Since the throat pressure is considerably higher than the back pressure, a Prandtl–Meyer expansion fan is attached to the throat cowling as shown. The plug is designed so that, at the design pressure ratio, the final expansion wave intersects the plug apex. Thus, under this operating condition, the pressure at the plug wall decreases continuously from throat pressure to ambient pressure, just as with the converging–diverging perfectly expanded nozzle.

To produce a maximum axial thrust, it is necessary for the exit flow to have an axial direction. Therefore, the flow at the throat cowling must be directed toward the axis so that the turning produced by the expansion fan will yield axial flow at the plug apex.

For the underexpanded case, the operation of the plug nozzle [Figure 8.15(a)] is similar to that of the converging–diverging nozzle. (See Section 4.4.) The pressure along the plug is the same as for the design case, just as the static pressure along the converging–diverging nozzle wall is the same as for the perfectly expanded case. With

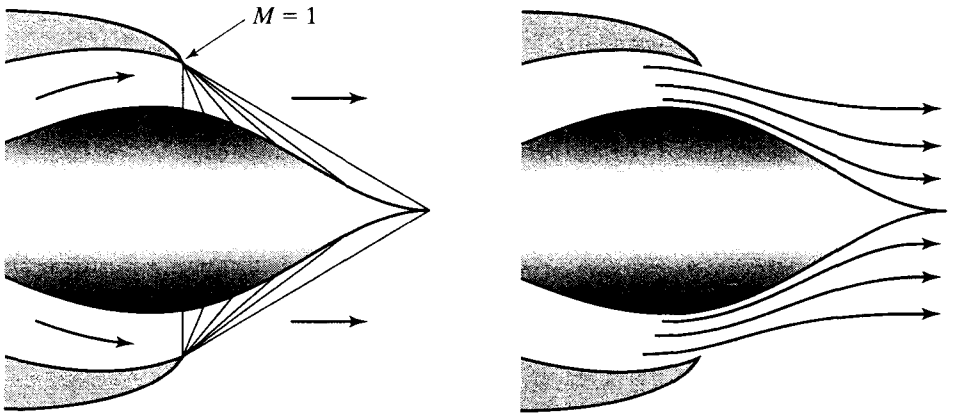


(a) Wave pattern for design (b) Streamlines for design

**Figure 8.14** Wave Pattern and Streamlines within a Plug Nozzle at Design

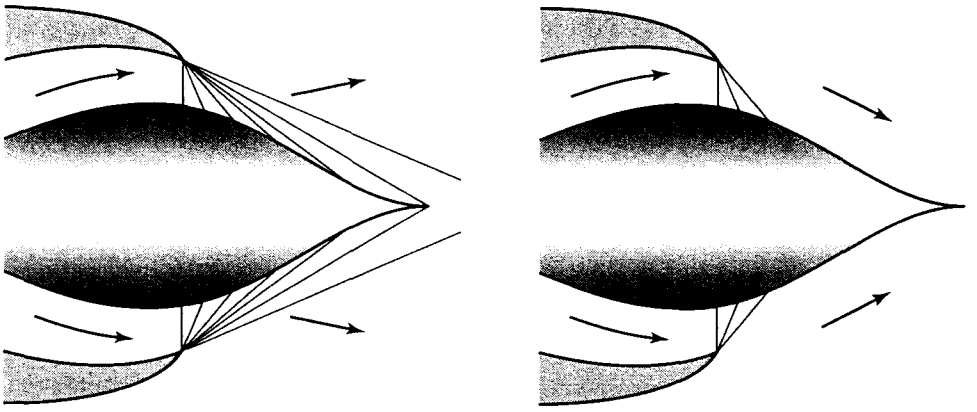

(a) Underexpanded (b) Overexpanded

**Figure 8.15** Wave Patterns of a Plug Nozzle Operating in Under- and Overexpanded Modes

a lower back pressure than that for the design case depicted in Figure 8.14, the flow continues to expand after the apex pressure, yielding a nonaxial jet velocity component, just as with the underexpanded supersonic converging–diverging nozzle.

The major improvement to be derived from the plug nozzle occurs with the overexpanded mode of operation. This is significant in that a rocket nozzle, for example, accelerating from sea level up to design speed and altitude must pass through the overexpanded regime. With the ambient pressure greater than the design back pressure, the flow expands along the plug only up to the design back pressure. The final wave of the expansion fan centered at the cowling intersects the plug at a point upstream of the apex. As shown in Figure 8.15(b), the outer boundaries of the exhaust jet are directed inward. Further weak compression and expansion waves occur downstream of the point of impingement of the final wave from the fan; the strength and location of these waves are dependent on the plug contour. Thus, the expansion along the

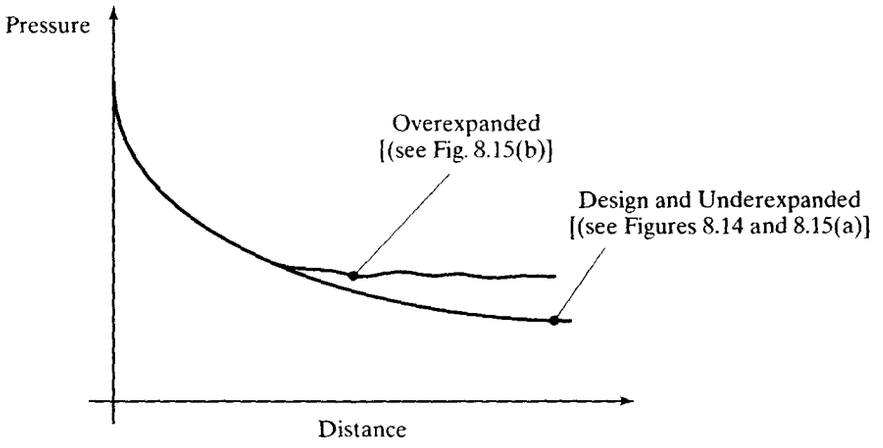


**Figure 8.16** Pressure Distribution within a Plug Nozzle

plug is controlled by the back pressure, whereas the converging–diverging nozzle expansion is controlled by nozzle geometry.

A sketch of the pressure along the plug surface versus distance is given in Figure 8.16. The pressure along the plug surface does not decrease below ambient pressure, so there is not a negative thrust term due to pressure difference. As a result, the plug nozzle provides improved thrust over the converging–diverging nozzle for the overexpanded case. (See Figure 8.17.)

It would appear desirable to design the plug so as to provide for isentropic expansion flow along its curved pointed surface. However, this design leads to a rather long plug and, in turn, to a heavy design. It has been shown [see Ref. (8.7)] that replacement of the curved shape with a simple cone results in only a small loss of thrust for cone half-angles up to 30°. Thus, it was recognized that the plug nozzle has the further advantage over the converging–diverging nozzle of being short and compact.

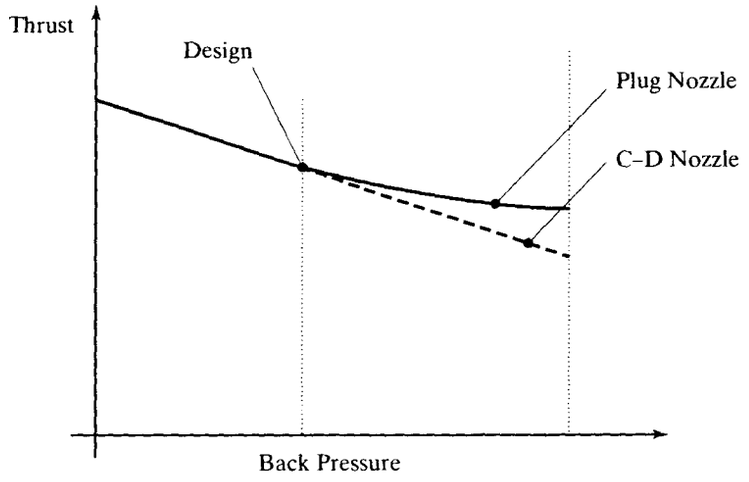


**Figure 8.17** Comparison of Thrust and Back Pressure for Plug and C–D Nozzles

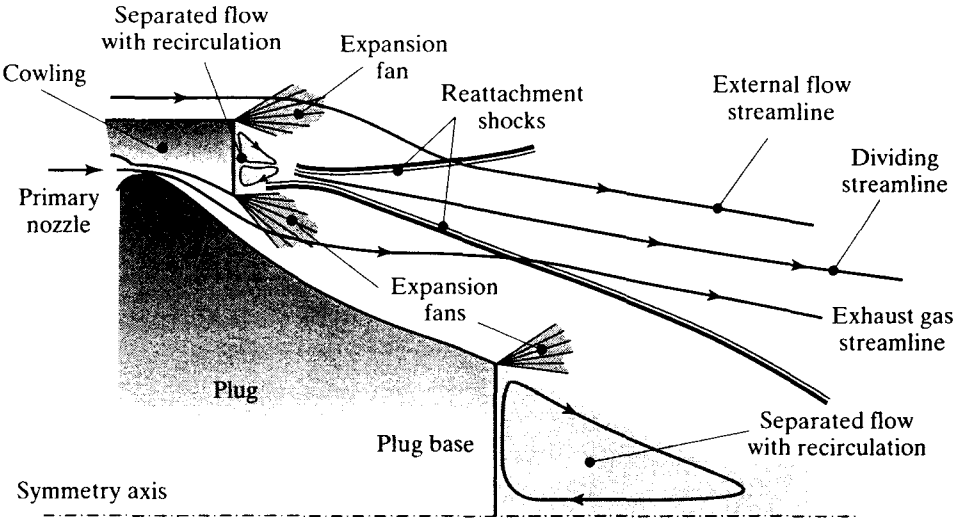


**Figure 8.18** Schematic Diagram of the Flow Field of a Truncated Annular Plug Nozzle [see Ref. (8.8)]

Further studies have revealed that more than one half of the plug length produces almost no thrust and only added weight. Consequently, truncated plugs have been considered. The flow field of these shortened plugs is rather complicated, involving lip shocks, regions of separated flow, and a variety of expansion and compression waves. Figure 8.18 is a sketch of the flow downstream of the plug. There is considerable research currently under way, largely using modern computational fluid dynamics, to study these flow fields [e.g., see Refs. (8.7)–(8.9)].

One major problem with the plug nozzle is that of designing a plug to withstand the high temperatures that exist, for example, in the exhaust gases of a rocket engine. This factor requires consideration for the cooling of the plug.

**Example 8.4. Performance computations comparing overexpanded plug and C–D nozzles**

A rocket nozzle is designed to operate with a ratio of chamber pressure to ambient pressure ($p_c/p_a$) of 50. Compare the performance of a plug nozzle with that of a converging–diverging nozzle for two cases where the nozzle is operating overexpanded: $p_c/p_a = 40$ and $p_c/p_a = 20$. Make the comparison on the basis of thrust coefficient $C_T = \mathbf{T}/(p_c A_t)$, where $\mathbf{T}$ is the thrust and $A_t$ is the area of throat. Assume that $\gamma = 1.4$, and in both cases neglect the effect of nonaxial exit velocity components.

**Solution**

*For the design case*:
From $p_e/p_o = p_a/p_c = 1/50 = 0.02$, and since in the design case the flow is isentropic, we can determine the Mach number at the exit [i.e., $M_e = 3.2077$; see Eq. (3.15)], and therefore $T_e/T_o = T_e/T_c = 0.3270$. Now, from the definition of the thrust coefficient,

$$C_T = \frac{(\dot{m}_t V_e)}{p_c A_t} = \frac{(\rho_t A_t V_t) V_e}{p_c A_t} = \left(\frac{p_t}{RT_t}\right)\frac{V_t V_e}{p_c} = \left(\frac{p_t}{p_c}\right)\left(\frac{p_c}{RT_o}\right)\left(\frac{T_o}{T_t}\right)\frac{(M_t a_t)(M_e a_e)}{p_c}$$

Because the nozzle is choked, $M_t = 1$, and therefore,

$$\frac{p_t}{p_c} = \left(\frac{\gamma + 1}{2}\right)^{\gamma/(1-\gamma)} = 0.5283$$

$$\frac{T_t}{T_c} = \frac{2}{\gamma + 1} = 0.8333$$

Using these values and the values at the exit, we get

$$C_T = \left[\frac{0.5283p_c}{R(0.8333T_c)}\right]\left[\frac{\sqrt{(1.4)(R)(0.8333)T_c}}{p_c}\right](3.2077)\sqrt{(1.4)(R)(0.3270)T_c} = 1.4862$$

Note that $R$, $p_c$, and $T_c$ drop out of the preceding expression.

*For the converging–diverging nozzle operating off design*:

$$C_T = (C_T)_{\text{design}} + \frac{A_e(p_e - p_a)}{A_t p_c} = 1.4862 + \frac{A_e}{A_t}\left(\frac{p_e}{p_c} - \frac{p_a}{p_c}\right)$$

where at $M_e = 3.2077$, $A_e/A_t = A_e/A^* = 5.1584$. So for $p_c/p_a = 40$,

$$C_T = 1.4862 + 5.1584\left(\frac{1}{50} - \frac{1}{40}\right) = 1.4604$$

For $p_c/p_a = 20$,

$$C_T = 1.4862 + 5.1584(0.02 - 0.05) = 1.3314$$

*For the plug nozzle*:

Flow in the plug nozzle does not continue to expand below ambient pressure, so there is no pressure term in the expression for thrust.

Now, at $\frac{p_c}{p_a} = 40$, $M_e = 3.0570$, $\frac{T_e}{T_c} = 0.3485$, and

$$C_T = \frac{\dot{m}_t V_e}{p_c A_t} = \left[\frac{0.5283p_c}{R(0.8333T_c)}\right]\left[\frac{A_t\sqrt{1.4(R)0.8333T_c}}{p_c A_t}\right]3.0570\sqrt{1.4R(0.3485T_c)} = 1.4622$$

whereas for $p_c/p_a = 20$, $M_e = 2.6015$, $\frac{T_e}{T_c} = 0.4249$, and $C_T = 1.3740$

The plug nozzle is marginally superior to the C–D nozzle near the design point when operating in the overexpanded regime; however, the gap widens as the chamber-to-ambient pressure ratio decreases.

## 8.5 SUPERSONIC AIRFOILS

The design of an airfoil should be such as to provide a lift force normal to the undisturbed flow, accompanied by low drag force in the direction of the undisturbed flow. The shape of a wing section to be used in low-speed, incompressible flow is the well-known teardrop, or streamlined, profile. This shape is predicated on incompressible aerodynamics, where, for example, drag is composed of skin friction on the airfoil surface and pressure or profile drag, due to the effects of flow separation at the rear of the airfoil. In supersonic flow, however, the design must be completely modified, owing to the occurrence of shocks. For example, if a streamlined profile with a rounded blunt nose were used in supersonic flow, either an attached shock of relatively high strength would occur at the nose or, if $\theta$ were great enough, a detached shock (Figure 8.19) would take occur in front of the airfoil. In both cases, the high pressures after the shockwave produce excessive drag forces on the airfoil. To minimize the drag due to the presence of shocks, the supersonic airfoil must have a pointed nose and be as thin as possible. The ideal case is a flat-plate airfoil possessing zero thickness.

Consider a two-dimensional flat plate at an *angle of attack* (AoA) to the approach flow as shown in Figure 8.20. Flow over the upper surface is turned through an expansion fan centered at the nose; flow over the lower surface is compressed through an oblique shock attached to the nose. The difference in pressure between the upper and lower surfaces causes a net upward force, directed normal to the flow direction, the *lift*, on the airfoil. A force opposing the motion of the airfoil, the *drag*, on the airfoil, accompanies this lift. The latter force is called *wave drag*, since it exists only because of the supersonic wave pattern involved with this flow.

Expressions for the lift and drag for supersonic flow past a flat-plate airfoil operating at an angle of attack $\alpha$ to the flow direction are given by

$$L = -(p_{\text{upper}}c)\cos\alpha + (p_{\text{lower}}c)\cos\alpha = c(p_{\text{lower}} - p_{\text{upper}})\cos\alpha \tag{8.2}$$

$$D = -(p_{\text{upper}}c)\sin\alpha + (p_{\text{lower}}c)\sin\alpha = c(p_{\text{lower}} - p_{\text{upper}})\sin\alpha \tag{8.3}$$

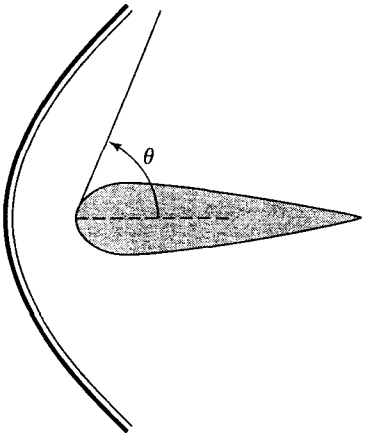


**Figure 8.19** Detached Shock in Front of a Streamlined Airfoil

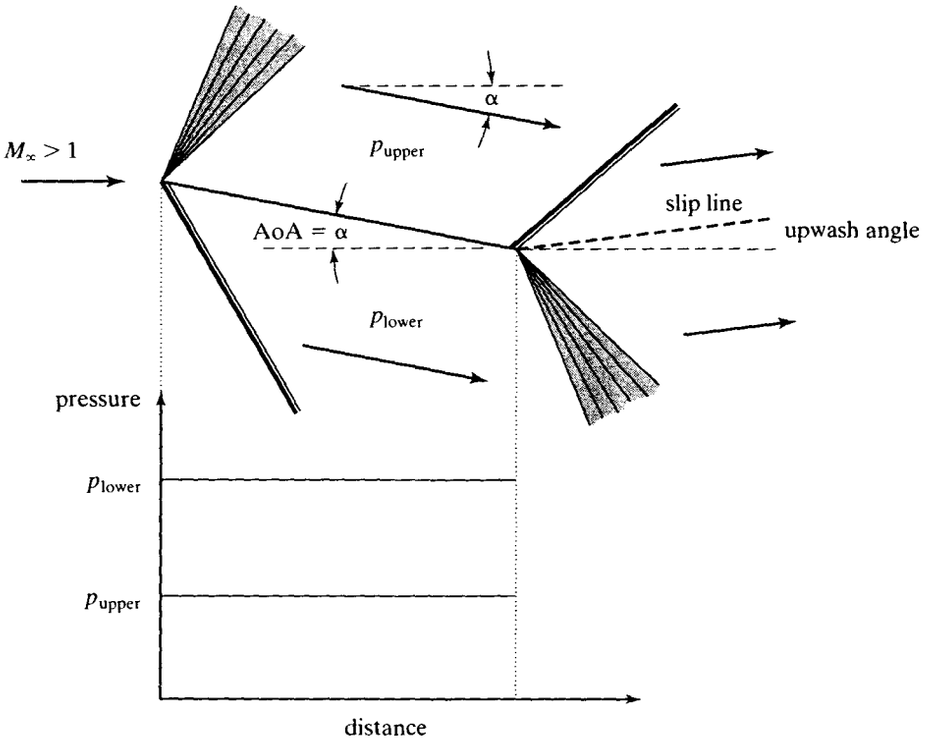


**Figure 8.20** Supersonic Flow Past a Flat Plate at an Angle of Attack

where $c$ is chord length. Note the various group of terms within each of these expressions. The lift force for this case is composed of two groups. Each is the product of pressure on the surface and the area—in this case, the chord length; the cosine of the angle of attack multiplied by each group provides the component in the direction normal to the flow direction. The only difference for the wave drag force is that the groups are multiplied by the sine of the angle of attack. Careful consideration of these groups and their components will enable more challenging geometries to be considered.

**Example 8.5. Computation of the lift and drag coefficients of a flat-plate airfoil at an angle of attack in a supersonic stream**

Compute the lift and drag coefficients

$$C_L = \frac{L}{\frac{1}{2}\rho V_\infty^2 c} \quad \text{and} \quad C_D = \frac{D}{\frac{1}{2}\rho_\infty V_\infty^2 c}$$

for a flat-plate airfoil of chord length $c = 1$ m in supersonic flow through air ($\gamma = 1.4$) at $M_\infty = 2.5$ and $\alpha = 10°$.

**Solution**

First, find the static pressure on the lower surface behind the oblique shock. Using the charts in Appendix D or an oblique shock solver from Chapter 6, for $M_\infty = 2.5$ and

$\delta = 10°$, the shock angle $\theta$ is found to be 31.8506°. With this and the oblique-shock relations, we can solve for the Mach number on the downstream side of the shock and the static pressure ratio across the shock (i.e, $M_{\text{lower}} = 2.0859$ and $p_{\text{lower}}/p_\infty = 1.8639$). For the expansion fan, using the Prandtl–Meyer table in Appendix E or the solver described in Chapter 7, at $M_\infty = 2.5$, we find that $\nu_\infty = 39.1236°$. Accordingly, $\nu_{\text{upper}} = 39.1236° + 10° = 49.1236°$. Reentering Table E.1 or the Prandtl–Meyer solver with this value, we find that $M_{\text{upper}} = 2.9674$. The flow through the expansion fan is isentropic; that is, $p_o$ is constant. Hence, at the freestream and upper region Mach numbers, we obtain from the isentropic flow expressions or an isentropic flow solver (see Appendix A) that $p_\infty/p_o = 0.0585$ and $p_{\text{upper}}/p_o = 0.0286$. Consequently,

$$\frac{p_{\text{upper}}}{p_\infty} = \left(\frac{p_{\text{upper}}}{p_o}\right)\left(\frac{p_o}{p_\infty}\right) = (0.0286)\left(\frac{1}{0.0585}\right) = 0.4885$$

$$C_L = \frac{L}{\frac{1}{2}\rho_\infty V_\infty^2 c} = \frac{L}{\frac{1}{2}\gamma p_\infty M_\infty^2 c} = \frac{(p_{\text{lower}} - p_{\text{upper}})\cos\alpha}{\frac{1}{2}\gamma p_\infty M_\infty^2}$$

$$= \frac{(1.8639 - 0.4885)\cos 10°}{4.3750} = 0.3096$$

$$C_D = \frac{D}{\frac{1}{2}\gamma p_\infty M_\infty^2 c} = \frac{(p_{\text{lower}} - p_{\text{upper}})\sin\alpha}{\frac{1}{2}\gamma p_\infty M_\infty^2} = C_L \tan\alpha = 0.0546$$

As a final set of computations for this example, we use the method described in Example 7.5 to determine the flow angle and the pressure ratio downstream of the airfoil. Basically, with that approach, the pressure–deflection diagram is drawn for the shock on the upper surface at the trailing edge of plate, as well as for the expansion fan on the lower surface of the plate at the trailing edge. The intersection of these diagrams provides the angle and pressure common to both sides of the dividing slip line. The result of this computation is

$$\alpha_3 = \alpha_4 = 0.0398°$$

$$p_3/p_\infty = p_4/p_\infty = 0.9998$$

Thus, the flow downstream of the airfoil has a slight upward angle (called the *upwash*), and the pressure is virtually equal to the free static pressure value. Explanation of the phenomena may be found in Anderson [Ref. (8.10)].

---

It should be noted that the flat plate is an idealization; structurally, such an airfoil is unsound. Again, for a supersonic airfoil, a thin airfoil with a pointed nose is required. The curved, symmetrical airfoil represents one possibility. For small angles of attack, oblique shocks are attached to the nose, with the stronger shock occurring on the lower surface, since the flow turning angle must be greater on this surface. (See Figure 8.21.) Due to the continuous curvature of the airfoil, flow over the airfoil continually changes direction, and a gradual expansion occurs over the upper and lower surfaces. Expansion waves are produced as shown in Figure 8.21. If the angle of attack becomes too great, or if the nose half-angle $\Delta$ is too large, the oblique shocks may detach from the nose, yielding excessive drag.

Another airfoil shape for supersonic flow is the diamond profile, shown in Figure 8.22. Flow over the upper surface is first expanded through a fan centered at

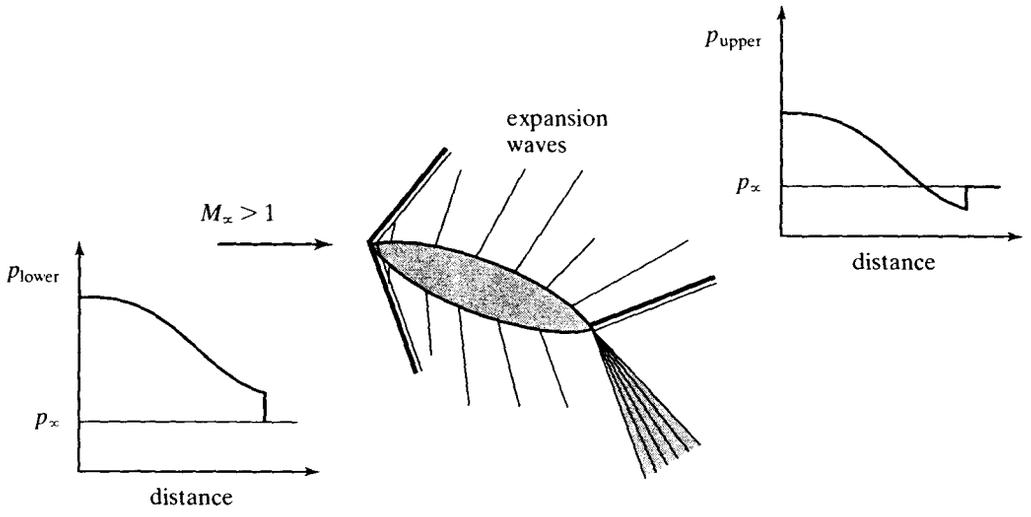


**Figure 8.21** Supersonic Flow Past a Curved, Symmetrical Airfoil at an Angle of Attack

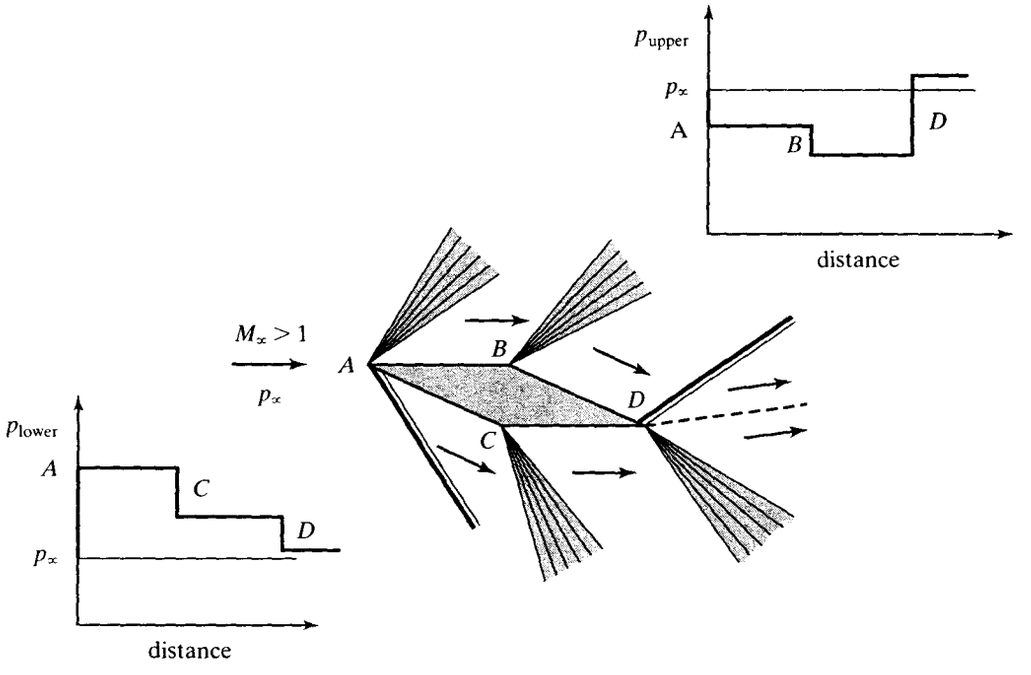


**Figure 8.22** Wave Pattern on a Supersonic Airfoil of Diamond Profile at an Angle of Attack

$A$ and then is turned through another expansion fan at $B$. If the angle of attack is small enough, or if the airfoil is thick enough, flow over the upper surface may first be compressed through an oblique shock attached at $A$. (See Figure 8.23.) Flow over the lower surface is turned through an oblique shock at $A$ and then through an expansion

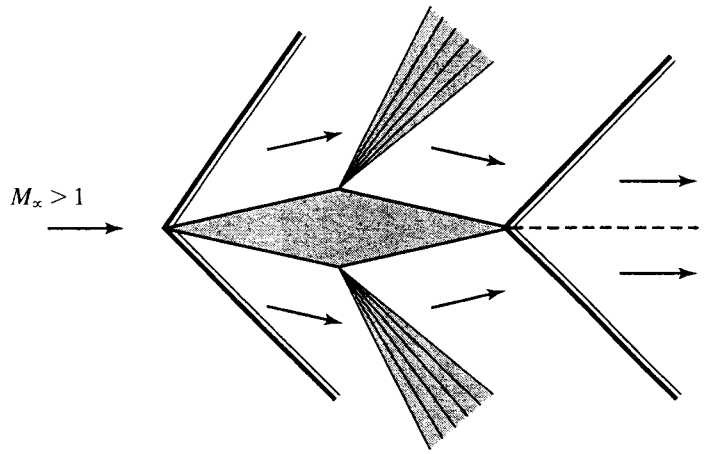


**Figure 8.23** Wave Pattern on a Supersonic Airfoil of Diamond Profile at Zero Angle of Attack

fan at *C*. As shown by the pressure distribution, higher pressures over the lower surfaces yield a lift force; higher pressures at the front surfaces cause a drag force.

**Example 8.6. Computation of the lift and drag coefficients of a supersonic airfoil with a diamond profile at an angle of attack**

For the two-dimensional symmetrical airfoil with a diamond profile $\Delta = 5°$, shown in Figure 8.22, compute the lift and drag coefficients in supersonic flow through air ($\gamma = 1.4$) at $M_\infty = 3.0$, with an angle of attack (AoA) = 10°.

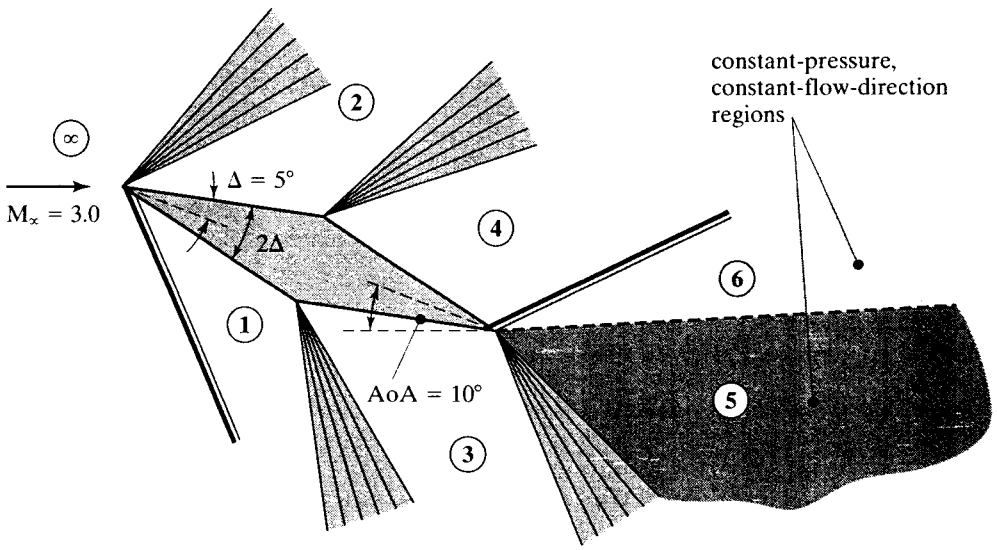


**Figure 8.24** Supersonic Flow Past an Airfoil with a Diamond Profile (Example 8.6)

**Solution**

On the *upper surface*, supersonic flow is first expanded through a Prandtl–Meyer fan. The Prandtl–Meyer function for the freestream conditions is obtained as

$$\nu_\infty = 49.7573°$$

The Prandtl–Meyer function in region 2 is therefore

$$\nu_2 = \nu_\infty + \Delta = 49.7573 + 5.0 = 54.7573°$$

and the value of the function in region 4 is

$$\nu_4 = \nu_2 + 2\Delta = 54.7573 + 10.0 = 64.7573°$$

Using the Prandtl–Meyer tables in Appendix E or a solver developed from relations in Chapter 7, we determine the respective Mach numbers for these functions to be

$$M_2 = 3.2731 \text{ and } M_4 = 3.9233$$

The static-to-total-pressure ratios at these two Mach numbers, as well as the freestream ratio, can be readily determined, and since the flow between the freestream and regions 2 and 4 is isentropic, we may write that

$$\frac{p_2}{p_\infty} = \left(\frac{p_2}{p_{o2}}\right)\left(\frac{p_{o2}}{p_{o\infty}}\right)\left(\frac{p_{o\infty}}{p_\infty}\right) = (0.0182)(1)\left(\frac{1}{0.0272}\right) = 0.6676$$

$$\frac{p_4}{p_\infty} = \left(\frac{p_4}{p_{o4}}\right)\left(\frac{p_{o4}}{p_{o\infty}}\right)\left(\frac{p_{o\infty}}{p_\infty}\right) = (0.0073)(1)\left(\frac{1}{0.0272}\right) = 0.2681$$

Flow on the *lower surface* is first compressed through an oblique shock, which turns the flow by an angle of 15°. For $M_\infty = 3.0$ and $\delta = 15°$, $\theta = 32.2404°$, so that $M_1 = 2.2549$, $p_{o1}/p_{o\infty} = 0.8950$, and $p_1/p_\infty = 2.8216$. Flow on the lower surface then expands through an expansion fan for which

$$\nu_1 = 33.1433°$$

$$\nu_3 = \nu_1 + 2\Delta = 43.1433°$$

The Mach number $M_3$ for this value of the Prandtl–Meyer function is determined to be 2.6780. The static-to-total-pressure ratio at $M_3$ is found to be 0.0444. Thus, we may write

$$\frac{p_3}{p_\infty} = \left(\frac{p_3}{p_{o3}}\right)\left(\frac{p_{o3}}{p_{o1}}\right)\left(\frac{p_{o1}}{p_{o\infty}}\right)\left(\frac{p_{o\infty}}{p_\infty}\right) = (0.0444)(1)(0.8950)\left(\frac{1}{0.0272}\right) = 1.4607$$

$$L = \left(p_1\frac{c/2}{\cos\Delta}\right)\cos(\alpha + \Delta) + \left(p_3\frac{c/2}{\cos\Delta}\right)\cos(\alpha - \Delta)$$
$$- \left(p_2\frac{c/2}{\cos\Delta}\right)\cos(\alpha - \Delta) - \left(p_4\frac{c/2}{\cos\Delta}\right)\cos(\alpha + \Delta)$$

Note that each group in parentheses in the expression represents a pressure times the corresponding area and that the flow direction in region 1 is $\alpha + \Delta$, in region 2 is $\alpha - \Delta$, in region 3 is $\alpha - \Delta$, and in region 4 is $\alpha + \Delta$. Now, multiplying and dividing by the

freestream static pressure, using the pressure ratios just determined, and employing the fact that $\alpha = 10°$ and $\Delta = 5°$, we find that

$$L = p_\infty c\left\{\left[\frac{2.8216}{(2)(0.9962)}\right]0.9659 + \left[\frac{1.4603}{(2)(0.9962)}\right]0.9962 - \left[\frac{0.6676}{(2)(0.9962)}\right]0.9962 - \left[\frac{0.2681}{(2)(0.9962)}\right]0.9659\right\}$$

$$L = 1.6345(p_\infty c)$$

Thus,

$$C_L = \frac{L}{\frac{1}{2}\gamma p_\infty M_\infty^2 c} = \frac{1.6345}{6.300} = 0.2594$$

$$D = \left(p_1\frac{c/2}{\cos\Delta}\right)\sin(\alpha + \Delta) + \left(p_3\frac{c/2}{\cos\Delta}\right)\sin(\alpha - \Delta) - \left(p_2\frac{c/2}{\cos\Delta}\right)\sin(\alpha - \Delta) - \left(p_4\frac{c/2}{\cos\Delta}\right)\sin(\alpha + \Delta)$$

$$D = p_\infty c\left\{\left[\frac{2.8216}{(2)(0.9962)}\right]0.2588 + \left[\frac{1.4603}{(2)(0.9962)}\right]0.0872 - \left[\frac{0.6676}{(2)(0.9962)}\right]0.0872 - \left[\frac{0.2681}{(2)(0.9962)}\right]0.2588\right\}$$

$$D = 0.3664(p_\infty c)$$

$$C_D = \frac{D}{\frac{1}{2}\gamma p_\infty M_\infty^2 c} = \frac{0.3664}{6.300} = 0.0582$$

As in the previous example, the angle of the slip line, and therefore the angle of the flow downstream of the airfoil, can be determined using the method described in Example 7.5. The results for the current problem are as follows:

$$\alpha_5 = \alpha_6 = 0.2853°$$

$$p_5/p_\infty = p_6/p_\infty = 0.9914$$

Thus, the flow downstream of the airfoil, as in the flat-plate case, has a slight upward angle, and the pressure is nearly equal to the free-static pressure. For smaller upstream Mach numbers, the flow can be pitched downwards.

It can be seen, then, that subsonic airfoil design cannot be applied to supersonic airfoils. The shape of a supersonic wing is determined mainly by the effect of shock-waves and thus requires a thin, pointed profile. The conventional teardrop shape used for subsonic flow would have extremely poor lift and drag characteristics in supersonic flow.

## 8.6 CHAPTER CAPSTONE APPLICATION: SURFACE PRESSURE DISTRIBUTION ON A BODY IN A HIGH-MACH-NUMBER FLOW

As noted previously, when a blunt body is immersed in a high-Mach-number (supersonic or hypersonic) stream, a bow shock surrounds the front portion of the body. The solution of supersonic *blunt-body problems* generally requires powerful computational fluid dynamics techniques. In this application, however, we will make use of a very simple technique that is widely used in conceptual hypersonic designs [e.g., see Refs. (8.11)–(8.13)]. The method that will be discussed was, curiously enough, originated by Newton long before compressible flow concepts such as shockwaves were even imagined. Thus, the modeling is known as *Newtonian theory*.

Newton considered a uniform stream of particles that collides inelastically with a surface. He hypothesized that when a particle hits a surface, it loses all of its momentum in a direction normal to the surface, but retains all of its momentum in the direction along the surface. He attempted, without success, to use this concept to determine the hydrodynamic forces on ship hulls.

The method was not widely used until the 1950s, when it was realized that a gas traveling at extremely high speeds behaves in a manner not unlike that proposed by Newton. It was found that at high Mach numbers, the bow shock surrounding a blunt body lies very close to the body. Accordingly, in a very high-speed flow, the gas particles are almost able to reach the body without any change in their velocity. After passing through the shock, the gas is forced to rapidly turn and form a thin region between the shock and the body, which is called the *shock layer*.

It is easy to demonstrate from oblique-shock theory that for a fixed wedge angle $\Delta = \delta$, as the freestream Mach number increases, the shock angle $\theta$ approaches the deflection angle $\delta$. For $M_\infty = \infty$ and $\gamma = 1$, it can be shown that $\theta = \delta$. Further justification of this theory comes from the fact that because of the high temperatures and pressures of very hypersonic flows, real-gas effects drive the value of $\gamma$ towards unity.

Consider a portion of the bow shock and shock layer surrounding the body, as shown in Figure 8.25. From a momentum balance in direction normal to the shock, we have, from Eq. (6.2),

$$p_1 - p_2 = \rho_2 V_{n2}^2 - \rho_1 V_{n1}^2 \tag{8.4}$$

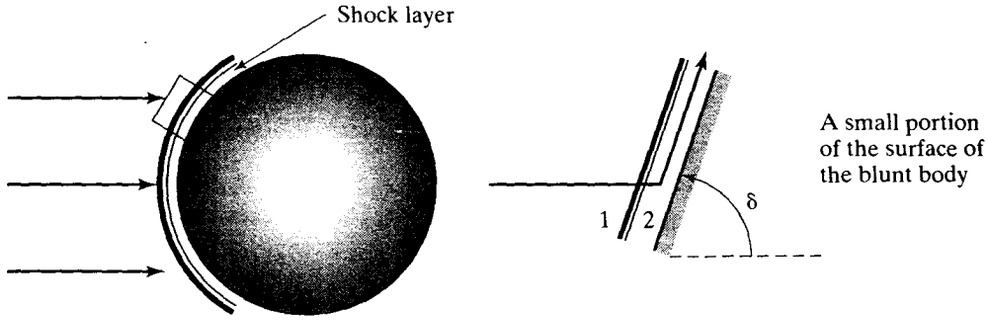


**Figure 8.25** Portion of Blunt Body in Supersonic Flow Used to Develop Newtonian Theory

Because the flow upstream is the freestream and because the gas downstream of the shock loses all of its normal momentum, we have in this case that

$$\begin{bmatrix} p_1 \\ V_{n1} \\ \rho_1 \end{bmatrix} = \begin{bmatrix} p_\infty \\ V_\infty \sin\delta \\ \rho_\infty \end{bmatrix} \quad \text{and} \quad \begin{bmatrix} p_2 \\ V_{n2} \\ \rho_2 \end{bmatrix} = \begin{bmatrix} p_{\text{surface}} \\ 0 \\ \rho_2 \end{bmatrix}$$

Note that the angle $\delta$ is the local inclination of the surface (i.e., the angle between the surface and the freestream velocity). Consequently, this method is also referred to as a *local surface inclination method.* Several other methods are also members of this family: the shock-expansion theory that we have already considered, as well as the tangent wedge and tangent cone theories. [See Ref. (8.13).] Inserting the foregoing conditions into the momentum equation, Eq. (8.4), produces

$$p_{\text{surface}} = p_\infty + \rho_\infty V_\infty^2 \sin^2\delta$$

It is not difficult to obtain this expression by directly applying control-volume methods. The expression may be rewritten as a *pressure coefficient*

$$C_p = \frac{p_{\text{surface}} - p_\infty}{\frac{\rho_\infty V_\infty^2}{2}} = 2\sin^2\delta \tag{8.5}$$

This expression is often referred to as *Newton's sine-squared law.* Note that the pressure coefficient is dependent solely on the geometry of the body and not on the freestream Mach number. Since the dynamic pressure $\rho_\infty V_\infty^2/2 = \gamma p_\infty M_\infty^2/2$, Eq. (8.5) may be expressed as

$$\frac{p_{\text{surface}}}{p_\infty} = 1 + \gamma M_\infty^2 \sin^2\delta \tag{8.6}$$

At the stagnation point, $\delta = 90°$ and $p_{\text{surface}} = p_o$, so

$$\frac{p_o}{p_\infty} = 1 + \gamma M_\infty^2 \tag{8.7}$$

Therefore, Newton's theory produces the following:

$$\frac{p_{\text{surface}}}{p_o} = \frac{p_\infty}{p_o} + \left(1 - \frac{p_\infty}{p_o}\right)\sin^2\delta = \frac{1 + \gamma M_\infty^2 \sin^2\delta}{1 + \gamma M_\infty^2} \tag{8.8}$$

To improve the accuracy of the method, Lees [Ref. (8.14)] proposed that Eq. (8.8) be replaced with *Rayleigh's formula* [see Eq. (16.7)]; that is, replace $p_o$ with $p_{o2}$. Hence, the pressure coefficient expression, Eq. (8.8), is written as

$$C_p = (C_p)_{\max}\sin^2\delta \tag{8.9}$$

Note that the 2 in Eq. (8.5) has been replaced with a coefficient that varies with $M_\infty$ and $\gamma$. In this form, the theory is generally known as *Newton's modified theory.* For $M_\infty = 4$ and $\gamma = 1.4$, $(C_p)_{\max} = 1.79179$; for $M_\infty = \infty$ and $\gamma = 1.4$, $(C_p)_{\max} = 1.83937$;

and for $M_\infty = \infty$ and $\gamma = 1$, $(C_p)_{max} = 2$. Thus, the uncorrected Newtonian theory is applicable at extreme conditions such as those encountered by reentry vehicles.

The predicted results of this model for a circular cylindrical body shape at a Mach number of 4 and $\gamma = 1.4$ are compared with measured values in Ref. (8.15). The predicted pressure ratio $p_{surface}/p_o$ is shown to be in excellent agreement with the experimental data for $\delta$ up to about 65°. It should also be mentioned that the Newtonian and modified Newtonian theory have been refined to predict lift and drag of bodies in hypersonic flow.

## 8.7 SUMMARY

Oblique shockwaves and expansion fans facilitate the turning of supersonic flows. Thus, there are numerous applications in which one or both of these appear. This chapter has sought to combine the fundamental concepts of Chapters 6 and 7 to solve a variety of flows in which the supersonic flow was required to change direction. Supersonic inlets and nozzles, as well as supersonic airfoils, are excellent examples to which the tools that were developed in earlier chapters can be applied. It was found that drag could occur on airfoils in supersonic flow even though the flow is assumed to be inviscid. This drag form (called wave drag) occurs because of an imbalance of forces acting on the surface of the airfoils caused by the wave pattern.

## 8.8 REFERENCES


**8.1** Wisse, M. E. N., and Bannink, W. J. "Half Model Restrictions for Linear Plug Nozzle Testing," *AIAA Journal* 2001; 39(11): 2148–2157.

**8.2** Rommel, G., Hagemann, C.-A., Krülle, G., and Manski, D. "Plug Nozzle Flowfield Analysis," *AIAA J Propul Power* 1997; 13(5): 629–634.

**8.3** Herman, K., and Neuffer, H., "Plug Nozzle Flexibility," *Astronautics* 1960; 5: pp. 30–31.

**8.4** Rao, G. "Recent Developments in Rocket Nozzle Configurations," *ARS Journal* 1961; 5: 1488–1494.

**8.5** Herman, K. "The Plug Nozzle: A New Approach to Engine Design," *Astronautics* 1960; 5: 22–24.

**8.6** Berman, K., and Crimp, F. W., "Performance of Plug-Type Rocket Exhaust Nozzles," *ARS Journal*, 1961; 31: 18–23.

**8.7** Nasuti, F., and Onofri, M. "Methodology to Solve Flowfields of Plug Nozzles for Future Launchers," *AIAA J Propul Power* 1998; 14(3): 318–326.

**8.8** Nasuti, F., and Onofri, M. "Analysis of In-Flight Behavior of Truncated Plug Nozzles," *AIAA J Propul Power* 2001; 17(4): 809–817.

**8.9** Ito, T., Fujii, K., and Hayashi, A. K. "Computations of Axisymmetric Plug-Nozzle Flowfields: Flow Structures and Thrust Performance," *AIAA J Propul Power* 2002; 18(2): 254–260.

**8.10** Anderson, Jr., J. D. *Modern Compressible Flow with Historical Perspectives*, 3d ed., McGraw-Hill Book Company, New York, 2002, pp. 176–178.

**8.11** *Ibid.*, pp. 443–418 and 559–565.

**8.12** Bertin, J. J., and Smith., M. L. *Aerodynamics for Engineers*, 3d ed., Prentice Hall, Upper Saddle River, NJ, 1998, pp. 516–540.

**8.13** Chernyi, G. G. *Introduction to Hypersonic Flow*, Academic Press, New York, 1961, pp. 95–120.

**8.14** Lees, L. "Hypersonic Flow," *Proceedings of the 5th International Aeronautical Conference*, Los Angeles, CA, Institute of the Aeronautical Sciences, 1955, pp. 241–275.

**8.15** Tannehill, J. C., Anderson, D. A., and Pletcher, R. H., *Computational Fluid Mechanics and Heat Transfer*, 2d ed., Taylor & Francis, Washington, DC, 1997, pp. 6–8.

## 8.9 PROBLEMS

**8.1** A supersonic inlet (see Figure P8.1) is to be designed to handle air ($\gamma = 1.4, R = 287$ J/kg · K) at Mach 1.75 with static pressure and temperature of 50 kPa and 250 K, respectively. Determine the diffuser inlet area $A_i$ if the device is to handle 10 kg/s of air.

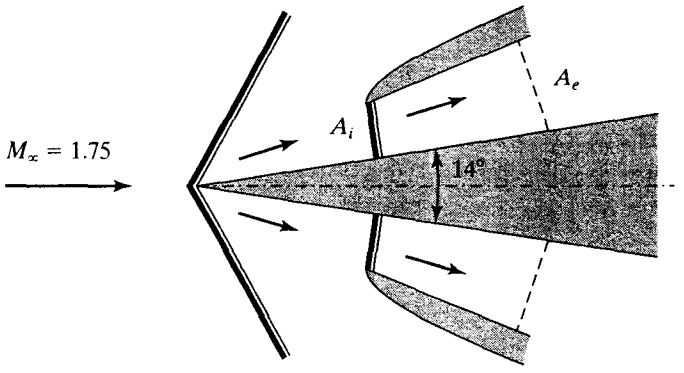


**Figure P8.1**

**8.2** The diffuser in Problem 8.1 is to further decelerate flow after the normal shock so that the velocity entering the compressor is not to exceed 25 m/s. Assuming isentropic flow after the shock, determine the area $A_e$ required. For this condition, find the static pressure $p_e$.

**8.3** Compare the loss in total pressure incurred by a one-shock spike diffuser with that incurred by a two-shock diffuser operating at Mach 2.0. Repeat at Mach 4.0. (See Figure 8.5.) Assume that each oblique shock turns the flow through an angle of 10°. Let $\gamma = 1.3$.

**8.4** A *converging nozzle* is supplied from a large air ($\gamma = 1.4, R = 287$ J/kg · K) reservoir maintained at 600 K and 2 MPa. If the nozzle back pressure is 101 kPa, determine the pressure and Mach number that exist at the nozzle exit plane. Since the nozzle is operating in the underexpanded regime, expansion waves occur at the nozzle exit. Determine the flow direction after the initial expansion fans and the flow Mach number. Also determine the fan angles.

**8.5** An oblique shockwave occurs in a supersonic flow in which $M_1 = 3$. The shock turns the supersonic stream through 10°. The shock impinges on a free surface along which the pressure is constant and equal to $p_1$ (i.e., the pressure upstream of the shock). The shock is reflected from the free surface as an expansion fan. Determine the Mach number and the angle of the flow just downstream on the leading wave of the fan. Assume that $\gamma = 1.4$. See Figure P8.5.

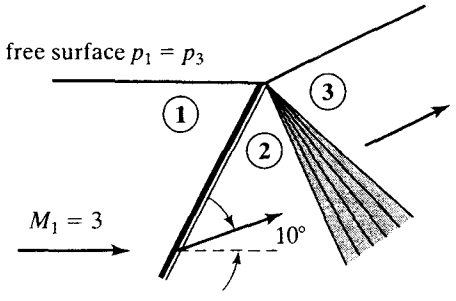


**Figure P8.5**

**8.6** A *converging–diverging* nozzle is designed to provide exit flow at Mach 2.2. With the nozzle exhausting to a back pressure of 101 kPa, however, and a reservoir pressure of 350 kPa, the nozzle is overexpanded, with oblique shocks appearing at the exit. Determine the flow direction, static pressure, and Mach number in regions 1, 2, and 3 of Figure P8.6.

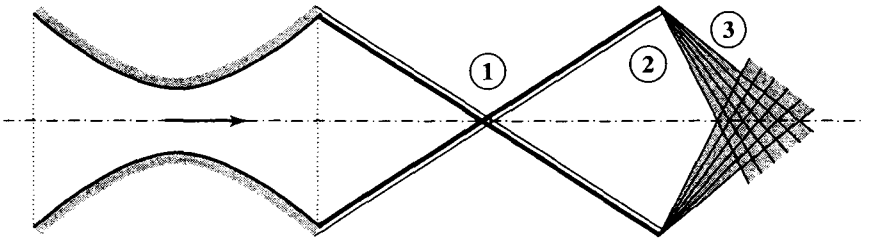


**Figure P8.6**

**8.7** Determine the flow directions in regions 1 and 3 of Figure P8.6 if the reservoir pressure were increased to 2 MPa.

**8.8** A plug nozzle is designed to produce Mach 2.5 flow in the axial direction at the plug apex. Flow at the throat cowling must therefore be directed toward the axis. Determine the flow direction at the throat cowling to produce axial flow at the apex. Assume that $\gamma = 1.4$.

**8.9** A rocket nozzle is designed to operate with a ratio of chamber pressure to ambient pressure ($p_c/p_a$) of 50. Compare the performance of a plug nozzle with that of a converging–diverging nozzle for two cases in which the nozzle is operating overexpanded: $p_c/p_a = 40$ and $p_c/p_a = 20$. Compare the cases on the basis of thrust coefficient $C_T = \mathbf{T}/(p_c A_{th})$, where $\mathbf{T}$ is the thrust and $A_{th}$ is the area of the throat. Assume that $\gamma = 1.3$, and in both cases neglect the effect of nonaxial exit velocity components.

**8.10** Compute the lift and drag coefficients for a flat-plate airfoil of chord length $c = 1$ m in supersonic flow through air ($\gamma = 1.4$) at $M_\infty = 3$ and $\alpha = 8°$.

**8.11** Compute the drag coefficient for a symmetric, diamond-shaped airfoil (see Figure P8.11) with a thickness-to-chord ratio $t/c$ equal to 0.10, flying at Mach 3.5 in air ($\gamma = 1.4$) at zero angle of attack.

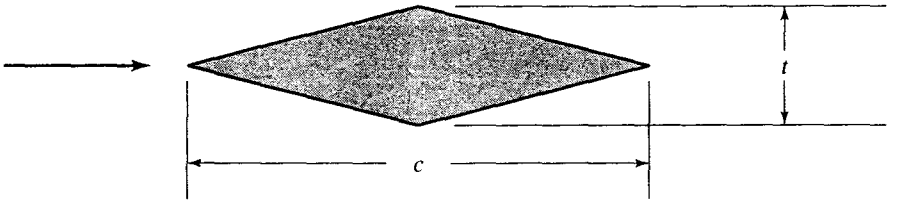


**Figure P8.11**

**8.12** Compute the lift and drag coefficients for the airfoil described in Problem 8.11 for an angle of attack of 5°.

**8.13** Compare the lift-to-drag ratio of the diamond airfoil in Problem 8.11 with that of a flat-plate airfoil for the same freestream Mach number of 3.5 and angle of attack of 5°. Assume that $\gamma = 1.4$.

**8.14** Consider a flat-plate supersonic airfoil with a flap, as shown in Figure P8.14. For a flap angle of 5°, an angle of attack of 10°, and a flight Mach number of 2.2, find the lift and drag coefficients of the airfoil. Assume that $\gamma = 1.4$.

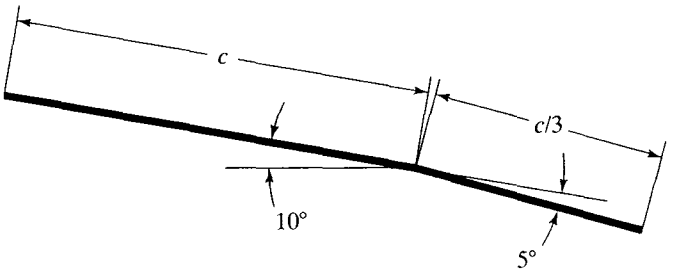


**Figure P8.14**

**8.15** Compute the lift and drag coefficients for the supersonic airfoil shown in Figure P8.15 flying in air ($\gamma = 1.4$) at Mach 2.5 at an angle of attack of 5°.

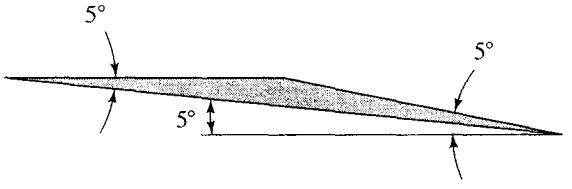


**Figure P8.15**

**8.16** A supersonic jet plane is flying horizontally at 150 m above ground level at a Mach number of 2.5. (See Figure P8.16.) The airfoil is symmetric and diamond shaped, with $2\Delta = 10°$ and a chord length of 4 m. As the plane passes over, an observer on the ground hears the "sonic boom" caused by the shockwaves. Find the time between the two booms, one from the shock at the leading edge and one from the shock at the trailing edge. Ambient pressure and temperature are 100 kPa and 20°C, respectively. Assume that $\gamma = 1.4$.

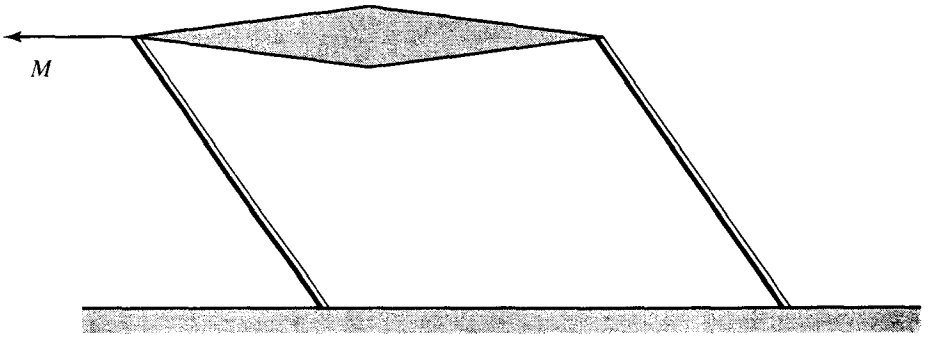


**Figure P8.16**

# Chapter 9

# Flow with Friction

## 9.1 INTRODUCTION

In previous chapters, compressible flow in ducts was analyzed for the case in which changes in flow properties were brought about solely by area change. In a real flow situation, however, frictional forces are present and may have a decisive effect on the resultant flow characteristics. Naturally, the inclusion of friction terms in the equations of motion makes the resultant analysis far more complex. For this reason, to study the effect of friction on compressible flow in ducts, certain restrictions will be placed on the flow.

The first portion of this chapter is concerned with compressible flow with friction in constant-area, insulated ducts, which eliminate the effects of area change and heat addition. In a practical sense, these restrictions limit the applicability of the resultant analysis; however, this approach enables certain problems, such as flow in short ducts, to be handled, and furthermore, it provides insight into the general effects of friction on a compressible flow.

The second section of this chapter investigates gas flow in a constant-area duct that is supplied by a nozzle. It is assumed that the nozzle flow is isentropic and that the flow in the duct is adiabatic. When a converging–diverging nozzle is connected to the duct, a wide range of possible flows emerge, including flows with normal shockwaves. A noniterative method to locate these shocks will be presented.

The third portion of the chapter relaxes the assumption that the flow in a variable-area channel is isentropic. Such flows occur in rocket or turbine nozzles. Numerical procedures for simultaneously handling friction and area change are presented. These procedures require the numerical solution of ordinary differential equations. Several different methods for doing so are introduced.

The analyses presented in this chapter will again be simplified by assuming one-dimensional, steady flow of a perfect gas with constant specific heats. Considerable use will be made of numerical methods facilitated through spreadsheet programs.

## 9.2 FANNO LINE FLOW

Consider one-dimensional, steady flow of a perfect gas with constant specific heats through a constant-area channel. (See Figure 9.1.) For the case of adiabatic flow with no external work, termed *Fanno line flow*, the energy equation [see, for example, Eq. (3.11)] can be written as

$$h + \frac{V^2}{2} = \text{constant} = h_o \tag{9.1}$$

The continuity equation for constant-area steady flow is given by

$$\rho V = \text{constant} \tag{9.2}$$

It is instructive to develop a $T$–$s$ or $h$–$s$ diagram for this flow. From Eq. (1.44), we have

$$Tds = dh - \frac{dp}{\rho} = du - \frac{p}{\rho^2}d\rho$$

so that, for a perfect gas,

$$ds = \frac{du}{T} - R\frac{d\rho}{\rho} \tag{9.3}$$

Assuming constant specific heats, with state 1 a reference state in the flow, Eq. (9.3) may be integrated to produce

$$s - s_1 = c_v \ln\frac{T}{T_1} - R\ln\frac{\rho}{\rho_1}$$

Using the continuity equation (i.e., $\rho/\rho_1 = V_1/V$), we obtain

$$s - s_1 = c_v \ln\frac{T}{T_1} + R\ln\frac{V}{V_1} \tag{9.4}$$

From the energy equation, we have

$$V = \sqrt{2(h_o - h)} = \sqrt{2c_p(T_o - T)} \tag{9.5}$$

so that

$$\frac{s - s_1}{c_v} = \ln\left(\frac{T}{T_1}\right) + \frac{\gamma - 1}{2}\ln\left(\frac{T_o - T}{T_o - T_1}\right) \tag{9.6}$$

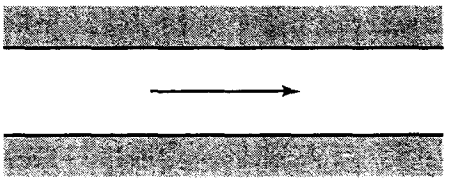

**Figure 9.1** Gas Flow in a Constant-Area, Insulated Duct

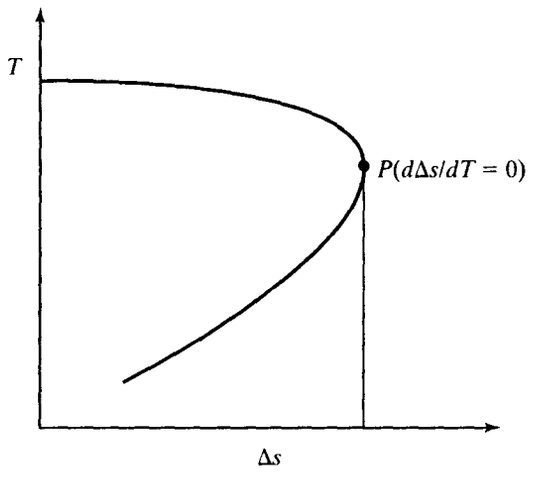


**Figure 9.2** Fanno Line

Since $c_p = \gamma c_v$, Eq. (9.6) may be written as

$$\frac{s - s_1}{c_p} = \frac{1}{\gamma}\ln\left(\frac{T}{T_1}\right) + \frac{\gamma - 1}{2\gamma}\ln\left(\frac{T_o - T}{T_o - T_1}\right) = \frac{1}{\gamma}\ln T + \frac{\gamma - 1}{2\gamma}\ln(T_o - T) + \text{constant} \tag{9.7}$$

Figure 9.2, a sketch of Eq. (9.7), depicts the Fanno line on $T$–$s$ coordinates. Note that for a perfect gas with constant specific heats, $\Delta h = c_p\,\Delta T$, so the $T$–$s$ and $h$–$s$ diagrams differ only by a scale factor.

The curve shown in Figure 9.2 represents the locus of states that can be obtained under the assumptions of Fanno flow for a fixed mass flow and total enthalpy. Consider the point of tangency $P$, where $d\Delta s/dT = 0$. To determine the characteristics of this point, differentiate Eq. (9.6):

$$\frac{1}{c_v}\frac{d\Delta s}{dT} = \frac{1}{T} - \frac{\gamma - 1}{2(T_o - T)} = 0 \quad \text{at point } P$$

However,

$$c_p(T_o - T) = \frac{V^2}{2}$$

Combining these expressions gives

$$V^2 = c_p(\gamma - 1)T$$

Since $c_p = \gamma R/(\gamma - 1)$,

$$V^2 = \gamma RT$$

or

$$V^2 = a^2 \quad \text{for} \quad ds = 0 \tag{9.8}$$

so that $M = 1$ at point $P$ in Figure 9.2.

According to the energy equation, Eq. (9.1), higher velocities are associated with lower enthalpies or temperatures, so the section of the Fanno line on $T$–$s$ coordinates that lies above point $P$ corresponds to subsonic flow, and the section below $P$ to supersonic flow. The Fanno line becomes a most useful tool in describing the variations in properties for this frictional compressible flow. Consider subsonic adiabatic flow in a constant-area tube. The flow is irreversible because of friction, so for this adiabatic case, $ds > 0$. In other words, the entropy increases in the flow direction. Returning to the $T$–$s$ diagram (see Figure 9.3), we see that for a given mass flow, the state of the fluid continually moves to the right, corresponding to an entropy rise. Thus, for subsonic flow with friction, the Mach number increases to unity. For supersonic flow, the entropy must again increase, so the flow Mach number here decreases to unity.

To understand how friction can accelerate a subsonic flow or decelerate a supersonic flow in a constant-area duct, it is helpful to examine the influence that the wall shear stress (which, as we shall soon see, is related to the friction), has on a real flow. Now, the flowfield of a real flow within a duct may be divided into two parts: an inner, very thin wall region where viscous effects are important and the fluid velocity varies with the distance from the wall, and an outer inviscid core region where the fluid velocity may be taken to be uniform. (See Figure 1.2.) The fluid velocity within the wall layer is zero at the pipe wall (this is called the *no-slip condition*) and increases to the value of the outer flow. (See Figure 1.1.) The wall layer is called a *boundary layer*, which grows thicker in the downstream direction. Accordingly, accounting for the wall layer results in a diminishment of the effective area to pass a given amount of flow. Hence, the cross-sectional area $A$ of the inviscid region becomes smaller in the downstream direction (i.e., $dA/dx < 0$). Recall that in Chapter 3, we found that for isentropic flows in geometries whose areas diminished in the flow direction (converging nozzles), subsonic flows were accelerated, while supersonic flows were decelerated. Thus, the effect of friction on subsonic and supersonic flows is attributable to the diminishment of the effective flow area.

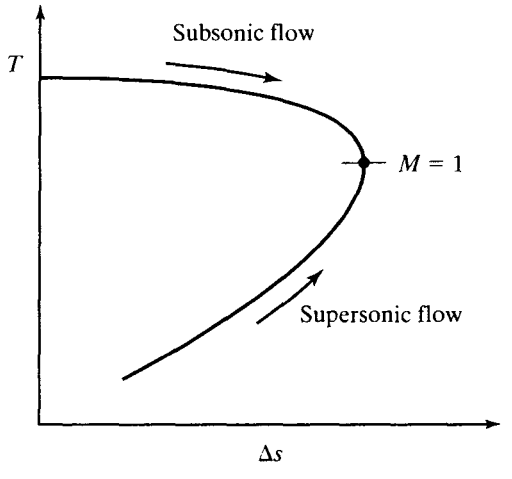


**Figure 9.3** Effect of Mach Number on Fanno Flow

**Example 9.1. Construction of the Fanno line for flow from a given reference state**

Draw the $T$–$s$ diagram for the adiabatic flow of a gas with $\gamma = 1.3$ in a constant-diameter pipe with friction. The reference Mach number $M_1$ for the flow is 3.0.

**Solution**

The reference Mach number is related to the stagnation-to-static-temperature ratio by the following relation:

$$\frac{T_o}{T_1} = 1 + \frac{\gamma - 1}{2} M_1^2 = 1 + \left(\frac{1.3 - 1}{2}\right)(3)^2 = 2.3500$$

Equation (9.7) may now be written as

$$\frac{\Delta s}{c_p} = \frac{1}{\gamma}\ln\left(\frac{T}{T_1}\right) + \frac{\gamma - 1}{2\gamma}\ln\left(\frac{T_o - T}{T_o - T_1}\right) = \ln\left\{\left(\frac{T_o/T_1}{T_o/T}\right)^{1/\gamma}\left[\left(\frac{T_o/T_1}{T_o/T}\right)\left(\frac{T_o/T - 1}{T_o/T_1 - 1}\right)\right]^{(\gamma-1)/2\gamma}\right\}$$

$$= \ln\left\{\left(\frac{2.35}{T_o/T}\right)^{1/1.3}\left[\left(\frac{2.35}{T_o/T}\right)\left(\frac{\frac{T_o}{T} - 1}{2.35 - 1}\right)\right]^{0.3/2.6}\right\} = \ln\left[\frac{2.0569}{(T_o/T)^{0.8846}}\left(\frac{T_o}{T} - 1\right)^{0.1154}\right]$$

In this expression, there are two values of $T_o/T$ that will cause $\Delta s/c_p$ to vanish. Clearly, both will cause the argument of the natural log function to be exactly equal to unity. One value occurs at $T_o/T_1$ (i.e., when $T = T_1$). Because of the nonlinearity of the function involving $T_o/T$, the other value must be found numerically. This task is readily accomplished using a spreadsheet program to implement the Newton–Raphson method. The results are

$$\left(\frac{T_o}{T}\right)_{\Delta s=0} = 1.001959 = 1 + \frac{1.3 - 1}{2} M_{\Delta s=0}^2$$

or

$$M_{\Delta s=0} = 0.1143$$

The coordinates for the Fanno line at this reference state are shown in Table 9.1. Figure 9.4 is a plot of these data.

**TABLE 9.1** Coordinates of the Fanno Line of Example 9.1

| $M$ | $\Delta s/c_p$ | $T/T_l$ | $M$ | $\Delta s/c_p$ | $T/T_l$ |
|---|---|---|---|---|---|
| 0.1143 | 0.0000 | 2.3454 | 1.65 | 0.3144 | 1.6666 |
| 0.31 | 0.2171 | 2.3173 | 1.85 | 0.2786 | 1.5553 |
| 0.50 | 0.3095 | 2.2654 | 2.04 | 0.2382 | 1.4479 |
| 0.69 | 0.3559 | 2.1928 | 2.23 | 0.1943 | 1.3457 |
| 0.88 | 0.3758 | 2.1035 | 2.42 | 0.1478 | 1.2496 |
| 1.08 | 0.3775 | 2.0022 | 2.62 | 0.0996 | 1.1600 |
| 1.27 | 0.3659 | 1.8930 | 2.81 | 0.0502 | 1.0768 |
| 1.46 | 0.3441 | 1.7801 | 3.00 | 0.0000 | 1.0000 |

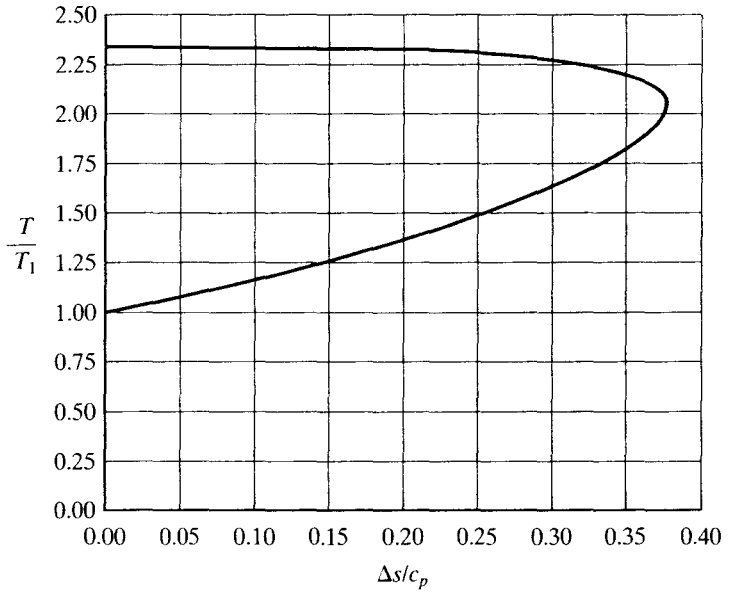


**Figure 9.4** Fanno Line for a Given Reference State

Suppose now that the duct is long enough for a flow initially subsonic to reach Mach 1 and that an additional length is added, as shown in Figure 9.5. Thus, $\Delta s = (\Delta s)_{1-\text{sonic}} + (\Delta s)_{\text{extra}}$. The flow Mach number for the given mass flow cannot exceed unity without decreasing the entropy [i.e., $(\Delta s)_{\text{extra}} < 0$]. However, from the second law of thermodynamics, this is impossible for an adiabatic flow. Hence, the additional length brings about a reduction in mass flow; the flow jumps to another Fanno line. (See Figure 9.6.) Essentially, the duct is choked due to friction. Corresponding to a given inlet subsonic Mach number, there is a certain maximum duct length $L_{\text{max}}$ beyond which a flow reduction occurs.

Now suppose the inlet flow is supersonic and the duct length is made greater than the $L_{\text{max}}$ required to produce Mach 1. With the supersonic flow unable to "sense" changes in duct length occurring ahead of it, the flow adjusts to the additional length by means of a normal shock rather than a flow reduction. The location of the shock in the duct is determined by the back pressure imposed on the duct. (This process will be covered in detail later in this chapter.)

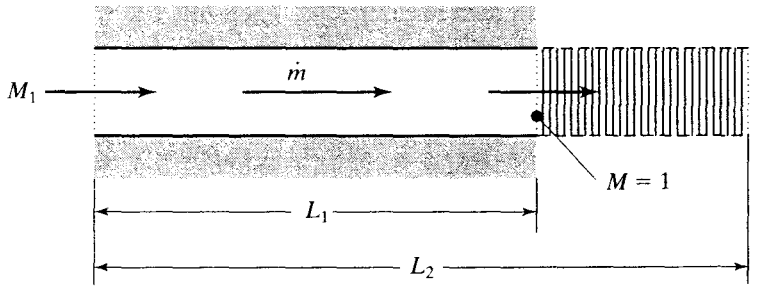


**Figure 9.5** Lengthening a Duct Containing a Subsonic Stream So That the Flow Can Reach Mach 1 at the Exit

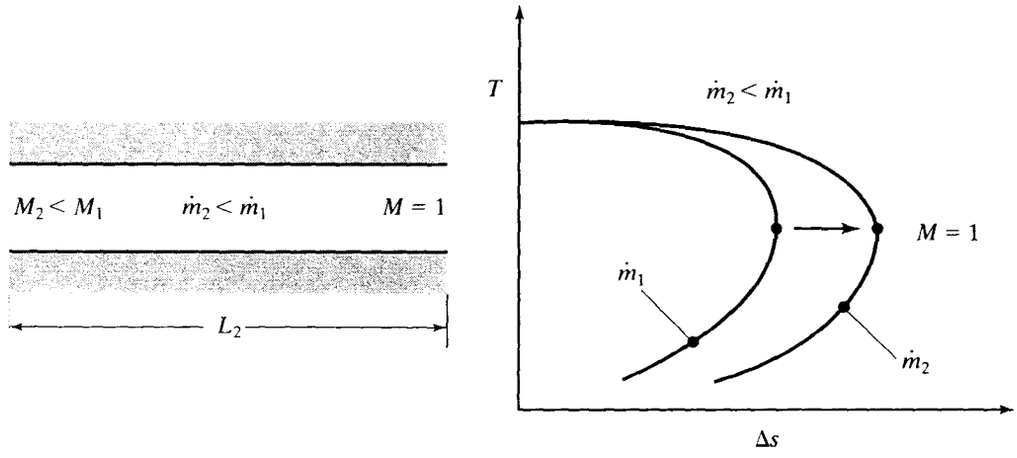


**Figure 9.6** Mass-Flow Rate Reduction Due to Lengthening of a Duct of a Flow That Has Reached Mach 1

**Historical Note: Gino Fanno** (1882–1962) was the son of a wholesale grocery dealer. His family lived in the Hebrew quarter of Conegliano. At age 13, Fanno was enrolled in a Venice technical institute. At age 17, he moved to Zürich to enroll in the Federal Polytechnic. He graduated officially (without a thesis) with a diploma in mechanical engineering in July 1904, and that October, he became Professor Aurel Stodola's (1859–1942) temporary assistant. In a footnote on p. 61 of Stodola's famous *Steam and Gas Turbines* (1927), Fanno's work on the Fanno line is described as *eine Diplomarbeit* (a diploma thesis). This was to be his only technical contribution, but one that has put him in all books describing compressible flows in tubes.

In 1907, Fanno joined the San Giorgio Company, where, by 1926, he had progressively risen to managing director of the Genova–Sestri branch, which manufactured large gas-turbine engines and electric motors. In July 1935, Fanno received the degree Dottore in Ingegneria Industriale from the Regia Istituto Superiore d'Ingegneria di Genova. In January 1939, the Fascist anti-Jewish policy in Italy compelled him to relinquish his position with San Giorgio. However, he was made "general consultant" to the company. During the Fascist years, to escape persecution, he moved to his farm near the village of Fucècchio and to other isolated villages. After the war, Fanno returned to San Giorgio. He was vice president of the company when he retired in 1953. At that time, he was appointed managing director and general manager of CO-GE-I, a company engaging in design and setup of plants abroad. In 1957, he retired to private life. In 1960, after a heart attack, Fanno became paralyzed in both legs. He died in Genoa in 1962. See Refs. (9.1)–(9.3).

## 9.3 WORKING RELATIONS FOR FANNO FLOW

From practical considerations, it is necessary to determine the change in properties with actual duct length. This requires the use of the momentum equation, with a term accounting for the frictional forces acting on the control volume. Select a control volume as shown

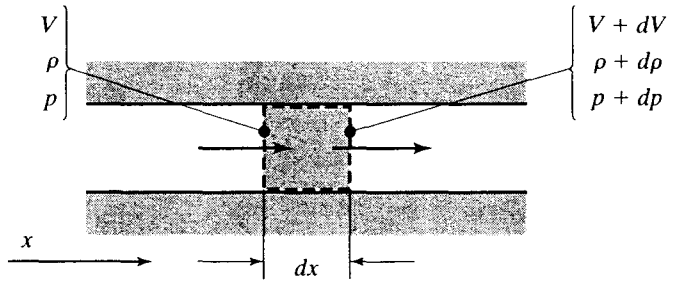


**Figure 9.7** Differential Control Volume for Fanno Flow Analysis

in Figure 9.7. The forces acting on the control volume are shown in Figure 9.8, where

$\tau_f$ = shear stress due to wall friction
$A_s$ = surface area over which the friction acts
$A$ = cross-sectional area of the duct

Applying the momentum equation for steady flow, we get

$$\sum F_x = \iint_{\text{C.S.}} V_x(\rho \mathbf{V} \cdot d\mathbf{A})$$

$$pA - (p + dp)A - \tau_f A_s = (\rho AV)(V + dV) - (\rho AV)V$$

$$-Adp - \tau_f A_s = \rho AV dV \tag{9.9}$$

Define the *hydraulic diameter* as

$$D_h = 4\frac{\text{Cross-Sectional Area}}{\text{Wetted Perimeter}} = \frac{4A}{P} \tag{9.10}$$

For a circular duct,

$$D_h = \frac{4(\pi D^2/4)}{\pi D} = D$$

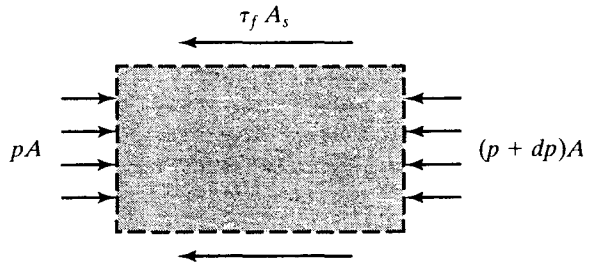


**Figure 9.8** Forces Acting on the Differential Control Volume Used in Fanno Flow Analysis

For a square duct, where $S$ = the width of each side,

$$D_h = \frac{4S^2}{4S} = S$$

Since the area over which friction acts, $A_s$, is equal to the perimeter of the duct times the incremental length $dx$, it may be replaced using the hydraulic diameter to obtain

$$-A dp - \tau_f (dx) \frac{4A}{D_h} = \rho A V dV \tag{9.11}$$

As is done for an incompressible flow [e.g., see Ref. (9.4)], define a *friction coefficient*

$$f \equiv 4\tau_f / (\tfrac{1}{2}\rho V^2)$$

where $f$ is dependent on the flow Reynolds number and the relative wall roughness $\varepsilon/D_h$. However, since $\text{Re} = \rho V D/\mu = 4\dot{m}/(\pi D\mu)$, for Fanno flow, the flow rate and the diameter are constant, and assuming constant dynamic viscosity $\mu$, we see that the Reynolds number is also constant and therefore does not affect the friction coefficient.

It should be noted that the grouping $\tau_f/(\frac{1}{2}\rho V^2)$ is defined as the *skin friction coefficient* $C_f$. [See Ref. (9.5).] In essence, it is a nondimensional shear stress. Thus, $f = 4C_f$. Some texts [e.g., see Refs. (9.6), (9.7), and (9.8)] define a friction coefficient "$f$" $= \tau_f/(\frac{1}{2}\rho V^2) = C_f$; that is, they use the skin friction coefficient as the friction coefficient. The friction coefficient in those texts is referred to as the *Fanning friction factor.* The friction coefficient used here is sometimes referred to as the *Darcy friction factor.* The relation between the two friction coefficients is $f = 4$"$f$".

Equation (9.11) therefore becomes

$$-dp - \frac{1}{2}\rho V^2 f \frac{dx}{D} = \rho V dV \tag{9.12}$$

It is desirable to integrate Eq. (9.12) to obtain, for example, an expression for Mach number and pressure change over a given duct length. First we divide the foregoing equation by $p$:

$$\frac{dp}{p} + \frac{1}{2}\gamma M^2 f \frac{dx}{D} + \gamma M^2 \frac{dV}{V} = 0 \tag{9.13}$$

To obtain an expression for $M$ in terms of $x$, $dV/V$ and $dp/p$ must be replaced in Eq. (9.13). From continuity, $\rho V$ = constant. Using the perfect-gas law ($\rho = p/RT$) and the definition of Mach number $\left(V = Ma = M\sqrt{\gamma RT}\right)$, we get

$$\rho V = \frac{p}{RT}\sqrt{\gamma RT}\frac{V}{\sqrt{\gamma RT}} = \sqrt{\frac{\gamma}{R}}\left(\frac{pM}{\sqrt{T}}\right) = \text{constant}$$

Taking the logarithm of this expression and then differentiating produces

$$\frac{dp}{p} = -\frac{dM}{M} + \frac{1}{2}\frac{dT}{T} = 0$$

Moreover, from the definition of the Mach number $\left(V = Ma = M\sqrt{\gamma RT}\right)$, we have

$$\frac{dV}{V} = \frac{dM}{M} + \frac{1}{2}\frac{dT}{T}$$

Substituting this expression into Eq. (9.13), we obtain

$$\left(-\frac{dM}{M} + \frac{1}{2}\frac{dT}{T}\right) + \frac{1}{2}\gamma M^2\left(f\frac{dx}{D}\right) + \gamma M^2\left(\frac{dM}{M} + \frac{1}{2}\frac{dT}{T}\right) = 0$$

or

$$\left(f\frac{dx}{D}\right) = -\frac{2}{\gamma M^2}\left(-\frac{dM}{M} + \frac{1}{2}\frac{dT}{T}\right) - 2\left(\frac{dM}{M} + \frac{1}{2}\frac{dT}{T}\right)$$

$$= \frac{2}{\gamma}\frac{dM}{M^3} - \frac{dM^2}{M^2} - \frac{dT}{T} - \frac{1}{\gamma M^2}\frac{dT}{T}$$

But, for this adiabatic flow, $T_o$ = constant, so

$$T\left(1 + \frac{\gamma - 1}{2}M^2\right) = \text{constant}$$

Taking the logarithm of this expression and then differentiating produces

$$\frac{dT}{T} + \frac{d\left(1 + \frac{\gamma - 1}{2}M^2\right)}{1 + \frac{\gamma - 1}{2}M^2} = 0 \tag{9.14}$$

Substituting and rearranging yields

$$f\frac{dx}{D} = \frac{2}{\gamma}\frac{dM}{M^3} - \frac{dM^2}{M^2} + \frac{d\left(1 + \frac{\gamma - 1}{2}M^2\right)}{1 + \frac{\gamma - 1}{2}M^2} + \left(\frac{1}{\gamma M^2}\right)\frac{d\left(1 + \frac{\gamma - 1}{2}M^2\right)}{1 + \frac{\gamma - 1}{2}M^2}$$

The coefficient of the last term may be written in an alternative form:

$$\frac{1}{(\gamma M^2)\left(1 + \frac{\gamma - 1}{2}M^2\right)} = \frac{c_1}{(\gamma M^2)} + \frac{c_2}{\left(1 + \frac{\gamma - 1}{2}M^2\right)}$$

Expanding the right-hand side and comparing the numerator of both sides reveals that $c_1 = 1$ and $c_2 = -(\gamma - 1)/(2\gamma)$. Thus, the last term in the friction differential equation may be expressed as two terms:

$$\left(\frac{1}{\gamma M^2}\right)\frac{d\left(1 + \dfrac{\gamma - 1}{2}M^2\right)}{1 + \dfrac{\gamma - 1}{2}M^2} = \frac{\gamma - 1}{2\gamma}\frac{d(M^2)}{M^2} - \frac{\gamma - 1}{2\gamma}\frac{d\left(1 + \dfrac{\gamma - 1}{2}M^2\right)}{1 + \dfrac{\gamma - 1}{2}M^2}$$

Finally, then,

$$f\frac{dx}{D} = \left(\frac{\gamma + 1}{2\gamma}\right)\frac{d\left(1 + \dfrac{\gamma - 1}{2}M^2\right)}{1 + \dfrac{\gamma - 1}{2}M^2} + \frac{2}{\gamma}\frac{dM}{M^3} - \left(\frac{\gamma + 1}{2\gamma}\right)\frac{d(M^2)}{M^2} \tag{9.15}$$

This equation may be integrated term by term to determine $M$ as a function of duct length. It is convenient for Fanno flow (frictional, constant-area, adiabatic flow) to choose, as a reference point, $M = 1$ and $L = L_{max}$. For the lower limit of integration, select $x = 0$ at $M = M$. Thus,

$$\frac{fL_{max}}{D} = \left(\frac{\gamma + 1}{2\gamma}\right)\ln\left(\frac{\dfrac{\gamma + 1}{2}}{1 + \dfrac{\gamma - 1}{2}M^2}\right) - \frac{1}{\gamma}\left(1 - \frac{1}{M^2}\right) - \left(\frac{\gamma + 1}{2\gamma}\right)\ln\left(\frac{1}{M^2}\right) \tag{9.16}$$

Values of $fL_{max}/D$ may be readily tabulated against $M$. Note that $M$ may be subsonic or supersonic. As $M \to \infty$, Eq. (9.16) reveals that $(fL_{max}/D) \to [(\gamma + 1)/(2\gamma)]$ $\ln[(\gamma + 1)/(\gamma - 1)] - 1/\gamma$. For $\gamma = 1.4$, this limiting value is 0.8215. Clearly, for $M = 1, fL_{max}/D = 0$. Thus, for supersonic flows, this factor lies between 0 and 0.8215 for $\gamma = 1.4$. For subsonic flows, $fL_{max}/D$ can be quite large for small Mach numbers (e.g., at $M = 0.1, fL_{max}/D = 66.9216$). Figure 9.9 is a plot of $fL_{max}/D$ against $M$ for $\gamma = 1.4$.

If it is required to find $p$ versus $M$ or $(fdx/D)$, $dV/V$ can be eliminated from Eq. (9.13):

$$\frac{dp}{p} + \frac{1}{2}\gamma M^2 f\frac{dx}{D} + \gamma M^2\frac{dM}{M} - \frac{1}{2}\frac{\gamma M^2(\gamma - 1)M^2}{1 + \dfrac{\gamma - 1}{2}M^2}\frac{dM}{M} = 0$$

To obtain a single expression for the pressure, written in terms of Mach number, we must eliminate $f(dx/D)$ from the preceding equation. To accomplish this, rewrite Eq. (9.15) in a more compact form:

$$f\frac{dx}{D} = \left[\frac{(1 - M^2)}{1 + \dfrac{\gamma - 1}{2}M^2}\right]\left(\frac{2}{\gamma M^2}\right)\frac{dM}{M}$$

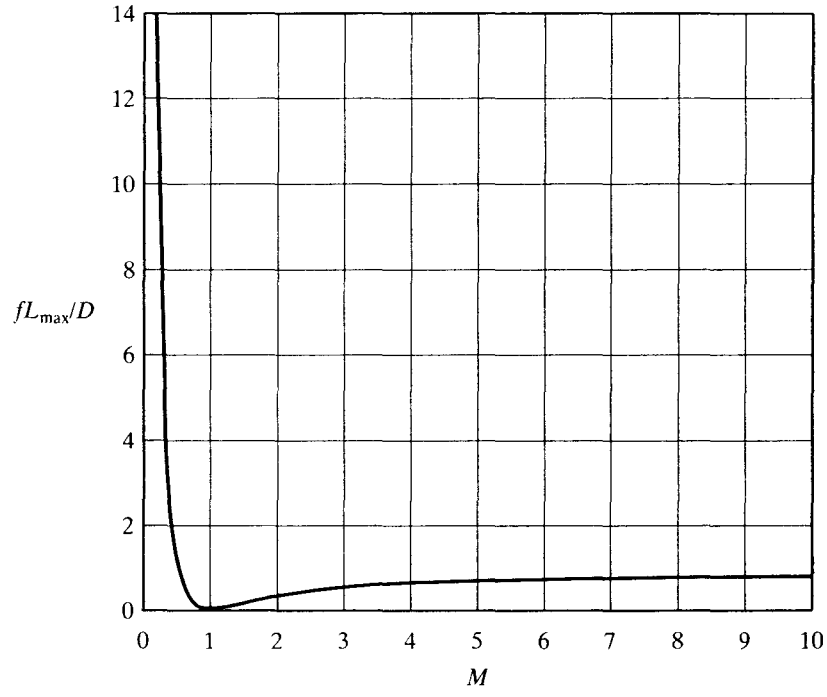


**Figure 9.9** $fL_{max}/D$ versus the Mach Number for $\gamma = 1.4$

Note that the coefficient of $dM/M$ is positive for $M < 1$ and negative for $M > 1$. This confirms the concept that for steady, adiabatic, frictional flows in a constant-area duct, the Mach number will increase with $x$ if the flow is subsonic and decrease with $x$ if the flow is supersonic. Substituting for $f(dx/D)$, we obtain

$$\frac{dp}{p} + \frac{1 - M^2}{1 + \dfrac{\gamma - 1}{2}M^2}\frac{dM}{M} + \gamma M^2\frac{dM}{M} - \frac{1}{2}\frac{\gamma M^2(\gamma - 1)M^2}{1 + \dfrac{\gamma - 1}{2}M^2}\frac{dM}{M} = 0$$

Collecting terms yields

$$\frac{dp}{p} = -\left[\frac{1 + (\gamma - 1)M^2}{1 + \dfrac{\gamma - 1}{2}M^2}\right]\frac{dM}{M} \tag{9.17}$$

The integration of this expression is easily accomplished by dividing the numerator on the right-hand side, $1 + (\gamma - 1)M^2$, into two pieces: $1 + (\gamma - 1)M^2/2$ and $(\gamma - 1)M^2/2$. The resulting expression may be directly integrated term by term. The

pressure limits of integration are $p$ and $p^*$, where $^*$ denotes the value of a property at Mach 1. Now we have

$$\int_p^{p^*} \frac{dp}{p} = -\int_M^1 \left[\frac{1 + \dfrac{\gamma - 1}{2}M^2}{1 + \dfrac{\gamma - 1}{2}M^2}\right]\frac{dM}{M} - \int_M^1 \left[\frac{\dfrac{\gamma - 1}{2}M^2}{1 + \dfrac{\gamma - 1}{2}M^2}\right]\frac{dM}{M}$$

$$\ln\left(\frac{p}{p^*}\right) = \ln\left(\frac{1}{M}\right) + \frac{1}{2}\ln\left[\frac{\gamma + 1}{2 + (\gamma - 1)M^2}\right] = \ln\left\{\left(\frac{1}{M}\right)\left[\frac{\gamma + 1}{2 + (\gamma - 1)M^2}\right]^{1/2}\right\} \quad (9.18)$$

Therefore,

$$\frac{p}{p^*} = \left(\frac{1}{M}\right)\left[\frac{\gamma + 1}{2 + (\gamma - 1)M^2}\right]^{1/2} \quad (9.19)$$

Equation (9.19) can be found by an alternative approach that has the advantage of not requiring integration. Since we are dealing with adiabatic flow of a perfect gas, the total temperature remains constant. Therefore, we may write the static temperature ratio for any two points in the flow as

$$\frac{T_1}{T_2} = \left(\frac{T_o}{T_2}\right)\left(\frac{T_1}{T_o}\right) = \frac{1 + \dfrac{\gamma - 1}{2}M_2^2}{1 + \dfrac{\gamma - 1}{2}M_1^2} = \frac{2 + (\gamma - 1)M_2^2}{2 + (\gamma - 1)M_1^2} \quad (9.20)$$

Because the flow area and flow rate are constant, we have from the continuity equation that

$$\rho_1 V_1 = \rho_2 V_2$$

The gas density can be expressed using the perfect-gas law, $\rho = p/(RT)$, and the velocity can be written in terms of the Mach number and the speed of sound: $V = Ma = M\sqrt{\gamma RT}$. Inserting these relations and rearranging gives

$$\frac{p_1}{p_2} = \frac{M_2}{M_1}\sqrt{\frac{T_1}{T_2}} \quad (9.21)$$

Combining Eqs. (9.20) and (9.21) gives the ratio of static pressures at any two points in the duct:

$$\frac{p_1}{p_2} = \frac{M_2}{M_1}\left[\frac{2 + (\gamma - 1)M_2^2}{2 + (\gamma - 1)M_1^2}\right]^{1/2} \quad (9.22)$$

The density ratio follows immediately from the perfect-gas relation:

$$\frac{\rho_1}{\rho_2} = \frac{p_1}{RT_1}\frac{RT_2}{p_2} = \frac{p_1}{p_2}\frac{T_2}{T_1} = \frac{M_2}{M_1}\left[\frac{2 + (\gamma - 1)M_1^2}{2 + (\gamma - 1)M_2^2}\right]^{1/2} = \frac{V_2}{V_1} \quad (9.23)$$

Because of the irreversibilities involved with Fanno flow, the total pressure will always decrease in the direction of flow, which is not the case for isentropic flow. An expression for this variation can be obtained as follows:

$$\frac{p_{o1}}{p_{o2}} = \frac{p_{o1}}{p_1}\frac{p_1}{p_2}\frac{p_2}{p_{o2}} = \left(1 + \frac{\gamma - 1}{2}M_1^2\right)^{\frac{\gamma}{\gamma-1}} \frac{M_2}{M_1}\left[\frac{2 + (\gamma - 1)M_2^2}{2 + (\gamma - 1)M_1^2}\right]^{1/2}\left(1 + \frac{\gamma - 1}{2}M_2^2\right)^{-\frac{\gamma}{\gamma-1}}$$

Simplification results in

$$\frac{p_{o1}}{p_{o2}} = \frac{M_2}{M_1}\left[\frac{2 + (\gamma - 1)M_1^2}{2 + (\gamma - 1)M_2^2}\right]^{\frac{\gamma+1}{2(\gamma-1)}} \tag{9.24}$$

Because the flow is also one dimensional and adiabatic, the equations for the conservation of mass and energy, but not momentum, for flow through a normal shock wave are the same as that for Fanno flow. Hence, from Chapter 4, we have

$$\frac{s_2 - s_1}{R} = -\ln\left(\frac{p_{o2}}{p_{o1}}\right) \tag{4.14}$$

Combining this relation with Eq. (9.24) enables the computation of the entropy change for this flow.

For computational purposes, the reference state where the Mach number reaches unity is used, and, as mentioned previously, the symbol for this state is $^*$. Removing the subscripts 1, allowing $M_2$ to be equal to unity, and replacing subscripts 2 with $^*$ will produce computational forms of the foregoing expressions. This process yields the following set of equations:

$$\frac{T_1}{T_2} = \frac{T}{T^*} = \frac{2 + (\gamma - 1)1^2}{2 + (\gamma - 1)M^2} = \frac{(\gamma + 1)}{2 + (\gamma - 1)M^2} \tag{9.25}$$

$$\frac{p}{p^*} = \left(\frac{1}{M}\right)\left[\frac{\gamma + 1}{2 + (\gamma - 1)M^2}\right]^{1/2} \tag{9.26}$$

$$\frac{\rho}{\rho^*} = \frac{V^*}{V} = \frac{1}{M}\left[\frac{2 + (\gamma - 1)M^2}{(\gamma + 1)}\right]^{1/2} \tag{9.27}$$

$$\frac{p_o}{p_o^*} = \frac{1}{M}\left[\frac{2 + (\gamma - 1)M^2}{(\gamma + 1)}\right]^{\frac{\gamma+1}{2(\gamma-1)}} \tag{9.28}$$

With pressure, temperature, density, velocity, total pressure, and the term $fL_{max}/D$ now calculated as functions of $M$ (see, for example, the tables in Appendix F), the variation of the flow variables in a duct can be found in terms of duct length.

Some qualitative conclusions can be drawn concerning the variation of these properties for Fanno flow. For *subsonic flow*, as shown by the $T$–$s$ diagram, static temperature decreases while the Mach number increases to unity. For *supersonic flow*, the opposite occurs; that is, temperature increases while the Mach number decreases to

unity. For subsonic flow, with $dM$ positive, Eq. (9.17) shows that the static pressure decreases. For supersonic flow, however, the static pressure increases. For adiabatic flow with friction, whether the Mach number is subsonic or supersonic, the stagnation pressure decreases, since for both cases there is a loss of available energy. (See Section 4.3.)

**Example 9.2. Determination of the exit conditions for gas flow in a constant-diameter pipe with friction**

Flow enters a constant-area, insulated duct (see Figure 9.10) with a Mach number of 0.60, static pressure of 150 kPa, and static temperature of 300 K. Assume a duct length of 45 cm, a duct diameter of 3 cm, and a friction coefficient of 0.02. Determine the Mach number, static pressure, and static temperature at the duct outlet. Assume that $\gamma = 1.4$.

**Solution**

From Eq. (9.16) (tabulated in Appendix F), at $M_1 = 0.60$, $(fL_{max}/D)_1 = 0.4908$, where $L_{max}$ is the duct length required to reach Mach 1. The actual $fL/D$ for the duct, however, is 0.30. Therefore, as can be seen from Figure 9.10,

$$(L_{max})_2 = (L_{max})_1 - L$$

or

$$\left(\frac{fL_{max}}{D}\right)_2 = \left(\frac{fL_{max}}{D}\right)_1 - \frac{fL}{D} = 0.4908 - 0.30 = 0.1908$$

Thus, from Eq. (9.16) (or the tables in Appendix F), $M_2 = 0.7093$. Also,

$$\frac{p_2}{p_1} = \frac{(p_2/p^*)}{(p_1/p^*)} = \frac{1.4722}{1.7634} = 0.8349$$

$$\frac{T_2}{T_1} = \frac{(T_2/T^*)}{(T_1/T^*)} = \frac{1.0903}{1.1194} = 0.9740$$

or

$$p_2 = (0.8349)150 = 125.2350 \text{ kPa}$$

and

$$T_2 = (0.9740)300 = 292.2012 \text{ K}$$

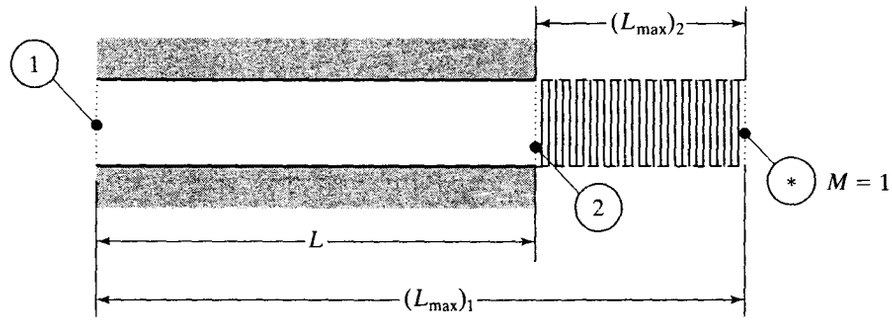


**Figure 9.10** Nomenclature for Calculations of Example 9.2

## 9.4 FLOW THROUGH A NOZZLE AND CONSTANT-AREA DUCT IN SERIES

Very often, a situation occurs where a duct is fed by a nozzle, with the duct back pressure and nozzle stagnation pressure the known quantities. Consider, for example, a duct supplied by a *converging nozzle*, with flow provided by a reservoir at pressure $p_r$. (See Figure 9.11.) Assuming isentropic nozzle flow, with Fanno flow in the duct, the system static pressure distribution $p$ versus the distance $x$ can be determined for various back pressures. ($p_r$ is maintained constant.)

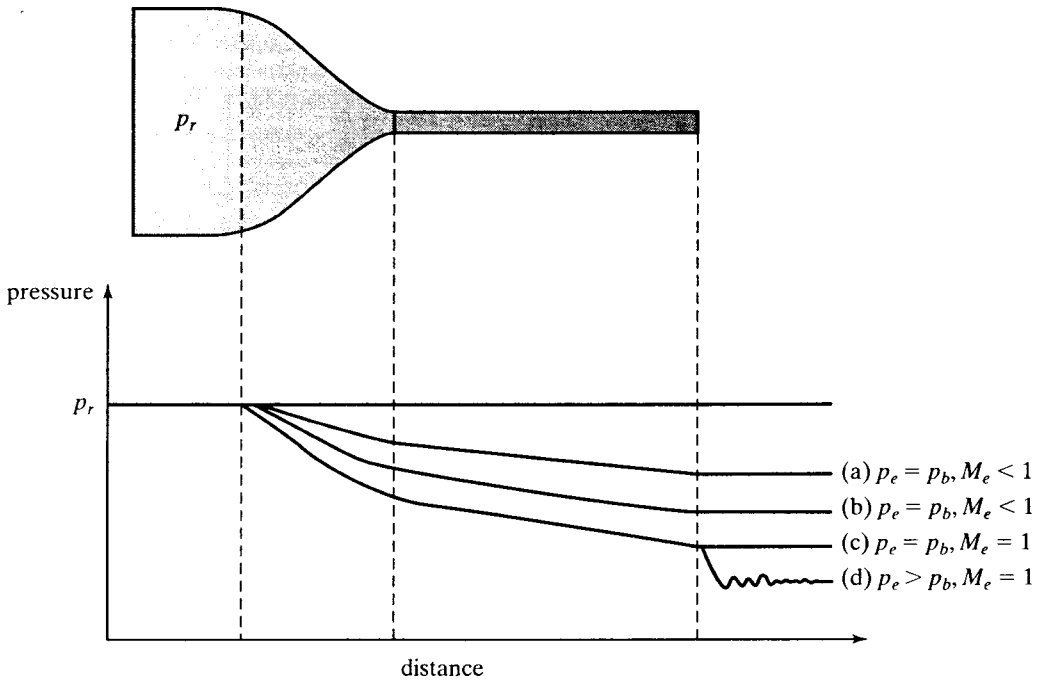


**Figure 9.11** Static Pressure in a Constant-Area Duct That Is Connected to a Reservoir by a Converging Nozzle for Various Back Pressures

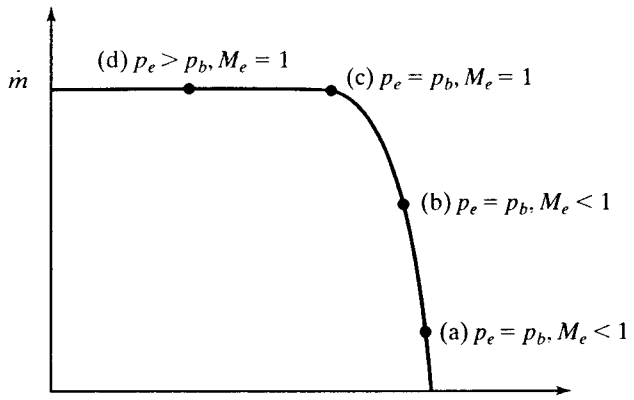


**Figure 9.12** Mass-Flow Rate in Constant-Area Duct $p_b$ That Is Connected to a Converging Nozzle for Various Back Pressures

As $p_b$ is lowered below $p_r$, curves (a) and (b) in Figure 9.11 are obtained, with pressure decreasing in both nozzle and duct. Eventually, when the back pressure is decreased to that of curve (c), Mach number 1 occurs at the *duct exit*. (Note that the Mach number at the *nozzle exit* is still less than unity.) Further decreases in back pressure cannot be "sensed" by the reservoir; for all back pressures below that of curve (c) [e.g., the underexpanded flow at curve (d)], the mass flow rate remains the same as that of curve (c). Figure 9.12 contains a plot of $\dot{m}$ versus $p_b$. The system here is choked by the duct, not by the converging nozzle. The maximum mass flow that can be passed by this system is less for the same reservoir pressure than that for a converging nozzle with no duct.

**Example 9.3. Determination of the maximum flow rate for gas flow in a constant-diameter pipe with friction that is connected to a converging nozzle**

A constant-area duct that is 20 cm in length by 2 cm in diameter is connected to a reservoir through a converging nozzle, as shown in Figure 9.13. For a reservoir pressure and temperature of 1 MPa and 500 K, determine the maximum air flow rate in kilograms per second through the system and the range of back pressures over which this flow is realized. Repeat these calculations for a converging nozzle with no duct. Assume that $f$ is equal to 0.032 and that $\gamma = 1.4$.

**Solution**

For maximum mass flow through the nozzle–duct system, $M_2$ is equal to unity. For this condition, the actual $fL/D$ of the duct becomes equal to $(fL_{max}/D)_1 = 0.32$. Solving Eq. (9.16) for the Mach number, we obtain $M_1 = 0.6517$. It is assumed that the nozzle flow is isentropic. At $M_1 = 0.6517$, $(p/p_o)_1 = 0.7518$ and $(T/T_o)_1 = 0.9217$, or, for a choked duct, $p_1 = (0.7518)1{,}000 = 751.8$ kPa and $T_1 = (0.9217)500 = 460.85$ K. Now,

$$\dot{m}_{max} = \left(\frac{p}{RT}\right)_1 A_1 M_1 \sqrt{\gamma R T_1}$$

$$= \left[\frac{(751.8)}{(0.287)(460.85)}\right]\left[\frac{\pi}{4}(4 \times 10^{-4})\right]\left[(0.6517)\sqrt{(1.4)(287)(460.85)}\right]$$

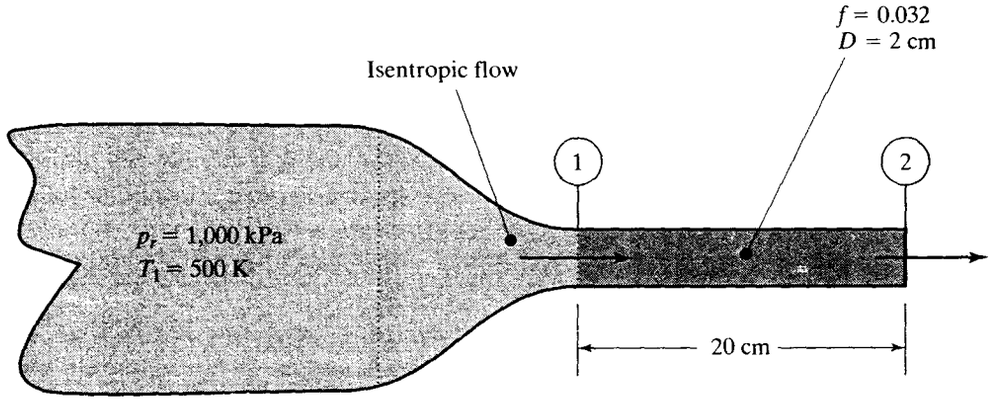


**Figure 9.13** Nomenclature and Physical Arrangement for the Flow of Example 9.3

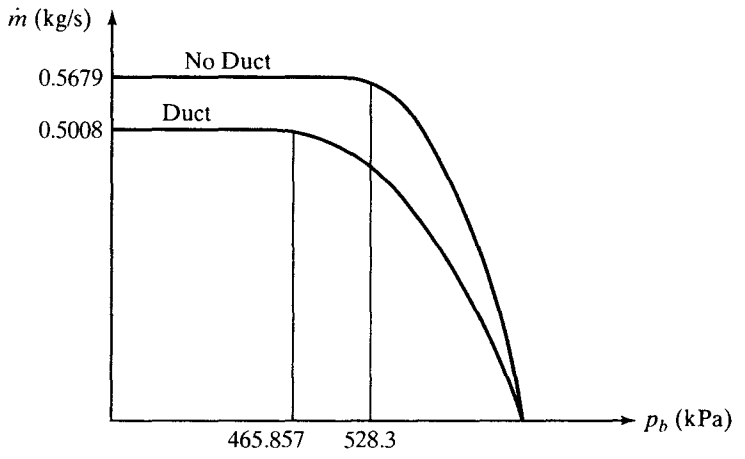


**Figure 9.14** Comparison of Mass Flow Rates in a Converging Nozzle with and without a Constant-Area Duct

$$\dot{m}_{max} = (5.6841 \text{ kg/m}^3)(0.00031416 \text{ m}^2)(280.4352 \text{ m/s})$$
$$= 0.5008 \text{ kg/s}$$

Also, $p_2/p_1 = p^*/p_1 = 1/1.6138$, or $p^* = 751.8/1.6138 = 465.8570$ kPa, so the system is choked over the range of back pressures from 0 to 465.8570 kPa.

If the duct were to be removed, choking would occur with Mach 1 at the nozzle exit. For this condition, $p_1 = (0.5283)(1{,}000) = 528.3$ kPa and $T_1 = 0.8333(500 \text{ K}) = 416.65$ K, so the maximum mass flow rate is $(4.4180)(0.00031416)(409.1576) = 0.5679$ kg/s. For this case, the system is choked over the back-pressure range from 0 to 528.3 kPa. The results are shown in Figure 9.14.

---

When a duct is connected to a reservoir through a *converging–diverging nozzle*, the situation becomes somewhat more complex. Consider first the case of subsonic flow in both nozzle and duct. A typical pressure distribution is shown in Figure 9.15. Depending on the duct length, the minimum pressure point, or point of maximum Mach number, can occur at the nozzle throat or duct exit. If the duct is long enough (see the dashed curve in the figure), the system reaches Mach 1 first at the duct exit; in this case, the nozzle is not choked. Once Mach 1 is reached, no further increase in mass flow rate can occur by reduction of the system back pressure. Supersonic flow in this system is impossible with the converging–diverging nozzle unchoked. Generally, however, the duct length required to cause choking is very long. For this reason, the more important case is that in which the system is choked at the nozzle throat and supersonic flow can occur in the duct.

With supersonic flow at the nozzle exit, there is the possibility of shocks in the duct. Note, however, that once the back pressure is just low enough to produce Mach 1 at the nozzle throat, the system is choked, with no further increase in mass

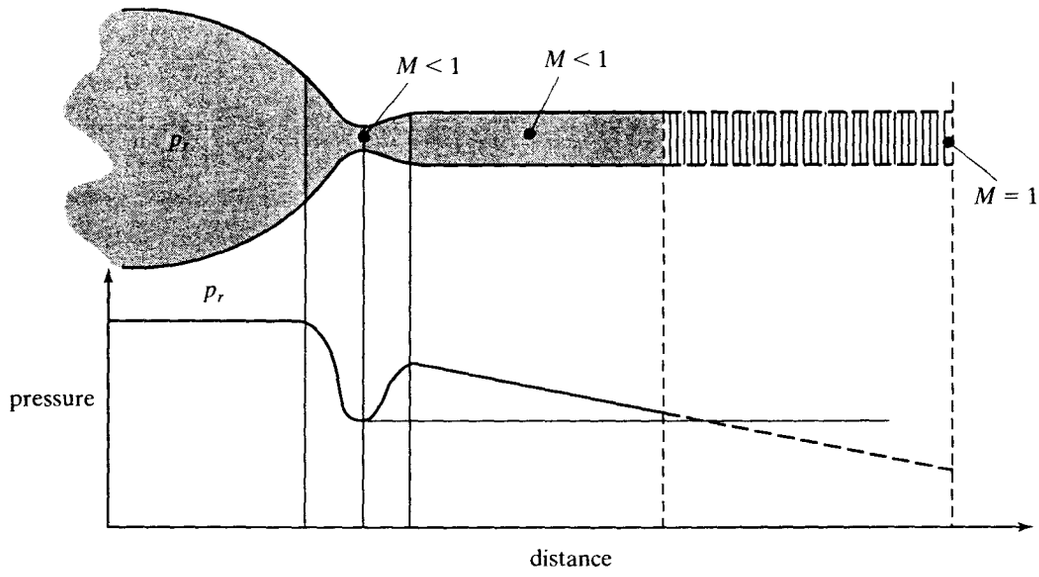


**Figure 9.15** Pressure Distribution of a Subsonic Flow in a Duct Connected to a Reservoir by a C–D Nozzle

flow possible. Unlike the case previously discussed, in which a converging nozzle exhausted into the duct and mass flow was affected by duct length, here, once the throat velocity reaches the velocity of sound, the mass flow rate is unaffected by duct length; that is, the conditions at the throat remain fixed, and therefore $\dot{m} = \rho_t A_t V_t$. Now the system is choked by the nozzle, not the duct.

Let us consider the flow pattern obtained with supersonic flow at the duct inlet.

First, suppose the duct length is less than the maximum length corresponding to the given duct inlet supersonic Mach number $M_i$ needed to reach Mach 1 at the exit i.e., $L < (L_{\max})_i$.

The change in flow pattern is to be described as the back pressure $p_b$ is increased from 0 kPa. A back pressure of 0 kPa, or a very low back pressure, implies the existence of expansion waves at the duct exit. This means that the exit Mach number must be either supersonic or unity. Since $L$ is less than $L_{\max}$, supersonic flow occurs at the duct exit, with the exit static pressure $p_e$ greater than $p_b$. [See curve (a) in Figure 9.16.] When $p_b$ is raised to a value corresponding to curve (b), the exit-plane pressure is equal to the back pressure. A further increase in back pressure yields oblique shockwaves at the duct exit [curve (c)] until eventually, for a back pressure equal to that of curve (d), a normal shock stands at the duct exit. It can be seen that the flow described is exactly the same as that obtained at the exit of a converging–diverging nozzle. (See Section 5.2.) Increases in back pressure over that of curve (d) cause the shock to move into the duct. For a high-enough back pressure, the shock moves into the nozzle, thus eliminating supersonic flow in the duct.

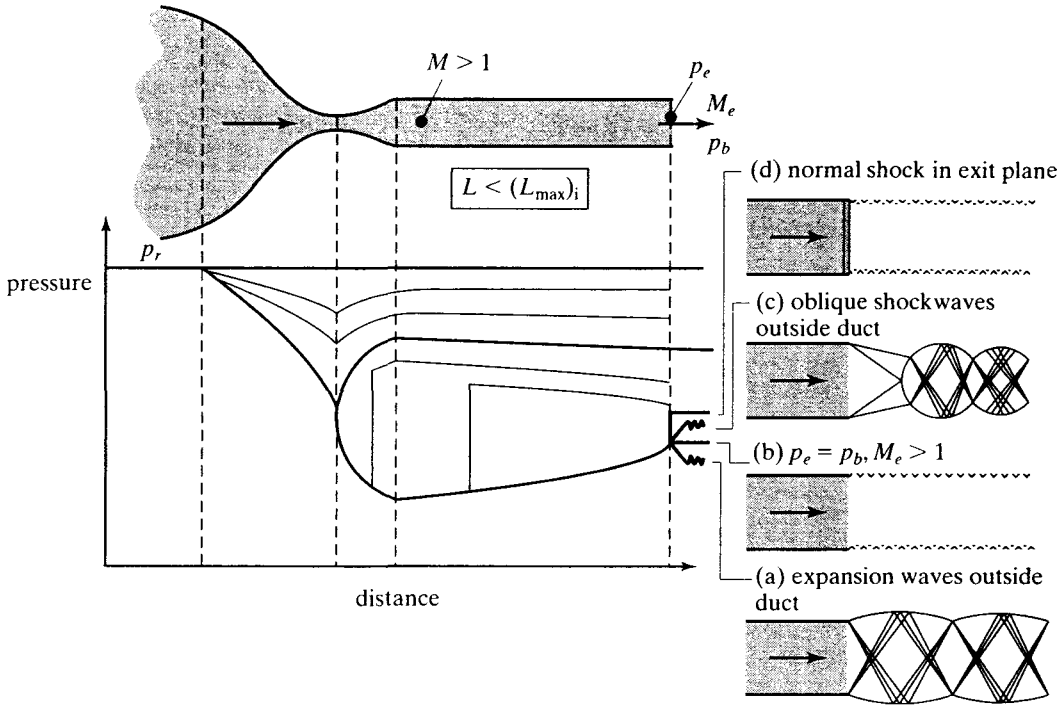


**Figure 9.16** Pressure Distribution in a Constant-Area Duct Connected to a Reservoir by a C–D Nozzle

**Example 9.4. Determination of the pressure range over which a normal shock appears in a constant-diameter duct with friction that is connected to reservoir by a C–D nozzle**

A converging–diverging nozzle with area ratio of 2 to 1 is supplied by a reservoir containing air at 500 kPa. The nozzle exhausts into a constant-area duct of length-to-diameter ratio of 10 and friction coefficient $f$ of 0.02. Determine the range of system back pressures over which a normal shock appears in the duct. Assume isentropic flow in the nozzle and Fanno flow in the duct. Assume that $\gamma = 1.4$.

**Solution**

From isentropic relations, at $(A/A^*)_1 = 2.0$, $M_1 = 2.1972$. At this Mach number, $(fL_{max}/D)_1 = \&0.3602$. For the duct under consideration, $fL/D = 0.20$, so that $L < (L_{max})_1$. Calculations must be made for two limiting cases (see Figure 9.17), one with shock at the duct inlet and the other with shock at the duct outlet.

*Shock at the duct inlet*: $M_1 = 2.1972$.

From the normal-shock relations, $M_2 = 0.5474$. At this Mach number, $(fL_{max}/D)_2 = 0.7429$. Thus,

$$\left(\frac{fL_{max}}{D}\right)_3 = \left(\frac{fL_{max}}{D}\right)_2 - \frac{fL}{D} = 0.7429 - 0.20 = 0.5427$$

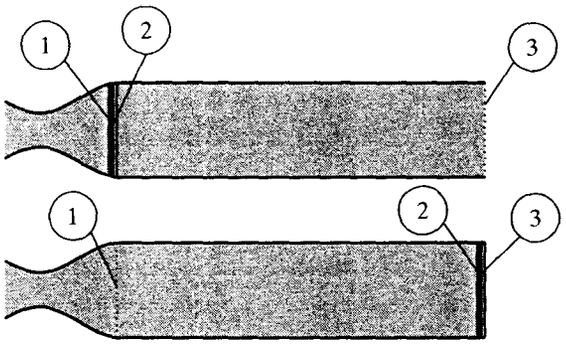


**Figure 9.17** Two Limiting Cases of a Normal Shock in a Constant-Area Duct with Friction for $L < (L_{max})_1$

From this value of $(fL_{max}/D)_3$, we can determine the corresponding Mach number $M_3 = 0.5874$. For this case,

$$p_b = p_3 = \left(\frac{p_3}{p^*}\right)\left(\frac{p^*}{p_2}\right)\left(\frac{p_2}{p_1}\right)\left(\frac{p_1}{p_{o1}}\right)\left(\frac{p_{o1}}{p_r}\right)p_r$$

Now, from Eq. (9.26), at $M_2$ and $M_3$, $(p/p^*)_2 = 1.9438$ and $(p/p^*)_3 = 1.8071$, respectively. From the normal-shock and the isentropic flow relations at $M_1$, $p_2/p_1 = 5.4656$ and $p_1/p_{o1} = 0.09393$. Inserting these values into the foregoing expression yields

$$p_b = (1.8071)\left(\frac{1}{1.9438}\right)(5.4656)(0.09393)(1)500 = 238.5961 \text{ kPa}$$

*Shock at the duct exit*: $M_1 = 2.1972$.
At this Mach number, $(fL_{max}/D)_1 = 0.3602$. Therefore,

$$\left(\frac{fL_{max}}{D}\right)_2 = \left(\frac{fL_{max}}{D}\right)_1 - \frac{fL}{D} = 0.3602 - 0.20 = 0.1602$$

From this value, we find that $M_2 = 1.5663$. From the normal-shock relations at this Mach number, $p_3/p_2 = 2.6955$, and from Eq. (9.26), at $M_1$ and $M_2$, $(p/p^*)_1 = 0.3556$ and $(p/p^*)_2 = 0.5728$, respectively. From the isentropic flow relations at $M_1$, $p_1/p_{o1} = 0.09393$. Using these values, we may form the following product of pressure ratios to compute $p_b$:

$$p_b = p_3 = \left(\frac{p_3}{p_2}\right)\left(\frac{p_2}{p^*}\right)\left(\frac{p^*}{p_1}\right)\left(\frac{p_1}{p_{o1}}\right)\left(\frac{p_{o1}}{p_r}\right)p_r$$

$$= (2.6955)\left(\frac{0.5728}{0.3556}\right)(0.09393)(1)500 = 203.9177 \text{ kPa}$$

Thus, a shock will appear in the duct over the back pressure range from 203.9177 to 238.6 kPa.

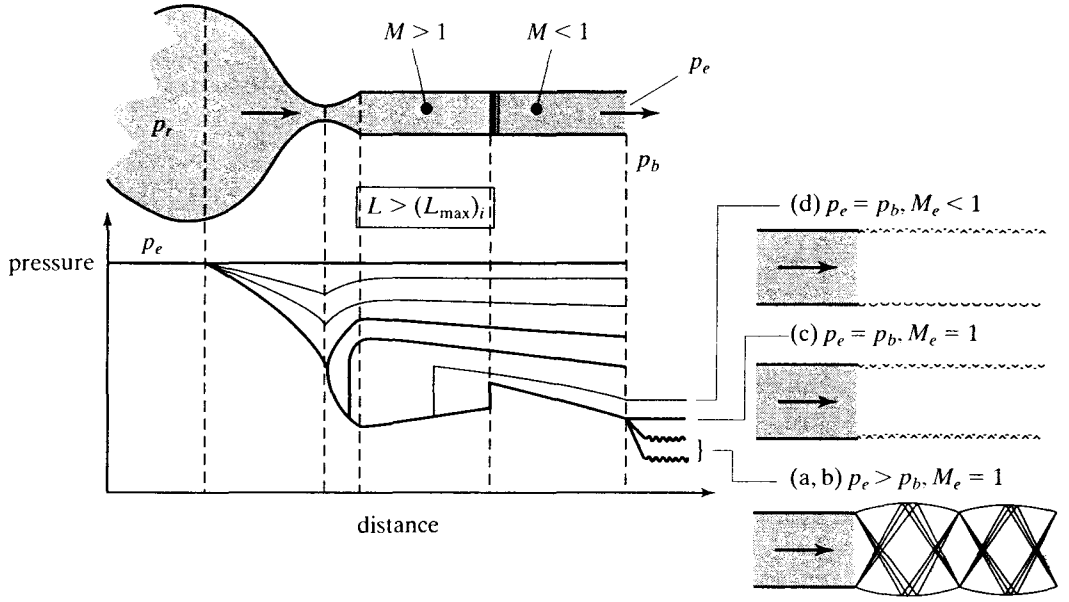


**Figure 9.18** Pressure Variation in a Constant-Area Pipe Connected to a C–D Nozzle

Next, suppose $L$ is greater than $(L_{max})_i$ and that the duct length is larger than that required to reach Mach 1 for supersonic duct flow.

For very low back pressures, for this case, there must be sonic or supersonic flow at the duct exit to provide expansion waves outside the duct. As was discussed previously, whereas for subsonic duct flow a reduction of flow occurs for $L > (L_{max})_i$, for supersonic flow, no such flow reduction can occur; instead, a normal shock appears in the duct. The resultant flow is as illustrated in Figure 9.18.

For a back pressure of 0 kPa and for very low back pressures, it is evident that the back pressure is less than the exit-plane pressure, so expansion waves must occur at the duct exit, with the exit-plane Mach number equal to unity. (Flow after the shock cannot reach supersonic velocities without violating the second law of thermodynamics.) For curves (a) and (b) in Figure 9.18, therefore, a normal shock occurs in the duct, with sonic flow at the duct exit and expansion waves outside the duct. For curve (c), the exit-plane pressure is equal to the back pressure. It should be noted that the location of the shock is the same for curves (a), (b), and (c). For this class of problem, this location represents the farthest downstream position that the normal shock is able to reach. As the back pressure is raised above curve (c), the normal shock moves upstream toward the duct inlet, with the exit Mach number subsonic and the back pressure equal to the exit-plane pressure. Again, for high-enough back pressures, the shock moves into the nozzle, eliminating supersonic flow in the aftersection of the duct.

## 9.5 A NONITERATIVE METHOD TO LOCATE A NORMAL SHOCK IN A CONSTANT-AREA DUCT WITH FRICTION THAT IS CONNECTED TO RESERVOIR BY A C–D NOZZLE

The location of a normal shock within the constant-area duct for both cases [$L < (L_{max})_i$ and $L > (L_{max})_i$] is generally found by a trial-and-error procedure. With this approach,

a shock location is assumed, and computations are then performed to determine whether the assumed location yields a solution that satisfies the given information. If it does not, then another position is assumed, and the process is repeated. Usually, several tries are needed to obtain an approximately accurate result.

There is an alternative procedure proposed by Na [Ref. (9.9)] that produces accurate results without iteration. This method makes use of both Fanno flow and normal-shock relations. Therefore, no additional information is required.

For the duct shown in Figure 9.19, the duct length can be written as

$$L = [(L_{\max})_2 - (L_{\max})_e] + [(L_{\max})_i - (L_{\max})_1]$$

Note that because the flow between the duct inlet, station $i$, and the upstream side of the shock, station 1, is supersonic and because the friction decelerates supersonic flows, $M_i > M_1$. In turn, as may be seen from Figure 9.9, $(L_{\max})_i > (L_{\max})_1$. Because the flow between the downstream side of the normal shock, station 2, and the duct exit, station $e$, is subsonic and because friction accelerates subsonic flows, $M_e > M_2$. Hence, as seen from Figure 9.9, $(L_{\max})_2 > (L_{\max})_e$.

Multiplying the foregoing expression by the average friction coefficient, dividing by the hydraulic diameter, and rearranging yields

$$\left(\frac{fL_{\max}}{D}\right)_2 - \left(\frac{fL_{\max}}{D}\right)_1 = \left(\frac{fL}{D}\right) + \left(\frac{fL_{\max}}{D}\right)_e - \left(\frac{fL_{\max}}{D}\right)_i \tag{9.29}$$

Now, from Eq. (9.16), we have

$$\left(\frac{fL_{\max}}{D}\right)_2 = \left(\frac{\gamma+1}{2\gamma}\right)\ln\left(\frac{\frac{\gamma+1}{2}M_2^2}{1+\frac{\gamma-1}{2}M_2^2}\right) - \frac{1}{\gamma}\left(1-\frac{1}{M_2^2}\right) \tag{9.30}$$

However, from the normal-shock relations, the Mach number on the downstream side of the shock, $M_2$, is related to the Mach number on the upstream side, $M_1$, as follows [see Eq. (4.9)]:

$$M_2^2 = \frac{M_1^2 + \frac{2}{\gamma-1}}{\frac{2\gamma}{\gamma-1}M_1^2 - 1} \tag{9.31}$$

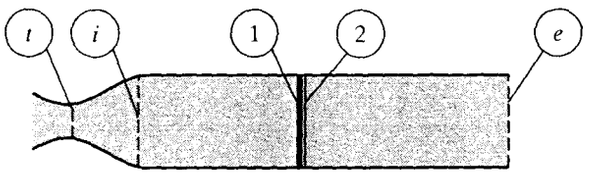


**Figure 9.19** Nomenclature to Locate a Normal Shock in the Duct

Combining Eqs. (9.30) and (9.31) and simplifying yields

$$\left(\frac{fL_{\max}}{D}\right)_2 = \left(\frac{\gamma+1}{2\gamma}\right)\ln\left(\frac{1+\frac{\gamma-1}{2}M_1^2}{\frac{\gamma+1}{2}M_1^2}\right) + \frac{(\gamma+1)(M_1^2-1)}{\gamma(\gamma-1)M_1^2+2\gamma} \tag{9.32}$$

Since both $(fL_{\max}/D)_2$ and $(fL_{\max}/D)_1$ depend only upon $M_1$, the left-hand side of Eq. (9.29) is a function of a single variable. This function can be obtained by combining Eqs. (9.32) and (9.16) to get

$$F(M_1) = \frac{\gamma+1}{\gamma}\ln\left[\frac{2+(\gamma-1)M_1^2}{(\gamma+1)M_1^2}\right] + \frac{2(1+\gamma M_1^2)(M_1^2-1)}{\gamma M_1^2[2+(\gamma-1)M_1^2]} \tag{9.33}$$

If $M_i$, $M_e$, and $fL/D$ are given, the right-hand side of Eq. (9.29) can be computed, and thus a numerical value of $F(M_1)$ is determined. From this value, we can, in turn, find $M_1$. (A spreadsheet program and the Newton–Raphson method may be used to accomplish this task.) With $M_1$ and $M_i$, we can determine the shock location from

$$L_s = [(L_{\max})_i - (L_{\max})_1] \tag{9.34}$$

If the back pressure $p_b$ is given rather than the exit Mach number $M_e$, an additional step to the preceding procedure is required. There are two possibilities: In one, $M_e = 1$ and $p_e > p_b$; in the other, $M_e \leq 1$ and $p_e = p_b$. The former is used for cases where the back pressure is very small, whereas in the latter, because the exit-plane pressure is known, we may determine the exit Mach number by first computing the following pressure ratio:

$$\frac{p_e}{p^*} = \left(\frac{p_e}{p_b}\right)\left(\frac{p_b}{p_r}\right)\left(\frac{p_r}{p_{oi}}\right)\left(\frac{p_{oi}}{p_i}\right)\left(\frac{p_i}{p^*}\right) \tag{9.35}$$

The fourth and fifth ratios on the right-hand side of the foregoing equation can be calculated from $M_i$; the third ratio is unity because the flow from the reservoir to the inlet of the duct is isentropic; and the second ratio is known because $p_r$ and $p_b$ are given individually. From the pressure ratio in Eq. (9.35), $M_e$ can be determined.

**Example 9.5. Locating a normal shock in a constant-area duct with friction that is connected to a reservoir by a C–D nozzle**

A converging–diverging nozzle with an area ratio of 2 to 1 is supplied by a reservoir containing air ($\gamma = 1.4$, $R = 0.287$ kJ/kg·K) at 500 kPa. The nozzle exhausts into a constant-area duct of length-to-diameter ratio $L/D$ of 25 and friction coefficient of 0.02. Determine the normal-shock location and exit-plane pressure for a back pressure of 0 kPa. Also, locate the shock for a back pressure of 180 kPa. Refer to Figure 9.19 for the nomenclature.

**Solution**

From isentropic relations, at $(A/A^*)_i = 2.0$, $M_i = 2.1972$. At this Mach number, $(fL_{max}/D)_i = 0.3602$, $(p/p^*)_i = 0.355615$, and $(p/p_o)_i = 0.093932$. For the duct under consideration, $fL/D = 0.02(25) = 0.50$, so that $L > (L_{max})_i$. For this type of problem, a normal shock usually stands in the C–D nozzle–duct system. The range of back pressures over which a normal shock exists within the duct can be established as follows: Consider a shock residing at the duct inlet. (See Example 9.4.) The Mach number on the downstream side of the shock is 0.5474. At this Mach number, $(fL_{max}/D)_2 = 0.7427$. Now,

$$\left(\frac{fL_{max}}{D}\right)_e = \left(\frac{fL_{max}}{D}\right)_2 - \left(\frac{fL}{D}\right) = 0.7427 - 0.5 = 0.2427$$

From this value, we can find that $M_e = 0.6832$ and that the corresponding pressure ratio $(p/p^*)_e = 1.53343$. Because the exit flow is subsonic, the exit static pressure is equal to the back pressure, which may be computed from

$$p_b = p_e = \left(\frac{p_e}{p^*}\right)\left(\frac{p^*}{p_i}\right)\left(\frac{p_i}{p_{oi}}\right)\left(\frac{p_{oi}}{p_r}\right)p_r$$

$$= (1.53343)\left(\frac{1}{0.355615}\right)(0.0939324)(1)500 = 202.5169 \text{ kPa}$$

Thus, a shock will reside within the duct for the following range of back pressures:

$$0 \leq p_b \leq 202.5169 \text{ kPa}$$

Now, if the exit Mach number is unity and the exit and back pressures are equal, then $p_e = p_b = p^*$, and hence

$$p_b = p_e = \left(\frac{p_e}{p^*}\right)\left(\frac{p^*}{p_i}\right)\left(\frac{p_i}{p_{oi}}\right)\left(\frac{p_{oi}}{p_r}\right)p_r$$

$$= (1)\left(\frac{1}{0.355615}\right)(0.0939324)(1)500 = 132.0702 \text{ kPa}$$

Case 1: $p_b = 0$ kPa

Since the back pressure for the first case of this example is 0 kPa, the exit Mach number is clearly unity and $p_e = p^*$. However, to reach the low value of $p_b$, further expansion must take place outside the duct, as shown in curve (a) of Figure 9.18. To determine the location of the shock for this case, first calculate the value of $F(M_1)$ from Eq. (9.29):

$$F(M_1) = \left(\frac{fL_{max}}{D}\right)_2 - \left(\frac{fL_{max}}{D}\right)_1 = \left(\frac{fL}{D}\right) + \left(\frac{fL_{max}}{D}\right)_e - \left(\frac{fL_{max}}{D}\right)_i$$

$$= 0.5 + 0 - 0.3602 = 0.1398$$

The value of $M_1$ can be obtained by numerically solving Eq. (9.33), using a spreadsheet program that implements the Newton–Raphson method. Because the derivative of $F(M_1)$ is complicated, it was obtained using the finite-difference approach. Table 9.2 contains the history of the iteration process.

**TABLE 9.2** Iterations to Obtain $M_1$ from $F(M_1)$ in Example 9.5

| Iteration | $M_{old}$ | $F(M)$ | $F(M + \Delta M)$ | $F(M-\Delta M)$ | $\Delta F/\Delta M$ | $M_{new}$ |
|---|---|---|---|---|---|---|
| 1 | 2.0000 | 0.14304 | 0.2878 | 0.2779 | 0.4960 | 1.7116 |
| 2 | 1.7116 | 0.008933 | 0.1530 | 0.1446 | 0.4217 | 1.6904 |
| 3 | 1.6904 | 8.95E-05 | 0.1441 | 0.1358 | 0.4132 | 1.6902 |
| 4 | 1.6902 | 5.93E-09 | 0.1440 | 0.1357 | 0.4131 | 1.6902 |
| 5 | 1.6902 | -2.5E-13 | 0.1440 | 0.1357 | 0.4131 | 1.6902 |
| 6 | 1.6902 | 0 | 0.1440 | 0.1357 | 0.4131 | 1.6902 |

At $M_1 = 1.6902$, $M_2$ is found from Eq. (9.31) to be 0.6431. At these Mach numbers, $(fL_{max}/D)_1 = 0.2044$ and $(fL_{max}/D)_2 = 0.3442$. The shock location is determined from Eq. (9.34):

$$\frac{L_s}{D} = \left(\frac{1}{f}\right)\left[\left(\frac{fL_{max}}{D}\right)_i - \left(\frac{fL_{max}}{D}\right)_1\right] = \frac{1}{0.02}(0.3602 - 0.2044) = 7.7892$$

As pointed out previously, this is as close to the duct exit as the shock can reach. It will maintain this position for the following range of back pressures: $0 \leq p_b \leq 132.0702$ kPa. Higher values of back pressure will cause the shock to be positioned farther upstream towards the nozzle, as we will see in the next case.

Case 2: $p_b = 180$ kPa

This case is similar to that of curve (d) in Figure 9.18. The first step is to determine the duct exit conditions. In particular, we need $M_e$. This value can be obtained from the pressure ratio $(p/p^*)_e$, which is simply 180/132.0702 = 1.3629. From this value, we find that $M_e = 0.7609$. With this Mach number, $(fL_{max}/D)_e = 0.1134$. Hence, $F(M_1) = 0.2532$. In turn, we use the root-solving process to determine that $M_1 = 1.9396$ and $(fL_{max}/D)_1 = 0.2867$. From this value and $(fL_{max}/D)_i$, the location is found to be $3.6744D$.

For back pressures up to 202.5169 kPa (at which a shock will stand at the inlet to the duct), we may proceed as before to locate the position of the shock. Higher back pressures will result in a shock appearing within the C–D nozzle. For a back pressure of 450.5889 kPa, a very weak shock will appear virtually at the throat. For back pressures between this value and the reservoir pressure, no shocks will appear in the duct or the nozzle.

---

**Example 9.6. Locating a normal shock in a C–D nozzle that is connected to a reservoir and a constant-area duct with friction**

For the same conditions as in the previous example, determine the location of a normal shock for $202.5465 \leq p_b \leq 450.5889$ kPa. Refer to Figure 9.19 for the nomenclature of the problem.

**Solution**

Over the given range of back pressures, a normal shock will reside in the diverging portion of the C–D nozzle. For the lower value, a shock will appear at $A_s/A_t = 2$, while for the

upper value a shock will appear at $A_s/A_t = 1$. We will determine a few shock locations for back pressures between these extremes. To accomplish this, we will combine the C–D shock locator process that was presented in Chapter 4 with the computational methods of the current chapter. Review of the former process reveals that the Mach number exiting the nozzle (i.e., $M_i$ in this case) can be determined provided that the reservoir pressure, the area ratio, and the nozzle exit pressure are given. Thus, for ease of calculation, the nozzle exit pressure will be specified and the back pressure on the duct subsequently computed. Moreover, we will develop results in stepwise fashion for a given nozzle exit pressure and then provide a table of corresponding results for other pressures.

Let $p_i = 350$ kPa. We begin by following the five-step process described in Chapter 4 (see Example 4.5):

1. Determine $M_e$ from Eq. (4.26).
2. Use $M_e$ to determine $p_e/p_{o2}$ from Eq. (4.23).
3. Since $M_e < 1$, $p_e = p_b$, so form the product $(p_b/p_{o1})(p_{o2}/p_e) = p_{o2}/p_{o1}$.
4. Use Eq. (4.15), with $p_{o2}/p_{o1}$ from step 3, to determine $M_1$.
5. Determine $A_s/A_1^* = A_s/A_t$ from Eq. (3.23).

The notation used in the process needs some revision to adapt it to the problem at hand: The subscript $e$ applies to the exit of the nozzle, so here it may be replaced with $i$, the duct inlet; the 1 and 2 refer to locations upstream and downstream, respectively, of the shock within the nozzle; the subscript $s$ indicates the shock location; and the subscript $t$ indicates the nozzle throat. Using the given information, we obtain the following:

1. $M_i = 0.4067$ (this is the Mach number at the nozzle exit and the duct inlet)
2. $p_i/p_{o2} = 0.8923$
3. $p_{o2}/p_{o1} = 0.7/0.8923 = 0.7845$ (Note: Since $p_{o1} = p_r = 500$ kPa, $p_{o2} = p_{oi} = 392.25$ kPa)
4. $M_1 = 1.8627$
5. $A_s/A_t = 1.5101$

Now, using Fanno flow relations at $M_i$, we find that $(fL_{max}/D)_i = 2.1902$, $(p/p^*)_i = 2.65002$, and $(p/p_o)_i = 0.89234$. For the duct under consideration, $fL/D = 0.02(25) = 0.50$; therefore, $(fL_{max}/D)_e = (fL_{max}/D)_i - fL/D = 1.6902$. From this value, we find

**TABLE 9.3** Results of Computations for Example 9.6 Used to Locate Shock in a C–D Nozzle

| $p_i$ | $M_i$ | $p_i/p_{oi}$ | $p_{oi}/p_r$ | $p_{oi}$ | $A_s/A_t$ | $(p/p^*)_i$ | $(fL_{max}/D)_i$ | $(fL_{max}/D)_e$ | $M_e$ | $(p/p^*)_e$ | $p_b$ |
|---|---|---|---|---|---|---|---|---|---|---|---|
| 256.7 | 0.5474 | 0.8157 | 0.6294 | 314.7000 | 2.0000 | 1.9438 | 0.7429 | 0.2429 | 0.6831 | 1.5336 | 202.5292 |
| 275 | 0.5128 | 0.8358 | 0.6581 | 329.0500 | 1.8932 | 2.0822 | 0.9694 | 0.4694 | 0.6055 | 1.7462 | 230.6406 |
| 300 | 0.4719 | 0.8586 | 0.6988 | 349.4000 | 1.7557 | 2.2713 | 1.3248 | 0.8248 | 0.5339 | 1.9958 | 263.6066 |
| 350 | 0.4067 | 0.8923 | 0.7845 | 392.2500 | 1.5101 | 2.6500 | 2.1902 | 1.6902 | 0.4401 | 2.4422 | 322.5733 |
| 400 | 0.3572 | 0.9156 | 0.8737 | 436.8500 | 1.2972 | 3.0284 | 3.2538 | 2.7538 | 0.3778 | 2.8591 | 377.6193 |
| 450 | 0.3183 | 0.9322 | 0.9655 | 482.7500 | 1.0988 | 3.4072 | 4.5125 | 4.0125 | 0.3320 | 3.2635 | 431.0398 |
| 468.58 | 0.3059 | 0.9372 | 1.0000 | 500.0000 | 1.0000 | 3.5480 | 5.0288 | 4.5288 | 0.3179 | 3.4118 | 450.6115 |

$M_e$ (i.e., the duct exit Mach number) to be 0.4401. At this Mach number, $(p/p^*)_e = 2.4422$. Finally, we may compute the back pressure, and since the exit flow is subsonic, it must be equal to the exit pressure.

$$p_b = p_e = \left(\frac{p_e}{p^*}\right)\left(\frac{p^*}{p_i}\right)\left(\frac{p_i}{p_{oi}}\right)p_{oi} = (2.4422)\left(\frac{1}{2.65002}\right)(0.89234)392.25$$

$$= 322.5733 \text{ kPa}$$

Additional values, calculated in the same manner, are contained in Table 9.3.

## 9.6 ADIABATIC FLOW WITH FRICTION AND AREA CHANGE

If the cross-sectional area is allowed to vary, for adiabatic flow with friction, the analysis becomes more complex than Fanno flow. Consider the control volume shown in Figure 9.20.

The pressure on the side walls of the control volume is assumed to be $p + dp/2$. (See Section 3.2.) The continuity equation is

$$\frac{d\rho}{\rho} + \frac{dA}{A} + \frac{dV}{V} = 0 \tag{9.36}$$

For steady flow, the momentum equation in the $x$ direction is

$$\sum F_x = \iint_{\text{c.s.}} V_x(\rho \mathbf{V} \cdot d\mathbf{A})$$

or

$$pA + \left(p + \frac{dp}{2}\right)dA - (p + dp)(A + dA) - \tau_f A_s = \rho A V dV \tag{9.37}$$

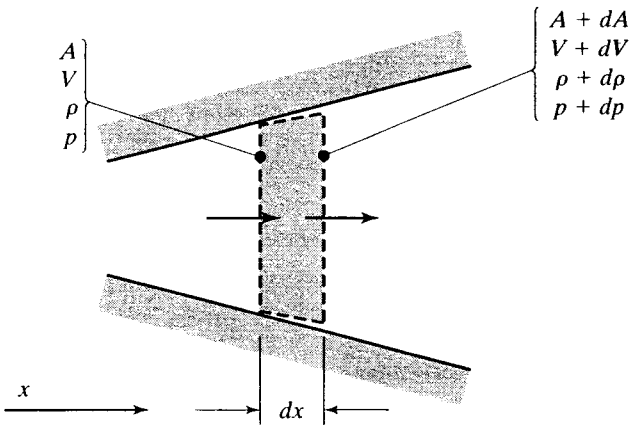


**Figure 9.20** Control Volume for the Analysis of Adiabatic Flow with Friction and Area Change

Substituting for $\tau_f$ from Eqs. (9.11) and (9.12) and simplifying and dropping second-order terms yields

$$-Adp - \frac{1}{2}\rho V^2 \frac{fA_s}{4} = \rho AV dV$$

For a circular duct, $A_s = \pi D dx = 4A dx/D$, and hence

$$dp + \frac{1}{2}\rho V^2 \frac{f dx}{D} + \rho V dV = 0$$

Following the same analysis as was carried out for Fanno flow (see Section 9.2), divide by $p$ and substitute for $dp/p$ from the perfect-gas law:

$$\frac{d\rho}{\rho} + \frac{dT}{T} + \gamma M^2 \frac{dV}{V} + \frac{1}{2}\gamma M^2 \frac{f dx}{D} = 0$$

Using continuity, we can eliminate $d\rho/\rho$:

$$-\frac{dA}{A} - \frac{dV}{V} + \frac{dT}{T} + \gamma M^2 \frac{dV}{V} + \frac{1}{2}\gamma M^2 \frac{f dx}{D} = 0 \tag{9.38}$$

By the definition of the Mach number, $V = Ma = M\sqrt{\gamma RT}$, so

$$\frac{dV}{V} = \frac{dM}{M} + \frac{1}{2}\frac{dT}{T}$$

Then we have

$$-\frac{dA}{A} - \frac{dM}{M} + \frac{1}{2}\frac{dT}{T} + \gamma M^2 \frac{dM}{M} + \frac{\gamma M^2}{2}\frac{dT}{T} + \frac{1}{2}\gamma M^2 \frac{f dx}{D} = 0$$

Substituting for $dT/T$ from Eq. (9.14) for this adiabatic flow, we obtain

$$\frac{1}{2}\gamma M^2 \frac{f dx}{D} = \frac{dA}{A} + \frac{2(1 - M^2)}{2 + (\gamma - 1)M^2}\frac{dM}{M} \tag{9.39}$$

or

$$\frac{1}{2}\gamma M^2 \frac{f}{D} = \frac{1}{A}\frac{dA}{dx} + \frac{2(1 - M^2)}{M[2 + (\gamma - 1)M^2]}\frac{dM}{dx} \tag{9.40}$$

Direct integration of this equation, except for in certain specialized cases, is not possible; however, numerical solution, as we see in the next section, can be used to obtain results. It is instructive at this point to discuss some special cases of Eq. (9.40).

*Constant-area flow* (i.e., $dA/dx = 0$): This case, of course, has already been discussed in detail; it is Fanno flow.

*Constant-Mach-number flow* (i.e., $dM/dx = 0$): This condition eliminates the second term on the right-hand side of Eq. (9.40). The resultant equation for a duct of circular cross-section is therefore

$$\frac{1}{2}\gamma M^2 \frac{f}{D} = \frac{1}{A}\frac{dA}{dx} = \frac{2}{D}\frac{dD}{dx} \tag{9.41}$$

Thus, if a duct is required to provide constant-Mach-number flow with friction, Eq. (9.41) gives a relationship for the diameter variation with $x$. Solving yields

$$\frac{dD}{dx} = \frac{\gamma M^2}{4} f \tag{9.42}$$

or

$$D = \left(\frac{\gamma M^2}{4} f\right) x + D_o$$

Therefore, the diameter varies linearly with distance, so the geometry for a constant-Mach-number flow with friction is a conical duct. (See Figure 9.21.)

*Nozzle flow with friction* is a flow of great interest. Although closed-form integration of Eq. (9.40) is not possible for this flow, several statements based on this equation can be made concerning nozzle flow. We must remember that, for isentropic flow ($f = 0$) in a converging–diverging nozzle, $M = 1$ corresponds to $dA/dx = 0$, or to the minimum area. For flow with friction, from Eq. (9.40), Mach 1 occurs for positive $dA/dx$, or in the diverging part of the nozzle. (See Figure 9.22.) At the throat, $dA/dx = 0$, but, for $M < 1$, $dM/dx$ is positive. With the throat area no longer suitable as a reference area, and with direct integration of Eq. (9.40) not possible, an exact solution of nozzle flow with friction becomes extremely difficult.

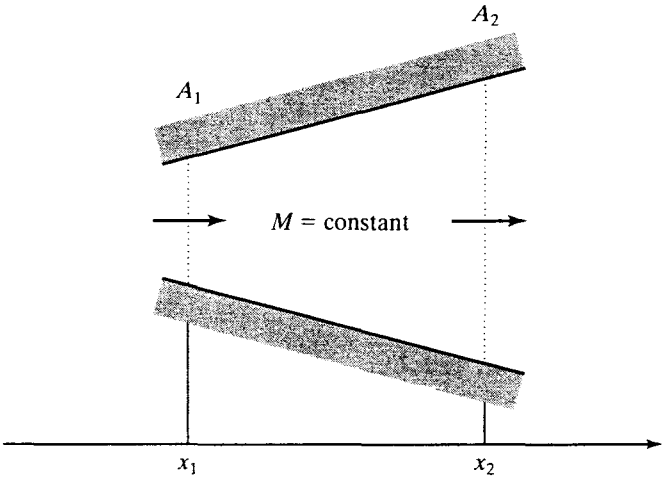


**Figure 9.21** Constant-Mach-Number Flow in a Variable-Area Duct with Friction

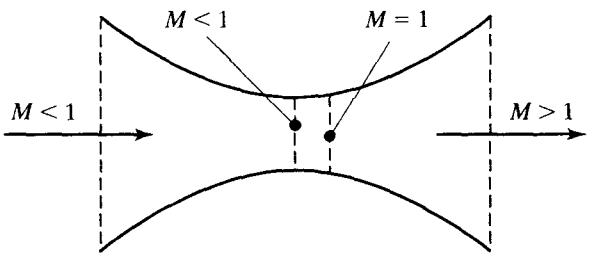


**Figure 9.22** Nozzle Flow with Friction

However, the engineer must still obtain at least an approximate solution to the problem of nozzle flow with friction. One procedure is to define a *nozzle velocity coefficient* $C_V$, which is equal to the ratio of actual nozzle exit velocity to the velocity that could be obtained in an isentropic expansion over the same overall pressure ratio. Alternatively, a *nozzle enthalpy coefficient* $C_h$ can be defined, relating the actual enthalpy drop in the nozzle to the enthalpy drop for an isentropic nozzle:

$$C_h = \frac{\Delta h_{\text{actual}}}{\Delta h_{\text{isentropic}}} \tag{9.43}$$

If the nozzle inlet velocity is negligible, for adiabatic flow [$\Delta h_o = 0 = \Delta h + \Delta(V^2/2)$],

$$\Delta h = -\frac{\Delta V^2}{2} = -\frac{V_{\text{inlet}}^2 - V_{\text{exit}}^2}{2} \cong \frac{V_{\text{exit}}^2}{2}$$

so that

$$C_h = \left(\frac{V_{\text{exit actual}}}{V_{\text{exit isentropic}}}\right)^2 \tag{9.44}$$

or

$$C_h = C_V^2 \tag{9.45}$$

In a well-designed nozzle, operating at or close to design pressure ratio, values of $C_V$ obtained are greater than 0.95 for Reynolds numbers based on nozzle diameter greater than $10^6$ (in the turbulent flow regime). With a favorable pressure gradient associated with nozzle expansion flows, the only losses are due to the small amount of skin friction at the nozzle walls.

**Example 9.7. Determination of the actual nozzle exit velocity in a jet engine**

Flow is expanded in a jet engine exhaust nozzle from a stagnation pressure and temperature of 300 kPa and 1,000 K, respectively, to an exhaust pressure of 100 kPa. For a velocity coefficient of 0.95, determine the actual nozzle exit velocity. Assume that $\gamma = 1.40$ and $R = 250$ J/kg · K.

**Solution**

First calculate the exit velocity for an isentropic expansion. For $(p/p_o)_e = 100/300 = 0.3333$, $M_e = 1.3578$ and $(T/T_o)_e = 0.7306$. Therefore, $(V_{\text{isentropic}})_e = 1.3578\sqrt{1.4(250)(0.7306)1{,}000} = 686.6609$ m/s, and from Eqs. (9.44) and (9.45), we obtain $(V_{\text{actual}})_e = 0.95(686.6609) = 652.2788$ m/s.

## 9.7 CHAPTER CAPSTONE APPLICATION: NUMERICAL SOLUTION OF THE ORDINARY DIFFERENTIAL EQUATION FOR ADIABATIC FLOW WITH FRICTION AND AREA CHANGE

Although the differential equation that governs steady, one-dimensional, adiabatic flow within a variable-area duct with friction [i.e., Eq. (9.40)] is too involved to be directly integrated, there is no such difficulty in obtaining numerical solutions. Because the governing equation is first order, it may be readily solved by a variety of methods; for example, see Ref. (9.10). Problems involving higher order equations are solved numerically by turning the higher order equation into a system of first-order equations and then applying one or more of the available methods. In this section, a few of these methods will be employed to solve one-dimensional gas-flow problems that include both friction and variable-area effects. However, the methods are equally amenable to problems for which one or the other of these effects is dominant (i.e., to isentropic or Fanno flows).

To effect a numerical solution of an ordinary differential equation such as Eq. (9.40), the equation needs to be written in the general form

$$\frac{dM}{dx} = F(x, M) \tag{9.46}$$

The Mach number is taken to be the dependent variable here, but we could have used pressure, temperature, etc., provided that an expression written exclusively in terms of those variables can be formulated. For compressible flows, Mach number usually represents the best choice of dependent variable. It is worth mentioning that because the dependent variable depends only on a single independent variable, *viz.*, the distance $x$, the equation is an *ordinary differential equation*. In a later chapter, we will present methods to solve compressible flows that are described in terms of *partial differential equations* (i.e., equations involving more than one independent variable).

Note that because Eq. (9.46) is first order, only one condition is required to complete the formulation:

$$M = M_1(x_1) \tag{9.47}$$

Because this condition is specified at the initial point of the calculation, it is naturally referred to as the *initial condition*. Further, problems governed by Eq. (9.46) subject to Eq. (9.47) are called *initial-value problems*. If a value is specified at a point other than the initial point, special procedures, often iterative, must be utilized.

The most basic method for solving a first-order ordinary differential equation is *Euler's method.* To obtain a solution, the length of the flow field is first subdivided into a number of pieces. This subdivided length is referred to as the *grid.* Each location $x_i$ is called a *grid point,* each piece is called a *grid cell,* and each cell has a width, or *grid spacing,* $\Delta x = x_{i+1} - x_i$. Although the grid spacing need not be uniform, here we will typically assume that $\Delta x$ is a constant equal to the length of the flow region, $L$, divided by the number of grid points, $n$, minus one—that is, $\Delta x = L/(n - 1)$. For example, if there are three grid points, the flow length is divided into two equal pieces.

Euler's method uses a one-sided difference (a *forward difference*) to represent the derivative in Eq. (9.46):

$$\frac{dM}{dx}(x) \cong \frac{M(x + \Delta x) - M(x)}{\Delta x} = \frac{M_{i+1} - M_i}{\Delta x} = F[x, M(x)] = F(x_i, M_i)$$

Hence, we obtain the very simple algorithm

$$M_{i+1} = M_i + F(x_i, M_i)\Delta x \tag{9.48}$$

The calculations begin at the initial point, say, $i = 1$, and using the initial information [i.e., Eq. (9.47)], we are able to find the Mach number at $i = 2$ (i.e., $M_2$). In turn, $M_2$ provides the initial information for the next interval, and with $x_2 = x_1 + \Delta x$ we are able to find $M_3$, and so on. It is easy to understand why this procedure is referred to as a *space-marching technique.* Basically, this method results in the ordinary differential equation being turned into a set of linear algebraic equations, one for each grid cell. Euler's method is called an *explicit method* because all terms on the right-hand side of Eq. (9.48) are known, and therefore we are able to compute the next $M$ directly.

Euler's method can be developed by an alternative approach that has the advantage of also providing the error with the method. To accomplish this, expand $M$ about the point $x$ in a Taylor series to obtain $M(x + \Delta x)$:

$$M_{i+1} = M_i + \left(\frac{dM}{dx}\right)_i (x_{i+1} - x_i) + \left(\frac{d^2M}{dx^2}\right)_i \frac{(x_{i+1} - x_i)^2}{2} + \cdots$$

Truncating the series after the second term on the right-hand side and using Eq. (9.46) to replace the first derivative produces Eq. (9.48). The Taylor-series approach reveals that the largest term that has been dropped is proportional to $(x_{i+1} - x_i)^2 = (\Delta x)^2$. Therefore, the method is regarded as being *locally second-order accurate.* However, because errors can accumulate as the computations progress, the method is regarded as being *globally first-order accurate*—that is, fairly inaccurate unless $\Delta x$ is made very small. Accordingly, other methods are preferred because they can more accurately solve ordinary differential equations. The real advantage of Euler's explicit method is that results can be obtained very quickly using the approach. On the other hand, as is the case with almost all explicit methods, unless care is exerted, the method can become unstable. (The usual terminology is that the method can "blow up.") It is beyond the scope of this volume to delve into the stability of the method. For such details, see Ref. (9.11). Suffice it to

say that if oscillations in the results appear, the method is becoming unstable. The simplest remedy for this problem is to reduce $\Delta x$. Alternatively, we could employ a *backwards difference* for the derivative in Eq. (9.46):

$$\frac{dM}{dx}(x + \Delta x) \cong \frac{M(x + \Delta x) - M(x)}{\Delta x} = \frac{M_{i+1} - M_i}{\Delta x} = F[x + \Delta x, M(x + \Delta x)]$$
$$= F(x_{i+1}, M_{i+1})$$

$$M_{i+1} = M_i + F(x_{i+1}, M_{i+1})\Delta x$$

It should be observed that $M_{i+1}$ appears on both sides of the equation. Thus, the next Mach-number value in a space march is not only dependent upon the previous value and the step size, but also upon its own value. Accordingly, this method is called an *implicit method.* Unless the function on the right side is linear in $M$, we will not be able to proceed as with the explicit method. In fact, we have obtained a nonlinear algebraic equation that must be solved somehow. To handle this difficulty, more involved procedures (and therefore more computational effort) are required. Often, these procedures are iterative in nature.

On the other hand, while the appearance of $M_{i+1}$ on both sides of the equation foils direct calculation of the next value of the Mach number, it turns out that it greatly benefits the stability of the method. In general, implicit methods are found to be quite stable, which allows us to use larger step sizes without concern that the method will blow up. However, large step sizes can produce results with poor numerical accuracy. The tug of war between accuracy and effort (or computer time) is a constant dilemma in numerical analysis. This condition helps to explain why there are so many methods available to numerically solve ordinary differential equations.

To improve the accuracy of the solution while also maintaining the simplicity of the explicit method, we can employ a multistep procedure called the *predictor–corrector* method; see, for example, Ref. (9.12). There are a number of versions of this approach. Here, we will first use Euler's method to obtain a first value (the prediction step) and then use a second method, which in this case is actually the *trapezoidal rule* from numerical integration, to obtain an improved value (the correction step). This method has been called *Heun's method* and the *modified Euler method.* The algorithm for this method is

$$\textit{Predictor step:} \quad \hat{M}_{i+1} = M_i + F(x_i, M_i)\Delta x$$

$$\textit{Corrector step:} \quad M_{i+1} = M_i + \left[\frac{F(x_i, M_i) + F(x_{i+1}, \hat{M}_{i+1})}{2}\right]\Delta x \qquad (9.49)$$

where $\hat{M}$ is the predicted Mach number. Observe the manner in which the predicted Mach number appears in the corrector. Because all terms on the right-hand side of the corrector are known, Heun's method is entirely explicit.

One other approach to obtaining the various forms of numerical solvers is to simply integrate Eq. (9.46) over one grid spacing; that is,

$$\int_{M_i}^{M_{i+1}} dM = M_{i+1} - M_i = \int_{x_i}^{x_{i+1}} F(x, M)dx$$

or

$$M_{i+1} = M_i + \overline{F}(x, M)\Delta x \tag{9.50}$$

where

$$\overline{F}(x, M) = \frac{1}{\Delta x}\int_{x_i}^{x_{i+1}} F(x, M)dx$$

is the cell average value of $F(x, M)$—physically the average slope of the $M(x)$ curve within the given cell. If the average slope $\overline{F}(x, M)$ is taken to be a constant at $F(x_i, M_i)$, Eq. (9.50) becomes Euler's explicit method; if the average slope is taken to be a constant at $F(x_{i+1}, M_{i+1})$, Eq. (9.50) becomes Euler's implicit method; and if the average slope is taken to be a constant equal to the arithmetic average of $F(x_i, M_i)$ and $F(x_{i+1}, M_{i+1})$—that is, $[F(x_i, M_i) + F(x_{i+1}, M_{i+1})]/2$—Eq. (9.50) yields the trapezoidal method.

Clearly, more accurate representation of the slope of $M(x)$ within each cell results in an improvement in the solver. Accordingly, the next method, which is generally regarded as the "gold standard" for numerically solving ordinary differential equations, uses a weighted average for the slope. How this weighted average is created (there are a number of variations) is too involved to be presented here; this development can be found in Ref. (9.13). The method is called the *Runge–Kutta fourth-order method*. Obviously, being fourth order, it is very accurate. Its algorithm is written

$$M_{i+1} = M_i + \frac{(k_1 + 2k_2 + 2k_3 + k_4)}{6}\Delta x \tag{9.51}$$

where $k_1$, $k_2$, $k_3$, and $k_4$ are slopes that are computed at various locations within each grid space interval as follows:

$$k_1 = F(x_i, M_i)$$

$$k_2 = F\left(x_i + \frac{\Delta x}{2}, M_i + k_1\frac{\Delta x}{2}\right)$$

$$k_3 = F\left(x_i + \frac{\Delta x}{2}, M_i + k_2\frac{\Delta x}{2}\right)$$

$$k_4 = F(x_i + \Delta x, M_i + k_3\Delta x)$$

**Historical Note: The Runge–Kutta Method**—In a paper published in 1895, Runge proposed an improved alternative to Euler's method for solving differential equations by using an analogy to the trapezoidal method and Simpson's rule for numerical integration. In 1900, based on Gauss's method of integration and the method of successive approximation, Heun introduced new formulas for integrating differential equations. The Runge "trapezoidal method" formulas were a particular case of Heun's formulas. The advantage of Heun's formulas is that they improve the accuracy of the quadrature without having to consider supplementary points. In 1901, Kutta perfected Heun's formula by introducing new parameters. The accuracy of the method can be increased by selecting these parameters in the right manner. In a book published by Runge and König, the method was called the Runge–Kutta method. The name stuck.

**Carle David Tolmé Runge** (1856–1927) studied mathematics and physics in Munich and mathematics in Berlin. He obtained his doctoral degree in 1880 in a subject dealing with differential geometry. After completing his secondary-school teacher's examinations, he returned to Berlin. There, he worked on a method to solve algebraic equations by using infinite series of rational functions. Between 1886 and 1925, he was a professor at the University of Hanover, where he turned from pure mathematics to experimental work. During this period, he studied the wavelength of the spectral lines of elements other than hydrogen. From 1904 to 1925, when he retired, he was a chair of applied mathematics at the University of Göttingen.

**Martin Wilhelm Kutta** (1867–1944) studied in Breslau and Munich. Later, he was an assistant to von Dyck in Munich. He also held various positions in Munich, Jena, and Aachen. Between 1911 and 1935, he was a professor in Stuttgart.

The most important of Kutta's achievements are his contributions to the Runge–Kutta method and the *Kutta–Joukowski theorem*, which is a mathematical expression for the lift on an airfoil. Apparently, Kutta developed this theorem in his dissertation in 1902, whereas Joukowski independently developed the relation in two papers in 1906. Further, imposing the correct amount of circulation to position the stagnation point at the trailing edge of an airfoil is termed the *Kutta condition*.

There are other numerical methods [e.g., see Ref. (9.14)] that could be presented to solve ordinary differential equations. However, many of these approaches are used for special purposes—for example, to obtain very high accuracy, to vary the width of the grid space as the computations proceed, or to treat equations that contain widely differing length scales (called *stiff ordinary differential equations*, which can be very challenging to solve). The few methods presented previously allow us to perform numerical solution of gas dynamics problems involving effects of area change and friction without too much difficulty, as will be illustrated in the next few examples.

**Example 9.8. Numerical solution of the ordinary differential equation for subsonic isentropic flow in a converging nozzle**

An airstream ($\gamma = 1.4$, $R = 287$ J/kg · K) flows in a conically shaped converging nozzle of length 10 cm from a cross-sectional area $A_{in}$ of 50 cm$^2$ to a cross-sectional area $A_{out}$ of

40 cm$^2$. If $T_{in}$ = 300 K and $V_{in}$ = 100 m/s, use Euler's explicit method to solve Eq. (9.40) to find $M_{out}$. For this example, assume steady, one-dimensional, isentropic flow.

**Solution**

Because the flow is isentropic, it is adiabatic and contains no losses. Keep in mind that all isentropic flows are adiabatic; however, not all adiabatic flows are isentropic. At any rate, the friction term vanishes from Eq. (9.40). Also, since the nozzle is conical, the local cross-sectional area $A(x)$ is $\pi[D(x)]^2/4 = \pi[D_{in} + (D_{out} - D_{in})x/L]^2/4$, and thus the area term in Eq. (9.40) can be written as

$$\frac{1}{A(x)}\frac{dA}{dx} = \frac{2}{D(x)}\frac{dD}{dx} = \frac{2\left(\dfrac{D_{out} - D_{in}}{L}\right)}{D(x)}$$

where $D(x) = D_{in} + (D_{out} - D_{in})x/L$. Consequently, Eq. (9.40) becomes

$$\frac{dM}{dx} = F(x, M) = -\left[\frac{(D_{out} - D_{in})/L}{D(x)}\right]\frac{[2 + (\gamma - 1)M^2]}{(1 - M^2)}M$$

Using the given area data, we find that $D_{in}$ = 7.9788 cm and $D_{out}$ = 7.1365 cm. The initial Mach number is computed by first determining the speed of sound from the given information to be 347.1887 m/s; thus, $M_{in} = V_{in}/a_{in} = (100)/(347.1887) = 0.2880 = M_1$.

Generally, a relatively coarse grid is first selected in order to work out any "bugs" in the calculations. For this problem, we will divide the length into 10 pieces of uniform length; that is, the grid spacing is $\Delta x$ = 1 cm.

Inserting $M_1$ and the given information into $F(x, M)$ at $x$ = 0 results in $F(0,0.2880)$ = 0.006742, and for the grid spacing we can compute the next Mach number (i.e., $M_2$ at $x$ = 1 cm) from Eq. (9.48) to be 0.2948. This value is then used to determine $M_3$ at $x$ = 2, and so on. The results of these calculations as obtained from a spreadsheet program are presented in Table 9.4.

Thus, we find the exiting Mach number $M_{out}$ to be 0.36982. This value can be compared with the exact value, determined in Example 3.4 to be 0.371930. Hence, the numerical value computed by Euler's explicit method is in error by −0.5682%. This is quite good, particularly when it is considered that Euler's explicit method is only first-order accurate and that a relatively coarse grid was used. The value can be improved upon by using a finer grid—say, by dividing the previous grid in half: $\Delta x_2 = \Delta x_1/2 = 0.5$. Using this grid spacing and proceeding as before, we find that $M_{out}$ = 0.370856, which differs from the exact value by −0.2887%.

*Richardson's extrapolation method* [see Ref. (9.15)] is a simple procedure that can be used to improve the results we obtained without much effort. The method had its origins in the work of Huygens in 1654. Richardson formalized the method in two papers: Refs. (9.16) and (9.17).

To use the method, two results, say, $R_1$ and $R_2$, must be available. These results must have been computed using the same method on two grids of known width, say, $\Delta x_1$ and $\Delta x_2$, respectively. Also, the accuracy of the method must be known; say it is of order $m$. The extrapolated value $E$ is given by

$$E = R_2 - \frac{R_2 - R_1}{1 - \left(\dfrac{\Delta x_1}{\Delta x_2}\right)^n}$$

**TABLE 9.4** Explicit Euler Calculations for Example 9.8

| pt | $x$ | $D_i$ | $M_i$ | $F(x_i, M_i)$ | $M_{i+1}$ |
|---|---|---|---|---|---|
| 1 | 0.0000 | 7.9788 | 0.2880 | 0.0067 | 0.2948 |
| 2 | 1.0000 | 7.8946 | 0.2948 | 0.0070 | 0.3018 |
| 3 | 2.0000 | 7.8104 | 0.3018 | 0.0073 | 0.3091 |
| 4 | 3.0000 | 7.7261 | 0.3091 | 0.0076 | 0.3167 |
| 5 | 4.0000 | 7.6419 | 0.3167 | 0.0079 | 0.3246 |
| 6 | 5.0000 | 7.5577 | 0.3246 | 0.0083 | 0.3328 |
| 7 | 6.0000 | 7.4734 | 0.3328 | 0.0086 | 0.3415 |
| 8 | 7.0000 | 7.3892 | 0.3415 | 0.0090 | 0.3505 |
| 9 | 8.0000 | 7.3050 | 0.3505 | 0.0094 | 0.3599 |
| 10 | 9.0000 | 7.2207 | 0.3599 | 0.0099 | 0.3698 |
| 11 | 10.0000 | 7.1365 | 0.36982 | | |

As just explained, Euler's method is first-order accurate; therefore, $m = 1$. From the computed results, $R_1 = 0.369817$, $R_2 = 0.370856$, and $\Delta x_1 = 2\Delta x_2$. Thus,

$$M_{\text{out}} = 2R_2 - R_1 = 2(0.370856) - 0.369817 = 0.3718944$$

The extrapolated value of the exit Mach number differs from the exact value by only $-0.00947\%$.

**Historical Note: Lewis Fry Richardson** (1881–1953) was born in Northumberland, England. He was the youngest of seven children in a Quaker family. He was educated at Bootham School, Durham College of Science, Newcastle, and King's College, Cambridge, where in 1903 he took a first class in natural science tripos. After graduating from Cambridge, he held a number of short research positions (in government, at the National Physical Laboratory; in academia, at Aberystwyth and Manchester; and in industry). In 1913, he became the superintendent of the Eskdalemuir Observatory of the Meteorological Office, located in southern Scotland. Because of his strong religious and personal beliefs, Richardson declared himself a conscientious objector at the outbreak of World War I. He joined the Society of Friends (Quakers) ambulance service in France and drove ambulances during the war from 1916 to 1919. At the conclusion of the war, Richardson returned to work at the Meteorological Office. However, he resigned his position in 1920 because the office became part of the Air Ministry (at the strong urging of Winston Churchill), and he did not want to become part of the military.

He published a book entitled *Weather Prediction by Numerical Process* in 1922. He was awarded a D.Sc. degree in physics from the University of London in 1926. He also obtained a special B.Sc. in psychology from the University of London in 1929. Richardson published nearly 30 papers on the

(*Continued*)

*(Continued)*

mathematics of the weather. His finite-difference numerical work is the foundation upon which modern weather prediction is built. Richardson's method for the solution of differential equations is a finite-difference technique that is discussed to this day in any course on numerical analysis. He was elected a Fellow to the Royal Society in 1926 and was the principal of Paisley Technical College from 1929 to 1940. After retiring in 1940, he applied mathematics to model the causes of wars and wrote extensively on the subject. Dr. Richardson died at his home in Kilmun, Argyllshire, Scotland. For an excellent, brief, and personal account of Lewis Richardson's life and work, see Ref. (9.18).

**Example 9.9. Numerical solution of the ordinary differential equation for subsonic gas flow in a constant-diameter pipe with friction (i.e., Fanno flow)**

Air ($\gamma = 1.4$) enters a constant-area, insulated duct (see Figure 9.9) with a Mach number of 0.60. The duct length is 45 cm; the duct diameter is 3 cm; and the friction coefficient is 0.02. Use Heun's predictor–corrector method to determine the Mach number at the duct outlet.

**Solution**

Because the duct has a constant diameter, the area term in Eq. (9.40) drops out, and upon rearrangement, the ordinary differential equation that we will solve is

$$\frac{dM}{dx} = F(x, M) = \frac{\gamma M^3[2 + (\gamma - 1)M^2]}{4(1 - M^2)} \frac{f}{D}$$

Again, we will begin with a relatively coarse grid, dividing the duct length into 10 evenly spaced increments (i.e., $\Delta x = 4.5$ cm). The computations are straightforward, and the results from a spreadsheet program are shown in Table 9.5.

**TABLE 9.5** Heun's Predictor–Corrector Calculations for Example 9.9

| Point | $x$ | $M_i$ | $F(x_i, M_i)$ | $M_p$ | $F(x_{i+1}, M_p)$ | $M_{i+1}$ |
|---|---|---|---|---|---|---|
| 1 | 0.0000 | 0.6000 | 0.0017 | 0.6076 | 0.0018 | 0.6078 |
| 2 | 4.5000 | 0.6078 | 0.0018 | 0.6158 | 0.0019 | 0.6161 |
| 3 | 9.0000 | 0.6161 | 0.0019 | 0.6246 | 0.0020 | 0.6249 |
| 4 | 13.5000 | 0.6249 | 0.0020 | 0.6339 | 0.0021 | 0.6342 |
| 5 | 18.0000 | 0.6342 | 0.0022 | 0.6439 | 0.0023 | 0.6442 |
| 6 | 22.5000 | 0.6442 | 0.0023 | 0.6546 | 0.0025 | 0.6550 |
| 7 | 27.0000 | 0.6550 | 0.0025 | 0.6663 | 0.0027 | 0.6667 |
| 8 | 31.5000 | 0.6667 | 0.0027 | 0.6789 | 0.0030 | 0.6795 |
| 9 | 36.0000 | 0.6795 | 0.0030 | 0.6929 | 0.0033 | 0.6935 |
| 10 | 40.5000 | 0.6935 | 0.0033 | 0.7083 | 0.0037 | 0.7092 |
| 11 | 45.0000 | 0.7092 | | | | |

It is seen that the results compare most favorably with the exact solution found in Example 9.4 (i.e., $M_{out} = 0.7093$). Hence, the numerical value of the exit Mach number differs from the exact value by −0.0179%. Again, it should be noted that the solution was obtained on a very coarse grid. Reducing the grid size by a factor of four (41 grid points instead of just 11) yields an exit Mach number of 0.70925, which differs from the exact value by a scant −0.0068%. The conclusion is that Heun's predictor corrector method can produce accurate results with very little effort for problems with friction.

---

Next, we will tackle a problem that contains both friction and area variation. To solve this problem, we will employ the Runge–Kutta fourth-order method. However, we could just as easily use either Euler's method (particularly if Richardson's extrapolation is included) or Heun's method. Of course, we expect to obtain more accuracy from the Runge–Kutta approach for the same grid.

Before proceeding to the next example, it is helpful to rearrange Eq. (9.40) as follows:

$$\frac{dM}{dx} = F(x, M) = \left\{\frac{M[2 + (\gamma - 1)M^2]}{2}\right\}\left\{\frac{\left[-\frac{1}{A}\left(\frac{dA}{dx}\right) + \frac{1}{2}\gamma M^2\left(\frac{f}{D}\right)\right]}{(1 - M^2)}\right\} \tag{9.52}$$

From this arrangement, we can observe that $F(x, M)$ is the product of two groups of terms: One group is solely a function of $M$ and $\gamma$, and the other is a ratio that includes both area and friction effects. Note that this ratio introduces a singularity when the Mach number becomes equal to unity, or, said another way, the right-hand side of Eq. (9.52) becomes infinite at $M = 1$. Thus, for problems involving a sonic point (e.g., choked flow in C–D nozzles), special treatment for the sonic point must be formulated. For all other points, Eq. (9.52) is numerically solved using the solver in the manner just described.

There are several approaches that have been used to resolve the difficulty at the sonic point [e.g., see Ref. (9.19)]; however, the *method of Beans* [see Ref. (9.20)] is generally accepted as the preferred approach. By this approach, *l'Hôpital's rule* is used to obtain a finite value for Eq. (9.52) as the Mach number approaches unity. To use this rule, the ratio on the right side of Eq. (9.52) is isolated and the Mach number is allowed to approach unity. To keep the value of the ratio bounded, both the numerator and denominator must approach zero. So, according to l'Hôpital's rule, the derivative of each is taken and we obtain in the limit

$$\lim_{M\to 1}\left[\frac{-\frac{1}{A}\left(\frac{dA}{dx}\right) + \frac{1}{2}\gamma M^2\left(\frac{f}{D}\right)}{(1 - M^2)}\right] = \lim_{M\to 1}\left\{\frac{\frac{d}{dx}\left[-\frac{1}{A}\left(\frac{dA}{dx}\right) + \frac{1}{2}\gamma M^2\left(\frac{f}{D}\right)\right]}{-2M\frac{dM}{dx}}\right\}$$

$$= \frac{\dfrac{d}{dx}\left[-\dfrac{1}{A}\left(\dfrac{dA}{dx}\right)\right]_{M\to 1} + \dfrac{1}{2}\gamma\dfrac{d}{dx}\left(\dfrac{f}{D}\right)_{M\to 1} + \gamma\left[\left(\dfrac{f}{D}\right)\left(\dfrac{dM}{dx}\right)\right]_{M\to 1}}{-2\left(\dfrac{dM}{dx}\right)_{M\to 1}}$$

Combining this expression with Eq. (9.52) results in a quadratic equation for $dM/dx$. [Note that $M[2 + (\gamma - 1)M^2]/2 \to (\gamma + 1)/2$ as $M \to 1$.] This is the limiting form of Eq. (9.52) that applies only at a sonic point (or, for numerical purposes, in the neighborhood of the point):

$$\frac{4}{\gamma + 1}\left(\frac{dM}{dx}\right)^2_{M\to 1} + \gamma\left(\frac{f}{D}\right)_{M\to 1}\left(\frac{dM}{dx}\right)_{M\to 1} - \frac{d}{dx}\left(\frac{1}{A}\frac{dA}{dx}\right)_{M\to 1} + \frac{\gamma}{2}\frac{d}{dx}\left(\frac{f}{D}\right)_{M\to 1} = 0 \tag{9.53}$$

The solution of this equation yields two roots for the slope of the Mach number distribution at the sonic point: $dM/dx > 0$ for accelerating flows (subsonic flows when $dA/dx < 0$ and supersonic flows when $dA/dx > 0$) and $dM/dx < 0$ for decelerating flows (subsonic flows when $dA/dx > 0$ and supersonic flows when $dA/dx < 0$).

The location of the sonic point is readily determined from the requirement that

$$\left(-\frac{1}{A}\frac{dA}{dx} + \frac{1}{2}\gamma M^2\frac{f}{D}\right)_{M\to 1} \to 0 \tag{9.54}$$

To demonstrate how to employ this method, suppose the shape of a symmetrical nozzle with a circular cross-section is specified by

$$D = 2\left[1 + \frac{1}{2}\cos\left(\pi\frac{x}{L}\right)\right]D_t \tag{9.55}$$

where $D_t$ is the diameter of the throat. When $x = 0$, $D = D_{in} = 3D_t$; when $x = L$, $D = D_t$; and when $x = 2L$, $D = D_{out} = 3D_t$. For a circular geometry, $(1/A)dA/dx = (2/D)dD/dx$. Accordingly, Eq. (9.54) becomes

$$\left(\frac{2}{D}\frac{dD}{dx}\right)_{M\to 1} = \left(\frac{\gamma}{2}\frac{f}{D}\right)_{M\to 1}$$

From the given nozzle profile, Eq. (9.55), differentiation yields $dD/dx = -(\pi D_t/L)\sin(\pi x/L)$. Thus,

$$\left(\frac{x}{L}\right)_{sp} = -\frac{1}{\pi}\sin^{-1}\left(\frac{\gamma f L}{4\pi D_t}\right)$$

For $\gamma = 1.4$, $f = 0.4$ (which is very large for illustrative purposes), and $L = 2D_t$, we find that $x_{sp} = 1.0284L$. (Care must be taken to obtain the correct angle that appears in the profile equation, *viz.*, 185.1134°.) As expected, this location is slightly downstream of the throat, which, as noted previously, is at $x = L$ (at an angle of 180° in the profile function).

Once the location of the sonic point is determined, the initial-value problem for the Mach number on either side of this point must be solved; that is, on the upstream side of the sonic point, the solution is marched towards the nozzle inlet, while on the downstream side of the sonic point it is marched towards the nozzle exit. The reason for this peculiar approach is that in an initial-value problem involving a first-order equation, information can be specified at only one location. For this problem, the initial information is $M = 1$ at the sonic point. Hence, the numerical procedure is used to determine the inlet and exiting values of Mach number. To handle the grid points on either side of the sonic point, the results of the solution of Eq. (9.53) are employed by use of either of the following equations, depending on whether we are marching backwards or forwards, respectively:

$$M_{i-1} = M_i - \left(\frac{dM}{dx}\right)_{M\to 1}(x_{sp} - x_{throat}) \tag{9.56}$$

$$M_{i+1} = M_i + \left(\frac{dM}{dx}\right)_{M\to 1}(x_{i+1} - x_{sp}) \tag{9.57}$$

Beyond each of these grid points, numerical solution of Eq. (9.52) is employed, as will be demonstrated in the next example.

**Example 9.10. Numerical solution of the ordinary differential equations for choked flow in a C–D nozzle with friction**

Air ($\gamma = 1.4$) flows through a symmetrical C–D nozzle with a circular cross-section. The shape of the nozzle is given by Eq. (9.55). Take the length of the nozzle to be equal to twice the throat diameter (i.e., $L = D_t$). Assuming that the nozzle is choked, determine the Mach number distribution for both subsonic and supersonic flow in the diverging portion of the nozzle. Assume that the friction coefficient is 0.4. Use the method of Beans and the fourth-order Runge–Kutta method to solve this problem on a grid in which $\Delta x/L = 0.05$.

**Solution**

The first step in the solution procedure is to determine the location of the sonic point $x_{sp}$ from the given information (in this case, however, that calculation was already performed, and thus the result need only be written here) and then to determine the various nozzle parameters, which are contained within the quadratic equation for $dM/dx$ at the sonic point:

$$\frac{x_{sp}}{L} = 1.0284$$

$$D_{sp} = 2\left[1 + \frac{\cos(\pi x_{sp}/L)}{2}\right]D_t = 1.0040D_t$$

$$\left(\frac{dD}{dx}\right)_{sp} = -\frac{\pi}{L}\sin\left(\pi\frac{x_{sp}}{L}\right)D_t = 0.2800\frac{D_t}{L}$$

$$\left(\frac{d^2D}{dx^2}\right)_{sp} = -\frac{\pi^2}{L^2}\cos\left(\pi\frac{x_{sp}}{L}\right)D_t = 9.8303\frac{D_t}{L^2}$$

Now Eq. (9.53) may be written as

$$a\left(\frac{dM}{dx}\right)_{sp}^2 + b\left(\frac{dM}{dx}\right)_{sp} + c = 0$$

where

$$a = \frac{4}{\gamma + 1} = 1.6667$$

$$b = \left(\frac{\gamma f}{D}\right)_{sp} = \frac{0.5578}{D_t}$$

$$c = -\left[\frac{d}{dx}\left(\frac{1}{A}\frac{dA}{dx}\right)\right]_{sp} + \left[\frac{d}{dx}\left(\frac{\gamma f}{2D}\right)\right]_{sp} = -2\left[\frac{d}{dx}\left(\frac{1}{D}\frac{dD}{dx}\right)\right]_{sp} + \frac{\gamma f}{2}\left[\frac{d}{dx}\left(\frac{1}{D}\right)\right]_{sp}$$

$$= -\left(\frac{2}{D}\frac{d^2D}{dx^2}\right)_{sp} + 2\left(\frac{1}{D}\frac{dD}{dx}\right)_{sp}^2 - \left(\frac{\gamma f}{2D^2}\frac{dD}{dx}\right)_{sp}$$

$$= -\frac{2}{(1.0040D_t)}\left(9.8303\frac{D_t}{L^2}\right) + 2\left(\frac{0.2799D_t/L}{1.0040D_t}\right)^2 - \frac{(1.4)(0.4)(0.2799D_t/L)}{2(1.0040D_t)^2}$$

$$= -\frac{19.5827}{L^2} - \frac{0.0777}{D_tL}$$

With these coefficients and $L = 2D_t$, the two roots for $(dM/dx)_{sp}$ are computed to be

$$\left(\frac{dM}{d(x/L)}\right)_{sp} = \frac{-b + \sqrt{b^2 - 4ac}}{2a} = 3.1094$$

$$\left(\frac{dM}{d(x/L)}\right)_{sp} = \frac{-b - \sqrt{b^2 - 4ac}}{2a} = -3.7787$$

The positive value (for accelerating flows) is inserted in Eq. (9.56), and the Mach number at $x/L = 1$ is found to be 0.9117. Backward solution is continued using the Runge–Kutta fourth-order method to solve Eq. (9.52). The solution procedure is implemented with the aid of a spreadsheet program, and the results are contained in Table 9.6. It must be kept in mind that the $k$'s in the table are slopes of $dM/dx$ at various locations within a given grid space. The location and Mach number coordinates that are to be used for each $k$ [refer to Eq. (9.51)] are listed above the corresponding column of values.

To complete the solution of this example, we return to the sonic point and use the positive root for $(dM/dx)_{sp}$ to compute the supersonic solution and the negative root to compute the subsonic distribution. The results are contained in Tables 9.7 and 9.8, respectively.

---

With the Mach number distribution in hand, we may accomplish the distribution of various flow properties by direct computation. The relationships needed for these computations are established from the local static-to-stagnation ratios of temperature and pressure, from the mass-flow relation, from the Mach number relation,

**TABLE 9.6** Runge–Kutta Solution of Subsonic Flow in the Converging Portion of a C–D Nozzle with Friction

| | | | | $x_i$ | $x_i$ | $x_i - \Delta x/2$ | $x_i - \Delta x/2$ | $x_i - \Delta x$ | |
|---|---|---|---|---|---|---|---|---|---|
| | | | | $M_i$ | $M_i$ | $M_i - k_1\Delta x/2$ | $M_i - k_2\Delta x/2$ | $M_i - k_3\Delta x$ | |
| Pt | $x/L$ | $D_i/D_t$ | $M_i$ | $F(x_i, M_i)$ | $k_1$ | $k_2$ | $k_3$ | $k_4$ | $M_{i-1}$ |
| 22 | 1.0284 | 1.0040 | 1.0000 | 3.1094 | 3.1094 | 3.1094 | 3.1094 | 3.1094 | 0.9117 |
| 21 | 1.0000 | 1.0000 | 0.9117 | 2.9306 | 2.9306 | 2.8451 | 2.8956 | 2.7385 | 0.7687 |
| 20 | 0.9500 | 1.0123 | 0.7687 | 2.7276 | 2.7276 | 2.5605 | 2.6135 | 2.4349 | 0.6395 |
| 19 | 0.9000 | 1.0489 | 0.6395 | 2.4221 | 2.4221 | 2.2382 | 2.2792 | 2.0936 | 0.5266 |
| 18 | 0.8500 | 1.1090 | 0.5266 | 2.0857 | 2.0857 | 1.9009 | 1.9334 | 1.7537 | 0.4307 |
| 17 | 0.8000 | 1.1910 | 0.4307 | 1.7482 | 1.7482 | 1.5748 | 1.6005 | 1.4366 | 0.3512 |
| 16 | 0.7500 | 1.2929 | 0.3512 | 1.4326 | 1.4326 | 1.2784 | 1.2985 | 1.1561 | 0.2867 |
| 15 | 0.7000 | 1.4122 | 0.2867 | 1.1532 | 1.1532 | 1.0219 | 1.0374 | 0.9183 | 0.2351 |
| 14 | 0.6500 | 1.5460 | 0.2351 | 0.9162 | 0.9162 | 0.8082 | 0.8198 | 0.7231 | 0.1943 |
| 13 | 0.6000 | 1.6910 | 0.1943 | 0.7215 | 0.7215 | 0.6349 | 0.6433 | 0.5664 | 0.1623 |
| 12 | 0.5500 | 1.8436 | 0.1623 | 0.5653 | 0.5653 | 0.4969 | 0.5030 | 0.4425 | 0.1372 |
| 11 | 0.5000 | 2.0000 | 0.1372 | 0.4417 | 0.4417 | 0.3882 | 0.3925 | 0.3452 | 0.1176 |
| 10 | 0.4500 | 2.1564 | 0.1176 | 0.3447 | 0.3447 | 0.3029 | 0.3059 | 0.2689 | 0.1024 |
| 9 | 0.4000 | 2.3090 | 0.1024 | 0.2686 | 0.2686 | 0.2359 | 0.2379 | 0.2089 | 0.0905 |
| 8 | 0.3500 | 2.4540 | 0.0905 | 0.2087 | 0.2087 | 0.1829 | 0.1843 | 0.1612 | 0.0813 |
| 7 | 0.3000 | 2.5878 | 0.0813 | 0.1611 | 0.1611 | 0.1405 | 0.1414 | 0.1228 | 0.0742 |
| 6 | 0.2500 | 2.7071 | 0.0742 | 0.1227 | 0.1227 | 0.1059 | 0.1066 | 0.0912 | 0.0689 |
| 5 | 0.2000 | 2.8090 | 0.0689 | 0.0912 | 0.0912 | 0.0772 | 0.0776 | 0.0646 | 0.0650 |
| 4 | 0.1500 | 2.8910 | 0.0650 | 0.0646 | 0.0646 | 0.0525 | 0.0527 | 0.0413 | 0.0624 |
| 3 | 0.1000 | 2.9511 | 0.0624 | 0.0413 | 0.0413 | 0.0305 | 0.0306 | 0.0202 | 0.0609 |
| 2 | 0.0500 | 2.9877 | 0.0609 | 0.0202 | 0.0202 | 0.0100 | 0.0101 | 0.0000 | 0.0604 |
| 1 | 0.0000 | 3.0000 | 0.0604 | | | | | | |

and from the equation of state. For convenience, we may write these relations as follows, respectively:

$$\frac{T_o}{T} = 1 + \frac{\gamma - 1}{2} M^2$$

$$\frac{p}{p_o} = \left(\frac{T}{T_o}\right)^{\gamma/(\gamma-1)}$$

**TABLE 9.7** Runge–Kutta Solution of Supersonic Flow in the Diverging Portion of a C–D Nozzle with Friction

| | | | | $x_i$ | $x_i$ | $x_i + \Delta x/2$ | $x_i + \Delta x/2$ | $x_i + \Delta x$ | |
|---|---|---|---|---|---|---|---|---|---|
| Supersonic Nozzle Solution | | | | $M_i$ | $M_i$ | $M_i + k_1\Delta x/2$ | $M_i + k_2\Delta x/2$ | $M_i + k_3\Delta x$ | |
| Pt | $x/L$ | $D_i/D_t$ | $M_i$ | $F(x_i, M_i)$ | $k_1$ | $k_2$ | $k_3$ | $k_4$ | $M_{i+1}$ |
| 23 | 1.0284 | 1.0040 | 1.0000 | 3.1094 | 3.1094 | 3.1094 | 3.1094 | 3.1094 | 1.0671 |
| 24 | 1.0500 | 1.0123 | 1.0671 | 3.2190 | 3.2190 | 3.2456 | 3.2289 | 3.2683 | 1.2291 |
| 25 | 1.1000 | 1.0489 | 1.2291 | 3.2733 | 3.2733 | 3.2851 | 3.2817 | 3.2706 | 1.3931 |
| 26 | 1.1500 | 1.1090 | 1.3931 | 3.2731 | 3.2731 | 3.2407 | 3.2465 | 3.1945 | 1.5551 |
| 27 | 1.2000 | 1.1910 | 1.5551 | 3.1946 | 3.1946 | 3.1256 | 3.1344 | 3.0501 | 1.7115 |
| 28 | 1.2500 | 1.2929 | 1.7115 | 3.0497 | 3.0497 | 2.9525 | 2.9618 | 2.8532 | 1.8592 |
| 29 | 1.3000 | 1.4122 | 1.8592 | 2.8527 | 2.8527 | 2.7348 | 2.7438 | 2.6178 | 1.9961 |
| 30 | 1.3500 | 1.5460 | 1.9961 | 2.6174 | 2.6174 | 2.4850 | 2.4933 | 2.3555 | 2.1206 |
| 31 | 1.4000 | 1.6910 | 2.1206 | 2.3551 | 2.3551 | 2.2131 | 2.2207 | 2.0751 | 2.2314 |
| 32 | 1.4500 | 1.8436 | 2.2314 | 2.0748 | 2.0748 | 1.9267 | 1.9335 | 1.7833 | 2.3279 |
| 33 | 1.5000 | 2.0000 | 2.3279 | 1.7830 | 1.7830 | 1.6313 | 1.6376 | 1.4848 | 2.4096 |
| 34 | 1.5500 | 2.1564 | 2.4096 | 1.4845 | 1.4845 | 1.3310 | 1.3368 | 1.1828 | 2.4763 |
| 35 | 1.6000 | 2.3090 | 2.4763 | 1.1826 | 1.1826 | 1.0285 | 1.0338 | 0.8796 | 2.5278 |
| 36 | 1.6500 | 2.4540 | 2.5278 | 0.8794 | 0.8794 | 0.7255 | 0.7304 | 0.5766 | 2.5642 |
| 37 | 1.7000 | 2.5878 | 2.5642 | 0.5765 | 0.5765 | 0.4231 | 0.4277 | 0.2747 | 2.5855 |
| 38 | 1.7500 | 2.7071 | 2.5855 | 0.2746 | 0.2746 | 0.1221 | 0.1264 | −0.0257 | 2.5917 |
| 39 | 1.8000 | 2.8090 | 2.5917 | −0.0258 | −0.0258 | −0.1775 | −0.1735 | −0.3248 | 2.5829 |
| 40 | 1.8500 | 2.8910 | 2.5829 | −0.3249 | −0.3249 | −0.4759 | −0.4721 | −0.6230 | 2.5592 |
| 41 | 1.9000 | 2.9511 | 2.5592 | −0.6231 | −0.6231 | −0.7739 | −0.7704 | −0.9214 | 2.5206 |
| 42 | 1.9500 | 2.9877 | 2.5206 | −0.9215 | −0.9215 | −1.0729 | −1.0696 | −1.2218 | 2.4671 |
| 43 | 2.0000 | 3.0000 | 2.4671 | | | | | | |

$$\dot{m} = \rho AV$$

$$V = Ma = M\sqrt{\gamma RT}$$

$$p = \rho RT$$

Now for steady, one-dimensional, adiabatic flow in a variable-area geometry with no mass addition, the relation between the stagnation temperature at location $x_j$ to

**TABLE 9.8** Runge–Kutta Solution of Subsonic Flow in the Diverging Portion of a C–D Nozzle with Friction

| | | | | $x_i$ | $x_i$ | $x_i + \Delta x/2$ | $x_i + \Delta x/2$ | $x_i + \Delta x$ | |
|---|---|---|---|---|---|---|---|---|---|
| Subsonic Solution | | | | $M_i$ | $M_i$ | $M_i$ | $M_i + k_2\Delta x/2$ | $M_i + k_3\Delta x$ | |
| Pt | $x/L$ | $D_i/D_t$ | $M_i$ | $F(x_i, M_i)$ | $k_1$ | $k_2$ | $k_3$ | $k_4$ | $M_{i+1}$ |
| 23 | 1.0284 | 1.0040 | 1.0000 | −3.7787 | −3.7787 | −3.7787 | −3.7787 | −3.7787 | 0.9184 |
| 24 | 1.0500 | 1.0123 | 0.9184 | −3.4585 | −3.4585 | −3.2307 | −3.3455 | −3.0517 | 0.7546 |
| 25 | 1.1000 | 1.0489 | 0.7546 | −3.0193 | −3.0193 | −2.7452 | −2.8198 | −2.5543 | 0.6154 |
| 26 | 1.1500 | 1.1090 | 0.6154 | −2.5366 | −2.5366 | −2.2843 | −2.3341 | −2.0964 | 0.4998 |
| 27 | 1.2000 | 1.1910 | 0.4998 | −2.0868 | −2.0868 | −1.8638 | −1.8994 | −1.6932 | 0.4056 |
| 28 | 1.2500 | 1.2929 | 0.4056 | −1.6871 | −1.6871 | −1.4966 | −1.5228 | −1.3494 | 0.3299 |
| 29 | 1.3000 | 1.4122 | 0.3299 | −1.3453 | −1.3453 | −1.1874 | −1.2066 | −1.0647 | 0.2699 |
| 30 | 1.3500 | 1.5460 | 0.2699 | −1.0619 | −1.0619 | −0.9342 | −0.9482 | −0.8346 | 0.2228 |
| 31 | 1.4000 | 1.6910 | 0.2228 | −0.8327 | −0.8327 | −0.7313 | −0.7414 | −0.6518 | 0.1858 |
| 32 | 1.4500 | 1.8436 | 0.1858 | −0.6504 | −0.6504 | −0.5710 | −0.5781 | −0.5081 | 0.1570 |
| 33 | 1.5000 | 2.0000 | 0.1570 | −0.5072 | −0.5072 | −0.4453 | −0.4503 | −0.3958 | 0.1346 |
| 34 | 1.5500 | 2.1564 | 0.1346 | −0.3953 | −0.3953 | −0.3471 | −0.3506 | −0.3081 | 0.1171 |
| 35 | 1.6000 | 2.3090 | 0.1171 | −0.3077 | −0.3077 | −0.2701 | −0.2725 | −0.2392 | 0.1035 |
| 36 | 1.6500 | 2.4540 | 0.1035 | −0.2389 | −0.2389 | −0.2093 | −0.2109 | −0.1845 | 0.0930 |
| 37 | 1.7000 | 2.5878 | 0.0930 | −0.1844 | −0.1844 | −0.1607 | −0.1618 | −0.1405 | 0.0849 |
| 38 | 1.7500 | 2.7071 | 0.0849 | −0.1404 | −0.1404 | −0.1211 | −0.1219 | −0.1043 | 0.0788 |
| 39 | 1.8000 | 2.8090 | 0.0788 | −0.1043 | −0.1043 | −0.0882 | −0.0887 | −0.0738 | 0.0744 |
| 40 | 1.8500 | 2.8910 | 0.0744 | −0.0738 | −0.0738 | −0.0599 | −0.0602 | −0.0472 | 0.0714 |
| 41 | 1.9000 | 2.9511 | 0.0714 | −0.0472 | −0.0472 | −0.0348 | −0.0349 | −0.0230 | 0.0696 |
| 42 | 1.9500 | 2.9877 | 0.0696 | −0.0230 | −0.0230 | −0.0114 | −0.0114 | 0.0001 | 0.0690 |
| 43 | 2.0000 | 3.0000 | 0.0690 | | | | | | |

that at location $x_k$ is $(T_o)_j = (T_o)_k$. Furthermore, the mass-flow rate is constant between these locations. Using these identities, it is an easy matter to show (except for the fact that the area is not constant, the development is the same as in Section 9.3) that the relationships needed to compute the flow variables at location $x_k$ are given as follows (note that $T_k = T(x_k)$, $p_j = p(x_j)$, etc.):

$$\frac{T_k}{T_j} = \frac{2 + (\gamma - 1)M_j^2}{2 + (\gamma - 1)M_k^2}$$

$$\frac{p_k}{p_j} = \frac{A_j M_j}{A_k M_k}\sqrt{\frac{T_k}{T_j}} = \frac{A_j M_j}{A_k M_k}\left[\frac{2 + (\gamma - 1)M_j^2}{2 + (\gamma - 1)M_k^2}\right]^{1/2}$$

$$\frac{p_{ok}}{p_{oj}} = \frac{p_{ok}}{p_k}\frac{p_k}{p_j}\frac{p_i}{p_{oj}} = \frac{A_j M_j}{A_k M_k}\left[\frac{2 + (\gamma - 1)M_k^2}{2 + (\gamma - 1)M_j^2}\right]^{\frac{\gamma+1}{2(\gamma-1)}}$$

$$\frac{\rho_k}{\rho_j} = \frac{p_k}{p_j}\frac{T_j}{T_k} = \frac{A_j M_j}{A_k M_k}\left[\frac{2 + (\gamma - 1)M_k^2}{2 + (\gamma - 1)M_j^2}\right]^{1/2} = \frac{A_j V_j}{A_k V_k}$$

$$\frac{s_k - s_j}{R} = -\ln\left(\frac{p_{ok}}{p_{oj}}\right) = \frac{\gamma}{\gamma - 1}\ln\left(\frac{T_k}{T_j}\right) - \ln\left(\frac{p_k}{p_j}\right)$$

To treat the case in which a normal shock resides in the diverging section of the C–D nozzle, a technique known as *shock fitting* may be used. By this approach, the location of the shock must be known. The solution proceeds as in the foregoing example using the supersonic solution for the diverging portion of the nozzle. However, the solution is marched to the upstream location of the shock, say, $x_j$. At that point, the normal-shock relations (the jump conditions) are utilized to compute the properties on the downstream side of the shock, $x_k$, and the solution marching procedure is continued to exit of the nozzle. The normal-shock relations are extracted directly from Chapter 4 and written here as

$$M_k^2 = \frac{M_j^2 + \dfrac{2}{\gamma - 1}}{\dfrac{2\gamma}{\gamma - 1}M_j^2 - 1}$$

$$\frac{T_k}{T_j} = \frac{\left(1 + \dfrac{\gamma - 1}{2}M_j^2\right)\left(\dfrac{2\gamma}{\gamma - 1}M_j^2 - 1\right)}{\left[\dfrac{(\gamma + 1)^2}{2(\gamma - 1)}\right]M_j^2}$$

$$\frac{p_k}{p_j} = \frac{2\gamma M_j^2}{\gamma + 1} - \frac{\gamma - 1}{\gamma + 1}$$

$$\frac{\rho_k}{\rho_j} = \frac{V_j}{V_k} = \frac{(\gamma + 1)M_j^2}{(\gamma - 1)M_j^2 + 2}$$

The combination of different effects into a single one-dimensional problem (e.g., area variation and friction), as we have done in this section, is part of a methodology that is called *generalized one-dimensional compressible flows*. This form of analysis not only includes area and frictional effects, but also incorporates effects of heat addition, mass-flow addition, and drag on the flow. Comprehensive treatment of generalized flows can be found in Refs. (9.6), (9.7), (9.8), and (9.20).

## 9.8 SUMMARY

This chapter has presented a study of compressible flows with friction. In each case, the analysis was started by referring to the continuity, momentum, and energy equations, with a term now included in the momentum equation to account for frictional effects acting on the control volume. Two basic flows were considered: first, adiabatic, constant-area, or Fanno flow, and second, variable-area, adiabatic flow. The phenomenon of choking was shown again to occur for frictional flows, even without area change.

At this point, the simplicity of the approach taken to analyze compressible flows should not be fully appreciated. Whether for isentropic flow, flow with friction, or, as we shall see in subsequent chapters, flows with heat addition and applied electrical and magnetic fields, the emphasis is on the use of the continuity, momentum, and energy equations and the organization of the resultant solutions into corresponding relations with the Mach number as the independent variable.

Also, the value and power of numerical techniques and their application in spreadsheet programs should be recognized as a significant engineering tool. This approach removes much of the drudgery associated with the computation of compressible flows, thus freeing time to delve more deeply into the physical relationships of these flows.

## 9.9 REFERENCES


**9.1** Downey, M. W., Gino Fanno, ETH E-Collection. Eidgenössische Technische Hochschule (Swiss Federal Institute of Technology, Zürich. http://e-collection.ethbib.ethz.ch/ecolpool/nala/nala_128.pdf.

**9.2** Tripp, W., Baehr, W. F., and Iotti, R. "Who Was Fanno?" *Eng Ed* 1965; 56(1): Commentary, p. xii.

**9.3** Tripp, W., Baehr, W. F., and Iotti, R. "Who Was Fanno?" *Eng Ed* 1966; 56(6): Commentary, p. xxiii.

**9.4** Alexandrou, A. N. *Principles of Fluid Mechanics*, Prentice Hall, Upper Saddle River, NJ, 2001, p. 317.

**9.5** *Ibid.*, p. 275.

**9.6** Shapiro, A. *The Dynamics and Thermodynamics of Compressible Fluid Flow*, Vol. 1, Ronald Press, New York, 1953, p. 163.

**9.7** Oosthuizen, P. H., and Carscallen, W. E. *Compressible Fluid Flow*, McGraw-Hill Book Company, New York, 1997, p. 231.

**9.8** Hodge, B. K., and Koenig, K. *Compressible Fluid Dynamics with Personal Computer Applications*, Prentice Hall, Upper Saddle River, NJ, 1995, p. 154.

**9.9** Na, T. Y. "A Simple Method for Locating Shock Waves in Constant Area Ducts with Friction," *Int J Mech Eng Ed* 1975; 3(2): 153–158.

**9.10** Hoffman, J. D. *Numerical Methods for Engineers and Scientists*, 2d ed., Marcel Dekker, New York, 2001, pp. 335–443.

**9.11** Moin, P. *Fundamentals of Engineering Numerical Analysis*, Cambridge University Press, Cambridge, UK, 2001, pp. 45–49.

**9.12** Ferziger, J. H. *Numerical Methods for Engineering Application*, 2d ed., John Wiley & Sons, New York, 1998, pp. 109–110.

**9.13** Schwarz, H. R. *Numerical Analysis: A Comprehensive Introduction*, John Wiley & Sons, New York, 1989, pp. 384–394.

**9.14** Iserles, A. *A First Course in the Numerical Analysis of Differential Equations*, Cambridge University Press, Cambridge, UK, 1996, pp. 1–102.

**9.15** Ferziger, J. H. *Numerical Methods for Engineering Application*, 2d ed., John Wiley & Sons, New York, 1998, pp. 50–53.

**9.16** Richardson, L. F. "The Approximate Arithmetical Solution of Finite Difference of Physical Problems Involving Differential Equations, with Applications to the Stresses of a Masonary Dam," *Philos Trans R Soc* 1911; 210: 307–357.

**9.17** Richardson, L. F. "The Deferred Approach to the Limit," *Philos Trans R Soc* 1927; 226: 299–361.

**9.18** Hunt, J. C. R. "Lewis Fry Richardson and His Contributions to Mathematics, Meteorology, and Models of Conflict," *Ann Rev Fluid Mech* 1998; 30: xiii–xxxvi.

**9.19** Zucrow, M. J., and Hoffman, J. D. *Gas Dynamics*, Vol. 1, John Wiley & Sons, New York, 1976, pp. 502–506.

**9.20** Beans, E. W. "Computer Solution to Generalized One-Dimensional Flow," *AIAA J Spacecraft Rockets* 1970; 7(12): 1460–1464.

## 9.10 PROBLEMS

**9.1** Draw the $T$–$s$ diagram for the adiabatic flow of a gas with $\gamma = 1.4$ in a constant-diameter pipe with friction. The reference Mach number $M_1$ for the flow is 3.0.

**9.2** Draw the $T$–$s$ diagram for the adiabatic flow of a gas with $\gamma = 1.3$ in a constant-diameter pipe with friction. The reference Mach number $M_1$ for the flow is 4.0.

**9.3** Air ($\gamma = 1.4$) flows into a constant-area insulated duct with a Mach number of 0.20. For a duct diameter of 1 cm and friction coefficient of 0.02, determine the duct length required to reach Mach 0.60. Then determine the length required to attain Mach 1. If an additional 75 cm is added to the duct length needed to reach Mach 1, while the initial stagnation conditions are maintained, determine the reduction in flow rate that would occur.

**9.4** Air ($\gamma = 1.4$, $R = 0.287$ kJ/kg·K) enters a constant-area insulated duct with a Mach number of 0.35, a stagnation pressure of 105 kPa, and stagnation temperature of 300 K. For a duct length of 50 cm, duct diameter of 1 cm, and friction coefficient of 0.022, determine the air force on the duct wall.

**9.5** Hydrogen ($\gamma = 1.4$, $R = 4{,}124$ J/kg·K) enters a constant-area insulated duct with a velocity of 2600 m/s, static temperature of 300 K, and stagnation pressure of 520 kPa. The duct is 2 cm in diameter and 10 cm long. For a friction coefficient of 0.02, determine the change of static pressure and temperature in the duct and the exit velocity of the hydrogen.

**9.6** A constant-area duct, 25 cm in length by 1.3 cm in diameter, is connected to an air reservoir through a converging nozzle, as shown in Figure P9.6. For a constant reservoir pressure of 1 MPa and constant reservoir temperature of 600 K, determine the flow rate through the duct for a back pressure of 101 kPa. Assume adiabatic flow in the tube, with $f = 0.023$.

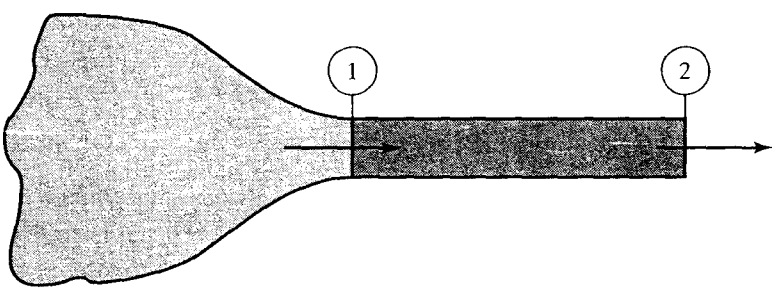


**Figure P9.6**

**9.7** Find the time required for the pressure in a tank filled with nitrogen ($\gamma = 1.4$, $R = 296.8$ J/kg·K), as shown in Figure P9.7, to drop from 1 MPa to 500 kPa. The tank volume is 8 $m^3$, and the tank temperature is 300 K. Assume that the tank

temperature remains constant and that the flow in the 3-m-long, 1-cm-diameter connecting tube is adiabatic, with $f = 0.018$. The back pressure is 101 kPa.

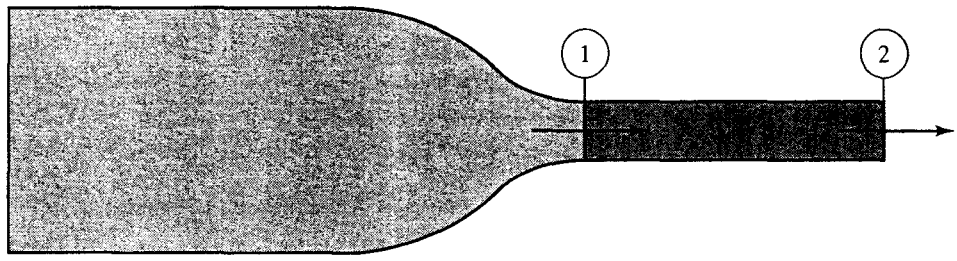


**Figure P9.7**

**9.8** A converging–diverging nozzle has an area ratio of 3.3; that is, the duct area = 3.3 times the throat area, which is 60 $cm^2$. The nozzle is supplied from a tank containing air ($\gamma = 1.4$, $R = 0.287$ kJ/kg·K) at 100 kPa at 270 K. For case *A* of Figure P9.8, find the maximum mass flow possible through the nozzle and the range of back pressures over which the mass flow can be attained. Repeat for case *B*, in which a constant-area insulated duct of length 1.5 m and $f = 0.022$ is added to the nozzle.

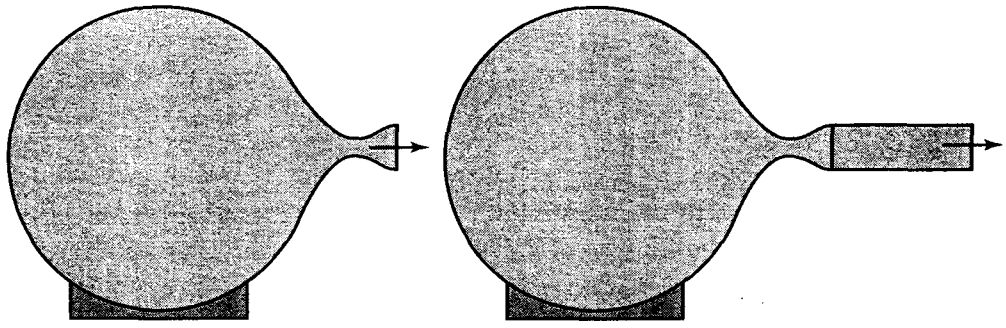


**Figure P9.8**

**9.9** A 3-$m^3$-volume tank *R* is to be filled to a pressure of 200 kPa. (The initial pressure is 0 kPa.) The tank is connected to a reservoir tank *L* containing air at 3 MPa and 300 K, whose volume is also 3 $m^3$. A 30-m length of 2.5-cm-diameter tubing is used to connect the two vessels, as shown in Figure P9.9. Determine the time required to fill the tank to 200 kPa. Assume Fanno flow with $f = 0.02$.

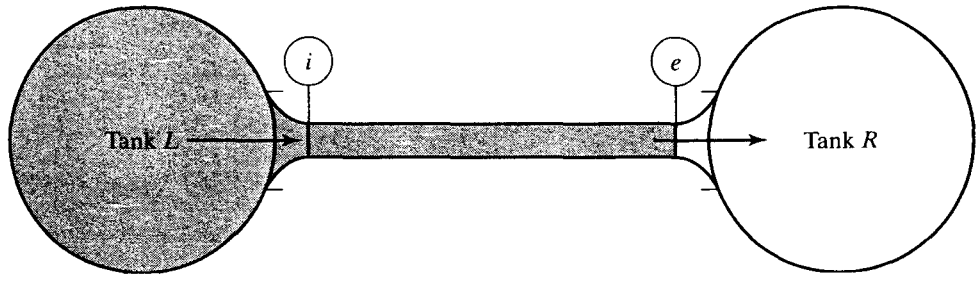


**Figure P9.9**

**9.10** Find the mass-flow rate of air ($\gamma = 1.4$, $R = 0.287$ kJ/kg · K) through the system shown in Figure P9.10. Assume Fanno line flow in the duct and isentropic flow in the converging sections, and take $f = 0.01$.

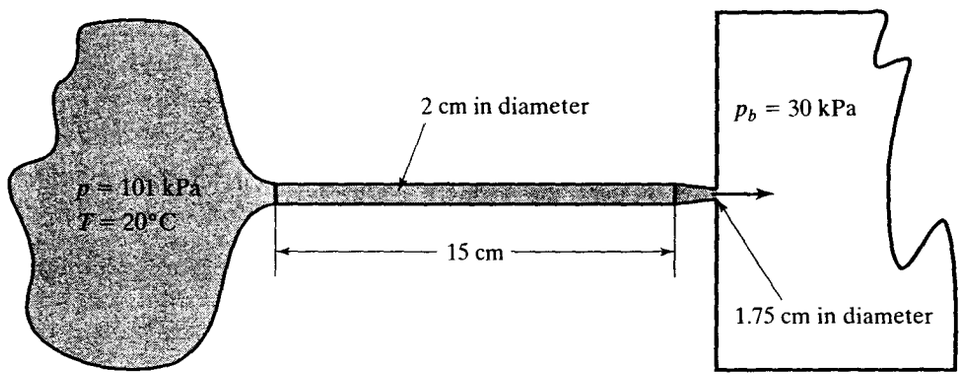


**Figure P9.10**

**9.11** For the flow of air ($\gamma = 1.4$, $R = 0.287$ kJ/kg · K) from the reservoir shown in Figure P9.11 at 650 kPa and 1,000 K, assume isentropic flow in the converging–diverging nozzle and Fanno flow in the constant-area duct, which has a length of 20 cm and a diameter of 1 cm. The area ratio $A_2/A_1$ of the C–D nozzle is 2.9. Take the friction factor to be 0.02.

(a) Find the mass-flow rate for a back pressure of 0 kPa.
(b) For part (a), find the pressure at the exit plane of the duct.
(c) Find the back pressure necessary for a normal shock to occur at the exit plane of the nozzle at point (2).
(d) Find the back pressure necessary for a normal shock to appear just downstream of the nozzle throat at point (1).

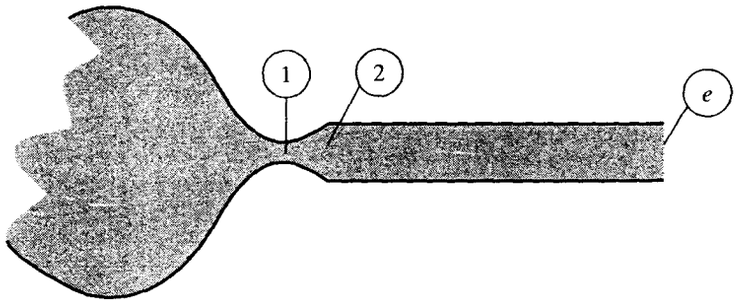


**Figure P9.11**

**9.12** In which configuration of Figure P9.12, (a) or (b), will the high-pressure tank empty faster? Explain.

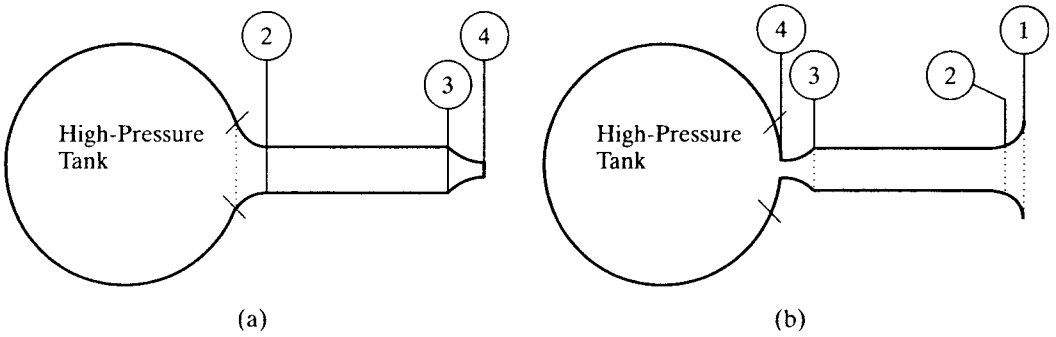


**Figure P9.12**

**9.13** Air ($\gamma = 1.4$, $R = 0.287$ kJ/kg · K) flows through a converging–diverging nozzle with an area ratio of 2.9. (See Figure P9.13.) The nozzle exhausts into a constant-area insulated duct with a length of 50 cm and diameter of 1 cm. If the system back pressure is 50 kPa, determine the range of reservoir pressures over which a normal shock will appear in the duct. Let $f = 0.02$ in the duct.

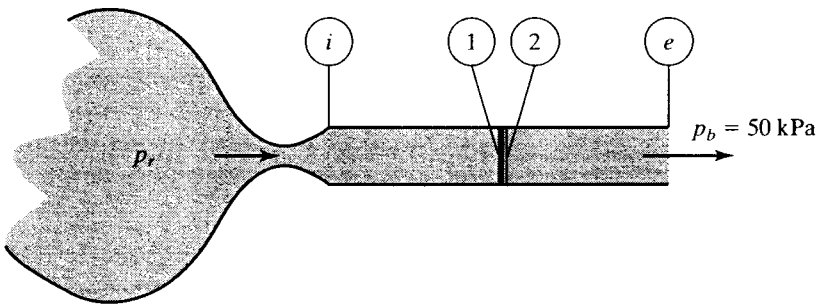


**Figure P9.13**

**9.14** A converging–diverging nozzle with area ratio of 3.2 (see Figure P9.14) exhausts air ($\gamma = 1.4$, $R = 0.287$ kJ/kg · K) into a constant-area insulated duct with a length of 50 cm and diameter of 1 cm. If the reservoir pressure is 500 kPa, determine the range of back pressures over which a normal shock will appear in the duct. Assume that $f = 0.02$.

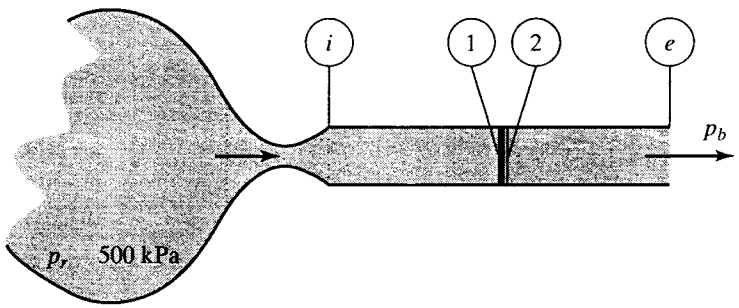


**Figure P9.14**

**9.15** A converging–diverging nozzle with an area ratio of 2 to 1 is supplied by a reservoir containing air ($\gamma = 1.4$, $R = 0.287$ kJ/kg · K) at 500 kPa. The nozzle exhausts into a constant-area duct of length-to-diameter ratio $L/D$ of 25 and friction coefficient of 0.02. Determine the normal-shock location and exit-plane pressure for a back pressure of 0 kPa. Also, locate the shock for a back pressure of 180 kPa. Refer to Figure 9.19 for the nomenclature.

**9.16** Air ($\gamma = 1.4$) enters a pipe of diameter 2 cm at a Mach number of $M_i = 3.0$. A normal shockwave stands in the pipe at a location where the Mach number on the upstream side of the shock is $M_1 = 2.0$. The Mach number exiting the pipe is $M_e = 1.0$. For steady, adiabatic, one-dimensional flow in the pipe (i.e., Fanno flow), determine the location of the shock and the total length of the pipe. Assume that $f = 0.02$.

**9.17** A rocket nozzle is operating with a stretched-out throat ($L = 50$ cm and $D = 10$ cm) as shown in Figure P9.17. If the inlet stagnation conditions are $p_{oi} = 1$ MPa and $T_{oi} = 1{,}500$ K, determine the nozzle exit velocity and mass-flow rate for a back pressure of 30 kPa. The diameter of the nozzle at the exit station is the same as at the inlet station: 30 cm. Treat the exhaust gases as perfect, with $\gamma = 1.4$ and $R = 0.50$ kJ/kg · K. Assume isentropic flow in variable-area sections and Fanno flow in constant-area sections, with $f = 0.022$.

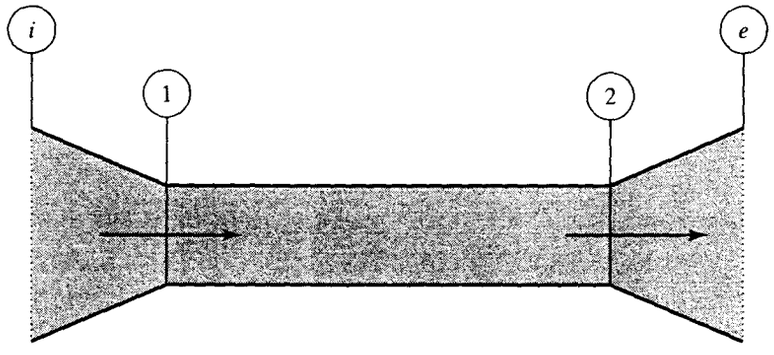


**Figure 9.17**

**9.18** Air ($\gamma = 1.4$, $R = 0.2598$ kJ/kg · K) flows adiabatically in a tube of circular cross-section with an initial Mach number of 0.5, initial static temperature $T_1 = 500$ K, and initial static pressure $p_1 = 600$ kPa. The cross-sectional area of the tube is to be varied so that, taking friction into account, there is no change in the temperature of the stream. Assume that the distance between inlet and exit, $L$, is equal to 100 $D_1$, with $D_1$ = initial duct diameter. Also, take $f = 0.02$. Find the following:

(a) the Mach number $M_2$
(b) $D_2/D_1$
(c) the static pressure $p_2$

**9.19** In a rocket nozzle of area ratio 8 to 1, combustion gases ($\gamma = 1.2$, $R = 0.50$ kJ/kg · K) are expanded from a chamber pressure and temperature of 5 MPa and 2,000 K, respectively. For a nozzle coefficient $C_h$ equal to 0.96, determine the rocket exhaust velocity in space.

**9.20** Air ($\gamma = 1.4$) enters a constant-area, insulated duct (see Figure 9.9) with a Mach number of 0.60. The duct length is 45 cm; the duct diameter is 3 cm; and the friction coefficient is 0.02. Use Euler's explicit method to determine the Mach number at the duct outlet.

**9.21** If Problem 9.21 is solved on finer grids, using the first-order Euler explicit method, the following results for the exit Mach number are obtained:

| $n$ | $\Delta x$ | $M_e$ |
|---|---|---|
| 11 | 4.5 | 0.542147 |
| 21 | 2.25 | 0.542529 |
| 41 | 1.125 | 0.542725 |
| 81 | 0.5625 | 0.542824 |

Determine the error when compared with the exact value of the exit Mach number: 0.542923. Use Richardson's extrapolation method to obtain improved values. Also, compute the error of these values.

**9.22** Heun's predictor–corrector method is of second order, and the Runge–Kutta method used in this chapter is of fourth order. Obtain an expression for each of these methods that could be used to perform Richardson's extrapolation of results $R_2$ and $R_1$ that were determined on two grids that differ by a factor of two (i.e., $\Delta x_2 = \Delta x_1/2$).

**9.23** An airstream ($\gamma = 1.4$, $R = 0.287$ kJ/kg · K) at Mach 2.0 with a pressure of 100 kPa and a temperature of 270 K enters a diverging, linear, conical channel with a ratio of exit area to inlet area of 3.0. (See Figure P9.23.) Determine the back pressure $p_b$ necessary to produce a normal shock in the channel at an area equal to twice the inlet area. Assume one-dimensional, steady flow, with the air behaving as a perfect gas with constant specific heats; assume isentropic flow except for the normal shock.

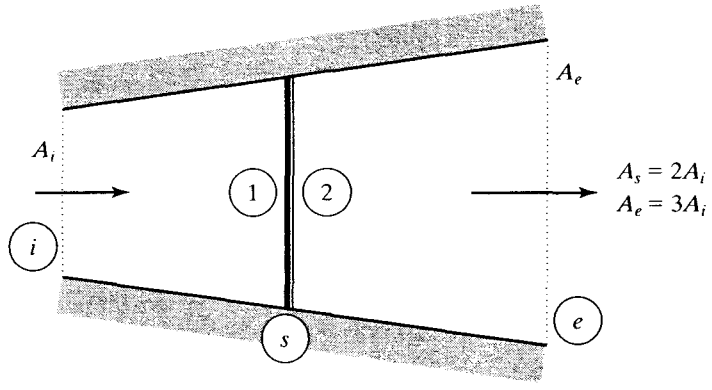


**Figure P9.23**

**9.24** Helium ($\gamma = 5/3$) flows through a symmetrical C–D nozzle with a circular cross-section. The shape of the nozzle is given by

$$D = 2\left[1 + \frac{1}{2}\cos\left(\pi\frac{x}{L}\right)\right]D_t$$

The nozzle length is two times the throat diameter (i.e., $L = 2D_t$). Assuming that the nozzle is choked, determine the Mach-number distribution for both subsonic and supersonic flow in the diverging portion of the nozzle. Assume that the friction coefficient is 0.4. Use the method of Beans [see Ref. (9.20)] and the fourth-order Runge–Kutta method to solve this problem on a grid in which $\Delta x/L = 0.05$.

# Chapter 10

# Flow with Heat Addition or Heat Loss

## 10.1 INTRODUCTION

We have studied in previous chapters the effects on a gas flow of area change and friction. For these cases, flows were assumed to be adiabatic. In this chapter, the effect of heat addition or loss on a one-dimensional gas flow will be investigated. Flows with heat transfer occur in a wide variety of situations—for example, combustion chambers, in which the heat addition is supplied internally by a chemical reaction, and heat exchangers, in which heat flow occurs across the system boundaries.

The analysis which follows will be similar to that of the previous chapter. The continuity, momentum, and energy equations will first be presented for the case of constant-area flow; later, combined effects of heat transfer and area change, as well as friction and heat exchange, will be considered. However, in the application of the flow equations, whereas the frictional force term showed up in the momentum equation, the heat-addition term will be present in the energy equation. Thus, in this chapter, the length of the duct, or, more properly, the term $fL/D_h$, will not be the significant parameter; rather, an expression containing the amount of heat addition and the resultant change of enthalpy of the flow will come into play.

The same simplifying assumptions will be made as in previous chapters: one-dimensional, steady flow of a perfect gas with constant specific heats. In a flow with heat addition, where large temperature changes may result, the assumption of a perfect gas with constant specific heats may produce considerable error. Furthermore, in any chemical reaction, the composition of the products is different from that of the reactants; again, the assumption of a perfect gas with constant specific heats breaks down. However, in cases such as that of the jet-engine combustion chamber, the fuel–air ratio is small enough that the chemical change involves only a small fraction of the overall flow; here, the perfect-gas assumption is reasonable. The assumptions made in the derivations of the flow equations must be kept in mind as we encounter new problems. One of the most important tasks of the engineer in any field is to be able to analyze what may be an extremely complex physical situation, make suitable approximations so as to reduce the overall equations describing the situation to simplified form, and solve these equations, subject to prescribed boundary conditions.

## 10.2 RAYLEIGH LINE FLOW

First we shall study constant-area steady flow with no friction. Refer to the control volume shown in Figure 10.1, in which a small amount of heat $\delta q$, expressed in joules per kilogram (J/kg), is added to the flow.

The continuity equation is

$$\rho V = (\rho + d\rho)(V + dV)$$

so that

$$\frac{d\rho}{\rho} + \frac{dV}{V} = 0 \tag{10.1}$$

or

$$\rho V = \text{constant}$$

The momentum equation is

$$dp + \rho V dV = 0$$

since the only forces acting on the control volume are pressure forces. With $\rho V$ = constant, we can integrate the preceding equation to obtain

$$p + \rho V^2 = \text{constant} \tag{10.2}$$

**Historical Note:** For a constant value of $\rho V$, Eq. (10.2), on a p-$v$ diagram (where $v = 1/\rho$), is a straight line with a negative slope and was named the *Rayleigh line* by Aurel Stodola in his classic book *Steam and Gas Turbines,* McGraw-Hill (1927), p. 84. The corresponding flow is thus called *Rayleigh line flow.*

The energy equation is

$$\delta q = dh + V dV \tag{10.3}$$

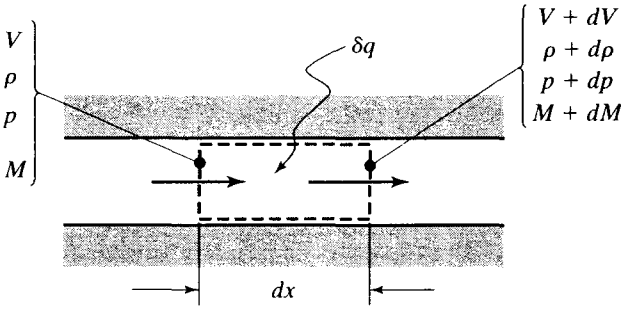


**Figure 10.1** Differential Control Volume for Analysis of Constant-Area Frictionless Flow with Heat Transfer

For a perfect gas,

$$dh = c_p\, dT$$

so that

$$\delta q = c_p dT + V dV \tag{10.4}$$

From the definition of stagnation enthalpy and stagnation temperature (see Section 3.4),

$$h_o = c_p T_o = h + \frac{V^2}{2} = c_p T + \frac{V^2}{2}$$

or

$$c_p dT_o = c_p dT + V dV$$

so that

$$\delta q = c_p dT_o \tag{10.5}$$

Note that if $\delta q = 0$, the flow is adiabatic, and Eq. (10.5) indicates that $T_o = \text{constant}$. Equations (10.1), (10.2), and (10.5) represent the basic equations for constant-area flow with heat exchange. It is now necessary to express these equations in terms of Mach number and arrange the results into a form suitable for application to engineering problems.

Referring to Eq. (10.2), we have

$$p + \rho V^2 = \text{constant}$$

or

$$p\left(1 + \frac{V^2}{RT}\right) = \text{constant}$$

and, since $a^2 = \gamma RT$,

$$p(1 + \gamma M^2) = \text{constant} \tag{10.6}$$

From the perfect-gas law,

$$T = \frac{p}{\rho R}$$

However,

$$\rho = \frac{\dot{m}}{AV}$$

where $V = M\sqrt{\gamma RT}$, so that

$$\sqrt{T} = (\text{constant})pM$$

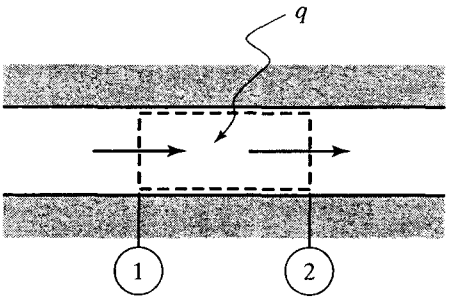


**Figure 10.2** Finite-Length Control Volume for Analysis of Constant-Area Frictionless Flow with Heat Transfer

or

$$T = (\text{constant})\frac{M^2}{(1 + \gamma M^2)^2} \tag{10.7}$$

Let us now apply Eqs. (10.6) and (10.7) to a control volume bounded by cross-sections 1 and 2, as shown in Figure 10.2, between which there is a heat addition $q$. Now,

$$p_1(1 + \gamma M_1^2) = p_2(1 + \gamma M_2^2)$$

or

$$\frac{p_2}{p_1} = \frac{(1 + \gamma M_1^2)}{(1 + \gamma M_2^2)} \tag{10.8}$$

$$\frac{T_1(1 + \gamma M_1^2)^2}{M_1^2} = \frac{T_2(1 + \gamma M_2^2)^2}{M_2^2}$$

or

$$\frac{T_2}{T_1} = \frac{M_2^2}{M_1^2}\frac{(1 + \gamma M_1^2)^2}{(1 + \gamma M_2^2)^2} \tag{10.9}$$

Also, Eq. (10.5) can be integrated for a perfect gas with constant specific heats to yield

$$q = c_p(T_{o2} - T_{o1}) \tag{10.10}$$

To facilitate computation, as well as any tabulation of these expressions, let state 2 be a reference state at which Mach number 1 occurs, as was done for both isentropic and Fanno flows. More physical significance will be attached to the Mach 1 state later. Denoting the properties at Mach 1 by (*), we see that Eqs. (10.8), (10.9), and (10.1) become

$$\frac{p}{p^*} = \frac{1 + \gamma}{1 + \gamma M^2} \tag{10.11}$$

$$\frac{T}{T^*} = \frac{(1+\gamma)^2 M^2}{(1+\gamma M^2)^2} \tag{10.12}$$

$$\frac{V}{V^*} = \frac{\rho^*}{\rho} = \frac{p^*}{p}\frac{T}{T^*}$$

So

$$\frac{V}{V^*} = \frac{(1+\gamma)M^2}{1+\gamma M^2} \tag{10.13}$$

Also, since

$$T_o = T\left(1 + \frac{\gamma - 1}{2} M^2\right)$$

we have

$$\frac{T_o}{T_o^*} = \frac{(1+\gamma)^2}{(1+\gamma M^2)^2}\frac{M^2}{1}\frac{\left(1 + \dfrac{\gamma-1}{2}M^2\right)}{\left(1 + \dfrac{\gamma-1}{2}\right)} = \frac{(1+\gamma)M^2[2 + (\gamma-1)M^2]}{(1+\gamma M^2)^2} \tag{10.14}$$

Finally, with

$$p_o = p\left(1 + \frac{\gamma - 1}{2} M^2\right)^{\gamma/(\gamma-1)}$$

we obtain

$$\frac{p_o}{p_o^*} = \left(\frac{1+\gamma M^2}{1+\gamma}\right)\left(\frac{1 + \dfrac{\gamma-1}{2}M^2}{1 + \dfrac{\gamma-1}{2}}\right)^{\gamma/(\gamma-1)}$$

$$= \left(\frac{1+\gamma M^2}{1+\gamma}\right)\left[\frac{2 + (\gamma-1)M^2}{\gamma+1}\right]^{\gamma/(\gamma-1)} \tag{10.15}$$

These equations are tabulated in Appendix G.

**Example 10.1. Calculation of subsonic flow in constant-area duct with heat addition**

Air ($\gamma = 1.4$, $R = 0.287$ kJ/kg · K, and $c_p = 1.004$ kJ/kg · K) is flowing in a constant-area duct at a Mach number of 0.20, a static temperature of 300 K, and a static pressure of 100 kPa. Heat is then added to the flow at a rate of 50 kJ/(kg of air). Assume frictionless flow and that the air behaves as a perfect gas with constant specific heats. Determine the state of the air at a downstream station. (See Figure 10.3.)

**Solution**

From the isentropic relations at $M_1 = 0.20$, $T/T_{o1} = 0.9921$, so that

$$T_{o1} = \frac{300}{0.9921} = 302.3889 \text{ K}$$

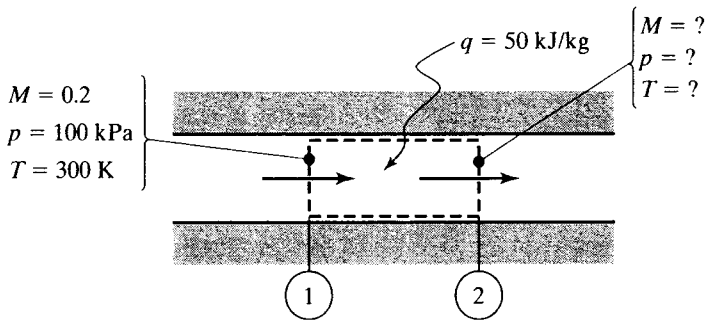


**Figure 10.3** Duct Nomenclature for Example 10.1

From Eq. (10.10),

$$T_{o2} - T_{o1} = \frac{q}{c_p} = \frac{50 \text{ kJ/kg}}{1.004 \text{ kJ/kg} \cdot \text{K}} = 49.8008 \text{ K}$$

so that $T_{o2} = 352.1897$ K. From the Rayleigh flow relations at $M_1 = 0.2$, $T_{o1}/T_o^* = 0.17355$. However,

$$\frac{T_{o2}}{T_o^*} = \left(\frac{T_{o2}}{T_{o1}}\right)\left(\frac{T_{o1}}{T_o^*}\right) = \left(\frac{352.1897}{302.3889}\right)0.17355 = 0.2021$$

Thus, from the Rayleigh flow relations (tabulated in Appendix G), we find that $M_2 = 0.2178$. Other properties at state 2 can be found in a similar fashion:

$$T_2 = \left(\frac{T_2}{T^*}\right)\left(\frac{T^*}{T_1}\right)T_1 = (0.2402)\left(\frac{1}{0.2066}\right)300 = 348.7899 \text{ K}$$

$$p_2 = \left(\frac{p_2}{p^*}\right)\left(\frac{p^*}{p_1}\right)p_1 = (2.2506)\left(\frac{1}{2.2727}\right)100 = 99.0276 \text{ kPa}$$

$$p_{o2} = \left(\frac{p_{o2}}{p_2}\right)p_2 = \left(\frac{1}{0.9675}\right)99.0276 = 102.3541 \text{ kPa}$$

Here, $p_{o2}/p_2$ was obtained from the isentropic flow relations. Since

$$p_{o1} = \left(\frac{p_{o1}}{p_1}\right)p_1 = \left(\frac{1}{0.9725}\right)100 = 102.8278 \text{ kPa}$$

the difference is

$$p_{o1} - p_{o2} = 102.8278 - 102.3541 = 0.4737 \text{ kPa}$$

---

To gain a better understanding of the effect of heat addition on Mach number, let us determine the locus of states for a given mass flow on a $T$–$s$ diagram; the resultant plot is termed the *Rayleigh line*. From Chapter 1, for a perfect gas,

$$ds = c_p\frac{dT}{T} - R\frac{dp}{p}$$

Integrating between a reference state (designated here by the subscript 1; however, we could have just as easily used the location where $M = 1$) and an arbitrary point and assuming constant specific heats [$c_p = \gamma R/(\gamma - 1)$], we get

$$\frac{s - s_1}{c_p} = \ln\frac{T}{T_1} - \frac{(\gamma - 1)}{\gamma}\ln\frac{p}{p_1} \tag{10.16}$$

To plot $s - s_1$ versus $T/T_1$, we must express $p/p_1$ in terms of $T/T_1$. From Eq. (10.8),

$$M^2 = \frac{1}{\gamma}\left[(1 + \gamma M_1^2)\frac{p_1}{p} - 1\right]$$

Also, combining Eqs. (10.8) and (10.9) yields

$$\frac{p}{p_1} = \frac{M_1}{M}\sqrt{\frac{T}{T_1}}$$

or

$$\frac{p}{p_1}\sqrt{\frac{1}{\gamma}\left[(1 + \gamma M_1^2)\frac{p_1}{p} - 1\right]} = M_1\sqrt{\frac{T}{T_1}}$$

Squaring yields

$$\gamma M_1^2\frac{T}{T_1} = \left(\frac{p}{p_1}\right)^2\left[(1 + \gamma M_1^2)\frac{p_1}{p} - 1\right]$$

Simplifying and arranging in quadratic form gives

$$\left(\frac{p}{p_1}\right)^2 - (1 + \gamma M_1^2)\left(\frac{p}{p_1}\right) + \gamma M_1^2\left(\frac{T}{T_1}\right) = 0$$

Solving for $p/p_1$ yields

$$\frac{p}{p_1} = \frac{(1 + \gamma M_1^2)}{2} \pm \frac{\sqrt{(1 + \gamma M_1^2)^2 - 4\gamma M_1^2(T/T_1)}}{2}$$

Returning to Eq. (10.16), we now have

$$\frac{s - s_1}{c_p} = \ln\frac{T}{T_1} - \frac{\gamma - 1}{\gamma}\ln\left[\frac{(1 + \gamma M_1^2) \pm \sqrt{(1 + \gamma M_1^2)^2 - 4\gamma M_1^2(T/T_1)}}{2}\right] \tag{10.17}$$

Note that in order not to obtain a negative square root in the foregoing expression, it is required that

$$\frac{T}{T_1} \le \frac{(1 + \gamma M_1^2)^2}{4\gamma M_1^2}$$

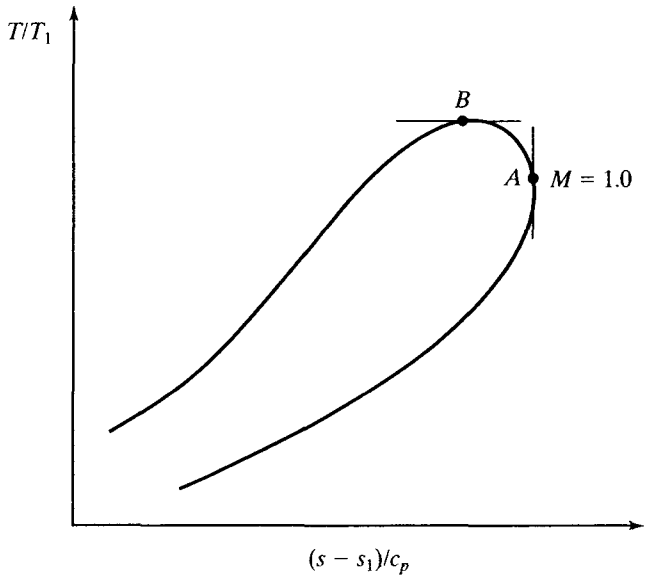


**Figure 10.4** The Rayleigh Line

Equation (10.17) has been sketched in Figure 10.4. To accomplish this, the + sign in Eq. (10.17) is used for the upper portion of the curve up to point $B$; the negative root is used to draw the remainder of the curve. Several features of this plot are to be seen immediately.

First, there is a point of tangency, denoted by $A$, at which $d(\Delta s)/dT$ is equal to zero. The Mach number at this point can be obtained from the continuity and momentum equations. Thus,

$$\frac{d\rho}{\rho} + \frac{dV}{V} = 0 \tag{10.1}$$

$$dp + \rho V dV = 0 \tag{10.2}$$

Rearranging the continuity equation, Eq. (10.1), yields

$$\rho dV = -V d\rho$$

Combining this expression with the momentum equation, Eq. (10.2), yields

$$dp = V^2 d\rho$$

or

$$V^2 = \frac{dp}{d\rho}$$

This expression is valid at any point in the flow. Also,

$$\left(\frac{\partial p}{\partial \rho}\right)_s = a^2$$

Thus, at point $A$, the point of tangency, where $ds/dT = 0$, the preceding two expressions can be equated, and therefore the Mach number is equal to 1. Also, point $B$ on Figure 10.4 represents a point of tangency at which $T/T_1$ is maximum. Since $T/T_1$ can be written exclusively in terms of $M$ [see Eq. (10.9)], to determine this maximum, we set

$$\frac{d(T/T_1)}{dM} = 0$$

Differentiating Eq. (10.9), with point 2 taken to be an arbitrary point, we obtain

$$\frac{d(T/T_1)}{dM} = \left[\frac{(1 + \gamma M_1^2)^2}{M_1^2}\right]\frac{(1 + \gamma M^2)^2 2M - M^2 2(1 + \gamma M^2)2\gamma M}{(1 + \gamma M^2)^2} = 0$$

Simplifying and setting the numerator equal to zero yields

$$1 + \gamma M^2 = 2\gamma M^2$$

or

$$M^2 = \frac{1}{\gamma}$$

$$M_B = \sqrt{\frac{1}{\gamma}} \tag{10.18}$$

The maximum value of $T/T_1$ is now obtained by substituting back into Eq. (10.9):

$$\left(\frac{T}{T_1}\right)_{\max} = \left[\frac{(1 + \gamma M_1^2)^2}{M_1^2}\right]\frac{\left(\frac{1}{\gamma}\right)}{2^2} = \frac{1}{4\gamma}\frac{(1 + \gamma M_1^2)^2}{M_1^2} \tag{10.19}$$

This result is in complete agreement with the relation that we obtained following Eq. (10.17).

Having determined the significant points on the Rayleigh line, we are now in a position to discuss completely the effect of heat addition on flow properties. Starting at state point (a) in Figure 10.5, suppose we add heat reversibly to flow in a constant-area duct. First, consider the velocity at (a) to be subsonic. Since $ds = (\delta q/T)_{\text{rev}}$, it follows that the addition of heat must result in an increase of entropy of the fluid, corresponding to a movement of the state point to the right on a $T$–$s$ diagram. The top point $B$ of the Rayleigh curve corresponds to subsonic flow [see Eq. (10.18)], so that as heat is added progressively to the flow, the state point moves from (a) to $B$ and finally to $A$, at which $M = 1$. Point $A$ represents a state of maximum entropy for the given mass-flow rate; any further heat addition can serve only to reduce the mass-flow rate in the duct—or, in other words, to jump to another Rayleigh line with a lower mass-flow. There results a maximum amount of heat that can be added to flow in a duct; this maximum is determined by the attainment of Mach 1. Thus, flow in a duct can be choked by heat addition, just as it was demonstrated in the last chapter that flow could be choked by friction.

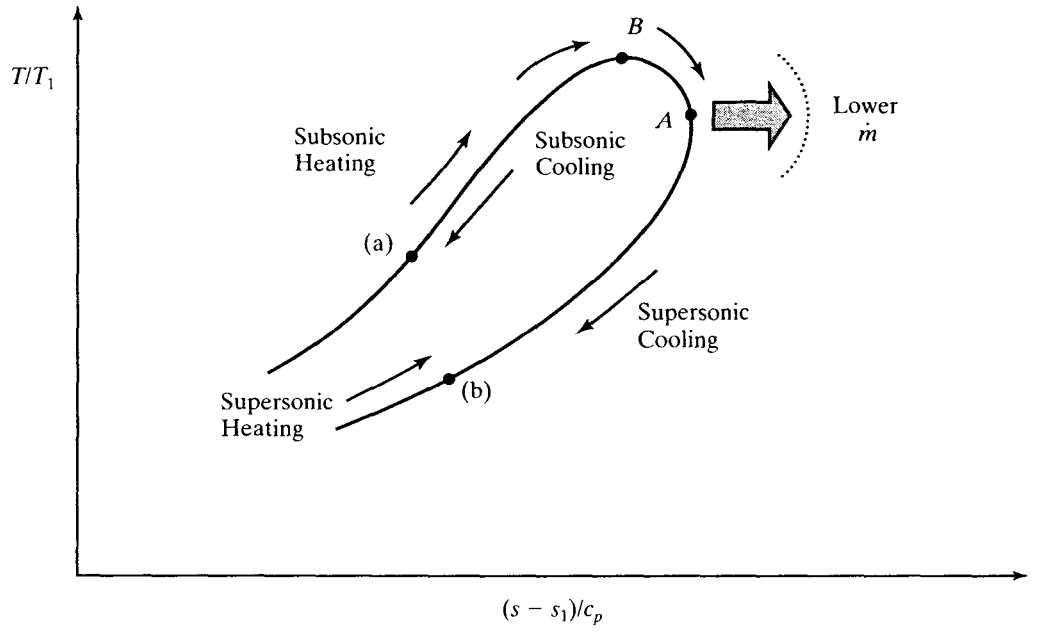


**Figure 10.5** Subsonic and Supersonic Heating and Cooling on the Rayleigh Line

Returning to Figure 10.5, we see that as heat is added to a subsonic flow, the Mach number increases to unity. From the momentum equation, an increase in velocity yields a decrease in static pressure. Note, however, from Figure 10.5, that the static temperature first increases [up to $(T/T_1)_{max}$ at $B$] and then decreases to $T^*/T_1$ at $A$. For cooling, the reverse of the aforementioned variations occur, as shown on the Rayleigh line. For supersonic flow, refer to the lower part of the curve, starting at point (b). As heat is added, the flow Mach number decreases to Mach 1. Thus, from momentum considerations, the static pressure increases up to $p^*$. From Figure 10.5, we see that the static temperature also increases up to $T = T^*$. Again, cooling has the reverse effect.

**Example 10.2. Construction of the Rayleigh line for flow from a given reference state**

Draw the $T$–$s$ diagram for the flow of a gas with $\gamma = 1.3$ in a constant-diameter pipe with heat addition or loss. The reference Mach number $M_1$ for the flow is 3.0.

**Solution**

To draw the Rayleigh line for the given reference state, we have two options: We can directly employ the temperature entropy relation just developed—that is,

$$\frac{s - s_1}{c_p} = \ln\frac{T}{T_1} - \frac{\gamma - 1}{\gamma}\ln\left[\frac{(1 + \gamma M_1^2) \pm \sqrt{(1 + \gamma M_1^2)^2 - 4\gamma M_1^2(T/T_1)}}{2}\right] \tag{10.17}$$

or we can construct a relation for the entropy that depends solely upon the Mach number. The latter option can be accomplished by combining Eqs. (10.8) and (10.9) with Eq. (10.16).

These three equations are reprinted as follows:

$$\frac{s - s_1}{c_p} = \ln\frac{T}{T_1} - \frac{(\gamma - 1)}{\gamma}\ln\frac{p}{p_1} = \ln\left[\left(\frac{T}{T_1}\right)\left(\frac{p_1}{p}\right)^{(\gamma-1)/\gamma}\right] \tag{10.16}$$

$$\frac{p}{p_1} = \frac{(1 + \gamma M_1^2)}{(1 + \gamma M^2)} \tag{10.8}$$

$$\frac{T}{T_1} = \frac{M^2}{M_1^2}\frac{(1 + \gamma M_1^2)^2}{(1 + \gamma M^2)^2} \tag{10.9}$$

So, combining the three equations, we obtain

$$\frac{s - s_1}{c_p} = \ln\left\{\left[\frac{M^2}{M_1^2}\frac{(1 + \gamma M_1^2)^2}{(1 + \gamma M^2)^2}\right]\left[\frac{(1 + \gamma M^2)}{(1 + \gamma M_1^2)}\right]^{(\gamma-1)/\gamma}\right\} = \ln\left[\left(\frac{M}{M_1}\right)^2\left(\frac{1 + \gamma M_1^2}{1 + \gamma M^2}\right)^{(\gamma+1)/\gamma}\right]$$

The corresponding temperature is then computed from Eq. (10.9). It should be noted that the entropy change is zero for $M = M_1$ and therefore zero at $T = T_1$ as well. However, there is a second value that is determined by setting the argument of the natural logarithm to unity and solving the nonlinear equation by using the Newton–Raphson method. The function that is solved and its derivative are, respectively,

$$F(M) = cM^b - \gamma M^2 - 1 = 0$$

$$\frac{dF}{dM} = bcM^{b-1} - 2\gamma M$$

where $c = (1 + \gamma M_1^2)/M_1^b$ and $b = 2\gamma/(\gamma + 1)$. For $M_1 = 3.0$ and $\gamma = 1.3$, the solution procedure yields $M = 0.3647$. The calculations to draw the Rayleigh line were performed within a spreadsheet program, and the results are contained in Table 10.1 and Figure 10.6.

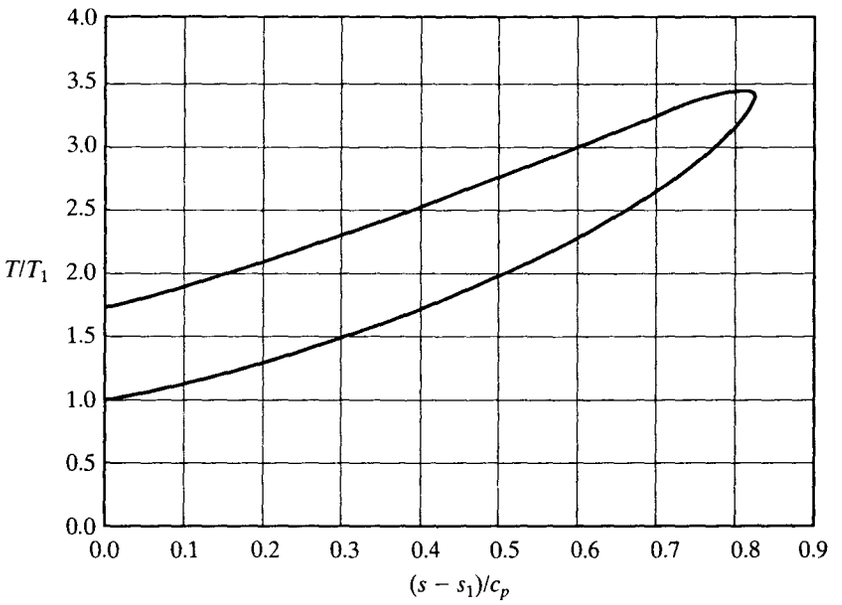


**Figure 10.6** The Rayleigh Line for a Reference Mach Number $M_1$of 3 and $\gamma = 1.3$

**TABLE 10.1** Rayleigh Line Coordinates for a Reference Mach Number $M_1 = 3$ and $\gamma = 1.3$

| | $M$ | $\Delta s/c_p$ | $T/T_1$ |
|---|---|---|---|
| | 0.3647 | 0.0000 | 1.7328 |
| | 0.4000 | 0.1325 | 1.9649 |
| | 0.5000 | 0.4153 | 2.5520 |
| | 0.6000 | 0.5986 | 2.9937 |
| | 0.7000 | 0.7141 | 3.2769 |
| | 0.8000 | 0.7821 | 3.4174 |
| point $B$ | 0.8771 | 0.8108 | 3.4464 |
| | 0.9000 | 0.8161 | 3.4441 |
| point $A$ | 1.0000 | 0.8258 | 3.3877 |
| | 1.1000 | 0.8180 | 3.2754 |
| | 1.2000 | 0.7975 | 3.1287 |
| | 1.4000 | 0.7319 | 2.7903 |
| | 1.6000 | 0.6474 | 2.4492 |
| | 1.8000 | 0.5541 | 2.1375 |
| | 2.0000 | 0.4577 | 1.8648 |
| | 2.2000 | 0.3613 | 1.6312 |
| | 2.4000 | 0.2666 | 1.4328 |
| | 2.6000 | 0.1746 | 1.2645 |
| | 2.8000 | 0.0856 | 1.1217 |
| | 3.0000 | 0.0000 | 1.0000 |

With Rayleigh line flow, changes are brought about by heat addition, which manifests itself as an increase in stagnation temperature. To determine the changes in properties brought about by a certain heat addition to a flow in a duct, the initial step is to calculate the change in stagnation temperature brought about by the heat addition, and hence the parameter $T_o/T_o^*$ at the duct exit. Equation (10.14) must be solved to determine the Mach number for this value of $T_o/T_o^*$. This Mach number enables other properties to be calculated in turn. This approach is analogous to the methods used for Fanno flow, where $fL_{max}/D_h$ was the critical parameter.

For Rayleigh flow, it can be seen that the same overall changes in properties result whether the heat is added at one cross-section (as a combustion flame front) or distributed over the length of the control volume (as a heat exchange). (See Figure 10.7.)

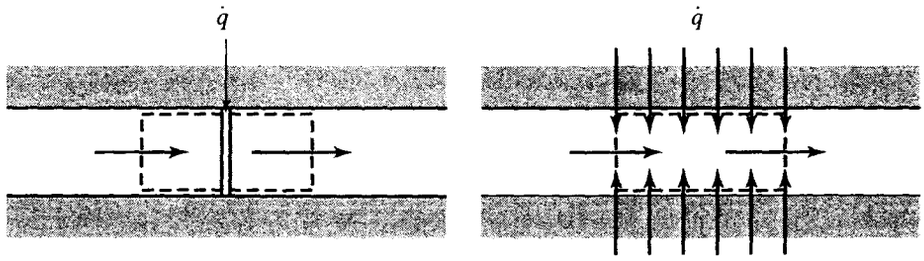


**Figure 10.7** Concentrated and Distributed Heat Exchanges

Also, no differentiation can be drawn between internal heat addition (a combustion reaction) or external heat addition (a heat exchanger). The following examples illustrate these points.

**Example 10.3. Mass-flow calculations within a ramjet combustion chamber**

Air ($\gamma = 1.4$, $R = 0.287$ kJ/kg · K, and $c_p = 1.004$ kJ/kg · K) enters a ramjet combustion chamber with a velocity of 100 m/s and static temperature of 400 K. Determine the maximum amount of heat that can be added in the combustion chamber without reducing the mass-flow rate. For this $q_{max}$, find the fuel–air ratio. If the fuel–air ratio were to be increased by 10 percent, determine the reduction in $\dot{m}$ for the same inlet stagnation pressure and temperature. Assume the heating value of the fuel to be 40 MJ/kg, neglect the fuel flow rate in comparison with the air flow rate, and assume the air to behave as a perfect gas with constant specific heats. Neglect friction.

**Solution**

First, the inlet Mach number is computed as follows:

$$M_1 = \frac{V_1}{a_1} = \frac{100}{\sqrt{(1.4)(287)(400)}} = 0.2494$$

From the isentropic flow relations, $(T/T_{o1}) = 0.9877$; thus,

$$T_{o1} = \left(\frac{T_{o1}}{T_1}\right)T_1 = \left(\frac{1}{0.9877}\right)400 = 404.9813 \text{ K}$$

Applying the energy equation to the flow in the combustion chamber, we get

$$\dot{q} = \dot{m}_{air}c_p(T_{o2} - T_{o1}) = \dot{m}_{fuel}(\text{HV})$$

where $\dot{q}$ = rate of heat transfer in kilowatts and HV (the heating value of the fuel) = 40,000 kJ/kg. For $q_{max} = \dot{q}_{max}/\dot{m}$, $T_{o2} = T_o^*$. From the Rayleigh flow relations, we have

$$T_{o2} = T_o^* = \left(\frac{T_o^*}{T_{o1}}\right)T_{o1} = \frac{404.9813}{0.2558} = 1{,}583.1950 \text{ K}$$

so that

$$\frac{\dot{m}_{\text{fuel}}}{\dot{m}_{\text{air}}} = \frac{c_p(T_{o2} - T_{o1})}{\text{HV}} = \frac{(1.004)(1{,}583.1950 - 404.9813)}{40{,}000} = 0.02957$$

and

$$q_{\max} = (1.004)(1{,}583.1950 - 404.9813) = 1{,}182.9265 \text{ kJ/kg}$$

If the fuel–air ratio were to be increased by 10 percent, the new ratio would be $\dot{m}_{\text{fuel}}/\dot{m}_{\text{air}} = (1.10)0.02957 = 0.03253$. Then, from the energy equation, we have

$$T_{o2} - T_{o1} = \frac{0.03253(40{,}000)}{1.004} = 1{,}295.8964 \text{ K}$$

or, since $T_{o2} = T_o^*$ for choked flow, $T_o^* = 1{,}295.8964 + 404.9813 = 1{,}700.8777$ K. Hence,

$$\frac{T_{o1}}{T_o^*} = \frac{404.9813}{1{,}700.8777} = 0.2381$$

From the Rayleigh flow relations, we find that $M_1 = 0.2392$, and from the isentropic relations at $M_1 = 0.2392$, $p_1/p_{o1} = 0.9610$ and $T_1/T_{o1} = 0.9887$. So, $T_1 = (0.9887)(404.9813) = 400.4050$ K. Also, from the isentropic relations at $M_1 = 0.2494$, $p_1/p_{o1} = 0.9577$. Thus, the 10-percent increase in fuel–air ratio results in a slight increase of inlet static pressure. Since

$$\dot{m} = \rho AV = \frac{p}{RT} A\left(M\sqrt{\gamma RT}\right)$$

the resultant effect of increasing fuel flow is a decrease in $\dot{m}$, given by

$$\frac{\dot{m}_{10\% \text{ increase}}}{\dot{m}} = \left(\frac{0.2392}{0.2494}\right)\left(\frac{0.9610}{0.9577}\right)\sqrt{\frac{400}{400.4050}} = 0.9619$$

corresponding to a 3.81 percent decrease of mass flow.

---

The heat exchange at a fluid–solid interface can be described by *Newton's law of cooling*,

$$\dot{q} = \bar{h}A(T_w - T_f)$$

where $\dot{q}$ is the rate of heat transfer, $\bar{h}$ is *the mean heat transfer coefficient* ($\text{W/m}^2 \cdot \text{K}$), $A$ is the surface area, $T_w$ is the wall temperature, and $T_f$ is the fluid temperature. [See Ref. (10.1).] When a fluid is made to flow over the surface, the heat exchange that occurs is termed a *forced convection*; when the heat exchange takes place as a result of fluid motion brought about by density differences within the fluid, it is termed a *natural convection*. The mean heat transfer coefficient depends upon the geometry, the flow conditions, and the fluid properties. Except in special cases—for example, see Ref. (10.2)—$\bar{h}$ is determined experimentally. For convective flows involving air, $\bar{h}$ ranges approximately from 10 to 500 $\text{W/m}^2 \cdot \text{K}$. This range is determined from what are usually termed "low-speed correlations." Low speed is defined

in terms of the *Eckert number*,

$$E = \frac{V^2}{c_p \Delta T}$$

[See Ref. (10.3).] When this nondimensional number is small (low $V$ or high $\Delta T$), the situation is regarded as "low speed." As may be easily verified, at speeds approaching sonic velocity (300 m/s for air) and for a temperature difference of 100°C, the Eckert number is close to unity. For Eckert numbers on the order of unity ("high-speed flows"), viscous dissipation terms within the energy equation become important and have a significant effect on the temperature distribution. In fact, for these "high-speed flows," the temperature of the surface can actually exceed the freestream static temperature even if the surface is perfectly insulated. [See Ref. (10.4).] This energy exchange is sometimes referred to as *aerodynamic* or *frictional heating*, and the temperature is called the *adiabatic wall temperature* $T_{aw}$. For gases, $T_{aw}$ is relatively close to the stagnation temperature $T_o$. (More will be said regarding this matter in Section 10.5.) So, for high-speed gas flows, the convective heat transfer may be expressed by

$$\dot{q} = \bar{h} A (T_w - T_o)$$

and the low-speed mean heat transfer coefficient may still be employed. Note that the sign of the temperature difference $T_w - T_o$ determines the direction of the heat exchange.

In ducts, through which gases flow, there can be a heat exchange at the inside surface as well as at the external surface. Moreover, heat must be conducted through the duct wall. To account for all of these heat exchanges, an *overall heat transfer coefficient* $U$ is often used. [See Ref. (10.5).] Overall heat transfer coefficients are widely used in the analysis and design of heat exchangers. The overall heat transfer coefficient based on the inside surface area of a circular pipe may be shown to be

$$U_i = \frac{1}{\frac{1}{\bar{h}_i} + \frac{D_i}{2k} \ln\left(\frac{D_o}{D_i}\right) + \left(\frac{D_i}{D_o}\right)\frac{1}{\bar{h}_o}}$$

where $k$ is the thermal conductivity of the pipe and $D_i$ and $D_o$ are the inside and outside diameters, respectively. When the wall thickness is small and the thermal conductivity is high, the overall heat transfer coefficient of the pipe is

$$U = \frac{1}{\frac{1}{\bar{h}_i} + \frac{1}{\bar{h}_o}}$$

**Example 10.4. Convective heat transfer calculations of subsonic flow in a constant-area duct**

Nitrogen ($\gamma = 1.4$, $R = 0.2968$ kJ/kg · K, and $c_p = 1.038$ kJ/kg · K) enters an uninsulated duct at Mach 2.0, with a stagnation temperature of 1,000 K and stagnation pressure of 1.4 MPa. Heat is lost from the nitrogen to the outside ambient air at 20°C, with the mean overall heat transfer coefficient $U$ equal to 60 W /m$^2$ · K. The duct's diameter is 5 cm, and its

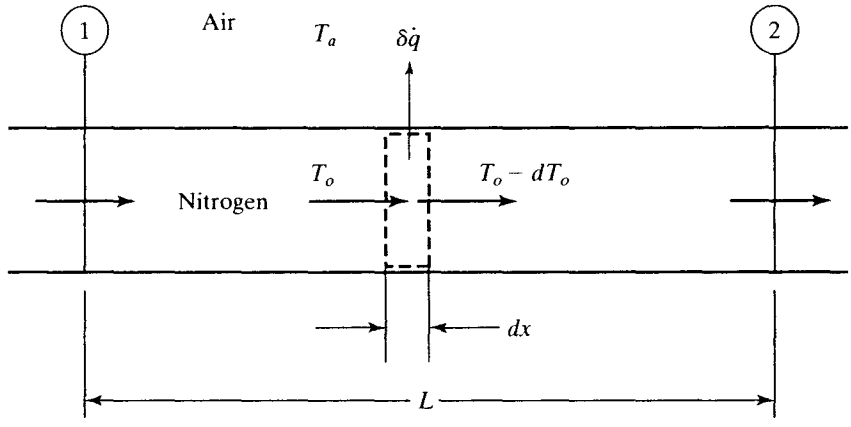


**Figure 10.8** Control Volume for Example 10.4

length is 2 m. Determine the outlet stagnation temperature, outlet Mach number, and percent of change of stagnation pressure. (See Figure 10.8.) Neglect friction.

**Solution**

Consider a differential control volume in the duct as shown in Figure 10.8, and write the energy equation

$$\delta\dot{q} = -\dot{m}c_p dT_o = U dA_p(T_o - T_a)$$

where

$$dA_p = \pi D\, dx$$

Assuming the nitrogen to have constant specific heat over the temperature range of interest, we can determine the overall change of stagnation temperature in the duct by separating variables and integrating the energy equation between locations 1 and 2 to obtain

$$-\int_1^2 \frac{dT_o}{T_o - T_a} = \int_1^2 \frac{U\pi D}{\dot{m}c_p} dx = \frac{U\pi D}{\dot{m}c_p}\int_1^2 dx$$

$$\ln\frac{T_{o1} - T_a}{T_{o2} - T_a} = \frac{U\pi D}{\dot{m}c_p}L$$

At $M_1 = 2$, from the isentropic relations, $(T/T_o)_1 = 0.5556$ and $(p/p_o)_1 = 0.1278$, so that $T_1 = 555.6$ K and $p_1 = 0.1789$ MPa. Then

$$V_1 = M_1\sqrt{\gamma RT_1} = 2.0\sqrt{1.4(296.8)(555.6)} = 960.9639 \text{ m/s}$$

$$\dot{m} = \frac{p_1}{RT_1}AV_1 = \frac{(178.9 \text{ kN/m}^2)\left(\frac{\pi}{4}0.05^2 \text{ m}^2\right)(960.9639 \text{ m/s})}{(0.2968 \text{ kJ/kg}\cdot\text{K})(555.6 \text{ K})} = 2.0470 \text{ kg/s}$$

$$\ln\frac{T_{o1} - T_a}{T_{o2} - T_a} = \frac{U\pi D}{\dot{m}c_p}L = \frac{(60 \text{ W/m}^2\cdot\text{K})\pi(0.05 \text{ m})2 \text{ m}}{(2.047 \text{ kg/s})(1.038 \text{ kJ/kg}\cdot\text{K})(1{,}000 \text{ J/kJ})} = 0.008871$$

$$\frac{T_{o1} - T_a}{T_{o2} - T_a} = 1.0089$$

or

$$T_{o2} - T_a = \frac{1{,}000 - 293}{1.0089} = 700.7557 \text{ K}$$

$$T_{o2} = 293 + 700.7557 = 993.7557 \text{ K}$$

To find $M_2$, use the Rayleigh relations, starting from

$$\frac{T_{o2}}{T_o^*} = \frac{T_{o2}}{T_{o1}} \frac{T_{o1}}{T_o^*} = \frac{993.7557}{1{,}000} 0.7934 = 0.7884$$

From this value, we find that $M_2 = 2.0251$. Accordingly, we may further write that

$$p_2 = \frac{p_2}{p^*} \frac{p^*}{p_1} p_1 = \frac{0.3560}{0.3636} 178.9 = 175.1606 \text{ kPa}$$

and

$$p_{o2} = \frac{p_{o2}}{p_2} p_2 = \frac{1}{0.1229} 175.1606 = 1{,}425.2288 \text{ kPa}$$

Hence,

$$\frac{p_{o2} - p_{o1}}{p_{o1}} = \frac{1{,}425.2288 - 1{,}400}{1{,}400} 100 = 1.8021\% \text{ increase}$$

---

**Example 10.5. Calculations within a constant-area duct connected to a reservoir by a converging nozzle and to which a given amount of heat is added**

A constant-area duct is connected to a high-pressure air ($\gamma = 1.4$, $R = 0.287$ kJ/kg · K, and $c_p = 1.004$ kJ/kg · K) reservoir through a converging nozzle. (See Figure 10.9.) The walls of the duct are heated so as to supply 250 kJ/kg to the air passing through the duct. If the reservoir pressure and temperature are, respectively, 750 kPa and 300 K, and the system back pressure is 300 kPa, determine whether the duct is choked or not. Also, find the mass-flow rate of air passing through the duct. The duct's diameter is 5 cm, and its length is 1.2 m. Assume isentropic flow in the nozzle and frictionless flow in the duct, with the air behaving as a perfect gas with constant specific heats.

**Solution**

First, consider a plot of pressure $p$ versus distance $x$ for this system. For a back pressure of 750 kPa, of course, there is no flow; as the back pressure is lowered, subsonic flow occurs in the nozzle and the duct, with the static pressure decreasing in both the nozzle and the duct, as shown by curves (a) and (b) in Figure 10.9. When the back pressure is decreased to that of curve (c), sonic flow occurs at the duct exit. Any further decrease in back pressure cannot be "sensed" by the reservoir, so for all back pressures below that of curve (c), the mass flow and pressure distribution in the duct remain the same as that for curve (c). For back pressures such as for curves (d) and (e), adjustment to the back pressure takes place via expansion waves outside the duct. Accordingly, the duct is choked when the back pressure is either equal to or below that of curve (c).

First, we shall calculate this back pressure necessary to choke the system. For $M_2 = 1$,

$$T_{o2} = T_o^*$$

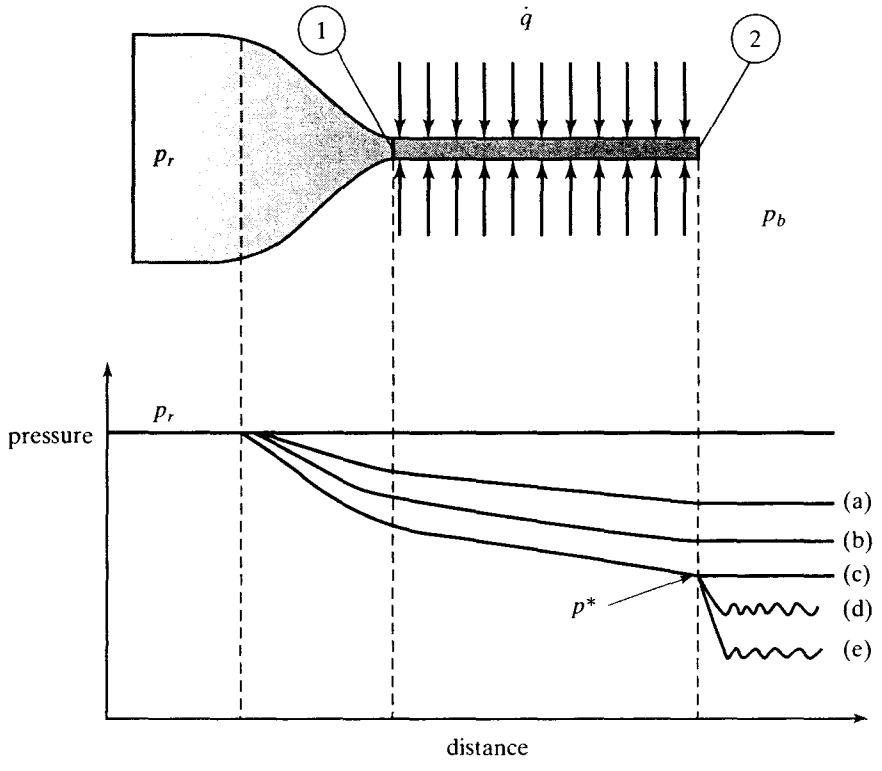


**Figure 10.9** Pressure Distribution within a Heated Constant-Area Duct Connected to a Reservoir by a Converging Nozzle

From the energy equation,

$$q = c_p(T_{o2} - T_{o1}) = c_p(T_o^* - T_{o1})$$

where $T_{o1} = 300$ K. Thus,

$$T_o^* - 300 = 250 \text{ kJ/kg}/1.004 \text{ kJ/kg} \cdot \text{K} = 249.0040 \text{ K}$$

or

$$T_o^* = 549.0040 \text{ K}$$

From the Rayleigh flow relations, at $T_{o1}/T_o^* = 300/549.004 = 0.5464$, $M_1 = 0.4099$ and $p_1/p^* = 1.9429$. From the isentropic flow relations, at $M_1 = 0.4099$, $p_1/p_{o1} = 0.8907$, or $p_1 = (0.8907)750 = 668.0250$ kPa. Therefore,

$$p_2 = p^* = 668.025/1.9429 = 343.8288 \text{ kPa}$$

In other words, the system is choked for all back pressures below 343.8288 kPa. Since the specified back pressure is 300 kPa, the duct is indeed choked and the pressure at the exit plane, $p_2$, is greater than the back pressure.

To calculate the mass-flow rate, consider the flow conditions at state 1: Mach number 0.4099, static pressure 668.025 kPa, and, from the isentropic flow relations, $T_1/T_{o1} = 0.9675$, so that $T_1 = 290.2500$ K. Therefore,

$$\dot{m} = \frac{p_1}{RT_1} A M_1 \sqrt{\gamma RT_1} = \frac{(668.025)\left(\frac{\pi}{4}0.05^2\right)(0.4099)\sqrt{1.4(287)(290.25\text{ K})}}{(0.287)(290.25\text{ K})}$$
$$= 2.2041 \text{ kg/s}$$

## 10.3 NORMAL SHOCK ON RAYLEIGH AND FANNO LINE *T–s* DIAGRAMS

To develop the *T–s* diagram for Fanno flow, we used the continuity and energy equations (a friction term does not appear in these equations) at two state points:

$$\rho_1 V_1 = \rho_2 V_2$$
$$c_p T_1 + \frac{V_1^2}{2} = c_p T_2 + \frac{V_2^2}{2}$$

To develop the *T–s* diagram for Rayleigh flow, the continuity and momentum equations were employed (a term containing heat addition $q$ does not appear in these equations) at two state points:

$$\rho_1 V_1 = \rho_2 V_2$$
$$p_1 + \rho_1 V_1^2 = p_2 + \rho_2 V_2^2$$

The Fanno continuity and energy equations and the Rayleigh continuity and momentum equations collectively are the same as the continuity, momentum, and energy equations developed for the normal shock in Chapter 4. Thus, the locus of states before and after a normal shock appears on a *T–s* diagram at the intersection of the Fanno and Rayleigh lines. Figure 10.10 shows the Rayleigh and Fanno lines on a *T–s* diagram for the same mass-flow rate. The intersections of the curves yield state points 1 and 2 for the flow ahead of and behind the shock, respectively. Whereas the increase of entropy for the shock is brought about by irreversibilities such as heat conduction and viscous dissipation occurring internal to the wave, the entropy rise for Fanno flow is brought about by friction and for Rayleigh flow by heat addition. The line between 1 and 2 is dashed; since the fluid inside the shock is not at thermodynamic equilibrium, its thermodynamic state is not defined.

## 10.4 FLOWS WITH HEAT ADDITION AND AREA CHANGE

There are many cases in which a flow involves both area variation and heat addition. A prime example is the exhaust of combustion gases through a rocket nozzle. As with flow with friction and area change, a combination of the two effects introduces additional complexity into the resultant analysis.

Select a control volume, as shown in Figure 10.11, with frictionless reversible, one-dimensional flow. We want to derive an expression relating Mach number variation to

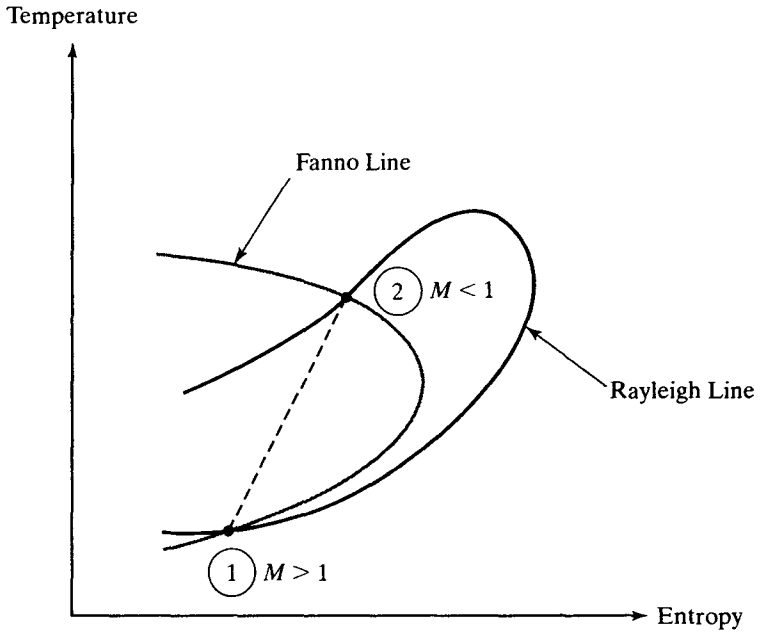


**Figure 10.10** Normal-Shock States on the $T$–$s$ Diagram

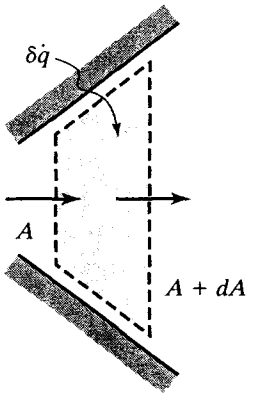


**Figure 10.11** Differential Control Volume for Variable-Area Flow with Heat Addition

changes in area and heat addition or loss. The continuity, momentum, and energy equations yield, respectively,

$$\frac{d\rho}{\rho} + \frac{dA}{A} + \frac{dV}{V} = 0 \tag{10.20}$$

$$dp + \rho V dV = 0 \tag{10.21}$$

$$\delta q = c_p dT_o \tag{10.22}$$

The perfect-gas law, in differential form, becomes

$$\frac{dp}{p} = \frac{d\rho}{\rho} + \frac{dT}{T} \tag{10.23}$$

Divide Eq. (10.21) by $p$ and substitute from Eq. (10.23) to obtain

$$\frac{d\rho}{\rho} + \frac{dT}{T} + \frac{\rho}{p} V dV = 0$$

By using Eq. (10.20) and the definition of Mach number, the foregoing expression can be written as

$$-\left(\frac{dA}{A} + \frac{dV}{V}\right) + \frac{dT}{T} + \gamma M^2 \frac{dV}{V} = 0$$

Since $V = (\text{constant}) M\sqrt{T}$, logarithmic differentiation yields

$$\frac{dV}{V} = \frac{dM}{M} + \frac{1}{2}\frac{dT}{T}$$

Hence,

$$-\frac{dA}{A} + (\gamma M^2 - 1)\frac{dM}{M} + \left(\frac{\gamma M^2 + 1}{2}\right)\frac{dT}{T} = 0 \tag{10.24}$$

But $\delta q = c_p\, dT_o$, where, for a perfect gas with constant specific heats,

$$T_o = T\left(1 + \frac{\gamma - 1}{2} M^2\right)$$

so that

$$\frac{dT_o}{T} = \left(1 + \frac{\gamma - 1}{2} M^2\right)\frac{dT}{T} + (\gamma - 1) M^2 \frac{dM}{M}$$

or

$$\frac{dT}{T} = \frac{\dfrac{\delta q}{c_p T}}{1 + \dfrac{\gamma - 1}{2} M^2} - \frac{M^2(\gamma - 1)\dfrac{dM}{M}}{1 + \dfrac{\gamma - 1}{2} M^2}$$

Substituting these results into Eq. (10.24), we get

$$-\frac{dA}{A} + \frac{(\gamma M^2 + 1)\dfrac{\delta q}{c_p T}}{2\left(1 + \dfrac{\gamma - 1}{2} M^2\right)} + \frac{(M^2 - 1)\dfrac{dM}{M}}{1 + \dfrac{\gamma - 1}{2} M^2} = 0 \tag{10.25}$$

The direct integration of this equation, except for special cases, is not possible. However, certain general conclusions can be drawn from Eq. (10.25). For $\delta q$ equal to zero, Eq. (10.25) reduces to the isentropic flow equation, and, as has been shown, Mach 1 occurs at the minimum area or the throat of a converging–diverging nozzle. On the other hand, with heat addition, it can be seen that the second term in Eq. (10.25) is positive, so that the sonic point now occurs at a position where $dA/A$ is positive (i.e., in the diverging portion of the nozzle). Conversely, if heat is rejected from the gas stream (as, for example, with hot gas flow through a rocket nozzle), the sonic point occurs in the converging part of the nozzle.

The question that the engineer must ask in trying to apply Eq. (10.25) concerns the relative importance of the term involving area change with respect to that containing heat addition. It is often the case that one effect far overrides the other. For example, with a rocket nozzle, sufficient accuracy can almost always be attained by neglecting heat losses from the gas stream; then the problem reduces to simple isentropic flow, as discussed in Chapter 3. If the effect of heat addition and area change are estimated to be of the same order of magnitude, numerical integration of Eq. (10.25) is required. To accomplish this, Eq. (10.25) can be rearranged into the following form:

$$\frac{dM}{dx} = \frac{M}{(1 - M^2)}\left[ -\frac{\left(1 + \dfrac{\gamma - 1}{2}M^2\right)}{A}\frac{dA}{dx} + \frac{(1 + \gamma M^2)}{2}\left(\frac{1}{c_p T}\frac{\delta q}{dx}\right)\right] \tag{10.26}$$

As we have seen in the previous chapter, numerical solutions are not difficult to obtain, particularly if no sonic point appears. If the flow field includes a location where $M = 1$, Eq. (10.26) contains a singularity, and the special approach described in Section 9.7 [the method of Beans; see Ref. (10.6)] to define a limiting form of this equation should be utilized prior to the computations.

**Example 10.6. Calculations within a diverging nozzle to which a given amount of heat is added**

A supersonic stream of air ($\gamma = 1.4$, $R = 0.287$ kJ/kg · K, and $c_p = 1.004$ kJ/kg · K) flows through a linear, conically shaped nozzle (i.e., $D = D_i + (D_e - D_i)x/L$). The diameter at the inlet is 2 cm, and the diameter at the exit is 5 cm. The nozzle is 10 cm long. The entering Mach number is 3. Heat is added to flow at a rate so that the stagnation temperature varies linearly with distance. The stagnation temperature at the inlet is 300 K and increases by 30 K per meter of nozzle. The pressure is such that a normal shockwave stands halfway down the nozzle. Use Heun's predictor–corrector scheme to determine the Mach number distribution within the duct.

**Solution**

The first step is to write an expression for $dM/dx$:

$$\frac{dM}{dx} = \frac{M[2 + (\gamma - 1)M^2]}{2(1 - M^2)}\left[ -\frac{1}{A}\frac{dA}{dx} + \frac{(1 + \gamma M^2)}{2}\left(\frac{1}{T_o}\frac{dT_o}{dx}\right)\right]$$

It should be noted that the heat transfer term has been replaced by an expression for the change in the stagnation temperature, using Eq. (10.22). Now, since the nozzle is conical, the

local cross-sectional area $A(x)$ is $\pi[D(x)]^2/4 = \pi[D_i + (D_e - D_i)x/L]^2/4$. Hence, the area variation term in the foregoing expression can be written as

$$\frac{1}{A(x)}\frac{dA}{dx} = \frac{2}{D(x)}\frac{dD}{dx} = \frac{2\left(\dfrac{D_e - D_i}{L}\right)}{D(x)} = \frac{2\alpha}{D(x)}$$

where $D(x) = D_i + \alpha x$ and $\alpha = (D_e - D_i)/L = 0.3$. Also, since the stagnation temperature varies linearly with nozzle distance, we may write that $T_o(x) = (T_o)_i + \beta x$, where $\beta = 30$ K/m. So, the stagnation temperature term may be written as

$$\frac{1}{T_o}\frac{dT_o}{dx} = \frac{\beta}{T_o(x)}$$

The governing equation for the Mach number variation becomes

$$\frac{dM}{dx} = F(x, M) = \frac{M[2 + (\gamma - 1)M^2]}{2(1 - M^2)}\left[-\left(\frac{2\alpha}{D_i + \alpha x}\right) + \frac{(1 + \gamma M^2)}{2}\left(\frac{\beta}{(T_o)_i + \beta x}\right)\right]$$

As described in the previous chapter, Heun's method is a multistep, explicit procedure in which a preliminary Mach number (the predicted value) is first computed and then an improved value (the corrector) is determined by using this preliminary value. The algorithm for this method is as follows:

$$\left.\begin{aligned} &\textit{Predictor:} \quad \hat{M}_{i+1} = M_i + F(x_i, M_i)\Delta x \\ &\textit{Corrector:} \quad M_{i+1} = M_i + \left[\frac{F(x_i, M_i) + F(x_{i+1}, M^*_{i+1})}{2}\right]\Delta x \end{aligned}\right\} \tag{9.49}$$

It is good technique to begin a numerical solution of a problem by using a relatively coarse grid. To validate the computational method, a problem with a known answer is generally used, and the predicted results are compared with this solution. Once the methodology (equations, initial conditions, and procedure) has been validated, the grid can be progressively refined to determine an appropriate grid size. Finally, we can attempt the actual problem on this grid.

For the validation problem, isentropic supersonic flow (no shock) in the nozzle is first computed. From the given areas, using isentropic relations, we find that the computed exit Mach number is 5.07154. Table 10.2 contains the results of the computations using Heun's method for this problem for progressively finer grids.

Clearly, a grid of 161 points produces very satisfactory accuracy. Accordingly, we will use this grid to predict adiabatic flow with a shock located at $x = 5$ cm. Again, using isentropic relations and the normal-shock relation for Mach number across the shock, we determine that the exit Mach number should be 0.193059. The computed value is 0.193061, which is larger by 0.001 percent.

Finally, we are in good position to solve the complete problem, which includes area variation, heat addition, and a normal shockwave. Table 10.3 contains a partial listing of the results of the computations performed with a spreadsheet program. Note that $M_p$ is the predicted Mach number $\hat{M}_{i+1}$. To assure oneself that the units and computations have been correctly worked out, it is good procedure to perform the computations for the first point by hand.

**TABLE 10.2** Effect of Grid Size on the Accuracy of the Exit-Mach-Number Prediction

| Pts | $\Delta x$ | $M(x = 10)$ | % Error |
|---|---|---|---|
| 11 | 0.01 | 5.07617 | 0.0912 |
| 21 | 0.005 | 5.07269 | 0.0225 |
| 41 | 0.0025 | 5.07182 | 0.0054 |
| 81 | 0.00125 | 5.07160 | 0.0012 |
| 161 | 0.000625 | 5.07155 | 0.0002 |

**TABLE 10.3** Selected Results of the Numerical Solution of Example 10.6, Using Heun's Method

| Pt | $x$ | $M_i$ | $F(x_i, M_i)$ | $M_p$ | $F(x_{i+1}, M_p)$ | $M_{i+1}$ |
|---|---|---|---|---|---|---|
| 1 | 0.0000 | 3.0000 | 30.7860 | 3.0192 | 30.4928 | 3.0191 |
| 17 | 0.0100 | 3.2868 | 26.7908 | 3.3035 | 26.5816 | 3.3034 |
| 33 | 0.0200 | 3.5393 | 23.8426 | 3.5542 | 23.6826 | 3.5541 |
| 49 | 0.0300 | 3.7657 | 21.5363 | 3.7792 | 21.4080 | 3.7792 |
| 65 | 0.0400 | 3.9714 | 19.6580 | 3.9837 | 19.5517 | 3.9837 |
| 81 | 0.0500 | 4.1599 | | | | 0.4309 |
| 82 | 0.0500 | 0.4309 | −9.3733 | 0.4250 | −9.1315 | 0.4251 |
| 98 | 0.0600 | 0.3530 | −6.5015 | 0.3489 | −6.3707 | 0.3490 |
| 114 | 0.0700 | 0.2970 | −4.8320 | 0.2940 | −4.7501 | 0.2940 |
| 130 | 0.0800 | 0.2545 | −3.7432 | 0.2521 | −3.6874 | 0.2521 |
| 146 | 0.0900 | 0.2210 | −2.9832 | 0.2192 | −2.9432 | 0.2192 |
| 162 | 0.1000 | 0.1941 | | | | |

## 10.5 FLOWS WITH FRICTION AND HEAT ADDITION

When heat is added to a gas flowing in a duct, whether it be external heat transfer, as in a heat exchanger, or internal heat addition, as via a chemical reaction, the effect of wall friction is present. As has been discussed previously, it is often possible to neglect the lesser of the two effects. However, there is an important class of problems wherein the effects may be of the same order of magnitude; a prime example is the heat exchanger, where often the designer must compromise the heat transfer design to minimize pressure drops due to friction and hence minimize pumping-power requirements.

For flow in a constant-area duct with heat transfer and friction, as shown in Figure 10.12, the equations of motion yield, for continuity,

$$\frac{d\rho}{\rho} + \frac{dV}{V} = 0$$

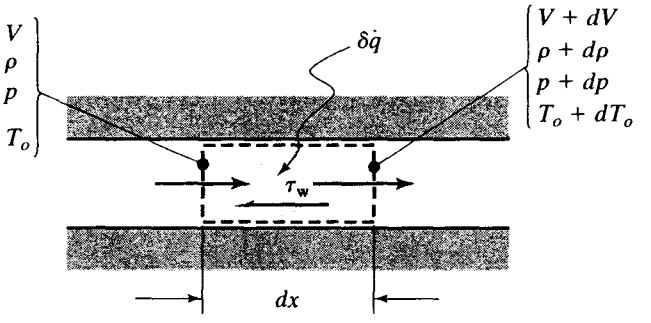


**Figure 10.12** Differential Control Volume for Flow in a Constant-Area Duct with Friction and Heat Addition

and for momentum,

$$dp + \frac{1}{2}\rho V^2 \frac{f dx}{D} + \rho V dV = 0$$

Or, since $V = M\sqrt{\gamma RT}$, logarithmic differentiation brings

$$\frac{dV}{V} = \frac{dM}{M} + \frac{1}{2}\frac{dT}{T}$$

so that

$$\frac{dp}{p} + \frac{1}{2}\gamma M^2 \frac{f dx}{D} + \gamma M^2 \frac{dM}{M} + \frac{1}{2}\gamma M^2 \frac{dT}{T} = 0 \tag{10.27}$$

For energy,

$$\delta q = c_p dT_o$$

or, since

$$T_o = T\left(1 + \frac{\gamma - 1}{2} M^2\right)$$

we find that

$$\frac{\delta q}{c_p T} = \left(1 + \frac{\gamma - 1}{2} M^2\right)\frac{dT}{T} + (\gamma - 1) M dM \tag{10.28}$$

For a perfect gas,

$$\frac{dp}{p} = \frac{d\rho}{\rho} + \frac{dT}{T}$$

Combining this expression with the differential version of the continuity equation, we get

$$\frac{dp}{p} = -\frac{dV}{V} + \frac{dT}{T}$$

and combining it with the definition of Mach number, we obtain

$$\frac{dp}{p} = -\frac{dM}{M} + \frac{1}{2}\frac{dT}{T}$$

Now we substitute this expression for $dp/p$ into Eq. (10.27), along with $dT/T$ from Eq. (10.28), to obtain

$$\frac{\delta q}{c_p T_o}\frac{1}{2}(1 + \gamma M^2) + \frac{1}{2}\gamma M^2\frac{f\,dx}{D} = \left[\frac{1 - \gamma M^2}{M} + \frac{(\gamma - 1)(1 + \gamma M^2)\frac{1}{2}M}{1 + \frac{\gamma - 1}{2}M^2}\right]dM$$

or

$$\frac{1}{2}(1 + \gamma M^2)\frac{\delta q}{c_p T_o} + \frac{1}{2}\gamma M^2\frac{f\,dx}{D} = \left[\frac{2(1 - M^2)}{2 + (\gamma - 1)M^2}\right]\frac{dM}{M} \tag{10.29}$$

Just as Eq. (10.25) indicated the relative effects of area change and heat addition on Mach number, Eq. (10.29) shows the effects of heat addition and friction. To afford a better comparison of the friction and heat addition terms, express $\delta q$ in terms of the mean convective heat transfer coefficient $\bar{h}$. For a compressible flow, the heat transfer rate between a differential wall area $dA_p = \pi D\,dx$ for a circular duct and the gas flowing in the duct is given by

$$\delta\dot{q} = \bar{h}(T_w - T_{\text{aw}})dA_p$$

where $T_w$ is the *duct wall temperature* and $T_{\text{aw}}$ the *adiabatic wall temperature.* [See, for example, Ref. (10.7).]

In an actual fluid (whether liquid or gas), viscous stresses will bring the flow to rest at the wall. If this process could be accomplished reversibly, the stagnation temperature would be recovered. However, because of viscous effects, this process is irreversible, and therefore the stagnation temperature is not completely recovered. To account for the losses, a *recovery factor* is defined as

$$r = \frac{T_{\text{aw}} - T}{T_o - T}$$

Since $T_o/T = 1 + (\gamma - 1)M^2/2$, it is easy to show that

$$T_{\text{aw}} = \left[\frac{2 + r(\gamma - 1)M^2}{2 + (\gamma - 1)M^2}\right]T_o$$

The recovery factor has been found to be related to the properties of the fluid as follows:

For laminar flow: $r = \text{Pr}^{1/2}$

For turbulent flow: $r = \text{Pr}^{1/3}$

Here, Pr is the *Prandtl number*, a nondimensional parameter that is the product of the specific heat at constant pressure, $c_p$, and the dynamic viscosity of the gas, $\mu$, divided by

the thermal conductivity $k$ (i.e., $\text{Pr} \equiv c_p\mu/k$). By multiplying and dividing by the fluid density $\rho$, the Prandtl number can also be written as the ratio of kinematic viscosity $\nu = \mu/\rho$ to the thermal diffusivity $\alpha = k/\rho c_p$ (i.e., $\text{Pr} = \nu/\alpha$). The Prandtl number of gases is close to unity. Hence, $r = 1$, and therefore $T_{\text{aw}} = T_o$. So, for gases,

$$\delta\dot{q} = \bar{h}(T_w - T_o)\pi D\, dx \tag{10.30}$$

where

$$\delta q = \frac{\delta\dot{q}}{\dot{m}} = \frac{\delta\dot{q}}{\rho AV}$$

A relation between the mean convective heat transfer coefficient $\bar{h}$ and the friction factor $f$ is given by *Reynolds's analogy*; see, for example, Refs. (10.8), (10.9), and (10.10). For Prandtl numbers close to unity,

$$\bar{h} = \frac{\rho V c_p f}{8} \tag{10.31}$$

Note that for flow in a constant-area duct, $\rho V$ is a constant; for variable-area ducts, $\rho V$ may be defined at a given location. Substituting Eqs. (10.30) and (10.31) into Eq. (10.29) yields

$$\frac{dM}{dx} = \left[\frac{2 + (\gamma - 1)M^2}{2(1 - M^2)}\right]M\left[\left(\frac{1 + \gamma M^2}{2}\right)\frac{1}{T_o}\frac{dT_o}{dx} + \left(\frac{1}{2}\gamma M^2\right)\frac{f}{D}\right] \tag{10.32}$$

Equation (10.32) can be solved by using the numerical procedures described in Sections 9.7 and 10.4. To accomplish this, however, we must know how the stagnation temperature varies with $x$. There are two common classes of problems in which $T_o(x)$ is readily determined: (1) constant-wall-temperature problems (i.e., $T_w$ = constant—these situations occur in heat exchangers where the heat transfer coefficient on the external surface is very large, a condition that can arise because of condensation or evaporation); and (2) constant-heat-rate problems (i.e., $q$ = constant—these situations occur when the duct wall is heated using electric resistance heating or radiant heating). We now consider each of these cases to determine $T_o(x)$ for the flow in a circular duct of diameter $D$.

*Constant-Wall-Temperature Problems*:

$$\delta\dot{q} = \dot{m}c_p dT_o = \bar{h}(T_w - T_o)\pi D\, dx$$

$$\frac{dT_o}{T_w - T_o} = \frac{\bar{h}\pi D\, dx}{\dot{m}c_p} \tag{10.33}$$

From Eq. (10.31),

$$\bar{h} = \frac{\rho V c_p f}{8} = \frac{\rho A V c_p f}{8A} = \frac{\dot{m}c_p f}{8A}$$

So,

$$\frac{\bar{h}\pi D}{\dot{m}c_p} = \frac{\pi D f}{8\frac{\pi D^2}{4}} = \frac{f}{2D}$$

Hence, Eq. (10.33) becomes

$$\frac{dT_o}{T_w - T_o} = \frac{f}{2D}dx$$

Integration and rearrangement produces the following exponential distribution of stagnation temperature:

$$T_o = T_w - (T_w - T_{o1})e^{-(f/2D)x}$$

Consequently,

$$\frac{1}{T_o}\frac{dT_o}{dx} = \frac{(T_w - T_{o1})}{T_w e^{(f/2D)x} - (T_w - T_{o1})}\frac{f}{2D}$$

*Constant-Heat-Rate Problems*:

$$\frac{1}{c_p}\frac{\delta q}{dx} = \frac{dT_o}{dx} = \beta$$

Integration gives

$$T_o = T_{o1} + \beta x$$

Consequently,

$$\frac{1}{T_o}\frac{dT_o}{dx} = \frac{\beta}{T_{o1} + \beta x}$$

where $\beta = (T_{o2} - T_{o1})/L = q/(c_p L)$. A constant-heat problem was assumed in Example 10.4.

To determine variations in pressure and other flow properties, the relations presented at the end of Section 9.7 may be employed, after slight modification, to account for the fact that the stagnation temperature is not constant and that the area varies in the flow direction:

$$\frac{T_k}{T_j} = \left(\frac{T_{ok}}{T_{oj}}\right)\frac{2 + (\gamma - 1)M_j^2}{2 + (\gamma - 1)M_k^2} \tag{10.34}$$

$$\frac{p_k}{p_j} = \frac{A_j M_j}{A_k M_k}\sqrt{\frac{T_k}{T_j}} = \left(\frac{A_j}{A_k}\right)\frac{M_j}{M_k}\left[\frac{2 + (\gamma - 1)M_j^2}{2 + (\gamma - 1)M_k^2}\right]^{1/2} \tag{10.35}$$

$$\frac{p_{ok}}{p_{oj}} = \frac{p_{ok}}{p_k}\frac{p_k}{p_j}\frac{p_j}{p_{oj}} = \left(\frac{A_j}{A_k}\right)\frac{M_j}{M_k}\left[\frac{2 + (\gamma - 1)M_k^2}{2 + (\gamma - 1)M_j^2}\right]^{\frac{\gamma+1}{2(\gamma-1)}} \tag{10.36}$$

$$\frac{\rho_k}{\rho_j} = \frac{p_k}{p_j}\frac{T_j}{T_k} = \left(\frac{A_j}{A_k}\right)\frac{M_j}{M_k}\left[\frac{2 + (\gamma - 1)M_k^2}{2 + (\gamma - 1)M_j^2}\right]^{1/2} = \left(\frac{A_j}{A_k}\right)\frac{V_j}{V_k} \tag{10.37}$$

$$\frac{s_k - s_j}{R} = -\ln\left(\frac{p_{ok}}{p_{oj}}\right) = \frac{\gamma}{\gamma - 1}\ln\left(\frac{T_k}{T_j}\right) - \ln\left(\frac{p_k}{p_j}\right) \tag{10.38}$$

## 10.6 CHAPTER CAPSTONE APPLICATION: ISOTHERMAL FLOW

During gas flow in long, noninsulated ducts and pipes, the gas is able to achieve temperature equilibrium with the surroundings. In other words, the temperature of the flow reaches a constant value and is therefore *isothermal.* This flow possesses characteristics that are different from either Fanno or Rayleigh flow because it involves *both* heat transfer *and* friction. A common misconception is to regard isothermal flow as flow that does not require any heat exchange. However, it is, in fact, the exchange of heat that allows the temperature to remain constant.

Consider the differential control volume, shown in Figure 10.13, of isothermal flow in a constant-area duct. The continuity, momentum, and energy equations are, respectively,

$$\frac{d\rho}{\rho} + \frac{dV}{V} = 0 \tag{10.1}$$

$$dp + \rho V dV + \frac{f\,dx}{2D_h}\rho V^2 = 0 \tag{10.39}$$

$$\delta\dot{q} = \dot{m}(dh_o) = \dot{m}(c_p dT_o) = \dot{m}\left[c_p dT + d\left(\frac{V^2}{2}\right)\right] = \dot{m}d\left(\frac{V^2}{2}\right) \tag{10.40}$$

The differential momentum equation, Eq. (10.39), may be rewritten as

$$\frac{dp}{p} + \frac{\gamma M^2}{2}\frac{f\,dx}{D_h} + \gamma M^2\frac{dV}{V} = 0 \tag{10.41}$$

Dividing by the mass-flow rate, which is constant, we find that the energy equation becomes

$$\frac{\delta\dot{q}}{\dot{m}} = \delta q = dh_o = c_p\,dT_o \tag{10.42}$$

Also, the perfect-gas law expressed in differential form is

$$\frac{dp}{p} = \frac{d\rho}{\rho} + \frac{dT}{T}$$

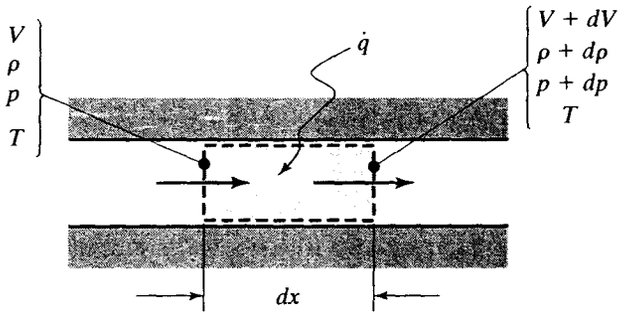


**Figure 10.13** Differential Control Volume Used for Isothermal Flow Analysis

Since the temperature is constant, $dT/T = 0$, and therefore,

$$\frac{dp}{p} = \frac{d\rho}{\rho} \tag{10.43}$$

From the definition of the Mach number, $M = V/a$. Since the temperature is constant, the speed of sound is also constant. Therefore, logarithmic differentiation yields

$$\frac{dM}{M} = \frac{dV}{V} \tag{10.44}$$

Combining Eqs. (10.40), (10.43), and (10.44) yields

$$\frac{dp}{p} = -\frac{dM}{M} \tag{10.45}$$

Substituting Eq. (10.45) into Eq. (10.41), we get

$$\frac{dM}{M} = \frac{(\gamma M^2/2)}{1 - \gamma M^2}\frac{f\,dx}{D} \tag{10.46}$$

Equation (10.46) shows that the critical Mach number for isothermal flow is not Mach 1, but $M = 1/\sqrt{\gamma}$ ( $= 0.8452$ for $\gamma = 1.4$). If $M < (1/\sqrt{\gamma})$, this flow is termed *subcritical flow*, and Eq. (10.46) indicates that $M$ increases with $x$, whereas if $M > (1/\sqrt{\gamma})$, we have *supercritical flow*, and $M$ decreases with $x$.

To determine the heat transfer necessary to maintain isothermal flow, refer to Eq. (10.42). Since

$$T_o = T\left(1 + \frac{\gamma - 1}{2}M^2\right)$$

we have

$$\frac{dT_o}{T_o} = \frac{(\gamma - 1)M\,dM}{1 + \dfrac{\gamma - 1}{2}M^2}$$

for isothermal flow with $dT/T = 0$. Substituting for $dM$ from Eq. (10.46), we obtain

$$\delta q = c_p dT_o = \frac{c_p T_o(\gamma - 1)M^4\dfrac{\gamma}{2}}{\left(1 + \dfrac{\gamma - 1}{2}M^2\right)(1 - \gamma M^2)}\left(\frac{f\,dx}{D}\right) \tag{10.47}$$

As $M \to 1/\sqrt{\gamma}$, it can be seen that $q \to \infty$, indicating that an infinite rate of heat transfer is necessary to maintain the isothermal flow at the critical Mach number. It is therefore apparent, then, that it is physically impossible to isothermally accelerate flow in a constant-area duct from a low Mach number up to $M = 1/\sqrt{\gamma}$. The assumption of isothermal flow is valid, however, and can be realized physically for small-velocity,

low-Mach-number flows. For such flows, it is desirable to obtain an expression for pressure drop and Mach-number variation as a function of $x$. Integrating Eq. (10.46) yields

$$\frac{fL}{D} = \int_{M_1}^{M_2} \frac{1 - \gamma M^2}{(\gamma M^2/2)} \left(\frac{dM}{M}\right) = 2\int_{M_1}^{M_2} \left(\frac{1}{\gamma M^3} - \frac{1}{M}\right) dM = -\left[\frac{1}{\gamma M^2} + 2\ln(M)\right]\Bigg|_{M_1}^{M_2}$$

This expression can be rewritten as

$$\frac{fL}{D} = \frac{1 - \gamma M_1^2}{\gamma M_1^2} - \frac{1 - \gamma M_2^2}{\gamma M_2^2} + \ln\frac{M_1^2}{M_2^2} = \frac{M_2^2 - M_1^2}{\gamma M_1^2 M_2^2} + \ln\frac{M_1^2}{M_2^2} \tag{10.48}$$

From Eq.(3.12), it is easy to show that

$$\frac{T_{o1}}{T_{o2}} = \left(\frac{T_{o1}}{T_1}\right)\left(\frac{T_2}{T_{o2}}\right) = \frac{1 + \dfrac{\gamma - 1}{2} M_1^2}{1 + \dfrac{\gamma - 1}{2} M_2^2} = \frac{2 + (\gamma - 1)M_1^2}{2 + (\gamma - 1)M_2^2} \tag{10.49}$$

Combine Eqs. (10.44) and (10.45) and the integrated continuity equation to get

$$\frac{p_1}{p_2} = \frac{M_2}{M_1} = \frac{\rho_1}{\rho_2} = \frac{V_2}{V_1} \tag{10.50}$$

Furthermore, from Eq. (10.50) and the stagnation-to-static-pressure ratio expression, we have

$$\frac{p_{o1}}{p_{o2}} = \frac{p_{o1}}{p_1}\frac{p_1}{p_2}\frac{p_2}{p_{o2}} = \left(1 + \frac{\gamma - 1}{2} M_1^2\right)^{\gamma/(\gamma-1)} \frac{M_2}{M_1} \left(1 + \frac{\gamma - 1}{2} M_2^2\right)^{-[\gamma/(\gamma-1)]}$$

Simplification of this expression results in

$$\frac{p_{o1}}{p_{o2}} = \frac{M_2}{M_1}\left[\frac{2 + (\gamma - 1)M_1^2}{2 + (\gamma - 1)M_2^2}\right]^{\gamma/(\gamma-1)} \tag{10.51}$$

The entropy change during the isothermal process can be determined from Eq. (1.45) as

$$\frac{s_2 - s_1}{R} = -\ln\left(\frac{p_2}{p_1}\right) = \ln\left(\frac{M_2}{M_1}\right) \tag{10.52}$$

For computational purposes, the reference state where the Mach number reaches $1/\sqrt{\gamma}$ is used, and the symbol for this state is $^*$. Removing the subscripts 1, allowing $M_2$ to be equal to $1/\sqrt{\gamma}$, and replacing the subscripts 2 with $^*$ will produce computational forms of the foregoing expressions. This process yields the following set of equations:

$$\frac{T_{o1}}{T_{o2}} = \frac{T_o}{T_o^*} = \frac{2 + (\gamma - 1)M^2}{2 + (\gamma - 1)\left(\dfrac{1}{\sqrt{\gamma}}\right)^2} = \left(\frac{\gamma}{3\gamma - 1}\right)[2 + (\gamma - 1)M^2] \tag{10.53}$$

$$\frac{p}{p^*} = \frac{\rho}{\rho^*} = \frac{V^*}{V} = \frac{1}{\sqrt{\gamma}M} \tag{10.54}$$

$$\frac{fL_{\max}}{D} = \frac{1 - \gamma M^2}{\gamma M^2} + \ln(\gamma M^2) \tag{10.55}$$

$$\frac{p_o}{p_o^*} = \frac{1}{\sqrt{\gamma}M}\left\{\frac{\gamma}{(3\gamma - 1)}[2 + (\gamma - 1)M^2]\right\}^{\gamma/(\gamma-1)} \tag{10.56}$$

**Example 10.7. Relations at small Mach numbers for isothermal flow in a constant-diameter pipe with friction**

Because of the unrealistic heat flow requirements [particularly at high speeds; see Eq. (10.47)] as $M \to 1/\sqrt{\gamma}$, isothermal flows are practical only at low Mach numbers. Develop the isothermal flow relations for low-velocity flows.

**Solution**

If the Mach number is small over the entire length of a duct or pipe (i.e., $M_1$ and $M_2 \ll 1$), then from Eq. (10.49), it is seen that $T_{o1} \cong T_{o2}$. Hence, the flow is virtually adiabatic. Said another way, small-Mach-number adiabatic flow is virtually isothermal. Moreover, from Eq. (10.53) at small Mach numbers,

$$\frac{T_o}{T_o^*} = \left(\frac{2\gamma}{3\gamma - 1}\right)$$

Hence, for small Mach numbers, this ratio is virtually constant. For $\gamma = 1.4$, the ratio is 0.8750.

When the Mach numbers within a pipe or duct are small, the drop of the stagnation pressure approaches that of the static pressure, as may be seen by considering first Eq. (10.51) and then Eq. (10.50). From this analysis, we find that

$$\frac{p_{o1}}{p_{o2}} = \frac{M_2}{M_1}\left(\frac{2}{2}\right)^{\gamma/(\gamma-1)} = \frac{M_2}{M_1} = \frac{p_1}{p_2}$$

Now, for isothermal flow in a constant-diameter pipe, $M_2 = M_1(p_1/p_2)$. Thus, Eq. (10.48) may be rewritten as

$$\frac{fL}{D} = \frac{1 - \gamma M_1^2}{\gamma M_1^2} - \frac{1 - \gamma M_2^2}{\gamma M_2^2} + \ln\frac{M_1^2}{M_2^2} = \frac{1 - \left(\frac{p_2}{p_1}\right)^2}{\gamma M_1^2} + \ln\left(\frac{p_2}{p_1}\right)^2$$

Accordingly, this equation provides an expression for the pressure at a downstream location for isothermal constant-area-duct flow. For small Mach numbers, the downstream pressure can be written as $p_2 = p_1 - (p_1 - p_2) = p_1(1 - \varepsilon)$, where $\varepsilon$ is a small number equal to the pressure drop divided by $p_1$ [i.e., $\varepsilon = (p_1 - p_2)/p_1 = \Delta p/p_1$]. Replacing $p_2/p_1$ with $(1 - \varepsilon)$ produces, for small pressure drops,

$$\frac{fL}{D} = \frac{1 - (1 - \varepsilon)^2}{\gamma M_1^2} + 2\ln(1 - \varepsilon) \approx \frac{2\varepsilon - \varepsilon^2}{\gamma M_1^2} + 2\left(-\varepsilon - \frac{\varepsilon^2}{2}\right)$$

$$= \frac{2\varepsilon}{\gamma M_1^2}\left[(1 - \gamma M_1^2) - \frac{(1 + \gamma M_1^2)}{2}\varepsilon\right]$$

or

$$\frac{fL}{D} = \frac{2}{\gamma M_1^2}\left(\frac{p_1 - p_2}{p_1}\right)\left[(1 - \gamma M_1^2) - \frac{(1 + \gamma M_1^2)}{2}\left(\frac{p_1 - p_2}{p_1}\right)\right]$$

If $M_1$ is very small, this expression becomes

$$(p_1 - p_2) = \Delta p = \frac{fL}{D}\rho_1\frac{V_1^2}{2}$$

This is the incompressible pressure-drop relation. [See Ref. (10.11).] It should be noted that to obtain this expression, the identity $p_1\gamma M_1^2/2 = \rho_1 V_1^2/2$ was used.

---

**Example 10.8. Pressure drop in an isothermal flow in a constant-diameter pipe with friction**

Methane enters a gas pipeline with a velocity of 15 m/s and static pressure of 500 kPa. The pipeline is 200 m long and 8 cm in diameter, with the gas temperature essentially constant at 288 K over the pipe length. Determine the pressure drop. For methane, $\gamma = 1.32$, and the molecular mass is 16. Assume that $f = 0.025$.

**Solution**

The inlet Mach number is

$$M_1 = \frac{V_1}{\sqrt{\gamma RT}} = \frac{15}{\sqrt{1.32\left(\frac{8{,}314}{16}\right)288}} = 0.033749$$

and

$$\frac{fL}{D} = (0.025)\frac{(200)}{(0.08)} = 62.5$$

Now, as with Fanno flow,

$$\left(\frac{fL_{\max}}{D}\right)_2 = \left(\frac{fL_{\max}}{D}\right)_1 - \frac{fL}{D}$$

or

$$\left(\frac{fL_{\max}}{D}\right)_2 = 657.6265 - 62.5 = 595.1265$$

Thus, from Eq. (10.55), $M_2 = 0.035459$. From Eq. (10.50),

$$\frac{p_2}{p_1} = \frac{M_1}{M_2} = \frac{0.033749}{0.035459} = 0.9518$$

So,

$$p_1 - p_2 = p_1\left(1 - \frac{p_2}{p_1}\right) = 500(1 - 0.9518) = 24.1124 \text{ kPa}$$

The computations may be checked against the result from the previous example, in which we obtained the following expression for small Mach numbers:

$$\frac{fL}{D} = \frac{2}{\gamma M_1^2}\left(\frac{p_1 - p_2}{p_1}\right)\left[(1 - \gamma M_1^2) - \frac{(1 + \gamma M_1^2)}{2}\left(\frac{p_1 - p_2}{p_1}\right)\right]$$

Inserting values produces an $fL/D$ of 62.4742, which is only 0.041 percent below the correct value of 62.5.

## 10.7 SUMMARY

This chapter has presented an analysis of compressible flow with heat addition. Using the continuity and momentum equations, we plotted the $T$–$s$ diagram for constant-area frictionless flow. It was found that the point of maximum entropy on this diagram corresponds to the sonic point. Thus, as heat is added to flow in a constant-area duct with a resultant increase of fluid entropy, the Mach number of the flow changes toward Mach 1. This change corresponds to an increase of Mach number for subsonic flow and a decrease for supersonic flow. If enough heat is added in the duct to reach Mach 1, the duct is choked. Any further heat addition can serve only to reduce the mass-flow rate through the duct.

Because of the significance for Rayleigh flow of the sonic point, this point was used as a reference state in the computation of tables expressing the variation of properties for this flow. From the continuity, momentum, and energy equations, the ratios $T/T^*$, $p/p^*$, and $T_o/T_o^*$ were found as functions of $M$; the resultant tables facilitate the solution of problems in this area.

Work in the subject of compressible flow with heat exchange was extended to cover the combined effects of heat addition and area change, as well as heat addition and friction. In the latter cases, it was impossible to integrate directly the flow equations to solve for property variations. Instead, numerical procedures were applied. For the important case of combined friction and heat transfer, an approximate method would be to calculate separately the change of a property incurred by each effect and then add the two together.

In conclusion, the similarity in the approaches used for handling isentropic flow with area change, Fanno flow, and Rayleigh flow should by now be apparent. In each case, continuity, momentum, and energy equations were written for a fixed-differential control volume in the fluid, with the resultant equations integrated using the sonic point as a reference state. Numerical values of property variations are readily determined from the developed relations incorporated into spreadsheet programs for each case, with area change manifesting itself in the term $A/A^*$ for isentropic flow, friction in the term $fL_{max}/D$ for Fanno flow, and heat addition in the term $T_o/T_o^*$ for Rayleigh flow.

## 10.8 REFERENCES

**10.1** Thomas, L. C. *Heat Transfer*, Prentice Hall, Upper Saddle River, NJ, 1992, p. 17.

**10.2** Kakac, S., and Yener, Y. *Convective Heat Transfer*, 2d ed., CRC Press, Boca Raton, FL, 1995, pp. 57–79 and 119–185.

**10.3** Eckert, E. R. G., and Drake, R. M., Jr. *Analysis of Heat and Mass Transfer*, McGraw-Hill Book Company, New York, 1972, pp. 276–277.

**10.4** Kreith, F., and Black, W. Z. *Basic Heat Transfer*, Harper & Row Publishers, New York, 1980, pp. 265–268.

**10.5** Ozisik, M. N. *Heat Transfer: A Basic Approach*, McGraw-Hill Book Company, New York, 1984, pp. 538–545.

**10.6** Beans, E. W. "Computer Solution to Generalized One-Dimensional Flow," *AIAA J Spacecr Rockets* 1970; 7(12): 1460–1464.

**10.7** White, F. M. *Heat Transfer and Mass Transfer*, Addison-Wesley Publishing Company, Reading, MA, 1988, p. 358–361.

**10.8** Cengel, Y. A. *Heat Transfer: A Practical Approach*, McGraw-Hill Book Company, New York, 2003, p. 758.

**10.9** Kays, W. M., and Crawford, M. E. *Convective Heat and Mass Transfer*, 3d ed., McGraw-Hill Book Company, New York, 1993, pp. 257–259.

**10.10** Arpaci, V. S., and Larsen, P. S. *Convection Heat Transfer*, Prentice Hall, Upper Saddle River, NJ, 1984, pp. 435–437.

**10.11** Alexandrou, A. N. *Principles of Fluid Mechanics*, Prentice Hall, Upper Saddle River, NJ, 2001, p. 317.

## 10.9 PROBLEMS

**10.1** Draw the $T$–$s$ diagram for the flow of a gas with $\gamma = 1.4$ in a constant-diameter pipe with heat addition or loss. The reference Mach number $M_1$ for the flow is 3.0.

**10.2** Draw the $T$–$s$ diagram for the flow of a gas with $\gamma = 1.3$ in a constant-diameter pipe with heat addition or loss. The reference Mach number $M_1$ for the flow is 4.0.

**10.3** Air ($\gamma = 1.4$, $R = 0.287$ kJ/kg · K) flows in a constant-area duct of 5 cm diameter at a rate of 2 kg/s. If the inlet stagnation pressure and temperature are, respectively, 700 kPa and 300 K, plot $T$ versus $s$ for Rayleigh line flow. For the same inlet conditions and mass-flow rate, plot a $T$–$s$ diagram for Fanno flow. From the points of intersection of Rayleigh and Fanno lines, show the states on either side of a normal shock. Assume the air to behave as a perfect gas with constant specific heats.

**10.4** Air ($\gamma = 1.4$, $R = 0.287$ kJ/kg · K) flows in a constant-area duct of diameter 1.5 cm with a velocity of 100 m/s, static temperature of 320 K, and static pressure of 200 kPa. Determine the rate of heat input to the flow necessary to choke the duct. Assume Rayleigh line flow; express your answer in kilowatts. Assume the air to behave as a perfect gas with constant specific heats.

**10.5** Air ($\gamma = 1.4$, $R = 0.287$ kJ/kg · K) flows in a constant-area duct of 10 cm diameter at a rate of 0.5 kg/s. The inlet stagnation pressure is 100 kPa, and the inlet stagnation temperature is 35°C.

(a) Find possible values of inlet Mach number.

(b) For each inlet Mach number of part (a), determine the heat addition rate, in kilowatts, necessary to choke the duct.

**10.6** A supersonic flow at $p_o = 1.0$ MPa and $T_o = 1{,}000$ K enters a 5-cm-diameter duct at Mach 1.8. Heat is added to the flow via a chemical reaction taking place inside the duct. Determine the heat transfer rate in kilowatts necessary to choke the duct. Assume the air ($\gamma = 1.4$, $R = 0.287$ kJ/kg · K) to behave as a perfect gas with constant specific heats; neglect changes in the composition of the gas stream caused by the chemical reaction.

**10.7** Heat is added to airflow ($\gamma = 1.4$, $R = 0.287$ kJ/kg · K) in a constant-area duct at the rate of 30 kJ/m. If flow enters at Mach 0.20, $T_1 = 300$ K, and $p_1 = 100$ kPa, plot $M$ versus $x$, $p$ versus $x$, $T$ versus $x$, and $p_1$ versus $x$.

**10.8** An airstream ($\gamma = 1.4, R = 0.287$ kJ/kg · K) passing through a 5-cm-diameter, thin-walled tube is to be heated by high-pressure steam condensing on the outer surface of the tube at 160°C. The overall heat transfer coefficient between steam and air can be assumed to be 140 W/m$^2$ · K, with the air entering at 30 m/s, 70 kPa, and 5°C. The air is to be heated to 65°C. Determine the tube length required. Assuming Rayleigh line flow, calculate the static pressure change due to heat addition. Also, for the same inlet conditions, calculate the pressure drop due to friction, assuming Fanno flow in the duct with $f = 0.018$. To obtain an approximation to the overall pressure drop in this heat exchanger, add the two results. Discuss the accuracy of this calculation.

**10.9** Air ($\gamma = 1.4, R = 0.287$ kJ/kg · K) enters a turbojet combustion chamber at 400 K and 200 kPa, with a temperature after combustion of 1,000 K. If the heating value of the fuel is 48,000 kJ/kg, determine the required fuel–air ratio (on a mass basis). Assume Rayleigh line flow in the combustion chamber. What fuel–air ratio would be required to choke the combustion chamber? The inlet velocity is 35 m/s.

**10.10** Air ($\gamma = 1.4, R = 0.287$ kJ/kg · K, and $c_p = 1.0045$ kJ/kg · K) flows through a constant-area duct connected to a reservoir at a temperature of 500°C and a pressure of 500 kPa by a converging nozzle, as shown in Figure P10.10. Heat is lost at the rate of 250 kJ/kg. (a) Determine the exit pressure, Mach number, and mass-flow rate for a back pressure of 0 kPa. (b) Determine the exit pressure and Mach number when a normal shock stands in the exit plane of the duct.

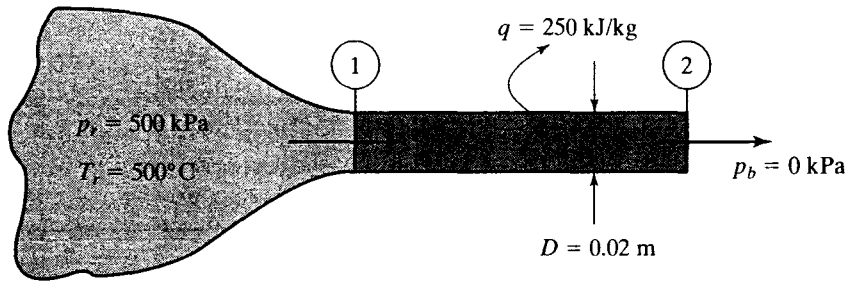


**Figure P10.10**

**10.11** Consider flow in a constant-area duct with friction and heat transfer. To maintain a constant subsonic Mach number, should heat be added or removed? Repeat for supersonic flow.

**10.12** For the system in Problem 10.10, determine the mass-flow rate if 250 kJ/kg of heat energy is added to the flow in the duct. Assume the duct diameter to be 2 cm. Repeat for a back pressure of 100 kPa. The working fluid is air ($\gamma = 1.4, R = 0.287$ kJ/kg · K).

**10.13** A detonation wave (Figure P10.13) represents a shock sustained by chemical reaction. Give the continuity, momentum, and energy equations for such a wave, assuming that a chemical reaction taking place in the wave liberates heat $q$. Denote properties of the unburned gas ahead of the wave by the subscript $u$ and those of the burned gases behind the wave by $b$. Write the equations for an observer traveling with the wave.

**10.14** Develop a computer program that will yield values of $p/p^*, T/T^*, T_o/T_o^*$, and $p_o/p_o^*$ for Rayleigh line flow, with the working fluid consisting of a perfect gas with constant $\gamma = 1.36$. Use Mach number increments of 0.10 over the range $M = 0$ to $M = 2.5$.

**10.15** Oxygen ($\gamma = 1.4, R = 0.2598$ kJ/kg · K) is to be pumped through an uninsulated 2.5-cm-diameter pipe that is 1,000 m long. (See Figure P10.15.) A compressor at the oxygen source is available capable of providing a pressure of 1 MPa. If the supply pressure is to be 101 kPa, determine the mass-flow rate through the system and the compressor power required. Assume isothermal flow at $T = 15$°C. Take the friction factor to be 0.018.

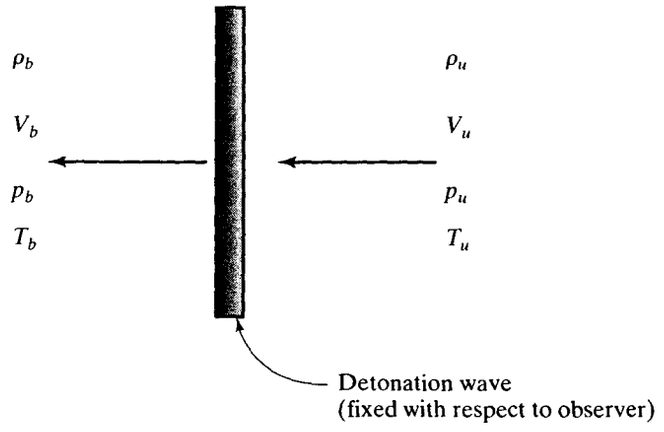


**Figure P10.13**

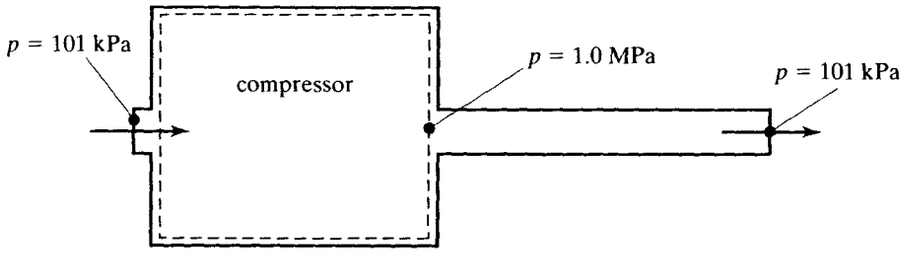


**Figure P10.15**

**10.16** Natural gas (assume the properties of methane: $\gamma = 1.32$ and $R = 0.5182$ kJ/kg · K) is to be pumped over a long distance through a 7.5-cm-diameter pipe. (See Figure P10.16.) Assume the gas flow to be isothermal, with $T = 15°C$. Compressor stations capable of delivering 20 kW to the flow are available, with each compressor capable of raising the gas pressure isothermally to 500 kPa. (The inlet compressor pressure is to be 120 kPa.) How far apart should the compressor stations be located? Assume isothermal compression in each compressor, with $f = 0.017$.

$p/p^*, fL_{max}/D, T_o/T_o^*, \quad p_o/p_o^*$
$\gamma = 1.34.$

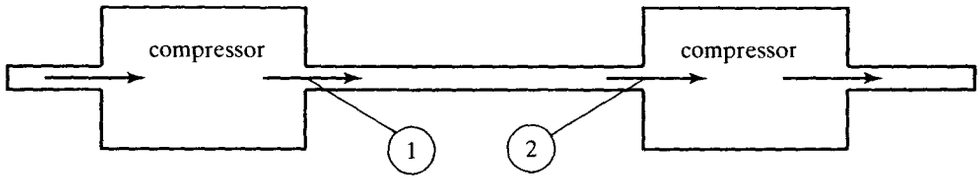


**Figure P10.16**

**10.17** Develop a computer program that will yield values of and for isothermal flow, with the working fluid consisting of a perfect gas with constant Use Mach number increments of 0.10 over the range $M = 0.1$ to $M = 2.5$.

**10.18** A subsonic stream of air ($\gamma = 1.4$, $R = 0.287$ kJ/kg · K, and $c_p = 1.0045$ kJ/kg · K) flows through a linear, conically shaped nozzle [i.e., $D = D_i + (D_e - D_i)x/L$]. The diameter at the inlet is 2 cm, and the diameter at the exit is 5 cm. The nozzle is 10 cm long. The entering Mach number is 0.6. Heat is added to flow at a rate so that the stagnation temperature varies linearly with distance. The stagnation temperature at the inlet is 300 K and increases 30 K per meter of nozzle. Use Heun's predictor–corrector scheme on a coarse grid that includes 11 grid points to determine the Mach number distribution within the duct. To verify the computations, determine the exit Mach number for the case when the heat transfer is zero, and compare it with the value determined from isentropic flow computations.

**10.19** A supersonic stream of air ($\gamma = 1.4$, $R = 0.287$ kJ/kg · K, and $c_p = 1.004$ kJ/kg · K) flows through a linear, conically shaped nozzle [i.e., $D = D_i + (D_e - D_i)x/L$]. The diameter at the inlet is 2 cm, and the diameter at the exit is 5 cm. The nozzle is 10 cm long. The entering Mach number is 3. Heat is added to flow at a rate so that the stagnation temperature varies linearly with distance. The stagnation temperature at the inlet is 300 K and increases 30 K per meter of nozzle. The pressure is such that a normal shockwave stands halfway down the nozzle. Use Euler's explicit method to determine the Mach number distribution within the duct.

**10.20** A supersonic stream of air ($\gamma = 1.3$, $R = 0.287$ kJ/kg · K, and $c_p = 1.004$ kJ/kg · K) flows through a linear, conically shaped nozzle [i.e., $D = D_i + (D_e - D_i)x/L$]. The diameter at the inlet is 2 cm, and the diameter at the exit is 5 cm. The nozzle is 10 cm long. The entering Mach number is 3. Heat is added to flow at a rate so that the stagnation temperature varies linearly with distance. The stagnation temperature at the inlet is 300 K and increases 30 K per meter of nozzle. The pressure is such that a normal shockwave stands halfway down the nozzle. Use Heun's predictor–corrector method to determine the Mach number distribution within the duct.

# Chapter 11

# Equations of Motion for Multidimensional Flow

## 11.1 INTRODUCTION

Previous chapters have dealt almost exclusively with one-dimensional flow. Exceptions were the treatment of oblique shocks in Chapter 6 and Prandtl–Meyer flow in Chapter 7, yet even these cases could be handled componentwise as equivalent one-dimensional flows. One-dimensional analysis has been shown to be useful for obtaining good engineering approximations to a wide variety of flow problems. However, such an analysis is necessarily an approximation; no real flow exists that is truly one dimensional. Furthermore, many problems cannot even be approached with a one-dimensional analysis. For example, whereas the procedures used in Chapter 3 enabled the prediction of supersonic nozzle area ratios for a required isentropic Mach number, the one-dimensional equations are inadequate for the design of the contour of such a nozzle ($A$ versus $x$). Likewise, the flow over a cambered supersonic wing cannot be predicted on the basis of a simple one-dimensional theory. For these, and a great many other, practical cases, we must develop the equations of motion for multidimensional gas dynamics and find means for solving these equations subject to prescribed boundary conditions.

In this chapter, we shall derive the equations of continuity, momentum, and energy for two- and three-dimensional compressible flows. Due to the complexity of these equations, we shall restrict ourselves to flows in which viscous forces, electromagnetic forces, heat transfer, and external work can be neglected. Later chapters will include methods for solving these partial differential equations.

## 11.2 CONTINUITY EQUATION

As we saw in Chapter 1, the continuity equation for a control volume is given by

$$0 = \frac{\partial}{\partial t}\underset{\text{C.V.}}{\iiint}\rho d\forall + \underset{\text{C.S.}}{\iint}\rho \mathbf{V}\cdot d\mathbf{A} \tag{1.21}$$

Consider a differential control volume of cubical shape in a compressible flow, as shown in Figure 11.1. Let the velocity components in the $x$, $y$, and $z$ directions at the center of the control volume be $u$, $v$, and $w$, respectively.

The *mass-flow rate* across each of the six faces of the control volume is given by the product of the density, velocity, and face area. Because the product of the density and the velocity represents a continuous variable, we may expand the product in a Taylor series [see Ref. (11.1)] to obtain mass-flow rate values on the faces of the cube. For example, in the $x$ direction, the mass flows crossing the left and right faces are

$$\left\{\begin{matrix}\text{mass flow into}\\ \text{left face of C.V.}\end{matrix}\right\} = \left(\rho u - \frac{\partial \rho u}{\partial x}\frac{dx}{2}\right)dy\,dz$$

$$\left\{\begin{matrix}\text{mass flow out of}\\ \text{right face of C.V.}\end{matrix}\right\} = \left(\rho u + \frac{\partial \rho u}{\partial x}\frac{dx}{2}\right)dy\,dz$$

Mass flows across the other four faces may be similarly written. The net flow rate in a given direction is found by taking the difference between the flows out of and into the control volume. In the $x$ direction, the net flow rate is

$$\left\{\begin{matrix}\text{net mass-flow rate in}\\ \text{the } x \text{ direction}\end{matrix}\right\} = \left(\rho u + \frac{\partial \rho u}{\partial x}\frac{dx}{2}\right)dy\,dz$$

$$-\left(\rho u - \frac{\partial \rho u}{\partial x}\frac{dx}{2}\right)dy\,dz = \frac{\partial \rho u}{\partial x}dx dy dz$$

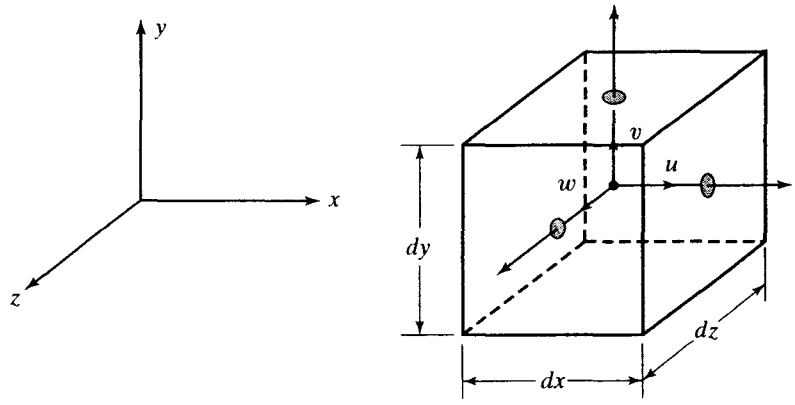


**Figure 11.1** Differential Control Volume for Three-Dimensional Flow in a Cartesian Coordinate System

Similar expressions are written for the other directions. From the continuity equation, then, we have

$$\iint_{\text{c.s.}} \rho \mathbf{V} \cdot d\mathbf{A} = \left( \frac{\partial \rho u}{\partial x} + \frac{\partial \rho v}{\partial y} + \frac{\partial \rho w}{\partial z} \right) dx dy dz$$

Now the rate of mass buildup inside the control volume may be written as

$$\frac{\partial}{\partial t} \iiint_{\text{c.v.}} \rho d\forall = \frac{\partial m}{\partial t} = \frac{\partial (\rho dx dy dz)}{\partial t} = \frac{\partial \rho}{\partial t} dx dy dz$$

Combining and dividing out the differential volume ($dxdydz$) yields

$$\frac{\partial \rho}{\partial t} + \frac{\partial \rho u}{\partial x} + \frac{\partial \rho v}{\partial y} + \frac{\partial \rho w}{\partial z} = 0 \tag{11.1}$$

Equation (11.1) is the three-dimensional continuity equation in a *Cartesian coordinate system*. We may rewrite it in a more general form using vector notation. To accomplish this, we introduce the *del operator* $\nabla$ [see Ref. (11.2)], which is defined for a Cartesian coordinate system as

$$\nabla \equiv \mathbf{i} \frac{\partial}{\partial x} + \mathbf{j} \frac{\partial}{\partial y} + \mathbf{k} \frac{\partial}{\partial z}$$

where $\mathbf{i}$, $\mathbf{j}$, and $\mathbf{k}$ are unit vectors in the $x$, $y$, and $z$ directions, respectively. Now, if the scalar, or dot product, of the del operator is taken and the *mass flux* (the product of the density $\rho$ and the velocity vector $\mathbf{V} = u\mathbf{i} + v\mathbf{j} + w\mathbf{k}$), we get

$$\nabla \cdot \rho \mathbf{V} = \frac{\partial \rho u}{\partial x} + \frac{\partial \rho v}{\partial y} + \frac{\partial \rho w}{\partial z}$$

Hence, Eq. (11.1) can be rewritten as

$$\frac{\partial \rho}{\partial t} + \nabla \cdot \rho \mathbf{V} = 0 \tag{11.2}$$

The *substantial*, or *material, derivative* of the density, $D\rho/Dt$, represents the time rate of change of the gas density as would be measured by an observer who moves with the flow. Since the density can vary with $x$, $y$, $z$, and $t$ [i.e., $\rho = \rho(x, y, z, t)$], the total derivative of $\rho$ is

$$\begin{aligned} d\rho &= \frac{\partial \rho}{\partial t} dt + \frac{\partial \rho}{\partial x} dx + \frac{\partial \rho}{\partial y} dy + \frac{\partial \rho}{\partial z} dz \\ &= \frac{\partial \rho}{\partial t} dt + \left( \frac{\partial \rho}{\partial x} \mathbf{i} + \frac{\partial \rho}{\partial y} \mathbf{j} + \frac{\partial \rho}{\partial z} \mathbf{k} \right) \cdot (dx\mathbf{i} + dy\mathbf{j} + dz\mathbf{k}) \\ &= \frac{\partial \rho}{\partial t} dt + \nabla \rho \cdot d\mathbf{r} \end{aligned}$$

where $d\mathbf{r} = dx\mathbf{i} + dy\mathbf{j} + dz\mathbf{k}$ is the differential position vector. The moving observer obtains the change of density of a fluid particle while following its motion. The instantaneous speed of the fluid and the observer are given by

$$\frac{dx}{dt} = u, \quad \frac{dy}{dt} = v, \quad \text{and} \quad \frac{dz}{dt} = w$$

Accordingly, we may write

$$d\mathbf{r} = \mathbf{V}dt$$

Now we replace the differential position vector in the equation for the differential density and divide by $dt$ to obtain the substantial derivative for the density:

$$\frac{D\rho}{Dt} = \frac{\partial \rho}{\partial t} + \mathbf{V} \cdot \nabla \rho = \frac{\partial \rho}{\partial t} + u\frac{\partial \rho}{\partial x} + v\frac{\partial \rho}{\partial y} + w\frac{\partial \rho}{\partial z}$$

Therefore, the continuity equation, Eq. (11.2), may also be written as

$$\frac{\partial \rho}{\partial t} + \nabla \cdot \rho\mathbf{V} = \frac{\partial \rho}{\partial t} + \mathbf{V} \cdot \nabla \rho + \rho \nabla \cdot \mathbf{V} = \frac{D\rho}{Dt} + \rho \nabla \cdot \mathbf{V} = 0$$

For steady flow, $\partial/\partial t = 0$, and the preceding equation simplifies to

$$\frac{\partial \rho u}{\partial x} + \frac{\partial \rho v}{\partial y} + \frac{\partial \rho w}{\partial z} = 0 \tag{11.3}$$

or

$$\nabla \cdot \rho\mathbf{V} = 0 \tag{11.4}$$

For steady, incompressible flow,

$$\frac{\partial u}{\partial x} + \frac{\partial v}{\partial y} + \frac{\partial w}{\partial z} = 0 \tag{11.5}$$

or

$$\nabla \cdot \mathbf{V} = 0 \tag{11.6}$$

which states that the *divergence* (i.e., $\nabla \cdot$)of the velocity field is zero.

**Example 11.1. Substantial derivative of the density of a gas**

At $t = 0$, a container of gas is located on a stationary surface. The density of the gas within the container is given by $\rho = \rho_o - \alpha z$, where $z$ is the distance in a stationary coordinate system fixed to the stationary surface. The container is allowed to move vertically with a speed $w = \beta t$. However, the density of the gas does not change at any point within the container as measured from the bottom of the container. Determine $D\rho/Dt$.

**Solution**

To solve this problem, we require a coordinate system that moves with the gas. We will label coordinates in this moving system $\zeta$, where distances are measured vertically from

the bottom of the container. Obviously, at $t = 0$, the stationary $z$-coordinate system and the moving $\zeta$-coordinate system are coincident. The relationship between the two coordinate measures is established as follows:

$$w = \frac{dz}{dt} = \beta t$$

Therefore,

$$\int_{z=\zeta}^{z} dz = \int_{t=0}^{t} w dt$$

$$z - \zeta = \int_{t=0}^{t} \beta t dt = \beta \frac{t^2}{2}$$

$$\zeta = z - \beta \frac{t^2}{2}$$

Since the density of the gas at any location depends only on the gas's position within the container, we may write

$$\rho = \rho_o - \alpha\zeta$$

$$= \rho_o - \alpha z + \alpha\beta \frac{t^2}{2}$$

Note that these two expressions tell us the following: (i) To an observer moving with the same speed as the container, the density remains the same at a given location above the bottom of the container (i.e, at a fixed value of $\zeta$), and (ii) to a stationary observer, the density at a given location within the container depends upon the time and location of the point. To determine the substantial derivative, we require the values of $\partial\rho/\partial t$ and $\partial\rho/\partial z$, which are easily obtained from the preceding equation:

$$\left(\frac{\partial \rho}{\partial t}\right)_z = \alpha\beta t$$

$$\left(\frac{\partial \rho}{\partial z}\right)_t = -\alpha$$

Hence,

$$\frac{D\rho}{Dt} = \frac{\partial \rho}{\partial t} + w\frac{\partial \rho}{\partial z} = \alpha\beta t + (\beta t)(-\alpha) = 0$$

This result indicates that the moving observer will measure no change in density.

## 11.3 MOMENTUM EQUATION

The momentum equation for the control volume is given by Eq. (1.31):

$$\sum \mathbf{F} = \frac{\partial}{\partial t} \iiint_{\text{C.V.}} \rho \mathbf{V} d\forall + \iint_{\text{C.S.}} \mathbf{V}(\rho \mathbf{V} \cdot d\mathbf{A}) \tag{1.31}$$

We shall neglect electromagnetic, gravity, and all other forces acting on the control volume, with the exception of the pressure forces. For the differential control volume shown in Figure 11.1, take $p$ to be the pressure at the center of the control volume. Consider the momentum equation in the $x$ direction, with pressure forces acting on the control surfaces perpendicular to the $x$-axis as shown in Figure 11.2. The pressure on the faces of the control volume (at $x = \pm dx/2$) are then obtained through the use of Taylor series expansions around the center point (i.e., at $x = 0$).

The net external force acting on the control volume in the $x$ direction is

$$F_{x,\text{left face}} - F_{x,\text{right face}} = \left(p - \frac{\partial p}{\partial x}\frac{dx}{2}\right)dydz - \left(p + \frac{\partial p}{\partial x}\frac{dx}{2}\right)dydz = -\frac{\partial p}{\partial x}dxdydz$$

The *x-momentum flux* (velocity component in the $x$ direction times the mass-flow rate) across the left- and right-hand faces of the control volume of Figure 11.1 are, respectively,

$$\left\{\begin{matrix}x\text{-momentum flux} \\ \text{into left face of C.V.}\end{matrix}\right\} = \left(u - \frac{\partial u}{\partial x}\frac{dx}{2}\right)\left(\rho u - \frac{\partial \rho u}{\partial x}\frac{dx}{2}\right)dy\,dz$$

$$\left\{\begin{matrix}x\text{-momentum flux out} \\ \text{of right face of C.V.}\end{matrix}\right\} = \left(u + \frac{\partial u}{\partial x}\frac{dx}{2}\right)\left(\rho u + \frac{\partial \rho u}{\partial x}\frac{dx}{2}\right)dy\,dz$$

The mass flows crossing the top and bottom faces, respectively, take with them an $x$-momentum flux:

$$\left\{\begin{matrix}x\text{-momentum flux into} \\ \text{bottom face of C.V.}\end{matrix}\right\} = \left(u - \frac{\partial u}{\partial y}\frac{dy}{2}\right)\left(\rho v - \frac{\partial \rho v}{\partial y}\frac{dy}{2}\right)dx\,dz$$

$$\left\{\begin{matrix}x\text{-momentum flux} \\ \text{out of top face of C.V.}\end{matrix}\right\} = \left(u + \frac{\partial u}{\partial y}\frac{dy}{2}\right)\left(\rho v + \frac{\partial \rho v}{\partial y}\frac{dy}{2}\right)dx\,dz$$

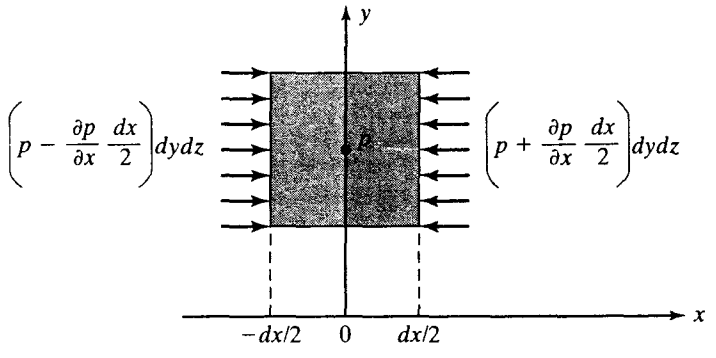


**Figure 11.2** Pressure Forces Acting in the $x$ Direction on the Surfaces of the Differential Control Volume

Similarly, the $x$-momentum flux crossing the rear and front faces, respectively, of the control volume are

$$\left\{\begin{matrix}x\text{-momentum flux} \\ \text{into rear face of C.V.}\end{matrix}\right\} = \left(u - \frac{\partial u}{\partial z}\frac{dz}{2}\right)\left(\rho w - \frac{\partial \rho w}{\partial z}\frac{dz}{2}\right)dx\,dy$$

$$\left\{\begin{matrix}x\text{-momentum flux out} \\ \text{of front face of C.V.}\end{matrix}\right\} = \left(u + \frac{\partial u}{\partial z}\frac{dz}{2}\right)\left(\rho w + \frac{\partial \rho w}{\partial z}\frac{dz}{2}\right)dx\,dy$$

The rate at which $x$-directed linear momentum builds up within the control volume is given by

$$\frac{\partial}{\partial t}\iiint_{\text{C.V.}} \rho u d\forall = \frac{\partial (mu)}{\partial t} = \frac{\partial (\rho u dx dy dz)}{\partial t} = \frac{\partial (\rho u)}{\partial t} dx dy dz$$

Combining, substituting into the $x$-momentum equation, and dropping second-order terms yields

$$-\frac{\partial p}{\partial x}dx\,dy\,dz = \frac{\partial}{\partial t}(\rho u)dx\,dy\,dz + \left(u\frac{\partial \rho w}{\partial z} + \rho w\frac{\partial u}{\partial z} + \rho v\frac{\partial u}{\partial y}\right.$$

$$\left. + u\frac{\partial \rho v}{\partial y} + \rho u\frac{\partial u}{dx} + u\frac{\partial \rho u}{\partial x}\right)dx\,dy\,dz$$

Canceling out the product $dxdydz$, the volume of the differential element, and using the continuity equation produces

$$-\frac{\partial p}{\partial x} = \frac{\partial \rho u}{\partial t} - u\frac{\partial \rho}{\partial t} + \rho\left(u\frac{\partial u}{\partial x} + v\frac{\partial u}{\partial y} + w\frac{\partial u}{\partial z}\right)$$

However,

$$\frac{\partial \rho u}{\partial t} = \rho\frac{\partial u}{\partial t} + u\frac{\partial \rho}{\partial t}$$

so that

$$-\frac{\partial p}{\partial x} = \rho\frac{\partial u}{\partial t} + \rho\left(u\frac{\partial u}{\partial x} + v\frac{\partial u}{\partial y} + w\frac{\partial u}{\partial z}\right)$$

or

$$-\frac{1}{\rho}\frac{\partial p}{\partial x} = \frac{\partial u}{\partial t} + u\frac{\partial u}{\partial x} + v\frac{\partial u}{\partial y} + w\frac{\partial u}{\partial z} \tag{11.7}$$

It should be noted that the terms on the right-hand side of Eq. (11.7) are acceleration components in the $x$ direction. The first term on the right-hand side, which vanishes

for steady flows, is the *local acceleration* (the time rate of change of the velocity component in the $x$ direction at a given location), whereas the last three terms on the right-hand are the *convective accelerations* in the $x$ direction. Thus, there are two principal means of changing the speed of a fluid particle: In one, the speed of the particle is changed at a given location (a local unsteady acceleration), and in the other, the speed is changed with position (convective acceleration).

The right-hand side of Eq. (11.7) can be recognized as the substantial derivative of $u$. Thus, the acceleration in the $x$-direction can be written as

$$\frac{Du}{Dt} = \frac{\partial u}{\partial t} + u\frac{\partial u}{\partial x} + v\frac{\partial u}{\partial y} + w\frac{\partial u}{\partial z}$$

The momentum equation in the $x$ direction may be written in a very compact form as

$$-\frac{1}{\rho}\frac{\partial p}{\partial x} = \frac{Du}{Dt}$$

Similar developments in the $y$ and $z$ directions yield, respectively,

$$-\frac{1}{\rho}\frac{\partial p}{\partial y} = \frac{Dv}{Dt} = \frac{\partial v}{\partial t} + u\frac{\partial v}{\partial x} + v\frac{\partial v}{\partial y} + w\frac{\partial v}{\partial z} \tag{11.8}$$

and

$$-\frac{1}{\rho}\frac{\partial p}{\partial z} = \frac{Dw}{Dt} = \frac{\partial w}{\partial t} + u\frac{\partial w}{\partial x} + v\frac{\partial w}{\partial y} + w\frac{\partial w}{\partial z} \tag{11.9}$$

By using vector notation, Eqs. (11.7), (11.8), and (11.9) can be written collectively as

$$-\frac{1}{\rho}\nabla p = \frac{D\mathbf{V}}{Dt} = \frac{\partial \mathbf{V}}{\partial t} + (\mathbf{V}\cdot\nabla)\mathbf{V} \tag{11.10}$$

where $\nabla p$ is the *gradient* of the pressure. This set of equations is called *Euler's equations*. We encountered the one-dimensional version of Euler's equation in Section 3.2. A considerable amount of research [see, for example, Refs. (11.3) and (11.4)] has been directed towards numerically solving this nonlinear set of equations.

## 11.4 ENERGY EQUATION

The energy equation for the control volume is given by Eq. (1.38):

$$\dot{Q} - \dot{W} = \frac{\partial}{\partial t}\iiint_{\text{C.V.}}\left(e + \frac{V^2}{2} + gz\right)\rho d\forall + \iint_{\text{C.S.}}\left(h + \frac{V^2}{2} + gz\right)(\rho\mathbf{V}\cdot d\mathbf{A}) \tag{1.38}$$

It should be noted that the symbol for internal energy that has been used in previous chapters, $u$, has been replaced by the symbol $e$ to avoid confusion with the velocity component $u$ in the $x$ direction. Also, $V^2 = u^2 + v^2 + w^2$.

In the upcoming text, in addition to the assumptions made at the end of Section 11.1, we assume that potential-energy effects are insignificant, as are the body forces, and that the rate of performing external work on the control volume, $\dot{W}$, is zero. Hence, the energy equation simplifies to

$$\dot{Q} = \frac{\partial}{\partial t}\iiint_{\text{C.V.}}\left(e + \frac{V^2}{2}\right)\rho d\forall + \iint_{\text{C.S.}}\left(h + \frac{V^2}{2}\right)(\rho \mathbf{V}\cdot d\mathbf{A})$$

or

$$\dot{Q} = \frac{\partial}{\partial t}\iiint_{\text{C.V.}} e_t \rho d\forall + \iint_{\text{C.S.}} h_o(\rho \mathbf{V}\cdot d\mathbf{A}) \tag{11.11}$$

where $e_t = e + V^2/2$ is the *total energy per unit mass* that is stored in the control volume and $h_o = h + V^2/2$ is the stagnation enthalpy.

Now the *flux of energy* (stagnation enthalpy times the mass-flow rate) that flows across the right- and left-hand faces of the control volume of Figure 11.1 are

$$\left\{\begin{matrix}\text{flow of energy into}\\ \text{left face of C.V.}\end{matrix}\right\} = \left(h_o - \frac{\partial h_o}{\partial x}\frac{dx}{2}\right)\left(\rho u - \frac{\partial \rho u}{\partial x}\frac{dx}{2}\right)dy\,dz$$

$$\left\{\begin{matrix}\text{flow of energy out of}\\ \text{right face of C.V.}\end{matrix}\right\} = \left(h_o + \frac{\partial h_o}{\partial x}\frac{dx}{2}\right)\left(\rho u + \frac{\partial \rho u}{\partial x}\frac{dx}{2}\right)dy\,dzy$$

Perform the multiplication within each of these expressions, drop the second-order terms, and take the difference of the resulting expressions to obtain the net flux of energy in the $x$ direction across the control volume:

$$\left\{\begin{matrix}\text{net flux of energy in}\\ \text{the } x \text{ direction}\end{matrix}\right\} = \left(h_o\frac{\partial \rho u}{\partial x}dx + \rho u\frac{\partial h_o}{\partial x}dx\right)dy\,dz = \frac{\partial(\rho u h_o)}{\partial x}dxdy\,dz$$

Repeating this process for the transport of energy across the top and bottom faces ($y$ direction) and the front and back faces ($z$ direction) of the control volume in Figure 11.1 gives, respectively,

$$\left\{\begin{matrix}\text{net flux of energy in}\\ \text{the } y \text{ direction}\end{matrix}\right\} = \frac{\partial(\rho v h_o)}{\partial y}dxdy\,dz$$

$$\left\{\begin{matrix}\text{net flux of energy in}\\ \text{the } z \text{ direction}\end{matrix}\right\} = \frac{\partial(\rho w h_o)}{\partial z}dxdy\,dz$$

Thus, the total flux of energy across the control surfaces is

$$\iint_{\text{C.S.}} h_o(\rho \mathbf{V}\cdot d\mathbf{A}) = \left[\frac{\partial(\rho u h_o)}{\partial x} + \frac{\partial(\rho v h_o)}{\partial y} + \frac{\partial(\rho w h_o)}{\partial z}\right]dxdy\,dz$$

Because the total energy per unit volume, $\rho e_t$, is uniform within the differential control volume, the rate of accumulation of total energy is given by

$$\frac{\partial}{\partial t}\iiint_{\text{c.v.}} e_t \rho d\forall = \frac{\partial(me_t)}{\partial t} = \frac{\partial(\rho dxdydze_t)}{\partial t} = \frac{\partial(\rho e_t)}{\partial t}dxdydz$$

The heat flow rate can be written as

$$\dot{Q} = \dot{q}dm = \dot{q}\rho dxdydz$$

where $\dot{q}$ is the *heat flow rate per unit mass*. Combining and substituting into Eq. (11.11) yields

$$\rho\dot{q} = \frac{\partial(\rho e_t)}{\partial t} + \frac{\partial(\rho u h_o)}{\partial x} + \frac{\partial(\rho v h_o)}{\partial y} + \frac{\partial(\rho w h_o)}{\partial z}$$

This expression may be rewritten using vector notation as

$$\rho\dot{q} = \frac{\partial(\rho e_t)}{\partial t} + \nabla\cdot(\rho h_o \mathbf{V}) = 0 \tag{11.12}$$

The energy equation can be expressed in various forms by using the substantial derivative; the continuity equation, Eq. (11.2); or the momentum equation, Eq. (11.10). We will develop a few of these forms and leave the others as problems at the end of this chapter.

Now,

$$h_o = h + \frac{V^2}{2} = e + \frac{p}{\rho} + \frac{V^2}{2} = \left(e + \frac{V^2}{2}\right) + \frac{p}{\rho} = e_t + \frac{p}{\rho}$$

Hence,

$$\nabla\cdot(\rho h_o \mathbf{V}) = \nabla\cdot(\rho e_t \mathbf{V}) + \nabla\cdot(p\mathbf{V})$$

Combining this expression with Eq. (11.12) gives

$$\rho\dot{q} = \frac{\partial(\rho e_t)}{\partial t} + \nabla\cdot(\rho e_t \mathbf{V}) + \nabla\cdot(p\mathbf{V}) \tag{11.13}$$

By multiplying the continuity equation, Eq. (11.2), by $e_t$ and subtracting it from Eq. (11.13), we obtain

$$\rho\dot{q} = \rho\frac{\partial e_t}{\partial t} + \rho\mathbf{V}\cdot\nabla e_t + \nabla\cdot(p\mathbf{V}) \tag{11.14}$$

The *substantial derivative operator* is

$$\frac{D}{Dt} = \frac{\partial}{\partial t} + \mathbf{V}\cdot\nabla$$

Thus, Eq. (11.14) can be expressed as

$$\rho\dot{q} - \nabla\cdot(p\mathbf{V}) = \rho\frac{De_t}{Dt} \tag{11.15}$$

Since

$$e_t = e + \frac{V^2}{2} = e + \frac{\mathbf{V}\cdot\mathbf{V}}{2}$$

we have

$$\rho\frac{De_t}{Dt} = \rho\frac{De}{Dt} + \rho\mathbf{V}\cdot\frac{D\mathbf{V}}{Dt} = \rho\dot{q} - \nabla\cdot(p\mathbf{V}) = \rho\dot{q} - p\nabla\cdot\mathbf{V} - \mathbf{V}\cdot\nabla p$$

or

$$\rho\frac{De}{Dt} + \rho\mathbf{V}\cdot\left(\frac{D\mathbf{V}}{Dt} + \frac{\nabla p}{\rho}\right) = \rho\dot{q} - p\nabla\cdot\mathbf{V} \tag{11.16}$$

The momentum equation in vector form is

$$\frac{D\mathbf{V}}{Dt} = -\frac{\nabla p}{\rho} \tag{11.10}$$

Thus, the term inside the brackets on the left of Eq. (11.16) is identically zero, and we have

$$\rho\frac{De}{Dt} = \rho\dot{q} - p\nabla\cdot\mathbf{V} \tag{11.17}$$

With the aid of the continuity equation, Eq. (11.16) can be rewritten as

$$\rho\frac{Dh}{Dt} = \rho\dot{q} + \frac{Dp}{Dt} \tag{11.18}$$

With the aid of the momentum equation, Eq. (11.16) can be rewritten as

$$\rho\frac{Dh_o}{Dt} = \rho\dot{q} + \frac{\partial p}{\partial t} \tag{11.19}$$

**Example 11.2. Total-enthalpy energy equation**

Derive Eq. (11.19), and use the result to demonstrate that the total enthalpy of a gas is constant if the flow is adiabatic and steady.

**Solution**

To develop the expression of Eq. (11.19), begin by adding $[\rho D(V^2/2)/Dt]$ to both sides of Eq. (11.18) to get

$$\rho\left[\frac{Dh}{Dt} + \frac{D(V^2/2)}{Dt}\right] = \rho\dot{q} + \frac{Dp}{Dt} + \rho\frac{D(V^2/2)}{Dt}$$

Since

$$\left[\frac{Dh}{Dt} + \frac{D(V^2/2)}{Dt}\right] = \frac{D}{Dt}\left(h + \frac{V^2}{2}\right) = \frac{Dh_o}{Dt}$$

$$\frac{Dp}{Dt} = \frac{\partial p}{\partial t} + \mathbf{V}\cdot\nabla p$$

$$\frac{D(V^2/2)}{Dt} = \frac{1}{2}\frac{D(\mathbf{V}\cdot\mathbf{V})}{Dt} = \mathbf{V}\cdot\frac{D\mathbf{V}}{Dt}$$

Combining, we obtain

$$\rho\frac{Dh_o}{Dt} = \rho\dot{q} + \frac{\partial p}{\partial t} + \mathbf{V}\cdot\nabla p + \rho\mathbf{V}\cdot\frac{D\mathbf{V}}{Dt} = \rho\dot{q} + \frac{\partial p}{\partial t} + \mathbf{V}\cdot\left(\nabla p + \rho\frac{D\mathbf{V}}{Dt}\right)$$

The group of terms on the far right is recognized as Euler's equations, which are identically zero. Finally, then,

$$\rho\frac{Dh_o}{Dt} = \rho\dot{q} + \frac{\partial p}{\partial t}$$

Therefore, for an inviscid flow with no body forces, the total or stagnation enthalpy can change only if heat is exchanged with the gas or if there is an unsteady variation of static pressure. If the flow is steady, $\partial p/\partial t = 0$, and if the flow is adiabatic, $\dot{q} = 0$, the total-enthalpy energy equation is reduced to

$$\frac{Dh_o}{Dt} = \frac{\partial h_o}{\partial t} + \mathbf{V}\cdot\nabla h_o = 0 + \mathbf{V}\cdot\nabla h_o = 0$$

This informs us that the total enthalpy is constant along a streamline for steady adiabatic flow. The value of the constant may vary from streamline to streamline, as illustrated in Figure 11.3; however, if the streamlines originate from the same reservoir, they will have a single value. Flows in which $\nabla h_o = 0$ are called *isoenergetic flows*.

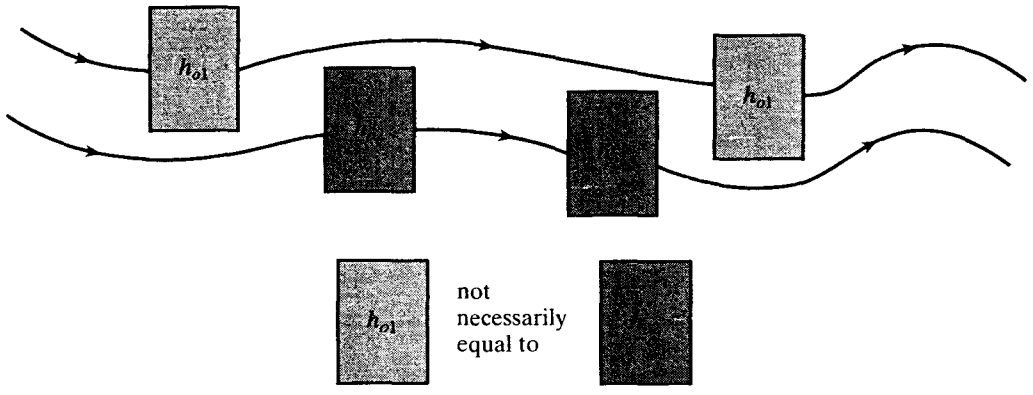


**Figure 11.3** Total Enthalpy on Streamlines in Steady, Inviscid, Adiabatic Flow with No Body Forces

## 11.5 CONSERVATION FORM OF THE GOVERNING EQUATIONS

The equations that govern inviscid, adiabatic, compressible flow are

$$\frac{\partial \rho}{\partial t} + \nabla \cdot \rho \mathbf{V} = 0 \tag{11.2}$$

$$\frac{\partial \mathbf{V}}{\partial t} + (\mathbf{V} \cdot \nabla)\mathbf{V} + \frac{\nabla p}{\rho} = 0 \tag{11.10}$$

$$\frac{\partial (\rho e_t)}{\partial t} + \nabla \cdot (\rho e_t \mathbf{V}) + \nabla \cdot (p\mathbf{V}) = 0 \tag{11.13}$$

For the numerical solution of these equations, it is more convenient to have them written in *conservation form* (a form in which all variables are contained within the derivatives). It may be observed that both the continuity and energy equations are in conservation form; the momentum equations, however, are not, because the density and velocity components appear outside of the derivatives. We will use the continuity equation and the $x$-momentum equation, written in Cartesian coordinates, to demonstrate how the $x$-momentum equation can be turned into the conservative form.

Now, earlier, we saw that

$$\frac{\partial \rho}{\partial t} + \frac{\partial \rho u}{\partial x} + \frac{\partial \rho v}{\partial y} + \frac{\partial \rho w}{\partial z} = 0 \tag{11.1}$$

Also,

$$\rho \frac{\partial u}{\partial t} + \rho u \frac{\partial u}{\partial x} + \rho v \frac{\partial u}{\partial y} + \rho w \frac{\partial u}{\partial z} + \frac{\partial p}{\partial x} = 0 \tag{11.20}$$

Multiply the continuity equation, Eq. (11.1), by $u$ and add the result to Eq. (11.20) to get

$$\left(\rho \frac{\partial u}{\partial t} + \rho u \frac{\partial u}{\partial x} + \rho v \frac{\partial u}{\partial y} + \rho w \frac{\partial u}{\partial z} + \frac{\partial p}{\partial x}\right) + \left(u \frac{\partial \rho}{\partial t} + u \frac{\partial \rho u}{\partial x} + u \frac{\partial \rho v}{\partial y} + u \frac{\partial \rho w}{\partial z}\right) = 0$$

Regrouping yields

$$\left(\rho \frac{\partial u}{\partial t} + u \frac{\partial \rho}{\partial t}\right) + \left(\rho u \frac{\partial u}{\partial x} + u \frac{\partial \rho u}{\partial x}\right) +$$

$$\left(\rho v \frac{\partial u}{\partial y} + u \frac{\partial \rho v}{\partial y}\right) + \left(\rho w \frac{\partial u}{\partial z} + u \frac{\partial \rho w}{\partial z}\right) + \frac{\partial p}{\partial x} = 0$$

or

$$\frac{\partial (\rho u)}{\partial t} + \frac{\partial (\rho u^2 + p)}{\partial x} + \frac{\partial (\rho u v)}{\partial y} + \frac{\partial (\rho u w)}{\partial z} = 0 \tag{11.21}$$

The same process may be followed for the $y$- and $z$-momentum equations, respectively:

$$\frac{\partial(\rho v)}{\partial t} + \frac{\partial(\rho uv)}{\partial x} + \frac{\partial(\rho v^2 + p)}{\partial y} + \frac{\partial(\rho vw)}{\partial z} = 0 \tag{11.22}$$

$$\frac{\partial(\rho w)}{\partial t} + \frac{\partial(\rho uw)}{\partial x} + \frac{\partial(\rho vw)}{\partial y} + \frac{\partial(\rho w^2 + p)}{\partial z} = 0 \tag{11.23}$$

The group of five equations can be written in the following form:

$$\frac{\partial \mathbf{Q}}{\partial t} + \frac{\partial \mathbf{E}}{\partial x} + \frac{\partial \mathbf{F}}{\partial y} + \frac{\partial \mathbf{G}}{\partial z} = 0 \tag{11.24}$$

where $\mathbf{Q}$ is called the *solution vector* and $\mathbf{E}$, $\mathbf{F}$, and $\mathbf{G}$ are called the *flux vectors*. These vectors each have five components that are obtained from the continuity, momentum, and energy equations. The vectors are defined as

$$\mathbf{Q} = \begin{bmatrix} \rho \\ \rho u \\ \rho v \\ \rho w \\ \rho e_t \end{bmatrix} \quad \mathbf{E} = \begin{bmatrix} \rho u \\ \rho u^2 + p \\ \rho uv \\ \rho uw \\ \rho u e_t + pu \end{bmatrix} \quad \mathbf{F} = \begin{bmatrix} \rho v \\ \rho uv \\ \rho v^2 + p \\ \rho vw \\ \rho v e_t + pv \end{bmatrix} \quad \mathbf{G} = \begin{bmatrix} \rho w \\ \rho uw \\ \rho vw \\ \rho w^2 + p \\ \rho w e_t + pw \end{bmatrix}$$

For flows that are not adiabatic, a source vector would have to be included in Eq. (11.24), which would appear as

$$\frac{\partial \mathbf{Q}}{\partial t} + \frac{\partial \mathbf{E}}{\partial x} + \frac{\partial \mathbf{F}}{\partial y} + \frac{\partial \mathbf{G}}{\partial z} = \mathbf{H} \tag{11.25}$$

where

$$\mathbf{H} = \begin{bmatrix} 0 \\ 0 \\ 0 \\ 0 \\ \rho \dot{q} \end{bmatrix}$$

The grouping of terms into this form is helpful in solving the set of equations because it allows us to solve first-order equations, a technique that was of considerable assistance in numerically solving the ordinary differential equations of Chapters 9 and 10, and because we are able to employ powerful linear algebra techniques to the set of equations expressed in this form.

## 11.6 IRROTATIONAL FLOW

Direct integration of the equations of motion over the entire flow field is difficult unless additional assumptions are made about the nature of the flow. An important type of flow—one that leads to simplification in the equations of motion—is *irrotational flow.*

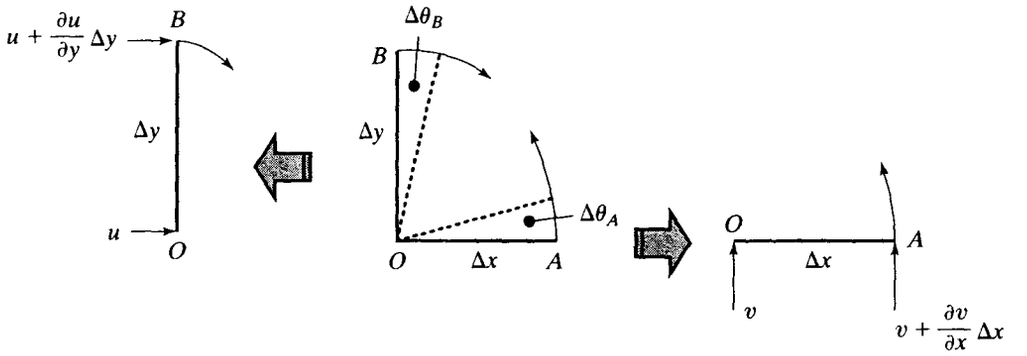


**Figure 11.4** Rotation of Two Mutually Perpendicular, Differential Line Elements

*Fluid rotation* is defined as the average angular velocity of two mutually perpendicular differential elements in a fluid. For example, consider the rotation in the $(x, y)$ plane about the origin, labeled $O$, of two elements $OA$ and $OB$ of lengths $\Delta x$ and $\Delta y$, respectively, as shown in Figure 11.4. Since the velocity components $u$ and $v$ are different at $O, A$, and $B$, the elements will move with respect to each other. Let the velocity components at $O$ be $u$ and $v$. Then, by using a two-term Taylor series, we find that the velocity component in the $x$ direction at $B$ is $u + (\partial u/\partial y)\Delta y$, and the $y$ component at $A$ is $v + (\partial v/\partial x)\Delta x$. After a time $\Delta t$, point $B$ will have moved in the $x$ direction a distance $\{[u + (\partial u/\partial y)\,\Delta y] - u\}\Delta t$ with respect to $O$, so that the angle $\Delta\theta_B$ is equal to $(\partial u/\partial y)\,\Delta t$. Likewise, point $A$ will have moved in the $y$ direction a distance $(\partial v/\partial x)\,\Delta x\Delta t$, so that $\Delta\theta_A = (\partial v/\partial x)\,\Delta t$. Using the right-hand rule to find the net rotation about the $z$-axis, we find that counterclockwise angles in Figure 11.4 are positive. So, a minus sign must be placed in front of $\Delta\theta_B$, because it is in the clockwise direction. Therefore, the rotation about the $z$-axis is

$$\omega_z = \frac{\dfrac{\Delta\theta_A}{\Delta t} + \dfrac{\Delta\theta_B}{\Delta t}}{2} = \frac{\dfrac{\partial v}{\partial x}\Delta t - \dfrac{\partial u}{\partial y}\Delta t}{2\Delta t} = \frac{1}{2}\left(\frac{\partial v}{\partial x} - \frac{\partial u}{\partial y}\right) \tag{11.26}$$

Similarly, it can be shown that

$$\omega_x = \frac{1}{2}\left(\frac{\partial w}{\partial y} - \frac{\partial v}{\partial z}\right) \tag{11.27}$$

$$\omega_y = \frac{1}{2}\left(\frac{\partial u}{\partial z} - \frac{\partial w}{\partial x}\right) \tag{11.28}$$

The *rotation vector* may be written as

$$\boldsymbol{\omega} = \mathbf{i}\omega_x + \mathbf{j}\omega_y + \mathbf{k}\omega_z \tag{11.29}$$

It should be understood that curved flows are not necessarily rotational and that straight flows are not necessary irrotational. For example, *pure shear flow*, called plane *Couette flow*, shown in Figure 11.5, is obviously rotational (because the average angular velocity of two mutually perpendicular differential elements is not zero) in a fluid even though the streamlines are all parallel straight lines.

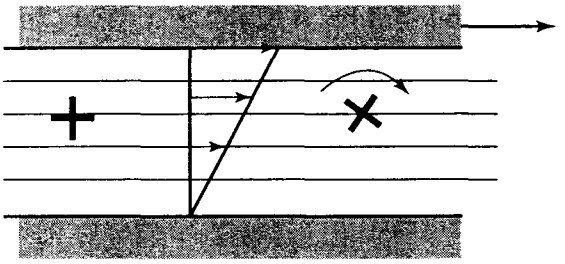

**Figure 11.5** Illustration that Plane Shear Flow Is Rotational

The *curl* (i.e., $\nabla \times$) *of a vector* $\mathbf{A} = \mathbf{i}A_1 + \mathbf{j}A_2 + \mathbf{k}A_3$ is defined by

$$\nabla \times \mathbf{A} = \begin{vmatrix} \mathbf{i} & \mathbf{j} & \mathbf{k} \\ \dfrac{\partial}{\partial x} & \dfrac{\partial}{\partial y} & \dfrac{\partial}{\partial z} \\ A_1 & A_2 & A_3 \end{vmatrix} = \left(\frac{\partial A_3}{\partial y} - \frac{\partial A_2}{\partial z}\right)\mathbf{i} + \left(\frac{\partial A_1}{\partial z} - \frac{\partial A_3}{\partial x}\right)\mathbf{j} + \left(\frac{\partial A_2}{\partial x} - \frac{\partial A_1}{\partial y}\right)\mathbf{k} \tag{11.30}$$

Therefore, by use of Eqs. (11.26) through (11.30), it is clear that the rotational vector is equal to one half of the curl of the velocity:

$$\boldsymbol{\omega} = \frac{1}{2}(\nabla \times \mathbf{V}) \tag{11.31}$$

Two times the rotation vector is called the *vorticity vector* ($\boldsymbol{\zeta} = 2\boldsymbol{\omega}$).

For irrotational flow, it follows [refer to Eqs. (11.26) to (11.28)] that

$$\frac{\partial u}{\partial z} = \frac{\partial w}{\partial x}, \quad \frac{\partial w}{\partial y} = \frac{\partial v}{\partial z}, \quad \text{and} \quad \frac{\partial u}{\partial y} = \frac{\partial v}{\partial x} \tag{11.32}$$

The simplification afforded by the assumption of irrotationality can be seen by substituting Eq. (11.32) into Eqs. (11.7), (11.8), and (11.9) to obtain

$$\begin{aligned} -\frac{1}{\rho}\frac{\partial p}{\partial x} &= \frac{\partial u}{\partial t} + u\frac{\partial u}{\partial x} + v\frac{\partial v}{\partial x} + w\frac{\partial w}{\partial x} \\ -\frac{1}{\rho}\frac{\partial p}{\partial y} &= \frac{\partial v}{\partial t} + u\frac{\partial u}{\partial y} + v\frac{\partial v}{\partial y} + w\frac{\partial w}{\partial y} \\ -\frac{1}{\rho}\frac{\partial p}{\partial z} &= \frac{\partial w}{\partial t} + u\frac{\partial u}{\partial z} + v\frac{\partial v}{\partial z} + w\frac{\partial w}{\partial z} \end{aligned} \tag{11.33}$$

For steady flow,

$$\frac{\partial u}{\partial t} = \frac{\partial v}{\partial t} = \frac{\partial w}{\partial t} = 0$$

Also,

$$dp = \frac{\partial p}{\partial x}dx + \frac{\partial p}{\partial y}dy + \frac{\partial p}{\partial z}dz$$

Furthermore,

$$u\frac{\partial u}{\partial x} + v\frac{\partial v}{\partial x} + w\frac{\partial w}{\partial x} = \frac{\partial}{\partial x}\left(\frac{u^2 + v^2 + w^2}{2}\right) = \frac{\partial}{\partial x}\left(\frac{V^2}{2}\right)$$

Adding and then substituting the preceding relations into Eq. (11.33) produces

$$-\frac{dp}{\rho} = d\left(\frac{V^2}{2}\right) \tag{11.34}$$

Integration of this expression yields

$$\int\left[\frac{dp}{\rho} + d\left(\frac{V^2}{2}\right)\right] = \text{constant}$$

Thus, the equations of motion can be integrated for the case of irrotational flow. The assumptions made in this derivation are that the flow is irrotational, steady, and frictionless, with no external forces except pressure acting on the control volume.

Equation (11.34) can also be derived from a vector point of view. From Eq. (11.10), we have

$$-\frac{1}{\rho}\nabla p = \frac{D\mathbf{V}}{Dt} = \frac{\partial \mathbf{V}}{\partial t} + (\mathbf{V}\cdot\nabla)\mathbf{V}$$

It is possible to establish the following vector identity [see Ref. (11.5)] for vectors **A** and **B**:

$$\nabla(\mathbf{A}\cdot\mathbf{B}) = (\mathbf{B}\cdot\nabla)\mathbf{A} + (\mathbf{A}\cdot\nabla)\mathbf{B} + \mathbf{B}\times(\nabla\times\mathbf{A}) + \mathbf{A}\times(\nabla\times\mathbf{B})$$

For our case, let $\mathbf{A} = \mathbf{B} = \mathbf{V}$, so that

$$\nabla(\mathbf{V}\cdot\mathbf{V}) = \nabla(V^2) = 2[\mathbf{V}\times(\nabla\times\mathbf{V})] + 2[(\mathbf{V}\cdot\nabla)\mathbf{V}]$$

or

$$(\mathbf{V}\cdot\nabla)\mathbf{V} = \nabla\left(\frac{V^2}{2}\right) - \mathbf{V}\times(\nabla\times\mathbf{V}) = \nabla\left(\frac{V^2}{2}\right) - 2(\mathbf{V}\times\boldsymbol{\omega}) \tag{11.35}$$

Substituting Eq. (11.35) into Eq. (11.10) yields

$$-\frac{\nabla p}{\rho} = \frac{\partial \mathbf{V}}{\partial t} + \nabla\left(\frac{V^2}{2}\right) - 2(\mathbf{V}\times\boldsymbol{\omega}) \tag{11.36}$$

For irrotational flow, $\omega = 0$. For steady flow, $\partial\mathbf{V}/\partial t = 0$. With the assumptions of steady, irrotational flow, the resultant equation is

$$-\frac{\nabla p}{\rho} = \nabla\left(\frac{V^2}{2}\right)$$

which agrees with Eq. (11.34).

## 11.7 CROCCO'S EQUATION

It is interesting to observe that the integral of Eq. (11.34) is the same equation already derived in Chapter 3, Eq. (3.2), from energy considerations for isentropic flow. This equality suggests a connection between irrotational flow and isentropic flow. Put another way, there is a connection between flow kinematics and flow thermodynamics. To demonstrate this connection, let us write the Gibbs identity, Eq. (1.22), in general form:

$$T\nabla s = \nabla h - \frac{\nabla p}{\rho} \tag{11.37}$$

Also, since

$$h_o = h + \frac{V^2}{2}$$

we have

$$\nabla h_o = \nabla h + \frac{\nabla(\mathbf{V}\cdot\mathbf{V})}{2} \tag{11.38}$$

Equation (11.36) may be rewritten as

$$-\frac{\nabla p}{\rho} = \frac{\partial \mathbf{V}}{\partial t} + \frac{\nabla(\mathbf{V}\cdot\mathbf{V})}{2} - 2(\mathbf{V}\times\boldsymbol{\omega})$$

Combining this expression with Eq. (11.38) and substituting into Eq. (11.37) gives

$$T\nabla s - \nabla h_o + \frac{\nabla(\mathbf{V}\cdot\mathbf{V})}{2} = \frac{\partial \mathbf{V}}{\partial t} + \frac{\nabla(\mathbf{V}\cdot\mathbf{V})}{2} - 2(\mathbf{V}\times\boldsymbol{\omega})$$

Simplifying yields *Crocco's equation*:

$$T\nabla s - \nabla h_o = \frac{\partial \mathbf{V}}{\partial t} - 2(\mathbf{V}\times\boldsymbol{\omega}) \tag{11.39}$$

Crocco's equation was derived in 1936 and is illustrated in Figure 11.6. This equation reveals that rotation ($\boldsymbol{\omega} = \nabla \times \mathbf{V}$) occurs only in flows that contain gradients of entropy, gradients of total enthalpy, or nonvanishing unsteady acceleration. Flows in which $\boldsymbol{\omega} = \nabla \times \mathbf{V} = 0$ are called *irrotational*.

As we have seen in Example 11.2, for adiabatic, steady flow, with no energy exchange, $\nabla h_o = 0$. This condition is realized when the stagnation enthalpy is uniform. Such flows are sometimes called *isoenergetic*. Therefore, Eq. (11.39) reduces to

$$T\nabla s = 2(\boldsymbol{\omega}\times\mathbf{V}) \tag{11.40}$$

Fluid motions in which the entropy is uniform, and therefore where $\nabla s = 0$, are termed *homentropic* flows. According to Eq. (11.40), steady ($\mathbf{V}$ does not change with time), isoenergetic ($h_o$ is uniform), homentropic ($s$ is uniform) flows are generally irrotational ($\boldsymbol{\omega} = 0$). The exception is an rotational flow in which $\mathbf{V}$ and $\boldsymbol{\omega}$ are parallel to each other. This case is termed *Beltrami flow*. [See Ref. (11.6).]

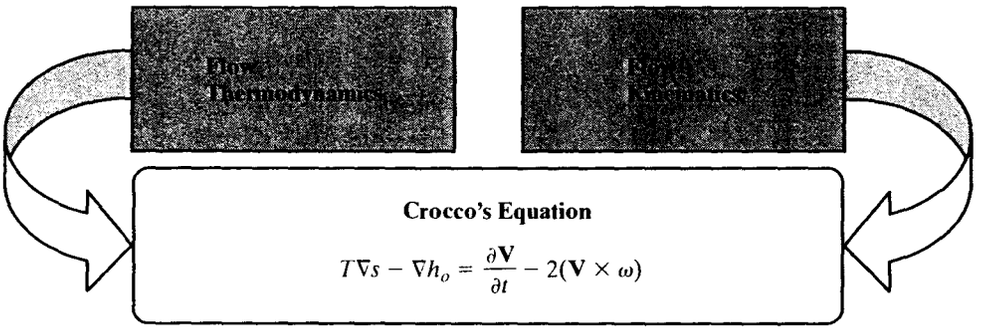


**Figure 11.6** Crocco's Equation: A Combination of Thermodynamics and Flow Kinematics

An *isentropic flow* is a flow in which the entropy remains constant along a streamline. Mathematically, this condition is expressed as $\mathbf{V} \cdot \nabla s = 0$, or $Ds/Dt = 0$. All homentropic flows must be isentropic, but not all isentropic flows are homentropic (because different streamlines can have different values of entropy). Finally, the flow in a boundary layer, with viscous dissipation, is irreversible and therefore nonisentropic. Hence, from Eq. (11.40), boundary-layer flow is rotational.

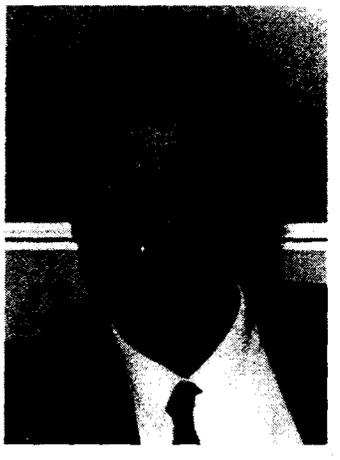

**Historical Note: Luigi Crocco** (1909–1986) began to conduct research as an undergraduate in mechanical engineering at the University of Rome, where he received his B.S. in 1932 and his Ph.D. in 1936. He remained at Rome as an assistant professor and became a full professor in 1939. During the 1930s, he became heavily involved in rocketry and generated a series of papers in theoretical aerodynamics. Among these papers are his derivations of the Crocco energy integral for boundary layers (1931), his vorticity theorem (1936), the Crocco point of gas dynamics (1937), and the Crocco transformation in boundary-layer theory (1939).

In 1949, he became a visiting professor at Princeton University, and there, in 1952, on Kármán's recommendation, he accepted the Goddard Chair of Jet Propulsion and became the director of the Guggenheim Jet Propulsion Center. While in that position, he developed the theory of combustion instability in rocket motors.

In addition, Crocco used his ability to combine elegant mathematics and numerical methods with insights into fluid physics to study problems associated with boundary-layer flows, separation, base flows, and transonic and supersonic aerodynamics. These abilities, along with his talent for making clear, at any level, the complex phenomena, made him an influential figure highly sought after as a consultant by industries and governments worldwide.

Crocco returned to Europe to facilitate his wife's medical treatments, and in 1968, he became a Fulbright Professor of the Faculté des Sciences of the University of Paris. After returning briefly to Princeton in 1969, he was a professor at l'École Centrale des Arts et Manufactures in Paris. In that post, he continued teaching and research. He retired in 1977, but remained active until his sudden death from a heart attack at the age of 77 in Rome. Crocco was gently mannered and cultured, with a warm handshake that made one feel special. For further detail, see Ref. (11.7).

## 11.8 VELOCITY POTENTIAL

The *velocity potential* $\phi$ is defined as a function of the space coordinates and time such that, when differentiated with respect to a space coordinate, it yields the velocity component in the coordinate direction. In Cartesian coordinate form,

$$u = \frac{\partial \phi}{\partial x}$$
$$v = \frac{\partial \phi}{\partial y}$$
$$w = \frac{\partial \phi}{\partial z} \tag{11.41}$$

In vector form,

$$\mathbf{V} = \nabla \phi \tag{11.42}$$

Thus, the velocity is the gradient of the velocity potential. If such a function can be defined at each point in the flow and has continuous derivatives, the flow is termed *potential flow*. The velocity potential is analogous to the electric potential in an electric field, in which current flow can be related to the potential gradient, or to the temperature in a heat-conducting material, where heat flow is proportional to temperature gradient. Some texts [e.g., see Refs. (11.8) and (11.9)] use a negative sign in Eqs. (11.41) and (11.42) to conform to the convention that flow is from a higher to a lower potential.

The advantage of introducing velocity potential into multidimensional fluid flow problems is simply the ability to express the flow in terms of one scalar variable instead of the three velocity components $u$, $v$, and $w$. For incompressible flow, the continuity equation has been shown to be

$$\frac{\partial u}{\partial x} + \frac{\partial v}{\partial y} + \frac{\partial w}{\partial z} = 0$$

In terms of $\phi$, this expression reduces to the simple form

$$\frac{\partial^2 \phi}{\partial x^2} + \frac{\partial^2 \phi}{\partial y^2} + \frac{\partial^2 \phi}{\partial z^2} = 0 \tag{11.43}$$

This equation can be recognized as *Laplace's equation* [$\nabla^2 \phi = \nabla \cdot \nabla(\phi) = 0$], a linear partial differential equation, for which the solutions are *harmonic functions*.

Let us now discuss the connection between irrotational and potential flow. From calculus, if a function is continuous and has continuous derivatives, the order of partial differentiation has no effect on the result. That is,

$$\frac{\partial^2 \phi}{\partial x\, \partial y} = \frac{\partial^2 \phi}{\partial y\, \partial x}$$
$$\frac{\partial^2 \phi}{\partial x\, \partial z} = \frac{\partial^2 \phi}{\partial z\, \partial x}$$
$$\frac{\partial^2 \phi}{\partial y\, \partial z} = \frac{\partial^2 \phi}{\partial z\, \partial y}$$

Substituting Eq. (11.41) into the foregoing expressions yields

$$\frac{\partial u}{\partial y} = \frac{\partial v}{\partial x}$$

$$\frac{\partial u}{\partial z} = \frac{\partial w}{\partial x}$$

$$\frac{\partial v}{\partial z} = \frac{\partial w}{\partial y}$$

But, according to Eq. (11.32), these are the conditions for the flow to be irrotational. In other words, a potential flow is also an irrotational flow. Let us now demonstrate the converse. We shall assume that the conditions for irrotational flow as given previously are satisfied. From calculus, if functions $P$, $Q$, and $R$, each functions of $x$, $y$, and $z$, satisfy the conditions

$$\frac{\partial P}{\partial y} = \frac{\partial Q}{\partial x}, \quad \frac{\partial Q}{\partial z} = \frac{\partial R}{\partial y}, \quad \text{and} \quad \frac{\partial R}{\partial x} = \frac{\partial P}{\partial z}$$

and are continuous with continuous partial derivatives, then $Pdx + Qdy + Rdz$ is an exact differential of some function $\phi$ of $x$, $y$, and $z$, where

$$d\phi = Pdx + Qdy + Rdz$$

For our case, with $P = u$, $Q = v$, and $R = w$,

$$d\phi = u\,dx + vdy + wdz$$

Also, since $\phi$ is a function of three space coordinates,

$$d\phi = \frac{\partial \phi}{\partial x}dx + \frac{\partial \phi}{\partial y}dy + \frac{\partial \phi}{\partial z}dz$$

Comparing, we have

$$u = \frac{\partial \phi}{\partial x}, \quad v = \frac{\partial \phi}{\partial y}, \quad \text{and} \quad w = \frac{\partial \phi}{\partial z}$$

which is the definition of velocity potential. Thus, we have proved the corollary—that for irrotational flow, a potential can be defined. In other words, potential flow and irrotational flow are equivalent and can be used interchangeably.

## 11.9 EQUATIONS OF MOTION IN TERMS OF VELOCITY POTENTIAL

We shall now take the equations of motion, as derived previously in this chapter, and reduce them to one partial differential equation for the velocity potential $\phi$. It will be assumed in this derivation that the flow is steady, irrotational, and isentropic and that the only forces acting on the control volume are pressure forces. (Viscous forces, magnetic forces, and so on, are assumed to be zero.)

Using Eq. (11.41), we see that the continuity equation for steady flow, Eq. (11.1), reduces to

$$\frac{\partial}{\partial x}\left(\rho\frac{\partial\phi}{\partial x}\right)+\frac{\partial}{\partial y}\left(\rho\frac{\partial\phi}{\partial y}\right)+\frac{\partial}{\partial z}\left(\rho\frac{\partial\phi}{\partial z}\right)=0$$

or, expanding, we find that

$$\frac{\partial\rho}{\partial x}\frac{\partial\phi}{\partial x}+\frac{\partial\rho}{\partial y}\frac{\partial\phi}{\partial y}+\frac{\partial\rho}{\partial z}\frac{\partial\phi}{\partial z}+\rho\left(\frac{\partial^2\phi}{\partial x^2}+\frac{\partial^2\phi}{\partial y^2}+\frac{\partial^2\phi}{\partial z^2}\right)=0 \tag{11.44}$$

To obtain a partial differential equation for $\phi$ alone, we shall have to eliminate $\rho$, using the momentum equation. Under the assumptions made, the momentum equation is given by Eq. (11.34) as

$$\frac{dp}{\rho}+\frac{d(u^2+v^2+w^2)}{2}=0$$

or

$$dp=-\frac{\rho}{2}d\left[\left(\frac{\partial\phi}{\partial x}\right)^2+\left(\frac{\partial\phi}{\partial y}\right)^2+\left(\frac{\partial\phi}{\partial z}\right)^2\right] \tag{11.45}$$

For isentropic flow,

$$\frac{dp}{d\rho}=a^2$$

so that

$$dp=a^2d\rho=-\frac{\rho}{2}d\left[\left(\frac{\partial\phi}{\partial x}\right)^2+\left(\frac{\partial\phi}{\partial y}\right)^2+\left(\frac{\partial\phi}{\partial z}\right)^2\right]$$

which upon differentiation yields

$$\begin{aligned}
\frac{\partial\rho}{\partial x}&=\frac{\rho}{a^2}\left(\frac{\partial\phi}{\partial x}\frac{\partial^2\phi}{\partial x^2}+\frac{\partial\phi}{\partial y}\frac{\partial^2\phi}{\partial y\,\partial x}+\frac{\partial\phi}{\partial z}\frac{\partial^2\phi}{\partial z\,\partial x}\right)\\
\frac{\partial\rho}{\partial y}&=\frac{\rho}{a^2}\left(\frac{\partial\phi}{\partial x}\frac{\partial^2\phi}{\partial x\,\partial y}+\frac{\partial\phi}{\partial y}\frac{\partial^2\phi}{\partial y^2}+\frac{\partial\phi}{\partial z}\frac{\partial^2\phi}{\partial z\,\partial y}\right)\\
\frac{\partial\rho}{\partial z}&=\frac{\rho}{a^2}\left(\frac{\partial\phi}{\partial x}\frac{\partial^2\phi}{\partial x\,\partial z}+\frac{\partial\phi}{\partial y}\frac{\partial^2\phi}{\partial y\,\partial z}+\frac{\partial\phi}{\partial z}\frac{\partial^2\phi}{\partial z^2}\right)
\end{aligned} \tag{11.46}$$

Substituting these expressions into Eq. (11.44) yields

$$\begin{aligned}
&\frac{\partial^2\phi}{\partial x^2}+\frac{\partial^2\phi}{\partial y^2}+\frac{\partial^2\phi}{\partial z^2}-\frac{1}{a^2}\left[\left(\frac{\partial\phi}{\partial x}\right)^2\frac{\partial^2\phi}{\partial x^2}+\left(\frac{\partial\phi}{\partial y}\right)^2\frac{\partial^2\phi}{\partial y^2}+\left(\frac{\partial\phi}{\partial z}\right)^2\frac{\partial^2\phi}{\partial z^2}\right]\\
&\qquad-\frac{2}{a^2}\left[\frac{\partial\phi}{\partial x}\frac{\partial\phi}{\partial y}\frac{\partial^2\phi}{\partial x\,\partial y}+\frac{\partial\phi}{\partial y}\frac{\partial\phi}{\partial z}\frac{\partial^2\phi}{\partial y\,\partial z}+\frac{\partial\phi}{\partial z}\frac{\partial\phi}{\partial x}\frac{\partial^2\phi}{\partial z\,\partial x}\right]=0
\end{aligned} \tag{11.47}$$

It can be seen that, for incompressible flow, in which $a \to \infty$, Eq. (11.47) reduces to Laplace's equation, $(\partial^2\phi/\partial x^2) + (\partial^2\phi/\partial y^2) + (\partial^2\phi/\partial z^2) = \nabla^2\phi = 0$, as mentioned previously.

To complete the derivation, it is necessary to obtain an expression for the velocity of sound in terms of the velocity potential and space coordinates. Such an expression can be obtained from the definition of the total enthalpy. For a perfect gas with constant specific heats,

$$c_pT_o = c_pT + \frac{V^2}{2}$$

where $c_p = \dfrac{R\gamma}{\gamma - 1}$ and $a^2 = \gamma RT$. Substitution yields

$$a^2 = \gamma RT_o - \frac{\gamma - 1}{2}V^2 = a_o^2 - \frac{\gamma - 1}{2}(u^2 + v^2 + w^2)$$

or

$$a^2 = a_o^2 - \frac{\gamma - 1}{2}\left[\left(\frac{\partial\phi}{\partial x}\right)^2 + \left(\frac{\partial\phi}{\partial y}\right)^2 + \left(\frac{\partial\phi}{\partial z}\right)^2\right] \tag{11.48}$$

where $a_o$ is the velocity of sound at the stagnation temperature.

Substituting Eq. (11.48) into Eq. (11.47), we obtain a partial differential equation for $\phi$ in terms of $x$, $y$, and $z$ for steady, irrotational, isentropic flow of a perfect gas with constant specific heats. Solution of this equation for $\phi$ will yield the entire flow for the prescribed boundary conditions:

$$\begin{aligned}&\left\{a_o^2 - \frac{\gamma - 1}{2}\left[\left(\frac{\partial\phi}{\partial x}\right)^2 + \left(\frac{\partial\phi}{\partial y}\right)^2 + \left(\frac{\partial\phi}{\partial z}\right)^2\right]\right\}\left(\frac{\partial^2\phi}{\partial x^2} + \frac{\partial^2\phi}{\partial y^2} + \frac{\partial^2\phi}{\partial z^2}\right)\\ &- \left[\left(\frac{\partial\phi}{\partial x}\right)^2\frac{\partial^2\phi}{\partial x^2} + \left(\frac{\partial\phi}{\partial y}\right)^2\frac{\partial^2\phi}{\partial y^2} + \left(\frac{\partial\phi}{\partial z}\right)^2\frac{\partial^2\phi}{\partial z^2}\right] - 2\left[\left(\frac{\partial\phi}{\partial x}\right)\left(\frac{\partial\phi}{\partial y}\right)\left(\frac{\partial^2\phi}{\partial x\,\partial y}\right)\right.\\ &\left. + \left(\frac{\partial\phi}{\partial y}\right)\left(\frac{\partial\phi}{\partial z}\right)\left(\frac{\partial^2\phi}{\partial y\,\partial z}\right) + \left(\frac{\partial\phi}{\partial z}\right)\left(\frac{\partial\phi}{\partial x}\right)\left(\frac{\partial^2\phi}{\partial z\,\partial x}\right)\right] = 0\end{aligned} \tag{11.49}$$

This expression can readily be recognized as a nonlinear equation, since terms such as $[(\partial\phi/\partial x)(\partial\phi/\partial y)(\partial^2\phi/\partial x\partial y)]$ appear and contain the products of the partial derivatives of the dependent variable. Furthermore, the partial differential equation for $\phi$ is of second order, since the highest order derivative is of the form $(\partial^2\phi/\partial x^2)$. The nonlinearity of the equation presents extreme mathematical difficulties, which render a general solution impossible. The advantage of linear equations, such as Laplace's equation, is that solutions may be added; complex solutions can thus be built up from the superposition of simple solutions.

One approach to solve Eq. (11.47) is to linearize the general partial differential equation by making suitable assumptions. This method necessarily restricts the validity of the solution to a special class of problems, but it does afford good engineering

approximations to cases that might otherwise prove very difficult to solve. In Chapter 13, methods of linearizing the potential equation will be discussed, as well as approximate methods for solving the general potential equation.

**Example 11.3. Vector development of the compressible flow velocity potential equation**

The compressible flow velocity potential equation, Eq. (11.49), was developed using a scalar approach; rederive this equation using a vector approach.

**Solution**

This derivation begins with the continuity equation for steady compressible flow:

$$\nabla \cdot \rho \mathbf{V} = 0 \tag{11.4}$$

Combining this expression with Eq. (11.42) produces

$$\nabla \cdot \rho \mathbf{V} = \nabla \cdot (\rho \nabla \phi) = \nabla \rho \cdot \nabla \phi + \rho \nabla^2 \phi = 0 \tag{11.44}$$

The potential flow equation will emerge from this expression by replacing the density terms. Now, for irrotational flow, we have seen that

$$-\frac{\nabla p}{\rho} = \nabla\left(\frac{V^2}{2}\right) = \nabla\left(\frac{\nabla \phi \cdot \nabla \phi}{2}\right) \tag{11.45}$$

Since the flow is isentropic, the pressure gradient is connected to the density gradient through the speed of sound, which may be written as

$$\nabla p = a^2 \nabla \rho$$

Hence,

$$\nabla \rho = -\frac{\rho}{a^2} \nabla\left(\frac{V^2}{2}\right) = -\frac{\rho}{2a^2} \nabla(\nabla \phi \cdot \nabla \phi) \tag{11.46}$$

Replacing the density gradient in Eq. (11.44), canceling the density, and rearranging brings

$$a^2 \nabla^2 \phi - \frac{1}{2} \nabla \phi \cdot \nabla(\nabla \phi \cdot \nabla \phi) = 0 \tag{11.47}$$

From Crocco's equation, the stagnation enthalpy $h_o$ is constant. Therefore, from the definition of the stagnation enthalpy, it is easy to show that

$$a_o^2 = a^2 + \frac{\gamma - 1}{2} \mathbf{V} \cdot \mathbf{V} = a^2 + \frac{\gamma - 1}{2} \nabla \phi \cdot \nabla \phi \tag{11.48}$$

Using this equation to replace the speed of sound squared results in the desired vector expression for the velocity potential equation:

$$2\left(a_o^2 - \frac{\gamma - 1}{2} \nabla \phi \cdot \nabla \phi\right) \nabla^2 \phi - \nabla \phi \cdot \nabla(\nabla \phi \cdot \nabla \phi) = 0 \tag{11.49}$$

The vector form of the potential equation, Eq. (11.49), is quite useful because the gradient and Laplacian operators can be related to various parameters of a given coordinate system. Consequently, by taking advantage of this feature, we will be able to write the potential equation for several other geometries.

In Ref. (11.10), it is shown for a scalar quantity, say, the velocity potential $\phi$, that

$$\nabla\phi = \frac{1}{h_1}\frac{\partial\phi}{\partial u_1}\mathbf{e}_1 + \frac{1}{h_2}\frac{\partial\phi}{\partial u_2}\mathbf{e}_2 + \frac{1}{h_3}\frac{\partial\phi}{\partial u_3}\mathbf{e}_3 \tag{11.50}$$

$$\nabla^2\phi = \frac{1}{h_1h_2h_3}\left[\frac{\partial}{\partial u_1}\left(\frac{h_2h_3}{h_1}\frac{\partial\phi}{\partial u_1}\right) + \frac{\partial}{\partial u_2}\left(\frac{h_1h_3}{h_2}\frac{\partial\phi}{\partial u_2}\right) + \frac{\partial}{\partial u_3}\left(\frac{h_1h_2}{h_3}\frac{\partial\phi}{\partial u_3}\right)\right] \tag{11.51}$$

and for a vector quantity, say, velocity $\mathbf{V} = (V_1, V_2, V_3)$, that

$$\nabla\cdot\mathbf{V} = \frac{1}{h_1h_2h_3}\left[\frac{\partial}{\partial u_1}(h_2h_3V_1) + \frac{\partial}{\partial u_2}(h_1h_3V_2) + \frac{\partial}{\partial u_3}(h_1h_2V_3)\right] \tag{11.52}$$

$$\begin{aligned}\nabla\times\mathbf{V} &= \frac{1}{h_1h_2h_3}\begin{vmatrix} h_1\mathbf{e}_1 & h_2\mathbf{e}_2 & h_3\mathbf{e}_3 \\ \dfrac{\partial}{\partial u_1} & \dfrac{\partial}{\partial u_2} & \dfrac{\partial}{\partial u_3} \\ h_1V_1 & h_2V_2 & h_3V_3 \end{vmatrix} \\ &= \left[\frac{\partial}{\partial u_2}(h_3V_3) - \frac{\partial}{\partial u_3}(h_2V_2)\right]\frac{\mathbf{e}_1}{h_2h_3} + \left[\frac{\partial}{\partial u_3}(h_1V_1) - \frac{\partial}{\partial u_1}(h_3V_3)\right]\frac{\mathbf{e}_2}{h_1h_3} \\ &\quad + \left[\frac{\partial}{\partial u_1}(h_2V_2) - \frac{\partial}{\partial u_2}(h_1V_1)\right]\frac{\mathbf{e}_3}{h_1h_2}\end{aligned} \tag{11.53}$$

where $u_1$, $u_2$, and $u_3$ are the *orthogonal curvilinear coordinates* and $h_1$, $h_2$, and $h_3$ are the *scale factors* relating the differential arc length to the differential coordinate length. That is, if $ds$ is the differential arc length, it can be shown that

$$(ds)^2 = h_1^2(du_1)^2 + h_2^2(du_2)^2 + h_3^2(du_3)^2$$

If we possess the various scale factors of a particular coordinate system, then by using the preceding equation, we will be able to directly express a given equation in that system. Table 11.1 lists the scale factors for the three most common coordinate

**TABLE 11.1** Coordinate Scale Factors

| Coordinate System | $u_1$ | $u_2$ | $u_3$ | $h_1$ | $h_2$ | $h_3$ |
|---|---|---|---|---|---|---|
| Cartesian | $x$ | $y$ | $z$ | 1 | 1 | 1 |
| Cylindrical | $r$ | $\theta$ | $z$ | 1 | $r$ | 1 |
| Spherical | $r$ | $\theta$ | $\varphi$ | 1 | $r$ | $r\sin\theta$ |

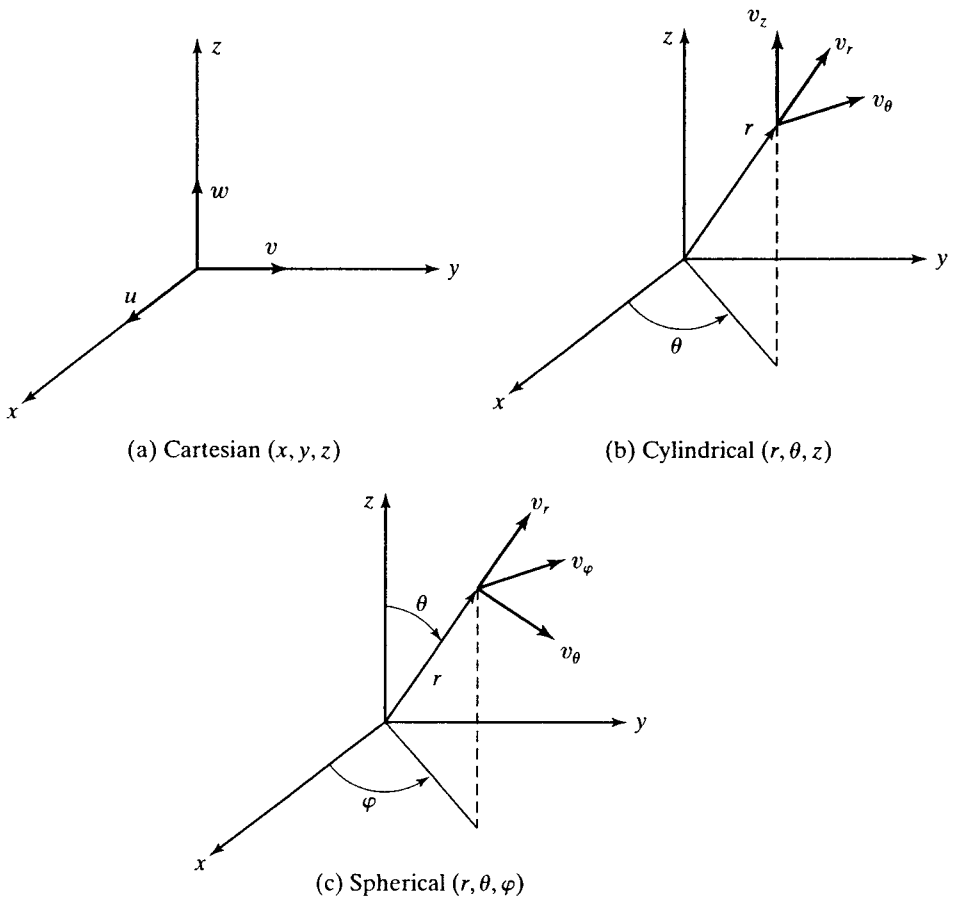


**Figure 11.7** Coordinate Systems

systems. Other sets of scale factors besides those shown in the table can be found in Ref. (11.11), along with a complete description of the coordinate surfaces. The coordinate systems are also illustrated in Figure 11.7.

**Example 11.4. Continuity equation in cylindrical coordinates**

Use the information within Table 11.1 to write the continuity equation in cylindrical coordinates.

**Solution**

The coordinates of the cylindrical coordinate system are $u_1 = r, u_2 = \theta$, and $u_3 = z$. The corresponding scale factors from Table 11.1 are $h_1 = 1, h_2 = r$, and $h_3 = 1$. Also, $V_1 = v_r, V_2 = v_\theta$, and $V_3 = v_\varphi$. Now, from Eq. (11.2),

$$\frac{\partial \rho}{\partial t} + \nabla \cdot \rho \mathbf{V} = 0 \tag{11.2}$$

To turn this equation into a scalar expression, we will use Eq. (11.52) for the divergence of $\rho\mathbf{V}$:

$$\nabla\cdot\rho\mathbf{V} = \frac{1}{(1)(r)(1)}\left[\frac{\partial}{\partial r}(r\rho V_r) + \frac{\partial}{\partial\theta}(\rho V_\theta) + \frac{\partial}{\partial z}(r\rho V_z)\right]$$
$$= \frac{1}{r}\frac{\partial}{\partial r}(r\rho V_r) + \frac{1}{r}\frac{\partial}{\partial\theta}(\rho V_\theta) + \frac{\partial}{\partial z}(\rho V_z)$$

Hence,

$$\frac{\partial\rho}{\partial t} + \frac{1}{r}\frac{\partial}{\partial r}(r\rho V_r) + \frac{1}{r}\frac{\partial}{\partial\theta}(\rho V_\theta) + \frac{\partial}{\partial z}(\rho V_z) = 0$$

or

$$\frac{\partial\rho}{\partial t} + \frac{\partial}{\partial r}(\rho V_r) + \frac{1}{r}\frac{\partial}{\partial\theta}(\rho V_\theta) + \frac{\partial}{\partial z}(\rho V_z) + \frac{\rho V_r}{r} = 0$$

These equations may be compared with expressions in other texts [e.g., Ref. (11.10)].

---

It is not difficult, using the aforementioned procedure, to develop expressions in various coordinate systems for component forms of the momentum equation from Eq. (11.10), the energy equation from Eq. (11.13), the velocity potential from Eq. (11.42), or the velocity potential equation from Eq. (11.49).

The following are the three-dimensional velocity potential equations, irrotational flow relations, and the velocity potential equation (written in terms of the velocity components rather than the potential) for the three coordinate systems listed in Table 11.1 and shown in Figure 11.7:

*Cartesian Coordinates*

$$u = \frac{\partial\phi}{\partial x}, v = \frac{\partial\phi}{\partial y}, w = \frac{\partial\phi}{\partial z} \tag{11.54}$$

$$\nabla\times\mathbf{V} = 0 \quad\Rightarrow\quad \left.\begin{aligned}\frac{\partial w}{\partial y} - \frac{\partial v}{\partial z} &= 0\\ \frac{\partial u}{\partial z} - \frac{\partial w}{\partial x} &= 0\\ \frac{\partial v}{\partial x} - \frac{\partial u}{\partial y} &= 0\end{aligned}\right\} \tag{11.55}$$

$$\left(1 - \frac{u^2}{a^2}\right)\frac{\partial u}{\partial x} + \left(1 - \frac{v^2}{a^2}\right)\frac{\partial v}{\partial y} + \left(1 - \frac{w^2}{a^2}\right)\frac{\partial w}{\partial z}$$
$$- \frac{vw}{a^2}\left(\frac{\partial w}{\partial y} + \frac{\partial v}{\partial z}\right) - \frac{uw}{a^2}\left(\frac{\partial u}{\partial z} + \frac{\partial w}{\partial x}\right) - \frac{uv}{a^2}\left(\frac{\partial v}{\partial x} + \frac{\partial u}{\partial y}\right) = 0 \tag{11.56}$$

$$a^2 = a_o^2 - \frac{\gamma - 1}{2}(u^2 + v^2 + w^2) \tag{11.57}$$

The derivatives of the velocity components in Eq. (11.56) may be replaced using the following expressions, which come from Eq. (11.54) and the irrotationality relations of Eq. (11.55):

$$\frac{\partial u}{\partial x} = \frac{\partial^2 \phi}{\partial x^2}, \quad \frac{\partial v}{\partial y} = \frac{\partial^2 \phi}{\partial y^2}, \quad \frac{\partial w}{\partial z} = \frac{\partial^2 \phi}{\partial z^2},$$

$$\frac{\partial w}{\partial y} = \frac{\partial v}{\partial z} = \frac{\partial^2 \phi}{\partial y \partial z}, \quad \frac{\partial u}{\partial z} = \frac{\partial w}{\partial x} = \frac{\partial^2 \phi}{\partial z \partial x}, \quad \frac{\partial v}{\partial x} = \frac{\partial u}{\partial y} = \frac{\partial^2 \phi}{\partial x \partial y} \tag{11.58}$$

*Cylindrical Coordinates*

$$v_r = \frac{\partial \phi}{\partial r}, \; v_\theta = \frac{1}{r}\frac{\partial \phi}{\partial \theta}, \; v_z = \frac{\partial \phi}{\partial z} \tag{11.59}$$

$$\nabla \times \mathbf{V} = 0 \quad \Rightarrow \quad \left.\begin{aligned} \frac{1}{r}\frac{\partial v_z}{\partial \theta} - \frac{\partial v_\theta}{\partial z} &= 0 \\ \frac{\partial v_r}{\partial z} - \frac{\partial v_z}{\partial r} &= 0 \\ \frac{1}{r}\left[\frac{\partial (r v_\theta)}{\partial r} - \frac{\partial v_r}{\partial \theta}\right] &= 0 \end{aligned}\right\} \tag{11.60}$$

$$\left(1 - \frac{v_r^2}{a^2}\right)\frac{\partial v_r}{\partial r} + \left(1 - \frac{v_\theta^2}{a^2}\right)\frac{1}{r}\frac{\partial v_\theta}{\partial \theta} + \left(1 - \frac{v_z^2}{a^2}\right)\frac{\partial v_z}{\partial z} - \frac{v_\theta v_z}{a^2}\left(\frac{1}{r}\frac{\partial v_z}{\partial \theta} + \frac{\partial v_\theta}{\partial z}\right)$$

$$- \frac{v_r v_z}{a^2}\left(\frac{\partial v_r}{\partial z} + \frac{\partial v_z}{\partial r}\right) - \frac{v_r v_\theta}{a^2}\frac{1}{r}\left[\frac{\partial (r v_\theta)}{\partial r} + \frac{\partial v_r}{\partial \theta}\right] + \left(1 + \frac{v_\theta^2}{a^2}\right)\frac{v_r}{r} = 0 \tag{11.61}$$

$$a^2 = a_o^2 - \frac{\gamma - 1}{2}(v_r^2 + v_\theta^2 + v_z^2) \tag{11.62}$$

The derivatives of the velocity components in Eq. (11.61) may be replaced using the following expressions, which come from Eq. (11.59) and the irrotationality relations of Eq. (11.60):

$$\frac{\partial v_r}{\partial r} = \frac{\partial^2 \phi}{\partial r^2}, \quad \frac{1}{r}\frac{\partial v_\theta}{\partial \theta} = \frac{1}{r^2}\frac{\partial^2 \phi}{\partial \theta^2}, \quad \frac{\partial v_z}{\partial z} = \frac{\partial^2 \phi}{\partial z^2},$$

$$\frac{1}{r}\frac{\partial v_z}{\partial \theta} = \frac{\partial v_\theta}{\partial z} = \frac{1}{r}\frac{\partial^2 \phi}{\partial \theta \partial z}, \quad \frac{\partial v_r}{\partial z} = \frac{\partial v_z}{\partial r} = \frac{\partial^2 \phi}{\partial z \partial r}, \quad \frac{1}{r}\frac{\partial (r v_\theta)}{\partial r} = \frac{1}{r}\frac{\partial v_r}{\partial \theta} = \frac{1}{r}\frac{\partial^2 \phi}{\partial r \partial \theta} \tag{11.63}$$

*Spherical Coordinates*

$$v_r = \frac{\partial \phi}{\partial r}, \; v_\theta = \frac{1}{r}\frac{\partial \phi}{\partial \theta}, \; v_\varphi = \frac{1}{r \sin \theta}\frac{\partial \phi}{\partial \varphi} \tag{11.64}$$

$$\nabla \times \mathbf{V} = 0 \quad \Rightarrow \quad \left.\begin{aligned} \frac{1}{r^2 \sin\theta}\left[\frac{\partial(rv_\varphi \sin\theta)}{\partial\theta} - \frac{\partial(rv_\theta)}{\partial\varphi}\right] &= 0 \\ \frac{1}{r\sin\theta}\left[\frac{\partial v_r}{\partial\varphi} - \frac{\partial(rv_\varphi \sin\theta)}{\partial r}\right] &= 0 \\ \frac{1}{r}\left[\frac{\partial(rv_\theta)}{\partial r} - \frac{\partial v_r}{\partial\theta}\right] &= 0 \end{aligned}\right\} \tag{11.65}$$

$$\left(1 - \frac{v_r^2}{a^2}\right)\frac{\partial v_r}{\partial r} + \left(1 - \frac{v_\theta^2}{a^2}\right)\frac{1}{r}\frac{\partial v_\theta}{\partial\theta} + \left(1 - \frac{v_\varphi^2}{a^2}\right)\frac{1}{r\sin\theta}\frac{\partial v_\varphi}{\partial\varphi}$$
$$- \frac{v_\varphi v_\theta}{a^2}\frac{1}{r^2\sin\theta}\left[\frac{\partial(rv_\theta)}{\partial\varphi} + \frac{\partial(rv_\varphi\sin\theta)}{\partial\theta}\right] - \frac{v_r v_\varphi}{a^2}\frac{1}{r\sin\theta}\left[\frac{\partial v_r}{\partial\varphi} + \frac{\partial(rv_\varphi\sin\theta)}{\partial r}\right]$$
$$- \frac{v_r v_\theta}{a^2}\frac{1}{r}\left[\frac{\partial(rv_\theta)}{\partial r} + \frac{\partial v_r}{\partial\theta}\right] + \left(2 + \frac{v_\theta^2}{a^2} + \frac{v_\varphi^2}{a^2}\right)\frac{v_r}{r} + \left(1 + \frac{v_\varphi^2}{a^2}\right)\frac{v_\theta\cot\theta}{r} = 0 \tag{11.66}$$

$$a^2 = a_o^2 - \frac{\gamma - 1}{2}(v_r^2 + v_\theta^2 + v_\varphi^2) \tag{11.67}$$

The derivatives of the velocity components in Eq. (11.66) may be replaced using the following expressions, which come from Eq. (11.64) and the irrotationality relations of Eq. (11.65):

$$\frac{\partial v_r}{\partial r} = \frac{\partial^2\phi}{\partial r^2}, \quad \frac{1}{r}\frac{\partial v_\theta}{\partial\theta} = \frac{1}{r^2}\frac{\partial^2\phi}{\partial\theta^2}, \quad \frac{1}{r\sin\theta}\frac{\partial v_\varphi}{\partial\varphi} = \frac{1}{r^2\sin^2\theta}\frac{\partial^2\phi}{\partial\varphi^2},$$
$$\frac{\partial(rv_\theta)}{\partial\varphi} = \frac{\partial(rv_\varphi\sin\theta)}{\partial\theta} = \frac{\partial^2\phi}{\partial\theta\partial\varphi}, \quad \frac{\partial v_r}{\partial\varphi} = \frac{\partial(rv_\varphi\sin\theta)}{\partial r} = \frac{\partial^2\phi}{\partial r\partial\varphi}, \quad \frac{\partial(rv_\theta)}{\partial r} = \frac{\partial v_r}{\partial\theta} = \frac{\partial^2\phi}{\partial r\partial\theta} \tag{11.68}$$

## 11.10 SUMMARY

This chapter has presented the generalized equations of motion for three-dimensional, inviscid, compressible flow. It is important to keep in mind the assumptions made in the various derivations—that is, isentropic, steady flow, with pressure forces as the only external forces acting on the control volume. When the complexity of the resultant nonlinear partial differential equations is seen, one can appreciate the great advantages inherent in the assumption of one-dimensional flow made in the first 10 chapters.

## 11.11 REFERENCES


**11.1** Hoffman, J. D. *Numerical Methods for Engineers and Scientists*, 2d ed., Marcel Dekker, New York, 2001, pp. 7–9.

**11.2** Schey, H. M. *Div, Grad, Curl and All That*, W.W. Norton & Company, New York and London, 1973, pp. 43–44.

**11.3** Toro, E. F. *Riemann Solvers and Numerical Methods for Fluid Dynamics,* 2d ed., Springer-Verlag, Berlin, Heidelberg, and New York, 1999.

**11.4** Culbert, L. B. *Computational Gasdynamics*, Cambridge University Press, Cambridge, UK, 1998.

**11.5** Spiegel, M. R. *Theory and Problems of Vector Analysis and an Introduction to Tensor Analysis*, Schaums Outline Series, McGraw-Hill Book Company, New York, 1959, p. 58.

**11.6** Saffman, P. G. *Vortex Dynamics*, Cambridge University Press, Cambridge, UK, 1992, p. 19.

**11.7** Bogdonoff, S. M., *Memorial Tributes: National Academy of Engineering*, Vol. 3 (1989), pp. 100–105, National Academy of Engineering (NAE). http://books.nap.edu/openbook/0309039398/html/100.html.

**11.8** Milne-Thompson, L. M. *Theoretical Hydrodynamics*, 4th ed., The MacMillan Company, New York, 1960, p. 50.

**11.9** Faber, T. E. *Fluid Dynamics for Physicists*, Cambridge University Press, Cambridge, UK, 1995, p. 22.

**11.10** Hoffman, K. A., Chiang, S. T., Siddiqui, S., and Papadakis, M. *Fundamental Equations of Fluid Mechanics*, Engineering Education System, Wichita, KS, 1996, p. 13.

**11.11** Spiegel, M. R. *Theory and Problems of Vector Analysis and an Introduction to Tensor Analysis*, Schaums Outline Series, McGraw-Hill Book Company, New York, 1959, pp. 137, 150, and 151.

## 11.12 PROBLEMS

**11.1** Prove that for a perfect gas,

(a) $p = \rho(\gamma - 1)e$

(b) $e_t = \dfrac{a^2}{\gamma(\gamma - 1)} + \dfrac{V^2}{2}$

**11.2** According to the generalized continuity equation given by Eq. (11.1), for steady, incompressible, one-dimensional flow, $\partial u/\partial x = 0$—or, in other words, $u$ is equal to a constant. Previously, for incompressible flow, however, it has been customary to assume that, for steady, one-dimensional flow, the product of velocity and cross-sectional area ($AV$) is a constant. Explain this seeming contradiction.

**11.3** The continuity equation for steady two-dimensional flow is

$$\frac{\partial \rho u}{\partial x} + \frac{\partial \rho v}{\partial y} = 0$$

A function $\psi$ (the compressible *stream function*) may be defined so that this equation is automatically satisfied. Show that the equations

$$u = \frac{\rho_{\text{ref}}}{\rho}\frac{\partial \psi}{\partial y} \quad \text{and} \quad v = -\frac{\rho_{\text{ref}}}{\rho}\frac{\partial \psi}{\partial x}$$

accomplish this objective, where $\rho_{\text{ref}}$ is a constant that is inserted so that the stream function has the same units as the incompressible flow stream function. What are the units of the stream function? What are the units of the velocity potential $\phi$?

**11.4** Expand Eq. (11.10) into the three component equations, and show that Eqs. (11.7), (11.8), and (11.9) result.

**11.5** Show that

$$\frac{dp}{\rho} + d\left(\frac{V^2}{2}\right) = 0$$

and

$$\frac{\nabla p}{\rho} + \nabla\left(\frac{V^2}{2}\right) = 0$$

are equivalent.

**11.6** Derive Eq. (11.18); that is, prove that

$$\rho\frac{Dh}{Dt} = \rho\dot{q} + \frac{Dp}{Dt}$$

**11.7** Under what conditions can it be assumed that $p + \frac{1}{2}\rho V^2$ is equal to a constant?

**11.8** Show that Crocco's equation along a streamline can be written as

$$\frac{1}{2}\frac{\partial V^2}{\partial t} = T\mathbf{V}\cdot\nabla s - \mathbf{V}\cdot\nabla h_o$$

**11.9** Using the substantial derivative operator within Crocco's equation, Eq. (11.39), develop the following equation for the entropy:

$$\frac{Ds}{Dt} = \frac{\partial s}{\partial t} + \mathbf{V}\cdot\nabla s = \frac{\partial s}{\partial t} + \frac{1}{T}\mathbf{V}\cdot\left(\nabla h_o + \frac{\partial \mathbf{V}}{\partial t}\right)$$

Under what conditions will the entropy remain constant along a streamline?

**11.10** From vector mechanics, it is known that the curl of a gradient ($\nabla \times \nabla f$) is identically zero. Demonstrate that this condition is true, and then use this fact to prove that if a velocity potential ($\mathbf{V} = \nabla\phi$) exists, the flow is irrotational.

**11.11** The velocity components for a possible flow field are given by $u = -3x^2 + 2y$ and $v = 2x + 2y$. Is the flow irrotational? If so, determine the velocity potential.

**11.12** Show that the velocity potential equation, Eq. (11.47), can be written in two-dimensional form as

$$\left(1 - \frac{u^2}{a^2}\right)\frac{\partial^2\phi}{\partial x^2} - 2\frac{uv}{a^2}\frac{\partial^2\phi}{\partial x\partial y} + \left(1 - \frac{v^2}{a^2}\right)\frac{\partial^2\phi}{\partial y^2} = 0$$

**11.13** Consider a steady, uniform flow of air ($\gamma = 1.4$, $R = 0.287$ kJ/kg · K) with velocity components $u = 120$ m/s and $v = w = 0$. Determine the velocity potential, substitute it into Eq. (11.48), and find the resultant difference between static and stagnation temperature.

**11.14** Using the stream function as defined in Problem 11.3, develop the following expression for steady, two-dimensional, irrotational flow:

$$\left(1 - \frac{u^2}{a^2}\right)\frac{\partial^2\psi}{\partial x^2} - 2\frac{uv}{a^2}\frac{\partial^2\psi}{\partial x\partial y} + \left(1 - \frac{v^2}{a^2}\right)\frac{\partial^2\psi}{\partial y^2} = 0$$

**11.15** Use the technique presented in Example 11.4 to write (a) the velocity components in terms of the velocity potential in spherical coordinates and (b) the steady energy equation for three-dimensional, adiabatic flow in cylindrical coordinates.

# Chapter 12

# Exact Solutions

## 12.1 INTRODUCTION

In the previous chapter, the equations for multidimensional flow of an inviscid compressible fluid were developed in Cartesian and vector forms. The vector forms enable the governing equations to be written in other coordinate systems. A typical two-dimensional compressible flow problem in the $(x, y)$ plane involves five dependent variables: $\rho$, $u$, $v$, $p$, and $T$. Accordingly, five equations are required to solve this problem: the continuity equation, the $x$ and $y$ momentum equations, the energy equation, and an equation of state. Even for steady, homentropic (uniform entropy) flows, the governing equations are complex.

The *velocity potential* $\phi$ is beneficial to the solution process, as its use allows a problem to be analyzed in terms of a single scalar quantity. It must be borne in mind, however, that $\phi$ can be used only in irrotational flows. Its use leads to a single equation, the *velocity potential equation*, Eq. (11.49). This equation manifests the flow physics of a problem; that is, it guarantees that the irrotational flow condition is satisfied, it is developed from the continuity equation, and it incorporates the momentum and energy equations.

One approach to solving irrotational compressible flow problems is to write the full velocity potential equation and then eliminate terms, based on the conditions of the problem. However, the velocity potential equation is nonlinear. This condition represents a major obstacle because there are no general analytical methods available to solve nonlinear partial differential equations (PDEs). Moreover, nonlinearity prevents the use of *the superposition principle*, which allows the buildup of a solution by combining the solutions of more elementary problems. The superposition principle is a cornerstone solution methodology for solving irrotational incompressible flow (*ideal-flow*) problems in hydrodynamics; see, for example, Ref. (12.1). Regrettably, that approach will not work in compressible flow.

To circumvent the difficulties imposed by nonlinearities in the governing equation, a method will be presented later in this chapter to transform the two-dimensional, nonlinear velocity potential equation from the *physical plane* (coordinates: $x$ and $y$)

to the *transformed plane*, or the *hodograph plane* (coordinates: the velocity components $u$ and $v$), in which the velocity potential equation is linear. The hodograph method was conceived in the 1890s and was widely explored in the 1930s, 1940s, and 1950s to solve subsonic, supersonic, and transonic flow problems. The method has fallen out of favor in recent times for three principal reasons: First, it is very difficult to impose the physical plane boundary conditions in the transformed plane; second, it applies only to two-dimensional flows; and third, and most importantly, numerical methods have been found to be superior.

In the next chapter, we will investigate an approach in which approximations are used to linearize the velocity potential equation. These approximations allow the solution to a special class of compressible flows (small-disturbance flows), which can provide useful engineering information. Because of the complexity of compressible flows, very few exact analytical solutions exist. A list of some of these flows is presented in Refs. (12.2) and (12.3).

In this chapter, we will consider several basic flows that represent exact solutions, including uniform flow, source/sink radial flow, irrotational vortex flow, spiral vortex flow, supersonic flow around a corner, and conical flow. It will be assumed that the flows considered are steady, irrotational, and have uniform entropy (i.e., are *homentropic*). Also, with few exceptions, the flows are all two dimensional.

## 12.2 SIMPLE HOMENTROPIC FLOWS

### Uniform Flow

Steady uniform flow in a plane is arguably the simplest of all flows. Suppose the flow is in the $x$ direction so that

$$u = \frac{\partial \phi}{\partial x} = V = \text{constant}$$

Integration gives

$$\phi = Vx + f(y)$$

Because the flow is along the $x$-axis, the transverse velocity component $v$ must vanish—that is, $v = \partial\phi/\partial y = 0$. Consequently, $f(y) =$ constant. We may arbitrarily set the constant to 0. So, for uniform flow in the $x$ direction, the velocity potential is

$$\phi = Vx \tag{12.1}$$

Similarly, for uniform flow in the $y$ direction, the velocity potential is

$$\phi = Vy$$

**Example 12.1. Velocity potential for an inclined uniform flow in the $(x, y)$ plane**

Develop an expression for the velocity potential in the $(x, y)$ plane for a flow inclined at an angle $\alpha$ to the $x$-axis as shown in Figure 12.1.

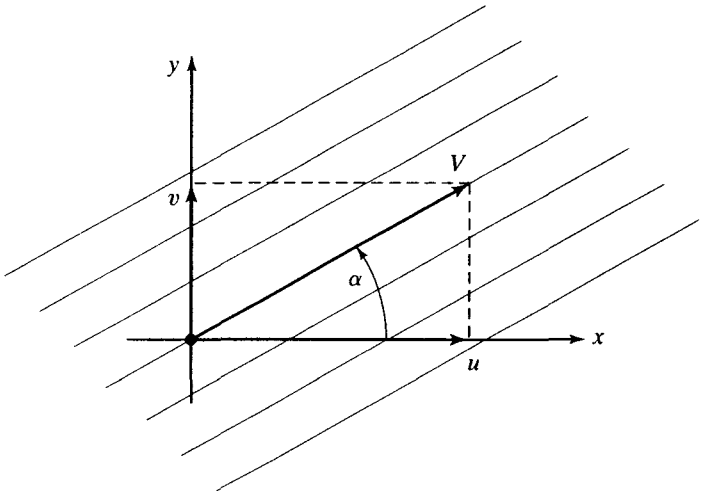


**Figure 12.1** Inclined Uniform Flow in the $(x, y)$ Plane

**Solution**

From Figure 12.1, it is clear that

$$u = \frac{\partial \phi}{\partial x} = V \cos \alpha$$

$$v = \frac{\partial \phi}{\partial y} = V \sin \alpha$$

**Notation Note:** Throughout this chapter, we use $\alpha$ as *the flow angle*—that is, the angle between the velocity vector and the $x$-axis—and $\theta$ as *the polar angle*—that is, the angle between the radial position vector and the $x$-axis.

Since $\phi = \phi(x, y)$, we may write

$$d\phi = \frac{\partial \phi}{\partial x} dx + \frac{\partial \phi}{\partial y} dy = (V \cos \alpha) dx + (V \sin \alpha) dy$$

Because the coefficients of the differentials are constant, we may integrate term by term to obtain

$$\phi = V(x \cos \alpha + y \sin \alpha) \tag{12.2}$$

**Example 12.2. Velocity potential for an inclined uniform flow in polar coordinates**

Develop an expression in terms of $r$ and $\theta$ for the velocity potential for a flow inclined at an angle $\alpha$ to the $x$-axis in the $(x, y)$ plane as shown in Figure 12.2.

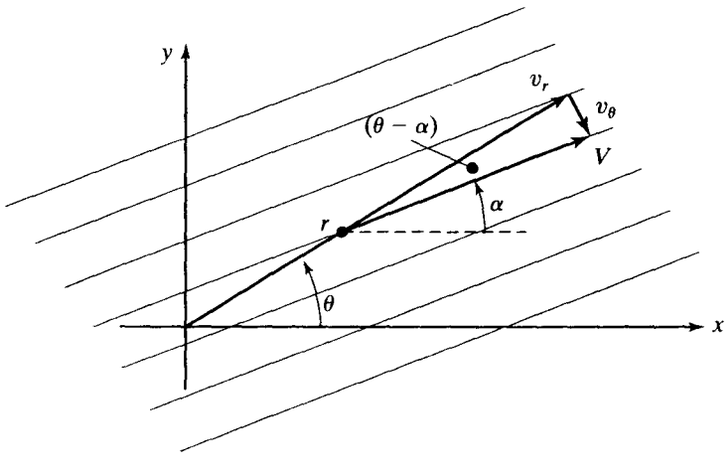


**Figure 12.2** Inclined Uniform Flow in the $(x, y)$ Plane

**Solution**

A simple method for obtaining $\phi(r, \theta)$ is to replace $x$ and $y$ in Eq. (12.2) with $r \cos \theta$ and $r \sin \theta$, respectively:

$$\phi = V(r \cos \theta \cos \alpha + r \sin \theta \sin \alpha) = Vr \cos(\theta - \alpha) \tag{12.3}$$

Alternatively, we may start with the radial and tangential velocity components:

$$v_r = \frac{\partial \phi}{\partial r} = V \cos(\theta - \alpha)$$

$$v_\theta = \frac{1}{r} \frac{\partial \phi}{\partial \theta} = -V \sin(\theta - \alpha)$$

Note that the tangential velocity component $v_\theta$ contains a minus sign, because the component is positive in the counterclockwise direction. Direct integration of the radial velocity component produces

$$\phi = Vr \cos(\theta - \alpha) + f(\theta)$$

Differentiation and comparison with the tangential velocity component reveal that $f(\theta) =$ constant. Thus, we have, as before,

$$\phi = Vr \cos(\theta - \alpha) = [V \cos(\theta - \alpha)]r = v_r r$$

## Pure Radial Flow

In the case of pure radial flow, it is assumed that the streamlines are radial lines that emerge from, or converge to, a common point. Moreover, only the radial component of velocity is nonzero. This type of flow is called *source*, or *sink*, *flow*, depending on whether the flow is directed away from, or toward, the origin, respectively. The flow may emanate from a line or from a point. (See Figure 12.3.) The former flow is two dimensional and is called a *line source* or *sink*, and the latter is three dimensional and

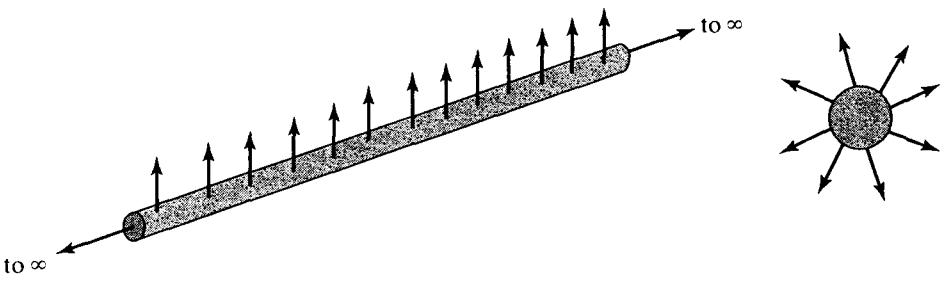


(a) line source (b) point source

**Figure 12.3** Line and Point Sources

is called a *point source* or *sink*. The former is described in terms of cylindrical coordinates (the $z$ direction is taken to lie along the line of the source or sink), and the latter is described in terms of spherical coordinates.

It is convenient here to begin with the continuity equation in cylindrical coordinates (for the line source/sink) and spherical coordinates (for the point source/sink) [see Ref. (12.4)]:

$$\frac{\partial \rho}{\partial t} + \frac{1}{r}\frac{\partial(\rho r v_r)}{\partial r} + \frac{1}{r}\frac{\partial(\rho v_\theta)}{\partial \theta} + \frac{\partial(\rho v_z)}{\partial z} = 0$$

$$\frac{\partial \rho}{\partial t} + \frac{1}{r^2}\frac{\partial(\rho r^2 v_r)}{\partial r} + \frac{1}{r \sin\theta}\frac{\partial(\rho \sin\theta v_\theta)}{\partial \theta} + \frac{1}{r \sin\theta}\frac{\partial(\rho v_\varphi)}{\partial \varphi} = 0$$

To obtain these equations, start with Eq. (11.2) and use the approach presented in Example 11.4. For steady radial flow, these expressions reduce to

$$\frac{d(\rho r v_r)}{dr} = 0$$

$$\frac{d(\rho r^2 v_r)}{dr} = 0$$

Integration of the pair of equations yields two expressions that may be written as a single equation, *viz.*,

$$\rho r^n v_r = \text{constant} = \frac{\dot{m}}{2^n \pi} \tag{12.4}$$

where $n = 1$ for the *line* source/sink, $n = 2$ for the *point* source/sink, and $\dot{m}$ is the mass flow respectively from/towards the source/sink per unit time. The term in the denominator on the right has been included to give the flow areas. Rearranging Eq. (12.4) yields

$$r^n = \frac{\dot{m}}{2^n \pi \rho v_r} = \left(\frac{\dot{m}}{2^n \pi \rho_o a_o}\right)\left(\frac{a}{v_r}\right)\left(\frac{\rho_o a_o}{\rho a}\right) = \left(\frac{\dot{m}}{2^n \pi \rho_o a_o}\right)\left(\frac{1}{M}\right)\left(\frac{\rho_o a_o}{\rho a}\right) \tag{12.5}$$

where $\rho_o$ and $a_o$ are the stagnation density and speed of sound, respectively. For isentropic flow of a perfect gas, we have

$$a^2 = \gamma RT = \gamma\frac{p}{\rho} = \gamma\frac{C\rho^\gamma}{\rho} = \gamma C\rho^{\gamma-1}$$

where $C$ is a constant. Consequently,

$$\frac{T_o}{T} = \frac{a_o^2}{a^2} = \left(\frac{\rho_o}{\rho}\right)^{\gamma-1}$$

Therefore,

$$\frac{\rho_o a_o}{\rho a} = \left(\frac{a_o}{a}\right)^{\frac{\gamma+1}{\gamma-1}} = \left(\frac{T_o}{T}\right)^{\frac{\gamma+1}{2(\gamma-1)}} = \left(1 + \frac{\gamma-1}{2}M^2\right)^{\frac{\gamma+1}{2(\gamma-1)}} \tag{12.6}$$

Combining Eqs. (12.5) and (12.6) produces

$$r^n = \left(\frac{\dot{m}}{2^n\pi\rho_o a_o}\right)\left(\frac{1}{M}\right)\left(1 + \frac{\gamma-1}{2}M^2\right)^{\frac{\gamma+1}{2(\gamma-1)}} \tag{12.7}$$

The Mach number can range from 0 to $\infty$. Inserting either of these extremes into Eq. (12.7) results in an infinite radius. This suggests that there is a minimum value of the radius that exists at an intermediate $M$. To locate this value, take the natural logarithm of Eq. (12.7) and differentiate the result to obtain

$$n\frac{dr}{r} = \frac{\gamma+1}{2(\gamma-1)}\frac{1}{1+\frac{\gamma-1}{2}M^2}\frac{(\gamma-1)}{2}2MdM - \frac{dM}{M}$$

Simplification brings

$$\frac{dr}{dM} = \frac{r}{n}\frac{M^2-1}{\left(1+\frac{\gamma-1}{2}M^2\right)M}$$

We now set the foregoing expression equal to zero. Ruling out the possibility that the radius is zero, we see that this expression amounts to zero at $M = 1$. Accordingly, the radius at this location, $r^*$, is

$$(r^*)^n = \left(\frac{\dot{m}}{2^n\pi\rho_o a_o}\right)\left(\frac{\gamma+1}{2}\right)^{\frac{\gamma+1}{2(\gamma-1)}} \tag{12.8}$$

Combining Eqs. (12.7) and (12.8) yields

$$\left(\frac{r}{r^*}\right)^n = \left(\frac{1}{M}\right)\left(\frac{2}{\gamma+1} + \frac{\gamma-1}{\gamma+1}M^2\right)^{\frac{\gamma+1}{2(\gamma-1)}} \tag{12.9}$$

This expression relates the Mach number to the radius. Further, the radius ratio on the left-hand side of Eq. (12.9) can be replaced with area ratios as follows:

*Cylindrical coordinates*: $n = 1$

$$\frac{r}{r^*} = \frac{2\pi r}{2\pi r^*} = \frac{A}{A^*}$$

*Spherical coordinates*: $n = 2$

$$\left(\frac{r}{r^*}\right)^2 = \frac{4\pi r^2}{4\pi (r^*)^2} = \frac{A}{A^*}$$

$$\frac{A}{A^*} = \frac{1}{M}\left[\left(\frac{2}{\gamma + 1}\right)\left(1 + \frac{\gamma - 1}{2}M^2\right)\right]^{\frac{\gamma+1}{2(\gamma-1)}}$$

This expression is identical to the area–Mach number relation of Eq. (3.23), which we developed in the chapter on isentropic flow. Thus, that one-dimensional flow represents an exact compressible flow solution. The remaining variables can be related to the Mach number through the isentropic flow relations:

$$\frac{T_o}{T} = 1 + \frac{\gamma - 1}{2}M^2$$

$$\frac{\rho_o}{\rho} = \left(1 + \frac{\gamma - 1}{2}M^2\right)^{1/(\gamma-1)}$$

$$\frac{p_o}{p} = \left(1 + \frac{\gamma - 1}{2}M^2\right)^{\gamma/(\gamma-1)}$$

There are four possible flow regimes, depending on whether the flow is inward (sink flow), outward (source flow), subsonic, or supersonic. As can be seen from Figure 12.4, in an inward flow (between two converging streamlines), the area decreases (a nozzle for subsonic flow; a diffuser for supersonic flow), and vice versa for outward flow. The minimum radius defines what is called the *limit line*, or *limit surface*. The mathematical solution cannot be continued beyond this radius. Source and sink flow exist only outside the circle

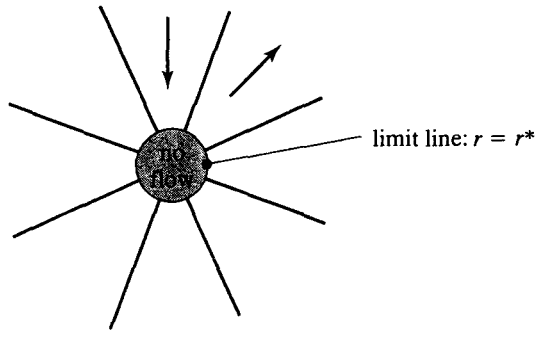


**Figure 12.4** Radial Flow Streamlines and Limit Line

or sphere defined by $r = r^*$. As is well known, a flow cannot pass from subsonic to supersonic or vice versa without the presence of a geometric throat.

The source/sink flow solution has been used in the design of minimum-length nozzles. [See Ref. (12.5).]

**Example 12.3. Solution of the velocity potential equation for radial flow**

Obtain an exact solution to the velocity potential equation in polar coordinates for radial potential flow in a plane [i.e., $\phi = \phi(r)$]. Also, develop the relation for the radial velocity.

**Solution**

The velocity potential equation in polar coordinates $(r, \theta)$ is obtained from Eq. (11.61) by removing all $z$ dependence—i.e., $\partial/\partial z = 0$ and $v_z = 0$—and by utilizing the relations of Eq. (11.63). This produces

$$\left(1 - \frac{v_r^2}{a^2}\right)\frac{\partial^2\phi}{\partial r^2} + \left(1 - \frac{v_\theta^2}{a^2}\right)\frac{1}{r^2}\frac{\partial^2\phi}{\partial\theta^2} - 2\frac{v_r v_\theta}{ra^2}\frac{\partial^2\phi}{\partial r\partial\theta} + \frac{v_r}{r}\left(1 + \frac{v_\theta^2}{a^2}\right) = 0 \tag{12.10}$$

where

$$v_r = \frac{\partial\phi}{\partial r} \quad v_\theta = \frac{1}{r}\frac{\partial\phi}{\partial\theta} \quad a^2 = a_o^2 - \frac{\gamma - 1}{2}(v_r^2 + v_\theta^2)$$

Now, for radial potential flow, $\phi = \phi(r)$; thus, the velocity potential equation is reduced to the following nonlinear ordinary differential equation:

$$(a^2 - v_r^2)\frac{dv_r}{dr} + \frac{a^2 v_r}{r} = 0$$

Rearranging and replacing the square of the speed of sound by $a^2 = a_o^2 - \dfrac{\gamma - 1}{2}v_r^2$ produces

$$\left(\frac{1}{v_r} - \frac{v_r}{a_o^2 - \dfrac{\gamma - 1}{2}v_r^2}\right)dv_r + \frac{dr}{r} = 0$$

This expression can be integrated to give

$$\ln(v_r) + \frac{1}{\gamma - 1}\ln\left(a_o^2 - \frac{\gamma - 1}{2}v_r^2\right) + \ln(r) = \text{constant}$$

or

$$rv_r\left(a_o^2 - \frac{\gamma - 1}{2}v_r^2\right)^{1/(\gamma-1)} = rv_r(a^2)^{1/(\gamma-1)} = \text{constant}$$

Finally, replacing the square of the speed of sound with its isentropic density relation gives

$$rv_r\rho = \text{constant}$$

So, we have

$$2\pi rv_r\rho = \rho Av_r = \text{constant}$$

### Pure Tangential Flow

This is the case of a *compressible irrotational vortex*. Here, the streamlines are concentric circles. Since the potential lines are orthogonal to the streamlines [see Ref. (12.6)], these lines are radial, and the velocity potential may be written as

$$\phi = C\theta \tag{12.11}$$

Previously, we gave the two-dimensional velocity potential equation in polar coordinates as

$$\left(1 - \frac{v_r^2}{a^2}\right)\frac{\partial^2\phi}{\partial r^2} + \left(1 - \frac{v_\theta^2}{a^2}\right)\frac{1}{r^2}\frac{\partial^2\phi}{\partial\theta^2} - 2\frac{v_r v_\theta}{ra^2}\frac{\partial^2\phi}{\partial r\partial\theta} + \frac{v_r}{r}\left(1 + \frac{v_\theta^2}{a^2}\right) = 0 \tag{12.10}$$

Substituting Eq. (12.11) into Eq. (12.10) and using the former to evaluate $v_r = \partial\phi/\partial r$ and $v_\theta = (1/r)(\partial\phi/\partial\theta)$ reveals that the velocity potential equation is satisfied exactly and that the velocity components for this flow are

$$v_r = 0$$

$$v_\theta = \frac{C}{r}$$

The constant in the tangential velocity component can be determined by computing the *circulation* $\Gamma$ of this flow. The circulation is the value of the line integral of the tangential velocity around a closed curve. Computing the circulation for this flow gives

$$\Gamma = \oint \mathbf{V}\cdot d\mathbf{s} = \oint v_\theta r d\theta = \oint \frac{C}{r} r d\theta = \oint C d\theta = C2\pi$$

Therefore,

$$C = \frac{\Gamma}{2\pi}$$

and so

$$v_\theta = \frac{\Gamma}{2\pi r} \tag{12.12}$$

This equation is identical to the expression for incompressible flow. [See Ref. (12.1).] From Eq. (12.12), we see that the maximum velocity occurs at the minimum radius. To determine an expression for the maximum velocity, we first write the energy equation

$$h_o = h + \frac{V^2}{2}$$

But $h = c_p T = \gamma RT/(\gamma - 1) = a^2/(\gamma - 1)$. Therefore, the foregoing expression can be written as

$$\frac{a_o^2}{\gamma - 1} = \frac{a^2}{\gamma - 1} + \frac{V^2}{2}$$

This is an equation of an ellipse in the $(a, V)$ plane:

$$\frac{a^2}{(a_o^2)} + \frac{V^2}{\left(\frac{2}{\gamma - 1} a_o^2\right)} = 1 \tag{12.13}$$

When $V = 0$, $a = a_o$ and the speed of sound is at a maximum; when $a = 0$ (when the temperature is at absolute zero, or there is a perfect vacuum), the velocity is at a maximum value equal to

$$V_{\max}^2 = \frac{2}{\gamma - 1} a_o^2 \tag{12.14}$$

Eq. (12.14) may be rewritten as

$$\frac{a^2}{a_o^2} + \frac{V^2}{V_{\max}^2} = 1$$

Now, by combining Eqs. (12.12) and (12.14) with $V = v_\theta$, we find that the minimum radius is

$$r_{\min} = \frac{\Gamma}{2\pi (v_\theta)_{\max}} = \frac{\Gamma}{2\pi V_{\max}} \tag{12.15}$$

This is the smallest radius possible for this flow. Inside this radius, irrotational vortex motion does not exist. For radii larger than $r_{\min}$, all Mach numbers are possible. In fact, at $r = r_{\min}$, $M = v_\theta/a = V_{\max}/0 = \infty$. The radius at which sonic conditions occur can be computed from

$$\frac{r}{r_{\min}} = \frac{(v_\theta)_{\max}}{v_\theta}$$

Using Eqs. (12.13) and (12.14) as well as $M = v_\theta/a$, it is not difficult to show that

$$\frac{(v_\theta)_{\max}}{v_\theta} = \sqrt{1 + \frac{2}{\gamma - 1} \frac{1}{M^2}}$$

Therefore,

$$\frac{r}{r_{\min}} = \sqrt{1 + \frac{2}{\gamma - 1} \frac{1}{M^2}} \tag{12.16}$$

At $M = 1, r = r^*$, so

$$\frac{r^*}{r_{\min}} = \sqrt{\frac{\gamma + 1}{\gamma - 1}}$$

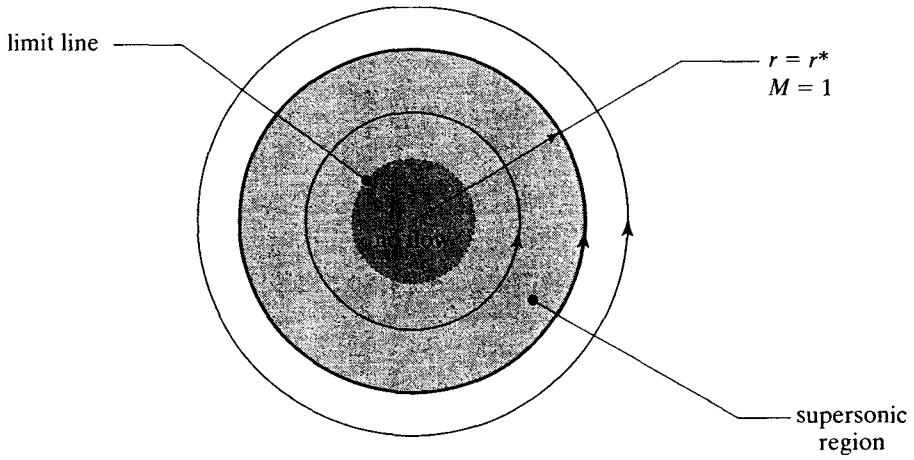


**Figure 12.5** The Compressible Irrotational Vortex Flow Field

The flow field for the compressible irrotational vortex is diagrammed in Figure 12.5. With the use of Eqs. (12.12) and (12.16), as well as the isentropic relations, we can compute the distribution of the flow variables.

Note that the limit line is not the line of sonic velocity as it was in source/sink flow.

## Spiral Flow

*Incompressible Flow*: The velocity potential $\phi$ and the stream function $\psi$ for elementary incompressible flows can be found in most books on fluid mechanics. The combination of a line source ($\phi = Q \ln r/2\pi$; $\psi = Q\theta/2\pi$) and an irrotational vortex ($\phi = \Gamma\theta/2\pi$; $\psi = -\Gamma \ln r/2\pi$) produces an outwardly directed spiral flow. Note that $Q$ is the *volume flow rate* and is related to the mass flow rate by $\dot{m} = \rho Q$. Because the governing equations for the velocity potential and the stream function in incompressible flow are linear—that is, $\nabla^2\phi = 0$ and $\nabla^2\psi = 0$ (Laplace's equation)—we are justified in adding source and vortex flows to obtain an additional flow. Hence,

$$\phi = \phi_{\text{source}} + \phi_{\text{vortex}} = \frac{Q}{2\pi}\ln r + \frac{\Gamma}{2\pi}\theta$$

$$\psi = \psi_{\text{source}} + \psi_{\text{vortex}} = \frac{Q}{2\pi}\theta - \frac{\Gamma}{2\pi}\ln r$$

Now, for $\psi = C/2\pi$ (a constant),

$$\ln r = \frac{Q\theta - C}{\Gamma}$$

or

$$r = e^{(Q\theta - C)/\Gamma} = ce^{Q/\Gamma\,\theta}$$

where $c = e^{-C/\Gamma}$, a constant. This is the equation of an *equiangular spiral.*

*Compressible Flow*: Although we have obtained solutions for the compressible source and the compressible irrotational vortex, we cannot simply add these solutions to obtain another solution as in the incompressible flow case, because the governing equations are nonlinear. Nevertheless, we can obtain a solution by properly combining the velocity components of the flow. Now, for source flow,

$$v_r = \frac{\dot{m}}{2\pi\rho r} = \frac{\dot{m}}{2\pi\rho_o}\frac{\rho_o}{\rho}\frac{1}{r} = \frac{\dot{m}}{2\pi\rho_o}\left(1 + \frac{\gamma - 1}{2}M^2\right)^{1/(\gamma-1)}\frac{1}{r} \tag{12.17}$$

Note that if $M = 0$, we obtain the same radial velocity as for the incompressible flow case. The tangential velocity component of spiral motion comes from the irrotational vortex, that is,

$$v_\theta = \frac{\Gamma}{2\pi r} \tag{12.18}$$

which is identical to the incompressible flow component. Vectorially adding the velocity components together produces the velocity of the flow:

$$V^2 = v_r^2 + v_\theta^2 = \left(\frac{\dot{m}}{2\pi\rho r}\right)^2 + \left(\frac{\Gamma}{2\pi r}\right)^2 \tag{12.19}$$

It is not difficult to show that by combining

$$V^2 = V_{\max}^2\left(1 - \frac{a^2}{a_o^2}\right) = V_{\max}^2\left[1 - \left(\frac{\rho}{\rho_o}\right)^{\gamma-1}\right]$$

with Eq. (12.19), we obtain

$$r^2 = \frac{1}{4\pi^2 V_{\max}^2}\frac{\dfrac{\dot{m}^2}{\rho_o^2} + \Gamma^2\left(\dfrac{\rho}{\rho_o}\right)^2}{\left(\dfrac{\rho}{\rho_o}\right)^2\left[1 - \left(\dfrac{\rho}{\rho_o}\right)^{\gamma-1}\right]} \tag{12.20}$$

To determine how the Mach number and the radius are related, we can combine the following isentropic relationship between the density and Mach number [see Eq. (3.17)] with Eq. (12.20):

$$\left(\frac{\rho_o}{\rho}\right) = \left(1 + \frac{\gamma - 1}{2}M^2\right)^{1/(\gamma-1)}$$

To find the limit line for this flow, we rewrite Eq. (12.19) as

$$4\pi^2 r^2 V^2 = \frac{\dot{m}^2}{\rho^2} + \Gamma^2$$

Now we differentiate this expression with respect to $V^2$ to get

$$4\pi^2 V^2 \frac{dr^2}{dV^2} + 4\pi^2 r^2 = -2\frac{\dot{m}^2}{\rho^3}\frac{d\rho}{dV^2} \tag{12.21}$$

Euler's equation may be written as

$$dp = -\rho V dV = -\frac{\rho}{2} dV^2$$

Since the flow is isentropic, the speed of sound enters through the relation

$$dp = a^2 d\rho$$

Hence,

$$\frac{d\rho}{dV^2} = -\frac{\rho}{2a^2}$$

Uniting this expression with Eq. (12.21) and setting $dr^2/dV^2 = 0$, we obtain the radius of the limit line (the minimum value of the radius for which the solution holds):

$$r_{\min} = \frac{\dot{m}}{2\pi\rho a} = \frac{\dot{m}}{2\pi\rho_o a_o}\frac{\rho_o}{\rho}\frac{a_o}{a} = \frac{\dot{m}}{2\pi\rho_o a_o}\left(\frac{\rho_o}{\rho}\right)^{(\gamma+1)/2}$$

$$= \frac{\dot{m}}{2\pi\rho_o a_o}\left(1 + \frac{\gamma - 1}{2}M^2\right)^{(\gamma+1)/[2(\gamma-1)]}$$

Comparison of the expression for the limit line with the radial velocity component expression of Eq. (12.17) reveals that at $r = r_{\min}$, $v_r = a$. Hence, the radial velocity component (not the velocity) reaches Mach 1 at the limit line for spiral flow.

It is useful to obtain an expression for the streamlines. To accomplish this, write the velocity components in terms of the stream function:

$$v_r = \frac{\rho_o}{\rho}\frac{1}{r}\frac{\partial\psi}{\partial\theta} = \frac{\dot{m}}{2\pi\rho_o}\frac{\rho_o}{\rho}\frac{1}{r}$$

$$v_\theta = -\frac{\rho_o}{\rho}\frac{\partial\psi}{\partial r} = \frac{\Gamma}{2\pi}\frac{1}{r}$$

Now, since $\psi = \psi(r, \theta)$, the total derivative is

$$d\psi = \frac{\partial\psi}{\partial r}dr + \frac{\partial\psi}{\partial\theta}d\theta$$

$$= -\frac{\Gamma}{2\pi}\frac{\rho}{\rho_o}\frac{dr}{r} + \frac{\dot{m}}{2\pi\rho_o}d\theta \tag{12.22}$$

To obtain an expression for $dr/r$, replace the density ratio in Eq. (12.20), using the isentropic relation

$$\frac{\rho}{\rho_o} = \left(\frac{a}{a_o}\right)^{2/(\gamma-1)} = A^{2/(\gamma-1)}$$

Note that $A = a/a_o$. Thus, Eq. (12.20) may be written as

$$r^2 = \frac{1}{4\pi^2 V_{\max}^2} \frac{\dfrac{\dot{m}^2}{\rho_o^2} + \Gamma^2 A^{4/(\gamma-1)}}{A^{4/(\gamma-1)}(1 - A^2)} \tag{12.23}$$

Differentiating the natural logarithm of Eq. (12.23), we obtain

$$\frac{dr}{r} = \left[ \frac{A^2}{(1 - A^2)} - \frac{\left(\dfrac{2}{\gamma - 1}\right)\dfrac{\dot{m}^2}{\rho_o^2}}{\dfrac{\dot{m}^2}{\rho_o^2} + \Gamma^2 A^{4/(\gamma-1)}} \right] \frac{dA}{A} \tag{12.24}$$

Uniting Eqs. (12.22) and (12.24) yields

$$d\psi = -\frac{\Gamma}{2\pi} A^{2/(\gamma-1)} \left[ \frac{A^2}{(1 - A^2)} - \frac{\left(\dfrac{2}{\gamma - 1}\right)\dfrac{\dot{m}^2}{\rho_o^2}}{\dfrac{\dot{m}^2}{\rho_o^2} + \Gamma^2 A^{4/(\gamma-1)}} \right] \frac{dA}{A} + \frac{\dot{m}}{2\pi\rho_o} d\theta$$

or

$$d\psi = -\frac{\Gamma}{2\pi} \left[ \frac{A^{(\gamma+1)/(\gamma-1)}}{(1 - A^2)} - \frac{\left(\dfrac{2}{\gamma - 1}\right)\dfrac{\dot{m}^2}{\rho_o^2} A^{(3-\gamma)/(\gamma-1)}}{\dfrac{\dot{m}^2}{\rho_o^2} + \Gamma^2 A^{4/(\gamma-1)}} \right] dA + \frac{\dot{m}}{2\pi\rho_o} d\theta \tag{12.25}$$

Equation (12.25) can be integrated term by term provided that the exponent $(\gamma + 1)/(\gamma - 1)$ is an integer. Further, the result depends on whether the integer is even or odd. For example, suppose $\gamma = 4/3$. Consequently, $(\gamma + 1)/(\gamma - 1) = 7$. Therefore, Eq. (12.25) may be written as

$$d\psi = -\frac{\Gamma}{2\pi} \left[ \frac{A^7}{(1 - A^2)} - \frac{6\dfrac{\dot{m}^2}{\rho_o^2} A^5}{\dfrac{\dot{m}^2}{\rho_o^2} + \Gamma^2 A^{12}} \right] dA + \frac{\dot{m}}{2\pi\rho_o} d\theta$$

$$= -\frac{\Gamma}{2\pi} \left[ -(A^5 + A^3 + A)dA + \frac{A\,dA}{(1 - A^2)} - \frac{\dot{m}^2}{\rho_o^2} \frac{1}{\Gamma} \frac{dB}{\dfrac{\dot{m}^2}{\rho_o^2} + B^2} \right] + \frac{\dot{m}}{2\pi\rho_o} d\theta$$

where $B = \Gamma A^6$, and therefore $dB = 6\Gamma A^5 dA$. Integration yields

$$\psi = \frac{\Gamma}{2\pi}\left[\frac{A^6}{6} + \frac{A^4}{4} + \frac{A^2}{2} + \frac{1}{2}\ln(1 - A^2) + \frac{\dot{m}^2}{\rho_o^2}\frac{1}{\Gamma}\tan^{-1}\left(\frac{\Gamma A^6}{\frac{\dot{m}}{\rho_o}}\right)\right] + \frac{\dot{m}}{2\pi\rho_o}\theta + \text{constant} \tag{12.26}$$

Setting $\psi$ = constant and using Eq. (12.23) allows the streamlines of the compressible spiral to be plotted for given values of $\dot{m}$, $\rho_o$, $\Gamma$, and $a_o$.

It should be noted that spiral vortex flow appears in actual compressible flows involving shockwaves and wedges. Furthermore, galaxies, including our own, take this geometric form.

**Example 12.4. Limiting form of spiral flow streamlines for $\gamma = 4/3$**

Prove that the incompressible streamlines of spiral flow are obtained for the case in which $A = a/a_o \to 1$. Use the stream function [Eq. (12.26)] and assume that $\gamma = 4/3$ to obtain the limiting form.

**Solution**

As may be seen from Eq. (12.23),

$$r^2 = \left(\frac{1}{4\pi^2 V_{\max}^2}\right)\left[\frac{\frac{\dot{m}^2}{\rho_o^2} + \Gamma^2 A^{4/(\gamma-1)}}{A^{4/(\gamma-1)}(1 - A^2)}\right]$$

So, as $A \to 1$, $r \to \infty$. However, if we take the logarithm of this expression and use the fact that $1 - A^2 = (1 + A)(1 - A)$, it is not hard to show that for this limiting situation,

$$2\ln r + \ln(1 - A) \to \text{constant}$$

Therefore, as $A \to 1$, $\ln(1 - A^2) = \ln(1 + A) + \ln(1 - A) \to (\text{constant} - 2\ln r)$. Using this condition in Eq. (12.26) yields

$$\psi = -\frac{\Gamma}{2\pi}\ln r + \frac{\dot{m}}{2\pi\rho_o}\theta + \text{constant} = \frac{Q}{2\pi}\theta - \frac{\Gamma}{2\pi}\ln r + \text{constant}$$

which is identical to the expression for the stream function for incompressible spiral flow. This result is also obtainable through direct integration of Eq. (12.22) by allowing $\rho/\rho_o \to 1$.

## 12.3 THE HODOGRAPH TRANSFORMATION

The situation confronting anyone who sought to analytically solve compressible flow problems many years ago was bleak. First, the governing equations are highly nonlinear, and second, there is no method available to analytically solve nonlinear equations. Moreover, the computing power of today was obviously not available back then. Consequently, the only possible recourse was somehow to linearize the equations. Two approaches were tried: In one, certain terms were dropped from the nonlinear equation, leaving a linear approximate expression. (This approach will be studied in the next chapter.) In the other approach, the nonlinear equation was transformed into a linear version. In 1890, Molenbroek [Ref. (12.7)] showed that by interchanging the dependent and independent variables, the velocity potential equation could be linearized. This concept was further exploited by Chaplygin [Ref. (12.8)] in his famous study of gas jets.

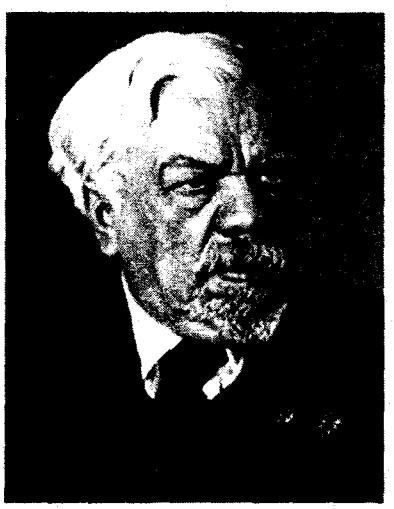

**Historical Note: Sergei Alekseevich Chaplygin** (1869–1942) had a difficult childhood, as his father, who was a shop assistant, died of cholera when Chaplygin was only two years old. Nevertheless, he was able to overcome this obstacle and in 1890 entered the University of Moscow. There, he impressed the famous Nikolai Zhukovsky (or Joukowski), who took Chaplygin under his wing and guided his work in hydrodynamics. Zhukovsky convinced Chaplygin to continue his studies and to become a teacher after graduation. Chaplygin became an assistant professor at the University of Moscow and taught in several colleges.

Chaplygin gained distinction by winning the Brashman Prize in 1893 (it had been won previously by Zhukovsky in 1885) for a long article he wrote on the motion of a solid body in a liquid. He was able to use much of this material for his master's dissertation in 1897. It should be noted that the Russian master's degree is the equivalent of today's Ph.D. Chaplygin taught mechanics at Moscow Technical College between 1896 and 1906. Also, in 1901, he became a professor at the Moscow Women's College. Four years later, he was appointed head of the college, a position he held until 1918.

In 1902, Chaplygin published his famous paper on gas jets. He employed the hodograph method to obtain the exact solution to compressible jet flow problems. This seminal work opened the way to the study of high-speed flow problems.

Chaplygin won numerous awards. For example, in 1899, he received the Gold Medal of the St. Petersburg Academy of Sciences. In 1924, he was elected to the USSR Academy of Sciences and five years later was given the title of Honored Scientist. Zhukovsky and Chaplygin created the Central Aerohydrodynamics Institute in 1918. When Zhukovsky passed away in 1921, Chaplygin became the director of the institute. In 1922, the institute was renamed the N. E. Zhukovsky Academy of Military and Aeronautical Engineering.

It should be mentioned that in 1847, Hamilton [Ref. (12.9)] graphically described the motion of a body via a curve, which was the locus of the end points of the velocity vector. He called the curve the *hodograph* of the body. The word "hodograph" is a combination of Greek words meaning "a way to describe." This appears to be the first occasion that the velocity plane was used as a tool in the solution of a problem. This method is still employed today in astronomy; for example, see Derbes [Ref. (12.10)].

The hodograph method, which has been used for two-dimensional flows, transforms the nonlinear velocity potential equation into an exact linear equation. In the original nonlinear potential equation, the velocity components $(u, v)$ are the dependent variables, while the space coordinates $(x, y)$ are the independent variables. The velocity potential equation is nonlinear because the coefficients of the velocity derivatives are functions of the velocity. The process to switch roles of the dependent and independent variables in this case is called the *hodograph transformation*. Besides the method that follows, several procedures have been used to perform the transformation; for example, see Example 12.5 and Problem 12.10.

We demonstrate the hodograph transformation by using the velocity potential and irrotational equations written in Cartesian coordinates:

$$\left(1 - \frac{u^2}{a^2}\right)\frac{\partial u}{\partial x} - \frac{uv}{a^2}\left(\frac{\partial v}{\partial x} + \frac{\partial u}{\partial y}\right) + \left(1 - \frac{v^2}{a^2}\right)\frac{\partial v}{\partial y} = 0$$

$$\frac{\partial v}{\partial x} - \frac{\partial u}{\partial y} = 0 \tag{12.27}$$

The physical and hodograph planes are shown in Figure 12.6. Again, it should be mentioned that $\alpha$ is the flow inclination angle and $\theta$ is the polar angle.

In the hodograph plane, the space coordinates $x$ and $y$ are considered functions of the velocity components $u$ and $v$; that is, $x = x(u, v)$ and $y = y(u, v)$. Thus, the total derivatives may be written as

$$dx = \frac{\partial x}{\partial u}du + \frac{\partial x}{\partial v}dv$$

$$dy = \frac{\partial y}{\partial u}du + \frac{\partial y}{\partial v}dv$$

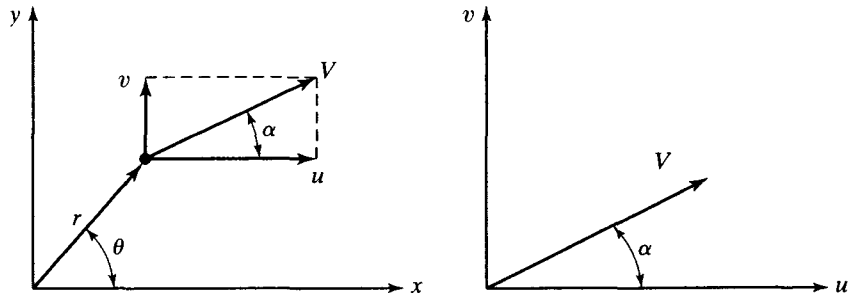


(a) Physical plane (b) Hodograph plane

**Figure 12.6** The Physical and Hodograph Planes

This pair of equations may be conveniently written in *vector–matrix form* as

$$\begin{bmatrix} dx \\ dy \end{bmatrix} = \begin{bmatrix} x_u & x_v \\ y_u & y_v \end{bmatrix} \begin{bmatrix} du \\ dv \end{bmatrix} \tag{12.28}$$

Note that the partial derivatives in the coefficient matrix on the right-hand side have been replaced using shorthand notation in which the subscript represents differentiation with respect to the independent variable—for example,

$$x_u \equiv \frac{\partial x}{\partial u}, \quad y_v = \frac{\partial y}{\partial v}, \text{ etc.}$$

In the physical plane, $u = u(x, y)$ and $v = v(x, y)$, and therefore,

$$\begin{bmatrix} du \\ dv \end{bmatrix} = \begin{bmatrix} u_x & u_y \\ v_x & v_y \end{bmatrix} \begin{bmatrix} dx \\ dy \end{bmatrix} \tag{12.29}$$

Another way to obtain Eq. (12.29) is to multiply Eq. (12.28) by the inverse of the coefficient matrix. For a $2 \times 2$ matrix, say $\mathbf{A}$, *the inverse* $\mathbf{A}^{-1}$ may be easily obtained from

$$\mathbf{A} = \begin{bmatrix} a & b \\ c & d \end{bmatrix} \qquad \mathbf{A}^{-1} = \frac{\mathbf{adjA}}{|\mathbf{A}|}$$

where $\mathbf{adjA} = \begin{bmatrix} d & -b \\ -c & a \end{bmatrix}$ is the *adjoint matrix* of $\mathbf{A}$ and $|\mathbf{A}| = \begin{vmatrix} a & b \\ c & d \end{vmatrix} = ad - bc$ is its *determinant*. Performing the operations on Eq. (12.28) results in

$$\begin{bmatrix} du \\ dv \end{bmatrix} = \frac{1}{J} \begin{bmatrix} y_v & -x_v \\ -y_u & x_u \end{bmatrix} \begin{bmatrix} dx \\ dy \end{bmatrix} \tag{12.30}$$

where $J$, the determinant of the coefficient matrix in Eq. (12.28), is the *Jacobian* of the transformation:

$$J = \frac{\partial(x, y)}{\partial(u, v)} = x_u y_v - x_v y_u \tag{12.31}$$

Since $J$ appears in the denominator of Eq. (12.30), for the transformation to be valid, $J$ must not be equal to zero. Comparing Eqs. (12.29) and (12.30) reveals that

$$\begin{aligned} \frac{\partial u}{\partial x} &= \frac{1}{J}\frac{\partial y}{\partial v}, \quad \frac{\partial u}{\partial y} = -\frac{1}{J}\frac{\partial x}{\partial v} \\ \frac{\partial v}{\partial x} &= -\frac{1}{J}\frac{\partial y}{\partial u}, \quad \frac{\partial v}{\partial y} = \frac{1}{J}\frac{\partial x}{\partial u} \end{aligned} \tag{12.32}$$

The partial derivatives of Eq. (12.32) may be inserted into Eq. (12.27) to obtain the transformed pair of equations:

$$(a^2 - u^2)\frac{\partial y}{\partial v} + uv\left(\frac{\partial x}{\partial v} + \frac{\partial y}{\partial u}\right) + (a^2 - v^2)\frac{\partial x}{\partial u} = 0$$

$$\frac{\partial x}{\partial v} - \frac{\partial y}{\partial u} = 0 \tag{12.33}$$

From the energy equation, we have

$$a^2 = a_o^2 - \frac{\gamma - 1}{2}V^2 = a_o^2 - \frac{\gamma - 1}{2}(u^2 + v^2)$$

Since $a_o$ is a constant, the speed of sound clearly depends only on $u$ and $v$; therefore, Eq. (12.33) is a linear system of equations. Unlike in the physical plane, where we determine the velocity field for a given geometry, solution of Eq. (12.33) in the hodograph plane yields the geometry of the flow field. Since we do not know *a priori* where the actual boundaries of the flow field are in the transformed plane, it is easy to understand why it would be difficult to impose physical boundary conditions in the hodograph method.

Generally, the dependent variables that have been employed to solve problems in the hodograph plane are the velocity potential $\phi$ and the stream function $\psi$. Use of the former assures that the flow is irrotational, and use of the latter assures that the continuity equation is satisfied. The independent variables are generally the magnitude of the velocity vector $V$ and the flow angle $\alpha$.

**Notation Note:** In most writings on the hodograph method, including writings dealing with inviscid streamline flows, the speed of the flow and the flow angle are respectively taken to be $q$ and $\theta$ rather than $V$ and $\alpha$ as used here.

The relations between the velocity potential, the stream function, and the velocity components, written in vector–matrix form, are

$$\begin{bmatrix} u \\ v \end{bmatrix} = V\begin{bmatrix} \cos\alpha \\ \sin\alpha \end{bmatrix} = \begin{bmatrix} \phi_x \\ \phi_y \end{bmatrix} = \frac{\rho_o}{\rho}\begin{bmatrix} \psi_y \\ -\psi_x \end{bmatrix} \tag{12.34}$$

Taking the total derivatives of both $\phi$ and $\psi$ with respect to $x$ and $y$ brings

$$\begin{bmatrix} d\phi \\ d\psi \end{bmatrix} = \begin{bmatrix} \phi_x & \phi_y \\ \psi_x & \psi_y \end{bmatrix}\begin{bmatrix} dx \\ dy \end{bmatrix} \tag{12.35}$$

The inverse of this expression may be found by employing the procedure described previously to obtain

$$\begin{bmatrix} dx \\ dy \end{bmatrix} = \frac{1}{J}\begin{bmatrix} \psi_y & -\phi_y \\ -\psi_x & \phi_x \end{bmatrix}\begin{bmatrix} d\phi \\ d\psi \end{bmatrix} \tag{12.36}$$

where $J$, the determinant of the coefficient matrix in Eq. (12.35), is the Jacobian of the transformation:

$$J = \frac{\partial(\phi, \psi)}{\partial(x, y)} = \begin{vmatrix} \phi_x & \phi_y \\ \psi_x & \psi_y \end{vmatrix} = \phi_x\psi_y - \phi_y\psi_x \tag{12.37}$$

Introducing the independent variables $V$ and $\alpha$ [i.e., $\phi = \phi(V, \alpha)$ and $\psi = \psi(V, \alpha)$] leads to

$$\begin{bmatrix} d\phi \\ d\psi \end{bmatrix} = \begin{bmatrix} \phi_V & \phi_\alpha \\ \psi_V & \psi_\alpha \end{bmatrix} \begin{bmatrix} dV \\ d\alpha \end{bmatrix} \tag{12.38}$$

Using Eq. (12.38) to replace the vector on the right side of Eq. (12.36) yields

$$\begin{bmatrix} dx \\ dy \end{bmatrix} = \frac{1}{J} \begin{bmatrix} \psi_y & -\phi_y \\ -\psi_x & \phi_x \end{bmatrix} \begin{bmatrix} \phi_V & \phi_\alpha \\ \psi_V & \psi_\alpha \end{bmatrix} \begin{bmatrix} dV \\ d\alpha \end{bmatrix} \tag{12.39}$$

Also, since $x = x(V, \alpha)$ and $y = y(V, \alpha)$, we have

$$\begin{bmatrix} dx \\ dy \end{bmatrix} = \begin{bmatrix} x_V & x_\alpha \\ y_V & y_\alpha \end{bmatrix} \begin{bmatrix} dV \\ d\alpha \end{bmatrix} \tag{12.40}$$

Comparing Eqs. (12.39) and (12.40) reveals that

$$\begin{bmatrix} x_V & x_\alpha \\ y_V & y_\alpha \end{bmatrix} = \frac{1}{J} \begin{bmatrix} \psi_y & -\phi_y \\ -\psi_x & \phi_x \end{bmatrix} \begin{bmatrix} \phi_V & \phi_\alpha \\ \psi_V & \psi_\alpha \end{bmatrix} \tag{12.41}$$

By performing the multiplications and using Eq. (12.36), it can be seen that Eq. (12.41) provides expressions for the derivatives in the hodograph plane. As an illustration, we will obtain an expression for $x_V$; however, first we evaluate the Jacobian of the transformation:

$$J = \phi_x\psi_y - \phi_y\psi_x = u\left(\frac{\rho}{\rho_o}u\right) - v\left(-\frac{\rho}{\rho_o}v\right) = \frac{\rho}{\rho_o}(u^2 + v^2) = \frac{\rho}{\rho_o}V^2$$

Now,

$$x_V = \frac{1}{J}(\psi_y\phi_V - \psi_V\phi_y) = \frac{\rho_o}{\rho V^2}\left(\frac{\rho}{\rho_o}u\phi_V - v\psi_V\right)$$

$$= \frac{u}{V^2}\phi_V - \frac{\rho_o}{\rho}\frac{v}{V^2}\psi_V = \frac{V\cos\alpha}{V^2}\phi_V - \frac{\rho_o}{\rho}\frac{V\sin\alpha}{V^2}\psi_V$$

Hence,

$$\frac{\partial x}{\partial V} = \frac{\cos\alpha}{V}\frac{\partial \phi}{\partial V} - \frac{\rho_o}{\rho}\frac{\sin\alpha}{V}\frac{\partial \psi}{\partial V} \tag{12.42}$$

Likewise,

$$\frac{\partial x}{\partial \alpha} = \frac{\cos\alpha}{V}\frac{\partial \phi}{\partial \alpha} - \frac{\rho_o}{\rho}\frac{\sin\alpha}{V}\frac{\partial \psi}{\partial \alpha} \tag{12.43}$$

$$\frac{\partial y}{\partial V} = \frac{\sin\alpha}{V}\frac{\partial \phi}{\partial V} + \frac{\rho_o}{\rho}\frac{\cos\alpha}{V}\frac{\partial \psi}{\partial V} \tag{12.44}$$

$$\frac{\partial y}{\partial \alpha} = \frac{\sin\alpha}{V}\frac{\partial \phi}{\partial \alpha} + \frac{\rho_o}{\rho}\frac{\cos\alpha}{V}\frac{\partial \psi}{\partial \alpha} \tag{12.45}$$

Now, since

$$\frac{\partial}{\partial \alpha}\left(\frac{\partial x}{\partial V}\right) = \frac{\partial}{\partial V}\left(\frac{\partial x}{\partial \alpha}\right) \tag{12.46}$$

and

$$\frac{\partial}{\partial \alpha}\left(\frac{\partial y}{\partial V}\right) = \frac{\partial}{\partial V}\left(\frac{\partial y}{\partial \alpha}\right) \tag{12.47}$$

we can perform the differentiations of this pair of equations to obtain two expressions relating the partial derivatives of $\phi$ and $\psi$ in the hodograph plane. However, these differentiations involve derivatives of the density ratio $\rho_o/\rho$. This ratio can be shown to be solely a function of $V$ as follows: From isentropic flow relations, we have

$$\frac{\rho_o}{\rho} = \left(\frac{T_o}{T}\right)^{1/(\gamma-1)} = \left(\frac{a_o^2}{a^2}\right)^{1/(\gamma-1)}$$

From the energy equation, we have

$$a_o^2 = a^2 + \frac{\gamma - 1}{2}V^2$$

Combining these expressions gives

$$\frac{\rho_o}{\rho} = \left(1 - \frac{\gamma - 1}{2}\frac{V^2}{a_o^2}\right)^{-[1/(\gamma-1)]} \tag{12.48}$$

As asserted, the density ratio varies only with $V$; therefore, the derivative of this ratio with respect to the flow angle $\alpha$ is zero. It is not hard to show (see Problem 12.11) that

$$\frac{\partial}{\partial V}\left(\frac{\rho_o}{\rho}\right) = \frac{d}{dV}\left(\frac{\rho_o}{\rho}\right) = \frac{\rho_o}{\rho}\frac{V}{a^2} \tag{12.49}$$

Performing the cross-differentiation required of Eqs. (12.46) and (12.47) yields, respectively,

$$-\frac{\sin\alpha}{V}\frac{\partial\phi}{\partial V}-\frac{\rho_o}{\rho}\frac{\cos\alpha}{V}\frac{\partial\psi}{\partial V}=-\frac{\cos\alpha}{V^2}\frac{\partial\phi}{\partial\alpha}+\frac{\rho_o}{\rho}\frac{\sin\alpha}{V^2}\frac{\partial\psi}{\partial\alpha}-\frac{\sin\alpha}{V}\frac{\rho_o}{\rho}\frac{V}{a^2}\frac{\partial\psi}{\partial\alpha} \tag{12.50}$$

$$\frac{\cos\alpha}{V}\frac{\partial\phi}{\partial V}-\frac{\rho_o}{\rho}\frac{\sin\alpha}{V}\frac{\partial\psi}{\partial V}=-\frac{\sin\alpha}{V^2}\frac{\partial\phi}{\partial\alpha}-\frac{\rho_o}{\rho}\frac{\cos\alpha}{V^2}\frac{\partial\psi}{\partial\alpha}+\frac{\cos\alpha}{V}\frac{\rho_o}{\rho}\frac{V}{a^2}\frac{\partial\psi}{\partial\alpha} \tag{12.51}$$

First, multiply Eq. (12.50) by cos $\alpha$ and Eq. (12.51) by sin $\alpha$ and add them together; then multiply Eq. (12.50) by sin $\alpha$ and Eq. (12.51) by cos $\alpha$ and subtract the latter from the former. This produces the following pair of equations, which are sometimes referred to as the *Chaplygin–Molenbroek equations*:

$$\frac{\partial\phi}{\partial\alpha}=\frac{\rho_o}{\rho}V\frac{\partial\psi}{\partial V} \tag{12.52}$$

$$\frac{\partial\phi}{\partial V}=-\frac{\rho_o}{\rho}\frac{1}{V}\left(1-\frac{V^2}{a^2}\right)\frac{\partial\psi}{\partial\alpha} \tag{12.53}$$

The velocity potential may be eliminated from the foregoing pair of equations by differentiating Eq. (12.52) with respect to $V$ and Eq. (12.53) with respect to $\alpha$. This operation produces a linear, second-order PDE for the stream function in the hodograph plane:

$$V\frac{\partial}{\partial V}\left(\frac{\rho_o}{\rho}V\frac{\partial\psi}{\partial V}\right)+\frac{\rho_o}{\rho}\left(1-\frac{V^2}{a^2}\right)\frac{\partial^2\psi}{\partial\alpha^2}=0$$

This equation can be rewritten as

$$V^2\frac{\partial^2\psi}{\partial V^2}+V\left(1+\frac{V^2}{a^2}\right)\frac{\partial\psi}{\partial V}+\left(1-\frac{V^2}{a^2}\right)\frac{\partial^2\psi}{\partial\alpha^2}=0 \tag{12.54}$$

Alternatively, we can eliminate $\psi$ from the Chaplygin–Molenbroek equations by differentiation with respect to $\alpha$ and V, respectively, to obtain a second-order, linear partial differential equation for the velocity potential $\phi$:

$$V^2\left(1-\frac{V^2}{a^2}\right)\frac{\partial^2\phi}{\partial V^2}+V\left(1+\gamma\frac{V^4}{a^4}\right)\frac{\partial\phi}{\partial V}+\left(1-\frac{V^2}{a^2}\right)^2\frac{\partial^2\phi}{\partial\alpha^2}=0 \tag{12.55}$$

It should be noted that in the physical plane, the velocity potential and the stream function equations have the same form. In the hodograph plane, however, these equations are found to be different from each other.

The obvious advantage in working with the transformed velocity potential equation is that it is linear. There are clear advantages—for example, various solutions can be combined—to working with a linear PDE. However, as mentioned previously, one of the difficulties with the hodograph method is that the boundary conditions within the physical plane are difficult to impose in the transformed plane. On the other hand, exact solutions for simple boundary conditions do exist.

**Example 12.5. Use of complex variables to perform the hodograph transformation**

Rederive the hodograph transformation by using complex variables.

**Solution**

Because the flow is two dimensional, complex variables may be effectively used to derive the hodograph equations. Begin by writing the following:

$$z = x + iy = r(\cos\theta + i\sin\theta) = re^{i\theta}$$

$$u + iv = V(\cos\alpha + i\sin\alpha) = Ve^{i\alpha}$$

Take the total derivative of $\phi$ and $\psi$ and use Eq. (12.34) to obtain

$$d\phi = \frac{\partial\phi}{\partial x}dx + \frac{\partial\phi}{\partial y}dy = udx + vdy$$

$$\frac{\rho_o}{\rho}d\psi = \frac{\rho_o}{\rho}\left(\frac{\partial\psi}{\partial x}dx + \frac{\partial\psi}{\partial y}dy\right) = -vdx + udy$$

Multiplying the latter equation by $i = \sqrt{-1}$ and combining the result with the expression for $d\phi$ yields

$$d\phi + i\frac{\rho_o}{\rho}d\psi = (u - iv)(dx + idy) = Ve^{-i\alpha}dz$$

Hence,

$$dz = \frac{e^{i\alpha}}{V}\left(d\phi + i\frac{\rho_o}{\rho}d\psi\right) = \frac{\partial z}{\partial V}dV + \frac{\partial z}{\partial\alpha}d\alpha$$

Replacing $d\phi$ and $d\psi$ by using Eq. (12.38) and comparing both sides of the resulting expression produces

$$\frac{\partial z}{\partial V} = \frac{e^{i\alpha}}{V}\left(\frac{\partial\phi}{\partial V} + i\frac{\rho_o}{\rho}\frac{\partial\psi}{\partial V}\right)$$

$$\frac{\partial z}{\partial\alpha} = \frac{e^{i\alpha}}{V}\left(\frac{\partial\phi}{\partial\alpha} + i\frac{\rho_o}{\rho}\frac{\partial\psi}{\partial\alpha}\right)$$

because

$$\frac{\partial}{\partial\alpha}\left(\frac{\partial z}{\partial V}\right) = \frac{\partial}{\partial V}\left(\frac{\partial z}{\partial\alpha}\right)$$

Perform the partial differentiation, cancel terms, and divide by $e^{i\alpha}$ to obtain

$$\frac{i}{V}\left(\frac{\partial\phi}{\partial V} + i\frac{\rho_o}{\rho}\frac{\partial\psi}{\partial V}\right) = -\frac{1}{V^2}\frac{\partial\phi}{\partial\alpha} + i\rho_o\frac{\partial}{\partial V}\left(\frac{1}{\rho V}\right)\frac{\partial\psi}{\partial\alpha}$$

Equating real and imaginary terms yields the following system of equations:

$$\frac{\partial\phi}{\partial V} = \frac{d}{dV}\left(\frac{\rho_o}{\rho V}\right)V\frac{\partial\psi}{\partial\alpha}$$

$$\frac{\partial\phi}{\partial\alpha} = \frac{\rho_o}{\rho}V\frac{\partial\psi}{\partial V}$$

Since $1/(\rho V)$ is a function of $V$, its derivative is easily found to be $-(1 - V^2/a^2)/\rho V^2$. (See Problem 12.6.) To obtain the hodograph equation in terms of $\psi$ [i.e., Eq. (12.54)], perform the following mixed differentiation:

$$\frac{\partial}{\partial \alpha}\left(\frac{\partial \phi}{\partial V}\right) = \frac{\partial}{\partial V}\left(\frac{\partial \phi}{\partial \alpha}\right)$$

---

**Example 12.6. An exact solution of the stream function PDE in the hodograph plane**

Obtain the exact solution of the stream function partial differential equation in the hodograph plane, Eq. (12.54), for the case in which $\psi = \psi(\alpha)$.

**Solution**

Equation (12.54) for this case reduces to

$$\frac{d^2\psi}{d\alpha^2} = 0$$

Hence, $\psi = C_1\alpha + C_2$. So,

$$\frac{\partial \psi}{\partial \alpha} = C_1 \quad \text{and} \quad \frac{\partial \psi}{\partial V} = 0$$

Insert these derivatives into Eqs. (12.52) and (12.53) to obtain expressions for the derivatives of the velocity potential:

$$\frac{\partial \phi}{\partial \alpha} = \frac{\rho_o}{\rho} V \frac{\partial \psi}{\partial V} = 0$$

$$\frac{\partial \phi}{\partial V} = -\frac{\rho_o}{\rho}\frac{1}{V}\left(1 - \frac{V^2}{a^2}\right)\frac{\partial \psi}{\partial \alpha} = -\frac{\rho_o}{\rho}\frac{1}{V}\left(1 - \frac{V^2}{a^2}\right)C_1$$

These derivatives in turn are inserted into Eqs. (12.42) and (12.43):

$$\frac{\partial x}{\partial V} = \frac{\cos\alpha}{V}\frac{\partial \phi}{\partial V} - \frac{\rho_o}{\rho}\frac{\sin\alpha}{V}\frac{\partial \psi}{\partial V} = -\frac{\rho_o}{\rho}\frac{\cos\alpha}{V^2}\left(1 - \frac{V^2}{a^2}\right)C_1 - 0$$

$$\frac{\partial x}{\partial \alpha} = \frac{\cos\alpha}{V}\frac{\partial \phi}{\partial \alpha} - \frac{\rho_o}{\rho}\frac{\sin\alpha}{V}\frac{\partial \psi}{\partial \alpha} = 0 - \frac{\rho_o}{\rho}\frac{\sin\alpha}{V}C_1$$

As we have seen, the density ratio is a function of $V$ only; therefore, the second expression can be directly integrated to obtain

$$x = \frac{\rho_o}{\rho}\frac{\cos\alpha}{V}C_1 + f(V)$$

This expression may be differentiated with respect to $V$, utilizing Eq. (12.49), to produce

$$\begin{aligned}\frac{\partial x}{\partial V} &= C_1 \frac{d}{dV}\left(\frac{\rho_o}{\rho}\right)\frac{\cos\alpha}{V} - C_1\left(\frac{\rho_o}{\rho}\right)\frac{\cos\alpha}{V^2} + \frac{df}{dV} \\ &= C_1\left(\frac{\rho_o}{\rho}\right)\frac{\cos\alpha}{a^2} - C_1\left(\frac{\rho_o}{\rho}\right)\frac{\cos\alpha}{V^2} + \frac{df}{dV} \\ &= -C_1\left(\frac{\rho_o}{\rho}\right)\frac{\cos\alpha}{V^2}\left(1 - \frac{V^2}{a^2}\right) + \frac{df}{dV}\end{aligned}$$

Comparing the result to $\partial x/\partial V$, we see that $df/dV = 0$. Hence, $f(V) = C_3$. So,

$$x = C_1 \frac{\rho_o}{\rho}\frac{\cos\alpha}{V} + C_3$$

Proceeding in a like manner with the derivatives of $y$ in Eqs. (12.44) and (12.45), it is not hard to show that

$$y = C_1 \frac{\rho_o}{\rho}\frac{\sin\alpha}{V} + C_4$$

We can set the constants $C_3$ and $C_4$ to zero, since they represent coordinate translations, and we can set $C_2$ to zero, because it only rotates the value of $\psi$. Consequently, taking the ratio of $y/x$, we find that

$$\frac{y}{x} = \frac{C_1 \dfrac{\rho_o}{\rho}\dfrac{\sin\alpha}{V}}{C_1 \dfrac{\rho_o}{\rho}\dfrac{\cos\alpha}{V}} = \tan\alpha$$

Therefore,

$$\psi = C_1\alpha = C_1 \tan^{-1}\left(\frac{y}{x}\right) = C_1\theta$$

As a result, the flow inclination $\alpha$ for this case is always in the direction of a line through the origin and the point $(x, y)$—that is, in the radial direction. This flow is, of course, the source/sink flow that we examined in the previous section. Now,

$$r^2 = x^2 + y^2 = \left(C_1 \frac{\rho_o}{\rho}\frac{\cos\theta}{V}\right)^2 + \left(C_1 \frac{\rho_o}{\rho}\frac{\sin\theta}{V}\right)^2 = C_1^2\left(\frac{\rho_o}{\rho}\right)^2 \frac{1}{V^2}$$

so that

$$V = C_1 \frac{\rho_o}{\rho}\frac{1}{r}$$

Utilizing Eq. (12.48), a relationship between the density ratio and the total speed, we have

$$V\left(1 - \frac{\gamma - 1}{2}\frac{V^2}{a_o^2}\right)^{1/(\gamma-1)} = \frac{C_1}{r}$$

An expression for the velocity potential may be developed from

$$\frac{\partial \phi}{\partial V} = -\frac{\rho_o}{\rho}\frac{1}{V}\left(1 - \frac{V^2}{a^2}\right)C_1$$

Since all terms on the right-hand side depend upon $V$, we may write

$$\phi = -C_1 \int \frac{\rho_o}{\rho}\left(1 - \frac{V^2}{a^2}\right)\frac{dV}{V}$$

---

There is a wealth of information that has been written about the hodograph method and various approaches in which it has been used to solve compressible flow problems. For example, refer to Refs. (12.11)–(12.16). As has been noted, the technique has fallen out of favor because computational techniques are able to deal directly with the nonlinearities, and therefore there is no need to linearize the governing equation. Nevertheless, any serious student of compressible flow is advised to spend some time becoming familiar with the hodograph method and the variety of analytical techniques that were developed to solve an assortment of compressible flow problems.

## 12.4 FLOWS AROUND CORNERS

In this section, we investigate an exact compressible flow solution of the flow around a corner. In particular, we reconsider supersonic flow around a convex corner (i.e., Prandtl–Meyer flow). This two-dimensional, steady, isentropic flow was the subject of Chapter 7. However, the analysis proceeds from a somewhat different perspective than that presented previously, as greater detail regarding the flow field will be provided. This will be accomplished by using the velocity potential equation written in polar coordinates.

As shown in Figure 12.7, the flow is turned through an angle $\Delta$. The flow field may be divided into three parts: two regions of uniform flow, in which the streamlines are straight and parallel to the bounding surfaces, and a pie-shaped expansion region, separating the uniform-flow regions, in which the streamlines are curved. The origin of the expansion region is at the corner of the bounding surface. The kinematic and thermodynamic variables of the flow vary within the expansion region.

The geometry and notation used in the analysis of the expansion region are illustrated in Figure 12.8. It should be noted that by standard convention, the polar angle $\theta$ and the tangential velocity component $v_\theta$ are positive in the counterclockwise (CCW) direction.

The flow within the expansion fan may be described in terms of the radius $r$ and the flow angle $\theta$. However, reference to Figure 12.8 reveals that there is no apparent characteristic length scale for this flow. As a result, the radius cannot be nondimensionalized, which in turn suggests that the flow is not described in terms of a length variable. Such flows are not uncommon in fluid dynamics [e.g., the flow due to a suddenly accelerated plane wall (Stokes's first problem), laminar boundary-layer flow, and flow near a rotating disk]. Such flows, called *self-similar flows*, can be analyzed by combining the independent variables into a single variable, which results in the replacement of the governing partial differential equation(s) with an ordinary differential equation(s).

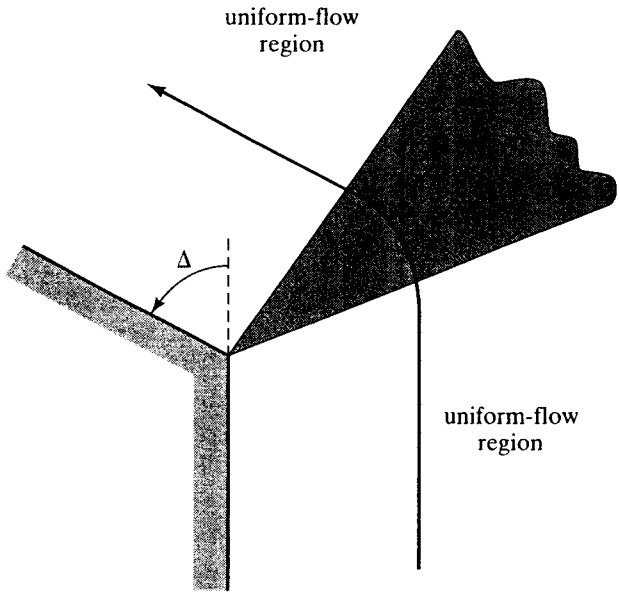


**Figure 12.7** Supersonic Flow around a Convex Corner

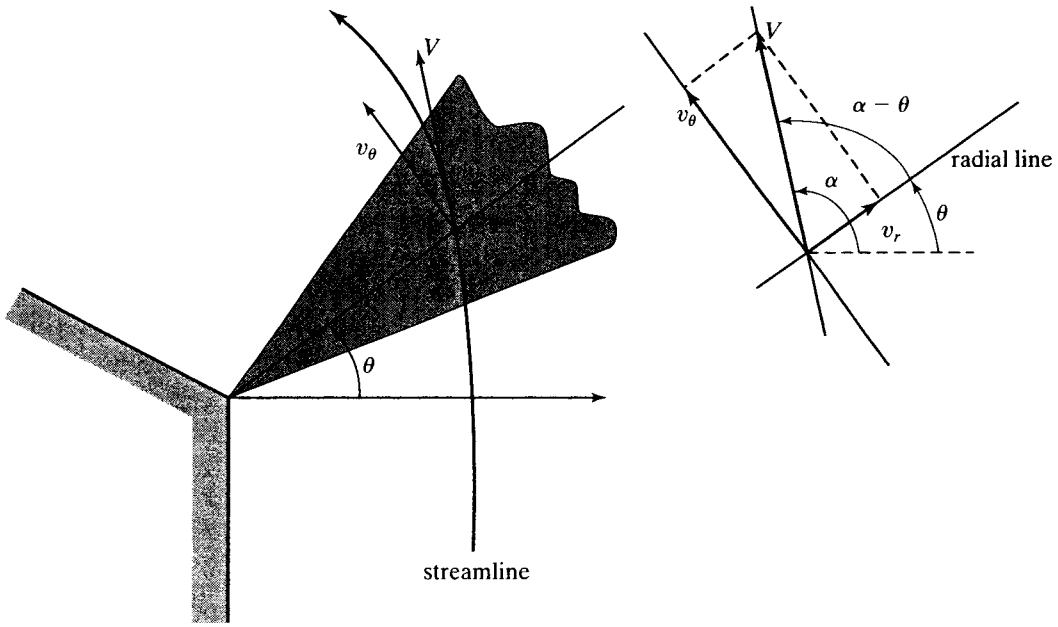


**Figure 12.8** Geometry of Supersonic Flow around a Corner

Here, we assume that the radial and tangential velocity components $v_r$ and $v_\theta$, respectively, as well as the pressure $p$, density $\rho$, and speed of sound $a$, depend only on the flow angle $\theta$. (That is, they do not depend on the distance from the corner.) The flow angle can be written as $\theta = \tan^{-1}(y/x)$, and therefore it is seen that $\theta$ does indeed combine independent variables $x$ and $y$ into a

single variable. The flow is assumed to be irrotational, so we begin with the following [refer to Eq. (11.60)]:

$$\frac{\partial(rv_\theta)}{\partial r} - \frac{\partial(v_r)}{\partial \theta} = v_\theta + r\frac{\partial v_\theta}{\partial r} - \frac{\partial v_r}{\partial \theta} = 0$$

Because the velocity components do not depend upon $r$, this equation reduces to

$$v_\theta - \frac{dv_r}{d\theta} = 0 \tag{12.56}$$

The radial velocity component is given by the following (note that $\phi$ is not taken to be independent of $r$):

$$v_r = \frac{\partial \phi}{\partial r} = v_r(\theta)$$

Integration brings

$$\phi = v_r r + g(\theta)$$

Differentiation of this expression with respect to the polar angle $\theta$ and use of Eq. (12.56) yields

$$\frac{\partial \phi}{\partial \theta} = r\frac{dv_r}{d\theta} + \frac{dg}{d\theta} = rv_\theta + \frac{dg}{d\theta} = r\left(\frac{1}{r}\frac{\partial \phi}{\partial \theta}\right) + \frac{dg}{d\theta} = \frac{\partial \phi}{\partial \theta} + \frac{dg}{d\theta}$$

Therefore, it is seen that $dg/d\theta = 0$, or $g =$ constant. We may set this constant to zero, since it will affect only the magnitude of the velocity potential and have no effect upon the flow variables. Consequently, the velocity potential for this flow has the form

$$\phi = v_r r$$

which is the same expression as that for uniform flow at an angle. [See Eq. (12.3).] Thus, the velocity potential has the same form for all three regions of the flow. For the uniform-flow regions, the velocity potential may be written as

$$\phi = rV\cos\left(\theta - \frac{\pi}{2}\right)$$

$$\phi = rV\cos\left(\theta - \frac{\pi}{2} - \Delta\right)$$

It is not difficult to determine the velocity components ($v_r$, $v_\theta$, $u$, and $v$) within the uniform-flow regions. (See Problem 12.2.)

The flow within the expansion region is described through the velocity potential equation, written in polar coordinates [i.e., the two-dimensional version of Eq. (11.61)], as

$$\left(1 - \frac{v_r^2}{a^2}\right)\frac{\partial v_r}{\partial r} + \left(1 - \frac{v_\theta^2}{a^2}\right)\frac{1}{r}\frac{\partial v_\theta}{\partial \theta} - \frac{v_r v_\theta}{a^2}\frac{1}{r}\left[\frac{\partial(rv_\theta)}{\partial r} + \frac{\partial v_r}{\partial \theta}\right] + \left(1 + \frac{v_\theta^2}{a^2}\right)\frac{v_r}{r} = 0$$

Eliminating radial dependence and utilizing Eq. (12.56) yields

$$(v_\theta^2 - a^2)\left(\frac{dv_\theta}{d\theta} + v_r\right) = 0 \tag{12.57}$$

The reduced momentum equation in the tangential direction is

$$\rho v_\theta\left(\frac{dv_\theta}{d\theta} + v_r\right) = -\frac{dp}{d\theta}$$

In order for the static pressure gradient not to vanish in the angular direction, it is clear that $dv_\theta/d\theta + v_r \neq 0$. Consequently, Eq. (12.57) informs us that within the expansion region,

$$v_\theta \equiv a$$

From the inset in Figure 12.8, it can be seen that $v_\theta = V\sin(\alpha - \theta) = a$. Consequently,

$$\sin(\alpha - \theta) = \frac{1}{M}$$

Hence,

$$\alpha - \theta = \sin^{-1}\left(\frac{1}{M}\right) = \mu$$

where $\mu$ is the Mach angle. Since the velocity, **V**, is tangent to a streamline, it is clear that the angle between the streamline and a radial line within the expansion region is the Mach angle. Therefore, all radial lines within the expansion region are Mach waves. The leading Mach wave is inclined at an angle $\theta_1 = \pi/2 - \mu_1$, where $\mu_1 = \sin^{-1}(1/M_1)$.

To determine expressions for the velocity components within the expansion region, start with the energy equation written as

$$a_o^2 = a^2 + \frac{\gamma - 1}{2}V^2 = \frac{\gamma - 1}{2}V_{\max}^2 = v_\theta^2 + \frac{\gamma - 1}{2}(v_r^2 + v_\theta^2)$$

Note that we have used Eq. (12.13) to obtain this expression. Rearranging yields

$$V_{\max}^2 = v_r^2 + \frac{\gamma - 1}{\gamma + 1}v_\theta^2$$

Combining this expression with Eq. (12.56) results in the first-order differential equation

$$\frac{dv_r}{d\theta} = b\sqrt{V_{\max}^2 - v_r^2}$$

where $b^2 = (\gamma - 1)/(\gamma + 1)$. This equation may be directly integrated to obtain

$$v_r = V_{\max} \sin b\theta + \text{constant}$$

The boundary condition at the leading edge of the expansion region, *viz.*, $v_r = v_{r1}$ at $\theta = \theta_1$, may be used to evaluate the constant. This evaluation results in

$$v_r = V_{\max} \sin\left[ b(\theta - \theta_1) + \sin^{-1}\left(\frac{v_{r1}}{V_{\max}}\right)\right] \tag{12.58}$$

This is a somewhat awkward expression that can be rewritten as

$$v_r = V_{\max} \sin b(\theta + \theta_{\text{ref}}) \tag{12.59}$$

where

$$\theta_{\text{ref}} = -\theta_1 + \frac{1}{b}\sin^{-1}\left(\frac{v_{r1}}{V_{\max}}\right) = -\left(\frac{\pi}{2} - \mu_1\right) + \frac{1}{b}\sin^{-1}\left(\frac{v_{r1}}{V_{\max}}\right) \tag{12.60}$$

Note that at $\theta = -\theta_{\text{ref}}$, $v_r = 0$, and since $v_\theta = a$, $M = 1$. This reference location is artificial unless $M_1 = 1$. Nevertheless, the use of this mathematical artifice greatly simplifies the relations within the expansion region. The tangential velocity distribution within the expansion region may be readily determined from

$$v_\theta = \frac{dv_r}{d\theta} = bV_{\max} \cos b(\theta + \theta_{\text{ref}}) = a \tag{12.61}$$

Using Eqs. (12.59) and (12.61), we may write the expansion fan Mach number distribution as

$$M^2 = \frac{V^2}{a^2} = \frac{v_r^2 + v_\theta^2}{v_\theta^2} = 1 + \frac{v_r^2}{v_\theta^2} = 1 + \left[\frac{V_{\max} \sin b(\theta + \theta_{\text{ref}})}{bV_{\max} \cos b(\theta + \theta_{\text{ref}})}\right]^2$$

$$= 1 + \frac{1}{b^2}\tan^2 b(\theta + \theta_{\text{ref}})$$

Hence,

$$\sqrt{M^2 - 1} = \frac{1}{b}\tan b(\theta + \theta_{\text{ref}}) \tag{12.62}$$

so that

$$\theta + \theta_{\text{ref}} = \frac{1}{b}\tan^{-1}\left(b\sqrt{M^2 - 1}\right) \tag{12.63}$$

Figure 12.9 presents the velocity triangle at a point within the expansion fan that is shown in the inset of Figure 12.8. Note that all velocities have been divided by the speed of sound to form Mach numbers.

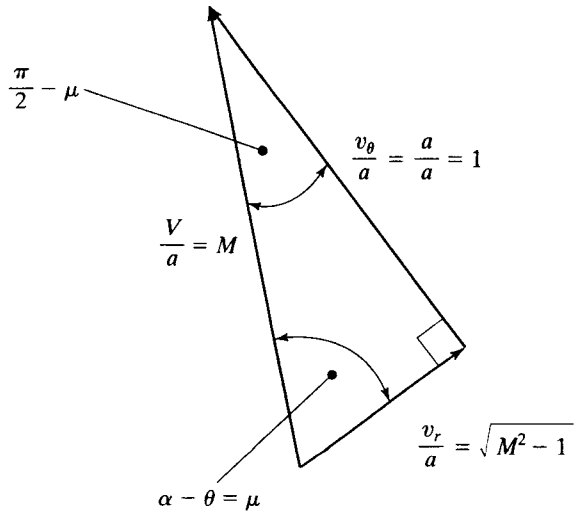


**Figure 12.9** Velocity Triangle at a Point within the Expansion Region

From Figure 12.9 and Eq. (12.62), it is evident that

$$\tan\left(\frac{\pi}{2} - \mu\right) = \frac{v_r/a}{v_\theta/a} = \sqrt{M^2 - 1} = \frac{1}{b}\tan b(\theta + \theta_{\text{ref}}) \tag{12.64}$$

The angle through which the flow is turned relative to the velocity direction at the reference angle (since the reference line is a radial line on which $v_r = 0$ and $v_\theta = a$, the velocity at this location is sonic and its direction is perpendicular to the radial line) is called the *deviation* and is written as

$$\nu = (\theta + \theta_{\text{ref}} + \mu) - \frac{\pi}{2} \tag{12.65}$$

As shown in Figure 12.10, the first group of terms, $\theta + \theta_{\text{ref}} + \mu$, is the angular distance from the reference line at $\theta = -\theta_{\text{ref}}$ to the velocity vector $\mathbf{V}$; the $\pi/2$ is the angular distance from the reference line to the velocity vector at the reference line.

Combining Eq. (12.65) with Eqs. (12.63) and (12.64) gives

$$\nu = (\theta + \theta_{\text{ref}}) - \left(\frac{\pi}{2} - \mu\right) = \frac{1}{b}\tan^{-1}\left(b\sqrt{M^2 - 1}\right) - \tan^{-1}\left(\sqrt{M^2 - 1}\right)$$

$$= \sqrt{\frac{\gamma + 1}{\gamma - 1}}\tan^{-1}\left(\sqrt{\frac{\gamma - 1}{\gamma + 1}}\sqrt{M^2 - 1}\right) - \tan^{-1}\left(\sqrt{M^2 - 1}\right) \tag{12.66}$$

This is the expression for the Prandtl–Meyer function that was developed and utilized in Chapter 7. The Prandtl–Meyer function, or the deviation at the leading edge of the expansion region, is $\nu_1 = \theta_1 + \theta_{\text{ref}} + \mu_1 - \pi/2$. Since the flow is turned through an angle $\Delta$, the Prandtl–Meyer function at the trailing edge of the expansion region is $\nu_2 = \nu_1 + \Delta$.

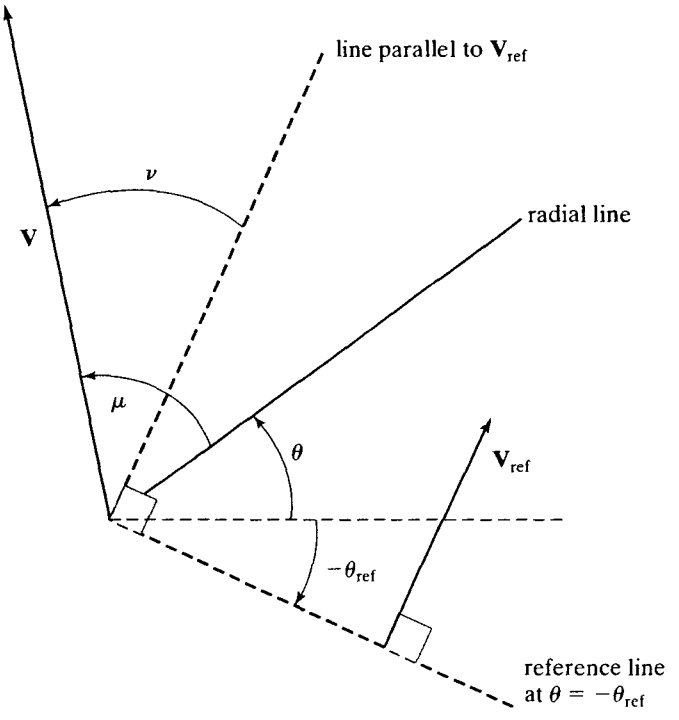


**Figure 12.10** Geometric Arrangement to Determine the Deviation Angle within the Expansion Region

To determine the location of the radial velocity component at the leading edge of the expansion region is first computed from

$$\frac{v_{r1}}{V_{max}} = \frac{V_1}{V_{max}}\sin\theta_1 = \frac{V_1}{a_1}\frac{a_1}{\sqrt{\frac{2}{\gamma-1}}a_o}\sin\left(\frac{\pi}{2}-\mu_1\right)$$

$$= M_1\sqrt{\frac{1}{\frac{2}{\gamma-1}+M_1^2}}\cos\mu_1 = \sqrt{\frac{M_1^2-1}{\frac{2}{\gamma-1}+M_1^2}}$$

Accordingly, from Eq. (12.60), we have

$$\theta_{ref} = -\left[\frac{\pi}{2} - \sin^{-1}\left(\frac{1}{M_1}\right)\right] + \sqrt{\frac{\gamma+1}{\gamma-1}}\sin^{-1}\left(\sqrt{\frac{M_1^2-1}{\frac{2}{\gamma-1}+M_1^2}}\right) \tag{12.67}$$

Hence, given $M_1$ and $\gamma$, $\theta_{ref}$, $\mu_1$, $\theta_1$, and $v_{r1}$ can all be directly determined.

To obtain the distribution of the thermodynamic variables, we begin with the continuity equation in polar coordinates:

$$\frac{\partial(\rho r v_r)}{\partial r} + \frac{\partial(\rho v_\theta)}{\partial \theta} = 0$$

The reduced version of this equation for Prandtl–Meyer flow is

$$\rho v_r + \frac{d(\rho v_\theta)}{d\theta} = 0$$

Making use of Eqs. (12.58) and (12.59) and rearranging yields

$$\int_{\rho^*}^{\rho} \frac{d\rho}{\rho} = \int_{-\theta_{\text{ref}}}^{\theta} \frac{b^2 \sin b(\theta + \theta_{\text{ref}}) - \sin b(\theta + \theta_{\text{ref}})}{b \cos b(\theta + \theta_{\text{ref}})} d\theta$$

$$= \left(\frac{b^2 - 1}{b}\right) \int_{-\theta_{\text{ref}}}^{\theta} \frac{\sin b(\theta + \theta_{\text{ref}})}{\cos b(\theta + \theta_{\text{ref}})} d\theta$$

Note that at $\theta = -\theta_{\text{ref}}$ (the reference line), the flow is sonic, and therefore $\rho = \rho^*$. Integrating and defining $\beta = 1/(\gamma - 1) = -(b^2 - 1)/(2b^2)$, we get

$$\frac{\rho}{\rho^*} = \cos^{2\beta} b(\theta + \theta_{\text{ref}}) \tag{12.68}$$

Employing the isentropic relation between density and the speed of sound (or static temperature), we find

$$\frac{a}{a^*} = \left(\frac{\rho}{\rho^*}\right)^{1/2\beta} = \left(\frac{\rho}{\rho^*}\right)^{(\gamma-1)/2} = \cos b(\theta + \theta_{\text{ref}}) \tag{12.69}$$

This expression can also be obtained from Eq. (12.61), since at $\theta = -\theta_{\text{ref}}$, $M = 1$, and therefore $a^* = bV_{\max}$. Using the perfect-gas relation, we may obtain the static pressure ratio:

$$\frac{p}{p^*} = \left(\frac{\rho}{\rho^*}\right)\left(\frac{T}{T^*}\right) = \left(\frac{\rho}{\rho^*}\right)\left(\frac{a}{a^*}\right)^2 = \cos^{2\beta+2} b(\theta + \theta_{\text{ref}}) \tag{12.70}$$

**Example 12.7. Shape of the streamlines in Prandtl–Meyer flow**

Determine the equation for the streamlines in supersonic flow around a convex corner.

**Solution**

The streamlines are lines of constant stream function. To determine the stream function, we use

$$v_r = \frac{\rho^*}{\rho}\frac{1}{r}\frac{\partial \psi}{\partial \theta} = V_{\max} \sin b(\theta + \theta_{\text{ref}})$$

$$v_\theta = -\frac{\rho^*}{\rho}\frac{\partial \psi}{\partial r} = bV_{\max} \cos b(\theta + \theta_{\text{ref}})$$

Integrating the foregoing, using the expression for the density ratio in Eq. (12.68), leads to

$$\psi = -[bV_{\max} \cos^{2\beta+1} b(\theta + \theta_{\text{ref}})]r$$

where the constant of integration has been set to zero. Since $2\beta + 1 = 1/b^2$, this expression can be written as

$$-\frac{\psi}{bV_{\max}} = [\cos^{2\beta+1} b(\theta + \theta_{\text{ref}})]r$$

Now at $\theta = -\theta_{\text{ref}}$, $r = r^*$, and therefore the foregoing equation becomes

$$\frac{r}{r^*} = \left[\frac{1}{\cos b(\theta + \theta_{\text{ref}})}\right]^{1/b^2}$$

---

Exact solutions of other compressible flows around corners exist. For example, in Ref. (12.2), Bickley describes two-dimensional flow past a convex boundary, as well as transitional flow from radial to uniform flow. The flow around a 180° bend (flow about the edge of a plate) is known as *Ringleb flow* and is described in Refs. (12.17) and (12.18).

## 12.5 CONICAL FLOW

For supersonic flow about a right circular cone at zero angle of attack with the oncoming stream, a conical shock is attached to the apex of the cone for small cone angles.

It is interesting to compare the resultant wedge and cone flows. (See Figure 12.11.) For a wedge, straight parallel flow exists both before and after the oblique shock. For the three-dimensional semi-infinite cone, this is not possible; streamlines after the conical shock must be curved in order for the three-dimensional continuity equation to be satisfied.

At each point on the conical shockwave, the oblique-shock equations presented in Chapter 6 are valid. Conical flow behind the wave is isentropic, with the static pressure increasing to the cone surface pressure. A solution for the conical shock thus requires fitting the isentropic compression behind the shock to the shock equations already derived.

Whereas the conical flow equations yield two shock solutions, the only one observed on an isolated conical body is the weak shock. As with wedge flow, for large-enough cone angles there is no solution; the shock stands detached from the cone.

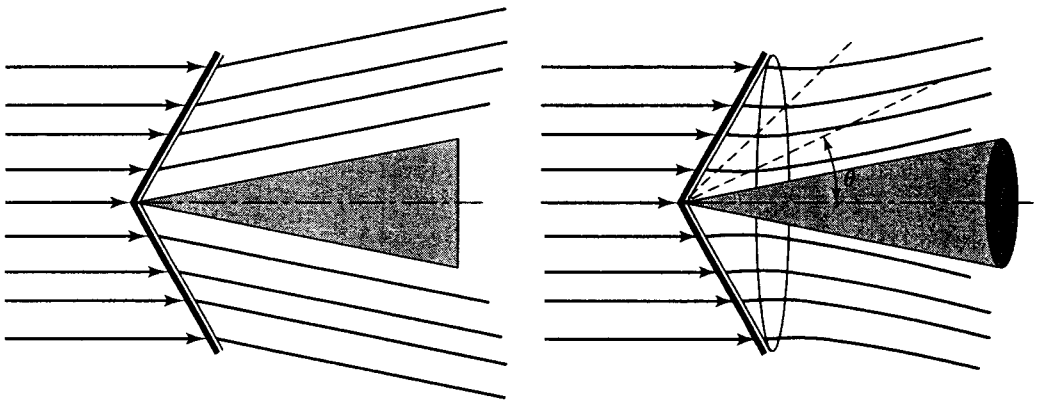

(a) Wedge (b) Cone

**Figure 12.11** Contrast of Supersonic Flow past a Two-Dimensional Wedge and an Axisymmetric Cone

For axisymmetric flow about a semi-infinite cone, with no characteristic length along the cone surface, conditions after the shock are dependent only on one conical coordinate: *the azimuthal angle* $\theta$. That is, along each radial line of constant $\theta$, the flow pressure, velocity, and so on, are constant. This condition indicates that the pressure on the surface of the cone after the shock is constant, independent of distance from the cone apex.

Taylor and Maccoll [Refs. (12.19) and (12.20)] solved the resultant nonlinear differential equations numerically for three cone angles, using a mechanical calculator. The solutions were tabulated by Kopal [Ref. (10.21)] and later by Sims [Ref. (10.22)].

Because the flow is axisymmetric, spherical coordinates can be used to analyze the flow between the shock and the cone. Figure 12.12 shows a cone within the coordinate system.

Symmetry about the $z$-axis requires that the flow be independent of the *meridional angle* $\varphi$. Consequently, expressions for the velocity potential, irrotational flow, and the

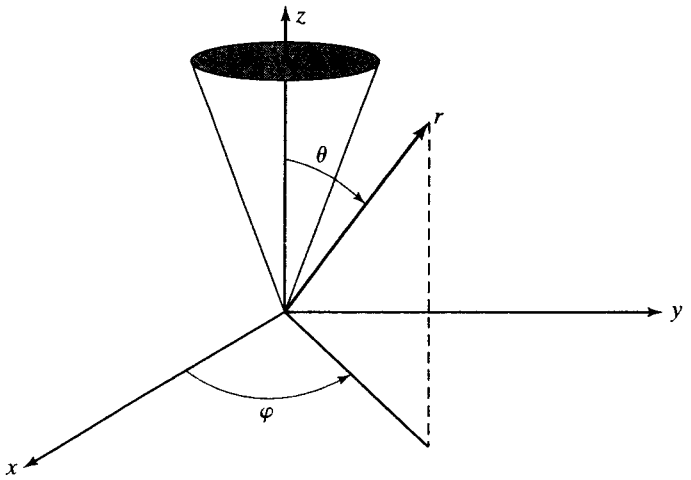


**Figure 12.12** Spherical Coordinate System

energy equations [Eqs. (11.64) to (11.67)] are respectively written in reduced form as follows:

$$v_r = \frac{\partial \phi}{\partial r}, \; v_\theta = \frac{1}{r}\frac{\partial \phi}{\partial \theta}, \; v_\varphi = 0 \tag{12.71}$$

$$\frac{1}{r}\left[\frac{\partial (r v_\theta)}{\partial r} - \frac{\partial v_r}{\partial \theta}\right] = 0 \tag{12.72}$$

$$\left(1 - \frac{v_r^2}{a^2}\right)\frac{\partial v_r}{\partial r} + \left(1 - \frac{v_\theta^2}{a^2}\right)\frac{1}{r}\frac{\partial v_\theta}{\partial \theta} - \frac{v_r v_\theta}{a^2}\frac{1}{r}\left[\frac{\partial (r v_\theta)}{\partial r} + \frac{\partial v_r}{\partial \theta}\right]$$
$$+ \left(2 + \frac{v_\theta^2}{a^2}\right)\frac{v_r}{r} + \frac{v_\theta \cot \theta}{r} = 0 \tag{12.73}$$

$$a^2 = a_o^2 - \frac{\gamma - 1}{2}(v_r^2 + v_\theta^2) \tag{12.74}$$

Now, as in Prandtl–Meyer flow as discussed in the previous section, it is assumed that the flow variables do not depend upon the distance from the apex of the cone. The removal of radial dependence is based on the notion that there is no apparent length scale with which to nondimensionalize the radial coordinate. Accordingly, the velocity components depend only upon the azimuthal angle $\theta$. Hence, Eqs. (12.72) and (12.73) are further reduced to the following, respectively:

$$v_\theta - \frac{dv_r}{d\theta} = 0 \tag{12.75}$$

$$(a^2 - v_\theta^2)\frac{dv_\theta}{d\theta} - v_r v_\theta\left(v_\theta + \frac{dv_r}{d\theta}\right) + (2a^2 + v_\theta^2)v_r + v_\theta a^2 \cot \theta = 0 \tag{12.76}$$

The tangential velocity component in Eq. (12.76) may be replaced using Eq. (12.75) to obtain a second-order, nonlinear, ordinary differential equation with variable coefficients

$$A\frac{d^2 v_r}{d\theta^2} + B\frac{dv_r}{d\theta} + C v_r = 0 \tag{12.77}$$

where

$$A = a^2 - v_\theta^2 = a^2 - \left(\frac{dv_r}{d\theta}\right)^2$$
$$B = a^2 \cot \theta$$
$$C = 2a^2 - v_\theta^2 = a^2 + A$$

Equation (12.77) is often referred to as the *Taylor–Maccoll equation*. Unfortunately, this equation cannot be solved analytically. On the other hand, a numerical solution, using procedures described in Chapters 9 and 10, is not difficult to construct. To accomplish this, the second-order equation must first be rewritten as a pair of first-order differential equations. Thus, Eq. (12.77) is rearranged and, along with Eq. (12.75), forms the following pair of equations:

$$\frac{dv_r}{d\theta} = v_\theta$$

$$\frac{dv_\theta}{d\theta} = -v_r + \frac{a^2(v_r + v_\theta \cot\theta)}{(v_\theta^2 - a^2)} \tag{12.78}$$

The energy equation in Eq. (12.74), which is written in terms of the speed of sound, can be expressed as

$$a^2 = \frac{\gamma - 1}{2}(V_{\max}^2 - V^2) = \frac{\gamma - 1}{2}[V_{\max}^2 - (v_r^2 + v_\theta^2)] \tag{12.79}$$

To facilitate the numerical solution, all velocity terms within the governing expressions will be nondimensionalized using $V_{\max}$ as the characteristic velocity. A bar over the velocity component is used to signify a nondimensional quantity. So, we have

$$\bar{v}_\theta \equiv \frac{v_\theta}{V_{\max}} \text{ and } \bar{v}_r \equiv \frac{v_r}{V_{\max}}$$

Consequently, Eqs. (12.78) and (12.79) are combined and written as

$$\frac{d\bar{v}_r}{d\theta} = \bar{v}_\theta$$

$$\frac{d\bar{v}_\theta}{d\theta} = -\bar{v}_r + \frac{\frac{\gamma - 1}{2}[1 - (\bar{v}_r^2 + \bar{v}_\theta^2)](\bar{v}_r + \bar{v}_\theta \cot\theta)}{\left\{\bar{v}_\theta^2 - \frac{\gamma - 1}{2}[1 - (\bar{v}_r^2 + \bar{v}_\theta^2)]\right\}} \tag{12.80}$$

To solve this pair of initial-value problems, two initial values (or in this application, two boundary conditions at the same angular location) are required. Since the oblique shock lies along a radial line, the velocity components on the downstream side of the shock (signified by a subscript of 2) may be written from Eqs. (6.7a) and (6.7b) at the angular location $\theta = \theta_s$ as follows:

$$\bar{v}_\theta = -\bar{V}_{n2} = -\bar{V}_2 \sin(\theta_s - \delta_s) \tag{12.81}$$

$$\bar{v}_r = \bar{V}_t = \bar{V}_2 \cos(\theta_s - \delta_s) \tag{12.82}$$

The minus sign that appears in Eq. (12.81) is due to the fact that the angular velocity component and the normal velocity component to the shock are in opposite directions. The quantity $\delta_s$ is the deflection of the flow at the shock location. For a wedge problem, $\delta_s$ is the wedge half-angle, as illustrated in Figure 12.11; for the cone, $\delta_s$ is not the cone half-angle.

The computations may commence at the shock and proceed in small increments of $\Delta\theta$ toward the cone surface. At the cone surface, which is also a radial line at $\theta = \theta_c$, the tangential velocity must vanish:

$$\overline{v}_\theta = 0 \tag{12.83}$$

Generally, in problems involving a compressible flow past a cone at zero angle of attack, we are given the freestream Mach number, say, $M_1$, and the cone half-angle $\delta_c$. These initial data present a minor problem because the value of shock angle $\theta_s$ needed in Eqs. (12.81) and (12.82) to determine the initial velocity components is not known, and there is no clear connection between the cone half-angle and the angle of the shock. Accordingly, in the solution strategy, we assume a value of $\theta_s$ and perform the computations until the condition of Eq. (12.83) is reached. This approach to solving initial-value problems is sometimes referred to as a *shooting method*. A typical computation proceeds beyond the value $\theta = \theta_c$, and interpolation is used to determine the cone half-angle. Of course, more than likely, the value $\theta_c$ that is obtained will not be the value that was specified in the problem, and therefore another shock angle must be assumed and the calculations repeated until the desired cone half-angle is obtained.

When the computations are started on the downstream side of the shock and proceed towards the cone, the procedure is often referred to as the *inverse method*. The method has this name because the geometric boundary is determined as part of the computations. The alternative method is to originate the computations at the cone surface and proceed towards the shock. This procedure is often called the *direct method*, because we are beginning the computations from the actual geometry.

In the direct method, we must assume a value for the radial velocity component at the cone surface and proceed in small increments of $\Delta\theta$ towards the shock. For this problem, either method is just as easy to implement; we will use the inverse method here.

The energy equation, Eq. (12.79), may be used to connect the velocity and Mach number anywhere within the conical computation region. Simply divide Eq. (12.79) by the velocity to obtain

$$\frac{a^2}{V^2} = \frac{1}{M^2} = \frac{\gamma - 1}{2}\left(\frac{V_{\max}^2}{V^2} - 1\right) = \frac{\gamma - 1}{2}\left(\frac{1}{\overline{V}^2} - 1\right)$$

or

$$\overline{V} = \frac{1}{\sqrt{1 + \dfrac{2}{(\gamma - 1)M^2}}} \tag{12.84}$$

From the freestream Mach number $M_1$ and the assumed value of the shock angle $\theta_s$ we may use the oblique-shock relations, Eqs. (6.17) and (6.18), as well as Eq. (12.84) to determine the conditions of the flow on the downstream side of the shock:

$$M_2^2 = \frac{1 + \dfrac{\gamma - 1}{2} M_1^2}{\gamma M_1^2 \sin^2\theta_s - \dfrac{(\gamma - 1)}{2}} + \frac{M_1^2 \cos^2\theta_s}{1 + \dfrac{\gamma - 1}{2} M_1^2 \sin^2\theta_s} \tag{12.85}$$

$$\overline{V}_2 = \frac{1}{\sqrt{1 + \dfrac{2}{(\gamma - 1)M_2^2}}} \tag{12.86}$$

$$\tan\delta_s = \cot\theta_s \frac{M_1^2 \sin^2\theta_s - 1}{\dfrac{\gamma + 1}{2} M_1^2 - (M_1^2 \sin^2\theta_s - 1)} \tag{12.87}$$

Therefore, Eqs. (12.81) and (12.82) provide the initial values that are used to begin the numerical solution of the governing pair of ordinary differential equations. Rewrite Eq. (12.80) as

$$\begin{aligned} \frac{d\overline{v}_r}{d\theta} &= \overline{v}_\theta \\ \frac{d\overline{v}_\theta}{d\theta} &= f(\overline{v}_r, \overline{v}_\theta) \end{aligned} \tag{12.88}$$

where

$$f(\overline{v}_r, \overline{v}_\theta) = -\overline{v}_r + \frac{\dfrac{\gamma - 1}{2}[1 - (\overline{v}_r^2 + \overline{v}_\theta^2)](\overline{v}_r + \overline{v}_\theta \cot\theta)}{\left\{\overline{v}_\theta^2 - \dfrac{\gamma - 1}{2}[1 - (\overline{v}_r^2 + \overline{v}_\theta^2)]\right\}}$$

As was discussed in Chapter 9, many numerical solution methods are available to solve ordinary differential equations. Here, we use a predictor–corrector scheme known as the *modified Euler method* in which Eq. (12.88) is rewritten for the predictor step as

$$\begin{aligned} (\overline{v}_r)_p &= (\overline{v}_r)_i - (\overline{v}_\theta)_i \Delta\theta \\ (\overline{v}_\theta)_p &= (\overline{v}_\theta)_i - f[(\overline{v}_r)_i, (\overline{v}_\theta)_i]\Delta\theta \end{aligned} \tag{12.89}$$

The grid system for the computations is shown in Figure 12.13. Note that the minus sign which appears in Eq. (12.89) is due to the fact that the solution direction is opposite to the $\theta$ direction.

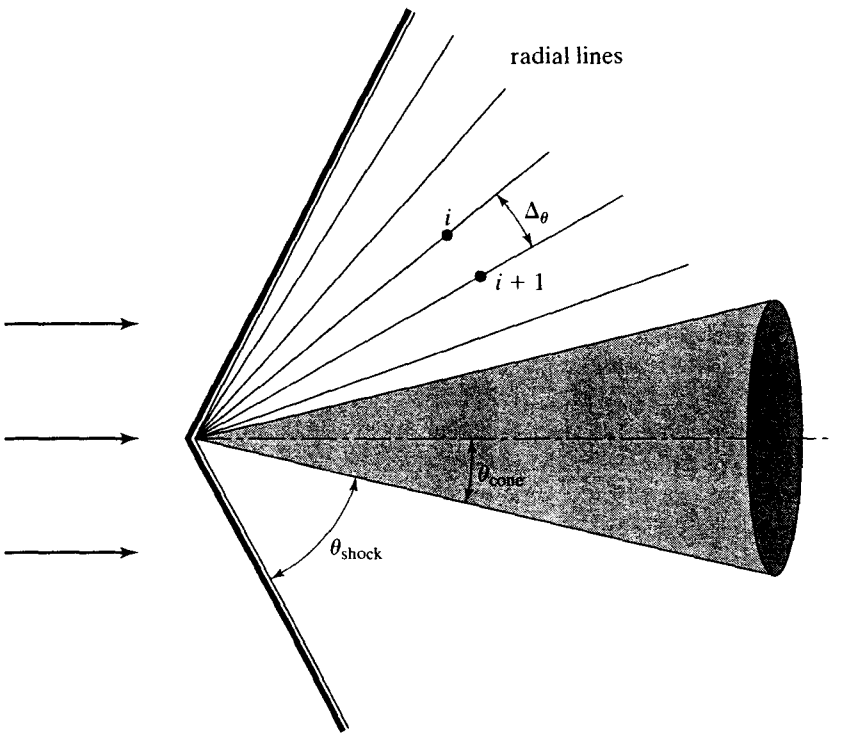


**Figure 12.13** Grid System for Conical Flow Computations

The predictor step is the Euler explict method introduced in Chapter 9. To improve the computations, we can employ a corrector step in which the predicted and initial increment values are used as follows:

$$(\bar{v}_r)_{i+1} = (\bar{v}_r)_i - \frac{(\bar{v}_\theta)_p + (\bar{v}_\theta)_i}{2}\Delta\theta$$

$$(\bar{v}_\theta)_{i+1} = (\bar{v}_\theta)_i - \frac{f[(\bar{v}_r)_i, (\bar{v}_\theta)_i] + f[(\bar{v}_r)_p, (\bar{v}_\theta)_p]}{2}\Delta\theta \qquad (12.90)$$

If we like, we may use these values to reevaluate the right-hand sides of Eq. (12.89) to determine improved predicted values. Equation (12.90) yields a second set of corrected velocity components.

A relatively small value of $\Delta\theta$ is selected and Eqs. (12.89) and (12.90) are marched in the direction of decreasing $\theta$ until it is determined that $v_\theta$ has changed sign. The location where the tangential velocity component has passed through zero identifies the cone surface.

The process is best illustrated by performing an actual computation, which is detailed in the following example.

**Example 12.8. Determination of the shock wave angle for a conical shock**

Uniform supersonic flow at Mach 3.0 and $p = 20$ kPa passes over a cone with a semivertex angle of 20° aligned parallel to the flow direction. Determine the shockwave angle, the

Mach number of the flow along the cone surface, and the surface pressure. Take $\gamma = 1.4$.

**Solution**

A spreadsheet program was developed to implement the methodology described previously. A partial sampling of the results of the program for a grid spacing of 0.1° is contained in the forthcoming tables.

To begin, an initial shock angle $\theta_s = 30°$ is assumed. At the freestream Mach number $M_1 = 3$ and the given shock angle, using Eqs. (12.85), (12.87), (12.86), (12.81), and (12.82), we find $M_2$, $\delta_s$, $V_2$, $v_r$, and $v_\theta$, respectively, as given in Table 12.1.

The computations are now initiated to compute new values of the velocity components, using Eqs. (12.89) and (12.90). The local velocity $\overline{V}$ may be readily calculated from the computed velocity components and, in turn, a local Mach number $M$ computed from Eq. (12.84) and a local deflection angle $\delta$ computed from $\tan^{-1}(v_\theta/v_r)$. The computations for the first few steps are contained in Table 12.2, and the results from the computations near the cone surface are presented in Table 12.3. Note that the computations require $\Delta\theta$ to be in radians.

**TABLE 12.1** Results of Calculations at the Shockwave for $\theta_s = 30°$, $M_1 = 3$, and $\gamma = 1.4$

| $M_2$ | $\tan(\delta_s)$ | $\delta_s$ (deg) | $V_2$ | $v_r$ | $v_\theta$ |
|---|---|---|---|---|---|
| 2.3673 | 0.2267 | 12.7735 | 0.7270 | 0.6944 | −0.2153 |

**TABLE 12.2** Calculation Results for the First Five Increments of $\Delta\theta = 0.1°$ for $\theta_s = 30°$, $M_1 = 3$, and $\gamma = 1.4$

| No. | $\theta$ (deg) | $(v_r)_p$ | $f[(v_r)_i,(v_\theta)_i]$ | $(v_\theta)_p$ | $f[(v_r)_p,(v_\theta)_p]$ | $(v_r)_{i+1}$ | $(v_\theta)_{i+1}$ | $V$ | $M$ | $\delta$ (rad) |
|---|---|---|---|---|---|---|---|---|---|---|
| 1 | 30.00 | 0.6944 | | −0.2153 | | 0.6944 | −0.2153 | 0.7270 | 2.3673 | −0.3007 |
| 2 | 29.90 | 0.6947 | −1.3266 | −0.2130 | −1.3191 | 0.6947 | −0.2130 | 0.7267 | 2.3651 | −0.2975 |
| 3 | 29.80 | 0.6951 | −1.3192 | −0.2107 | −1.3123 | 0.6951 | −0.2107 | 0.7263 | 2.3629 | −0.2943 |
| 4 | 29.70 | 0.6955 | −1.3123 | −0.2084 | −1.3059 | 0.6955 | −0.2084 | 0.7260 | 2.3608 | −0.2911 |
| 5 | 29.60 | 0.6958 | −1.3059 | −0.2061 | −1.3000 | 0.6958 | −0.2061 | 0.7257 | 2.3587 | −0.2880 |
| 6 | 29.50 | 0.6962 | −1.3000 | −0.2039 | −1.2945 | 0.6962 | −0.2039 | 0.7254 | 2.3567 | −0.2849 |

**TABLE 12.3** Calculation Results Near the Cone Surface for $\Delta\theta = 0.1°$, $\theta_s = 30°$, $M_1 = 3$, and $\gamma = 1.4$

| No. | $\theta$ (deg) | $(v_r)_p$ | $f[(v_r)_i, (v_\theta)_i]$ | $(v_\theta)_p$ | $f[(v_r)_p, (v_\theta)_p]$ | $(v_r)_{i+1}$ | $(v_\theta)_{i+1}$ | $V$ | $M$ | $\delta$ (rad) |
|---|---|---|---|---|---|---|---|---|---|---|
| 95 | 20.6 | 0.7126 | −1.4069 | −0.0046 | −1.4131 | 0.7126 | −0.0046 | 0.7127 | 2.2716 | −0.0065 |
| 96 | 20.5 | 0.7127 | −1.4131 | −0.0022 | −1.4196 | 0.7127 | −0.0022 | 0.7127 | 2.2716 | −0.0030 |
| 97 | 20.4 | 0.7127 | −1.4196 | 0.0003 | −1.4262 | 0.7127 | 0.0003 | 0.7127 | 2.2716 | 0.0005 |
| 98 | 20.3 | 0.7127 | −1.4262 | 0.0028 | −1.4330 | 0.7126 | 0.0028 | 0.7127 | 2.2716 | 0.0040 |

From Table 12.3, it may be observed that the tangential velocity component $v_\theta$ changes sign at step number 97. Also note that the local deflection angle $\delta$ also changes sign.

Interpolating, we find that the tangential velocity component vanishes at $\theta = 20.4133°$. This is the cone half-angle for the assumed 30° shock angle. This value is too large, and therefore other shock angles were tried until a value of $\theta_s = 29.6145°$ produced the desired cone half-angle of $\theta_c = 20°$. Performing these iterations within the spreadsheet program is a simple matter. The same values shown in Tables 12.1, 12.2, and 12.3, only at the correct shock angle, are presented in Tables 12.4, 12.5, and 12.6, respectively.

Since the velocity at the surface is equal to the radial velocity component, we may readily compute the Mach number on the surface from Eq. (12.84). The results are contained in Table 12.7.

**TABLE 12.4** Results of Calculations at the Shockwave for $\theta_s = 29.6145°$, $M_1 = 3$, and $\gamma = 1.4$

| $M_2$ | $\tan(\delta_s)$ | $\delta_s$ (deg) | $V_2$ | $v_r$ | $v_\theta$ |
|---|---|---|---|---|---|
| 2.3872 | 0.2194 | 12.3773 | 0.7298 | 0.6970 | 0.2163 |

**TABLE 12.5** Calculation Results for the First Five Increments of $\Delta\theta = 0.1°$ for $\theta_s = 29.6145°$, $M_1 = 3$, and $\gamma = 1.4$

| No. | $\theta$ (deg) | $(v_r)_p$ | $f[(v_r)_i, (v_\theta)_i]$ | $(v_\theta)_p$ | $f[(v_r)_p, (v_\theta)_p]$ | $(v_r)_{i+1}$ | $(v_\theta)_{i+1}$ | $V$ | $M$ | $\delta$ (rad) |
|---|---|---|---|---|---|---|---|---|---|---|
| 1 | 29.6145 | 0.6970 | | −0.2163 | | 0.6970 | −0.2163 | 0.7298 | 2.3872 | −0.3008 |
| 2 | 29.5145 | 0.6974 | −1.3307 | −0.2139 | −1.3229 | 0.6974 | −0.2140 | 0.7295 | 2.3849 | −0.2977 |
| 3 | 29.4145 | 0.6978 | −1.3229 | −0.2116 | −1.3158 | 0.6978 | −0.2116 | 0.7292 | 2.3827 | −0.2945 |
| 4 | 29.3145 | 0.6982 | −1.3158 | −0.2094 | −1.3091 | 0.6982 | −0.2094 | 0.7289 | 2.3805 | −0.2913 |
| 5 | 29.2145 | 0.6985 | −1.3091 | −0.2071 | −1.3030 | 0.6985 | −0.2071 | 0.7286 | 2.3784 | −0.2882 |
| 6 | 29.1145 | 0.6989 | −1.3030 | −0.2048 | −1.2973 | 0.6989 | −0.2048 | 0.7283 | 2.3763 | −0.2851 |

**TABLE 12.6** Calculation Results Near the Cone Surface for $\Delta\theta = 0.1°$, $\theta_s = 29.6145°$, $M_1 = 3$ and $\gamma = 1.4$

| No. | $\theta$ (deg) | $(v_r)_p$ | $f[(v_r)_i, (v_\theta)_i]$ | $(v_\theta)_p$ | $f[(v_r)_p, (v_\theta)_p]$ | $(v_r)_{i+1}$ | $(v_\theta)_{i+1}$ | $V$ | $M$ | $\delta$ (rad) |
|---|---|---|---|---|---|---|---|---|---|---|
| 96 | 20.1145 | 0.7155 | −1.4167 | −0.0029 | −1.4232 | 0.7155 | −0.0029 | 0.7155 | 2.2900 | −0.0040 |
| 97 | 20.0145 | 0.7155 | −1.4232 | −0.0004 | −1.4299 | 0.7155 | −0.0004 | 0.7155 | 2.2900 | −0.0005 |
| 98 | 19.9145 | 0.7155 | −1.4300 | 0.0021 | −1.4369 | 0.7155 | 0.0021 | 0.7155 | 2.2900 | 0.0030 |
| 99 | 19.8145 | 0.7155 | −1.4369 | 0.0046 | −1.4440 | 0.7155 | 0.0047 | 0.7155 | 2.2900 | 0.0065 |

**TABLE 12.7** Calculation Results at Cone Surface for $\Delta\theta = 0.1°$, $\theta_s = 29.6145°$, $M_1 = 3$, and $\gamma = 1.4$

| $\theta_c$ (deg) | $M_c$ | $V_c$ | $v_r$ | $v_\theta$ |
|---|---|---|---|---|
| 20.0000 | 2.2900 | 0.7155 | 0.7155 | 0.0000 |

The surface pressure may be determined by noting that the flow behind the conical shock is isentropic. Therefore, the ratio of static pressure at the surface to the static pressure just downstream of the shock is

$$\frac{p_s}{p_2} = \frac{p_s}{p_o}\frac{p_o}{p_2} = \left[\frac{2 + (\gamma - 1)M_2^2}{2 + (\gamma - 1)M_s^2}\right]^{\gamma/(\gamma-1)} \tag{12.91}$$

The static pressure ratio across the shock may be computed from Eq. (6.10):

$$\frac{p_2}{p_1} = \frac{2\gamma M_1^2 \sin^2\theta}{\gamma + 1} - \frac{\gamma - 1}{\gamma + 1} \tag{12.92}$$

Multiplying Eqs. (12.91) and (12.92) by the given value $p_1 = 20$ kPa yields the surface pressure:

$$p_s = \left(\frac{p_s}{p_2}\right)\left(\frac{p_2}{p_1}\right)p_1 = (1.1641)(2.3974)(20) = 55.8175 \text{ kPa}$$

If we again compare the wedge and cone solutions, it can be shown that, for a given half-angle and $M_1$, the shock on the wedge is inclined at a greater angle to the flow direction than the shock on the cone. As an illustration, in the foregoing example, the shock angle for a 20° wedge at the given Mach number is 37.7636°; the value for the cone is 29.6145°. This indicates that a stronger compression takes place across the wedge oblique shock. In other words, the wedge presents a greater flow disturbance than the cone. Again, this condition results from three-dimensional effects. From a physical standpoint, the flow is unable to pass around the side of the two-dimensional wedge, since it extends to infinity in the third dimension. Flow can pass around the sides of the three-dimensional cone, however, so the cone presents less overall disruption to the supersonic flow.

---

**Historical Note:** Conical supersonic flows were first solved graphically by Busemann in 1929. In 1933, Taylor and Maccoll obtained results on a hand-operated mechanical calculator for cone angles of 20°, 40°, and 60°. Fourteen years later, Kopal, in the first extensive use of a digital computer, numerically solved the Taylor–Maccoll equation at the MIT Center for Analysis. He had a large staff, and the work lasted several years. The effort produced a set of tables, but they were constructed in terms of unrounded five-digit freestream Mach numbers [Ref. (12.23)]. Seventeen years later, Sims, working alone, repeated the calculations and obtained an improved set of values.

**John Watson Maccoll** (1903–1977) was born in Aberdeenshire, Scotland. He started at the University of Glasgow in 1921, studying mathematics, natural philosophy, engineering, drawing, electricity, and electrical engineering. He graduated with a B.Sc. in 1924 and went on to study at Imperial College, London, where he received his Ph.D. Following his studies, Dr. Maccoll worked as a ballistic research officer for the Ordnance Board from 1929. Shortly after beginning at the armamanets, he began working with G. I. Taylor. (Refer to Chapter 4, Table 4.1.) They collaborated on their seminal papers on conical shocks and wrote a chapter on compressible flow together [Ref. (12.24)]. Dr. Maccoll retired in 1963 as senior superintendent of basic research. He died in 1977 in Tunbridge Wells, Kent, England. See Ref. (12.25).

## 12.6 SUMMARY

As we have observed, the equations that govern flows of compressible fluids are nonlinear. Consequently, there are relatively few analytical approaches available to obtain solutions, and, not surprisingly, there are only a few exact solutions of these equations. In this chapter, we considered several special geometries (uniform flow, source/sink flow, the irrotational vortex, and the spiral vortex) that lead to exact solutions. However, these flows have limited applications.

It was found that the governing equations could be linearized through use of the hodograph transformation, in which the velocity components become the independent variables and the spatial coordinates become the dependent variables. However, this role reversal creates major difficulties with the boundary conditions, and the method has fallen out of favor.

The last two exact solutions presented in this chapter—Prandtl–Meyer flow and conical shock flows—are more widely used. The former was covered in a different manner in Chapter 7. The latter was obtained by solving an ordinary differential equation. Even though it is obtained numerically, the conical shock flow solution is regarded as exact.

In the next chapter, we will again consider linearized equations, but these equations will not be obtained by a transformation, but rather by neglecting small terms in the governing equations. That chapter will be followed by one that deals with numerical methods that can directly confront nonlinearies.

## 12.7 REFERENCES


**12.1** Vallentine, H. R. *Applied Hydrodynamics, S.I. Edition*, Butterworths, London, 1969, pp. 102–132.

**12.2** Howarth, L., ed. *Modern Developments in Fluid Dynamics*, Vol. I, Oxford at the Clarendon Press, 1953; Bickley, W. G., Chapter V, "Some Exact Solutions of the Equations of Steady Homentopic Flow of an Inviscid Gas," pp. 158–189.

**12.3** Thompson, P. A. *Compressible-Fluid Dynamics*, McGraw-Hill Book Company, New York, 1972, p. 515.

**12.4** Hoffmann, K. A., Chiang, S. T., Siddiqui, S., and Papadakis, M. *Fundamental Equations of Fluid Mechanics*, Engineering Education System, Wichita, KS, 1996, pp. 89–91.

**12.5** Emanuel, G. *Gasdynamics: Theory and Applications*, AIAA Education Series, 1986, pp. 307–328.

**12.6** Shapiro, A. H. *The Dynamics and Thermodynamics of Compressible Fluid Flow*, Vol. 1, Ronald Press, New York, 1953, pp. 295–296.

**12.7** Molenbroek, P. "Uber eninige Bewegungen eines Gases mit Annahme eines Geswindigkeitspotentials," *Arch d Math u Phys* 1890; 9: 157–195.

**12.8** Chaplygin, C. T. "On Gaseous Jets," *Ann. Math. Phys. Sect. Sci. Imperial University Moscow*, 21, 1904, pp. 1–121, English translation, NACA Tech. Note, No. 1063, 1944.

**12.9** Hamilton, W. R. "The Hodograph, or a New Method of Expressing in Symbolical Language the Newtonian Law of Attraction," *Proc R Ir Acad* 1847; 3: 344–353.

**12.10** Derbes, D. "Reinventing the Wheel: Hodograph Solutions to the Kepler Problems," *Am J Phys* 2001; 69(4): 481–489.

**12.11** Courant, R., and Friedrichs, K. O. *Supersonic Flow and Shock Waves*, Interscience Publishers, New York, 1948, pp. 247–259.

**12.12** Shapiro, A. H. *The Dynamics and Thermodynamics of Compressible Fluid Flow*, Vol. 1, Ronald Press, New York, 1953, pp. 336–363.

**12.13** Von Mises, R. *Mathematical Theory of Compressible Fluid Flow*, Academic Press, New York, 1958, pp. 249–278.

**12.14** Pai, S. I. *Introduction to the Theory of Compressible Flow*, D. Van Nostrand Company, New Jersey, 1959, pp. 132–152.

**12.15** Schiffer, M. "Analytical Theory of Subsonic and Supersonic Flows," *Encyclopedia of Physics, Vol. IX, Fluid Dynamics III*, Springer-Verlag, Berlin, 1960, pp. 56–92.

**12.16** Chapman, C. J. *High Speed Flow*, Cambridge University Press, Cambridge, UK, 2000, pp. 206–221.

**12.17** Shivamoggi, B. K. *Theoretical Fluid Dynamics*, 2d ed., John Wiley & Sons, New York, 1998, pp. 271–273.

**12.18** Chapman, C. J. *High Speed Flow*, Cambridge University Press, Cambridge, UK, 2000, pp. 211–214.

**12.19** Taylor, G. I., and Maccoll, J. W. "The Air Pressure on a Cone Moving at High Speed," *Proc R Soc* A, 1933; 139: 278–311.

**12.20** Maccoll, J. W. "The Conical Shock Wave Formed by a Cone Moving at High Speed," *Proc R Soc* A, 1937; 159: 459–472.

**12.21** Kopal, Z. *Tables of Supersonic how around Cones*, M.I.T. Department of Electrical Engineering, Center of Analysis, Report No. 1, 1947.

**12.22** Sims, J. "Tables for Supersonic Flow around Right Circular Cones at Zero Angle of Attack," *NASA* SP-3004, 1964.

**12.23** Brower, W. B. *Tables and Data for Compressible Flow*, Hemisphere Publishing Corporation, New York, 1990, pp. 65–70.

**12.24** Taylor, G. I., and Maccoll, J. W., "The Mechanics of Compressible Fluids," in Durand, W. F., ed. *Aerodynamic Theory Vol. III, Div. H.*, Springer-Verlag, Berlin, 1934, pp. 229–231.

**12.25** Archive Services, University of Glasgow, 2002. http://www.archives.gla.ac.uk/collects/catalog/ugc/001-050/ugc005.html.

**12.26** Zwillinger, D. *Handbook of Differential Equations*, Academic Press, San Diego, CA, 1989, pp. 353–356.

## 12.8 PROBLEMS

**12.1** The velocity potential equation can be written in a variety of forms. For example, Taylor and Maccoll [Ref. (12.24)] used the following form for problems in Cartesian coordinates:

$$\frac{\partial^2\phi}{\partial x^2} + \frac{\partial^2\phi}{\partial y^2} = \frac{1}{2a^2}\left[\left(\frac{\partial\phi}{\partial x}\right)\frac{\partial V^2}{\partial x} + \left(\frac{\partial\phi}{\partial y}\right)\frac{\partial V^2}{\partial y}\right]$$

Derive this expression and then show that it may be written as

$$\frac{\partial^2\phi}{\partial x^2} + \frac{\partial^2\phi}{\partial y^2} = \frac{1}{a^2}\left[\left(\frac{\partial\phi}{\partial x}\right)^2\frac{\partial^2\phi}{\partial x^2} + 2\left(\frac{\partial\phi}{\partial x}\right)\left(\frac{\partial\phi}{\partial y}\right)\frac{\partial^2\phi}{\partial x\partial y} + \left(\frac{\partial\phi}{\partial y}\right)^2\frac{\partial^2\phi}{\partial y^2}\right]$$

**12.2** Show that the polar velocity components $v_r$ and $v_\theta$ are related to the Cartesian velocity components $u$ and $v$ by

$$v_r = u\cos\theta + v\sin\theta$$

$$v_\theta = -u\sin\theta + v\cos\theta$$

Then find the inverse of these relationships; that is, develop expressions for $u = u(v_r, v_\theta)$ and $v = v(v_r, v_\theta)$.

**12.3** For a uniform flow in the $+y$ direction, show that the expressions for the velocity components in Problem 12.2 give

$$v = V, \quad u = 0, \quad v_r = V \sin\theta, \quad \text{and} \quad v_\theta = V \cos\theta$$

Obtain expressions for the velocity components for a uniform flow that is directed at an angle $\pi/2 + \Delta$.

**12.4** Prove that as the limit line for radial flow is approached, the acceleration of the flow approaches $\infty$.

**12.5** Starting from the concept that the streamlines are straight for radial flow and therefore have the form $\psi = c\theta = c \tan^{-1}(y/x)$, develop an equation for the velocity field of a compressible fluid.

**12.6** Sketch the ellipse of Eq. (12.13) in the first quadrant. Indicate roughly subsonic and hypersonic regimes. Use the sketch to explain which effect, thermodynamic or inertial, dominates in subsonic and hypersonic accelerations.

**12.7** Develop expressions for the flow variables in terms of the radius $r$ for the irrotational vortex.

**12.8** Plot the incompressible flow equiangular spiral. Assume $Q = \Gamma$ and that the constant $c$ is unity.

**12.9** Use the hodograph transformation to obtain a solution for the case in which $\psi = \psi(V)$. Show that for this case, $\phi = c\alpha$.

**12.10** Another method to obtain the hodograph equations is to make use of the *Legrendre transformation* [Zwillinger, Ref. (12.26)]. In this approach, a function $\Phi(u, v)$ in the hodograph plane is related to the velocity potential $\phi(x, y)$ by

$$\Phi = xu + yv - \phi$$

Use this relation to show that

(a) $\dfrac{\partial\Phi}{\partial u} = x$ and $\dfrac{\partial\Phi}{\partial v} = y$

$$\frac{\partial^2\phi}{\partial x^2} = \frac{1}{J}\frac{\partial^2\Phi}{\partial v^2}$$

(b) $$\frac{\partial^2\phi}{\partial x\partial y} = -\frac{1}{J}\frac{\partial^2\Phi}{\partial u\partial v}$$

$$\frac{\partial^2\phi}{\partial y^2} = \frac{1}{J}\frac{\partial^2\Phi}{\partial u^2}$$

where $J = \begin{vmatrix} \Phi_{uu} & \Phi_{uv} \\ \Phi_{uv} & \Phi_{vv} \end{vmatrix}$.

(c) Finally, show that Eq. (12.27) is transformed into the following linear equation:

$$\left(1 - \frac{u^2}{a^2}\right)\frac{\partial^2\Phi}{\partial v^2} + 2\frac{uv}{a^2}\frac{\partial^2\Phi}{\partial u\partial v} + \left(1 - \frac{v^2}{a^2}\right)\frac{\partial^2\Phi}{\partial u^2} = 0$$

**12.11** Prove Eq. (12.49).

**12.12** In the solution of problems using the hodograph equations, the resulting expressions often contain the following two parameters: $\tau = (V/V_{\max})^2$ and $\beta = 1/(\gamma - 1)$. Show that

(a) $\dfrac{\rho}{\rho_o} = (1 - \tau)^{\beta}$ and (b) $M^2 = \dfrac{2\beta\tau}{1 - \tau}$.

**12.13** Using Eq. (12.79), show that Eq. (12.77) can be written as

$$\left(\frac{dv_r}{d\theta}\right)^2\left(v_r + \frac{d^2v_r}{d\theta^2}\right) = \frac{\gamma - 1}{2}\left[V_{\max}^2 - v_r^2 - \left(\frac{dv_r}{d\theta}\right)^2\right]\left(\frac{d^2v_r}{d\theta^2} + \cot\theta\frac{dv_r}{d\theta} + 2v_r\right)$$

Verify that this expression is identically satisfied by a uniform stream given by $v_r = V\cos\theta$.

**12.14** A steady, two-dimensional, supersonic flow uniformly streams along a horizontal wall that is aligned with the $x$-axis. The stream encounters a sharp corner located at $x = 0$. Show that the maximum angle through which the flow may turn is given by $\pi/2b - \pi/2$, where $b^2 = (\gamma - 1)/(\gamma + 1)$. Also show that the maximum angle can occur only if the original flow is sonic.

**12.15** Uniform supersonic flow at Mach 3.0 and $p = 20$ kPa passes over a cone with a semivertex angle of 20° aligned parallel to the flow direction. Determine the shockwave angle, the Mach number of the flow along the cone surface, and the surface pressure. Take $\gamma = 1.3$.

**12.16** Uniform supersonic flow at Mach 4.0 and $p = 20$ kPa passes over a cone with a semivertex angle of 20° aligned parallel to the flow direction. Determine the shockwave angle, the Mach number of the flow along the cone surface, and the surface pressure. Take $\gamma = 1.4$.

**12.17** Uniform supersonic flow at Mach 3.0 and $p = 20$ kPa passes over a cone with a semivertex angle of 30° aligned parallel to the flow direction. Determine the shockwave angle, the Mach number of the flow along the cone surface, and the surface pressure. Take $\gamma = 1.4$.

**12.18** A supersonic diffuser contains a conical spike of semivertex angle 5°; the spike is aligned with the flow. (See Figure P12.18.) Determine the Mach number of the flow along the cone surface and the static pressure at the surface of the cone. Take the altitude = 5 km and $\gamma = 1.4$.

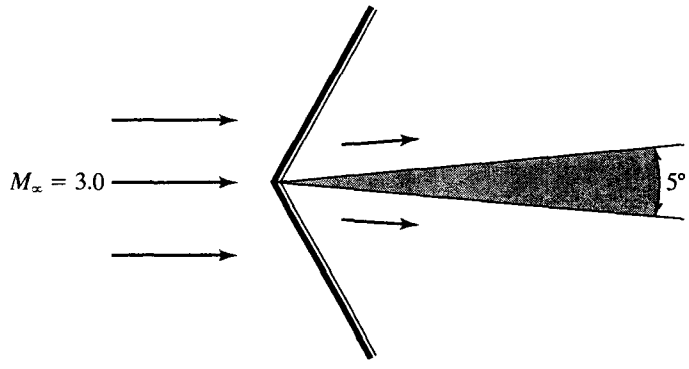


**Figure P12.18**

# Chapter 13

# Linearized Flows

## 13.1 INTRODUCTION

The equations of motion for two-dimensional, compressible, steady flow, as derived in Chapter 11, are *nonlinear* partial differential equations—that is, they contain products of the dependent variables and their derivatives. The mathematics associated with the solution of a system of nonlinear partial differential equations is extremely complex; in virtually all cases, solutions are possible only through the application of advanced numerical techniques. To reduce the equations to a more workable form, we shall, in this chapter, place certain restrictions on the flow and thereby *linearize* the partial differential equations.

If a body, when placed in a uniform flow, causes only *small disturbances* to that flow, then it is possible to linearize the equations of fluid motion and thereby effect a solution. According to this method of small disturbances, or *small perturbations*, the flow is considered to be made up of a uniform flow on which are superposed perturbation velocities. We shall first discuss the assumptions inherent in small-perturbation theory, as regards both the flow and the body shape. Then we shall develop solutions, for both subsonic and supersonic flows, of the linearized equations. Of interest here is the contrast between the respective natures of subsonic and supersonic flow. Although the method of small perturbations is approximate, it does succeed in pointing out the very basic differences between the two types of flow. Furthermore, it will be shown possible, at least for subsonic flow, to derive similarity laws relating a compressible flow to the corresponding incompressible flow. This relatability is quite important because incompressible solutions are already available for a wide variety of physical situations.

## 13.2 LINEARIZATION OF THE POTENTIAL EQUATION

One case for which the potential equation, Eq. (11.47), for isentropic steady flow can be linearized is that of flow over a body that presents only a small disturbance to the flow. Let us consider uniform parallel flow in the positive $x$ direction over a thin body

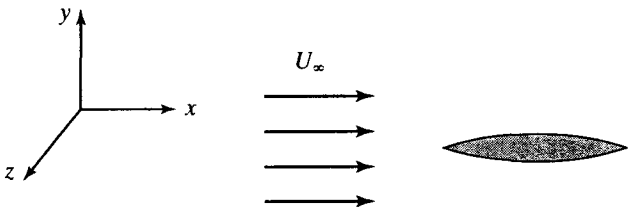


**Figure 13.1** Uniform Flow past a Thin Body Aligned with the Flow

aligned with the flow. (See Figure 13.1.) The potential of the total velocity field can be considered to be composed of two parts, one due to the uniform flow and the other due to the perturbation introduced into the flow by the thin body. We shall assume that the flow is steady and in the $(x, y)$ plane—i.e., two dimensional—so flow properties do not vary in the $z$ direction. The presence of the body gives rise to small-perturbation velocities $u_p$ and $v_p$ in the $x$ and $y$ directions, respectively. From the definition of the velocity potential $\phi$ (see Section 11.8), we have

$$\frac{\partial \phi}{\partial x} = U_\infty + u_p$$

$$\frac{\partial \phi}{\partial y} = v_p \tag{13.1}$$

Substituting into the two-dimensional flow version of Eq. (11.47) yields

$$\frac{\partial^2 \phi}{\partial x^2} + \frac{\partial^2 \phi}{\partial y^2} - \frac{1}{a^2}\left[(U_\infty + u_p)^2 \frac{\partial^2 \phi}{\partial x^2} + v_p^2 \frac{\partial^2 \phi}{\partial y^2}\right] - \frac{2}{a^2}(U_\infty + u_p)(v_p)\frac{\partial^2 \phi}{\partial x\, \partial y} = 0 \tag{13.2}$$

We also need an expression for the velocity of the sound. From Eq. (11.48), we have

$$a^2 = a_o^2 - \frac{\gamma - 1}{2}[(U_\infty + u_p)^2 + (v_p)^2] \tag{13.3}$$

where

$$a_o^2 = \gamma R T_o$$

From the energy equation for steady, adiabatic flow, we have demonstrated that

$$c_p T_o = c_p T_\infty + \frac{U_\infty^2}{2} = \text{constant}$$

so that

$$a_o^2 = \gamma R\left(T_\infty + \frac{U_\infty^2}{2c_p}\right) = a_\infty^2 + \frac{\gamma - 1}{2}U_\infty^2 \tag{13.4}$$

We can now combine Eqs. (13.3) and (13.4) to yield

$$a^2 = a_\infty^2 - \frac{\gamma - 1}{2}(u_p^2 + 2u_p U_\infty + v_p^2) \tag{13.5}$$

Substituting Eq. (13.5) into Eq. (13.2), we obtain

$$a_\infty^2\left(\frac{\partial^2\phi}{\partial x^2}+\frac{\partial^2\phi}{\partial y^2}\right)=\left(\frac{\gamma-1}{2}\right)(u_p^2+2u_pU_\infty+v_p^2)\left(\frac{\partial^2\phi}{\partial x^2}+\frac{\partial^2\phi}{\partial y^2}\right)$$
$$+(U_\infty+u_p)^2\frac{\partial^2\phi}{\partial x^2}+v_p^2\frac{\partial^2\phi}{\partial y^2}+2(U_\infty+u_p)v_p\frac{\partial^2\phi}{\partial x\,\partial y} \tag{13.6}$$

We now divide Eq. (13.6) by $a_\infty^2$, use $M_\infty=U_\infty/a_\infty$, and simplify to obtain

$$(1-M_\infty^2)\frac{\partial^2\phi}{\partial x^2}+\frac{\partial^2\phi}{\partial y^2}=\frac{\gamma-1}{2}M_\infty^2\left(\frac{u_p^2}{U_\infty^2}+\frac{2u_p}{U_\infty}+\frac{v_p^2}{U_\infty^2}\right)\left(\frac{\partial^2\phi}{\partial x^2}+\frac{\partial^2\phi}{\partial y^2}\right)$$
$$+M_\infty^2\left(\frac{u_p^2}{U_\infty^2}+\frac{2u_p}{U_\infty}\right)\frac{\partial^2\phi}{\partial x^2}+M_\infty^2\left(\frac{v_p^2}{U_\infty^2}\right)\frac{\partial^2\phi}{\partial y^2}$$
$$+2M_\infty^2\left(\frac{v_p}{U_\infty}+\frac{u_pv_p}{U_\infty^2}\right)\frac{\partial^2\phi}{\partial x\,\partial y} \tag{13.7}$$

The perturbation velocities $u_p$ and $v_p$ are assumed small compared with $U_\infty$. Accordingly, *multiples* of these velocities may be taken to be much smaller than $a_\infty^2$; in other words,

$$M_\infty^2\left(\frac{u_p^2}{U_\infty^2}\right)\ll 1,\quad M_\infty^2\left(\frac{v_p^2}{U_\infty^2}\right)\ll 1,\text{ and }M_\infty^2\left(\frac{u_pv_p}{U_\infty^2}\right)\ll 1 \tag{13.8}$$

Using these relations and by comparing the coefficients of like terms on both sides of the equation, we may eliminate five terms from the right-hand side of Eq. (13.7). This operation leaves

$$(1-M_\infty^2)\frac{\partial^2\phi}{\partial x^2}+\frac{\partial^2\phi}{\partial y^2}=\frac{\gamma-1}{2}M_\infty^2\left(\frac{2u_p}{U_\infty}\right)\left(\frac{\partial^2\phi}{\partial x^2}+\frac{\partial^2\phi}{\partial y^2}\right)$$
$$+M_\infty^2\left(\frac{2u_p}{U_\infty}\right)\frac{\partial^2\phi}{\partial x^2}+2M_\infty^2\left(\frac{v_p}{U_\infty}\right)\frac{\partial^2\phi}{\partial x\,\partial y}$$
$$=\left[M_\infty^2(\gamma+1)\frac{u_p}{U_\infty}\right]\frac{\partial^2\phi}{\partial x^2}+\left[M_\infty^2(\gamma-1)\frac{u_p}{U_\infty}\right]\frac{\partial^2\phi}{\partial y^2}$$
$$+2M_\infty^2\left(\frac{v_p}{U_\infty}\right)\frac{\partial^2\phi}{\partial x\,\partial y} \tag{13.9}$$

Unfortunately, because it contains terms of the form $u_p(\partial^2\phi/\partial x^2)$, this equation is still nonlinear. To linearize the equation, it is necessary to place additional restrictions on the flow. If we assume that

$$\left[\frac{M_\infty^2(u_p/U_\infty)}{1-M_\infty^2}\right]\ll 1 \tag{13.10}$$

then terms containing the nonlinear term $(u_p/U_\infty)(\partial^2\phi/\partial x^2)$ are eliminated. If we further assume that

$$M_\infty^2 \frac{u_p}{U_\infty} \ll 1 \quad \text{and} \quad M_\infty^2 \frac{v_p}{U_\infty} \ll 1$$

then terms containing $u_p(\partial^2\phi/\partial y^2)$ and $v_p(\partial^2\phi/\partial x\,\partial y)$ are likewise eliminated. The resultant equation is

$$(1 - M_\infty^2)\frac{\partial^2\phi}{\partial x^2} + \frac{\partial^2\phi}{\partial y^2} = 0 \tag{13.11}$$

Equation (13.11) is valid for steady, two-dimensional, irrotational, and isentropic flow of a perfect gas with constant specific heats around a thin body. From the assumptions made in Eq. (13.10), it is further necessary to state that for Eq. (13.11) to hold, $M_\infty$ cannot be unity or close to unity, so Eq. (13.11) is not valid for transonic flow. For transonic flow, the term containing $(u_p/U_\infty)(\partial^2\phi/\partial x^2)$ would have to be retained. Hence, for transonic flow,

$$(1 - M_\infty^2)\frac{\partial^2\phi}{\partial x^2} + \frac{\partial^2\phi}{\partial y^2} = M_\infty^2(\gamma + 1)\frac{u_p}{U_\infty}\frac{\partial^2\phi}{\partial x^2} \tag{13.12}$$

Furthermore, for $M_\infty^2(u_p/U_\infty) \ll 1$, $M_\infty$ cannot be too great, so neither Eq. (13.11) nor Eq. (13.12) hold for hypersonic flow—that is, a flow in which $M_\infty \gg 3$ to 5.

Under these assumptions, then, we are left with Eq. (13.11), a linear partial differential equation (PDE). Briefly, linear second-order PDEs of the form

$$A(x, y)\frac{\partial^2\phi}{\partial x^2} + B(x, y)\frac{\partial^2\phi}{\partial x\partial y} + C(x, y)\frac{\partial^2\phi}{\partial y^2} = F\left(\frac{\partial\phi}{\partial x}, \frac{\partial\phi}{\partial y}, \phi, x, y\right)$$

are classified according to the value of the discriminant of the PDE [see Ref. (13.1)], which is constructed from the coefficients of the second derivative terms: $D = B^2 - AC$. If $D > 0$, the PDE is called *hyperbolic*; if $D = 0$, the PDE is called *parabolic*; and if $D < 0$, the PDE is called *elliptic*. For $M_\infty < 1$, the PDE is seen to be of the *elliptic type*, with solutions possessing similarity to the solutions of Laplace's equation (incompressible flow). For supersonic flow, however, with $M_\infty^2 - 1 > 0$, the PDE is of the *hyperbolic type*, which can be transformed into the *wave equation*, which has the form

$$\frac{\partial^2\phi}{\partial x^2} = c^2\frac{\partial^2\phi}{\partial y^2}$$

where $c = \sqrt{M_\infty^2 - 1}$ is the *wave speed*. Thus, supersonic solutions are similar to solutions for a vibrating string or other wave phenomena. Needless to say, subsonic solutions have entirely different features than supersonic solutions.

It is advantageous to split the potential $\phi$ into two parts, one due to the uniform flow and the other due to the perturbation. For the linearized equation, for which solutions can be added,

$$\phi = \phi_p + U_\infty x$$

with

$$u_p = \frac{\partial \phi_p}{\partial x}, \quad v_p = \frac{\partial \phi_p}{\partial y}$$

Note that $\phi_p$ satisfies Eq. (13.11):

$$(1 - M_\infty^2)\frac{\partial^2 \phi_p}{\partial x^2} + \frac{\partial^2 \phi_p}{\partial y^2} = 0 \tag{13.13}$$

A solution of Eq. (13.13) for $\phi_p$ requires a specification of the boundary conditions both on the body and at infinity. For this irrotational flow, in which we neglect the effects of viscosity and hence the boundary layer on the body, the boundary conditions on the body surface require that the flow velocity at the surface be tangent to the body. Place the body on the $x$-axis, as shown in Figure 13.2. The slope of the body surface, $(dy/dx)_b$, must be equal to the slope of the velocity vector at the surface:

$$\left(\frac{dy}{dx}\right)_b = \frac{v_p}{u_p + U_\infty} \tag{13.14}$$

Since

$$\frac{u_p}{U_\infty} \ll 1$$

we have

$$\left(\frac{dy}{dx}\right)_b = \frac{v_p}{U_\infty} \tag{13.15}$$

According to the assumptions necessary for small-perturbation flow, the $y$-coordinate of the body, $y_b$, must be small. It is possible, then, to write a Taylor's series expansion for the perturbation velocities at a point $(x_b, y_b)$ on the body surface in terms of a corresponding point $(x_b, 0)$ located on the axis:

$$v_p(x_b, y_b) = v_p(x_b, 0) + \left(\frac{\partial v_p}{\partial y}\right)_{x_b, 0}(y_b - 0) + \cdots$$

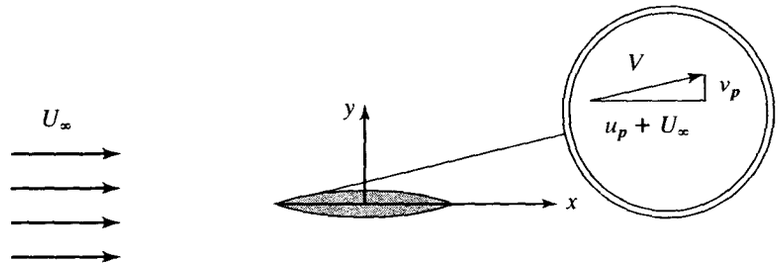


**Figure 13.2** Uniform Flow past a Thin Symmetrical Body Located on the $x$-Axis

Neglecting all terms but the first yields

$$v_p(x_b, y_b) = v_p(x_b, 0)$$

The linearized boundary condition in Eq. (13.15) then becomes

$$\left(\frac{dy}{dx}\right)_b = \frac{v_p(x_b, 0)}{U_\infty} \tag{13.16}$$

The boundary condition at infinity for linearized flow is that the perturbation velocities must be finite or zero; they cannot go to infinity in magnitude.

Before proceeding to an example, we shall first derive an expression for pressure in a linearized two-dimensional flow. It is customary to express pressure in terms of a nondimensional pressure coefficient $C_p$ where

$$C_p = \frac{p - p_\infty}{\frac{1}{2}\rho_\infty U_\infty^2} = \frac{p/p_\infty - 1}{\frac{1}{2}\gamma M_\infty^2} \tag{13.17}$$

The energy equation for isentropic flow may be written as

$$c_p T_\infty + \frac{U_\infty^2}{2} = c_p T + \frac{(U_\infty + u_p)^2 + v_p^2}{2}$$

Simplifying gives

$$T_\infty - T = \frac{2U_\infty u_p + u_p^2 + v_p^2}{2c_p}$$

Now, for a perfect gas,

$$c_p = \frac{\gamma}{\gamma - 1} R$$

Combining and dividing by $T_\infty$ produces

$$\frac{T}{T_\infty} = 1 - \frac{\gamma - 1}{2} \frac{2U_\infty u_p + u_p^2 + v_p^2}{\gamma R T_\infty}$$

$$= 1 - \frac{\gamma - 1}{2} M_\infty^2 \left(2\frac{u_p}{U_\infty} + \frac{u_p^2 + v_p^2}{U_\infty^2}\right)$$

For an isentropic process and a perfect gas with constant specific heats,

$$\frac{p}{p_\infty} = \left(\frac{T}{T_\infty}\right)^{\gamma/(\gamma-1)}$$

so that

$$C_p = \frac{\left[1 - \dfrac{\gamma - 1}{2} M_\infty^2 \left( 2\dfrac{u_p}{U_\infty} + \dfrac{u_p^2 + v_p^2}{U_\infty^2} \right) \right]^{\gamma/(\gamma-1)} - 1}{\dfrac{1}{2}\gamma M_\infty^2}$$

The term in brackets can be expanded using the binomial theorem (for $x < 1$, $(1 + x)^m = 1 + mx + m(m - 1)x^2/2! + \cdots$). Consequently, we obtain the following simplification:

$$\left[1 - \frac{\gamma - 1}{2} M_\infty^2 \left( 2\frac{u_p}{U_\infty} + \frac{u_p^2 + v_p^2}{U_\infty^2} \right) \right]^{\gamma/(\gamma-1)} = 1 - \frac{\gamma M_\infty^2}{2} \left( 2\frac{u_p}{U_\infty} + \frac{u_p^2 + v_p^2}{U_\infty^2} \right) + \cdots$$

Under the assumptions of the small-perturbation theory described previously, the higher order terms in the series can be dropped, so that

$$C_p = -\left( 2\frac{u_p}{U_\infty} + \frac{u_p^2 + v_p^2}{U_\infty^2} \right) \tag{13.18}$$

Utilizing the approximations indicated in Eq. (13.8), we obtain

$$\frac{u_p^2}{U_\infty^2} \ll 1 \text{ and } \frac{v_p^2}{U_\infty^2} \ll 1$$

The linearized pressure coefficient is thus

$$C_p = -\frac{2u_p}{U_\infty} \tag{13.19}$$

Having established the linearized partial differential equation for small perturbations and the appropriate boundary conditions, we are now in a position to solve a simple *boundary-value problem*. In the next section, we shall discuss such a simple problem for subsonic flow and then return, in a later section, to the same problem for supersonic flow.

## 13.3 SUBSONIC FLOW OVER A WAVY WALL

Consider a uniform subsonic flow in the positive $x$ direction of magnitude $U_\infty$, as shown in Figure 13.3. The flow passes over a two-dimensional wave-shaped wall, with the equation of the wall given by

$$y_b = A \sin\left( \frac{2\pi x}{\lambda} \right)$$

where $A$ is the *wave amplitude* and $\lambda$ the *wave length*. We shall treat this case using small-perturbation theory, so we must assume that $A \ll \lambda$. Bourque [Ref. (13.2)] has

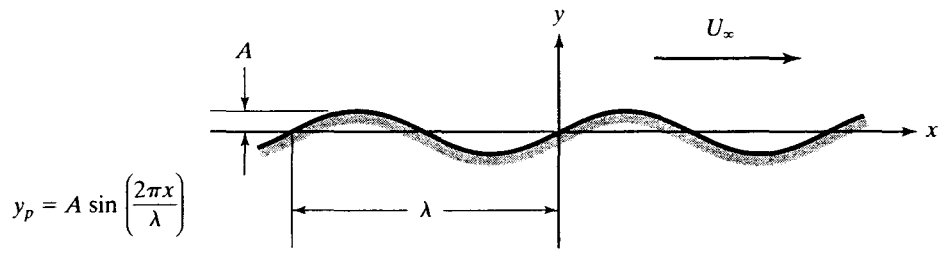


**Figure 13.3** Subsonic Uniform Flow over a Wavy Wall

developed expressions that provide the maximum value that the ratio $A/\lambda$ may have for a given level of accuracy. We wish to solve the partial differential equation

$$(1 - M_\infty^2)\frac{\partial^2 \phi_p}{\partial x^2} + \frac{\partial^2 \phi_p}{\partial y^2} = 0$$

subject to the boundary conditions

$$v_p(x_b, 0) = U_\infty\left(\frac{dy}{dx}\right)_b = U_\infty A\frac{2\pi}{\lambda}\cos\frac{2\pi x}{\lambda}$$

and the requirement that $u_p(x, \infty)$ and $v_p(x, \infty)$ are finite.

One of the methods of solving a linear partial differential equation is to assume that the dependent variable (in this case, the velocity potential function $\phi$) can be written as the product of individual functions of the independent variables (here, $x$ and $y$)—that is, $X(x)Y(y)$. This method is called *separation of variables*; for examples of its uses see Refs. (13.3) and (13.4). The assumption of the product form can be justified only if it is possible (1) to replace the original PDE with an equation in which the independent variables appear individually on each side of the equation and (2) to find a solution with this product form that satisfies the boundary conditions.

Assume $\phi_p = X(x)Y(y)$ and substitute into

$$\frac{\partial^2 \phi_p}{\partial x^2} + \frac{1}{1 - M_\infty^2}\frac{\partial^2 \phi_p}{\partial y^2} = 0$$

to produce

$$\frac{1}{X}\frac{d^2X}{dx^2} = -\frac{1}{1 - M_\infty^2}\frac{1}{Y}\frac{d^2Y}{dy^2}$$

We observe that the independent variables $x$ and $y$ have indeed been separated. In this expression, partial derivatives are not used, since $X$ and $Y$ are each functions of a single variable. Since the left-hand side of the preceding equation is dependent on $x$ alone, the right-hand side is dependent on $y$ alone, and $x$ and $y$ may vary independently

of each other, it follows that both sides must be equal to a constant. Selecting this constant to be $-k^2$, we have the following:

$$\frac{d^2X}{dx^2} + k^2X = 0 \tag{13.20}$$

$$\frac{d^2Y}{dy^2} - (1 - M_\infty^2)k^2Y = 0 \tag{13.21}$$

Now we have to solve these two ordinary differential equations. The solution to Eq. (13.20) is

$$X = c_1 \cos(kx) + c_2 \sin(kx) \tag{13.22}$$

The solution to Eq. (13.21) is

$$Y = c_3 e^{\sqrt{1-M_\infty^2}(ky)} + c_4 e^{-\sqrt{1-M_\infty^2}(ky)} \tag{13.23}$$

Multiplying these solutions together yields

$$\phi_p = (c_1 \cos kx + c_2 \sin kx)\left(c_3 e^{\sqrt{1-M_\infty^2}\,ky} + c_4 e^{-\sqrt{1-M_\infty^2}\,ky}\right) \tag{13.24}$$

The constants $c_1$, $c_2$, $c_3$, and $c_4$ are determined from the boundary conditions.

At the wall,

$$v_p(x_b, y_b) \cong v_p(x_b, 0) = \frac{\partial \phi_p}{\partial y}(x_b, 0) = U_\infty A \frac{2\pi}{\lambda} \cos \frac{2\pi x}{\lambda}$$

At infinity, $\partial\phi_p/\partial x$ and $\partial\phi_p/\partial y$ must be finite or zero.

From the conditions at infinity, it is clear that $c_3$ is equal to zero. From the conditions at the wall, we have

$$[(c_1 \cos kx + c_2 \sin kx)]\left[-c_4\sqrt{1 - M_\infty^2}k\right] = U_\infty A \frac{2\pi}{\lambda} \cos \frac{2\pi x}{\lambda}$$

Matching like terms, we observe that there is only one sine term, and thus

$$c_2 = 0$$

Moreover, comparison of the arguments of the cosine terms reveals that $k = 2\pi/\lambda$. Also,

$$-c_1 c_4 \sqrt{1 - M_\infty^2} \frac{2\pi}{\lambda} = U_\infty A \frac{2\pi}{\lambda}$$

so that

$$c_1 c_4 = \frac{-U_\infty A}{\sqrt{1 - M_\infty^2}}$$

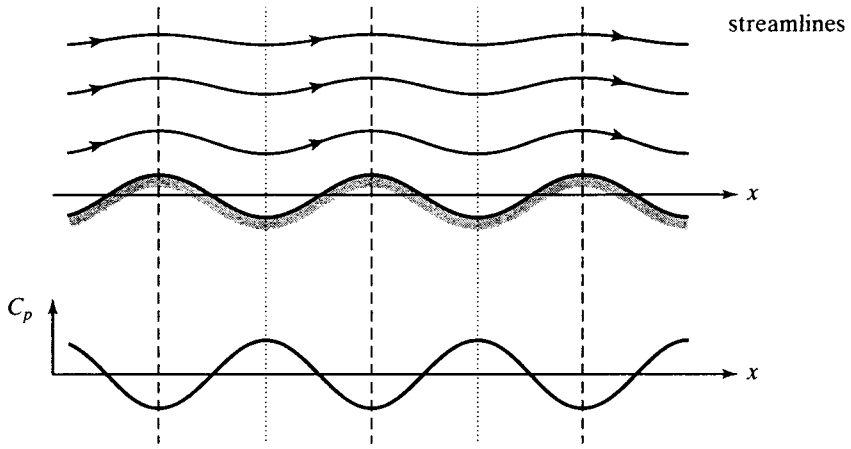


**Figure 13.4** Subsonic Flow Streamlines and Pressure Variation along a Wavy Wall

Therefore,

$$\phi_p = -\frac{U_\infty A}{\sqrt{1 - M_\infty^2}} e^{-\left(\sqrt{1-M_\infty^2}\frac{2\pi}{\lambda}y\right)} \cos\left(\frac{2\pi x}{\lambda}\right) \tag{13.25}$$

For the pressure distribution on the wall, we use Eq. (13.19):

$$C_p = -\frac{2u_p}{U_\infty} = -\frac{2}{U_\infty}\left(\frac{\partial \phi_p}{\partial x}\right)_{y=0}$$

Differentiation of the perturbation potential function brings

$$C_p = -\frac{4\pi A}{\lambda\sqrt{1 - M_\infty^2}} \sin\left(\frac{2\pi x_b}{\lambda}\right) \tag{13.26}$$

The flow streamlines and the pressure variation along the wall have been sketched in Figure 13.4. It can be seen that, for subsonic flow, the disturbance created by the wall dies out as $y$ goes to infinity. Also, the pressure peaks occur in the troughs of the wall, and vice versa, so the pressure is in phase with the wall. Thus, as may be expected for an inviscid flow, there is no drag force (force in the $x$ direction) on the wall.

**Example 13.1. Streamlines for subsonic flow over a wavy wall**

Develop an expression for the streamlines of the subsonic flow over the wavy wall shown in Figure 13.3.

**Solution**

The velocity components in the $x$ and $y$ directions may be written in terms of the stream function (see Problem 11.3) as

$$u = \frac{\rho_\infty}{\rho}\frac{\partial \psi}{\partial y}$$

$$v = -\frac{\rho_\infty}{\rho}\frac{\partial \psi}{\partial x}$$

As we have seen, the velocity components may be written as $u = U_\infty + u_p$ and $v = v_p$. The perturbation velocity potential, with $\beta^2 = 1 - M_\infty^2$ and $k = 2\pi/\lambda$ inserted for simplicity, can be written as

$$\phi_p = -\frac{U_\infty A}{\beta} e^{-(\beta k y)} \cos(kx)$$

This expression enables us to determine the perturbation velocity components by differentiation:

$$v_p = \frac{\partial \phi_p}{\partial y} = U_\infty A k e^{-(\beta k y)} \cos(kx)$$

$$u_p = \frac{\partial \phi_p}{\partial x} = \frac{U_\infty A}{\beta} k e^{-(\beta k y)} \sin(kx)$$

Now, for an isentropic process involving a perfect gas with constant specific heats, we have

$$\frac{T}{T_\infty} = \left(\frac{\rho}{\rho_\infty}\right)^{(\gamma - 1)}$$

The energy equation for isentropic flow yields

$$\frac{T}{T_\infty} = 1 - \left(\frac{\gamma - 1}{2}\right) M_\infty^2 \left(\frac{u^2 + v^2}{U_\infty^2} - 1\right)$$

Combining this expression with the relation for the density ratio, using the binomial expansion along with the assumptions that $u_p \ll U_\infty$ and $v_p \ll U_\infty$, leads to the following approximate expression:

$$\frac{\rho}{\rho_\infty} \cong 1 - M_\infty^2 \frac{u_p}{U_\infty}$$

This density relation and the expression for the velocity component in the $x$ direction produce

$$\frac{\partial \psi}{\partial y} = \frac{\rho}{\rho_\infty} u = \left(1 - M_\infty^2 \frac{u_p}{U_\infty}\right)(U_\infty + u_p)$$

$$\cong U_\infty + (1 - M_\infty^2) u_p = U_\infty + \beta U_\infty A k e^{-(\beta k y)} \sin(kx)$$

Integrate this expression with respect to $y$ to obtain

$$\psi = U_\infty y - U_\infty A e^{-(\beta k y)} \sin(kx) + f(x)$$

To determine the arbitrary function $f(x)$, differentiate this expression with respect to $x$ and equate the result to the negative of the product of the perturbation velocity component in the $y$ direction and the density ratio $\rho/\rho_\infty$. This operation yields

$$\frac{\partial \psi}{\partial x} = -U_\infty A k e^{-(\beta k y)} \cos(kx) + \frac{df}{dx} = -\frac{\rho}{\rho_\infty} v_p = -U_\infty A k e^{-(\beta k y)} \cos(kx)$$

Hence, $df/dx = 0$, and therefore $f(x)$ is a constant arbitrarily set to zero. The streamlines may be obtained by setting the stream function equal to a constant. Thus, we have

$$\psi = U_\infty y - U_\infty A e^{-(\beta k y)} \sin(kx) = C$$

When $C = 0$, we obtain the expression for the wall. Moreover, we see that the streamlines are harmonic and oscillate with the same frequency as the wall. Note, however, that the amplitude $A$ is multiplied by an exponential that gradually fades to zero for increasing values of $y$. Hence, far from the wall, the streamlines will be practically horizontal straight lines given by $U_\infty y$, which corresponds to a uniform, constant velocity flow in the $x$ direction.

## 13.4 SIMILARITY LAWS FOR SUBSONIC FLOW

For small-perturbation, linearized, compressible flow, it has been shown that

$$(1 - M_\infty^2)\frac{\partial^2 \phi}{\partial x^2} + \frac{\partial^2 \phi}{\partial y^2} = 0 \tag{13.11}$$

For incompressible, two-dimensional, steady potential flow, the potential equation reduces to Laplace's equation,

$$\frac{\partial^2 \phi_i}{\partial x_i^2} + \frac{\partial^2 \phi_i}{\partial y_i^2} = 0 \tag{13.27}$$

where $\phi_i$ is the velocity potential and $x_i$ and $y_i$ the space coordinates for an incompressible flow field. Solutions to Laplace's equation are available for a wide variety of boundary conditions. Thus, it would seem logical to try to transform the linearized, compressible potential equation into the incompressible potential equation, so as to utilize available incompressible flow solutions for problems in compressible flow. Consider a thin body in the $(x, y)$ plane immersed in a uniform compressible flow $U_\infty$ of Mach number $M_\infty$. We shall transform this flow to the incompressible plane $(x_i, y_i)$. Let

$$\begin{aligned} x_i &= k_1 x \\ y_i &= k_2 y \\ \phi_i &= k_3 \phi \\ U_{\infty_i} &= k_4 U_\infty \end{aligned} \tag{13.28}$$

where $k_1$, $k_2$, $k_3$, and $k_4$ are scale factors of the transformation. Substitute Eq. (13.28) into Eq. (13.11) to obtain

$$k_1^2 \frac{(1 - M_\infty^2)}{k_3}\frac{\partial^2 \phi_i}{\partial x_i^2} + \frac{k_2^2}{k_3}\frac{\partial^2 \phi_i}{\partial y_i^2} = 0 \tag{13.29}$$

In order to transform Eq. (13.11) into Laplace's equation, using the relationships given by Eq. (13.28), it follows that

$$\frac{k_1}{k_2} = \frac{1}{\sqrt{1 - M_\infty^2}} \tag{13.30}$$

Notice that the term $\sqrt{1 - M_\infty^2}$ becomes imaginary for supersonic flow; hence, the transformation can be applied only to subsonic flow. Physically, we have shown that, if a thin two-dimensional body is present in a subsonic compressible flow of Mach number $M_\infty$, the transformed body in an incompressible flow field will have its dimensions altered according to Eq. (13.30). For example, consider compressible flow over a thin airfoil of chord $c$ and thickness $t$. The transformed airfoil in incompressible flow will have its thickness-to-chord ratio $t/c$ altered so that

$$\frac{t_i}{c_i} = \frac{k_2 t}{k_1 c} = \frac{t}{c}\sqrt{1 - M_\infty^2} \tag{13.31}$$

As shown in Figure 13.5, if the same chord is maintained, then the incompressible thickness will be less: $t_i = \sqrt{1 - M_\infty^2}t$. However, if the same thickness is maintained, the chord will be stretched: $c_i = c/\sqrt{1 - M_\infty^2}$.

It is necessary for the compressible flow in the $(x, y)$ plane and the transformed flow in the $(x_i, y_i)$ plane to satisfy the boundary conditions on the body. We have established

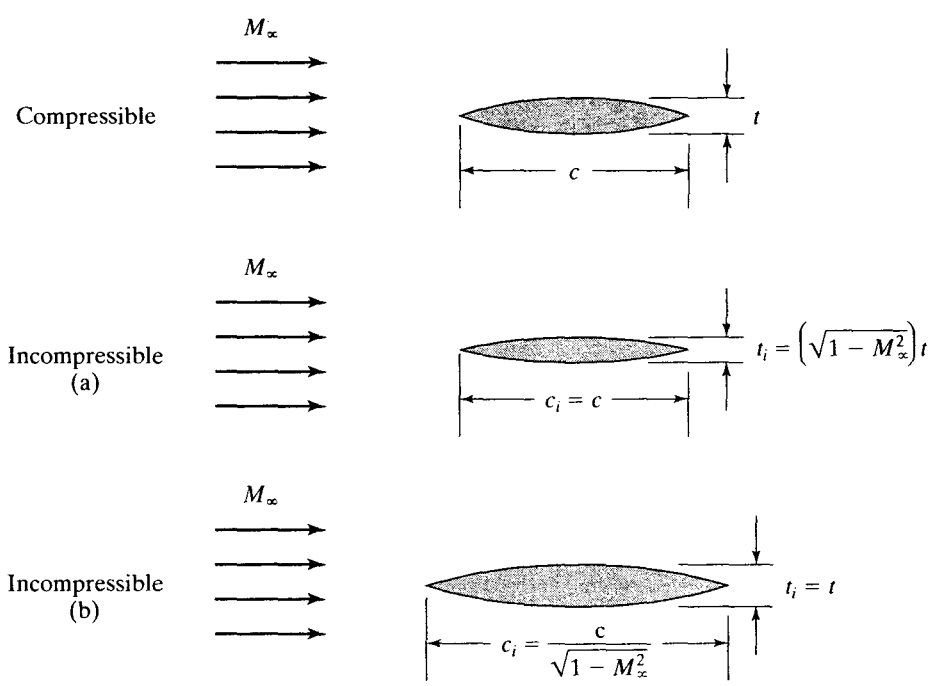


**Figure 13.5** Similarity Relationships between the Incompressible and Compressible Flow Chord $c$ and Thickness $t$ Dimensions of an Airfoil

that, for small perturbation flows,

$$\left(\frac{dy}{dx}\right)_b = \frac{v_p}{U_\infty} \tag{13.15}$$

where $v_p = \partial\phi_p/\partial y$. Using Eq. (13.28) to transform this boundary condition to the incompressible plane, we obtain

$$\frac{k_1}{k_2}\left(\frac{dy_i}{dx_i}\right)_b = \frac{k_4}{U_\infty}\frac{k_2}{k_3}\frac{\partial\phi_{p_i}}{\partial y_i}$$

To satisfy the boundary conditions at the body surface in the incompressible plane, it is necessary that

$$\frac{k_1}{k_2} = \frac{k_4 k_2}{k_3}$$

However, since

$$\frac{k_1}{k_2} = \frac{1}{\sqrt{1 - M_\infty^2}}$$

it follows that

$$\frac{k_2 k_4}{k_3} = \frac{1}{\sqrt{1 - M_\infty^2}} \tag{13.32}$$

It is important also to compare the pressure coefficients in the two planes. For compressible flow, it has been shown that $C_p = -2u_p/U_\infty$. For incompressible irrotational flow, Bernoulli's equation in the form $p + \frac{1}{2}\rho V^2 = \text{constant}$ can be applied. By definition,

$$C_{p_i} = \frac{(p - p_\infty)_i}{\frac{1}{2}\rho U_{\infty_i}^2}$$

Now, from Bernoulli's equation for incompressible flow, we have

$$p_{\infty_i} + \frac{1}{2}\rho U_{\infty_i}^2 = p_i + \frac{1}{2}\rho V_i^2 = p_i + \frac{1}{2}\rho\left[(u_{p_i} + U_{\infty_i})^2 + v_{p_i}^2\right]$$

Hence,

$$(p - p_\infty)_i = -\frac{1}{2}\rho U_{\infty_i}^2\left[2\frac{u_{p_i}}{U_{\infty_i}} + \left(\frac{u_{p_i}}{U_{\infty_i}}\right)^2 + \left(\frac{v_{p_i}}{U_{\infty_i}}\right)^2\right]$$

Dropping smaller terms, we obtain

$$C_{p_i} = -\frac{2u_{p_i}}{U_{\infty_i}} \tag{13.33}$$

For the compressible plane,

$$C_p = -\frac{2u_p}{U_\infty} = -\frac{2\dfrac{\partial \phi_p}{\partial x}}{U_\infty} = -\frac{2\dfrac{k_1 k_4}{k_3}\dfrac{\partial \phi_{pi}}{\partial x_i}}{U_{\infty i}} = -\frac{k_1}{k_2}\frac{k_2 k_4}{k_3}\frac{2u_{pi}}{U_{\infty i}}$$

So, we have the result that

$$C_p = \frac{C_{pi}}{1 - M_\infty^2} \tag{13.34}$$

From the transformation relationships given in Eq. (13.28), it is possible to determine the geometrical properties of an airfoil in the $(x_i, y_i)$ plane from those in the compressible plane. If we assume the chord length to be the same in the two planes, then the thickness ratio $t_i/c_i$ for the incompressible airfoil has been shown to be $\sqrt{1 - M_\infty^2}$ times the thickness ratio for the compressible airfoil. The same relationship holds for other airfoil characteristics involving a ratio of the $y$ dimension to the $x$ dimension. For example, the angles of attack of the airfoils (see Figure 13.6) are related by

$$\alpha_i = \alpha\sqrt{1 - M_\infty^2} \tag{13.35}$$

Similarly, the camber ratios (see Figure 13.7) are in proportion:

$$\frac{(\text{camber}/c)_i}{(\text{camber}/c)} = \sqrt{1 - M_\infty^2} \tag{13.36}$$

The lift $L$ of an airfoil, the upward force normal to the uniform-flow direction, is obtained by integrating the pressure over the airfoil surface. Thus,

$$L = \int_0^c p_l\, dx - \int_0^c p_u\, dx$$

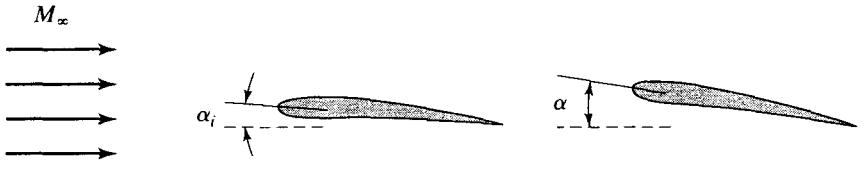


**Figure 13.6** Incompressible and Compressible Angles of Attack of an Airfoil

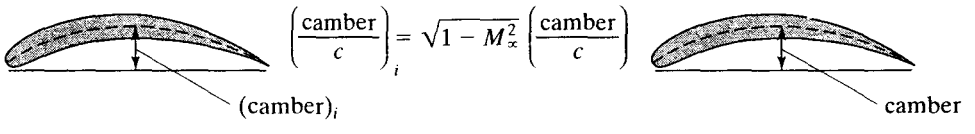


---- Mean line (equidistant between upper and lower surfaces)

**Figure 13.7** Incompressible and Compressible Camber of an Airfoil

where $p_u$ and $p_l$ are the pressures on the upper and lower airfoil surfaces, respectively. Define a lift coefficient $C_L$ as

$$C_L \equiv \frac{L}{\frac{1}{2}\rho U_\infty^2 c} = \frac{L}{\frac{1}{2}\rho U_\infty^2 c} = \int_0^c C_{p_l} \frac{dx}{c} - \int_0^c C_{p_u} \frac{dx}{C} \tag{13.37}$$

Thus, the lift coefficients for the airfoils in the compressible and incompressible planes are in the same ratio as the pressure coefficient:

$$C_{Li} = C_L(1 - M_\infty^2) \tag{13.38}$$

The similarity relations as stated here [Eqs. (13.34), (13.35), (13.36), and (13.38)] are called the *Goethert rules*. It must be emphasized that these rules are valid only for thin airfoils with small angles of attack, small camber ratios, and so on. Also, the Goethert rules only apply to subsonic flow, for which $\sqrt{1 - M_\infty^2}$ is real. The extension of these rules to three-dimensional flow will be left as an exercise. The following example illustrates the application of the Goethert rules to a two-dimensional airfoil.

**Example 13.2. Application of Goethert similarity rules for subsonic flow past a two-dimensional airfoil**

A two-dimensional airfoil has a thickness ratio (maximum thickness to chord) of 0.04 and a camber ratio of 0.015. When tested in a low-speed wind tunnel (incompressible flow, $M_\infty = 0$) at an angle of attack of 3°, the lift coefficient $C_L$ is measured to be 0.6. It is desired to determine the performance of a similar airfoil at $M_\infty = 0.5$. Using the Goethert rules, determine the geometrical characteristics of the related airfoil in compressible flow at the given $M_\infty$, and determine the lift coefficient.

**Solution**

First, we have

$$\sqrt{1 - M_\infty^2} = \sqrt{1 - (0.5)^2} = 0.8660$$

From Eq. (13.31),

$$\left(\frac{t}{c}\right)_{M_\infty = 0.5} = \left(\frac{t}{c}\right)_i \frac{1}{\sqrt{1 - M_\infty^2}} = \left(\frac{t}{c}\right)_i \frac{1}{0.8660} = (0.04)(1.1547) = 0.0462$$

From Eq. (13.36),

$$\left(\frac{\text{camber}}{c}\right)_{M_\infty = 0.5} = \left(\frac{\text{camber}}{c}\right)_i \frac{1}{\sqrt{1 - M_\infty^2}} = (0.015)(1.1547) = 0.0173$$

From Eq. (13.35),

$$\alpha_{M_\infty = 0.5} = \alpha_i \frac{1}{\sqrt{1 - M_\infty^2}} = (3)(1.1547) = 3.4641°$$

From Eq. (13.38),

$$C_{L_{M_\infty=0.5}} = \frac{C_{Li}}{1 - M_\infty^2} = \frac{0.6}{0.75} = 0.80$$

Although the Goethert rules have been shown to possess some application, it would seem far more useful to have a comparison between performance of the same airfoil in compressible and incompressible flows. So far, the airfoils have been distorted according to Eq. (13.28), as shown in Figure 13.5.

To this end, let us consider two airfoils in the incompressible plane, related to a third foil in the compressible plane. The first incompressible airfoil—call it $A$, as shown in Figure 13.8—is distorted according to Eq. (13.28), with its thickness-to-chord ratio, for example, given by

$$\left(\frac{t}{c}\right)_{iA} = \frac{t}{c}\sqrt{1 - M_\infty^2}$$

The second incompressible foil—call it $B$—is assumed to possess exactly the same dimensions as the compressible foil, so that, for example,

$$\left(\frac{t}{c}\right)_{iB} = \frac{t}{c}$$

or

$$\left(\frac{t}{c}\right)_{iA} = \sqrt{1 - M_\infty^2}\left(\frac{t}{c}\right)_{iB}$$

Since we have a relationship between the pressure coefficients for the compressible airfoil and incompressible airfoil $A$, we need a relation between the pressure coefficients for the incompressible airfoils. It can be shown that for thin bodies in incompressible, two-dimensional potential flow, related by $(y/c)_i = Kf(x/c)_i$, with $f$ being the same

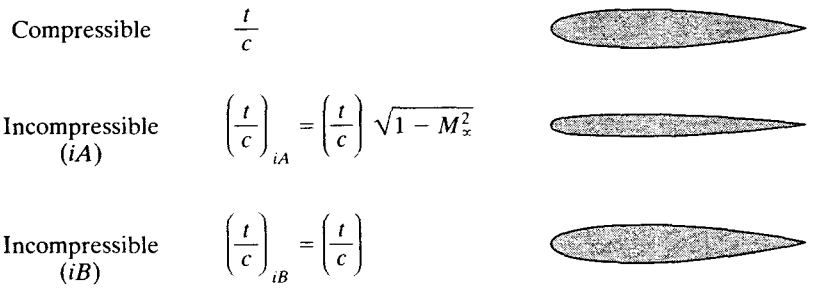


**Figure 13.8** Similarity Relations for the Thickness-to-Chord Ratio of an Airfoil

function for all bodies, the potential $\phi_i$, and therefore $C_{pi}$ at corresponding points $x/c$, is proportional to $K$. [See Ref. (13.5).] For our case,

$$\frac{\left(\frac{y}{c}\right)_{iB}}{\left(\frac{y}{c}\right)_{iA}} = \frac{K_{iB}}{K_{iA}} = \frac{1}{\sqrt{1 - M_\infty^2}}$$

which means that

$$\frac{C_{piA}}{C_{piB}} = \frac{K_{iA}}{K_{iB}} = \sqrt{1 - M_\infty^2} \tag{13.39}$$

From Eq. (13.34) we have

$$C_{piA} = C_p(1 - M_\infty^2)$$

then

$$C_{piB} = C_p\sqrt{1 - M_\infty^2}$$

$$C_p = \frac{C_{pi}}{\sqrt{1 - M_\infty^2}} \tag{13.40}$$

This expression relates the pressure coefficient on a body immersed in two-dimensional compressible flow of Mach number $M_\infty$ to the pressure coefficient on the same body immersed in an incompressible flow.

Let us now attempt to determine the shape of a third incompressible airfoil—call it $C$—that has the same pressure coefficient at corresponding points as the compressible foil:

$$C_{piC} = C_p$$

From Eq. (13.40),

$$\frac{C_{piC}}{C_{piB}} = \frac{1}{1 - M_\infty^2}$$

But, from Eq. (13.39),

$$\frac{C_{piC}}{C_{piB}} = \frac{\left(\frac{y}{c}\right)_{iC}}{\left(\frac{y}{c}\right)_{iB}} = \frac{\left(\frac{t}{c}\right)_{iC}}{\left(\frac{t}{c}\right)_{iB}}$$

Therefore, for $C_{piC} = C_p$, it follows that

$$\left.\begin{aligned} \left(\frac{t}{c}\right)_{iC} &= \frac{1}{\sqrt{1 - M_\infty^2}}\left(\frac{t}{c}\right)_{iB} = \frac{1}{\sqrt{1 - M_\infty^2}}\frac{t}{c} \\ \alpha_{iC} &= \frac{1}{\sqrt{1 - M_\infty^2}}\alpha \\ \left(\frac{\text{camber}}{c}\right)_{iC} &= \frac{1}{\sqrt{1 - M_\infty^2}}\frac{\text{camber}}{c} \end{aligned}\right\} \tag{13.41}$$

The similarity laws for subsonic compressible flow, as given by Eqs. (13.40) and (13.41), are called the *Prandtl–Glauert rules*. Their validity is restricted to two-dimensional flows, since Eq. (13.39) is not valid for three-dimensional flows. Based on the assumptions that underlie the development, the Prandtl–Glauert rules apply only to flows with small perturbations—that is, to thin bodies—at small angles of attack. Moreover, they also are limited to small values of freestream Mach numbers. Because of these restrictions, other compressibility correction formulas have been derived. For example, Laitone [Ref. (13.6)] wrote the pressure coefficient in Eq. (13.40) in terms of the local Mach number rather than $M_\infty$:

$$C_p = \frac{C_{pi}}{\sqrt{1 - M^2}}$$

The implications of the Laitone modification is that the linearized equations are not applicable over the entire flowfield, but rather only to a small local region of approximately uniform flow.

The local Mach number $M$ is connected to the freestream Mach number $M_\infty$ by the isentropic relation

$$\frac{p}{p_\infty} = \left(\frac{1 + \dfrac{\gamma - 1}{2}M_\infty^2}{1 + \dfrac{\gamma - 1}{2}M^2}\right)^{\gamma/(\gamma-1)}$$

This expression is then introduced into Eq. (13.17) and the result rearranged to give

$$M^2 = \frac{[2 + (\gamma - 1)M_\infty^2]\left(1 + \dfrac{\gamma M_\infty^2}{2}C_p\right)^{(1-\gamma)/\gamma} - 2}{(\gamma - 1)}$$

Next, the binominal theorem is used and the result incorporated into the pressure coefficient expression to produce Laitone's formula:

$$C_p = \frac{C_{pi}}{\sqrt{1 - M_\infty^2} + \dfrac{M_\infty^2\left[1 + \dfrac{(\gamma - 1)}{2}M_\infty^2\right]}{2\sqrt{1 - M_\infty^2}}C_{pi}} \tag{13.42}$$

This expression approaches the Prandtl–Glauert expression, Eq. (13.40), for small values of $C_{pi}$. Comparison of the results using both Prandtl–Glauert and Laitone can be found in Ref. (13.7). Other correction formulas have also been developed, such as the Karman–Tsien rule [Ref. (13.8)].

**Example 13.3. Application of the Prandtl-Glauert similarity rule for subsonic flow past a two-dimensional airfoil**

The two-dimensional airfoil of Example 13.2, when tested in a low-speed wind tunnel at an angle of attack of 3°, is found to have a lift coefficient $C_L$ of 0.6. Determine the lift coefficient of the same airfoil at $M_\infty = 0.50$.

**Solution**

From the Prandtl–Glauert similarity rule, Eq. (13.40), we can write

$$C_{L_{M_\infty=0}} = C_{Li} = C_L\sqrt{1 - M_\infty^2}$$

Therefore,

$$C_L = \frac{0.6}{\sqrt{1 - (0.5)^2}} = \frac{0.6}{0.8660} = 0.6928$$

Note that in Example 13.2 we compared the lift coefficients of two different airfoils, one in incompressible flow and the other, of different dimensions, in compressible flow. In Example 13.3, we are comparing the lift coefficients of the same airfoil in incompressible and compressible flow.

---

The upper limit of applicability of the similarity laws for subsonic flow is reached when the Mach number at some point on the airfoil is unity. The Mach number increases over the airfoil surface and reaches a maximum at the point of minimum pressure, so that Mach 1 will occur at a point on the surface when $M_\infty$ is somewhat less than unity. Once Mach 1 or greater is reached at a point on the airfoil (presumably on the upper surface), a shock will form (Figure 13.9), and the assumption of irrotational, isentropic flow will be invalid. With the pressure increase on the upper surface due to the shock (an adverse pressure gradient), the boundary layer will separate and cause a resultant decrease in airfoil lift–drag ratio. It becomes important to be able to calculate the critical freestream Mach number $M_{\infty_{crit}}$ at which the Mach number will be equal to unity at a point on the airfoil surface.

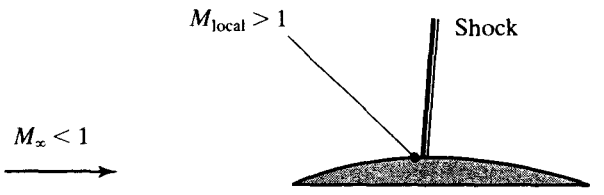


**Figure 13.9** Limit of Applicability of Subsonic Similarity Rules

Assuming isentropic flow from $M_\infty$ up to the point at which sonic flow is first reached on the airfoil (at the point of minimum pressure), we obtain, for $p_o$ equal to a constant,

$$p_\infty\left(1 + \frac{\gamma - 1}{2}M^2_{\infty_{crit}}\right)^{\gamma/(\gamma-1)} = p_{M=1}\left(1 + \frac{\gamma - 1}{2}\right)^{\gamma/(\gamma-1)} \tag{13.43}$$

We have defined the pressure coefficient as

$$C_p = \frac{p - p_\infty}{\frac{1}{2}\rho U^2_\infty} = \frac{2(p - p_\infty)}{\gamma p_\infty M^2_\infty}$$

or

$$C_{p_{M=1}} = \frac{2}{\gamma M^2_{\infty_{crit}}}\left(\frac{p_{M=1}}{p_\infty} - 1\right)$$

Substituting from Eq. (13.43), we obtain

$$C_{p_{M=1}} = \frac{2}{\gamma M^2_{\infty_{crit}}}\left[\frac{\left(1 + \frac{\gamma - 1}{2}M^2_{\infty_{crit}}\right)^{\gamma/(\gamma-1)}}{\left(1 + \frac{\gamma - 1}{2}\right)^{\gamma/(\gamma-1)}} - 1\right] \tag{13.44}$$

The minimum pressure coefficient for incompressible flow can be determined from low-speed wind-tunnel tests; then the minimum pressure coefficient for the same airfoil in compressible flow can be calculated from the Prandtl–Glauert rule:

$$C_{p_{M_\infty}} = \frac{C_{p_{M_\infty=0}}}{\sqrt{1 - M^2_\infty}} \tag{13.40}$$

**Example 13.4. Determination of the critical Mach number and minimum pressure coefficient on a two-dimensional airfoil in subsonic flow**

The minimum pressure coefficient on a two-dimensional airfoil, as measured in a low-speed wind tunnel ($M_\infty = 0$), is $-0.8$. Determine the critical Mach number for the airfoil.

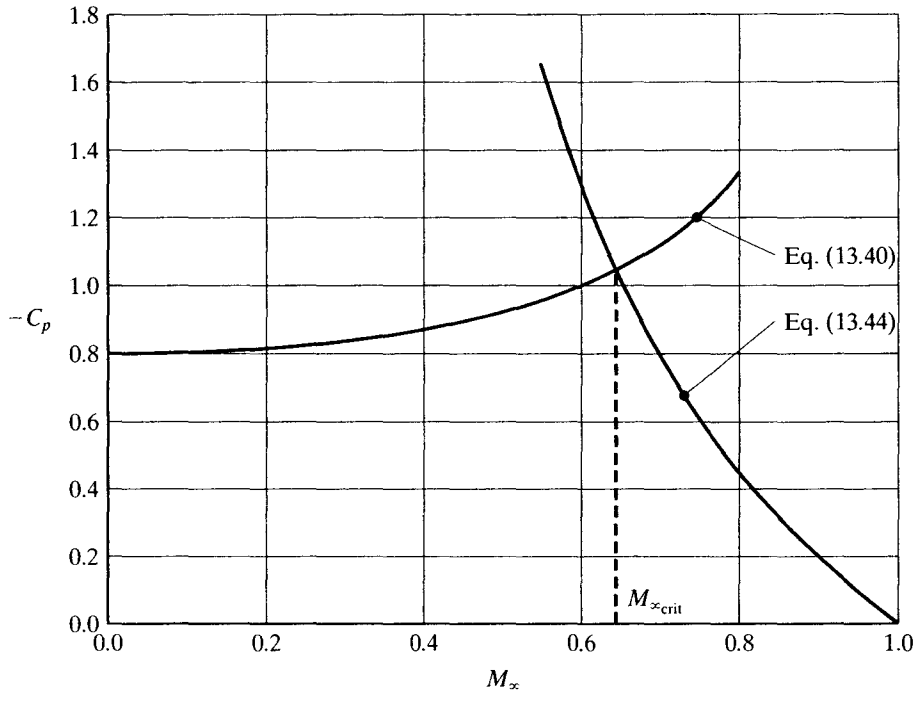


**Figure 13.10** Graphical Determination of the Critical Mach Number

**Solution**

From Eq. (13.40), we have

$$C_{p_{M_\infty}} = \frac{C_{pi}}{\sqrt{1 - M_\infty^2}} = \frac{-0.8}{\sqrt{1 - M_\infty^2}}$$

This expression is plotted in Figure 13.10 and gives the minimum pressure coefficient as a function of the freestream Mach number. From Eq. (13.43), we have the pressure coefficient at which Mach 1 occurs versus the freestream Mach number. This relationship is also plotted in Figure 13.10; the intersection of the two curves is the solution to the problem. It can be seen that $M_{\infty_{crit}} = 0.64$. This value is somewhat high for the Prandtl–Glauert formula.

## 13.5 SUPERSONIC FLOW OVER A WAVY WALL

The equation for the small-perturbation velocity potential for isentropic steady flow was found to be

$$(1 - M_\infty^2)\frac{\partial^2 \phi_p}{\partial x^2} + \frac{\partial^2 \phi_p}{\partial y^2} = 0 \tag{13.13}$$

This equation is valid for supersonic as well as subsonic flow, with the aforementioned restriction that it becomes invalid for transonic and hypersonic flows. Furthermore, shocks

that might occur in this supersonic flow must be assumed to be extremely weak so as not to cause a significant departure from isentropic flow. For flows in which $M_\infty > 1$, the coefficient of the first term in Eq. (13.13) becomes negative. This changes the entire nature of the partial differential equation. As described in Section 13.2, for $M_\infty < 1$, Eq. (13.13) is an elliptic type of PDE and, as we have shown, may be reduced to Laplace's equation by suitable transformation. However, for $M_\infty > 1$, Eq. (13.13) is of the hyperbolic type, with the form of that of the wave equation. The general solution to this equation can be obtained in a variety of ways; see, for example, Ref. (13.9). A simple approach is to write the potential as the sum of two arbitrary functions $f$ and $g$ such that

$$\phi_p = f(\xi) + g(\eta) \tag{13.45}$$

where $\xi = x + y\sqrt{M_\infty^2 - 1}$ and $\eta = x - y\sqrt{M_\infty^2 - 1}$. Rather than develop the solution, we will instead verify Eq. (13.45) by substituting it into Eq. (13.13), making use of the chain rule:

$$\frac{\partial \phi_p}{\partial x} = \frac{\partial}{\partial x}[f(\xi) + g(\eta)] = \frac{\partial \xi}{\partial x}\frac{\partial}{\partial \xi}[f(\xi) + g(\eta)] + \frac{\partial \eta}{\partial x}\frac{\partial}{\partial \eta}[f(\xi) + g(\eta)]$$

$$= \frac{\partial \xi}{\partial x}\left(\frac{df}{d\xi} + 0\right) + \frac{\partial \eta}{\partial x}\left(0 + \frac{dg}{d\eta}\right) = (1)\frac{df}{d\xi} + (1)\frac{dg}{d\eta} = \frac{df}{d\xi} + \frac{dg}{d\eta}$$

$$\frac{\partial^2 \phi_p}{\partial x^2} = \frac{\partial}{\partial x}\left(\frac{\partial \phi_p}{\partial x}\right) = \frac{\partial \xi}{\partial x}\frac{d}{d\xi}\left(\frac{df}{d\xi} + \frac{dg}{d\eta}\right) + \frac{\partial \eta}{\partial x}\frac{d}{d\eta}\left(\frac{df}{d\xi} + \frac{dg}{d\eta}\right) = \frac{d^2 f}{d\xi^2} + \frac{d^2 g}{d\eta^2}$$

$$\frac{\partial \phi_p}{\partial y} = \frac{\partial}{\partial y}[f(\xi) + g(\eta)] = \frac{\partial \xi}{\partial y}\frac{\partial}{\partial \xi}[f(\xi) + g(\eta)] + \frac{\partial \eta}{\partial y}\frac{\partial}{\partial \eta}[f(\xi) + g(\eta)]$$

$$= \frac{\partial \xi}{\partial y}\left(\frac{df}{d\xi} + 0\right) + \frac{\partial \eta}{\partial y}\left(0 + \frac{dg}{d\eta}\right) = \left(\sqrt{M_\infty^2 - 1}\right)\frac{df}{d\xi} + \left(-\sqrt{M_\infty^2 - 1}\right)\frac{dg}{d\eta}$$

$$= \sqrt{M_\infty^2 - 1}\left(\frac{df}{d\xi} - \frac{dg}{d\eta}\right)$$

$$\frac{\partial^2 \phi_p}{\partial y^2} = \sqrt{M_\infty^2 - 1}\left[\frac{\partial \xi}{\partial y}\frac{d}{d\xi}\left(\frac{df}{d\xi} - \frac{dg}{d\eta}\right) + \frac{\partial \eta}{\partial y}\frac{d}{d\eta}\left(\frac{df}{d\xi} - \frac{dg}{d\eta}\right)\right]$$

$$= (M_\infty^2 - 1)\left(\frac{d^2 f}{d\xi^2} + \frac{d^2 g}{d\eta^2}\right)$$

It can be seen that

$$(1 - M_\infty^2)\frac{\partial^2 \phi_p}{\partial x^2} = -\frac{\partial^2 \phi_p}{\partial y^2}$$

and therefore the identified solution, Eq.(13.45), satisfies the governing equation, Eq. (13.13).

For this linearized flow, lines of constant $f$, or lines for which $\xi = x + y\sqrt{M_\infty^2 - 1}$ = constant, are straight with the following slope:

$$\frac{dy}{dx} = -\frac{1}{\sqrt{M_\infty^2 - 1}} \tag{13.46}$$

Lines of constant $g$ are also straight, inclined to the flow direction by

$$\frac{dy}{dx} = +\frac{1}{\sqrt{M_\infty^2 - 1}} \tag{13.47}$$

From the expressions for the slopes, there appears to be a connection between lines of constant $f$ and $g$ and the Mach waves or lines discussed in Chapter 2. There, we found that if a point disturbance were placed in a uniform flow, the disturbance would be felt in the zone of action, defined by the Mach waves. This situation is depicted for two-dimensional flow in Figure 13.11.

From Eq. (2.19), the Mach angle $\mu$ is given by

$$\sin \mu = \frac{1}{M_\infty}$$

Using trigonometry, we obtain

$$\tan \mu = \frac{1}{\sqrt{M_\infty^2 - 1}} = \frac{dy}{dx}$$

or

$$\tan(-\mu) = -\frac{1}{\sqrt{M_\infty - 1}}$$

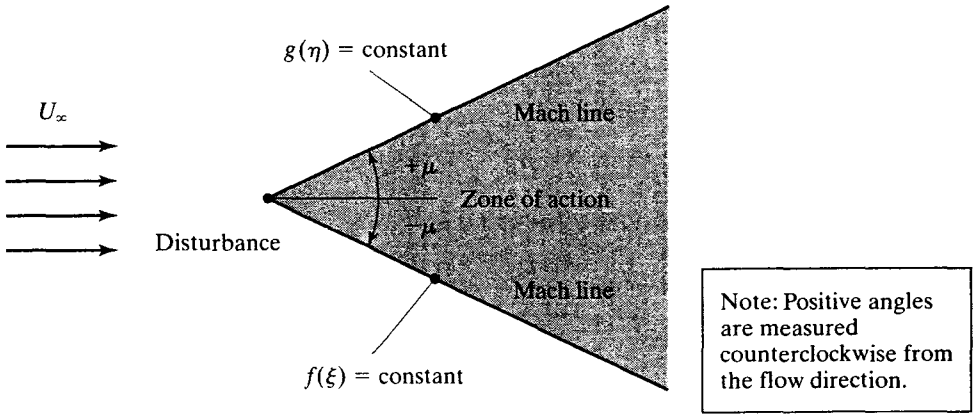


**Figure 13.11** Connection between Mach Lines and the Functions $f(\xi)$ and $g(\eta)$

We see, therefore, that a line of constant $g$ is the Mach line or wave in Figure 13.11 that makes a positive angle with the flow direction, and a line of constant $f$ is the Mach wave that makes a negative angle with the flow direction.

For a linearized supersonic flow over a thin body, lines of constant $f$ and $g$ form a network as shown in Figure 13.12. These lines extend to infinity in both directions. However, from Figure 13.11, it can be seen that an $f$ = constant line is not a Mach wave above and to the left of the disturbance, since this would imply that the effect of the disturbance could be felt outside the zone of action. Likewise, a line of $g$ = constant is not a Mach wave below and to the left of the disturbance.

For flow over a thin body, as shown in Figure 13.13, we need consider only the lines of $g$ = constant above the body, since these are the only lines physically present in the flow as Mach waves. Likewise, below the body, we need consider only lines of $f$ = constant.

The nature of the functions $f$ and $g$ is arbitrary; their particular form is dependent on the boundary conditions. To illustrate this point we shall return to the problem of

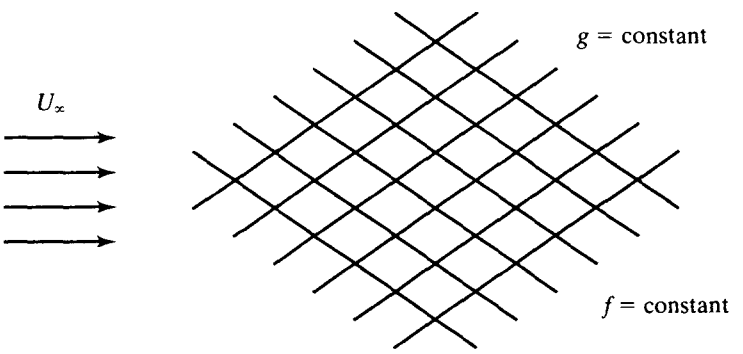


**Figure 13.12** Network of Lines Formed by the Functions $f(\xi)$ and $g(\eta)$ in a Linearized Supersonic Flow

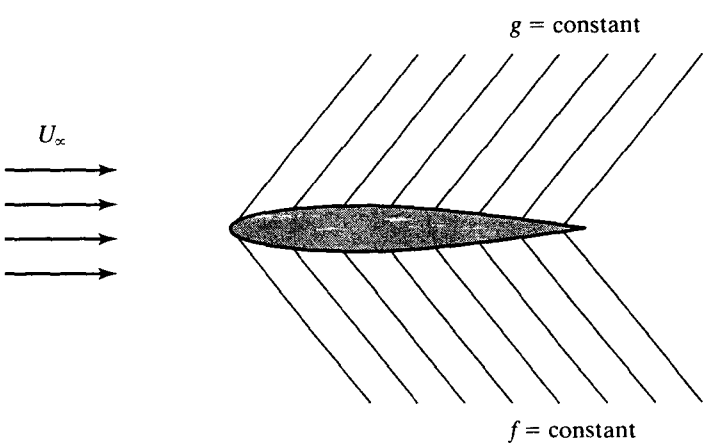


**Figure 13.13** Supersonic Flow over a Thin Airfoil

flow over a wavy wall. Consider uniform, irrotational supersonic flow over a wavy wall, as shown in Figure 13.3. The boundary condition at the wall, just as with the subsonic case, is

$$\left(\frac{\partial \phi_p}{\partial y}\right)_{y=0} = U_\infty A \frac{2\pi}{\lambda} \cos \frac{2\pi x}{\lambda} \tag{13.48}$$

As shown in Figure 13.14, and discussed previously, only the $g$ function is applicable for this case, so

$$\phi_p = g\left(x - y\sqrt{M_\infty^2 - 1}\right) = g(\eta) \tag{13.49}$$

Substituting Eq. (13.49) into Eq. (13.48) and applying the chain rule yields

$$\left(\frac{\partial \phi_p}{\partial y}\right)_{y=0} = \left(\frac{\partial \eta}{\partial y}\frac{dg}{d\eta}\right)_{y=0} = -\sqrt{M_\infty^2 - 1}\left(\frac{dg}{d\eta}\right)_{y=0} = U_\infty A \frac{2\pi}{\lambda} \cos \frac{2\pi x}{\lambda}$$

Therefore,

$$\left(\frac{dg}{d\eta}\right)_{y=0} = -\frac{U_\infty}{\sqrt{M_\infty^2 - 1}} \frac{2\pi A}{\lambda} \cos \frac{2\pi x}{\lambda}$$

or, at any $y$, simply replace each $x$ in the expression with $x - y\sqrt{M_\infty^2 - 1}$:

$$\frac{dg}{d\eta} = -\frac{U_\infty}{\sqrt{M_\infty^2 - 1}} \frac{2\pi A}{\lambda} \cos\left[\frac{2\pi\left(x - y\sqrt{M_\infty^2 - 1}\right)}{\lambda}\right]$$

$$= -\frac{U_\infty}{\sqrt{M_\infty^2 - 1}} \frac{2\pi A}{\lambda} \cos\left(\frac{2\pi\eta}{\lambda}\right)$$

Integrating with respect to $\eta$, we obtain

$$g = -\frac{U_\infty}{\sqrt{M_\infty^2 - 1}} \frac{2\pi A}{\lambda} \frac{\lambda}{2\pi} \sin\left(\frac{2\pi\eta}{\lambda}\right) + \text{constant}$$

$$= -\frac{U_\infty A}{\sqrt{M_\infty^2 - 1}} \sin\left[\frac{2\pi}{\lambda}\left(x - y\sqrt{M_\infty^2 - 1}\right)\right] + \text{constant}$$

$$= \phi_p \tag{13.50}$$

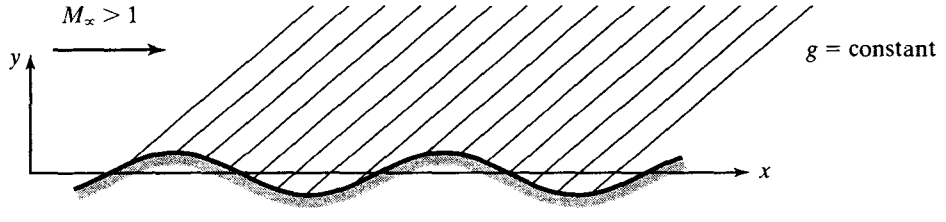


**Figure 13.14** Supersonic Flow over a Wavy Wall

Note that the boundary conditions at infinity, as given in Section 13.3, are also satisfied. The perturbation velocities $u_p$ and $v_p$ are obtained by differentiation:

$$u_p = \frac{\partial \phi_p}{\partial x} = -\frac{U_\infty A}{\sqrt{M_\infty^2 - 1}} \frac{2\pi}{\lambda} \cos \frac{2\pi}{\lambda} \left( x - y\sqrt{M_\infty^2 - 1} \right) \tag{13.51}$$

$$v_p = \frac{\partial \phi_p}{\partial y} = +U_\infty A \frac{2\pi}{\lambda} \cos \left[ \frac{2\pi}{\lambda} \left( x - y\sqrt{M_\infty^2 - 1} \right) \right] \tag{13.52}$$

Also, it has been shown that, for small-perturbation flow,

$$C_p = -\frac{2u_p}{U_\infty}$$

so that, for supersonic flow over a wave-shaped wall,

$$C_p = \frac{4A\pi}{\sqrt{M_\infty^2 - 1}\lambda} \cos \frac{2\pi}{\lambda} \left( x - y\sqrt{M_\infty^2 - 1} \right) \tag{13.53}$$

At the wall, $y$ is approximately zero, so

$$C_{p_{\text{wall}}} = \frac{4A\pi}{\sqrt{M_\infty^2 - 1}\lambda} \cos \frac{2\pi x}{\lambda} \tag{13.54}$$

Streamlines and pressure distribution on the wall are shown in Figure 13.15 for uniform supersonic flow over a wavy wall.

By referring to Eqs. (13.51), (13.52), and (13.53), we can observe that along lines of $\eta = x - y\sqrt{1 - M_\infty^2}$ = constant, the perturbation velocities and pressure coefficient are constant. In other words, the disturbance introduced into the uniform flow by the presence of the wall is felt equally (out to infinity) along these lines. Thus, the presence of a disturbance in supersonic linearized flow is propagated along the Mach lines or waves.

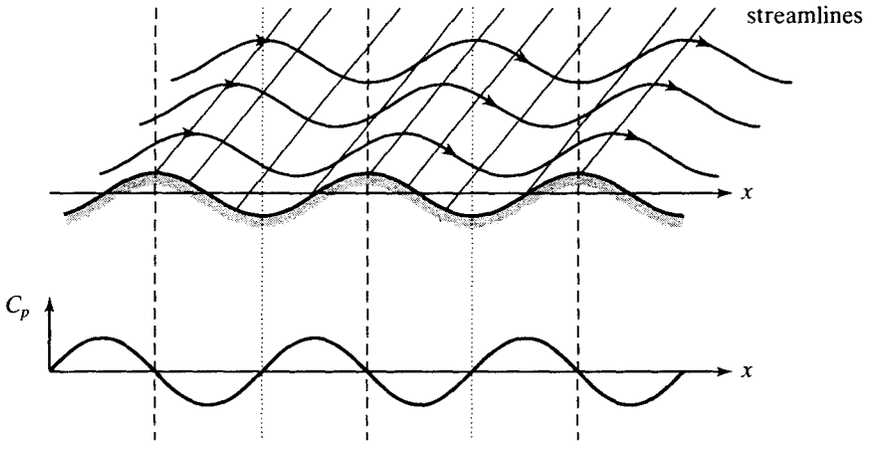


**Figure 13.15** Supersonic Flow Streamlines and Pressure Variation along a Wavy Wall

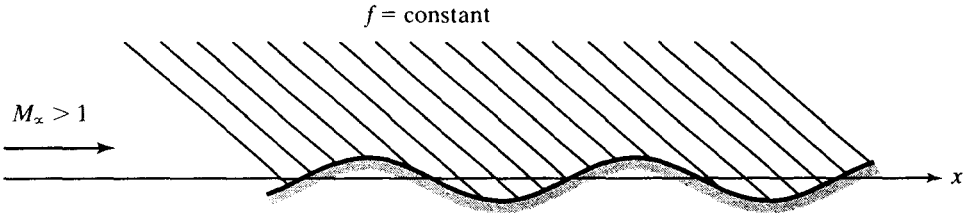


**Figure 13.16** Impossibility of the Existence of $f(\xi)$ = Constant Lines in Supersonic Flow over a Wavy Wall

Once again, it can be seen why lines of $f$ = constant were ruled out of the solution. These lines would be inclined to the flow as shown in Figure 13.16. For such lines to exist as Mach waves, it would be possible for the presence of the wall to be propagated back upstream into the supersonic flow, and thus the supersonic flow would be able to "sense" the presence of the wall before reaching it. But from the discussion in Chapter 2, we know that this condition is physically impossible; thus, for this situation, only lines of $g$ = constant are physically present.

Several of the basic differences between supersonic and subsonic flow become evident from the example of flow over a wavy wall. In subsonic flow, the perturbation velocities die out as $y$ gets very large. In supersonic flow, the disturbance of the wall is felt along Mach lines inclined to the flow direction. The disturbance, or perturbation, does not die out, but remains constant, even as $y$ approaches infinity. Thus, for supersonic flow, the Mach lines or waves have great significance; such Mach lines do not exist for subsonic flow.

In subsonic flow, the pressure coefficient is in phase with the wall shape, so there is no drag force on the wall. In supersonic flow, the pressure coefficient is out of phase with the wall shape, so there is a drag force on the wall. (See Figure 13.17.)

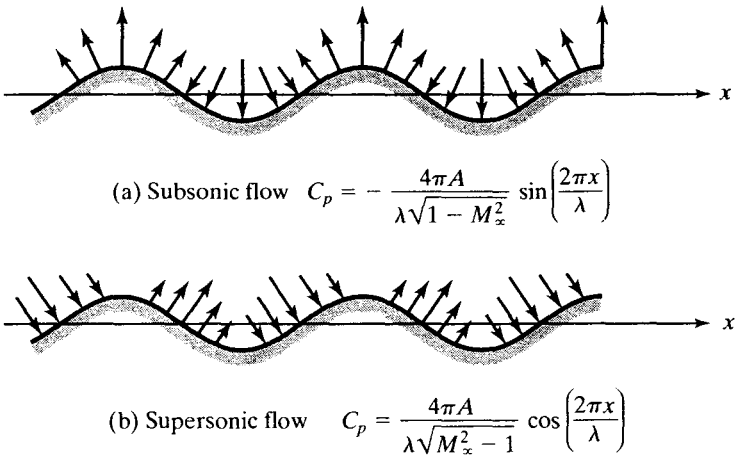


**Figure 13.17** Comparison of Pressure Forces Acting on a Wavy Wall in Subsonic and Supersonic Flow

## 13.6 THIN AIRFOILS IN SUPERSONIC FLOW

The general solution of the linearized potential equation for isentropic, irrotational supersonic flow has been shown to be

$$\phi_p = f\left(x + y\sqrt{M_\infty^2 - 1}\right) + g\left(x - y\sqrt{M_\infty^2 - 1}\right) = f(\xi) + g(\eta) \quad (13.45)$$

where $f(\xi)$ and $g(\eta)$ are arbitrary functions dependent on the boundary conditions. Let us apply this result to supersonic flow over a thin, two-dimensional airfoil. (See Figure 13.18.) Since a disturbance cannot be propagated upstream into a supersonic flow, the solution over the top of the foil will consist of lines of constant $g$, and the solution under the foil will consist of lines of constant $f$.

Now, for $y > 0$ (i.e., on the upper side of the airfoil),

$$\phi_p = g\left(x - y\sqrt{M_\infty^2 - 1}\right) = g(\eta)$$

For $y < 0$ (i.e., on the lower side of the airfoil),

$$\phi_p = f(x + y\sqrt{M_\infty^2 - 1}) = f(\xi) \quad (13.55)$$

The boundary condition on the upper foil surface, designated by the subscript $u$, is

$$\left(\frac{dy}{dx}\right)_u = \frac{v_u}{U_\infty} = \frac{1}{U_\infty}\frac{\partial \phi_p}{\partial y}$$

Applying the chain rule, we obtain

$$\left(\frac{\partial \phi_p}{\partial y}\right)_{y>0} = \frac{\partial \eta}{\partial y}\frac{dg}{d\eta} = -\sqrt{M_\infty^2 - 1}\left(\frac{dg}{d\eta}\right) = U_\infty\left(\frac{dy}{dx}\right)_u \quad (13.56)$$

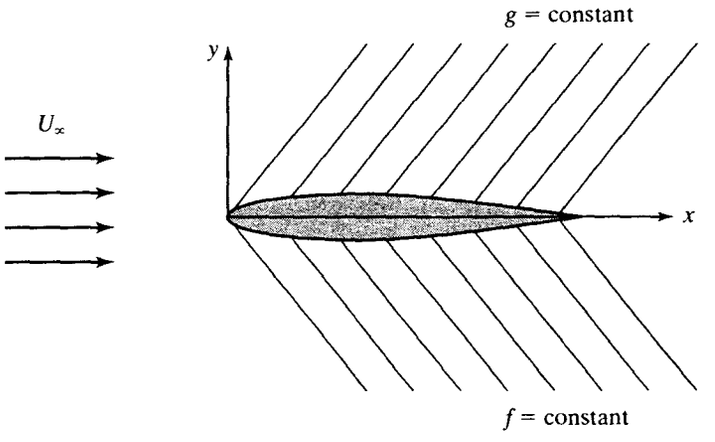


**Figure 13.18** Supersonic Flow over a Thin Airfoil

The pressure coefficient on the upper surface of the foil, $C_{p_u}$, is given by

$$C_{p_u} = -\frac{2u_u}{U_\infty} = -\frac{2}{U_\infty}\left(\frac{\partial \phi_p}{\partial x}\right)_{y=0}$$

$$= -\frac{2}{U_\infty}\frac{\partial \eta}{\partial x}\frac{dg}{d\eta} = \frac{2}{U_\infty}(1)\frac{dg}{d\eta} \tag{13.57}$$

Substituting Eq. (13.56) into Eq. (13.57), we obtain

$$C_{p_u} = \frac{2}{U_\infty}\frac{U_\infty\left(\frac{dy}{\partial x}\right)_u}{\sqrt{M_\infty^2 - 1}} = \frac{2}{\sqrt{M_\infty^2 - 1}}\left(\frac{dy}{dx}\right)_u \tag{13.58}$$

Similarly, for the pressure coefficient on the lower surface, $C_{p_l}$, we have

$$C_{p_l} = -\frac{2u_l}{U_\infty} = -\frac{2}{U_\infty}\left(\frac{df}{d\xi}\right)_{y=0}$$

where

$$\left(\frac{df}{d\xi}\right)_{y=0}\sqrt{M_\infty^2 - 1} = U_\infty\left(\frac{dy}{dx}\right)_l$$

Hence,

$$C_{p_l} = -\frac{2}{\sqrt{M_\infty^2 - 1}}\left(\frac{dy}{dx}\right)_l \tag{13.59}$$

There are also other approaches to develop the pressure coefficients on airfoils in supersonic flow. The following example illustrates a second approach.

**Example 13.5. Determination of an expression for the linearized pressure coefficient from oblique-shock relations**

Using oblique-shock relations, rederive Eq. (13.58) for the linearized pressure coefficient in supersonic flow over the upper portion of an airfoil.

**Solution**

Figure 13.19 depicts a weak oblique shock occurring at a convex corner, which is the same configuration as that at the leading edge of an airfoil in a supersonic flow. The corner angle $\delta$ is very small, while the shock angle $\theta$ may be approximated by the Mach angle $\mu$.

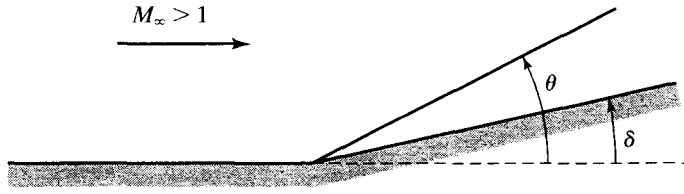


**Figure 13.19** A Weak Oblique Shock at a Convex Corner

Equation (6.18) provides a relation between the freestream Mach number $M_\infty$ (the Mach number on the upstream side of the shock) and the corner and the shock angles:

$$\tan\delta = \cot\theta \frac{M_\infty^2 \sin^2\theta - 1}{\frac{\gamma+1}{2}M_\infty^2 - (M_\infty^2 \sin^2\theta - 1)} \tag{6.18}$$

Rearranging gives

$$(M_\infty^2 \sin^2\theta - 1)(1 + \tan\theta\tan\delta) = \frac{\gamma+1}{2}M_\infty^2 \tan\theta\tan\delta$$

Since $\delta$ is small, we may make the approximation that $\tan\delta \cong \delta$ and that $\tan\theta \cong \tan\mu = 1/\sqrt{M_\infty^2 - 1}$. Therefore, the second product on the left may be approximated by

$$1 + \tan\theta\tan\delta \cong 1 + \frac{\delta}{\sqrt{M_\infty^2 - 1}} \cong 1$$

Accordingly, we have

$$(M_\infty^2 \sin^2\theta - 1) \cong \frac{\gamma+1}{2}M_\infty^2 \frac{\delta}{\sqrt{M_\infty^2 - 1}}$$

The strength of the shock is given by the ratio of the static-pressure difference across the shock divided by the static pressure on the upstream side:

$$\frac{p - p_\infty}{p_\infty} = \frac{2\gamma}{\gamma+1}(M_\infty^2 \sin^2\theta - 1) \cong \frac{2\gamma}{\gamma+1}\left(\frac{\gamma+1}{2}M_\infty^2 \frac{\delta}{\sqrt{M_\infty^2 - 1}}\right) = \frac{\gamma M_\infty^2}{\sqrt{M_\infty^2 - 1}}\delta$$

The pressure coefficient is defined in Eq. (13.17) as

$$C_p = \frac{p - p_\infty}{\frac{1}{2}\rho_\infty U_\infty^2} = \left(\frac{1}{\frac{1}{2}\gamma M_\infty^2}\right)\left(\frac{p - p_\infty}{p_\infty}\right) \cong \frac{1}{\frac{1}{2}\gamma M_\infty^2}\frac{\gamma M_\infty^2}{\sqrt{M_\infty^2 - 1}}\delta$$

$$= \frac{2}{\sqrt{M_\infty^2 - 1}}\delta$$

Finally, since

$$\delta \cong \tan\delta = \frac{dy}{dx}$$

we have

$$C_p = \frac{2}{\sqrt{M_\infty^2 - 1}}\frac{dy}{dx}$$

---

From the expressions for pressure coefficients, it is possible to calculate *lift* and *drag coefficients* for a thin airfoil in uniform supersonic flow. The slope $dy/dx$ at a point on the surface of an airfoil is dependent on the angle of attack of the foil and the thickness

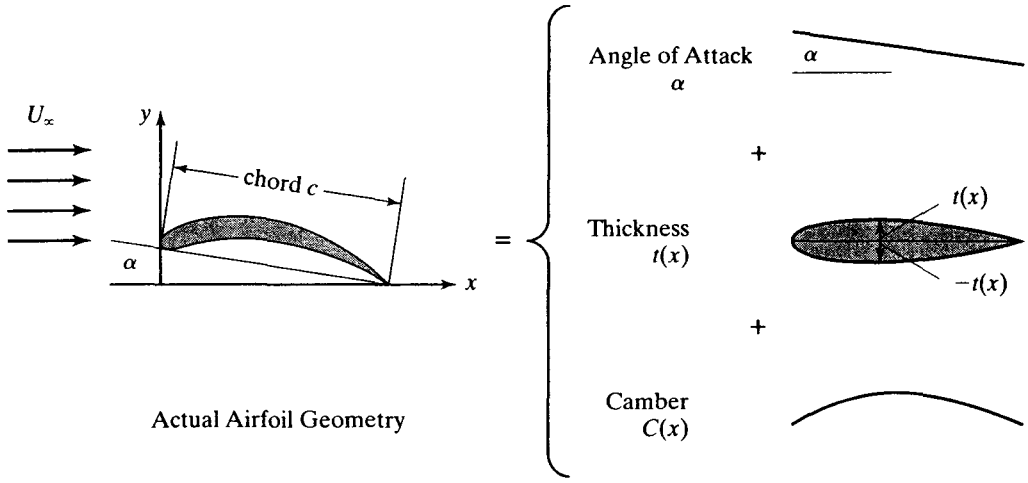


$$\left(\frac{dy}{dx}\right)_u = -\alpha + \frac{dt}{dx} + \frac{dC}{dx}$$

$$\left(\frac{dy}{dx}\right)_l = -\alpha - \frac{dt}{dx} + \frac{dC}{dx}$$

**Figure 13.20** Linear Separation of Airfoil Angle of Attack, Thickness, and Camber Effects

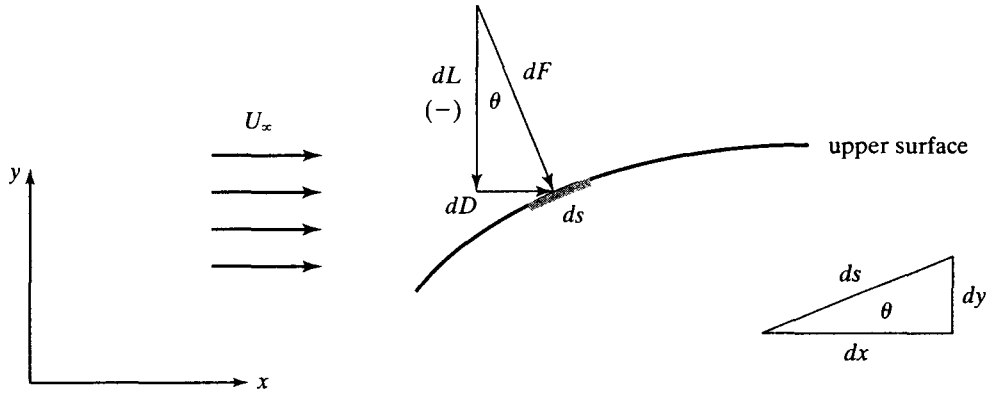


**Figure 13.21** Forces Acting on a Differential Surface Element on the Upper Portion of an Airfoil

and camber at the point. It is instructive to separate these airfoil properties in the way shown in Figure 13.20. [See Ref. (13.10) or (13.11).]

Consider a differential force $dF$ acting on a differential element of length $ds$ on the upper airfoil surface, as shown in Figure 13.21:

$$dF = p\,ds = C_{p_u}\frac{1}{2}\gamma p_\infty M_\infty^2 ds + p_\infty ds$$

The differential lift force $dL$ ($= -dF \cos\theta$) is given by

$$dL = -C_{p_u}\frac{1}{2}\gamma p_\infty M_\infty^2 dx - p_\infty dx$$

where lift is defined to be positive upward. Also note that $ds \cos\theta = dx$. The differential drag force $dD$ ($= dF \sin\theta$) is

$$dD = C_{p_u}\frac{1}{2}\gamma p_\infty M_\infty^2\left(\frac{dy}{dx}\right)_u dx + p_\infty\left(\frac{dy}{dx}\right)_u dx$$

where drag is positive in the flow direction. Note that $ds \sin\theta = dy = (dy/dx)dx$.

For an element on the lower surface, as shown in Figure 13.22, we have

$$dL = C_{p_l}\frac{1}{2}\gamma p_\infty M_\infty^2 dx + p_\infty dx$$

$$dD = -C_{p_l}\frac{1}{2}\gamma p_\infty M_\infty^2\left(\frac{dy}{dx}\right)_l dx - p_\infty\left(\frac{dy}{dx}\right)_l dx$$

We can now add the two contributions to lift and drag and integrate to obtain the lift and drag for the airfoil:

$$L = \frac{1}{2}\gamma p_\infty M_\infty^2 \int_0^c (C_{p_l} - C_{p_u})dx \tag{13.60}$$

$$D = \frac{1}{2}\gamma p_\infty M_\infty^2 \int_0^c \left[C_{p_u}\left(\frac{dy}{dx}\right)_u - C_{p_l}\left(\frac{dy}{dx}\right)_l\right]dx + p_\infty \int_0^c \left[\left(\frac{dy}{dx}\right)_u - \left(\frac{dy}{dx}\right)_l\right]dx \tag{13.61}$$

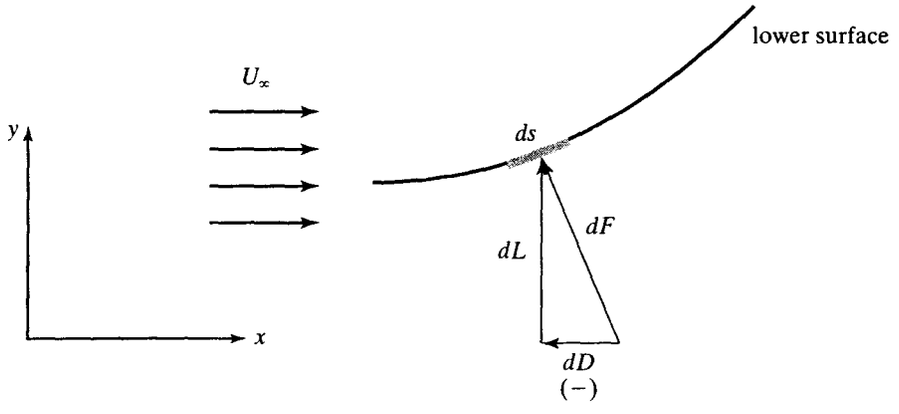


**Figure 13.22** Forces Acting on a Differential Surface Element on the Lower Portion of an Airfoil

The upper limit of the integration has been taken as $x = c$, where $c$ is the chord length. (See Figure 13.20.) Actually, the upper limit should be $x = c \cos \alpha$. However, the small-perturbation theory can be used only for small angles of attack, so $\cos \alpha \approx 1$.

We now substitute Eqs. (13.58) and (13.59) into Eq. (13.60):

$$L = \frac{1}{2}\gamma p_\infty M_\infty^2 \int_0^c \left(-\frac{2}{\sqrt{M_\infty^2 - 1}}\right)\left\{\left(\frac{dy}{dx}\right)_l + \left(\frac{dy}{dx}\right)_u\right\} dx$$

$$= -\frac{\gamma p_\infty M_\infty^2}{\sqrt{M_\infty^2 - 1}}\left[\int_0^c (-2\alpha)dx + \int_0^c \left(\frac{dt}{dx} + \frac{dC}{dx}\right)_u dx - \int_0^c \left(\frac{dt}{dx} - \frac{dC}{dx}\right)_l dx\right]$$

For an airfoil with sharp, or only slightly rounded, leading and trailing edges, the thickness and camber are both 0 at $x = 0$ and at $x = c$. For this case, the foregoing relation produces

$$L = \frac{2\gamma p_\infty M_\infty^2 \alpha c}{\sqrt{M_\infty^2 - 1}} \tag{13.62}$$

Defining a lift coefficient as

$$C_L = \frac{L}{\frac{1}{2}\rho_\infty U_\infty^2 A} = \frac{L}{\frac{1}{2}\gamma p_\infty M_\infty^2 c}$$

we get

$$C_L = \frac{4\alpha}{\sqrt{M_\infty^2 - 1}} \tag{13.63}$$

For a thin airfoil in supersonic linearized flow, with sharp leading and trailing edges, the lift coefficient depends only on the angle of attack and the freestream Mach number. It does not depend on the camber or thickness of the foil.

An expression for the drag coefficient can be found in a similar fashion. Using Eqs. (13.58), (13.59), and (13.61), we have

$$D = \frac{1}{2}\gamma p_\infty M_\infty^2 \int_0^c \frac{2}{\sqrt{M_\infty^2 - 1}}\left[\left(\frac{dy}{dx}\right)_u^2 + \left(\frac{dy}{dx}\right)_l^2\right] dx + p_\infty \int_0^c \left[\left(\frac{dy}{dx}\right)_u - \left(\frac{dy}{dx}\right)_l\right] dx$$

$$= \frac{\gamma p_\infty M_\infty^2}{\sqrt{M_\infty^2 - 1}} \int_0^c \left\{\left[-\alpha + \frac{dt}{dx} + \frac{dC}{dx}\right]_u^2 + \left[-\alpha - \frac{dt}{dx} + \frac{dC}{dx}\right]_l^2\right\} dx$$

Note that the integral involving $[(dy/dx)_u - (dy/dx)_l]$ vanishes when integrated from 0 to $c$. (See the inset in Figure 13.20.) Expanding this expression for drag, we obtain

$$D = \frac{\gamma p_\infty M_\infty^2}{\sqrt{M_\infty^2 - 1}}\left\{\int_0^c \left[2\alpha^2 + 2\left(\frac{dt}{dx}\right)^2 + 2\left(\frac{dC}{dx}\right)^2\right] dx - \int_0^c 4\alpha \frac{dC}{dx} dx\right\}$$

However,

$$\int_0^c \alpha \frac{dC}{dx} dx = 0$$

for a foil with sharp, or only slightly rounded, leading and trailing edges. Also, we can write the integrals of the squares of $dt/dx$ and $dC/dx$ as chord average values—that is,

$$\int_0^c \left(\frac{dt}{dx}\right)^2 dx = \overline{\left(\frac{dt}{dx}\right)^2} c \quad \text{and} \quad \int_0^c \left(\frac{dC}{dx}\right)^2 dx = \overline{\left(\frac{dC}{dx}\right)^2} c$$

so that

$$D = \frac{2\gamma p_\infty M_\infty^2}{\sqrt{M_\infty^2 - 1}} \left[\alpha^2 c + \overline{\left(\frac{dt}{dx}\right)^2} c + \overline{\left(\frac{dC}{dx}\right)^2} c\right]$$

or

$$C_D = \frac{4}{\sqrt{M_\infty^2 - 1}} \left[\alpha^2 + \overline{\left(\frac{dt}{dx}\right)^2} + \overline{\left(\frac{dC}{dx}\right)^2}\right] \tag{13.64}$$

There is thus a contribution to drag from the angle of attack, thickness, and camber. The *total drag* coefficient is the sum of the *induced drag*, the *form drag*, and the *frictional drag*. However, since we have assumed a frictionless flow, there is no skin-friction drag present. The drag coefficient in Eq. (13.64) may be written as

$$C_D = (C_D)_{\text{induced}} + (C_D)_{\text{form}}$$

$$(C_D)_{\text{induced}} = \frac{4\alpha^2}{\sqrt{M_\infty^2 - 1}} = \alpha C_L$$

$$(C_D)_{\text{form}} = \frac{4}{\sqrt{M_\infty^2 - 1}} \left[\overline{\left(\frac{dt}{dx}\right)^2} + \overline{\left(\frac{dC}{dx}\right)^2}\right]$$

**Example 13.6. Determination of the linearized lift and drag coefficients for a flat plate in supersonic flow**

Using the linearized theory, calculate the lift and drag coefficients for a flat-plate airfoil at an angle of attack of 10° and $M_\infty = 2.5$. Compare the result with the exact solution obtained from oblique shock theory in Example 8.5.

**Solution**

We start with

$$C_L = \frac{4\alpha}{\sqrt{M_\infty^2 - 1}}$$

with $\alpha$ expressed in radians; that is, $\alpha(\pi/180) = 0.1745$. Thus,

$$C_L = \frac{4(0.1745)}{\sqrt{(2.5)^2 - 1}} = 0.3046$$

Since a flat-plate airfoil has no thickness and no camber, there is only an induced drag component, which may be determined from Eq. (13.64) as

$$C_D = \frac{4\alpha^2}{\sqrt{M_\infty^2 - 1}} = \alpha C_L = (0.1745)(0.3046) = 0.0532$$

The exact solution in Example 8.5 yielded

$$C_L = 0.3096 \quad \text{and} \quad C_D = 0.0546$$

It can be seen that, even at an angle of attack as large as 10°, the linearized theory gives results that are within 3 percent of the exact solution.

---

**Example 13.7. Determination of the linearized lift and drag coefficients for a diamond-shaped airfoil in supersonic flow**

Using the linearized theory, compute the lift and drag coefficients for the symmetrical, diamond-shaped airfoil shown in Figure 13.23. Assume $M_\infty = 2.0$, with an angle of attack of 7°.

**Solution**

As diagrammed in Figure 13.24, the analysis of the symmetrical diamond-shaped airfoil at an angle of attack is equivalent to the analysis of a flat plate at an angle of attack (lift + induced drag) and a symmetrical diamond at zero angle of attack (no lift + form drag).

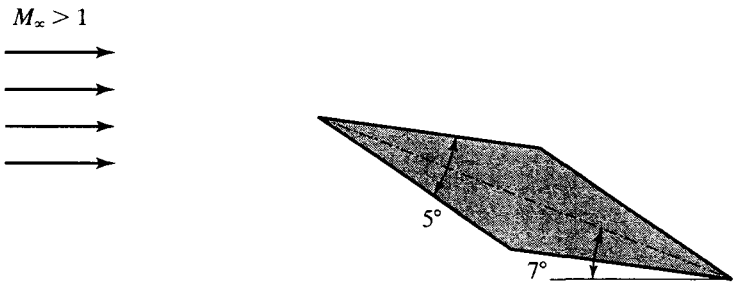


**Figure 13.23** Supersonic flow past a Symmetrical Diamond-Shaped Airfoil

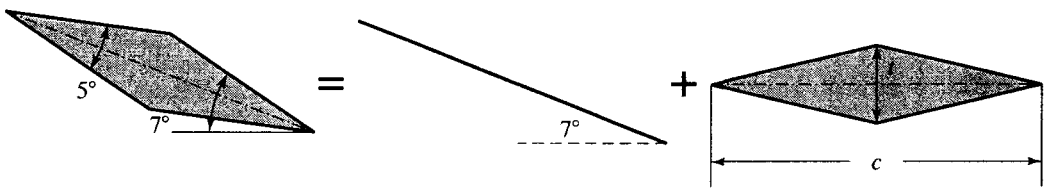


**Figure 13.24** Supersonic Flow past a Symmetrical Diamond-Shaped Airfoil

The lift coefficient can be computed from Eq. (13.63):

$$C_L = \frac{4\alpha}{\sqrt{M_\infty^2 - 1}} = \frac{(4)(7\pi/180)}{\sqrt{3}} = 0.2821$$

The diamond-shaped airfoil has thickness, but no camber. Thus, the mean square slope of the thickness profile is

$$\left(\frac{dt}{dx}\right)^2 = \left(\frac{t/2}{c/2}\right)^2 = \left(\frac{t}{c}\right)^2 = (\tan 2.5°)^2 = (0.04366)^2 = 0.001906$$

Thus, from Eq. (13.64),

$$C_D = \frac{4}{\sqrt{M_\infty^2 - 1}}\left[\alpha^2 + \left(\frac{\overline{dt}}{dx}\right)^2\right] = \frac{4}{\sqrt{3}}(0.1222^2 + 0.001906) = 0.03887$$

It is easy to show that for a symmetrical diamond-shaped airfoil, $(C_D)_{\text{induced}}/(C_D)_{\text{form}} = (\alpha c/t)^2$, where $c$ is the chord length and $t$ is the thickness at midspan.

## 13.7 SUMMARY

In this chapter, we have presented certain approximate methods for handling problems in two-dimensional compressible flow. Again, it is very important to recognize the nature of the approximation that we were forced to make in order to linearize the partial differential equation—that is, that the body introduced into the flow causes only small perturbations in the flow.

Certain results from this analysis are important to recognize. Among these results are (1) the change in the nature of the partial differential equation upon going from subsonic to supersonic flow, (2) the possibility of deriving similarity relationships between subsonic compressible flow and the corresponding incompressible flow, and (3) the importance of Mach waves in a supersonic solution.

## 13.8 REFERENCES


**13.1** Jeffrey, A. *Applied Partial Differential Equations: An Introduction*, Academic Press, Burlington, MA, 2003, pp. 103–125.

**13.2** Bourque, C. "Limitations of the Linearized Theory for the Flow Over a Wavy Wall," *Int J Mech Eng Ed* 1991; 20(1): 68–73.

**13.3** Arpaci, V. S. *Conduction Heat Transfer*, Addison-Wesley Publishing Company, Reading, MA, 1966, pp. 180–217.

**13.4** Zill, D. G., and Cullen, M. R. *Advanced Engineering Mathematics*, 2d ed., Jones and Bartlett Publishers, Sudbury, MA, 2000, pp. 688–691.

**13.5** Cheers, F. *Elements of Compressible Flow,* John Wiley & Sons, New York, 1963, p. 131.

**13.6** Laitone, E. V. "New Compressibility Correction for Two-Dimensional Subsonic Flow," *J Aeronaut Sci* 1951; 18(5): 350.

**13.7** Shapiro, A. *The Dynamics and Thermodynamics of Compressible Fluid Flow*, Vol. 1, Ronald Press Company, New York, 1953, pp. 324–327.

**13.8** Ibid., pp. 344–351.

**13.9** Duffy, D. G. *Advanced Engineering Mathematics*, CRC Press, Boca Raton, FL, 1998, pp. 325–388.

**13.10** Liepmann, H., and Roshko, A. *Elements of Gas Dynamics*, John Wiley & Sons, New York, 1957, p. 111.

**13.11** Ashley, H., and Landahl, M. *Aerodynamics of Wings and Bodies*, Dover Publications, New York, 1985, pp. 86–87.

## 13.9 PROBLEMS

**13.1** The lift coefficient versus angle of attack for an airfoil, as measured in a low-speed wind tunnel, is given in Figure P13.1. Sketch this curve for the same airfoil at a Mach number of 0.45.

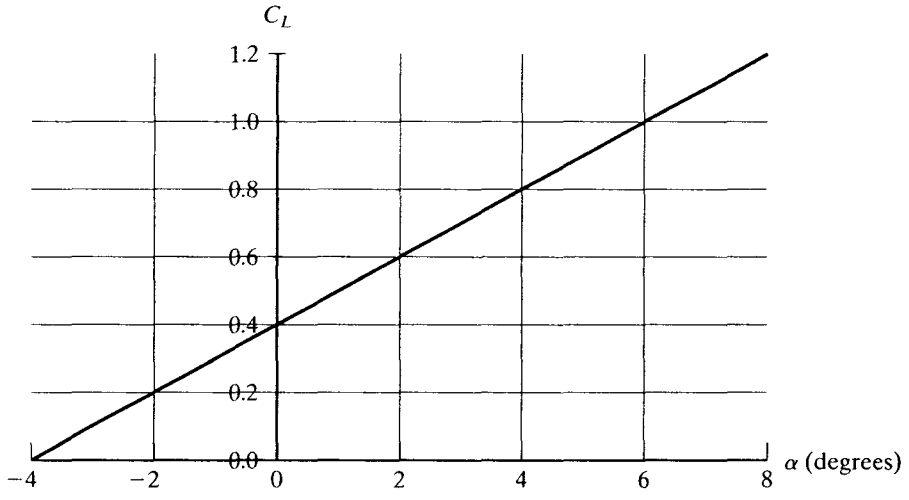


**Figure P13.1**

**13.2** Using the potential equation

$$\frac{\partial^2 \phi_p}{\partial x^2}(1 - M_\infty^2) + \frac{\partial^2 \phi_p}{\partial y^2} + \frac{\partial^2 \phi_p}{\partial z^2} = 0$$

develop the Goethert similarity rules for three-dimensional potential subsonic flow.

**13.3** Tests run at $M_\infty = 0.3$ show that the lift coefficient versus angle of attack for an airfoil is given by $C_L = 0.1(\alpha + 1)$, with $\alpha$ in degrees. Using the appropriate similarity laws, derive an expression for $C_L$ versus $\alpha$ for this airfoil at $M_\infty = 0.50$.

**13.4** For the airfoil of Problem 13.3, plot $C_L$ versus $M_\infty$ from $M_\infty = 0$ to $M_\infty = 0.60$ at angles of attack of 0°, 2°, and 4°.

**13.5** During the testing of a two-dimensional, streamlined shape, it is found that sonic flow first occurs on the surface for $M_\infty = 0.70$. Calculate the pressure coefficient at this point, as well as the minimum pressure coefficient for this shape in incompressible flow.

**13.6** Two-dimensional, subsonic, linearized potential flow takes place between two wavy walls as shown Figure P13.6. Solve for $\phi_p$ and determine the pressure distribution along the centerline.

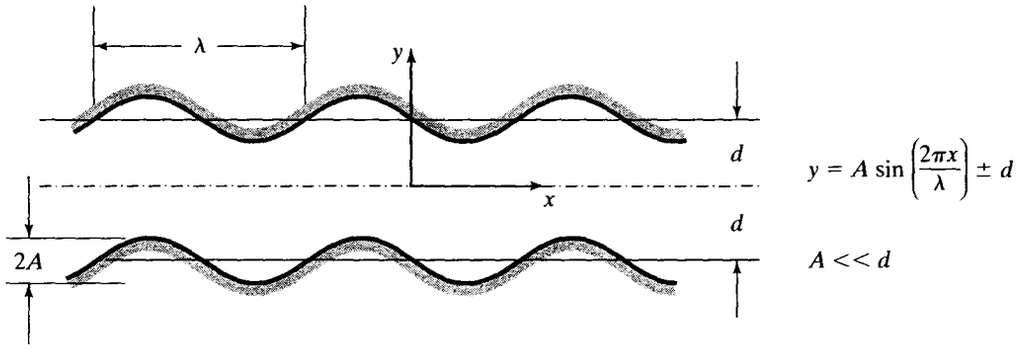


**Figure P13.6**

**13.7** Consider two-dimensional, supersonic, linearized flow under a wavy wall, as shown in Figure P13.7. Solve for the velocity potential of the flow and pressure coefficient along the wall. Derive an expression for the lift and drag per wavelength.

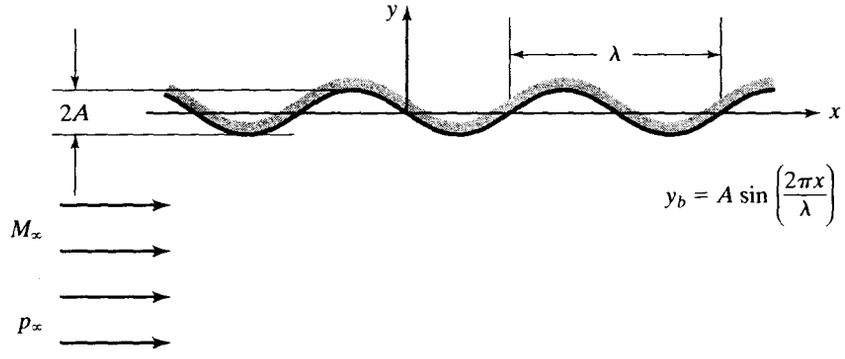


**Figure P13.7**

**13.8** A wing has the shape of a sine wave, as shown in Figure P13.8. Compute the lift and drag for supersonic flow. Assume linearized, two-dimensional flow above and below the foil.

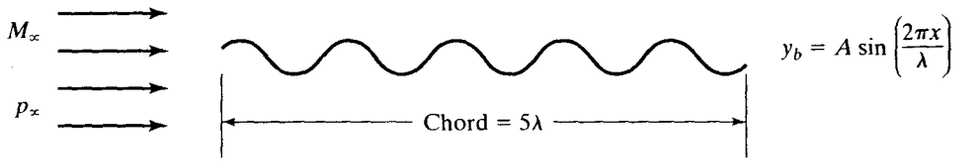


**Figure P13.8**

**13.9** Using thin-airfoil theory, find $C_L$ and $C_D$ for a two-dimensional, flat-plate airfoil with deflected flap in supersonic flow of Mach number $M_\infty$. Plot $C_L$ versus $\alpha$ for various $\delta$ for $F = 0.25$. (See Figure P13.9.)

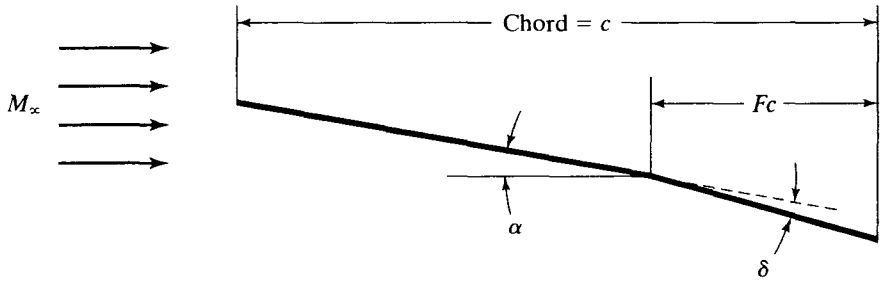


**Figure P13.9**

**13.10** Consider uniform supersonic flow over a wall in which there exists a bump, as shown in Figure P13.10. Assuming linearized, two-dimensional potential flow, calculate the vertical and horizontal components of the force on the bump. Assume $M_\infty = 2.0$, with $p_\infty = 50$ kPa.

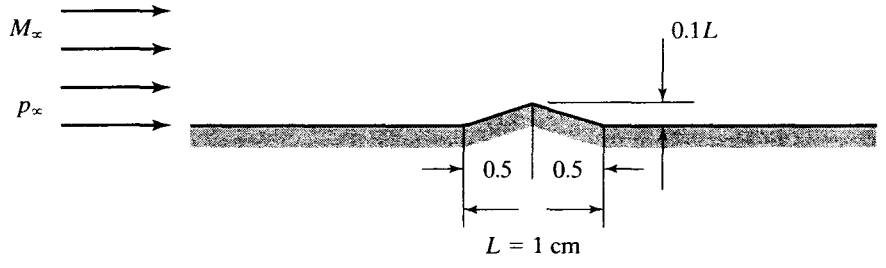


**Figure P13.10**

**13.11** A supersonic airfoil consists of a circular arc, as shown in Figure P13.11. Compute the lift and drag coefficients of the foil versus angle of attack.

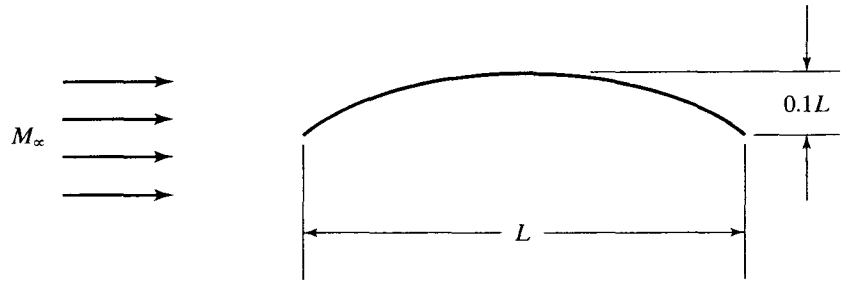


**Figure P13.11**

**13.12** For the airfoil shown in Figure P13.12, determine $C_L$ and $C_D$ versus the angle of attack in supersonic flow.

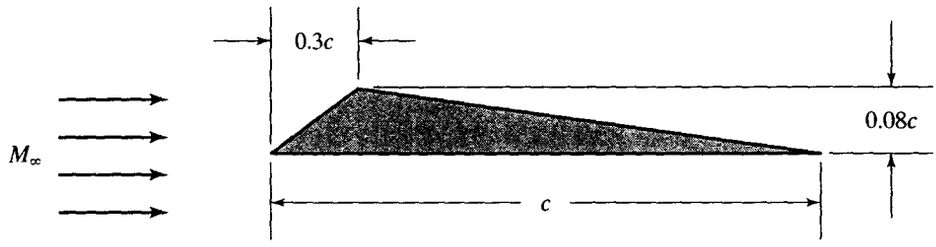


**Figure P13.12**

# Chapter 14

# Characteristics

## 14.1 INTRODUCTION

In Chapter 11, we derived the partial differential equation for the velocity potential $\phi$ for the case of steady, irrotational, and isentropic flow, in the absence of gravitational, viscous, electric, and magnetic forces. Several exact solutions to the governing equations were presented in Chapter 12. Linearization of these equations in Chapter 13 allowed approximate solutions to be worked out for several types of flow problems. Linearized solutions were found for both subsonic and supersonic flows, with the nature of the solutions being quite different for the two types of flow. In a variety of cases, however, approximate solutions obtained by linearization are not adequate, and greater accuracy is necessary. Instead of dropping terms to obtain an approximate model of a flow, we must consider the complete nonlinear velocity potential equation. In those cases, the solution can be accomplished only through numerical methods.

In this chapter, we consider a numerical procedure to solve certain classes of flow problems. This procedure enables solutions to be obtained for two-dimensional, planar and axisymmetric, and three-dimensional supersonic flows. The procedure may also be employed for all one-dimensional unsteady flows. The procedure is called the *method of characteristics* (*MOC*). MOC has been used for many years to solve problems, in various fields of study, that are described by hyperbolic partial differential equations (PDEs).

In this chapter, we shall first discuss a few properties of *characteristics* (lines or curves in two-dimensional flows and surfaces in three-dimensional flows) that are used to build a solution at discrete points in the field by application of a predetermined numerical procedure. The equations of motion developed in Chapter 11 will be used in various ways to develop the MOC procedure for the case of two-dimensional, supersonic, steady flow of a perfect gas with constant specific heats. We shall assume that the flow is irrotational and isentropic and that it contains no shockwaves. Several applications of the MOC procedure will be presented.

## 14.2 PROPERTIES OF CHARACTERISTICS

Characteristics have very special and important properties that may be utilized to derive the equations that form the basis of the method of characteristics. To provide a foundation for the discussion of these properties, we will use some of the concepts regarding the physical nature of supersonic flow, as already covered in previous chapters, as well as a very simple mathematical model.

It is imperative to keep in mind that characteristics, and therefore MOC, can be used to solve only particular types of gas flow problems, *viz.*, those that are governed by hyperbolic partial differential equations. In the upcoming text, if not stated otherwise, it should be understood that we are dealing with two-dimensional supersonic flows, which, as we will see, are governed by hyperbolic PDEs.

***Property 1:*** *A characteristic in a two-dimensional supersonic flow is a curve or line along which physical disturbances are propagated at the local speed of sound relative to the gas.*

It was shown in Chapter 2 that when a small disturbance is introduced into a subsonic flow, the effect of the disturbance is felt throughout the entire flowfield. However, when a small disturbance is introduced into a supersonic flow, the effect of the disturbance is confined to that portion of the flowfield contained within a Mach cone defined by the Mach lines or waves (*the zone of influence*).

Likewise, for linearized supersonic flow—for example, flow over a wavy wall, discussed in Section 13.5—the effect of the disturbance (in that case, the wall) was propagated to infinity along straight lines inclined at the Mach angle to the flow. (See Figure 14.1.)

It may be useful to contrast pathlines (or, equivalently, streamlines in steady flow) of a flow with Mach lines or waves. Fluid particles travel along pathlines propagating information regarding the condition of the flow, such as $\rho$, $h$, and $s$. In supersonic flow, acoustic waves travel along Mach lines (or characteristics) propagating information regarding flow disturbances.

Mach lines = characteristics: lines of disturbance propagation

The existence of characteristics (Mach lines for supersonic flows) is an attribute of the solution of hyperbolic partial differential equations. The solution of supersonic flow problems by MOC depends on determination of the direction of the Mach lines or characteristics, as well as on the information that is propagated along them. For linearized two-dimensional flow, the Mach lines are straight and relatively easy to determine.

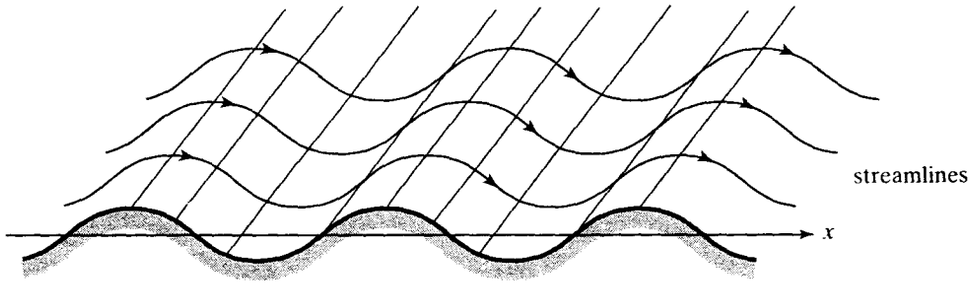


**Figure 14.1** Linearized Supersonic Flow over a Wavy Wall

However, if the nonlinear terms in the equations of motion are taken into account, the determination of the Mach lines, and therefore the characteristic lines, becomes more complex, as they are no longer straight lines.

***Property 2:*** *A characteristic is a curve across which flow properties are continuous, although they may have discontinuous first derivatives, and along which the derivatives are indeterminate.*

In the discussion of Prandtl–Meyer flow in Chapter 7, we considered a weak disturbance that was introduced into a supersonic, two-dimensional flow by a small change in the direction of the wall, as illustrated in Figure 14.2. The effect of the disturbance is felt in the flow behind the Mach line, with uniform, but different, conditions prevailing before and after the wave.

For isentropic flow, with no finite shockwaves possible, there can be no finite discontinuity in the velocity components across the wave, so the first derivatives of the velocity potential—that is, $\partial\phi/\partial x = u$ and $\partial\phi/\partial y = v$—are continuous. However, the infinitesimal change in wall direction, $d\alpha$, does bring about an infinitesimal expansion and a resultant infinitesimal increase in velocity to $V + dV$. This infinitesimal velocity increase, occurring normal to a Mach line of infinitesimal thickness, indicates the presence of a finite velocity gradient $\partial V/\partial n$, where $n$ is the direction normal to the Mach line. In the flow field ahead of the wave for this flow, the spatial derivatives of velocity are zero, since the flow is uniform. In the flow field behind the wave, again the velocity derivatives are zero, since the flow here, too, is uniform. The presence of a finite derivative at the wave itself, however, indicates that there is a discontinuity in the velocity derivative across a Mach line.

If there is a discontinuity in the derivative of a variable, but not in the variable itself, the discontinuity is said to be weak. Thus, a Mach line is a *weak discontinuity*. Because of the discontinuity in the velocity derivative, supersonic flows are also considered to be *nonsmooth*. The infinitesimally thin Mach wave may be thought of as patching smooth regions of the flow together.

Consider a problem governed by the following first-order PDE [first-order equations are classified as hyberbolic; see Ref. (14.1)]:

$$a\frac{\partial u}{\partial x} + b\frac{\partial u}{\partial y} = c \tag{14.1}$$

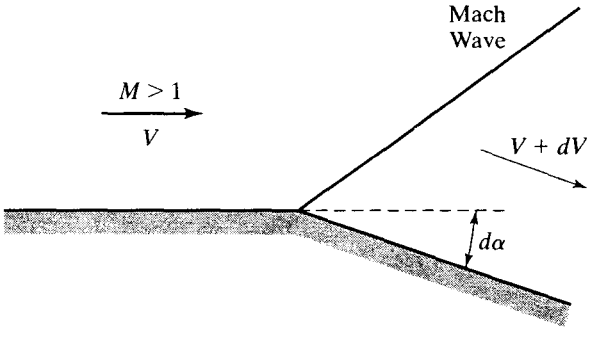


**Figure 14.2** Infinitesimal Change of Wall Angle to Create a Mach Wave

If the coefficients $a$, $b$, and $c$ are constants or functions of $x$ and $y$, then Eq. (14.1) is *linear*; if $a$, $b$, and $c$ are functions of $x$, $y$, and $u$, Eq. (14.1) is *quasilinear* (linear in the highest derivative). If $c$ is zero, Eq. (14.1) is *homogeneous*. Assume that the dependent variable $u(x, y)$ is everywhere continuous. Accordingly, we may take its total derivative:

$$dx\frac{\partial u}{\partial x} + dy\frac{\partial u}{\partial y} = du \tag{14.2}$$

Thus, Eqs. (14.1) and (14.2) form two equations written in terms of two unknown partial derivatives. We can solve for each derivative by applying Cramer's rule [see Ref. (14.2)] and obtain

$$\frac{\partial u}{\partial x} = \frac{N_x}{D} = \frac{\begin{vmatrix} c & b \\ du & dy \end{vmatrix}}{\begin{vmatrix} a & b \\ dx & dy \end{vmatrix}} = \frac{cdy - bdu}{ady - bdx} = \frac{\left(\frac{c}{a}\right)\frac{dy}{dx} - \left(\frac{b}{a}\right)\frac{du}{dx}}{\frac{dy}{dx} - \left(\frac{b}{a}\right)} \tag{14.3}$$

$$\frac{\partial u}{\partial y} = \frac{N_y}{D} = \frac{\begin{vmatrix} a & c \\ dx & du \end{vmatrix}}{\begin{vmatrix} a & b \\ dx & dy \end{vmatrix}} = \frac{adu - cdx}{ady - bdx} = \frac{\frac{du}{dx} - \left(\frac{c}{a}\right)}{\frac{dy}{dx} - \left(\frac{b}{a}\right)} \tag{14.4}$$

It is apparent from Eqs. (14.3) and (14.4) that at any point $(x, y)$ in the field, curves with the slope $dy/dx = b/a$ will result in the denominator of each first derivative becoming zero. Along such curves, it would appear that the derivatives are unbounded, which is physically and mathematically unacceptable. On all other curves, the derivatives are finite. Hence, this PDE has yielded a particular set of curves that are different from all others.

Now, along a curve whose slope is $b/a$, in order to avoid both partial derivatives from becoming unbounded, we require that the numerators in Eqs. (14.3) and (14.4) also be zero. From Eq. (14.4), it is evident that by setting $du/dx = c/a$ the derivative $\partial u/\partial y$ is equal to 0/0—that is, it is *indeterminate*. As may be readily shown, this condition forces the derivative $\partial u/\partial x$ in Eq. (14.3) to have an indeterminate form as well.

Hence, for a first-order PDE, we have demonstrated that at any point $(x, y)$ in the field, along curves with the slope $dy/dx = b/a$, the dependent variable $u$ must satisfy the ordinary differential equation $du/dx = c/a$. These curves satisfy the second property and are termed the *characteristic curves* of this problem.

To complete the solution, we must solve both of these ordinary differential equations (ODEs). For a simple problem as represented by the first-order PDE in Eq. (14.1), this might be accomplished by direct integration. However, for a supersonic flow problem (or for an unsteady flow problem), numerical solution of the ODEs is generally required.

***Property 3:*** *A characteristic is a curve along which the governing partial differential equation(s) may be manipulated into an ordinary differential equation(s).*

Put another way, this property states that a characteristic is a curve along which the governing PDE become an ODE. This property is significant because ODEs are often easier to solve than PDEs.

To demonstrate this property, reconsider a slightly rearranged version of Eq. (14.1):

$$\frac{\partial u}{\partial x} + \frac{b}{a}\frac{\partial u}{\partial y} = \frac{c}{a} \tag{14.5}$$

Contrast this expression with the total derivative in Eq. (14.2), written as

$$\frac{\partial u}{\partial x} + \frac{dy}{dx}\frac{\partial u}{\partial y} = \frac{du}{dx} \tag{14.6}$$

It is apparent that if $dy/dx = b/a$ in Eq. (14.6), then the grouping on the left-hand side of Eq. (14.5) may be replaced by $du/dx$, and therefore, as before, we obtain

$$\frac{du}{dx} = \frac{c}{a}$$

Note that we first obtained the equation for the slope of the characteristic, that is, $dy/dx$. Next, we determined how the flow variables change along the characteristic. This resulting expression is called the *compatibility equation*. Finally, we would have to solve the pair of ordinary differential equations. This three-step procedure is the MOC.

For more complicated situations than the one we just examined, there is a variety of methods available for determining both the slopes of the characteristics and the compatibility equations. In the next section, we consider three methods: the first based on Property 2, the second on Property 3, and the third, arguably the most modern and general approach, based on both Properties 2 and 3.

## 14.3 THEORY OF CHARACTERISTICS

The nonlinear potential equation for isentropic, irrotational, steady flow of a perfect gas with constant specific heats was found in Chapter 11 to be

$$\frac{\partial^2\phi}{\partial x^2} + \frac{\partial^2\phi}{\partial y^2} + \frac{\partial^2\phi}{\partial z^2} - \frac{1}{a^2}\left[\left(\frac{\partial\phi}{\partial x}\right)^2\frac{\partial^2\phi}{\partial x^2} + \left(\frac{\partial\phi}{\partial y}\right)^2\frac{\partial^2\phi}{\partial y^2} + \left(\frac{\partial\phi}{\partial z}\right)^2\frac{\partial^2\phi}{\partial z^2}\right]$$
$$- \frac{2}{a^2}\left[\frac{\partial\phi}{\partial x}\frac{\partial\phi}{\partial y}\frac{\partial^2\phi}{\partial x\,\partial y} + \frac{\partial\phi}{\partial y}\frac{\partial\phi}{\partial z}\frac{\partial^2\phi}{\partial y\partial z} + \frac{\partial\phi}{\partial z}\frac{\partial\phi}{\partial x}\frac{\partial^2\phi}{\partial z\partial x}\right] = 0 \tag{11.47}$$

For two-dimensional flow, this equation reduces to

$$\frac{\partial^2\phi}{\partial x^2} + \frac{\partial^2\phi}{\partial y^2} - \frac{1}{a^2}\left[\left(\frac{\partial\phi}{\partial x}\right)^2\frac{\partial^2\phi}{\partial x^2} + \left(\frac{\partial\phi}{\partial y}\right)^2\frac{\partial^2\phi}{\partial y^2}\right] - \frac{2}{a^2}\left[\frac{\partial\phi}{\partial x}\frac{\partial\phi}{\partial y}\frac{\partial^2\phi}{\partial x\,\partial y}\right] = 0 \tag{14.7}$$

or

$$\left[a^2 - \left(\frac{\partial\phi}{\partial x}\right)^2\right]\frac{\partial^2\phi}{\partial x^2} - 2\frac{\partial\phi}{\partial x}\frac{\partial\phi}{\partial y}\frac{\partial^2\phi}{\partial x\,\partial y} + \left[a^2 - \left(\frac{\partial\phi}{\partial y}\right)^2\right]\frac{\partial^2\phi}{\partial y^2} = 0 \tag{14.8}$$

This partial differential equation is of the general form

$$C_1\frac{\partial^2\phi}{\partial x^2} + 2C_2\frac{\partial^2\phi}{\partial x\,\partial y} + C_3\frac{\partial^2\phi}{\partial y^2} = 0 \tag{14.9}$$

where $C_1$, $C_2$, and $C_3$ depend on $a^2$, $\partial\phi/\partial x$ and $\partial\phi/\partial y$, respectively. We shall assume, as discussed previously, that for this isentropic flow, the velocity components, and hence the derivatives $\partial\phi/\partial x$ and $\partial\phi/\partial y$, are continuous. Thus we can write, for the differential changes in velocity components,

$$d\left(\frac{\partial\phi}{\partial x}\right) = \frac{\partial^2\phi}{\partial x^2}dx + \frac{\partial^2\phi}{\partial x\,\partial y}dy \tag{14.10}$$

and

$$d\left(\frac{\partial\phi}{\partial y}\right) = \frac{\partial^2\phi}{\partial y\,\partial x}dx + \frac{\partial^2\phi}{\partial y^2}dy \tag{14.11}$$

---

**Method 1**—*The Method of Indeterminate Derivatives*: This method uses the property that along a characteristic, the derivatives of the flow variables are indeterminate.

This procedure is a generalization of the approach applied to Eqs. (14.1) and (14.2). From Eqs. (14.9), (14.10), and (14.11), we obtain three linear equations for determining

$$\frac{\partial^2\phi}{\partial x^2},\quad \frac{\partial^2\phi}{\partial y^2}\quad \text{and}\quad \frac{\partial^2\phi}{\partial y\,\partial x}$$

According to Cramer's rule, if there exists a set of $n$ linear equations in the unknowns $x_1, x_2, \ldots, x_n$, namely,

$$\begin{aligned}
a_{11}x_1 + a_{12}x_2 + \cdots + a_{1n}x_n &= k_1\\
a_{21}x_1 + a_{22}x_2 + \cdots + a_{2n}x_n &= k_2\\
&\vdots\\
a_{n1}x_1 + a_{n2}x_2 + \cdots + a_{nn}x_n &= k_n
\end{aligned}$$

then the system has a unique solution if the determinant of the system

$$|A| = \begin{vmatrix} a_{11} & a_{12} & \cdots & a_{1n}\\ a_{21} & a_{22} & \cdots & a_{2n}\\ \vdots & \vdots & \ddots & \vdots\\ a_{n1} & a_{n2} & \cdots & a_{nn} \end{vmatrix}$$

is not equal to zero. The solution for, say, $x_1$, is given by

$$x_1 = \frac{|A_1|}{|A|}$$

where the numerator $|A_1|$, for example, is the determinant formed by replacing the elements $a_{11}, a_{21}, \ldots, a_{n1}$ in the first column of $|A|$ by $k_1, k_2, \ldots, k_n$, respectively.

For our case, we have the following set of three linear equations in the unknowns $\partial^2\phi/\partial x^2$, $\partial^2\phi/\partial y^2$, and $\partial^2\phi/\partial x\,\partial y$:

$$\begin{aligned} dx\frac{\partial^2\phi}{\partial x^2} + dy\frac{\partial^2\phi}{\partial x\,\partial y} + 0\frac{\partial^2\phi}{\partial y^2} &= d\left(\frac{\partial\phi}{\partial x}\right) \\ 0\frac{\partial^2\phi}{\partial x^2} + dx\frac{\partial^2\phi}{\partial x\,\partial y} + dy\frac{\partial^2\phi}{\partial y^2} &= d\left(\frac{\partial\phi}{\partial y}\right) \\ C_1\frac{\partial^2\phi}{\partial x^2} + 2C_2\frac{\partial^2\phi}{\partial x\,\partial y} + C_3\frac{\partial^2\phi}{\partial y^2} &= 0 \end{aligned} \tag{14.12}$$

According to Property 2, we are interested in obtaining expressions for the characteristics, lines across which there may be a discontinuity in the velocity derivatives—or, expressed another way, lines on which there is not a unique solution for the velocity derivative. Furthermore, we are interested in determining under what conditions such characteristics exist.

The determinant of the coefficients of the partial derivatives in Eqs. (14.12) is

$$|A| = \begin{vmatrix} dx & dy & 0 \\ 0 & dx & dy \\ C_1 & 2C_2 & C_3 \end{vmatrix} = C_3(dx)^2 - 2C_2 dx\,dy + C_1(dy)^2$$

If there is not to be a unique solution for the velocity derivatives ($\partial^2\phi/\partial x^2$, $\partial^2\phi/\partial y^2$, and $\partial^2\phi/\partial x\,\partial y$), then $|A|$ must equal zero. Therefore, the slope of a characteristic line in the $(x, y)$ plane, $dy/dx$, is given by

$$C_1\left(\frac{dy}{dx}\right)^2 - 2C_2\frac{dy}{dx} + C_3 = 0 \tag{14.13}$$

Solving this quadratic, we obtain

$$\frac{dy}{dx} = \frac{2C_2 \pm \sqrt{4C_2^2 - 4C_1C_3}}{2C_1} = \frac{C_2 \pm \sqrt{C_2^2 - C_1C_3}}{C_1} \tag{14.14}$$

Notice that, unlike in the simple model of the previous section, in which we obtained a single family of characteristics ($dy/dx = b/a$), here we obtain two families, one corresponding to the plus sign in Eq. (14.14) and the other to the minus sign. It should also be noticed that for $C_2^2 - C_1C_3 < 0$, $dy/dx$ will be imaginary, and for $C_2^2 - C_1C_3 > 0$, $dy/dx$ will be real. Referring to Eq. (14.8), we see that

$$C_1 = a^2 - \left(\frac{\partial\phi}{\partial x}\right)^2 = a^2 - u^2$$

$$C_2 = -\frac{\partial\phi}{\partial x}\frac{\partial\phi}{\partial y} = -uv$$

$$C_3 = a^2 - \left(\frac{\partial\phi}{\partial y}\right)^2 = a^2 - v^2$$

so that Eq. (14.14) can be rewritten as

$$\frac{dy}{dx} = \frac{-uv \pm \sqrt{(uv)^2 - (a^2 - u^2)(a^2 - v^2)}}{a^2 - u^2}$$

or

$$\frac{dy}{dx} = \frac{-uv \pm \sqrt{a^2u^2 + a^2v^2 - a^4}}{a^2 - u^2} \tag{14.15}$$

To acknowledge that at each point in the flow there exist two characteristics, we will label one "I" and the other "II," with slopes given respectively by

$$\left(\frac{dy}{dx}\right)_{\text{I}} = \frac{-\left(\frac{uv}{a^2}\right) + \sqrt{M^2 - 1}}{1 - \left(\frac{u^2}{a^2}\right)} \tag{14.16}$$

and

$$\left(\frac{dy}{dx}\right)_{\text{II}} = \frac{-\left(\frac{uv}{a^2}\right) - \sqrt{M^2 - 1}}{1 - \left(\frac{u^2}{a^2}\right)} \tag{14.17}$$

where $M^2 = (u^2 + v^2)/a^2$. We can see that, for $M > 1$, there exist characteristic lines along which a unique value of the velocity derivatives does not exist. For $M < 1$, these lines are imaginary. According to the mathematical theory of partial differential equations, if $\sqrt{C_2^2 - C_1C_3}$ is real, the equation is of the *hyperbolic type*; if $\sqrt{C_2^2 - C_1C_3} = 0$, the equation is *parabolic*; and if $\sqrt{C_2^2 - C_1C_3}$ is imaginary, the equation is *elliptic*. Thus, for supersonic flow, we are dealing with *a hyperbolic partial differential equation*. As a result, characteristics may be used to classify partial differential equations. [See Ref. (14.3).]

For the general case, we have determined the slope of the characteristic lines in the $(x, y)$ plane in terms of the velocity components $u$ and $v$, or $\partial\phi/\partial x$ and $\partial\phi/\partial y$. To fully establish the characteristic lines, we must find how the velocity components vary with $x$ and $y$. To this end, let us now return to the set of three linear equations

in Eq. (14.12) and develop an expression for one of the velocity derivatives. For example, for $\partial u/\partial x = \partial^2\phi/\partial x^2$,

$$\frac{\partial^2\phi}{\partial x^2} = \frac{\begin{vmatrix} du & dy & 0 \\ dv & dx & dy \\ 0 & 2C_2 & C_3 \end{vmatrix}}{\begin{vmatrix} dx & dy & 0 \\ 0 & dx & dy \\ C_1 & 2C_2 & C_3 \end{vmatrix}} \tag{14.18}$$

It will now be assumed that the velocity derivatives $\partial^2\phi/\partial x^2$, $\partial^2\phi/\partial y^2$, and $\partial^2\phi/\partial x\,\partial y$, with no shocks present, must be finite throughout the entire flow field. Since the denominator of Eq. (14.18) is zero, for these derivatives to remain finite the determinant of the numerator must also be zero. Thus, the derivatives of the velocity components are indeterminate—that is, 0/0—along the characteristic. Consequently,

$$\begin{vmatrix} du & dy & 0 \\ dv & dx & dy \\ 0 & 2C_2 & C_3 \end{vmatrix} = du dx\, C_3 - du dy\, 2C_2 - dv dy\, C_3 = 0$$

or

$$\frac{dv}{du} = \frac{dx}{dy} - \frac{2C_2}{C_3} \tag{14.19}$$

Combining this expression with Eq. (14.15) produces

$$\begin{aligned} \frac{dv}{du} &= \frac{C_1}{C_2 \pm \sqrt{C_2^2 - C_1C_3}} - \frac{2C_2}{C_3} \\ &= \frac{C_1}{C_2 \pm \sqrt{C_2^2 - C_1C_3}}\left(\frac{-C_2 \pm \sqrt{C_2^2 - C_1C_3}}{-C_2 \pm \sqrt{C_2^2 - C_1C_3}}\right) - \frac{2C_2}{C_3} \\ &= \frac{C_1\left(-C_2 \pm \sqrt{C_2^2 - C_1C_3}\right)}{-C_2^2 + C_2^2 - C_1C_3} - \frac{2C_2}{C_3} \\ &= \frac{-\left(-C_2 \pm \sqrt{C_2^2 - C_1C_3}\right) - 2C_2}{C_3} \end{aligned}$$

Hence,

$$\frac{dv}{du} = \frac{-C_2 \mp \sqrt{C_2^2 - C_1C_3}}{C_3} \tag{14.20}$$

Replacing $C_1$, $C_2$ and $C_3$, we obtain

$$\frac{dv}{du} = \frac{uv \mp \sqrt{a^2(u^2 + v^2) - a^4}}{a^2 - v^2} \tag{14.21}$$

Thus, for Characteristic I,

$$\left(\frac{dv}{du}\right)_{\mathrm{I}} = \frac{-uv + a\sqrt{u^2 + v^2 - a^2}}{v^2 - a^2} \tag{14.22}$$

and for Characteristic II,

$$\left(\frac{dv}{du}\right)_{\mathrm{II}} = \frac{-uv - a\sqrt{u^2 + v^2 - a^2}}{v^2 - a^2} \tag{14.23}$$

Equations (14.22) and (14.23) present the slopes of the characteristics in the *hodograph*, or *velocity plane* ($u$ versus $v$); recall the hodograph transformation in Section 12.4, in which we switched the roles of the independent variables $x$ and $y$ with the dependent variables $u$ and $v$ in order to obtain a linear governing equation.

Given initial values of velocity, $u$, $v$, and $a$ at some point in the flow field, Eqs. (14.16) and (14.17), the physical characteristics, and Eqs. (14.22), and (14.23), the hodograph characteristics can be simultaneously numerically integrated to obtain the characteristic curves in the physical $(x, y)$ plane and in the hodograph $(u, v)$ plane, respectively. Note that, since $dy/dx$ has been shown to be a function of $u$ and $v$, the solution for the characteristics in the $(x, y)$ plane is dependent on the simultaneous solution for the characteristic curves in the $(u, v)$ plane.

---

**Method 2**—*The Method of Linear Combination*: This method uses the sum of constant multiples of the equations that govern the flow to determine the characteristic and compatibility equations.

We now repeat the foregoing analysis of two-dimensional supersonic flow, using a different approach [called *the Friedrichs theory*; see Ref. (14.4)] that employs Property 3 to obtain the characteristic and the compatibility equations. This method, arguably the simplest approach to apply, has been thoroughly described by Zucrow and Thompson in Ref. (14.5). In this case, we rewrite Eq. (14.9) as a pair of first-order partial differential equations directly involving the velocity derivatives rather than the derivatives of the velocity potential:

$$C_1\frac{\partial u}{\partial x} + C_2\frac{\partial u}{\partial y} + C_2\frac{\partial v}{\partial x} + C_3\frac{\partial v}{\partial y} = 0$$

$$\frac{\partial v}{\partial x} - \frac{\partial u}{\partial y} = 0 \tag{14.24}$$

The second expression is the irrotational equation.

To obtain the desired ODEs that govern the characteristics, the set of PDEs must be manipulated somewhat. To accomplish this, multiply the first equation by an unknown parameter $\sigma_1$, the second by a second unknown parameter $\sigma_2$, and add the results to get

$$\sigma_1\left(C_1\frac{\partial u}{\partial x} + C_2\frac{\partial u}{\partial y} + C_2\frac{\partial v}{\partial x} + C_3\frac{\partial v}{\partial y}\right) + \sigma_2\left(\frac{\partial v}{\partial x} - \frac{\partial u}{\partial y}\right) = 0$$

Basically, we are forming a linear combination of the two equations. Alternatively, this task can be accomplished by utilizing a single parameter $\sigma$ $(= \sigma_2/\sigma_1)$; that is, we could

multiply the second equation by $\sigma$ and add it to the first equation. Grouping like derivatives gives

$$\left[C_1\sigma_1\frac{\partial u}{\partial x} + (C_2\sigma_1 - \sigma_2)\frac{\partial u}{\partial y}\right] + \left[(C_2\sigma_1 + \sigma_2)\frac{\partial v}{\partial x} + C_3\sigma_1\frac{\partial v}{\partial y}\right] = 0$$

or

$$C_1\sigma_1\left[\frac{\partial u}{\partial x} + \frac{(C_2\sigma_1 - \sigma_2)}{C_1\sigma_1}\frac{\partial u}{\partial y}\right] + (C_2\sigma_1 + \sigma_2)\left[\frac{\partial v}{\partial x} + \frac{C_3\sigma_1}{(C_2\sigma_1 + \sigma_2)}\frac{\partial v}{\partial y}\right] = 0 \quad (14.25)$$

Compare the group of terms within the square brackets to the following total derivatives:

$$\frac{\partial u}{\partial x} + \frac{dy}{dx}\frac{\partial u}{\partial y} = \frac{du}{dx}$$

$$\frac{\partial v}{\partial x} + \frac{dy}{dx}\frac{\partial v}{\partial y} = \frac{dv}{dx} \quad (14.26)$$

From the comparison of Eqs. (14.25) and (14.26), we may write the slope $dy/dx$, denoted as $\lambda$, as

$$\frac{dy}{dx} = \lambda = \frac{(C_2\sigma_1 - \sigma_2)}{C_1\sigma_1} = \frac{C_3\sigma_1}{(C_2\sigma_1 + \sigma_2)}$$

Expanding this pair of equations produces two equations for $\sigma_1$ and $\sigma_2$:

$$(C_1\lambda - C_2)\sigma_1 + \sigma_2 = 0$$

$$(C_2\lambda - C_3)\sigma_1 + \lambda\sigma_2 = 0 \quad (14.27)$$

A unique solution for $\sigma_1$ and $\sigma_2$ will be obtained if and only if the determinant of their coefficients vanishes—that is,

$$\begin{vmatrix}(C_1\lambda - C_2) & 1\\ (C_2\lambda - C_3) & \lambda\end{vmatrix} = 0$$

Expanding and rearranging the result produces the quadratic equation

$$C_1\lambda^2 - 2C_2\lambda + C_3 = 0$$

[See Eq. (14.13).] Solution of this expression yields

$$\lambda = \frac{dy}{dx} = \frac{2C_2 \pm \sqrt{4C_2^2 - 4C_1C_3}}{2C_1} = \frac{C_2 \pm \sqrt{C_2^2 - C_1C_3}}{C_1} \quad (14.28)$$

which was previously obtained as Eq. (14.14).

To derive the compatibility equation, combine Eqs. (14.25) and (14.26) to obtain

$$C_1\sigma_1 du + (C_2\sigma_1 + \sigma_2)dv = 0$$

or

$$C_1 du + \left(C_2 + \frac{\sigma_2}{\sigma_1}\right) dv = 0 \tag{14.29}$$

In order for this result to be useful, we must determine the relationship between $\sigma_1$ and $\sigma_2$. To accomplish this, combine Eq. (14.28) with either equation in Eq. (14.27) (*Note*: Both equations return the same result, but use of the first equation involves less algebra) to find

$$\frac{\sigma_2}{\sigma_1} = \mp\sqrt{C_2^2 - C_1 C_3} \tag{14.30}$$

Substituting Eq. (14.29) into Eq. (14.30), the details of which are left as a homework exercise, leads to

$$\frac{dv}{du} = \frac{-C_2 \mp \sqrt{C_2^2 - C_1 C_3}}{C_3}$$

This is the same compatibility equation as obtained by the Method of Indeterminate Derivatives [Eq. (14.20)]. It should be understood that by combining Eqs. (14.25) and (14.26), we are computing the change in the velocity components in particular directions, that is, along the characteristics. Such derivatives are termed *directional derivatives*. [See Ref. (14.6).]

**Historical Note: Richard Courant** was born on January 8, 1888 in Lublinitz, Prussia, Germany (now Lubliniec, Poland). During his youth, his family lived in Glatz and Breslau, and he entered the university in Breslau. The courses were not challenging to him, so he continued his studies at Zürich and, finally, Göttingen, where he became David Hilbert's assistant. He earned his doctorate in 1910. He fought in World War I, was soon wounded, and returned to research at Göttingen, where he remained except for the two years he spent as a professor in Münster. In 1919, he married Carle Runge's daughter. He founded Göttingen's Mathematics Institute, where he served as director from 1928 until 1933.

Courant was Jewish and, after being expelled from his position, left Germany in 1933—earlier than most Jews did. After one year in Cambridge, he went to New York and became, in 1936, a professor at New York University. There, he was given the task to found an institute for graduate studies in mathematics; the Courant Institute for Mathematical Sciences (as it was renamed in 1964) continues to be one of the most respected research centers in applied mathematics. In addition, he authored, with Hilbert, the influential textbook *Methods of Mathematical Physics*. His name is also attached to the finite-element method, which he set on a solid mathematical foundation. He died on January 27, 1972, in New Rochelle, NY, after suffering a stroke two months earlier.

**Friedrichs and Courant in 1965**
They wrote the classic text: *Supersonic Flow and Shock Waves*, Interscience (1948).

(*Continued*)

**Kurt Otto Friedrichs**, the son of a lawyer, was born in Kiel, Germany, on September 28, 1901. Friedrichs attended four universities before completing his mathematics studies at Göttingen. There, he met Richard Courant, director of the Institute of Mathematics, who admired his talent, but found him somewhat unworldly and extremely shy. Thus began their lifelong friendship. In his first five years at Göttingen, he wrote two papers and his dissertation (1927). In 1928, while investigating whether difference schemes for a time-varying partial differential equation yielded good approximate solutions, Courant, Friedrichs, and Hans Lewy were led to consider the stability of the difference scheme. After Friedrichs completed his dissertation and two years of an assistantship, Courant advised his young friend that in the severe competition for positions at German universities, Friedrichs would need some special advantage and therefore he should become an applied mathematician. Thus, Friedrichs followed Theodore von Kármán to Aachen, where the latter had become the first professor of aeronautical engineering. Friedrichs returned to Göttingen two years later with a deep knowledge of aerodynamics.

In 1931, Friedrichs was called to Braunschweig as a full professor, a rarity in prewar Germany for a man of just 30. But the Hitler era was about to begin. After five years of increasing political difficulties at Braunschweig; a visit to Courant, who had emigrated to New York; and, most important, meeting his future wife, Nellies, who was Jewish, Friedrichs saw clearly that he, too, would have to emigrate. He joined Courant in New York in 1937 and was later joined by Nellie.

Until the end of World War II, Friedrichs's main contributions were in fluid dynamics (with Courant) and in elasticity (with J. J. Stoker). By 1951, his spectral theory work led him into his fundamental work in the quantum theory of fields.

In 1954, Friedrichs gave the Gibbs Lecture at the American Mathematical Society on asymptotic theory. There, he surveyed the role of discontinuities in many physical phenomena, pointing out how important they are to us as observers. Shockwaves, boundary layers, shadowgraphs, edge effects, and Stokes phenomena in ordinary differential equations are all examples of discontinuities. This theoretical and applied mathematician died on December 31, 1982, in New Rochelle, NY.

For more information, see Refs. (14.7)–(14.9).

---

**Method 3**—*Eigenanalysis*: This method uses linear algebra to determine the characteristic and compatibility equations.

Paralleling the analytical model of Section 14.2, Method 3 takes advantage of the form of the first-order PDEs. However, because this approach involves a system of equations, principles from linear algebra are used throughout the method. The method was presented by Whitham in Ref. (14.10) along with a collection of examples; it is a more general procedure to determine the characteristics than the previous methods, and it is widely used in the field of computational fluid dynamics [e.g., see Refs. (14.11)–(14.13)].

The first step in the procedure is to write the governing system of PDEs in vector–matrix form. To demonstrate the methodology, let us reconsider the equations used in the analysis of Method 2, *viz.*, Eq. (14.24):

$$C_1\frac{\partial u}{\partial x} + C_2\frac{\partial u}{\partial y} + C_2\frac{\partial v}{\partial x} + C_3\frac{\partial v}{\partial y} = 0$$

$$\frac{\partial v}{\partial x} - \frac{\partial u}{\partial y} = 0 \qquad (14.24)$$

These equations may be combined into matrix–vector form as

$$\begin{bmatrix} C_1 & C_2 \\ 0 & 1 \end{bmatrix} \frac{\partial \mathbf{w}}{\partial x} + \begin{bmatrix} C_2 & C_3 \\ -1 & 0 \end{bmatrix} \frac{\partial \mathbf{w}}{\partial y} = 0$$

where the dependent-column vector is $\mathbf{w} = \begin{bmatrix} u \\ v \end{bmatrix}$. Defining the coefficient matrices as

$$\mathbf{A} = \begin{bmatrix} C_1 & C_2 \\ 0 & 1 \end{bmatrix} \qquad \mathbf{B} = \begin{bmatrix} C_2 & C_3 \\ -1 & 0 \end{bmatrix}$$

We may write the foregoing equation as

$$\mathbf{A} \frac{\partial \mathbf{w}}{\partial x} + \mathbf{B} \frac{\partial \mathbf{w}}{\partial y} = 0$$

Note that although it is more complex, this expression resembles a homogeneous version of Eq. (14.1). To write this equation in *characteristic equation form*, we multiply the entire expression by the inverse of matrix **A** to obtain

$$\frac{\partial \mathbf{w}}{\partial x} + \mathbf{A}^{-1}\mathbf{B} \frac{\partial \mathbf{w}}{\partial y} = 0$$

or

$$\frac{\partial \mathbf{w}}{\partial x} + \mathbf{C} \frac{\partial \mathbf{w}}{\partial y} = 0 \tag{14.31}$$

Matrix **C** is seen to be the product of the inverse of matrix **A** and matrix **B**. Because **A** is a $2 \times 2$ matrix, as described in Section 12.3, it is a simple matter to determine its inverse. Consider the following $2 \times 2$ matrix **M**:

$$\mathbf{M} = \begin{bmatrix} a & b \\ c & d \end{bmatrix}$$

The inverse matrix of **M** may be determined as follows:

$$\mathbf{M}^{-1} = \frac{\text{adj } \mathbf{M}}{\det \mathbf{M}} = \frac{1}{(ad - bc)} \begin{bmatrix} d & -b \\ -c & a \end{bmatrix}$$

Hence, for the case at hand,

$$\mathbf{A}^{-1} = \frac{1}{C_1} \begin{bmatrix} 1 & -C_2 \\ 0 & C_1 \end{bmatrix}$$

Multiplying $\mathbf{A}^{-1}$ by **B** gives

$$\mathbf{C} = \mathbf{A}^{-1}\mathbf{B} = \frac{1}{C_1} \begin{bmatrix} 1 & -C_2 \\ 0 & C_1 \end{bmatrix} \begin{bmatrix} C_2 & C_3 \\ -1 & 0 \end{bmatrix} = \begin{bmatrix} \dfrac{2C_2}{C_1} & \dfrac{C_3}{C_1} \\ -1 & 0 \end{bmatrix}$$

As Whitham [Ref. (14.10)] has shown, the equation for the characteristic directions is obtained by determining the *eigenvalues* of matrix **C**—that is, by solving

$$|\mathbf{C} - \lambda\mathbf{I}| = 0 \tag{14.32}$$

which for this case is

$$\begin{vmatrix} \dfrac{2C_2}{C_1} - \lambda & \dfrac{C_3}{C_1} \\ -1 & -\lambda \end{vmatrix} = 0 \tag{14.33}$$

Expanding the determinant yields the same quadratic expression [Eq. (14.13)] as obtained by the two previous methods:

$$-\left(\frac{2C_2}{C_1} - \lambda\right)\lambda + \frac{C_3}{C_1} = 0$$

$$C_1\lambda^2 - 2C_2\lambda + C_3 = 0$$

Solution of this equation brings two eigenvalues, $\lambda_{\mathrm{I}}$ and $\lambda_{\mathrm{II}}$, which are the slopes of the characteristic curves $(dy/dx)_{\mathrm{I}}$ and $(dy/dx)_{\mathrm{II}}$.

To derive the compatibility equation, begin with Eq. (14.31):

$$\frac{\partial \mathbf{w}}{\partial x} + \mathbf{C}\frac{\partial \mathbf{w}}{\partial y} = 0 \tag{14.31}$$

This system of PDEs is hyperbolic (an essential requirement for the existence of characteristics) if and only if matrix **C** is *diagonalizable*—that is, provided that

$$\mathbf{X}^{-1}\mathbf{C}\mathbf{X} = \mathbf{\Lambda} \tag{14.34}$$

where $\mathbf{\Lambda}$ is the diagonal matrix containing the eigenvalues of **C** on its main diagonal (i.e., $\mathbf{\Lambda} = \lambda\mathbf{I}$); **X** is a matrix composed of columns $\mathbf{r}_i$ that are the *right eigenvectors* of **C**; and $\mathbf{X}^{-1}$ is a matrix composed of rows $\mathbf{l}_i^{\mathbf{T}}$ (the superscript **T** stands for the *transpose*) that are the *left eigenvectors* of **C**. [See Ref. (14.14).] From linear algebra, the right eigenvectors corresponding to eigenvalue $\lambda_i$ of matrix **C** are determined from

$$\mathbf{C}\mathbf{r}_i = \lambda_i\mathbf{r}_i$$

or

$$(\mathbf{C} - \lambda_i\mathbf{I})\mathbf{r}_i = 0$$

whereas the left eigenvectors corresponding to eigenvalue $\lambda_i$ of matrix **C** are determined from

$$\mathbf{l}_i^{\mathbf{T}}\mathbf{C} = \lambda_i\mathbf{l}_i^{\mathbf{T}}$$

or

$$\mathbf{l}_i^{\mathbf{T}}(\mathbf{C} - \lambda_i\mathbf{I}) = 0 \tag{14.35}$$

Now premultiply Eq. (14.31) by $\mathbf{X}^{-1}$ and postmultiply matrix **C** by $\mathbf{X}\mathbf{X}^{-1}$ (note that the latter is equal to the identity matrix **I**, or the equivalent of unity) to get

$$\mathbf{X}^{-1}\frac{\partial \mathbf{w}}{\partial x} + \mathbf{X}^{-1}\mathbf{C}\mathbf{X}\mathbf{X}^{-1}\frac{\partial \mathbf{w}}{\partial y} = 0 \tag{14.36}$$

Because this is a hyperbolic system of equations, the grouping of terms $\mathbf{X}^{-1}\mathbf{C}\mathbf{X}$ within Eq. (14.36) may be replaced with the diagonal matrix $\Lambda$. Moreover, the *characteristic variables* are defined by $d\Gamma = \mathbf{X}^{-1}d\mathbf{w}$. Therefore, Eq. (14.36) may be rewritten as

$$\frac{\partial \Gamma}{\partial x} + \Lambda \frac{\partial \Gamma}{\partial y} = 0 \tag{14.37}$$

Equation (14.37) is called the *characteristic form* of Eq. (14.31). The $i$th component of this equation is

$$\frac{\partial \Gamma_i}{\partial x} + \lambda_i \frac{\partial \Gamma_i}{\partial y} = 0$$

Note that if there are $n$ equations within the system, then there will be $n$ eigenvalues and consequently $n$ characteristics; however, some of the eigenvalues may not be distinct.

The compatibility equation, which, as we have seen, provides the information that is passed along the characteristic lines, is produced from

$$d\Gamma = \mathbf{X}^{-1}d\mathbf{w} = 0 \tag{14.38}$$

Thus, to derive the compatibility equation, the left eigenvectors must first be determined. For the case at hand, there are two left eigenvectors corresponding to each of the two eigenvalues, say, $\lambda_{\mathrm{I}}$ and $\lambda_{\mathrm{II}}$. Each eigenvector contains two components that are determined by applying Eq. (14.35). Thus,

$$\mathbf{X}^{-1} = \mathbf{L} = [\mathbf{l}_{\mathrm{I}} \quad \mathbf{l}_{\mathrm{II}}] = \begin{bmatrix} l_{1\mathrm{I}} & l_{1\mathrm{II}} \\ l_{2\mathrm{I}} & l_{2\mathrm{II}} \end{bmatrix}$$

So, for characteristics in the family denoted by I,

$$\mathbf{l}_{\mathrm{I}}^{\mathrm{T}}(\mathbf{C} - \lambda_{\mathrm{I}}\mathbf{I}) = 0$$

or

$$[l_{1\mathrm{I}} \quad l_{2\mathrm{I}}]\begin{bmatrix} \dfrac{2C_2}{C_1} - \lambda_{\mathrm{I}} & \dfrac{C_3}{C_1} \\ -1 & -\lambda_{\mathrm{I}} \end{bmatrix} = 0$$

Expanding gives two equations:

$$\left(2\frac{C_2}{C_1} - \lambda_{\mathrm{I}}\right)l_{1\mathrm{I}} - l_{2\mathrm{I}} = 0$$

$$\frac{C_3}{C_1}l_{1\mathrm{I}} - \lambda_{\mathrm{I}}l_{2\mathrm{I}} = 0$$

Hence,

$$l_{2\mathrm{I}} = \left(2\frac{C_2}{C_1} - \lambda_{\mathrm{I}}\right)l_{1\mathrm{I}} \tag{14.39}$$

$$l_{2\mathrm{I}} = \left(\frac{C_3}{\lambda_{\mathrm{I}} C_1}\right) l_{1\mathrm{I}}$$

The group of coefficients on the right side of Eq. (14.39) are equal to each other, as may be seen by examining the eigenvalue expansion in Eq. (14.33). Therefore, the equations are not independent of each other. Accordingly, we may arbitrarily assign a value to either $l_{1\mathrm{I}}$ or $l_{2\mathrm{I}}$ and then use the foregoing equations to determine the remaining component. Let $l_{1\mathrm{I}} = 1$, so that

$$l_{2\mathrm{I}} = \left(2\frac{C_2}{C_1} - \lambda_{\mathrm{I}}\right) = \left(\frac{C_3}{\lambda_{\mathrm{I}} C_1}\right).$$

The compatibility equation for characteristics of the I family is then determined from Eq. (14.38) to be

$$\mathbf{l}_{\mathrm{I}}^{\mathrm{T}} d\mathbf{w} = 0$$

or

$$[l_{1\mathrm{I}} \quad l_{2\mathrm{I}}]\begin{bmatrix} du \\ dv \end{bmatrix} = \left[1\left(2\frac{C_2}{C_1} - \lambda_{\mathrm{I}}\right)\right]\begin{bmatrix} du \\ dv \end{bmatrix} = du + \left(2\frac{C_2}{C_1} - \lambda_{\mathrm{I}}\right)dv = 0$$

Consequently,

$$\left(\frac{dv}{du}\right)_{\mathrm{I}} = \frac{1}{\lambda_{\mathrm{I}} - 2\dfrac{C_2}{C_1}} = \frac{1}{\lambda_{\mathrm{I}}} + \frac{2\dfrac{C_2}{C_1}}{\lambda_{\mathrm{I}}\left(\lambda_{\mathrm{I}} - 2\dfrac{C_2}{C_1}\right)}$$

Since $\left(2\dfrac{C_2}{C_1} - \lambda_{\mathrm{I}}\right) = \left(\dfrac{C_3}{\lambda_{\mathrm{I}} C_1}\right)$, the foregoing equation becomes

$$\left(\frac{dv}{du}\right)_{\mathrm{I}} = \frac{1}{\lambda_{\mathrm{I}}} + \frac{2\dfrac{C_2}{C_1}}{\lambda_{\mathrm{I}}\left(-\dfrac{C_3}{\lambda_{\mathrm{I}} C_1}\right)} = \frac{1}{\lambda_{\mathrm{I}}} - \frac{2C_2}{C_3}$$

which is the same relation that was obtained by the other methods [Eq. (4.19)]. A similar expression can be developed for characteristics of the II family.

By comparing eigenanalysis to the method of linear combination, it can be seen that the left eigenvectors and the $\sigma$ values are related to each other. Expanding Eq. (14.38) for either eigenvalue gives

$$l_1 du + l_2 dv = 0$$

whereas from Eqs. (14.29) and (14.30), we have

$$C_1 du + \left(C_2 + \frac{\sigma_2}{\sigma_1}\right)dv = C_1 du + \left(C_2 \mp \sqrt{C_2^2 - C_1 C_3}\right)dv = 0$$

Clearly, $l_1$ is proportional to $C_1$, and $l_2$ is proportional to $C_2 + \sigma_2/\sigma_1 = C_2 \mp \sqrt{C_2^2 - C_1 C_3}$.

---

It is more useful to express the slope of the characteristic lines in polar coordinates $(V, \alpha)$ where $V$ is the flow speed and $\alpha$ is the flow inclination. Using the system shown in Figure 14.3, with positive $\alpha$ counterclockwise, we see that $u = V\cos\alpha$, $v = V\sin\alpha$, and $\tan\alpha = v/u$. As was demonstrated in Chapter 2, $\sin\mu = 1/M = a/V$ (where $\mu$ = Mach angle), or $\tan\mu = 1/\sqrt{M^2 - 1}$. (See Figure 14.4.)

Starting from Eq. (14.15), multiply the numerator and denominator by $M^2/[u^2(M^2 - 1)]$ and rearrange the result slightly to obtain

$$\frac{dy}{dx} = \frac{-uv \pm a\sqrt{u^2 + v^2 - a^2}}{a^2 - u^2} = \frac{\left(\frac{v}{u}\right)\left(\frac{M^2}{M^2-1}\right) \mp \left(\frac{a^2}{u^2}\sqrt{M^2 - 1}\right)\left(\frac{M^2}{M^2-1}\right)}{\left(\frac{M^2}{M^2-1}\right) - \left(\frac{a^2}{u^2}\right)\left(\frac{M^2}{M^2-1}\right)} \tag{14.40}$$

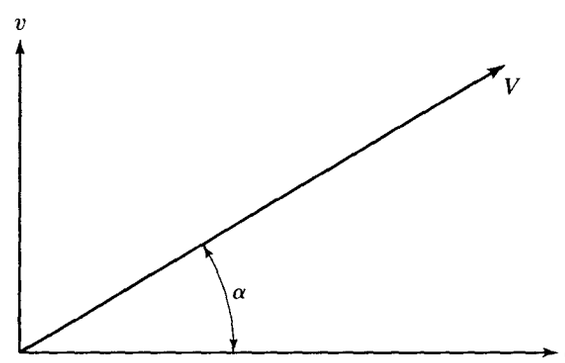


**Figure 14.3** Polar Coordinates $V$ and $\alpha$ in the Hodograph Plane

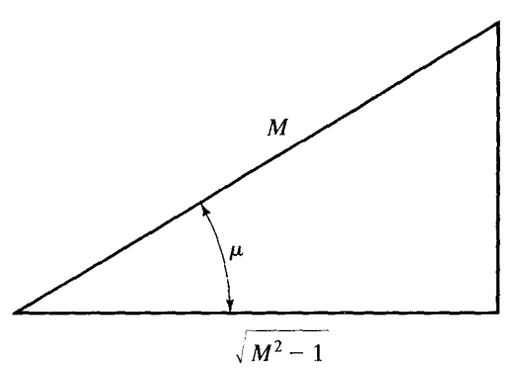


**Figure 14.4** Mach Triangle

Note that $M^2 = (u^2 + v^2)/a^2$; also, $M^2/(M^2 - 1) = 1 + 1/(M^2 - 1)$ and $(u^2 + v^2)/u^2 = 1 + v^2/u^2$. Utilizing these relationships allows Eq. (14.40) to be rewritten as

$$\frac{dy}{dx} = \frac{\frac{v}{u}\left(1 + \frac{1}{M^2 - 1}\right) \mp \left(1 + \frac{v^2}{u^2}\right)\frac{1}{\sqrt{M^2 - 1}}}{1 + \frac{1}{M^2 - 1} - \left(1 + \frac{v^2}{u^2}\right)\frac{1}{M^2 - 1}}$$

Rearrange terms in the numerator and cancel terms in the denominator to obtain

$$\frac{dy}{dx} = \frac{\left(\frac{v}{u} \mp \frac{1}{\sqrt{M^2 - 1}}\right) + \frac{v}{u}\frac{1}{\sqrt{M^2 - 1}}\left(\frac{1}{\sqrt{M^2 - 1}} \mp \frac{v}{u}\right)}{1 - \frac{v^2}{u^2}\frac{1}{M^2 - 1}}$$

Factor the terms in both the numerator and denominator to yield

$$\frac{dy}{dx} = \frac{\left(\frac{v}{u} \mp \frac{1}{\sqrt{M^2 - 1}}\right)\left(1 \mp \frac{v}{u}\frac{1}{\sqrt{M^2 - 1}}\right)}{\left(\frac{v}{u} + \frac{1}{\sqrt{M^2 - 1}}\right)\left(\frac{v}{u} - \frac{1}{\sqrt{M^2 - 1}}\right)}$$

Multiply the numerator and denominator by $\left(1 \pm \frac{v}{u}\frac{1}{\sqrt{M^2 - 1}}\right)$ and cancel terms to get

$$\frac{dy}{dx} = \frac{\left(\frac{v}{u} \mp \frac{1}{\sqrt{M^2 - 1}}\right)}{\left(1 \pm \frac{v}{u}\frac{1}{\sqrt{M^2 - 1}}\right)}$$

Make the replacements $v/u = V\sin\alpha/V\cos\alpha = \tan\alpha$ and $1/\sqrt{M^2 - 1} = \tan\mu$ to obtain

$$\frac{dy}{dx} = \frac{\tan\alpha \mp \tan\mu}{1 \pm \tan\alpha\tan\mu} \tag{14.41}$$

Use the trigonometric identity

$$\tan(\alpha \mp \mu) = \frac{\tan\alpha \mp \tan\mu}{1 \pm \tan\alpha\tan\mu} \tag{14.42}$$

to arrive at the equations for the slopes of the physical characteristics:

$$\left(\frac{dy}{dx}\right)_I = \tan(\alpha - \mu) \tag{14.43}$$

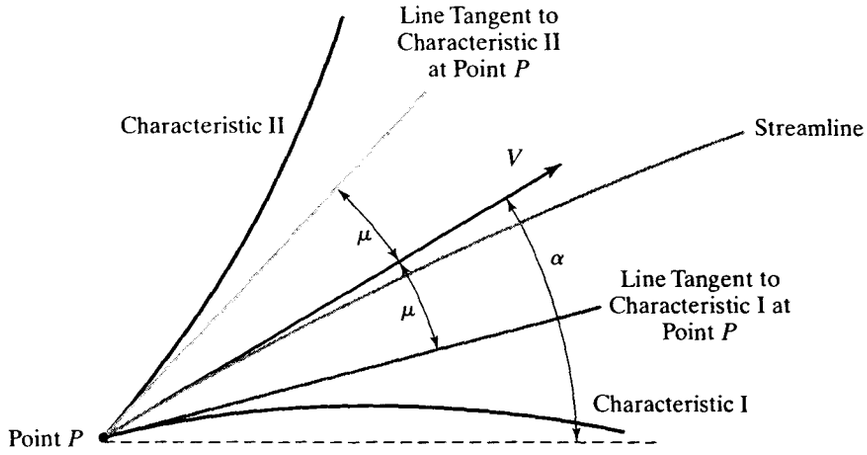


**Figure 14.5** Geometry of Characteristics at a Point

$$\left(\frac{dy}{dx}\right)_{\text{II}} = \tan(\alpha + \mu) \tag{14.44}$$

In other words, at each point in the flow, the characteristic lines are inclined at the Mach angle to the flow direction, as shown in Figure 14.5, with characteristics of Type I (sometimes referred to as *right running*) making a negative acute angle with the flow direction, and characteristics of Type II (sometimes referred to as *left running*) making a positive acute angle with the flow direction.

Using the mathematical approach, we have so far demonstrated the existence of characteristics for supersonic flow and have shown their equivalence with the Mach waves.

It should be noted that, whereas the mathematics shows the existence of two characteristics at each point in a supersonic flow field, there may exist only one Mach wave, since from physical considerations a disturbance in a supersonic flow cannot propagate back upstream. This situation was shown in Chapter 13, for example, for supersonic flow over a wave-shaped wall, where lines of $f$ = constant, corresponding to Mach lines making a negative angle with the flow direction, were ruled out.

To demonstrate the utility of the characteristics for the solution of flow problems, we must obtain a workable expression for velocity or Mach number along a characteristic. Let us write an expression for the slope of the characteristic in the hodograph plane in polar coordinates.

We have shown that

$$\frac{dv}{du} = \frac{-uv \pm a\sqrt{u^2 + v^2 - a^2}}{v^2 - a^2} \tag{14.21}$$

Multiply the numerator and denominator by $uv \pm a\sqrt{u^2 + v^2 - a^2}$ and simplify to obtain

$$\frac{dv}{du} = \frac{\left(-uv \pm a\sqrt{u^2 + v^2 - a^2}\right)}{(v^2 - a^2)} \frac{\left(uv \pm a\sqrt{u^2 + v^2 - a^2}\right)}{\left(uv \pm a\sqrt{u^2 + v^2 - a^2}\right)}$$

So,

$$\frac{dv}{du} = \frac{-u^2v^2 + a^2(u^2 + v^2) - a^4}{(v^2 - a^2)\left(uv \pm a\sqrt{u^2 + v^2 - a^2}\right)}$$

$$= \frac{-(v^2 - a^2)(u^2 - a^2)}{(v^2 - a^2)\left(uv \pm a\sqrt{u^2 + v^2 - a^2}\right)} = \frac{(a^2 - u^2)}{\left(uv \pm a\sqrt{u^2 + v^2 - a^2}\right)}$$

Thus,

$$\left(\frac{dv}{du}\right)_{\mathrm{I}} = \frac{1 - \dfrac{u^2}{a^2}}{\dfrac{uv}{a^2} + \sqrt{M^2 - 1}} \tag{14.45}$$

$$\left(\frac{dv}{du}\right)_{\mathrm{II}} = \frac{1 - \dfrac{u^2}{a^2}}{\dfrac{uv}{a^2} - \sqrt{M^2 - 1}} \tag{14.46}$$

Comparing Eqs. (14.45) and (14.46) with Eqs. (14.16) and (14.17), we see that

$$\left(\frac{dv}{du}\right)_{\mathrm{I}} = -\frac{1}{\left(\dfrac{dy}{dx}\right)_{\mathrm{II}}} \quad \text{and} \quad \left(\frac{dv}{du}\right)_{\mathrm{II}} = -\frac{1}{\left(\dfrac{dy}{dx}\right)_{\mathrm{I}}} \tag{14.47}$$

It is well known that two lines are perpendicular if their slopes are negative reciprocals of each other. Hence, *physical* Characteristic II is *orthogonal* to *hodograph* Characteristic I, and *physical* Characteristic I is orthogonal to *hodograph* Characteristic II. So, from Eqs. (14.43) and (14.44), we have

$$\left(\frac{dv}{du}\right)_{\mathrm{I}} = -\cot(\alpha + \mu) \tag{14.48}$$

$$\left(\frac{dv}{du}\right)_{\mathrm{II}} = -\cot(\alpha - \mu) \tag{14.49}$$

Since $u = V\cos\alpha$ and $v = V\sin\alpha$, then $du = \cos\alpha dV - V\sin\alpha d\alpha$ and $dv = \sin\alpha dV + V\cos\alpha d\alpha$, and we can write

$$\frac{dv}{du} = \frac{\sin\alpha dV + V\cos\alpha d\alpha}{\cos\alpha dV - V\sin\alpha d\alpha} = \frac{\tan\alpha \dfrac{1}{V}\dfrac{dV}{d\alpha} + 1}{\dfrac{1}{V}\dfrac{dV}{d\alpha} - \tan\alpha} \tag{14.50}$$

Combining Eq. (14.50) with Eqs. (14.48) and (14.49), and using the trigonometric identity in Eq. (14.42), we obtain

$$\frac{1}{V}\frac{dV}{d\alpha} = \frac{\tan\alpha - \tan(\alpha \pm \mu)}{1 + \tan\alpha\tan(\alpha \pm \mu)} = \tan[\alpha - (\alpha \pm \mu)] \tag{14.51}$$

Therefore,

$$\frac{1}{V}\frac{dV}{d\alpha} = \mp\tan\mu = \mp\frac{1}{\sqrt{M^2 - 1}} \tag{14.52}$$

where, once again, we have used the relation between $\tan\mu$ and Mach number. So, along Characteristic I, we can write

$$\frac{1}{V}\frac{dV}{d\alpha} = -\frac{1}{\sqrt{M^2 - 1}} \tag{14.53}$$

and along Characteristic II, we have

$$\frac{1}{V}\frac{dV}{d\alpha} = +\frac{1}{\sqrt{M^2 - 1}} \tag{14.54}$$

We now wish to integrate Eqs. (14.53) and (14.54) to obtain Mach number as a function of $\alpha$ *along* the characteristics. Fortunately, we have already come across a similar integral in dealing with Prandtl–Meyer flow in Chapter 7, where it was shown that, *across* a Mach wave,

$$d\nu = \sqrt{M^2 - 1}\frac{dV}{V} \tag{7.2}$$

or

$$\Delta\nu = \int \sqrt{M^2 - 1}\frac{dV}{V}$$

It is very important to appreciate the difference between Eq. (7.2) and Eqs. (14.53) and (14.54). In Chapter 7, we integrated across the waves, or characteristics, to find changes taking place normal to the waves. In Eqs. (14.53) and (14.54), we are integrating *along* the characteristic, not across or normal to it. The reason that the resultant equation for the two cases is similar will be discussed later in this chapter, when we derive expressions for changes taking place across the characteristics. Returning to the integration, we have

$$\int_a^b d\alpha = -\int_a^b \sqrt{M^2 - 1}\frac{dV}{V} \qquad \text{along a characteristic of Type I}$$

$$\int_a^b d\alpha = +\int_a^b \sqrt{M^2 - 1}\frac{dV}{V} \qquad \text{along a characteristic of Type II}$$

where $a$ and $b$ are points on the characteristics. Using the results from Chapter 7, for the Type I characteristic, we have

$$\alpha_b - \alpha_a = -(\nu_b - \nu_a) \tag{14.55}$$

Let $a$ be a reference state, so that $\alpha + \nu = \alpha_{\text{ref}} + \nu_{\text{ref}}$. Hence, along a characteristic of Type I, the sum of $\nu$ and $\alpha$ remains constant:

$$\nu + \alpha = \text{constant} = C_{\text{I}} \tag{14.56}$$

Similarly, along a characteristic of Type II, the difference between $\nu$ and $\alpha$ is constant:

$$\nu - \alpha = \text{constant} = C_{\text{II}} \tag{14.57}$$

The groupings $\nu \pm \alpha$ in Eqs. (14.56) and (14.57) are called *Riemann invariants*.

**Example 14.1. The method of linear combination applied to steady two-dimensional supersonic flow**

Write the continuity, momentum, and energy equations for two-dimensional, steady, supersonic flow of a perfect gas, and then use the method of linear combination to develop the characteristic and compatibility equations.

**Solution**

Starting from Eqs. (11.2) and (11.10) and a version of Eq. (11.18), the governing equations may be written as

$$\frac{\partial \rho}{\partial t} + \nabla \cdot \rho \mathbf{V} = 0$$

$$\rho \frac{D\mathbf{V}}{Dt} + \nabla p = \rho \left[ \frac{\partial \mathbf{V}}{\partial t} + \left( \mathbf{V} \cdot \nabla \right) \mathbf{V} \right] + \nabla p = 0$$

$$\rho \frac{Dh}{Dt} = \frac{Dp}{Dt}$$

The enthalpy for a perfect gas is $h = [\gamma/(\gamma - 1](p/p)$ Use this expression to replace the enthalpy in the energy equation, take the substantial derivative of the pressure–density expression, and use the speed-of-sound relation ($a^2 = \gamma p/\rho$) to obtain

$$\frac{Dp}{Dt} - a^2 \frac{D\rho}{Dt} = 0$$

Now, for two-dimensional, steady flow, the foregoing set of equations becomes

$$u \frac{\partial \rho}{\partial x} + v \frac{\partial \rho}{\partial y} + \rho \frac{\partial u}{\partial x} + \rho \frac{\partial v}{\partial y} = 0$$

$$\rho u \frac{\partial u}{\partial x} + \rho v \frac{\partial u}{\partial y} + \frac{\partial p}{\partial x} = 0$$

$$\rho u\frac{\partial v}{\partial x} + \rho v\frac{\partial v}{\partial y} + \frac{\partial p}{\partial y} = 0$$

$$u\frac{\partial p}{\partial x} + v\frac{\partial p}{\partial y} - a^2\left(u\frac{\partial \rho}{\partial x} + v\frac{\partial \rho}{\partial y}\right) = 0$$

It should be noted that to solve this problem using the method of indeterminate derivatives (Method 1), we would need four additional equations: the total derivatives of $\rho$, $u$, $v$, and $p$. To determine the characteristic equations by this approach, we would then have to expand two $8 \times 8$ determinants—a somewhat daunting task, as it requires more than 2.5 million multiplications and divisions.

The method of linear combinations is much simpler; the procedure requires that we (1) multiply each of the foregoing equations in turn by parameters $\sigma_1, \sigma_2, \sigma_3$, and $\sigma_4$; (2) add the resulting expressions together (that is, linearly combine the governing equations); and (3) group all like derivatives. The result of these steps is the following expression:

$$\left[(\rho\sigma_1 + \rho u\sigma_2)\frac{\partial u}{\partial x} + (\rho v\sigma_2)\frac{\partial u}{\partial y}\right] + \left[(\rho u\sigma_3)\frac{\partial v}{\partial x} + (\rho\sigma_1 + \rho v\sigma_3)\frac{\partial v}{\partial y}\right]$$
$$\left[(u\sigma_1 - ua^2\sigma_4)\frac{\partial \rho}{\partial x} + (v\sigma_1 - va^2\sigma_4)\frac{\partial \rho}{\partial y}\right] + \left[(\sigma_2 + u\sigma_4)\frac{\partial p}{\partial x} + (\sigma_3 + v\sigma_4)\frac{\partial p}{\partial y}\right] = 0$$

This equation can be rewritten by extracting the coefficients of all $x$-derivative terms from each of the [ ] terms, leaving

$$(\rho\sigma_1 + \rho u\sigma_2)\left[\frac{\partial u}{\partial x} + \frac{(\rho v\sigma_2)}{(\rho\sigma_1 + \rho u\sigma_2)}\frac{\partial u}{\partial y}\right] + (\rho u\sigma_3)\left[\frac{\partial v}{\partial x} + \frac{(\rho\sigma_1 + \rho v\sigma_3)}{(\rho u\sigma_3)}\frac{\partial v}{\partial y}\right] +$$
$$(u\sigma_1 - ua^2\sigma_4)\left[\frac{\partial \rho}{\partial x} + \frac{(v\sigma_1 - va^2\sigma_4)}{(u\sigma_1 - ua^2\sigma_4)}\frac{\partial \rho}{\partial y}\right] + (\sigma_2 + u\sigma_4)\left[\frac{\partial p}{\partial x} + \frac{(\sigma_3 + v\sigma_4)}{(\sigma_2 + u\sigma_4)}\frac{\partial p}{\partial y}\right] = 0$$

The coefficients of the $y$-derivative terms are taken to be the slopes ($dy/dx$) of the physical characteristics. This factor results in the following equations:

$$\frac{dy}{dx} = \lambda = \frac{(\rho v\sigma_2)}{(\rho\sigma_1 + \rho u\sigma_2)} = \frac{(\rho\sigma_1 + \rho v\sigma_3)}{(\rho u\sigma_3)} = \frac{(v\sigma_1 - va^2\sigma_4)}{(u\sigma_1 - ua^2\sigma_4)} = \frac{(\sigma_3 + v\sigma_4)}{(\sigma_2 + u\sigma_4)}$$

Expanding these equations and writing the resulting expressions in matrix form yields

$$\begin{bmatrix} \lambda & (u\lambda - v) & 0 & 0 \\ -1 & 0 & (u\lambda - v) & 0 \\ (u\lambda - v) & 0 & 0 & -(u\lambda - v)a^2 \\ 0 & \lambda & -1 & (u\lambda - v) \end{bmatrix}\begin{bmatrix} \sigma_1 \\ \sigma_2 \\ \sigma_3 \\ \sigma_4 \end{bmatrix} = 0$$

For this set of equations to produce nonzero values for the $\sigma$'s, the determinant of the coefficient matrix must vanish. Expanding the $4 \times 4$ determinant and letting $b = u\lambda - v$ yields

$$b^2(-a^2\lambda^2 - a^2 + b^2) = 0$$

Now, $b^2 = (u\lambda - v)^2 = u^2\lambda^2 - 2uv\lambda - v^2$, so the foregoing expression may be rewritten as

$$(u\lambda - v)^2[(u^2 - a^2)\lambda^2 - 2uv\lambda + (v^2 - a^2)] = 0$$

This equation contains four roots:

$$\lambda_{1,2} = \left(\frac{dy}{dx}\right)_{1,2} = \frac{v}{u}$$

$$\lambda_{3,4} = \left(\frac{dy}{dx}\right)_{3,4} = \frac{-uv \pm \sqrt{(uv)^2 - (a^2 - u^2)(a^2 - v^2)}}{a^2 - u^2}$$

Since $u = V\cos\alpha$ and $v = V\sin\alpha$, we see that the double root ($\lambda_1$ and $\lambda_2$) is simply the slope of the streamline. The other two roots are the slopes of the Mach lines. Hence, at each point, there are three characteristics: the streamline and two Mach lines.

To complete this problem, we must determine the compatibility equations. These are obtained from

$$(\rho\sigma_1 + \rho u\sigma_2)\left[\frac{\partial u}{\partial x} + \frac{(\rho v\sigma_2)}{(\rho\sigma_1 + \rho u\sigma_2)}\frac{\partial u}{\partial y}\right] + \quad (\rho u\sigma_3)\left[\frac{\partial v}{\partial x} + \frac{(\rho\sigma_1 + \rho v\sigma_3)}{(\rho u\sigma_3)}\frac{\partial v}{\partial y}\right]$$

$$+(u\sigma_1 - ua^2\sigma_4)\left[\frac{\partial \rho}{\partial x} + \frac{(v\sigma_1 - va^2\sigma_4)}{(u\sigma_1 - ua^2\sigma_4)}\frac{\partial \rho}{\partial y}\right] + (\sigma_2 + u\sigma_4)\left[\frac{\partial p}{\partial x} + \frac{(\sigma_3 + v\sigma_4)}{(\sigma_2 + u\sigma_4)}\frac{\partial p}{\partial y}\right]$$

$$= (\rho\sigma_1 + \rho u\sigma_2)[du] + (\rho u\sigma_3)[dv] + (u\sigma_1 - ua^2\sigma_4)[d\rho] + (\sigma_2 + u\sigma_4)[dp] = 0$$

Clearly, the values of the $\sigma$'s must be known in order to obtain the desired expressions.

Now, on a streamline, $\lambda_{1,2} = v/u$—that is, $u\lambda - v = 0$. Inserting this expression into the four equations for the $\sigma$'s and solving reveals that $\sigma_1 = 0$ and $\sigma_3 = \lambda\sigma_2$, whereas $\sigma_2$ and $\sigma_4$ are arbitrary, but nonzero. Hence,

$$(\rho\sigma_1 + \rho u\sigma_2)[du] + (\rho u\sigma_3)[dv] + (u\sigma_1 - ua^2\sigma_4)[d\rho] + (\sigma_2 + u\sigma_4)[dp] =$$

$$(0 + \rho u\sigma_2)[du] + \left(\rho u\frac{v}{u}\sigma_2\right)[dv] + (0 - ua^2\sigma_4)[d\rho] + (\sigma_2 + u\sigma_4)[dp] =$$

$$\sigma_2[\rho(udu + vdv) + dp] + u\sigma_4[dp - a^2 d\rho] = 0$$

Because $\sigma_2$ and $\sigma_4$ are nonzero, the groupings within the [ ] terms must vanish; therefore,

$$\rho(udu + vdv) + dp = 0$$

$$dp - a^2 d\rho = 0$$

The first expression is Bernoulli's equation, and the second is the speed-of-sound equation. Thus, as we should have anticipated, these results demonstrate that Bernoulli's equation and the isentropic speed-of-sound equation apply along a streamline. Furthermore, it is a simple matter to show that the entropy is constant along the streamline as well. However, it should be noted that this condition does not imply that the entropy is the same everywhere, which is the case for homentropic flow. Instead, the entropy can vary from streamline to streamline. According to Crocco's equation, Eq. (11.39), if

the entropy varies across streamlines—that is, there is a entropy gradient—the flow is rotational.

Now, on the Mach lines, $b^2 - a^2(1 + \lambda^2) = 0$, where, as before, $b = u\lambda - v$. Inserting this expression into the four equations for the $\sigma$'s and solving reveals that $\sigma_1 = b\sigma_3$, $\sigma_2 = -\lambda\sigma_3$, and $\sigma_4 = b\sigma_3/a^2$. Hence,

$$(\rho\sigma_1 + \rho u\sigma_2)[du] + (\rho u\sigma_3)[dv] + (u\sigma_1 - ua^2\sigma_4)[d\rho] + (\sigma_2 + u\sigma_4)[dp] =$$

$$\rho(b\sigma_3 - u\lambda\sigma_3)[du] + \rho(u\sigma_3)[dv] + u(b\sigma_3 - b\sigma_3)[d\rho] + \left(-\lambda\sigma_3 + \frac{ub}{a^2}\sigma_3\right)[dp] =$$

$$\rho(u\lambda - v - u\lambda)[du] + \rho(u)[dv] + u(0)[d\rho] + \left(-\lambda + \frac{ub}{a^2}\right)[dp] =$$

$$\rho v du + \rho u dv + \left(-\lambda + \frac{u^2\lambda - uv}{a^2}\right)dp = 0$$

Since Bernoulli's equation is applicable at any point within the field, we may replace $dp$ in the foregoing expression with $-\rho(udu + vdv)$. This replacement gives

$$\left[v + \left(\lambda - \frac{ub}{a^2}\right)u\right]du + \left[u + \left(\lambda - \frac{ub}{a^2}\right)v\right]dv + = 0$$

The coefficient of $du$ can readily be shown to equal $(1 + \lambda^2)(u^2 - a^2)/b$, whereas the coefficient of $dv$ is more difficult to reduce to $(1 + \lambda^2)(v^2 - a^2)/b\lambda$. The coefficient-reduction algebra uses the relationships $b = u\lambda - v$, $b^2/a^2 = 1 + \lambda^2$, and $(u^2 - a^2)\lambda^2 - 2uv\lambda = -(v^2 - a^2)$. Consequently, as obtained previously, we obtain

$$\frac{dv}{du} = \lambda\frac{(a^2 - u^2)}{(v^2 - a^2)} = \frac{-uv \pm a\sqrt{u^2 + v^2 - a^2}}{v^2 - a^2}$$

---

**Example 14.2. Eigenanalysis applied to steady two-dimensional supersonic flow**

Repeat Example 14.1, using eigenanalysis to develop the characteristic and compatibility equations for steady, two-dimensional, rotational, supersonic flow.

**Solution**

The governing set of equations given in Example 14.1 are first written in vector–matrix form as

$$\mathbf{A}\frac{\partial \mathbf{w}}{\partial x} + \mathbf{B}\frac{\partial \mathbf{w}}{\partial y} = 0$$

where

$$\mathbf{w} = \begin{bmatrix} u \\ v \\ p \\ \rho \end{bmatrix}, \quad \mathbf{A} = \begin{bmatrix} u & \rho & 0 & 0 \\ 0 & u & 0 & 1/\rho \\ 0 & 0 & u & 0 \\ 0 & \rho a^2 & 0 & u \end{bmatrix} \quad \text{and} \quad \mathbf{B} = \begin{bmatrix} v & 0 & \rho & 0 \\ 0 & v & 0 & 0 \\ 0 & 0 & v & 1/\rho \\ 0 & 0 & \rho a^2 & v \end{bmatrix}$$

To put this expression into characteristic equation form, we multiply it by $\mathbf{A}^{-1}$ to obtain

$$\frac{\partial \mathbf{w}}{\partial x} + \mathbf{A}^{-1}\mathbf{B}\frac{\partial \mathbf{w}}{\partial y} = 0$$

or

$$\frac{\partial \mathbf{w}}{\partial x} + \mathbf{C}\frac{\partial \mathbf{w}}{\partial y} = 0$$

Matrix $\mathbf{C}$ is seen to be the product of the inverse of matrix $\mathbf{A}$ and matrix $\mathbf{B}$. In this case, $\mathbf{A}$ is a $4 \times 4$ matrix, and obtaining its inverse is not easily accomplished by hand. It is better to employ a computer symbolic language program such as Maple or Mathematica to perform this operation. From this operation, we obtain

$$\mathbf{A}^{-1} = \begin{bmatrix} \frac{1}{u} & \frac{\rho}{a^2 - u^2} & 0 & \frac{1}{u(u^2 - a^2)} \\ 0 & \frac{u}{u^2 - a^2} & 0 & \frac{1}{\rho(a^2 - u^2)} \\ 0 & 0 & \frac{1}{u} & 0 \\ 0 & \frac{\rho a^2}{a^2 - u^2} & 0 & \frac{u}{u^2 - a^2} \end{bmatrix}$$

It is good practice to take the product of $\mathbf{A}$ and $\mathbf{A}^{-1}$ to see that this operation gives the identity matrix $\mathbf{I}$. Now, we multiply the inverse of matrix $\mathbf{A}$ and matrix $\mathbf{B}$ (the components are the coefficients of the $y$-derivative terms) to produce matrix $\mathbf{C}$:

$$\mathbf{C} = \frac{1}{(u^2 - a^2)} \begin{bmatrix} uv & -a^2 & -v/\rho & 0 \\ 0 & v(u^2 - a^2)/u & (u^2 - a^2)/\rho u & 0 \\ -\rho v a^2 & \rho u a^2 & uv & 0 \\ -\rho v & \rho u & v/u & v(u^2 - a^2)/u \end{bmatrix}$$

Next, the four eigenvalues of this matrix are determined. This operation requires that we solve

$$|\mathbf{C} - \lambda \mathbf{I}| = 0$$

Again, for this case, the process is more readily performed using a computer symbolic language program. The results of this step are the following four eigenvalues:

$$\lambda_{1,2,3,4} = \frac{v}{u}, \frac{v}{u}, \frac{-uv + \sqrt{(uv)^2 - (a^2 - u^2)(a^2 - v^2)}}{a^2 - u^2}, \text{ and } \frac{-uv - \sqrt{(uv)^2 - (a^2 - u^2)(a^2 - v^2)}}{a^2 - u^2}$$

These eigenvalues are the same as those obtained in Example 14.1 by the method of linear combination. Using these results, we next obtain the left eigenvectors that will in turn

produce the compatibility equations. Although use of a computer symbolic language program is recommended to remove the algebraic burden of obtaining the left eigenvectors, in order to get a feel for the procedure, we will go through the steps to determine the left eigenvectors corresponding to $\lambda_1$ and $\lambda_2$. Now, from Eq. (14.35),

$$[\mathbf{l}_i^1]^T(\mathbf{C} - \lambda_1\mathbf{I}) = 0$$

or

$$\frac{[l_1^1 \quad l_2^1 \quad l_3^1 \quad l_4^1]}{(u^2 - a^2)} \begin{bmatrix} uv - v(u^2 - a^2)/u & -a^2 & -v/\rho & 0 \\ 0 & 0 & (u^2 - a^2)/\rho u & 0 \\ -\rho v a^2 & \rho u a^2 & uv - v(u^2 - a^2)/u & 0 \\ -\rho v & \rho u & v/u & 0 \end{bmatrix} = 0$$

Note that the superscript on the left-eigenvector components indicates that we are working with $\lambda_1$. Also, note that $uv - v(u^2 - a^2)/u = va^2/u$. Expanding the foregoing expression yields three equations [not four because the last column in the $(\mathbf{C} - \lambda_1\mathbf{I})$ matrix consists of all zeros] in terms of four unknown components:

$$\left(\frac{va^2}{u}\right)l_1^1 + (0)l_2^1 - (\rho v a^2)l_3^1 - (\rho v)l_4^1 = 0$$

$$(-a^2)l_1^1 + (0)l_2^1 - (\rho u a^2)l_3^1 - (\rho u)l_4^1 = 0$$

$$\left(-\frac{v}{\rho}\right)l_1^1 + \left(\frac{u^2 - a^2}{\rho u}\right)l_2^1 - \left(\frac{va^2}{u}\right)l_3^1 - \left(\frac{v}{u}\right)l_4^1 = 0$$

It is easy to see that the first two expressions differ by a multiple $(-v/u)$ and therefore are not independent of each other. Hence, the foregoing set of expressions actually provides only two equations in terms of four unknowns. Consequently, we may arbitrarily set two of the components. From the last two expressions, it can be shown that

$$l_1^1 = \left(\frac{\rho u}{a^2}\right)(a^2 l_3^1 + l_4^1)$$

$$l_2^1 = \left(\frac{v}{u}\right)l_1^1 = \left(\frac{\rho v}{a^2}\right)(a^2 l_3^1 + l_4^1)$$

For simplicity, we set $l_3^1 = 1$ and $l_4^1 = 0$. Thus,

$$[l_1^1 \quad l_2^1 \quad l_3^1 \quad l_4^1] = [\rho u \quad \rho v \quad 1 \quad 0]$$

For the left eigenvector corresponding to $\lambda_2$ (also equal to $v/u$ and therefore yielding the same equations as before), we may set $l_3^2 = -1/a^2$ and $l_4^2 = 1$. This step produces the following:

$$[l_1^2 \quad l_2^2 \quad l_3^2 \quad l_4^2] = [0 \quad 0 \quad -1/a^2 \quad 1]$$

The left eigenvectors corresponding to $\lambda_3$ and $\lambda_4$ are algebraically more complicated, and therefore use of a computer symbolic language program is recommended. The results

may be assembled into the following matrix:

$$\mathbf{L} = \begin{bmatrix} \rho u & 0 & \dfrac{-1}{\sqrt{(u^2+v^2)-a^2}} & \dfrac{1}{\sqrt{(u^2+v^2)-a^2}} \\ \rho v & 0 & \dfrac{u/v}{\sqrt{(u^2+v^2)-a^2}} & \dfrac{-u/v}{\sqrt{(u^2+v^2)-a^2}} \\ 1 & -1/a^2 & 1/\rho v a & 1/\rho v a \\ 0 & 1 & 0 & 0 \end{bmatrix}$$

The compatibility equations are established by application of Eq. (14.38) for each left eigenvector corresponding to a particular eigenvalue. For example, along the characteristic given by $dy/dy = \lambda_1$,

$$\mathbf{l}_1^{\mathrm{T}} d\mathbf{w} = [l_1^1 \quad l_2^1 \quad l_3^1 \quad l_4^1] \begin{bmatrix} du \\ dv \\ dp \\ d\rho \end{bmatrix} = [\rho u \quad \rho v \quad 1 \quad 0] \begin{bmatrix} du \\ dv \\ dp \\ d\rho \end{bmatrix} = \rho u du + \rho v dv + dp = 0$$

This expression, as discussed in Example 14.1, is Bernoulli's equation. It is left as an exercise to determine the other three compatibility equations.

## 14.4 CALCULATION PROCEDURES

We are now in a position to demonstrate how the method of characteristics can be used to determine a two-dimensional supersonic flow field. Just as there were several ways to develop the equations that form the MOC, it is also possible to develop several distinct calculation procedures.

### Procedure 1—The Point-to-Point Method

When a characteristic of one family extends into a flow field, it can encounter (1) a characteristic of another family, (2) a boundary, (3) a free surface, or (4) a shockwave. Each of these encounters or interactions leads to a set of computational rules that are called *unit processes*. Application of the unit processes allow the solution to be gradually advanced into the flow field. Therefore, the procedure is generally called the *Point-to-Point Method*. We now consider the first three types of interaction. Consult Ref. (14.15) for an explanation of the unit process of a characteristic and a shockwave.

### An Interior-Field-Point Unit Process

We begin by considering the calculation at an interior field point. Suppose that, along a curve $LM$, we know the flow conditions—that is, the velocity and its direction, pressure, temperature, Mach number, and so on. This curve is called the *initial value line* and must not be a characteristic curve or else the problem is ill posed. Now select points $A$ and $B$ on the initial value curve, as shown in Figure 14.6.

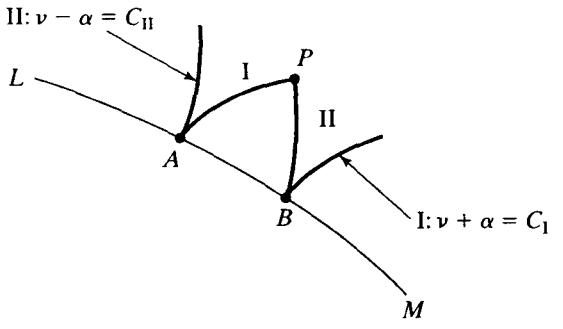


**Figure 14.6** Extending the Solution at an Interior Field Point by the Point-to-Point Procedure

With velocity (magnitude and direction) and Mach number known at points $A$ and $B$, $\alpha$ and $\nu(M)$ are known, so the Riemann invariants $C_I$ and $C_{II}$ can be calculated from Eqs. (14.56) and (14.57), respectively. Characteristic I from point $A$ intersects with Characteristic II from point $B$ at point $P$, as shown in the figure. Since $\nu + \alpha$ = constant along a characteristic of Type I and $\nu - \alpha$ = constant along a characteristic of Type II, it follows that, at point $P$,

$$C_I = \nu_A + \alpha_A = \nu_P + \alpha_P$$

$$C_{II} = \nu_B - \alpha_B = \nu_P - \alpha_P$$

So, we have two equations with two unknowns, $\nu_p$ and $\alpha_p$, which may be readily solved to obtain

$$\nu_P = \frac{C_I + C_{II}}{2} \tag{14.58}$$

$$\alpha_P = \frac{C_I - C_{II}}{2} \tag{14.59}$$

Since, from

$$\nu_p = \left\{\sqrt{\frac{\gamma+1}{\gamma-1}}\tan^{-1}\left[\sqrt{\frac{\gamma-1}{\gamma+1}(M_p^2-1)}\right] - \tan^{-1}\left(\sqrt{M_p^2-1}\right)\right\} \tag{7.10}$$

$v = v(M)$, the Mach number at $P$ can be determined. Moreover, the direction of the velocity at $P$ is known from Eq. (14.59). For isentropic flow, the Mach number can be used to determine the values of the stagnation-to-static-temperature and -pressure ratios at point $P$. Since $T_o$ and $p_o$ are constants for this flow, the static temperature and pressure at $P$ can be calculated. By working outward from the initial value curve $LM$, it is then possible to build a net or mesh, with points connected by the characteristics. (See Figure 14.7.) Of course, to complete the process, we need to determine the direction of the characteristics. Since Mach number varies throughout the flow field, the

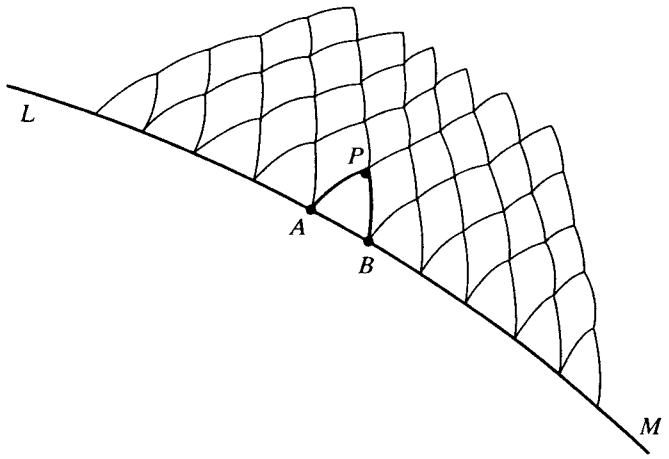


**Figure 14.7** Characteristic Mesh

characteristic lines $AP$ and $BP$ are not necessarily straight, but rather may be curved. However, if the size of the mesh is kept small enough, the lines $AP$ and $BP$ can be approximated by straight lines (see Figure 14.8) inclined at the Mach angle to the flow direction. Naturally, the accuracy of this procedure depends on the mesh size: The smaller the mesh, the more accurate the solution is.

To find the direction of the characteristics, we employ Eqs. (14.43) and (14.44):

$$\left(\frac{dy}{dx}\right)_{\text{I}} = \tan(\alpha - \mu) \tag{14.43}$$

$$\left(\frac{dy}{dx}\right)_{\text{II}} = \tan(\alpha + \mu) \tag{14.44}$$

As we have seen, these equations tell us that at a given point the characteristics of family I are inclined to the $x$-axis at an angle of $\alpha - \mu$, whereas at a given point the characteristics of family II are inclined to the $x$-axis at an angle of $\alpha + \mu$.

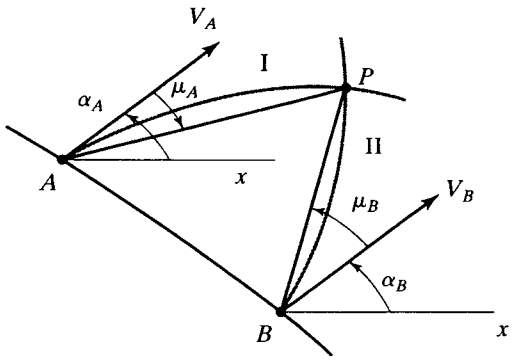


**Figure 14.8** Straight-Line Approximations of the Characteristics

To solve the foregoing pair of equations, we may use the explicit Euler method that was used to solve ordinary differential equations in Chapters 9 and 10. However, this situation is somewhat different because we must solve the pair of equations simultaneously. Thus, instead of selecting a set value of the difference $\Delta x$, here we write the finite-difference versions of the equations as follows (refer to Figure 14.8):

$$\left(\frac{dy}{dx}\right)_{\mathrm{I}} = \frac{y_P - y_A}{x_P - x_A} = \tan(\alpha - \mu)_A = m_{\mathrm{I}}$$

$$\left(\frac{dy}{dx}\right)_{\mathrm{II}} = \frac{y_P - y_B}{x_P - x_B} = \tan(\alpha - \mu)_B = m_{\mathrm{II}}$$

*Note*: Because characteristics can be curved, there are other ways to evaluate the right-hand side of Eqs. (14.43) and (14.44). For example, we could base the inclination angle on the average value between the initial value line and the target point. This approach leads to an improved calculation of the location of the target point. Applying this method to Eqs. (14.43) and (14.44) yields

$$\left(\frac{dy}{dx}\right)_{\mathrm{I}} = \frac{y_P - y_A}{x_P - x_A} = \tan\left[\frac{(\alpha - \mu)_A + (\alpha - \mu)_P}{2}\right] = m_{\mathrm{I}} \tag{14.60}$$

$$\left(\frac{dy}{dx}\right)_{\mathrm{II}} = \frac{y_P - y_B}{x_P - x_B} = \tan\left[\frac{(\alpha - \mu)_B + (\alpha - \mu)_P}{2}\right] = m_{\mathrm{II}}$$

These variations will result in a slightly different characteristic net and will cause the target point $P$ to appear at a different location from that shown in Figure 14.8.

Eqs. (14.60) give two equations for the $y$ location of point $P$:

$$y_P = y_A + m_{\mathrm{I}}(x_P - x_A) \tag{14.61}$$

$$y_P = y_B + m_{\mathrm{II}}(x_P - x_B)$$

Solving this pair of equations simultaneously yields $x_p$, the $x$ location of point $P$:

$$x_P = \frac{y_A - y_B + m_{\mathrm{II}}x_B - m_{\mathrm{I}}x_A}{m_{\mathrm{II}} - m_{\mathrm{I}}} \tag{14.62}$$

Example 14.3 will illustrate the computational procedure.

### A Boundary-Point Unit Process

What distinguishes the interactions of this unit process is that the angle at point $P$ is known because $P$ is on a boundary. The boundary may be a solid wall, or it could be the centerline. So for this unit process is that we know the value of $\alpha_p$ and must determine the Prandtl–Meyer function $\nu_p$.

If a characteristic of family I located at a known point, say, point $A$, intersects the boundary, the unit process is

$$C_{\mathrm{I}} = \nu_A + \alpha_A = \nu_P + \alpha_P$$

or

$$\nu_P = C_{\mathrm{I}} - \alpha_P \tag{14.63}$$

On the other hand, if a characteristic of family II located at a known point, say, point $B$, intersects the boundary, the unit process is

$$C_{\mathrm{II}} = \nu_B - \alpha_B = \nu_P - \alpha_P$$

or

$$\nu_P = C_{\mathrm{II}} + \alpha_P \tag{14.64}$$

Example 14.3 will demonstrate how to determine the direction of the characteristics in either situation.

### A Free-Surface Point-Unit Process

The static pressure along a free surface is constant. For example, when a gas jet exits a nozzle, its boundary is a free surface because the boundary must be in mechanical equilibrium with the surroundings. Since the static pressure along the free-surface boundary is known, and since the stagnation pressure is constant throughout the flow, we know the value of the static-to-stagnation-pressure ratio. From this ratio, we can compute a Mach number and, in turn, use Eq. (7.10) to determine the value of the Prandtl–Meyer function on the free-surface boundary. So the distinguishing feature of this unit process is that we know the value of $\nu_p$ and must determine the flow angle $\alpha_p$.

Consequently, when a characteristic of family I located at a known point, say, point $A$, intersects a free-surface boundary, the unit process is

$$C_{\mathrm{I}} = \nu_A + \alpha_A = \nu_P + \alpha_P$$

or

$$\alpha_P = C_{\mathrm{I}} - \nu_P \tag{14.65}$$

On the other hand, if a characteristic of family II located at a known point, say, point $B$, intersects the boundary, the unit process is

$$C_{\mathrm{II}} = \nu_B - \alpha_B = \nu_P - \alpha_P$$

or

$$\alpha_P = C_{\mathrm{II}} + \nu_P \tag{14.66}$$

**Example 14.3. Point-to-point MOC applied to radial supersonic flow in a diverging channel**

Uniform radial flow at Mach 2.0 enters a two-dimensional diverging channel with straight walls. Compute the variation of Mach number in this radial flow field, assuming isentropic, steady flow. The walls are inclined at a total angle of 12°, as shown in Figure 14.9, and $\gamma = 1.4$.

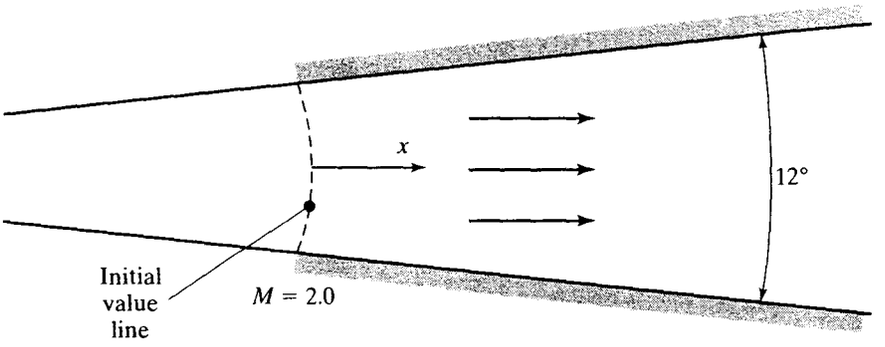


**Figure 14.9** Radial Supersonic Flow in a Diverging Two-Dimensional Channel

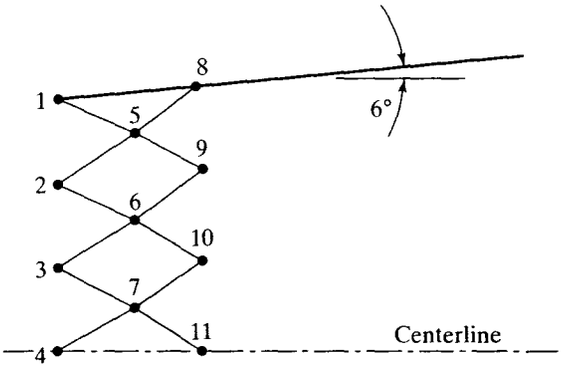


**Figure 14.10** Grid Network Downstream of the Initial Value Line

**Solution**

From symmetry, it is only necessary to consider one half of the flow field. (See Figure 14.10.) The initial value arc is a radial line on which the flow is known, so we can work outward from this line. To begin, select four equally spaced points on the initial value line, $\alpha_4 = 0°, \alpha_3 = 2°, \alpha_2 = 4°$, and $\alpha_1 = 6°$. Accordingly, $M_1 = M_2 = M_3 = M_4 = 2.0$. From the *Prandtl–Meyer Spreadsheet Solver* of Chapter 7 (for brevity, this program will be hereby be referred to as *PMSS*), $\nu_1 = \nu_2 = \nu_3 = \nu_4 = 26.3798°$.

Along the characteristic line 2–5, the Riemann invariant $C_{II}$ = constant = $\nu_2 - \alpha_2$ = 26.3798 − 4 = 22.3798°. Along the characteristic line 1–5, the Riemann invariant $C_I$ = constant = $\nu_1 + \alpha_1$ = 26.3798 + 6 = 32.3798°. Thus, $C_I$ and $C_{II}$ are known at point 5. From the interior-field-point unit process of Eqs. (14.58) and (14.59), we find that $\nu_5 = 27.3798°$ and $\alpha_5 = 5°$. From PMSS, at this value of $\nu_5$, we compute $M_5 = 2.0365$.

In the MOC numerical procedure, the line 1–5 is assumed straight, as shown in Figure 14.11, making an angle $-\mu_1$ with the flow direction at 1, or an angle $\alpha_1 - \mu_1$ with the horizontal. $\mu_1$ can be found from $\sin \mu_1 = 1/M_1$. The angle between lines such as 2–5, which make a positive (counterclockwise) acute angle with the flow direction, and the horizontal is $\alpha_2 + \mu_2$. The angle between lines such as 2–6, which make a negative acute angle with the flow direction, and the horizontal is $\alpha_2 - \mu_2$. (See Figure 14.11.)

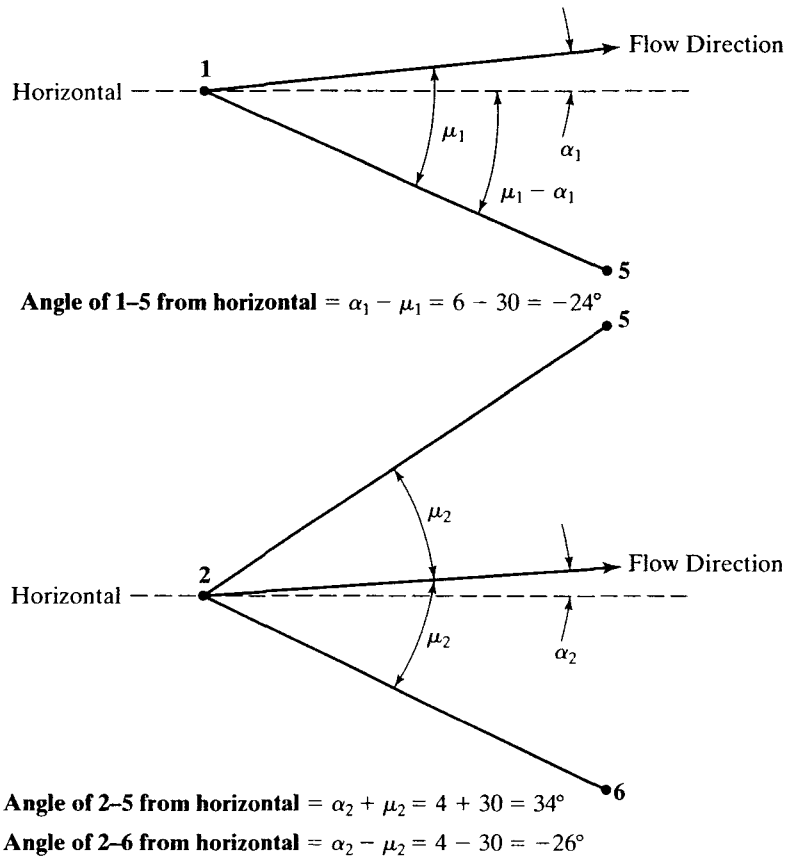


**Figure 14.11** Geometry of Characteristic Lines

At points such as 8 and 11, we apply the boundary-point unit process. The Riemann invariant at each point is known from previous calculations ($C_{II} = \nu_5 - \alpha_5$ at point 8; $C_I = \nu_7 + \alpha_7$ at point 11). At these two boundary points, we have additional boundary conditions, since the flow must follow the walls. At point 8, $\alpha_8 = 6°$; at point 11, $\alpha_{11} = 0°$. Using Eqs. (14.61) and (14.60), respectively, we can calculate the values of $\nu_8$ and $\nu_{11}$. Table 14.1 shows the results of the numerical procedure for points 1 to 18. Note that the bold entries indicate known information for the given point. Figure 14.12 is a sketch showing the grid point numbering.

Next, we determine the locations of the characteristic points. Because the channel walls are radial lines, the initial value line is taken to be on an arc of length $R\Delta\theta$. The equation for the upper wall is $y = x \tan \theta$. To fix point 1 (Figure 14.12), let $y_1 = 1.0$; therefore, $x_1 = 1/\tan \Delta\theta = 9.51436$. Consequently the $(x, y)$ coordinates of point 1 are (9.51436, 1.0). The radius of the initial value line is $R_{IVL} = \sqrt{x_1^2 + y_1^2} = 9.56677$. Other points on the initial value line may be computed using $x = R \cos \theta$ and $y = R \sin \theta$. The points within the interior field points are determined using Eqs. (14.60) through (14.62). Values for points from 1 to 18 are shown in Table 14.2.

To determine the accuracy of the MOC computations, we can compare the Mach number along the centerline of the channel with the results from the exact radial source flow solution presented in Section 12.2. The area ratio $A_4/A^*$ depends only on $M_4$ and $\gamma$. The

**TABLE 14.1** Computations for Example 14.3

| Point | $\alpha = (C_I + C_{II})/2$ deg | $\nu = (C_I - C_{II})/2$ deg | $C_I = \alpha + \nu$ deg | $C_{II} = \alpha - \nu$ deg | $M$ | $\mu$ deg | $\alpha + \mu$ deg | $\alpha - \mu$ deg |
|---|---|---|---|---|---|---|---|---|
| 1 | **6** | 26.3798 | 32.3798 | 20.3798 | **2** | 30 | 36 | −24 |
| 2 | **4** | 26.3798 | 30.3798 | 22.3798 | **2** | 30 | 34 | −26 |
| 3 | **2** | 26.3798 | 28.3798 | 24.3798 | **2** | 30 | 32 | −28 |
| 4 | **0** | 26.3798 | 26.3798 | 26.3798 | **2** | 30 | 30 | −30 |
| 5 | 5 | 27.3798 | **32.3798** | **22.3798** | 2.0365 | 29.4095 | 34.4095 | −24.4095 |
| 6 | 3 | 27.3798 | **30.3798** | **24.3798** | 2.0365 | 29.4095 | 32.4095 | −26.4095 |
| 7 | 1 | 27.3798 | **28.3798** | **26.3798** | 2.0365 | 29.4095 | 30.4095 | −28.4095 |
| 8 | **6** | 28.3798 | 34.3798 | **22.3798** | 2.0733 | 28.8370 | 34.8370 | −22.8370 |
| 9 | 4 | 28.3798 | **32.3798** | **24.3798** | 2.0733 | 28.8370 | 32.8370 | −24.8370 |
| 10 | 2 | 28.3798 | **30.3798** | **26.3798** | 2.0733 | 28.8370 | 30.8370 | −26.8370 |
| 11 | **0** | 28.3798 | **28.3798** | 28.3798 | 2.0733 | 28.8370 | 28.8370 | −28.8370 |
| 12 | 5 | 29.3798 | **34.3798** | **24.3798** | 2.1106 | 28.2815 | 33.2815 | −23.2815 |
| 13 | 3 | 29.3798 | **32.3798** | **26.3798** | 2.1106 | 28.2815 | 31.2815 | −25.2815 |
| 14 | 1 | 29.3798 | **30.3798** | **28.3798** | 2.1106 | 28.2815 | 29.2815 | −27.2815 |
| 15 | **6** | 30.3798 | 36.3798 | **24.3798** | 2.1483 | 27.7419 | 33.7419 | −21.7419 |
| 16 | 4 | 30.3798 | **34.3798** | **26.3798** | 2.1483 | 27.7419 | 31.7419 | −23.7419 |
| 17 | 2 | 30.3798 | **32.3798** | **28.3798** | 2.1483 | 27.7419 | 29.7419 | −25.7419 |
| 18 | **0** | 30.3798 | **30.3798** | 30.3798 | 2.1483 | 27.7419 | 27.7419 | −27.7419 |

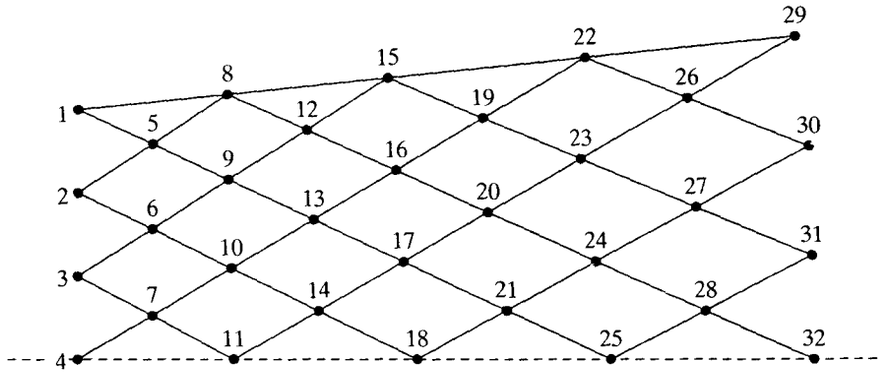


**Figure 14.12** Characteristic Grid Network in Channel

**TABLE 14.2** Physical Characteristic Computations for Example 14.3

| Point | $\alpha$ deg | $\mu$ | $\alpha + \mu$ | $\alpha - \mu$ | $m_{\mathrm{I}}$ | $m_{\mathrm{II}}$ | $x$ | $y$ |
|---|---|---|---|---|---|---|---|---|
| 1 | 6 | 30 | 36 | −24 | | | 9.5144 | 1.0000 |
| 2 | 4 | 30 | 34 | −26 | | | 9.5435 | 0.6673 |
| 3 | 2 | 30 | 32 | −28 | | | 9.5609 | 0.3339 |
| 4 | 0 | 30 | 30 | −30 | | | 9.5668 | 0.0 |
| **5** | **5** | **29.4095** | **34.4095** | **−24.4095** | **−0.4495** | **0.6797** | **9.8265** | **0.8597** |
| **6** | **3** | **29.4095** | **32.4095** | **−26.4095** | **−0.4922** | **0.6298** | **9.8505** | **0.5162** |
| **7** | **1** | **29.4095** | **30.4095** | **−28.4095** | **−0.5363** | **0.5821** | **9.8625** | **0.1722** |
| 8 | 6 | 28.8370 | 34.8370 | −22.8370 | 0.1051 | 0.6905 | 10.1222 | 1.0639 |
| 9 | 4 | 28.8370 | 32.8370 | −24.8370 | −0.4750 | 0.6106 | 10.1563 | 0.7030 |
| 10 | 2 | 28.8370 | 30.8370 | −26.8370 | −0.5186 | 0.6401 | 10.1541 | 0.3588 |
| 11 | 0 | 28.8370 | 28.8370 | −28.8370 | −0.5457 | 0.0 | 10.1779 | 0.0 |
| **12** | **5** | **28.2815** | **33.2815** | **−23.2815** | **−0.4257** | **0.6509** | **10.4780** | **0.9124** |
| **13** | **3** | **28.2815** | **31.2815** | **−25.2815** | **−0.4676** | **0.6023** | **10.4768** | **0.5532** |
| **14** | **1** | **28.2815** | **29.2815** | **−27.2815** | **−0.5108** | **0.5557** | **10.5030** | **0.1806** |
| 15 | 6 | 27.7419 | 33.7419 | −21.7419 | 0.1051 | 0.6622 | 10.8171 | 1.1369 |
| 16 | 4 | 27.7419 | 31.7419 | −23.7419 | −0.4351 | 0.6131 | 10.8201 | 0.7636 |
| 17 | 2 | 27.7419 | 29.7419 | −25.7419 | −0.4772 | 0.5660 | 10.8481 | 0.3760 |
| 18 | 0 | 27.7419 | 27.7419 | −27.7419 | −0.5208 | 0.0 | 10.8497 | 0.0 |

other ratios are determined by multiplication. For example, $A_{11}/A^* = (A_{11}/A_4)(A_4/A^*) = (R_{11}\Delta\theta/R_4\Delta\theta)(A_4/A^*) = (x_{11}/x_4)(A_4/A^*)$.

The MOC results are seen to be very accurate even though a coarse grid was used. Completion of the remaining points (that is, from 19 to 32) is left as a homework exercise.

**TABLE 14.3** Comparison of Results with Exact Solution for Example 14.3

| Point | Area | $A/A^*$ | $M$ (exact solution) | $M$ (MOC) | % Error |
|---|---|---|---|---|---|
| 4 | $A_4$ | 1.6875 | 2.0 | 2.0 | |
| 11 | $1.06395A_4$ | 1.7953 | 2.0733 | 2.0733 | 0.0000 |
| 18 | $1.1341A_4$ | 1.9138 | 2.1472 | 2.1483 | 0.0514 |

### Procedure 2—The Region-to-Region Method

The method we just examined involves calculating the flow properties at points in the flow field, with the points determined by the intersection of characteristic lines. In many cases, however, it is easier to use a slightly different procedure in which properties are found in the *regions* bounded by characteristics. Therefore, the procedure is called the *region-to-region method*, but is also known as the *field method*.

For example, suppose we have a continuously varying flow along a curved wall, as shown in Figure 14.13(a). Several Mach waves (characteristics of Type II) are illustrated in the figure; for this flow, the characteristics of Type I are not Mach waves, since, as has been discussed previously, a disturbance cannot propagate back upstream in a supersonic flow. If the wall is smooth, there will be an infinite number of Mach waves between $M_{\text{upstream}}$ and $M_{\text{downstream}}$. In order to analyze the flow, let us break the continuous curved wall into segments, as shown in Figure 14.13(b). Expansion fans will emanate from the corner of each segment. To carry this procedure one step further, let us replace each expansion fan in Figure 14.13(b) by a single wave, as shown in Figure 14.14. These pseudowaves are not truly characteristics or Mach waves, since they separate regions between which small but finite changes take place. However, let us assume that the wall is divided into enough segments, say, $n - 1$, that the waves can be approximated as characteristics. (Strictly speaking, only if the wall were divided into an infinite number of segments would the waves be characteristics.) Four pseudowaves ($a$, $b$, $c$, and $d$) are used in Figure 14.14 to segregate the flow into five regions, in each of which Mach number and flow direction are uniform.

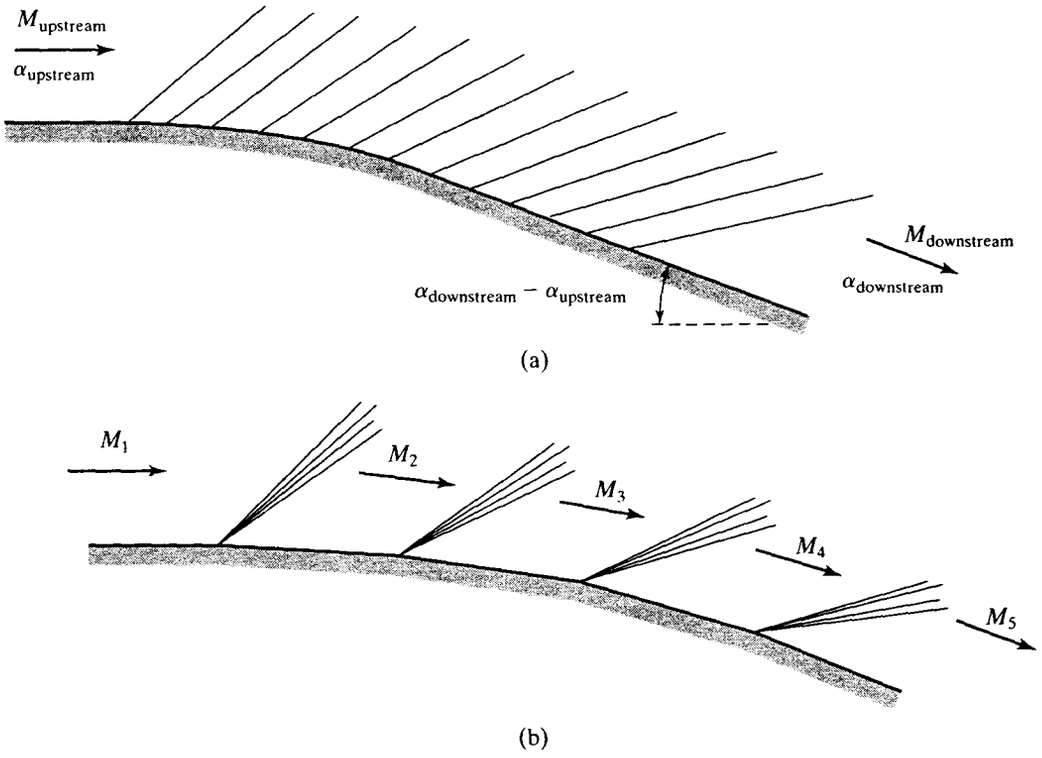


**Figure 14.13** Supersonic Flow over a Curved Wall

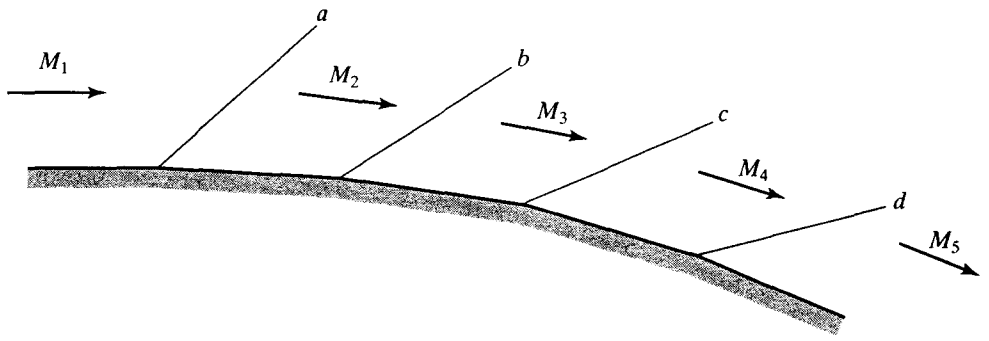


**Figure 14.14** Segregated Supersonic Flow along a Curved Surface

We wish to determine the changes in $\nu$ and $\alpha$ in going from one region to another across the pseudowaves. Consider regions 1 and 2 shown in Figure 14.15. It is evident from the results of Chapter 7 that, across this wave, $\Delta\nu = -\Delta\alpha$, where again $\alpha$ is defined to be positive counterclockwise. This result can be seen also by sketching in the characteristics of Type I. (See Figure 14.16.) Notice that, in order to go from region 1 to

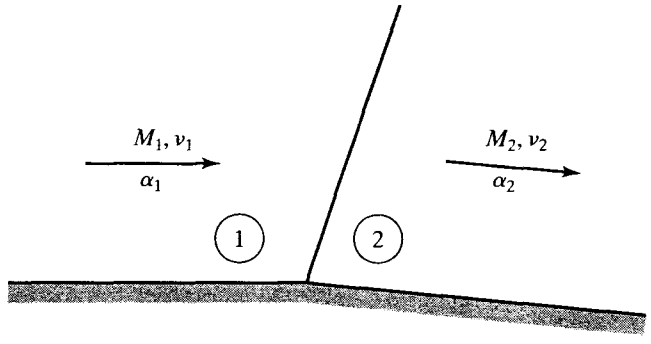


**Figure 14.15** Flow across a Pseudowave between Two Regions of Supersonic Flow

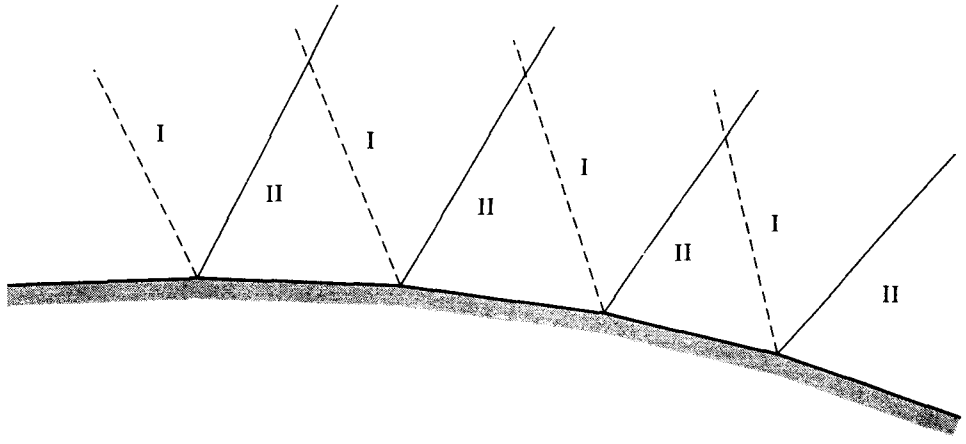


**Figure 14.16** Crossing of Characteristics in Supersonic Flow along a Curved Wall by the Region-to-Region Method

region 2, we must go *across* a characteristic of Type II. However, by proceeding *along* a characteristic of Type I, we can also go from region 1 to region 2. Thus, when we talk about changes taking place *across* characteristics of Type II, we are also talking about changes that take place *along* characteristics of Type I. We have shown from Eq. (14.56) that *along* Type I characteristics, $\Delta\nu = -\Delta\alpha$. Likewise, *across* Type II characteristics,

$$\Delta\nu = -\Delta\alpha \tag{14.67}$$

From Eq. (14.57), *along* a characteristic of Type II, $\Delta\nu = \Delta\alpha$, so that *across* a Type I characteristic, we have

$$\Delta\nu = \Delta\alpha \tag{14.68}$$

It thus becomes possible to work out a procedure involving the computation of a supersonic flow from region to region across characteristics, rather than from point to point along the characteristics.

To illustrate the use of the region-to-region method, we will compute the flow field within an underexpanded jet ($p_{exit} > p_{back}$). However, before embarking on such an example, it is useful to discuss a few details regarding the geometry and physics of this flow.

Figure 14.17 is a sketch showing several important features of an unexpanded jet. As drawn, the jet is perfectly periodic. The periodicity requires the flow to be reversible and shock free. Expansion fans exist at the lip of the nozzle to turn the flow outward and to reduce the higher exit pressure to the lower back pressure. The outline of the jet is a constant-pressure boundary—that is, a *free surface*. Across this boundary, the pressure is constant, but the velocity is discontinuous. Mach waves that intersect the free surface change form; expansion (rarefaction) waves are reflected as compression waves, and vice versa. Recall that expansion waves diverge from each other, while compression waves converge. The reflected set of expansion waves is seen to converge at a downstream point, and the pattern is repeated.

Figure 14.17 also reveals that there are three distinct types of areas within the jet. Areas within which the flow conditions are the same are called *uniform flow regions* and are shown unshaded. Areas that contain only one type of characteristic are called *simple wave regions* and are lightly shaded. It may be shown [see Ref. (14.16)] that simple wave regions always border uniform flow regions. Areas that contain

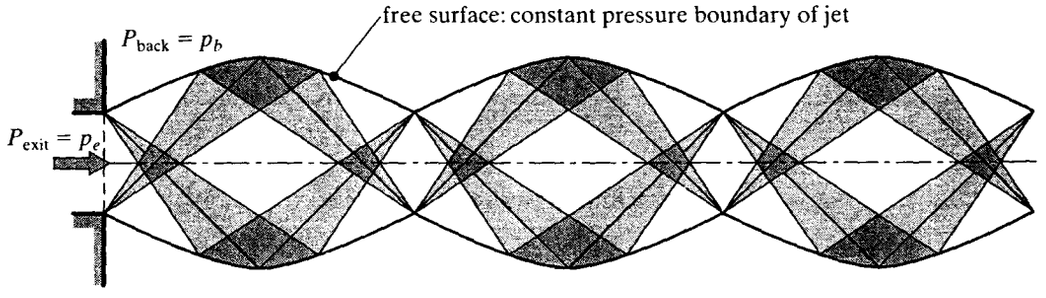


**Figure 14.17** Flow Features of a Hypothetical Supersonic Jet from an Underexpanded Nozzle

interactions of both types of characteristics are called *Nonsimple Wave Regions* and are darkly shaded.

Although all of the characteristics in Figure 14.17 are drawn as straight lines, when characteristics of different families intersect each other in the nonsimple wave regions, they are bent. Mathematically, the nonlinear terms in the governing equations are the root cause of this effect. Were the governing equations linear, the characteristics would remain straight lines.

Because of the curved nature of the characteristics that pass through the nonsimple wave regions, the wave pattern does not appear as that sketched in Figure 14.17. Rather, for all pressure ratios above unity, the compression waves, shown in Figure 14.17 converging at a single point on the free surface, can cross each other before reaching the boundary. When characteristics of the same family intersect one another in the flow field, a shockwave is formed.

The problem of shocks forming in supersonic jets was studied by Pack in Ref. (14.17), using MOC for an exit Mach number $M_e$ of 1.5, $\gamma = 1.3$, and two pressure ratios $p_e/p_b = 2$ and 7.5. Figure 14.18 is a sketch of three shock patterns that can occur in a supersonic jet, depending upon the size of the pressure ratio. As $p_e/p_b$ is elevated above unity, the characteristics of a single family (of compression waves) will not meet at a single point on the free surface as illustrated in Figure 14.17, but will cross each other at a location upstream of that point, signaling the formation of weak shocks, as shown in Figure 14.18(a). Pack obtained this pattern for the lower pressure ratio. Increasing the pressure ratio causes the characteristics to cross farther upstream and can result in the shocks coalescing, as shown in Figure 14.18(b). For a still larger pressure ratio, shocks will occur farther upstream, as illustrated in Figure 14.18(c). This was the pattern Pack obtained for the pressure ratio of 7.5. Figure 14.19 is an illustration of the underexpanded supersonic jet for that case. Note that when shocks intersect the free surface, they are reflected as expansion fans.

If the pressure ratio is raised to a high value, the regular shock reflection shown in Figure 14.18(c) is not possible, and instead a Mach reflection (see Figure 6.14) occurs, resulting in the formation of a normal shock at the center of the jet (or a *Mach disk* for an axisymmetric flow), as illustrated in Figure 14.20. Because the temperature of the gas passing through the normal shock (also known as the *Mach stem*) is elevated, excess fuel in the supersonic exhaust of a jet aircraft can be ignited. This ignition in

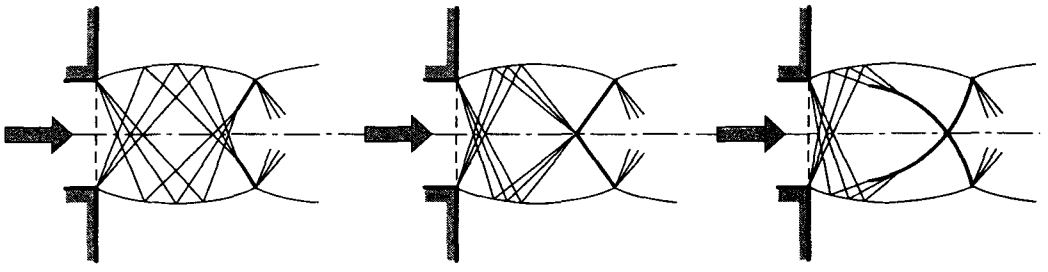

(a) Formation of Weak Shocks (b) Coalescing Shocks (c) Formation of Reflecting Shocks

**Figure 14.18** Shock Formation within an Underexpanded Jet

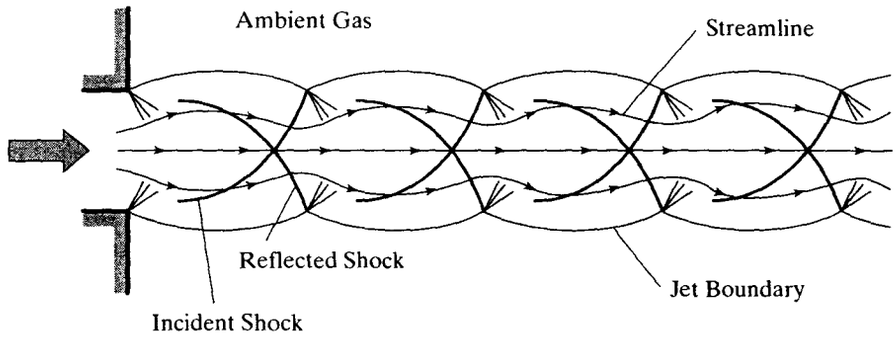


**Figure 14.19** Flow Pattern within a Supersonic Jet from an Underexpanded Jet

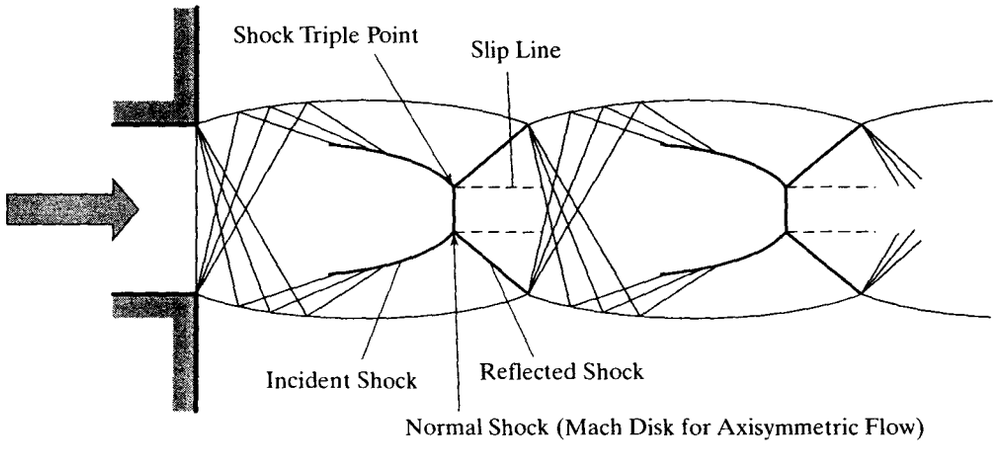


**Figure 14.20** Mach Disk Flow Pattern within a Supersonic Jet from an Underexpanded Jet for a Large Pressure Ratio

turn causes a visible glow that is referred to as a *shock diamond.* What is being seen are actually the Mach disks. Some regard the number of shock diamonds that can be observed in the exhaust of high-performance jet aircraft as an indication of the quality of the engine.

**Example 14.4. Region-to-region MOC applied to supersonic flow at the exit of an underexpanded nozzle**

The flow exiting an underexpanded supersonic nozzle has a Mach number of 1.5 and is expanded from an exit plane pressure of 200 kPa to a back pressure of 100 kPa. Use the region-to-region method to determine the flow just downstream of the nozzle exit. Take $\gamma$ to be 1.4.

**Solution**

From symmetry, we need consider only the upper half of the flow. First, divide the Prandtl–Meyer expansion fan at the nozzle exit into equal segments. Only four segments

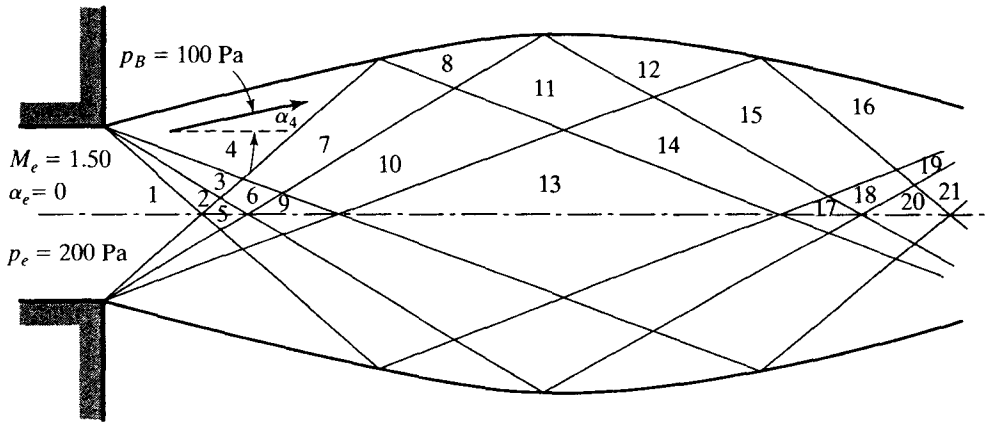


**Figure 14.21** Supersonic Outflow from an Underexpanded Nozzle

will be used here because we wish only to demonstrate the method. If more accuracy is needed, this number could be readily increased, as the methodology would be the same. The various regions are numbered in Figure 14.21. Because region 4 is a uniform flow region bordering the free surface, $p_4 = 100$ kPa. For isentropic flow at $M_1 = 1.5$ and $\gamma = 1.4$,

$$\frac{p_4}{p_o} = \left(\frac{p_4}{p_1}\right)\left(\frac{p_1}{p_o}\right) = \left(\frac{100}{200}\right)(0.2724) = 0.1362$$

so using the isentropic flow relations or a solver for this pressure ratio, we find that $M_4 = 1.9590$.

At this Mach number, from the Prandtl–Meyer Spreadsheet Solver (PMSS), we have $\nu_4 = 25.2444°$ and $\mu_4 = \sin^{-1}(1/M_4) = 30.6940°$. Also, at $M_1 = 1.5$, the PMSS gives $\nu_1 = 11.9052°$ and $\mu_1 = \sin^{-1}(1/M_1) = 41.8103°$. Hence,

$$\alpha_4 = \alpha_1 + \nu_4 - \nu_1 = 0.0 + 25.2444 - 11.9052 = 13.3392°$$

As seen in Figure 14.21, the expansion fan has been represented by three waves with equal turns so that

$$\alpha_2 = \frac{13.3392}{3} = 4.4464° \text{ and } \alpha_3 = 8.8928°$$

In going from *regions 1 to 2*, we cross a Type I wave or pseudocharacteristic, so that $\Delta\nu = \Delta\alpha$. Since $\alpha_2 = 4.4464°$, $\Delta\alpha = \alpha_2 - \alpha_1 = 4.4464°$ and $\Delta\nu = \nu_2 - \nu_1 = 4.4464°$; hence, $\nu_2 = \nu_1 + \Delta\nu = 11.9052 + 4.4464 = 16.3516°$. From the PMSS, we find that this value corresponds to $M_2 = 1.6505$ and $\mu_2 = 37.2929°$.

In going from *regions 2 to 3*, we again cross a Type I characteristic where $\nu_3 - \nu_2 = \alpha_3 - \alpha_2 = 4.4464°$. Hence, $\nu_3 = \nu_2 + 4.4464 = 16.3516 + 4.4464 = 20.7980°$, which, in turn, gives $M_3 = 1.8025$ and $\mu_3 = 33.6954°$ from the PMSS.

In going from *regions 2 to 5*, we traverse a Type II wave or characteristic; across this wave, $\Delta\nu = -\Delta\alpha$. From the boundary condition at the centerline, we have $\alpha_5 = 0°$, so from 2 to 5, $\Delta\alpha = -4.4464°$ and $\Delta\nu = 4.4464°$. Therefore, $\nu_5 = \nu_2 + \Delta\nu = 16.3516 + 4.4464 = 20.7980°$, yielding $M_5 = 1.8025$ and $\mu_5 = 33.6954°$.

In going from *region 5 to 6*, $\Delta\nu = \Delta\alpha$, so that $\nu_6 - \nu_5 = \alpha_6 - \alpha_5$, or $\nu_6 - \alpha_6 = \nu_5 - \alpha_5$. In going from *region 3 to 6*, $\Delta\nu = -\Delta\alpha$, so that $\nu_6 - \nu_3 = \alpha_3 - \alpha_6$, or $\nu_6 + \alpha_6 = \nu_3 + \alpha_3$. Combining and eliminating $\alpha_6$, we can solve for $\nu_6$:

$$\nu_6 = \frac{(\nu_5 - \alpha_5) + (\nu_3 + \alpha_3)}{2} = \frac{(20.7980 - 0) + (20.7980 + 8.8928)}{2} = 25.2444°$$

Consequently, from the PMSS, we have $M_6 = 1.9590$, $\mu_6 = 30.6940°$, and

$$\alpha_6 = \nu_6 - (\nu_5 - \alpha_5) = 4.4464°$$

In going from *region 6 to 7*, the procedure is the same as going from region 5 to 6 and therefore need not be shown here.

In going from *region 7 to 8*, the procedure is virtually the same as the computations for region 4. Because region 8 borders the free surface, the pressure in this region must equal the back pressure, and so $p_8/p_o = 0.1362$. Therefore, $M_8 = M_4 = 1.9590$ and $\nu_8 = \nu_4 = 25.2444°$. In fact, any region that borders the free surface will have the same pressure, Mach number, and Prandtl–Meyer function. The flow angle for this region is computed from

$$\alpha_8 = \nu_8 - \nu_7 + \alpha_7 = 25.2444 - 29.6908 + 8.8928 = 4.4464°$$

Results of the remainder of the computations are shown in Table 14.4. It should be noted that the calculations for the block containing regions 5, 6, 7, and 8 (shown in bold in Table 14.4) may be copied and pasted into the calculation worksheet to obtain the respective values for regions 9, 10, 11, and 12, as well as for regions 13, 14, 15, and 16, and so forth.

**TABLE 14.4** Computations for Example 14.4

| Region | $\alpha$ deg | $\nu$ deg | $M$ | $\mu$ deg | $\alpha + \mu$ deg | $\alpha - \mu$ deg |
|---|---|---|---|---|---|---|
| 1 | 0.0 | 11.9052 | 1.5 | 41.8103 | 41.8103 | −41.8103 |
| 2 | 4.4464 | 16.3516 | 1.6505 | 37.2929 | 41.7393 | −32.8465 |
| 3 | 8.8928 | 20.7980 | 1.8025 | 33.6954 | 42.5882 | −24.8026 |
| 4 | 13.3392 | 25.2444 | 1.9590 | 30.6940 | 44.0332 | −17.3549 |
| **5** | **0.0** | **20.7980** | **1.8025** | **33.6954** | **33.6954** | **−33.6954** |
| **6** | **4.4464** | **25.2444** | **1.9590** | **30.6940** | **35.1404** | **−26.2476** |
| **7** | **8.8928** | **29.6908** | **2.1223** | **28.1120** | **37.0048** | **−19.2193** |
| **8** | **4.4464** | **25.2444** | **1.9590** | **30.6940** | **35.1404** | **−26.2476** |
| 9 | 0.0 | 29.6908 | 2.1223 | 28.1120 | 28.1120 | −28.1120 |
| 10 | 4.4464 | 34.1372 | 2.2942 | 25.8415 | 30.2878 | −21.3951 |
| 11 | 0.0000 | 29.6908 | 2.1223 | 28.1120 | 28.1120 | −28.1120 |

(continued)

TABLE 14.4 (continued)

| | | | | | | |
|---|---|---|---|---|---|---|
| 12 | −4.4464 | 25.2444 | 1.9590 | 30.6940 | 26.2476 | −35.1404 |
| **13** | **0.0** | **38.5836** | **2.4770** | **23.8110** | **23.8110** | **−23.8110** |
| **14** | **−4.4464** | **34.1372** | **2.2942** | **25.8415** | **21.3951** | **−30.2878** |
| **15** | **−8.8928** | **29.6908** | **2.1223** | **28.1120** | **19.2193** | **−37.0048** |
| **16** | **−13.3392** | **25.2444** | **1.9590** | **30.6940** | **17.3549** | **−44.0332** |
| 17 | 0.0 | 29.6908 | 2.1223 | 28.1120 | 28.1120 | −28.1120 |
| 18 | −4.4464 | 25.2444 | 1.9590 | 30.6940 | 26.2476 | −35.1404 |
| 19 | −8.8928 | 20.7980 | 1.8025 | 33.6954 | 24.8026 | −42.5882 |
| **20** | **0.0** | **29.6908** | **2.1223** | **28.1120** | **28.1120** | **−28.1120** |
| **21** | **−4.4464** | **25.2444** | **1.9590** | **30.6940** | **26.2476** | **−35.1404** |

Examination of the computed flow angles reveals that, within regions that border the free surface, the flow having passed though the expansion fan at the nozzle lip is turned upward at +13.3392° in region 4 and continuously declines to point downward at −13.3392° in region 16. The flow is horizontal within regions 1, 5, 9, 11, 13, 17, and 20. The computations were terminated before the leading-edge Mach line of the Prandtl–Meyer expansion at the nozzle lip was intersected by a characteristic of the same family—that is, prior to the formation of a shock.

To establish the physical boundaries of the regions, we must determine the wave angles. Since a single wave separates two regions, approximate the angle that the single wave makes with the horizontal by averaging the values from each side. For a wave that makes a negative acute angle with the flow direction—that is, a Type I characteristic—the angle that the wave makes with the horizontal is $\alpha - \mu$. [See Figure 14.22(a).] For a wave that makes a positive acute angle with the flow direction—that is, a Type II characteristic—the angle that the wave makes with the horizontal is $\alpha + \mu$. [See Figure 14.22(b).]

For the flow in region 1, $\alpha_1 = 0.0°$, $M_1 = 1.5$, and $\mu_1 = \sin^{-1}(1/M_1) = \sin^{-1}(1/1.5) = 41.8103°$. For region 2, $\alpha_2 = 4.4456°$, $M_2 = 1.6505$, and $\mu_2 = \sin^{-1}(1/M_2) = \sin^{-1}(1/1.6505) = 37.2929°$. So the wave between regions 1 and 2, in actuality a Prandtl–Meyer fan, is at an angle of

$$\frac{(\alpha - \mu)_1 + (\alpha - \mu)_2}{2} = \frac{-41.8103 + (-32.8465)}{2} = -37.3284°$$

with the horizontal. The wave between regions 2 and 5 is at an angle of

$$\frac{(\alpha + \mu)_2 + (\alpha + \mu)_5}{2} = \frac{41.7393 + 33.6954}{2} = 37.7174°$$

The angles for all of the waves shown in Figure 14.21 are contained in Table 14.5.

Note that the Type I characteristic between regions 6 and 7 is parallel to that between regions 7 and 8, and the Type I characteristic between regions 9 and 10 is parallel to that between regions 10 and 11. This is because, for characteristics intersecting the free surface, the angle of incidence, which is the local Mach angle, is equal to the angle of reflection.

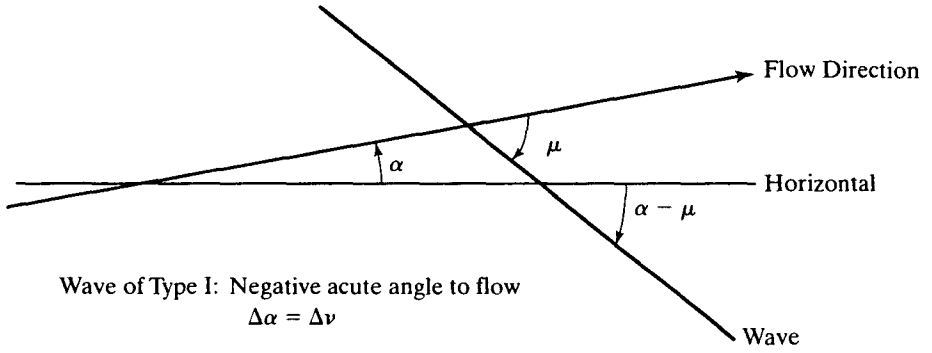


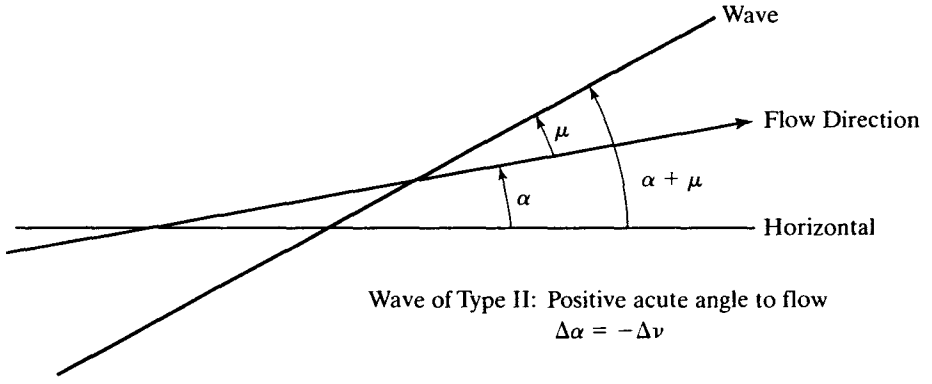


(b)

**Figure 14.22** Geometry across Type I and II Waves

**TABLE 14.5** Angles of Waves for the Underexpanded Nozzle of Example 14.4

| Type I: $\alpha - \mu$ | | | Type II: $\alpha + \mu$ | | |
|---|---|---|---|---|---|
| Regions | Angle deg | $\text{Slope}_\text{I}$ | Regions | Angle deg | $\text{Slope}_\text{II}$ |
| 1–2 | −37.3284 | −0.7626 | 2–5 | 37.7174 | 0.7734 |
| 2–3 | −28.8246 | −0.5503 | 3–6 | 38.8643 | 0.8059 |
| 3–4 | −21.0787 | −0.3854 | 4–7 | 40.5190 | 0.8547 |
| 5–6 | −29.9715 | −0.5767 | 6–9 | 31.6262 | 0.6158 |
| 6–7 | −22.7335 | −0.4190 | 7–10 | 33.6463 | 0.6656 |
| 7–8 | −22.7335 | −0.4190 | 8–11 | 31.6262 | 0.6158 |
| 9–10 | −24.7536 | −0.4611 | 10–13 | 27.0494 | 0.5106 |
| 10–11 | −24.7536 | −0.4611 | 11–14 | 24.7536 | 0.4611 |
| 11–12 | −31.6262 | −0.6158 | 12–15 | 22.7335 | 0.4190 |
| 13–14 | −29.4757 | −0.5652 | 14–17 | 24.7536 | 0.4611 |
| 14–15 | −27.0494 | −0.5106 | 15–18 | 22.7335 | 0.4190 |
| 15–16 | −33.6463 | −0.6656 | 16–19 | 21.0787 | 0.3854 |
| 17–18 | −40.5190 | −0.8547 | 18–20 | 27.1798 | 0.5135 |
| 18–19 | −36.0726 | −0.7285 | 19–21 | 25.5251 | 0.4775 |
| 20–21 | −31.6262 | −0.6158 | | | |

From the preceding example, a property of the waves becomes apparent: The *strength of the wave*, as measured by $\Delta\alpha$ across the wave, is undiminished by intersection with other weak waves or by reflection. For example, the initial wave separating regions 1 and 2 is reflected from the centerline, with the reflected wave intersected by two other waves. Yet $\alpha_2 - \alpha_1 = \alpha_4 - \alpha_7$. This result really follows from our assumption that the waves are very weak—that they behave as characteristics.

## 14.5 SUPERSONIC-NOZZLE DESIGN

One application of the method of characteristics is the design of the *contour* of supersonic nozzles. One-dimensional isentropic flow theory, as presented in Chapter 3, provided useful information regarding the change of flow variables within variable-area nozzles; however, one-dimensional theory is unable to provide information as to how nozzles should be shaped in order to produce particular results. For example, it is essential that the flow exiting a wind tunnel nozzle (test section) be parallel and free of Mach waves at the desired Mach number. The presence of waves is undesirable, in that these weak waves can coalesce to form a finite shock and prevent uniform flow in the test section. By properly shaping the nozzle, a uniform exit flow can be established.

Let us now examine how a nozzle contour can be designed so as to cancel an incident wave. If a weak wave of turning angle $\Delta\alpha$ is incident upon a plane surface, as shown in Figure 14.23, a reflected wave of turning angle $\Delta\alpha$ must be present so as to satisfy the boundary conditions at the wall.

To cancel the incident wave, let the wall turn exactly through an angle $\Delta\alpha$ at the point of impingement of the incident wave. (See Figure 14.24.) There is no reflected

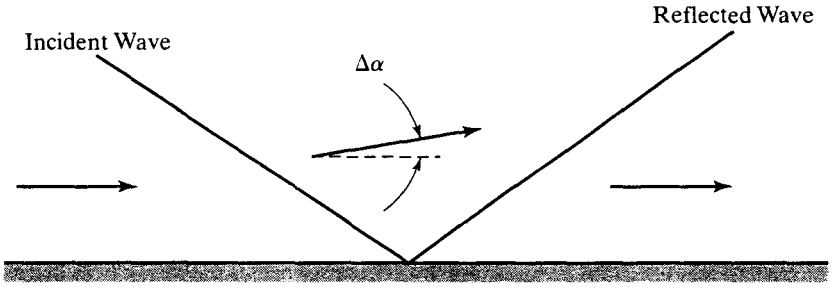


**Figure 14.23** Incident Wave Reflected from a Plane Surface

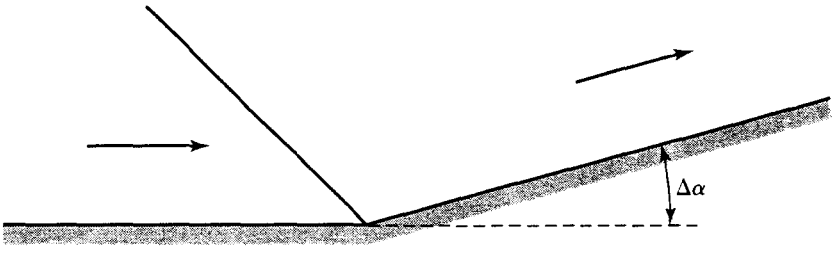


**Figure 14.24** Incident Wave Canceled through Wall Turning

wave, since the boundary condition at the wall is satisfied without it—that is, the flow is parallel to the wall; the incident wave is effectively canceled. Recall that in Chapter 6 we used the same technique to cancel an incident oblique shockwave.

Now let us turn our attention to a converging–diverging supersonic nozzle, as illustrated in Figure 14.25. We shall assume parallel, sonic flow at the nozzle throat. A second form of analysis assumes that the sonic line is an arc of a circle. [See Ref. (14.18).] From symmetry, we need consider only one half of the flow; that is, the centerline is a streamline, and therefore we can represent the centerline as a plane wall.

The supersonic flow first expands within the shaded region denoted by corner points $a, b, e$, and $f$. This portion of the nozzle is called the *expansion section*. Within this section, the wall angle increases from point a to a maximum value, say, $\alpha_{w,\max}$ at point $f$. Four expansion waves (Type I characteristics) have been sketched within the expansion section of the nozzle. Fluid particles on streamlines are continuously accelerated as they pass through the waves in this section. The expansion waves intersect the centerline at points $b, c, d$, and $e$ and are reflected, as characteristics of Type II, impinging on the nozzle wall at points $g, h, i$, and $j$, respectively. The waves are regarded as being reflected, but in actuality there is an interaction of the Type I waves from the portion of the nozzle with Type II waves from the lower portion. Thus, the waves reflected from the centerline turn the flow back to the horizontal between points $e$ and $j$. The unshaded region of the nozzle denoted by corner points $e, f$, and $j$ is called the *straightening*

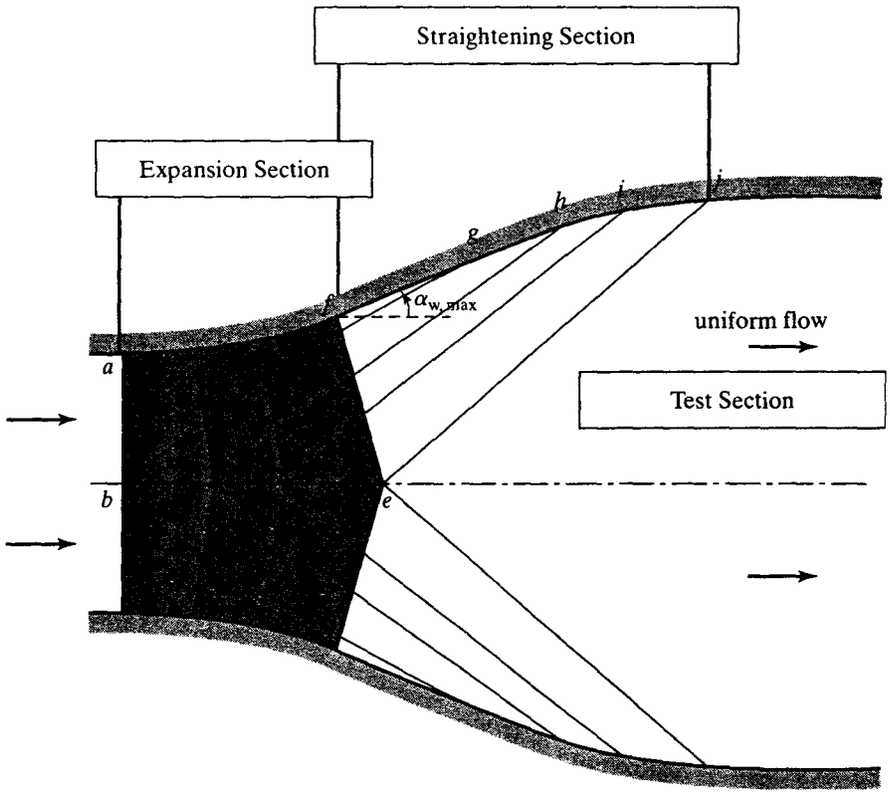


**Figure 14.25** Wave Pattern in a Supersonic Nozzle Containing Both Expansion and Straightening Sections

*section*. The wall contours at points $g, h, i$, and $j$ must turn the flow through the same $\Delta\alpha$ as the incident waves so as to cancel those waves. (Recall Figure 14.24.) The uniform flow region is the *test section*.

Naturally, the more waves that are considered, the smoother and more exact the resultant contour will be. Here, we are interested only in wave cancellations, so the initial expansion (from points $a$ to $f$) is arbitrary. In fact, some nozzles—for example, rocket nozzles—have no expansion section at all, in order to minimize weight. Such nozzles are called *minimum length nozzles* (MLNs), and the initial expansion is created by a sharp corner at the nozzle throat, as illustrated in Figure 14.26. These nozzles, which are also called *rapid expansion nozzles*, have been used in gas-dynamic lasers [see Ref. (14.19)] and hypersonic wind tunnels.

We now develop a simple expression that relates the design Mach number in the test section, $M_e$, and the expansion angle of the wall on the downstream side of the nozzle lip, $\alpha_{\text{max, MLN}}$.

Since the flow is expanded from sonic conditions, the expansion angle of the wall, $\alpha_{\text{max, MLN}}$, and the Prandtl–Meyer function at the corner point $a$ in Figure 14.26, $\nu_a$, are equal (see also Figure 7.10):

$$\nu_a = \alpha_a = \alpha_{\text{max, MLN}} \tag{14.69}$$

For a Type I characteristic between point $a$ and point $c$, we may write

$$\nu_a + \alpha_a = \nu_c + \alpha_c \tag{14.70}$$

Because point $c$ is on the centerline and a corner point of the test section, we have $\alpha_c = 0$ and $\nu_c = \nu(M_e)$. Using these values in Eq. (14.70) and combining the result with Eq. (14.69) produces

$$\alpha_{\text{max, MLN}} = \frac{\nu(M_e)}{2} \tag{14.71}$$

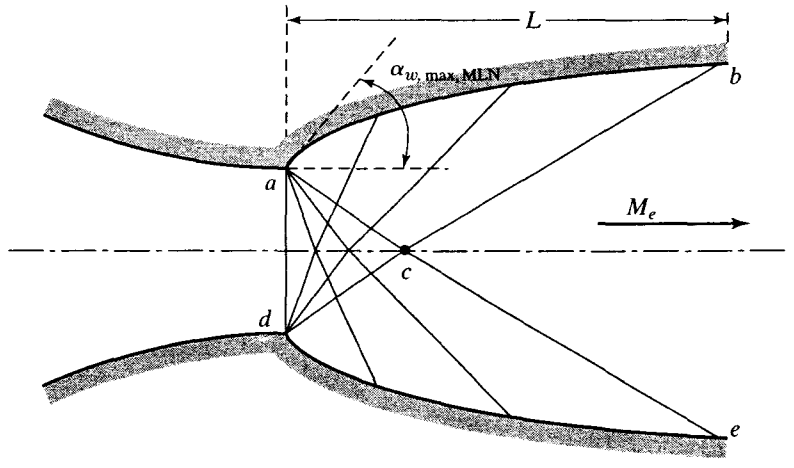


**Figure 14.26** Straight Sonic Line Minimum Length Supersonic Nozzle

**Example 14.5. Design of supersonic-flow minimum length nozzle**

Design the diverging section of a supersonic nozzle to produce a uniform Mach 1.8 flow of $\gamma = 1.2$. Assume that the length of the nozzle is to be kept to a minimum.

**Solution**

To design a nozzle, the coordinates of the boundary surface must be computed. Since the point-to-point method is more appropriate for this purpose, it will be used to solve this example.

As discussed previously, for the shortest possible nozzle, the expansion is assumed to take place as a Prandtl–Meyer expansion fan that is centered at the corner of the throat, as shown in Figure 14.26.

To obtain a first estimate of the nozzle contour, the expansion fan will be represented by four waves. This number is far too few for an actual design; however, it is ideal to illustrate computational procedures. According to the numbering system illustrated in Figure 14.27, four waves will require the determination of 14 grid points within the nozzle and on its boundary. In fact, it is easy to show that if the number of waves is $n$, then the number of computed points would be $n(n + 3)/2$. Hence if seven waves were selected, the computations would involve 35 grid points.

As with all previous examples, to accomplish the computations, a simple spreadsheet program may be used. Spreadsheet programming without logic commands (Visual Basic techniques) is not the best tool for the calculations that follow, for, as we will see, at each grid point a supersonic Mach number must be extracted from a computed Prandtl–Meyer function. Although this is a straightforward process involving a Newton–Raphson iteration procedure, as demonstrated in Chapter 7, having to perform this computation at each grid point with simple spreadsheet programming can become tedious as the number of waves is increased.

Because the flow at the nozzle throat is sonic, the first expansion wave is a vertical characteristic, which obviously is unable to convey disturbance information downstream. To circumvent this difficulty, the first expansion wave is taken to be nonvertical and allowed to turn the flow by a small angle. Consequently, the first grid point on the centerline, instead of being set to 0°, is equated to this small angle. This procedure, while not correct, does enable the computations to start. Both computations and experiments have shown

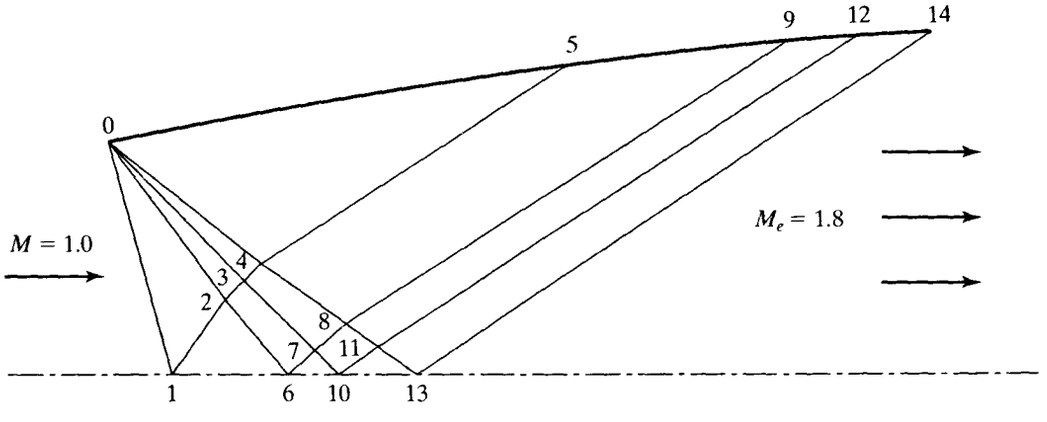


**Figure 14.27** Grid Point Numbering for Example 14.5

that the sonic line in the throat of the nozzle is not a straight line, as it is taken to be here. This refinement, too, should be considered in the final design.

For $M_e = 1.8$ and $\gamma = 1.2$, the Prandtl–Meyer Spreadsheet Solver is used to obtain $\nu(M_e) = 24.30252°$. Therefore, from Eq.(14.71), $\alpha_{\max, \text{MLN}} = 12.1512°$. It is assumed that the flow angle at point 1 is 0.1512°. Each succeeding wave in the expansion fan is assumed to turn the flow by 4°.

The computations at grid points 2, 3, and 4 all follow the unit-process expressions of Eqs. (14.58) and (14.59). The same procedure is used to determine information at grid points 7, 8, and 11.

To assure that there is no reflection from the boundary, the flow angle at point 5 is set equal to that at point 4. Likewise, $\alpha_9 = \alpha_8$, $\alpha_{12} = \alpha_{11}$, and $\alpha_{14} = \alpha_{13} = 0°$. Because the boundary with known flow angle is intercepted by a Type II characteristic, we use Eq. (14.57) to compute $\nu_5$, $\nu_9$, $\nu_{12}$, and $\nu_{14} = 24.30252°$.

The flow angle at points 6, 10, and 13 is 0°, and since each of these points is intercepted by a Type I characteristic, we use Eq. (14.56) to determine the corresponding $\nu$ values.

Finally, the coordinates of all of the grid points are computed using Eqs. (14.61) and (14.62). To provide more accurate slopes ($m_\text{I}$ and $m_\text{II}$), the values of $\tan(\alpha \pm \mu)$ are averaged between points on connecting characteristics. The slopes of points on the boundary of the nozzle are also averaged. Note that the expansion is assumed to be centered at the location (0, 1).

The results of the calculations are contained in Tables 14.6 and 14.7.

It should be noted that uniform, one-dimensional flow is present at the throat of the nozzle and at the exit, with isentropic flow in between. So we may find $A_\text{exit}/A_\text{throat}$ by using the isentropic flow solver of Chapter 3. At $M = 1.80$ and $\gamma = 1.2$, we find $A/A^* = 1.5398$. From Table 14.7, $A/A^* = A_{14}/A_0 = y_{14}/y_0 = 1.5367/1 = 1.5367$. Thus,

**TABLE 14.6** Minimum Length Supersonic-Nozzle Design Calculations of Example 14.5

| Point | $\alpha$ | $\nu$ | $C_\text{I} = \nu + \alpha$ | $C_\text{II} = \nu - \alpha$ | $M$ | $\mu$ | $\alpha + \mu$ | $\alpha - \mu$ |
|---|---|---|---|---|---|---|---|---|
| 1 | **0.151** | **0.151** | 0.3025 | 0.0000 | 1.0213 | 78.2681 | 78.4194 | −78.1169 |
| 2 | **4.151** | 4.151 | 8.3025 | **0.0000** | 1.2071 | 55.9379 | 60.0892 | −51.7867 |
| 3 | **8.151** | 8.151 | 16.3025 | **0.0000** | 1.3387 | 48.3298 | 56.4810 | −40.1785 |
| 4 | **12.151** | 12.151 | 24.3025 | **0.0000** | 1.4583 | 43.2931 | 55.4444 | −31.1419 |
| 5 | **12.151** | 12.151 | 24.3025 | **0.0000** | 1.4583 | 43.2931 | 55.4444 | −31.1419 |
| 6 | **0.000** | 8.302 | **8.3025** | 8.3025 | 1.3434 | 48.1063 | 48.1063 | −48.1063 |
| 7 | 4.000 | 12.302 | **16.3025** | **8.3025** | 1.4627 | 43.1312 | 47.1312 | −39.1312 |
| 8 | 8.000 | 16.302 | **24.3025** | **8.3025** | 1.5769 | 39.3571 | 47.3571 | −31.3571 |
| 9 | 8.000 | 16.302 | **24.3025** | **8.3025** | 1.5769 | 39.3571 | 47.3571 | −31.3571 |
| 10 | **0.000** | 16.302 | **16.3025** | 16.3025 | 1.5769 | 39.3571 | 39.3571 | −39.3571 |
| 11 | 4.000 | 20.302 | **24.3025** | **16.3025** | 1.6888 | 36.3081 | 40.3081 | −32.3081 |
| 12 | 4.000 | 20.302 | **24.3025** | **16.3025** | 1.6888 | 36.3081 | 40.3081 | −32.3081 |
| 13 | **0.000** | 24.302 | **24.3025** | **24.3025** | 1.8000 | 33.7490 | 33.7490 | −33.7490 |
| 14 | 0.000 | 24.302 | **24.3025** | **24.3025** | 1.8000 | 33.7490 | 33.7490 | −33.7490 |

**TABLE 14.7** Slopes of the Characteristics and Grid Point Coordinates for the MLN of Example 14.5

| Point | $m_{\mathrm{I}}$ | $m_{\mathrm{II}}$ | $x$ | $y$ |
|---|---|---|---|---|
| 1 | −4.7523 | 4.8800 | 0.2104 | 0.0000 |
| 2 | −1.2702 | 2.6400 | 0.3978 | 0.4947 |
| 3 | −0.8444 | 1.6182 | 0.4666 | 0.6060 |
| 4 | −0.6042 | 1.4805 | 0.5203 | 0.6856 |
| 5 | 0.2153 | 1.4520 | 0.8652 | 1.1863 |
| 6 | −1.1895 | 1.1148 | 0.8137 | 0.0000 |
| 7 | −0.8289 | 1.0959 | 1.0436 | 0.2519 |
| 8 | −0.6068 | 1.0816 | 1.1124 | 0.3263 |
| 9 | 0.1777 | 1.0859 | 2.1077 | 1.4071 |
| 10 | −0.8169 | 0.8202 | 1.3519 | 0.0000 |
| 11 | −0.6208 | 0.8341 | 1.3935 | 0.0347 |
| 12 | 0.1051 | 0.8483 | 3.1391 | 1.5155 |
| 13 | −0.6501 | 0.6682 | 1.4468 | 0.0000 |
| 14 | 0.0349 | 0.6682 | 3.7467 | 1.5367 |

even for this extremely coarse grid, the difference is only 0.2%. Naturally, the more waves considered, the smoother will be the resultant nozzle contour, and the more adequate will be the design.

## 14.6 SUMMARY

In this chapter, characteristics have been presented in order to develop a method for solving problems in two-dimensional isentropic, supersonic flow. Characteristics are defined as lines along which there exist discontinuities in velocity derivatives.

By treating the complete equations of motion for isentropic, two-dimensional flow, expressions were derived for the characteristics in the $(x, y)$ plane and in the hodograph, or $(u, v)$, plane. Three methods were presented for deriving the governing equations: the method of indeterminant derivatives, the method of linear combination, and eigenanalysis. The first of these is simple to understand, but impractical for most problems; the second method is probably the easiest to use; and the third method is the most modern and is commonly used today in the field of computational fluid dynamics.

It was shown that in steady flow, characteristics exist only in the real plane for supersonic flow and that the characteristics are inclined at the local Mach angle to the flow direction, thereby establishing a relationship between the characteristics and Mach waves.

After expressions for the velocity vector along the characteristics were found, the point-to-point method of computation was presented to effect a solution for a

supersonic flow. An equivalent procedure called the region-to-region method was also discussed, in which regions of the flow are separated by Mach waves or characteristics. If the necessary relationships for $\Delta\alpha$ and $\Delta\nu$ across such waves are known, problems in two-dimensional supersonic flow can be solved.

The advent of powerful numerical solution techniques has reduced the importance of the method of characteristics from the front line of solution techniques that are currently used to solve gas-dynamics problems. Instead, the Euler equations (for inviscid gas flows) and the Navier–Stokes equations (for viscous gas flows) are directly solved. Nevertheless, concepts upon which characteristics are based are still used to this day. For example, the boundary conditions of problems described by hyberbolic partial differential equations, which often prove to be a challenging aspect of the numerical solution of fluid flow problems, may be established through application of characteristics. So, although the numerical method has been somewhat supplanted, it is important that we have an understanding of the methodology of characteristics.

If nothing else, coverage of characteristics indicates very real differences between subsonic flow and supersonic flow. Since, from experience, we are somewhat more accustomed to dealing with low-velocity flows, it follows that some of the relationships between the various properties may be more easily understood for subsonic flow. However, it should also be realized that the solution of a general two-dimensional, compressible flow problem for supersonic flow, for which the method of characteristics is available, is often easier than the solution of a similar problem in subsonic flow, where no such procedure exists.

## 14.7 REFERENCES


**14.1** Tannehill, J. C., Anderson, D. A., and Pletcher, R. H. *Computational Fluid Mechanics and Heat Transfer,* 2d ed., Taylor & Francis, Washington, DC, 1997, p. 37.

**14.2** Hoffman, J. D. *Numerical Methods for Engineers and Scientists*, 2d ed., Marcel Dekker, New York, 2001, p. 31.

**14.3** Tannehill, J. C., Anderson, D. A., and Pletcher, R. H. *Computational Fluid Mechanics and Heat Transfer,* 2d ed., Taylor & Francis, Washington, DC, 1997, pp. 22–39.

**14.4** Chapman, C. J. *High Speed Flow,* Cambridge University Press, Cambridge, UK, 2000, pp. 166–169.

**14.5** Zucrow, M. J., and Hoffman, J. D. *Gas Dynamics,* Vol. II, John Wiley & Sons, New York, 1977, pp. 188–192.

**14.6** Davis, J. L. *Finite Difference Methods in Dynamics of Continuous Media*, Macmillan Publishing Company, New York, 1986, p. 28.

**14.7** MacTutor, School of Mathematics and Statistics, University of St. Andrews, Fife, Scotland.

**14.8** Reid, C. "K. O. Friedrichs," *Mathematical Intelligencer* 5: (1983): 23–30.

**14.9** Morawetz, C. S. "Kurt Otto Friedrichs," Biographical Memoirs, Vol. 67, 1995, National Academy of Sciences, National Academy Press, Washington, DC.

**14.10** Whitham, G. B. *Linear and Nonlinear Waves*, John Wiley & Sons, New York, 1999, pp. 114–124.

**14.11** Culbert, L. B. *Computational Gasdynamics*, Cambridge University Press, Cambridge, UK, 1998.

**14.12** Toro, E. F. *Riemann Solvers and Numerical Methods for Fluid Dynamics,* 2d ed., Springer-Verlag, Berlin, Heidelberg, and New York, 1999.

**14.13** Hirsch, C. *Fluid Numerical Computation of Internal and External Flows*, Vol. I, John Wiley & Sons, New York, 1988, pp. 135–152.

**14.14** Lomax, H., Pulliam, T. H., and Zingg, D. W. *Fundamentals of Computational Fluid Dynamics,* Springer-Verlag, Berlin, Heidelberg, and New York, 2001, pp. 233–234.

**14.15** Hodge, B. K., and Koenig, K. *Compressible Fluid Dynamics with Personal Computer Applications*, Prentice Hall, Upper Saddle River, NJ, 1995, pp. 446–447.

**14.16** Meyer, R. E. "Theory of Characteristics of Inviscid Gas Dynamics," *Encyclopedia of Physics*, Vol. IX: "Fluid Dynamics III," Springer-Verlag, Berlin, 1960, p. 252.

**14.17** Pack, D. C. "On the Formation of Shock-Waves in Supersonic Gas Jets," *Quarterly Journal of Mechanics and Applied Mathematics*, Vol. 1, 1948, pp. 1–17.

**14.18** Emanuel, G. *Gasdynamics: Theory and Applications*, AIAA Education Series, 1986, pp. 307–328.

**14.19** Anderson, J. D., Jr. *Gasdynamic Lasers: An Introduction*, Academic, New York, 1976.

## 14.8 PROBLEMS

**14.1** Use the method of indeterminate derivatives to obtain equations of the characteristics for the following equation in the hodograph plane:

$$\left(1 - \frac{u^2}{a^2}\right)\frac{\partial^2 \Phi}{\partial v^2} + 2\frac{uv}{a^2}\frac{\partial^2 \Phi}{\partial u \partial v} + \left(1 - \frac{v^2}{a^2}\right)\frac{\partial^2 \Phi}{\partial u^2} = 0$$

In this equation, the function $\Phi(u, v)$ in the hodograph plane is related to the velocity potential $\phi(x, y)$ by

$$\Phi = xu + yv - \phi$$

so that

$$\frac{\partial \Phi}{\partial u} = x \text{ and } \frac{\partial \Phi}{\partial v} = y$$

(See Problem 12.10.)

**14.2** Use the method of indeterminate derivatives to obtain the equation for the slope of the characteristics in the hodograph plane in terms of the flow speed $V$ and the flow angle $\alpha$. Develop the equation starting with the potential equation in the hodograph plane, that is, Eq. (12.55):

$$V^2\left(1 - \frac{V^2}{a^2}\right)\frac{\partial^2 \phi}{\partial V^2} + V\left(1 + \gamma\frac{V^4}{a^4}\right)\frac{\partial \phi}{\partial V} + \left(1 - \frac{V^2}{a^2}\right)^2\frac{\partial^2 \phi}{\partial \alpha^2} = 0$$

**14.3** Use the method of linear combination to obtain equations of the characteristics for the following set of equations in the hodograph plane:

$$(a^2 - u^2)\frac{\partial y}{\partial v} + uv\left(\frac{\partial x}{\partial v} + \frac{\partial y}{\partial u}\right) + (a^2 - v^2)\frac{\partial x}{\partial u} = 0$$

$$\frac{\partial x}{\partial v} - \frac{\partial y}{\partial u} = 0$$

**14.4** Use eigenanalysis to resolve Problem 14.3.

**14.5** The continuity and momentum equations for one-dimensional unsteady flow are, respectively,

$$\frac{\partial \rho}{\partial t} + \rho\frac{\partial u}{\partial x} + u\frac{\partial \rho}{\partial x} = 0$$

$$\rho\frac{\partial u}{\partial t} + \rho u\frac{\partial u}{\partial x} = -\frac{\partial p}{\partial x}$$

(a) For an isentropic flow, show that this pair can be written as

$$\frac{\partial \rho}{\partial t} + \rho\frac{\partial u}{\partial x} + u\frac{\partial \rho}{\partial x} = 0$$

$$\frac{\partial u}{\partial t} + u\frac{\partial u}{\partial x} = -\frac{a^2}{\rho}\frac{\partial \rho}{\partial x}$$

(b) If the Riemann variable $R$ is defined as

$$dR = a\frac{d\rho}{\rho}$$

show that the pair of equations in part (a) becomes

$$\frac{\partial R}{\partial t} + u\frac{\partial R}{\partial x} + a\frac{\partial u}{\partial x} = 0$$

$$\frac{\partial u}{\partial t} + u\frac{\partial u}{\partial x} + a\frac{\partial R}{\partial x} = 0$$

(c) Add and subtract the pair of equations in part (b) to obtain

$$\frac{\partial(u + R)}{\partial t} + (u + a)\frac{\partial(u + R)}{\partial x} = 0$$

$$\frac{\partial(u - R)}{\partial t} + (u - a)\frac{\partial(u - R)}{\partial x} = 0$$

(d) From the results of part (c), determine the slope of the characteristics—that is, $dx/dt$—as well as the information that is propagated along the characteristics.

(e) For isentropic flow of a perfect gas, show that if $R(0) = a(0) = 0$, then

$$R = \frac{2}{\gamma - 1}a$$

**14.6** Obtain the characteristic equations of the pair of PDEs in part (b) of Problem 14.5 by using the method of indeterminate derivatives.

**14.7** Obtain the characteristic equations of the pair of PDEs in part (b) of Problem 14.5 by using the method of linear combination.

**14.8** Obtain the characteristic equations of the pair of PDEs in part (b) of Problem 14.5 by using eigenanalysis.

**14.9** (a) Combine Eq. (14.28) with both expressions in Eq. (14.27) to obtain Eq. (14.30).
(b) Substitute Eq. (14.30) into Eq. (14.29) to obtain

$$\frac{dv}{du} = \frac{-C_2 \mp \sqrt{C_2^2 - C_1 C_3}}{C_3}$$

**14.10** In Example 14.2, only one of four compatibility equations was determined. Complete this example by determining the remaining three.

**14.11** Use the method of indeterminate derivatives to determine the equations of the characteristics for linearized, two-dimensional, supersonic flow described by

$$(1 - M_\infty^2)\frac{\partial^2 \phi}{\partial x^2} + \frac{\partial^2 \phi}{\partial y^2} = 0$$

**14.12** (a) Show that each dependent variable in the following pair of equations must satisfy the wave equation and that therefore the set is hyperbolic:

$$\frac{\partial u}{\partial x} - \frac{\partial v}{\partial y} = 0$$

$$\frac{\partial u}{\partial y} - \frac{\partial v}{\partial x} = 0$$

(b) Use the method of linear combination to determine the equations of the characteristics for this set of equations.

**14.13** Use eigenanalysis to determine the equations of the characteristics in Problem 14.12.

**14.14** Complete Example 14.3 by determining the solution at points 19 to 32. Check the accuracy of the results.

**14.15** Using the same number of points repeat Example 14.3 for

(a) $M_{\text{initial}} = 2.0$, a total wedge angle of 12°, and $\gamma = 1.3$;
(b) $M_{\text{initial}} = 4.0$, a total wedge angle of 12°, and $\gamma = 1.4$;
(c) $M_{\text{initial}} = 2.0$, a total wedge angle of 24°, and $\gamma = 1.4$.

**14.16** A supersonic flow at Mach 1.8 and $\gamma = 1.4$ enters the channel shown in Figure P14.16(a). Using the point-to-point method of characteristics, determine the Mach number distribution throughout the flow for the pattern shown in Figure P14.16(b).

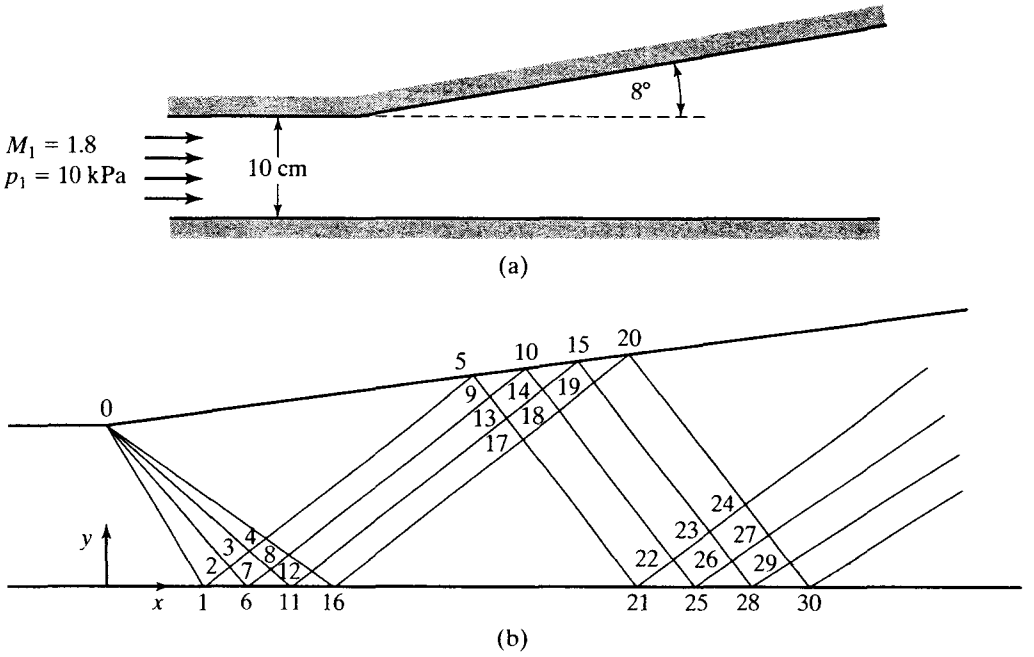


**Figure P14.16**

**14.17** The values of the flow angle $\alpha$, the Mach angle $\mu$, and the angles of the characteristics $\alpha \pm \mu$ for the first 15 points of the Problem 14.16 are shown in Table P14.17. Compute the slopes $m_{\mathrm{I}}$ and $m_{\mathrm{II}}$ and the $(x, y)$ coordinates for each of the points.

**TABLE P14.17**

| Point | $\alpha$ | $\mu$ | $\alpha + \mu$ | $\alpha - \mu$ | $m_{\mathrm{I}}$ | $m_{\mathrm{II}}$ | $x$ | $y$ |
|---|---|---|---|---|---|---|---|---|
| 1 | 0.0 | 33.7490 | 33.7490 | −33.7490 | | | | |
| 2 | 2.0 | 32.3339 | 34.3339 | −30.3339 | | | | |
| 3 | 4.0 | 31.0204 | 35.0204 | −27.0204 | | | | |
| 4 | 6.0 | 29.7940 | 35.7940 | −23.7940 | | | | |
| 5 | 8.0 | 28.6433 | 36.6433 | −20.6433 | | | | |
| 6 | 0.0 | 31.0204 | 31.0204 | −31.0204 | | | | |
| 7 | 2.0 | 29.7940 | 31.7940 | −27.7940 | | | | |
| 8 | 4.0 | 28.6433 | 32.6433 | −24.6433 | | | | |
| 9 | 6.0 | 27.5591 | 33.5591 | −21.5591 | | | | |
| 10 | 8.0 | 26.5337 | 34.5337 | −18.5337 | | | | |
| 11 | 0.0 | 28.6433 | 28.6433 | −28.6433 | | | | |
| 12 | 2.0 | 27.5591 | 29.5591 | −25.5591 | | | | |
| 13 | 4.0 | 26.5337 | 30.5337 | −22.5337 | | | | |
| 14 | 6.0 | 25.5605 | 31.5605 | −19.5605 | | | | |
| 15 | 8.0 | 24.6340 | 32.6340 | −16.6340 | | | | |

**14.18** Repeat Problem 14.16 using the region-to-region method for the regions shown in Figure P14.18.

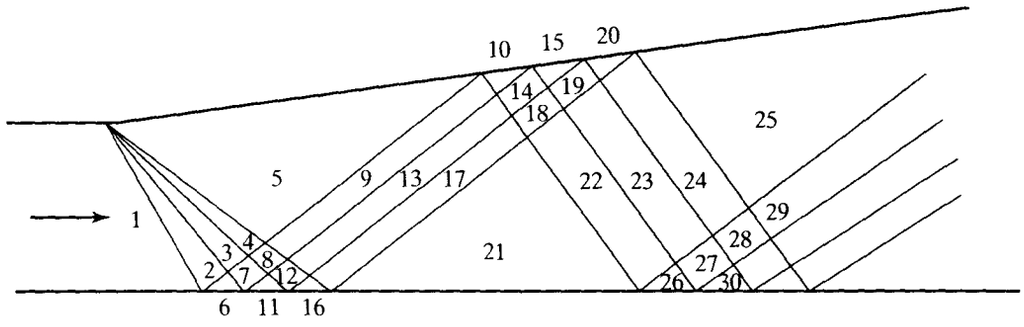


**Figure P14.18**

**14.19** Compute the supersonic flow past the curved contour of the two-dimensional plug nozzle shown in Figure P14.19(a). The contour is shaped so as to produce cancellation of the waves incident on the plug. The nozzle is to provide a flow of air ($\gamma = 1.4$) at Mach 1.9502856. The Mach number at the throat of the nozzle is sonic. Use the region-to-region method for a five-wave expansion as indicated in Figure 14.19(b). Determine the Mach number distribution and the inclinations of the characteristics.

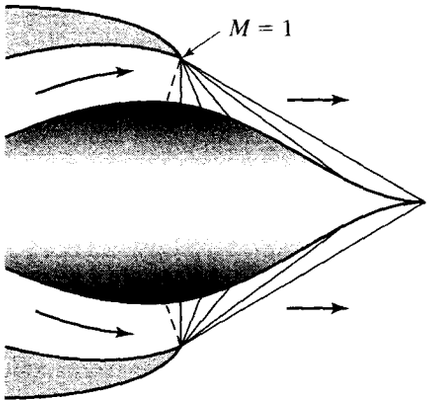


**Figure P14.19(a)**

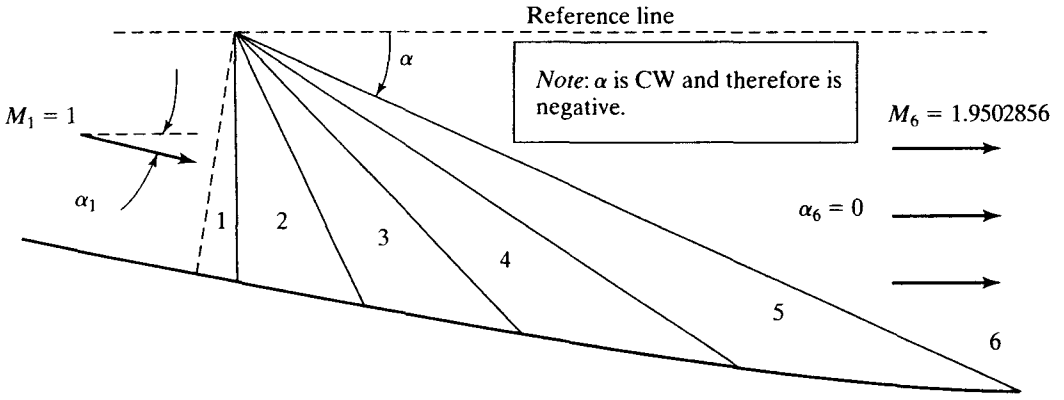


**Figure P14.19(b)**

**14.20** A thin airfoil has the form of a circular arc, as shown in Figure P14.20. Use segregated supersonic flow along a curved surface to determine the lift and drag coefficients for the foil at a Mach number of 1.851177. Take $\gamma = 1.4$, and divide the circular arc into five linear pieces of equal length. A characteristic will emerge from each of the corners of these lengths on both the upper and lower sides on the foil.

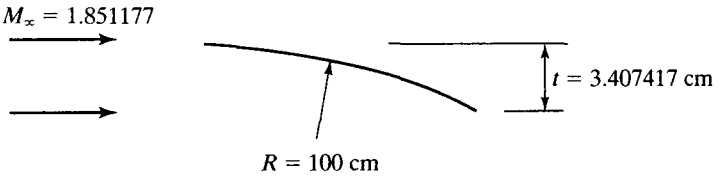


**Figure P14.20**

**14.21** A converging–diverging nozzle discharges a uniform supersonic flow at Mach 2.2 and static pressure of 101 kPa two dimensionally into a back-pressure region of 69.28701 kPa. Use the region-to-region method to determine the flow just downstream of the nozzle exit for the same configuration as employed in Example 14.4. Assume that $\gamma = 1.4$.

**14.22** Use the region-to-region method to repeat Example 14.5. Compare the results with those obtained in the example.

# Chapter 15

# Measurements in Compressible Flow

## 15.1 INTRODUCTION

In this chapter, we shall discuss some of the methods used for measuring the properties of a compressible flow. Important variables that require measurement are pressure, temperature, velocity, density, and flow rate. We shall restrict ourselves to the more conventional techniques used in continuum flow measurements. Several of the devices to be mentioned here should be familiar from studies of the fluid mechanics of an incompressible flow. It is important to keep in mind, then, the differences due to compressibility effects, in both subsonic and supersonic flow.

It should also be noted that in previous chapters, most of the flows that we considered were inviscid and adiabatic. Exceptions included flows through shockwaves, frictional flows through tubes (Fanno flow), and flows through tubes with heat exchange (Rayleigh flow). In each of these types of flow, the entropy varied due to viscous or heat transfer effects. Accordingly, when discussing measuring devices, we will encounter shear stress $\tau$, heat flux $q$, and the real fluid properties of dynamic viscosity $\mu$ thermal conductivity $k$ must be considered as well. Moreover, we will encounter various nondimensional groups such as the Reynolds number $\mathrm{Re} = \rho V L/\mu = V L/\nu$, (kinematic viscosity $\nu = \mu/\rho$), the Prandtl number $\mathrm{Pr} = c_p\mu/k = \nu/\alpha$ (thermal diffusivity $\alpha = k/\rho c_p$), the Nusselt number $\mathrm{Nu} = hL/k$ (the convective heat transfer coefficient $h$), and the Eckert number $\mathrm{Ec} = V^2/c_p\Delta T$.

## 15.2 PRESSURE MEASUREMENT

*Static pressure* is the pressure indicated by a measuring device moving at the flow velocity or, in other words, by a device that introduces no disturbance or velocity change to the flow. The usual method for measuring the static pressure of a flow along a wall is

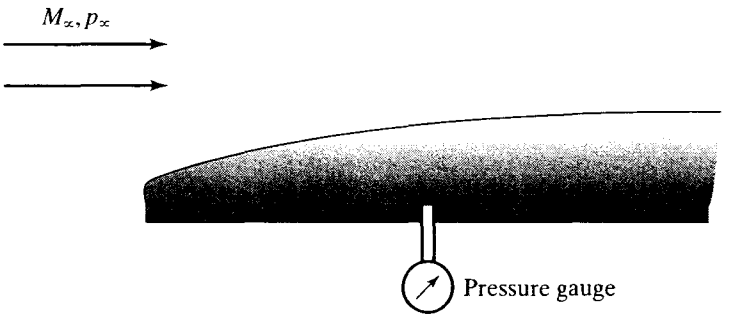


**Figure 15.1** Measurement of Static Pressure

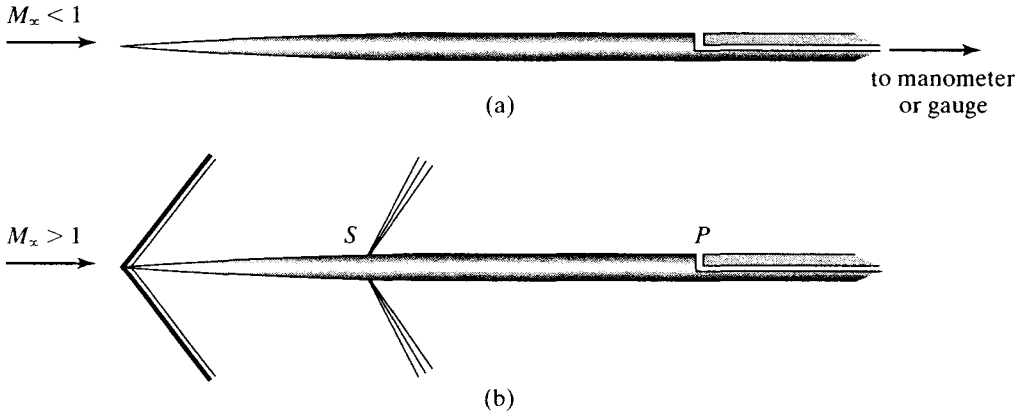


**Figure 15.2** Conical-Nose Static Pressure Probe in Subsonic and Supersonic Flows

to drill a small hole normal to the surface of the wall and connect this hole to a manometer, pressure gauge, or other similar device. (See Figure 15.1.) The hole must be small with respect to the boundary-layer thickness (say, 20 percent of the local laminar boundary-layer thickness) and must be free from roughness or burrs that might disturb the flow. Since there is no pressure change through a boundary layer in a direction normal to the wall, the pressure indicated is a true measure of the freestream static pressure $p_\infty$.

If there is no wall present in the flow, static pressure can be measured in a similar fashion by introducing a probe, which, in a sense, creates a wall in the flow. Such a probe must be very thin and aligned with the flow direction so as to introduce a minimum disturbance into the flow. A typical *static pressure probe* is shown in Figure 15.2(a). The tip or nose of the probe may have a round, wedge, or conical configuration; the body of the probe is generally cylindrical. Because the pressure varies along the surface of the probe, a *pressure tap* is located far enough downstream (say 5 to 10 probe diameters for subsonic operation and 10 to 15 probe diameters for supersonic flow) so that the surface pressure recovers to the freestream static pressure.

For a narrow wedge- or conical-shaped probe in supersonic flow, there will be an attached shock at the nose, as shown in Figure 15.2(b). However, there will be an

expansion where the nose joins the cylindrical section of the probe at $S$, so the pressure measurement at the tap at $P$, at least for a weak attached shock, will be very close to the freestream static pressure $p_\infty$.

The static pressure probe is very sensitive to flow alignment; it can be seen that the more the probe is misaligned, the greater will be the disturbance introduced into the flow by the probe. This sensitivity can be reduced by drilling several holes (typically, eight equally spaced holes are used) around the circumference of the probe, as illustrated in Figure 15.3, so that the resultant measured pressure is an average pressure. However, even with this configuration, if accuracy to within 1 percent is desired, the misalignment cannot exceed 5°. [See Ref. (15.1).]

Care must be exercised in the interpretation of the results of static pressure probe measurements in a supersonic flow field in which a shock is present. Consider such a supersonic flow field in which there occurs a normal shock, as shown in Figure 15.4(a). If we move the probe along the line $ABCD$, we should obtain a static pressure curve like the one shown in Figure 15.4(b). Actually, however, a boundary layer builds up on the probe, so the actual velocity at the fixed probe surface is zero. In the subsonic part of the

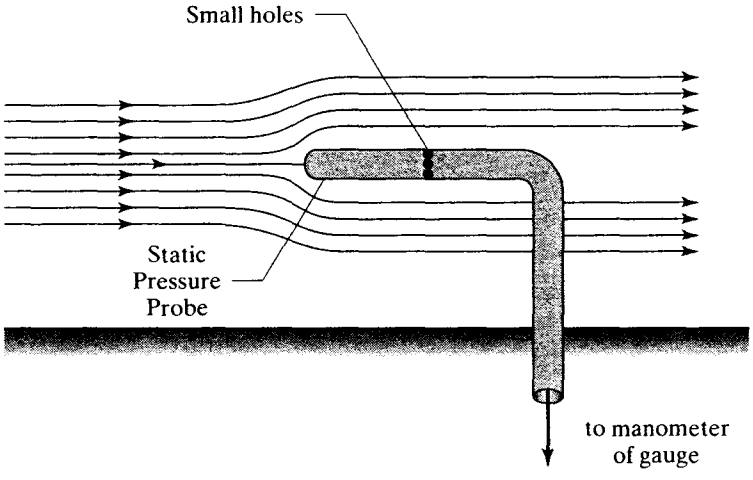


**Figure 15.3** Round-Nose Static Pressure Probe

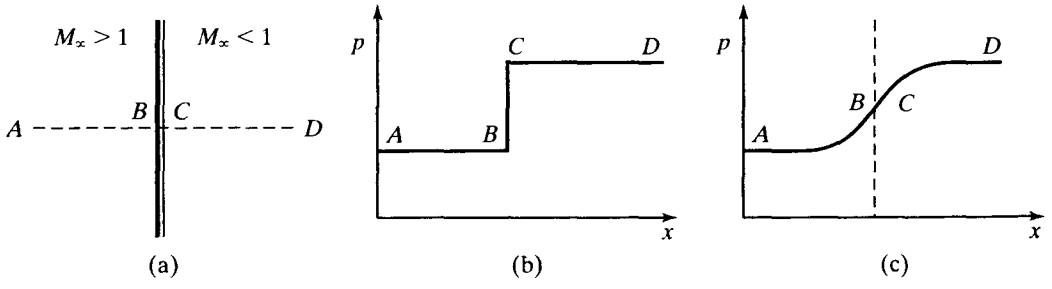


**Figure 15.4** Pressure Measurement in a Supersonic Flow Containing a Normal Shock Wave

boundary layer, with no shock present, the effect of the pressure change occurring outside the boundary layer can be "felt" upstream. In other words, in the presence of a shock, the pressure changes that occur in the boundary layer are not the same as the pressure changes that occur across the shock outside the boundary layer. Instead of a sudden pressure rise, the pressure probe indicates a more gradual pressure rise, as shown in Figure 15.4(c). Consequently, in the presence of a shock, the static pressure indicated by the probe can be taken as a true reading only when the probe is either far upstream or downstream of the shock or the shock is very weak.

The *stagnation* (or *total*) *pressure* is the pressure measured by an instrument that brings the flow isentropically to rest. Such a device is called the *Pitot tube*, an open-ended tube facing directly into the flow, as shown in Figure 15.5. This instrument was invented by Henri Pitot in 1732 in order to determine whether the velocity of a river stream was larger near the bottom or near the surface. However, it was not regarded as a useful instrument until it was modified by Henry Darcy in 1858. The history of the Pitot tube is described by Brown in Ref. (15.2), and the literature on the Pitot tube up to the 1950s has been reviewed by Folsom in Ref. (15.3).

The Pitot tube consists of three components: (1) the instrument tip; (2) the body, which includes the stem and the hardware to fasten the instrument to the wall, as well as the lines that connect the tip to a measuring device; and (3) the measuring device. The choice of the size of the orifice (tube diameter) is dependent on the fineness of the measurement to be taken; for stagnation pressure measurements in a boundary layer, a probe with a diameter as small as 0.5 mm might be used. The stagnation pressure probe is not as sensitive to misalignment as the static probe; 1 percent accuracy can be achieved for angles up to 20°. [See Ref. (15.1).]

The static pressure probe and the stagnation pressure tube may be combined to form the *Pitot–static tube*, which is sketched in Figure 15.6. As the figure illustrates, the instrument contains a tube within a tube; the inner tube measures the stagnation pressure, while the outer tube measures the static pressure.

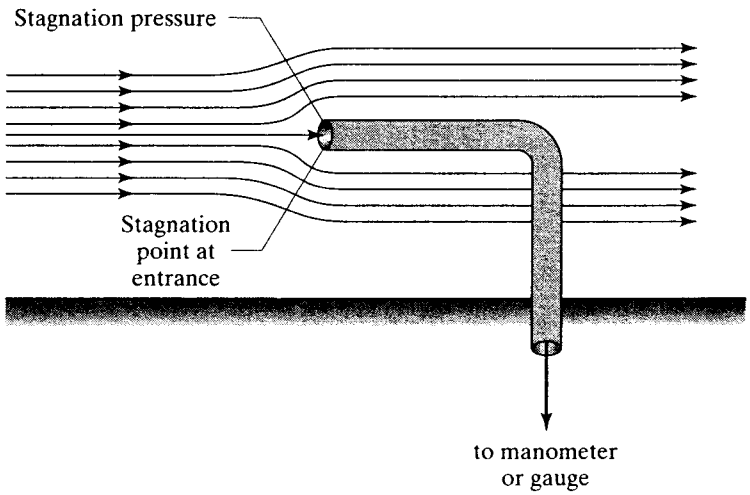


**Figure 15.5** Pitot Tube in a Compressible Flow

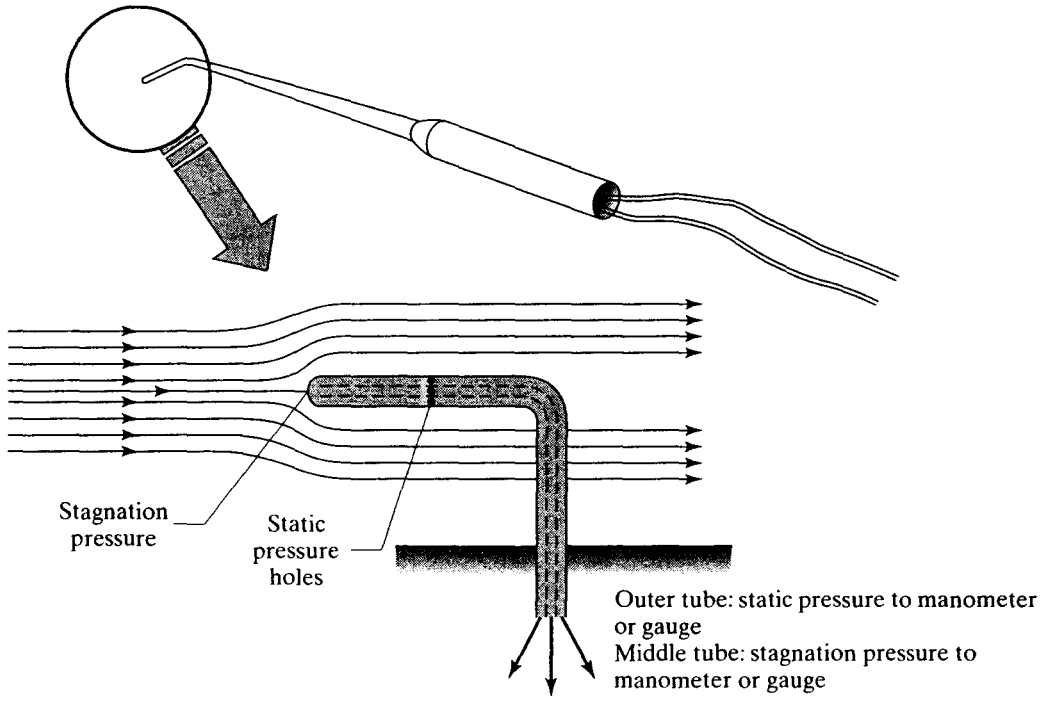


**Figure 15.6** Pitot–Static Tube

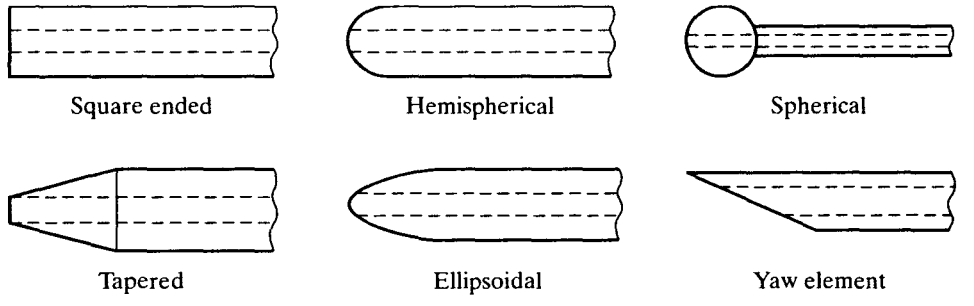


**Figure 15.7** Various Pitot–Static Tube Tip Configurations

The *Pitot tube* and the *Pitot–static tube* may have various tip geometries. Figure 15.7 illustrates a variety of these configurations. It should also be mentioned that there are various designs, such as the Prandtl design. [See Ref. (15.4).]

To remove sensitivity to flow angularity—that is, to yaw and pitch angles—a shield is placed around a total-pressure tube. This instrument is called a *Kiel tube*, after its originator, and can tolerate flow-angle variations as large as ±45°. (See Figure 15.8.) This instrument has been used to measure stagnation pressures within high-gradient total-pressure regions as might be found in boundary-layer flows or in turbomachinery applications. To simultaneously measure uneven pressure distributions within particular regions, several Pitot probes may be ganged together to form a *pressure rake* or a *boundary-layer mouse*. [See Ref. (15.4).] Moreover, a probe may be placed in a traversing mechanism and manipulated to survey various regions of a flow.

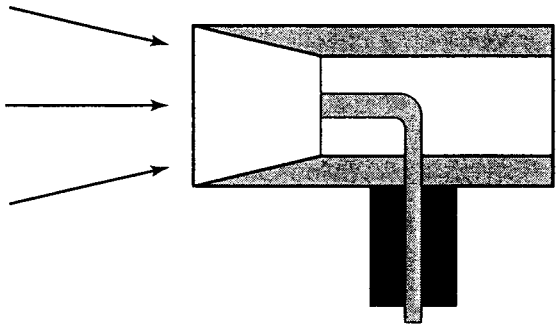

**Figure 15.8** Kiel Total-Pressure Tube

From the measured pressures, a pressure ratio

$$\frac{p_o}{p} = \left(1 + \frac{\gamma - 1}{2} M^2\right)^{\gamma/(\gamma-1)} \tag{15.1}$$

may be formed that enables determination of the Mach number as follows:

$$M^2 = \frac{2}{\gamma - 1}\left[\left(\frac{p_o}{p}\right)^{(\gamma-1)/\gamma} - 1\right] \tag{15.2}$$

With the Mach number and the static pressure, the dynamic pressure can be computed from

$$\frac{1}{2}\rho V^2 = \frac{\gamma}{2}\frac{V^2}{(\gamma p/\rho)}p = \frac{\gamma}{2}\left(\frac{V^2}{a^2}\right)p = \frac{\gamma}{2}M^2 p = \frac{\gamma}{\gamma - 1}\left[\left(\frac{p_o}{p}\right)^{(\gamma-1)/\gamma} - 1\right]p \tag{15.3}$$

In supersonic flow, since the Pitot–static tube is essentially a blunt-nosed body, there will be a detached bow shock in front of the probe, as illustrated in Figure 15.9.

In this case, the stagnation pressure indicated on the manometer or gauge connected to the Pitot–static tube will be the stagnation pressure downstream of the portion

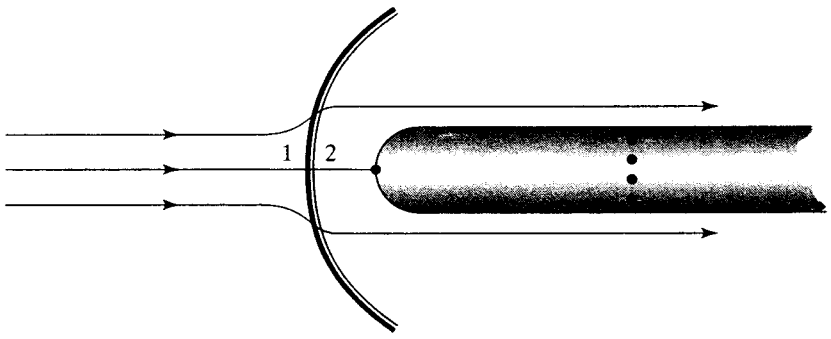


**Figure 15.9** Bow Shock in Front of a Pitot–Static Tube in Supersonic Flow

of the shock that is normal to the flow direction. That is to say, it is assumed that the stagnation pressure on the rear side of the shock is unchanged from the pressure at the probe tip. If the Reynolds number based on the probe diameter is too low, say, smaller than 400, this assumption is not valid. Assuming a large-enough Reynolds number, we may write

$$(\text{pressure})_{\text{measured}} = p_{o2} = \left(\frac{p_{o2}}{p_2}\right)\left(\frac{p_2}{p_1}\right)p_1 \tag{15.4}$$

where $p_1$ is the free static pressure $p_\infty$. Now the stagnation-to-static-pressure ratio on the downstream side of the shock can be written in terms of the freestream Mach number $M_\infty = M_1$ by using Eq. (4.10):

$$\frac{p_{o2}}{p_2} = \left(1 + \frac{\gamma - 1}{2}M_2^2\right)^{\gamma/(\gamma-1)} = \left[1 + \left(\frac{\gamma - 1}{2}\right)\left(\frac{M_1^2 + \dfrac{2}{\gamma - 1}}{\dfrac{2\gamma}{\gamma - 1}M_1^2 - 1}\right)\right]^{\gamma/(\gamma-1)} \tag{15.5}$$

Also, the static pressure ratio across a normal shock is given by Eq. (4.8), so we have

$$\frac{p_2}{p_1} = \frac{2\gamma}{\gamma + 1}M_1^2 - \frac{\gamma - 1}{\gamma + 1} \tag{15.6}$$

Combining Eqs. (15.4), (15.5), and (15.6) yields the *Rayleigh–Pitot formula*:

$$\frac{p_{o2}}{p_1} = \left(\frac{\dfrac{\gamma + 1}{2}M_1^2}{\dfrac{2\gamma}{\gamma + 1}M_1^2 - \dfrac{\gamma - 1}{\gamma + 1}}\right)^{\gamma/(\gamma-1)} \left(\frac{2\gamma}{\gamma + 1}M_1^2 - \frac{\gamma - 1}{\gamma + 1}\right)$$

$$= \frac{\gamma + 1}{2}M_1^2\left[\frac{(\gamma + 1)^2 M_1^2}{4\gamma M_1^2 - 2(\gamma - 1)}\right]^{1/(\gamma-1)} \tag{15.7}$$

**Example 15.1. Determination of Mach number from pressure measurements**

The Mach number of a compressible flow is to be determined from measurements made by a Pitot–static tube. If the static probe indicates 20 kPa and the Pitot tube 32 kPa, determine the flow Mach number. Repeat for a Pitot pressure of 80 kPa. Assume that $\gamma = 1.4$.

**Solution**

The first step in this problem is to compute the critical pressure ratio—that is, Eq. (15.1)—at $M = 1$ and $\gamma = 1.4$:

$$\left(\frac{p_o}{p}\right)_{\text{critical}} = \left(\frac{\gamma + 1}{2}\right)^{\gamma/(\gamma-1)} = 1.89293$$

If the actual pressure ratio $p_{o2}/p_1$ is below the critical value, a subsonic Mach number is computed from Eq. (15.2), whereas if the pressure ratio is above the critical value, we must extract the supersonic Mach number from the Rayleigh–Pitot formula [Eq. (15.7)]. To accomplish this, we now develop a method that uses the Newton–Raphson procedure and is easily incorporated into a spreadsheet program. Equation (15.7) may be written in the form

$$f(M) = AM^{2\gamma} - BM^2 + C = 0$$

where the coefficients in this expression are

$$A = \frac{(\gamma + 1)^{\gamma+1}}{2^{\gamma-1}}, \qquad B = 4\gamma\left(\frac{p_{o2}}{p_1}\right)^{\gamma-1}, \qquad C = 2(\gamma - 1)\left(\frac{p_{o2}}{p_1}\right)^{\gamma-1}$$

The derivative of this function is

$$\frac{df}{dM}(M) = 2\gamma AM^{2\gamma-1} - 2BM$$

The Newton–Raphson algorithm is

$$M_{\text{new}} = M_{\text{old}} - \frac{f(M_{\text{old}})}{\dfrac{df}{dM}(M_{\text{old}})} = \frac{(2\gamma - 1)AM_{\text{old}}^{2\gamma} - BM_{\text{old}}^2 - C}{2(\gamma AM_{\text{old}}^{2\gamma-1} - BM_{\text{old}})}$$

For the case in which $p_{o2} = 32$ kPa and $p_1 = 20$ kPa, the pressure ratio is 1.600, which is below the critical pressure ratio for the given ratio of specific heats. Hence, computing the subsonic Mach number from Eq. (15.2) produces $M_\infty = M_1 = 0.8477$.

For the case in which $p_{o2} = 80$ kPa and $p_1 = 20$ kPa, the pressure ratio is 4.000, which is above the critical pressure ratio for the given ratio of specific heats. It should be noted that the computed coefficients for this case are

$$A = 6.195766$$

$$B = 9.750166$$

$$C = 1.392881$$

The results of the iterative computations are presented in Table 15.1. Hence, the computed Mach number for this case is $M_\infty = M_1 = 1.64736$.

**TABLE 15.1** Rayleigh–Pitot Formula Computations for Example 15.1

| $n$ | $M$(old) | $f(M)$ | $df/dM$ | $M$(new) |
|---|---|---|---|---|
| 1 | 2.00000 | 5.54203 | 21.40908 | 1.74114 |
| 2 | 1.74114 | 1.10498 | 13.11811 | 1.65690 |
| 3 | 1.65690 | 0.10122 | 10.74129 | 1.64748 |
| 4 | 1.64748 | 0.00121 | 10.48532 | 1.64736 |
| 5 | 1.64736 | 0.00000 | 10.48220 | 1.64736 |

## 15.3 TEMPERATURE MEASUREMENT

Temperature is a fundamental variable in the study of gas dynamics. We have considered various analytical and numerical methods to predict temperature. Many of the techniques were applied to models or simplifications of actual flow situations. To assess the validity of the results of these models, we need either exact solutions or reliable experimental data. Unfortunately, as observed in Chapter 12, there are very few exact compressible flow solutions available. Therefore, we must consider experimental methods to provide the validation temperature information we require.

In this section, we discuss some of the methodology and devices that are used in the measurement of the temperature of moving gases. The range of environments in which temperature-measuring devices are exposed, as well as the wide variation of temperature values, presents great challenges for thermometric instrumentation. For example, temperatures on aircraft surfaces can range from 200 to 1,500 K and in extreme cases from 20 to 2,000 K. [See Ref. (15.5).]

The direct measurement of the *static temperature* of a gas flow would have to be made by a device that does not disturb the flow—in other words, by an instrument that would travel at the velocity of the flow. As with static pressure measurement, however, moving a probe at the speed of the fluid is impractical. Consequently, it is safe to say that there is no method for the direct measurement of the static temperature of a moving gas.

As an alternative, we might consider performing the temperature measurement just as was done with the static pressure measurement; that is, locate a thermocouple or other thermometric device at the wall surface, as illustrated in Figure 15.10. As shown in the figure, the thermocouple is located inside the boundary layer on a fixed wall, where the flow velocity is zero. Accordingly, we would expect the measured wall temperature to be closer to the freestream stagnation temperature $T_{o\infty}$ than to the freestream static temperature $T_\infty$. This condition differs from the situation of static pressure measurement previously considered, because the static pressure does not vary across the boundary layer. It should be noted that, because of viscous effects, the gas is not brought to rest adiabatically, and so the temperature at the wall would not be the stagnation temperature. For the same reasons, we cannot simply insert a thermometer into a gas flow and expect to measure the freestream static temperature; the thermometer will produce a reading above $T_\infty$.

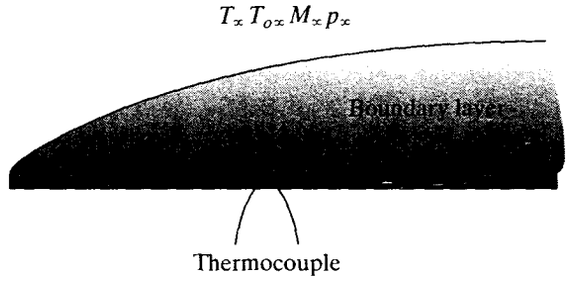


**Figure 15.10** Thermocouple Located within the Wall

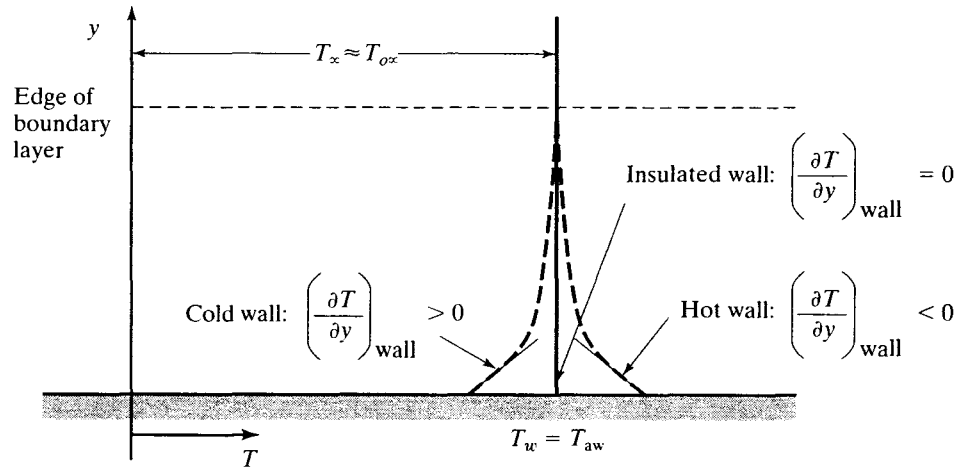


**Figure 15.11** Low-Mach-Number Temperature Distributions within a Boundary Layer on an Insulated Wall

To gain additional perspective, it is helpful to view illustrations of the temperature distributions within a compressible-flow boundary layer. The sketches to be presented depend, however, on whether the gas is moving slowly or rapidly over the surface, as well as on the conditions that are imposed at the wall. Two broad classes of wall conditions are generally considered: one in which the wall temperature $T_w$ is specified, and one in which the wall heat flux $q_w$ is specified.

Figure 15.11 presents the temperature distribution within the boundary layer on an insulated surface over which a low-Mach-number gas flows. Since the surface is insulated, no heat flows into or out of the wall—that is, $q_w = 0$. The boundary condition at the wall ($y = 0$) is $\partial T/\partial y = 0$. The surface temperature for the case shown is called the *adiabatic wall temperature* $T_{aw}$. Because the Mach number is very small, the freestream static and stagnation temperatures are nearly the same. Further, we see in this case that the freestream temperature and the wall temperature are virtually the same. Thus, this is not a very involved case. Also shown are the static temperature distribution if the temperature gradient at the wall is negative [i.e., heat flows from the wall to the gas (the hot wall case)] and the distribution if the temperature gradient is positive [i.e., heat flows from the gas to the wall (the cold wall case)].

The temperature distribution within the boundary layer is illustrated in Figure 15.12 for the case when a gas with large Mach number flows over an insulated surface. The flow physics is more complex than that of Figure 15.11. Since the fluid near the wall is at a higher temperature than the fluid near the outer edge of the boundary layer, there will be a heat flow in the $y$ direction, due to conduction. For this case, there is also appreciable frictional heating of the fluid. In such cases, the faster moving layers in the boundary layer do significant work on the slower moving layers, which causes the static temperature to rise above the freestream value. Within the boundary layer, mechanical energy is converted to thermal energy, with attendant heat conduction transporting energy away from the insulated wall. The temperature difference $T_{aw} - T_\infty$ is a measure of the rate of this dissipation. Note that this difference is increased as the wall is approached.

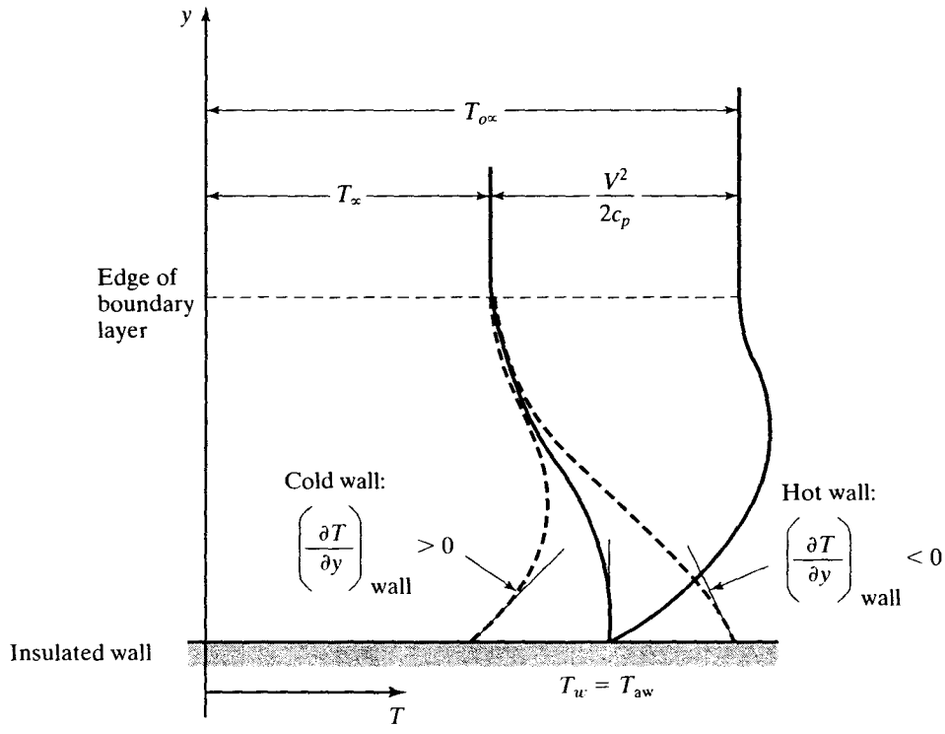


**Figure 15.12** High-Mach-Number Temperature Distributions within a Boundary Layer on an Insulated Wall

Also shown in Figure 15.12 is a sketch of the distribution of the stagnation temperature. The fact that it varies within the boundary layer is an indication that the process is neither adiabatic nor reversible. Again, the frictional heating is the reason for the variation.

To determine the relative importance of viscous or frictional heating (expressed by the viscous dissipation terms in the energy equation), a size comparison can be made with the heat conduction through the fluid. To accomplish this, form the ratio of terms that characterize each within the boundary layer. The viscous dissipation terms for two-dimensional flow in the $(x, y)$ plane are given by

$$\mu\Phi = 2\mu\left[\left(\frac{\partial u}{\partial x}\right)^2 + \left(\frac{\partial v}{\partial y}\right)^2\right] + \mu\left(\frac{\partial u}{\partial y} + \frac{\partial v}{\partial x}\right)^2$$

where $\Phi$ is called the *dissipation function*. [See Ref. (15.6).] In the boundary layer, changes in the streamwise $x$ direction are smaller than changes in the transverse $y$ direction. Also, the velocity component in the $x$ direction, $u$, is larger than the velocity component in the $y$ direction, $v$. By performing an order-of-magnitude analysis, we find that the largest viscous dissipation term in the foregoing equation is $\mu(\partial u/\partial y)^2$.

The heat conduction terms for two-dimensional flow are

$$-\nabla \cdot \vec{q} = \frac{\partial}{\partial x}\left(k\frac{\partial T}{\partial x}\right) + \frac{\partial}{\partial y}\left(k\frac{\partial T}{\partial y}\right)$$

Assuming that the thermal conductivity $k$ is constant, a boundary-layer order-of-magnitude analysis reveals that $k\partial^2T/\partial y^2$ is the larger of the two conduction terms. Taking the ratio of the viscous dissipation and the heat conduction across a boundary layer of thickness $\delta$, we obtain the following:

$$\frac{\mu\left(\frac{\partial u}{\partial y}\right)^2}{k\left(\frac{\partial^2 T}{\partial y^2}\right)} = \frac{\frac{\mu}{\rho c_p}\left(\frac{\partial u}{\partial y}\right)^2}{\frac{k}{\rho c_p}\left(\frac{\partial^2 T}{\partial y^2}\right)} \sim \frac{\frac{\nu}{c_p}\left(\frac{V-0}{\delta}\right)^2}{\frac{\alpha}{\left(\frac{T_w - T_\infty}{\delta^2}\right)}} = \left(\frac{V^2}{c_p \Delta T}\right)\left(\frac{\nu}{\alpha}\right) = (\text{Ec})(\text{Pr})$$

Thus, the importance of the viscous dissipation within the boundary layer as compared with the heat conduction within the layer is determined by the product of the Eckert $(V^2/c_p\Delta T)$ and Prandtl $(c_p\mu/k = \nu/\alpha)$ numbers. When $(\text{Ec})(\text{Pr}) \gg 1$, frictional heating should be taken into account, whereas when $(\text{Ec})(\text{Pr}) \ll 1$, it can be neglected.

From Figures 15.11 and 15.12, it may be observed that

$$\text{when} \quad T_w = T_{\text{aw}}, \quad q_w = 0 \quad \text{(the insulated wall case)}$$

$$\text{when} \quad T_w > T_{\text{aw}}, \quad q_w > 0 \quad \text{(the hot wall case)}$$

$$\text{when} \quad T_w < T_{\text{aw}}, \quad q_w < 0 \quad \text{(the cold wall case)}$$

Accordingly, Newton's law of cooling, used in convection heat transfer and generally written as $q_w = h(T_w - T_\infty)$, is more appropriately written as $q_w = h(T_w - T_{\text{aw}})$. Use of the temperature difference $(T_w - T_{\text{aw}})$ rather than $(T_w - T_\infty)$ prevents the heat transfer coefficient $h$, and therefore the Nusselt number $\text{Nu} = hL/k$, from becoming negative. In low-Mach-number cases (and therefore also for incompressible flows), $T_{\text{aw}} = T_\infty$, as shown in Figure 15.11.

For the limiting situation in which the energy gain by viscous heating is just canceled by the energy loss due to heat conduction, throughout the boundary layer the gas can be considered to be brought to rest adiabatically at the wall. For this situation, which is diagrammed in Figure 15.13, because the overall process is net adiabatic, the stagnation temperature remains constant throughout the layer. In this case, it is said that the static temperature at the wall fully recovers the freestream stagnation temperature—that is, $T_w = T_{\text{aw}} = T_{o\infty}$ or $T_{\text{aw}} - T_\infty = T_{o\infty} - T_\infty$. This limiting situation is then used as a metric for the adiabatic wall temperature by defining a *recovery factor* $r$ as follows:

$$r \equiv \frac{T_{\text{aw}} - T_\infty}{T_{o\infty} - T_\infty} \tag{15.8}$$

Since

$$T_{o\infty} = T_\infty + \frac{V^2}{2c_p} = T_\infty + \frac{\gamma - 1}{2} M_\infty^2 T_\infty = T_\infty\left(1 + \frac{\gamma - 1}{2} M_\infty^2\right) \tag{15.9}$$

it follows that

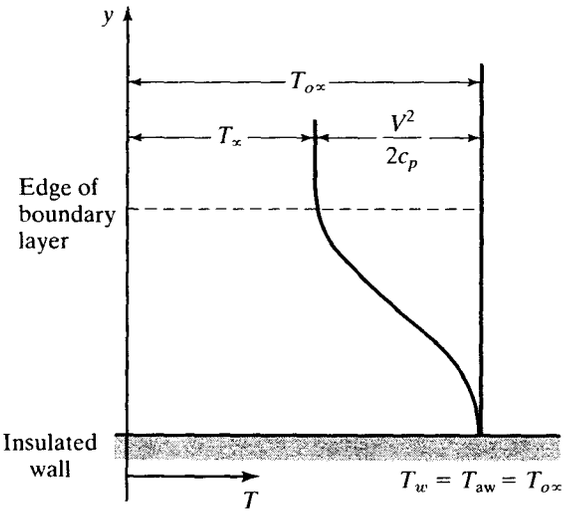


**Figure 15.13** Temperature Distributions within an Adiabatic Boundary Layer on an Insulated Wall

$$r = \frac{T_{aw} - T_\infty}{\frac{V^2}{2c_p}} = \frac{T_{aw} - T_\infty}{\frac{\gamma - 1}{2} M_\infty^2 T_\infty}$$

or

$$T_{aw} = T_\infty \left( 1 + r \frac{\gamma - 1}{2} M_\infty^2 \right) \tag{15.10}$$

Analytical work on boundary-layer flow over an insulated plate [see Refs. (15.7) and (15.8)] reveals that

$$T_{aw} = T_\infty + \frac{V^2}{2c_p} f(\text{Pr}) = T_\infty \left[ 1 + f(\text{Pr}) \frac{\gamma - 1}{2} M_\infty^2 \right]$$

Hence, we see that the recovery factor depends only upon the Prandtl number. For a laminar compressible boundary layer, over the range of Prandtl numbers between 0.5 and 10, the recovery factor may be approximated by $r = \sqrt{\text{Pr}}$, whereas for a turbulent boundary layer, the recovery factor may be approximated by $r = \sqrt[3]{\text{Pr}}$. Note that at $\text{Pr} = 1$, $r = 1$, so $T_{aw} = T_{o\infty}$.

Although a direct measurement of freestream static temperature is not possible, the foregoing analysis suggests that an indirect method is possible. The process is first to measure $p_{o\infty}$ and $p_\infty$ by using the methods of the previous section and then to determine $M_\infty$ by using Eq. (15.1) if the pressure ratio is below the critical pressure ratio and Eq. (15.7) if the pressure ratio is above the critical pressure ratio. A measurement of the adiabatic wall temperature $T_{aw}$ and a value of the Prandtl number (and therefore the recovery factor $r$ as well) are then sufficient to permit the calculation of both $T_\infty$ and $T_{o\infty}$ from Eqs. (15.10) and (15.9), respectively.

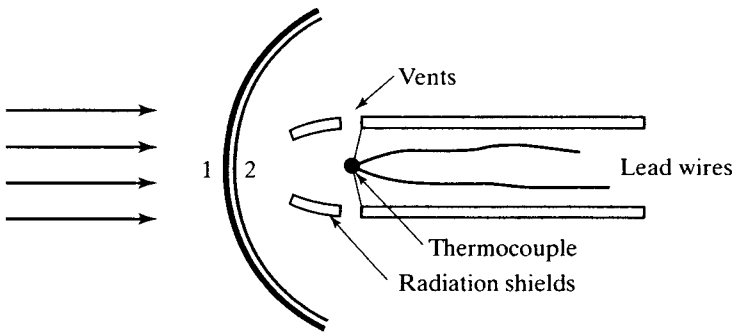


**Figure 15.14** Illustration of Stagnation Temperature Probe in Supersonic Flow

In the absence of a wall, a *stagnation temperature probe*, as illustrated in Figure 15.14, can be used to determine $T_{o\infty}$. The measurement of $T_{o\infty}$ is unaffected by the presence of the detached shock in front of the probe, since shock flow is adiabatic. The flow is brought to rest within the tube. Vent holes are provided in the sides of the probe to allow for proper ventilation of the space inside the probe; if the gas were allowed to stagnate, it would cool and yield a false reading. It is necessary that the flow be slowed down to zero velocity at the thermocouple, with no gain or loss of heat. Shields are provided to prevent radiation heat loss from the thermocouple; also, the thermocouple lead wires must be made as thin as possible so as to minimize heat flow by conduction back along the wires. Nevertheless, it is appropriate to define a *correction factor* $K$ such that

$$K = \frac{T_{o,\,\text{indicated}} - T_\infty}{T_{o\infty} - T_\infty} \tag{15.11}$$

where $T_{o,\,\text{indicated}}$ is the temperature indicated by the probe. By suitable design, $K$ can be made very close to unity for air; in any case, such a probe must be calibrated to define $K$ as a function of Reynolds number, Prandtl number, and Mach number.

Two designs of the *total air temperature (TAT) probe* as used on aircraft are diagrammed in Figure 15.15. [See Ref. (15.5).] This instrument is used to measure stagnation temperatures external to aircraft. In turn, these data, along with Pitot–static data, are sent to an onboard computer to determine true air speed. Accordingly, the TAT is a key component of the autopilot system. The TAT probes have a tube-shaped housing that is mounted parallel to the external stream and extends outside the boundary layer of the aircraft. The air that enters the probe is decelerated adiabatically such that the total temperature is recovered with very little error. The internal construction of the TAT probes is also presented in Figure 15.15. It should be noticed that the flow is turned by 90° before it passes through the measuring element. This configuration helps protect the measuring element from rain and foreign materials. The flows are exhausted with excess air out of the rear openings of the TAT. Most models also contain heaters for protection from ice.

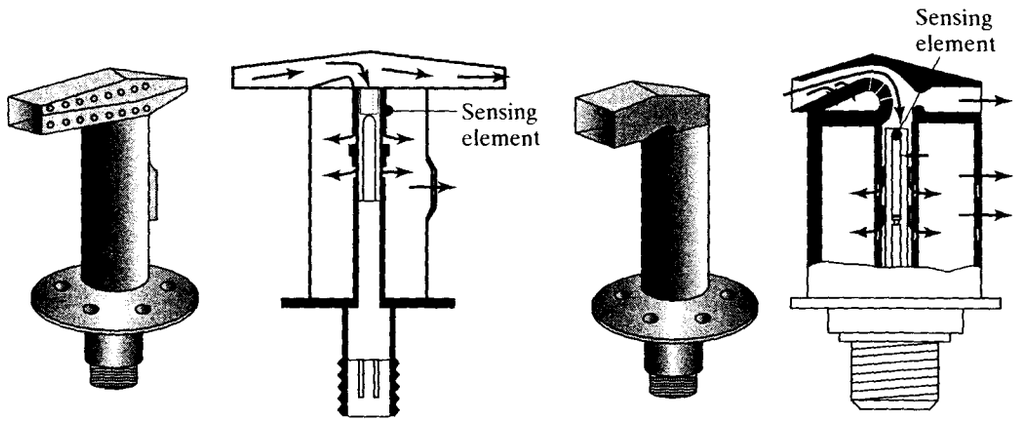


**Figure 15.15** Two Styles of Total Air Temperature Probes

**Example 15.2. Determination of static temperature**

A total-temperature probe is found to have $K = 0.95$ over a wide range of operating conditions. A Pitot tube inserted into a supersonic flow indicates a pressure of 300 kPa; a static probe indicates 60 kPa. If the indicated temperature of the total-temperature probe is 600 K when inserted into the same supersonic flow, determine $T_\infty$.

**Solution**

For $p_1/p_{o2} = 60/300 = 0.2$, we solve Eq. (15.7) to find that $M_1 = M_\infty = 1.87056$. From the isentropic relations, at $M_\infty = 1.87056$, $T_\infty/T_{o\infty} = 0.58830$, so we have

$$K = 0.95 = \frac{T_{o,\,\text{indicated}} - T_\infty}{T_{o\infty} - T_\infty} = \frac{T_{o.\,\text{indicated}} - T_\infty}{\dfrac{T_\infty}{0.5883} - T_\infty} = \frac{600 - T_\infty}{0.69981 T_\infty}.$$

Solving, we obtain $T_\infty = 360.3988$ K.

---

**Example 15.3. Couette flow of a compressible fluid**

Develop a simple model for high-Mach-number boundary-layer flow. Represent the outer freestream with a thin plate that moves with a constant speed $U$. The plate moves parallel to a stationary wall. This arrangement is called *plane Couette flow*. Assume that perfect-gas relations apply.

**Solution**

A significant difference between boundary-layer flow and a Couette flow approximation is that boundary layers grow in thickness in the $x$ direction, while plane Couette flow is of constant thickness. This simplification allows us to observe the effects of compressibility without having to manipulate the actual boundary-layer equations.

Plane Couette flow is shear driven. The shearing is supplied by the relative motion of two parallel plates as shown in Figure 15.16. A gas resides in the constant-width space between the plates. It is assumed here that the pressure is constant. Accordingly, this

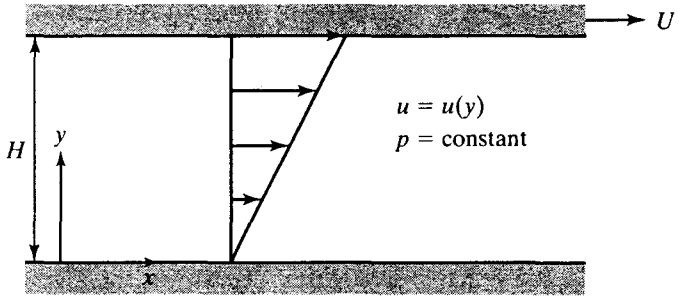


**Figure 15.16** Plane Couette Flow

configuration models the actual pressure within a boundary layer of a flat plate. It is further assumed that the velocity components in the $y$ and $z$ directions vanish—that is, $v = 0$ and $w = 0$. Also, the velocity in the $x$ direction depends only on the gas's location above the stationary plate—that is, $u = u(y)$. With these conditions, it is easy to see that the acceleration terms in the momentum equations vanish (e.g., $u\partial u/\partial x + v\partial u/\partial y + w\partial u/\partial z = 0$). Further assume that $T = T(y)$ and, in turn, $\mu = \mu(T)$ and $k = k(T)$; thus, the governing $x$-momentum equation and the energy equation reduce respectively to

$$0 = \frac{d}{dy}\left(\mu\frac{du}{dy}\right) = \frac{d\tau}{dy} \tag{15.12}$$

$$0 = \frac{d}{dy}\left(k\frac{dT}{dy}\right) + \mu\left(\frac{du}{dy}\right)^2 = \frac{d}{dy}\left(k\frac{dT}{dy}\right) + \tau\left(\frac{du}{dy}\right) \tag{15.13}$$

Designating the lower surface by the symbol $L$ and the upper surface by the symbol $U$, we readily integrate Eq. (15.12) to give

$$\tau = \text{constant} = \tau_L = \tau_U = \mu\frac{du}{dy}$$

For constant viscosity, it follows that $du/dy = \text{constant}$. Solving for $u$ and applying the velocity boundary conditions yields the well-known linear velocity profile for plane Couette flow:

$$u = U\frac{y}{H}$$

However, in a compressible flow, because of the variation in the temperature, $\mu$ does not remain constant. Instead, we find that

$$u = U\frac{\int_0^y dy/\mu}{\int_0^H dy/\mu}$$

Integrating the energy equation, Eq. (15.13), yields

$$k\frac{dT}{dy} + \tau u = C$$

At the lower boundary, $y = 0, u = 0$, and from Fourier's law, $-(kdT/dy)_L = q_L$. Thus, $C = -q_L$. We can rewrite the integrated viscous dissipation term as follows:

$$\tau u = \mu \frac{du}{dy} u = \frac{\mu}{2} \frac{d(u^2)}{dy}$$

Combining expressions and using Newton's law of viscosity, we can now write the integrated energy equation as

$$\frac{k}{\mu} \frac{dT}{dy} + \frac{d}{dy}\left(\frac{u^2}{2}\right) = -\frac{q_L}{\mu}$$

or

$$\frac{k}{\mu} dT + d\left(\frac{u^2}{2}\right) = -q_L \frac{dy}{\mu} = -q_L \frac{du}{\tau_L}$$

Integrating from the lower surface where $T = T_L$ and $u = 0$ gives

$$\frac{u^2}{2} + \int_{T_L}^{T} \frac{k}{\mu} dT = -\frac{q_L}{\tau_L} u$$

At the upper surface, $y = H, u = U$, and $T = T_U$; thus,

$$\frac{\tau_U}{U}\left(\frac{U^2}{2} + \int_{T_L}^{T_H} \frac{k}{\mu} dT\right) = -q_L$$

Although both the thermal conductivity $k$ and the viscosity $\mu$ vary with temperature, we may approximate their ratio as a constant: $k/\mu = c_p/\text{Pr} = \text{constant}$. This enables the integral in the foregoing expression to be completed, and we obtain

$$q_L = \frac{c_p}{\text{Pr}} \frac{\tau_L}{U}\left[(T_L - T_U) - \frac{\text{Pr}\, U^2}{2c_p}\right]$$

Now, if the heat flux at the lower surface, $q_L$, is zero (i.e., $dT/dy = 0$), the wall is adiabatic. Thus, $T_L = T_{aw}$ and the previous equation can be written as

$$T_L - T_U = T_{aw} - T_U = \frac{\text{Pr}\, U^2}{2c_p} = \text{Pr}\left(\frac{\gamma - 1}{2}\right) M_U^2 T_U \tag{15.14}$$

where $M_U$ is the Mach number at the upper wall. This value is based on the upper wall speed and the static temperature of the upper wall, $T_U$. Rearranging Eq. (15.14) informs us that for an adiabatic wall in plane Couette flow,

$$\frac{U^2}{c_p(T_{aw} - T_H)} \text{Pr} = (\text{Ec})(\text{Pr}) = 2 \tag{15.15}$$

The difference between the stagnation temperature at the upper wall, $T_{oU}$, and the static temperature at the upper wall, $T_U$, may be written as

$$T_{oU} - T_U = \frac{U^2}{2c_p} = \left(\frac{\gamma - 1}{2}\right) M_U^2 T_U \tag{15.16}$$

The ratio of Eq. (15.15) to Eq. (15.16) is the recovery factor $r$:

$$\frac{T_{aw} - T_U}{T_{oU} - T_U} = r = \text{Pr}$$

So, we see that the recovery factor for Couette flow is simply equal to the Prandtl number. It should be mentioned that in keeping with the use of Couette flow as a model of boundary-layer flow, $T_{oU}$ plays the role of $T_{o\infty}$, and $T_U$ plays the role of $T_\infty$.

## 15.4 VELOCITY MEASUREMENT

The velocity of a moving gas may be measured by using mechanical or laser/optical probes. The Pitot–static tube is still the most widely used mechanical device for measuring the mean velocity of a moving gas. *Hot wire anemometers* (HWA) are used to perform detailed, high-frequency or high-resolution flow-field velocity measurements. As mentioned in Ref. (15.9), HWAs have been used to measure the variables that occur in turbulent flows, such as mean and fluctuating velocity components, mean and fluctuating temperatures, and vorticity.

Over the past few decades, laser/optical devices have been developed, allowing the noninvasive measurement of instantaneous velocity. Laser/optical techniques measure the local velocity components of tracer particles (naturally occurring or artificially seeded) transported by the flow. There are two main categories of laser/optical measuring systems: *laser Doppler anemometers* (referred to here as velocimeters, with the acronym LDV) and *particle image velocimetry* (PIV). LDVs determine the velocity from the frequency shift of a laser beam that is traversed by a moving object. PIV is a photographic technique that measures the velocity by determining the displacement of seeded particles over time. To accomplish this, the particles are illuminated with a planar (2D) light or laser sheet, and the flow field is photographed at short time intervals.

Both HWAs and LDVs have good frequency response, typically more than 1 MHz for hot wires and 30 kHz for LDVs. They are both capable of performing point measurements. The HWA wire is around 5 $\mu$m in diameter and 2 mm in length; the measuring volume of an LDV is about 50 $\mu \times 0.25$ mm. Both instruments are capable of providing reasonably accurate velocities, within, say, a few percent. The resolution is typically 1 part in 10,000 for the HWA and below 1 part in 1000 for the LDV. Both techniques can be used over a very wide range of velocities. The LDV has the advantage at very low velocities, when the natural convection can introduce disturbances, and in the transonic flow regime, where the thermal probes are sensitive to recovery or adiabatic wall temperatures. However, the LDV has limitations due to its requiring seed particles in the fluid, while hot wires have limitations dictated by the maximum operating temperature of the sensor (typically about 300°C). Hot wire probes are very fragile; however, the HWA is still significantly less expensive compared with an LDV system.

### Hot Wire Anemometry

The hot wire anemometer, which began to appear around 1900, is essentially a small probe containing a thin, electrically heated wire located within a fluid stream. The convective heat transfer from the heated wire depends principally upon the velocity of the fluid and the temperature of the wire. Electronic circuitry monitors the signal in the

transducers and computes the convective heat loss, as well as the temperature of the heat-exchange surfaces. An energy balance and empirical heat transfer correlations provide the equations connecting the convective heat loss, the temperature variations, the fluid velocity, and the fluid properties.

The fundamental equation of a hot wire anemometer is the *temperature law of the resistivity* $\chi$ for the hot wire materials. To a good approximation, $\chi$ varies linearly with temperature of the wire as

$$\chi_w = \chi_{\text{ref}}[1 + \alpha(T_w - T_{\text{ref}})]$$

where $\alpha$ is the temperature *coefficient of resistivity*. Consequently, the resistance of a wire of length $L$ and cross-sectional area $A$ at a mean temperature $T_w$ is

$$\frac{\chi_w L}{A} = R_w = R_{\text{ref}}[1 + \alpha(T_w - T_{\text{ref}})]$$

Therefore,

$$\Delta R = R_w - R_{\text{ref}} = \alpha(T_w - T_{\text{ref}})R_{\text{ref}}$$

Hot wire probes are typically connected to a *Wheatstone bridge*. At reference conditions, the bridge is balanced, so the output voltage is zero. When a fluid streams over the heated wire of the probe, the convective heat exchange produces a variation in the temperature, which in turn generates a variation in the resistance of the hot wire. The bridge becomes unbalanced and generates an output voltage that is proportional to the resistance variation—that is,

$$\Delta e \sim \Delta R$$

The output voltage can easily be measured, and hence all of the parameters of the circuit can be determined.

Neglecting all heat losses except for the convection, we can write a heat balance on a wire of length $L$ as

$$\dot{Q}_{\text{generated}} = \dot{Q}_{\text{convected to the fluid}}$$

That is,

$$I^2 R_w = hA(T_w - T_f) = h(L\pi d)(T_w - T_f) = \pi L k(T_w - T_f)\text{Nu}$$

where $I$ is the probe current, $d$ the diameter of the wire, $k$ the thermal conductivity of the fluid, Nu ($= hd/k$) the Nusselt number, and $T_w$ and $T_f$ the wire and fluid temperatures, respectively. Taking the reference temperature to be the same as the fluid temperature $T_f$, we have

$$T_w - T_{\text{ref}} = T_w - T_f = \frac{R_w - R_f}{\alpha R_f}$$

The Nusselt number (and therefore the heat transfer coefficient $h$) are provided by heat transfer correlations of experimental data. For forced convection from a heated wire, we may write a general relation for the Nusselt number that depends upon the

flow regime. For low-velocity flows, the Nusselt number depends upon the Reynolds number (based on the wire diameter) and on the Prandtl number. On the other hand, for higher speed compressible flows (subsonic, transonic, and low supersonic), we may write

$$\text{Nu} = \text{Nu}[\text{Re}, \text{Pr}, M, \gamma, L/d, (T_w - T_{\text{aw}})/T_o] \tag{15.17}$$

The properties are evaluated at either the film temperature or the stagnation temperature. It should be noted that because the wire is very thin, small Re values are encountered (say, between 2 and 40) and that there can be departures from continuum flow. The flow regime of continuum flow is determined by the value of the *Knudsen number* $\text{Kn} = \lambda/d = \left(\sqrt{\pi\gamma/2}\right)M/\text{Re}$, where $\lambda$ is the *molecular mean free path* of the gas. *Continuum flow* exists if $\text{Kn} < 0.01$; *slip flow* exists if $0.01 < \text{Kn} < 1$; and *free molecular flow* exists if $\text{Kn} > 1$. The ratio $L/d$ is termed the *aspect ratio of the wire*, and $(T_w - T_{\text{aw}})/T_o$—that is, the difference between the wire temperature and the adiabatic wall temperature, divided by the stagnation temperature—is called the *overheat ratio of the wire*. It is assumed in Eq. (15.17) that the velocity is normal to the wire; if it is not, an additional parameter would have to be included in the formulation. For supersonic and hypersonic flows, a normal shock resides in front of the probe, and the correlation is found to be independent of the Mach number. [See Ref. (15.10).]

There are numerous correlations that have been developed to relate the heat transfer from a cylinder to the flow parameters. [See Ref. (15.11) to gain an appreciation for the extent of this body of work.] The oldest, and so perhaps the best known, correlation is *King's law*,

$$\text{Nu} = A + B\,\text{Re}^{0.5}$$

where $A$ and $B$ are empirical constants and $Re = pvd/\mu$ [See Ref. (15.12).] Because this correlation provides reliable values only over a limited range of velocities, it is rarely used today. A more accurate correlation, however, exclusively for air, has been provided by Collis and Williams [see Ref. (15.13)] as

$$\text{Nu} = (A + B\,\text{Re}^n)\left[1 + \frac{1}{2}\left(\frac{T_w + T_{\text{air}}}{T_{\text{air}}}\right)\right]^{0.17}$$

where the values for the Re range, $A$, $B$, and $n$ are given in Table 15.2.

Note that there is a discontinuity at $\text{Re} = 44$, because of vortex shedding behind the wire. A more general relation than the two presented previously was developed by Kramers [see Ref. (15.14)]:

$$\text{Nu} = 0.42\,\text{Pr}^{0.26} + 0.57\,\text{Pr}^{0.33}\,\text{Re}^{0.50} \tag{15.18}$$

**TABLE 15.2** Empirical Constants in the Collis and Williams Correlation

| Re Range | $A$ | $B$ | $n$ |
|---|---|---|---|
| 0.02–44 | 0.24 | 0.56 | 0.45 |
| 44–140 | 0 | 0.48 | 0.51 |

This correlation is applicable to both gases and liquids: $0.71 < \text{Pr} < 525$ and $2 < \text{Nu} < 20$. The properties are evaluated at the film temperature—that is, $(T_w + T_f)/2$. Using Kramers's correlation, we can write the heat balance on the wire as

$$\frac{I^2 R_w}{R_w - R_f} = A + BV^{0.5}$$

where

$$A = 0.42\frac{\pi k L}{\alpha_0 R_0}\text{Pr}^{0.26} \quad \text{and} \quad B = 0.57\frac{\pi k L}{\alpha_0 R_0}\text{Pr}^{0.33}\left[\frac{\rho d}{\mu}\right]^{0.5}$$

Experience has shown that the characteristics of apparently identical probes vary enough to require separate calibration for each transducer. Calibration devices are commercially available. They typically provide the curve connecting the velocity to the bridge voltage,

$$\Delta e^2 = a + bV^n$$

The values of the constants $a$, $b$, and $n$ are obtained by curve fitting.

There are two main types of electronic circuitry, each controlling the probe in a different way. In a *constant temperature anemometer* (CTA), a differential feedback amplifier detects the bridge unbalance and modifies the current to keep the sensor temperature constant. In a *constant current anemometer* (CCA), the bridge current is provided by a constant current source. As explained previously, for both cases, the voltage difference across the Wheatstone bridge is proportional to the velocity. Recently, a *constant voltage anemometer* (CVA) has been considered.

The typical hot wire transducer (see Figure 15.17) is a wire, usually made of tungsten, platinum, or platinum–iridium. The typical diameter of the sensing element is 0.5–5 microns (1 micron = 1 $\mu$m = $1 \times 10^{-6}$ m), with a length of 1 to 2 mm. The wire is attached to the tips of two support needles. The two electrical connectors are located at the other end of the body of the probe, opposite the hot wire.

Relations have been developed that enable an HWA to sense the direction of a flow as well as the velocity. [See Ref. (15.15).] In order to measure two velocity components, usually an *X hot wire probe* is used. An *X* hot wire probe consists of two wire sensors placed in the same plane and oriented at angle of 90° to each other. The plane of the *X* probe is either parallel to the probe stem, as shown in Figure 15.18(a), or perpendicular to the probe stem, as shown in Figure 15.18(b). Similarly, three velocity components can be measured by introducing a third sensor.

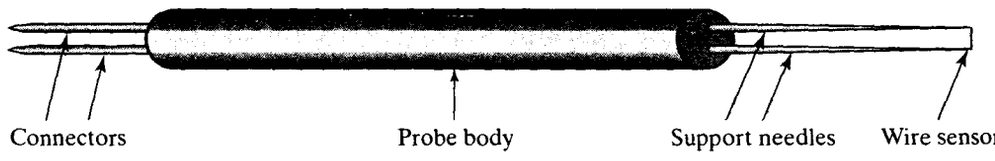


**Figure 15.17** Typical Hot Wire Probe

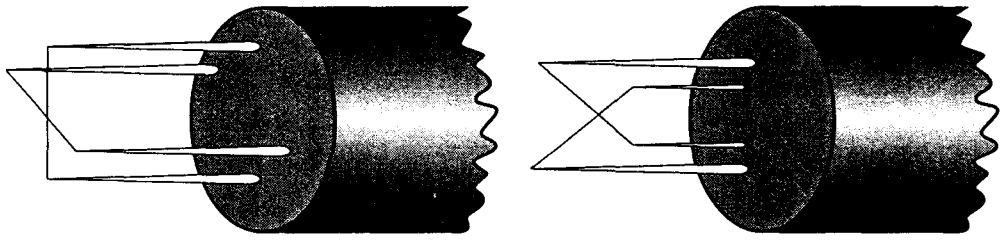

(a) $X$ probe: plane parallel to probe stem

(b) $X$ probe: plane perpendicular to probe stem

**Figure 15.18** $X$ Hot Wire Probes

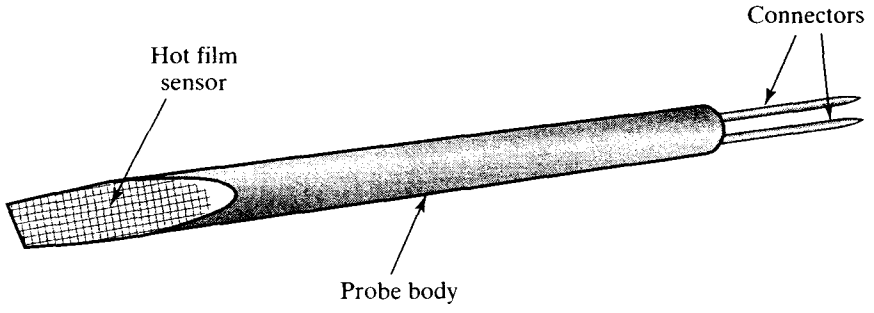


**Figure 15.19** Hot Film Probe

Hot wire sensors are generally used in gas flow applications. For measurements in conducting liquids and in liquids or gases with particle contamination, the *hot film sensor probe* (see Figure 15.19) is used, as the fragile wire of the HWA could otherwise be broken. In this case, the sensor is a thin ($\sim$0.1 $\mu$m) conducting film (platinum or nickel) deposited on thermally insulating backing material (usually quartz). In order to protect the film from damage by abrasion or by chemical reactions, a thin coating layer of insulating material is often added.

For additional information regarding HWAs, see Refs. (15.15)–(15.18).

### Laser Doppler Velocimetry

Laser Doppler velocimeters began to be used in the mid-1960s. The fundamental phenomenon of laser Doppler velocimetry (LDV) is the *Doppler shift* of the light that is scattered from small particles moving with the fluid. The sizes of the particles that are used to seed the flow are typically from 0.1 to 10 microns. Figure 15.20 shows an arrangement in which the particles have a velocity $\vec{\mathbf{V}}$ and the shift is recorded on a sensor situated a distance $\vec{\mathbf{r}}_d$ from a fixed coordinate system $Oxyz$. The position of the particles with respect to the fixed laser source is given by the vector $\vec{\mathbf{r}}_1$.

If the laser has a wavelength $\lambda$ and the frequency of the illuminating beam is $\nu_o$, the frequency of the scattered light detected at the location $\vec{\mathbf{r}}_d$ is

$$\nu = \nu_o + \frac{\vec{\mathbf{V}} \cdot (\vec{\mathbf{i}}_1 - \vec{\mathbf{i}}_d)}{\lambda}$$

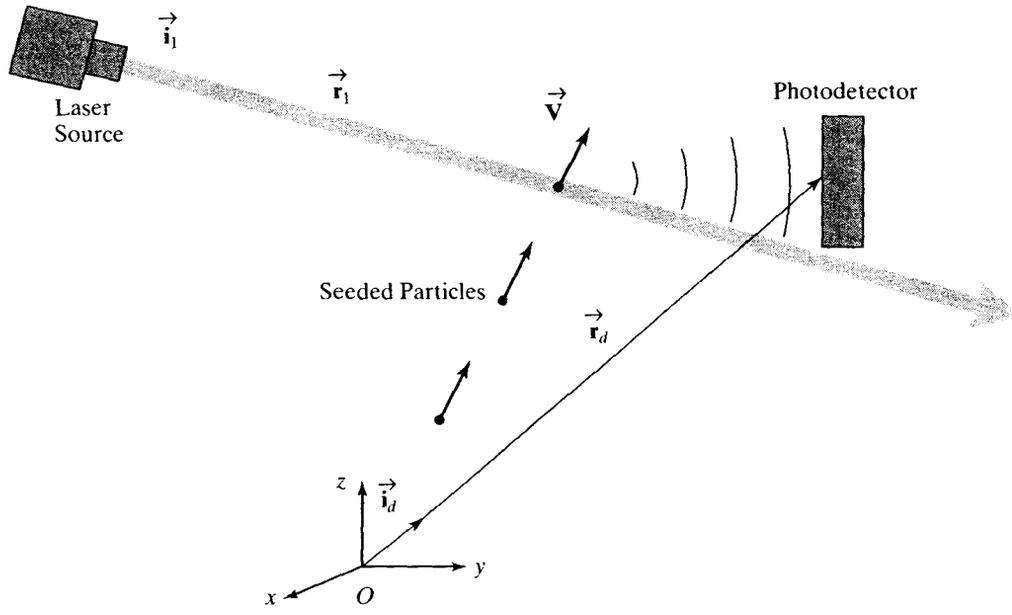


**Figure 15.20** The Principle of the Laser Doppler Velocimeter

where $\vec{i}_1$ and $\vec{i}_d$ are the unit vectors of $\vec{r}_1$ and $\vec{r}_d$, respectively. [See Ref. (15.19).] Since the Doppler frequency shift depends linearly upon the velocity component in the direction $(\vec{i}_1 - \vec{i}_d)$, by measuring $\Delta\nu$ we can obtain the component of velocity along the external bisector of the angle formed between the illumination and the observation directions.

The standard method for measuring the Doppler shift frequency is *optical mixing*, or the *optical heterodyne detection technique*. This technique consists of combining two light waves on the surface of an electronic *photodetector*. This device has an output signal that oscillates at a frequency equal to the difference between the frequencies of the two light inputs. Consequently, although other LDV systems are available, most LDV systems are based on the so-called dual-beam system. The fundamental principle of the *dual-beam LDV* is to irradiate the scattering particle with two plane waves, propagating in two directions, $\vec{i}_1$ and $\vec{i}_2$. (See Figure 15.21.) The waves come from a single monochromatic

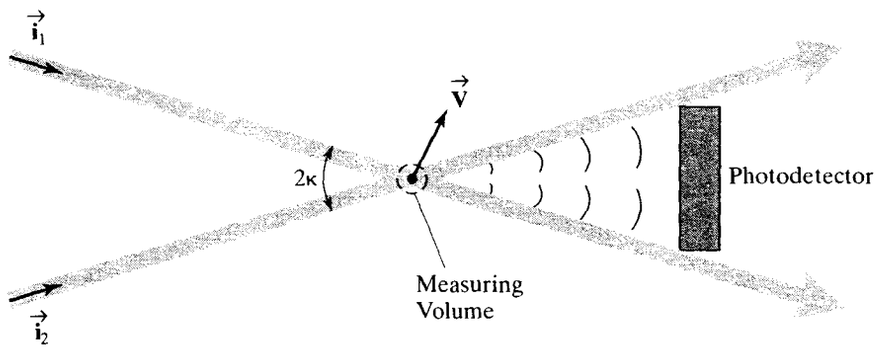


**Figure 15.21** The Dual-Beam LDV

laser source that sends a laser beam to a *beam splitter*. The resulting beams intersect to form a measuring volume, as illustrated in Figure 15.21.

The particle scatters two waves, one from each beam. The frequencies of these scattered waves in the scattering direction $\vec{\mathbf{i}}_d$ (refer to Figure 15.20) are

$$\nu_1 = \nu_{o1} + \frac{\vec{\mathbf{V}} \cdot (\vec{\mathbf{i}}_d - \vec{\mathbf{i}}_1)}{\lambda}$$

and

$$\nu_2 = \nu_{o2} + \frac{\vec{\mathbf{V}} \cdot (\vec{\mathbf{i}}_d - \vec{\mathbf{i}}_2)}{\lambda}$$

The heterodyne mixing produces the frequency difference

$$\nu_1 - \nu_2 = \nu_{o1} - \nu_{o2} + \frac{\vec{\mathbf{V}} \cdot (\vec{\mathbf{i}}_2 - \vec{\mathbf{i}}_1)}{\lambda}$$

Thus, the difference between the Doppler shifts,

$$\nu_D = \frac{\vec{\mathbf{V}} \cdot (\vec{\mathbf{i}}_2 - \vec{\mathbf{i}}_1)}{\lambda} \equiv \frac{\vec{\mathbf{V}} \cdot \vec{\mathbf{K}}}{2\pi}$$

is independent of the direction $\vec{\mathbf{r}}_d$. (Again, refer to Figure 15.20.) Here,

$$\vec{\mathbf{K}} = \frac{2\pi(\vec{\mathbf{i}}_2 - \vec{\mathbf{i}}_1)}{\lambda}$$

is the *wave vector* in the direction $(\vec{\mathbf{i}}_2 - \vec{\mathbf{i}}_1)$. If $V(t)$ is the component of the velocity in the $(\vec{\mathbf{i}}_2 - \vec{\mathbf{i}}_1)$ direction, then

$$\nu_D = \frac{KV(t)}{2\pi}$$

where

$$K = |\vec{\mathbf{K}}| = \frac{4\pi \sin \kappa}{\lambda}$$

Consequently, the difference $\nu_D$ between the two Doppler shifts is a measure of the velocity component $V$, which lies in the plane of the illuminating beams and is perpendicular to their bisector.

As with other optical devices, the operation of the dual LDV can be explained from an optical perspective, in terms of *interferometry*. The *fringe model* can explain the operation of the dual-beam LDV without making any reference to the Doppler frequency shift effect.

The fringe model is based on the fact that an interference fringe appears in the measuring volume—that is, at the intersection of the two beams. The space between fringes is

$$d_f = \frac{\lambda}{2 \sin \kappa}$$

When a very small particle intersects the fringes, it will generate a scattered light flux. As the particle traverses the fringes, the scattered light flux oscillates sinusoidally. The time for the particle to traverse one fringe is $V/d_f$. So, the frequency of the sinusoidal oscillation of the light flux is

$$\nu_D = \frac{V}{d_f} = \frac{2u \sin \kappa}{\lambda}$$

which is the same as that obtained from the Doppler model.

As before, $V$ represents the velocity component perpendicular to the fringes, which is also located in the plane of the two intersecting beams and perpendicular to their bisector.

Thus far, we have considered only the measurement of a single velocity component. The measurement of the other two components requires a combination of several single-velocity systems. The illuminating beams must have different properties—typically, different wavelengths (that is, different colors)—in order to allow for identification of the one-component system corresponding to the signal.

### Particle Image Velocimetry

The PIV technique was initiated in the 1980s, being derived from the *laser speckle* systems, which have been used to study the motion of solid surfaces. The fundamental principle of the PIV technique is the calculation of the velocity from a sequence of photographs of a seeded and illuminated flow field. Complete PIV systems are commercially available and have been used in a wide variety of flows, including wind tunnel flows, supersonic jet expansions, flows inside a combustion cylinder of an engine, flames, two-phase flows, waves, and rotating and turbulent flows.

In solid-surface applications, the *speckle phenomenon* is created by the interference of coherent light—that is, a laser beam—scattered from a surface element roughness that is large compared with the wavelength of the laser. When the rough surface is illuminated, the interference of the light creates an image called a *speckle pattern*. The *speckle size* is a statistical average of the distance between adjacent regions of maximum and minimum brightness. A doubly exposed photograph of the speckle pattern is taken, one before and one after a lateral displacement is given to the solid. This photograph, or *specklegram*, contains two correlated grids that can be analyzed as a nonuniform diffracting grating to obtain displacement and, therefore, strain data. [See Ref. (15.20).]

The first attempts to implement laser speckle measurements in fluid mechanics were reported in the 1970s. When the concentration of the particles in the laser-illuminated field is large, and the scattered light is coherent, interference signals begin to appear. When many images interfere, the resulting pattern is the laser speckle phenomenon. However, researchers realized that the fluid often did not contain enough scattering particles and that the photograph of the flow field contained only images of the particles. This observation led to the creation of a new velocity measurement technique, which is now called particle image velocimetry (PIV).

The basic setup of a PIV measurement is shown in Figure 15.22. A double-pulsed light beam (preferably a laser) is focused onto an optical device, such as a cylindrical lens, to create a laser sheet. The sheet of light illuminates the seeded flow field, which is photographed. The plane of the photograph is parallel to the light sheet. Any medium can be used for the photography; both photographic film and digital cameras have been

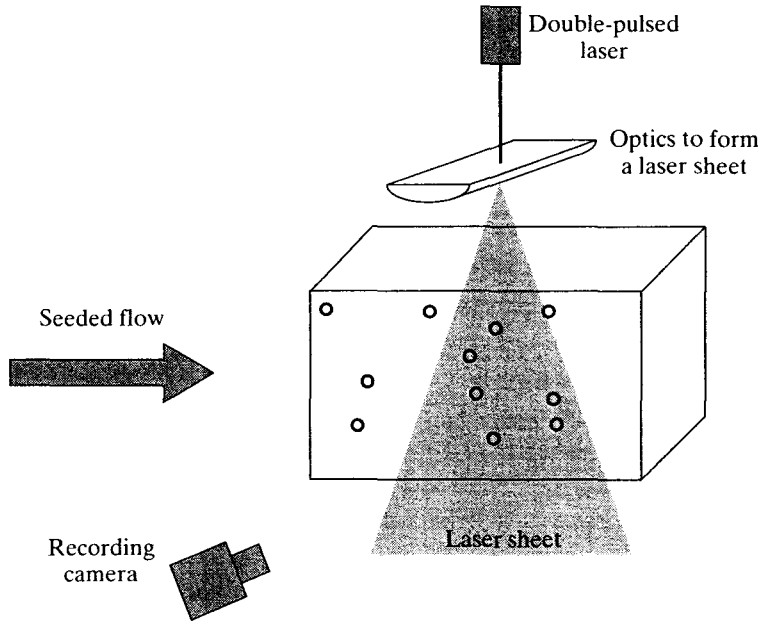


**Figure 15.22** PIV Measurement Arrangement

successfully used. However, modern commercial systems incorporate computer-driven "frame grabber" systems. These devices basically consist of electronic digital cameras connected to data acquisition boards dedicated to video recording.

The laser pulse has to be very short in order to be capable of "freezing" the motion of the particles in high-velocity flows. After a short time interval $\Delta t$, a second image of the flow field is recorded. The images are analyzed and the displacements $\Delta x$ of the particles are computed. Since the time interval is known, the velocity can be computed from $u = \Delta x/\Delta t$. The process is illustrated in Figure 15.23(a).

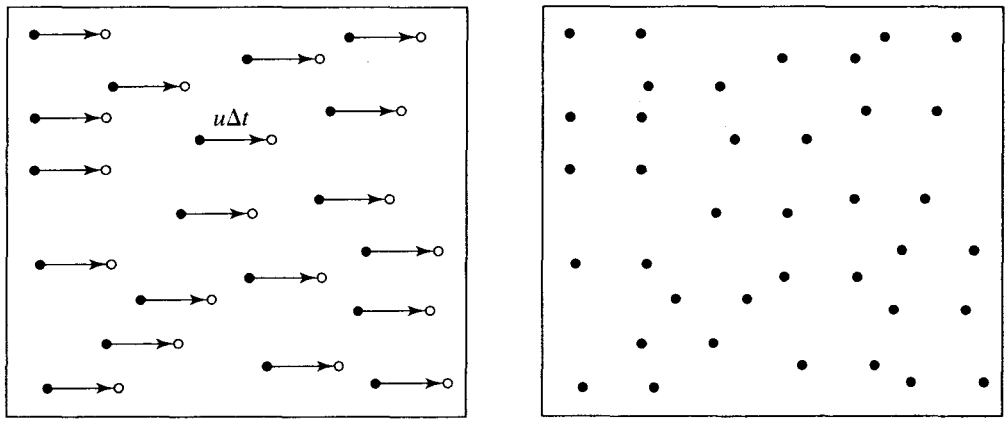


**Figure 15.23** PIV Process and Double-Exposure Example

The measuring process is simple for low-particle-density PIV. However, for very complex flows, a higher particle density is generally required. When the density of the particles is large, the doubly exposed high-density-image photographs [see Figure 15.23(b)] become more difficult to analyze; the analysis of the data becomes more involved and requires special algorithms.

Initially, the analysis algorithms were inspired by *Young's method of fringes*, currently used in speckle analysis. Additional algorithms were also developed. Other techniques used currently include *matching methods* (based on maximization and cross-correlations), *Fourier analyses*, and *statistical methods*, based on constructing a two-dimensional histogram of the distances between two particle pairs and assigning the local velocity to the most frequent distance.

A full discussion of the procedures and techniques of PIV is well beyond the scope of this section. Refs. (15.21)–(15.23) contain detailed information regarding PIV.

**Example 15.4. Determination of velocity from hot-wire-anemometer measurements**

A hot wire anemometer is placed in an airstream at atmospheric pressure and a temperature of 20°C. The electric current in the wire is 4 mA, and the temperature of the wire is 180°C. The diameter of the wire is 2 $\mu$m, and the length is 1.5 mm. Determine the velocity of the air flow. For air at the mean film temperature, take $\rho = 0.9458\ \text{kg/m}^3$, $c_p = 1.013\ \text{kJ/kg} \cdot \text{K}$, $k = 0.0314\ \text{W/m} \cdot \text{K}$, and $\mu = 2.18 \cdot 10^{-5}\ \text{kg/m} \cdot \text{s}$. The resistivity of the wire is $0.22\ \mu\Omega \cdot \text{m}$.

**Solution**

The resistance of the wire is

$$R = \frac{\chi_w L}{(\pi d^2/4)} = \frac{(0.22 \cdot 10^{-6}\ \Omega \cdot \text{m})(1.5 \cdot 10^{-3}\ \text{m})}{[\pi(2 \cdot 10^{-6})^2/4]} = 105.0423\ \Omega$$

The heat loss from the wire is computed as

$$q = I^2 R = (0.004A)^2(105.0423\ \Omega) = 0.0016807\ \text{W}$$

The heat transfer coefficient is determined as follows:

$$h = \frac{q}{A(T_w - T_\infty)} = \frac{q}{\pi dL(T_w - T_\infty)} = \frac{0.0016807\ \text{W}}{\pi \cdot (2 \cdot 10^{-6}\ \text{m}) \cdot (1.5 \cdot 10^{-3}\ \text{m})(180 - 20)\ \text{K}}$$

$$= 1{,}114.5330\ \text{W/m}^2 \cdot \text{K}$$

Consequently, the Nusselt number is

$$\text{Nu} = \frac{hd}{k} = \frac{(1114.533\ \text{W/m}^2 \cdot \text{K})(2 \cdot 10^{-6}\ \text{m})}{0.0314\ \text{W/m} \cdot \text{K}} = 0.07099$$

The Prandtl number is

$$\text{Pr} = \frac{\mu c_p}{k} = \frac{(2.18 \cdot 10^{-5}\ \text{kg/m} \cdot \text{s})(1.013 \cdot 10^3\ \text{J/kg} \cdot \text{K})}{0.0314\ \text{W/m} \cdot \text{K}} = 0.7033$$

With the Nusselt and Prandtl numbers, we can determine the Reynolds number from Eq. (15.18):

$$\mathrm{Re} = \left(\frac{\mathrm{Nu} - 0.42 \cdot \mathrm{Pr}^{0.26}}{0.57 \cdot \mathrm{Pr}^{0.33}}\right)^2 = \left(\frac{0.07099 - 0.42 \cdot 0.7033^{0.26}}{0.57 \cdot 0.7033^{0.33}}\right)^2 = 0.3786$$

Having the Reynolds number, we can compute the velocity of the air flow:

$$V = \frac{\mathrm{Re}\mu}{\rho d} = \frac{0.3786 \cdot (2.18 \cdot 10^{-5}\ \mathrm{kg/m \cdot s})}{(0.9458\ \mathrm{kg/m^3}) \cdot (2 \cdot 10^{-6}\ \mathrm{m})} = 4.3637\ \mathrm{m/s}$$

---

**Example 15.5. Determination of velocity from LDV measurements**

A dual-beam LDV uses a laser with a wavelength of 6,000 Angstroms ($1\text{Å} = 10^{-10}$ m). The angle between the intersecting beams is 10°. When the seeds cross the fringes from the measuring volume, they scatter a light flux that oscillates sinusoidally with a frequency of 20 MHz. What is the velocity of the flow?

**Solution**

The space between the fringes is

$$d_f = \frac{\lambda}{2 \sin \kappa} = \frac{6{,}000 \cdot 10^{-10}\ \mathrm{m}}{2 \sin 5^0} = 3.442 \cdot 10^{-6}\ \mathrm{m}$$

The velocity of the flow (i.e., the velocity of the particle) is

$$V = d_f \nu = (3.442 \cdot 10^{-6}\ \mathrm{m}) \cdot (20 \cdot 10^6\ \mathrm{s^{-1}}) = 68.842\ \mathrm{m/s}$$

---

## 15.5 DENSITY AND OPTICAL METHODS OF MEASUREMENT

The actual measurement of density seems superfluous at this point. Certainly, by measuring or determining pressure and temperature, density can be calculated from the perfect-gas law or some other equation of state. However, the optical methods to be discussed here, which depend on the variation of density or its derivatives throughout the flow field, are extremely important techniques for the investigation of compressible flows. The use of any of the three optical methods to be discussed—the *Schlieren*, *shadowgraph*, and *interferometer* methods—allows one to "see" phenomena such as shockwaves, temperature gradients, and natural convection patterns in liquids without introducing any object or disturbance into the flow.

The three optical methods depend on the principle that the speed of light in a medium is dependent on the density of that medium. The *index of refraction*, $n$, relates the speed of light in vacuum, $c_0$ ($= 3 \times 10^8$ m/s), to the speed of light in a medium, $c$:

$$n = \frac{c_0}{c} \tag{15.19}$$

The *Lorenz–Lorentz equation* provides a relation between the index of refraction of a homogenous medium and the density of the medium:

$$\frac{n^2 - 1}{n^2 + 2} = C\rho \tag{15.20}$$

For values of $n$ near unity, an approximate linear relationship, known as the *Gladstone–Dale equation*, may be obtained from Eq. (15.20) as

$$n = 1 + K\rho \tag{15.21}$$

where $K$ is a positive constant (*the Gladstone–Dale constant*) that depends on gas composition, temperature, density, and the wavelength of the light, $\lambda$. ($K$ increases with increasing $\lambda$, and hence infrared light may be used to detect small disturbances.) For air at standard conditions, $K$ is about 0.23 $cm^3/g$ (for other gases, $K$ ranges from about 0.1 to 1.5 $cm^3/g$), and the index of refraction, $n$, is very close to 1. Table 15.3 presents the index-of-refraction values for air for several temperatures and the Gladstone–Dale constant for a few gases.

As is well known, if light rays pass from one medium into another of a different density, the rays are turned—that is, they are *refracted*. Consider a series of light rays passing from one medium (air) into another medium (water), as shown in Figure 15.24.

**TABLE 15.3** Values for the Index of Refraction and the Gladstone–Dale Constant

| Air, $T$ (K) | $n$ | Gas | $K$ ($cm^3/g$) | $T$ (K) |
|---|---|---|---|---|
| 258 | 1.0003094 | He | 0.196 | 295 |
| 273 | 1.0002924 | $H_2$ | 1.55 | 273 |
| 288 | 1.0002771 | $O_2$ | 0.190 | 273 |
| 303 | 1.0002634 | $N_2$ | 0.238 | 273 |
| 333 | 1.0002396 | $CO_2$ | 0.229 | 295 |

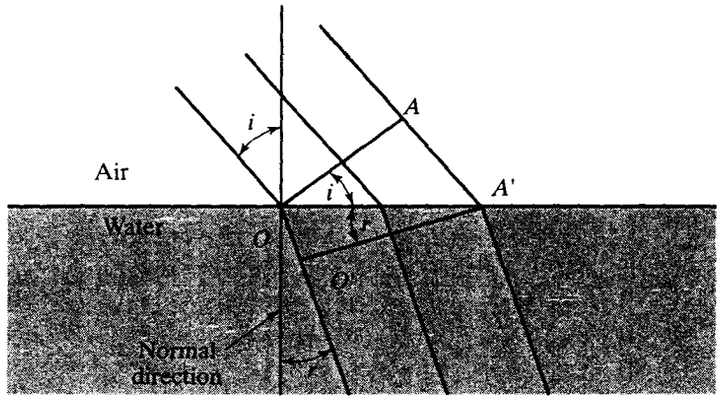


**Figure 15.24** Bending of Light Waves Passing from Air through Water

The plane wave front $\overline{OA}$ has been shown at the instant the light is incident on the surface. A short time later, the wave front reaches the position $\overline{O'A'}$. Since the velocity of light in water, $c_{water}$, is less than that in air, $c_{air}$, the distance $\overline{OO'}$ is less than $\overline{AA'}$, so the wave front turns, with

$$\frac{\sin(i)}{\sin(r)} = \frac{\overline{AA'}/\overline{OA'}}{\overline{OO'}/\overline{OA'}} = \frac{\overline{AA'}}{\overline{OO'}} = \frac{c_{air}\Delta t}{c_{water}\Delta t} = \frac{c_{air}}{c_{water}}$$

Using Eq. (15.19), we obtain a relation between the *angle of incidence*, $i$; the angle of refraction, $r$; and the respective indices of refraction:

$$\frac{\sin(i)}{\sin(r)} = \frac{c_{air}}{c_{water}} = \frac{n_{water}}{n_{air}} \tag{15.22}$$

Equation (15.22) is known as *Snell's law*. As may be observed, the light rays from the less dense medium are turned towards the normal (formed at the interface between the two media) within the denser medium; that is, since $\rho_{water} > \rho_{air}$, $n_{water} > n_{air}$, so angle $i >$ angle $r$.

Now suppose that, instead of passing through a region such that there is a sudden change in the index $n$, the light passes through a region in which there exists a gradual change of index of refraction, as illustrated in Figure 15.25. In this case, there is a smooth turning of the light rays, with the angle through which the rays have been turned clearly dependent on the gradient of $n$, which, in turn, is dependent on the density gradient in the $y$ direction.

Next, we develop a relation between the *angular deflection of a wave front* and the density gradient. To develop this expression, consider a flow in the $z$ direction [as shown in Figure 15.26(a)] with a density gradient in the $y$ direction. As may be seen from the figure, light is passed in the $x$ direction. For this flow, it is assumed that the density gradually decreases with $y$, and since the index of refraction, $n$ (and therefore the density $\rho$), is inversely related to $c$, the local velocity of light for Ray 1 is slightly smaller than that for Ray 2.

The density variation causes a turning of the wave front, $\theta_2 - \theta_1 = \Delta\varepsilon$, which is an extremely small angle; hence, we may use the approximation $\sin(\theta_2 - \theta_1) \cong (\theta_2 - \theta_1)$.

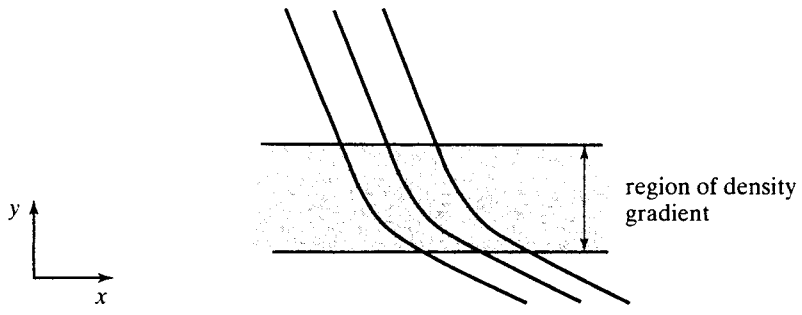


**Figure 15.25** Gradual Bending of Light Waves Passing Through a Fluid of Variable Density

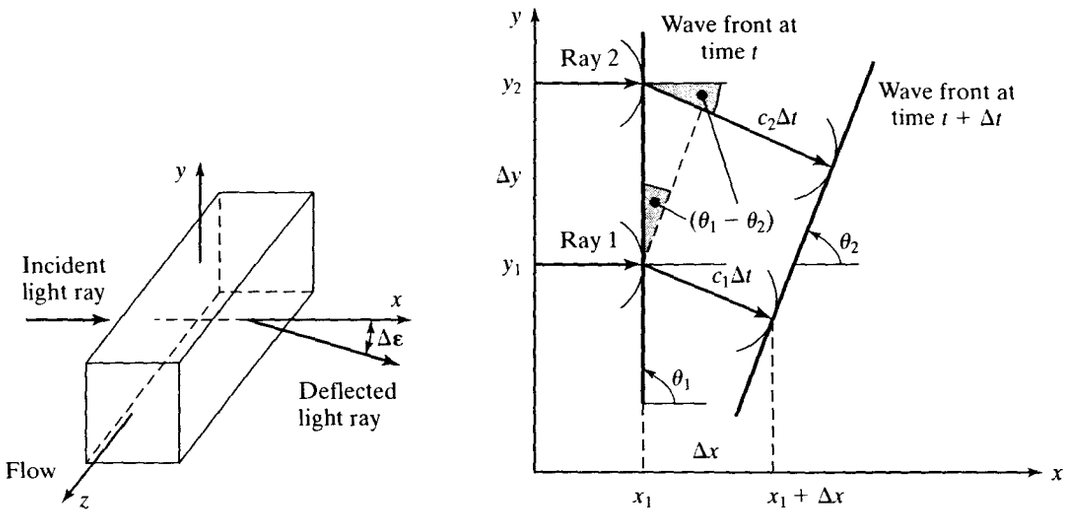


**Figure 15.26** Deflected Light Rays through a Fluid of Variable Density: Two-Dimensional Flow

Since the rays are always normal to the local wave front, the rays are also turned by this amount. Assume that the density changes are relatively small, so that the rays can be treated as straight lines. The local velocity of light for Ray 2 is $c_2 = c_0/n_2$, and the local velocity of light for Ray 1 is $c_1 = c_0/n_1$. The angular deflection of the wave front—that is, the small angle $\Delta\varepsilon$ through which the light rays are turned—is

$$\sin(\theta_1 - \theta_2) \cong (\theta_1 - \theta_2) \cong -\Delta\varepsilon = \frac{(c_2 - c_1)\Delta t}{\Delta y} = \frac{c_0\left(\frac{1}{n_2} - \frac{1}{n_1}\right)\Delta t}{\Delta y}$$

$$= -\frac{c_0}{n_2 n_1}\frac{(n_2 - n_1)}{\Delta y}\Delta t \tag{15.23}$$

where $\Delta t$ is the time interval required for the light rays to pass through the distance $\Delta x$. Now, from the geometry of Figure 15.26, we have

$$\Delta x = c_1 \Delta t \cos(\theta_1 - \theta_2) \cong c_1 \Delta t = \frac{c_0}{n_1}\Delta t$$

Thus,

$$n_1 \Delta x = c_0 \Delta t$$

Combining this expression with Eq. (15.23) yields

$$\Delta\varepsilon = \frac{1}{n_2}\frac{(n_2 - n_1)}{\Delta y}\Delta x$$

By allowing $\Delta x$ and $\Delta y$ to approach zero, the expression becomes

$$\frac{d\varepsilon}{dx} = \frac{1}{n}\frac{dn}{dy}$$

Finally, use of the Gladstone–Dale equation, Eq. (15.21), produces

$$\frac{d\varepsilon}{dx} = \frac{K}{n}\frac{d\rho}{dy}$$

This equation may be integrated to obtain an expression for the angle through which the light rays will be turned due to the density gradient in the transverse (in this case, $y$) direction:

$$\varepsilon_x = K\int \frac{1}{n}\frac{d\rho}{dy}dx \tag{15.24}$$

Because the index of refraction for gases is close to unity, the value of $n$ in the integrand is sometimes omitted. The important result is that the angular deflection of the light rays is dependent on the first derivative of the gas density in the direction normal to the light ray.

If the density $\rho$ is uniform in the test section, an entering light ray will not be deflected; if the gradient of the density, $\partial\rho/\partial y$, is uniform across the height of the test section, all rays passing through the section will be deflected through the same angle; if the curvature of the density, $\partial^2\rho/\partial y^2$, is uniform across the height of the test section, all rays passing through the section will diverge or converge uniformly; if the curvature of the density, $\partial^2\rho/\partial y^2$, is variable across the height of the test section, entering rays passing through the section can interfere with each other. The relative light intensity as sensed at a screen is proportional to the distance between the rays: It is brighter if the rays are close to each other and darker if they are separated. These cases are illustrated in Figure 15.27.

For a three-dimensional flow, the angular deflection is dependent on the density gradients in both the $x$ and $y$ directions. Consider light rays passing through a medium as illustrated in Figure 15.28. The light rays will be deflected by the disturbance in the field. For each light ray, three quantities may be recorded at a screen:

- the deflection angles of the light ray, $\varepsilon_x$ and $\varepsilon_y$, measured by a *Schlieren system*;
- the displacements $\Delta x$ and $\Delta y$ of the deflected light ray with respect to an undisturbed light beam, measured by a *shadowgraph instrument*;
- the difference in time between a deflected and an undisturbed light ray, measured by *optical interferometers*.

Having established a few basic optical principles, we are now in position to consider the Schlieren, shadowgraph, and interferometer systems individually.

## Schlieren System

Settles [see Ref. (15.24)] has presented the history of the Schlieren instrument, as well as a very detailed account of the system. Apparently, the origin of instrument dates back to the 17th century when Robert Hooke used a primitive form of the device `to

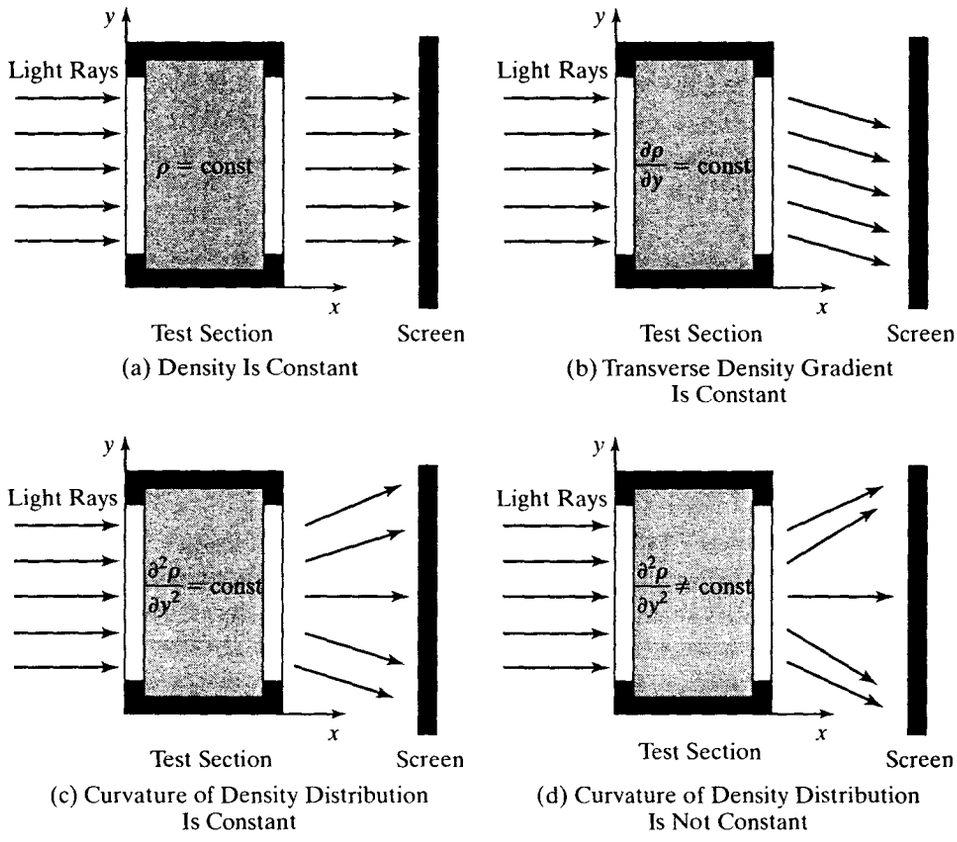


**Figure 15.27** Deflections of Light Rays in Media with Various Density Gradients

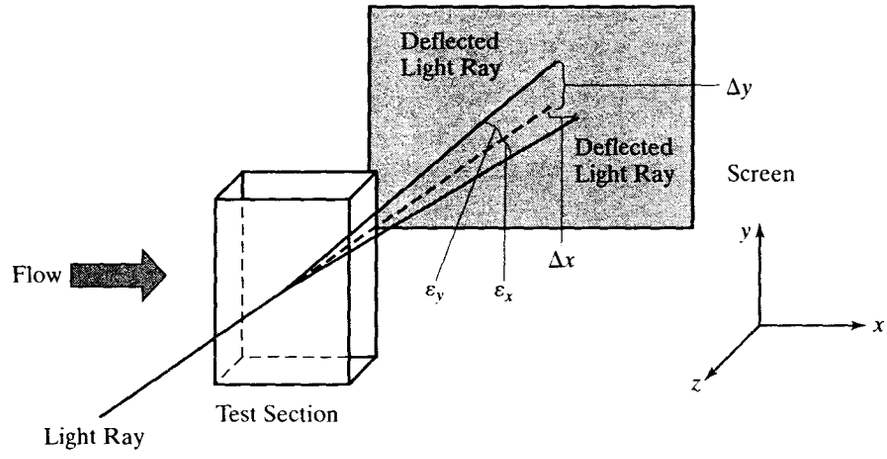


**Figure 15.28** Deflected Light Rays through a Three-Dimensional Flow of Variable Density

view thermal convection from a lighted candle. Some 200 years later, Toepler brought the instrument to a more practical and useful level. It should be noted that Schlieren is not the name of a person, but rather is derived from the German word for "streak." With the Schlieren system, we are able to visualize density variations (and therefore index-of-refraction variations) within a transparent medium. This visualization is possible by sensing the refraction of light rays as they pass through a region with a density-gradient distribution.

The Schlieren system has been used in supersonic/hypersonic flows. It is especially effective in visualizing shocks and expansion waves that do not possess large gradients in density. Another application is in subsonic flows, where the system can be used to visualize natural convection phenomena. In this application, the changes in the density are due to temperature gradients. Photographs from Schlieren systems can provide considerable detail about the flow field.

To understand the basics of the Schlieren technique, it helps to begin with a simplified system that uses a point light source (see Figure 15.29) and then proceed to a more practical system that uses an extended light source.

As shown in Figure 15.29, a first lens, labeled $L_1$, whose focal point coincides with the location of the source, *collimates* light from a point source. This lens provides parallel light beams through the test section. After passing through the test section, the rays are refocused by lens $L_2$. If a screen were located at the focal point of this second lens, it would contain the image of the light source. After passing through $L_2$, the light is then projected onto the screen or camera, providing an inverted image of the test section. In this form, the optical system is similar to a simple projector, imaging opaque objects within the test section as silhouettes onto the screen.

Now place the edge of a knife (an ordinary razor blade), identified as $K$, in the focal plane of $L_2$. The knife edge is such that it can be vertically raised or lowered or it can be rotated to another position. If in the vertical position, $K$ is raised too far, it will obstruct all the light, and the screen will be dark. Instead, imagine that $K$ obstructs approximately half of the incident light. In this way, the image of the test section on the screen will be darker than it would be without the presence of $K$, but still uniformly illuminated.

Suppose that gas flows through the test section (say, out of the plane of the paper) such that there is a density disturbance at the center of the section. As we have seen, transverse density gradients cause the light rays to be bent from their original paths;

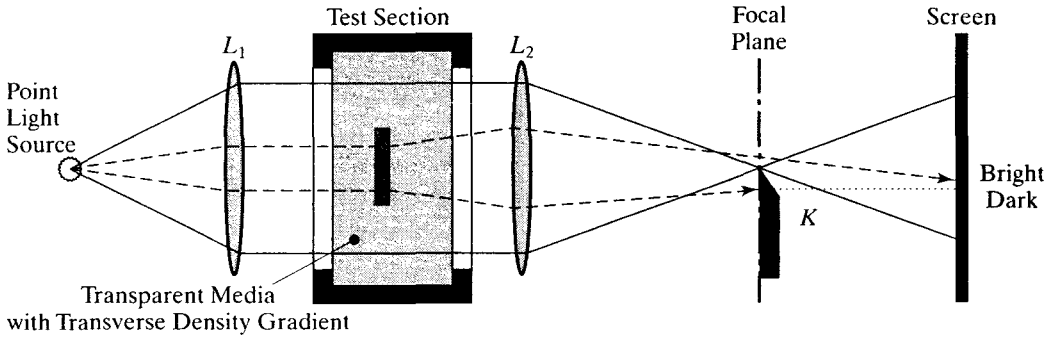


**Figure 15.29** Basic Schlieren System with a Point Light Source

however, the lens $L_2$ focuses the rays from each point in the test section to a corresponding point on the screen. Two rays are shown as dashed lines in Figure 15.29. The ray deflected upward passes over $K$ and therefore brightens a point on the screen, while the ray deflected downward is obstructed by $K$ and results in an image that is darker than before, but still uniformly illuminated. Thus, the phenomenon within the test section, which could not be seen by the naked eye, becomes visible on a screen by converting angular difference, caused by the density gradient in the test section, into an intensity difference.

A *Schlieren* system with an extended light source, such as light from a rectangular slit or from a filament, is shown in Figure 15.30. As may be seen by comparison with Figure 15.29, the pattern of light rays is more complicated. Nonetheless, similarities between the two configurations may be observed. Light from the source, labeled $ab$, is collimated by lens $L_1$, providing a parallel light beam through the test section. Two extreme light rays from $a$ and $b$ are shown in Figure 15.30, rays from each point passing parallel through the test section. After passing through the test section, the rays are focused by lens $L_2$ at $a'b'$, which is an inverted image of the light source. The light is then focused onto the screen or photographic plate by lens $L_3$, providing a uniformly illuminated, but inverted, image of the test section. By placing a knife edge $K$ in the $L_2$ focal plane and letting the knife edge obstruct approximately half the incident light, the image of the test section on the screen will be darker than before, but still uniformly illuminated. Let there be a transverse density gradient in the test section in the plane of $r$ (at the same $y$ coordinate as $r$). In this case, the rays from $r$ will be deflected so that, for example, a ray shown with a dotted line will be turned downward. Now, as seen previously, this ray is intercepted by the knife edge, so the image of $r$ on the screen will be darker than the rest of the image of the test section. If the density gradient had the opposite sign, the rays from $r$ would be bent upward, so some rays that had been obstructed by the knife edge would now pass over it and give a brighter image of $r$ on the screen. Thus, it must be emphasized that the Schlieren system, unlike the shadowgraph and interferometer devices, involves the visualization of density gradients (in this case, $\partial\rho/\partial y$) in a flow.

Figure 15.31 shows images of the extended light source at the knife edge. Two views are shown: one in which there is no disturbance in the test section (the basic image) and another in which a disturbance causes some of the light to be deflected (the

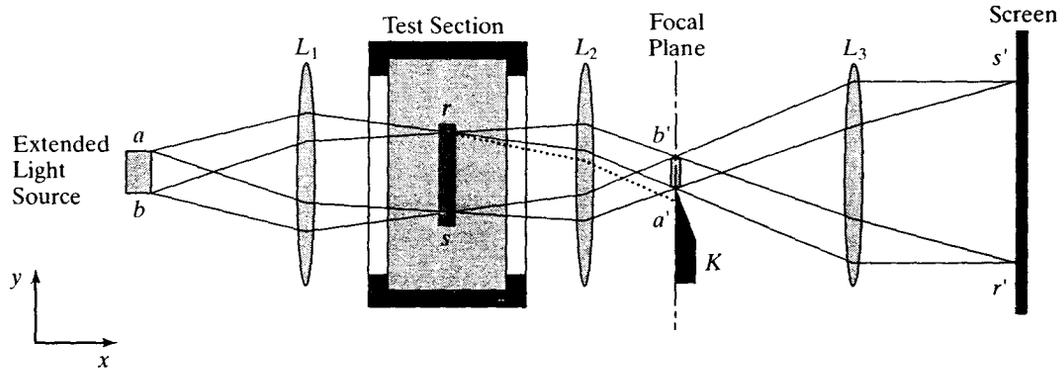


**Figure 15.30** Schlieren System with an Extended Light Source

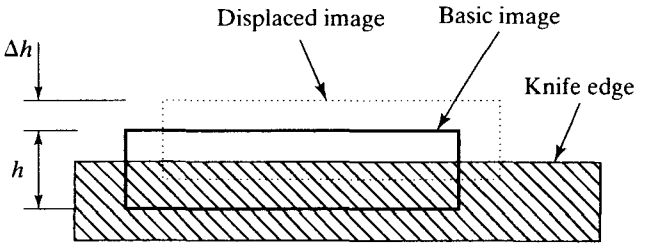


**Figure 15.31** Displacement of the Light Source Image at the Knife Edge

displaced image). Light rays in the latter case are shifted vertically and horizontally because of the density gradients in those directions.

As indicated in Ref. (15.25), the *relative displacement* $\Delta h/h$ can be equated to the *relative change in light intensity*, $\Delta I/I$, or *contrast*:

$$\frac{\Delta I}{I} = \frac{\Delta h}{h}$$

Since the knife edge is located at the focal point of $L_2$, this distance (along the $x$-axis between $L_2$ and $K$) is labeled $f_2$. The expression for the displacement of a light beam at the knife edge is $\Delta h = f_2 \tan \varepsilon_x \cong f_2 \varepsilon_x$. Hence, the foregoing expression, with the aid of Eq. (15.24), yields

$$\frac{\Delta I}{I} = \frac{\Delta h}{h} \cong \frac{f_2}{h}\varepsilon_x = \frac{K f_2}{h}\int \frac{1}{n}\frac{\partial \rho}{\partial y}dx$$

Since the index of refraction for gases is very nearly unity, the foregoing equation becomes

$$\frac{\Delta I}{I} = \frac{K f_2}{h}\int \frac{\partial \rho}{\partial y}dx \tag{15.25}$$

So, we see that the contrast at the screen for the Schlieren system depends upon the first derivative of the density in the direction normal to the path of the light ray.

In actual practice, it is found beneficial to use mirrors, which are less expensive than lenses, especially if the test section is large. A classical Schlieren system using concave mirrors is presented in Figure 15.32. The light source and the knife edge $K$ must be in the same plane and on opposite sides of the axis of the mirrors, in a "Z" arrangement. The angles between the light source and the mirrors' axis and between the screen and the mirrors' axis must be equal. The light from the source falls on the first mirror $M_1$ and then is projected, as parallel light rays, through the test section onto the second mirror $M_2$. The knife edge $K$ is placed at the focal plane of the mirror $M_2$. If there is flow (out of the plane of the paper), some of the light rays will be deflected toward, or away from, $K$, and the resulting image on the screen will be a Schlieren image.

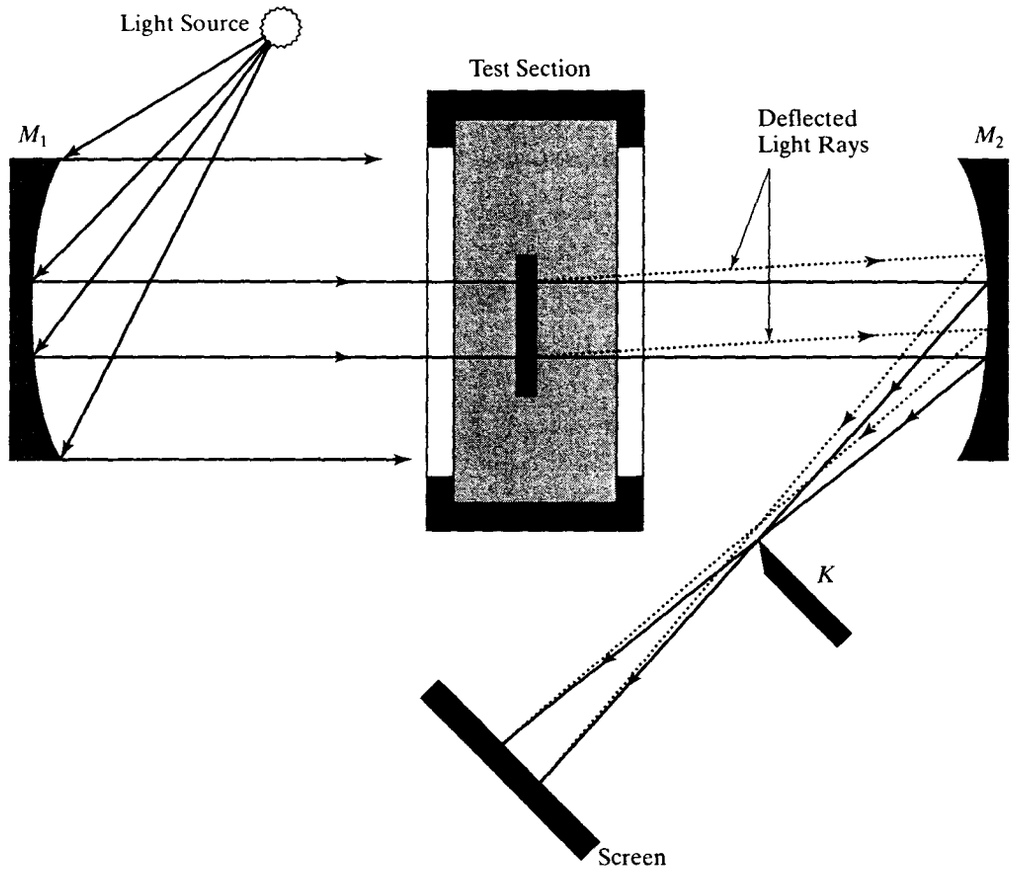


**Figure 15.32** A Schlieren System with Mirrors

It should be noted that there are improved versions of the Schlieren optical system. For example, there are color Schlieren systems that use a colored bull's-eye filter instead of a knife edge. In this case, the deflection of the light beam gives rise to a spectrum of colors on the screen, the colors being related to the angle of deflection and thus to the density gradient. Furthermore, a large Schlieren system [see Ref. (15.25)] has been constructed that is capable of visualizing full-scale objects (e.g., vehicles, equipment, and people). Description of these systems, as well as more details on the fundamentals of optics, can be found in Refs. (15.24) and (15.26)–(15.28).

### The Shadowgraph Instrument

The use of a shadowgraph, another technique to visualize flow fields, was first initiated by Dvorak (a coworker of Mach) in 1880. This method is suitable for use in flows with large, sudden changes in density, such as flows across strong shockwaves. The shadowgraph is the simplest and the least expensive of the three methods considered herein. The basic system is presented in Figure 15.33. Parallel light beams pass through the test section and illuminate the screen. Without flow in the test area, the screen is uniformly illuminated. When there is flow in the test section, the light rays will be deflected because of the density gradient, and therefore dark and light spots will appear on the

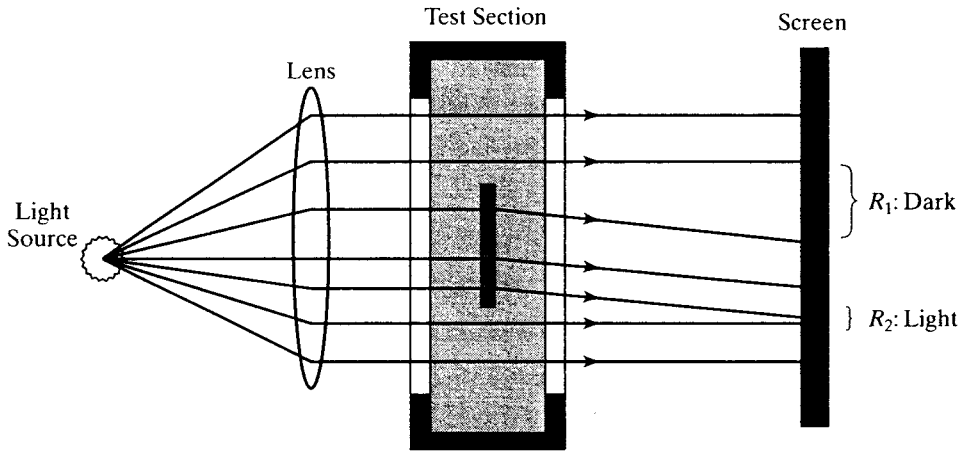


**Figure 15.33** Basic Shadowgraph System

screen, creating shadow patterns. (Therefore, the image on the screen is called a shadowgraph.) In region $R_1$, the light rays have diverged, so there is a decrease in illumination on the screen. In region $R_2$, the rays have converged, so there is an increase in illumination.

Let us consider two parallel light rays separated by a distance $\Delta y$, as shown in Figure 15.34. Without flow, the light rays pass through the test section undisturbed, and the illumination on the screen is uniform. If there is flow in the test section, which results in a density gradient in the $y$ direction, the two light rays are refracted at very small angles $\varepsilon$ and $\varepsilon + \Delta\varepsilon$. The ratio of intensity at the screen, $I_{scr}$, to the intensity at the disturbance, $I_{ts}$, is given as follows [see Ref. (15.26)]:

$$\frac{I_{scr}}{I_{ts}} = \frac{\Delta y}{\Delta y_{scr}}$$

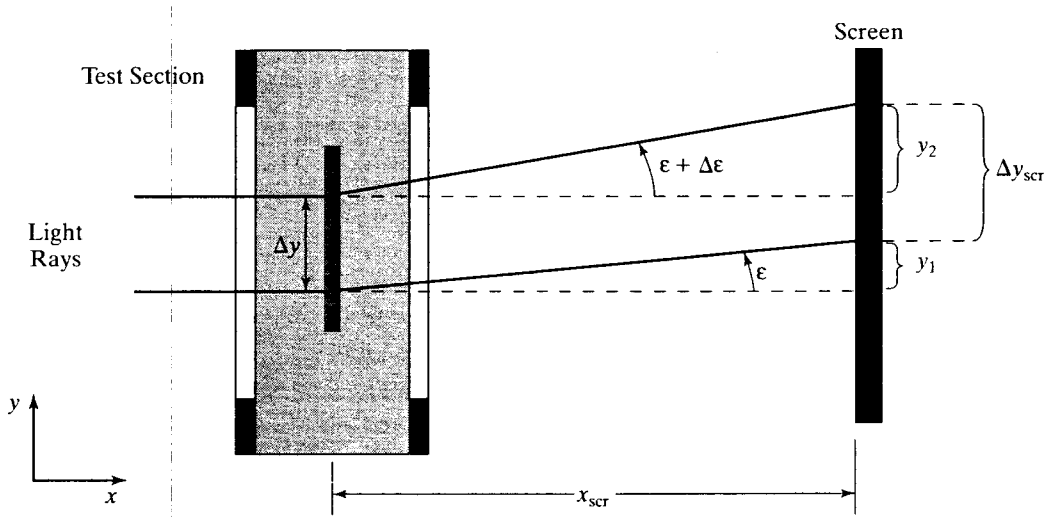


**Figure 15.34** Light Ray Refraction Using the Shadowgraph

Note that the larger the value of $\Delta y_{scr}$, the smaller is the value of the intensity at the screen.

The contrast is expressed as the ratio of the difference in the intensities to the initial intensity [see Ref. (15.26)]:

$$\frac{I_{scr} - I_{ts}}{I_{ts}} = \frac{\Delta I}{I_{ts}} = \frac{\Delta y}{\Delta y_{scr}} - 1$$

From Figure 15.34, it is seen that $\Delta y_{scr} = y_2 + (\Delta y - y_1)$. Furthermore, for small angles, $y_1 = x_{scr} \tan \varepsilon \cong x_{scr}\varepsilon$ and $y_2 = x_{scr} \tan(\varepsilon + \Delta\varepsilon) \cong x_{scr}(\varepsilon + \Delta\varepsilon)$. Thus, the foregoing equation becomes

$$\frac{\Delta I}{I_{ts}} = \frac{\Delta y}{\Delta y_{scr}} - 1 \cong \frac{\Delta y}{\Delta y + x_{scr}\Delta\varepsilon} - 1 = -\frac{x_{scr}\Delta\varepsilon}{\Delta y + x_{scr}\Delta\varepsilon} = -\frac{x_{scr}\dfrac{\Delta\varepsilon}{\Delta y}}{1 + x_{scr}\dfrac{\Delta\varepsilon}{\Delta y}} \cong -x_{scr}\frac{\Delta\varepsilon}{\Delta y}$$

Taking the limit as $\Delta y \to 0$ and utilizing Eq. (15.24) produces

$$\frac{\Delta I}{I_{ts}} = -K x_{scr} \int \frac{\partial^2 \rho}{\partial y^2} dx \tag{15.26}$$

Hence, the screen illumination is related to the second derivative of the density. If there is a uniform density gradient in the test section, all the light rays will be deflected with the same angle, and therefore the screen will be evenly illuminated. The shadowgraph, indicating the second derivative of density, is more suitable for use in flows with

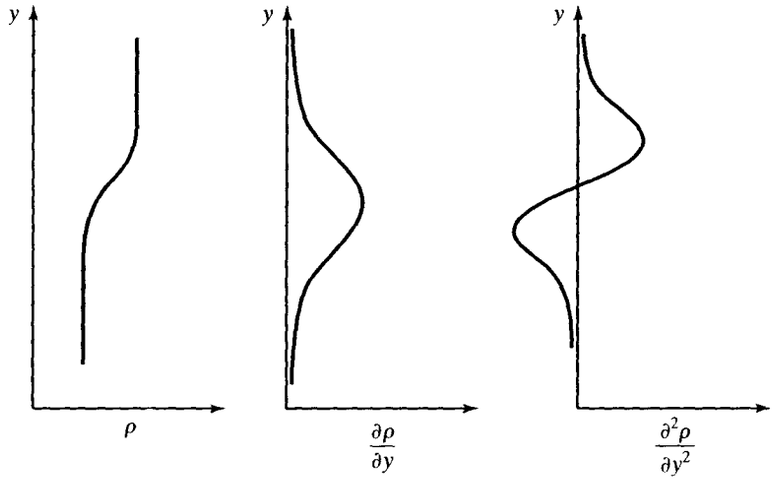


**Figure 15.35** Distributions of Density and First and Second Density Derivatives across a Shockwave

large, sudden changes in density, such as strong shockwaves. For flows with slowly varying density, the Schlieren system is a better choice.

By using a shadowgraph, a shockwave can be seen on a screen as a dark region followed by a bright region. To better understand this aspect, it should be noted that if light rays diverge, illumination will be decreased (refer to Figure 15.33), which occurs when $\partial\varepsilon/\partial y > 0$ [i.e., from Eq. (15.26), when $\partial^2\rho/\partial y^2$ is positive]. On the other hand, if light rays converge, illumination will be increased, which occurs when $\partial\varepsilon/\partial y < 0$ (i.e., when $\partial^2\rho/\partial y^2$ is negative). Figure 15.35 presents the density variation across a shock, as well as the distributions of its first and second derivatives.

Alternative shadowgraph instruments, based on the same principle described previously, are used in practice. Two types are shown in Figure 15.36: one that uses a point light source without any lens or mirrors and another with a concave mirror to create a parallel beam of light.

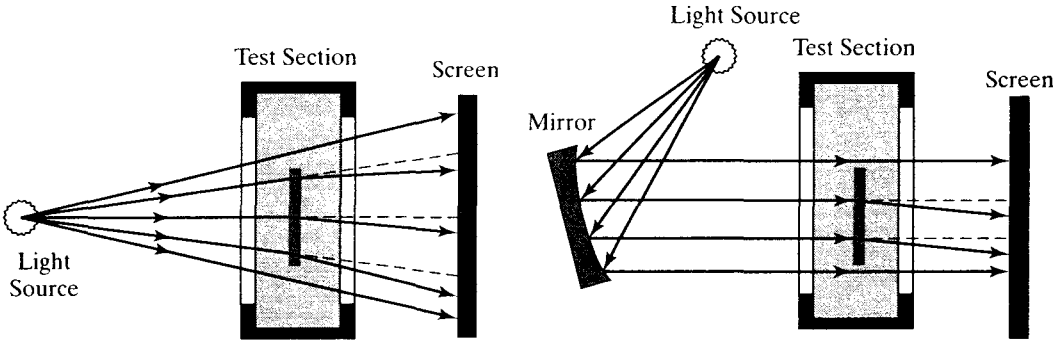


(a) Shadowgraph without Lens or Mirror (b) Shadowgraph with Mirror

**Figure 15.36** Types of Shadowgraph

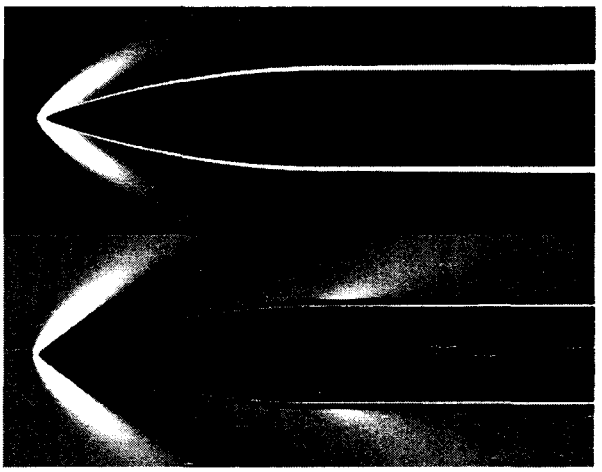

**Figure 15.37** Simulated Schlieren (top) and shadowgraph (bottom) of the CFD results of a Mach 2 flow around a missile-shaped body [http://www.tecplot.com/showcase/contours/issue_10/article02.htm]

Today, many postprocessing programs allow the simulation of the Schlieren (density gradient) or the shadowgraph (the Laplacian of the density) representations of the numerical results obtained after running computational fluid dynamic (CFD) codes. Figure 15.37 shows the simulated experimental results of a missile-shaped object at Mach 2. The top portion is a simulated Schlieren image, made from contours of the density gradient. The bottom is a simulated shadowgraph, made from contours of the Laplacian of the density, using the commercial CFD analyzer Tecplot 3.0.

**Historical Note: Ernst Waldfried Josef Wenzel Mach** (1838–1916) was born in Chirlitz–Turas, Moravia (Chirlice–Turany, Czech Republic), near Brünn (Brno), in the Austro–Hungarian empire. Except for one year, Ernst Mach was home educated until age 14 by his father, who raised silkworms. At age 15, he entered the public gymnasium, and, at age 17, he entered the University of Vienna to study mathematics, philosophy, and physics. He received a doctorate in physics in 1860; his thesis was titled, "On electrical charge and induction." From 1860 to 1862, he worked in his mentor's laboratory and derived income from popular scientific lectures on optics, musical acoustics, and psychophysics. Having declined a professorship in surgery at Salzburg, Mach accepted a full professorship in mathematics at the University of Graz in 1864 and became a professor of physics in 1866. In 1867, he left Graz to become professor of experimental physics at Prague.

In 1887, Mach presented the paper "Photographische Fixierung der durch Projektile in der Luft eingeleiteten Vorgänge" ("Photographic Record of Processes Induced by Projectiles in Air"). To Mach, no statement in science was admissible unless it was empirically verifiable. Mach and Dr. P. Salcher (1848–1928), professor of physics at the Imperial Royal Naval Academy in Rijeka, used a shadowgraph arrangement developed by Salcher by which invisible shockwaves were made visible. In the aforementioned paper, Mach showed a photograph of a bullet moving supersonically (shown in the accompanying photograph). This historic photo allowed scientists, for the first time, to actually see a shockwave. Yet Mach's contributions to supersonic aerodynamics were not limited to experimental methods. He was also the first physicist to understand the basic characteristics of supersonic flow. He was also the first to note

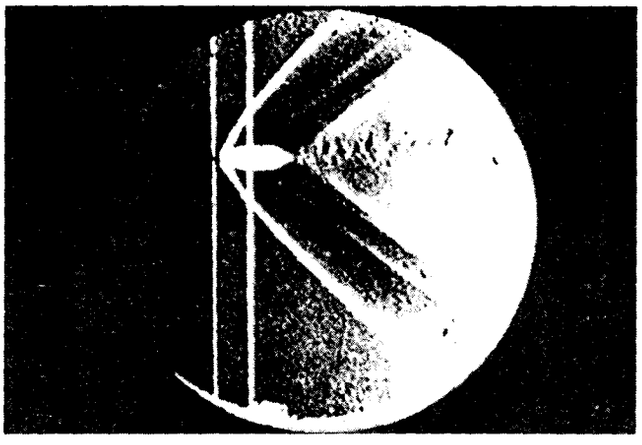

**Ernst Mach's photo of a bullet in supersonic flight**
This photograph demonstrates the strong shockwave formed by the nose of the bullet, the weaker shockwave created at the aft end of the bullet, and the turbulent wake downstream of the bullet's base. Also visible in the photo are two vertical lines made by the trip wires that triggered the camera as the projectile passed by.

*(Continued)*

*(Continued)*

the sudden and discontinuous changes in the airflow behavior when the flow went from subsonic to supersonic.

Mach returned to the University of Vienna as professor of inductive philosophy in 1895. In 1898, he suffered a stroke and retired from active research in 1901. In 1913, he moved to Vaterstetten to be with his son Ludwig, a medical doctor who became his father's devoted assistant. Mach's criteria of verifiability led him to reject Newton's concepts of absolute time and space and prepared the way for Einstein's relativity theory. His studies also included physical optics, the history of science, mechanics, philosophy, physiology, thermodynamics, the sugar cycle in grapes, the physics of music, classical literature, and epistemology (the study of knowledge).

Mach died on February 19, 1916, in Vaterstetten, near Munich, Germany. [Refs. (15.29) and (15.30)]

## The Interferometer

The *interferometer*, invented about 150 years ago, is an optical instrument that is used to perform measurements by utilizing wave properties of light. The interferometer operates by dividing a light beam into two or more parts, which then travel along different paths until they are recombined to form an *interference fringe pattern*. Interference phenomena are commonly encountered when observing the colors within a soap bubble or on the surface of an oil slick. Interference is also observed in the thin film of air captured between two flat glass surfaces that are brought into contact. Description of the observed pattern, called *Newton's rings*, dates back to the 17th century. A variety of interferometers are used in practice, including the Fizeau interferometer, the Twyman–Green interferometer, the Fabry–Perot interferometer, and others, descriptions of which may be found in Refs. (15.31)–(15.33).

The *Mach–Zehnder interferometer*, shown in Figure 15.38, has been widely used to study flows in wind tunnels and shock tubes. It has also been employed to experimentally study natural convection heat transfer.

The instrument consists of two adjustable mirrors $M_1$ and $M_2$ and two splitter plates $SP_1$ and $SP_2$, usually positioned in the corners of a rectangle. The splitter plates

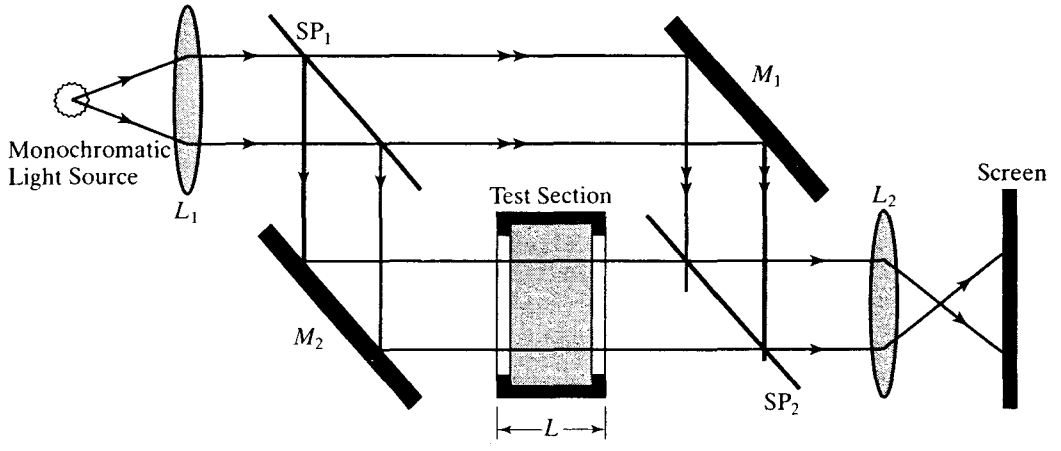


**Figure 15.38** Mach–Zehnder Interferometer

(half-silvered mirrors) reflect about one half the incident light and transmit the rest. A light beam, from a *monochromatic* (single-frequency) light source, can take two possible paths to reach the screen. The system is arranged so that the optical path lengths (*optical path length* is the product of the geometric distance traveled and the index of refraction) of the two legs are as equal as possible.

One path, marked with double arrows, is that of the *reference beam*. Along this path, the light beam is transmitted, without phase change, through splitter plate $SP_1$. The light beam is then reflected by the first mirror, $M_1$, which causes a phase change of one half of a wavelength. The beam is then reflected again by splitter plate $SP_2$, where the phase is further changed by one half of a wavelength. From the second splitter plate, the light ray is projected, after passing through the second lens, $L_2$, onto the screen.

The second path, marked with single arrows, is that of the *test beam*, which passes through the test section. Along this path, the light beam is first reflected by splitter plate $SP_1$ and experiences a phase change of one half of a wavelength. The beam is then reflected by the second mirror, $M_2$, and has an additional phase change of one half of a wavelength. From $M_2$, the light ray is transmitted without phase change through splitter plate $SP_2$. From there, the test light beam follows a similar course to reach the screen as that of the reference beam.

If the light waves on each path arrive at the screen in phase, they will reinforce one another (*constructive interference*) and in turn brighten the screen. If the waves are one half of a wavelength out of phase, they will cancel one another (*destructive interference*) and the screen will be dark.

With no flow through the test section, the geometry of the system may be arranged to yield a regular, uniform pattern of *fringes* that are seen as alternating bands of parallel dark and light stripes. If there is flow and the density changes within the test section, the speed with which the light rays traverse the path of the test beam is altered, and a distorted fringe pattern emerges. By increasing the density of the test section, the effective optical path of the test beam is increased, and therefore the time for the light beam to traverse the path through the test section is increased by an amount

$$\Delta t = \frac{L}{c_f} - \frac{L}{c_{\text{nf}}} = \frac{L}{c_0}(n_f - n_{\text{nf}})$$

where $L$ is the width of the test section and $c_{\text{nf}}$, $c_f$, and $c_0$ are the respective velocities of light through the test section with no flow, with flow, and through a vacuum. Thus, there is an effective increase in the optical path of the amount $\Delta L = c_0 \Delta t$. This difference in optical-path length produces, in turn, $N$ fringe shifts for the monochromatic light. In essence, the fringes of an interferometer measure the difference in the optical-path length in units of wavelength; that is,

$$N = \frac{\Delta L}{\lambda} = \frac{L}{\lambda}(n_f - n_{\text{nf}}) \tag{15.27}$$

where $\lambda$ is the wavelength of light. Combining the Gladstone–Dale equation, Eq. (15.21), with Eq. (15.27) yields an expression for the density of flow within the test section:

$$\rho_f = \rho_{\text{nf}} + \frac{N\lambda}{LK} \tag{15.28}$$

**TABLE 15.4** Comparison of the Shadowgraph, the Schlieren, and the Interferometer

| Shadowgraph | Schlieren | Interferometer |
|---|---|---|
| • Measures $\partial^2\rho/\partial y^2$ | • Measures $\partial\rho/\partial y$ | • Measures $\rho$ |
| • Easy to operate | • Easy to operate | • Is difficult to set up |
| • Displays shadows | • Displays a focused image | • Displays sharp images |
| • Is precise | • Has good precision | • Is the most precise system |
| • Is suitable for use in flows with large, sudden changes in density (strong shockwaves) | • Is suitable for use in flows with changes in density (shocks or expansion waves) or to visualize convection phenomena | • Is suitable for use in flows in wind tunnels, mixing regions, and boundary layers |

Thus, the density at different points throughout the test section can be determined by counting the number of fringe shifts from the reference (no flow) condition. These fringes, which are photographically recorded (the photo is called an *interferogram*), are useful for both qualitative flow-field visualization and quantitative studies of shockwaves, mixing regions, boundary layers, and heat transfer. The desire for a monochromatic, small, *coherent* (single-source) light source makes a laser suitable for application with the interferometer. Also, a compensatory section is often inserted into the path of the reference beam during the setup. Greater detail regarding the interferometer can be found in Refs. (15.26), (15.27), and (15.31)–(15.33).

Table 15.4 provides a brief summary of important features of the three optical systems considered in this section.

## 15.6 FLOW RATE MEASUREMENT

*Flow rate* is a fundamental parameter in gas dynamics; its measurement is therefore of considerable importance. Flow rate measurements fall into two categories: mass flow rate and volume flow rate. There are numerous devices and techniques available for flow rate measurement. Some of these devices can be used only for liquids (such as for weighing a liquid), whereas others can be used for both liquids and gases. Figure 15.39 diagrams a sampling of various flow rate measuring devices.

Each fluid flow measurement device consists of two main parts: the *primary element* and the *secondary element.* The primary element is in contact with fluid and interacts with the fluid to produce a measurable signal. The associated secondary part converts the signal(s) produced by the primary part into a quantity that is observable by the user. Orifice plates and turbine rotors are two common primary elements. Manometers and electromagnetic devices have been used as secondary elements. The electromagnetic device senses the number of rotations of the turbine blades within a specific period of time (e.g., rpm) and can then easily convert this value to a flow rate.

Because of their widespread application, simplicity, low cost, and limited maintenance requirements, two *differential pressure meters* will be considered here: the Venturi meter and the orifice plate.

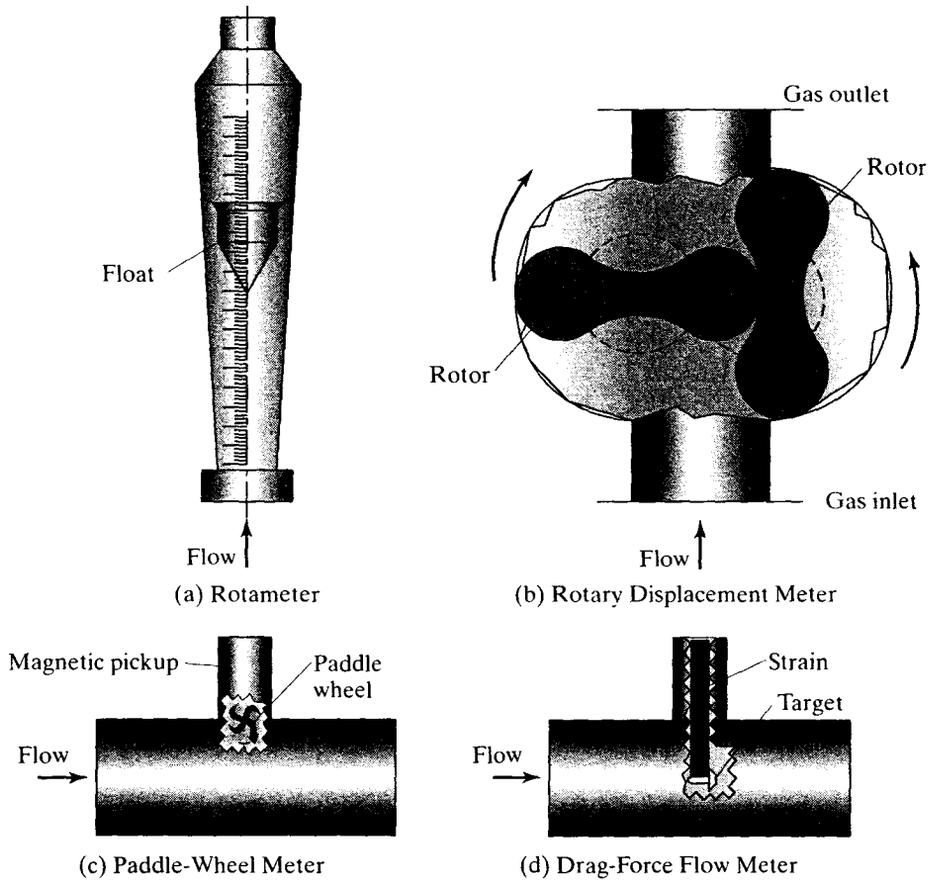


**Figure 15.39** Four Types of Flow Rate Meters

The *Venturi tube* (see Figure 15.40) is regarded as one of the oldest types of differential flow rate measurement devices. It was actually invented by Clemens Herschel in 1898 [see Ref. (15.34)]; the name of the device derives from the practice in those days of calling the pressure at the throat the "Venturi," after the Italian physicist Giovanni Venturi, who experimentally studied water flow through a converging–diverging pipe section. Herschel decided to retain this name for the device.

A Venturi meter is essentially an instrumented converging–diverging nozzle. The volume flow rate ($\dot{m}/\rho = VA$) can be simply determined from the flow velocity and the area of the cross-section. Of course, this approach presumes that the flow velocity in a flow cross-section has a single value. (The average value is required.) A Pitot–static tube can be used for this purpose.

To develop an expression for the mass flow rate, begin by applying the law of conservation of mass to the control volume shown in Figure 15.40:

$$\dot{m} = \rho_{th} V_{th} A_{th} = \rho_1 V_1 A_1 \tag{15.29}$$

For steady, one-dimensional flow, the momentum equation can be written as

$$V dV = -\frac{dp}{\rho} \tag{15.30}$$

For isentropic flow of an ideal gas, we have

$$\frac{p}{\rho^{\gamma}} = \text{constant} \tag{15.31}$$

Using Eq. (15.31), we may integrate Eq. (15.30) between an upstream point 1 and the throat th to produce

$$V_{\text{th}}^2 - V_1^2 = \frac{2\gamma}{\gamma - 1}\left(\frac{p_1}{\rho_1} - \frac{p_{\text{th}}}{\rho_{\text{th}}}\right) \tag{15.32}$$

An expression for the velocity at the throat can be obtained by using the continuity equation to eliminate $V_1$ from Eq. (15.32):

$$V_{\text{th}}^2 = \frac{\dfrac{2\gamma}{\gamma - 1}\left(\dfrac{p_1}{\rho_1} - \dfrac{p_{\text{th}}}{\rho_{\text{th}}}\right)}{1 - \left(\dfrac{\rho_{\text{th}} A_{\text{th}}}{\rho_1 A_1}\right)^2}$$

Finally, the continuity and the isentropic relations at the throat are applied to get

$$\dot{m} = \frac{A_{\text{th}}\sqrt{\dfrac{2\gamma\rho_1 p_1}{\gamma - 1}\left[\left(\dfrac{p_{\text{th}}}{p_1}\right)^{2/\gamma} - \left(\dfrac{p_{\text{th}}}{p_1}\right)^{(\gamma+1)/\gamma}\right]}}{\sqrt{1 - \left(\dfrac{A_{\text{th}}}{A_1}\right)^2\left(\dfrac{p_{\text{th}}}{p_1}\right)^{2/\gamma}}} \tag{15.33}$$

This equation provides the theoretical value of the mass flow rate of a compressible fluid. Note that static pressures must be measured at the throat and at another point upstream of the nozzle. Also the density must be available at the upstream location.

To obtain the actual flow, multiply Eq. (15.33) by an appropriate *discharge coefficient* $C_d$. Accordingly, the discharge coefficient is defined as the ratio of the actual mass-flow rate to the theoretical mass-flow rate. The discharge coefficient is a function of the geometry and the Reynolds number. For the Venturi tube, $C_d$ is close to unity, typically 0.95.

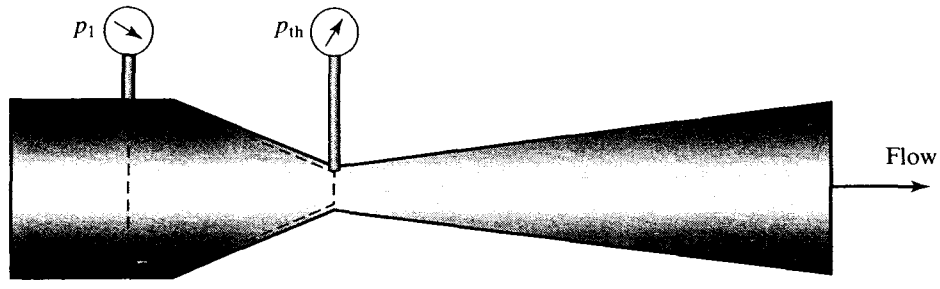


**Figure 15.40** Venturi Tube

Because of its geometry, a well-designed Venturi tube causes a very small pressure drop in the flow. Its disadvantages are its cost and size.

One of the most common, and perhaps the best known, differential pressure meters is the *orifice meter*. [See Ref. (15.35).] Figure 15.41(a) is a sketch of an orifice plate in a pipe. Figure 15.41(b) shows two common profiles of an orifice plate: the *sharp-edged orifice* and the *quadrant-edged orifice*. The orifice plate should be thin, and the profile and dimensions should be precise. Because of its simplicity and low cost of manufacturing, the sharp-edged orifice is widely used for flow metering.

Brower et al. [Ref. (15.36)] presented a novel approach for analyzing compressible flow of a perfect gas through an orifice. An idealized geometry is shown in Figure 15.42. As may be observed, the gas flow cannot follow the solid surface; instead, the flow separates from the orifice plate's edge to form a free jet. The static pressure on the boundary of the jet is equal to the static pressure of the surrounding gas. The area of this jet reaches a minimum at a distance equal to few pipe diameters downstream of the orifice (the *vena contracta*). The mass-flow rate can be determined using flow parameters at cross-section 4:

$$\dot{m} = \rho_4 V_4 A_4 = \frac{\rho_4}{\rho_o}\frac{V_4}{a_4}\frac{a_4}{a_o}\rho_o a_o A_4 \tag{15.34}$$

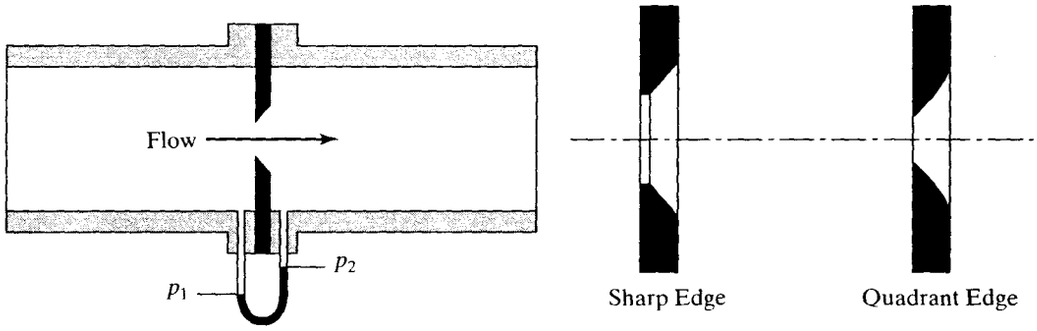


(a) Instrumented Orifice Plate in Pipe (b) Two Styles of Orifice Profiles

**Figure 15.41** Orifice Plate Arrangement and Two Plate Geometries

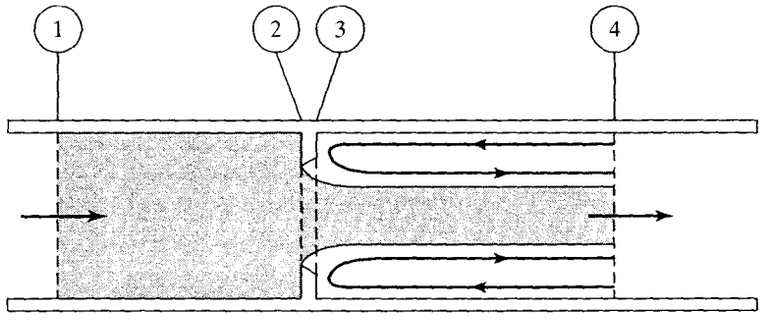


**Figure 15.42** Flow through an Orifice Plate

Assuming isentropic flow of an ideal gas, we have

$$\frac{\rho_4}{\rho_o} = \left(\frac{p_4}{p_o}\right)^{1/\gamma} = \left(\frac{a_4}{a_o}\right)^{2/(\gamma-1)} \tag{15.35}$$

or

$$\frac{\rho_4}{\rho_o}\frac{a_4}{a_o} = \left(\frac{p_4}{p_o}\right)^{(\gamma-1)/2\gamma} \tag{15.36}$$

Also, the conservation of energy gives

$$a_o^2 = a_4^2 + \frac{\gamma - 1}{2}V_4^2 \tag{15.37}$$

Combining Eqs. (15.35) and (15.37), we obtain

$$M_4 = \frac{V_4}{a_4} = \sqrt{\frac{2}{\gamma - 1}\left[\left(\frac{p_o}{p_4}\right)^{(\gamma-1)/\gamma} - 1\right]} \tag{15.38}$$

Substituting Eqs. (15.36) and (15.38) into Eq. (15.34) produces the following expression for the theoretical mass flow:

$$\dot{m} = \rho_4 V_4 A_4 = \rho_o a_o A_4 \sqrt{\frac{2}{\gamma - 1}\left(\frac{p_4}{p_o}\right)^{2/\gamma}\left[\left(\frac{p_o}{p_4}\right)^{(\gamma-1)/\gamma} - 1\right]} \tag{15.39}$$

Therefore, to calculate the mass-flow rate, $p_4$, $p_o$, $\rho_o$, $a_o$, and $A_4$ must all be known. The static pressure at location 4 can be easily obtained experimentally. Further, by using the ideal-gas law, $p = \rho RT$, and the speed-of-sound equation at stagnation conditions, $a_o = \sqrt{\gamma RT_o}$, we are able to form the following product:

$$\rho_o a_o = \frac{p_o}{RT_o}\sqrt{\gamma RT_o} = p_o\sqrt{\frac{\gamma}{RT_o}} \tag{15.40}$$

Because $p_o$ and $T_o$ can be measured directly, Eq. (15.40) can be easily calculated. The ratio of the minimum area $A_4$ to the area of the orifice $A_2$ is the contraction coefficient of the jet. Unfortunately, to date, there is no closed-form, theoretically based expression available for the contraction coefficient of a compressible axisymmetric jet. However, in 1937, Busemann [see Ref. (15.36)] used the hodograph method (briefly described in Section 12.3) to obtain the following relation for the contraction coefficient of a compressible free jet for two-dimensional planar flow:

$$\frac{A_4}{A_2} = \frac{\pi}{\pi + 2\dfrac{\rho_4}{\rho_o}} \tag{15.41}$$

The one dimensionality of the flow at cross-section 4 is reached (theoretically) infinitely far downstream of the orifice. Equation (15.41) is valid only in the limit of an infinite upstream plenum ($A_2/A_1 \to 0$). Moreover, it is limited to subcritical flow—i.e., $M_4 \leq 1$.

Lacking an analytical expression for the axisymmetric case, Brower et al. [Ref. (15.36)] used the planar-flow relation as a surrogate. To justify this approach, they first considered the incompressible flow case. For that situation, Eq. (15.41) gives

$$\lim_{(p_4/p_o)\to 1} \frac{A_4}{A_2} = \frac{\pi}{\pi + 2} = 0.6110 \tag{15.42}$$

Bloch [Ref. (15.37)] numerically investigated the incompressible, axisymmetric flow case and found that

$$\frac{A_4}{A_2} = 0.59135 \pm 0.00004 \tag{15.43}$$

As can be seen, for an incompressible jet, the axisymmetric value of $A_4/A_2$ in Eq. (15.43) is only 3 percent smaller than the planar flow value of Eq. (15.42). Accordingly, it was surmised that the same idea could be applied to the compressible jet of an orifice flow meter. By combining Eqs. (15.39) and (15.41), the following is obtained:

$$\dot{m} = \frac{\sqrt{\dfrac{2}{\gamma - 1}\left(\dfrac{p_4}{p_o}\right)^{2/\gamma}\left[\left(\dfrac{p_o}{p_4}\right)^{(\gamma-1)/\gamma} - 1\right]}}{1 + \dfrac{2}{\pi}\left(\dfrac{p_4}{p_o}\right)^{1/\gamma}} \rho_o a_o A_2 \tag{15.44}$$

Substituting Eq. (15.40) into Eq. (15.44), we produce an expression for the theoretical mass-flow rate that is based on direct measurements:

$$\dot{m} = \frac{\sqrt{\dfrac{2\gamma RT_o}{\gamma - 1}\left(\dfrac{p_4}{p_o}\right)^{2/\gamma}\left[\left(\dfrac{p_o}{p_4}\right)^{(\gamma-1)/\gamma} - 1\right]}}{1 + \dfrac{2}{\pi}\left(\dfrac{p_4}{p_o}\right)^{1/\gamma}} p_o A_2 \tag{15.45}$$

Unlike the mass-flow rate through the C–D nozzle, it has been theoretically and experimentally demonstrated [see Refs. (15.38) and (15.39)] that the mass-flow rate through an orifice meter continues to increase as the downstream pressure $p_4$ is decreased below the critical pressure $p^*$. In other words, it does not reach a maximum, choked value when the pressure at the throat reaches the critical value. The critical pressure ratio $p^*/p_o$ is given by

$$\frac{p^*}{p_o} = \lim_{M_4 \to 1}\left(\frac{p_4}{p_o}\right) = \left(\frac{2}{\gamma + 1}\right)^{\gamma/(\gamma-1)} \tag{15.46}$$

When the downstream pressure $p_4$ is lower than the critical pressure (this condition is termed *supercritical flow*), the flow within the jet downstream of the minimum area becomes supersonic. Also, the area of the low-pressure jet expands to accommodate a higher flow rate. In this case, the flow becomes extremely complex, and the assumption of

one dimensionality is no longer valid. Consequently, there is a practical limitation on the theoretical mass-flow rate in the subcritical regime, $\dot{m}_{\max} = \lim_{p_4 \to p^*}(\dot{m})$:

$$\dot{m}_{\max} = \frac{\left(\frac{2}{\gamma+1}\right)^{\frac{\gamma+1}{2(\gamma-1)}}}{1 + \frac{2}{\pi}\left(\frac{\gamma}{\gamma+1}\right)^{\frac{1}{\gamma-1}}} \rho_o a_o A_2 \tag{15.47}$$

For cases where $p_4/p_o > 0.7$, the discharge coefficient $C_d$ is almost 1.0; therefore, Eq. (15.45) can be used directly to calculate the actual mass-flow rate. As the pressure ratio $p_4/p_o$ decreases below 0.7, $C_d$ has been experimentally found to increase [see Ref. (15.36)], reaching a value of about 1.2 for $p_4/p_o \approx 0.2$. The discharge coefficient is also a function of the duct-to-orifice area ratio $A_2/A_1$; however, the dependency of the discharge coefficient on this area ratio is taken to be small.

Additional information regarding the two flow meters considered in this section, as well as several others, can be found in Refs. (15.35) and (15.40).

## 15.7 SUMMARY

This chapter has provided an introduction to a variety of topics dealing with the measurement of flow quantities that are important in compressible fluid flows. A range of flow devices and instruments have been discussed. Some of the theory associated with these measurement devices has also been presented. As has been shown, direct measurement of a flow quantity is often not possible or practical (e.g., static temperature of a moving gas); in those cases, indirect measurements combined with analytical relations provided the vehicle for obtaining the desired quantity.

Space limitations do not permit comprehensive coverage of much of the material presented in this chapter. Consequently, many important topics, including accuracy, calibration, experimental uncertainty, data acquisition, data reduction, holography, three-dimensional imaging, pressure-sensitive paints, and measurement of shear stress, have not even been mentioned.

The subject of compressible fluid flow measurements is simply too broad to be thoroughly covered in a single chapter. Where additional information is required, the references provided should be consulted, as they generally contain the missing information or at least can point to other references that may contain the needed material.

## 15.8 REFERENCES

**15.1** Liepmann, H. W., and Roshko, A. *Elements of Gasdynamics*, John Wiley & Sons, New York, 1957, pp. 145 and 148.

**15.2** Brown, G. O. "Henry Darcy's Perfection of the Pitot Tube," in *Henry P. G. Darcy and Other Pioneers in Hydraulics: Contributions in Celebration of the 200th Birthday of Henry Pilibert Gaspard Darcy*, G. O. Brown, J. D. Garbrecht, and W. H. Hagers, Eds., ASCE, Reston, VA, pp. 14–23.

**15.3** Folsom, R. G. "Review of the Pitot Tube," *Trans ASME* 1956; 78: 1447–1460.

**15.4** Rae, W. H., Jr., and Pope, A. *Low-Speed Wind Tunnel Testing*, 2d ed., John Wiley & Sons, New York, 1984, pp. 102–103 and 112–113.

**15.5** Trenkle, F., and Reinhardt, M. "In-Flight Temperature Measurements—AGARD Flight Test Instrumentation Series (Vol. 2), NATO Advisory Group for Aerospace Research and Development AGARD, AGARDograph No. 160, 1973.

**15.6** Bejan, A. *Convection Heat Transfer*, John Wiley & Sons, New York, 1984, p. 11.

**15.7** Kakac, S., and Yener, Y. *Convection Heat Transfer*, 2d ed., CRC Press, Boca Raton, FL, 1995, pp. 378–388.

**15.8** Kays, W., Crawford, M., and Weigand, B. *Convective Heat and Mass Transfer*, 4th ed., McGraw-Hill, New York, 2005, pp. 344–363.

**15.9** Comte-Bellot, G. "Hot-Wire Anemometry," *Ann Rev Fluid Mech* 1976; 8: 209–231.

**15.10** Kovasznay, L. S. G. "The Hot-Wire Anemometer in Supersonic Flows," *J Aeronautl Sci* 1950; 17: 565–573.

**15.11** Morgan, V. T. "The Overall Convective Heat Transfer from Smooth Cylinders," *Advances in Heat Transfer*, Vol. 11, Academic Press, New York, 1975, pp. 199–264.

**15.12** King, L. V. "On the Convection of Heat from Small Cylinders in a Stream of Fluid: Determination of the Convection Constant of Small Platinum Wires with Applications to Hot-Wire Anemometry," *Phil Trans R Soc* A 1914; 214: 373–432.

**15.13** Collis, D. C., and Williams, M. J. "Two-Dimensional Convection from Heated Wires at Low Reynolds Numbers," *J Fluid Mech* 1959; 6: 357–384.

**15.14** Kramers, H. "Heat Transfer from Spheres to Flowing Media," *Physica* 1946; 12: 61–120.

**15.15** Hinze, J. O. *Turbulence*, 2d ed., McGraw-Hill, New York, 1975, Chapter 2.

**15.16** Fingerson, L. M., and Freymuth, P. "Thermal Anemometers," *Fluid Mechanics Measurements*, 2d ed., R. J. Goldstein, Ed., Taylor & Francis, Washington, DC, 1996, Chapter 3, pp. 115–173.

**15.17** Lomas, C. G. *Fundamentals of Hot Wire Anemometry*, Cambridge University Press, Cambridge, UK, 1986.

**15.18** Brunn, H. H. *Hot-Wire Anemometry*, Oxford University Press, Oxford, UK, 1995.

**15.19** Adrian, R. J. "Laser Velocimetry," *Fluid Mechanics Measurements*, 2d ed., R. J. Goldstein, Ed., Taylor & Francis, Washington, DC, 1996, Chapter 4, pp. 175–299.

**15.20** Kihm, K. D. "Laser Speckle Photography Technique, Applied for Heat and Mass Transfer Problems," *Adv Heat Trans* 1997; 30: 255–311.

**15.21** Reithmuller, M. L., Ed., *Particle Image Velocimetry and Associated Techniques. Lecture Series 2000–2001*, Von Karman Institute, Belgium, 2000.

**15.22** Adrian, R. J. "Particle-Imaging Techniques for Experimental Fluid Mechanics," *Ann Rev Fluid Mech* 1991; 23: 261–304.

**15.23** Raffel, M., Willert, C., and Kompenhaus, J. *Particle Image Velocimetry*, Springer-Verlag, Berlin, 1998.

**15.24** Settles, G. S. *Schlieren and Shadowgraph Techniques: Visualizing Phenomena in Transparent Media*, Springer-Verlag, Berlin, 2001.

**15.25** Settles, G. S. "The Penn State Full-Scale Schlieren System," The 11th International Symposium on Flow Visualization, University of Notre Dame, Notre Dame, IN, August 9–12, 2004, pp. 1–12.

**15.26** Goldstein, R. J., and Kuehn, T. H. "Optical Systems for Flow Measurement: Shadowgraph, Schlieren and Interferometric Techniques," *Fluid Mechanics Measurements*, 2d ed., R. J. Goldstein, Ed., Taylor & Francis, Washington, DC, 1996, Chapter 7, pp. 451–508.

**15.27** Merkirch, W. *Flow Visualization*, 2d ed., Academic Press, Orlando, FL, 1987.

**15.28** Bachalo, W. D. "Methods for Compressible Flow," *Flow Visualization: Techniques and Examples*, A. J. Smits and T. T. Lim, Eds., Imperial College Press, London, 2000, Chapter 9, pp. 205–243.

**15.29** Anderson, J. D. "Research in Supersonic Flight and the Breaking of the Sound Barrier," NASA SP-4219, Chapter 3.

**15.30** Scott, J. "Ernst Mach and Mach Number," http://www.aerospaceweb.org, November 2003.

**15.31** Cook, A. H. *Interference of Electromagnetic Waves*, Clarendon Press, Oxford, UK, 1971.

**15.32** Hariharan, P. *Optical Interferometry*, Academic Press, Orlando, FL, 1985.

**15.33** Hariharan, P. *Basics of Interferometry*, Academic Press, Orlando, FL, 1992.

**15.34** Rouse, H., and Ince, S. *History of Hydraulics*, Dover Publications, New York, 1963, pp. 188–189.

**15.35** Tse, F. S., and Morse, I. E. *Measurements and Instrumentation in Engineering, Principles and Basic Laboratory Experiments*, Marcel Dekker, New York, 1989, pp. 478–494.

**15.36** Brower, W. B., Jr., Eisler, E., Filkorn, J. E., Gonenc, J., Plati, C., and Stagnitti, J. "On the Compressible Flow Through an Orifice," *Transactions of the ASME* 1993; 115: pp. 660–664.

**15.37** Bloch, E. "Numerical Solution of Free Boundary Problems by the Method of Steepest Descent," *Physics of Fluids*, Supplement II, Vol. 12, 1967, pp. 129–132.

**15.38** Perry, J. A. "Critical Flow Through Sharp-Edged Orifices," *Trans ASME* 1949; 71: 757–764.

**15.39** Mattingly, G. E. "Volume Flow Measurements," *Fluid Mechanics Measurements*, 2d ed., R. J. Goldstein, Ed., Taylor & Francis, Washington, DC, 1996, Chapter 5, pp. 301–366.

## 15.9 PROBLEMS

**15.1** A Pitot tube is placed in a uniform air flow of Mach 2.5. If the Pitot tube indicates a pressure of 500 kPa, find the static pressure of the flow. Take $\gamma = 1.40$.

**15.2** A Pitot tube is placed in a uniform helium flow. If the Pitot tube indicates a pressure of 280 kPa and the static pressure of the flow is measured to be 20 kPa, find the Mach number. Take $\gamma = 1.40$.

**15.3** A uniform flow of air at Mach 2.0 passes over an insulated wall. The static temperature and pressure in the freestream outside the boundary layer are, respectively, 250 K and 20 kPa. Determine the freestream stagnation temperature, adiabatic wall temperature, and static pressure at the wall surface. Take $\gamma = 1.40$.

**15.4** A total-temperature probe is inserted into the flow of Problem 15.3. If the probe has $K$ [see Eq. (15.11)] equal to 0.97, what temperature will be indicated by the probe?

**15.5** Sketch a plot of $p/p_o$ versus $M$ for isentropic flow. On the same coordinates, plot $p_\infty/p_{\text{Pitot}}$ versus $M_\infty$. Take $\gamma = 1.40$.

**15.6** Derive the Gladstone–Dale relation, Eq. (15.21), from the Lorenz–Lorentz relation, Eq. (15.20).

**15.7** Compute the index of refraction at atmospheric pressure for the gases contained in Table 15.3 for the given Gladstone–Dale constants and temperatures.

**15.8** The wire of a hot wire anemometer is placed to an air flow at atmospheric pressure with a temperature of 30°C and a velocity of 80 m/s. The wire is heated to a constant temperature of 210°C. The diameter of the wire is 4 $\mu$m, and the length of the wire is 2 mm. Determine the electric current in the wire. The air properties at the mean film temperature are $\rho = 0.898\ \text{kg/m}^3$, $\mu = 2.27 \cdot 10^{-5}\ \text{kg/m} \cdot \text{s}$, $k = 0.0328\ \text{W/m} \cdot \text{K}$, and $c_p = 1.013\ \text{kJ/kg} \cdot \text{K}$. The resistivity of the wire is $0.22\ \mu\Omega \cdot \text{m}$.

**15.9** A symmetrical wedge of 10° total included angle is placed in a uniform Mach 2.0 flow with a static pressure of 60 kPa. If the axis of the wedge is misaligned with the flow direction by 3°, determine the static pressure difference between the top and bottom surfaces of the wedge. Take $\gamma = 1.40$.

**15.10** The temperature of the wire of an anemometer placed perpendicular to an air flow of 20°C is 100°C. The wire dissipates 20 mW of heat to the flow. The diameter of the wire is 3 $\mu$m,

and the length is 1 mm. What is the velocity of the flow? The properties of the air at the mean temperature between the fluid and the wire are $\rho = 1.0595$ kg/m$^3$, $c_p = 1.009$ kJ/kg, $k = 0.0285$ W/m · K, and $\mu = 2 \cdot 10^{-5}$ kg/m · s.

**15.11** The sensing element of a hot wire anemometer is a platinum wire 4 $\mu$m in diameter and 2 mm in length. The wire is placed perpendicular to an air flow at atmospheric pressure with a temperature of 20°C and a velocity of 60 m/s. If the temperature of the wire is 100°C, determine the power dissipated by the wire. The properties of the air at the mean film temperature are $\rho = 1.0595$ kg/m$^3$, $c_p = 1.009$ kJ/kg · K, $k = 0.0285$ W/m · K, and $\mu = 2 \cdot 10^{-5}$ kg/m · s.

**15.12** A dual-beam LDV system with a wavelength of 3000 Å and a 20° angle between the intersecting beams records a difference of 30 MHz between the two Doppler shifts. What is the velocity of the flow field?

**15.13** What is the minimum frequency that a dual-beam LDV system has to have in order to measure a 1,000-m/s velocity with a 5,000-Å laser with a 5° angle between the beams? Explain using both theoretical explanations of the LDV instrument.

**15.14** Determine the vorticity of the flow field, based on the double-exposed PIV photograph shown in Figure P15.14. The interval between the two exposures is $\Delta t = 0.001$ s. The grid size equals 1 mm in both directions.

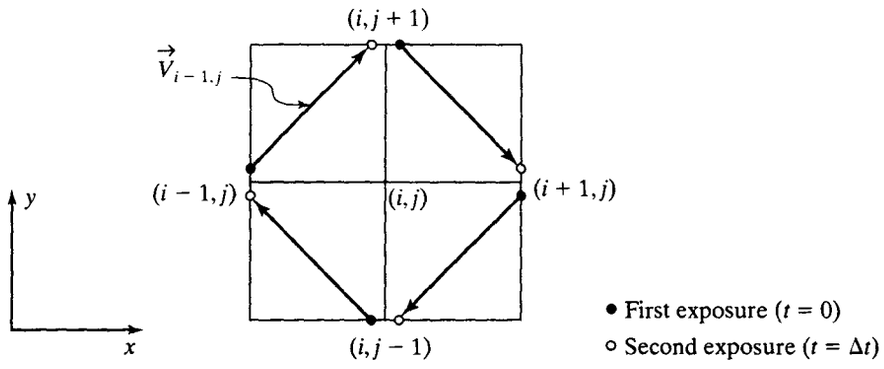


**Figure P15.14**

**15.15** A double-exposed PIV photograph contains the flow field illustrated in Figure P15.15. Show that if the grid size is equal in the $x$ and $y$ directions (i.e., $\Delta x = \Delta y$), the vorticity at $(i, j)$ is dependent only upon the time interval $\Delta t$ between the two exposures.

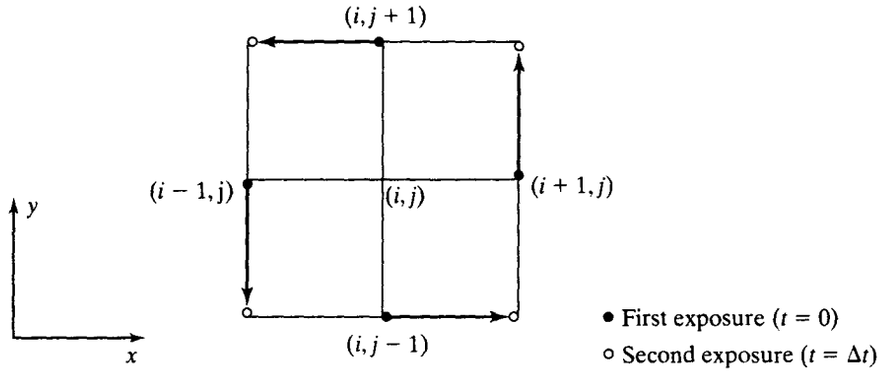


**Figure P15.15**

# Appendix A

# One-Dimensional Equations of Gas Dynamics for Use in Spreadsheet Programs

Many texts have been written to describe the theory and applications of compressible fluid flow. In most books, a good deal of attention is generally given to one-dimensional, steady flows. Because of the nonlinear relation between flow variables and the Mach number, the solution of these one-dimensional problems is accomplished through the use of tables and charts. These "tools" are found at the back of every text on the subject (including this one). There are tables for isentropic flows, normal shockwaves, Prandtl–Meyer flows, flows with friction, and flows with heat transfer. Moreover, oblique-shock problems are solved either by making use of the normal-shock tables or through the use of charts.

The solution of even simple problems is painfully slow because of the use of these "tools." Much time is spent learning how to navigate through these tables and charts. A fair amount of time is often required to interpolate between table values, and the charts require a very keen eye or else the results of the computations are flawed. Unfortunately, this process diminishes the amount of time available for the study of compressible flow physics.

In this appendix, the equations of gas dynamics are presented in a form that will aid the creation of simple spreadsheet programs. Spreadsheet programs are relatively easy to build, very easy to use, and fast. Simply put, a spreadsheet is essentially a calculator. For most problems, all that is required are +, −, *, /, and ∧ operations. Some programs require the trigonometric, logarithmic, or exponential functions. Also, the $ function is very important.

After creating a spreadsheet solver, one finds that problems which could be very time consuming are solved in just a few minutes. The outcome is a more efficient

use of one's time, which allows one more time to concentrate on the actual subject matter.

In this appendix, we present the equations of isentropic flow (see Chapter 3), normal shockwaves (see Chapter 4), oblique shockwaves (see Chapter 6), Prandtl–Meyer flow (see Chapter 7), Fanno flow (see Chapter 9), and Rayleigh flow (see Chapter 10).

## A.1 ISENTROPIC FLOW

If the flow Mach number $M$ and the ratio of specific heats, $\gamma$, are known, the stagnation-to-static-temperature, -pressure, and -density ratios, as well as the area ratio, may be directly calculated from the following equations:

$$\frac{T_o}{T} = 1 + \frac{\gamma - 1}{2} M^2 \tag{A.1}$$

$$\frac{p_o}{p} = \left(1 + \frac{\gamma - 1}{2} M^2\right)^{\gamma/(\gamma-1)} \tag{A.2}$$

$$\frac{\rho_o}{\rho} = \left(1 + \frac{\gamma - 1}{2} M^2\right)^{1/(\gamma-1)} \tag{A.3}$$

$$\frac{A}{A^*} = \frac{1}{M}\left[\left(\frac{2}{\gamma + 1}\right)\left(1 + \frac{\gamma - 1}{2} M^2\right)\right]^{\frac{\gamma+1}{2(\gamma-1)}} \tag{A.4}$$

If the property ratios are known, the Mach number can be directly determined from any of the following expressions:

$$M = \sqrt{\frac{2}{\gamma - 1}\left(\frac{T_o}{T} - 1\right)} \tag{A.5}$$

$$M = \sqrt{\frac{2}{\gamma - 1}\left[\left(\frac{p_o}{p}\right)^{(\gamma-1)/\gamma} - 1\right]} \tag{A.6}$$

$$M = \sqrt{\frac{2}{\gamma - 1}\left[\left(\frac{\rho_o}{\rho}\right)^{(\gamma-1)} - 1\right]} \tag{A.7}$$

If the area ratio $A/A^*$ and $\gamma$ are known, the Mach number can be determined only through a root-solving technique. Some spreadsheet programs contain root solvers. If no solver is available, one can be built from the forthcoming equations, using the Newton–Raphson technique. Here, we seek the Mach-number roots (one subsonic and one supersonic) of Eq. (A.4), which is rewritten in the following form:

$$F(M) = \alpha M - c^b\left(1 + \frac{M^2}{2bc}\right)^b \tag{A.8}$$

$$\frac{dF}{dM} = F' = \alpha - c^{b-1} M\left(1 + \frac{M^2}{2bc}\right)^{b-1} \tag{A.9}$$

$$\alpha = \frac{A}{A^*}$$

$$b = \frac{\gamma + 1}{2(\gamma - 1)}$$

$$c = \frac{2}{\gamma + 1}$$

The relation that provides the new value of the Mach number from an assumed or previous value is the Newton–Raphson algorithm:

$$M_{\text{new}} = M_{\text{old}} - \frac{F(M_{\text{old}})}{\frac{dF}{dM}(M_{\text{old}})} \tag{A.10}$$

Because two roots are sought, there should be two parallel sets of calculations. One begins with a subsonic initial guess (say, 0.2), while the other starts with a supersonic first guess (say, 4.0).

Figure A.1 shows a layout of an isentropic flow solver. It is presented to demonstrate a potential arrangement of the sheet, as well as to provide actual values that can be compared in order to validate the solver.

In the first column of the fifth row, $M = 0.4770$, and the various ratios are shown to the right for $\gamma = 1.4$. In the eighth row, property ratios are given, and the $M$ corresponding to each is contained in the ninth row. To find the $M$ for the given $A/A^*$, we have to perform a root-solving method as described previously. Figure A.2 shows results of the iterative scheme to find the two Mach numbers.

| $\gamma$ | 1.4 | | | |
|---|---|---|---|---|
| **isentropic flow calculations** | | | | |
| **Given $M$, find the property ratio** | | | | |
| Given: | $p/p_o$ | $T/T_o$ | $A/A^*$ | |
| 0.4770 | 0.8558 | 0.9565 | 1.3865 | |
| **Given the property ratio, find $M$** | | | | |
| | $p/p_o$ | $T/T_o$ | $A/A^*$ | |
| Given: | 0.7143 | 0.55556 | 1.3865 | |
| $M$ | 0.7103 | 2.0000 | 0.4770 | $M < 1$ |
| | | | 1.7500 | $M > 1$ |

**Figure A.1** Spreadsheet Layout of an Isentropic Flow Solver

| $\gamma$ | 1.4 | | $A/A^*$ | 1.3865 |
|---|---|---|---|---|
| **subsonic solution** | | | | |
| **Iteration** | $M_{old}$ | $F(M)$ | $dF/dM$ | $M_{new}$ |
| 1 | 0.2000 | −0.31541 | 1.245 | 0.4533 |
| 2 | 0.4533 | −0.02457 | 1.045 | 0.4768 |
| 3 | 0.4768 | −0.00024 | 1.025 | 0.4770 |
| 4 | 0.4770 | 0.00000 | 1.024 | 0.4770 |
| 5 | 0.4770 | 0.00000 | 1.024 | 0.4770 |
| 6 | 0.4770 | 0.00000 | 1.024 | 0.4770 |
| 7 | 0.4770 | 0.00000 | 1.024 | 0.4770 |
| 8 | 0.4770 | 0.00000 | 1.024 | 0.4770 |

| $b$ | 3.0000 | | $c$ | 0.8333 |
|---|---|---|---|---|
| **supersonic solution** | | | | |
| **Iteration** | $M_{old}$ | $F(M)$ | $dF/dM$ | $M_{new}$ |
| 1 | 4.0000 | −37.32903 | −47.614 | 3.2160 |
| 2 | 3.2160 | −12.26147 | −19.642 | 2.5918 |
| 3 | 2.5918 | −3.85422 | −8.498 | 2.1382 |
| 4 | 2.1382 | −1.09555 | −4.055 | 1.8681 |
| 5 | 1.8681 | −0.24273 | −2.353 | 1.7649 |
| 6 | 1.7649 | −0.02696 | −1.842 | 1.7503 |
| 7 | 1.7503 | −0.00049 | −1.775 | 1.7500 |
| 8 | 1.7500 | 0.00000 | −1.773 | 1.7500 |

**Figure A.2** Eight Iterations Using the Newton–Raphson Method to Find $M$ for a Given Area Ratio and $\gamma$

## A.2 NORMAL SHOCKWAVES

The normal-shock equations can be expressed exclusively in terms of the flow Mach number upstream of the shock, $M_1$, and the ratio of specific heats, $\gamma$. It is straightforward to calculate the Mach number downstream of the shock, $M_2$; ratios of downstream to upstream static temperature, static pressure, and density; and the ratio of stagnation pressure across the shock from the following relations [*Note*: The parameter $\Gamma = (\gamma - 1)/(\gamma + 1)$ may be used to simplify several of the expressions]:

$$M_2^2 = \frac{M_1^2 + \dfrac{2}{\gamma - 1}}{\dfrac{2\gamma}{\gamma - 1}M_1^2 - 1} = \frac{\Gamma M_1^2 + (1 - \Gamma)}{(1 + \Gamma)M_1^2 - \Gamma} \tag{A.11}$$

$$\frac{T_2}{T_1} = \frac{\left(1 + \dfrac{\gamma - 1}{2}M_1^2\right)\left(\dfrac{2\gamma}{\gamma - 1}M_1^2 - 1\right)}{\left[\dfrac{(\gamma + 1)^2}{2(\gamma - 1)}\right]M_1^2} \tag{A.12}$$

$$\frac{p_2}{p_1} = \frac{2\gamma M_1^2}{\gamma + 1} - \frac{\gamma - 1}{\gamma + 1} = (1 + \Gamma)M_1^2 - \Gamma \tag{A.13}$$

$$\frac{\rho_2}{\rho_1} = \frac{V_1}{V_2} = \frac{(\gamma + 1)M_1^2}{(\gamma - 1)M_1^2 + 2} = \frac{M_1^2}{\Gamma M_1^2 + (1 - \Gamma)} \tag{A.14}$$

$$\frac{p_{o2}}{p_{o1}} = \left[\frac{\frac{\gamma + 1}{2}M_1^2}{1 + \frac{\gamma - 1}{2}M_1^2}\right]^{\gamma/(\gamma-1)} \left[\frac{1}{\frac{2\gamma}{\gamma + 1}M_1^2 - \frac{\gamma - 1}{\gamma + 1}}\right]^{1/(\gamma-1)} \tag{A.15}$$

The foregoing equations can be used to create a table of values with $M_1$ in one column and the various ratios in parallel columns. However, to build a useful solver, we must be able to compute the upstream Mach number from whatever information is supplied. The following relations will be needed in creating a spreadsheet solver:

$$M_1 = \sqrt{\frac{\Gamma M_2^2 + (1 - \Gamma)}{(1 + \Gamma)M_2^2 - \Gamma}} \tag{A.16}$$

$$M_1 = \sqrt{\frac{-\left[\frac{-\gamma^2 + 6\gamma - 1}{2(\gamma - 1)} - \frac{(\gamma + 1)^2}{2(\gamma - 1)}\frac{T_2}{T_1}\right] + \sqrt{\left[\frac{-\gamma^2 + 6\gamma - 1}{2(\gamma - 1)} - \frac{(\gamma + 1)^2}{2(\gamma - 1)}\frac{T_2}{T_1}\right]^2 + 4\gamma}}{2\gamma}} \tag{A.17}$$

$$M_1 = \sqrt{\frac{\frac{p_2}{p_1} + \Gamma}{1 + \Gamma}} \tag{A.18}$$

$$M_1 = \sqrt{\frac{(1 - \Gamma)\frac{\rho_2}{\rho_1}}{1 - \Gamma\frac{\rho_2}{\rho_1}}} = \sqrt{\frac{(1 - \Gamma)\frac{V_1}{V_2}}{1 - \Gamma\frac{V_1}{V_2}}} \tag{A.19}$$

If the total pressure ratio $p_{o2}/p_{o1}$ and $\gamma$ are known, the Mach number $M_1$ can be determined using a root-solving technique. If no solver is available, one can be built using the Newton–Raphson technique. To utilize this method, we create a function $F(M_1)$ by rearranging the relationship between $p_{o2}/p_{o1}$ and $M_1$—that is, by rewriting Eq. (A.15). Because the derivative of this function would yield a complicated expression that would be tedious to program, we may adopt an alternative approach and construct a central difference to compute the derivative of the function. To accomplish

this, we select a small increment $\Delta M_1$ (say, 0.01) and evaluate $F(M_1)$ at $M_1 \pm \Delta M_1$. The derivative is then the difference between these values, divided by $2\Delta M_1$:

$$F(M_1) = \left[\frac{\frac{\gamma+1}{2}M_1^2}{1+\frac{\gamma-1}{2}M_1^2}\right]^{\gamma/(\gamma-1)}\left[\frac{1}{\frac{2\gamma}{\gamma+1}M_1^2-\frac{\gamma-1}{\gamma+1}}\right]^{1/(\gamma-1)} - \frac{p_{o2}}{p_{o1}} \tag{A.20}$$

$$\frac{dF}{dM_1} = \frac{F(M_1+\Delta M_1) - F(M_1-\Delta M_1)}{2\Delta M_1} \tag{A.21}$$

The relation that provides the new value of Mach number from an assumed or previous value is as follows:

$$M_{1\,\text{new}} = M_{1\,\text{old}} - \frac{F(M_{1\,\text{old}})}{\frac{dF}{dM_1}(M_{1\,\text{old}})} \tag{A.22}$$

Figure A.3 shows a layout of a normal-shockwave solver. It is presented to demonstrate a potential spreadsheet arrangement as well as to provide actual values that can be compared against in order to validate the normal-shockwave solver. In the first column of the fifth row, $M_1 = 2.0$, and the various ratios are shown to the right for $\gamma = 1.4$. In the eighth row, property ratios are given, and the $M_1$ corresponding to each is contained in the ninth row.

To find $M_1$ for a given $p_{o2}/p_{o1}$, we have to perform a root-solving method as described previously. Figure A.4 shows the 10 iterations, starting from a guess of $M_1 = 3.00$. The far right-hand column contains the updated value, which becomes the value for the next round of calculations. Note that success is realized when an $M_1$ is inserted into $F(M_1)$ and the result is very close to zero.

| $\gamma$ | 1.4 | | | | |
|---|---|---|---|---|---|
| **normal-shockwave calculations** | | | | | |
| **Given *M*, find the property ratio** | | | | | |
| Given: | $p_2/p_1$ | $\rho_2/\rho_1$ | $T_2/T_1$ | $p_{o2}/p_{o1}$ | $M_2$ |
| 2.00 | 4.5000 | 2.6667 | 1.6875 | 0.7209 | 0.57735 |
| **Given the property ratio, find *M*** | | | | | |
| | $p_2/p_1$ | $\rho_2/\rho_1$ | $T_2/T_1$ | $p_{o2}/p_{o1}$ | $M_2$ |
| Given: | 4.0000 | 3.0000 | 2.0000 | 0.8000 | 0.6000 |
| $M_1$ | 1.8898 | 2.2361 | 2.3574 | 1.8284 | 1.8778 |

**Figure A.3** Spreadsheet Layout of a Normal-Shockwave Solver

| | $p_{o2}/p_{o1}$ | 0.8000 | | | | | | |
|---|---|---|---|---|---|---|---|---|
| | $\gamma$ | 1.4 | $(\gamma + 1)/2$ | $(\gamma - 1)/2$ | $\gamma/(\gamma - 1)$ | $1/(\gamma - 1)$ | | |
| | $\Delta$ | 0.01 | 1.2000 | 0.2000 | 3.5000 | 2.5000 | | |
| $n$ | $(M_1)_{old}$ | $M_1 + \Delta$ | $M_1 - \Delta$ | $F(M_1)$ | $F(M_1 + \Delta)$ | $F(M_1 - \Delta)$ | $dF/dM_1$ | $(M_1)_{new}$ |
| 1 | 3.00 | 3.0100 | 2.9900 | −0.4717 | −0.4745 | −0.4688 | −0.2824 | 1.3301 |
| 2 | 1.33 | 1.3401 | 1.3201 | 0.1738 | 0.1718 | 0.1757 | −0.1967 | 2.2136 |
| 3 | 2.21 | 2.2236 | 2.2036 | −0.1780 | −0.1826 | −0.1735 | −0.4537 | 1.8212 |
| 4 | 1.82 | 1.8312 | 1.8112 | 0.0032 | −0.0013 | 0.0077 | −0.4484 | 1.8284 |
| 5 | 1.83 | 1.8384 | 1.8184 | 0.0000 | −0.0045 | 0.0045 | −0.4498 | 1.8284 |
| 6 | 1.83 | 1.8384 | 1.8184 | 0.0000 | −0.0045 | 0.0045 | −0.4498 | 1.8284 |
| 7 | 1.83 | 1.8384 | 1.8184 | 0.0000 | −0.0045 | 0.0045 | −0.4498 | 1.8284 |
| 8 | 1.83 | 1.8384 | 1.8184 | 0.0000 | −0.0045 | 0.0045 | −0.4498 | 1.8284 |
| 9 | 1.83 | 1.8384 | 1.8184 | 0.0000 | −0.0045 | 0.0045 | −0.4498 | 1.8284 |
| 10 | 1.83 | 1.8384 | 1.8184 | 0.0000E + 00 | −0.0045 | 0.0045 | −0.4498 | 1.8284 |

**Figure A.4** Ten Iterations for Mach Number, Using Newton–Raphson for a Given Total-Pressure Ratio and $\gamma$

## A.3 OBLIQUE SHOCKWAVES

Examination of the equations for the oblique shock (Chapter 6) reveals that two independent parameters are required to fully describe the conditions on either side of the front. The working relations for an oblique shock as a function of $M_1$ and $\theta$ are as follows:

$$\frac{p_2}{p_1} = \frac{2\gamma M_1^2 \sin^2\theta}{\gamma + 1} - \frac{\gamma - 1}{\gamma + 1} \tag{A.23}$$

$$\frac{\rho_2}{\rho_1} = \frac{V_{n1}}{V_{n2}} = \frac{V_1 \sin\theta}{V_2 \sin(\theta - \delta)} = \frac{(\gamma + 1)M_1^2 \sin^2\theta}{(\gamma - 1)M_1^2 \sin^2\theta + 2} \tag{A.24}$$

$$\frac{T_2}{T_1} = \left(\frac{a_2}{a_1}\right)^2 = \frac{p_2}{p_1}\cdot\frac{\rho_1}{\rho_2} = \frac{\left(1 + \dfrac{\gamma - 1}{2}M_1^2 \sin^2\theta\right)\left(\dfrac{2\gamma}{\gamma - 1}M_1^2 \sin^2\theta - 1\right)}{\left[\dfrac{(\gamma + 1)^2}{2(\gamma - 1)}\right]M_1^2 \sin^2\theta} \tag{A.25}$$

$$\frac{p_{o2}}{p_{o1}} = e^{-(\Delta s/R)} = \frac{p_2}{p_1}\left(\frac{T_2}{T_1}\right)^{\gamma/(1-\gamma)}$$

$$= \left[\frac{\frac{\gamma+1}{2}M_1^2\sin^2\theta}{1+\frac{\gamma-1}{2}M_1^2\sin^2\theta}\right]^{\gamma/(\gamma-1)}\left[\frac{1}{\frac{2\gamma}{\gamma+1}M_1^2\sin^2\theta - \frac{\gamma-1}{\gamma+1}}\right]^{\gamma/(\gamma-1)} \tag{A.26}$$

$$\frac{T_{o2}}{T_{o1}} = 1 \tag{A.27}$$

$$M_2^2 = \frac{1+\frac{\gamma-1}{2}M_1^2}{\gamma M_1^2\sin^2\theta - \frac{(\gamma-1)}{2}} + \frac{M_1^2\cos^2\theta}{1+\frac{\gamma-1}{2}M_1^2\sin^2\theta} \tag{A.28}$$

$$\tan\delta = \cot\theta\frac{M_1^2\sin^2\theta - 1}{\frac{\gamma+1}{2}M_1^2 - (M_1^2\sin^2\theta - 1)} \tag{A.29}$$

It is not much more difficult to develop working relations for oblique shocks in terms of the deflection angle $\delta$ and the shock angle $\theta$—that is, $\xi = f(\delta, \theta)$. However, once the $M_1$ value is calculated from a function of $\delta$ and $\theta$, the flow conditions can be determined using the foregoing expressions. Considerable rearrangement of Eq. (A.29) brings the desired functional relation between $M_1$ and the two angles:

$$\frac{1}{M_1^2} = \sin^2\theta - \left(\frac{\gamma+1}{2}\right)\frac{1}{1+(\cot\delta)(\cot\theta)} \tag{A.30}$$

In most cases, the shock angle is not known; rather, $M_1$ and $\delta$ are the independent variables. Therefore, it is more advantageous to be able to work in terms of $M_1$ and $\delta$—that is, $\xi = f(M_1, \delta)$. Unfortunately, the calculation of the shock angle $\theta$ for a given deflection angle $\delta$ cannot be done directly. One way to overcome this difficulty is to use Collar's method, which was described in Chapter 6. This method can be readily utilized to determine the shock angle $\theta$ for a given $\delta$ and $M_1$ from Eq. (A.29). To use Collar's method, first rewrite Eq.(A.29) as a cubic equation in terms of cot $\theta$:

$$f(x) = x^3 + Cx^2 - Ax + (B - AC) = 0 \tag{A.31}$$

$$x = \cot\theta$$

$$A = M_1^2 - 1$$

$$B = [(\gamma + 1)/2]M_1^4 \tan \delta$$

$$C = \{1 + [(\gamma + 1)/2]M_1^2\}\tan \delta$$

Then it is a simple matter to solve the cubic. Here, we employ Collar's successive approximation technique.

The largest root can be found by starting from a computed initial value—that is, $x_0 = \sqrt{A} = \sqrt{M_1^2 - 1}$. The right-hand side of Eq. (A.32) may then be computed, which yields $x_1$. This value is then used to determine $x_2$, and so on. The process continues

| $\gamma$ | $\gamma + 1$ | $\gamma - 1$ |
|---|---|---|
| 1.4 | 2.4 | 0.4 |

**Option One: $M_1$ and $\delta$ are given**

**Weak-Shock Solution**

| $\gamma$ | $M_1$ | $\delta$ (deg) | $\theta$ (deg) | $p_2/p_1$ | $\rho_2/\rho_1$ | $T_2/T_1$ | $p_{o2}/p_{o1}$ | $M_2$ |
|---|---|---|---|---|---|---|---|---|
| 1.4000 | 4.0000 | 30.0000 | 45.2241 | 9.2397 | 3.7034 | 2.4949 | 0.3767 | 1.8485 |
| | | 0.5236 | 0.9922 | | | | | |
| | | radians | cot $\theta$ | | | | | |

**Strong-Shock Solution**

| $\gamma$ | $M_1$ | $\delta$ (deg) | $\theta$ | $p_2/p_1$ | $\rho_2/\rho_1$ | $T_2/T_1$ | $p_{o2}/p_{o1}$ | $M_2$ |
|---|---|---|---|---|---|---|---|---|
| 1.4000 | 4.0000 | 30.0000 | 79.22751 | 17.8479 | 4.5324 | 3.9379 | 0.1473 | 0.5769 |
| | | 0.5236 | 0.1903 | | | | | |
| | | radians | cot $\theta$ | | | | | |

**Option Two: $M_1$ and $\theta$ are given**

| $\gamma$ | $M_1$ | $\theta$ (deg) | $\delta$ (deg) | $p_2/p_1$ | $\rho_2/\rho_1$ | $T_2/T_1$ | $p_{o2}/p_{o1}$ | $M_2$ |
|---|---|---|---|---|---|---|---|---|
| 1.4000 | 4.0000 | 45.0000 | 29.8459 | 9.1667 | 3.6923 | 2.4826 | 0.3802 | 1.8598 |
| | radians | 0.7854 | 0.5209 | | | | | |
| | cot ($\theta$) | 1.0000 | | | | | | |
| | $M_1^2 \sin^2 \theta - 1$ | 7.0000 | | | | | | |

**Option Three: $\theta$ and $\delta$ are given**

| $\gamma$ | $\delta$ (deg) | $\theta$ (deg) | $M_1$ | $p_2/p_1$ | $\rho_2/\rho_1$ | $T_2/T_1$ | $p_{o2}/p_{o1}$ | $M_2$ |
|---|---|---|---|---|---|---|---|---|
| 1.4000 | 10.0000 | 20.0000 | 4.7347 | 2.8927 | 2.0642 | 1.4014 | 0.8879 | 3.8163 |
| $(\gamma + 1)/2$ | 0.1745 | 0.3491 | radians | | | | | |
| 1.2000 | | 2.7475 | cot ($\theta$) | | | | | |

**Figure A.5** Spreadsheet Layout of an Oblique-Shockwave Solver

until the value used on the right, $x_n$, yields virtually the same value as that on the left, $x_{n+1}$, resulting in the weak shock:

$$x_0 = \sqrt{A}$$

$$x_{n+1} = \sqrt{A - \frac{B}{(x_n + C)}} \tag{A.32}$$

The second root (the strong-shock result) is obtained by root extraction:

$$x_{II} = \frac{1}{2}\left[ -(x_I + C) + \sqrt{(x_I + C)(C - 3x_I) + 4A}\right] \tag{A.33}$$

*Note*: There is also a negative root, but it is not meaningful.

Figure A.5 shows a potential spreadsheet layout for an oblique-shockwave solver. It contains three options that depend upon what information is available. The values presented are actual results for the cases shown.

The four left-hand columns of Figure A.6 present the first 7 iterations of the Collar successive approximation for the case in which $M_1 = 4.0$ and $\delta = 30°$. Note that the computations shown are not yet converged. Extended calculation shows that 20 iterations are required in order to obtain a converged value of $x = 0.9922$. The last five columns on the right present Newton–Raphson iterations starting from the same initial guess, for comparison.

Finally, Figure A.7 shows the three roots for the example case ($M_1 = 4.0$ and $\delta = 30°$).

| **Collar's Method** | | | | | | | | |
|---|---|---|---|---|---|---|---|---|
| ***A*** | ***B*** | ***C*** | ***B* − *AC*** | **First guess** | | | | |
| 15.0000 | 177.3620 | 11.6625 | 2.4249 | 3.8730 | | **Newton–Raphson** | | |
| **Iteration** | $x_{old}$ | $x_{new}$ | | **Iteration** | $x_{old}$ | ***F*** | ***F'*** | $x_{new}$ |
| 1 | 3.8730 | 1.8930 | | 1 | 3.8730 | 177.3620 | 120.3371 | 2.3991 |
| 2 | 1.8930 | 1.3841 | | 2 | 2.3991 | 47.3728 | 58.2262 | 1.5855 |
| 3 | 1.3841 | 1.1855 | | 3 | 1.5855 | 11.9455 | 29.5234 | 1.1809 |
| 4 | 1.1855 | 1.0933 | | 4 | 1.1809 | 2.6217 | 16.7279 | 1.0242 |
| 5 | 1.0933 | 1.0467 | | 5 | 1.0242 | 0.3696 | 12.0355 | 0.9935 |
| 6 | 1.0467 | 1.0220 | | 6 | 0.9935 | 0.0139 | 11.1332 | 0.9922 |
| 7 | 1.0220 | 1.0087 | | 7 | 0.9922 | 2.273E−05 | 11.0967 | 0.9922 |

**Figure A.6** Calculation of cot $\theta$ for Given Mach and Deflection Angles

| | cot $\theta$ | tan $\theta$ | angle (deg) |
|---|---|---|---|
| *weak* | 0.9922087 | 1.00785249 | 45.22 |
| *strong* | 0.1902626 | 5.25589488 | 79.23 |
| *negative root* | −12.84495 | −0.07785163 | −4.45 |

**Figure A.7** Numerical Determination of the Shockwave Angles

## A.4 PRANDTL–MEYER FLOW

For a given value of Mach number, the wave angle is as follows:

$$\mu = \sin^{-1}\left(\frac{1}{M}\right) = \tan^{-1}\left(\frac{1}{\sqrt{M^2 - 1}}\right) \tag{A.34}$$

Hence,

$$M = \frac{1}{\sin \mu} \tag{A.35}$$

The angle $\nu$ through which a stream, initially at Mach 1, must be expanded to reach a supersonic Mach number $M$ is given by the Prandtl–Meyer function:

$$\nu = \left\{\sqrt{\frac{\gamma + 1}{\gamma - 1}}\tan^{-1}\left[\sqrt{\frac{\gamma - 1}{\gamma + 1}(M^2 - 1)}\right] - \tan^{-1}\left(\sqrt{M^2 - 1}\right)\right\} \tag{A.36}$$

For given values of the Prandtl–Meyer function $\nu$ and the ratio specific heats $\gamma$, the Mach number $M$ can be computed using a root solver. If no solver is available, then one can be built using the Newton–Raphson method. We seek the Mach number root of Eq. (A.36), which can be rewritten in function form and then differentiated, resulting in Eqs. (A.37) and (A.38), respectively.

$$F(M) = \left\{\sqrt{\frac{\gamma + 1}{\gamma - 1}}\tan^{-1}\left[\sqrt{\frac{\gamma - 1}{\gamma + 1}(M^2 - 1)}\right] - \tan^{-1}\left(\sqrt{M^2 - 1}\right)\right\} - \nu \tag{A.37}$$

$$\frac{dF}{dM} = \frac{\gamma + 1}{2 + (\gamma - 1)M^2}\frac{M}{\sqrt{M^2 - 1}} - \frac{1}{M\sqrt{M^2 - 1}} \tag{A.38}$$

Instead of using the foregoing analytical formula for the derivative, we might also consider using the central-difference alternative,

$$\frac{dF}{dM} = \frac{F(M + \Delta M) - F(M - \Delta M)}{2\Delta M}$$

| **Inputs:** $\nu$ (deg) and $\gamma$ | | $\gamma$ | $\nu$ | |
|---|---|---|---|---|
| | | 1.4 | 30.0000 | degrees |
| $\gamma + 1/\gamma - 1$ | $\gamma - 1/\gamma + 1$ | $\Delta M$ | | |
| 6 | 0.1667 | 0.01 | | |

| **Uses the Newton-Raphson Method to find M for a given value of $\nu$** | | | | | | |
|---|---|---|---|---|---|---|
| **Iteration** | $M_{old}$ | $F(M)$ | $F(M + \Delta M)$ | $F(M - \Delta M)$ | $\Delta F/\Delta M$ | $M_{new}$ |
| 1 | 4.0000 | 0.6246 | 0.6269 | 0.6223 | 0.2305 | 1.2908 |
| 2 | 1.2908 | −0.4203 | −0.4155 | −0.4250 | 0.4742 | 2.1770 |
| 3 | 2.1770 | 0.0198 | 0.0244 | 0.0152 | 0.4560 | 2.1336 |
| 4 | 2.1336 | −0.0001 | 0.0045 | −0.0048 | 0.4624 | 2.1339 |
| 5 | 2.1339 | −6.255E−09 | 0.0046 | −0.0046 | 0.4623 | 2.1339 |
| 6 | 2.1339 | 1.343E−14 | 0.0046 | −0.0046 | 0.4623 | 2.1339 |
| 7 | 2.1339 | 0.000E+00 | 0.0046 | −0.0046 | 0.4623 | 2.1339 |
| 8 | 2.1339 | 0.000E+00 | 0.0046 | −0.0046 | 0.4623 | 2.1339 |
| | | | | | | **Answer** |

**Figure A.8** Determination of $M$ for Given Values of $\nu$ and $\gamma$

where $\Delta M$ is a small value (say, 0.01). The relation that provides the new value of the Mach number from an assumed or previous value is as follows:

$$M_{new} = M_{old} - \frac{F(M_{old})}{\frac{dF}{dM}(M_{old})} \tag{A.39}$$

Figure A.8 shows a potential spreadsheet layout for a Prandtl–Meyer flow solver. The calculations for this case (i.e., $\nu = 30°$, with $\gamma = 1.4$) begin from an assumed Mach number of 4.0000. (Other values should be tried to get a feel for how the solver responds.) Note that the value of $\nu$ used in the calculations must be in radians (i.e., multiply $\nu$ by $\pi/180$). The values presented are actual results for the case shown.

Figure A.9 presents the calculation of $\nu$ and $\mu$ for the given $M$ and $\gamma$. These values are computed directly from Eqs. (A.36) and (A.34), respectively. It is easy to see how a table of $\nu$ and $\mu$ values for given $M$ may be created.

| **Prandtl–Meyer values** | | | | |
|---|---|---|---|---|
| $M$ | $\nu$ **(rad)** | $\nu$ **(deg)** | $\mu$ **(rad)** | $\mu$ **(deg)** |
| 4.0000 | 1.1482 | 65.7848 | 0.2527 | 14.4775 |

**Figure A.9** Prandtl–Meyer Flow Parameters

## A.5 FANNO FLOW

It is convenient for Fanno flow (frictional, constant-area, adiabatic flow) to choose as a reference point $M = 1$ at $L = L_{max}$. We use the symbol $^*$ for this state. The length of the duct as function of Mach number is given as follows:

$$\frac{fL_{max}}{D} = \left(\frac{\gamma+1}{2\gamma}\right)\ln\left(\frac{\frac{\gamma+1}{2}}{1+\frac{\gamma-1}{2}M^2}\right) - \frac{1}{\gamma}\left(1-\frac{1}{M^2}\right) - \left(\frac{\gamma+1}{2\gamma}\right)\ln\left(\frac{1}{M^2}\right) \tag{A.40}$$

The temperature, pressure, density, velocity, and total pressure can be calculated as functions of Mach number from the following equations:

$$\frac{T}{T^*} = \frac{2+(\gamma-1)1^2}{2+(\gamma-1)M^2} = \frac{(\gamma+1)}{2+(\gamma-1)M^2} \tag{A.41}$$

$$\frac{p}{p^*} = \left(\frac{1}{M}\right)\left[\frac{\gamma+1}{2+(\gamma-1)M^2}\right]^{1/2} \tag{A.42}$$

$$\frac{\rho}{\rho^*} = \frac{V^*}{V} = \frac{1}{M}\left[\frac{2+(\gamma-1)M^2}{(\gamma+1)}\right]^{1/2} \tag{A.43}$$

$$\frac{p_o}{p_o^*} = \frac{1}{M}\left[\frac{2+(\gamma-1)M^2}{(\gamma+1)}\right]^{\frac{\gamma+1}{2(\gamma-1)}} \tag{A.44}$$

If the temperature, pressure, density, velocity, or total-pressure ratio is known, then the Mach number can be determined directly from the following expressions:

$$M^2 = \frac{\gamma+1-2\frac{T}{T^*}}{(\gamma-1)\frac{T}{T^*}} \tag{A.45}$$

$$M^2 = \frac{1}{\gamma-1}\left[-1+\sqrt{1+\frac{\gamma^2-1}{\left(\frac{p}{p^*}\right)^2}}\right] \tag{A.46}$$

$$M^2 = \frac{2}{\left(\frac{\rho}{\rho^*}\right)^2(\gamma + 1) - (\gamma - 1)} \tag{A.47}$$

$$M^2 = \frac{2}{\left(\frac{V^*}{V}\right)^2(\gamma + 1) - (\gamma - 1)} \tag{A.48}$$

If the $p_o/p_o^*$ ratio is given, then the Mach number can be determined using a root solver. We may use the Newton–Raphson method once again, with $F(M)$ and its derivative $dF/dM$ in the following respective forms:

$$F(M) = M\frac{p_o}{p_o^*} - \left[\frac{2 + (\gamma - 1)M^2}{(\gamma + 1)}\right]^{\frac{\gamma+1}{2(\gamma-1)}} \tag{A.49}$$

$$\frac{dF}{dM} = \frac{p_o}{p_o^*} - M\left[\frac{2 + (\gamma - 1)M^2}{(\gamma + 1)}\right]^{\frac{3-\gamma}{2(\gamma-1)}} \tag{A.50}$$

The new value of the Mach number can be computed from an assumed or previous value from the following expression:

$$M_{\text{new}} = M_{\text{old}} - \frac{F(M_{\text{old}})}{\frac{dF}{dM}(M_{\text{old}})}$$

Similarly, given a value of $fL_{\max}/D$, we can determine the Mach number by using a root-solving technique. For this case, the function and derivative used within the Newton–Raphson technique are as follows, respectively:

$$F(M) = \left(\frac{\gamma + 1}{2\gamma}\right)\ln\left(\frac{\frac{\gamma + 1}{2}}{1 + \frac{\gamma - 1}{2}M^2}\right) - \frac{1}{\gamma}\left(1 - \frac{1}{M^2}\right)$$

$$- \left(\frac{\gamma + 1}{2\gamma}\right)\ln\left(\frac{1}{M^2}\right) - \frac{fL_{\max}}{D} \tag{A.51}$$

$$\frac{dF}{dM} = -\frac{\gamma^2 - 1}{2\gamma}\frac{M}{1 + \frac{\gamma - 1}{2}M^2} - \frac{2}{\gamma}\frac{1}{M^3} + \frac{\gamma + 1}{\gamma}\frac{1}{M} \tag{A.52}$$

| **Fanno flow calculations** | | | | | | $\gamma$ | 1.4 |
|---|---|---|---|---|---|---|---|
| **Given $M$, find the property ratio** | | | | | | $(\gamma + 1)$ | 2.4 |
| Given: | $p/p^*$ | $T/T^*$ | $\rho/\rho^*$ | $p_o/p_o^*$ | $fL_{max}/D$ | $(\gamma - 1)$ | 0.4 |
| 0.5000 | 2.13809 | 1.1429 | 1.8708 | 1.3398 | 1.0691 | $1/\gamma$ | 0.7143 |
| **Given the property ratio, find $M$** | | | | | | $(\gamma + 1)/(2\gamma)$ | 0.8571 |
| | $p/p^*$ | $T/T^*$ | $\rho/\rho^*$ | $p_o/p_o^*$ | $fL_{max}/D$ | $(\gamma + 1)/(\gamma - 1)$ | 6.0000 |
| Given: | 2.1381 | 1.1000 | 2.0000 | 20.0000 | 0.8000 | $(\gamma - 1)/(\gamma + 1)$ | 0.1667 |
| $M$ | 0.5000 | 0.6742 | 0.4663 | 0.0289 | 0.5378 | $M < 1$ | |
| | | | | 4.7255 | 12.7693 | $M > 1$ | |
| | | | | **Note: For $M > 1$, the largest $fL_{max}/D$ is** | | | |
| | | | | $([\gamma + 1)/2\gamma]\ln[(\gamma + 1)/(\gamma - 1)] - 1/\gamma$ | | | **0.8215** |

**Figure A.10** Spreadsheet Layout of a Fanno Flow Solver

Instead of using the foregoing expression for the derivative, a central-difference representation can be used instead:

$$\frac{dF}{dM} = \frac{F(M + \Delta M) - F(M - \Delta M)}{2\Delta M}$$

The new value of the Mach number is computed from an assumed or previous value from the following equation:

$$M_{new} = M_{old} - \frac{F(M_{old})}{\frac{dF}{dM}(M_{old})}$$

Figure A.10 presents a Fanno flow solver that follows arrangements similar to those just described.

Figure A.11 provides tables of results for both subsonic and supersonic flow iterations for the specific Fanno flow case in which $fL_{max}/D = 0.8$ and $\gamma = 1.4$. Obviously, starting guesses that are close to the converged results minimize the number of iterations.

Figure A.12 provides results of the $p_o/p_o^*$ iterations.

## A.6 RAYLEIGH FLOW

$$\frac{p}{p^*} = \frac{1 + \gamma}{1 + \gamma M^2} \tag{A.53}$$

$$\frac{T}{T^*} = \frac{(1 + \gamma)^2 M^2}{(1 + \gamma M^2)^2} \tag{A.54}$$

| $M < 1$ Solution | | $fL_{max}/D$ | 0.8 | | | | |
|---|---|---|---|---|---|---|---|
| **Iteration** | $M_{old}$ | $F(M)$ | $F(M + \Delta M)$ | $F(M - \Delta M)$ | $dF/dM$ | $M_{new}$ | |
| 1 | 0.2000 | 13.7333 | 12.1560 | 15.5752 | −170.9571 | 0.2803 | |
| 2 | 0.2803 | 5.5377 | 4.9814 | 6.1612 | −58.9885 | 0.3742 | |
| 3 | 0.3742 | 2.0341 | 1.8160 | 2.2729 | −22.8438 | 0.4633 | |
| 4 | 0.4633 | 0.6152 | 0.5111 | 0.7278 | −10.8341 | 0.5200 | |
| 5 | 0.5200 | 0.1171 | 0.0494 | 0.1901 | −7.0373 | 0.5367 | |
| 6 | 0.5367 | 0.0070 | −0.0530 | 0.0715 | −6.2273 | 0.5378 | |
| 7 | 0.5378 | 0.0000 | −0.0595 | 0.0641 | −6.1764 | 0.5378 | |
| 8 | 0.5378 | 0.0000 | −0.0595 | 0.0640 | −6.1762 | 0.5378 | **Answer** |
| $M > 1$ Solution | | $fL_{max}/D$ | 0.8 | | | | |
| **Iteration** | $M_{old}$ | $F(M)$ | $F(M + \Delta M)$ | $F(M - \Delta M)$ | $dF/dM$ | $M_{new}$ | |
| 1 | 2.0000 | −0.4950 | −0.4920 | −0.4980 | 0.2976 | 3.6632 | |
| 2 | 3.6632 | −0.1967 | −0.1958 | −0.1977 | 0.0980 | 5.6712 | |
| 3 | 5.6712 | −0.0801 | −0.0798 | −0.0805 | 0.0328 | 8.1116 | |
| 4 | 8.1116 | −0.0304 | −0.0303 | −0.0305 | 0.0122 | 10.5947 | |
| 5 | 10.5947 | −0.0095 | −0.0094 | −0.0095 | 0.0057 | 12.2587 | |
| 6 | 12.2587 | −0.0018 | −0.0018 | −0.0018 | 0.0037 | 12.7399 | |
| 7 | 12.7399 | −0.0001 | −0.0001 | −0.0001 | 0.0033 | 12.7692 | |
| 8 | 12.7692 | 0.0000 | 0.0000 | 0.0000 | 0.0033 | 12.7693 | **Answer** |

**Figure A.11** Fanno Flow Newton–Raphson Solver for the Mach Number for $fL_{max}/D = 0.8$

$$\frac{V}{V^*} = \frac{\rho^*}{\rho} = \frac{p^*}{p}\frac{T}{T^*} \tag{A.55}$$

$$\frac{T_o}{T_o^*} = \frac{(1+\gamma)M^2[2+(\gamma-1)M^2]}{(1+\gamma M^2)^2} \tag{A.56}$$

$$\frac{p_o}{p_o^*} = \left(\frac{1+\gamma}{1+\gamma M^2}\right)\left[\frac{2+(\gamma-1)M^2}{\gamma+1}\right]^{\gamma/(\gamma-1)} \tag{A.57}$$

When a property ratio is known, the Mach number can be determined from one of the following equations:

$$M = \sqrt{\frac{1+\gamma}{\gamma}\frac{p^*}{p} - \frac{1}{\gamma}} \tag{A.58}$$

| $p_o/p_o^*$ | 20.0000 | | | | |
|---|---|---|---|---|---|
| $M < 1$ | | | | | |
| **Iteration** | $M_{old}$ | $F(M)$ | $dF/dM$ | $M_{new}$ | |
| 1 | 0.7000 | 13.2339 | 19.4139 | 0.0183 | |
| 2 | 0.0183 | −0.2123 | 19.9873 | 0.0289 | |
| 3 | 0.0289 | 0.0000 | 19.9799 | 0.0289 | |
| 4 | 0.0289 | 0.0000 | 19.9799 | 0.0289 | |
| 5 | 0.0289 | 0.0000 | 19.9799 | 0.0289 | **Answer** |
| $M > 1$ | | | | | |
| **Iteration** | $M_{old}$ | $F(M)$ | $dF/dM$ | $M_{new}$ | |
| 1 | 4.0000 | 37.1250 | −29.0000 | 5.2802 | |
| 2 | 5.2802 | −58.9665 | −138.5678 | 4.8546 | |
| 3 | 4.8546 | −10.8418 | −90.0515 | 4.7342 | |
| 4 | 4.7342 | −0.6860 | −78.8234 | 4.7255 | |
| 5 | 4.7255 | −0.0034 | −78.0501 | 4.7255 | **Answer** |

**Figure A.12** Newton–Raphson Solver for $M$ for a Given Stagnation Pressure Ratio $p_o/p_o^* = 20.00$

$$M = \frac{1}{\sqrt{\frac{\rho}{\rho^*}(1+\gamma) - \gamma}} \tag{A.59}$$

$$M = \frac{1 + \gamma \pm \sqrt{(1+\gamma)^2 - 4\gamma\frac{T}{T^*}}}{2\gamma\sqrt{\frac{T}{T^*}}} \tag{A.60}$$

$$M^2 = \frac{(1+\gamma)\left(1 \pm \sqrt{1 - \frac{T_o}{T_o^*}}\right) - \gamma\frac{T_o}{T_o^*}}{\gamma^2\left(\frac{T_o}{T_o^*} - 1\right) + 1} \tag{A.61}$$

The calculation of the Mach number from the stagnation pressure ratio can be done only numerically, using, for example, the Newton–Raphson algorithm. Equation (A.57) can be written as function of the ratio of the stagnation pressures $p_o/p_o^*$ and $M$. (Note that a variety of such functions can be constructed; some, however, are not as

| **Rayleigh flow calculations** | | | | | | | |
|---|---|---|---|---|---|---|---|
| **Given $M$, find the property ratio** | | | | | | $\gamma$ | 1.4 |
| Given: | $p/p^*$ | $T/T^*$ | $\rho/\rho^*$ | $T_o/T_o^*$ | $p_o/p_o^*$ | $(\gamma + 1)$ | 2.4 |
| 0.1000 | 2.36686 | 0.05602 | 42.2500 | 0.04678 | 1.2591 | $(\gamma - 1)$ | 0.4 |
| 0.5000 | 1.77778 | 0.79012 | 2.2500 | 0.6914 | 1.1141 | $1/\gamma$ | 0.7143 |
| 2.0000 | 0.36364 | 0.52893 | 0.6875 | 0.7934 | 1.5031 | $(\gamma + 1)/(2\gamma)$ | 0.8571 |
| **Given the property ratio, find $M$** | | | | | | $(\gamma + 1)/(\gamma - 1)$ | 6.0000 |
| | $p/p^*$ | $T/T^*$ | $\rho/\rho^*$ | $T_o/T_o^*$ | $p_o/p_o^*$ | $(\gamma - 1)/(\gamma + 1)$ | 0.1667 |
| Given: | 2.3669 | 0.0552 | 42.2500 | 0.7934 | 1.1141 | $(\gamma)/(3\gamma - 1)$ | 0.4375 |
| $M$ | 0.1000 | 0.09922 | 0.1000 | 0.5774 | 0.5000 | **subsonic** | $M_{critical}$ |
| | | 7.1993 | | 2.0000 | 1.4844 | **supersonic** | 0.845154 |

**Figure A.13** Layout of the Spreadsheet Solver for Rayleigh Flow

"friendly" to work with as others.) The derivative of the function can be taken and the pair written as follows:

$$F(M) = 2 + (\gamma - 1)M^2 - (\gamma + 1)^{1/\gamma}\left[\frac{p_o}{p_o^*}(1 + \gamma M^2)\right]^{(\gamma-1)/\gamma} \tag{A.62}$$

$$\frac{dF}{dM}(M) = 2(\gamma - 1)M - 2(\gamma - 1)(\gamma + 1)^{1/\gamma}\left[\frac{p_o}{p_o^*}(1 + \gamma M^2)\right]^{-(1/\gamma)} M\frac{p_o}{p_o^*} \tag{A.63}$$

Figure A.13 presents a potential spreadsheet arrangement for a Rayleigh Flow solver. The arrangement is one of personal preference, and the solver's creator can insert those computations which help in its construction. Thus, on the far right are various quantities involving $\gamma$ that were used in the calculation formulas.

As pointed out previously, the Mach number can be extracted from the $p_o/p_o^*$ expression, Eq. (A.57), by numerical procedures only. Figure A.14 presents subsonic and supersonic iterations for a specific case.

## A.7 ISOTHERMAL FLOW

$$M^* = \frac{1}{\sqrt{\gamma}} \tag{A.64}$$

$$\frac{T_o}{T_o^*} = \frac{2 + (\gamma - 1)M^2}{2 + (\gamma - 1)\left(\frac{1}{\sqrt{\gamma}}\right)^2} = \left(\frac{\gamma}{3\gamma - 1}\right)[2 + (\gamma - 1)M^2] \tag{A.65}$$

| $p_o/p_o^*$ | 1.1141 | | | | |
|---|---|---|---|---|---|
| $M < 1$ | | | | | |
| **Iteration** | $M_{old}$ | $F(M)$ | $dF/dM$ | $M_{new}$ | |
| 1 | 0.2000 | 0.0583 | −0.1366 | 0.6269 | |
| 2 | 0.6269 | −0.0274 | −0.2053 | 0.4933 | |
| 3 | 0.4933 | 0.0015 | −0.2223 | 0.5000 | |
| 4 | 0.5000 | 0.0000 | −0.2222 | 0.5000 | |
| 5 | 0.5000 | 0.0000 | −0.2222 | 0.5000 | **Answer** |
| $M > 1$ | | | | | |
| **Iteration** | $M_{old}$ | $F(M)$ | $dF/dM$ | $M_{new}$ | |
| 1 | 3.0000 | 1.5370 | 1.6830 | 2.0868 | |
| 2 | 2.0868 | 0.3679 | 0.8757 | 1.6666 | |
| 3 | 1.6666 | 0.0779 | 0.5061 | 1.5127 | |
| 4 | 1.5127 | 0.0102 | 0.3738 | 1.4853 | |
| 5 | 1.4853 | 0.0003 | 0.3506 | 1.4844 | |
| 6 | 1.4844 | 0.0000 | 0.3499 | 1.4844 | **Answer** |

**Figure A.14** Newton–Raphson Solver for Mach Number for a Given Stagnation Pressure Ratio $p_o/p_o^* = 1.1141$

$$\frac{p}{p^*} = \frac{\rho}{\rho^*} = \frac{V^*}{V} = \frac{1}{\sqrt{\gamma}M} \tag{A.66}$$

$$\frac{fL_{\max}}{D} = \frac{1 - \gamma M^2}{\gamma M^2} + \ln(\gamma M^2) \tag{A.67}$$

$$\frac{p_o}{p_o^*} = \frac{1}{\sqrt{\gamma}M}\left\{\frac{\gamma}{(3\gamma - 1)}[2 + (\gamma - 1)M^2]\right\}^{\gamma/(\gamma-1)} \tag{A.68}$$

When a property ratio is given, the Mach number can be determined from the following expressions:

$$M = \frac{1}{\sqrt{\gamma}}\frac{p^*}{p} \tag{A.69}$$

$$M = \frac{1}{\sqrt{\gamma}}\frac{\rho^*}{\rho} \tag{A.70}$$

$$M = \sqrt{\frac{(3\gamma - 1)\dfrac{T_o}{T_o^*} - 2\gamma}{\gamma(\gamma - 1)}} \tag{A.71}$$

When the Mach number has to be computed from a known value of $fL_{max}/D$, Eq. (A.67) has to be solved numerically. To accomplish this, a function $F(M)$ is created and its derivative is taken to give the following:

$$F(M) = \gamma M^2\left[\frac{fL_{max}}{D} + 1 - \ln(\gamma M^2)\right] - 1 \tag{A.72}$$

$$\frac{dF}{dM}(M) = 2\gamma M\left[\frac{fL_{max}}{D} - \ln(\gamma M^2)\right] \tag{A.73}$$

Also, if the stagnation pressure ratio $p_o/p_o^*$ for isothermal flow is known, we can determine the corresponding $M$ by constructing a function $F(M)$ and taking its derivative:

$$F(M) = 2 + (\gamma - 1)M^2 - \left(\sqrt{\gamma}\frac{p_o}{p_o^*}M\right)^{(\gamma-1)/\gamma}\frac{1}{\dfrac{\gamma}{3\gamma - 1}} \tag{A.74}$$

$$\frac{dF}{dM}(M) = 2(\gamma - 1)M - \left(\sqrt{\gamma}\frac{p_o}{p_o^*}\right)^{(\gamma-1)/\gamma}\frac{\gamma - 1}{\gamma}\cdot\frac{1}{\dfrac{\gamma}{3\gamma - 1}}\cdot\frac{1}{M^{1/\gamma}} \tag{A.75}$$

Figure A.15 presents a potential spreadsheet arrangement for an isothermal flow solver.

Figure A.16 presents the iterations required to extract Mach numbers (subcritical and supercritical) from Eq. (A.72) for an $fL_{max}/D = 0.901338$ and $\gamma = 1.4$.

| **Isothermal flow calculation** | | | | | | $\gamma$ | 1.4 |
|---|---|---|---|---|---|---|---|
| **Given $M$, find the property ratio** | | | | | | $(\gamma + 1)$ | 2.4 |
| Given: | $p/p^*$ | $T_o/T_o^*$ | $\rho/\rho^*$ | $p_o/p_o^*$ | $fL_{max}/D$ | $(\gamma - 1)$ | 0.4 |
| 2.0000 | 0.42258 | 1.5750 | 0.4226 | 2.0720 | 0.9013 | $1/\gamma$ | 0.7143 |
| 0.4880 | 1.73203 | 0.9167 | 1.7320 | 1.2773 | 0.9013 | $(\gamma + 1)/(2\gamma)$ | 0.8571 |
| **Given the property ratio, find $M$** | | | | | | $(\gamma + 1)/(\gamma - 1)$ | 6.0000 |
| | $p/p^*$ | $T_o/T_o^*$ | $\rho/\rho^*$ | $p_o/p_o^*$ | $fL_{max}/D$ | $(\gamma - 1)/(\gamma + 1)$ | 0.1667 |
| Given: | 0.4226 | 1.5750 | 0.4226 | 2.0720 | 0.9013 | $(\gamma)/(3\gamma - 1)$ | 0.4375 |
| $M$ | 2.0000 | 2.0000 | 2.0000 | 0.2688 | 0.4880 | **subcritical** | $M_{critical}$ |
| | | | | 2.0000 | 2.0000 | **supercritical** | 0.845154 |

**Figure A.15** Layout of a Spreadsheet Solver for Isothermal Flow

| $fL_{max}/D$ | 0.90133803 | | | | |
|---|---|---|---|---|---|
| **Subcritical Solution** | | | | | |
| **Iteration** | $M_{old}$ | $F(M)$ | $dF/dM$ | $M_{new}$ | |
| 1 | 0.2000 | −0.7321 | 2.1189 | 0.5455 | |
| 2 | 0.5455 | 0.1569 | 2.7141 | 0.4877 | |
| 3 | 0.4877 | −0.0007 | 2.7325 | 0.4880 | |
| 4 | 0.4880 | 0.0000 | 2.7325 | 0.4880 | |
| 5 | 0.4880 | 0.0000 | 2.7325 | 0.4880 | **Answer** |
| **Supercritical Solution** | | | | | |
| **Iteration** | $M_{old}$ | $F(M)$ | $dF/dM$ | $M_{new}$ | |
| 1 | 4.0000 | −28.0530 | −24.7265 | 2.8655 | |
| 2 | 2.8655 | −7.2143 | −12.3607 | 2.2818 | |
| 3 | 2.2818 | −1.6202 | −6.9327 | 2.0481 | |
| 4 | 2.0481 | −0.2305 | −4.9833 | 2.0019 | |
| 5 | 2.0019 | −0.0086 | −4.6147 | 2.0000 | |
| 6 | 2.0000 | 0.0000 | −4.6000 | 2.0000 | **Answer** |

**Figure A.16** Newton–Raphson Solver to Find Mach Numbers for a Given Value of $fL_{max}/D$ in Isothermal Flow

As pointed out previously, the Mach number can be extracted from the $p_o/p_o^*$ expression, Eq. (A.68), by numerical procedures only. Figure A.17 presents subcritical and supercritical iterations for a specific case.

| $p_o/p_o^*$ | 2.0720 | | | | |
|---|---|---|---|---|---|
| **Subcritical** | | | | | |
| **Iteration** | $M_{old}$ | $F(M)$ | $dF/dM$ | $M_{new}$ | |
| 1 | 0.2000 | 0.1514 | −2.5037 | 0.2605 | |
| 2 | 0.2605 | 0.0164 | −1.9973 | 0.2687 | |
| 3 | 0.2687 | 0.0002 | −1.9426 | 0.2688 | |
| 4 | 0.2688 | 0.0000 | −1.9418 | 0.2688 | **Answer** |
| **Supercritical** | | | | | |
| **Iteration** | $M_{old}$ | $F(M)$ | $dF/dM$ | $M_{new}$ | |
| 1 | 3.0000 | 1.5578 | 2.0150 | 2.2269 | |
| 2 | 2.2269 | 0.2714 | 1.3052 | 2.0190 | |
| 3 | 2.0190 | 0.0208 | 1.1044 | 2.0002 | |
| 4 | 2.0002 | 0.0002 | 1.0859 | 2.0000 | |
| 5 | 2.0000 | 0.0000 | 1.0857 | 2.0000 | **Answer** |

**Figure A.17** Newton–Raphson Iteration for Mach Number for a Given Stagnation Pressure Ratio $p_o/p_o^*$

# Appendix B

# Isentropic Flow Tables

**TABLE B.1** Isentropic Flow Table ($\gamma = 1.4$)

| $M$ | $T/T_o$ | $p/p_o$ | $\rho/\rho_o$ | $A/A^*$ |
|---|---|---|---|---|
| 0.00 | 1.0000 | 1.0000 | 1.0000 | $\infty$ |
| 0.02 | 0.9999 | 0.9997 | 0.9998 | 28.9421 |
| 0.04 | 0.9997 | 0.9989 | 0.9992 | 14.4815 |
| 0.06 | 0.9993 | 0.9975 | 0.9982 | 9.6659 |
| 0.08 | 0.9987 | 0.9955 | 0.9968 | 7.2616 |
| 0.10 | 0.9980 | 0.9930 | 0.9950 | 5.8218 |
| 0.12 | 0.9971 | 0.9900 | 0.9928 | 4.8643 |
| 0.14 | 0.9961 | 0.9864 | 0.9903 | 4.1824 |
| 0.16 | 0.9949 | 0.9823 | 0.9873 | 3.6727 |
| 0.18 | 0.9936 | 0.9776 | 0.9840 | 3.2779 |
| 0.20 | 0.9921 | 0.9725 | 0.9803 | 2.9635 |
| 0.22 | 0.9904 | 0.9668 | 0.9762 | 2.7076 |
| 0.24 | 0.9886 | 0.9607 | 0.9718 | 2.4956 |
| 0.26 | 0.9867 | 0.9541 | 0.9670 | 2.3173 |
| 0.28 | 0.9846 | 0.9470 | 0.9619 | 2.1656 |
| 0.30 | 0.9823 | 0.9395 | 0.9564 | 2.0351 |
| 0.32 | 0.9799 | 0.9315 | 0.9506 | 1.9219 |
| 0.34 | 0.9774 | 0.9231 | 0.9445 | 1.8229 |
| 0.36 | 0.9747 | 0.9143 | 0.9380 | 1.7358 |
| 0.38 | 0.9719 | 0.9052 | 0.9313 | 1.6587 |
| 0.40 | 0.9690 | 0.8956 | 0.9243 | 1.5901 |
| 0.42 | 0.9659 | 0.8857 | 0.9170 | 1.5289 |
| 0.44 | 0.9627 | 0.8755 | 0.9094 | 1.4740 |
| 0.46 | 0.9594 | 0.8650 | 0.9016 | 1.4246 |
| 0.48 | 0.9559 | 0.8541 | 0.8935 | 1.3801 |
| 0.50 | 0.9524 | 0.8430 | 0.8852 | 1.3398 |
| 0.52 | 0.9487 | 0.8317 | 0.8766 | 1.3034 |
| 0.54 | 0.9449 | 0.8201 | 0.8679 | 1.2703 |
| 0.56 | 0.9410 | 0.8082 | 0.8589 | 1.2403 |
| 0.58 | 0.9370 | 0.7962 | 0.8498 | 1.2130 |
| 0.60 | 0.9328 | 0.7840 | 0.8405 | 1.1882 |
| 0.62 | 0.9286 | 0.7716 | 0.8310 | 1.1656 |
| 0.64 | 0.9243 | 0.7591 | 0.8213 | 1.1451 |
| 0.66 | 0.9199 | 0.7465 | 0.8115 | 1.1265 |
| 0.68 | 0.9153 | 0.7338 | 0.8016 | 1.1097 |
| 0.70 | 0.9107 | 0.7209 | 0.7916 | 1.0944 |
| 0.72 | 0.9061 | 0.7080 | 0.7814 | 1.0806 |
| 0.74 | 0.9013 | 0.6951 | 0.7712 | 1.0681 |
| 0.76 | 0.8964 | 0.6821 | 0.7609 | 1.0570 |
| 0.78 | 0.8915 | 0.6691 | 0.7505 | 1.0471 |
| 0.80 | 0.8865 | 0.6560 | 0.7400 | 1.0382 |
| 0.82 | 0.8815 | 0.6430 | 0.7295 | 1.0305 |
| 0.84 | 0.8763 | 0.6300 | 0.7189 | 1.0237 |
| 0.86 | 0.8711 | 0.6170 | 0.7083 | 1.0179 |
| 0.88 | 0.8659 | 0.6041 | 0.6977 | 1.0129 |
| 0.90 | 0.8606 | 0.5913 | 0.6870 | 1.0089 |
| 0.92 | 0.8552 | 0.5785 | 0.6764 | 1.0056 |
| 0.94 | 0.8498 | 0.5658 | 0.6658 | 1.0031 |
| 0.96 | 0.8444 | 0.5532 | 0.6551 | 1.0014 |
| 0.98 | 0.8389 | 0.5407 | 0.6445 | 1.0003 |
| 1.00 | 0.8333 | 0.5283 | 0.6339 | 1.0000 |
| 1.02 | 0.8278 | 0.5160 | 0.6234 | 1.0003 |
| 1.04 | 0.8222 | 0.5039 | 0.6129 | 1.0013 |
| 1.06 | 0.8165 | 0.4919 | 0.6024 | 1.0029 |
| 1.08 | 0.8108 | 0.4800 | 0.5920 | 1.0051 |
| 1.10 | 0.8052 | 0.4684 | 0.5817 | 1.0079 |
| 1.12 | 0.7994 | 0.4568 | 0.5714 | 1.0113 |
| 1.14 | 0.7937 | 0.4455 | 0.5612 | 1.0153 |
| 1.16 | 0.7879 | 0.4343 | 0.5511 | 1.0198 |
| 1.18 | 0.7822 | 0.4232 | 0.5411 | 1.0248 |
| 1.20 | 0.7764 | 0.4124 | 0.5311 | 1.0304 |
| 1.22 | 0.7706 | 0.4017 | 0.5213 | 1.0366 |
| 1.24 | 0.7648 | 0.3912 | 0.5115 | 1.0432 |
| 1.26 | 0.7590 | 0.3809 | 0.5019 | 1.0504 |
| 1.28 | 0.7532 | 0.3708 | 0.4923 | 1.0581 |
| 1.30 | 0.7474 | 0.3609 | 0.4829 | 1.0663 |
| 1.32 | 0.7416 | 0.3512 | 0.4736 | 1.0750 |
| 1.34 | 0.7358 | 0.3417 | 0.4644 | 1.0842 |
| 1.36 | 0.7300 | 0.3323 | 0.4553 | 1.0940 |
| 1.38 | 0.7242 | 0.3232 | 0.4463 | 1.1042 |
| 1.40 | 0.7184 | 0.3142 | 0.4374 | 1.1149 |
| 1.42 | 0.7126 | 0.3055 | 0.4287 | 1.1262 |
| 1.44 | 0.7069 | 0.2969 | 0.4201 | 1.1379 |
| 1.46 | 0.7011 | 0.2886 | 0.4116 | 1.1501 |
| 1.48 | 0.6954 | 0.2804 | 0.4032 | 1.1629 |
| 1.50 | 0.6897 | 0.2724 | 0.3950 | 1.1762 |
| 1.52 | 0.6840 | 0.2646 | 0.3869 | 1.1899 |
| 1.54 | 0.6783 | 0.2570 | 0.3789 | 1.2042 |
| 1.56 | 0.6726 | 0.2496 | 0.3710 | 1.2190 |
| 1.58 | 0.6670 | 0.2423 | 0.3633 | 1.2344 |
| 1.60 | 0.6614 | 0.2353 | 0.3557 | 1.2502 |
| 1.62 | 0.6558 | 0.2284 | 0.3483 | 1.2666 |
| 1.64 | 0.6502 | 0.2217 | 0.3409 | 1.2836 |
| 1.66 | 0.6447 | 0.2151 | 0.3337 | 1.3010 |
| 1.68 | 0.6392 | 0.2088 | 0.3266 | 1.3190 |
| 1.70 | 0.6337 | 0.2026 | 0.3197 | 1.3376 |
| 1.72 | 0.6283 | 0.1966 | 0.3129 | 1.3567 |
| 1.74 | 0.6229 | 0.1907 | 0.3062 | 1.3764 |
| 1.76 | 0.6175 | 0.1850 | 0.2996 | 1.3967 |
| 1.78 | 0.6121 | 0.1794 | 0.2931 | 1.4175 |
| 1.80 | 0.6068 | 0.1740 | 0.2868 | 1.4390 |
| 1.82 | 0.6015 | 0.1688 | 0.2806 | 1.4610 |
| 1.84 | 0.5963 | 0.1637 | 0.2745 | 1.4836 |
| 1.86 | 0.5910 | 0.1587 | 0.2686 | 1.5069 |

**TABLE B.1** *(Continued)*

| $M$ | $T/T_o$ | $p/p_o$ | $\rho/\rho_o$ | $A/A^*$ |
|---|---|---|---|---|
| 1.88 | 0.5859 | 0.1539 | 0.2627 | 1.5308 |
| 1.90 | 0.5807 | 0.1492 | 0.2570 | 1.5553 |
| 1.92 | 0.5756 | 0.1447 | 0.2514 | 1.5804 |
| 1.94 | 0.5705 | 0.1403 | 0.2459 | 1.6062 |
| 1.96 | 0.5655 | 0.1360 | 0.2405 | 1.6326 |
| 1.98 | 0.5605 | 0.1318 | 0.2352 | 1.6597 |
| 2.00 | 0.5556 | 0.1278 | 0.2300 | 1.6875 |
| 2.02 | 0.5506 | 0.1239 | 0.2250 | 1.7160 |
| 2.04 | 0.5458 | 0.1201 | 0.2200 | 1.7451 |
| 2.06 | 0.5409 | 0.1164 | 0.2152 | 1.7750 |
| 2.08 | 0.5361 | 0.1128 | 0.2104 | 1.8056 |
| 2.10 | 0.5313 | 0.1094 | 0.2058 | 1.8369 |
| 2.12 | 0.5266 | 0.1060 | 0.2013 | 1.8690 |
| 2.14 | 0.5219 | 0.1027 | 0.1968 | 1.9018 |
| 2.16 | 0.5173 | 0.0996 | 0.1925 | 1.9354 |
| 2.18 | 0.5127 | 0.0965 | 0.1882 | 1.9698 |
| 2.20 | 0.5081 | 0.0935 | 0.1841 | 2.0050 |
| 2.22 | 0.5036 | 0.0906 | 0.1800 | 2.0409 |
| 2.24 | 0.4991 | 0.0878 | 0.1760 | 2.0777 |
| 2.26 | 0.4947 | 0.0851 | 0.1721 | 2.1153 |
| 2.28 | 0.4903 | 0.0825 | 0.1683 | 2.1538 |
| 2.30 | 0.4859 | 0.0800 | 0.1646 | 2.1931 |
| 2.32 | 0.4816 | 0.0775 | 0.1609 | 2.2333 |
| 2.34 | 0.4773 | 0.0751 | 0.1574 | 2.2744 |
| 2.36 | 0.4731 | 0.0728 | 0.1539 | 2.3164 |
| 2.38 | 0.4688 | 0.0706 | 0.1505 | 2.3593 |
| 2.40 | 0.4647 | 0.0684 | 0.1472 | 2.4031 |
| 2.42 | 0.4606 | 0.0663 | 0.1439 | 2.4479 |
| 2.44 | 0.4565 | 0.0643 | 0.1408 | 2.4936 |
| 2.46 | 0.4524 | 0.0623 | 0.1377 | 2.5403 |
| 2.48 | 0.4484 | 0.0604 | 0.1346 | 2.5880 |
| 2.50 | 0.4444 | 0.0585 | 0.1317 | 2.6367 |
| 2.52 | 0.4405 | 0.0567 | 0.1288 | 2.6865 |
| 2.54 | 0.4366 | 0.0550 | 0.1260 | 2.7372 |
| 2.56 | 0.4328 | 0.0533 | 0.1232 | 2.7891 |
| 2.58 | 0.4289 | 0.0517 | 0.1205 | 2.8420 |
| 2.60 | 0.4252 | 0.0501 | 0.1179 | 2.8960 |
| 2.62 | 0.4214 | 0.0486 | 0.1153 | 2.9511 |
| 2.64 | 0.4177 | 0.0471 | 0.1128 | 3.0073 |
| 2.66 | 0.4141 | 0.0457 | 0.1103 | 3.0647 |
| 2.68 | 0.4104 | 0.0443 | 0.1079 | 3.1233 |
| 2.70 | 0.4068 | 0.0430 | 0.1056 | 3.1830 |
| 2.72 | 0.4033 | 0.0417 | 0.1033 | 3.2440 |
| 2.74 | 0.3998 | 0.0404 | 0.1010 | 3.3061 |
| 2.76 | 0.3963 | 0.0392 | 0.0989 | 3.3695 |
| 2.78 | 0.3928 | 0.0380 | 0.0967 | 3.4342 |
| 2.80 | 0.3894 | 0.0368 | 0.0946 | 3.5001 |
| 2.82 | 0.3860 | 0.0357 | 0.0926 | 3.5674 |
| 2.84 | 0.3827 | 0.0347 | 0.0906 | 3.6359 |
| 2.86 | 0.3794 | 0.0336 | 0.0886 | 3.7058 |
| 2.88 | 0.3761 | 0.0326 | 0.0867 | 3.7771 |
| 2.90 | 0.3729 | 0.0317 | 0.0849 | 3.8498 |
| 2.92 | 0.3696 | 0.0307 | 0.0831 | 3.9238 |
| 2.94 | 0.3665 | 0.0298 | 0.0813 | 3.9993 |
| 2.96 | 0.3633 | 0.0289 | 0.0796 | 4.0763 |
| 2.98 | 0.3602 | 0.0281 | 0.0779 | 4.1547 |
| 3.00 | 0.3571 | 0.0272 | 0.0762 | 4.2346 |

| $M$ | $T/T_o$ | $p/p_o$ | $\rho/\rho_o$ | $A/A^*$ |
|---|---|---|---|---|
| 3.02 | 0.3541 | 0.0264 | 0.0746 | 4.3160 |
| 3.04 | 0.3511 | 0.0256 | 0.0730 | 4.3989 |
| 3.06 | 0.3481 | 0.0249 | 0.0715 | 4.4835 |
| 3.08 | 0.3452 | 0.0242 | 0.0700 | 4.5696 |
| 3.10 | 0.3422 | 0.0234 | 0.0685 | 4.6573 |
| 3.12 | 0.3393 | 0.0228 | 0.0671 | 4.7467 |
| 3.14 | 0.3365 | 0.0221 | 0.0657 | 4.8377 |
| 3.16 | 0.3337 | 0.0215 | 0.0643 | 4.9304 |
| 3.18 | 0.3309 | 0.0208 | 0.0630 | 5.0248 |
| 3.20 | 0.3281 | 0.0202 | 0.0617 | 5.1210 |
| 3.22 | 0.3253 | 0.0196 | 0.0604 | 5.2189 |
| 3.24 | 0.3226 | 0.0191 | 0.0591 | 5.3186 |
| 3.26 | 0.3199 | 0.0185 | 0.0579 | 5.4201 |
| 3.28 | 0.3173 | 0.0180 | 0.0567 | 5.5234 |
| 3.30 | 0.3147 | 0.0175 | 0.0555 | 5.6286 |
| 3.32 | 0.3121 | 0.0170 | 0.0544 | 5.7358 |
| 3.34 | 0.3095 | 0.0165 | 0.0533 | 5.8448 |
| 3.36 | 0.3069 | 0.0160 | 0.0522 | 5.9558 |
| 3.38 | 0.3044 | 0.0156 | 0.0511 | 6.0687 |
| 3.40 | 0.3019 | 0.0151 | 0.0501 | 6.1837 |
| 3.42 | 0.2995 | 0.0147 | 0.0491 | 6.3007 |
| 3.44 | 0.2970 | 0.0143 | 0.0481 | 6.4198 |
| 3.46 | 0.2946 | 0.0139 | 0.0471 | 6.5409 |
| 3.48 | 0.2922 | 0.0135 | 0.0462 | 6.6642 |
| 3.50 | 0.2899 | 0.0131 | 0.0452 | 6.7896 |
| 3.52 | 0.2875 | 0.0127 | 0.0443 | 6.9172 |
| 3.54 | 0.2852 | 0.0124 | 0.0434 | 7.0471 |
| 3.56 | 0.2829 | 0.0120 | 0.0426 | 7.1791 |
| 3.58 | 0.2806 | 0.0117 | 0.0417 | 7.3135 |
| 3.60 | 0.2784 | 0.0114 | 0.0409 | 7.4501 |
| 3.62 | 0.2762 | 0.0111 | 0.0401 | 7.5891 |
| 3.64 | 0.2740 | 0.0108 | 0.0393 | 7.7305 |
| 3.66 | 0.2718 | 0.0105 | 0.0385 | 7.8742 |
| 3.68 | 0.2697 | 0.0102 | 0.0378 | 8.0204 |
| 3.70 | 0.2675 | 0.0099 | 0.0370 | 8.1691 |
| 3.72 | 0.2654 | 0.0096 | 0.0363 | 8.3202 |
| 3.74 | 0.2633 | 0.0094 | 0.0356 | 8.4739 |
| 3.76 | 0.2613 | 0.0091 | 0.0349 | 8.6302 |
| 3.78 | 0.2592 | 0.0089 | 0.0342 | 8.7891 |
| 3.80 | 0.2572 | 0.0086 | 0.0335 | 8.9506 |
| 3.82 | 0.2552 | 0.0084 | 0.0329 | 9.1148 |
| 3.84 | 0.2532 | 0.0082 | 0.0323 | 9.2817 |
| 3.86 | 0.2513 | 0.0080 | 0.0316 | 9.4513 |
| 3.88 | 0.2493 | 0.0077 | 0.0310 | 9.6237 |
| 3.90 | 0.2474 | 0.0075 | 0.0304 | 9.7990 |
| 3.92 | 0.2455 | 0.0073 | 0.0299 | 9.9771 |
| 3.94 | 0.2436 | 0.0071 | 0.0293 | 10.1581 |
| 3.96 | 0.2418 | 0.0069 | 0.0287 | 10.3420 |
| 3.98 | 0.2399 | 0.0068 | 0.0282 | 10.5289 |
| 4.00 | 0.2381 | 0.0066 | 0.0277 | 10.7188 |
| 4.02 | 0.2363 | 0.0064 | 0.0271 | 10.9117 |
| 4.04 | 0.2345 | 0.0062 | 0.0266 | 11.1077 |
| 4.06 | 0.2327 | 0.0061 | 0.0261 | 11.3068 |
| 4.08 | 0.2310 | 0.0059 | 0.0256 | 11.5091 |
| 4.10 | 0.2293 | 0.0058 | 0.0252 | 11.7147 |
| 4.12 | 0.2275 | 0.0056 | 0.0247 | 11.9234 |
| 4.14 | 0.2258 | 0.0055 | 0.0242 | 12.1354 |

**TABLE B.1** *(Continued)*

| $M$ | $T/T_o$ | $p/p_o$ | $\rho/\rho_o$ | $A/A^*$ |
|---|---|---|---|---|
| 4.16 | 0.2242 | 0.0053 | 0.0238 | 12.3508 |
| 4.18 | 0.2225 | 0.0052 | 0.0234 | 12.5695 |
| 4.20 | 0.2208 | 0.0051 | 0.0229 | 12.7916 |
| 4.22 | 0.2192 | 0.0049 | 0.0225 | 13.0172 |
| 4.24 | 0.2176 | 0.0048 | 0.0221 | 13.2463 |
| 4.26 | 0.2160 | 0.0047 | 0.0217 | 13.4789 |
| 4.28 | 0.2144 | 0.0046 | 0.0213 | 13.7151 |
| 4.30 | 0.2129 | 0.0044 | 0.0209 | 13.9549 |
| 4.32 | 0.2113 | 0.0043 | 0.0205 | 14.1984 |
| 4.34 | 0.2098 | 0.0042 | 0.0202 | 14.4456 |
| 4.36 | 0.2083 | 0.0041 | 0.0198 | 14.6965 |
| 4.38 | 0.2067 | 0.0040 | 0.0194 | 14.9513 |
| 4.40 | 0.2053 | 0.0039 | 0.0191 | 15.2099 |
| 4.42 | 0.2038 | 0.0038 | 0.0187 | 15.4724 |
| 4.44 | 0.2023 | 0.0037 | 0.0184 | 15.7388 |
| 4.46 | 0.2009 | 0.0036 | 0.0181 | 16.0092 |
| 4.48 | 0.1994 | 0.0035 | 0.0178 | 16.2837 |
| 4.50 | 0.1980 | 0.0035 | 0.0174 | 16.5622 |
| 4.52 | 0.1966 | 0.0034 | 0.0171 | 16.8449 |
| 4.54 | 0.1952 | 0.0033 | 0.0168 | 17.1317 |
| 4.56 | 0.1938 | 0.0032 | 0.0165 | 17.4228 |
| 4.58 | 0.1925 | 0.0031 | 0.0163 | 17.7181 |
| 4.60 | 0.1911 | 0.0031 | 0.0160 | 18.0178 |
| 4.62 | 0.1898 | 0.0030 | 0.0157 | 18.3218 |
| 4.64 | 0.1885 | 0.0029 | 0.0154 | 18.6303 |
| 4.66 | 0.1872 | 0.0028 | 0.0152 | 18.9433 |
| 4.68 | 0.1859 | 0.0028 | 0.0149 | 19.2608 |
| 4.70 | 0.1846 | 0.0027 | 0.0146 | 19.5828 |
| 4.72 | 0.1833 | 0.0026 | 0.0144 | 19.9095 |
| 4.74 | 0.1820 | 0.0026 | 0.0141 | 20.2409 |
| 4.76 | 0.1808 | 0.0025 | 0.0139 | 20.5770 |
| 4.78 | 0.1795 | 0.0025 | 0.0137 | 20.9179 |
| 4.80 | 0.1783 | 0.0024 | 0.0134 | 21.2637 |
| 4.82 | 0.1771 | 0.0023 | 0.0132 | 21.6144 |
| 4.84 | 0.1759 | 0.0023 | 0.0130 | 21.9700 |
| 4.86 | 0.1747 | 0.0022 | 0.0128 | 22.3306 |
| 4.88 | 0.1735 | 0.0022 | 0.0125 | 22.6963 |
| 4.90 | 0.1724 | 0.0021 | 0.0123 | 23.0671 |
| 4.92 | 0.1712 | 0.0021 | 0.0121 | 23.4431 |
| 4.94 | 0.1700 | 0.0020 | 0.0119 | 23.8243 |
| 4.96 | 0.1689 | 0.0020 | 0.0117 | 24.2109 |
| 4.98 | 0.1678 | 0.0019 | 0.0115 | 24.6027 |
| 5.00 | 0.1667 | 0.0019 | 0.0113 | 25.0000 |
| 6.00 | 0.1220 | 0.0006 | 0.0052 | 53.1798 |
| 7.00 | 0.0926 | 0.0002 | 0.0026 | 104.1429 |
| 8.00 | 0.0725 | 0.0001 | 0.0014 | 190.1094 |
| 9.00 | 0.0581 | 0.0000 | 0.0008 | 327.1893 |
| 10.00 | 0.0476 | 0.0000 | 0.0005 | 535.937 |

**TABLE B.2** Isentropic Flow Table ($\gamma = 1.3$)

| $M$ | $T/T_o$ | $p/p_o$ | $\rho/\rho_o$ | $A/A^*$ |
|---|---|---|---|---|
| 0.00 | 1.0000 | 1.0000 | 1.0000 | $\infty$ |
| 0.05 | 0.9996 | 0.9984 | 0.9988 | 11.7214 |
| 0.10 | 0.9985 | 0.9935 | 0.9950 | 5.8860 |
| 0.15 | 0.9966 | 0.9855 | 0.9888 | 3.9522 |
| 0.20 | 0.9940 | 0.9744 | 0.9803 | 2.9940 |
| 0.25 | 0.9907 | 0.9604 | 0.9694 | 2.4262 |
| 0.30 | 0.9867 | 0.9435 | 0.9563 | 2.0537 |
| 0.35 | 0.9820 | 0.9241 | 0.9411 | 1.7930 |
| 0.40 | 0.9766 | 0.9023 | 0.9240 | 1.6023 |
| 0.45 | 0.9705 | 0.8784 | 0.9051 | 1.4586 |
| 0.50 | 0.9639 | 0.8525 | 0.8845 | 1.3479 |
| 0.55 | 0.9566 | 0.8251 | 0.8625 | 1.2614 |
| 0.60 | 0.9488 | 0.7962 | 0.8392 | 1.1932 |
| 0.65 | 0.9404 | 0.7662 | 0.8148 | 1.1395 |
| 0.70 | 0.9315 | 0.7354 | 0.7895 | 1.0972 |
| 0.75 | 0.9222 | 0.7040 | 0.7634 | 1.0644 |
| 0.80 | 0.9124 | 0.6722 | 0.7367 | 1.0395 |
| 0.85 | 0.9022 | 0.6403 | 0.7097 | 1.0214 |
| 0.90 | 0.8917 | 0.6084 | 0.6823 | 1.0092 |
| 0.95 | 0.8808 | 0.5769 | 0.6549 | 1.0022 |
| 1.00 | 0.8696 | 0.5457 | 0.6276 | 1.0000 |
| 1.05 | 0.8581 | 0.5152 | 0.6004 | 1.0021 |
| 1.10 | 0.8464 | 0.4854 | 0.5735 | 1.0083 |
| 1.15 | 0.8345 | 0.4565 | 0.5470 | 1.0184 |
| 1.20 | 0.8224 | 0.4285 | 0.5211 | 1.0321 |
| 1.25 | 0.8101 | 0.4015 | 0.4957 | 1.0495 |
| 1.30 | 0.7978 | 0.3757 | 0.4709 | 1.0703 |
| 1.35 | 0.7853 | 0.3509 | 0.4468 | 1.0948 |
| 1.40 | 0.7728 | 0.3273 | 0.4235 | 1.1227 |
| 1.45 | 0.7602 | 0.3049 | 0.4010 | 1.1543 |
| 1.50 | 0.7477 | 0.2836 | 0.3793 | 1.1895 |
| 1.55 | 0.7351 | 0.2635 | 0.3585 | 1.2284 |
| 1.60 | 0.7225 | 0.2446 | 0.3385 | 1.2712 |
| 1.65 | 0.7100 | 0.2268 | 0.3194 | 1.3180 |
| 1.70 | 0.6976 | 0.2100 | 0.3011 | 1.3690 |
| 1.75 | 0.6852 | 0.1944 | 0.2836 | 1.4243 |
| 1.80 | 0.6729 | 0.1797 | 0.2671 | 1.4841 |
| 1.85 | 0.6608 | 0.1660 | 0.2513 | 1.5486 |
| 1.90 | 0.6487 | 0.1533 | 0.2363 | 1.6182 |
| 1.95 | 0.6368 | 0.1415 | 0.2222 | 1.6929 |
| 2.00 | 0.6250 | 0.1305 | 0.2087 | 1.7732 |
| 2.05 | 0.6134 | 0.1203 | 0.1961 | 1.8593 |
| 2.10 | 0.6019 | 0.1108 | 0.1841 | 1.9514 |
| 2.15 | 0.5905 | 0.1020 | 0.1728 | 2.0501 |
| 2.20 | 0.5794 | 0.0939 | 0.1621 | 2.1556 |
| 2.25 | 0.5684 | 0.0865 | 0.1521 | 2.2682 |
| 2.30 | 0.5576 | 0.0795 | 0.1427 | 2.3885 |
| 2.35 | 0.5469 | 0.0732 | 0.1338 | 2.5168 |

**TABLE B.2** *(Continued)*

| $M$ | $T/T_o$ | $p/p_o$ | $\rho/\rho_o$ | $A/A^*$ |
|---|---|---|---|---|
| 2.40 | 0.5365 | 0.0673 | 0.1255 | 2.6535 |
| 2.45 | 0.5262 | 0.0619 | 0.1176 | 2.7993 |
| 2.50 | 0.5161 | 0.0569 | 0.1103 | 2.9545 |
| 2.55 | 0.5062 | 0.0523 | 0.1034 | 3.1197 |
| 2.60 | 0.4965 | 0.0481 | 0.0969 | 3.2954 |
| 2.65 | 0.4870 | 0.0443 | 0.0909 | 3.4824 |
| 2.70 | 0.4777 | 0.0407 | 0.0852 | 3.6811 |
| 2.75 | 0.4685 | 0.0374 | 0.0799 | 3.8922 |
| 2.80 | 0.4596 | 0.0344 | 0.0749 | 4.1165 |
| 2.85 | 0.4508 | 0.0317 | 0.0702 | 4.3546 |
| 2.90 | 0.4422 | 0.0291 | 0.0659 | 4.6073 |
| 2.95 | 0.4338 | 0.0268 | 0.0618 | 4.8754 |
| 3.00 | 0.4255 | 0.0247 | 0.0580 | 5.1598 |
| 3.50 | 0.3524 | 0.0109 | 0.0309 | 9.1098 |
| 4.00 | 0.2941 | 0.0050 | 0.0169 | 15.9441 |
| 4.50 | 0.2477 | 0.0024 | 0.0095 | 27.3870 |
| 5.00 | 0.2105 | 0.0012 | 0.0056 | 45.9565 |
| 6.00 | 0.1563 | 0.0003 | 0.0021 | 120.0965 |
| 7.00 | 0.1198 | 0.0001 | 0.0008 | 285.3372 |
| 8.00 | 0.0943 | 0.0000 | 0.0004 | 623.1235 |
| 9.00 | 0.0760 | 0.0000 | 0.0002 | 1265.6040 |
| 10.00 | 0.0625 | 0.0000 | 0.0001 | 2416.1184 |

**TABLE B.3** Isentropic Flow Table ($\gamma = 5/3$)

| $M$ | $T/T_o$ | $p/p_o$ | $\rho/\rho_o$ | $A/A^*$ |
|---|---|---|---|---|
| 0.00 | 1.0000 | 1.0000 | 1.0000 | $\infty$ |
| 0.05 | 0.9992 | 0.9979 | 0.9988 | 11.2688 |
| 0.10 | 0.9967 | 0.9917 | 0.9950 | 5.6626 |
| 0.15 | 0.9926 | 0.9815 | 0.9889 | 3.8065 |
| 0.20 | 0.9868 | 0.9674 | 0.9803 | 2.8880 |
| 0.25 | 0.9796 | 0.9498 | 0.9695 | 2.3447 |
| 0.30 | 0.9709 | 0.9288 | 0.9566 | 1.9892 |
| 0.35 | 0.9608 | 0.9048 | 0.9417 | 1.7411 |
| 0.40 | 0.9494 | 0.8782 | 0.9250 | 1.5603 |
| 0.45 | 0.9368 | 0.8493 | 0.9067 | 1.4244 |
| 0.50 | 0.9231 | 0.8186 | 0.8869 | 1.3203 |
| 0.55 | 0.9084 | 0.7865 | 0.8658 | 1.2394 |
| 0.60 | 0.8929 | 0.7533 | 0.8437 | 1.1760 |
| 0.65 | 0.8766 | 0.7194 | 0.8207 | 1.1263 |
| 0.70 | 0.8596 | 0.6851 | 0.7970 | 1.0875 |
| 0.75 | 0.8421 | 0.6508 | 0.7728 | 1.0576 |
| 0.80 | 0.8242 | 0.6167 | 0.7482 | 1.0351 |
| 0.85 | 0.8059 | 0.5831 | 0.7235 | 1.0189 |
| 0.90 | 0.7874 | 0.5502 | 0.6987 | 1.0081 |
| 0.95 | 0.7687 | 0.5181 | 0.6740 | 1.0019 |
| 1.00 | 0.7500 | 0.4871 | 0.6495 | 1.0000 |
| 1.05 | 0.7313 | 0.4573 | 0.6253 | 1.0018 |
| 1.10 | 0.7126 | 0.4286 | 0.6015 | 1.0071 |
| 1.15 | 0.6940 | 0.4013 | 0.5782 | 1.0154 |
| 1.20 | 0.6757 | 0.3753 | 0.5554 | 1.0268 |
| 1.25 | 0.6575 | 0.3506 | 0.5332 | 1.0408 |
| 1.30 | 0.6397 | 0.3272 | 0.5116 | 1.0575 |
| 1.35 | 0.6221 | 0.3052 | 0.4907 | 1.0767 |
| 1.40 | 0.6048 | 0.2845 | 0.4704 | 1.0983 |
| 1.45 | 0.5879 | 0.2651 | 0.4508 | 1.1222 |
| 1.50 | 0.5714 | 0.2468 | 0.4320 | 1.1484 |
| 1.55 | 0.5553 | 0.2298 | 0.4138 | 1.1769 |
| 1.60 | 0.5396 | 0.2139 | 0.3963 | 1.2076 |
| 1.65 | 0.5242 | 0.1990 | 0.3796 | 1.2404 |
| 1.70 | 0.5093 | 0.1851 | 0.3635 | 1.2754 |
| 1.75 | 0.4948 | 0.1723 | 0.3481 | 1.3126 |
| 1.80 | 0.4808 | 0.1603 | 0.3334 | 1.3520 |
| 1.85 | 0.4671 | 0.1491 | 0.3192 | 1.3935 |
| 1.90 | 0.4539 | 0.1388 | 0.3058 | 1.4372 |
| 1.95 | 0.4410 | 0.1292 | 0.2929 | 1.4831 |
| 2.00 | 0.4286 | 0.1202 | 0.2806 | 1.5313 |
| 2.05 | 0.4165 | 0.1120 | 0.2688 | 1.5816 |
| 2.10 | 0.4049 | 0.1043 | 0.2576 | 1.6342 |
| 2.15 | 0.3936 | 0.0972 | 0.2469 | 1.6890 |
| 2.20 | 0.3827 | 0.0906 | 0.2367 | 1.7462 |
| 2.25 | 0.3721 | 0.0845 | 0.2270 | 1.8057 |
| 2.30 | 0.3619 | 0.0788 | 0.2177 | 1.8675 |
| 2.35 | 0.3520 | 0.0735 | 0.2088 | 1.9317 |
| 2.40 | 0.3425 | 0.0686 | 0.2004 | 1.9984 |
| 2.45 | 0.3332 | 0.0641 | 0.1924 | 2.0675 |
| 2.50 | 0.3243 | 0.0599 | 0.1847 | 2.1391 |
| 2.55 | 0.3157 | 0.0560 | 0.1774 | 2.2132 |
| 2.60 | 0.3074 | 0.0524 | 0.1704 | 2.2898 |
| 2.65 | 0.2993 | 0.0490 | 0.1638 | 2.3691 |
| 2.70 | 0.2915 | 0.0459 | 0.1574 | 2.4510 |
| 2.75 | 0.2840 | 0.0430 | 0.1514 | 2.5356 |
| 2.80 | 0.2768 | 0.0403 | 0.1456 | 2.6229 |
| 2.85 | 0.2697 | 0.0378 | 0.1401 | 2.7129 |
| 2.90 | 0.2629 | 0.0354 | 0.1348 | 2.8058 |
| 2.95 | 0.2564 | 0.0333 | 0.1298 | 2.9015 |
| 3.00 | 0.2500 | 0.0313 | 0.1250 | 3.0000 |
| 3.50 | 0.1967 | 0.0172 | 0.0873 | 4.1529 |
| 4.00 | 0.1579 | 0.0099 | 0.0627 | 5.6406 |
| 4.50 | 0.1290 | 0.0060 | 0.0463 | 7.5078 |
| 5.00 | 0.1071 | 0.0038 | 0.0351 | 9.8000 |
| 6.00 | 0.0769 | 0.0016 | 0.0213 | 15.8438 |
| 7.00 | 0.0577 | 0.0008 | 0.0139 | 24.1429 |
| 8.00 | 0.0448 | 0.0004 | 0.0095 | 35.0703 |
| 9.00 | 0.0357 | 0.0002 | 0.0067 | 49.0000 |
| 10.00 | 0.0291 | 0.0001 | 0.0050 | 66.3062 |

# Appendix C

# Normal-Shock Tables

**TABLE C.1** Normal-Shock Table ($\gamma = 1.4$)

| $M_1$ | $M_2$ | $p_2/p_1$ | $T_2/T_1$ | $\rho_2/\rho_1$ | $p_{o2}/p_{o1}$ | $p_{o2}/p_1$ |
|---|---|---|---|---|---|---|
| 1.00 | 1.0000 | 1.0000 | 1.0000 | 1.0000 | 1.0000 | 1.8929 |
| 1.02 | 0.9805 | 1.0471 | 1.0132 | 1.0334 | 1.0000 | 1.9379 |
| 1.04 | 0.9620 | 1.0952 | 1.0263 | 1.0671 | 0.9999 | 1.9844 |
| 1.06 | 0.9444 | 1.1442 | 1.0393 | 1.1009 | 0.9998 | 2.0325 |
| 1.08 | 0.9277 | 1.1941 | 1.0522 | 1.1349 | 0.9994 | 2.0819 |
| 1.10 | 0.9118 | 1.2450 | 1.0649 | 1.1691 | 0.9989 | 2.1328 |
| 1.12 | 0.8966 | 1.2968 | 1.0776 | 1.2034 | 0.9982 | 2.1851 |
| 1.14 | 0.8820 | 1.3495 | 1.0903 | 1.2378 | 0.9973 | 2.2388 |
| 1.16 | 0.8682 | 1.4032 | 1.1029 | 1.2723 | 0.9961 | 2.2937 |
| 1.18 | 0.8549 | 1.4578 | 1.1154 | 1.3069 | 0.9946 | 2.3500 |
| 1.20 | 0.8422 | 1.5133 | 1.1280 | 1.3416 | 0.9928 | 2.4075 |
| 1.22 | 0.8300 | 1.5698 | 1.1405 | 1.3764 | 0.9907 | 2.4663 |
| 1.24 | 0.8183 | 1.6272 | 1.1531 | 1.4112 | 0.9884 | 2.5263 |
| 1.26 | 0.8071 | 1.6855 | 1.1657 | 1.4460 | 0.9857 | 2.5875 |
| 1.28 | 0.7963 | 1.7448 | 1.1783 | 1.4808 | 0.9827 | 2.6500 |
| 1.30 | 0.7860 | 1.8050 | 1.1909 | 1.5157 | 0.9794 | 2.7136 |
| 1.32 | 0.7760 | 1.8661 | 1.2035 | 1.5505 | 0.9758 | 2.7784 |
| 1.34 | 0.7664 | 1.9282 | 1.2162 | 1.5854 | 0.9718 | 2.8444 |
| 1.36 | 0.7572 | 1.9912 | 1.2290 | 1.6202 | 0.9676 | 2.9115 |
| 1.38 | 0.7483 | 2.0551 | 1.2418 | 1.6549 | 0.9630 | 2.9798 |
| 1.40 | 0.7397 | 2.1200 | 1.2547 | 1.6897 | 0.9582 | 3.0492 |
| 1.42 | 0.7314 | 2.1858 | 1.2676 | 1.7243 | 0.9531 | 3.1198 |
| 1.44 | 0.7235 | 2.2525 | 1.2807 | 1.7589 | 0.9476 | 3.1915 |
| 1.46 | 0.7157 | 2.3202 | 1.2938 | 1.7934 | 0.9420 | 3.2643 |
| 1.48 | 0.7083 | 2.3888 | 1.3069 | 1.8278 | 0.9360 | 3.3382 |
| 1.50 | 0.7011 | 2.4583 | 1.3202 | 1.8621 | 0.9298 | 3.4133 |
| 1.52 | 0.6941 | 2.5288 | 1.3336 | 1.8963 | 0.9233 | 3.4894 |
| 1.54 | 0.6874 | 2.6002 | 1.3470 | 1.9303 | 0.9166 | 3.5667 |
| 1.56 | 0.6809 | 2.6725 | 1.3606 | 1.9643 | 0.9097 | 3.6450 |
| 1.58 | 0.6746 | 2.7458 | 1.3742 | 1.9981 | 0.9026 | 3.7244 |
| 1.60 | 0.6684 | 2.8200 | 1.3880 | 2.0317 | 0.8952 | 3.8050 |
| 1.62 | 0.6625 | 2.8951 | 1.4018 | 2.0653 | 0.8877 | 3.8866 |
| 1.64 | 0.6568 | 2.9712 | 1.4158 | 2.0986 | 0.8799 | 3.9693 |
| 1.66 | 0.6512 | 3.0482 | 1.4299 | 2.1318 | 0.8720 | 4.0531 |
| 1.68 | 0.6458 | 3.1261 | 1.4440 | 2.1649 | 0.8639 | 4.1379 |
| 1.70 | 0.6405 | 3.2050 | 1.4583 | 2.1977 | 0.8557 | 4.2238 |
| 1.72 | 0.6355 | 3.2848 | 1.4727 | 2.2304 | 0.8474 | 4.3108 |
| 1.74 | 0.6305 | 3.3655 | 1.4873 | 2.2629 | 0.8389 | 4.3989 |
| 1.76 | 0.6257 | 3.4472 | 1.5019 | 2.2952 | 0.8302 | 4.4880 |
| 1.78 | 0.6210 | 3.5298 | 1.5167 | 2.3273 | 0.8215 | 4.5782 |
| 1.80 | 0.6165 | 3.6133 | 1.5316 | 2.3592 | 0.8127 | 4.6695 |
| 1.82 | 0.6121 | 3.6978 | 1.5466 | 2.3909 | 0.8038 | 4.7618 |
| 1.84 | 0.6078 | 3.7832 | 1.5617 | 2.4224 | 0.7948 | 4.8552 |
| 1.86 | 0.6036 | 3.8695 | 1.5770 | 2.4537 | 0.7857 | 4.9497 |
| 1.88 | 0.5996 | 3.9568 | 1.5924 | 2.4848 | 0.7765 | 5.0452 |
| 1.90 | 0.5956 | 4.0450 | 1.6079 | 2.5157 | 0.7674 | 5.1418 |

**TABLE C.1** *(Continued)*

| $M_1$ | $M_2$ | $p_2/p_1$ | $T_2/T_1$ | $\rho_2/\rho_1$ | $p_{o2}/p_{o1}$ | $p_{o2}/p_1$ |
|---|---|---|---|---|---|---|
| 1.92 | 0.5918 | 4.1341 | 1.6236 | 2.5463 | 0.7581 | 5.2394 |
| 1.94 | 0.5880 | 4.2242 | 1.6394 | 2.5767 | 0.7488 | 5.3381 |
| 1.96 | 0.5844 | 4.3152 | 1.6553 | 2.6069 | 0.7395 | 5.4378 |
| 1.98 | 0.5808 | 4.4071 | 1.6713 | 2.6369 | 0.7302 | 5.5386 |
| 2.00 | 0.5774 | 4.5000 | 1.6875 | 2.6667 | 0.7209 | 5.6404 |
| 2.02 | 0.5740 | 4.5938 | 1.7038 | 2.6962 | 0.7115 | 5.7433 |
| 2.04 | 0.5707 | 4.6885 | 1.7203 | 2.7255 | 0.7022 | 5.8473 |
| 2.06 | 0.5675 | 4.7842 | 1.7369 | 2.7545 | 0.6928 | 5.9523 |
| 2.08 | 0.5643 | 4.8808 | 1.7536 | 2.7833 | 0.6835 | 6.0583 |
| 2.10 | 0.5613 | 4.9783 | 1.7705 | 2.8119 | 0.6742 | 6.1654 |
| 2.12 | 0.5583 | 5.0768 | 1.7875 | 2.8402 | 0.6649 | 6.2735 |
| 2.14 | 0.5554 | 5.1762 | 1.8046 | 2.8683 | 0.6557 | 6.3827 |
| 2.16 | 0.5525 | 5.2765 | 1.8219 | 2.8962 | 0.6464 | 6.4929 |
| 2.18 | 0.5498 | 5.3778 | 1.8393 | 2.9238 | 0.6373 | 6.6042 |
| 2.20 | 0.5471 | 5.4800 | 1.8569 | 2.9512 | 0.6281 | 6.7165 |
| 2.22 | 0.5444 | 5.5831 | 1.8746 | 2.9784 | 0.6191 | 6.8298 |
| 2.24 | 0.5418 | 5.6872 | 1.8924 | 3.0053 | 0.6100 | 6.9442 |
| 2.26 | 0.5393 | 5.7922 | 1.9104 | 3.0319 | 0.6011 | 7.0597 |
| 2.28 | 0.5368 | 5.8981 | 1.9285 | 3.0584 | 0.5921 | 7.1762 |
| 2.30 | 0.5344 | 6.0050 | 1.9468 | 3.0845 | 0.5833 | 7.2937 |
| 2.32 | 0.5321 | 6.1128 | 1.9652 | 3.1105 | 0.5745 | 7.4122 |
| 2.34 | 0.5297 | 6.2215 | 1.9838 | 3.1362 | 0.5658 | 7.5319 |
| 2.36 | 0.5275 | 6.3312 | 2.0025 | 3.1617 | 0.5572 | 7.6525 |
| 2.38 | 0.5253 | 6.4418 | 2.0213 | 3.1869 | 0.5486 | 7.7742 |
| 2.40 | 0.5231 | 6.5533 | 2.0403 | 3.2119 | 0.5401 | 7.8969 |
| 2.42 | 0.5210 | 6.6658 | 2.0595 | 3.2367 | 0.5317 | 8.0207 |
| 2.44 | 0.5189 | 6.7792 | 2.0788 | 3.2612 | 0.5234 | 8.1455 |
| 2.46 | 0.5169 | 6.8935 | 2.0982 | 3.2855 | 0.5152 | 8.2713 |
| 2.48 | 0.5149 | 7.0088 | 2.1178 | 3.3095 | 0.5071 | 8.3982 |
| 2.50 | 0.5130 | 7.1250 | 2.1375 | 3.3333 | 0.4990 | 8.5261 |
| 2.52 | 0.5111 | 7.2421 | 2.1574 | 3.3569 | 0.4911 | 8.6551 |
| 2.54 | 0.5092 | 7.3602 | 2.1774 | 3.3803 | 0.4832 | 8.7851 |
| 2.56 | 0.5074 | 7.4792 | 2.1976 | 3.4034 | 0.4754 | 8.9161 |
| 2.58 | 0.5056 | 7.5991 | 2.2179 | 3.4263 | 0.4677 | 9.0482 |
| 2.60 | 0.5039 | 7.7200 | 2.2383 | 3.4490 | 0.4601 | 9.1813 |
| 2.62 | 0.5022 | 7.8418 | 2.2590 | 3.4714 | 0.4526 | 9.3155 |
| 2.64 | 0.5005 | 7.9645 | 2.2797 | 3.4937 | 0.4452 | 9.4506 |
| 2.66 | 0.4988 | 8.0882 | 2.3006 | 3.5157 | 0.4379 | 9.5869 |
| 2.68 | 0.4972 | 8.2128 | 2.3217 | 3.5374 | 0.4307 | 9.7241 |
| 2.70 | 0.4956 | 8.3383 | 2.3429 | 3.5590 | 0.4236 | 9.8624 |
| 2.72 | 0.4941 | 8.4648 | 2.3642 | 3.5803 | 0.4166 | 10.0017 |
| 2.74 | 0.4926 | 8.5922 | 2.3858 | 3.6015 | 0.4097 | 10.1421 |
| 2.76 | 0.4911 | 8.7205 | 2.4074 | 3.6224 | 0.4028 | 10.2835 |
| 2.78 | 0.4896 | 8.8498 | 2.4292 | 3.6431 | 0.3961 | 10.4259 |
| 2.80 | 0.4882 | 8.9800 | 2.4512 | 3.6636 | 0.3895 | 10.5694 |
| 2.82 | 0.4868 | 9.1111 | 2.4733 | 3.6838 | 0.3829 | 10.7139 |
| 2.84 | 0.4854 | 9.2432 | 2.4955 | 3.7039 | 0.3765 | 10.8594 |
| 2.86 | 0.4840 | 9.3762 | 2.5179 | 3.7238 | 0.3701 | 11.0060 |
| 2.88 | 0.4827 | 9.5101 | 2.5405 | 3.7434 | 0.3639 | 11.1536 |
| 2.90 | 0.4814 | 9.6450 | 2.5632 | 3.7629 | 0.3577 | 11.3022 |
| 2.92 | 0.4801 | 9.7808 | 2.5861 | 3.7821 | 0.3517 | 11.4519 |
| 2.94 | 0.4788 | 9.9175 | 2.6091 | 3.8012 | 0.3457 | 11.6026 |
| 2.96 | 0.4776 | 10.0552 | 2.6322 | 3.8200 | 0.3398 | 11.7544 |
| 2.98 | 0.4764 | 10.1938 | 2.6555 | 3.8387 | 0.3340 | 11.9072 |
| 3.00 | 0.4752 | 10.3333 | 2.6790 | 3.8571 | 0.3283 | 12.0610 |
| 3.02 | 0.4740 | 10.4738 | 2.7026 | 3.8754 | 0.3227 | 12.2158 |
| 3.04 | 0.4729 | 10.6152 | 2.7264 | 3.8935 | 0.3172 | 12.3717 |

**TABLE C.1** *(Continued)*

| $M_1$ | $M_2$ | $p_2/p_1$ | $T_2/T_1$ | $\rho_2/\rho_1$ | $p_{o2}/p_{o1}$ | $p_{o2}/p_1$ |
|---|---|---|---|---|---|---|
| 3.06 | 0.4717 | 10.7575 | 2.7503 | 3.9114 | 0.3118 | 12.5286 |
| 3.08 | 0.4706 | 10.9008 | 2.7744 | 3.9291 | 0.3065 | 12.6865 |
| 3.10 | 0.4695 | 11.0450 | 2.7986 | 3.9466 | 0.3012 | 12.8455 |
| 3.12 | 0.4685 | 11.1901 | 2.8230 | 3.9639 | 0.2960 | 13.0055 |
| 3.14 | 0.4674 | 11.3362 | 2.8475 | 3.9811 | 0.2910 | 13.1666 |
| 3.16 | 0.4664 | 11.4832 | 2.8722 | 3.9981 | 0.2860 | 13.3287 |
| 3.18 | 0.4654 | 11.6311 | 2.8970 | 4.0149 | 0.2811 | 13.4918 |
| 3.20 | 0.4643 | 11.7800 | 2.9220 | 4.0315 | 0.2762 | 13.6559 |
| 3.22 | 0.4634 | 11.9298 | 2.9471 | 4.0479 | 0.2715 | 13.8211 |
| 3.24 | 0.4624 | 12.0805 | 2.9724 | 4.0642 | 0.2668 | 13.9873 |
| 3.26 | 0.4614 | 12.2322 | 2.9979 | 4.0803 | 0.2622 | 14.1546 |
| 3.28 | 0.4605 | 12.3848 | 3.0234 | 4.0963 | 0.2577 | 14.3228 |
| 3.30 | 0.4596 | 12.5383 | 3.0492 | 4.1120 | 0.2533 | 14.4921 |
| 3.32 | 0.4587 | 12.6928 | 3.0751 | 4.1276 | 0.2489 | 14.6625 |
| 3.34 | 0.4578 | 12.8482 | 3.1011 | 4.1431 | 0.2446 | 14.8339 |
| 3.36 | 0.4569 | 13.0045 | 3.1273 | 4.1583 | 0.2404 | 15.0063 |
| 3.38 | 0.4560 | 13.1618 | 3.1537 | 4.1734 | 0.2363 | 15.1797 |
| 3.40 | 0.4552 | 13.3200 | 3.1802 | 4.1884 | 0.2322 | 15.3542 |
| 3.42 | 0.4544 | 13.4791 | 3.2069 | 4.2032 | 0.2282 | 15.5297 |
| 3.44 | 0.4535 | 13.6392 | 3.2337 | 4.2179 | 0.2243 | 15.7062 |
| 3.46 | 0.4527 | 13.8002 | 3.2607 | 4.2323 | 0.2205 | 15.8838 |
| 3.48 | 0.4519 | 13.9621 | 3.2878 | 4.2467 | 0.2167 | 16.0624 |
| 3.50 | 0.4512 | 14.1250 | 3.3151 | 4.2609 | 0.2129 | 16.2420 |
| 3.52 | 0.4504 | 14.2888 | 3.3425 | 4.2749 | 0.2093 | 16.4227 |
| 3.54 | 0.4496 | 14.4535 | 3.3701 | 4.2888 | 0.2057 | 16.6044 |
| 3.56 | 0.4489 | 14.6192 | 3.3978 | 4.3026 | 0.2022 | 16.7871 |
| 3.58 | 0.4481 | 14.7858 | 3.4257 | 4.3162 | 0.1987 | 16.9708 |
| 3.60 | 0.4474 | 14.9533 | 3.4537 | 4.3296 | 0.1953 | 17.1556 |
| 3.62 | 0.4467 | 15.1218 | 3.4819 | 4.3429 | 0.1920 | 17.3415 |
| 3.64 | 0.4460 | 15.2912 | 3.5103 | 4.3561 | 0.1887 | 17.5283 |
| 3.66 | 0.4453 | 15.4615 | 3.5388 | 4.3692 | 0.1855 | 17.7162 |
| 3.68 | 0.4446 | 15.6328 | 3.5674 | 4.3821 | 0.1823 | 17.9051 |
| 3.70 | 0.4439 | 15.8050 | 3.5962 | 4.3949 | 0.1792 | 18.0951 |
| 3.72 | 0.4433 | 15.9781 | 3.6252 | 4.4075 | 0.1761 | 18.2860 |
| 3.74 | 0.4426 | 16.1522 | 3.6543 | 4.4200 | 0.1731 | 18.4781 |
| 3.76 | 0.4420 | 16.3272 | 3.6836 | 4.4324 | 0.1702 | 18.6711 |
| 3.78 | 0.4414 | 16.5031 | 3.7130 | 4.4447 | 0.1673 | 18.8652 |
| 3.80 | 0.4407 | 16.6800 | 3.7426 | 4.4568 | 0.1645 | 19.0603 |
| 3.82 | 0.4401 | 16.8578 | 3.7723 | 4.4688 | 0.1617 | 19.2564 |
| 3.84 | 0.4395 | 17.0365 | 3.8022 | 4.4807 | 0.1589 | 19.4536 |
| 3.86 | 0.4389 | 17.2162 | 3.8323 | 4.4924 | 0.1563 | 19.6518 |
| 3.88 | 0.4383 | 17.3968 | 3.8625 | 4.5041 | 0.1536 | 19.8510 |
| 3.90 | 0.4377 | 17.5783 | 3.8928 | 4.5156 | 0.1510 | 20.0513 |
| 3.92 | 0.4372 | 17.7608 | 3.9233 | 4.5270 | 0.1485 | 20.2526 |
| 3.94 | 0.4366 | 17.9442 | 3.9540 | 4.5383 | 0.1460 | 20.4549 |
| 3.96 | 0.4360 | 18.1285 | 3.9848 | 4.5494 | 0.1435 | 20.6583 |
| 3.98 | 0.4355 | 18.3138 | 4.0158 | 4.5605 | 0.1411 | 20.8627 |
| 4.00 | 0.4350 | 18.5000 | 4.0469 | 4.5714 | 0.1388 | 21.0681 |
| 4.02 | 0.4344 | 18.6871 | 4.0782 | 4.5823 | 0.1364 | 21.2745 |
| 4.04 | 0.4339 | 18.8752 | 4.1096 | 4.5930 | 0.1342 | 21.4820 |
| 4.06 | 0.4334 | 19.0642 | 4.1412 | 4.6036 | 0.1319 | 21.6905 |
| 4.08 | 0.4329 | 19.2541 | 4.1729 | 4.6141 | 0.1297 | 21.9001 |
| 4.10 | 0.4324 | 19.4450 | 4.2048 | 4.6245 | 0.1276 | 22.1106 |
| 4.12 | 0.4319 | 19.6368 | 4.2368 | 4.6348 | 0.1254 | 22.3223 |
| 4.14 | 0.4314 | 19.8295 | 4.2690 | 4.6450 | 0.1234 | 22.5349 |
| 4.16 | 0.4309 | 20.0232 | 4.3014 | 4.6550 | 0.1213 | 22.7486 |
| 4.18 | 0.4304 | 20.2178 | 4.3339 | 4.6650 | 0.1193 | 22.9633 |

**TABLE C.1** *(Continued)*

| $M_1$ | $M_2$ | $p_2/p_1$ | $T_2/T_1$ | $\rho_2/\rho_1$ | $p_{o2}/p_{o1}$ | $p_{o2}/p_1$ |
|---|---|---|---|---|---|---|
| 4.20 | 0.4299 | 20.4133 | 4.3666 | 4.6749 | 0.1173 | 23.1790 |
| 4.22 | 0.4295 | 20.6098 | 4.3994 | 4.6847 | 0.1154 | 23.3958 |
| 4.24 | 0.4290 | 20.8072 | 4.4324 | 4.6944 | 0.1135 | 23.6135 |
| 4.26 | 0.4286 | 21.0055 | 4.4655 | 4.7040 | 0.1116 | 23.8324 |
| 4.28 | 0.4281 | 21.2048 | 4.4988 | 4.7135 | 0.1098 | 24.0522 |
| 4.30 | 0.4277 | 21.4050 | 4.5322 | 4.7229 | 0.1080 | 24.2731 |
| 4.32 | 0.4272 | 21.6061 | 4.5658 | 4.7322 | 0.1062 | 24.4950 |
| 4.34 | 0.4268 | 21.8082 | 4.5995 | 4.7414 | 0.1045 | 24.7180 |
| 4.36 | 0.4264 | 22.0112 | 4.6334 | 4.7505 | 0.1028 | 24.9420 |
| 4.38 | 0.4260 | 22.2151 | 4.6675 | 4.7595 | 0.1011 | 25.1670 |
| 4.40 | 0.4255 | 22.4200 | 4.7017 | 4.7685 | 0.0995 | 25.3930 |
| 4.42 | 0.4251 | 22.6258 | 4.7361 | 4.7773 | 0.0979 | 25.6201 |
| 4.44 | 0.4247 | 22.8325 | 4.7706 | 4.7861 | 0.0963 | 25.8482 |
| 4.46 | 0.4243 | 23.0402 | 4.8053 | 4.7948 | 0.0947 | 26.0773 |
| 4.48 | 0.4239 | 23.2488 | 4.8401 | 4.8034 | 0.0932 | 26.3075 |
| 4.50 | 0.4236 | 23.4583 | 4.8751 | 4.8119 | 0.0917 | 26.5387 |
| 4.52 | 0.4232 | 23.6688 | 4.9102 | 4.8203 | 0.0902 | 26.7709 |
| 4.54 | 0.4228 | 23.8802 | 4.9455 | 4.8287 | 0.0888 | 27.0041 |
| 4.56 | 0.4224 | 24.0925 | 4.9810 | 4.8369 | 0.0874 | 27.2384 |
| 4.58 | 0.4220 | 24.3058 | 5.0166 | 4.8451 | 0.0860 | 27.4737 |
| 4.60 | 0.4217 | 24.5200 | 5.0523 | 4.8532 | 0.0846 | 27.7101 |
| 4.62 | 0.4213 | 24.7351 | 5.0882 | 4.8612 | 0.0832 | 27.9475 |
| 4.64 | 0.4210 | 24.9512 | 5.1243 | 4.8692 | 0.0819 | 28.1859 |
| 4.66 | 0.4206 | 25.1682 | 5.1605 | 4.8771 | 0.0806 | 28.4253 |
| 4.68 | 0.4203 | 25.3861 | 5.1969 | 4.8849 | 0.0793 | 28.6658 |
| 4.70 | 0.4199 | 25.6050 | 5.2334 | 4.8926 | 0.0781 | 28.9073 |
| 4.72 | 0.4196 | 25.8248 | 5.2701 | 4.9002 | 0.0769 | 29.1498 |
| 4.74 | 0.4192 | 26.0455 | 5.3070 | 4.9078 | 0.0756 | 29.3934 |
| 4.76 | 0.4189 | 26.2672 | 5.3440 | 4.9153 | 0.0745 | 29.6380 |
| 4.78 | 0.4186 | 26.4898 | 5.3811 | 4.9227 | 0.0733 | 29.8836 |
| 4.80 | 0.4183 | 26.7133 | 5.4184 | 4.9301 | 0.0721 | 30.1303 |
| 4.82 | 0.4179 | 26.9378 | 5.4559 | 4.9374 | 0.0710 | 30.3779 |
| 4.84 | 0.4176 | 27.1632 | 5.4935 | 4.9446 | 0.0699 | 30.6267 |
| 4.86 | 0.4173 | 27.3895 | 5.5313 | 4.9518 | 0.0688 | 30.8764 |
| 4.88 | 0.4170 | 27.6168 | 5.5692 | 4.9589 | 0.0677 | 31.1272 |
| 4.90 | 0.4167 | 27.8450 | 5.6073 | 4.9659 | 0.0667 | 31.3790 |
| 4.92 | 0.4164 | 28.0741 | 5.6455 | 4.9728 | 0.0657 | 31.6318 |
| 4.94 | 0.4161 | 28.3042 | 5.6839 | 4.9797 | 0.0647 | 31.8857 |
| 4.96 | 0.4158 | 28.5352 | 5.7224 | 4.9865 | 0.0637 | 32.1406 |
| 4.98 | 0.4155 | 28.7671 | 5.7611 | 4.9933 | 0.0627 | 32.3965 |
| 5.00 | 0.4152 | 29.0000 | 5.8000 | 5.0000 | 0.0617 | 32.6535 |
| 6.00 | 0.4042 | 41.8333 | 7.9406 | 5.2683 | 0.0297 | 46.8152 |
| 7.00 | 0.3974 | 57.0000 | 10.4694 | 5.4444 | 0.0154 | 63.5526 |
| 8.00 | 0.3929 | 74.5000 | 13.3867 | 5.5652 | 0.0085 | 82.8655 |
| 9.00 | 0.3898 | 94.3333 | 16.6927 | 5.6512 | 0.0050 | 104.7536 |
| 10.00 | 0.3876 | 116.5000 | 20.3875 | 5.7143 | 0.0030 | 129.2170 |

**TABLE C.2** Normal-Shock Table ($\gamma = 1.3$)

| $M_1$ | $M_2$ | $p_2/p_1$ | $T_2/T_1$ | $\rho_2/\rho_1$ | $p_{o2}/p_{o1}$ | $p_{o2}/p_1$ |
|---|---|---|---|---|---|---|
| 1.00 | 1.00000 | 1.00000 | 1.00000 | 1.00000 | 1.00000 | 1.83242 |
| 1.05 | 0.95297 | 1.11587 | 1.02566 | 1.08795 | 0.99985 | 1.94068 |
| 1.10 | 0.91120 | 1.23739 | 1.05065 | 1.17774 | 0.99891 | 2.05780 |
| 1.15 | 0.87388 | 1.36457 | 1.07521 | 1.26911 | 0.99660 | 2.18319 |
| 1.20 | 0.84033 | 1.49739 | 1.09953 | 1.36184 | 0.99258 | 2.31638 |
| 1.25 | 0.81003 | 1.63587 | 1.12377 | 1.45570 | 0.98661 | 2.45706 |
| 1.30 | 0.78253 | 1.78000 | 1.14805 | 1.55046 | 0.97858 | 2.60495 |
| 1.35 | 0.75749 | 1.92978 | 1.17246 | 1.64592 | 0.96845 | 2.75987 |
| 1.40 | 0.73459 | 2.08522 | 1.19710 | 1.74189 | 0.95627 | 2.92166 |
| 1.45 | 0.71358 | 2.24630 | 1.22204 | 1.83816 | 0.94211 | 3.09019 |
| 1.50 | 0.69425 | 2.41304 | 1.24732 | 1.93458 | 0.92610 | 3.26536 |
| 1.55 | 0.67642 | 2.58543 | 1.27301 | 2.03097 | 0.90838 | 3.44710 |
| 1.60 | 0.65992 | 2.76348 | 1.29914 | 2.12717 | 0.88911 | 3.63533 |
| 1.65 | 0.64463 | 2.94717 | 1.32574 | 2.22304 | 0.86847 | 3.83000 |
| 1.70 | 0.63041 | 3.13652 | 1.35285 | 2.31845 | 0.84664 | 4.03107 |
| 1.75 | 0.61718 | 3.33152 | 1.38050 | 2.41328 | 0.82380 | 4.23849 |
| 1.80 | 0.60484 | 3.53217 | 1.40870 | 2.50740 | 0.80014 | 4.45224 |
| 1.85 | 0.59330 | 3.73848 | 1.43747 | 2.60073 | 0.77582 | 4.67229 |
| 1.90 | 0.58251 | 3.95043 | 1.46684 | 2.69316 | 0.75102 | 4.89860 |
| 1.95 | 0.57238 | 4.16804 | 1.49682 | 2.78461 | 0.72589 | 5.13117 |
| 2.00 | 0.56288 | 4.39130 | 1.52741 | 2.87500 | 0.70057 | 5.36997 |
| 2.05 | 0.55394 | 4.62022 | 1.55863 | 2.96427 | 0.67521 | 5.61500 |
| 2.10 | 0.54553 | 4.85478 | 1.59050 | 3.05236 | 0.64992 | 5.86622 |
| 2.15 | 0.53760 | 5.09500 | 1.62302 | 3.13922 | 0.62481 | 6.12364 |
| 2.20 | 0.53011 | 5.34087 | 1.65619 | 3.22480 | 0.59998 | 6.38725 |
| 2.25 | 0.52304 | 5.59239 | 1.69002 | 3.30906 | 0.57552 | 6.65703 |
| 2.30 | 0.51635 | 5.84957 | 1.72453 | 3.39197 | 0.55150 | 6.93298 |
| 2.35 | 0.51001 | 6.11239 | 1.75972 | 3.47351 | 0.52799 | 7.21509 |
| 2.40 | 0.50400 | 6.38087 | 1.79558 | 3.55365 | 0.50504 | 7.50335 |
| 2.45 | 0.49831 | 6.65500 | 1.83213 | 3.63238 | 0.48269 | 7.79776 |
| 2.50 | 0.49290 | 6.93478 | 1.86938 | 3.70968 | 0.46098 | 8.09831 |
| 2.55 | 0.48775 | 7.22022 | 1.90731 | 3.78555 | 0.43994 | 8.40500 |
| 2.60 | 0.48286 | 7.51130 | 1.94594 | 3.85998 | 0.41958 | 8.71783 |
| 2.65 | 0.47820 | 7.80804 | 1.98528 | 3.93298 | 0.39993 | 9.03679 |
| 2.70 | 0.47377 | 8.11043 | 2.02531 | 4.00454 | 0.38099 | 9.36187 |
| 2.75 | 0.46954 | 8.41848 | 2.06605 | 4.07467 | 0.36276 | 9.69308 |
| 2.80 | 0.46550 | 8.73217 | 2.10750 | 4.14338 | 0.34525 | 10.03042 |
| 2.85 | 0.46164 | 9.05152 | 2.14966 | 4.21068 | 0.32844 | 10.37387 |
| 2.90 | 0.45796 | 9.37652 | 2.19252 | 4.27659 | 0.31233 | 10.72344 |
| 2.95 | 0.45444 | 9.70717 | 2.23611 | 4.34111 | 0.29691 | 11.07912 |
| 3.00 | 0.45107 | 10.04348 | 2.28040 | 4.40426 | 0.28216 | 11.44092 |
| 3.50 | 0.42411 | 13.71739 | 2.76295 | 4.96476 | 0.16775 | 15.39484 |
| 4.00 | 0.40577 | 17.95652 | 3.31805 | 5.41176 | 0.09933 | 19.95890 |
| 4.50 | 0.39275 | 22.76087 | 3.94619 | 5.76780 | 0.05939 | 25.13253 |
| 5.00 | 0.38319 | 28.13043 | 4.64764 | 6.05263 | 0.03613 | 30.91547 |
| 6.00 | 0.37039 | 40.56522 | 6.27095 | 6.46875 | 0.01422 | 44.30868 |
| 7.00 | 0.36248 | 55.26087 | 8.18861 | 6.74850 | 0.00610 | 60.13786 |
| 8.00 | 0.35726 | 72.21739 | 10.40087 | 6.94340 | 0.00283 | 78.40273 |
| 9.00 | 0.35364 | 91.43478 | 12.90786 | 7.08365 | 0.00140 | 99.10318 |
| 10.00 | 0.35103 | 112.91304 | 15.70964 | 7.18750 | 0.00074 | 122.23913 |

**TABLE C.3** Normal-Shock Table ($\gamma = 5/3$)

| $M_1$ | $M_2$ | $p_2/p_1$ | $T_2/T_1$ | $\rho_2/\rho_1$ | $p_{o2}/p_{o1}$ | $p_{o2}/p_1$ |
|---|---|---|---|---|---|---|
| 1.00 | 1.00000 | 1.00000 | 1.00000 | 1.00000 | 1.00000 | 2.05280 |
| 1.05 | 0.95349 | 1.12813 | 1.04946 | 1.07495 | 0.99986 | 2.18654 |
| 1.10 | 0.91305 | 1.26250 | 1.09817 | 1.14964 | 0.99899 | 2.33058 |
| 1.15 | 0.87759 | 1.40313 | 1.14650 | 1.22383 | 0.99691 | 2.48423 |
| 1.20 | 0.84624 | 1.55000 | 1.19479 | 1.29730 | 0.99335 | 2.64701 |
| 1.25 | 0.81837 | 1.70313 | 1.24328 | 1.36986 | 0.98815 | 2.81856 |
| 1.30 | 0.79343 | 1.86250 | 1.29218 | 1.44136 | 0.98127 | 2.99860 |
| 1.35 | 0.77101 | 2.02813 | 1.34165 | 1.51166 | 0.97274 | 3.18694 |
| 1.40 | 0.75076 | 2.20000 | 1.39184 | 1.58065 | 0.96261 | 3.38340 |
| 1.45 | 0.73239 | 2.37813 | 1.44285 | 1.64821 | 0.95100 | 3.58785 |
| 1.50 | 0.71568 | 2.56250 | 1.49479 | 1.71429 | 0.93802 | 3.80021 |
| 1.55 | 0.70041 | 2.75313 | 1.54774 | 1.77881 | 0.92381 | 4.02037 |
| 1.60 | 0.68643 | 2.95000 | 1.60176 | 1.84173 | 0.90851 | 4.24829 |
| 1.65 | 0.67358 | 3.15313 | 1.65691 | 1.90301 | 0.89226 | 4.48389 |
| 1.70 | 0.66175 | 3.36250 | 1.71325 | 1.96265 | 0.87521 | 4.72714 |
| 1.75 | 0.65083 | 3.57813 | 1.77081 | 2.02062 | 0.85749 | 4.97799 |
| 1.80 | 0.64072 | 3.80000 | 1.82963 | 2.07692 | 0.83922 | 5.23641 |
| 1.85 | 0.63135 | 4.02813 | 1.88975 | 2.13157 | 0.82053 | 5.50239 |
| 1.90 | 0.62264 | 4.26250 | 1.95119 | 2.18457 | 0.80153 | 5.77588 |
| 1.95 | 0.61454 | 4.50313 | 2.01397 | 2.23594 | 0.78231 | 6.05688 |
| 2.00 | 0.60698 | 4.75000 | 2.07813 | 2.28571 | 0.76298 | 6.34536 |
| 2.05 | 0.59992 | 5.00313 | 2.14366 | 2.33391 | 0.74362 | 6.64132 |
| 2.10 | 0.59331 | 5.26250 | 2.21061 | 2.38057 | 0.72429 | 6.94473 |
| 2.15 | 0.58712 | 5.52813 | 2.27897 | 2.42571 | 0.70507 | 7.25558 |
| 2.20 | 0.58132 | 5.80000 | 2.34876 | 2.46939 | 0.68601 | 7.57388 |
| 2.25 | 0.57586 | 6.07813 | 2.41999 | 2.51163 | 0.66717 | 7.89960 |
| 2.30 | 0.57073 | 6.36250 | 2.49268 | 2.55247 | 0.64858 | 8.23274 |
| 2.35 | 0.56590 | 6.65313 | 2.56683 | 2.59196 | 0.63028 | 8.57329 |
| 2.40 | 0.56134 | 6.95000 | 2.64245 | 2.63014 | 0.61231 | 8.92125 |
| 2.45 | 0.55704 | 7.25313 | 2.71954 | 2.66704 | 0.59468 | 9.27661 |
| 2.50 | 0.55298 | 7.56250 | 2.79813 | 2.70270 | 0.57743 | 9.63937 |
| 2.55 | 0.54913 | 7.87812 | 2.87820 | 2.73717 | 0.56056 | 10.00952 |
| 2.60 | 0.54549 | 8.20000 | 2.95976 | 2.77049 | 0.54409 | 10.38706 |
| 2.65 | 0.54204 | 8.52812 | 3.04283 | 2.80269 | 0.52803 | 10.77199 |
| 2.70 | 0.53877 | 8.86250 | 3.12740 | 2.83382 | 0.51238 | 11.16429 |
| 2.75 | 0.53566 | 9.20312 | 3.21349 | 2.86391 | 0.49716 | 11.56398 |
| 2.80 | 0.53270 | 9.55000 | 3.30108 | 2.89299 | 0.48235 | 11.97104 |
| 2.85 | 0.52989 | 9.90312 | 3.39020 | 2.92111 | 0.46796 | 12.38548 |
| 2.90 | 0.52721 | 10.26250 | 3.48083 | 2.94829 | 0.45399 | 12.80729 |
| 2.95 | 0.52466 | 10.62813 | 3.57299 | 2.97458 | 0.44043 | 13.23646 |
| 3.00 | 0.52223 | 11.00000 | 3.66667 | 3.00000 | 0.42728 | 13.67301 |
| 3.50 | 0.50310 | 15.06250 | 4.68782 | 3.21311 | 0.31657 | 18.44342 |
| 4.00 | 0.49041 | 19.75000 | 5.86328 | 3.36842 | 0.23725 | 23.94948 |
| 4.50 | 0.48158 | 25.06250 | 7.19387 | 3.48387 | 0.18056 | 30.19068 |
| 5.00 | 0.47519 | 31.00000 | 8.68000 | 3.57143 | 0.13966 | 37.16673 |
| 6.00 | 0.46677 | 44.75000 | 12.11979 | 3.69231 | 0.08751 | 53.32287 |
| 7.00 | 0.46164 | 61.00000 | 16.18367 | 3.76923 | 0.05789 | 72.41729 |
| 8.00 | 0.45829 | 79.75000 | 20.87207 | 3.82090 | 0.04007 | 94.44973 |
| 9.00 | 0.45598 | 101.00000 | 26.18519 | 3.85714 | 0.02879 | 119.42007 |
| 10.00 | 0.45433 | 124.75000 | 32.12313 | 3.88350 | 0.02133 | 147.32824 |

# Appendix D

# Oblique-Shock Charts

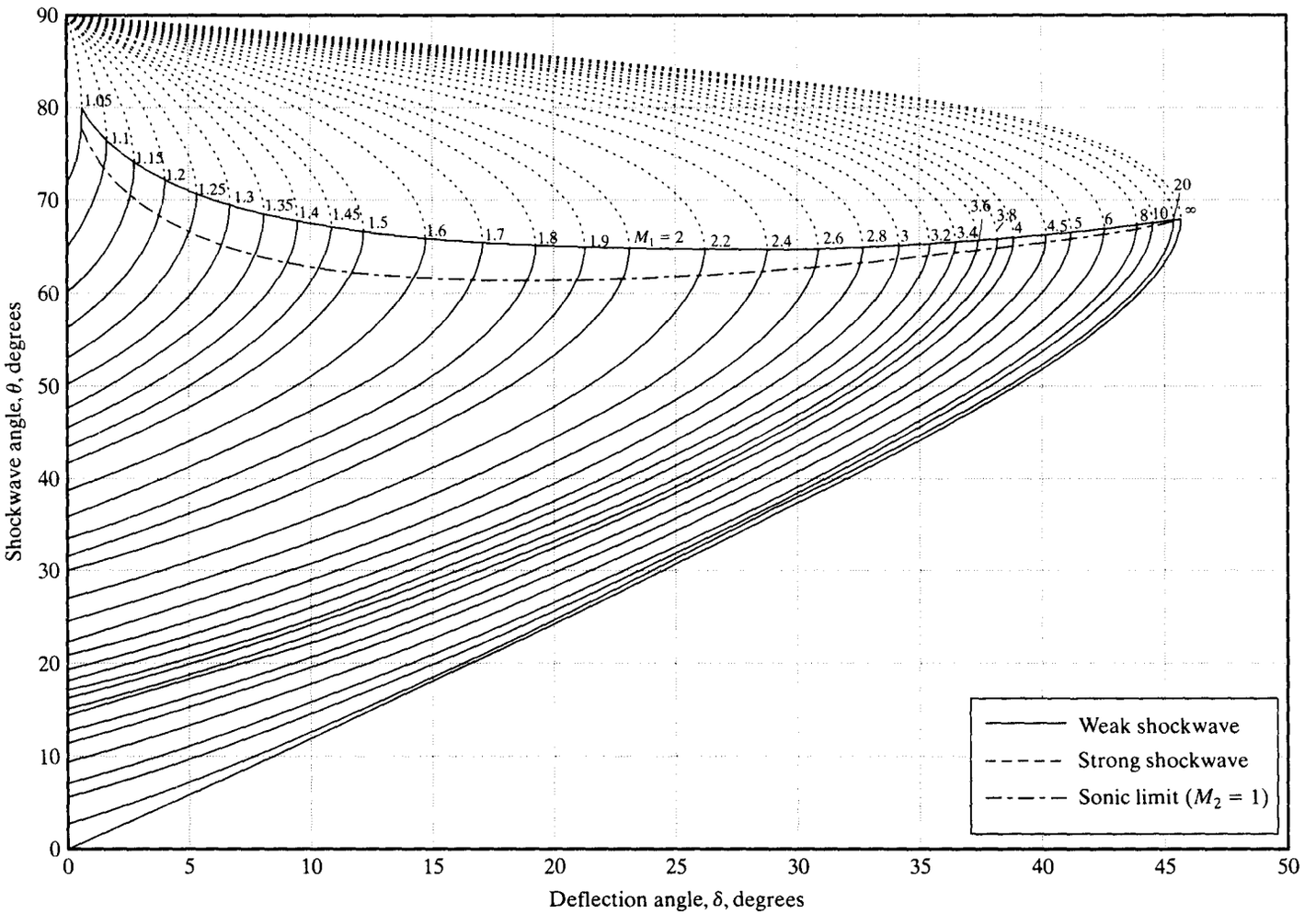


**Figure D.1** Variation of shockwave angle with flow-deflection angle for various upstream Mach numbers ($\gamma = 1.4$)

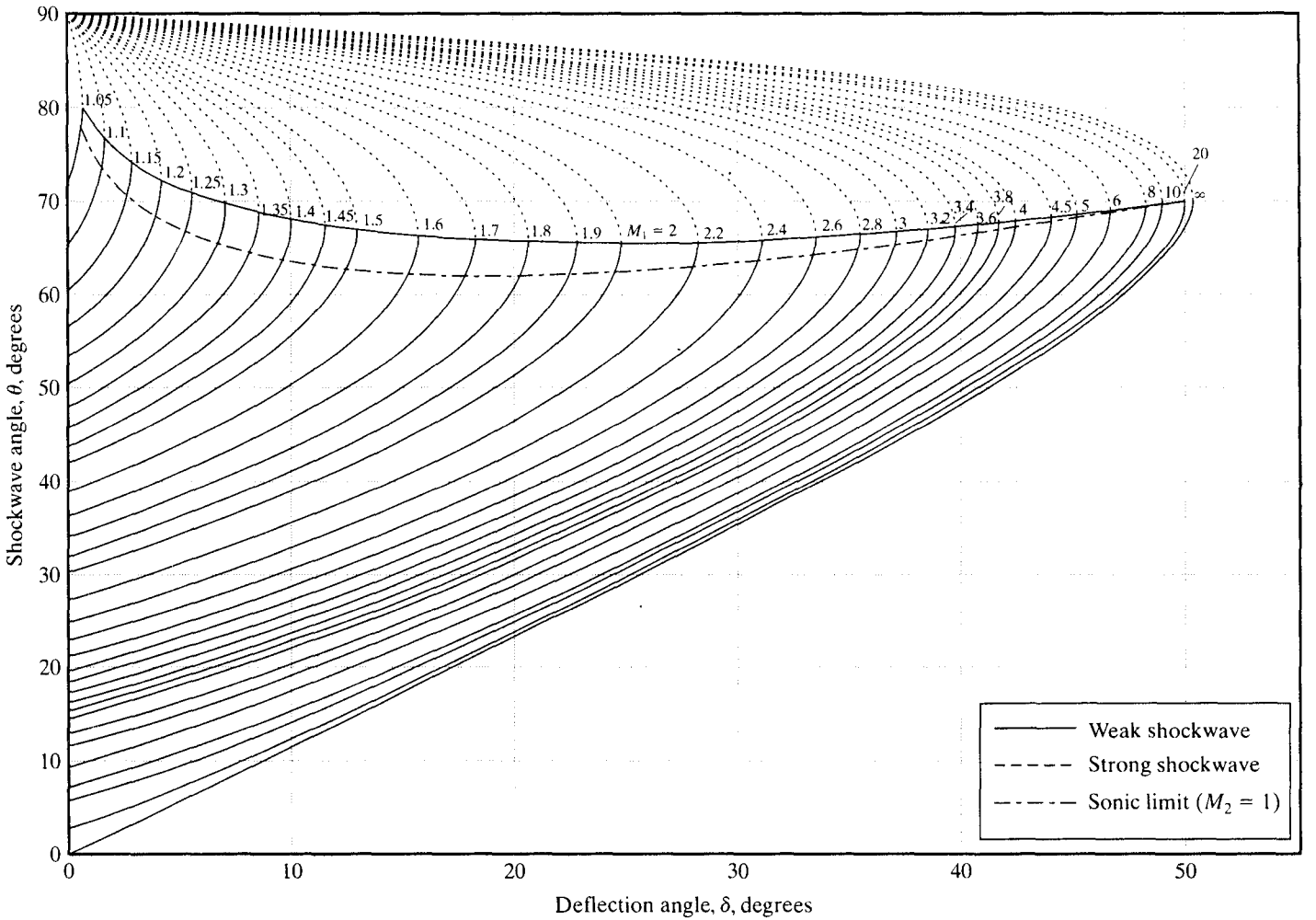


**Figure D.2** Variation of shockwave angle with flow-deflection angle for various upstream Mach numbers ($\gamma = 1.3$)

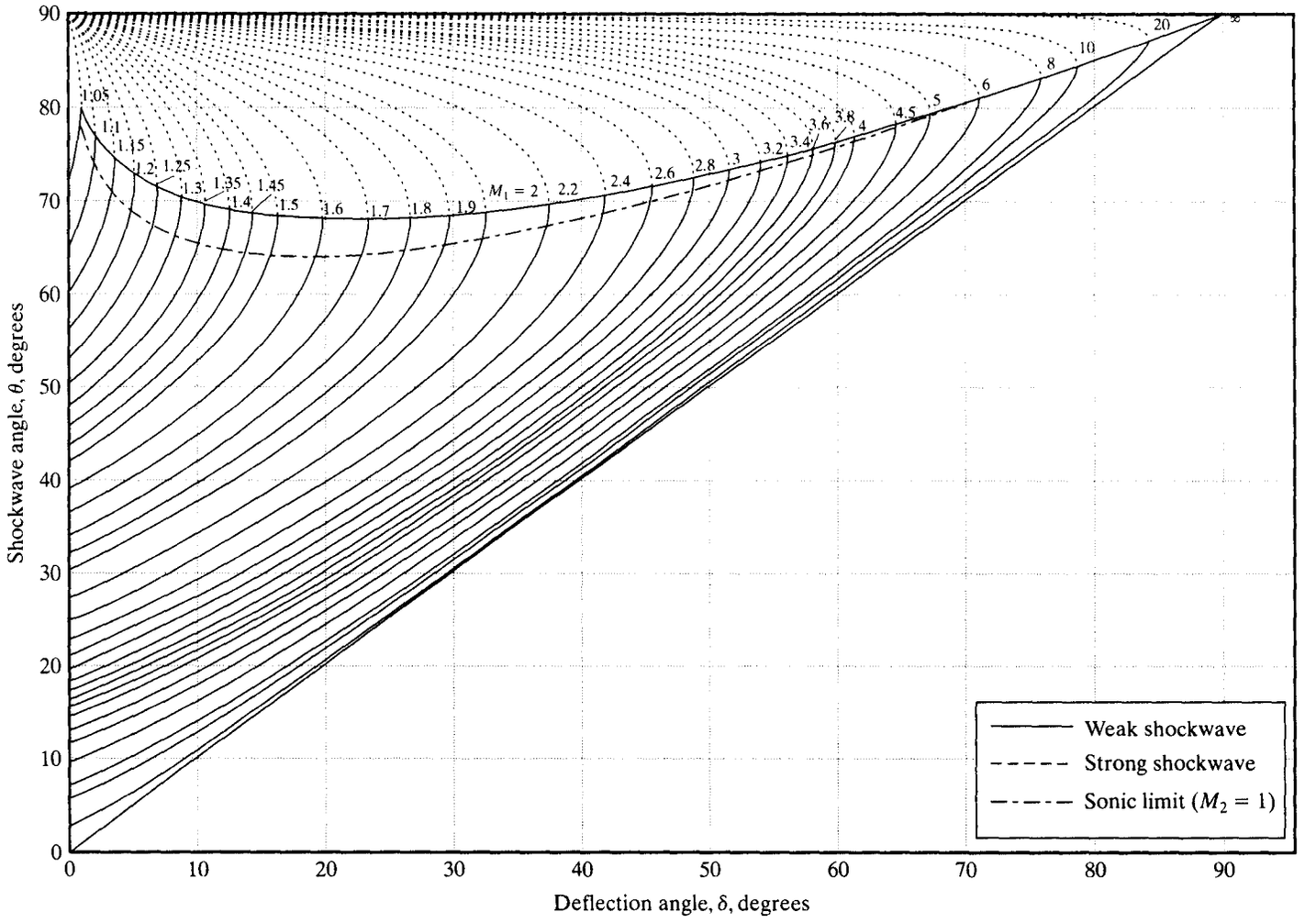


**Figure D.3** Variation of shockwave angle with flow-deflection angle for various upstream Mach numbers ($\gamma = 5/3$)

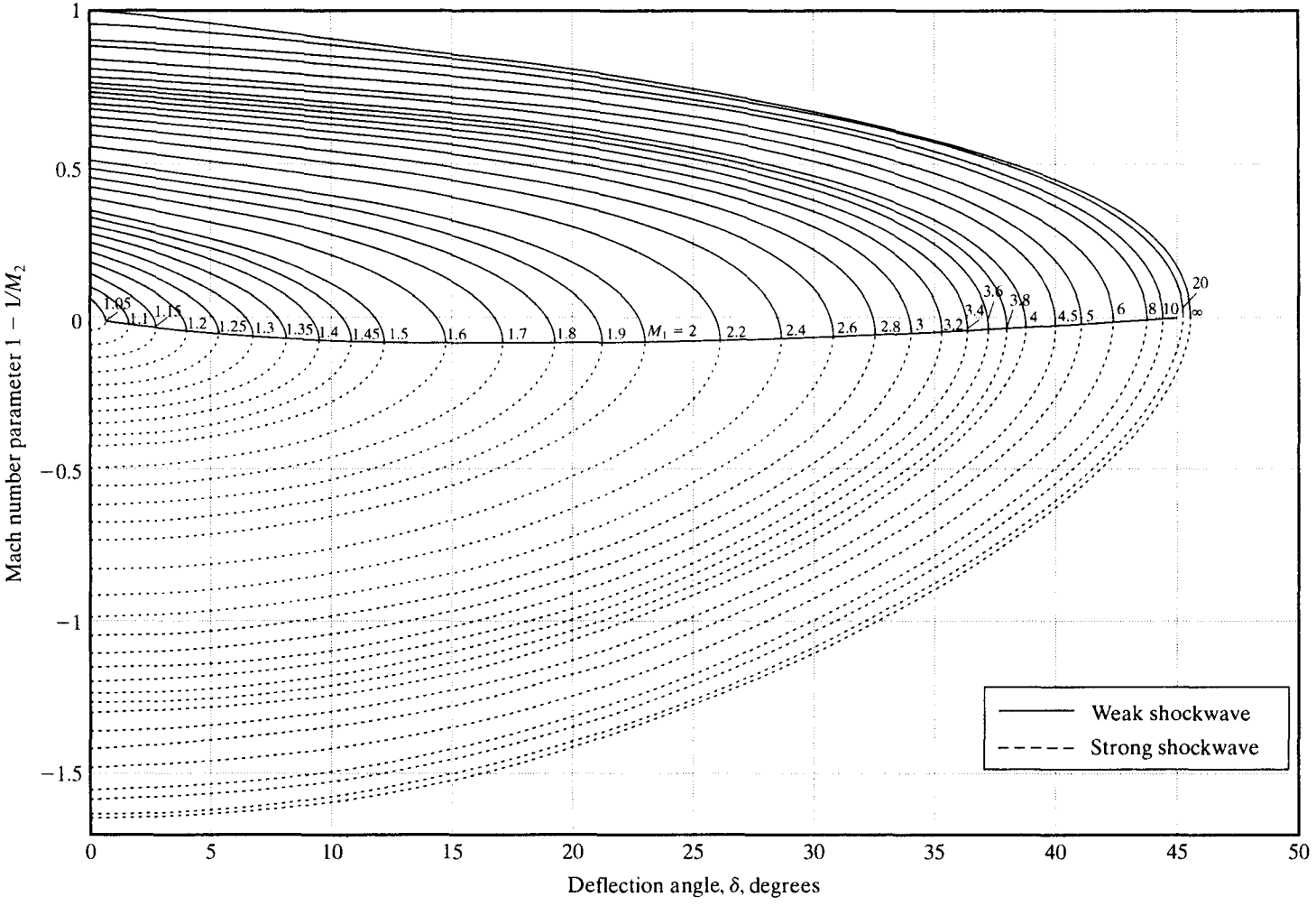


**Figure D.4** Variation of Mach number downstream of a shockwave with flow-deflection angle for various upstream Mach numbers ($\gamma = 1.4$)

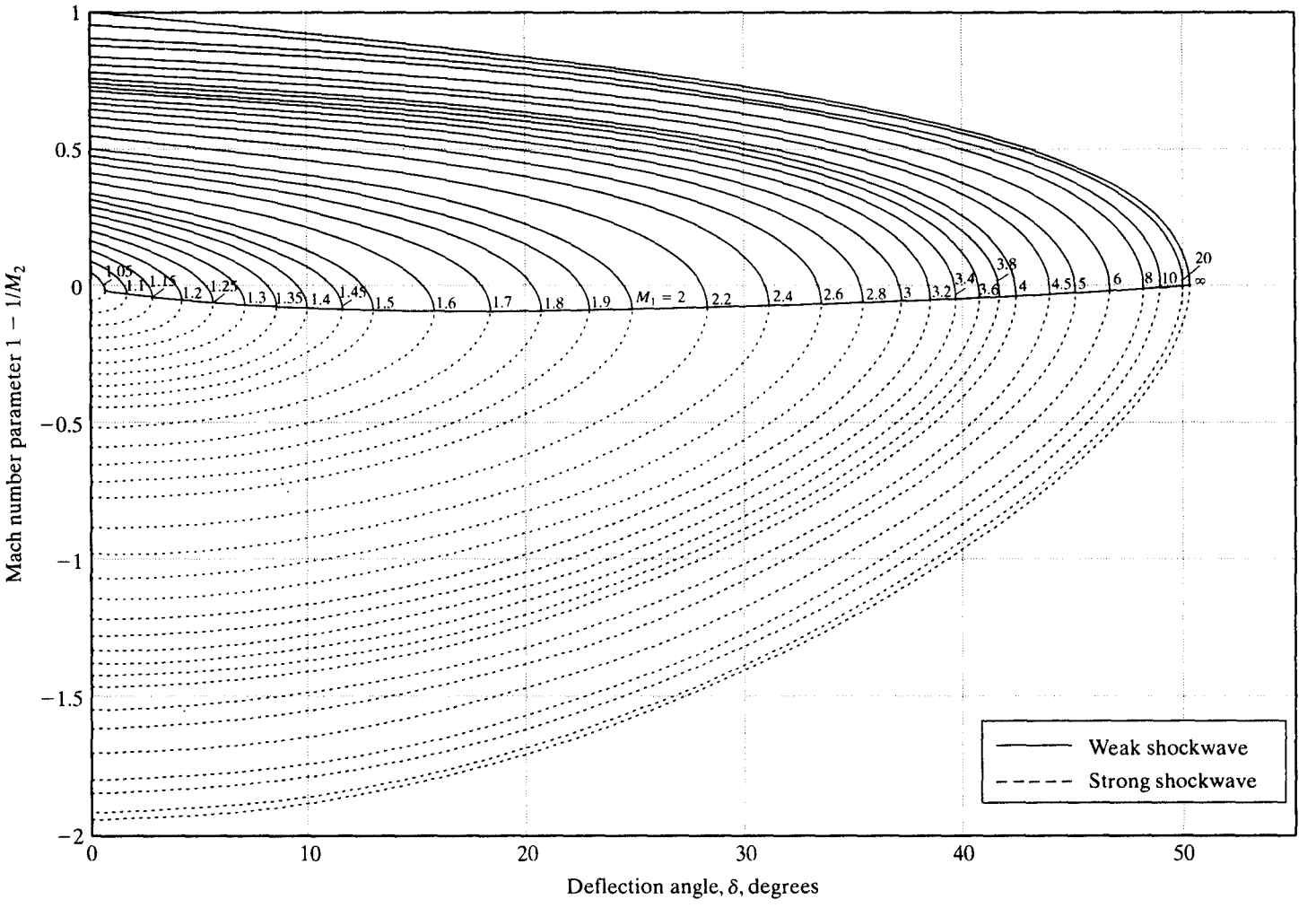


**Figure D.5** Variation of Mach number downstream of a shockwave with flow-deflection angle for various upstream Mach numbers ($\gamma = 1.3$)

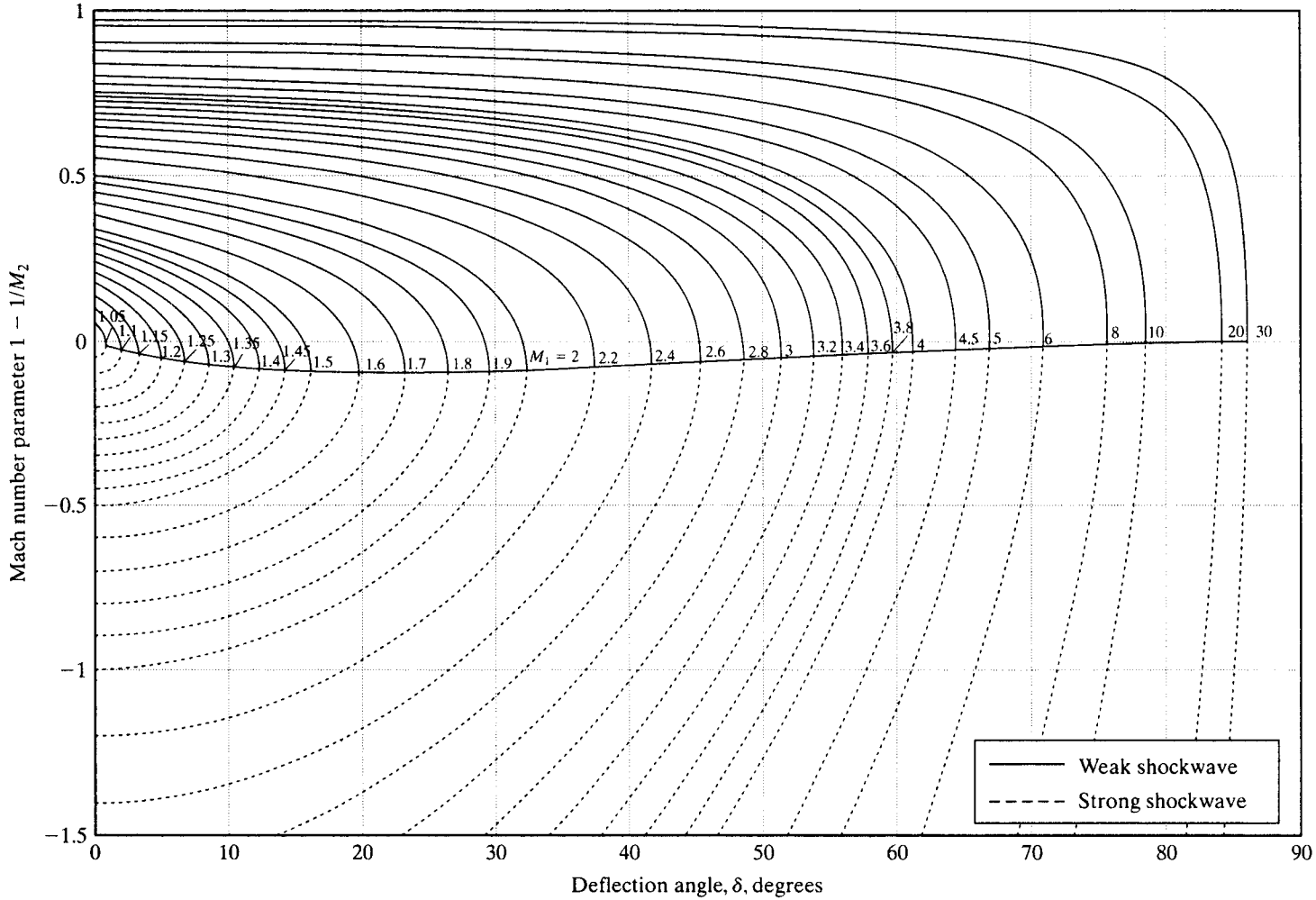


**Figure D.6** Variation of Mach number downstream of a shockwave with flow-deflection angle for various upstream Mach numbers ($\gamma = 5/3$)

# Appendix E

# Prandtl–Meyer Functions

**TABLE E.1** Prandtl–Meyer Functions ($\gamma = 1.4$)

| $M$ | $\nu$ | $\mu$ | $M$ | $\nu$ | $\mu$ |
|---|---|---|---|---|---|
| 1.00 | 0.0000 | 90.0000 | 1.92 | 24.1506 | 31.3882 |
| 1.02 | 0.1257 | 78.6351 | 1.94 | 24.7123 | 31.0285 |
| 1.04 | 0.3510 | 74.0576 | 1.96 | 25.2711 | 30.6774 |
| 1.06 | 0.6367 | 70.6300 | 1.98 | 25.8269 | 30.3347 |
| 1.08 | 0.9680 | 67.8084 | 2.00 | 26.3798 | 30.0000 |
| 1.10 | 1.3362 | 65.3800 | 2.02 | 26.9295 | 29.6730 |
| 1.12 | 1.7350 | 63.2345 | 2.04 | 27.4762 | 29.3535 |
| 1.14 | 2.1600 | 61.3056 | 2.06 | 28.0197 | 29.0411 |
| 1.16 | 2.6073 | 59.5497 | 2.08 | 28.5600 | 28.7357 |
| 1.18 | 3.0743 | 57.9362 | 2.10 | 29.0971 | 28.4369 |
| 1.20 | 3.5582 | 56.4427 | 2.12 | 29.6308 | 28.1446 |
| 1.22 | 4.0572 | 55.0520 | 2.14 | 30.1613 | 27.8585 |
| 1.24 | 4.5694 | 53.7507 | 2.16 | 30.6884 | 27.5785 |
| 1.26 | 5.0931 | 52.5280 | 2.18 | 31.2121 | 27.3043 |
| 1.28 | 5.6272 | 51.3752 | 2.20 | 31.7325 | 27.0357 |
| 1.30 | 6.1703 | 50.2849 | 2.22 | 32.2494 | 26.7726 |
| 1.32 | 6.7213 | 49.2509 | 2.24 | 32.7629 | 26.5148 |
| 1.34 | 7.2794 | 48.2682 | 2.26 | 33.2730 | 26.2621 |
| 1.36 | 7.8435 | 47.3321 | 2.28 | 33.7796 | 26.0144 |
| 1.38 | 8.4130 | 46.4387 | 2.30 | 34.2828 | 25.7715 |
| 1.40 | 8.9870 | 45.5847 | 2.32 | 34.7825 | 25.5332 |
| 1.42 | 9.5650 | 44.7670 | 2.34 | 35.2787 | 25.2995 |
| 1.44 | 10.1464 | 43.9830 | 2.36 | 35.7715 | 25.0702 |
| 1.46 | 10.7305 | 43.2302 | 2.38 | 36.2607 | 24.8452 |
| 1.48 | 11.3169 | 42.5066 | 2.40 | 36.7465 | 24.6243 |
| 1.50 | 11.9052 | 41.8103 | 2.42 | 37.2289 | 24.4075 |
| 1.52 | 12.4949 | 41.1395 | 2.44 | 37.7077 | 24.1945 |
| 1.54 | 13.0856 | 40.4927 | 2.46 | 38.1831 | 23.9854 |
| 1.56 | 13.6770 | 39.8683 | 2.48 | 38.6551 | 23.7800 |
| 1.58 | 14.2686 | 39.2652 | 2.50 | 39.1236 | 23.5782 |
| 1.60 | 14.8604 | 38.6822 | 2.52 | 39.5886 | 23.3799 |
| 1.62 | 15.4518 | 38.1181 | 2.54 | 40.0503 | 23.1850 |
| 1.64 | 16.0427 | 37.5719 | 2.56 | 40.5085 | 22.9934 |
| 1.66 | 16.6328 | 37.0427 | 2.58 | 40.9633 | 22.8051 |
| 1.68 | 17.2220 | 36.5296 | 2.60 | 41.4147 | 22.6199 |
| 1.70 | 17.8099 | 36.0319 | 2.62 | 41.8628 | 22.4377 |
| 1.72 | 18.3964 | 35.5487 | 2.64 | 42.3074 | 22.2586 |
| 1.74 | 18.9814 | 35.0795 | 2.66 | 42.7488 | 22.0824 |
| 1.76 | 19.5646 | 34.6235 | 2.68 | 43.1868 | 21.9090 |
| 1.78 | 20.1458 | 34.1802 | 2.70 | 43.6215 | 21.7385 |
| 1.80 | 20.7251 | 33.7490 | 2.72 | 44.0529 | 21.5706 |
| 1.82 | 21.3021 | 33.3293 | 2.74 | 44.4810 | 21.4053 |
| 1.84 | 21.8768 | 32.9207 | 2.76 | 44.9059 | 21.2427 |
| 1.86 | 22.4492 | 32.5227 | 2.78 | 45.3275 | 21.0825 |
| 1.88 | 23.0190 | 32.1349 | 2.80 | 45.7459 | 20.9248 |
| 1.90 | 23.5861 | 31.7569 | 2.82 | 46.1611 | 20.7695 |

**TABLE E.1** *(Continued)*

| $M$ | $\nu$ | $\mu$ | $M$ | $\nu$ | $\mu$ |
|---|---|---|---|---|---|
| 2.84 | 46.5731 | 20.6166 | 3.94 | 64.9836 | 14.7029 |
| 2.86 | 46.9820 | 20.4659 | 3.96 | 65.2526 | 14.6270 |
| 2.88 | 47.3877 | 20.3175 | 3.98 | 65.5197 | 14.5519 |
| 2.90 | 47.7903 | 20.1713 | 4.00 | 65.7848 | 14.4775 |
| 2.92 | 48.1898 | 20.0272 | 4.02 | 66.0480 | 14.4039 |
| 2.94 | 48.5863 | 19.8852 | 4.04 | 66.3093 | 14.3311 |
| 2.96 | 48.9796 | 19.7452 | 4.06 | 66.5688 | 14.2590 |
| 2.98 | 49.3700 | 19.6072 | 4.08 | 66.8263 | 14.1876 |
| 3.00 | 49.7573 | 19.4712 | 4.10 | 67.0820 | 14.1170 |
| 3.02 | 50.1417 | 19.3371 | 4.12 | 67.3359 | 14.0470 |
| 3.04 | 50.5231 | 19.2049 | 4.14 | 67.5879 | 13.9778 |
| 3.06 | 50.9016 | 19.0745 | 4.16 | 67.8381 | 13.9092 |
| 3.08 | 51.2771 | 18.9459 | 4.18 | 68.0866 | 13.8414 |
| 3.10 | 51.6497 | 18.8191 | 4.20 | 68.3332 | 13.7741 |
| 3.12 | 52.0195 | 18.6939 | 4.22 | 68.5782 | 13.7076 |
| 3.14 | 52.3864 | 18.5705 | 4.24 | 68.8213 | 13.6417 |
| 3.16 | 52.7505 | 18.4487 | 4.26 | 69.0628 | 13.5764 |
| 3.18 | 53.1118 | 18.3285 | 4.28 | 69.3026 | 13.5118 |
| 3.20 | 53.4703 | 18.2100 | 4.30 | 69.5406 | 13.4477 |
| 3.22 | 53.8261 | 18.0929 | 4.32 | 69.7770 | 13.3843 |
| 3.24 | 54.1791 | 17.9774 | 4.34 | 70.0118 | 13.3215 |
| 3.26 | 54.5294 | 17.8634 | 4.36 | 70.2449 | 13.2593 |
| 3.28 | 54.8770 | 17.7508 | 4.38 | 70.4763 | 13.1976 |
| 3.30 | 55.2220 | 17.6397 | 4.40 | 70.7062 | 13.1366 |
| 3.32 | 55.5643 | 17.5300 | 4.42 | 70.9344 | 13.0761 |
| 3.34 | 55.9040 | 17.4216 | 4.44 | 71.1611 | 13.0161 |
| 3.36 | 56.2411 | 17.3147 | 4.46 | 71.3862 | 12.9567 |
| 3.38 | 56.5756 | 17.2090 | 4.48 | 71.6097 | 12.8979 |
| 3.40 | 56.9075 | 17.1046 | 4.50 | 71.8317 | 12.8396 |
| 3.42 | 57.2369 | 17.0016 | 4.52 | 72.0522 | 12.7818 |
| 3.44 | 57.5639 | 16.8997 | 4.54 | 72.2712 | 12.7246 |
| 3.46 | 57.8883 | 16.7991 | 4.56 | 72.4887 | 12.6678 |
| 3.48 | 58.2102 | 16.6997 | 4.58 | 72.7046 | 12.6116 |
| 3.50 | 58.5298 | 16.6015 | 4.60 | 72.9192 | 12.5559 |
| 3.52 | 58.8469 | 16.5045 | 4.62 | 73.1322 | 12.5006 |
| 3.54 | 59.1616 | 16.4086 | 4.64 | 73.3438 | 12.4459 |
| 3.56 | 59.4739 | 16.3139 | 4.66 | 73.5540 | 12.3916 |
| 3.58 | 59.7838 | 16.2202 | 4.68 | 73.7628 | 12.3378 |
| 3.60 | 60.0915 | 16.1276 | 4.70 | 73.9701 | 12.2845 |
| 3.62 | 60.3968 | 16.0361 | 4.72 | 74.1761 | 12.2316 |
| 3.64 | 60.6998 | 15.9456 | 4.74 | 74.3807 | 12.1792 |
| 3.66 | 61.0005 | 15.8562 | 4.76 | 74.5839 | 12.1273 |
| 3.68 | 61.2990 | 15.7678 | 4.78 | 74.7858 | 12.0758 |
| 3.70 | 61.5953 | 15.6804 | 4.80 | 74.9863 | 12.0247 |
| 3.72 | 61.8893 | 15.5939 | 4.82 | 75.1855 | 11.9741 |
| 3.74 | 62.1812 | 15.5084 | 4.84 | 75.3833 | 11.9239 |
| 3.76 | 62.4709 | 15.4239 | 4.86 | 75.5799 | 11.8741 |
| 3.78 | 62.7584 | 15.3402 | 4.88 | 75.7752 | 11.8247 |
| 3.80 | 63.0438 | 15.2575 | 4.90 | 75.9691 | 11.7757 |
| 3.82 | 63.3271 | 15.1757 | 4.92 | 76.1619 | 11.7272 |
| 3.84 | 63.6083 | 15.0948 | 4.94 | 76.3533 | 11.6790 |
| 3.86 | 63.8874 | 15.0147 | 4.96 | 76.5435 | 11.6313 |
| 3.88 | 64.1645 | 14.9355 | 4.98 | 76.7325 | 11.5839 |
| 3.90 | 64.4395 | 14.8572 | 5.00 | 76.9202 | 11.5370 |
| 3.92 | 64.7125 | 14.7796 | | | |

# Appendix F

# Fanno Line Flow

**TABLE F.1** Fanno Line Flow ($\gamma = 1.4$)

| $M$ | $T/T^*$ | $p/p^*$ | $p_o/p_o^*$ | $\rho/\rho^*$ | $fL_{max}/D$ |
|---|---|---|---|---|---|
| 0.00 | 1.2000 | $\infty$ | $\infty$ | $\infty$ | $\infty$ |
| 0.02 | 1.1999 | 54.7701 | 28.9421 | 45.6454 | 1778.4499 |
| 0.04 | 1.1996 | 27.3817 | 14.4815 | 22.8254 | 440.3522 |
| 0.06 | 1.1991 | 18.2508 | 9.6659 | 15.2200 | 193.0311 |
| 0.08 | 1.1985 | 13.6843 | 7.2616 | 11.4182 | 106.7182 |
| 0.10 | 1.1976 | 10.9435 | 5.8218 | 9.1378 | 66.9216 |
| 0.12 | 1.1966 | 9.1156 | 4.8643 | 7.6182 | 45.4080 |
| 0.14 | 1.1953 | 7.8093 | 4.1824 | 6.5333 | 32.5113 |
| 0.16 | 1.1939 | 6.8291 | 3.6727 | 5.7200 | 24.1978 |
| 0.18 | 1.1923 | 6.0662 | 3.2779 | 5.0879 | 18.5427 |
| 0.20 | 1.1905 | 5.4554 | 2.9635 | 4.5826 | 14.5333 |
| 0.22 | 1.1885 | 4.9554 | 2.7076 | 4.1694 | 11.5961 |
| 0.24 | 1.1863 | 4.5383 | 2.4956 | 3.8255 | 9.3865 |
| 0.26 | 1.1840 | 4.1851 | 2.3173 | 3.5347 | 7.6876 |
| 0.28 | 1.1815 | 3.8820 | 2.1656 | 3.2857 | 6.3572 |
| 0.30 | 1.1788 | 3.6191 | 2.0351 | 3.0702 | 5.2993 |
| 0.32 | 1.1759 | 3.3887 | 1.9219 | 2.8818 | 4.4467 |
| 0.34 | 1.1729 | 3.1853 | 1.8229 | 2.7158 | 3.7520 |
| 0.36 | 1.1697 | 3.0042 | 1.7358 | 2.5684 | 3.1801 |
| 0.38 | 1.1663 | 2.8420 | 1.6587 | 2.4367 | 2.7054 |
| 0.40 | 1.1628 | 2.6958 | 1.5901 | 2.3184 | 2.3085 |
| 0.42 | 1.1591 | 2.5634 | 1.5289 | 2.2115 | 1.9744 |
| 0.44 | 1.1553 | 2.4428 | 1.4740 | 2.1145 | 1.6915 |
| 0.46 | 1.1513 | 2.3326 | 1.4246 | 2.0261 | 1.4509 |
| 0.48 | 1.1471 | 2.2313 | 1.3801 | 1.9451 | 1.2453 |
| 0.50 | 1.1429 | 2.1381 | 1.3398 | 1.8708 | 1.0691 |
| 0.52 | 1.1384 | 2.0519 | 1.3034 | 1.8024 | 0.9174 |
| 0.54 | 1.1339 | 1.9719 | 1.2703 | 1.7391 | 0.7866 |
| 0.56 | 1.1292 | 1.8975 | 1.2403 | 1.6805 | 0.6736 |
| 0.58 | 1.1244 | 1.8282 | 1.2130 | 1.6260 | 0.5757 |
| 0.60 | 1.1194 | 1.7634 | 1.1882 | 1.5753 | 0.4908 |
| 0.62 | 1.1143 | 1.7026 | 1.1656 | 1.5279 | 0.4172 |
| 0.64 | 1.1091 | 1.6456 | 1.1451 | 1.4836 | 0.3533 |
| 0.66 | 1.1038 | 1.5919 | 1.1265 | 1.4421 | 0.2979 |
| 0.68 | 1.0984 | 1.5413 | 1.1097 | 1.4032 | 0.2498 |
| 0.70 | 1.0929 | 1.4935 | 1.0944 | 1.3665 | 0.2081 |
| 0.72 | 1.0873 | 1.4482 | 1.0806 | 1.3320 | 0.1721 |
| 0.74 | 1.0815 | 1.4054 | 1.0681 | 1.2994 | 0.1411 |
| 0.76 | 1.0757 | 1.3647 | 1.0570 | 1.2686 | 0.1145 |
| 0.78 | 1.0698 | 1.3261 | 1.0471 | 1.2395 | 0.0917 |
| 0.80 | 1.0638 | 1.2893 | 1.0382 | 1.2119 | 0.0723 |
| 0.82 | 1.0578 | 1.2542 | 1.0305 | 1.1858 | 0.0559 |
| 0.84 | 1.0516 | 1.2208 | 1.0237 | 1.1609 | 0.0423 |
| 0.86 | 1.0454 | 1.1889 | 1.0179 | 1.1373 | 0.0310 |
| 0.88 | 1.0391 | 1.1583 | 1.0129 | 1.1148 | 0.0218 |
| 0.90 | 1.0327 | 1.1291 | 1.0089 | 1.0934 | 0.0145 |

**TABLE F.1** *(Continued)*

| $M$ | $T/T^*$ | $p/p^*$ | $p_o/p_o^*$ | $\rho/\rho^*$ | $fL_{max}/D$ |
|---|---|---|---|---|---|
| 0.92 | 1.0263 | 1.1011 | 1.0056 | 1.0730 | 0.0089 |
| 0.94 | 1.0198 | 1.0743 | 1.0031 | 1.0535 | 0.0048 |
| 0.96 | 1.0132 | 1.0485 | 1.0014 | 1.0348 | 0.0021 |
| 0.98 | 1.0066 | 1.0238 | 1.0003 | 1.0170 | 0.0005 |
| 1.00 | 1.0000 | 1.0000 | 1.0000 | 1.0000 | 0.0000 |
| 1.02 | 0.9933 | 0.9771 | 1.0003 | 0.9837 | 0.0005 |
| 1.04 | 0.9866 | 0.9551 | 1.0013 | 0.9681 | 0.0018 |
| 1.06 | 0.9798 | 0.9338 | 1.0029 | 0.9531 | 0.0038 |
| 1.08 | 0.9730 | 0.9133 | 1.0051 | 0.9387 | 0.0066 |
| 1.10 | 0.9662 | 0.8936 | 1.0079 | 0.9249 | 0.0099 |
| 1.12 | 0.9593 | 0.8745 | 1.0113 | 0.9116 | 0.0138 |
| 1.14 | 0.9524 | 0.8561 | 1.0153 | 0.8988 | 0.0182 |
| 1.16 | 0.9455 | 0.8383 | 1.0198 | 0.8865 | 0.0230 |
| 1.18 | 0.9386 | 0.8210 | 1.0248 | 0.8747 | 0.0281 |
| 1.20 | 0.9317 | 0.8044 | 1.0304 | 0.8633 | 0.0336 |
| 1.22 | 0.9247 | 0.7882 | 1.0366 | 0.8524 | 0.0394 |
| 1.24 | 0.9178 | 0.7726 | 1.0432 | 0.8418 | 0.0455 |
| 1.26 | 0.9108 | 0.7574 | 1.0504 | 0.8316 | 0.0517 |
| 1.28 | 0.9038 | 0.7427 | 1.0581 | 0.8218 | 0.0582 |
| 1.30 | 0.8969 | 0.7285 | 1.0663 | 0.8123 | 0.0648 |
| 1.32 | 0.8899 | 0.7147 | 1.0750 | 0.8031 | 0.0716 |
| 1.34 | 0.8829 | 0.7012 | 1.0842 | 0.7942 | 0.0785 |
| 1.36 | 0.8760 | 0.6882 | 1.0940 | 0.7856 | 0.0855 |
| 1.38 | 0.8690 | 0.6755 | 1.1042 | 0.7773 | 0.0926 |
| 1.40 | 0.8621 | 0.6632 | 1.1149 | 0.7693 | 0.0997 |
| 1.42 | 0.8551 | 0.6512 | 1.1262 | 0.7615 | 0.1069 |
| 1.44 | 0.8482 | 0.6396 | 1.1379 | 0.7540 | 0.1142 |
| 1.46 | 0.8413 | 0.6282 | 1.1501 | 0.7467 | 0.1215 |
| 1.48 | 0.8344 | 0.6172 | 1.1629 | 0.7397 | 0.1288 |
| 1.50 | 0.8276 | 0.6065 | 1.1762 | 0.7328 | 0.1361 |
| 1.52 | 0.8207 | 0.5960 | 1.1899 | 0.7262 | 0.1433 |
| 1.54 | 0.8139 | 0.5858 | 1.2042 | 0.7198 | 0.1506 |
| 1.56 | 0.8071 | 0.5759 | 1.2190 | 0.7135 | 0.1579 |
| 1.58 | 0.8004 | 0.5662 | 1.2344 | 0.7074 | 0.1651 |
| 1.60 | 0.7937 | 0.5568 | 1.2502 | 0.7016 | 0.1724 |
| 1.62 | 0.7869 | 0.5476 | 1.2666 | 0.6958 | 0.1795 |
| 1.64 | 0.7803 | 0.5386 | 1.2836 | 0.6903 | 0.1867 |
| 1.66 | 0.7736 | 0.5299 | 1.3010 | 0.6849 | 0.1938 |
| 1.68 | 0.7670 | 0.5213 | 1.3190 | 0.6796 | 0.2008 |
| 1.70 | 0.7605 | 0.5130 | 1.3376 | 0.6745 | 0.2078 |
| 1.72 | 0.7539 | 0.5048 | 1.3567 | 0.6696 | 0.2147 |
| 1.74 | 0.7474 | 0.4969 | 1.3764 | 0.6648 | 0.2216 |
| 1.76 | 0.7410 | 0.4891 | 1.3967 | 0.6601 | 0.2284 |
| 1.78 | 0.7345 | 0.4815 | 1.4175 | 0.6555 | 0.2352 |
| 1.80 | 0.7282 | 0.4741 | 1.4390 | 0.6511 | 0.2419 |
| 1.82 | 0.7218 | 0.4668 | 1.4610 | 0.6467 | 0.2485 |
| 1.84 | 0.7155 | 0.4597 | 1.4836 | 0.6425 | 0.2551 |
| 1.86 | 0.7093 | 0.4528 | 1.5069 | 0.6384 | 0.2616 |
| 1.88 | 0.7030 | 0.4460 | 1.5308 | 0.6344 | 0.2680 |
| 1.90 | 0.6969 | 0.4394 | 1.5553 | 0.6305 | 0.2743 |
| 1.92 | 0.6907 | 0.4329 | 1.5804 | 0.6267 | 0.2806 |
| 1.94 | 0.6847 | 0.4265 | 1.6062 | 0.6230 | 0.2868 |
| 1.96 | 0.6786 | 0.4203 | 1.6326 | 0.6193 | 0.2929 |
| 1.98 | 0.6726 | 0.4142 | 1.6597 | 0.6158 | 0.2990 |
| 2.00 | 0.6667 | 0.4082 | 1.6875 | 0.6124 | 0.3050 |
| 2.02 | 0.6608 | 0.4024 | 1.7160 | 0.6090 | 0.3109 |
| 2.04 | 0.6549 | 0.3967 | 1.7451 | 0.6057 | 0.3168 |
| 2.06 | 0.6491 | 0.3911 | 1.7750 | 0.6025 | 0.3225 |
| 2.08 | 0.6433 | 0.3856 | 1.8056 | 0.5994 | 0.3282 |

**TABLE F.1** *(Continued)*

| $M$ | $T/T^*$ | $p/p^*$ | $p_o/p_o^*$ | $\rho/\rho^*$ | $fL_{max}/D$ |
|---|---|---|---|---|---|
| 2.10 | 0.6376 | 0.3802 | 1.8369 | 0.5963 | 0.3339 |
| 2.12 | 0.6320 | 0.3750 | 1.8690 | 0.5934 | 0.3394 |
| 2.14 | 0.6263 | 0.3698 | 1.9018 | 0.5905 | 0.3449 |
| 2.16 | 0.6208 | 0.3648 | 1.9354 | 0.5876 | 0.3503 |
| 2.18 | 0.6152 | 0.3598 | 1.9698 | 0.5848 | 0.3556 |
| 2.20 | 0.6098 | 0.3549 | 2.0050 | 0.5821 | 0.3609 |
| 2.22 | 0.6043 | 0.3502 | 2.0409 | 0.5794 | 0.3661 |
| 2.24 | 0.5989 | 0.3455 | 2.0777 | 0.5768 | 0.3712 |
| 2.26 | 0.5936 | 0.3409 | 2.1153 | 0.5743 | 0.3763 |
| 2.28 | 0.5883 | 0.3364 | 2.1538 | 0.5718 | 0.3813 |
| 2.30 | 0.5831 | 0.3320 | 2.1931 | 0.5694 | 0.3862 |
| 2.32 | 0.5779 | 0.3277 | 2.2333 | 0.5670 | 0.3911 |
| 2.34 | 0.5728 | 0.3234 | 2.2744 | 0.5647 | 0.3959 |
| 2.36 | 0.5677 | 0.3193 | 2.3164 | 0.5624 | 0.4006 |
| 2.38 | 0.5626 | 0.3152 | 2.3593 | 0.5602 | 0.4053 |
| 2.40 | 0.5576 | 0.3111 | 2.4031 | 0.5580 | 0.4099 |
| 2.42 | 0.5527 | 0.3072 | 2.4479 | 0.5558 | 0.4144 |
| 2.44 | 0.5478 | 0.3033 | 2.4936 | 0.5537 | 0.4189 |
| 2.46 | 0.5429 | 0.2995 | 2.5403 | 0.5517 | 0.4233 |
| 2.48 | 0.5381 | 0.2958 | 2.5880 | 0.5497 | 0.4277 |
| 2.50 | 0.5333 | 0.2921 | 2.6367 | 0.5477 | 0.4320 |
| 2.52 | 0.5286 | 0.2885 | 2.6865 | 0.5458 | 0.4362 |
| 2.54 | 0.5239 | 0.2850 | 2.7372 | 0.5439 | 0.4404 |
| 2.56 | 0.5193 | 0.2815 | 2.7891 | 0.5421 | 0.4445 |
| 2.58 | 0.5147 | 0.2781 | 2.8420 | 0.5402 | 0.4486 |
| 2.60 | 0.5102 | 0.2747 | 2.8960 | 0.5385 | 0.4526 |
| 2.62 | 0.5057 | 0.2714 | 2.9511 | 0.5367 | 0.4565 |
| 2.64 | 0.5013 | 0.2682 | 3.0073 | 0.5350 | 0.4604 |
| 2.66 | 0.4969 | 0.2650 | 3.0647 | 0.5333 | 0.4643 |
| 2.68 | 0.4925 | 0.2619 | 3.1233 | 0.5317 | 0.4681 |
| 2.70 | 0.4882 | 0.2588 | 3.1830 | 0.5301 | 0.4718 |
| 2.72 | 0.4839 | 0.2558 | 3.2440 | 0.5285 | 0.4755 |
| 2.74 | 0.4797 | 0.2528 | 3.3061 | 0.5269 | 0.4791 |
| 2.76 | 0.4755 | 0.2498 | 3.3695 | 0.5254 | 0.4827 |
| 2.78 | 0.4714 | 0.2470 | 3.4342 | 0.5239 | 0.4863 |
| 2.80 | 0.4673 | 0.2441 | 3.5001 | 0.5225 | 0.4898 |
| 2.82 | 0.4632 | 0.2414 | 3.5674 | 0.5210 | 0.4932 |
| 2.84 | 0.4592 | 0.2386 | 3.6359 | 0.5196 | 0.4966 |
| 2.86 | 0.4552 | 0.2359 | 3.7058 | 0.5182 | 0.5000 |
| 2.88 | 0.4513 | 0.2333 | 3.7771 | 0.5169 | 0.5033 |
| 2.90 | 0.4474 | 0.2307 | 3.8498 | 0.5155 | 0.5065 |
| 2.92 | 0.4436 | 0.2281 | 3.9238 | 0.5142 | 0.5097 |
| 2.94 | 0.4398 | 0.2256 | 3.9993 | 0.5129 | 0.5129 |
| 2.96 | 0.4360 | 0.2231 | 4.0763 | 0.5116 | 0.5160 |
| 2.98 | 0.4323 | 0.2206 | 4.1547 | 0.5104 | 0.5191 |
| 3.00 | 0.4286 | 0.2182 | 4.2346 | 0.5092 | 0.5222 |
| 3.50 | 0.3478 | 0.1685 | 6.7896 | 0.4845 | 0.5864 |
| 4.00 | 0.2857 | 0.1336 | 10.7188 | 0.4677 | 0.6331 |
| 4.50 | 0.2376 | 0.1083 | 16.5622 | 0.4559 | 0.6676 |
| 5.00 | 0.2000 | 0.0894 | 25.0000 | 0.4472 | 0.6938 |
| 6.00 | 0.1463 | 0.0638 | 53.1798 | 0.4357 | 0.7299 |
| 7.00 | 0.1111 | 0.0476 | 104.1429 | 0.4286 | 0.7528 |
| 8.00 | 0.0870 | 0.0369 | 190.1094 | 0.4239 | 0.7682 |
| 9.00 | 0.0698 | 0.0293 | 327.1893 | 0.4207 | 0.7790 |
| 10.00 | 0.0571 | 0.0239 | 535.9375 | 0.4183 | 0.7868 |
| $\infty$ | 0 | 0 | $\infty$ | 0.40824 | 0.8215 |

# Appendix G

# Rayleigh Line Flow

**TABLE G.1** Rayleigh Line Flow ($\gamma = 1.4$)

| $M$ | $T_o/T_o^*$ | $T/T^*$ | $p_o/p_o^*$ | $p/p^*$ | $V/V^*$ |
|---|---|---|---|---|---|
| 0.00 | 0.0000 | 0.0000 | 1.2679 | 2.4000 | 0.0000 |
| 0.02 | 0.0019 | 0.0023 | 1.2675 | 2.3987 | 0.0010 |
| 0.04 | 0.0076 | 0.0092 | 1.2665 | 2.3946 | 0.0038 |
| 0.06 | 0.0171 | 0.0205 | 1.2647 | 2.3880 | 0.0086 |
| 0.08 | 0.0302 | 0.0362 | 1.2623 | 2.3787 | 0.0152 |
| 0.10 | 0.0468 | 0.0560 | 1.2591 | 2.3669 | 0.0237 |
| 0.12 | 0.0666 | 0.0797 | 1.2554 | 2.3526 | 0.0339 |
| 0.14 | 0.0895 | 0.1069 | 1.2510 | 2.3359 | 0.0458 |
| 0.16 | 0.1151 | 0.1374 | 1.2461 | 2.3170 | 0.0593 |
| 0.18 | 0.1432 | 0.1708 | 1.2406 | 2.2959 | 0.0744 |
| 0.20 | 0.1736 | 0.2066 | 1.2346 | 2.2727 | 0.0909 |
| 0.22 | 0.2057 | 0.2445 | 1.2281 | 2.2477 | 0.1088 |
| 0.24 | 0.2395 | 0.2841 | 1.2213 | 2.2209 | 0.1279 |
| 0.26 | 0.2745 | 0.3250 | 1.2140 | 2.1925 | 0.1482 |
| 0.28 | 0.3104 | 0.3667 | 1.2064 | 2.1626 | 0.1696 |
| 0.30 | 0.3469 | 0.4089 | 1.1985 | 2.1314 | 0.1918 |
| 0.32 | 0.3837 | 0.4512 | 1.1904 | 2.0991 | 0.2149 |
| 0.34 | 0.4206 | 0.4933 | 1.1822 | 2.0657 | 0.2388 |
| 0.36 | 0.4572 | 0.5348 | 1.1737 | 2.0314 | 0.2633 |
| 0.38 | 0.4935 | 0.5755 | 1.1652 | 1.9964 | 0.2883 |
| 0.40 | 0.5290 | 0.6151 | 1.1566 | 1.9608 | 0.3137 |
| 0.42 | 0.5638 | 0.6535 | 1.1480 | 1.9247 | 0.3395 |
| 0.44 | 0.5975 | 0.6903 | 1.1394 | 1.8882 | 0.3656 |
| 0.46 | 0.6301 | 0.7254 | 1.1308 | 1.8515 | 0.3918 |
| 0.48 | 0.6614 | 0.7587 | 1.1224 | 1.8147 | 0.4181 |
| 0.50 | 0.6914 | 0.7901 | 1.1141 | 1.7778 | 0.4444 |
| 0.52 | 0.7199 | 0.8196 | 1.1059 | 1.7409 | 0.4708 |
| 0.54 | 0.7470 | 0.8469 | 1.0979 | 1.7043 | 0.4970 |
| 0.56 | 0.7725 | 0.8723 | 1.0901 | 1.6678 | 0.5230 |
| 0.58 | 0.7965 | 0.8955 | 1.0826 | 1.6316 | 0.5489 |
| 0.60 | 0.8189 | 0.9167 | 1.0753 | 1.5957 | 0.5745 |
| 0.62 | 0.8398 | 0.9358 | 1.0682 | 1.5603 | 0.5998 |
| 0.64 | 0.8592 | 0.9530 | 1.0615 | 1.5253 | 0.6248 |
| 0.66 | 0.8771 | 0.9682 | 1.0550 | 1.4908 | 0.6494 |
| 0.68 | 0.8935 | 0.9814 | 1.0489 | 1.4569 | 0.6737 |
| 0.70 | 0.9085 | 0.9929 | 1.0431 | 1.4235 | 0.6975 |
| 0.72 | 0.9221 | 1.0026 | 1.0376 | 1.3907 | 0.7209 |
| 0.74 | 0.9344 | 1.0106 | 1.0325 | 1.3585 | 0.7439 |
| 0.76 | 0.9455 | 1.0171 | 1.0278 | 1.3270 | 0.7665 |
| 0.78 | 0.9553 | 1.0220 | 1.0234 | 1.2961 | 0.7885 |
| 0.80 | 0.9639 | 1.0255 | 1.0193 | 1.2658 | 0.8101 |
| 0.82 | 0.9715 | 1.0276 | 1.0157 | 1.2362 | 0.8313 |
| 0.84 | 0.9781 | 1.0285 | 1.0124 | 1.2073 | 0.8519 |
| 0.86 | 0.9836 | 1.0283 | 1.0095 | 1.1791 | 0.8721 |
| 0.88 | 0.9883 | 1.0269 | 1.0070 | 1.1515 | 0.8918 |
| 0.90 | 0.9921 | 1.0245 | 1.0049 | 1.1246 | 0.9110 |

**TABLE G.1** *(Continued)*

| $M$ | $T_o/T_o^*$ | $T/T^*$ | $p_o/p_o^*$ | $p/p^*$ | $V/V^*$ |
|---|---|---|---|---|---|
| 0.92 | 0.9951 | 1.0212 | 1.0031 | 1.0984 | 0.9297 |
| 0.94 | 0.9973 | 1.0170 | 1.0017 | 1.0728 | 0.9480 |
| 0.96 | 0.9988 | 1.0121 | 1.0008 | 1.0479 | 0.9658 |
| 0.98 | 0.9997 | 1.0064 | 1.0002 | 1.0236 | 0.9831 |
| 1.00 | 1.0000 | 1.0000 | 1.0000 | 1.0000 | 1.0000 |
| 1.02 | 0.9997 | 0.9930 | 1.0002 | 0.9770 | 1.0164 |
| 1.04 | 0.9989 | 0.9855 | 1.0008 | 0.9546 | 1.0325 |
| 1.06 | 0.9977 | 0.9776 | 1.0017 | 0.9327 | 1.0480 |
| 1.08 | 0.9960 | 0.9691 | 1.0031 | 0.9115 | 1.0632 |
| 1.10 | 0.9939 | 0.9603 | 1.0049 | 0.8909 | 1.0780 |
| 1.12 | 0.9915 | 0.9512 | 1.0070 | 0.8708 | 1.0923 |
| 1.14 | 0.9887 | 0.9417 | 1.0095 | 0.8512 | 1.1063 |
| 1.16 | 0.9856 | 0.9320 | 1.0124 | 0.8322 | 1.1198 |
| 1.18 | 0.9823 | 0.9220 | 1.0157 | 0.8137 | 1.1330 |
| 1.20 | 0.9787 | 0.9118 | 1.0194 | 0.7958 | 1.1459 |
| 1.22 | 0.9749 | 0.9015 | 1.0235 | 0.7783 | 1.1584 |
| 1.24 | 0.9709 | 0.8911 | 1.0279 | 0.7613 | 1.1705 |
| 1.26 | 0.9668 | 0.8805 | 1.0328 | 0.7447 | 1.1823 |
| 1.28 | 0.9624 | 0.8699 | 1.0380 | 0.7287 | 1.1938 |
| 1.30 | 0.9580 | 0.8592 | 1.0437 | 0.7130 | 1.2050 |
| 1.32 | 0.9534 | 0.8484 | 1.0497 | 0.6978 | 1.2159 |
| 1.34 | 0.9487 | 0.8377 | 1.0561 | 0.6830 | 1.2264 |
| 1.36 | 0.9440 | 0.8269 | 1.0629 | 0.6686 | 1.2367 |
| 1.38 | 0.9391 | 0.8161 | 1.0701 | 0.6546 | 1.2467 |
| 1.40 | 0.9343 | 0.8054 | 1.0777 | 0.6410 | 1.2564 |
| 1.42 | 0.9293 | 0.7947 | 1.0856 | 0.6278 | 1.2659 |
| 1.44 | 0.9243 | 0.7840 | 1.0940 | 0.6149 | 1.2751 |
| 1.46 | 0.9193 | 0.7735 | 1.1028 | 0.6024 | 1.2840 |
| 1.48 | 0.9143 | 0.7629 | 1.1120 | 0.5902 | 1.2927 |
| 1.50 | 0.9093 | 0.7525 | 1.1215 | 0.5783 | 1.3012 |
| 1.52 | 0.9042 | 0.7422 | 1.1315 | 0.5668 | 1.3095 |
| 1.54 | 0.8992 | 0.7319 | 1.1419 | 0.5555 | 1.3175 |
| 1.56 | 0.8942 | 0.7217 | 1.1527 | 0.5446 | 1.3253 |
| 1.58 | 0.8892 | 0.7117 | 1.1640 | 0.5339 | 1.3329 |
| 1.60 | 0.8842 | 0.7017 | 1.1756 | 0.5236 | 1.3403 |
| 1.62 | 0.8792 | 0.6919 | 1.1877 | 0.5135 | 1.3475 |
| 1.64 | 0.8743 | 0.6822 | 1.2002 | 0.5036 | 1.3546 |
| 1.66 | 0.8694 | 0.6726 | 1.2131 | 0.4940 | 1.3614 |
| 1.68 | 0.8645 | 0.6631 | 1.2264 | 0.4847 | 1.3681 |
| 1.70 | 0.8597 | 0.6538 | 1.2402 | 0.4756 | 1.3746 |
| 1.72 | 0.8549 | 0.6445 | 1.2545 | 0.4668 | 1.3809 |
| 1.74 | 0.8502 | 0.6355 | 1.2692 | 0.4581 | 1.3870 |
| 1.76 | 0.8455 | 0.6265 | 1.2843 | 0.4497 | 1.3931 |
| 1.78 | 0.8409 | 0.6176 | 1.2999 | 0.4415 | 1.3989 |
| 1.80 | 0.8363 | 0.6089 | 1.3159 | 0.4335 | 1.4046 |
| 1.82 | 0.8317 | 0.6004 | 1.3324 | 0.4257 | 1.4102 |
| 1.84 | 0.8273 | 0.5919 | 1.3494 | 0.4181 | 1.4156 |
| 1.86 | 0.8228 | 0.5836 | 1.3669 | 0.4107 | 1.4209 |
| 1.88 | 0.8185 | 0.5754 | 1.3849 | 0.4035 | 1.4261 |
| 1.90 | 0.8141 | 0.5673 | 1.4033 | 0.3964 | 1.4311 |
| 1.92 | 0.8099 | 0.5594 | 1.4222 | 0.3895 | 1.4360 |
| 1.94 | 0.8057 | 0.5516 | 1.4417 | 0.3828 | 1.4408 |
| 1.96 | 0.8015 | 0.5439 | 1.4616 | 0.3763 | 1.4455 |
| 1.98 | 0.7974 | 0.5364 | 1.4821 | 0.3699 | 1.4501 |
| 2.00 | 0.7934 | 0.5289 | 1.5031 | 0.3636 | 1.4545 |
| 2.02 | 0.7894 | 0.5216 | 1.5246 | 0.3575 | 1.4589 |
| 2.04 | 0.7855 | 0.5144 | 1.5467 | 0.3516 | 1.4632 |
| 2.06 | 0.7816 | 0.5074 | 1.5693 | 0.3458 | 1.4673 |
| 2.08 | 0.7778 | 0.5004 | 1.5924 | 0.3401 | 1.4714 |

**TABLE G.1** *(Continued)*

| $M$ | $T_o/T_o^*$ | $T/T^*$ | $p_o/p_o^*$ | $p/p^*$ | $V/V^*$ |
|---|---|---|---|---|---|
| 2.10 | 0.7741 | 0.4936 | 1.6162 | 0.3345 | 1.4753 |
| 2.12 | 0.7704 | 0.4868 | 1.6404 | 0.3291 | 1.4792 |
| 2.14 | 0.7667 | 0.4802 | 1.6653 | 0.3238 | 1.4830 |
| 2.16 | 0.7631 | 0.4737 | 1.6908 | 0.3186 | 1.4867 |
| 2.18 | 0.7596 | 0.4673 | 1.7168 | 0.3136 | 1.4903 |
| 2.20 | 0.7561 | 0.4611 | 1.7434 | 0.3086 | 1.4938 |
| 2.22 | 0.7527 | 0.4549 | 1.7707 | 0.3038 | 1.4973 |
| 2.24 | 0.7493 | 0.4488 | 1.7986 | 0.2991 | 1.5007 |
| 2.26 | 0.7460 | 0.4428 | 1.8271 | 0.2945 | 1.5040 |
| 2.28 | 0.7428 | 0.4370 | 1.8562 | 0.2899 | 1.5072 |
| 2.30 | 0.7395 | 0.4312 | 1.8860 | 0.2855 | 1.5103 |
| 2.32 | 0.7364 | 0.4256 | 1.9165 | 0.2812 | 1.5134 |
| 2.34 | 0.7333 | 0.4200 | 1.9476 | 0.2769 | 1.5165 |
| 2.36 | 0.7302 | 0.4145 | 1.9794 | 0.2728 | 1.5194 |
| 2.38 | 0.7272 | 0.4091 | 2.0119 | 0.2688 | 1.5223 |
| 2.40 | 0.7242 | 0.4038 | 2.0451 | 0.2648 | 1.5252 |
| 2.42 | 0.7213 | 0.3986 | 2.0789 | 0.2609 | 1.5279 |
| 2.44 | 0.7184 | 0.3935 | 2.1136 | 0.2571 | 1.5306 |
| 2.46 | 0.7156 | 0.3885 | 2.1489 | 0.2534 | 1.5333 |
| 2.48 | 0.7128 | 0.3836 | 2.1850 | 0.2497 | 1.5359 |
| 2.50 | 0.7101 | 0.3787 | 2.2218 | 0.2462 | 1.5385 |
| 2.52 | 0.7074 | 0.3739 | 2.2594 | 0.2427 | 1.5410 |
| 2.54 | 0.7047 | 0.3692 | 2.2978 | 0.2392 | 1.5434 |
| 2.56 | 0.7021 | 0.3646 | 2.3370 | 0.2359 | 1.5458 |
| 2.58 | 0.6995 | 0.3601 | 2.3770 | 0.2326 | 1.5482 |
| 2.60 | 0.6970 | 0.3556 | 2.4177 | 0.2294 | 1.5505 |
| 2.62 | 0.6945 | 0.3512 | 2.4593 | 0.2262 | 1.5527 |
| 2.64 | 0.6921 | 0.3469 | 2.5018 | 0.2231 | 1.5549 |
| 2.66 | 0.6896 | 0.3427 | 2.5451 | 0.2201 | 1.5571 |
| 2.68 | 0.6873 | 0.3385 | 2.5892 | 0.2171 | 1.5592 |
| 2.70 | 0.6849 | 0.3344 | 2.6343 | 0.2142 | 1.5613 |
| 2.72 | 0.6826 | 0.3304 | 2.6802 | 0.2113 | 1.5634 |
| 2.74 | 0.6804 | 0.3264 | 2.7270 | 0.2085 | 1.5654 |
| 2.76 | 0.6781 | 0.3225 | 2.7748 | 0.2058 | 1.5673 |
| 2.78 | 0.6760 | 0.3186 | 2.8235 | 0.2030 | 1.5693 |
| 2.80 | 0.6738 | 0.3149 | 2.8731 | 0.2004 | 1.5711 |
| 2.82 | 0.6717 | 0.3111 | 2.9237 | 0.1978 | 1.5730 |
| 2.84 | 0.6696 | 0.3075 | 2.9752 | 0.1953 | 1.5748 |
| 2.86 | 0.6675 | 0.3039 | 3.0278 | 0.1927 | 1.5766 |
| 2.88 | 0.6655 | 0.3004 | 3.0813 | 0.1903 | 1.5784 |
| 2.90 | 0.6635 | 0.2969 | 3.1359 | 0.1879 | 1.5801 |
| 2.92 | 0.6615 | 0.2934 | 3.1914 | 0.1855 | 1.5818 |
| 2.94 | 0.6596 | 0.2901 | 3.2481 | 0.1832 | 1.5834 |
| 2.96 | 0.6577 | 0.2868 | 3.3058 | 0.1809 | 1.5851 |
| 2.98 | 0.6558 | 0.2835 | 3.3646 | 0.1787 | 1.5867 |
| 3.00 | 0.6540 | 0.2803 | 3.4245 | 0.1765 | 1.5882 |
| 3.50 | 0.6158 | 0.2142 | 5.3280 | 0.1322 | 1.6198 |
| 4.00 | 0.5891 | 0.1683 | 8.2268 | 0.1026 | 1.6410 |
| 4.50 | 0.5698 | 0.1354 | 12.5023 | 0.0818 | 1.6559 |
| 5.00 | 0.5556 | 0.1111 | 18.6339 | 0.0667 | 1.6667 |
| 6.00 | 0.5363 | 0.0785 | 38.9459 | 0.0467 | 1.6809 |
| 7.00 | 0.5244 | 0.0583 | 75.4138 | 0.0345 | 1.6897 |
| 8.00 | 0.5165 | 0.0449 | 136.6235 | 0.0265 | 1.6954 |
| 9.00 | 0.5110 | 0.0356 | 233.8840 | 0.0210 | 1.6993 |
| 10.00 | 0.5070 | 0.0290 | 381.6149 | 0.0170 | 1.7021 |
| $\infty$ | 0.4898 | 0.0000 | $\infty$ | 0.0000 | 1.7143 |

# Appendix H

# Physical Properties of Gases

**TABLE H.1** Ideal-Gas Properties of Various Gases

| Gas | Chemical formula | Molecular mass | Gas constant, $R$ kJ/kg · K | $c_p$ kJ/kg · K | $\gamma = c_p/c_v$ |
|---|---|---|---|---|---|
| Acetylene | $C_2H_2$ | 26.038 | 0.3193 | 1.711 | 1.23 |
| Air | | 28.967 | 0.2870 | 1.004 | 1.40 |
| Ammonia | $NH_3$ | 17.030 | 0.4882 | 2.092 | 1.30 |
| Argon | Ar | 39.948 | 0.2081 | 0.519 | 1.67 |
| Butane | $C_4H_{10}$ | 58.124 | 0.1430 | 1.674 | 1.09 |
| Carbon dioxide | $CO_2$ | 44.009 | 0.1889 | 0.845 | 1.30 |
| Carbon monoxide | CO | 28.010 | 0.2968 | 1.042 | 1.40 |
| Ethane | $C_2H_6$ | 30.070 | 0.2765 | 1.766 | 1.18 |
| Ethylene | $C_2H_4$ | 28.054 | 0.2964 | 1.720 | 1.21 |
| Helium | He | 4.003 | 2.0770 | 5.200 | 1.67 |
| Hydrogen | $H_2$ | 2.016 | 4.1240 | 14.350 | 1.40 |
| Methane | $CH_4$ | 16.043 | 0.5182 | 2.223 | 1.32 |
| Nitrogen | $N_2$ | 28.014 | 0.2968 | 1.038 | 1.40 |
| Oxygen | $O_2$ | 31.998 | 0.2598 | 0.916 | 1.40 |
| Propane | $C_3H_8$ | 44.097 | 0.1885 | 1.690 | 1.12 |
| Water vapor | $H_2O$ | 18.015 | 0.4615 | 1.866 | 1.33 |

*Note*: $c_p$ and $c_v$ are taken at 25°C.
This table has been adapted from Haberman, W. L., and John, J. E. A., *Engineering Thermodynamics*, Allyn and Bacon, Boston, 1980, p. 443.

**TABLE H.2** Ideal-Gas Specific-Heat Ratio $\gamma$ of Several Gases as a Function of Temperature

| $T$ (K) | Nitrogen ($N_2$) | Oxygen ($O_2$) | Hydrogen ($H_2$) | Water vapor 200 |
|---|---|---|---|---|
| 1.400 | 1.399 | 1.439 | 1.332 | |
| 400 | 1.397 | 1.382 | 1.398 | 1.321 |
| 600 | 1.381 | 1.350 | 1.396 | 1.297 |
| 800 | 1.360 | 1.327 | 1.390 | 1.274 |
| 1000 | 1.341 | 1.313 | 1.380 | 1.253 |

This table is taken from Hilsenrath et al., *Tables of Thermodynamic and Transport Properties*, Pergamon Press, Elmsford, NY, 1960. Originally published as National Bureau of Standards Circular 564.

**TABLE H.3** Thermodynamic Properties of Air at 1 Atmosphere ($R$ for Air = 0.2870 kJ/kg • K)

| $T$ (K) | $c_p/R$ | $\gamma$ | $\frac{(h - h_{ref})}{\text{kJ/kg}}$ | $\frac{s - s_{ref}}{R}$ |
|---|---|---|---|---|
| 200 | 3.506 | 1.406 | 199.7 | 22.497 |
| 300 | 3.506 | 1.402 | 300.2 | 23.917 |
| 400 | 3.533 | 1.396 | 401.2 | 24.929 |
| 500 | 3.588 | 1.387 | 503.3 | 25.723 |
| 600 | 3.663 | 1.376 | 607.4 | 26.383 |
| 700 | 3.746 | 1.365 | 713.7 | 26.954 |
| 800 | 3.828 | 1.354 | 822.4 | 27.460 |
| 900 | 3.906 | 1.345 | 933.4 | 27.915 |
| 1000 | 3.979 | 1.336 | 1046.6 | 28.330 |
| 1200 | 4.109 | 1.322 | 1278.8 | 29.068 |
| 1400 | 4.230 | 1.310 | 1518.2 | 29.711 |
| 1600 | 4.352 | 1.299 | 1764.5 | 30.284 |
| 1800 | 4.487 | 1.288 | 2018.2 | 30.804 |
| 2000 | 4.662 | 1.274 | 2280.6 | 31.284 |

This table is taken from Hilsenrath et al., *Tables of Thermodynamic and Transport Properties*, Pergamon Press, Elmsford, NY, 1960. Originally published as National Bureau of Standards Circular 564.

**TABLE H.4** Thermodynamic Properties of Air at 10 Atmospheres ($R$ for Air = 0.2870 kJ/kg • K)

| $T$ (K) | $c_p/R$ | $\gamma$ | $\frac{(h - h_{ref})}{\text{kJ/kg}}$ | $\frac{s - s_{ref}}{R}$ |
|---|---|---|---|---|
| 200 | 3.643 | 1.449 | 195.3 | 20.139 |
| 300 | 3.555 | 1.418 | 298.2 | 21.594 |
| 400 | 3.558 | 1.404 | 400.2 | 22.616 |
| 500 | 3.603 | 1.392 | 502.9 | 23.414 |
| 600 | 3.673 | 1.379 | 607.3 | 24.077 |
| 700 | 3.753 | 1.366 | 713.8 | 24.649 |
| 800 | 3.834 | 1.355 | 822.7 | 25.155 |
| 900 | 3.910 | 1.345 | 933.8 | 25.610 |
| 1000 | 3.983 | 1.336 | 1047.1 | 26.025 |
| 1200 | 4.111 | 1.322 | 1279.5 | 26.763 |
| 1400 | 4.232 | 1.310 | 1519.0 | 27.404 |
| 1600 | 4.351 | 1.299 | 1765.3 | 27.977 |
| 1800 | 4.478 | 1.288 | 2018.7 | 28.740 |
| 2000 | 4.613 | 1.278 | 2279.5 | 28.974 |

This table is taken from Hilsenrath et al., *Tables of Thermodynamic and Transport Properties*, Pergamon Press, Elmsford, NY, 1960. Originally published as National Bureau of Standards Circular 564.

**TABLE H.5** Thermodynamic Properties of Nitrogen at 1 Atmosphere ($R$ for Nitrogen = 0.2968 kJ/kg·K)

| $T$ (K) | $\frac{(h - h_{ref})}{\text{kJ/kg}}$ | $\frac{s - s_{ref}}{R}$ |
|---|---|---|
| 200 | 207.0 | 21.6249 |
| 250 | 259.1 | 22.4085 |
| 300 | 311.2 | 23.0482 |
| 350 | 363.3 | 23.5892 |
| 400 | 415.4 | 24.0586 |
| 450 | 467.8 | 24.4741 |
| 500 | 520.4 | 24.8479 |
| 550 | 573.4 | 25.1884 |
| 600 | 626.9 | 25.5020 |
| 650 | 681.0 | 25.7935 |
| 700 | 735.6 | 26.0662 |
| 750 | 790.8 | 26.3228 |
| 800 | 846.6 | 26.5656 |
| 900 | 960.8 | 27.0154 |
| 1000 | 1075.6 | 27.4260 |
| 1100 | 1193.3 | 27.8039 |
| 1200 | 1312.9 | 28.1543 |
| 1300 | 1434.0 | 28.4811 |
| 1400 | 1556.6 | 28.7872 |
| 1500 | 1680.4 | 29.0751 |
| 1600 | 1805.3 | 29.3467 |
| 1700 | 1931.2 | 29.6037 |
| 1800 | 2057.9 | 29.8477 |
| 1900 | 2185.3 | 30.0799 |
| 2000 | 2313.4 | 30.3013 |

This table is taken from Hilsenrath et al., *Tables of Thermodynamic and Transport Properties*, Pergamon Press, Elmsford, NY, 1960. Originally published as National Bureau of Standards Circular 564.

**TABLE H.6** Thermodynamic Properties of Nitrogen at 10 Atmospheres ($R$ for Nitrogen = 0.2968 kJ/kg·K)

| $T$ (K) | $\frac{(h - h_{ref})}{\text{kJ/kg}}$ | $\frac{s - s_{ref}}{R}$ |
|---|---|---|
| 200 | 202.7 | 19.2682 |
| 250 | 256.2 | 20.0741 |
| 300 | 309.2 | 20.7248 |
| 350 | 361.9 | 21.2721 |
| 400 | 414.5 | 21.7454 |
| 450 | 467.1 | 22.1634 |
| 500 | 520.0 | 22.5390 |
| 550 | 573.2 | 22.8807 |
| 600 | 626.9 | 23.1953 |
| 650 | 681.1 | 23.4875 |
| 700 | 735.8 | 23.7607 |
| 750 | 791.1 | 24.0178 |
| 800 | 847.0 | 24.2609 |
| 900 | 960.5 | 24.7113 |
| 1000 | 1076.2 | 25.1223 |
| 1100 | 1194.0 | 25.5004 |
| 1200 | 1313.7 | 25.8511 |
| 1300 | 1434.9 | 26.1780 |
| 1400 | 1557.5 | 26.4842 |
| 1500 | 1681.3 | 26.7721 |
| 1600 | 1806.3 | 27.0438 |
| 1700 | 1932.1 | 27.3009 |
| 1800 | 2058.9 | 27.5449 |
| 1900 | 2186.3 | 27.7772 |
| 2000 | 2314.4 | 27.9986 |

This table is taken from Hilsenrath et al., *Tables of Thermodynamic and Transport Properties*, Pergamon Press, Elmsford, NY, 1960. Originally published as National Bureau of Standards Circular 564.

# Appendix I

# Standard Atmosphere

**TABLE I.1** Standard Atmosphere Properties

| Altitude Z (km) | $T$ (K) | $p$ (kPa) | $\rho$ (kg/m³) | $\mu \times 10^5$ (N·s/m²) |
|---|---|---|---|---|
| 0 | 288.2 | 101.3 | 1.225 | 1.79 |
| 5 | 255.7 | 54.05 | 0.736 | 1.63 |
| 10 | 223.3 | 26.50 | 0.414 | 1.46 |
| 15 | 216.7 | 12.11 | 0.195 | 1.42 |
| 20 | 216.7 | 5.53 | 0.0889 | 1.42 |
| 25 | 221.6 | 2.55 | 0.0401 | 1.45 |
| 30 | 226.5 | 1.20 | 0.0184 | 1.48 |
| 35 | 236.5 | 0.575 | 0.00846 | 1.53 |
| 40 | 250.4 | 0.287 | 0.00400 | 1.60 |
| 45 | 264.2 | 0.149 | 0.00197 | 1.67 |
| 50 | 270.7 | 0.0798 | 0.00103 | 1.70 |
| 55 | 260.8 | 0.0425 | 0.000568 | 1.65 |
| 60 | 247.0 | 0.0220 | 0.000310 | 1.58 |

Reference: U.S. Standard Atmosphere 1976; NOAA, NASA, USAF, Washington, DC, October 1976.

Approximate formulas are available for standard atmosphere descriptions. The following analysis is adapted from Boiffier, J. L., *The Dynamics of Flight: The Equations*, John Wiley & Sons, New York, 1998.

**Assumptions:**

(1) It is assumed that the air is completely immobile (the Taylor hypothesis).

(2) It is assumed that air is an ideal gas; therefore, $p = \rho RT$. (I.1)

(3) It is assumed that the atmosphere is subject to the hydrostatic equation:

$$dp = -\rho g\, dZ \tag{I.2}$$

(4) It is assumed that temperature variation with altitude (sometimes called Toussaint's law), is characterized by a temperature gradient

$$T_z = dT/dZ \tag{I.3}$$

where the gradient is given in Table I.2.

**TABLE I.2** Altitude Variation of the Temperature Gradient

| Altitude $Z$ | Gradient of Temperature $T_Z \equiv dT/dZ$ |
|---|---|
| $0 \text{ km} \leq Z \leq 11 \text{ km}$ | $-6.5 \times 10^{-3}$ K/m |
| $11 \text{ km} \leq Z \leq 20 \text{ km}$ | 0 K/m |
| $20 \text{ km} \leq Z \leq 32 \text{ km}$ | $1 \times 10^{-3}$ K/m |
| $32 \text{ km} \leq Z \leq 47 \text{ km}$ | $2.8 \times 10^{-3}$ K/m |

The acceleration of gravity can be taken as $g = 9.806 \text{ m/s}^2$.

The altitude variation of pressure, density, and temperature can be estimated from the following:

(1) For an altitude $0 \text{ m} \leq Z \leq 11{,}000 \text{ m}$, we use Eqs. (I.1), (I.2), and (I.3) to find that

$$p = p_0\left(1 + \frac{T_Z}{T_0}Z\right)^{\frac{-g}{RT_Z}}$$

$$\rho = \frac{p}{RT} = \rho_0\left(1 + \frac{T_Z}{T_0}Z\right)^{\frac{-g}{RT_Z}-1}$$

$$T = T_0 + T_Z Z = T_0\left(1 + \frac{T_Z}{T_0}Z\right)$$

where $Z$ is given in meters and $p_0$, $\rho_0$, and $T_0$ are the values at sea level.

(2) For $11{,}000 \text{ m} \leq Z \leq 20{,}000 \text{ m}$,

$$p = p_{11}e^{\frac{-g}{RT_{11}}(Z-11{,}000)}$$

$$\rho = \frac{p}{RT} = \rho_{11}e^{\frac{-g}{RT_{11}}(Z-11{,}000)}$$

$$T = T_{11} = 216.7 \text{ K}$$

where the state variables at 11 km are $p_{11} = 22{,}631.7$ Pa, $\rho_{11} = 0.3639 \text{ kg/m}^3$, and $T_{11} = 216.7$ K.

(3) For $20{,}000 \text{ m} \leq Z \leq 32{,}000 \text{ m}$,

$$p = p_{20}\left[1 + \frac{T_Z}{T_{20}}(Z - 20{,}000)\right]^{\frac{-g}{RT_Z}}$$

$$\rho = \frac{p}{RT} = \rho_{20}\left[1 + \frac{T_Z}{T_{20}}(Z - 20{,}000)\right]^{\frac{-g}{RT_Z}-1}$$

$$T = T_{20}\left[1 + \frac{T_Z}{T_{20}}(Z - 20{,}000)\right]$$

where the atmosphere parameters at 20 km are, approximately, $p_{20} = 5{,}474.7$ Pa, $\rho_{20} = 0.08803$ kg/m$^3$, and $T_{20} = 216.7$ K.

4. For 32,000 m $\leq Z \leq$ 47,000 m,

$$p = p_{32}\left[1 + \frac{T_Z}{T_{32}}(Z - 32{,}000)\right]^{\frac{-g}{RT_Z}}$$

$$\rho = \frac{p}{RT} = \rho_{32}\left[1 + \frac{T_Z}{T_{32}}(Z - 32{,}000)\right]^{\frac{-g}{RT_Z}-1}$$

$$T = T_{32}\left[1 + \frac{T_Z}{T_{32}}(Z - 32{,}000)\right]$$

where the values at 32 km are, approximately, $p_{32} = 867.98$ Pa, $\rho_{32} = 0.01322$ kg/m$^3$, and $T_{32} = 228.7$ K.

Some variation may exist between the values provided by the approximate equations and the "standard" atmospheric data from the tables; however, for many engineering applications, the differences are insignificant.

# Appendix J

# Conversion Factors

**TABLE J.1** Conversion Factors

| | |
|---|---|
| Length | 1 ft = 0.3048 m<br>1 m = 3.281 ft |
| Volume | 1 $ft^3$ = 0.02832 $m^3$<br>1 $m^3$ = 35.315 $ft^3$ = 1000 liters<br>1 liter = 1.057 qt |
| Mass | 1 lbm = 0.45359 kg<br>1 kg = 2.2046 lb |
| Density | 1 $lbm/ft^3$ = 16.02 $kg/m^3$<br>1 $kg/m^3$ = 0.06243 $lbm/ft^3$ |
| Force | 1 lbf = 4.448 N<br>1 N = 0.2248 lbf |
| Pressure | 1 $lbf/in^2$ = 6.8948 $kN/m^2$<br>1 $N/m^2$ = 1 Pa = 0.02089 $lbf/in^2$<br>1 atm = 101.3 kPa |
| Energy | 1 Btu = 1.055 kJ<br>1 kJ = 0.9478 Btu |
| Power | 1 horsepower = 0.7457 kW<br>1 Btu/s = 1.055 kW<br>1 W = 3.412 Btu/h |
| Specific energy | 1 Btu/lbm = 2.326 kJ/kg<br>1 kJ/kg = 0.4299 Btu/lbm |
| Velocity | 1 ft/s = 0.3048 m/s<br>1 m/s = 3.281 ft/s |
| Temperature | °F = 1.8(°C) + 32<br>°C = (°F − 32)/1.8<br>K = °R / 1.8<br>°R = 1.8 K<br>°R = °F + 459.67<br>K = °C + 273.15 |

# Index

## D

## E



## F



## G



## H

## I



## J



## K



## L



## M

## N



## O



## P

## Q



## R



## S